ICPES 2025

40th INTERNATIONAL CONFERENCE ON PRODUCTION ENGINEERING – SERBIA 2025

Nis, Serbia, 18th - 19th September 2025

Society of Production Engineering

University of Nis
Faculty of Mechanical Engineering

CONFERENCE PROCEEDINGS

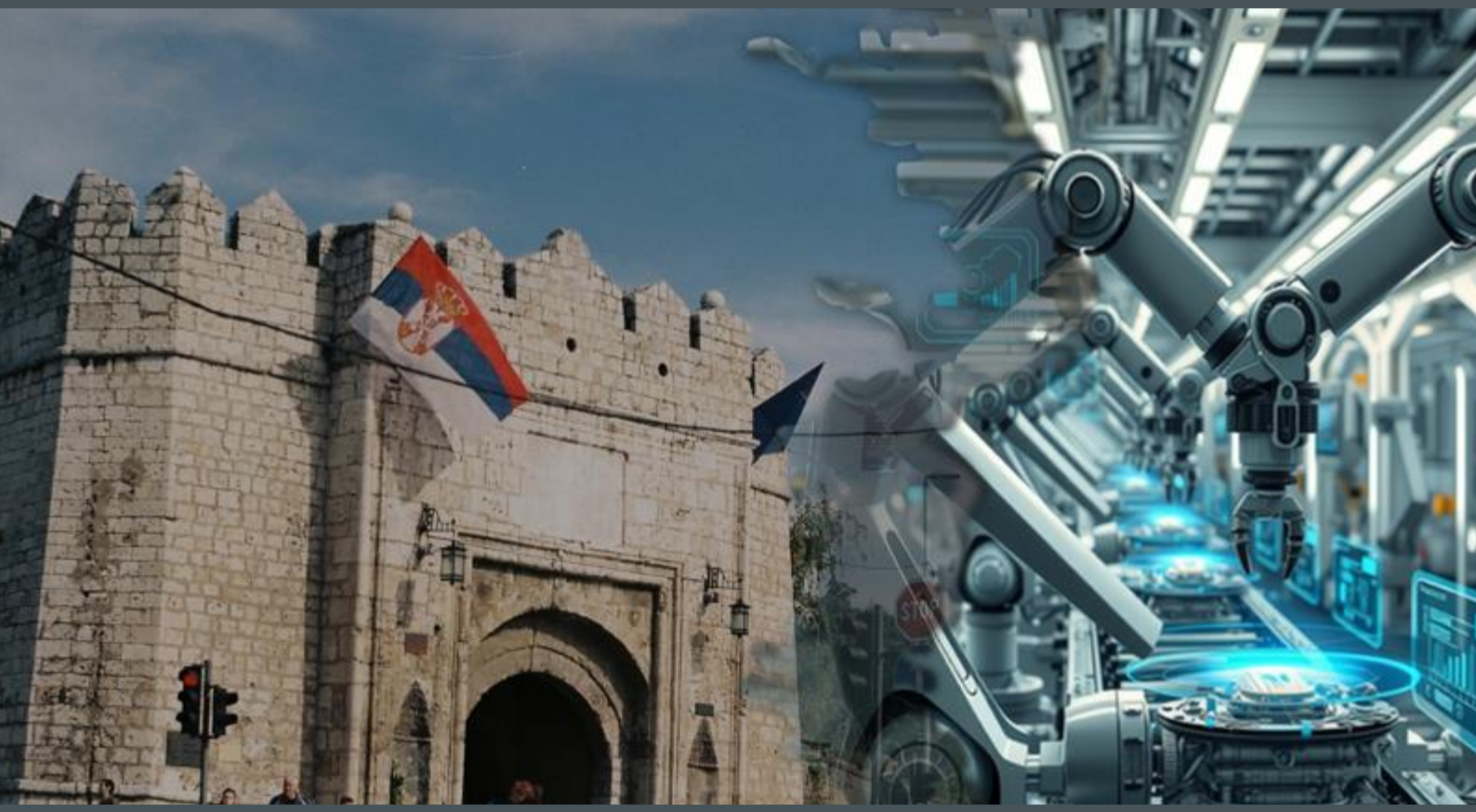

60th Anniversary of the Association of Production Engineering of Serbia

Editors:

Prof. dr Miodrag T. Manić, University of Niš, Faculty of Mechanical Engineering,

Prof. dr Saša S. Ranđelović, University of Niš, Faculty of Mechanical Engineering,

Publisher:

Faculty of Mechanical Engineering, Aleksandra Medvedeva 14, 18000 Niš, Serbia

For the Publisher:

Prof. dr Goran Janevski, Dean, University of Niš, Faculty of Mechanical Engineering,

Technical editor:

The Organizing Committee of ICPES2025

Cover design:

Ass. Rajko Turudija

Printing: Grafika Galeb , Niš

CIP - Каталогизација у публикацији
Народна библиотека Србије, Београд

621.7/.9(082)(0.034.2)
621.7/.9:669(082)(0.034.2)
681.5(082)(0.034.2)
005.6(082)(0.034.2)
004.896(082)(0.034.2)

INERNATIONAL Conference on Production Engineering (40 ; 2025 ; Niš)
Conference proceedings [Elektronski izvor] : 60th Anniversary of the Association of Production Engineering of Serbia / 40th International Conference of Production Engineering ICPES 2025 - Serbia 2025, Nis, Serbia, 18th - 19th September 2025 ; [organizer] The University of Niš, Faculty of Mechanical Engineering, Department for production and information technology ; [editors Miodrag T. Manić, Saša S. Ranđelović]. - Niš : Faculty of Mechanical Engineering, 2025 (Niš : Galeb). - 1 USB fleš memorija ; 1 x 1 x 6 cm

Sistemski zahtevi: Nisu navedeni. - Nasl. sa naslovne strane dokumenta. - Tiraž 100. - Foreword / Saša S. Ranđelović. - Bibliografija uz svaki rad.

ISBN 978-86-6055-197-1

a) Производно машинство -- Зборници b) Метали -- Обрада -- Зборници v) Системи аутоматског управљања -- Зборници g) Управљање квалитетом -- Зборници

COBISS.SR-ID 179507721

Financing of the Proceedings was sponsored by the Ministry of Education, Science and Technological Development of the Republic of Serbia.

The Association of Production Engineering of Serbia
UNIVERSITY OF NIŠ, Faculty of Mechanical Engineering

CONFERENCE PROCEEDINGS

40th INTERNATIONAL CONFERENCE ON PRODUCTION ENGINEERING SERBIA 2025

ICPES2025

Niš, September 2025

Organizing Institution:

The Association of Production Engineering of Serbia

Founders Institutions:

- Faculty of Mechanical Engineering, University of Belgrade, Department for production engineering, Serbia
- Faculty of technical science, University of Novi Sad, Department of production engineering, Serbia
- Faculty of Technical science, University of Novi Sad, Department of industrial engineering and management, Serbia
- Faculty of Mechanical Engineering, University of Niš, Department of production and information technology, Serbia
- Faculty of Technical sciences Čačak, University of Kragujevac, Department of mechatronic, Serbia
- Faculty of engineering science, University of Kragujevac, Department of production engineering, Kragujevac, Serbia
- Faculty of mechanical and civil engineering in Kraljevo, University of Kragujevac, Department of production engineering, Serbia
- Faculty of Technical science, Kosovska Mitrovica, University of Priština, Serbia
- LOLA institute, Belgrade, Serbia

Accompanied Institutions:

- Faculty of Mechanical engineering, Podgorica, University of Montenegro, Montenegro
- Faculty of Production and management Trebinje, University of East Sarajevo, Bosnia and Hercegovina
- Faculty of Mechanical engineering, Banja Luka, University of Banja Luka, Department of production and computer aided technology, Bosnia and Hercegovina
- Faculty of Mechanical engineering, University of East Sarajevo, Bosnia and Hercegovina
- Polytechnic faculty, University of Zenica, Bosnia and Hercegovina
- Faculty of Mechanical engineering, University of Skopje, North Macedonia
- Technical faculty Bitola, University saint Kliment Ohridski, North Macedonia
- Technical faculty Mihajlo Pupin, Zrenjanin, University of Novi Sad, Serbia
- Technical faculty, Department of mechanical engineering, University of Bihać, Bosnia and Hercegovina
- Technical faculty Bor, University of Belgrade
- Academy of Professional Studies SUMADIJA, Department of mechanical and industrial engineering, Serbia

ORGANIZER:

THE UNIVERSITY OF NIŠ, Faculty of Mechanical Engineering,

Department for production and information technology

www: masfak.ni.ac.rs, **e mail:** icpespms25@gmail.com

Hotel Cristal Light, Niš

International Scientific Committee

President:

dr Miodrag Manić, University of Niš, Faculty of Mechanical Engineering, Serbia

Memebers:

dr Aco Antić, University of Novi Sad, Serbia
dr Zoran Miljković, University of Belgrade, Serbia
dr Živana Jakovljević, University of Belgrade, Serbia
dr Saša Živanović, University of Belgrade, Serbia
dr Dragan Đurđanović, University Austin, USA
dr Dejan Lukić, University of Novi Sad, Serbia
dr Radovan Puzović, University of Belgrade, Serbia
dr Ilija Ćosić, University of Novi Sad, Serbia
dr Filip Gorski, University Poznan, Poland
dr Sebastian Baloš, University of Novi Sad, Serbia
dr Milenko Sekulić, University of Novi Sad, Serbia
dr Georg Weichhart, Primetals, Austria
dr Slobodan Tabaković, University of Novi Sad, Serbia
dr Branko Škorić, University of Novi Sad, Serbia
dr Miodrag Hadžistević, University of Novi Sad, Serbia
dr Đorđe Vukelić, University of Novi Sad, Serbia
dr Igor Budak, University of Novi Sad, Serbia
dr Bojan Lalić, University of Novi Sad, Serbia
dr Razvan Pacurar, University Cluj-Napoca, Romania
dr Mijodrag Milošević, University of Novi Sad, Serbia
dr Samir Lemeš, University of Zenica, B&H
dr Obrad Spaić, University of East Sarajevo, B&H
dr Radoslav Vučurević, University of East Sarajevo, B&H
dr Milija Kraišnik, University of East Sarajevo, B&H
dr Aleksandar Košarac, University of East Sarajevo, B&H
dr Stojanče Nusev, University Bitola, North Macedonia
dr Damir Hodžić, University of Bihać, B&H
dr Sanel Gredelj, University of Bihać, B&H
dr Branislav Sredanović, University of Banja Luka, B&H
dr Mileta Janjić, University of Podgorica, MNG
dr Radmil Polenakovikj, University Sv.Ki.Me., N Macedonia
dr Dejan Tanikić, University of Belgrade, Serbia
dr Saša S. Ranđelović, University of Niš, Serbia
dr Predrag Janković, University of Niš, Serbia
dr Vladislav Blagojević, University of Niš, Serbia
dr Miloš Stojković, University of Niš, Serbia
dr Nikola Korunović, University of Niš, Serbia
dr Milan Zdravković, University of Niš, Serbia
dr Nikola Vitković, University of Niš, Serbia
dr Jelena Stojković, University of Niš, Serbia
dr Milan Trifunović, University of Niš, Serbia
dr Miloš Madić, University of Niš, Serbia
dr Santiago C. Gutiérrez, University of Valencia, Spain
dr Solano G. Lorenzo, University of Valencia, Spain
dr Dragan Adamović, Unive of Kragujevac, Serbia
dr Goran Devedžić, University of Kragujevac, Serbia
dr Milan Erić, University of Kragujevac, Serbia
dr Branko Radičević, University of Kragujevac, Serbia
dr Mirko Đapić, University of Kragujevac, Serbia
dr Snežana Dragićević, University of Kragujevac, Serbia
dr Jasmina Vesić-Vasović, University of Kragujevac, Serbia
dr Miladin Stefanović, University of Kragujevac, Serbia
dr Maja Trstenjak, University of Zagreb, Croatia
dr Vojislav Petrović Filipović, FH Wiener Neustadt, Austria
dr Fernando G. Warchomicka, University of Graz, Austria
dr Bojan Ačko, University of Maribor, Slovenia
dr Biserka Runje, University of Zagreb, Croatia
dr Pilar Rey Rodriguez, Technology center AIMEN, Spain
dr Srećko Manasijević, LOLA Institute, Serbia
dr Lazar Kovačević, University of Novi Sad, Serbia
dr Nenad Simeunović, University of Novi Sad, Serbia
dr Ivan Milićević, University of Kragujevac, Serbia
dr Ognjan Lužanin, University of Novi Sad, Serbia
dr Mihajlo Popović, University of Belgrade, Serbia
dr Nikola Slavković, University of Belgrade, Serbia
dr Slavenko Stojadinović, University of Belgrade, Serbia
dr Goran Miladinović, University of Belgrade, Serbia
dr Branko Kokotović, University of Belgrade, Serbia
dr Milica Petrović, University of Belgrade, Serbia
dr Mladomir Milutinović, Unive of Novi Sad, Serbia
dr Tomaž Pepelnjak, Unive of Ljubljana, Slovenia
dr Davorin Kramar, University of Ljubljana, Slovenia
dr Đorđe Čiča, University of Banja Luka, B&H
dr Stevo Borojević, University of Banja Luka, B&H
dr Sven Maričić, Unive of Juraj Dobrila in Pula, Croatia
dr Slobodan Mitrović, Unive of Kragujevac, Serbia
dr Srećko Čurčić, Unive of Kragujevac, Serbia
dr Zoran Dimić, LOLA Institute, Serbia

Honorary Committee

dr Milisav Kalajdžić, University of Belgrade, Serbia
dr Pavao Bojanić, University of Belgrade, Serbia
dr Dragan Milutinović, University of Belgrade, Serbia
dr Miroslav Pilipović, University of Belgrade, Serbia
dr Miloš Glavonjić, University of Belgrade, Serbia
dr Petar Petrović, University of Belgrade, Serbia
dr Velimir Todić, University of Novi Sad, Serbia
dr Dragoje Milikić, University of Novi Sad, Serbia
dr Bogdan Sovilj, University of Novi Sad, Serbia
dr Velimir Todić, University of Novi Sad, Serbia
dr Bogdan Nedić, University of Kragujevac, Serbia
dr Goran Putnik, University Minho, Portugal
dr Velibor Marinković, University of Niš, Serbia
dr Dragan Domazet, University of Niš, Serbia
dr Dragan Temeljkovski, University of Niš, Serbia
dr Tihomir Pantelić, University of Kragujevac, Serbia
dr Ratomir Ječmenica, University of Kragujevac, Serbia
dr Snežana Radonjić, University of Kragujevac, Serbia
dr Miomir Vukićević, University of Kragujevac, Serbia
dr Dragiša Vilotić, University of Novi Sad, Serbia
dr Miroslav Plančak, University of Novi Sad, Serbia
dr Miodrag Lazić, University of Kragujevac, Serbia
dr Milentije Stefanović, University of Kragujevac, Serbia
dr Ratko Mitrović, University of Kragujevac, Serbia
dr Slavko Arsovski, University of Kragujevac, Serbia
dr Branislav Jeremić, University of Kragujevac, Serbia
dr Ljubodrag Tanović, University of Belgrade, Serbia
dr Ljubomir Lukić, University of Kragujevac, Serbia
dr Vidosav Majstorović, University of Belgrade, Serbia
dr Pavel Kovač, University of Novi Sad, Serbia
dr Marin Gostimirović, University of Novi Sad, Serbia
dr Svetislav Dekić, University of Pristina, Serbia
dr Vid Jovišević, University Banja Luka
dr Milan Zeljković, University of Novi Sad, Serbia
dr Miroslav Radovanović, University of Niš, Serbia
dr Vladimir Kvrgić, Mihajlo Pupin Institute, Serbia
dr Slavica Cvetković, University of Pristina, Serbia

Organizing Committee

President:

dr Saša S. Ranđelović, University of Niš, Faculty of Mechanical Engineering, Serbia

Memebers:

dr Miloš Simonović,
dr Dušan Petković,
dr Miloš Tasić,
M.Sc. Rajko Turudija
M.Sc. Jovan Aranđelović
M.Sc. Vladimir Mitrović
M.Sc. Aleksandar Trajković
M.Sc. Dejan Žikić

ORGANIZERS OF THE CONFERENCE ON PRODUCTION ENGINEERING OF SERBIA

from 1965 to 2025

No.	Place	Year	No.	Place	Year
I	Beograd	1965	XXI	Opatija	1987
II	Zagreb	1966	XXII	Ohrid	1989
III	Ljubljana	1967	XXIII	Zagreb	1991 (not perform)
IV	Sarajevo .	1968	XXIV	Novi Sad	1992
V	Kragujevac	1969	XXV	Beograd	1994
VI	Opatija	1970	XXVI	Podgorica	1996
VII	Novi Sad.	1971	**XXVII**	**Niš**	**1998**
VIII	Ljubljana	1973	XXVIII	Kraljevo	2000
IX	**Niš**	**1974**	XXIX	Beograd	2002
X	Beograd	1975	XXX	Čačak	2005
XI	Ohrid	1977	XXXI	Kragujevac	2006
XII	Maribor	1978	XXXII	Novi Sad	2008
XIII	Banja Luka	1979	XXXIII	Beograd	2009
XIV	Čačak	1980	**XXXIV**	**Niš**	**2011**
XV	Novi Sad	1981	XXXV	Kraljevo	2013
XVI	Mostar	1982	XXXVI	Beograd	2015
XVII	Budva	1983	XXXVII	Kragujevac	2018
XVIII	**Niš**	**1984**	XXXVIII	Čačak	2021
XIX	Kragujevac	1985	XXXIX	Novi Sad	2023
XX	Beograd	1986	**XL**	**Niš**	**2025**

Pavle P. Stanković (1909 - 1969)

"Prof. dr Pavle Stanković" charter & plaque:

2025
Prof. dr Dragiša Vilotić, Faculty of Technical Sciences, Novi Sad

Previous laureates:

2023
Prof. dr Mirko Đapić, LOLA Institute, Beograd
Prof. dr Srećko Ćurčić, Faculty of Technical Sciences, Čačak
Prof dr Bojan Babić, Faculty of Mechanical Engineering, Beograd

2021
Prof. dr Velimir Todić, Faculty of Mechanical and Civil Engineering, Kraljevo
Prof. dr Milan Zeljković, Faculty of Technical Sciences, Novi Sad
Prof. dr Miodrag Manić, Faculty of Mechanical Engineering, Niš

2018
Prof. dr Vidosav Majstorović, Faculty of Mechanical Engineering, Beograd
Prof. dr Miroslav Radovanović, Faculty of Mechanical Engineering, Niš

2015
Prof. dr Janko Hodolič, Faculty of Technical Sciences, Novi Sad
Prof. dr Bogdan Nedić, Faculty of Engineering, Kragujevac

2013
Prof. dr Bogdan Sovilj, Faculty of Technical Sciences, Novi Sad
Prof. dr Miroslav Trajanović, Faculty of Mechanical Engineering, Niš

2011
Prof. dr Miodrag Lazić, Faculty of Mechanical Engineering, Kragujevac
Prof. dr LJubodrag Tanović, Faculty of Mechanical Engineering, Beograd

2009
Prof. dr Velimir Todić, Faculty of Technical Sciences, Novi Sad
Prof. dr Velibor Marinković, Faculty of Mechanical Engineering, Niš
Проф. др Сергею А. Клименко, Институт сверхтвердых материалов, НАН Украине

2008
Prof. dr Dragan Milutinović, Faculty of Mechanical Engineering, Beograd
Prof. dr Milentije Stefanović, Faculty of Mechanical Engineering, Kragujevac

2006
Prof. dr Miroslav Plančak, Faculty of Technical Sciences, Novi Sad
Prof. dr Ratomir Ječmenica, Technical Faculty, Čačak

2005
Prof. dr Dragan Domazet, Faculty of Mechanical Engineering, Niš
Prof. dr Pavao Bojanić, Faculty of Mechanical Engineering, Beograd

2002
Prof. dr Vojislav Stojiljković, Faculty of Mechanical Engineering, Niš
Prof. dr Ilija Ćosić, Faculty of Technical Sciences, Novi Sad

2000
Prof. dr Mihailo Milojević, Faculty of Mechanical Engineering, Kraljevo
Prof. dr Dragoje Milikić, Faculty of Technical Sciences, Novi Sad

1998
Prof. dr Ratko Gatalo, Faculty of the Technical Sciences, Novi Sad
Prof. dr Vučko Mečanin, Faculty of Mechanical Engineering, Kraljevo

1996
Prof. dr Milisav Kalajdžić, Faculty of Mechanical Engineering, Beograd
Prof. dr Dragutin Zelenović, Faculty of Technical Sciences, Novi Sad

1994
Mile Benedetić, LOLA Institute, Beograd
Prof. dr Vuko Domazetović, Faculty of Mechanical Engineering, Podgorica
Prof. dr Milenko Jovičić, Faculty of Mechanical Engineering, Beograd

1992
Prof. dr Jožef Rekecki, Faculty of the Technical Sciences, Novi Sad
Prof. dr Sava Sekulić, Faculty of the Technical Sciences, Novi Sad
Prof. dr Joko Stanić, Faculty of Mechanical Engineering, Beograd
Prof. dr Vlado Vujović, Faculty of Technical Sciences, Novi Sad

1988
Prof. dr Branislav Devedžić, Faculty of Mechanical Engineering, Kragujevac
Prof. dr Elso Kuljanić, Faculty of Mechanical Engineering, Rijeka
Prof. dr Zoran Seljak, Faculty of Mechanical Engineering, Ljubljana

1987
Prof. dr Svetislav Zarić, Faculty of Mechanical Engineering, Beograd
Prof. dr Josip Hribar, Faculty of Mechanical Engineering

1986
Prof. dr Branko Ivković, Faculty of Mechanical Engineering, Kragujevac
Prof. dr Strezo Trajkovski, Faculty of Mechanical Engineering, Skoplje

1985
Prof. dr Predrag Popović, Faculty of Mechanical Engineering, Niš
Prof. dr Vladimir Milačić, Faculty of Mechanical Engineering, Beograd

1984
Prof. dr Janez Peklenik, Faculty, Ljubljana
Prof. dr Binko Musafija, Faculty of Mechanical Engineering, Sarajevo

1983
Prof. dr Rudolf Zdenkovic, Faculty of Mechanical Engineering, Zagreb
Prof. dr Vladimir Šolaja, Faculty of Mechanical Engineering, Beograd
Prof. dr Julije Kremer, Faculty of the Technical Sciences, Beograd

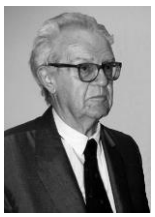

Prof. dr Vladimir Šolaja (1920 -1998)

"Prof. dr Vladimir Šolaja" medal:

2025
dr Petar Janjatović, Faculty of Technical Sciences, Novi Sad

Previous laureates:

2021
Prof dr Milica Petrović, Faculty of Mechanical Engineering, Beograd, Serbia

FOREWORD

This year marks the 60th anniversary of the Serbian Association of Production Engineering and the 40th gathering of its members at scientific and professional conferences. It all began on October 7, 1965, when the Institute for Machine Tools from Belgrade, the Faculty of Mechanical Engineering in Belgrade, and the Institute for Machine Tools from Zagreb jointly organized the first conference. It was then that the Yugoslav Association of Scientific and Research Institutions of Production Engineering was founded. The first president and bearer of the initiative was Prof. dr Vladimir Šolaja, full professor at the Faculty of Mechanical Engineering in Belgrade and director of the Institute for Machine Tools. After the first gathering of production engineers, and in accordance with the goals for which it was founded, the Association took over the organization of future gatherings, which continues to this day.

Production engineering in Serbia has a long and successful tradition that has gone through various periods of growth and prosperity, but also stagnation due to socio-political circumstances and events in this region.

Today, production engineering is the driving force behind the economic development of modern society as a whole, both locally and globally. This is exactly what the world's most powerful economies recognize, where industrial production and the development of new technologies break down all borders and divisions in order to conquer new markets.

Faced with these facts, the Serbian Association of Production Engineering has initiated the process of integration and connection in this region so that scientific and educational institutions and the economy as a whole can keep pace with developed countries. On initiative the Department of production and information technology, Faculty of mechanical engineering Niš, and Prof. dr Miodrag Manić and Prof. dr Saša S. Ranđelović, during 2024., 11 institutions from region has thus far signed the accession to the Association, and these institutions today, together with the founders, participate in the work of the 40th International Conference, where authors from a dozen countries will present 78 scientific papers.

In the time of ubiquitous artificial intelligence, ongoing research into new materials, and the development of smart technologies aimed at optimizing resources and sustainable development, production engineers face new opportunities and challenges for multidisciplinary scientific research.

In that light, this 40th Conference has brought together domestic and foreign authors, reviewers, business organizations, and companies to offer new prospects and a hope for a better tomorrow, through joint work and support.

in Niš, september 2025 **President of the Executive Committee of the Association**

Prof. dr Saša S. Ranđelović

The "prof. dr Pavle Stanković" charter & plaque

Prof. dr Dragiša Vilotić

He was born on April 12, 1950 in the village of Bojić, municipality of Šabac. He graduated from high school in Šabac in 1969, majoring in mechanical engineering, and then enrolled at the Faculty of Mechanical Engineering in Novi Sad. He graduated in 1974 with an average grade of 9.19 and defended his master's thesis in 1981. He defended his doctoral thesis entitled "Contribution to the investigation of the behavior of steel materials in different cold volumetric deformation processing systems" in 1986 at the Faculty of Technical Sciences in Novi Sad.

He began his career on January 1, 1975 at the Faculty of Technical Sciences as an assistant in scientific work in the field of deformation processing technologies. He was elected to the title of assistant professor in 1988, and to the title of full professor in the field of plastic deformation technology in 1998. In the past period, he taught in the field of plastic deformation technologies, additive technologies and plastics processing technologies at various levels of education (OAS, MAS and DAS) in a total of 16 subjects. In student surveys for the quality of teaching in the last five years of work, he was rated 9.80. He was a mentor in the preparation of more than 100 diploma and four master's theses. He was a mentor for the preparation of doctoral theses on three occasions.

Professor Vilotić's narrower scientific field was plastic deformation technologies, additive and virtual technologies. In his research work, Professor Vilotić dealt with the theoretical analysis of deformation processing processes, their technology, and especially the issue of material deformability during cold volumetric deformation, which resulted in the development of numerous experimental tests and devices for assessing the plastic properties of materials under various stress conditions. In the narrow scientific field, as an author and co-author, he published a total of 385 papers (data from the APV Researcher's Card), of which 21 are papers in international journals from the SCI list (category M20). There are 6 invited lectures at international conferences printed in full (category M31), and 92 papers from international conferences printed in full (M33). There are 88 published papers in category M50, and 135 papers from national conferences (category M60). As an author and co-author, Professor Vilotić has published six university textbooks and one monograph in the field of plastic deformation technologies.

As Vice-Dean for Education at the Faculty of Technical Sciences, as an author and co-author, he participated in writing 6 monographic publications on the topic of improving the teaching process in the field of higher education and 26 papers relevant to higher education. He has been a member of the editorial board of the Journal for Technology of Plasticity since 1995, published by FTN Novi Sad, and a reviewer in two international journals. The total citation index of Professor Vilotić is 142 citations and the total scientific competence index according to data from the scientific worker's file of the APV is 567.

Professor Vilotić participated in the implementation of more than forty national scientific research and development projects. In the period 2002–2011, he was the project manager of the technological development program on three occasions. In addition, Professor Vilotić participated in the implementation of about a dozen international projects. In the period 2000–2014, he was the manager of scientific research projects on five occasions that were implemented under the protocol on cooperation between the Russian Academy of Sciences (RAS), the Serbian Academy of Sciences (SASA) and the Faculty of Technical Sciences in Novi Sad. In the research program ERA.Net RUS Plus (2017), he led the project entitled: Development of a method for improving material properties by combined bulk and surface plastic deformation.

He was a member of the Registry Board for Mechanical Engineering and Industrial Software of the Ministry of Education, Science and Technological Development of the Republic of Serbia from 2010 to 2016. In the period from 1998 to 2002, Professor Vilotić was the head of the Institute for Production Engineering, and for many years the head of the Laboratory for Plastic Deformation Technologies.

In 2017/18, Professor Vilotić actively participated in the establishment and construction of a modern Laboratory for Polymer Processing Technologies in cooperation with the company Neofiton from Novi Sad and the Faculty of Technology of the University of Novi Sad. Professor Vilotić was the Vice-Dean for Education at the Faculty of Technical Sciences from 2012 to 2020, when he actively worked on improving the teaching process in numerous study programs and resolving student issues. He actively participated in the preparation of documentation for the accreditation of 86 study programs of the Faculty of Technical Sciences of various levels (OAS, MAS, DAS, etc.), which resulted in their accreditation by the National Academy of Sciences of the Republic of Serbia in 2013.

In addition to teaching and scientific activities, Professor Vilotić actively participated in cooperation with industry in the introduction of new deformation processing technologies into production. On this occasion, he points out the introduction of cold stamping technology for the needs of making tools for molding plastics, then the introduction of the technology of rotary drawing of conical parts for the needs of the automotive industry and the introduction of the technology of profile bending of thin aluminum sheet for the production of parabolas for neon lamps. After 45 years of work at FTN, Professor Vilotić retired on September 30, 2020.

After retiring in the period 2023–2024, Professor Vilotić was engaged by Beihang University in Beijing on the project Prediction technology of flexible forming and welding and formability for thin-walled hollow components based on process requirements as an expert in deformation processing. The goal of this engagement was to develop a method for testing the deformability of difficult-to-deform materials (titanium alloys) in a wider range of negative values of stress state indicators.

The "prof. dr Vladimir Šolaja" medal

dr Petar Janjatovć, Assistant Professor

Dr Petar Janjatović was born on February 17, 1991, in Ogulin. He graduated from the Faculty of Technical Sciences, University of Novi Sad, in 2014, majoring in Production Engineering, with an average grade of 9.61, and was awarded the Dositeja Scholarship for academic excellence. He completed his master's studies in 2016 and defended his doctoral dissertation entitled "Influence of Water on the Embrittlement of Conventional and Dual-Phase ADI Materials" on December 13, 2023.

He has been employed at the Faculty of Technical Sciences since 2014, where he currently works as an Assistant Professor at the Chair of Materials and Joining Technologies. He is involved in teaching several courses in the fields of materials science and manufacturing technology.

Dr Janjatović has participated in several research projects, including the national project "Innovative Scientific and Artistic Research in the Field of FTN Activities", a continuation of the project "Design, Development, and Application of a New Generation of ADI Materials" supported by the Ministry of Science, Technological Development and Innovation, as well as international COST Actions CA18120 – Reliable Roadmap for Certification of Bonded Primary Structures and CA15102 – Solutions for Critical Raw Materials Under Extreme Conditions (CRM-EXTREME).

Dr Janjatović is the author and co-author of more than 70 scientific papers. In the past five years, Dr. Janjatović has authored or co-authored one paper published in an M21a journal, nine papers in M21 journals, two papers in M22 journals, and six papers in M23 journals.

According to the SCOPUS database, his works have been cited 84 times, including 59 independent citations, and his h-index is 5. His research interests include the microstructure and mechanical properties of advanced materials for the automotive industry and technologies for their processing.

In memoriam

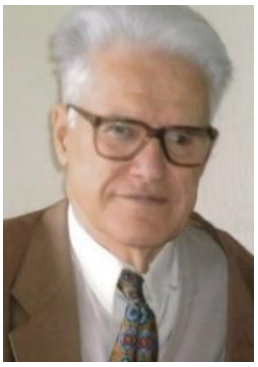

Prof. dr Milenko Jovičić (1935 – 2024)

Prof. dr Milenko Jovicic was born in Jezevica, near Pozega, where he finished elementary school. In the spring of 1949, he participated in the construction of Belgrade with the Pozega Youth Labor Brigade. From there, he was sent to continue his education at the School of Students in Economics at the Trepca Mine in Stari Trg. He continued his education at the "Petar Drapsin" Secondary School in Belgrade and graduated with excellent results while working at the companies "Metal" and "Industrija prezisne mehanike".

He enrolled in the Faculty of Mechanical Engineering in Belgrade in 1956. He received a scholarship from the University of Belgrade and the Motor Industry in Rakovica. During his studies, he worked at the companies Industrija prezisne mehanike, IMT, "David Pajic" and "Geomašina". He did his internship in West Germany. He graduated in 1960. In the same year, he started working at the Faculty of Mechanical Engineering in Belgrade as a professional associate, and in 1961 he was elected as an assistant. He received his master's degree in 1966. He was elected as an assistant professor in 1970. He defended his doctoral dissertation at the same faculty in 1975. He was elected as an associate professor in 1977 and promoted to full professor in 1983 for the subject group of production engineering.

At the Faculty of Mechanical Engineering in Belgrade and the departments of the Faculty in Kragujevac, Kraljevo, Valjevo, Užice and Žarkovo, he taught subjects from the subject group of production engineering, as well as in postgraduate studies. He also taught at the Higher Metal School in New Belgrade, as well as at the Department of Mechanization of the Faculty of Agriculture in Zemun. After retiring from the Faculty of Mechanical Engineering in Belgrade at the end of 1997, he was engaged for four years as a full professor by invitation at the Faculty of Mechanical Engineering of the University of Srpski Sarajevo. He was a mentor for over 550 diploma theses, 12 master's theses and 8 doctoral dissertations. He published (as author and co-author) 15 textbooks and manuals, which had a large number of editions: for secondary schools of mechanical engineering, higher mechanical technical schools and university teaching.

He was actively engaged in professional and scientific work in the field of production engineering, participating in the implementation of over 30 scientific research projects. He published about 90 papers in journals and publicly announced at professional and scientific conferences in the country and abroad. He wrote as an author and co-author two monographs: "Grinding, identification of state characteristics and process optimization", and "Cutting processing of difficult-to-machine metals and alloys", and as a co-author of two publications: "Prof. Dr. Pavle P. Stanković - pedagogical and scientific contributions to the field of production engineering" and "Prof. Dr. Vladimir B. Šolaja - pedagogical and scientific contributions to the field of production engineering and the study of the historiography of engineering in Serbia". He wrote over 25 reviews. As a contributor to the Serbian Encyclopedia, he wrote nine biographical entries in the field of production engineering.

He has made several short and long visits to university centers in Europe: TU Berlin, TU Braunschweig, TH Darmstadt, TH Karlsruhe, TU Dresden, the Institute for Superhard Materials in Kiev, TU Braunschweig and TH Darmstadt as a Humboldt Foundation scholarship holder.

He was active in social work at the Faculty of Mechanical Engineering in Belgrade, the University of Belgrade, professional organizations and associations. At the Faculty, he served as Vice-Dean for Finance. He was also the chairman of several commissions and boards, including the board for publishing, the head of the OOUR for production and commercial mechanical engineering and the chairman of the Executive Board of the Council of the Faculty of Mechanical

Engineering. He was also a member of the Educational Council of the Republic of Serbia, President of the Commission for Mechanical and Energy Professions of Secondary Education of the Educational Council, Head of the Department of the Faculty of Mechanical Engineering in Užice, as well as President of the City Board of the Association of Toolmakers and Secretary of the Republic Board of the Association of Toolmakers of Serbia. He was also a member of the Commission for Tools of the Yugoslav Institute for Standardization, as well as a member of the Editorial Board of the journal "Technology" and editor-in-chief of the "Mechanical Engineering" section.

He is the recipient of numerous awards and recognitions, including: the Belgrade Chamber of Commerce Award for the best doctoral dissertation in technical sciences defended in 1975, the October Award of the Belgrade City Assembly for the monograph "Grinding, Identification of Condition Characteristics and Process Optimization" as the best work in the field of technical sciences published in Belgrade in 1987, the "Prof. dr. Pavle P. Stanković" plaque and charter awarded by the Association of Production Engineering Institutions of Yugoslavia in 1994 for his overall contribution to the development of production engineering, and the Special Plaque of the Faculty of Mechanical Engineering Council in 1995 on the occasion of Faculty Day for 35 years of work at the Faculty and mentoring 500 diploma theses.

He dedicated the last 10 years of his life to writing valuable testimonies about one of the most successful stages of the Faculty's development. He greatly influenced the awareness of the importance of recording significant historical dates and facts, not only for Serbian science, but also for the entire national discourse.

Prof. Jovićić's exceptional work in teaching, profession and science will be remembered by generations of students, colleagues, professors and engineers. He will remain in the lasting memory of his colleagues from the Department of Production Engineering, and the Faculty of Mechanical Engineering will be forever grateful to him for his commitment to the faculty and dedication to the study of its history.

Prof. dr Mihajlo Popović

In memoriam

Prof. Emerita dr Leposava Šiđanin (1940 - 2023)

In Novi Sad, on November 10, 2023, our esteemed and beloved Professor Emeritus dr Leposava Šiđanin passed away at the age of 83. She was a cherished educator whose wisdom and guidance touched the lives of many students and colleagues. Her dedication to teaching and her passion for knowledge left an indelible mark on the academic community. Professor Šiđanin's legacy will continue to inspire future generations, and her memory will be held in the highest regard by all who had the privilege of knowing her.

She was born on April 6, 1940, in Skopje, now North Macedonia. After completing high school in Skopje in 1959, she enrolled in the Faculty of Natural Sciences and Engineering, Department of Metallurgy, at the University of Ljubljana, Slovenia, where she was the only girl among 60 students in her generation. She graduated in June 1965.

In Ljubljana, at the Department of Metallurgy (now Metallurgy and Materials) of the Faculty of Natural Sciences and Engineering, she defended her Master's thesis titled "Research of Optimal Dimensions in Fine Wire Drawing" in January 1976, and her doctoral dissertation "Morphology and Mechanisms of Fracture of Low-Carbon Killed Steel" was defended in June 1983. At the University of Ljubljana, she met her husband, Dušan Šiđanin, master engineer of metallurgy, and they were married until his passing in 2012. They had one daughter, dr Duška Šiđanin, Ph.D., who is a professor of Genetics at the Medical College of Wisconsin, Milwaukee, USA. Duška is married to Michael Maier, and they have two children, Mark and Alex.

After marriage, Professor Šiđanin moved to Novi Sad and began her teaching career on September 1, 1965, as a high school teacher at the Mechanical Technical School in Novi Sad, where she worked until August 30, 1972. Following her appointment as a teaching assistant, she joined the Faculty of Technical Sciences on September 1, 1972, where she worked until her retirement on September 30, 2007, after 42 years of employment.

At the Faculty, she become assistant professor in 1984, associate professor in 1989, and a full professor in 1994. On January 24, 2008, she was honored with the title of emeritus professor at the University of Novi Sad, becoming one of the inaugural six to receive this distinction. Her scientific field was Material Science, Engineering Materials, and Microscopy.

Since 2008, as a professor emeritus at the Faculty of Technical Sciences, she teaches at master's and doctoral studies, passing on her knowledge to students until the very last moment. She also formerly lectured at the Technical Faculty "Mihajlo Pupin" in Zrenjanin, and at the Faculty of Agriculture and the Faculty of Sciences in Novi Sad. At the University of California at Berkeley, Department of Material Science and Mineral Engineering, she held a portion of the laboratory exercises for the course Engineering Materials and their Applications under Prof. Gareth Thomas during the 1986/87 school year. Throughout her long teaching career, she was always highly esteemed and beloved by students.

At the Faculty of Technical Sciences, she introduces new subjects into the curriculum: Metallography, Fracture Mechanics of Materials, Microscopic Aspects of Fracture, Selected Chapters from Phase and Structural Transformations, Advanced Materials, Advanced Methods of Material Testing, Light and Electron Microscopy, and Electron Microanalysis. In 1975, at the Faculty she established a Metallographic Laboratory with high-quality equipment that is still in intensive use today and has been recognized as a reference laboratory by the Committee for Interlaboratory Material Testing (KOMIM) thanks to its successful work. At the University level, in 1978, she participated in the procurement of SEM and TEM microscopes and the establishment of an Electron Microscopy Laboratory. Through her tireless efforts and with the help

of colleagues from the University, a new SEM microscope was acquired in 2003, and the University Center for Electron Microscopy - Novi Sad was formed. Since 2003, she has been the first President of the Center's Council. In 2002, thanks to her dedication and the support of the Dean of the Faculty of Technical Sciences, Professor Ilija Ćosić, the Chair of Materials and Joining Technologies, at the Department of Production Engineering was established, and she was appointed as its first head. This highlighted the importance of materials in manufacturing technologies, which further contributed to the development of all interconnected areas of Production Engineering.

Throughout her scientific career, she participated in numerous scientific exchange programs, notably at the University of Birmingham, UK, and at the University of California, Berkeley, USA, where she specialized in electron microscopy. She spent a total of 20 months at the University of Birmingham from 1977 to 1995, under Professor Ray (Raymond Edward) Smallman. Initially supported by the University of Novi Sad, her training was later funded by the British Council, the Royal Society, and the University of Birmingham. In recognition of a long-standing successful collaboration, on the recommendation of Prof. Šiđanin and members of the Department of Production Engineering, FTN, Novi Sad, the University of Novi Sad awarded Professor R.E. Smallman an honorary doctorate in 1990. She spent 13 months at Berkeley during the 1986/87 academic year as a recipient of the prestigious Fulbright Scholarship, under Professor Gareth Thomas.

She collaborates with Prof. Surya Kalindindi, head of the Department of Material Science and Engineering at Drexel University, USA. As part of this collaboration, four students from FTN were admitted to doctoral studies and successfully completed their PhDs.

Prof. dr Šiđanin has worked throughout her career on the advancement of many young individuals who are now eminent experts in their field, both in the country and abroad. She participates as a mentor and as a member of committees in the creation of a large number of bachelor's, master's, and doctoral theses, not only at the Faculty of Technical Sciences but also at the Faculty of Sciences and the Faculty of Technology in Novi Sad; as well as at faculties in Belgrade, Podgorica, and Sarajevo.

The scientific work of Prof. dr Šiđanin was primarily focused on the characterization of microstructures, especially of metals and alloys, obtained through various processing technologies. For characterization, she utilizes advanced research techniques, among which the results achieved using electron microscopy (SEM and TEM) and electron microanalysis stand out. In the field of microscopy, she is recognized both domestically and internationally, and her involvement has been of great significance in affirming the University of Novi Sad as a leading center for microscopy in the region. Additionally, notable results have been observed in the characterization of the microstructure and mechanical properties of metallic glasses, traditional ceramics, and polymers. Her most significant contribution has been in the research of iron-based alloys, steels, cast irons, and particularly ADI materials.

Working with her was an exceptional experience; she knew all the microstructures, all the conditions of transformation, all the methods of preparation, etching, and had a photographic memory. She always shared her knowledge selflessly and was always there to help everyone.

Professor dr Šiđanin is the author of 430 scientific, review, and professional papers both domestically and internationally, including 70 works in prestigious international journals. He has authored several textbooks, books, and other professional literature, and has been a leader and participant in numerous scientific and professional workshops, conferences, and projects.

Within the scope of social activities, Prof. dr Šiđanin served in the Department of Production Machinery as a member of the executive board and assistant director. She was the president of the FTN union from 1994. to 2002., and the president of the University of Novi Sad union from 1998. to 2002. She was a member of the executive board of the Serbian Society for Electron Microscopy from 1992. to 2006., and the General Secretary of the Society, during which time the Society became a member of the European Microscopy Society, from 1996. to 2006. In 2011, the Accreditation Body of Serbia appointed Prof. dr Šiđanin as a member of the Sectoral Commission for the Accreditation of Material Testing Laboratories.

She was a member of professional associations: European Microscopy Society, European Ceramic Society, Serbian Society for Microscopy, Serbian Chemical Society, Serbian Society for Tribology, Society for the Advancement of Welding in Serbia, and the Committee for Interlaboratory Material Testing of Serbia.

Professor Šiđanin received various recognitions and awards, both national and international, among which are noteworthy: The Lifetime Achievement Award in the field of technical sciences by the Association of University Teachers and Scientists of Vojvodina, 2014, and The Award for exceptional results in science and 45 years of work at FTN, Novi Sad, 2016. As well as the selection for Honorary Senior Research Fellow, University of Birmingham, UK, 1993, and the Plaque for special contribution to the development of the Faculty of Technical Sciences Novi Sad on the occasion of the faculty's 50th anniversary in 2010.

As we bid farewell to Prof. Emeritus dr Leposava Šiđanin, we are reminded of the lasting mark she left in the world of academia and beyond, on to all of us who had the opportunity to meet her, to work with her, and to learn from her example. Her unwavering dedication to education, her pioneering research, and her compassionate mentorship have shaped countless minds and futures. Her spirit, preserved in her work and the people she influenced, will continue to guide the path of education and discovery.

Rest in peace, esteemed scholar and cherished friend.

Prof. dr Dragan Rajnović

In memoriam

Prof. dr Vojislav Stoiljković (1945 – 2024)

Professor dr Vojislav Stoiljković, graduated in mechanical engineering, was born on may 21, 1945 year in Niš. After a difficult childhood in a working-class family of five, he graduated from primary and secondary mechanical technical school in Niš, where he showed excellent results and was declared one of the best students. During that short time, he studied part-time in the first year of the Faculty of Mechanical Engineering in Niš and graduated with excellent grades. Very quickly he was noticed by his colleagues and managers at work as well as professors at the university, after which he made the decision to transit on regular scholarship studies of mechanical engineering, finishing with an average grade of 9.47.

After completing his studies, he worked at the Faculty of Mechanical Engineering in Niš, at the Department of production engineering as an assistant, but also at "EI Niš" as a designer of mechanical systems. He received his Master's degree under the mentorship of professor dr Vladimir Šolaja, at the Faculty of Mechanical Engineering in Belgrade with the topic: "Stress-deformation state during the manufacture of elements by deep drawing with incompressible fluid and identification of the optimal pressure", in 1974, and he defended his doctoral thesis in april 1977 at the Faculty of Mechanical Engineering in Niš before an eminent commission: prof. dr Vladimir Šolaja, prof. dr Binko Musafia, prof. dr Branislav Devedžić, prof. dr Predrag Popović and prof. dr Milan Nedeljković with the topic "Stress-deformation state during the production of elements by deep drawing with an incompressible fluid with a holder and the identification of influential factors with the establishment of their correlation relationships". He passed all academic degrees at the Faculty of Mechanical Engineering in Niš, where he was elected full professor in 1987. Initiative and creativity in work were never lacking in professor Stoiljković's career, which he demonstrated both at the faculty and by participating in numerous domestic and foreign scientific gatherings. In 1991., he founded the private company CIM College d.o.o. which dealt with the transfer of top knowledge and technologies of plastic deformation, but also software development in the field of CAD CAM, quality management and business management of companies on a global level.

At the Faculty of Mechanical Engineering in Niš, he was the head of the main department of production engineering for four terms, from 1993 to 2001, where he taught a large number of subjects in the older years of undergraduate studies as well as in doctoral studies. He was the mentor of numerous graduate theses, master's theses and doctoral dissertations. He showed his creativity and innovation in his work with students, assistants and colleagues, where he was always looking for new and modern solutions. He has publicly presented and published his scientific work at the Faculty of Mechanical Engineering through numerous scientific papers (over 170) at conferences, professional journal of domestic and foreign publishers in the field of conventional technologies of metal forming of sheet deformation, forming by fluid, by explosives, deformation theory, etc. He spoke and wrote in german and english, which helped him to quickly convey foreign solutions and successful practices to domestic engineers and experts in the economy through numerous seminars, professional lectures, thematic conferences, trainings, etc.

In the 1980s, he translated his scientific and pedagogical work into three books in the field of plastic deformation theory and measurement, which were the basis for many advanced researches and technological measurements. Later, he devoted his work to management, which in the nineties was increasingly present in the areas of former and current countries. From that period, numerous books and software were created, primarily in the field of industrial management and the economy, which was at the beginning of a new era where managers entered through the back door. CIM Company Strategy, from 1993, CAQ - Computer Aided Quality, 1994, CAD Computer Aided Design, from 1995., ISO 9000 and ISO 14000, from 1996., Q Manager's guide, from 1996, Q Tools - Quality Tools, from 1996, TQM Excellence Models,

from 1997., Changes to World Class - Process Improvement and reengineering, from 1998, Lean six sigma 2011., ISO 9001:2015 and Lean 2016, Lean in health 2018, mainly published by the Faculty of Mechanical Engineering in Niš and CIM College. All these publications from that period clearly indicated that a new era was coming, primarily from the west and the far east, which was accepted by our community and where professor Stoiljković was one of the pioneers of the scientific application of management theory at the Faculty of Mechanical Engineering in Niš, but also much more widely.

He was vice-dean for cooperation with the economy at the Faculty of Mechanical Engineering in Niš from 1979 to 1983 He is the recipient of numerous awards, among which the "plaque and charter of Prof. Dr. Pavle Stanković" for 2002 should be singled out, which was then awarded by the Association of production engineering of Yugoslavia and now of Serbia.

He led numerous scientific research projects financed by the Ministry of science and technology of the Republic of Serbia. Initially, these were projects in the field of plastic deformation such as: "Research and development of sheet metal forming methods by deforming and pressing profiles using maximum workability", 1980-1984, "Improving the technology of plastic processing of hard-to-press aluminum alloys", 1986-1990, "Integral system for the development of new technologies by forming sheet metal with an incompressible fluid", "Generating product models by applying knowledge and defining production equipment for the implementation of developed technologies in production", 1994-1998.

At the end of the last century and at the beginning of this century, these were projects in the field of management: "CIM models for managing business-production systems and their transfer to other branches of industry", "CIM concept of DP NITEX Niš", 1994-1998, "Development of software to improve the performance of industrial processes", 2001-2003, Development of an information system for planning, management and supervision of production business systems, 2001-2003, all as their leader.

In addition to scientific research projects, there were also projects for the economy where professor Stoiljković dominated with his leadership role and managerial approach to solving problems. Some of them are: "Project the technology of making the electrode of the electrostatic filter of the Obrenovac thermal power plant - block B", 1978, Project the production of a suspended ceiling made of profiled aluminum for the clinical center Belgrade, 1979., Project the technology of making a sphere for accumulating gas under a pressure of 320 bar for controlling a guided missile, 1982-1985, Explosive joining of metals - conquest of technology at the surface mine in Bor and the construction of a plating range in Aleksinac, 1983-1988, The main technological project of the TIR Bor tool shop, 1988, The global project of the CIM concept of S.P. "Fabrika duvana Niš", 1991, The global project of the CIM concept "Mačkatica" Surdulica, 1992., The global project of the CIM concept "NITEX Niš", 1994., Production rocket launcher tubes of various calibers for the needs of the Yugoslav Army, 1994-1995 etc.

One thing is certain, professor Stoiljković left a deep scientific mark on the area of Western Balkans, where he transmitted technological inventiveness, persistence and work enthusiasm for generations, which is very often not accepted with enthusiasm. Nevertheless, his work represented a roadmap for further research and directions, primarily at the Faculty of Mechanical Engineering in Niš, where a special study program was formed in 2012, from the first year of study, entitled Engineering Management, whose subjects and concepts originate from the works of professor Stoiljković. He was married to his wife Gordana, a german language teacher, and is the father of three children.

Dear professor, rest in peace.

Prof. dr Saša S. Ranđelović

In memoriam

Prof. dr Dragan Mišić (1963 - 2024)

Dr Dragan Mišić, a mechanical engineer, full professor at the Faculty of Mechanical Engineering in Niš, was born in 1964 in Niš. He enrolled at the Faculty of Mechanical Engineering in Niš in 1996. He graduated in 1991.

He defended his master's thesis entitled "Simultaneous design of rotating parts and technological processes of cutting" in 1998 at the Faculty of Mechanical Engineering in Niš. He defended his doctoral dissertation entitled "Adaptable systems for managing production business processes" in 2010 at the Faculty of Mechanical Engineering in Niš.

After graduating from 1991 to 1993, he worked as an associate on projects within the Laboratory for Intelligent Manufacturing Systems at the Faculty of Mechanical Engineering in Niš. In 1993, he was elected to the position of assistant trainee at the Department of Production Engineering. In the period from 1993 to 2010, he conducted exercises in the subjects "Computer-aided production design", "Modeling and optimization of production systems", "Machining", "Introduction to information systems", "Basics of programming".

He received his doctorate in 2010 at the Faculty of Mechanical Engineering in Niš and in the same year he was elected to the position of assistant professor, and in 2016 to the position of associate professor. He was re-elected to the position of associate professor in 2021. He was elected to the position of full professor in 2022.

He taught the subjects "Business Information Systems", "Information Systems Design", "Production Process Management", "Object-Oriented Programming", "Fundamentals of Information and Communication Technologies" at the Mechanical Engineering studies, as well as lectures on the subjects "Information Technologies 1", "Information Technologies 2", "Enterprise Information Systems" and "Process Management" at the Industrial Management studies.

After being elected to the title of associate professor, in addition to his engagement in the previously mentioned undergraduate academic subjects, he was engaged in doctoral academic subjects in the subjects: Ubiquitous Computing and Selected Chapters in Production and Information Technologies and Industrial Management.

He is the author of more than 80 scientific and professional papers in domestic and international journals, and has participated in a number of domestic and international scientific and research projects. He has been a mentor and member of committees in a number of master's and diploma theses. He has participated as a member of the committee for assessing the scientific basis and defense of several doctoral dissertations, and the committee for selecting assistants and teachers. He has also been a reviewer of papers in the international journal Enterprise Information Systems. He was a reviewer of papers and participated in the organization of international conferences: ICIST 2017, ICIST 2018, ICIST 2019, ICIST 2020, ICIST 2021. He reviewed technical solutions for the Ministry of Education, Science and Technological

Development, as well as several publications published by the Faculty of Mechanical Engineering in Niš. He was a member of the board of directors of the Informatics Society from 2017 to 2020.

He was a co-author of university textbooks "Information and Communication Technologies". Faculty of Mechanical Engineering in Niš, 2022, “Web Programming Practicum”, Faculty of Mechanical Engineering in Niš, 2017, “Introduction to Object-Oriented Programming”, Faculty of Mechanical Engineering in Niš, 2015.

Rest in peace.

Prof. dr Miodrag Manić

In memoriam

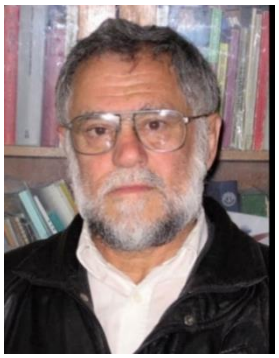

Prof. dr Milorad Jovanović (1941 - 2024)

Born on August 30, 1941, in the village of Rašković, municipality of Knić. He completed elementary school in his native village and high school in Kragujevac. He enrolled in the Faculty of Engineering in Kragujevac in the 1960-61 school year and graduated in 1965. After completing his military service, he worked briefly in Razvoj ZCZ Kragujevac, and then moved to the Faculty of Engineering in Kragujevac as an assistant (1965-1974). After completing his master's studies at the Faculty of Engineering in Belgrade, he worked as a lecturer at the Faculty of Engineering in Kragujevac (1974-1978). He defended his doctoral dissertation in 1978 at his home Faculty, where he worked as a teacher in the positions of Assistant Professor, Associate Professor, and Full Professor (1978-2006).

He taught courses in: Material Technology, Welding Technology, Plant Engineering, Engineering Materials, Welding Science, etc. He introduced several new courses into the Faculty's curriculum, such as: Welding Technology, Surface Regeneration, Casting Technology, Heat Treatment, etc.

He was the mentor for a large number of diploma theses (over 250) in Welding Technology, Engineering Materials, Plant Engineering, and Surface Regeneration. He was a reviewer for a large number of university books, handbooks, and monographs from almost all universities in Serbia.

He published more than 150 original scientific and professional papers, which were published in international and domestic journals or presented at international and domestic conferences. He is the author of 7 university textbooks, 8 auxiliary university textbooks, as well as several handbooks, practicums, and scripts. He participated in the realization of several international and domestic research projects. He was the mentor for 3 doctoral dissertations and a member of several defense committees. He was the mentor for 3 master's theses and a member of several defense committees. He had many years of experience working with measuring equipment for testing materials, welded joints, and castings using destructive and non-destructive methods.

He specialized in the field of materials and welding at the VÚZ Institute in Bratislava (Czechoslovakia, 1976-1977) and the Krakow Polytechnic (Poland, 1983-1984).

In addition to participating in teaching, he actively participated in conducting numerous seminars for engineers, training/retraining programs for the unemployed in welding and related processes, within which over 400 welders were trained. He made a significant contribution to the development of the materials and welding laboratories at his home faculty. He had knowledge and spoke several foreign languages: English, French, Polish, Czech, and Slovak.

Prof. dr Vukić Lazić,

Prof. dr Dušan Arsić

In memoriam

Prof. dr Miroslav Trajanović (1954 - 2025)

Dr Miroslav Trajanović was born on December 24, 1954, in Niš. He graduated from the Faculty of Mechanical Engineering in Niš, Production Department, in 1978. He defended his master's thesis in 1986 at the same faculty and earned his PhD in 1995 with a dissertation titled: "Expert System for Modeling Elements of Machine Tool Supporting Structures for Static Analysis Using the Finite Element Method."

Dr Trajanović began his professional career in 1978 as a junior assistant at the Department of Production Engineering. He was elected Assistant Professor in 1996, Associate Professor in 2001, and Full Professor in 2006.

He authored more than 300 scientific papers and numerous books and served as editor of prestigious international conference proceedings and journals. His teaching career was marked by exceptional dedication to students, delivering lectures on a wide range of subjects - many of which he introduced himself - in line with his passion for curriculum innovation, particularly while considering the ongoing trends of digitalization and the development and application of information technologies in industry, which marked his academic path. He made a lasting impact as professor of courses such as Machine Tools I, Modeling and Optimization of Production Systems, Systems for Rapid Product Development, Fundamentals of Information and Communication Technologies, Computer-Aided Product Design, Finite Element Method Applications, Fundamentals of Biomedical Engineering, Additive Technologies, Reverse Engineering, and others. A particularly important contribution to teaching was his role as Chair of the Department of Production-Information Technologies and Management (2007–2013), where he stood out as one of the few professors fully aware of emerging technological transformations and the need to reform the scientific field of production systems and technologies.

Throughout his career, he greatly contributed to the development of educational, research, and administrative infrastructure at the faculty and university levels. He was appointed Head of the Laboratory for Machine Tools and Machining twice (1983 and 1985). From 1993 to 2006, he successfully served as Director of the Computing Center (i.e., the Information System of the Faculty of Mechanical Engineering in Niš). In 2003, he initiated the establishment of the Innovation Center for Development and Application of Information Technologies (ICIT) at the faculty, where he served as Director until 2009. In 2005, he was appointed Manager of the Training Center Niš, as part of the Serbia and Montenegro Army's PRISMA Program for redundant military personnel retraining. From 2005 to 2008, 350 officers were educated through this center. Between 2007 and 2009, he was Chair of the Council of UNIS (the Unified University Information System of the University of Niš).

He made an immense contribution to the development of both the national and European science and research ecosystems through various roles within the national Ministry of Science and the European Commission. From 2001 to 2003, he chaired the Expert Committee for Mechanical Engineering and Industrial Software of the Ministry of Science, Technology, and Development of the Republic of Serbia, and from 2003 to 2007, he served as Chair of the Expert Committee for Industrial Software. From 2007 to 2010, he was Chair of the Scientific Council for Industrial Software and Informatics of the Ministry of Science, and from 2010 onward, Chair of the Scientific Council for Electronics, Telecommunications, and Information Technologies. Between 2007 and 2013, he represented the Ministry of Science of the Republic of Serbia in the Program Committees of the EU's 7th Framework Programme and the HORIZON framework (PEOPLE, ERC, FET, and MSCA programs). He played a key role in Serbia's EU integration process by participating in the preparation of the negotiating position for Chapter 25 – Science and Research — a chapter opened and immediately closed in 2016. From 2008 to 2017, he was Serbia's representative in the EU's high-level body responsible for researcher

mobility and human resources: the Steering Group on Human Resources and Mobility in the European Research Area. In 2009, he founded the national EURAXESS network to support researcher mobility and career development. Following Serbia's accession to the European Framework Programme for Research and Innovation (FP7), he coordinated the first and subsequent international cooperation projects within the large European EURAXESS network of over 40 countries.

Thanks to his initiative and leadership, the Faculty of Mechanical Engineering in Niš became a recognized research and educational institution in the field of biomedical engineering. From 2008 to 2020, he led projects in the area of computer-aided technologies for surgery of the human musculoskeletal system and their application in clinical and pre-clinical practice, resulting in new services, software tools, and products for predictive, preventive, diagnostic, and therapeutic applications, particularly in orthopedic surgery. One initiative stemming from these projects was the formation of the student group BestCAD, which developed various technical solutions in the field of bone fixation, published its results in several scientific papers, and even participated in the production of protective visors during the COVID-19 pandemic.

Dr Miroslav Trajanović is recognized in the scientific community also for his pioneering work in computer-aided tire and vulcanization-tool design - a project that propelled the company Tigar to the top of innovation in the tire industry. This project began in 2002 with support from the Ministry of Science and Technology.

Since 2022, he has served as State Secretary at the Ministry of Science, Technological Development, and Innovation. In this role, he has made an invaluable contribution to the development of Serbia's science policy, understanding science and innovation as pillars of a modern society. Thanks to his efforts and international presence, Serbia became the Chair country of the Global Partnership on Artificial Intelligence (GPAI) and in 2024 hosted the GPAI Summit in Belgrade, attended by over 1,500 participants and 44 foreign delegations, where the Belgrade Declaration on Artificial Intelligence - conceptually initiated by Professor Trajanović - was adopted.

Dear professor rest in peace.

Prof. dr Milan Zdravković

Table of Contents

FOREWORD ix

Plenary lecture 1

COGNITIVE MOBILE ROBOTICS BASED ON INTELLIGENT MECHANISMS OF LEARNING, Zoran Miljković, Aleksandar Jokić, Đorđe Jevtić 2

ONTOLOGIES IN MANUFACTURING, Lorenzo Solano García 9

FROM PRACTICAL INSIGHTS TO FUTURE INNOVATIONS IN ADDITIVE MANUFACTURING FOR MEDICAL APPLICATIONS, Razvan Pacurar 18

DIGITALISATION AND SENSING IN ADDITIVE MANUFACTURING - DATA COLLECTION FOR PRODUCTION OPTIMIZATION, Vojislav Petrović Filipović 23

Session 1: Material removal and nonconventional technologies 29

AI-BASED PREDICTION OF KERF WIDTH AND SURFACE ROUGHNESS IN CO2 LASER CUTTING OF STAINLESS STEEL, A. Nagadeepan, C.S. Tamil Selvan, S. Viswanathan, B.Vishnu, V. Senthilkumar . 30

CNC TURNING DYNAMICS: MODELING WITH NEWTON'S LINEAR INTERPOLATION AND MATLAB, Violeta Krcheva, Miša Tomić 36

MODELS FOR PREDICTING THE MAXIMUM HEIGHT OF THE SURFACE ROUGHNESS PROFILE BASED ON AXIAL DRILLING FORCE, Radoslav Vučurević, Zdravko Krivokapić, Saša Ranđelović, Mirjana Miljanović, Brankica Čomić 42

MEASURING MILLING FORCE WITH TWO C9C FORCE TRANSDUCERS, Attila Rétfalvi, Tamás Tornai 47

DIMENSIONAL ANALYSIS BASED PREDICTION MODEL OF THE MAIN CUTTING FORCE: COMPARISON AND VALIDATION, Jelena Stanojković, Miloš Madić, Milan Trifunović 55

MODELLING AND CUTTING PARAMETER OPTIMISATION OF THE INCONEL 718 MICROMILLING PROCESS, Branislav Sredanović, Gordana Globočki Lakić, Jelena Marković, Dejan Vujasin, Davorin Kramar 62

ELECTROMAGNETIC FIELD ANALYSIS AND PREDICTIVE MODELING IN FIBER LASER CUTTING OF REFRACTORY STEELS, Constantin Cristinel Girdu, Miloš Madić, Catalin Gheorghe, Daniel Lateș, Bogdan Cătălin Iacob 72

ANALYSIS OF THE IMPACT OF FRICTION ON THE QUALITY OF REGULATION DEPENDING ON THE USED FRICTION MODEL AND THE CONTROL LAW, Igor Kocić, Saša S. Nikolić, Darko Mitić, Nikola Danković, Staniša Perić, Miloš Madić , Milan Trifunović 84

APPLICATION OF RANDOM FOREST REGRESSION FOR PREDICTION OF SURFACE ROUGHNESS IN FIBER LASER CUTTING, Dragan Rodić, Milenko Sekulić, Borislav Savković, Anđelko Aleksić, Aleksandra Kosanović 91

INFLUENCE OF COOLING FLUID TYPE ON THE TEMPERATURE OF HIGH SPEED MOTORIZED SPINDLE, Miloš Knežev, Cvijetin Mlađenović, Dejan Marinković, Aco Antić, Aleksandar Živković . 100

MULTILAYER LASER CUTTING OF STEEL PLATES, Jelena Baralić, Bogdan Nedić 104

QUANTITATIVE ANALYSIS OF TOOL WEAR IN DEEP HOLE DRILLING, Milan Ivković, Strahinja Đurović, Bogdan Živković, Stefan Đurić, Aleksandar Đorđević, Goran Devedžić, Suzana Petrović Savić 112

Session 2: Metal forming and joining technologies 118

DETERMINATION OF THE FLOW CURVE USING THE MODIFIED RASTEGAEV TEST, Mladomir Milutinović, Dejan Movrin, Milica Panić, Marko Vilotić, Nemanja Prodanović 119

MODELING DEFORMATION FORCE IN OPEN DIES USING NEURAL NETWORKS, Mileta Janjić 124

THERMOMECHANICAL PROCESSING OF NEAR BETA TITANIUM ALLOYS, Fernando Warchomicka, Esmaeil Shahryari, Ricardo Henrique Buzolin, Franz Ferraz, Miller Branco, Cecilia Poletti 132

CRITERIA FOR SELECTING GEAR MANUFACTURING METHODS, Aleksandar Miltenović, Damjan Rangelov, Marko Perić 139

HYDROGEN EMBRITTLEMENT OF RECYCLED PRESSURE VESSEL STEEL P460NL1, Tobias Walder, Fabian BOBNER, Thomas Staubmann, Hamdi Elsayed, Fernando Wachomicka, Rudolf Vallant 145

IMPACT OF GATING SYSTEM DESIGNA ON MECHANICAL PROPERTIES OF ALUMINIUM SAND CASTINGS, Marko Zagoričnik, Lazar Kovačević, Vladimir Terek, Zoran Bobić, Pal Terek 150

ANALYSIS OF THE PREFORMING STAGE IN THE CLOSED-DIE HOT FORGING PROCESS, Mihajlo Milojković, Saša Ranđelović 157

Session 3: Materials and surface engineering and tribology 163

EFFECT OF THE MAXIMUM TEMPERATURE ON THE HARDNESS AT THE HEAT AFFECTED ZONE OF THREE DIFFERENT CARBON STEELS AFTER A SLOW COOLING, Nima Poursalimi, Juan Carlos Ferrero-Taberner, Lorenzo Solano-García, Norberto Feito-Sánchez, Miguel Ángel Pérez-Puig, Fidel Salas-Vicente 164

NANOCORROSION EFFECT ON NiTi ARCHWIRE EXPOSED TO VARIOUS MOUTHWASHES, Zoran Bobić, Lazar Kovačević, Vladimir Terek, Marko Zagoričnik, Sanja Kojić, Goran Stojanović, Bojan Petrović, Pal Terek 171

A COMPARATIVE STUDY ON THE TRIBOLOGICAL BEHAVIOR OF NEW AND USED 10W-40 ENGINE OIL APPLIED IN GASOLINE AND DIESEL ENGINES, Dragan Džunić, Vladimir Kočović, Živana Jovanović Pešić, Slobodan Mitrović, Milan Erić 177

ASSESSMENT OF MEASUREMENT UNCERTAINTY IN MECHANICAL MATERIAL TESTING – THEORETICAL FRAMEWORK AND PRACTICAL APPLICATION, Dušan Petković, Predrag Janković 182

Session 4: Process planning and production control, logistics and optimization 187

DEEP LEARNING TECHNIQUES FOR DEFECT DETECTION IN AUTOMATED QUALITY CONTROL SYSTEMS A. Gandhi Manikandan, V. Sandhiya, P. Harine, R. Ajay Dhisone, M. Sathyaprakash 188

MULTI-CRITERIA OPTIMIZATION OF CO2 LASER CUTTING OF METALS USING HYBRID AHP–TOPSIS APPROACH A. Nagadeepan, M. Pranav, P. Santhosh, S. SivaShankaran, V. Senthilkumar 193

INFORMATION SYSTEMS IN THE FUNCTION OF BUSINESS LOGISTICS
Srećko Ćurčić, Dejan Ž. Veljković 199

DEFINING PRODUCTION LOGISTICS FOR INDUSTRY 4.0 Srećko Ćurčić..... 208

APPLICATION OF THE MATHEMATICAL CONVOLUTION OPERATOR IN THE OPTIMIZATION OF RESOURCE PLANNING AND SCHEDULING,
Aleksandar Stanković, Milica Milunović, Goran Petrović 217

BLOCKCHAIN APPLICATION IN SUPPLY CHAIN MANAGEMENT Miodrag Manić, Nikola Vitković, Zorana Stanković, Vladimir Mitrović..... 224

Session 5: Artificial intelligence in manufacturing 229

ARTIFICIAL INTELLIGENCE AND CNC MANUFACTURING, Milica Utvić, Bojan Stojčetović, Milan Mišić, Aleksandar Sekulić, A. Kokić Arsić, Martina Petković, Strahinja Đurović 230

USE OF GENERATIVE AI IN THE CROATIAN MANUFACTURING INDUSTRY, Maja Trstenjak, Biljana Cvetić, Vanina Macowski Durski Silva, Bernhard Axmann..... 235

DYNAMIC FLEXIBLE JOB SHOP SCHEDULING PROBLEM BASED ON GENETIC ALGORITHM,
Katarina Brenjo, Aleksandar Jokić, Milica Petrović..... 243

RECENT ADVANCES IN ARTIFICEL INTELIGENCE AND MACHINE LEARNING FOR PROCESS, OPTIMIZATION IN TURNING Aleksandar Trajković, Miloš Madić 255

Session 6: Machine tools and automation, flexible technological systems 263

DEVELOPMENT OF A 2-AXIS SCARA ROBOT MOTION CONTROLLER BASED ON MCU, Bogdan Momčilović, Nikola Slavković 264

HOW THE LOLA 8A COMPUTER WAS MADE — A REVERSE ENGINEERING STUDY,
Stevan Parojčić, Dragan Pavlović 273

EXPLAINABLE ARTIFICIAL INTELLIGENCE IN INDUSTRIAL AUTOMATION AND ROBOTICS: STATE, PROSPECTS AND A CASE-STUDY, Nemanja Marković, Emilija Ćojbašić, Dejan Rančić, Nedeljko Dučić, Žarko Ćojbašić 278

FROM MODULAR LEGACY TO OPEN INNOVATION: EVOLUTION OF THE LOLA CNC SYSTEM ARCHITECTURE, Zoran Dimić, Andrija Dević, Saša Živanović, Aleksa Krošnjar, Stevan Parojčić, Dragan Pavlović 283

MATHEMATICAL MODEL OF PNEUMATIC CARTESIAN ROBOT,
Vladislav Blagojević, Saša Ranđelović, Srđan Mladenović 288

Session 7: CAx and smart technologies 292

PROGRAMMING AND VERIFICATION OF MILLING OPERATIONS FOR CNC MACHINES WITH HORIZONTAL ROTARY AXIS, Sasa Živanović, Julija Maletić, Nikola Vorkapić, Nikola Slavković, Zoran Dimić, Radovan Puzović 293

CNC SIMULATOR BASED ON LINUXCNC CONTROL AND PROGRAMMING SYSTEM, Goran Vasilić, Milan Milutinović, Saša Živanović, Zoran Dimić..... 300

THE CONCEPT OF SMART INFORMATION SYSTEMS IN PRODUCTION ENGINEERING: THE METAVERSE APPROACH, Nikola Vitković, Miodrag Manić, Milan Mitković, Sven Maričić, Marek Chodnicki, George Vosniakos, Panorios Benardos, Manolis Stathatos 307

RAPID PROTOTYPING OF A DEVICE FOR TESTING THE CONNECTION OF REINFORCED CONCRETE AND ANCHOR BOLT, Nikola Šibalić, Marko Mumović 318

A BRIEF HISTORY OF CAD AND RELATED TECHNOLOGIES, Nikola Korunović, Miloš Stojković, Nikola Vitković, Jovan Aranđelović 324

VIRTUAL REALITY ENVIRONMENT FOR TEACHING ASSEMBLY SEQUENCE ANALYSIS TO PRODUCTION ENGINEERING STUDENTS, Živojin Suvajac, Lazar Matijašević, Dušan Nedeljković, Živana Jakovljević 335

Session 8: Additive manufacturing technologies 345

OPTIMIZATION OF THE DELTA 3D PRINTER STRUCTURE, Natalija Lazarević, Aleksandar Lazić, Mihajlo Popović, Miloš Pjević 346

IMPLEMENTATION AND OPTIMIZATION OF THE DELTA 3D PRINTER CONTROL SYSTEM, Aleksandar Lazić, Natalija Lazarević, Mihajlo Popović, Miloš Pjević 355

THE INFLUENCE AND ADJUSTMENT OF 3D PRINTER TEMPERATURES DURING MODEL PRINTING WITH REFERENCE TO THE USED MATERIAL, Saša Vasiljević, Milan Đorđević, Marina Karić, Milan Radenković, Marko Maslać 363

INFLUENCE OF LAYER HEIGHT ON THE SURFACE ROUGHNESS OF FDM PRINTED PETG PARTS, Strahinja Đurović, Nikolaj Velikanac, Milan Ivković, Dragan Lazarević, Milan Mišić, Bojan Stojčetović, Martina Petković 371

ADVANCED DESIGN OF 3D-PRINTED COMPONENTS FOR ROBOTIC END- EFFECTORS: A TAGUCHI-BASED MASS AND VOLUME OPTIMIZATION Dejan Bozic, Mijodrag Milosevic, Zeljko Santosi, Grigor Stambolov, Dejan Lukic 375

EXPERIMENTAL EVALUATION OF TENSILE PROPERTIES OF 3D-PRINTED PLA THREADS Miroslav Mijajlović, Gordana Jović, Aleksandar Trajković, Miloš Madić, Jovan Aranđelović, Nikola Korunović 397

PERSONALIZED CHRONIC WOUNDS TREATMENT BY APPLICATION OF ADDITIVE TECHNOLOGIES Nikola Vitković, Sanja Stojanović, Miloš Madić, Zoran Damnjanović, Răzvan Păcurar, Filip Górski, Joaquín Francisco Roca González 407

INFLUENCE OF EXTRUSION TEMPERATURE ON THE INTERLAYER ADHESION OF PLA AND TPU IN FDM TECHNOLOGY, Milica Panić, Dejan Movrin, Mladomir Milutinović, Sanja Bojić 416

EFFECT OF LAYER HEIGHT ON GEOMETRIC ACCURACY OF FDM 3D PRINTED POROUS STRUCTURES, Nikola Kotorčević, Fatima Živić, Petar Todorović, Nenad Grujović 422

INFLUENCE OF STRUT CROSS-SECTION GEOMETRY ON THE MECHANICAL PROPERTIES OF MSLA-FABRICATED BONE SCAFFOLDS, Aleksandra Veličković, Rajko Turudija, Jovan Aranđelović, Jelena Stojković 430

RELATIONSHIP BETWEEN POROSITY AND MECHANICAL PERFORMANCE OF CUSTOM LATTICE-LIKE BONE SCAFFOLDS, Rajko Turudija, Jovan Aranđelović, Miloš Stojković, Jelena Stojković, Nikola Korunović 438

Session 9: Metrology and quality, cutting tools 444

COMPARISON OF LASER INTERFEROMETER SYSTEMS FOR MEASURING POSITIONAL ACCURACY OF MACHINE TOOLS, Alexander Buda Budimir, Slobodan Tabaković, Milan Zeljković, Saša Živanović, Zoran Dimić 445

MULTISENSOR TECHNOLOGIES IN COORDINATE METROLOGY: MEASUREMENT DIMENSIONAL QUALITY CHARACTERISTICS, Vidoje Kasalica, Slavenko Stojadinović, Radovan Puzović 452

MEASUREMENT OF NOISE AND VIBRATION IN THE CUTTING ZONE DURING TURNING, Zvonko Petrović, Branko Radičević, Bogdan Nedić, Radovan Nikolić 461

REVIEW OF METHODS AND APPROACHES FOR EVALUATING MEASUREMENT UNCERTAINTY OF CMM, Branko Štrbac, Miloš Ranisavljev, Biserka Runje, Goran Jotić, Branislav Dudić, Miodrag Hadžistević 465

ACCURACY OF SOUND POWER DETERMINATION USING DIFFERENT SOUND INTENSITY METHODS: A CASE STUDY ON A VACUUM PUMP, Tanja Dulović, Branko Radičević, Jovana Perić, Mladen Rasinac, Vladan Grković 473

IMPLEMENTATION OF INDUSTRY 4.0 ELEMENTS IN THE AUTOMOTIVE INDUSTRY ACCORDING TO ISO 16949, Natalija Stanković, Saša Ranđelović, Goran Stanković, Branislav Marković, Radoslav Vučurević 480

ANALYSIS OF MEASUREMENT SYSTEM CAPABILITY WITH NEGLIGIBLE OPERATOR INFLUENCE: A CASE STUDY USING A COORDINATE MEASURING MACHINE, Predrag Janković, Miloš Madić 487

Session 10: Management for sustainable manufacturing 495

SMART ENERGY PRODUCTION AND INDUSTRY 5.0: XAI AND IRREGULAR TIME SERIES FORECASTING, Milica Tasić, Ivan Ćirić, Vladan Jovanović, Miloš Simonović, Marko Ignjatović 496

PACKAGING OPTIMIZATION AS A TOOL FOR SUSTAINABLE PRODUCTION ON A GLOBAL SCALE, Maja Branković, Miloš Paunović, Saša Ranđelović 506

ANALYSIS OF TECHNICAL RISKS IN SMALL HYDROPOWER PLANTS IN THE CONTEXT OF SUSTAINABLE DEVELOPMENT, Natalija Anđelković, Saša Ranđelović, Radica Stojanović 512

INTEGRATING RENEWABLE ENERGY SOURCES INTO INDUSTRIAL MANUFACTURING: TECHNOLOGIES, CHALLENGES, AND BEST PRACTICES, Milan Grozdanović, Dejan Tanikić, Ana Kitić 520

ROADMAP FOR SUSTAINABLE MANUFACTURING IN THE INDUSTRY 4.0 AND 5.0 ERA: CONCEPTS, METRICS, AND OPPORTUNITIES FOR SMES, 7Ana Kitić, Mladen Radišić, Milan Grozdanović, Ivana Janković 527

SUSTAINABLE WATER MANAGEMENT IN THE COSMETIC INDUSTRY, Jelena Nedeljković, Neda Desić, Iva Jevtić, Jelena Nikolić, Saša Ranđelović 535

Plenary lectures

Society of Production Engineering

ICPES 2025

40th INTERNATIONAL CONFERENCE ON PRODUCTION ENGINEERING – SERBIA 2025

DOI: 10.46793/ICPES25.002M

University of Nis Faculty of Mechanical Engineering

Nis, Serbia, 18 - 19th September 2025

COGNITIVE MOBILE ROBOTICS BASED ON INTELLIGENT MECHANISMS OF LEARNING

Zoran MILJKOVIĆ[1*], Aleksandar JOKIĆ[1], Đorđe JEVTIĆ[1]

Orcid: 0000-0001-9706-6134; **Orcid:** 0000-0002-7417-4244; **Orcid:** 0000-0002-6917-1663

[1]University of Belgrade – Faculty of Mechanical Engineering, Serbia, Belgrade

*Corresponding author: zmiljkovic@mas.bg.ac.rs

Abstract: *The purpose of this contribution is the deployment of digital manufacturing through new cognitive intelligence mechanisms. With the implementation of Industry 4.0 principles, mobile intelligent robots utilized as transportation vehicles in the manufacturing system need a higher degree of autonomy to fulfill all the requirements of the contemporary market. Although industrial robots are common in manufacturing systems, mobile robotics requires the expertise of specialists in cognitive robotics issues to gain international competitiveness, particularly for small and medium-sized enterprises. The industrial mobile robots' autonomous subsystems based on deep machine learning provide significantly more flexibility as well as more accurate and robust real-time decisions compared to common deterministic sensor-based algorithms. The main goal of this paper is to create artificial intelligence-based solutions for cognitive mobile robotics within Industry 4.0 using a Machine Learning (ML) based approach, particularly deep learning (convolutional neural networks, recurrent neural networks, etc.). The focus of the paper is the generation of new ML-based cognitive intelligence mechanisms for obstacle avoidance, decision-making, and visual control of intelligent mobile robots, whereas the main goal of the paper is to demonstrate the possibility of integrating intelligent ML-based algorithms into a high-level cognitive architecture by enabling better understanding of the environment in real-time through the processing of higher-quality and more complex sensory data, thereby enhancing the overall flexibility of mobile robotic systems within intelligent manufacturing systems.*

Keywords: *mobile robots, intelligent control systems, digital manufacturing, cognitive intelligence mechanisms, deep learning, autonomous systems, visual servoing.*

1. INTRODUCTION

In the era of rapid development of technological innovation, the cognitive mobile robots have enormous potential to influence both the industrial and service sectors. In the industrial sector, intelligent mobile robots with learning mechanisms can support the declining workforce with repetitive, dull, and physically tiring tasks. However, for intelligent mobile robots to be effective in the manufacturing sector, many essential skills need to be acquired, such as highly accurate positioning [1], obstacle avoidance [2], perception [3], and decision-making [4]. One of the most promising research directions within the robotics domain that can fulfill the skills is the utilization of machine learning techniques. The limits and potential of deep machine learning within robotics systems are analyzed in great detail in [5]. The three primary axes of research

development are learning, embodiment, and reasoning, with an aim to reach active learning, active manipulation, and integration of semantic and geometric reasoning. Active learning represents the process of learning through interaction with the environment or online learning, which differs from the standard learning pipeline where the model is trained and statically utilized in robotics application. Active manipulation is the process of adjusting robots pose, to increase the accuracy of the environment perception and the probability of the successful manipulation process. Integration of semantic and geometric reasoning includes the process of mapping and utilizing not only the geometric properties of the environment but also the human-centered meaning of the objects and their semantic relationships. Two primary approaches to achieving the aforementioned skills include the development of individual skills and their integration trough cognitive high-level architectures such as, subsampling architecture [6], cognitive maps [7], and Soar [8], or utilizing novel deep learning based Vision-Language-Action (VLA) models [9]. The main primary deficiency of the VLA models is in their lack of reliability stemming form their black box nature and their sensitivity to environmental factors. Therefore, in this paper we will analyze the three developed deep machine learning-based algorithm utilized to achieve the necessary skills for the implementation of cognitive mobile robots within the manufacturing environment.

2. SEMANTIC SEGMENTATION BASED OBSTACLE AVOIDANCE

For a mobile robot to work autonomously in a dynamic and unstructured industrial environment, it needs to be able to avoid different obstacles in its path. Therefore, a globally optimally planned path needs to have local minor deviations necessary to avoid obstacles detected with the robot's sensors.

In this section, we analyze one of the approaches for obstacle avoidance based on semantic segmentation [2]. The custom version of the ResNet model is trained on the SunRGBD indoor dataset [10]. Since the experimental evaluation is performed on the mobile robot RAICO (Robot with Artificial Intelligence based COgnition), which has the Nvidia Jetson Nano development board, the utilized convolutional neural network needed to be lightweight. The state machine utilized for the obstacle avoidance algorithm is shown in Fig. 1.

The path the mobile robot takes during the obstacle avoidance process can be seen in Fig. 2. The obstacle detection is performed by analyzing semantic maps and checking if there is something other than class "floor" in the mobile robot's path. An example of one obstacle avoidance procedure, shown from RAICO's perspective, is illustrated in Fig. 3. As can be seen, the floor is labeled with red, yellow represents the obstacle, black denotes the tables, and teal represents the walls. Images generated by the mobile robot and the transformation of the image space occupancy grid defined with a semantic map to a 2D occupancy grid in the mobile robot frame are shown in Fig. 4. Green represents the free space, while red represents the occupied grids.

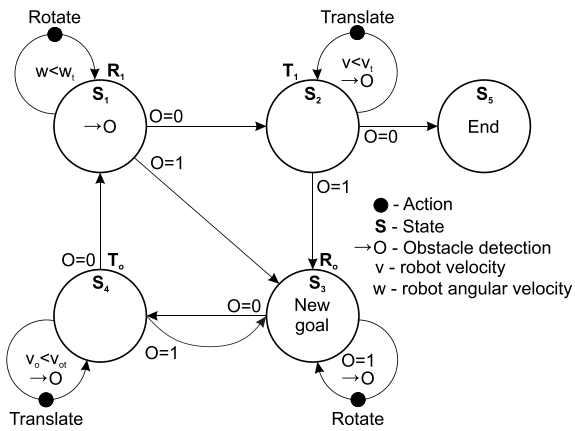

Figure 1. State machine for obstacle avoidance algorithm.

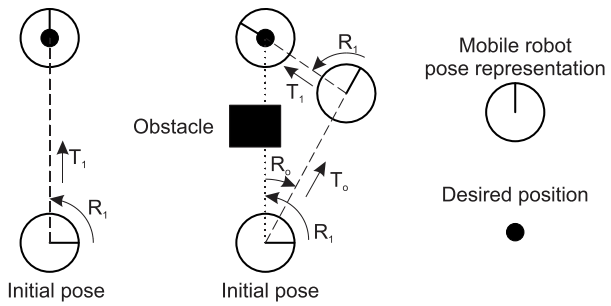

Figure 2. Mobile robot during path following (left) and during obstacle avoidance algorithm (right).

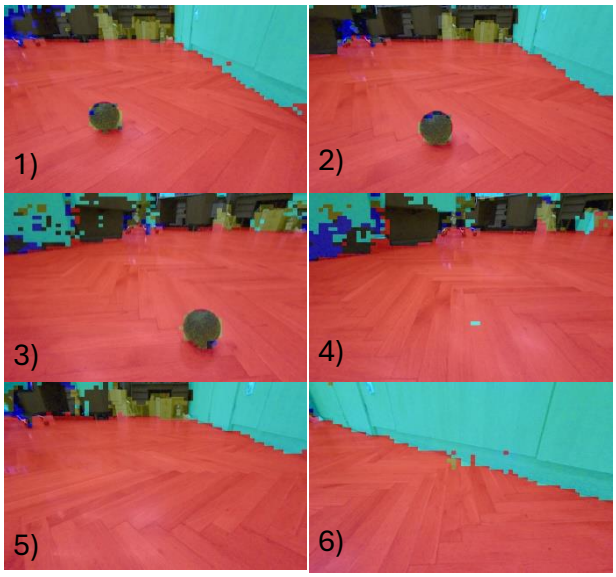

Figure 3. Semantic segmentation of the mobile robot's scene.

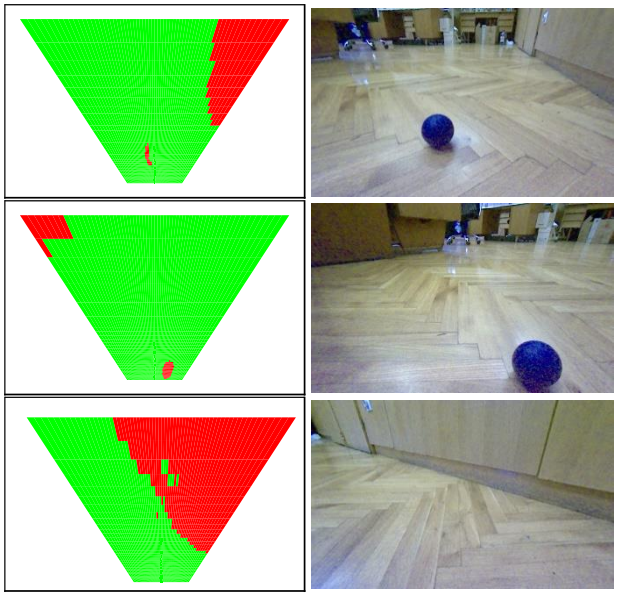

Figure 4. Visualization of the occupancy grid generated from the visual system.

The path the mobile robot took during the experimental evaluation can be seen in Fig. 5.

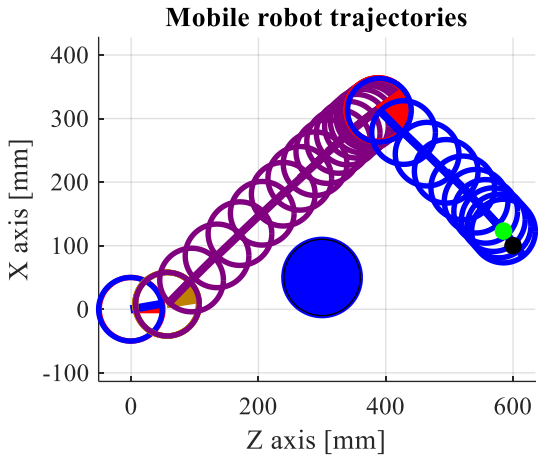

Figure 5. Mobile robot path.

3. SEMANTIC SEGMENTATION-BASED VISUAL SERVOING

One of the key requirements for the efficient utilization of cognitive architectures is to reuse the data for multiple behaviors. Having that in mind, the second behavior considers accurate positioning of the mobile robot, based on semantic stereo visual servoing. Since the standard odometry-based mobile robot positioning system cannot provide high levels of accuracy, needed for the manipulation tasks in the manufacturing environment, the stereo visual servoing based on semantic segmentation is employed [1].

The images generated in the laboratory manufacturing environment are converted into semantic maps by utilizing a convolutional neural network (Fig. 6). The dataset comprises five classes: four machine tool classes and one background class.

Afterwards, semantic maps generated in the desired and current pose (position and orientation) are registered [11]. The registration represents the process of image transformation with an objective function to align two images. The semantic maps registration can be seen in Fig. 7 for both images of the stereo vision system. Combined semantic maps of two images (current and desired) are shown in the first row. One of the initially generated semantic maps is shown with shades of pink, while the other is shown with green. After the registration process is completed, the images are displayed in the

second row. If the green and pink elements are aligned accurately, they are displayed in gray.

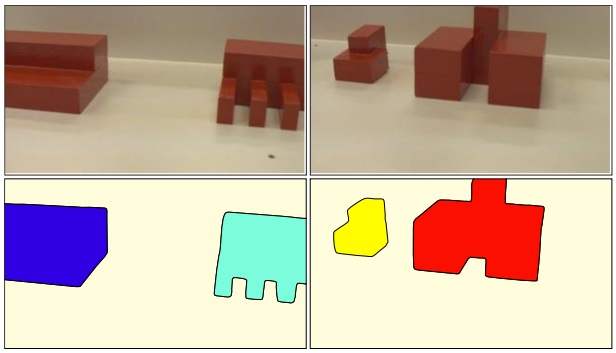

Figure 6. Images and semantic maps generated from the stereo visual system.

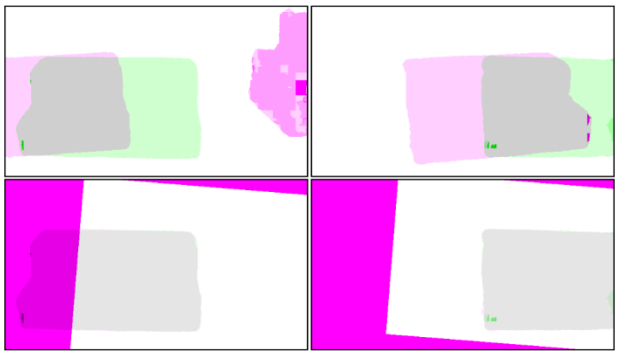

Figure 7. Semantic map registration process.

The output of the image registration process is the transformation matrix $\mathbf{T} \in \mathbb{R}^{3\times3}$. That transformation matrix is utilized to align all the control pixels belonging to the same machine in the current $\mathbf{c}_c = (u_c, v_c, 1)^T$ and desired $\mathbf{c}_d = (u_d, v_d, 1)^T$ image (1):

$$\mathbf{c}_c = \mathbf{T}\mathbf{c}_d. \tag{1}$$

After the registration is performed and the pixels are connected by utilizing the transformation matrix, the difference between those pixels can be used to determine the necessary velocities in the camera frame (2):

$$\dot{\mathbf{c}} = \mathbf{J}\mathbf{v}_{cam}, \tag{2}$$

where $\dot{\boldsymbol{c}}$ is the difference between current and desired control pixels, $\mathbf{J}$ is the image Jacobian matrix [12], and $\mathbf{V}_{cam}$ are the velocities generated in the camera frame. Finally, the velocities in the mobile robot frame ($\mathbf{V}_{mr} \in \mathbb{R}^{6\times1}$) are generated by utilizing a visual servoing controller for k defined control pixels (3):

$$\mathbf{v}_{mr} = \lambda \begin{pmatrix} \mathbf{J}_1\mathbf{M} \\ \vdots \\ \mathbf{J}_k\mathbf{M} \end{pmatrix}^{-1} \begin{pmatrix} \dot{\mathbf{c}}_1 \\ \vdots \\ \dot{\mathbf{c}}_k \end{pmatrix}, \tag{3}$$

where λ is the gain value, and $\mathbf{M} \in \mathbb{R}^{6\times6}$ is the velocity transformation matrix from the camera to the mobile robot frame.

Both simulation and real-world experimental evaluations with the semantic segmentation-based stereo visual servoing algorithm show high levels of accuracy [1]. Initial pose of mobile robot RAICO in simulated and real-world experiment can be seen in Fig. 8. The path mobile robot took during the first experiment can be seen in Fig. 9. The accuracy of the final pose can also be shown by visualizing the absolute pixel difference between the final and the desired images (Fig. 10).

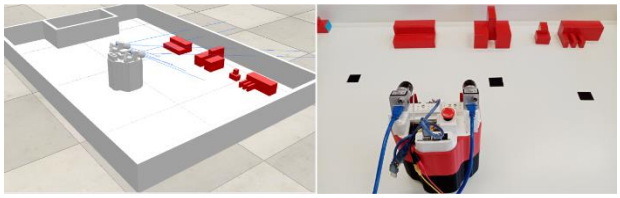

Figure 8. Initial pose of mobile robot RAICO in the simulation (left) and real-world (right) experimental setup.

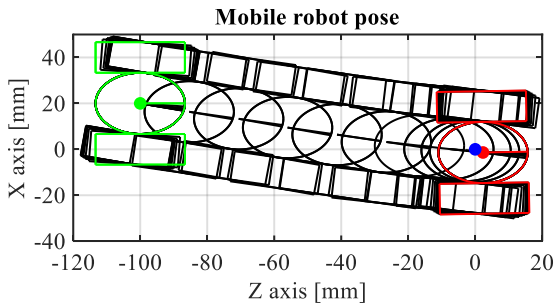

Figure 9. The path RAICO took from starting (green), intermediate (black), to the final (red) pose. The desired position is shown with a blue dot.

Figure 10. Absolute pixel difference between the desired and final images.

The black color represents a low difference between pixels, while light blue represents the parts of the image with noticeable differences. An additional important feature of the semantic segmentation-based stereo visual servoing is the ability to utilize the images generated in simulation for visual servoing, which is provided in the last experimental evaluation [1]. The desired images (Fig. 11) are generated in simulation and utilized in the real-world environment.

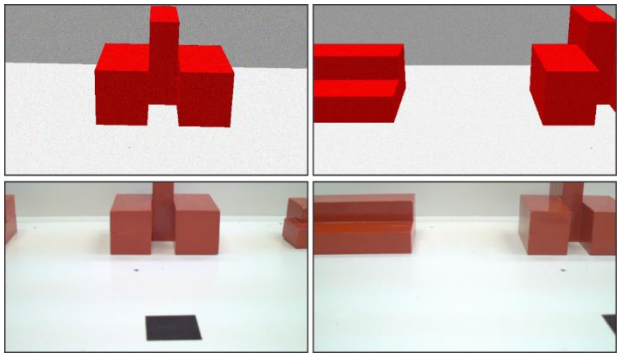

Figure 11. Desired images generated in simulation (first row) and real-world current images (second row).

The mobile robot managed to achieve the desired pose, which opens a possibility to change the desired image adaptably, significantly increasing the flexibility of the visual servoing algorithm.

4. ACCURACY ESTIMATION SYSTEM BASED ON DEEP LEARNING

The last system that utilizes deep learning in mobile robot applications is the accuracy estimation system that predicts the probability of a successful pickup procedure [4]. The input variables include the pose of the mobile robot, as well as the image of the final scene before the pickup procedure is initiated. The standard ResNet18 model (Fig. 12) is adapted and trained on the custom dataset to predict if the pickup procedure will be successful with a standard softmax output function.

The output of the model is utilized to assess if the current pose of the mobile robot is adequate for the pickup procedure.

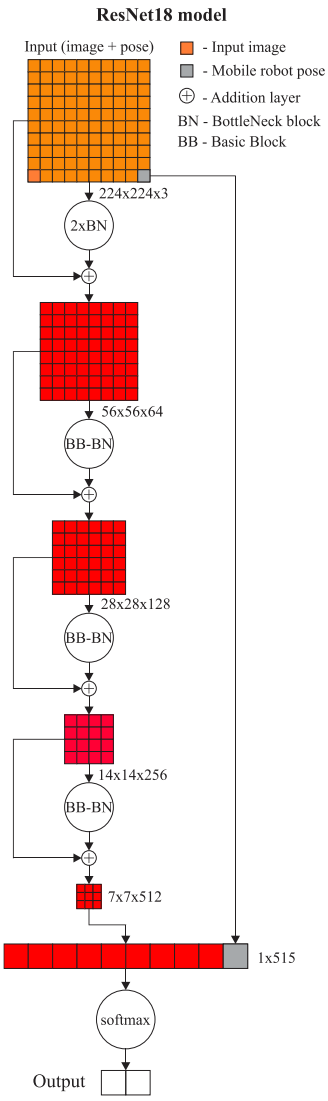

Figure 12. ResNet18 model for the probability of the pickup success prediction.

The experimental evaluation showed that high confidence of the model is highly correlated with the gripping success.

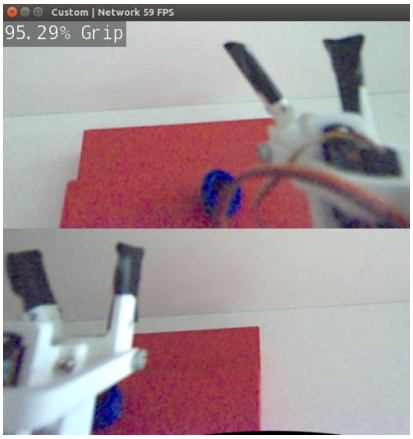

Figure 13. Mobile robot's view of the scene and gripping accuracy prediction.

However, the overall accuracy of the model is 70%. Figures 13 and 14 show the mobile robot performing the pickup procedure from the mobile robot's perspective and from the side view, respectively.

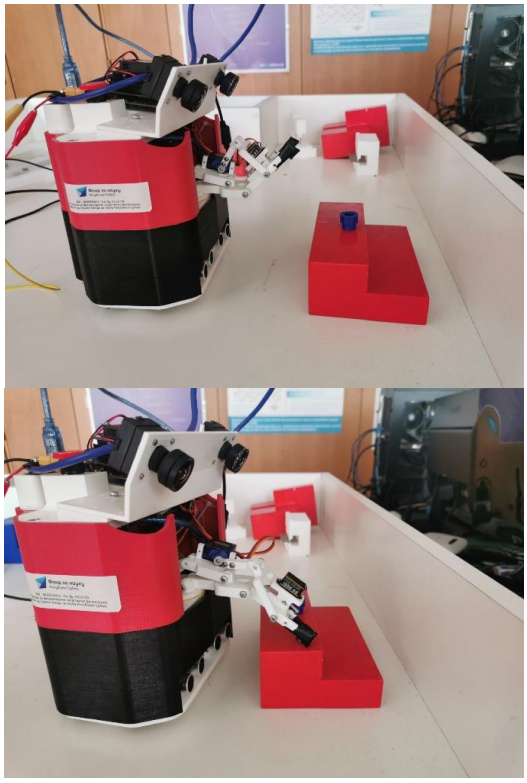

Figure 14. Side view of mobile robot RAICO during the gripping procedure.

5. CONCLUSION

In this paper, we have presented the results regarding the utilization of the intelligent learning mechanisms within the cognitive mobile robot domain. Three primary subsystems utilized to demonstrate the advantages of the deep machine learning approaches are obstacle avoidance, visual servoing, and prediction of the accuracy of pickup operation. The obstacle avoidance is performed by utilizing semantic segmentation of the scene, where the mobile robot RAICO can determine the difference between the classes of objects in its environment and the floor class. After successful semantic segmentation, the image is projected to a 2D occupancy grid and utilized within the obstacle avoidance procedure. The second algorithm regards the accurate positioning of the mobile robot. For that, we utilized stereo visual servoing based on semantic segmentation. After the registration of semantic maps, it is possible to determine the velocities the mobile robot needs to achieve to position itself accurately. Lastly, the standard ResNet18 model is utilized in the image classification problem to determine if the current pose is adequate for the pickup procedure. Mobile robot pose and image information represent the input into the desired model. The future research direction includes the integration of the developed algorithm into a cognitive control architecture.

ACKNOWLEDGEMENT

This research was supported by the Science Fund of the Republic of Serbia, grant No. 17801, Cybersecurity of Motion Control Systems in Industry 4.0 – MCSecurity, and by the Ministry of Science, Technological Development and Innovations of the Serbian Government under the contract No. 451-03-137/2025-03/200105.

REFERENCES

[1] A. Jokić, M. Petrović, Z. Miljković, Semantic segmentation based stereo visual servoing of nonholonomic mobile robot in intelligent manufacturing environment, Expert Systems with Applications, Vol. 190, p. 116203, 2022.

[2] M. Petrović, Z. Miljković, A. Jokić, Efficient Machine Learning of Mobile Robotic Systems based on Convolutional Neural Networks, in Artificial intelligence for Robotics and Autonomous Systems. Studies in Computational Intelligence, A. Koubaa and A. T. Azar, Eds., Springer, 2023, pp. 1–26.

[3] A. Jokić, M. Petrović, Z. Miljković, Real-time Mobile Robot Perception based on Deep Learning Detection Model, in New Technologies, Development and Application V (NT 2022). Lecture Notes in Networks and Systems, Springer, Cham, 2022, pp. 670–677.

[4] A. Jokić, M. Petrović, Z. Miljković, Mobile robot decision-making system based on deep machine learning, in 9th International

Conference on Electrical, Electronics and Computing Engineering (IcETRAN 2022), 2022, pp. 653–656.

[5] N. Sünderhauf et al., The limits and potentials of deep learning for robotics, International Journal of Robotics Research, Vol. 37, No. 4–5, pp. 405–420, 2018.

[6] R. Brooks, A robust layered control system for a mobile robot, IEEE journal on robotics and automation, Vol. 2, No. 1, pp. 14–23, 2003.

[7] S. Vasudevan, S. Gächter, V. Nguyen, R. Siegwart, Cognitive maps for mobile robots—an object based approach, Robotics and Autonomous Systems, Vol. 55, No. 5, pp. 359–371, 2007.

[8] J. E. Laird, The Soar cognitive architecture. MIT press, 2019.

[9] G. R. Team et al., Gemini robotics: Bringing ai into the physical world, arXiv preprint arXiv:2503.20020, 2025.

[10] S. Song, S. P. Lichtenberg, J. Xiao, SUN RGB-D: A RGB-D scene understanding benchmark suite, in Proceedings of the IEEE Conference on Computer Vision and Pattern Recognition, 2015, pp. 567–576.

[11] Z. Miljković, A. Jokić, M. Petrović, Image Registration Algorithm for Deep Learning-Based Stereo Visual Control of Mobile Robots, in Deep Learning for Unmanned Systems. Studies in Computational Intelligence, A. Koubaa and A. T. Azar, Eds., Springer, Cham, 2021, pp. 447–479.

[12] F. Chaumette, S. Hutchinson, Visual servo control. I. Basic approaches, IEEE Robotics and Automation Magazine, Vol. 13, No. 4, pp. 82–90, 2006.

Society of Production Engineering

ICPES 2025

40th INTERNATIONAL CONFERENCE ON PRODUCTION ENGINEERING - SERBIA 2025

DOI: 10.46793/ICPES25.009SG

University of Nis
Faculty of Mechanical Engineering

Nis, Serbia, 18 - 19th September 2025

ONTOLOGIES IN MANUFACTURING

Lorenzo SOLANO-GARCÍA[*1]
Orcid: 0000-0003-0535-314X
[1]Institute of Design and Manufacturing, Universitat Politècnica de València, Spain
*Corresponding author: isolano@mcm.upv.es

Abstract: *This paper presents an application of ontologies in the manufacturing field, specifically in collaborative process planning. To this end, it first examines the concept of ontology through its definition, purpose, and classification. After it presents the tools used to implement the developed ontologies and the upper ontologies used for their development. Finally, a brief description of these ontologies is provided: PPDRC ontology (ontology for collaborative Development of Products and Processes focused on Resource Capabilities) and MIRC ontology (ontology for integrated Machining and Inspection process planning focusing on Resource Capabilities).*

Keywords: *Ontologies, manufacturing, collaborative process planning, PPDRC ontology, MIRC ontology, resource capabilities.*

1. INTRODUCTION

Process planning, as a link between design and manufacturing, is a key function to ensuring that the characteristics of manufactured products meet customer needs. Multiple factors converge in the tasks of manufacturing process planning. When these factors are combined with the diversity of possible strategies and approaches, they form a particularly complex scenario.

Taking as a starting point the above, this paper presents a contribution in the field of collaborative process planning. For this, an ontological approach is proposed. This ontology gives support and consistency to the co-planning tools used in creating process plans, especially in decision-making related to the optimal and dynamics resource allocation based on resource capabilities.

2. ONTOLOGIES

This section shows an overview of ontologies, intended to provide a general and integrative vision of them. Since the relatively recent presence of ontologies in the field of engineering, and particularly in manufacturing engineering, means that they may not be sufficiently well known in these fields.

2.1 Definition

Some authors agree on the extreme difficulty of establishing a general definition for the concept of ontology, since there are many and diverse realities to which this term can

refer, usually linked to their different uses: the integration of data sets; the sharing of knowledge bases; enabling communication between software agents; decision-making support; semantic frameworks for enterprise architectures; the representation of a natural language vocabulary; the representation of semantics for complex software services and applications; or the provision of a conceptual framework for indexing content.

According to Gruber, an ontology is an explicit specification of a conceptualization [1]. This conceptualization can be understood as a set of objects, concepts, and other entities that are assumed to exist in some area of interest, along with the relationships they maintain among themselves. Terms with a precise, shared interpretation and meaning are established and used to refer to all of these entities and relationships.

Formalisms facilitate the sharing of certain common knowledge between humans and machines in a structured and precise manner, as they use a rigorous syntax for representing entities and relationships, ensuring unambiguous interpretation of their semantics. Logic uses these formalisms to reach certain conclusions through reasoning processes.

Among the definitions of ontology that are based on logical theories or formalisms, the one by Uschold and Gruninger stands out: 'an ontology is a formal description of the entities within a given domain, with the properties they have, the relationships in which they participate, the restrictions to which they are subject, and the patterns of behavior they exhibit' [2].

2.2 Purpose of ontologies

Ontologies aim to rationally establish the principles that organize and guide knowledge of being, as a part of reality, through its properties, principles, and causes.

Ontologies allow the relevant concepts and terms of a given domain to be identified and defined unambiguously. In this sense, they constitute the technological key to describing the semantics of information, overcoming the problem of implicit and lost knowledge and enabling the exchange of semantic content.

For other authors, the main purpose of an ontology is to enable communication between computer systems, making it independent of the technologies of the individual systems, the information architectures and the application domain [3].

According to Guarino, the purpose of an ontology is the characterization of a conceptualization, with the aim of establishing a consensus about the knowledge described by that language [4]. In fact, the set of terms and definitions of an ontology are shared by all participants in the domain and, therefore, constitute a basis for communication about said domain.

However, an ontology must be understood as more than just an effective and efficient means of transmitting information. An ontology allows us to capture knowledge in a domain of interest, and although in its practical applications in engineering this has also involved data storage and maintenance. Ontologies are situated at a higher level than information systems, as they also allow reasoning based on the information they contain. Furthermore, this captured knowledge can be shared and reused for various purposes and applications related to its domain. Therefore, ontologies occupy an important place among modeling and representation techniques of knowledge.

Ontologies facilitate the representation of a body of knowledge in a formal and declarative manner, and constitute the foundation for building the bases of knowledge, representing the terminology specific to a domain and facilitating communication and the transmission of knowledge between heterogeneous agents in a knowledge-based system.

2.3 Types of ontologies and classification criteria

Based on the relationship between ontology and language, Fox and Gruninger proposed classifying ontologies into informal, semi-formal and formal, considering the degree of

precision with which both their syntax and semantics are established. In this context, natural language would be an example of an informal ontology, logical-mathematical languages would be formal ontologies and semi-informal ontologies would be found halfway between the two [5].

On the other hand, ontologies can be classified according to their degree of specificity [6]: upper ontologies, which define concepts applicable to most or all domains; core ontologies, which define concepts shared by several similar or related domains; domain ontologies, which contain concepts specific to a particular domain of interest; and application ontologies, which specialize the concepts of a domain ontology with application-specific variants (Figure 1).

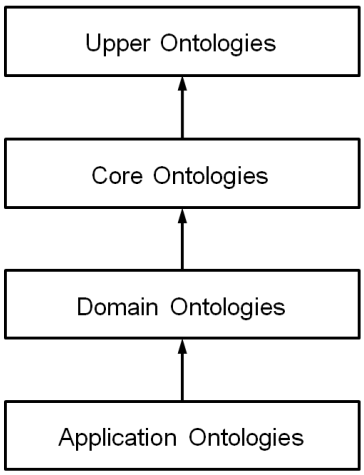

Figure 1. Types of ontologies according to the degree of specificity [6]

Taking this classification as a reference, high-level models can be obtained from the adaptation of a base ontology (upper ontology) that describes the basic concepts (foundational concepts), which are sufficiently general to be applied in a wide range of domains, and is designed so that it can be extended and meet the additional requirements introduced by a specific domain.

This aspect is fundamental when developing ontologies in engineering, because the use of different ontologies without a common basis necessarily leads to misunderstandings.

3. LANGUAGES AND TOOLS FOR THE IMPLEMENTATION OF ONTOLOGIES

This section addresses aspects related to the practical use of ontologies in engineering, from those linked to applications based on knowledge inference to those related to software tools for editing, presenting, and sharing ontologies.

3.1 Ontology editors. Protégé

There are several ontology development environments or ontology editors: OntoEdit, WebODE, Hozo, etc. Among them, Protégé stands out.

Protégé [7] offers significant features in the ontology utilization phase. Its features include: extensibility, which allows users to redefine representative primitives; a semi-automatic tool for merging and aligning ontology components; the ability to perform some tasks automatically and guide the user through the development of others; a customizable output file format capable of adapting to any formal language; a customizable user interface; and a powerful and sophisticated plug-in architecture capable of integration with other applications. Protégé, which uses, among others, the OWL and RDF syntaxes, allows the construction of domain ontologies, since, as can be seen in Figure 2, with this editor you can define classes, class hierarchies, properties, restrictions for the value of properties, relationships between classes and the properties of these relationships.

Protégé allows concepts to be described and also provides new facilities or services. It has a rich set of operators, for example, intersection, union, and negation. Since Protégé is based on a logical model that allows concepts to be defined and described, complex concepts can be built on the definitions of other simpler concepts. Furthermore, the logical model allows the use of a reasoner that can check whether all the ontology declarations and definitions are consistent with each other and can also recognize that concepts fit within each definition. The reasoner can therefore help maintain the hierarchy correctly. This is

particularly useful when dealing with cases where classes may have more than one superclass.

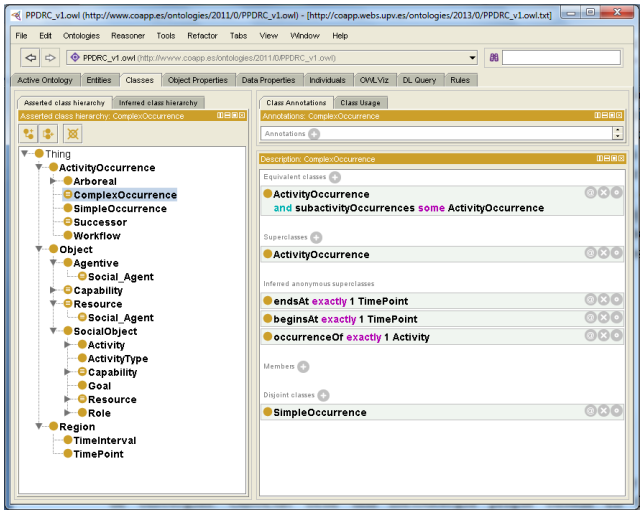

Figure 2. User interface of the Protégé ontology editor, with the PPDRC ontology class taxonomy and the defining axioms of the 'ComplexOccurrence' class, which constrain its semantics

3.2 Reasoners

In addition to a suitable user interface and mechanisms to facilitate and systematize communication between collaborators, the main aid for the design and maintenance of ontology provided by current tools is an interface with reasoning systems or reasoners, most of which are based on OWL DL. Reasoners support the testing layer of the Semantic Web and can return examples of objects that meet defined constraints or perform checks to determine the veracity of an assumption. The main function of reasoners is to classify ontology concepts by establishing subclass and superclass relationships and to detect logical errors that indicate modeling flaws. That is, the validation and analysis of ontology.

Among the reasoners that work with ontologies written in OWL DL are Racer and Fact++, which are, along with Pellet, the three most commonly used reasoners with OWL. As indicated above, they check the ontology to automatically compute the classification hierarchy and also to verify its logical consistency. The class hierarchy described in the ontology is called the *asserted hierarchy*, while the class hierarchy resulting from the reasoning process is called the *inferred hierarchy*. After the reasoner checks, it can be seen whether any class has been reclassified (i.e., if its superclass has changed) or if it is inconsistent.

4. UPPER ONTOLOGIES

Upper ontologies facilitate the integration of other, lower-level ontologies, as they allow for shared vocabulary to describe the semantics of ontological entities unambiguously and in a machine-processable manner. This is the case with DOLCE (Descriptive Ontology for Linguistic and Cognitive Engineering) and PSL (Process Specification Language).

4.1 DOLCE

The DOLCE ontology is intended to support the design of domain ontologies and has been successfully used in industrial and academic projects and in diverse domains such as law, biomedicine, and agriculture. As its name suggests, 'Descriptive Ontology for Linguistic and Cognitive Engineering,' DOLCE has a clear cognitive bias and aims to capture the ontological categories that underlie human natural language and common sense. DOLCE represents the world as it is perceived by humans rather than as it is seen from the perspective of scientific theories.

DOLCE is an ontology of *particulars* in the sense that its domain of discourse is restricted to *particulars*, or entities that cannot have instances. However, *universals*, or entities that can have instances, appear in an ontology of *particulars* such as DOLCE, to the extent that they are used to organize and characterize that ontology. In other words, when designing this ontology, the classes of its taxonomy and their predicates are established (predicates are the properties of the classes and the relationships between them), which are *universals*, while the use of the ontology is based on the instances of

these classes and predicates, which are *particulars*.

DOLCE's ontological classification of the world is extensive. DOLCE's four high-level categories are: *endurant*, *perdurant*, *quality*, and *abstract* (Figure 3). *Endurants* are particulars in space, which participate in at least one *perdurant*. *Endurants* are classified as physical versus non-physical, and agentive versus non-agentive. *Perdurants* are particulars in time, which have at least one participant. *Qualities* are particulars inherent in other *endurants* or *perdurants*. *Abstracts* are entities that do not extend in space or time, have no spatial or temporal quality, and are not qualities [8].

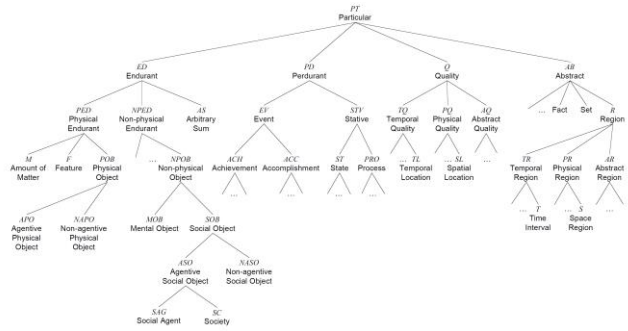

Figure 3. DOLCE Basic Categories Taxonomy [8]

4.2 PSL

PSL ontology was developed with the goal of creating a common process representation for all manufacturing applications, finding its most genuine scope in discrete manufacturing processes.

The PSL methodology is based on the identification of intuitions related to manufacturing processes, which are subsequently translated into elements of an algebraic or combinatorial mathematical structure, and finally formalized through definitions and axioms written in first-order logic that ensure rigorously developed semantics.

The PSL ontology consists of a series of interdependent modules built from a core that captures the high-level primitive concepts inherent to process specification. Each module refines this core by capturing sets of concepts specific to a specific area related to process specification [9], [10].

PSL is the result of a project initiated in 1995 by the National Institute for Standards and Technology (NIST) to create a neutral, standardized, high-level process specification language that would allow for the integration of multiple related process applications throughout the product lifecycle, such as CAD/CAPP/CAM/CNC. This requires identifying the semantic relationships between the terms in these manufacturing applications.

Regarding its consideration as an exchange language, Figure 4 illustrates the information translation mechanism, based on the semantics of PSL and the syntax of KIF (Knowledge Interchange Format).

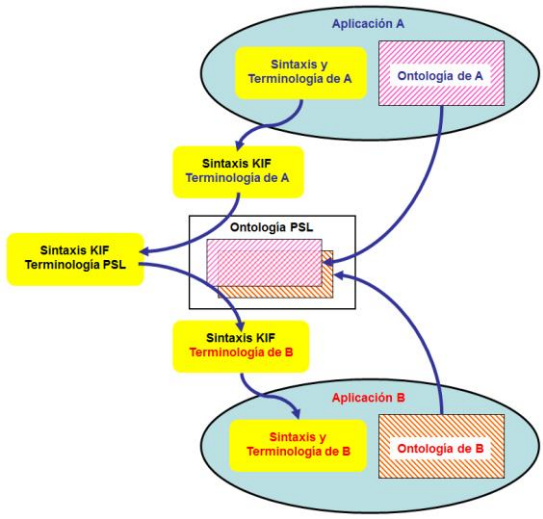

Figure 4. Using KIF syntax in the process of exchanging process information using the PSL ontology [11]

4.3 PSL-Core

The purpose of the PSL-Core is to transform into axioms a set of intuitive semantic primitives suitable for describing basic processes. These intuitive semantic primitives are: (a) there are four types of entities required for reasoning about processes: activities, activity occurrences, timepoints, and objects; (b) activities can have multiple realizations, and there may be activities that never occur; (c) points in time are ordered linearly, forward into the future and backward into the past; and (d) realizations and objects are associated with

unique points in time, which mark the start and end of the realization or object.

Despite the simplicity of PSL-Core, the set of its axioms written in the formal language of PSL provides a primitive semantics that is sufficient to describe the basic processes.

5. ONTOLOGIES IN THE MANUFACTURING DOMAIN

This section is dedicated to the PPDRC and MIRC ontologies, both focused on manufacturing process planning.

5.1 PPDRC ontology

PPDRC (Product and Processes Development Resource Capabilities) is an ontology for collaborative development of products and processes focused on resource capabilities [11].

The PPDRC ontology supports the planning of the integrated new product development process in collaborative environments deployed within the context of a virtual OKP (One-of-a-Kind Production) enterprise, where communication and cooperation between different actors is possible thanks to the high connectivity offered by Web technologies. In general terms, it can be stated that PPDRC supports the planning of any type of process, such as the manufacturing process of a product or a process. A schematic representation of the predicates of the PPDRC ontology can be seen in Figure 5.

In the case of process planning activities, the requirements outlined are particularly important, both due to their complexity, as they are subject to continuous feedback and adaptations, and due to the collaborative nature of the process and the agentic nature of the actors involved.

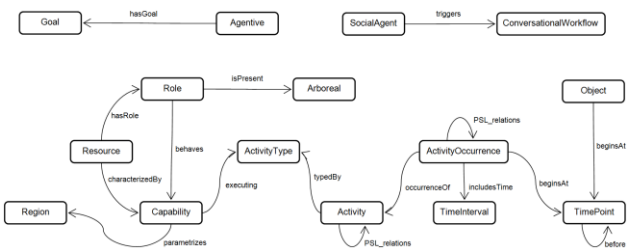

Figure 5. Predicates of the PPDRC ontology [11]

In the development of PPDRC, ontological concepts from other proposals specific to the process and resource domains are incorporated and integrated into the DOLCE+DnS Ultralite (DUL) base ontology. These include those from PSL and those from MANDATE. The use of the DUL ontology facilitates the semantic interoperability of PPDRC with ontologies from other domains.

5.2 MIRC ontology

MIRC (Manufacturing and Inspection Resource Capabilities) is an ontology for integrated machining and inspection process planning focusing on resource capabilities [11].

MIRC is a specialization of the PPDRC ontology (Figure 6). Therefore, it inherits from the latter the ability to support collaborative planning activities developed in the context of a virtual OKP and to represent the social and agentic nature of the required resources—in this case, machining and inspection equipment and tools. The specialization of PPDRC concepts provides the MIRC ontology with the semantic interoperability required for its integration with other ontologies in the manufacturing and product development domains.

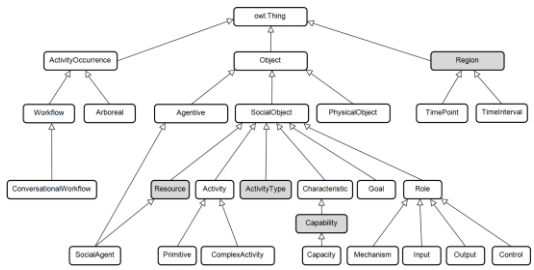

Figure 6. Basic entities of the MIRC ontology (Resource, ActivityType, Capability and Region) in the PPDRC ontology taxonomy [11]

The MIRC ontology represents both machining and inspection resources and their dimensional and geometric capabilities, as well as the activities involved in a machining and inspection plan for a part. This is because, to ensure that a part meets established quality requirements, expressed through the corresponding dimensional and geometric

requirements, it is not sufficient to assign resources compatible with the required performance level to each activity. This assignment must be made within the context of a plan, which establishes the structure (phase, subphase, and operation) and dependencies between these activities. The selection and allocation of these resources within a machining and inspection plan determines its efficiency, especially in distributed and collaborative environments, such as the integrated and collaborative product development process in a virtual OKP.

In the MIRC ontology, four entities of the PPDRC ontology are specialized: Resource, ActivityType, Capability and Region (Figures 6 and 7), which represent the essential concepts used in the definition of a process plan (resources and types of activities) and those that are necessary for the allocation of resources to activities in the creation and validation of the process plan (capabilities and their quantification).

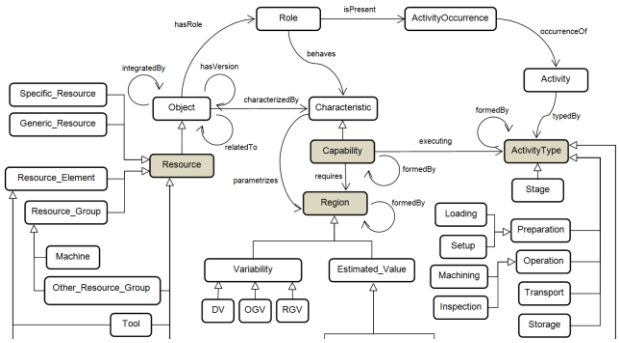

Figure 7. Predicates of the PPDRC ontology, and taxonomy of the entities Resource, Region and ActivityType in the MIRC ontology [11]

In the ontology, a resource is an object that can perform an activity by exhibiting active behavior. However, it can also exhibit passive behavior when, while involved in the activity, it is not responsible for its execution. Active behavior corresponds to a mechanism-type participation role in the activity, while input, output, and control roles correspond to passive behavior.

In the first of these behaviors (active), the resource transmits the values that quantify its capabilities to the characteristics of the resulting object. This transmission of characteristics in the execution of the activity materializes through an interface between the resource and the processed object, which introduces additional dispersion conditioned by the type of control under which the activity is executed. In the second behavior (passive), the resource is the object that receives the activity, as occurs in Preparation-type activities oriented toward resource configuration.

The MIRC ontology considers two types of activities: Operation activities and Preparation activities. The former include activities performed on the part to modify its characteristics, while the Preparation type includes activities performed on resources to modify their characteristics (Figure 8).

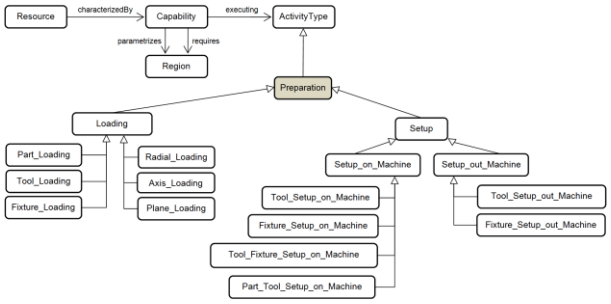

Figure 8. Preparation activities in the MIRC ontology [11]

On the other hand, resources are considered at different levels of aggregation and can be simple or complex (Figure 9). The latter are configured through Preparation activities, which modify their capacities. These capacities, for both simple and complex resources, also vary over time depending on the performance of their functions. In this sense, the preparation activities (loading and setup) of machining and inspection resources (Figure 8) are essential for determining the adequacy of the assigned resources according to technological criteria related to their dimensional and geometric capacities. Therefore, it can be stated that the MIRC ontology supports all the necessary knowledge for decision-making concerning the preparation and allocation of resources during the development of an integrated machining and inspection process plan, and is capable of

supporting the evaluation and validation of any plan.

For this evaluation and validation of the plan, a methodology is established that facilitates understanding of the conceptual framework of the MIRC ontology. This methodology is supported by graphical representations (Figure 9) that allow viewing both the plan as a whole, showing the sequence of processing activities and resource configuration, and the details of each of its component stages. Furthermore, the detailed graphical representations show the type and quantification of the characteristics associated with the resources and objects involved in the execution of the activities. Specifically, these graphs serve to show the effect of resource capabilities and activity execution (interface) on the characteristics of the resulting objects or resources.

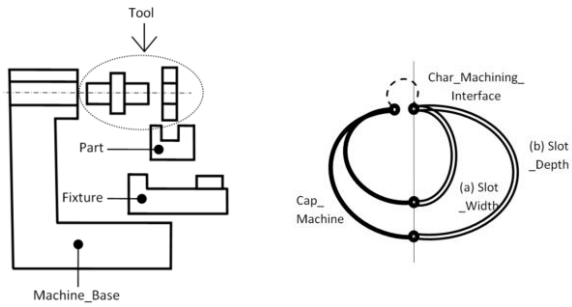

Figure 9. Physical representation of the resource participating in the machining of the slot (left) and graph with the characteristics of the machined slot (right) [11]

6. CONCLUSION

The PPDRC ontology provides an efficient response to the needs arising from product development in distributed and collaborative environments.

The MIRC ontology, which is a specialization of PPDR, supports the planning of machining and inspection processes in the field of integrated and collaborative product, process, and resource development.

Both ontologies, PPDRC and MIRC, have been built from upper ontologies (DOLCE and PSL), taking advantage of its semantic richness and bringing together concepts from these and other non-ontological initiatives. Among them, the consideration of the social nature inherent to the DOLCE ontology, the treatment of resources and roles derived from the MANDATE initiative, and the description of activities and process plans derived from the PSL ontology stand out.

REFERENCES

[1] Gruber, T. R. 1993. “A Translation Approach to Portable Ontologies.” Knowledge Acquisition 5 (2): 199–220.

[2] Uschold, M. y M. Gruninger. 1996. “Ontologies: Principles, Methods y Applications.” Knowledge Engineering Review 11 (2): 93–136.

[3] Deshayes, L. M., O. El Beqqali y A. Bouras. 2005. “The Use of Process Specification Language for Cutting Processes.” International Journal of Product Development 2 (3): 236–253.

[4] Guarino, N. 1997. “Understanding, Building and Using Ontologies.” International Journal of Human-Computer Studies 46 (2–3): 293–301.

[5] Fox, M. S. y M. Gruninger. 1998. “Enterprise modeling.” AI Magazine 19 (3): 109–121

[6] Bräuer, M. 2007. “Design of a Semantic Connector Model for Composition of Metamodels in the Context of Software Variability.” PhD diss., Technische Universität Dresden.

[7] Musen, M. A., R. W. Fergerson, W. E. Grosso, M. Crubezy, H. Eriksson, N. F. Noy y S. W. Tu. 2003. “The Evolution of Protégé: An Environment for Knowledge-Based Systems Development.” International Journal of Human-Computer Interaction 58 (1): 89–123.

[8] Masolo, C., S. Borgo, A. Gangemi, N. Guarino y A. Oltramari. 2003. WonderWeb Deliverable D18. Ontology Library (final). Laboratory for Applied Ontology ISTC CNR.

[9] Bock, C. y M. Gruninger. 2005. “PSL: A Semantic Domain for Flow Models.” Journal of Software and Systems Modeling 4 (2): 209–231. doi: 10.1007/s10270-004-0066-x.

[10] PSL. 2010. National Institute of Standards and Technology. Consultada en Diciembre.

[11] Solano García, L. 2015. “Definition of an

integrated ontology of processes and resources for the collaborative development of process plans." PhD diss., Universitat Politècnica de València.

Society of Production Engineering

ICPES 2025

40th INTERNATIONAL CONFERENCE ON PRODUCTION ENGINEERING - SERBIA 2025

DOI: 10.46793/ICPES25.018P

University of Nis Faculty of Mechanical Engineering

Nis, Serbia, 18 - 19th September 2025

FROM PRACTICAL INSIGHTS TO FUTURE INNOVATIONS IN ADDITIVE MANUFACTURING FOR MEDICAL APPLICATIONS

Răzvan PĂCURAR[1,*]
Orcid: 0000-0002-0554-6120
[1]Technical University of Cluj-Napoca, Romania
*Corresponding author: razvan.pacurar@tcm.utcluj.ro

Abstract: *Additive Manufacturing (AM) has transformed the medical domain by enabling the creation of patient-specific implants, prosthetics, surgical tools and bioprinted scaffolds. This paper critically reviews the main AM technologies applied in medicine, highlighting their advantages, limitations and future development needs. Material extrusion, photopolymerization, powder bed fusion and bioprinting methods are discussed with emphasis on their applicability in producing medical applications. Special attention is given to issues such as biocompatibility, sterilization, regulatory frameworks and mechanical reliability. Based on the realized analysis opportunities for design improvements, material innovation and technological optimization are emphasized. Looking ahead, emerging approaches such as 4D printing, multi-material systems, AI-driven design and advanced bioprinting are explored as potential solutions that are considered as reliable alternatives to address the current limitations of AM technological solutions that are used for medical applications. This paper emphasizes therefore the ongoing need for innovation to meet evolving medical requirements and ensure safe, sustainable and personalized healthcare solutions.*

Keywords: *Additive manufacturing, biomedical engineering, medical applications, innovations, future trends*

1. INTRODUCTION

Additive Manufacturing (AM), commonly known as 3D printing enables the fabrication of complex medical applications with a level of customization such as cranial implants, dental restorations, prosthetics, surgical guides, and tissue engineering scaffolds with one design freedom that is hard to be reached by conventional methods [1]. In recent years, the integration of digital imaging, computer-aided design and advanced simulation tools has further enhanced the ability to create patient-specific devices that match anatomical and functional requirements [2]. AM's unique capacity to produce porous and patient-specific structures allows for improved osseointegration, comfort and surgical outcomes [3]. Despite its growing success, AM technologies face significant limitations regarding material biocompatibility, mechanical performance, regulatory approval and scalability. This paper aims to provide one synthetic presentation of current AM technologies that are used for medical applications, in order to identify limitations while proposing directions for future innovations aligned with the medical needs.

2. ADDITIVE MANUFACTURING SOLUTIONS FOR MEDICAL APPLICATIONS

2.1 Material Extrusion Technologies

Material extrusion (MEX) includes Fused Deposition Modeling (FDM), Fused Filament Fabrication (FFF) and Metal Extrusion (ME). These are among the most widely used AM processes due to their accessibility. Applications range from anatomical models and orthoses made of PLA, ABS or TPU to high-performance implants produced from PEEK or PEKK material. Metal Extrusion further extends the possibilities of this approach to titanium and stainless-steel components, which are consolidated after debinding and sintering. The main advantages of material extrusion technologies lie in their relatively low cost, the wide range of available materials and the ease capacity to produce patient-specific prototypes. However, these processes are not free of drawbacks. Components often display anisotropic mechanical behavior, a rough surface finish and limited options for sterilization, while their mechanical strength is generally inferior to that of parts obtained through powder bed fusion methods [4]. To overcome these limitations, improvements are needed in several directions. Stronger composites and improved interlayer adhesion could enhance performance, while hybrid reinforcement strategies and validated medical-grade extrusion systems are essential for meeting the strict requirements of biomedical applications.

2.2 Photopolymerization Technologies

Photopolymerization processes include Stereolithography (SLA), Digital Light Processing (DLP), PolyJet and Carbon Digital Light Synthesis (DLS). These methods are widely used in the medical field for the production of surgical guides, dental devices, prosthetics and highly accurate anatomical models. The strengths of photopolymerization technologies lie in their high precision, smooth surface finish, the ability to fabricate highly complex geometries and, in the case of PolyJet, the capability to print with multiple materials simultaneously. Despite these advantages, several limitations persist. The resins used are often brittle, they have restricted long-term biocompatibility and the materials and equipment tend to be costly. Moreover, extensive post-processing steps such as washing and curing add both time and complexity to the workflow [5]. Addressing these challenges requires the development of stronger and more durable biocompatible resins, scalable and efficient post-processing methods, and materials with improved resistance to degradation in biological environments.

2.3 Powder Bed Fusion Technologies

Powder Bed Fusion (PBF) comprises several technologies, including Selective Laser Sintering (SLS), Selective Laser Melting (SLM), Electron Beam Melting (EBM), Binder Jetting and Multi Jet Fusion (MJF). Among additive manufacturing processes, PBF has established itself as one of the standard alternative for producing metallic implants, particularly those made from titanium and cobalt-chrome alloys, which are widely used in orthopedic and dental applications. The major advantages of PBF lie in its ability to deliver high mechanical strength and to design porous structures that promote osseointegration, thereby improving the long-term stability and functionality of implants. These characteristics contribute significantly to the reliability and longevity of medical devices manufactured with this technology. However, PBF also presents important drawbacks. The equipment and raw materials are costly, powder recycling remains a challenge and the process is exposed to the development of residual stresses that may compromise mechanical characteristics of realized parts [6]. Furthermore, extensive post-processing steps, such as support removal and surface finishing are often required to achieve clinically acceptable results. Future improvements should therefore focus on the establishment of standardized powder reuse protocols, the

development of advanced finishing techniques, methods to reduce residual stresses and simulation tools that enable optimized process control for medical applications.

2.4 Bioprinting Technologies

Bioprinting extends additive manufacturing into the field of regenerative medicine by using bioinks composed of living cells, hydrogels and growth factors. Several approaches exist, including extrusion-based bioprinting, inkjet printing, photopolymerization techniques and laser-assisted methods. More recently, 4D printing has emerged as a promising frontier, introducing constructs that can adapt their shape or function over time in response to environmental stimuli. The advantages of bioprinting are particularly significant in the biomedical context. It enables the fabrication of tissue scaffolds and organ-like constructs, provides patient-specific regenerative solutions and allows for the deposition of multiple materials in a single structure. Nevertheless, the technology still faces important challenges. Bioinks typically lack sufficient mechanical strength, scalability remains limited and maintaining high levels of cell viability throughout the printing process is difficult [7]. Moreover, standardized protocols for clinical translation are still lacking. To move forward, research and development must focus on creating robust bioinks with customizable properties, developing reliable vascularization techniques and implementing real-time monitoring systems. The integration of bioreactors for tissue maturation is also crucial to bridge the gap between laboratory research and clinical application.

3. FUTURE DIRECTIONS IN ADDITIVE MANUFACTURING FOR MEDICAL APPLICATIONS

3.1 Design Innovations using Artificial Intelligence

Future progress in biomedical additive manufacturing will be closely tied to advances in digital design methods. The use of generative design, topology optimization and patient-specific modeling is already redefining the way implants and scaffolds are conceived [8]. Artificial Intelligence (AI) is expected to play a key role by enabling predictive models for defect detection, automated optimization of process parameters and rapid customization of devices based on patient data. Coupled with digital twins and simulation tools, AI-driven design will allow for virtual validation of implants before fabrication, significantly reducing trial-and-error approaches and accelerating clinical translation [9]. The key challenge in this area is integrating medical imaging data, computational design and process control into a seamless workflow that meets regulatory standards.

3.2 Development of Advanced Materials

Another major direction for innovation lies in the development of new customized materials which are adapted to medical needs. Multi-material printing is gaining importance, as it allows the combination of rigid structural materials with flexible or bioactive ones in a single construct. Smart and intelligent materials, such as shape-memory polymers or stimuli-responsive hydrogels are being investigated for their potential to adapt to physiological conditions and improve patient outcomes [10]. In the field of bioprinting, research is focused on bioinks that combine mechanical strength with high cell viability, as well as functional additives like nanoparticles or growth factors [11]. Despite these promising directions, challenges remain in ensuring long-term stability, biocompatibility and regulatory approval of novel materials. Standardization and scalability will be critical for widespread adoption in clinical practice.

3.3 Emerging Technological Variants

Beyond materials and design, new technological variants are reshaping the future of biomedical AM. Hybrid manufacturing systems, which integrate additive processes with subtractive machining, coating, or surface treatments offer a pathway to improve surface

quality and functional performance. 4D printing, which incorporates time-dependent transformations into printed structures, holds promise for developing adaptive implants and scaffolds that respond dynamically to changes in the biological environment. In bioprinting, progress is moving toward the fabrication of vascularized tissues, organoids and functional organ models through the integration of microfluidics and bioreactors [12]. However, scaling these approaches from laboratory demonstrations to clinically relevant applications remains a formidable challenge and leaves lot of open rooms for innovations. On-going research will have to address reproducibility, cost-efficiency and the integration of these technologies into existing medical workflows in the future.

4. CONCLUSION

Additive Manufacturing has already reshaped biomedical engineering by enabling customized, patient-specific solutions. Each technology provides unique opportunities but also faces significant limitations. Improvements in design, materials and process control are crucial to unlock the full potential of AM technologies. Emerging innovations such as multi-material and 4D printing, combined with AI-driven optimization, will push the boundaries of personalized medicine and regenerative healthcare in the future. Collaboration between engineers, material scientists and clinicians remains essential to align technological progress with clinical needs in this context.

ACKNOWLEDGEMENT

This research was supported by the ERASMUS+ Partnerships for cooperation and exchanges of practices (KA220) - “Biomedical Innovations through Digital Transformation of Additive Technologies and Knowledge Exchange - BIOMEDIX” — Project No. 2024-1-LV01-KA220-HED-000255929.

REFERENCES

[1] M. Salmi: AM Processes in Medical Applications, Materials, Vol. 14, 191, 2021.

[2] F.J. Birbe: Advances in 3D-Printed Implants for Facial Plastic Surgery, Surgical Techniques Development, Vol. 14, 22, 2025.

[3] E. Khorasani, B. Vahidi: 3D-Printed Scaffolds for Cranial Bone Regeneration: A Systematic Review of Design, Materials & Computational Optimization, Biotechnology &Bioengineering, Vol. 122, No. 8, pp. 1982–2008, 2025

[4] Debreceni, A., Z. Buri, S. Bodzás: Linking Process Parameters, Structure & Properties in Material Extrusion AM of Polymers & Composites: A Review, Journal of Manufacturing & Materials Processing, Vol. 9, Art. 286, 2025.

[5] Y. Hu,X. Wang: Trends in Photopolymerization 3D Printing for Advanced Biomedical Applications: Biocompatible Resins & Process Optimization, Biomacromolecules, Vol. 25, pp. 1023–1045, 2024.

[6] N.D. Dejene, H.G. Lemu: Current Status and Challenges of Powder Bed Fusion-Based Metal Additive Manufacturing: Literature Review. Metals, Vol. 13, 424, 2023.

[7] J. Halper: Narrative Review & Guide: State of the Art & Emerging Opportunities of Bioprinting in Tissue Regeneration & Medical Instrumentation,Bioengineering,Vol. 12, 2025.

[8] P. Koul: A Review of Generative Design Using Machine Learning for Additive Manufacturing, Advances in Mechanical and Materials Engineering, Vol. 41, pp. 145–159, 2024.

[9] M.S. Ahmmed, L. Khan, L., M.A. Mahmood, F. Liou: Digital Twins, AI & Cybersecurity in AM: A Comprehensive Review of Current Trends & Challenges. Machines, Vol. 13, 691, 2025.

[10] G. A. Appuhamillage, S. S. Ambagaspitiya, R. S. Dassanayake, A. Wijenayake: 3D and 4D Printing of Biomedical Materials: Current Trends, Challenges, and Prospects, Exploration Engineering Journal, Vol. 5, pp. 17–47, 2024.

[11] T. M. Castiblanco, J. P. M. Marín, M. Osorio: Natural Macromolecule-Based Bioinks for 3D Bioprinting: A Systematic Review, Biofabrication, Vol. 48, e00407, 2025.

[12] R. Kumar, H. Mehdi, S. S. Bhati, M. Arunkumar, S. Mishra, M. K. Lohumi: A Comprehensive Review of Advancements in Additive Manufacturing for Biomedical Components, Discover Materials, Vol. 5, 152, 2025.

Society of Production Engineering

ICPES 2025

40th INTERNATIONAL CONFERENCE ON PRODUCTION ENGINEERING - SERBIA 2025

DOI: 10.46793/ICPES25.023PF

University of Nis
Faculty of Mechanical Engineering

Nis, Serbia, 18 - 19th September 2025

DIGITALISATION AND SENSING IN ADDITIVE MANUFACTURING: DATA COLLECTION FOR PRODUCT(ION) OPTIMISATION

Vojislav PETROVIĆ-FILIPOVIĆ[1*]
Orcid: 0000-0003-0238-7934
[1]Fachhochschule Wiener Neustadt, Austria
*Corresponding author: vojislav.petrovic@fhwn.ac.at

Abstract: *Additive Manufacturing (AM) has evolved into a robust industrial production technology, but its inherent process complexity poses significant challenges to ensuring consistent part quality and repeatability. Traditional quality control methods often take place in the post-process phase, being time-consuming and costly. This paper argues that the future of AM lies in the adoption of real-time, in-situ monitoring and closed-loop control systems and offers several examples to fundament this claim. The AM systems leverage a network of sensors to collect vast amounts of data during the build process, enabling immediate analysis and corrective measures to prevent defect propagation. The methodology of this data-driven approach is explored, distinguishing between different in-situ monitoring solutions (optical, acoustic, and infrared sensors) and their practical implementation. A robust data management pipeline, incorporating advanced data reduction and AI/ML models, is essential to make this approach viable. The paper is discussed through four key research projects—CUSTODIAN, QuaL-DED, WAVETAILOR, and crystAIr—to illustrate these concepts in practice. These projects collectively demonstrate the importance of sensor fusion, AI-driven models and digital twins in establishing a self-optimising ecosystem that can significantly reduce scrap, accelerate development, and pave the way for a zero-defect manufacturing paradigm in AM. The conclusion is that digitalisation in AM is a critical shift that will secure the technology's future in advanced industrial production.*

Keywords: *additive manufacturing, digital technologies, monitoring, sensors*

1. INTRODUCTION

Additive Manufacturing (AM), commonly known as 3D printing, has transitioned from a rapid prototyping technology to an established industrial production method, covering the applications that conventional processes cannot attend. This shift is particularly evident in processes like Laser Powder Bed Fusion (L-PBF) and Laser Directed Energy Deposition (L-DED), which together accounted for a significant portion of the global AM market in 2025, that is 74% of all installed systems [1].

The increasing adoption of AM in critical sectors, such as aerospace, medical devices, and energy, highlights the need for robust quality assurance and process control [2]. However, the complexity of AM processes, which involve numerous interdependent parameters like laser power, scan speed, powder flow, and temperature, makes it

challenging to ensure part quality and repeatability [3, 4].

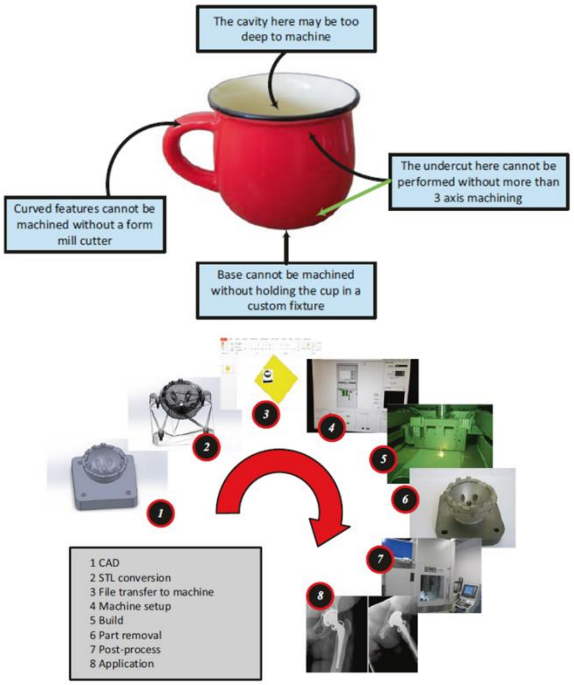

Figure 1. The niche of AM technologies [2] and the AM production steps [3]

The fundamental challenge in AM is the link between process variables, part quality, and machine health. Traditional quality control methods, such as post-process inspection using Computed Tomography (CT) or metallography, are time-consuming and costly, making them unsuitable for large-scale production. This has driven the industry towards real-time, in-situ monitoring and closed-loop control systems. These systems rely on a network of sensors to collect vast amounts of data during the build process, enabling instantaneous analysis and decision-making. Real-time monitoring can detect critical errors and stop the process, thereby preventing further defects from propagating. Alternatively, by non-critical errors, it can register an alert and notify the end user that an error has occurred at a specific location. The ideal scenario, as illustrated in a simplified closed-loop model (**Figure 2**), involves sensors providing real-time feedback to a data processing unit, which in turn can implement corrective measures on the AM machine to prevent defect propagation and ensure the production of zero-defect components.

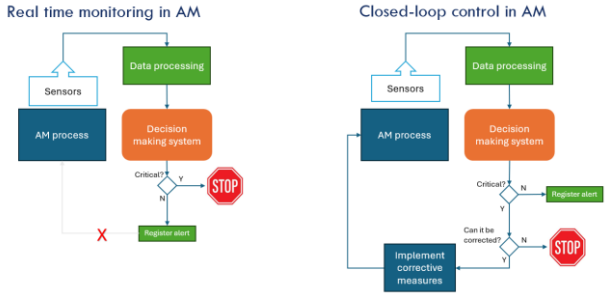

Figure 2. Schematic view and comparison of real-time monitoring and closed-loop control in AM.

The present paper outlines a data-driven approach to enhance AM process control. It details the methodologies for data collection and analysis and presents a discussion of four key research projects that demonstrate the application of these concepts in real-world scenarios.

2. METHODOLOGY

Effective data collection in AM is a multi-faceted process that can be broadly categorized into two main types of monitoring: *in-situ* and *ex-situ*. Ex-situ monitoring concepts, such as Computerized Tomography (CT), metallography, surface profilometry are limited, given that they offer an analysis when the possibility of intervention during the process is already gone. In-situ Monitoring, on the other hand, involves collecting data *during* the AM process itself and, as such, allows for a swift intervention when the process gets affected by an event. The goal is to capture transient process events and material behavior in real time. Common sensors used for in-situ monitoring include:

- Optical sensors: High-speed cameras and pyrometers are used to capture images of the melt pool, spatter, and thermal behavior. This data can reveal inconsistencies in melting, potential defects, and temperature gradients [6,11].
- Acoustic sensors: Microphones or acoustic emission sensors can detect sound waves generated by the process, such as spatter or

keyhole formation, which are often correlated with defect formation [7].

- Infrared sensors: Thermal cameras and photodiodes measure temperature distribution on the powder bed and within the melt pool, providing crucial feedback on energy input and heat dissipation [8].
- Piezoelectric sensors: Generation of impulse or signal by the collision between raw material and piezo crystal can also be successfully used for monitoring in AM [10]

The successful implementation of a data-driven approach requires robust data collection, processing and management. Raw sensor data, often in the form of high-resolution images or high-frequency signals, can be enormous. Advanced data reduction and processing techniques are useful to extract meaningful information without losing critical detail. This data is used for direct process evaluation in Real-Time, but also to train Machine Learning (ML) and Artificial Intelligence (AI) models to correlate process parameters and quality metrics. These models perform tasks such as defect prediction, process anomaly classification, and predictive maintenance [9]. The goal is to move from a *reactive* quality control paradigm to a *proactive* one, where the process is dynamically adjusted to prevent defects before they occur.

3. RESULTS & DISCUSSION

The concepts of digitalization, sensing, and data-driven process control have been demonstrated in several key research projects, which are discussed in the following section, highlighting their unique contributions to the field of AM monitoring.

3.1. Project CUSTODIAN: Real-Time Laser-Matter Interaction Monitoring

The CUSTODIAN project [12] is an example of an advanced laser-matter interaction. Its objectives were to study the role of laser beam shaping in L-PBF. The project's focus, among other challenges, was to develop advanced sensing techniques to monitor the melt pool dynamics and the flow of material and energy during laser-based AM. The project leverages an MWIR camera based on an uncooled PbSe sensor to collect data on the melt pool geometry, temperature, and spectral emission. The data is then analyzed in real-time to identify anomalies (size, shape, etc.) that could lead to porosity or improper fusion. These sensory inputs are then linked with the final mechanical properties of the part, aiming at a data-driven feedback loop that ensures part quality without extensive post-process inspection. Additional to monitoring, a closed-loop control of the laser source was established, trying to control the melt pool properties by changing the laser power in RT. Although in the case of L-DED process this has worked correctly [13], in case of L-PBF the high process speed was a relevant obstacle.

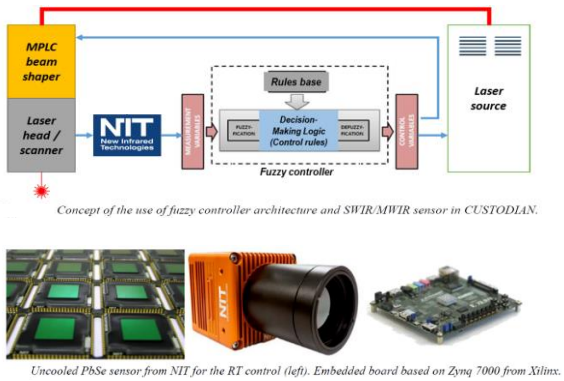

Figure 3. Concept of the use of fuzzy controller architecture and MWIR sensor in CUSTODIAN (up). Uncooled PbSe sensor by NIT Europe for the RT control, together with the embedded board based on Zynq 7000 from Xilinx. © 2018 CUSTODIAN Consortium. All rights reserved.

3.2. Project QuaL-DED: Towards Zero-Defect Components

The QuaL-DED project [14], aimed to develop a full Quality Assessment (QA) system for the L-DED process. The project's central objective was to ensure process stability and pave the way for manufacturing zero-defect

metallic components. The system integrated three key concepts:

- Beam Quality Monitoring: Constant real-time monitoring of the laser beam's quality and stability using MWIR camera approach.
- Energy Input Control: A monitoring system for both the melt pool and powder flux. The novelty was the combined monitoring of the energy-per-mass input, measuring the powder flux by laser scattering principle and the melt pool aspect by the MWIR images reconstructed in 3D.
- Inline Quality Monitoring: A special novelty was the use of Laser-Induced Breakdown spectroscopy to monitor the composition of the consolidated material as it is being built layer-by-layer, being this performed in near real time.

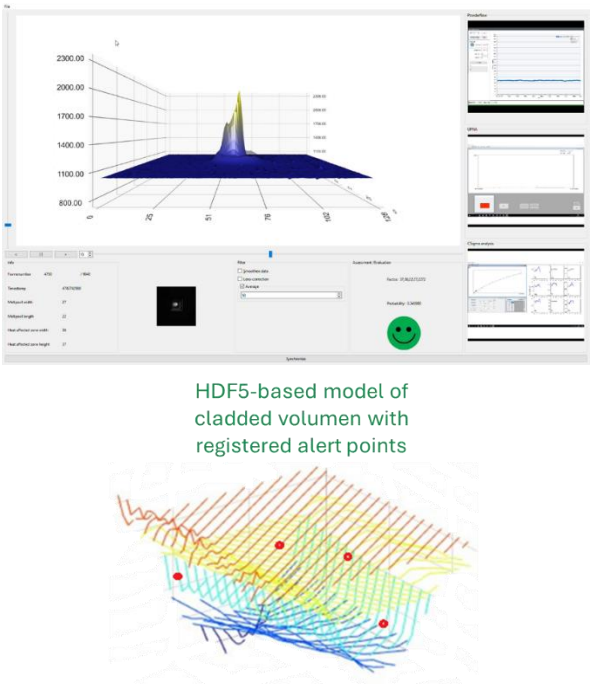

Figure 4. A 3D reconstruction of the melt pool, shown together with the powder flow values and momentaneous values of main chemical constituents in the recently deposited material. © 2023 QuaL-DED Consortium. All rights reserved.

This approach, which leverages big data analytics and machine learning to analyze process parameters and sensor data, has two aims. The first one is to record all events, that is, mismatches in the process parameters, in an HDF5 data structure, and to enable the L-DED technician to analyze what went wrong after the job, helping also the certification of the part. Another goal was to identify behavioral patterns for process optimization and analyze the influence of component design on process stability.

3.3. Project WAVETAILOR: Digital Twins and Sensor Fusion

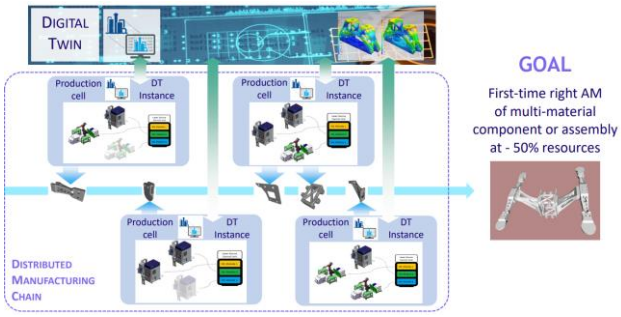

Figure 5. A schematic view of a digital twin concept operating over a delocalized LBAM facility. © 2023 WAVETAILOR Consortium. All rights reserved.

WAVETAILOR is another pioneering project about digitalization in AM, specifically in L-PBF and L-DED [15]. This ongoing project's key innovation is the use of a robust Digital Twin, a virtual replica of the manufacturing process that allows for real-time simulation and optimization. By integrating multi-scale models with machine learning algorithms, the digital twin can accurately predict outcomes and optimise component designs, thereby reducing the reliance on a trial-and-error approach.

The core component of WAVETAILOR is sensor signal fusion. The idea is to combine data from multiple disparate sensors to enhance the AI/ML algorithms, leading to more precise process parameter optimization with two main outcomes: less deformation in L-PBF parts and better assembly of L-PBF parts which have been manufactured in different machines at different locations (delocalized manufacturing). This approach is instrumental in ensuring a substantial reduction in scrap, by as much as 80%. WAVETAILOR's application of

Digital Twin technology and sensor fusion represents a significant step towards creating more reliable AM processes.

3.4. Project crystAIr: Sensing in Related Fields

While not directly referring to monitoring and control of AM production, crystAIr demonstrates the application of AI and sensing in a related high-tech field: *combustion burners made by L-PBF*. The project is focused on developing an AI- and sensing-driven combustion burner to address the challenges of hydrogen combustion, such as increased temperatures and faster combustion, which can lead to dangerous flashbacks. The methodology is based on a generic, data-driven three-step process: unsupervised learning of the intended combustion state, classification of different combustion states, and detection of early indicators of irregularities which could lead to a flashback. This is achieved through a distributed network of sensors, including a Piezoelectric crystal sensor with a sensitivity of 18.5 pC/bar and capable of operating up to 600°C [17].

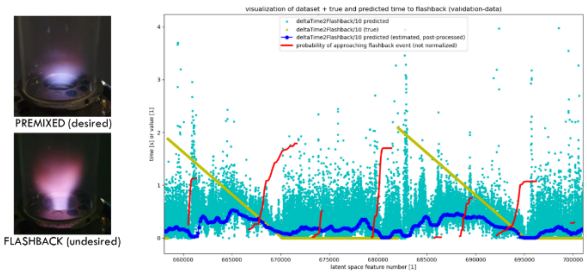

Figure 6. Hydrogen combustor in premixed and flashback mode (left). Prediction of flashback using data from a sensorized combustion burner (right) [16]. © 2024 crystAIr Consortium. All rights reserved.

The project's approach of creating a hybrid digital twin for unsupervised mixture and flame control provides a valuable blueprint for AM. The integration of sensors, AI, and digital twin technology to monitor a dynamic, high-temperature process for early anomaly detection is a directly transferable concept to the AM environment, particularly in L-PBF and L-DED, where process stability is paramount.

4. CONCLUSION

The transition of Additive Manufacturing into an established industrial technology hinges on the ability to ensure consistent quality and process reliability. Real-time monitoring and data collection are not merely beneficial but are essential for the future of AM. The move from post-process inspection to in-situ, closed-loop control is a critical paradigm shift that enables the production of complex, high-performance parts with a high degree of confidence. Monitoring in even not so mature AM technologies is a reality, which is shown through the projects discussed in this paper provide compelling examples realized. However, the closed loop control remains a complex challenge, mostly because of process speed (e.g. L-PBF).

The examples shown collectively demonstrate that by leveraging sensor technology, Big Data analytics, Artificial Intelligence, and Digital Twins, it becomes possible to achieve unparalleled levels of production control. The conclusions drawn from these projects in terms of monitoring are clear:

1. Combining data from multiple sensor types provides a more comprehensive picture of the process than any single sensor could offer, hence, the sensor fusion is key.
2. Machine learning and AI are indispensable for making sense of the large and complex datasets generated by AM processes. They enable the detection of subtle anomalies and the prediction of potential defects, at the production and part-in-service level.
3. The use of Digital Twins creates a virtual environment and a meeting point for process monitoring data, drastically reducing trial-and-error and improving efficiency.
4. Although the ultimate goal remains to establish a closed-loop control system that can automatically adjust process parameters in real-time, moving AM closer

to a zero-defect manufacturing paradigm, the path is complex due to significant process speed.

ACKNOWLEDGMENT

The presented projects have been funded in the framework of the H2020 (CUSTODIAN, Grant Nr. 825103), Horizon Europe (WAVETAILOR, Grant Nr. 101137974) and the Austrian Research Funding Agency (QuaL-DED and crystAIr).

REFERENCES

[1] Market Growth Reports, Laser Market Size & Growth, and Industry Analysis, Aug 2025.
[2] Gibson, I. Additive Manufacturing Technologies, Springer, 2014.
[3] Vincent, J., et al. 3D Printing in Orthopedics: A Review of the Current State and Future Perspectives, Journal of Orthopaedic Case Reports, 2018.
[4] FormNext Trends, FormNext, 2025.
[6] Grasso, M., et al. Laser Powder Bed Fusion Process Monitoring: A Review on Sensors and Systems, Journal of Manufacturing Science and Engineering, 2021.
[7] Shevchik, S. A., et al. Acoustic emission for process monitoring of additive manufacturing, Additive Manufacturing, 2019.
[8] Tapia, G., et al. In-Situ Monitoring of Laser-Based Additive Manufacturing, Journal of Advanced Manufacturing Technology, 2019.
[9] Lidong L, Alexander C.A., Additive Manufacturing and Big Data. December 2016. International Journal of Mathematical Engineering and Management Sciences 1(3):107-121
[10] Petrovic-Filipovic V. et al. Monitoring concept for powder flow monitoring in Laser-Directed Energy Deposition (L-DED) process based on flexible piezoelectric sensors, Materials Open Research, 2022
[11] Montero et al. Inspection of Powder Flow During LMD Deposition by High-Speed Imaging. December 2016. Physics Procedia 83:1319-1328
[12]. CUSTODIAN project official webpage: www.shapeyourlaser.eu
[13] Pallas A et al. A convolutional approach to quality monitoring for laser manufacturing. Journal of Intelligent Manufacturing 31 (3-4). 2020
[14] QuaL-DED Projekt, Project Database: https://projekte.ffg.at/projekt/3701237
[15] WAVETAILOR official project webpage: http://wavetailor.eu
[16] Giuliani F, Petrovic-Filipovic V. et al. Combining Machine Learning, Embedded Sensor Networks and Additive Burner Design for Combustor Structural Health Monitoring. Journal of Engineering for Gas Turbines and Power, Vol 147 (3). 2025
[17] High Temperature Pressure Sensor CP5X, Datasheet: https://www.piezocryst.com/en/product/CP5x1

Session 1:

Material removal and nonconventional technologies

Society of Production Engineering

ICPES 2025

40th INTERNATIONAL CONFERENCE ON PRODUCTION ENGINEERING - SERBIA 2025

DOI: 10.46793/ICPES25.030N

University of Nis Faculty of Mechanical Engineering

Nis, Serbia, 18 - 19th September 2025

AI-BASED PREDICTION OF KERF WIDTH AND SURFACE ROUGHNESS IN CO_2 LASER CUTTING OF STAINLESS STEEL

A. Nagadeepan[1], C.S. Tamil Selvan [2], S. Viswanathan[3], B.Vishnu[4], V. Senthilkumar [5]
Orcid: 0000-0002-7442-2658; **…; Orcid:** 0000-0003-1673-3180
[1]SRM TRP Engineering College, Trichy, Tamilnadu, India – 621105
*Corresponding author: nagadeepan.a@gmail.com

Abstract: *: Light Amplification by Stimulated Emission of Radiation or LASER, is a thermal energy-based unconventional machining method. CO_2 laser cutting of AISI 314 Stainless steel is carried out to evaluate the variation of kerf width in the cut section. Back-propagation Artificial Neural Networks are used to analyse and predict the kerf width during CO_2 laser cutting. In this study, input parameters considered were cutting speed, power, stand off distance and gas pressure. For experimental database of artificial neural network L_{16} taguchi orthogonal array with four levels for each input parameter was proposed. Among the 16 datasets, 12 datasets were used for training the network and the remaining 4 datasets were used for testing the network. The results of predicted roughness and kerf width by back propagation neural network were compared with experimental data and the average predicting error on training datas was 0.37% and the average predicting error on testing datas was 4.34%, which confirms that the predicted ANN model might be utilised to study the impact of CO_2 laser cutting settings on kerf width.*

Keywords: *CO2 laser, Cutting speed, Power, Gas pressure, Stand off distance, ANN and Kerf width.*

1. INTRODUCTION

Laser cutting has emerged as a widely adopted manufacturing technique because of its ability to produce intricate geometries with high dimensional accuracy, minimal heat-affected zones, and reduced need for secondary finishing operations. It is extensively applied in industries such as shipbuilding, automotive, aerospace, and medical devices, where both efficiency and cut quality are critical.

Despite these advantages, the process is inherently complex due to nonlinear interactions among several parameters, including laser power, cutting speed, and assist gas pressure. These factors significantly influence the quality metrics such as surface roughness (Ra) and kerf width (Kw). Achieving an optimal balance between these responses is challenging

since improvements in one often lead to trade-offs in another.

Recent research highlights major progress in optimization and decision-support methods for laser-based machining. Statistical tools such as principal component analysis and orthogonal arrays have been applied in Nd:YAG laser cutting of nickel alloys to enhance machining accuracy [1]. Studies on fiber and CO_2 lasers reveal strong parameter sensitivity and its impact on stainless-steel cut quality [2]. Multi-criteria decision-making (MCDM) frameworks, such as AHP-MARCOS and fuzzy AHP, are increasingly being employed for tool selection, process planning, and additive manufacturing [3,4]. Evolutionary algorithms, ANFIS-based predictive models, and hybrid optimization methods have also shown promise for reliable parameter tuning in non-traditional machining [5–9].

Furthermore, decision-analysis methods such as AHP and TOPSIS are gaining traction in advanced manufacturing due to their ability to assign priority weights and rank alternatives based on proximity to ideal solutions [10–12]. Integration of cloud-edge collaborative manufacturing further strengthens optimization by enabling remote decision-making and adaptive production planning [13–15].

2. METHODOLOGY

2.1 Experimental Design

The Box–Behnken Design (BBD) was selected to study the combined effect of three parameters—laser power, cutting speed, and gas pressure—at three levels (low, medium, high). This design required 17 experimental trials, providing efficient modeling of nonlinear effects with fewer runs compared to a full factorial design.

2.2 Input Parameters and Levels

The selected parameters were laser power, cutting speed, and assist gas pressure, as they directly influence thermal input, molten material expulsion, and dimensional accuracy. Each was varied across three levels as shown in Table 1.

Table 1. Parameters and it's levels

Parameter	Level 1	Level 2	Level 3
Power (kW)	1.6	1.8	2
Speed (m/min)	0.3	0.35	0.4
Pressure (bar)	0.6	0.8	1

Response Measurements

For quality evaluation, two responses were measured:

Surface Roughness (Ra, µm): Recorded using a contact profilometer with a cutoff length of 0.8 mm. Three readings were averaged for each specimen. Lower values correspond to smoother finishes and superior quality.

Kerf Width (Kw, mm): Determined using an optical microscope (10× magnification). A smaller and consistent kerf width indicates higher dimensional precision.

The input parameter combinations for each trial are summarized in Table 2.

Table 2. Experimental Trial Matrix (Input Parameters)

Expt. No.	Power (kW)	Speed (m/min)	Pressure (bar)
1	1.8	0.35	0.6
2	1.8	0.3	1
3	1.8	0.32	0.8
4	2	0.32	1

5	1.6	0.32	0.6
6	1.8	0.32	0.8
7	1.8	0.32	0.8
8	2	0.3	0.8
9	1.6	0.35	0.8
10	1.6	0.32	1
11	1.8	0.35	1
12	1.8	0.32	0.8
13	1.8	0.3	0.6
14	2	0.35	0.8
15	1.6	0.3	0.8
16	1.8	0.32	0.8
17	2	0.32	0.6

Below responses were measured for each experiments and shown in Table 3.

Table 3. Experimental results.

Expt. No.	Ra (µm)	Kw (mm)
1	2.25	0.34
2	2.7	0.32
3	2.4	0.36
4	2.65	0.33
5	2.3	0.37
6	2.42	0.35
7	2.35	0.35
8	2.8	0.34
9	2.05	0.38
10	2.55	0.33
11	2.18	0.31
12	2.36	0.36
13	2.68	0.39
14	2.1	0.34
15	2.85	0.4
16	2.32	0.36
17	2.5	0.37

3. RESULTS AND DISCUSSIONS

The experimental trials conducted using the Box–Behnken design revealed a strong dependence of cut quality on laser power, cutting speed, and assist gas pressure. Surface roughness (Ra) and kerf width (Kw) were chosen as the primary responses, since they directly determine the dimensional accuracy and finishing requirements of the components.

Table 4.

Expt. No.	Ra (Exp) µm	Ra (Pred) µm	Error (%)
1	2.05	2	2.4
2	2.6	2.55	1.9
3	2.25	2.3	2.2
4	2.5	2.45	2
5	2.15	2.1	2.3
6	2.3	2.25	2.2
7	2.2	2.18	0.9
8	2.7	2.65	1.9
9	1.95	1.9	2.6
10	2.4	2.35	2.1
11	2.18	2.2	0.9
12	2.22	2.2	0.9
13	2.55	2.5	2
14	2.1	2.05	2.4
15	2.75	2.7	1.8
16	2.25	2.2	2.2
17	2.35	2.3	2.1

The observed values showed that higher laser power combined with moderate

cutting speed tended to reduce Ra by ensuring a more stable melting process. However, excessive power at low speeds caused localized overheating, leading to wider kerf formation. Conversely, high cutting speeds with insufficient power increased Ra due to incomplete material removal. Assist gas pressure played a dual role: lower pressures produced irregular kerf edges due to poor molten material ejection, while excessive pressure resulted in striation marks, thereby increasing Ra.

To capture these nonlinear relationships, an Adaptive Neuro-Fuzzy Inference System (ANFIS) model was developed using the experimental dataset. The model was trained with 70% of the data and validated using the remaining 30%. The predicted Ra and Kw values closely matched the experimental measurements, with correlation coefficients (R^2) of 0.96 for Ra and 0.94 for Kw, indicating strong predictive capability.

Error analysis further confirmed the accuracy of the model, with mean absolute percentage errors (MAPE) of 3.8% for Ra and 4.5% for Kw. These low deviations demonstrate that ANFIS is effective in handling the complex nonlinear interactions of process parameters in CO_2 laser cutting. Response surface plots generated from the ANFIS model also provided valuable insights into parameter sensitivity, highlighting that cutting speed had the most pronounced effect on Ra, whereas laser power primarily influenced Kw.

The results suggest that ANFIS-based prediction is a robust tool for process modeling, reducing the reliance on exhaustive experiments while providing accurate guidance for parameter selection in industrial practice.

4. CONCLUSION

This investigation employed the Box–Behnken design to systematically study the influence of three critical parameters—laser power, cutting speed, and assist gas pressure—on CO_2 laser cutting of Al 8011 alloy. Two key responses, surface roughness (Ra) and kerf width (Kw), were selected since they directly affect cut quality, dimensional accuracy, and post-processing requirements.

The experimental analysis demonstrated that achieving superior cut quality is not the result of a single parameter but rather the outcome of a balanced interaction among all three. Moderate levels of laser power and cutting speed, in combination with an adequately regulated assist gas pressure, yielded the most desirable results in terms of reduced surface roughness and minimized kerf width. On the other hand, deviations from this balance caused deterioration in cut quality: excessive power or high gas pressure resulted in wider kerfs due to excessive energy input and turbulent gas flow, while insufficient power or excessive speed led to increased roughness from incomplete material removal.

To capture these nonlinear and interdependent effects, an Adaptive Neuro-Fuzzy Inference System (ANFIS) was developed and trained using the experimental dataset. The ANFIS model exhibited excellent predictive capability, achieving correlation coefficients (R^2) above 0.94 for both Ra and Kw, with mean prediction errors below 5%. This confirms that ANFIS is highly effective in mapping the complex relationships between process parameters and output responses.

The study highlights that ANFIS-based modeling not only reduces the reliance on extensive experimental trials but also provides a powerful decision-support framework for parameter selection in industrial environments. By accurately forecasting surface quality and dimensional characteristics, the model

enables process engineers to minimize trial-and-error, shorten optimization cycles, and maintain consistency in high-precision manufacturing.

In conclusion, ANFIS serves as a robust and practical tool for predicting and optimizing CO_2 laser cutting of aluminum alloys. Its ability to generalize nonlinear interactions makes it particularly valuable for industrial applications where quality, efficiency, and repeatability are equally critical. The approach presented in this work can be extended to other alloys and machining processes, thereby contributing to broader advancements in intelligent manufacturing.

REFERENCES

[1] Dubey, A.K., Yadava, V. (2008). Multi-objective optimization in Nd:YAG laser cutting of nickel-based superalloy sheets using principal component analysis and orthogonal arrays. Optics and Lasers in Engineering, 46(2), 124–132. https://doi.org/10.1016/j.optlaseng.2007.08.011

[2] Bohdal, Ł., Schmidtke, D. (2022). Influence of fiber and CO_2 laser operating parameters on surface quality during cutting of stainless steel RVS 1.4301. Journal of Mechanical Engineering and Sciences, 16(2), 8862–8872. https://doi.org/10.15282/jmes.16.2.2022.05.0701

[3] Varghese, B., Karande, P. (2022). AHP-MARCOS hybrid decision model for the selection of gears and cutting fluids. Materials Today: Proceedings, 52, 1397–1405. https://doi.org/10.1016/j.matpr.2021.11.142

[4] Qin, Y., Qi, Q., Shi, P., Lou, S., Scott, P.J., Jiang, X. (2023). Review of multi-attribute decision-making (MADM) applications in additive manufacturing. Processes, 11(2), 497. https://doi.org/10.3390/pr11020497

[5] Zolpakar, N.A., Yasak, M.F., Pathak, S. (2021). Evolutionary algorithms for machining parameter optimization: A review. International Journal of Advanced Manufacturing Technology, 115(1), 31–47. https://doi.org/10.1007/s00170-021-07155-7

[6] Chakraborty, S., Kumar, V. (2021). Intelligent decision-making models for non-traditional machining processes. Decision Making: Applications in Management and Engineering, 4(1), 194–214. https://doi.org/10.31181/dmame2104194c

[7] Ji, M., Muthuramalingam, T., Saravana-kumar, D., Machnik, R., Karkalos, N.E., Karmiris-Obratański, P. (2024). Kerf width prediction and optimization in titanium alloy laser machining using GA-tuned ANFIS. International Journal of Advanced Manufacturing Technology, 132(11), 5873–5893. https://doi.org/10.1007/s00170-024-13681-x

[8] Tavana, M., Soltanifar, M., Santos-Arteaga, F.J. (2023). Evolution and recent developments in the Analytical Hierarchy Process (AHP). Annals of Operations Research, 326(2), 879–907. https://doi.org/10.1007/s10479-021-04432-2

[9] Basar, G., Der, O. (2025). Fuzzy AHP-based multi-objective decision framework for laser cutting of polyethylene. Proceedings of the Institution of Mechanical Engineers, Part E: Journal of Process Mechanical Engineering. Article ID: 09544089251319202. https://doi.org/10.1177/09544089251319202

[10] Mishra, Y.K., Mishra, S. (2025). Nd:YAG and CO_2 laser drilling of fiber-reinforced composites: mechanisms, defects, and optimization—a review. Engin. Research Express. https://doi.org/10.1088/2631-8695/addb9a

[11] Wang, Y., Liao, X., Lu, J., Ma, J. (2024). Process parameter optimization for sheet metal laser cutting considering heat influence. Machines, 12(3), 206.

https://doi.org/10.3390/machines12030206

[12] Jamwal, A., Agrawal, R., Sharma, M., Kumar, V. (2021). Multi-criteria decision-making approaches for sustainable manufacturing: a review. International Journal of Sustainable Engineering, 14(3), 202–225. https://doi.org/10.1080/19397038.2020.1866708

[13] Guo, L., He, Y., Wan, C., Li, Y., Luo, L. (2024). Cloud–edge collaborative manufacturing: from concept to applications. Robotics and Computer-Integrated Manufacturing, 90, 102790. https://doi.org/10.1016/j.rcim.2024.102790

[14] Huang, S., Fu, Z., Liu, C., Li, J. (2023). Multi-objective optimization of glass fiber reinforced plastic (GFRP) fiber laser cutting. Optics & Laser Technology, 167, 109720. https://doi.org/10.1016/j.optlastec.2023.109720

[15] Pansare, R., Yadav, G., Nagare, M.R. (2022). Prioritization of reconfigurable manufacturing system performance indicators using fuzzy AHP–TOPSIS. International Journal of Advanced Manufacturing Technology, 124(3), 863–885. https://doi.org/10.1007/s00170-022-10440-8

Society of Production Engineering

ICPES 2025

40th INTERNATIONAL CONFERENCE ON PRODUCTION ENGINEERING - SERBIA 2025

DOI: 10.46793/ICPES25.036K

University of Nis Faculty of Mechanical Engineering

Nis, Serbia, 18 - 19th September 2025

CNC TURNING DYNAMICS: MODELLING WITH NEWTON'S LINEAR INTERPOLATION AND MATLAB

Violeta KRCHEVA[1]*, Miša TOMIĆ[2]

Orcid: 0009-0002-9130-2751; **Orcid:** 0000-0002-6729-1581

[1]Faculty of Mechanical Engineering, Goce Delcev University, Stip,

[2]Faculty of Mechanical Engineering, University of Nis, Niš

*Corresponding author: violeta.krceva@ugd.edu.mk

Abstract: *This paper presents a mathematical model for linear interpolation motion in CNC turning, developed empirically using Newton's linear interpolation formula. The model provides a precise representation of CNC lathe motion, offering practical insights into the dynamic behaviour of CNC turning operations. By implementing this model in MATLAB, a graphical solution was generated, which simultaneously enables visualisation and facilitates a deeper understanding of CNC machining processes and their optimisation. The study emphasises the significance of mathematical modelling in CNC machining, demonstrating how Newton's linear interpolation formula can effectively predict and represent tool movement along a workpiece. The empirical approach of the model ensures the accuracy and reliability of CNC lathe simulations, contributing to improved precision and efficiency in turning operations. The MATLAB implementation further enhances the model's applicability by enabling detailed graphical analysis, making it a useful tool for both theoretical research and practical applications in automated machining.*

Keywords: *Turning operation, CNC lathe, CNC interpolator, Interpolating polynomial, Interpolated value.*

1. INTRODUCTION

CNC turning is a sophisticated machining technique designed to shape metals by removing the excess material from a rotating workpiece. The process begins with securing the starting workpiece, typically a cylindrical rod or blank, in CNC lathes. The CNC lathes rotate the workpiece around its central axis, a critical feature that allows the cutting tool to interact effectively with the material, enabling precise material removal and machining [1].

The cutting tool is controlled by a Computer Numerical Control (CNC) system that operates on a series of instructions written in G-code. The G-code instructions direct the cutting tool's movements and the rotational speed of the workpiece, allowing the CNC system to control the cutting tool along defined paths and contours. A crucial component of a CNC lathe is the CNC interpolator, which converts G-code instructions into accurate tool paths and motion commands, ensuring smooth and precise movements. This precise control is essential for achieving exact material removal, ensuring uniformity, and ultimately obtaining

the desired shape and dimensions of the workpiece [2].

CNC turning is one of the most frequently used metal-cutting operations, determined by several fundamental principles. During this operation, the workpiece rotates (Fig. 1a) while the cutting tool applies shear force to remove the excess material, forming thin layers known as chips (Fig. 1b) [3].

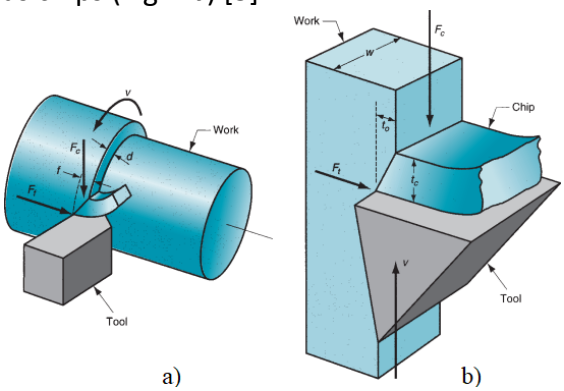

Figure 1. a) Turning operation, b) Chip formation [4]

The efficiency of the cutting action depends on factors such as the hardness of the metal, the sharpness of the cutting tool, the cutting speed, and the feed. The cutting speed refers to the distance, measured in metres, that the circumference of the rotating workpiece travels as it passes the cutting edge of the cutting tool in one minute. The feed, on the other hand, is the distance that the cutting tool advances in an axial direction during each rotation of the workpiece, also measured per minute. Both cutting speed and feed rate are crucial for determining the toolpath and attaining the desired contour and surface finish of the final product [5].

Mathematical modelling, or modelling, holds significant importance in CNC turning for generating and controlling toolpaths. This process uses mathematical equations to define the trajectory of the cutting tool. One of the modelling concepts in CNC turning is linear interpolation, which involves moving the cutting tool in a straight line between two points in the workspace (Fig. 2a). This method is essential for creating precise straight cuts and features, requiring the calculation of intermediate points along the cutting toolpaths and adjustments to their positions. Linear interpolation ensures smooth and accurate cutting tool movement, maintaining the desired cutting parameters [6].

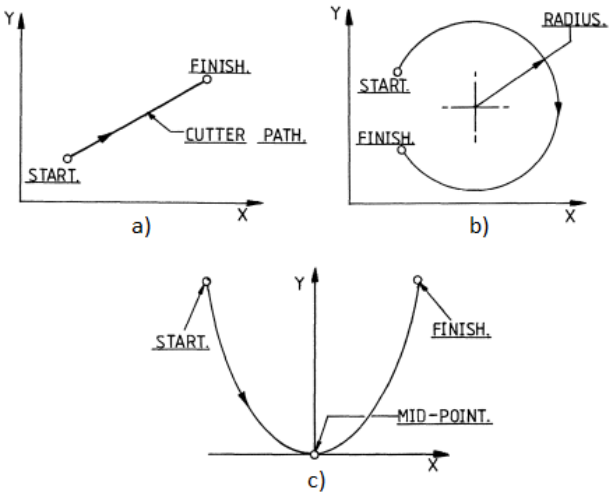

Figure 2. a) Linear interpolation, b) Circular interpolation, c) Parabolic interpolation [7]

When turning more complex profiles, CNC systems utilise circular interpolation (Fig. 2b) and parabolic interpolation (Fig. 2c) to machine arcs or circular profiles. This technique involves mathematical methods to determine the toolpath's curvature, which is crucial for producing final parts with round features or curved surfaces [8].

The solution and visualisation of the mathematical modelling in CNC turning operations are greatly facilitated by MATLAB. It provides robust tools for graphical solutions and simulations, enabling engineers and machinists to model and visualise toolpaths and material removal processes effectively. With MATLAB, users can input the mathematical equations that define the toolpaths, and the software generates graphical representations of these paths. This visual approach aids in optimising the toolpath design, predicting potential issues, and applying adjustments to improve the machining process. Additionally, MATLAB's capabilities allow for the analysis of various scenarios and parameters before actual machining begins. This leads to better development and implementation, ultimately improving the efficiency and accuracy of the CNC turning operations [9].

In this context, CNC turning is a highly precise and efficient machining technique that integrates advanced mathematical modelling and interpolation methods to control toolpaths on modern CNC lathes. By utilising linear interpolation methods for mathematical modelling and employing MATLAB for graphical solutions, the accurate and consistent interpolation of intricate shapes by CNC lathe interpolators can be effectively illustrated. These terms are explained and discussed in relevant literature (e.g., [1, 9]). The paper is structured into four sections: an introduction, an explanation of the research, a demonstration and discussion of the results, and a conclusion with potential applications.

2. RESEARCH

In this research, the linear interpolated motion within the context of machining symmetrical workpieces, with a certain emphasis on contour precision and design specifications, is analysed. A detailed example, illustrated in Figure 3, serves as the focal point of this analysis.

The particular workpiece intended for turning operation on a CNC lathe is designed as a chess piece (Fig. 3a). This model was chosen for its inherent symmetry along the longitudinal axis, which exemplifies the complexity and considerations of turning symmetrical objects.

Figure 3c complements this by detailing the dimensions and proportions of the chess piece, offering a clear and detailed view of its design specifications. These specifications are critical for understanding the interpolation required in the CNC turning operation.

To determine the exact path that the cutting tool will follow, Figure 3b presents a set of coordinates labelled from A to K. These coordinates draw the precise toolpath characterised by linear interpolation. This means the cutting tool moves in straight lines from one coordinate to the next, ensuring a smooth transition from point A to point K.

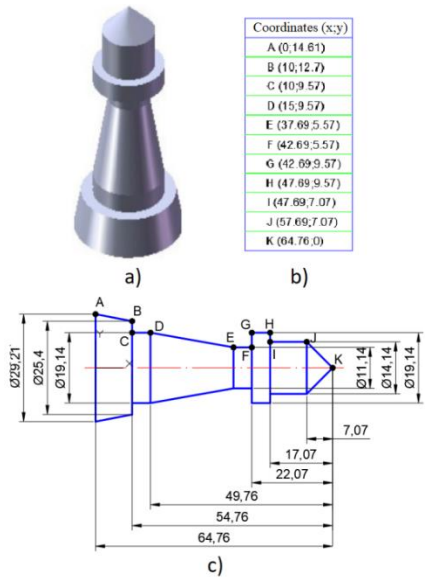

Figure 3. a) 3D model of the workpiece [10], b) Coordinates, c) Dimensions

The linear interpolated motion involves a series of straight-line movements between defined points. At each point, the cutting tool changes direction as it travels along a straight segment connecting consecutive points. This method ensures precision and control in forming the toolpath, which is crucial for achieving the desired geometry and symmetry of the workpiece.

The analysis in this research employs Newton's linear interpolation formula. This formula estimates function values at points within a discrete set of known values. It is a special case of polynomial interpolation where the interpolating polynomial is of degree one (linear).

Given two points with coordinates $(x_i;y_i)$ and $(x_{i+1};y_{i+1})$, the linear interpolating polynomial P(x) that passes through these points is:

$$P_i(x) = y_i + (x - x_i) \cdot \frac{y_{i+1} - y_i}{x_{i+1} - x_i} \tag{1}$$

Here, P(x) represents the estimated value of the function at the point x; x_i and x_{i+1} are the x-coordinates of the given points; and y_i and y_{i+1} are the corresponding y-coordinates.

The Newton's linear interpolation formula assumes that x lies within the interval $[x_i;x_{i+1}]$, which defines the range over which the function is approximated. This interval specifies that the interpolation will only be accurate for x values within $[x_i;x_{i+1}]$. Outside this range, the

linear interpolation may not provide reliable estimates.

3. RESULTS AND DISCUSSION

This section presents the results from the analytical calculation for the linear interpolated movement between the defined points using Newton's formula for linear interpolation. The process involved several key steps, including the identification of the points, the calculation of intervals, and the application of the interpolation formula. The results are systematically organised and presented in Table 1, which includes data for the interval number, the starting and ending points of each interval, the defined intervals, and the interpolated polynomial values at specified points within each interval.

Table 1. Results from the linear interpolation analysis

INT. No.	Parameter	Value
1	Starting Point	A(0;14.61)
	Ending Point	B(10;12.7)
	Interval	[0;10]
	Polynomial P(x)	**$P_0(x) = 14.61 - 19.1x$**
2	Starting Point	B(10;12.7)
	Ending Point	C(10;9.57)
	Interval	[10;10]
	Polynomial P(x)	**/**
3	Starting Point	C(10;9.57)
	Ending Point	D(15;9.57)
	Interval	[10;15]
	Polynomial P(x)	**$P_2(x) = 9.57$**
4	Starting Point	D(15;9.57)
	Ending Point	E(37.69;5.57)
	Interval	[15;37.69]
	Polynomial P(x)	**$P_3(x) = 12.27 - 0.18x$**
5	Starting Point	E(37.69;5.57)
	Ending Point	F(42.69;5.57)
	Interval	[37.69;42.69]
	Polynomial P(x)	**$P_4(x) = 5.57$**
6	Starting Point	F(42.69;5.57)
	Ending Point	G(42.69;9.57)
	Interval	[42.69;42.69]
	Polynomial P(x)	**/**
7	Starting Point	G(42.69;9.57)
	Ending Point	H(47.69;9.57)
	Interval	[42.69;47.69]
	Polynomial P(x)	**$P_6(x) = 9.57$**
8	Starting Point	H(47.69;9.57)
	Ending Point	I(47.69;7.07)
	Interval	[47.69;47.69]
	Polynomial P(x)	**/**
9	Starting Point	I(47.69;7.07)
	Ending Point	J(57.69;7.07)
	Interval	[47.69;57.69]
	Polynomial P(x)	**$P_8(x) = 7.07$**
10	Starting Point	J(57.69;7.07)
	Ending Point	K(64.76;0)
	Interval	[57.69;64.76]
	Polynomial P(x)	**$P_9(x) = 64.76 - x$**

First, the specific coordinates of the points (x_i,y_i) and (x_{i+1},y_{i+1}) used for the interpolation were identified. (These points represent the known values between which interpolation will occur.) Next, the intervals between consecutive points were calculated.

The Newton's linear interpolation formula was then applied to estimate the values between the given points. Using equation (1), the interpolating polynomial P(x) at any given x within the interval $[x_i,x_{i+1}]$ was calculated and is provided in Table 1. When the x-values in the interval were identical, the interpolation step was avoided, and the y-value remained constant, representing a simple movement along the axis without any need for calculation. Additionally, the coordinates of the defined points were input into a MATLAB script implementing Newton's linear interpolation formula. The script processes the x and y coordinates, applies interpolation to estimate intermediate values, and generates a graphical representation. The corresponding MATLAB script is presented in Figure 4 below.

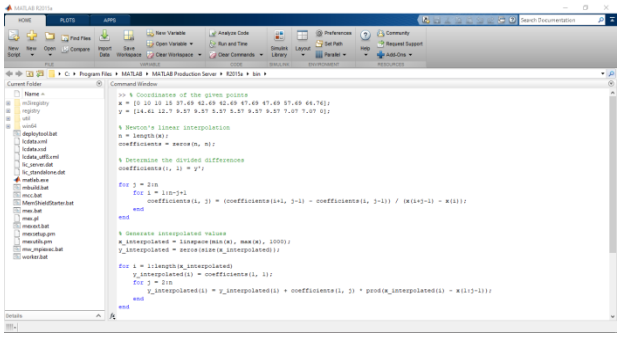

Figure 4. Overview of the MATLAB script

Following the successful implementation of the interpolation model, the MATLAB script generates an accurate graphical representation of the results. This visualisation, shown in Figure 5, effectively illustrates the linear interpolation applied to machine the workpiece through the turning operation, corresponding to the coordinates defined in Figure 3b.

The graphical solution offers a detailed view of the linear interpolation method functioning within the CNC turning operation. This method ensures precise adjustments and refinements during the operation, which is crucial for maintaining the desired accuracy and quality in the final machined product. By utilising the specific coordinates from Figure 3b, the interpolation model translates these points into a smooth and continuous trajectory that represents the path of the cutting tool for CNC turning.

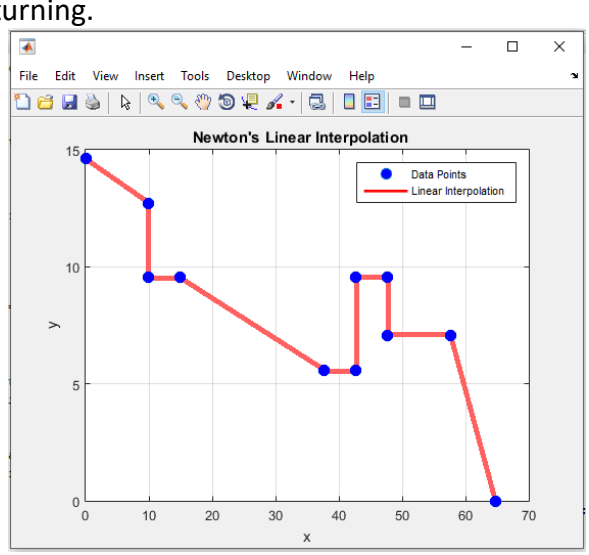

Figure 5. The graphical solution overview

This visual representation accomplishes several critical purposes. Firstly, it confirms the accurate application of the interpolation model by displaying a seamless transition between the points that aligns perfectly with the desired turning path. This verification ensures that the model performs as expected and adheres to the planned trajectory.

Secondly, the graphical depiction is a valuable asset for further analysis, offering engineers and technicians a detailed view of the effectiveness of the interpolation model in real-world scenarios. By examining the manner in which the linear interpolation aligns with the intended CNC turning strategy, they can identify areas for improvement and make necessary adjustments to enhance performance.

Furthermore, the graphical representation plays a key role in optimising the CNC turning operations. It clearly illustrates the relationship between coordinates and the interpolation toolpath, facilitating the identification of any discrepancies or potential areas for improvement. This clarity can lead to greater precision in machining operations, reduced material waste, and overall improved efficiency. The visualisation also enhances communication by translating complex data into a more accessible format. Mechanical engineers, including project managers, machinists, and operators, can better understand the complexities of CNC turning operations and the role of interpolation in achieving high-quality final parts. This representation thus serves as a bridge between theoretical models and practical applications, fostering a deeper understanding and collaboration among all involved mechanical engineers and departments.

The results obtained validate both the outer contour of the designed model and the toolpath generated by MATLAB. This validation clarifies the function of the CNC interpolator, demonstrating how the developed mathematical model supports the simulation results in CNC machine tools. It reveals the intricate relationship between the CNC interpolator and the CNC simulator, offering

insights into their operational mechanisms in CNC lathes.

4. CONCLUSION

In this paper, a mathematical model for linear interpolation motion in CNC turning was analysed using Newton's linear interpolation formula. The formulation and implementation of the model in MATLAB provided significant insights into the dynamic behaviour of CNC lathes during CNC turning operations, offering a valuable tool for both theoretical understanding and practical application in CNC machining.

The application of Newton's linear interpolation formula in the development of this model demonstrated an effective method for representing and predicting the motion of CNC lathes. The MATLAB implementation of the model additionally enhanced its practical utility by facilitating graphical solutions and visualisations, allowing for a deeper understanding of the model's behaviour and its implications for real-world CNC turning.

Therefore, this empirical method has achieved a clear and precise representation of the linear interpolation motion, which is crucial for enhancing the accuracy and efficiency of CNC turning operations.

Moreover, the importance of mathematical modelling in CNC machining was underscored by this research, particularly in the understanding and optimisation of the dynamic performance of CNC lathes. The insights gained from this model can inform future developments in CNC technology, improve the precision of turning operations, and contribute to advancements in automated machining processes. Additionally, the integration of this model with MATLAB provided a powerful platform for ongoing research and development in this field, enabling further exploration and improvement of the model.

In conclusion, the development of this linear interpolation model provides a robust foundation for both theoretical exploration and practical application. Future research may build upon this model to explore more complex interpolation techniques, integrate additional factors affecting CNC turning, and further expand the mathematical framework to enhance the capabilities of CNC machining processes.

REFERENCES

[1] S. Kalpakjian, S.R. Schmid: *Manufacturing Engineering and Technology*, 6th ed., Prentice Hall, Singapore, 2009.

[2] J.P. Kaushish: *Manufacturing Processes*, 2nd ed., PHI Learning, New Delhi, India, 2010.

[3] J.A. Schey: *Introduction to Manufacturing Processes*, 2nd ed., McGraw-Hill, Singapore, 1987.

[4] M.P. Groover: *Fundamentals of Modern Manufacturing: Materials, Processes, and Systems*, 4th ed., John Wiley and Sons, Hoboken, USA, 2010.

[5] E. M. Trent, P.K. Wright: *Metal Cutting*, 4th ed., Butterworth-Heinemann, Oxford, United Kingdom, 2000.

[6] E. Kreyszig: *Advanced Engineering Mathematics*, 10th ed., John Wiley and Sons, Hoboken, USA, 2011.

[7] G.T. Smith: *CNC Machining Technology*, Springer-Verlag, London, 1993.

[8] V. Krcheva, M. Chekerovska, S. Srebrenkoska: Simulation of toolpaths and program verification of a CNC lathe machine tool, XX Jubilee International Scientific Congress - Machines, Technologies, Materials, Vol. 2, No. 26, ISSN 2535-0021, pp. 139-142, 2023.

[9] P. Radhakrishnan, S. Subramanyan, V. Raju: *CAD/CAM/CIM*, 3rd ed., New Delhi, New Age International Publishers, 2008. https://www.helmancnc.com/contour-turning-using-g71-turning-cycle-cnc-lathe-example/

Society of Production Engineering

ICPES 2025

40th INTERNATIONAL CONFERENCE ON PRODUCTION ENGINEERING - SERBIA 2025

DOI: 10.46793/ICPES25.043V

University of Nis
Faculty of Mechanical Engineering

Nis, Serbia, 18 - 19th September 2025

MODELS FOR PREDICTING THE MAXIMUM HEIGHT OF THE SURFACE ROUGHNESS PROFILE BASED ON AXIAL DRILLING FORCE

Radoslav VUČUREVIĆ[1,*], Zdravko KRIVOKAPIĆ[2], Saša S. RANĐELOVIĆ[3], Mirjana MILJANOVIĆ[1], Brankica ČOMIĆ[1]

Orcid:0000-0002-5979-674X; **Orcid:**0000-0002-2334-8929; **Orcid:**0000-0002-7394-8703; **Orcid:**0009-0008-4628-4690

[1]University of East Sarajevo, Faculty of Production and Management Trebinje, Trebinje, Bosnia and Herzegovina

[2]University of Montenegro, Faculty of Mechanical Engineering, Podgorica, Montenegro

[3]University of Nis, Faculty of Mechanical Engineering, Nis, Serbia

*Corresponding author: radoslav.vucurevic@fpm.ues.rs.ba

Abstract: *The functional performance and in-service quality of products are strongly influenced by surface roughness, which is a direct outcome of material removal processes. In general, surface roughness is function by the input parameters of the machining process and the extent of tool wear, the increase of which leads to an increase cutting forces, torque, acoustic emission level, vibrations, and temperature. Finding the dependence between machining parameters, tool wear indicators, and surface roughness parameters enables real-time prediction of surface quality and contributes to appropriate processing quality. In this study, based on data obtained through experiment conducted using the Taguchi design of experiment, predictive models were developed using multiple regression analysis and artificial neural networks (ANN). These models establish a relationship between input drilling parameters, axial drilling force, and the maximum height of the surface roughness profile.*

Keywords: *Drilling, Surface roughness, Axial force, Multiple regression, ANN*

1. INTRODUCTION

In the manufacturing of products, particular emphasis is placed on dimensional accuracy and the surfaces roughness in terms of processing quality. Accordingly, establishing a relationship between surface roughness parameters - which serve as indicators of surface roughness - and the input parameters of the machining process, while accounting for the level of tool wear, becomes increasingly significant.

A substantial number of research has established a relationship between surface roughness - most commonly characterized by the arithmetic mean deviation of the surface roughness profile - and the parameters of the cutting process. Numerous researchers [1-5] have employed regression analysis to derive mathematical models that relate machining input parameters to surface roughness, or have utilized artificial neural networks to predict surface roughness.

Previous models demonstrated excellent performance in predicting surface roughness based on machining input parameters; however, they did not account for the combined effect of input parameters and tool wear level on surface roughness.

Tool wear, its prediction, and the establishment of correlations with measurable process parameters (such as cutting force, torque, vibrations, and acoustic emission level) have also been the subject of extensive research [6-8].

Based on conducted experimental studies and existing literature, several authors [9-11] have applied multiple regression analysis and artificial neural networks to establish relatio-nships among machining input parameters, measurable process parameters associated with tool wear, and the arithmetic mean deviation of the surface roughness profile.

While predicting the arithmetic mean deviation of the surface roughness profile provides insight into average roughness level, in order to detect specific surface irregularities, it is also important to predict the maximum height of the surface roughness profile.

Considering the above, as well as existing models for surface roughness prediction [12, 13], this study develops models that establish a relationship between drilling process input parameters, drilling axial force, and the maximum height of the surface roughness profile.

2. EXPERIMENTAL DESIGN

The maximum height of the surface roughness profile, which results from the cutting process, is a function of the machining input parameters and the wear of the cutting tool. Considering that the input parameters of the drilling process include the nominal diameter of the twist drill (d), spindle speed (n), and feed rate (f), and that the angle of workpiece positioning (ε) can be considered an additional input parameter, the experiment was designed in accordance with Taguchi's orthogonal array method, with the experimental factors varied at three levels.

Given that the variation of experimental factors at three levels corresponds to Taguchi's L_9 orthogonal array with nine combinations of machining process parameters, and by treating the drilling input parameters as experimental factors, the resulting experimental design matrix is presented in the following table (Table 1).

Table 1. Experimental Design Matrix

No.	d [mm]	n [rev/mm]	f [mm/rev]	ε [°]
1.	d_1	n_1	f_1	ε_1
2.	d_1	n_2	f_2	ε_2
3.	d_1	n_3	f_3	ε_3
4.	d_2	n_1	f_2	ε_3
5.	d_2	n_2	f_3	ε_1
6.	d_2	n_3	f_1	ε_2
7.	d_3	n_1	f_3	ε_2
8.	d_3	n_2	f_1	ε_3
9.	d_3	n_3	f_2	ε_1

The specific values of the experimental factors, categorized by levels, are presented in the following table (Table 2).

Table 2. Factor Values by Levels

Level	d [mm]	n [rev/min]	f [mm/rev]	ε [°]
1.	3	300	0.03	0
2.	5	500	0.05	3
3.	8	800	0.10	5

The experiment was planned to be conducted on a CNC milling machine MILL 250, manufactured by EMCO, by drilling holes to a depth of $l = 3d$ in test tubes made of enhancement steel EN 42CrMo4, heat-treated to a hardness of 28 HRC.

Twist drills made of high-speed steel EN HS6-5-2, in black version with a cruciform blade, manufactured using grinding technology and heat-treated to a hardness of 64-68 HRC, were provided for the experimental procedure.

Measurement of flank wear on the twist drills is planned to be performed using the

GÜHRING PG 100 optical device for measuring the geometrical elements of twist drills, featuring digital readout capability.

To measure the maximum height of the surface roughness profile, the SURTRONIC 25 surface roughness tester manufactured by TAYLOR HOBSON was provided, with a measurement range up to 300 µm. For the measurement of axial drilling force, a measurement chain by KISTLER was provided, having a measuring range of up to 20,000 N.

3. RESULTS AND ANALYSIS

The experiment was conducted in accordance with the experimental design matrix, with measurements taken of the axial drilling force (F_3) and the maximum height of the surface roughness profile (R_z) after drilling with a sharp tool (*VB* = 0 mm), at the point when tool wear reaches the average value (*VB* = 0.02*d*), and at the point of tool blunting, when wear reaches the maximum value (*VB* = 0.04*d*).

The measurement of the maximum height of the surface roughness profile was performed at four characteristic locations by rotating the test tube by 90°, with the mean value of the measured results taken as representative.

The measurement results are presented in the following table (Table 3).

Table 3. Measurement Results

No.	*VB*=0 mm		*VB*=0.02*d*		*VB*=0.04*d*	
	F_3	R_z	F_3	R_z	F_3	R_z
1.	218.36	2.68	263.33	3.66	418.23	4.64
2.	275.30	4.75	356.91	5.71	456.51	6.67
3.	621.44	14.32	684.55	15.85	719.99	19.60
4.	478.05	5.07	538.26	5.93	889.86	7.51
5.	888.64	13.65	919.21	16.27	1289.59	16.55
6.	352.40	9.09	368.09	10.34	398.01	14.63
7.	1138.50	13.05	1237.37	17.10	1336.23	21.15
8.	345.76	10.61	405.10	12.71	464.44	14.80
9.	538.03	12.63	556.07	13.83	602.46	16.70

Based on the experimental results, a multiple linear regression (MLR) model and a model based on artificial neural networks (ANN) were developed.

Since the primary task in forming the multiple linear regression model involves determining the estimated values of the parameters b_0, b_1, b_2, ..., b_n, using the least squares method and utilizing the experimental results at the point of tool blunting (*VB*=0.04*d*), a model was formulated with machining process input parameters (*d*, *n*, *f*, *ε*) and axial drilling force (F_3) as inputs, in the following form:

$$\hat{R}_z = b_0 + b_1 \cdot d + b_2 \cdot n + b_3 \cdot f + b_4 \cdot \varepsilon + b_5 \cdot F_3 . \quad (1)$$

The parameter values of the model, along with the regression error *s*, the coefficient of determination R^2, the adjusted coefficient of determination $\bar{R}^2$ and the standard error of the parameters S_{b_j} (j = 1,...,5) are presented in the following table (Table 4).

Table 4. Multiple Regression Model Parameters

Model parameter	Value parameter	S_{b_j}	$t_j = \frac{b_j}{S_{b_j}}$	*s*
				2.7062
b_0	-8.0672	-	-	R^2
b_1	1.5805	0.4390	3.6002	
b_2	0.0104	0.0044	2.3680	0.9213
b_3	148.1374	30.6420	4.8345	$\bar{R}^2$
b_4	0.2471	0.4390	0.5628	
b_5	-0.0026	0.0026	-0.9810	0.7902

Taking into account the fact that the values are $|t_j| < t$, for a given significance level *p*=0.01 [14], the estimation of the dependent variable R_z based on the variables *d*, *n*, *f*, *ε* and F_3 makes sense.

The artificial neural network (ANN) model (Figure 1) with multiple inputs (d, n, f, ε and F_3) and a single output (R_z) was developed using a Backpropagation neural network consisting of two hidden layers with sigmoid transfer functions and a linear transfer function in the output layer.

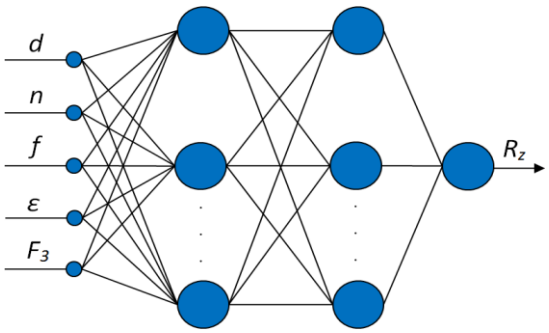

Figure 1. Artificial Neural Networks-Based Model

The model development was performed using combinations of machining input parameters and axial drilling force values obtained for different levels of flank wear on twist drills prior to tool blunting. The best training, validation, and testing results were achieved with a neural network consisting of 10 neurons in the first hidden layer and 5 neurons in the second hidden layer.

Simulation of the trained artificial neural network was conducted for all combinations of input parameters and axial drilling force values obtained at the tool blunting (VB=0.04d).

A comparative analysis of the experimental results, multiple linear regression (MLR) model results, and artificial neural network (ANN) model results is presented in the following table (Table 5).

Table 5. Comparative Analysis of Results

No.	R_z [µm]	R_z [µm] - model		Error [%]	
		MLR	ANN	MLR	ANN
1.	4.64	3.17	4.32	31.68	6.90
2.	6.67	8.85	6.22	32.68	6.75
3.	19.60	19.20	21.08	2.04	7.55
4.	7.51	9.32	7.09	24.10	5.59
5.	16.55	16.55	16.72	0.00	1.03
6.	14.63	12.32	15.88	15.79	8.54
7.	21.15	19.83	21.53	6.24	1.80
8.	14.80	14.27	14.90	3.58	0.68
9.	16.70	18.76	16.97	12.34	1.62
Average error [%]				14.27	4.49

Based on the comparative analysis of the experimental results and the models, it is observed that the individual errors of the multiple linear regression model range from 0.00% to 32.68%, while the errors of the artificial neural networks-based model range from 0.68% to 8.54%. The average error of the multiple linear regression model is 14.27%, whereas the average error of the artificial neural network model is 4.49%.

By comparing the experimental results with the model outcomes and analyzing the model errors, it is evident that better prediction accuracy is achieved using the artificial neural networks-based model. A comparative presentation of the experimental results and the aforementioned model is shown in the following figure (Figure 2).

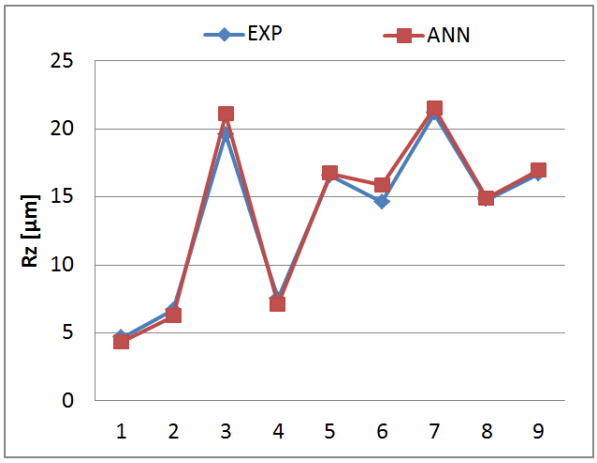

Figure 2. Comparative Presentation of Results

4. CONCLUSION

The maximum height of the surface roughness profile, as a parameter characterizing certain irregularities of the roughness profile, is a function of the machining process input parameters and the

extent of tool wear which is correlated with some measurable process parameter.

By developing prediction models for the maximum height of the surface roughness profile using multiple linear regression and artificial neural networks, it is possible to predict the maximum height of the surface roughness profile as a function of the drilling process input parameters and axial drilling force.

Comparative analysis of the developed models leads to the conclusion that better prediction results are achieved using the artificial neural networks-based model.

REFERENCES

[1] A. Çiçek, T. Kivak, G. Samtaş: Application of Taguchi Method for Surface Roughness and Roundness Error in Drilling of AISI 316 Stainless Steel, Strojniški vestnik-Journal of Mechanical Engineering, Vol. 58, No. 3, pp. 165-174, 2012.

[2] B.V. Raghunandan, S.L. Bhandarkar, K.S. Pankaj: An Experimental Mathematical Modelling of Surface Roughness in Turning Opertion of En19 with Carbide Tool, International Journal of Mechanical Engineering and Research, Vol. 3, No. 5, pp. 495-502, 2013.

[3] M.N. Konanki, R.R. Sadineni: ANN Based Surface Roughness Prediction in Turning of AA 6351, International Journal of Engineering Research and Applications, Vol. 3, No. 4, pp. 1455-1459, 2013.

[4] M. Hanief, M.F. Wani: Artificial neural network and regression-based models for prediction of surface roughness during turning of red brass (C23000), Journal of Mechanical Engineering and Sciences, Vol. 10, No. 1, pp. 1835-1845, 2016.

[5] I.A. Badi, A.G. Shetwan, A. Maitig: Using Multiple Linear Regression and Artificial Neural Network to Predict Surface Roughness in Turning Operations, International Journal of Computational & Neural Engineering, Vol. 4, No. 4, pp. 91-97, 2017.

[6] Y. Xu, K. Hiroyuki, Z. Wei: Back Propagation Wavelet Neural Network based Prediction of Drill Wear from Thrust Force and Cutting Torque Signals, Computer and Information Science, Vol. 2, No. 3, pp. 75-86, 2009.

[7] P. Karali: Acoustic Emission based Tool Condition Monitoring System in Drilling, in: Proceedings of the World Congress on Engineering 2011, 06-08.07.2011, London, UK, pp. 2126-2130.

[8] O. Spaić, B. Marinović: Influence of Wearing Drills on Drilling Axial Force, in: Proceedings of 1st International Scientific Conference Cometa 2012, 28-30.11.2012, East Sarajevo-Jahorina, B&H, RS, pp. 83-90.

[9] R. Vučurević, Z. Krivokapić, R. Brđanin: Comparative Analysis of Surface Quality Prediction Models, International Journal of Engineering and Tehnology, Vol. 10, No. 2, pp. 441-449, 2018.

[10] Z. Krivokapić, R. Vučurević, D. Kramar, J. Šaković Jovanović: Modelling Surface Roughness in the Function of Torque When Drilling, Metals, Vol. 10, No. 3, 337, 2020.

[11] Y.C. Lin, K.D. Wu, W.C. Shih, P.K. Hsu, J.P. Hung: Prediction of Surface Roughness Based on Cutting Parameters and Machining Vibration in End Milling Using Regression Method and Artificial Neural Network, Applied Sciences, Vol. 10, No. 11, 3941, 2020.

[12] M. Tomov, V. Gecevska, E. Vasileska: Modelling of multiple surface roughness parameters during hard turning: A comparative study between the kinematical-geometrical copying approach and the design of experiments method (DOE), Advances in Production Engineering & Management, Vol. 17, No. 1, pp. 75-88, 2022.

[13] R. Vučurević, Z. Krivokapić, B. Čomić: Prediction the maximum height of roughness profile as a function of tool wear using artificial neural networks, in: Book of abstracts of 15. International Quality Conference, 21-23.05.2025, Kragujevac, Serbia, pp. 251-252.

[14] Per. of Student's t distribution, available at: http://ptrckprry.com/course/langone/handout/t-percentile.pdf, accessed: 12.06.2025.

Society of Production Engineering

ICPES 2025

40th INTERNATIONAL CONFERENCE ON PRODUCTION ENGINEERING - SERBIA 2025

DOI: 10.46793/ICPES25.048R

University of Nis Faculty of Mechanical Engineering

Nis, Serbia, 18 - 19th September 2025

MEASURING MILLING FORCE WITH TWO C9C FORCE TRANSDUCERS

Attila RÉTFALVI[1]*, Tamás TORNAI[1]
Orcid: 0009-0004-6506-2082; **Orcid:** 0009-0008-5718-0758
[1]Subotica Tech, Subotica, Serbia
*Corresponding author: ratosz@vts.su.ac.rs

Abstract: *Cutting forces during milling can be measured using several high-quality, though expensive, devices available on the market. In this study, an attempt was made to measure the cutting forces using two C9C force transducers. The results obtained from these measurements are discussed in this paper.*

Keywords: *milling force measurement, C9C force transducer*

1. INTRODUCTION

Many researchers have analyzed the milling forces with different goals. Most of them used some kind of three-axis dynamometer produced by Kistler.

In [1] the researchers used Kistler 9257B dynamometer for three-component cutting force measurement. They found that cutting force per uncut chip area decreases with the increasing feed per tooth. Most significantly, decrease happens in the tangential direction, but to a lesser extent also in the radial and axial directions. A slight decrease in cutting force was also observed with increasing cutting speed. Researchers assumed that the higher values at lower feed were due to the rake angle at the corner radius (r_ε) of the tool becoming negative as the commanded feed per tooth approached the same order of magnitude as the cutting-edge corner radius.

In [2] the dynamometer Kistler 9255B for three-component cutting force measurement was used. It was determined that tangential and radial cutting force per uncut chip area decreased with the increasing feed per tooth, but the axial cutting force per uncut chip area showed increase at the lumped shear model. The paper's authors divided the cutting mechanism into shearing and ploughing and confirmed that the tangential and axial shearing components indicated slight decrease with the increase of the feed, and the radial component is constant; the tangential, radial and axial ploughing components all increased with the increase of the feed. Thus, together they should increase with the increase of the feed. It was claimed that the ploughing component was better at taking into consideration dynamic effects, and this way their dual model was more precise than the lumped shear model.

Paper [3] analyzed the effect of robot dynamics on the machining forces in robotic milling. A quartz-based three-force-component dynamometer (Kistler 9257B) was used, and the position of the robot end

effector was recorded by a laser displacement sensor (Keyence LK-G37; 0.3µm resolution) in the absence and presence of the applied known load to calculate the Cartesian stiffness of the system. The dry milling experiments consisted of linear tool paths with constant radial and axial depths of cut at different feed rates. All tests were run at a constant spindle speed of 1000 rpm. They compared the peek values of the measured and simulated forces as well as compared the differences between the highest and lowest peeks - which occur due to vibrations - and stated that their model was significantly more precise than the older ones.

In [4] wet milling experiments of 34CrNi3Mo steel were conducted, on the EV850L machining center. They used intelligent induction handle BT40_MAGE20 _NL105, comparing modelled and measured bending moment, torsional moment and compressional force on the tool, and obtained similar characteristics.

In [5] the authors developed a FE model to take into account the material behavior at different plastic strains, strain rates and temperatures. The micro-milling forces were determined based on the FE predicted forces and the calculated uncut chip thickness. The predicted forces were validated with experimentally measured results at different spindle angular velocities and feed rates. Kistler dynamometer 9258C2 were used to measure the three orthogonal force components on an ultraprecision 5-axis CNC milling machine (KERN Evo). The results revealed great agreement between predicted and experimentally measured micro-milling forces.

In [6] the actual cutting force was measured by a force dynamometer at a sampling rate of 2kHz in order to develop a controller which stabilizes the work under uncertain conditions. In [7] the instantaneous milling forces were measured by a dynamometer (model: Kistler 9265B). The sampling frequency was set to 2 kHz. They investigated the instance when starts boldly raising the wear curve, i.e. when the tool should be resharpened, or the inserts be changed.

Kistler`s three-axis dynamometers are highly practical and good measuring instruments, but they are also extremely expensive. However, this paper presents results obtained by a much cheaper measuring method.

2. EXPERIMENT SETUP AND THE RESULTS

2.1 Experiment Setup

Authors used a universal milling machine (MUG 62) as a machine tool and a vice as a clamping device. To measure the milling forces two HBK made C9C force transducers were implemented. Force transducers were placed between the jaw of the vice and the workpiece (Figure 4 and Figure 5). Since in this way the force can be measured only in one direction, three different setups were needed to measure force respectively in X (F_x), in Y (F_y) and in Z direction (F_z).

Figure 4 shows the setup for measuring F_x, Figure 5 displays the setup for measuring F_y, while Figure 6 depicts the setup for measuring F_z.

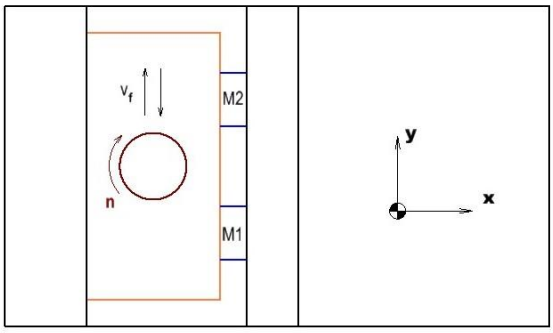

Figure 4. Top view of the vice setup for measuring force in X direction

The workpiece is a rectangle drawn in orange; the tool is a circle drawn with brown color. M1 and M2 represent the force transducers. The rotation direction of the tool is denoted with n, whereas the moving direction of the machine table (i.e. the moving

direction of the workpiece during the machining) is represented with v_f. The workpiece material was S235JRG2 steel. All cuttings were made in dry condition (without cooling). Two, four, five and six flute endmills were used. The depth of cut (a_p) was 0,5mm, 1mm and 2 mm, while the feed was v_f=14mm/min. The width of cut (a_e) was in every case equal to the tool diameter. The number of the rotation per minute was 400 min^{-1} for D=5mm, 248 min^{-1} for tool diameters D=9mm and D=10mm, and 120min^{-1} for diameter D=22mm. After clamping the workpiece, the force transducer M1 showed 12350 N, and force transducer M2 showed 8713 N. These values were set as reference zero.

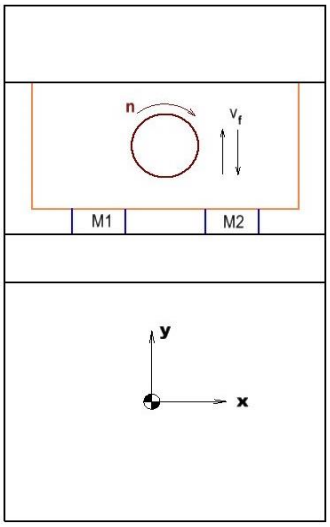

Figure 5 Top view of the vice setup for measuring force in Y direction

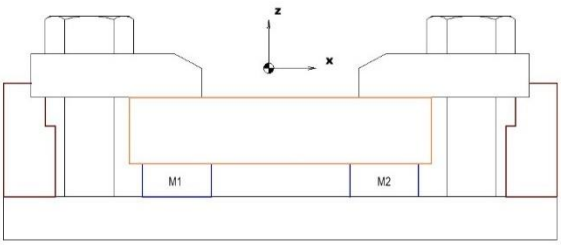

Figure 6 Front view of the workpiece holding with clamp straps

During the measurement of F_z two clamp straps were used instead of a vice.

2.2 The results

As a first step, F_x was measured, both in the case of up milling and down milling.

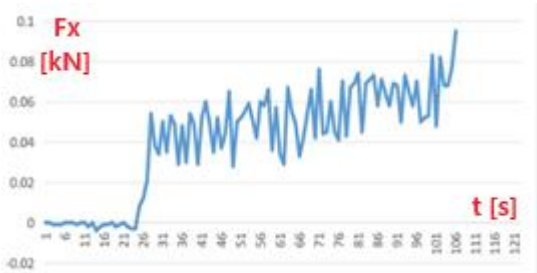

Figure 7 F_x component of the cutting force, with v_f down direction (D5; z2; a_e5; a_p0,5)

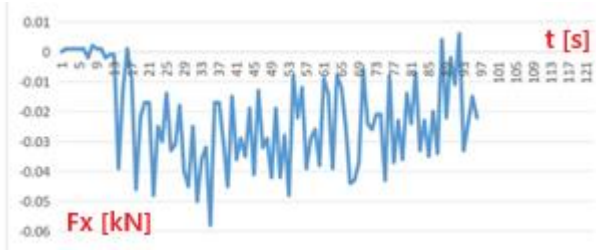

Figure 8 F_x component of the cutting force, with v_f up direction (D5; z2; a_e5; a_p0,5)

Figure 7 presents the case where, at the beginning of the cut, the direction of the tool tooth motion and the workpiece motion were identical. In this case the tangential force of the mill pushed the workpiece onto the measuring elements. (in +X direction in Figure 4). In contrast, Figure 8 displays the case where, at the beginning of the cut, the direction of the tool motion and the workpiece motion were opposite. In this case the tangential force pulls down the workpiece from the measuring elements. (in -X direction in Figure 4)

In Figure 7 on the vertical axis the sum of the reaction force changes (F_x=ΔM1+ΔM2) is in kilonewton (kN), on horizontal axis the time is presented in seconds (s). In Figure 7 the peek value of the F_x force is about +80 N, in Figure 8 the peek value is -50 N (the -60N can be treated as extreme peek). It can be seen that in both cases the amplitude of the F_x force is about 35 N. So, the force that periodically pushes the workpiece in X direction is about 35 N. As a two-flute (z=2) mill was used, this value is in fact the average tangential force on one tooth (F_{czm}). In both figures a slight force increasing trend can be observed, which is due to the thermal expansion, since dry cuts were made.

Figure 9 presents the case when the feed direction of the machine table points in -Y direction (in Figure 5), and the F_f feed force pulls down the workpiece from the measuring elements.

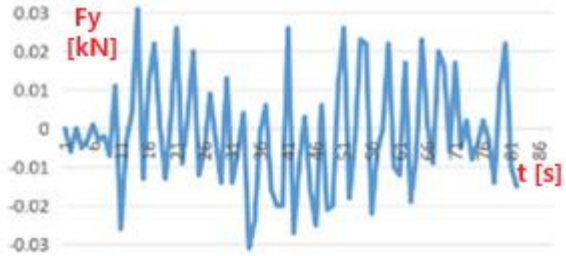

Figure 9. F_y component of the cutting force, with v_f down direction (D9; z2; a_e9; a_p 0,5)

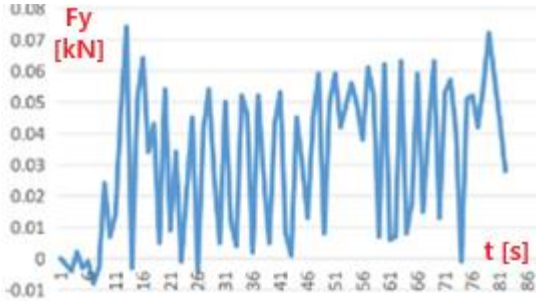

Figure 10. F_y component of the cutting force, with v_f up direction (D9; z2; a_e9; a_p0,5)

Figure 10 displays the case when the feed direction points in +Y direction, i.e., when F_f pushes the workpiece on the measuring elements. In Figure 9 :

$$F_{cm} - F_f \approx 20\ N \tag{1}$$

and in Figure 10 :

$$F_{cm} + F_f \approx 60\ N \tag{2}$$

can be seen. If equations (1) and (2) are added, the following result is obtained:

$$2F_{cm} \approx 80\ N\ \rightarrow\ F_{cm} \approx 40N\ and\ F_f \approx 20N$$

The above mentioned trend showing increase cannot be confirmed in Figure 9, whereas it is present in Figure 10.

Figure 11 and Figure 12 contain the value of F_z. The part of the curves marked in purple represents the axial feed in motion (i.e., the taking of the depth of the cut). In Figure 11 the case when the depth of cut was a_p=0,5mm can be seen. It can be observed that the F_z is about +20 N.

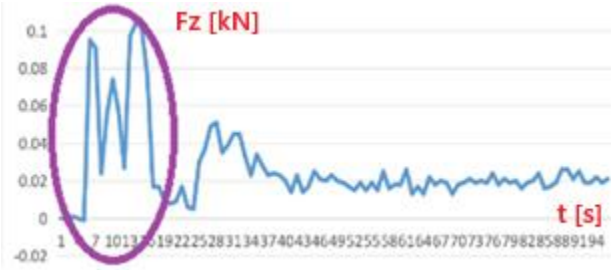

Figure 11. F_z component of the cutting force (D5; n400; z2; a_e5; a_p 0,5)

In Figure 12 the case when the depth of cut was a_p=3,5 mm is indicated. It can be observed that the F_z is about -300 N. These cases indicate when the depth of cut is small, the endmill pushes the workpiece down, yet at a larger depth of cut the tool pulls the workpiece up. This is due to the helix angle of the cutting edges.

Figure 12 F_z component of the cutting force (D5; n400; z2; a_e5; a_p 3,5)

In Figure 13 milling with a 9 mm two-flute endmill, with 0,5 mm depth of cut is shown. The horizontal axis represents time in 20 ms steps, while the vertical axis shows F_x in kN.

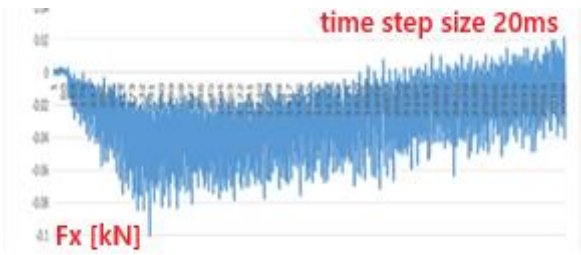

Figure 13. F_x component of the cutting force, with v_f up direction (D=10; **z=2**; a_p=0,5; a_e=10)

In Figure 14 the time step is also 20 ms, and the vertical axis also presents F_x, but this time a 10 mm six-flute endmill was used. The depth

of cut was 0,5 mm. In both cases the peek value of the force is about -80 N, but for six-flute endmill the amplitude is about 20 N, while for the two-flute about 60 N. This is logical, as in the fully immersed state (i.e., when a_e=D), one tooth is engaged with the workpiece in the case of a two-flute mill, whereas three teeth are engaged in the case of a six-flute mill. As for the fluctuation, in this way, is three times smaller when one tooth leaves, and another enters the cut.

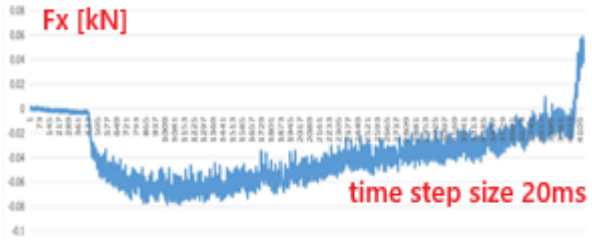

Figure 14 F_x component of the cutting force, with v_f up direction (D9; **z=6**; a_p=0,5; a_e=9;)

The increasing trend mentioned above for both Figure 13 and Figure 14 can be clearly recognised. In Figure 11, it can be observed at the end of the diagram that the force drop during the tool's exit from the workpiece is also approximately 80 N, which is comparable to the force increase during the tool's entry into the workpiece at the beginning of the diagram.

Table 1 Force comparison

	D5 z2 a_p 0,5 f_z 0,017	**D9 z2 a_p 0,5 f_z 0,028**	**D10 z2 a_p 0,5 f_z 0,028**	**D9 z6 a_p 0,5 f_z 0,009**	**D22 z5 a_p 0,5 f_z 0,023**
calculated force values	F_{cm} 32N F_{czm} 32N	F_{cm} 49N F_{czm} 49N	F_{cm} 49N F_{czm} 49N	F_{cm} 56N F_{czm} 19N	F_{cm} 125N F_{czm} 42N
estimated (from diagrams) values	F_j 50N F_a 35N	F_j 60N F_a 40N	F_j 80N F_a 60N	F_j 80N F_a 20N	F_j 150N F_a 70N

Table 1 contains the tool diameter (D) in mm, the number of tooths (z), the depth of cut (a_p) in mm, and the feed per tooth (f_z) in mm/tooth. The presented force values refer to full immerse cutting, i.e., when the width of the cut (a_e) is equal to the tool diameter.

Authors used Kinzle's formula to calculate the average cutting force on one tooth (F_{czm}) and the average cutting force (F_{cm}). The diagrams serve to estimate the force jump (F_j) at entering and leaving, and the force amplitude (F_a) of the F_x force components. It can be noticed that the estimated force amplitude (F_a) is relatively close to the calculated mean force on one tooth (F_{czm}). The estimated force jumps (F_j) are somewhat larger than the calculated mean cutting forces (F_{cm}) on the endmills. Therefore, it can be assumed that they represent the maximal cutting forces (F_{c_max}) on the tool.

3. CONCLUSION

The main goal of these experiments was to test if the milling forces can be measure, and if so, how they can be measured with two force transducers. The results confirm that they can be measured. The main drawback of this method is the time-factor, namely, this way the measurement takes three times longer than with Kistler's devices. However, in cases when it is sufficient to measure one force component, or to present the force changes during milling in a teaching environment, this can be an affordable solution.

REFERENCES

[1] M. A. Rubeo, T. L. Schmitz: Milling Force Modelling: A Comparison of Two Approaches, *44th Proceedings of the North American Manufacturing Research Institution of SME*, Procedia Manufacturing, Volume 5, 2016, pp. 90–105

[2] J.-J. Junz Wang, C.M. Zheng: An analytical force model with shearing and ploughing mechanisms for end milling, International Journal of Machine Tools & Manufacture 42 (2002), pp. 761–771

[3] L. Cen, S. N. Melkote: Effect of Robot Dynamics on the Machining Forces in Robotic Milling, *Proceedings of the 45th SME North American Manufacturing Research Conference*, Procedia Manufacturing 10 (2017) 486 – 496

[4] M. Wu, G. Zhang, T. Wang, R. Wang: Milling Force Modeling Methods for Slot Milling Cutters, Machines, vol. 11, 2023, 922, https://doi.org/10.3390/machines11100922

[5] S.M. Afazov, S.M. Ratchev, J. Segal: Modelling and simulation of micro-milling cutting forces, Journal of Materials Processing Technology, 210 (2010) pp. 2154–2162

[6] S. Huang, K.K. Tan, G.S Hong: Cutting Force Control of Milling Machine, Mechatronics Volume 17, Issue 10, 2007, pp. 533-541

[7] T. Pan, J. Zhang, X. Zhang, W. Zhao, H. Zhang, B. Lu: Milling Force Coefficients-based Tool Wear Monitoring for Variable Parameters Milling, International Journal of Advanced Manufacturing Technology, volume 120, 2022, pp 4565-4580

Society of Production Engineering

ICPES 2025

40th INTERNATIONAL CONFERENCE ON PRODUCTION ENGINEERING - SERBIA 2025

DOI: 10.46793/ICPES25.054S

University of Nis Faculty of Mechanical Engineering

Nis, Serbia, 18 - 19th September 2025

DIMENSIONAL ANALYSIS BASED PREDICTION MODEL OF THE MAIN CUTTING FORCE: COMPARISON AND VALIDATION

Jelena STANOJKOVIĆ[1,*], Miloš MADIĆ[2], Milan TRIFUNOVIĆ[2]

Orcid: 0000-0002-2323-493X; **Orcid:** 0000-0002-2310-2590; **Orcid:** 0000-0002-4653-6957

[1]University of Priština, Faculty of Technical Sciences, Kosovska Mitrovica, Serbia

[2]University of Niš, Faculty of Mechanical Engineering in Niš, Serbia

*Corresponding author: jelena.stanojkovic@pr.ac.rs

Abstract: *Cutting force acting on the cutting tool is an important aspect in machining. Its knowledge provides information about the machinability of the workpiece material and also enables determination of cutting power and cutting energy. Empirical modelling of cutting forces and the development of prediction models remain active area of research. For the purpose of cutting force model development, researchers have used various methods and approaches of various levels of complexity. This study presents the comparison and validation results of the dimensional analysis (DA) based model for the main cutting force prediction. The aim was to demonstrate the applicability of the DA-based cutting force prediction model on different case studies that have used different empirical models of different complexity.*

Keywords: *turning, cutting force, dimensional analysis, prediction, comparison.*

1. INTRODUCTION

Today, machining processes should satisfy all the strictest production requirements, including: productivity, efficiency, machining quality, reliability, and economy. The turning process, as one of the oldest and most widely used machining processes, is still widely used in industry and is a field of research for many researchers [1].

Cutting force plays a key role in the turning process. Knowledge of cutting force is necessary for machine tool manufacturers to assess the requirements for power, bearing loads on machine tools, as well as for designing machine tool elements, cutting tool holders, and fixture assemblies to be sufficiently rigid and to prevent vibrations [2]. Cutting force plays a significant role in improving machining performance, as it affects the tool wear and tool life, surface finish, dimensional accuracy and energy consumption to obtain the final product [3]. Moreover, a priori estimation of cutting forces helps prevent chatter and allows for achieving higher production rates.

Accurate prediction of cutting forces during turning, therefore, becomes an essential factor for process optimization and characterization, and above all for improving machining efficiency [2, 4]. Moreover, monitoring of

cutting forces is often used to detect tool wear and breakage. In the literature, there are various methods and models used for modelling the cutting force [5]. For cutting force estimation in turning, different models are used, ranging from simple analytical models to data-driven models, such as empirical models, FEM models, AI models, as well as hybrid models [6], which combine different modelling paradigms. The aforementioned types of cutting force prediction models differ in complexity, required data for model development, prediction accuracy, interpolation and extrapolation capabilities, interpretability, etc. Empirical models are widely used for predicting cutting force with appropriate accuracy [2, 7]. The estimation of cutting force values based on empirical models is common in practice due to the ease of application and satisfactory accuracy for a wide range of workpiece materials, as well as the interval of variation of the cutting parameters [2].

This paper analyses the applicability of the dimensional analysis (DA) based models for the main cutting force prediction. To this aim, six case studies from the literature, that used different empirical models, different process parameters, different workpiece materials and cutting tools, different types of turning operations etc., were considered for comparison and validation of the proposed DA-based cutting force prediction models.

2. DA - BASED MODEL OF THE MAIN CUTTING FORCE

A model of the main cutting force in turning was developed using an approach based on DA [2], and can be represented by the following equation:

$$F_c = C \cdot R_m \cdot f^2 \left(\frac{v}{v_f}\right)^{x_1} \cdot \left(\frac{a_p}{f}\right)^{x_2} \cdot \left(\frac{\kappa}{\gamma_0}\right)^{x_3} \quad (1)$$

As given in Eq. 1, the main cutting force prediction model considered parameters related to the workpiece material (tensile strength - R_m), machining process (cutting speed - v, feed velocity - v_f, depth of cut -a_p, and feed rate - f), and geometry of the cutting tool (cutting edge angle - κ and rake angle -γ_o) [2].

The unknown coefficients (C, x_1, x_2 and x_3) are to be determined based on experimental data by minimizing the sum of squared errors.

3. CASE STUDIES

Six case studies were considered to validate and compare the prediction results of the DA-based models of the main cutting force. These case studies were taken from the referential literature, and they originally used different types of prediction models for the estimation of the main cutting force in turning of steels (Table 1).

Based on the analysis of results from previous research [2] it was observed that the ratio of the depth of cut and feed rate, which represents the chip slenderness ratio, was the most important parameter affecting the main cutting force. Therefore, by using an experimental design with only 6 trials, for all six case studies, the unknown coefficients (C, x_1, x_2 and x_3) of the DA-based models for predicting the main cutting force were determined. The tensile strength (R_m) values of workpiece materials were taken from the manual [8].

Table 1. Considered case studies

Case study	Model	Exp. trials	Workpiece material	Operation
1	RSM	27	AISI 4340	roughing
2	OLS GP	20	AISI 1045	roughing
3	GPR SVM ANN	60	AISI 4340	roughing
4	FL	27	AISI 1040	roughing
5	Power model	21	C45 KO36 AS12	finishing
6	RSM Kienzle	20	34CrNiMo6	semi-finishing
Ordinary Least Squares (OLS) regression analysis, Genetic programming (GP), Gaussian Process				

Regression (GRP), Support Vector Machine (SVM), Artificial Neural Network (ANN), Fuzzy Logic (FL), Response Surface Methodology (RSM)

4.1 Case Study 1

For case study 1, experimental data from the study of Suresh et al. [9] were used. The authors developed the model of the main cutting force for hard turning of AISI 4340 steel using RSM. The cutting parameters were varied at three levels: cutting speed (v) = [140, 200, 260] m/min, feed rate (f) = [0.1, 0.18, 0.26] mm/rev, depth of cut (a_p) = [0.6, 0.8, 1.0] mm.

The predicted values of the DA-based main cutting force model were compared with the experimentally obtained values to determine the mean absolute percentage error (MAPE). The MAPE value for 6 trials, which were used for estimation of unknown model coefficients, is about 3.02%.

The MAPE values for the RSM model and the DA-based prediction model for the entire experimental plan of 27 trials, as well as the minimum and maximum absolute percentage error of the DA-based prediction model, are shown in Figure 1.

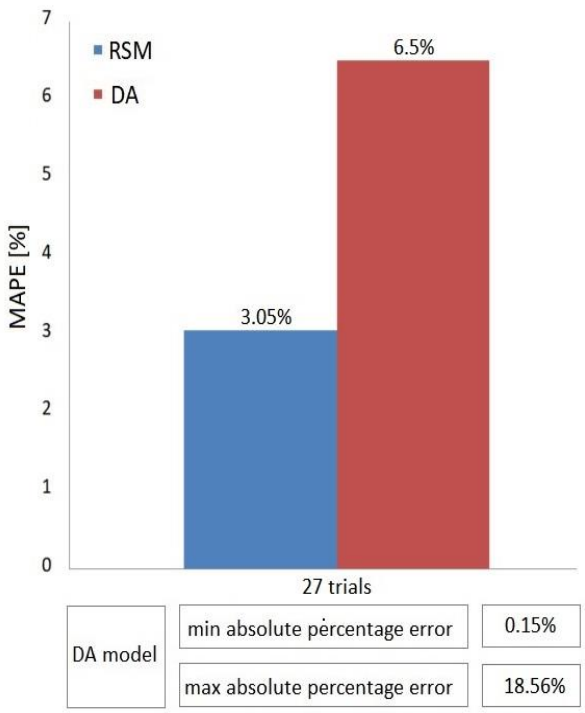

Figure 1. MAPE values of RSM and DA-based model of the main cutting force

Given that selected six trials for estimation of model coefficients considered the same cutting speed, the results indicate that the cutting speed has no significant effect on the main cutting force.

The DA-based model of the main cutting force provides satisfactory results, although the chip slenderness was very low (below 5) in over half of the experimental trials.

4.2 Case Study 2

The experimental study conducted by Cukor and Jurkovic [10] was considered as case study 2. In their study, the authors used OLS regression and GP models for predicting the main cutting force in rough longitudinal turning of AISI 1045 steel. Rotatable central composite design with 20 trials was used to arrange three cutting parameters: cutting speed (v), feed rate (f) and the depth of cut (a_p) at five levels. The predictive capabilities of the developed models were tested with an additional set of 26 experimental trials.

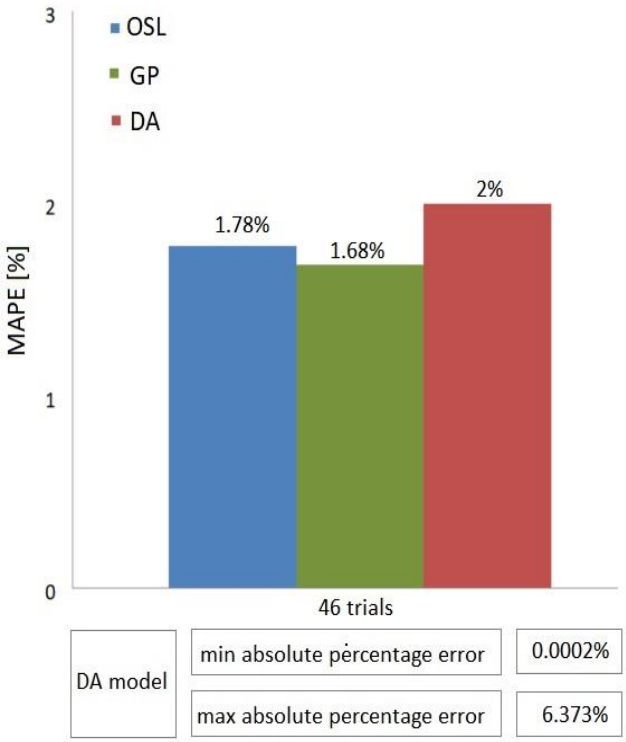

Figure 2. MAPE values of OLS, GP and DA-based models of the main cutting force

The MAPE value of the DA-based prediction model for initial 6 trials is below 0.05% and for

the initial experimental plan with 20 trials is about 2.18%.

The MAPE values for the initial experimental design with 20 trials and an additional set of 26 trials are shown in Figure 2.

Again, the application of the DA-based model in this study showed that the cutting speed doesn't play a decisive role in the prediction of the main cutting force.

4.3 Case Study 3

For case study 3, the experimental study of Alajmi and Almeshal [11] was considered. The authors developed prediction models for the main cutting force in turning of AISI 4340 alloy steel using GPR, SVM and ANN. To this aim, an experimental design with 60 trials was used while considering four input parameters: cutting speed (v) = [75, 90] m/min, feed rate (f) = [0.04, 0.06, 0.08, 0.1, 0.12] mm/rev, depth of cut (a_p) = [0.5, 1.0, 1.5] mm, and tool nose radius (r_ε) = [0.4, 0.8] mm.

The MAPE value of the DA-based prediction model for 6 trials is below 0.05% and for the initial experimental plan with 20 trials is about 2.18%.

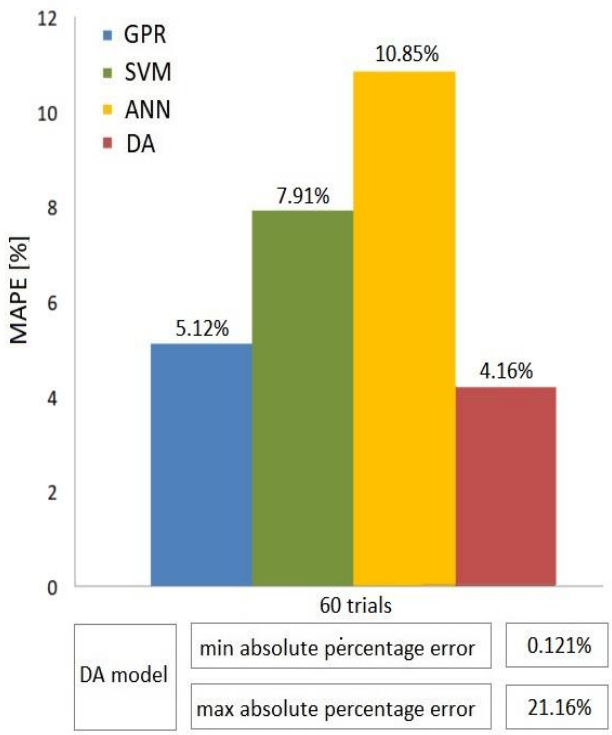

Figure 3. MAPE values of GPR, SVM, ANN and DA-based models of the main cutting force

The MAPE values for the entire 60 trials are shown in Figure 3.

Even though the range of chip slenderness ratio in the experiment was high (from 4 to 37.5) and the effect of tool nose radius was omitted, the DA-based model provided very good prediction results.

4.4 Case Study 4

For case study 4, the cutting force experimental data obtained by Yaldiz et al. [12] were considered. FL model was used in this study for predicting the main cutting force in turning of AISI 1040 steel. In the experiment, three cutting parameters were considered: cutting speed (v) = [96, 143, 203] m/min, feed rate (f) = [0.12, 0.16, 0.2] mm/rev and depth of cut (a_p) = [1.0, 1.5, 2.0] mm.

The MAPE value of the DA-based prediction model for 6 trials is about 2.89 %.

The MAPE values for the entire 27 trials are shown in Figure 4.

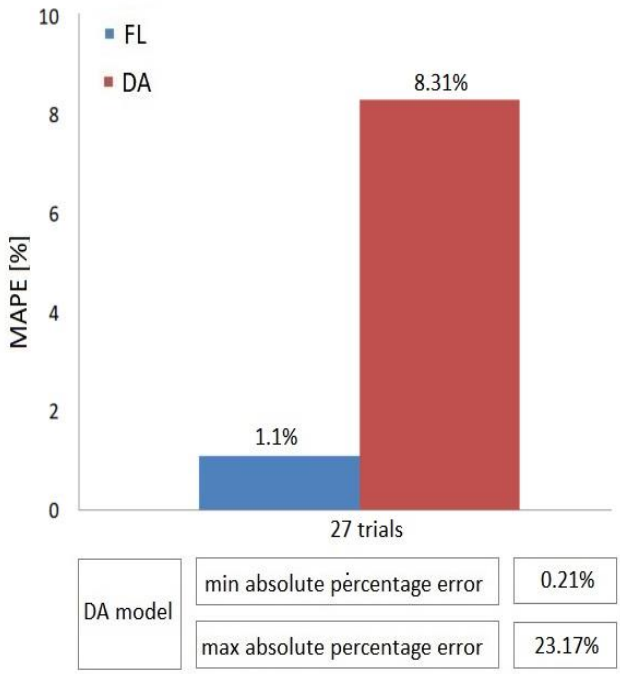

Figure 4. MAPE values of FL and DA-based models of the main cutting force

4.5 Case Study 5

The experimental study conducted by Horvath and Lukacs [13] was considered as case study 5. The authors created the adapted model of cutting force based on the theoretical parameters of the undeformed chip cross-section (h_{eq} is equivalent chip thickness and l_{eff} effective length of the edge of the tool) in fine turning of three different workpiece materials (C45 and KO36 steels and AS12 die-cast aluminum alloy).

The Victor-Kienzle model is suitable for estimating the main cutting force in the case of roughing, where the effect of the nose radius on the chip cross-section is neglected. However, in the case of finishing, where the chip removal takes places primarily not on the side cutting edge, but also on the tool nose radius ($a_p > r_\varepsilon$), or only on the tool nose radius ($a_p << r_\varepsilon$), the abovementioned Victor-Kienzle model cannot be used [13, 14].

The MAPE value of the DA-based prediction model for 6 trials is 2.68% for C45 steel, 4.57% for KO36 steel, and 1.68% for cast aluminum alloy AS12.

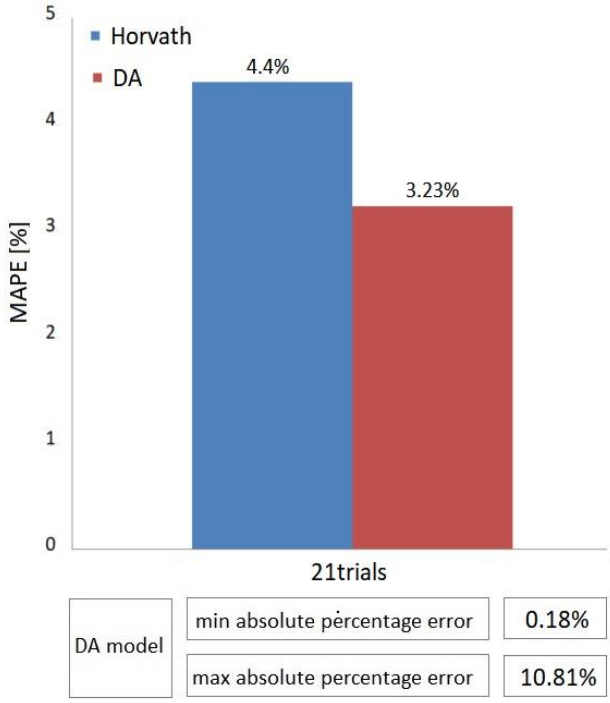

Figure 5. MAPE values of proposed and DA-based models of the main cutting force (C45 steel)

The MAPE values for the entire 21 trials for all workpiece materials are shown in Figures 5-7.

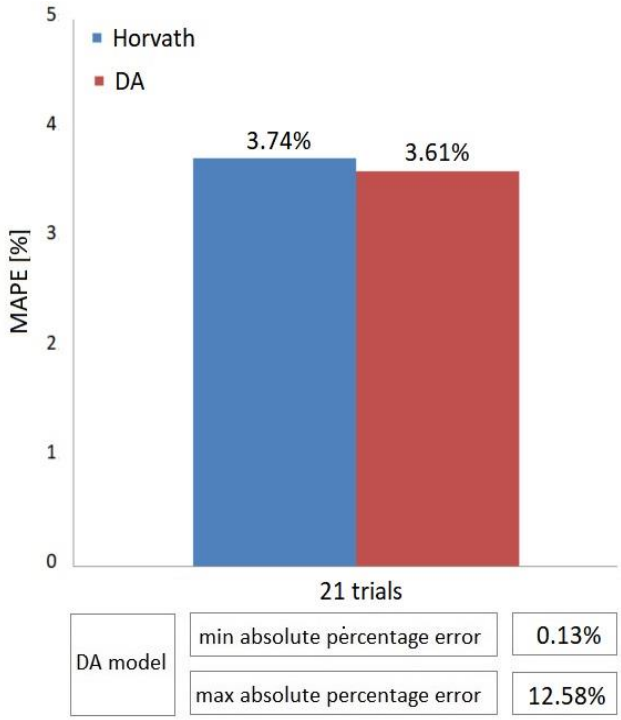

Figure 6. MAPE values of proposed and DA-based models of the main cutting force (KO36 steel)

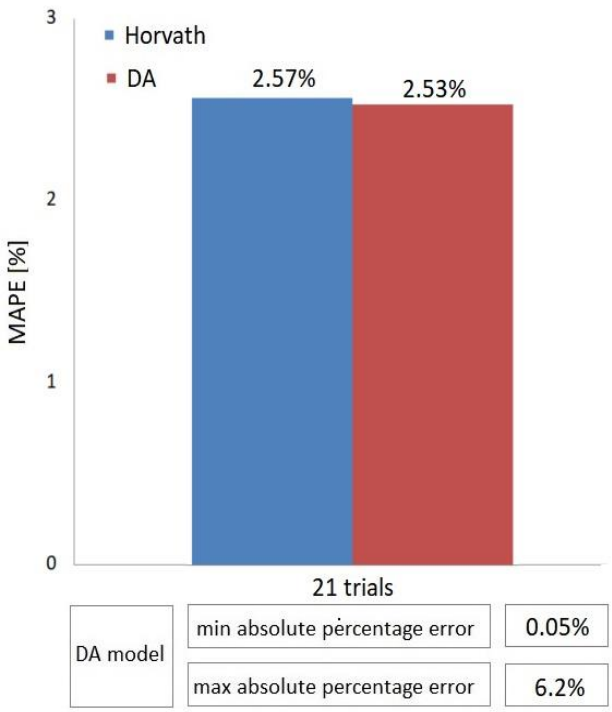

Figure 7. MAPE values of proposed and DA-based models of the main cutting force (cast aluminium AS12)

The DA-based model provided similar results to the newly proposed model for estimating the

main cutting force in finishing based on geometrical parameters, such as equivalent chip thickness and effective cutting length.

4.6 Case Study 6

For case study 6, experimental data from the study of Cebalo et al. [15] were considered. The authors used RSM and well-known Victor-Kienzle models for predicting the main cutting force in semi-finish turning of 34CrNiMo6 steel. The three cutting parameters were varied at five levels: cutting speed (v) = [0.401, 0.821, 1,437, 2.0525, 2.4727] m/s, feed rate (f) = [0.12, 0.16, 0.22, 0.28, 0.32] mm/rev and depth of cut (a_p) = [0.4, 0.6, 0.9, 1.12, 1.4] mm.

The MAPE value of the DA-based prediction model for 6 trials is about 2.04%.

The MAPE values for the entire 20 trials are shown in Figure 8.

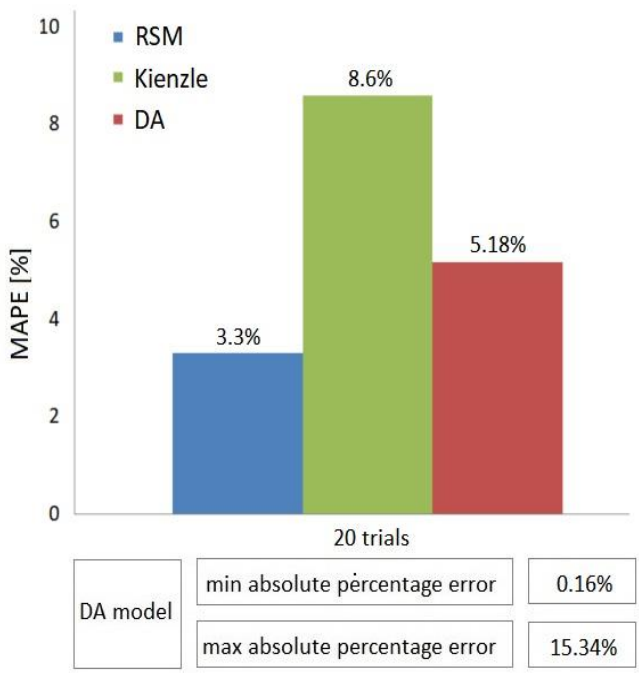

Figure 8. MAPE values of RSM, Victor-Kienzle and DA-based models of the main cutting force

Again, given that selected six trials for estimation of model coefficients considered the same cutting speed, the results indicate minor effect of the cutting speed on the resulting main cutting force.

5. CONCLUSION

This study presents the results of the comparison and validation of the DA-based models for predicting the main cutting force in turning operations. The DA-based models were not developed through a designed experiment, but only using a small fraction of data from previously conducted turning experiments.

From the analysis of the application of DA-based main cutting force prediction models to various case studies, the following conclusions can be drawn:

- In general, the DA-based models at least provide comparable results to other, more complex empirical models. One may argue that power-based models may be sufficient for cutting force modeling in turning.
- The chip slenderness ratio is a significant parameter in the DA-based model and is of essential importance for the prediction of the main cutting force in turning.
- The DA-based model yields good results across a wide range of cutting parameter values, workpiece materials, chip slenderness ratios, and can be applied in roughing, semi-finishing, and even finishing operations, where the removed chip cross-section is significantly smaller compared to roughing.
- The effects of the cutting speed and the tool nose radius on the resulting main cutting force are not so pronounced.

From the stated conclusions, it can be observed that the DA model is easily adaptable for incorporating additional factors that are shown to have a significant influence on the main cutting force. Since the DA approach for predicting the main cutting force in turning uses a smaller number of experimental trials with satisfactory accuracy, it plays an important role with high cost-efficiency ratio, reduced experimentation time, and material and energy savings. The proposed DA-based cutting force models are useful in the planning of technological processes to estimate the

generated cutting force with satisfactory accuracy.

ACKNOWLEDGEMENT

This research was financially supported by the Ministry of Science, Technological Development and Innovation of the Republic of Serbia (451-03-137/2025-03/200109 and 451-03-18/2025-03/200155).

REFERENCES

[1] S. Wang, Z. Tao, D. Wenping, S. Zhanwen: Analytical modeling and prediction of cutting forces in orthogonal turning: a review, The International Journal of Advanced Manufacturing Technology, Vol. 119, pp. 1407-1434, 2022.

[2] J. Stanojković, M. Madić, M. Trifunović, P. Janković, D. Petković: A novel approach to predicting the cutting force in turning using dimensional analysis, Facta Universitatis, Series: Mechanical Engineering, online first, 2025.

[3] L. Tang, Z. Cheng, j. Huang, C. Gao, W. Chang: Empirical models for cutting forces in finish dry hard turning of hardened tool steel at different hardness levels, The International Journal of Advanced Manufacturing Technology, Vol. 76, pp. 691-703, 2015.

[4] B.Y. Lee, Y.S. Tarng: Prediction of specific cutting force and cutting force ratio in turning, Journal of Materials Processing Technology, Vol. 41, No. 1, pp. 71-82, 1994.

[5] R.W. Invester, M. Kenedy, M. Davies, R. Stevenson, J. Thiele, R. Furness, S. Athavale: Assessment of machining models: Progress report, Machining Science and Technology, Vol. 4, No. 3, pp. 511-538, 2020.

[6] S.V.A Laakso, A. Mityakov, T. Niinimäki, K. S. B Ribeiro, W.M. Bessa: Hybrid FE-ML model for turning of 42CrMo4 steel, CIRP Journal of Manufacturing Science and Technology, Vol. 55, pp. 333-346, 2024.

[7] J. Stanojković, M. Madić, D. Lazarević: *Empirical modeling methods of turning process: a review*, 18th International Conference on Tribology, 17-19.05.2023. Kragujevac, Serbia.

[8] M. Kalajdžić, Lj. Tanović, B. Babić, M. Glavonjić, Z. Miljković, R. Puzović, B. Kokotović, M. Popović, S. Živanović, D. Tošić, I. Vasić: Tehnologija obrade rezanjem-Priručnik, IX izdanje. Mašinski fakultet u Beogradu, Beograd, 1999.

[9] R. Suresh, S. Basavarajappa, G.L. Samuel: Some studies on hard turning of AISI 4340 steel using multilayer coated carbide tool, Measurement, Vol. 45, No. 7, pp. 1872-1884, 2012.

[10] G. Cukor, Z. Jurković,: Optimization of turning using evolutionary algorithms, Engineering Review, Vol. 30, No. 2, pp. 1-10, 2010.

[11] M.S. Alajmi, A.M. Almeshal: Modeling of cutting force in the turning of AISI 4340 using Gaussian Process Regression Algorithm, Applied Sciences, Vol. 11, No. 9, 4055, 2021.

[12] S. Yaldiz. F. Unsacar, H. Saglam: Comparison of experimental results obtained by designed dynamometer fo fuzzy model for predicting cutting force in turning, Materials and Design, Vol. 27, pp. 1139-1147, 2006.

[13] R. Horváth, J. Lukács: Application of a Force model adapted for the precise turning of various metallic materials, Journal of Mechanical Engineering, Vol. 63, No. 9, pp. 489-500, 2017.

[14] R. Horváth: A new model for fine turning forces, Acta Polytechnica Hungarica, Vol.12, No. 7, pp. 109-128, 2015.

[15] R. Cebalo, D. Bajić, B. Bilić: *Mathematical modelling of cutting force in the longitudinal turning process*, 10th International Scientific Conference on Production Engineering, 15-17.06.2025, Croatia, pp. 131-140.

Society of Production Engineering

ICPES 2025

40th INTERNATIONAL CONFERENCE ON PRODUCTION ENGINEERING - SERBIA 2025

DOI: 10.46793/ICPES25.062S

University of Nis Faculty of Mechanical Engineering

Nis, Serbia, 18 - 19th September 2025

MODELLING AND CUTTING PARAMETER OPTIMISATION OF THE INCONEL 718 MICROMILLING PROCESS

Branislav SREDANOVIĆ[1]*, Gordana GLOBOČKI LAKIĆ[1], Jelena MARKOVIĆ[1], Dejan VUJASIN[1], Davorin KRAMAR[2]

Orcid: 0000-0003-0618-8596; **Orcid:** 0000-0001-8143-4406; **Orcid:** 0009-0001-3608-4213; **Orcid:** 0009-0008-4181-9190; **Orcid:** 0000-0002-1323-4514

[1]University of Banja Luka, Faculty of Mechanical Engineering, Banja Luka, Bosnia and Herzegovina

[2]University of Ljubljana, Faculty of Mechanical Engineering, Ljubljana, Slovenia

*Corresponding author: branislav.sredanovic@mf.unibl.org

Abstract: *Micromachining is taking an increasing area in the mechanical engineering and production technologies. Understanding the workpiece material mechanical removal process during micromilling is one of the main tasks on the way to successful optimization and control of the cutting process. In this paper, the micromilling process of the superalloy Inconel 718 is analysed. This superalloy has low machinability, due to its special mechanical and chemical properties. In the framework of the experimental research, the depth of cut and feed per tooth were varied on tree level, while the milling width and cutting speed were kept at the constant level. Based on the experimental data, a significant influence of the depth of cut and feed per tooth on the cutting forces, and the feed per tooth on the roughness of the machined surface was observed. Using logarithmic transformation and the least squares method, exponential models with sufficient response accuracy were developed. Using the models, the input cutting process parameters were optimized using the classical gradient method. Optimization resulted in parameters that ensure maximizing the quality of the machined surface and minimizing dimensional errors.*

Keywords: *micromilling, super-alloy, roughness, accuracy, analysis, modelling.*

1. INTRODUCTION

Microcomponents, i.e. parts with at least two perpendicular dimensions below 1 mm, are occupying an increasingly significant area of the global industrial market [1]. The use of special materials for microcomponents manufacturing, such are heat-treated steels, superalloys, aluminium alloys, composites, etc., contributes to enhanced reliability and functionality under extremal exploitation conditions. On the other hand, mentioned materials are characterized by difficulties in machining. The high efficiency and success of the machining process depend on the workpiece material properties largely. These market trends are

accompanied by increasingly strictly demands for development of new, and improvement of existing micromachining methods and processes.

The micromilling process enables rough, semi-finish, and finish machining of metallic microcomponents. Due to the complex kinematics of relative movements, it allows for relatively more flexible process, and more productive manufacturing of microparts with complex geometries. Compared to other production methods, micromilling provides relative high machined surface quality, high dimensional accuracy, avoidance of thermal effects on the part surface layers which are typical for non-conventional methods, and etc.

The mechanism of mechanical workpiece material removal process, and consequently, the dependence of cutting process output parameters differs between machining on macro and micro level significantly. In microcutting process, a phenomenon known as the size effect occurs (Figure 1).

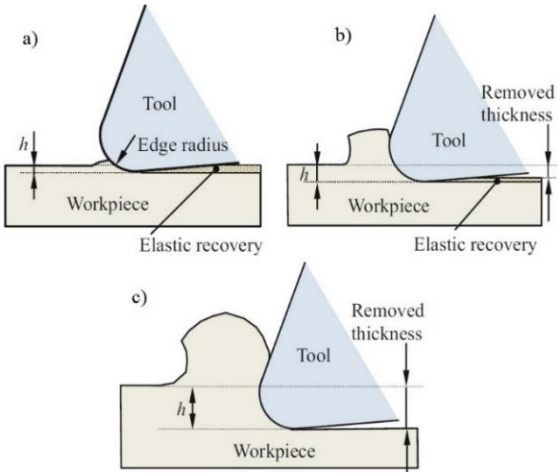

Figure 1. Size effect [2]

This effect refers to the disproportion between the technological cutting process parameters and the cutting tool geometrical parameters, as well as the workpiece material crystal structure. As a result of the size effect, the workpiece material ploughing phenomenon becomes increasingly significant during machining, and cannot be neglected.

In accordance with the above, it can be concluded that the special alloys micromilling process efficiency depends on the synergistic interaction between cutting process parameters, cutting tool properties, and machining conditions [3, 4]. The analysis of performance and the characterization of micromilling process behaviour indicators is one of the key factors in achieving maximum machining efficiency. At the microscale, the influence of indicators, such as surface roughness and dimensional accuracy on the functionality of microcomponents becomes even more pronounced. The key performance indicators of the machining process include factors connected to machined surface quality, part dimension accuracy, process productivity and economy, ecology, and similar factors.

Numerous scientific studies have focused on the analysis, modelling, and optimization of the special alloys micromilling process, with the aim of establishing a foundation for production process control, and achieving the required part properties. These studies have examined the influence of machining parameters, cutting tool properties, and cooling strategies on the machining process indicators that define the microcomponent quality and accuracy, as well as on the productivity, cost-efficiency, and environmental sustainability of the cutting process. In [5], the micromilling of Inconel 718 alloy was analysed. A dynamic analysis was performed, and a part deformation model based on cutting forces was established. Authors developed surface roughness model connected to tool deformation. In [6], experimental analysis and modelling of deformation in thin-walled microcomponents was conducted. Appropriate wall deflection models were

developed using the so-called birth/death technique. Lu et al. [7] employed a Taguchi experimental design to modelling the effect of cutting process parameters on surface roughness and material removal rate. The developed first-order models served as the basis for genetic algorithm optimization. The study identified depth of cut as the most influential factor affecting surface roughness. In [8], the influence of cutting process parameters and various tool coatings on the surface topography of Inconel 718 was investigated. Similar to the previous study, a significant impact of both depth of cut and cutting speed was observed. In addition to cutting process parameters, also considered the initial surface condition of the workpiece in [9]. Among other findings, the study revealed that the initial surface condition significantly affects the final surface roughness. The results also indicated that high tool loading leads to poorer surface quality and increased tool wear. In [10], the influence of process and tool parameters on the geometry of the dead metal zone and cutting forces was examined. The authors developed mechanistic models, which were then integrated into a finite element micromilling model. The analysis showed a significant influence of feed per tooth and cutting edge radius on cutting forces. Kiswanto et al. [11] studied micromachining of Inconel 718 at low cutting speeds. They found a notable influence of both feed per tooth and cutting speed on surface roughness. A comprehensive experimental performance analysis of the micromilling process for Inconel 718 was conducted in [12]. There are highlighting the significant impact of milling parameters and cooling strategies on process performance. Liang et al. [13] analysed and optimized micromilling performance using a finite element method model to simulate chip formation, and to conclude the output cutting parameters values.

The aim of this research is to analyse the machining quality and accuracy in the micromilling of Inconel 718. The focus is placed on the development of appropriate mathematical models that describe the influence of cutting process input parameters on dimensional accuracy and surface quality indicators. Furthermore, the goal is to use the developed models as a basis for the cutting parameters optimization. Machining time is analysed in order to provide a reference for the micromilling process productivity, and comparison with other manufacturing methods.

2. EXPERIMENTAL SETUP

For experimental setup machining centre Sodick MC430L with LN2X control was used (Figure 2). It is three axis micro-milling CNC tool machine, with high speed main spindle. In experiments was used coated two flute extra-long end micro-mill cuter, with diameter of 600 µm, and neck length of 8 mm. Its cutting edge length is 0.8 mm, helix revolution angle is 7.25°, and tool tip corner radius 0.05 mm. Cutting tool was mounted in HSK holder.

Workpiece was nickel-chromium super alloy Inconel 718, with tensile strength 1350 MPa, and hardness 40 HRc. Its chemical composition consist next chemical elements: 53% Ni, 19% Cr, 18% Fe, 5.1% Nb, 3% Mo, 1.1% Ti, 1% Co, 0.5% Al, 0.35% Si, and 0.08% C). Inconel has excellent oxidation and high temperature resistance. Regard to this, it is used for responsible mechanical parts that operates in extreme mechanical and thermal conditions.

As experimental plan full factorial plan is used [14]. Two controlled milling process input parameters, was used: depth of cut a_p (mm), and feed per tooth f_z (mm/tooth),

each on tree level. Varied values of depth of cut were: 0.01, 0.02, and 0.03 mm. Varied values of feed per tooth were: 0.008, 0.012, and 0.018 mm/tooth.

Figure 2. Experimental setup

Experimental plan was results in nine experimental combinations (runs). Cutting speed was set to constant value of v_c = 40 m/min (spindle speed n = 21222 rev/min), and milling width of 0.6 mm. Microchannel milling was used for each experimental run. Channel was 10 mm long. MQL technique was used for lubrication of cutting zone. The synthetic oil aerosol was supplied under flow ratio of Q = 25 ml/h, and pressure of p = 5 bar.

For measuring of cutting force component Kistler 9257B dynamometer was used. It was mounted on machine table, and aligned with the axis of the tool machine. Measuring axis for cutting force component F_y is directed in milling tool auxiliary movement. Cutting force signals were collected using A/D devices and *LabView* software. Measuring of surface roughness was performed on *Alicona Infinite Focus SL* device optical scanning device. It measures according to the standard ISO 4287. This device work on principle photographing of machined surface with focus variations, and image sharped regions separating. Based on separated regions on images, algorithm generates a three-dimensional representation of scanned surface, on micro-level resolution. Experimental and measuring data processing, statistical analysis, model development, and optimization were carried out using Design Express 7 software.

3. RESULTS AND DISCUSSION

On Figure 3, the dependence of F_x cutting force component values on the variation of feed per tooth and depth of cut is shown. It can be observed that cutting forces component increase with the increase of both depth of cut and feed per tooth. For the smallest depth of cut value, the cutting force component exhibits an almost linear dependence on the feed per tooth. However, at higher depths of cut, a nonlinear relationship becomes evident. At lower feed per tooth values, the cutting forces component values that corresponding to minimum and medium depth of cuts are relatively close. On the other hand, at higher feed per tooth values, the cutting forces component values associated with medium and maximum depth of cuts are closer in values.

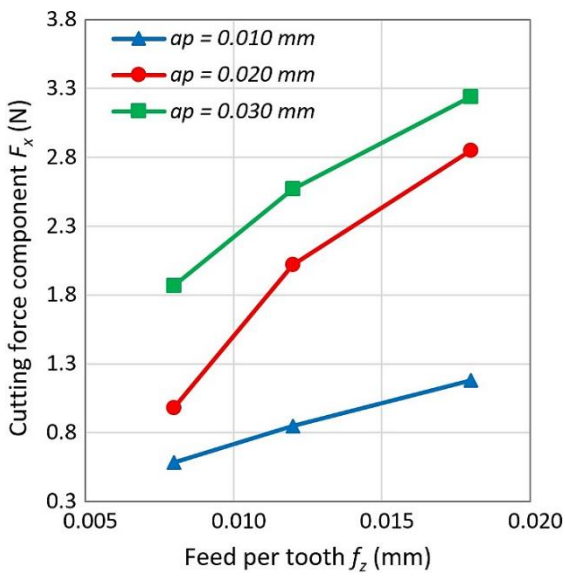

Figure 3. Cutting force component F_x

Similar conclusions can be noted for the F_y cutting force component, as cutting force component that acts along the direction of the cutting tool auxiliary movement, by examining the dependency diagram shown in Figure 4. A relative more uniform variation of the cutting force component values, with respect to changes in the depth of cut, can be observed. Similar to previous, at lower feed per tooth values, the cutting forces component values that corresponding to minimum and medium depth of cuts are relatively close. At higher feed per tooth values, the cutting forces component values have a more uniform difference.

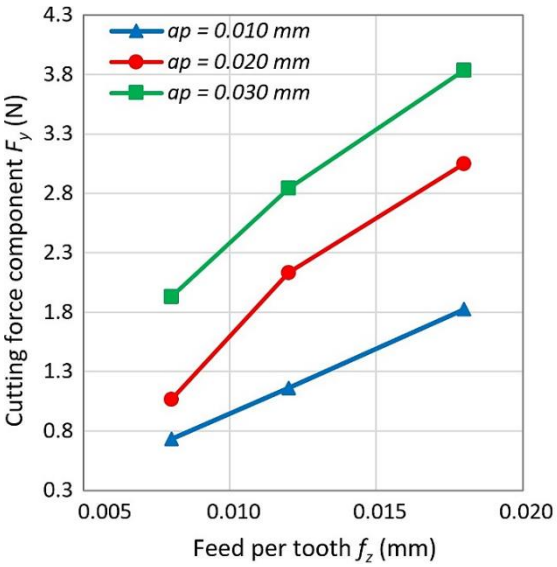

Figure 4. Cutting force component F_y

For cutting force values, it is evident that both analyzed components increase with the increase of depth of cut and feed per tooth. However, an increase in these cutting process parameters leads to a larger uncut chip cross-section area. As the uncut chip cross-section area increases, so the force required for chip mechanical separation increases. The influence of depth of cut, and especially feed per tooth cannot be considered as linear. This is consequences of mechanistic and the complex thermo-mechanical phenomena occurring in the cutting zone. During microcutting process, not only mechanical chip separation occur, but also material deformation through the ploughing mechanism, which is primarily caused by the size effect.

The influence of depth of cut and feed per tooth on the average surface roughness height R_a is shown on the diagram in Figure 5. Analysis of the diagram reveals a significant impact of feed per tooth on mentioned output parameter. In most cases, an increase in feed per tooth results in a sudden increase in surface roughness. Changes in depth of cut do not lead to sudden variations in surface roughness. Although minimal, the effect of depth of cut varies depending on the feed per tooth value. As can be observed, at different feed levels, maximum surface roughness occurs at different depth of cut values. At the lowest feed per tooth, the maximum surface roughness is recorded at a medium depth of cut. At this point, the maximum of surface roughness parameter value deviates significantly from the values that corresponding to the other two depth of cut levels. At the medium feed per tooth, the highest surface roughness occurs at the smallest depth of cut, while at the maximum feed per tooth, it is observed at the maximum depth of cut value.

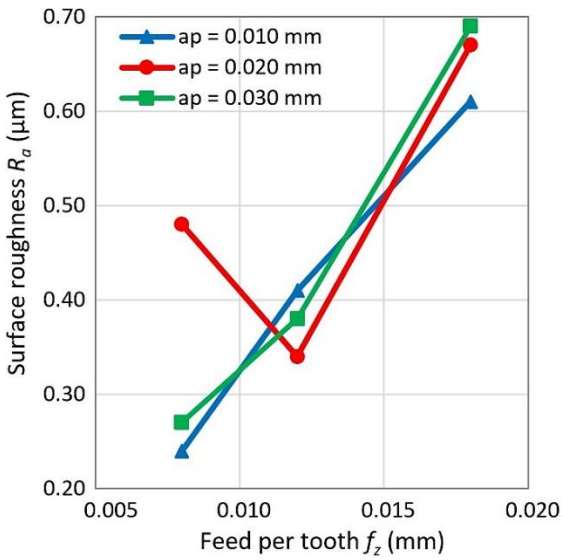

Figure 5. Surface roughness R_a

Previous concluded variations in the influence of feed per tooth and depth of cut on average surface roughness height, can be attributed to the pronounced influence of the size effect. It becomes more significant at lower uncut chip thicknesses, i.e., at lower feed per tooth values. Size effect may also be intensified by the disproportion between the feed per tooth and depth of cut values. Such significant variations and data dispersion can lead to difficulties in the mathematical modelling of the influence of cutting process parameters on the process output indicators.

3.1 Modelling and optimisation

As the initial model function that describing the influence of input parameters on the output variables of the micromilling process, an exponential function was selected. This function includes one coefficient and exponents of the two input variables: depth of cut and feed per tooth. For the purpose of determining the model coefficient and exponents, the initial function was linearized to enable the application of the least squares method.

Based on experimentally obtained data, a model for the cutting force component in the direction perpendicular to the cutting tool auxiliary movement F_x [N] was developed. It is mathematical function with variables depth of cut a_p [mm], and feed per tooth f_z [mm/tooth]:

$$F_x = 5892 \cdot a_p^{1.005} \cdot f_z^{0.953} \quad (1)$$

A statistical analysis of variance (ANOVA) was conducted based on the experimental data and the response of the developed model. Based on the p-values, the model was determined to be significant, with a notable significant influence of depth of cut and feed per tooth (Table 1). The given abbreviations refer to statistical next parameters: sum of squares (SoS), degree of freedom (DoF), and mean square (MSQ).

Table 1. Statistical parameters for F_x model

Source	SoS	DoF	MSQ	*t* value	*p* value
Model	2.77	2	1.38	79.92	< 0.0001
ln (f_z)	1.87	1	1.87	108.13	< 0.0001
ln (a_p)	0.90	1	0.90	51.71	0.0004
Residual	0.10	6	0.017		
Total	2.87	8			

Mean value of data is $\bar{x}$ = 1.79, and standard deviation of *SD* = 1.01. Coefficient of determination is R^2 = 0.97, and signal to noise value is *S/N* = 24.7. Model response mean absolute percentage error is *MAPE* = 8%. Based on previous statistical parameters, can be concluded that model is adequate. Model response diagraph is given on Figure 6.

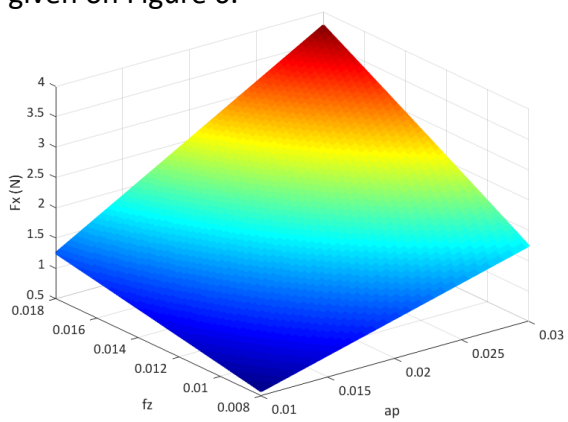

Figure 6. Response of F_x model

Following a same procedure, a model was developed for the cutting force component in the direction of the cutting tool auxiliary movement F_y [N]. Model is in form of mathematical function with

variables depth of cut a_p [mm], and feed per tooth f_z [mm/tooth]:

$$F_y = 5244 \cdot a_p^{0.784} \cdot f_z^{1.090} \quad (2)$$

The results of the statistical analysis of the model and variables significance are presented in Table 2. Based on the given data, a significant influence of both depth of cut and feed per tooth can be concluded.

Table 2. Statistical parameters for F_y model

Source	SoS	DoF	MSQ	*t* value	*p* value
Model	2.31	2	1.15	116.81	< 0.0001
ln (f_z)	1.14	1	1.14	115.05	< 0.0001
ln (a_p)	1.17	1	1.17	118.58	< 0.0001
Residual	0.059	6	$9.9 \cdot 10^{-3}$		
Total	2.37	8			

The other determined statistical parameters are: mean value of $\bar{x}$ = 2.07, standard deviation of *SD* = 1.09, coefficient of determination of R^2 = 0.98, signal to noise value of *S/N* = 30.4. Model response mean absolute percentage error is *MAPE* = 6%. On Figure 6 is shown model response diagraph.

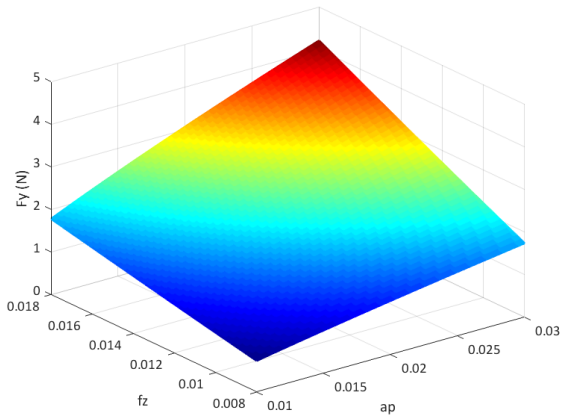

Figure 7. Response of F_y model

The surface roughness model was developed using the previous procedure. Statistical analysis showed that the depth of cut doesn't have a significant effect on the values of R_a. To avoid large model errors and low correlation between experimental data and corresponding model responses, the depth of cut, was excluded from the model. Consequently, model of R_a [µm] is obtained, and depends on feed per tooth f_z [mm/tooth]:

$$R_a = 23.46 \cdot f_z^{0.916} \quad (3)$$

Statistical parameters values for surface roughness parameter are given in Table 3. It is evident that feed per tooth has a statistically significant influence on model responses.

Table 3. Statistical parameters for *Ra* model

Source	SoS	DoF	MSQ	*t* value	*p* value
Model	0.81	1	0.81	15.19	0.0059
ln (f_z)	0.81	1	0.81	15.19	0.0059
Residual	0.37	7	0.053		
Total	1.18	8			

Based on obtained data, there are calculated: mean value of $\bar{x}$ = 0.43, standard deviation of SD = 0.13, coefficient R^2 = 0.87, signal to noise value of S/N = 6.75. Surface roughness model response has *MAPE* = 13%. Despite a slightly higher model response error, it can be concluded that the previous model is adequate. Model response graph is shown on Figure 8.

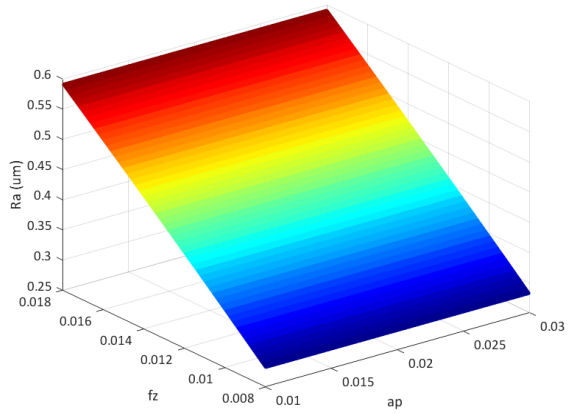

Figure 8. Response of R_a model

In addition to the previously mentioned output parameters of the micromilling process, the machining time was also taken into consideration. There, it is referred to the time required to machining of the one micro-channel. The machining time t_c [min] was obtained through analytical calculation, as the ratio of the channel length to the feed rate. The feed rate is the product of the cutter teeth number, feed per tooth, and spindle speed.

The optimization was carried out with the aim of minimizing dimensional error during machining and maximizing the quality of the machined surface. Minimization of machining time was considered as an objective also. The mathematical framework for the process parameters optimization is shown in Table 4.

Table 4. Optimization framework

Name	Goal	Limit		Weight	
		Lower	Upper	Low	Up
a_p	in range	0.010	0.030	1	1
f_z	in range	0.008	0.018	1	1
ln (R_a)	minimize	-1.4271	-0.3711	1	1
ln (F_x)	minimize	-0.5361	1.1756	1	1
ln (F_y)	minimize	-0.3119	1.3444	1	1
ln (t_c)	minimize	-0.2416	0.5693	1	1

Indirectly, minimizing dimensional accuracy was represented as the minimization of tool deflection, i.e., cutting forces. Maximizing quality was expressed as the minimization of surface roughness. All input parameters and their domains boundaries were assigned equal importance. According to the previously, it is clear that the minimization of machining time is in opposite with the minimizing of cutting forces and maximizing of surface quality [1]. The optimization was performed using the gradient method, which gave ten possible solutions. The optimal results of the process parameters were obtained as follows: depth of cut a_p = 0.010 mm, and feed per tooth f_z = 0.011 mm/tooth. Optimisation aims achievement is 61%. The optimization results desirability diagram, with respect to the values of the input process parameters, is shown in Figure 9.

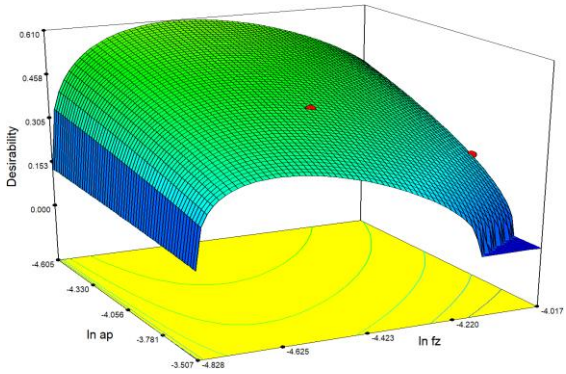

Figure 9. Desirability of results in optimisation

4. CONCLUSION

This paper presents an experimental study of the superalloy Inconel 718 micromilling. The experimental research was conducted with the aim of analysing the influence of depth of cut and feed per tooth on the micromilling process performance indicators. There are measured and analysed the cutting force component in the cutting tool auxiliary movement direction, and the cutting force component perpendicular to mentioned direction. The average surface roughness height was analysed also.

Based on the experimental data, and using the least squares method, models were developed. Statistical analysis shown a significant influence of the input cutting parameters on the process indicators. Depth of cut, and feed per tooth have significantly influence on cutting forces. Surface roughness was influenced by the feed per tooth.

Based on the models, optimization of the input parameters was performed. The obtained optimal process parameters were depth of cut of a_p = 0.010 mm, and feed per

tooth of f_z = 0.011 mm/tooth. Future research is planned to investigate the influence of other process parameters and conditions, as well as different modelling and optimization methods.

REFERENCES

[1] K. Cheng, D. Huo, *Micro-Cutting: Fundamentals and Applications*, John Wiley and Sons, New York, 2013. https://doi.org/10.1002/9781118 536605

[2] J. Chae, S.S. Park, T. Freiheit, Investigation of micro-cutting operations, International Journal of Machine Tools and Manufacture, Vol. 46, No. 3-4, pp. 313–332, 2006. https://doi.org/10.1016/j.ijmachtools.2005.05.015

[3] D. Serje, J. Pacheco, E. Diez, Micromilling research: current trends and future prospects, The International Journal of Advanced Manufacturing Technology, Vol. 111, pp. 1889-1916, 2020. https://doi.org/10.1007/s00170-020-06205-w

[4] N. Ullah, M. Rehan, M.U. Farooq, H. Li, W.S. Yip, S.S. To, A comprehensive review of micro-milling: fundamental mechanics, challenges, and future prospective, The International Journal of Advanced Manufacturing Technology, Vol. 137, pp. 4309-4351, 2025. https://doi.org/10.1007/ s00170 -025-15388-z

[5] X. Lu, X. Hu, Z. Jia, M. Liu, S. Gao, C. Qu, S.Y. Liang, Model for the prediction of 3D surface topography and surface roughness in micro-milling Inconel 718, The International Journal of Advanced Manufacturing Technology, Vol. 94, pp. 2043-2056, 2018. https://doi.org/10.1007/s00170-017-1001-y

[6] Z. Jia, X. Lu, H. Gu, F. Ruan, S.Y. Liang, Deflection prediction of micro-milling Inconel 718 thin-walled parts, Journal of Materials Processing Technology, Vol. 291, 7003, 2021. https://doi.org/10.1016/j.jmatprotec.2020.117003

[7] X. Lu, F. R. Wang, L. Xue, Y. Feng, S. Y. Liang, Investigation of material removal rate and surface roughness using multi-objective optimization for micro-milling of Inconel 718, Industrial Lubrication and Tribology, Vol. 71, No. 6, pp. 787-794, 2019. https://doi.org/ 10.1108/ILT-07-2018-0259

[8] A. Muhammad, M.K. Gupta, T. Mikołajczyk, D.Y. Pimenov, K. Giasin, Effect of tool coating and cutting parameters on surface roughness and burr formation during micromilling of Inconel 718, Metals, Vol. 11, No. 1, 167, 2021. https://doi.org/10.3390/met11010167

[9] D. de Oliveira, M. Ziberov, R.L. de Paiva, M. B. da Silva, An experimental evaluation of cutting parameters influence on the surface integrity and tool wear mechanisms on the dry micromilling of austenitic alloy Inconel 718, Wear, Vol. 571, 205789, 2025. https://doi.org/10.1016/j.wear.2025.205789

[10] K.V. Rao, B.H. Babu, V.U.V. Prasad, A study on effect of dead metal zone on tool vibration, cutting and thrust forces in micro milling of Inconel 718, Journal of Alloys and Compounds, Vol. 793, pp. 343-351, 2019. https://doi.org/10.1016/j.jallcom.2019.04.194

[11] G. Kiswanto, M. Azmi, A. Mandala, T.J. Ko, The effect of machining parameters to the surface roughness in low speed machining micro-milling Inconel 718, IOP Conference Series: Materials Science and Engineering, Vol. 654, 012014, 2019. https://doi.org/10.1088/1757-899X/654/1/012014

[12] M. Gueli, J. Ma, N. Cococcetta, D. Pearl, M.P. Jahan, Experimental investigation into tool wear, cutting forces, and resulting surface finish during dry and flood coolant slot milling of Inconel 718, Procedia Manufacturing, Vol. 53, pp. 236-245, 2021. https://doi.org/10.1016/j.promfg.2021.06.026

[13] J. Liang, X. Cheng, Y. Tian, W. Wang, Q. Yang, Z. Mu, J. Sun, M. Tang, Study on the chip morphology and machining quality of micro helical milling of superalloy small holes, Materials Today Communications, Vol. 43, 111834, 2025. https://doi.org/10.1016/j.mtcomm.2025.111834

[14] B. Sredanović, D. Cica, S. Borojevic, S. Tesic, D. Kramar, Optimization of superalloy Inconel 718 micro-milling process by combined Taguchi and multi-criteria decision making method, Journal of the Brazilian society of mechanical sciences and engineering, Vol. 46, pp. 1 - 14, 2024. https://doi.org/10.1007/s40430-024-04996-7

Society of Production Engineering

ICPES 2025

40th INTERNATIONAL CONFERENCE ON PRODUCTION ENGINEERING - SERBIA 2025

DOI: 10.46793/ICPES25.072G

University of Nis
Faculty of Mechanical Engineering

Nis, Serbia, 18 - 19th September 2025

ELECTROMAGNETIC FIELD ANALYSIS AND PREDICTIVE MODELING IN FIBER LASER CUTTING OF REFRACTORY STEELS

Constantin CRISTINEL GIRDU[1], Miloš MADIĆ[2], Catalin GHEORGHE[3*], Daniel LATEȘ[4], Bogdan CĂTĂLIN IACOB[5]

Orcid: 0000-0002-4653-6957; **Orcid:** 0000-0002-2310-2590; **Orcid:** 0000-0003-4090-1439,

[1]Department of Manufacturing Engineering, Transilvania University of Brasov, Eroilor Street 29, 500036 Brasov, Romania

[2]Faculty of Mechanical Engineering, University of Niš, A. Medvedeva 14, 18000 Niš, Serbia

[3]Department of Engineering and Industrial Management, Transilvania University of Brasov, Eroilor Street 29, 500036 Brasov, Romania

[4]IRUM SA, Axente Sever 6, 545300 Reghin, Romania

[5]Oltenia Energy Complex SA, Alexandru Ioan Cuza 5, 210140 Targu-Jiu, Romania

*Corresponding author: gheorghe.c@unitbv.ro

Abstract: *This study presents a theoretical and experimental framework for modelling the electromagnetic field generated by a high-power fiber laser beam and for predicting the hardness variations in refractory steels subjected to laser cutting. Based on Maxwell's equations, a mathematical model is developed to describe the propagation of electric and magnetic fields in space and time, linking beam parameters, such as power, focal position, and cutting speed, with the physical characteristics of laser radiation. This theoretical foundation is applied to analyse the behaviour of an X10AlCr180 alloy, commonly used in high-temperature industrial applications. Changes in hardness within the heat-affected zone after oxygen-assisted laser cutting are investigated. Experimental data are statistically processed, and a quasi-linear predictive model is developed, achieving a determination coefficient* R^2*= 99.52%. The results indicate that laser power and focal position have the most significant influence on hardness. This work highlights the relevance of integrating electromagnetic wave theory with thermal-material interactions in advanced manufacturing processes.*

Keywords: *fiber laser cutting; electromagnetic field modelling; refractory steels; hardness.*

1. INTRODUCTION

High-power laser cutting is one of the most advanced methods for processing metallic materials, highly valued for its precision, speed, and adaptability to challenging materials such as refractory steels. Controlling the surface quality and post-cutting mechanical properties is essential in critical industrial applications, such as steam boiler components or energy system installations.

In this context, the alloyed steel X10AlCr180 is frequently used due to its excellent resistance to high temperatures and corrosion. However, its behaviour during laser cutting presents challenges related to

microstructural changes and the reduction of hardness in the heat-affected zone (HAZ). Several studies have shown that the choice of technological parameters, such as laser power, cutting speed, and focal position, directly influences the mechanical characteristics of the processed surfaces [1], [2].

To optimize the cutting process, recent research has employed methods such as statistical modeling using RSM (Response Surface Methodology) [3], artificial intelligence algorithms [4], or multi-objective optimization techniques [5]. Nevertheless, few studies address the phenomenon from a fundamental perspective, starting with the modelling of electromagnetic field propagation generated by the laser beam, based on Maxwell's equations [6]. For instance, Turkkan et al. (2023) applied a multi-objective optimization using Taguchi methods and Grey Relational Analysis for laser cutting of AISI 304L stainless steel, identifying duty cycle and frequency as the most influential parameters for reducing roughness and kerf width [7].

This study proposes an integrated theoretical–experimental approach, combining mathematical modelling of the electromagnetic field generated by the laser beam with the analysis of the hardness of X10AlCr180 steel after fiber laser cutting. Quasi-linear predictive equations for hardness are formulated and empirically validated based on a factorial experimental design with eight processing variants, using a BySmart Fiber Bystronic laser cutting machine. The correlation of theoretical and experimental results provides a comprehensive view of the influence of cutting parameters on the material's hardness, thus contributing to the optimization of the process applied to advanced steels. According to Pimenov et al. (2023), heat-resistant steels with complex structures and high alloying element content (Cr, Ni, Al) are considered difficult-to-machine materials, requiring the use of advanced technologies such as high-precision laser cutting [8].

2. LITERATURE REVIEW

2.1. Optimization of technological parameters in laser cutting

Fiber laser cutting has gained significant traction in the processing of advanced materials due to its ability to deliver high-precision cuts, minimized HAZ, and precise control over microstructural changes. Numerous studies have highlighted the direct influence of technological parameters, particularly laser power, cutting speed, and focal position, on local hardness, surface topography, and mechanical behaviour of the processed material [9].

Research on structural steels has shown that varying these parameters can significantly alter the hardness within the heat-affected zone. For example, Safari et al. demonstrated that in Hardox 400 steel, process optimization can be effectively achieved using robust statistical models that reveal the sensitivity of HAZ hardness to changes in process parameters [1]. Similarly, Yurdakul et al. combined the RSM methodology with the Analytic Hierarchy Process, resulting in an efficient multicriteria framework for optimizing the cutting of St-52 steel [2].

Advancements in artificial intelligence have introduced new tools for modelling the complex relationships within the cutting process. Sket et al. implemented neural networks to predict thermal and geometric behaviour in stainless steels, achieving better performance than traditional regression models [3]. Other approaches focused on improving experimental data distribution through methods like Latin Hypercube Sampling, contributing to more effective calibration of predictive models [4].

For difficult to cut materials such as 904L super-austenitic steel, Balasubramaniyan and Rajkumar (2025) showed that simultaneous optimization of laser power, feed rate, and

pulse frequency led to higher material removal rates and improved surface hardness, highlighting the effects of the resolidified layer [10]. In a recent review, Alsaadawy et al. (2024) reported that using low laser power combined with high cutting speed, moderate assist gas pressure, and nitrogen gas significantly reduced machining defects, including excessive roughness and burr formation [11].

Basak et al. (2025) analyzed the impact of intrinsic material properties on surface quality, concluding that these can have a greater influence than process parameters [12]. In their study, hardness decreased by up to 22.7% in SS316 stainless steel, suggesting a strong dependence of thermomechanical response on material composition. Additionally, Mahrle et al. (2021), through a factorial experimental design, identified a significant correlation between cut edge roughness and kerf geometry, emphasizing that internal process parameters may outweigh external factors such as assist gas pressure [13].

Overall, the literature shows a continuous effort to identify optimal configurations of technological parameters to improve the quality of laser-cut surfaces. However, most studies focus on empirical or statistical approaches and tend to overlook a fundamental perspective based on modelling the electromagnetic field generated by the laser beam. This gap underscores the need for a combined approach that links process parameters with the behaviour of electromagnetic waves, enabling a deeper understanding of the interaction between the laser beam and the material.

2.2 Theoretical modelling of laser beam propagation

A central objective of this research is the formulation of a rigorous theoretical model of the electromagnetic field generated by the laser beam during the cutting process. To achieve this, the starting point is the fundamental equations of electromagnetism developed by James Clerk Maxwell, which describe how electromagnetic waves are generated and propagate in a vacuum. The laser beam is interpreted as a plane electromagnetic wave, composed of synchronized oscillations of the electric and magnetic fields, propagating at the speed of light ccc.

According to classical theory, a time-varying electric field induces a time-varying magnetic field, and this reciprocal process gives rise to the propagation of an electromagnetic wave. Maxwell's equations, in their differential form for vacuum conditions, are expressed as follows:

$$\mathrm{rot}H=\nabla\times H=\frac{\partial D}{\partial t} \quad (1)$$

$$\mathrm{rot}E=\nabla\times E=-\frac{\partial B}{\partial t} \quad (2)$$

$$\mathrm{div}D=\nabla\cdot D=0 \quad (3)$$

$$\mathrm{div}B=\nabla\cdot B=0 \quad (4)$$

We start from the equation involving differential operators i:

$$\nabla\times(\nabla\times H)=\nabla\cdot(\nabla\cdot H)-\Delta H \quad (5)$$

in which E is the electric field intensity, D the electric displacement field, H the magnetic field intensity, and B the magnetic flux density.

$$D=\varepsilon_0\cdot E, B=\mu_0\cdot H \quad (6)$$

These relations are combined, resulting in:

$$\nabla\times\frac{\partial D}{\partial t}=\nabla\cdot(\nabla\cdot H)-\Delta H \quad (7)$$

For a stationary field: $\nabla\cdot H=0$

$$\Delta H+\nabla\times\frac{\partial D}{\partial t}=0 \quad (8)$$

$$\Delta H+\nabla\times\varepsilon_0\frac{\partial E}{\partial t}=0 \quad (9)$$

$$\Delta H+\varepsilon_0\frac{\partial}{\partial t}(\nabla\times E)=0 \quad (10)$$

$$\Delta H+\varepsilon_0\frac{\partial}{\partial t}\left(-\frac{\partial B}{\partial t}\right)=0 \quad (11)$$

$$\Delta H-\varepsilon_0\frac{\partial^2 B}{\partial t^2}=0 \quad (12)$$

$$\Delta H-\varepsilon_0\mu_0\frac{\partial^2 H}{\partial t^2}=0 \quad (13)$$

In Cartesian coordinates, the equation becomes:

$$\frac{\partial^2 H}{\partial x^2}+\frac{\partial^2 H}{\partial y^2}+\frac{\partial^2 H}{\partial z^2}-\varepsilon_0\mu_0\frac{\partial^2 H}{\partial t^2}=0 \quad (14)$$

$$\frac{\partial^2 H}{\partial x^2}+\frac{\partial^2 H}{\partial y^2}+\frac{\partial^2 H}{\partial z^2}-\frac{1}{c^2}\frac{\partial^2 H}{\partial t^2}=0 \quad (15)$$

The solution of the second-order differential

equation:

$$H=H_0\cos(\omega t-kz) \quad (16)$$

where H_0 is the magnetic amplitude, ω is the angular frequency, k is the wave number, and z is the direction of laser wave propagation.

At the origin of the axes, where the laser source is located, electromagnetic waves are generated with the following components:

$$H=H_0\cos(\omega t) \quad (17)$$

$$E=E_0\cos(\omega t) \quad (18)$$

At a distance z from the origin of the Cartesian system, the following waves of the coupled fields are generated:

$$H=H_0\cos(\omega t-kz) \quad (19)$$

$$E=E_0\cos(\omega t-kz) \quad (20)$$

Based on previous relations we can develop the field equation:

$$H=H_0\cos\left(\frac{2\pi}{T}t-\frac{2\pi}{\lambda}z\right)=H_0\cos 2\pi\left(\frac{t}{T}-\frac{z}{\lambda}\right) \quad (21)$$

The relationship between the electric field and the magnetic field is governed by the principle of cause and effect, where one acts as the cause and the other as the effect, resulting in the propagation of laser light. These fields are in phase and simultaneously reach their maximum and minimum values. An important relation can be obtained by setting the phase as:

$$\phi=\omega t-kz \quad (22)$$

When we apply Fermat's theorem to the phase of the wave, we obtain an extremum point:

$$\frac{\partial\phi}{\partial t}=0 \quad (23)$$

$$c=\frac{\partial z}{\partial t}=\frac{\omega}{k}=\frac{\lambda}{T} \quad (24)$$

When the wavelength of electromagnetic radiation is very short, the oscillation period of the associated field becomes extremely brief. Lasers operating in the ultraviolet region of the electromagnetic spectrum are characterized by short oscillation periods and high electric field amplitudes, which grant them a high energy density. The intensity of laser radiation is directly influenced by the rapid temporal variation of the electric and magnetic fields, and the synchronization of these fields in space and time leads to the formation of a high-energy coherent beam. The electric field plays a crucial role in the spatial displacement of the magnetic field lines, while the magnetic field loops around the beam in a circular manner, thereby defining the geometry of the laser beam.

This mutual interaction leads to the generation of a collimated beam, directed along the longitudinal axis (the Oz direction), which propagates at the speed of light in a vacuum. The electric field oscillates in a plane perpendicular to the direction of propagation (along the Ox axis), while the magnetic field oscillates perpendicular to it (along the Oy direction), the two being orthogonal both to each other and to the propagation direction. From a physical standpoint, the electric field can be interpreted as a magnetic moment generated by the cross product between the speed of light and the magnetic field intensity, according to the relation:

$$E=c \times B=c \times \mu_0 H=\mu_0(c \times H) \quad (25)$$

Depending on the values of E and B (or H), laser light is concentrated into a very small diameter and is characterized by different wavelengths. The laser light spectrum spans the infrared, visible, and ultraviolet regions. The amplitude of the electric field is much greater than that of the magnetic field, by a factor of c (speed of light).

$$E_0=c \times B_0 \quad (26)$$

The greater the value of E_0, the higher the frequency of the laser light, which gives rise to high-power lasers possessing strong electric fields of significant magnitude. When the amplitudes E_0 and B_0 increase, this results in a strong concentration of laser light in a small space, with higher luminous excitation and intensity. The circular cross-section of the beam is primarily due to the magnetic field. This flash, sometimes of different colours or invisible, is generated by a laser light source with beam directionality confined to a narrow parallel path. The wavelength is the same for both the electric and magnetic fields. When the wavelength drops below 1 nm, it is observed that the energy of the flash increases while the distance between two field maxima decreases.

When laser radiation interacts with matter, collisions occur between laser photons and electrons, as well as between laser photons and ions, resulting in physical phenomena such as absorption and reflection. The laser energy density is defined as the amount of light energy per unit volume:

$$w=\frac{E}{V}=\frac{Nh\vartheta}{V}=nh\vartheta \quad (27)$$

Taking into account the field laws, the energy density is expressed as follows:

$$w=\varepsilon_0 \cdot E^2 \quad (28)$$

The maximum energy density is obtained when the amplitudes of the electric and magnetic fields reach their peak values and are in perfect phase synchronization cos(ωt-kz)=1,

$$w_m=\varepsilon_0 \cdot E_0^2=\varepsilon_0 \cdot I_0 \quad (29)$$

Incident laser intensity is:

$$I_0=\frac{4P}{\pi \cdot d^2}=E_0^2 \quad (30)$$

We can calculate the amplitude E of the radiation field:

$$E_0=\left(\frac{4P}{\pi \cdot d^2}\right)^{1/2} \quad (31)$$

where P is the laser power, and d is the spot diameter, an important parameter of the laser light field. In vacuum, the electric field quantifies the magnetic field by the value of c. Based on the operating parameters of the laser, we can calculate the maximum value of the electric field.

3. MATERIAL AND DESIGN OF EXPERIMENTS

3.1 Material

The material analysed in this study is a sheet of alloy steel of type X10AlCr180, characterized by a high content of chromium (approximately 18%), aluminium, and silicon. This alloy is intended for use under extreme temperature and corrosion conditions and is commonly used in the construction of reinforcements and support elements for the refractory linings of pulverized coal burners in boilers used for generating superheated steam. The initial hardness of the sheet, determined using the Vickers method, falls within the range of 220–280 HV, which is typical for refractory materials with high thermal stability.

3.2 Experimental setup

The cutting experiments were carried out using a fiber laser with a maximum radiation power of P = 5200 W and a focused spot with a diameter of d = 0.38 mm, within which a maximum electric field intensity of $E_o = 2.17 \times 10^5$ V/m was achieved. Following interaction with the material, this electric field instantaneously generates, through relativistic effects, a magnetic induction field of $B_o = 0.7 \times 10^{-3}$ T. The energy delivered by the laser beam heats, melts, and vaporizes the surface of the metallic target, and collisions with atomic electrons result in excitations and ionizations, also producing intense luminous effects.

Theoretical modelling of the electromagnetic field propagation, based on specific operating parameters, enables a detailed understanding of energy transfer and the effects induced in the material. This approach allows the correlation of field distribution with the microstructural and mechanical changes that occur after cutting.

Figure 1. BySmart Fiber Bystronic laser cutting machine used in the experiments.

The tests were conducted using the BySmart Fiber Bystronic equipment designed for high-precision processing. It enables fine, clean cuts with high tolerances and virtually no burr formation, eliminating, in most cases, the need for subsequent machining. Its non-contact operation ensures minimal wear of

components and significantly reduces technological losses. The image of the equipment used is shown in Figure 1.

For a comparative evaluation of performance, the results obtained with the conventional Zinser 2325 equipment, based on oxy-gas cutting, were also analysed. This machine, shown in Figure 2, is significantly slower, involves direct contact with the material, and often produces burrs and thermal deformations, requiring additional processing (grinding, deburring).

Figure 2. Zinser 2325 cutting machine used for performance evaluation comparison

An essential advantage of laser technology is the minimal material loss, due to the extremely thin beam that produces narrow cutting kerfs. This enables optimized nesting of parts on the sheet, contributing to process efficiency and cost reduction. Moreover, the absence of mechanical contact eliminates tool wear, an important benefit compared to conventional machining methods.

3.3 Experimental design

Hardness was selected as the main evaluation criterion for assessing the quality of parts obtained through oxygen-assisted laser cutting, given its direct impact on mechanical performance in critical applications. Due to the unstable behavior of the material in its molten state, conventional oxy-fuel cutting does not allow for clean and precise edges. This is why laser technology was chosen, as it offers superior accuracy and minimal material loss by narrowing the cutting kerf.

To quantify the efficiency of the process, a removal index (I_s) was introduced, defined as the ratio between the amount of usable material remaining in the part and the total amount of material cut:

$$I_s = \frac{\text{Amount of cut material remaining in the part}}{\text{Total amount of material cut}}$$

An index close to 1 reflects an efficient cutting process, with high precision and minimal losses, essential characteristics for high-performance industrial machining. The novelty of this research lies in the detailed experimental analysis of surface hardness on parts cut with high-power fiber laser, correlated with microstructural changes induced in the HAZ.

Hardness measurements were performed using a portable KrautKramer MIC 10 hardness tester equipped with a diamond-tipped probe, as illustrated in Figure 3. The recorded values showed a slight decrease in hardness within the HAZ, a phenomenon attributed to annealing and local softening effects. These changes are associated with the migration of alloying atoms (Cr, Al, Si), increased interatomic distances, and reduced bonding forces, processes induced by the high thermal concentration generated by the laser beam.

Figure 3. Portable KrautKramer MIC 10 device used for hardness measurement.

The average hardness obtained after cutting was approximately 150 HV, which is

lower compared to the initial values of the raw material. For the experimental design, a 2^3 factorial matrix was applied, from which 8 relevant experimental points (out of a possible 27) were analysed, as shown in Table 1. Based on these data, the main and interaction effects of the independent variables (laser power, cutting speed, focal position) were estimated, and the resulting statistical model allows for the prediction of hardness values.

The resulting factorial model enables the exploration of hardness variations in response to controlled changes in technological parameters and provides a foundation for optimizing the cutting process in high-reliability industrial applications.

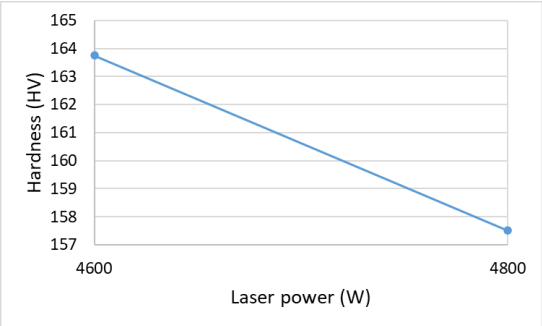

a) Effect of laser power on hardness

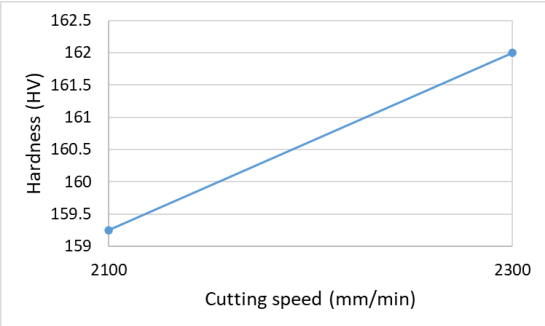

b) Effect of cutting speed on hardness

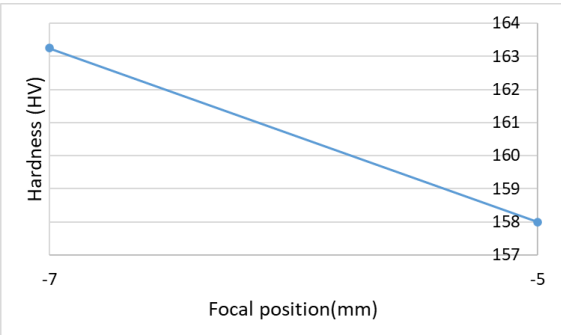

c) Effect of focal position on hardness

Figure 4. Main effects of process parameters on hardness

Table 1. Experimental data

Design point	Laser power, P (W)	Cutting speed, v (mm/min)	Focal position, f (mm)	Hardness (HV)
1	4600	2100	-7	170
19	4800	2100	-7	159
3	4600	2300	-7	165
21	4800	2300	-7	159
7	4600	2100	-5	158
25	4800	2100	-5	150
9	4600	2300	-5	162
27	4800	2300	-5	162

4. RESULTS AND DISCUSSION

This subsection analyses the main effects of the three technological factors, laser power, cutting speed, and focal position, on the hardness of X10AlCr18 steel, using a 2^3 factorial design. Hardness was considered a key indicator of the quality of the resulting parts, given the potential structural changes induced by thermal energy in the HAZ.

Based on experimental observations, it is evident that laser power significantly influences material hardness, as shown in Figure 4a, where an increase in power from

4600 W to 4800 W leads to a decrease in hardness from 164 HV to 157 HV. This behaviour suggests that higher energy input promotes annealing and thermal softening of the local microstructure. Regarding cutting speed, Figure 4b shows that as the speed increases from 2100 mm/min to 2300 mm/min, hardness slightly increases from 159 HV to 162 HV. This is due to the reduced interaction time between the laser beam and the material, which limits thermal diffusion and the extension of the HAZ. In Figure 4c, modifying the focal position from –7 mm to –5 mm results in a decrease in hardness from 164 HV to 158 HV, suggesting that focusing closer to the material surface leads to a broader energy distribution in depth, which promotes extended melting and reduces local hardness.

The graphical interpretation of these relationships uses a Cartesian coordinate system, where the Ox axis represents each technological parameter, and the Oy axis indicates the measured hardness values. Comparing the slopes of the three graphs highlights that laser power has the greatest influence on hardness, followed by focal position and cutting speed.

The results suggest that maximum hardness can be achieved when the ratio between laser power and cutting speed (P/v) is minimized. In this case, a value of Pmin/vmax = 2 determines the optimal conditions for preserving the mechanical properties of the material.

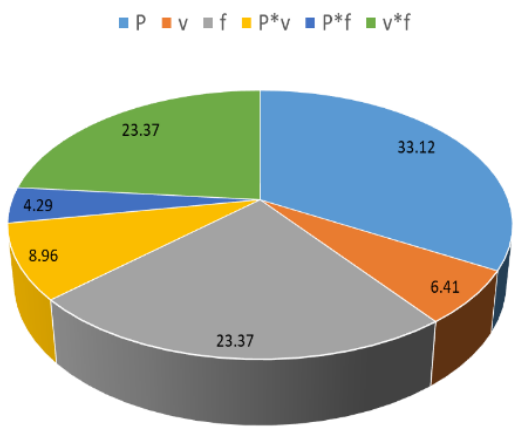

Figure 5. Contribution of model terms to hardness

Figure 5 summarizes the percentage contribution of each term within the statistical model.

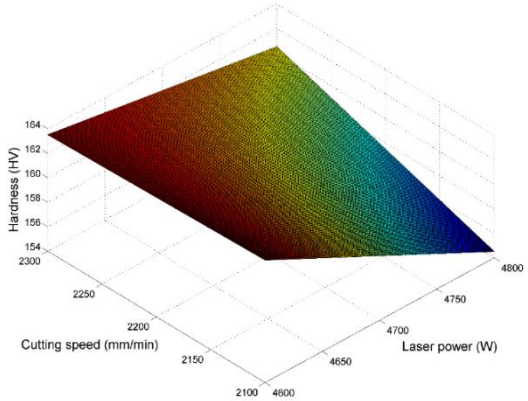

a) Interaction effect of laser power and cutting speed (for focal position of f=-6 mm)

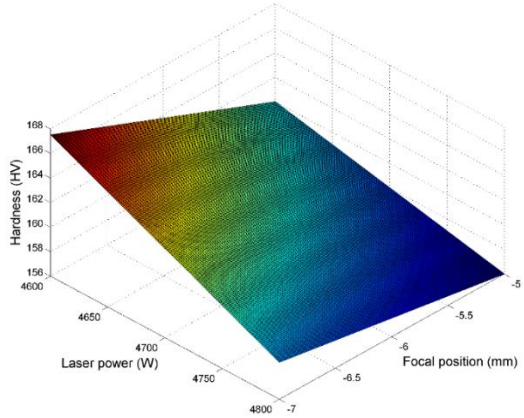

b) Interaction effect of laser power and focal position (for cutting speed of v=2200 mm/min)

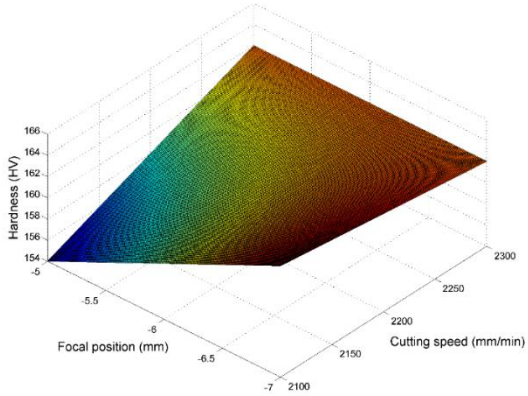

c) Interaction effect of cutting speed and focal position (for laser power of P=4700 W)

Figure 6. Effects of laser cutting parameters on material hardness

According to the results, laser power (P) has the highest influence on hardness, accounting for 33.12%, followed by focal position (f) and the interaction between cutting speed and focal position (v*f), each contributing 23.37%. In contrast, the interactions P*f and P*v had a reduced impact, and cutting speed (v) on its own contributed only 6.41% to the variability in hardness.

The 3D chart in Figure 5 provides an intuitive visual representation of each factor's weight in explaining the experimental response. Each sector is distinctly coloured to highlight the influence intensity of each predictor or their combinations. This representation facilitates the quick identification of critical parameters in the laser cutting process, emphasizing that hardness optimization is primarily determined by the delivered energy and the geometry of the focused beam.

For the qualitative and quantitative evaluation of the main and interaction effects of the process parameters, the following quasi-linear regression model was developed for hardness prediction:

$$\text{Hardness}=1278-0.32125*P-0.5925*v-113.25*f+0.0001625*P*v+0.01125*P*f+0.02625*v*f$$

The model presents a coefficient of determination R^2 of 99.52%, an adjusted R^2 of 96.66%, and a predicted R^2 of 69.48%.

These values indicate a strong predictive capability of the model and a solid correlation between the estimated and experimental values.

The regression coefficient analysis enabled the ranking of each predictor's influence. Among the processed parameters, laser power exerts the strongest effect on hardness, followed by the interaction between cutting speed and focal position. The coefficients associated with the interaction terms are subunitary, suggesting moderate but significant effects. The negative sign of the laser power coefficient confirms an inverse relationship with hardness, indicating a decrease in hardness at higher power levels, most likely due to thermal effects in the HAZ.

The developed model is graphically represented in Figure 6, where three surface plots illustrate the bidirectional interaction effects between parameters. These graphs were constructed using the RSM, keeping one parameter constant while varying the other two. The resulting surfaces highlight the combined impact of parameters on hardness, with differences in slope and contour reflecting the response sensitivity depending on the cutting regime. Broad zones with pronounced variations indicate factor pairs with significant influence, an essential aspect for process optimization and property control of the material.

The quasi-linear graphs presented were developed using RSM to highlight the combined effects of technological parameters on hardness. The resulting three-dimensional surfaces illustrate hardness variations in a colour spectrum, where chromatic gradients reflect the value levels of the response. The morphology of these surfaces, ranging from uniform planes to slightly distorted geometries, suggests a different dependence of hardness on each parameter pair. Areas with wide extension and significant variation in the response indicate strong interactions between predictors, emphasizing the importance of these combinations in controlling the properties of the processed material.

The results align with previous studies from the literature. For instance, Li (2021) applied the RSM methodology to optimize fiber laser cutting parameters for duplex stainless steel, a material characterized by superior thermophysical properties due to its high chromium and molybdenum content [14]. According to the author's conclusions, laser power exerts the greatest influence on the thermal distribution near the kerf edge, and a focal length of 0.4 mm, associated with maximum energy density, led to minimal surface roughness. However, excessive laser power values (>900 W) can generate defects such as slag and cavities, compromising the

quality of the cut surface. In a recent study, Liao et al. (2024) investigated high-power laser cutting (10 kW) applied to 20CrNiMo steel without the use of assist gas [15]. The authors demonstrated that both cutting speed and focal position have a direct impact on cut quality and the efficiency of slag ejection from the kerf.

5. CONCLUSION

This study analysed the influence of high-power laser cutting process parameters, beam power, cutting speed, and focal position, on the hardness of X10AlCr180 steel, using a linear regression model with interaction terms, supplemented by graphical representations generated through Response Surface Methodology (RSM).

The main results can be summarized as follows:

- The generated response surfaces highlighted significant relationships between hardness and each of the analysed parameters. Each graph illustrated a sloped plane, where the angle reflects the sensitivity of hardness to changes in process parameters.
- Bidirectional interactions between parameter pairs (power–speed, power–focal position, speed–focal position) were represented by 3D surfaces that revealed nonlinear behaviours and favourable operating regimes for optimizing hardness.
- The proposed mathematical model allows the identification of optimal parameter configurations based on application-specific requirements, thus facilitating the fine adjustment of laser equipment to achieve superior performance.
- Hardness prediction proved to be an effective tool not only due to the accuracy of the estimates obtained but also due to its ability to provide an intuitive visualization of hardness variations in relation to operational parameters.
- The maximum hardness value was achieved under conditions of minimum laser power and minimum focal position, while the lowest hardness was associated with low cutting speed and a maximum focal position.
- From an energy standpoint, operating the laser at minimum power is more economical, and the influence of focal position on cutting quality is essential, a focus near the lower edge of the part leads to cleaner and more precise cuts.

Future research directions:

- Extending experiments to other types of advanced or heat-treated materials to generalize and validate the proposed model.
- Integrating additional parameters such as assist gas pressure and type, optical characteristics of the lens, or laser pulse frequency into predictive models.
- Using nonlinear prediction models (neural networks, higher-order polynomial regressions, fuzzy systems) to more accurately capture local hardness behaviour.
- Correlating hardness values with advanced microstructural analyses to substantiate the link between local structural changes and the applied technological parameters.

By deepening these research directions, future studies can contribute to increasing the efficiency, quality, and sustainability of high-power industrial laser cutting processes.

REFERENCES

[1] M. Safari, S. M. Abtahi, and J. Joudaki, Experimental modeling, statistical analysis, and optimization of the laser-cutting process of Hardox 400 steel, *Materials*, vol. 17, no. 12, p. 2798, 2024.

[2] M. Yurdakul, T. Tukel, and Y. T. Iç, Development of a goal programming model based on response surface and analytic hierarchy process approaches for laser cutting process optimization, *Journal of Advanced Manufacturing Systems*, vol. 21, pp. 293–316, 2022.

[3] A. R. Patel and S. N. Bhavsar, Laser machining of die steel (EN-31): An experimental approach to optimise process parameters using response surface methodology, *International Journal of Automotive and Mechanical Engineering*, vol. 18, no. 1, pp.

8563–8576, 2021.

[4] K. Sket, D. Potocnik, L. Berus, *et al.*, Optimizing laser cutting of stainless steel using Latin hypercube sampling and neural networks, *Optics and Laser Technology*, vol. 182, p. 112220, 2025.

[5] D. Itner, M. Nießen, and G. Vossen, Mathematical modeling and stability analysis for laser cutting via asymptotic expansion, *International Journal of Mechanical Sciences*, vol. 219, p. 107062, 2022.

[6] D. Halliday and R. Resnick, *Physics*, vol. I, Bucharest, Romania: Didactic and Pedagogical Publishing House, 1975.

[7] Y. A. Turkkan, M. Aslan, A. Tarkan, Ö. Aslan, C. Yuce, and N. Yavuz, Multi-objective optimization of fiber laser cutting of stainless-steel plates using Taguchi-based grey relational analysis, *Metals*, vol. 13, no. 1, p. 132, 2023. https://doi.org/10.3390/met13010132

[8] D. Y. Pimenov, L. F. Berti, G. Pintaude, G. X. Peres, Y. Chaurasia, N. Khanna, and K. Giasin, Influence of selective laser melting process parameters on the surface integrity of difficult-to-cut alloys: Comprehensive review and future prospects, *International Journal of Advanced Manufacturing Technology*, vol. 127, pp. 1071–1102, 2023. https://doi.org/10.1007/s00170-023-11541-8

[9] P. Zuo, T. Liu, F. Li, G. Wang, K. Zhang, X. Li, W. Han, H. Tian, and D. Zhu, Research progress on laser processing of carbon fiber composite materials, *Polymer Composites*, 2024. https://doi.org/10.1002/pc.29287

[10] C. Balasubramaniyan and K. Rajkumar, Identification of parametric conditions and the influence of laser interaction on the material removal and surface characteristics of 904L super austenitic stainless steel, *International Journal on Interactive Design and Manufacturing*, vol. 19, pp. 3527–3539, 2025.

[11] M. Alsaadawy, M. Dewidar, A. Said, I. Maher, and T. A. Shehabeldeen, A comprehensive review of studying the influence of laser cutting parameters on surface and kerf quality of metals, *International Journal of Advanced Manufacturing Technology*, vol. 130, pp. 1039–1074, 2024.

[12] A. K. Basak, K. Lightbody, and A. Pramanik, The effect of material intrinsic properties on the quality of machined surface during laser beam cutting, *Materials Chemistry and Physics*, vol. 336, p. 130546, 2025. https://doi.org/10.1016/j.matchemphys.2025.130546

[13] A. Mahrle, M. Borkmann, and P. Pfohl, Factorial analysis of fiber laser fusion cutting of AISI 304 stainless steel: Evaluation of effects on process performance, kerf geometry and cut edge roughness, *Materials*, vol. 14, no. 10, p. 2669, 2021. https://doi.org/10.3390/ma14102669

[14] M. Li, Evaluation of the effect of process parameters on the cut quality in fiber laser cutting of duplex stainless steel using response surface method (RSM), *Infrared Physics & Technology*, vol. 118, p. 103896, 2021. https://doi.org/10.1016/j.infrared.2021.103896

[15] W. Liao, G. Wang, L. Zhong, Y. Chen, and J. Wang, Feasibility analysis and cutting process research on laser cutting medium-thick 20CrNiMo steel plates using a high-power fiber laser without assisted blowing, *Journal of Manufacturing Processes*, vol. 111, pp. 130–138, 2024. https://doi.org/10.1016/j.jmapro.2024.01.020

Society of Production Engineering

ICPES 2025

40th INTERNATIONAL CONFERENCE ON PRODUCTION ENGINEERING - SERBIA 2025

DOI: 10.46793/ICPES25.084K

University of Nis Faculty of Mechanical Engineering

Nis, Serbia, 18 - 19th September 2025

ANALYSIS OF THE IMPACT OF FRICTION ON THE QUALITY OF REGULATION DEPENDING ON THE USED FRICTION MODEL AND THE CONTROL LAW

Igor KOCIĆ[1], Saša S. NIKOLIĆ[1]*, Darko MITIĆ[1], Nikola DANKOVIĆ[1], Staniša PERIĆ[1], Miloš MADIĆ[2], Milan TRIFUNOVIĆ[2]

Orcid: 0009-0002-8569-1180; **Orcid:** 0000-0003-2745-3862; **Orcid:** 0000-0001-9483-0176; **Orcid:** 0000-0003-0986-5695; **Orcid:** 0000-0003-4766-195Xc; **Orcid:** 0000-0002-2310-2590; **Orcid:** 0000-0002-4653-6957;

[1]Univerity of Niš, Faculty of Electronic Engineering, Niš, Republic of Serbia

[2]Univerity of Niš, Faculty of Mechanical Engineering, Niš, Republic of Serbia

*Corresponding author: sasa.s.nikolic@elfak.ni.ac.rs

Abstract: *This paper analyses the effects of friction, i.e. the friction model, on control performance. The analysis was carried out using the model of the control object and the friction model with the application of different control laws. The Stribeck and LuGre friction models were considered. Position responses, control signals and friction force are shown as a function of the control laws of PID, SMC and TS LQR controllers. All simulations were performed using the MATLAB software package. The possibility of modeling a nonlinear system with friction using the Takagi-Sugeno fuzzy system and the method of generating a control signal using an LQR controller for each individual linear subsystem based on parallel distributed control (PDC) are shown. Control signals are generated using PID, SMC and TS-LQR control laws respectively. Instead of setting poles for each individual rule of the TS controller, the LQR method is used at the level of each individual rule by selecting unique Q and R matrices based on optimality criteria.*

Keywords: *friction, Striebeck model, LuGre model, PID, SMC, Takagi-Sugeno LQR, friction compensation.*

1. INTRODUCTION

In this paper, a simulation analysis of the effect of friction on the quality and performance of the regulation was performed based on the selected friction model. Knowledge of the effects of friction and its compensation is very important for design and control of servo mechanisms, robots, and precise pneumatic and hydraulic systems. Due to its nonlinearity, it causes a static error, leads to oscillation around the set value as a result of a rapid transition from the range of static to the range of dynamic friction due to the difference between the force of static and dynamic friction and the occurrence of limit cycles. The control

object used is a simplified model of a DC motor with independent excitation, which is controlled by the current in the rotor and drives the positioning system via a gearbox. All simulations were performed with Matlab and Simulink using the friction models of Stribeck and LuGre. The analysis of the effect of friction on the performance of the controlled variable as well as the compensation method was carried out using the classical PID controller, which is considered the standard industrial controller, then the SMC (Sliding Mode Controller) controller and finally the Takagi-Sugeno controller (TSLQR) was used. The model of the nonlinear system is derived using the Euler-Lagrange equations. The TS model was created using fuzzy if-then rules according to the local TS approximation method, which is based on the properties of TS fuzzy models as universal approximators. Based on the obtained fuzzy model, the fuzzy controller was designed using the same if-then rules, where the control signals were obtained based on the given optimality criterion and the parallel distributed control (PDC) method based on the TS fuzzy model. Position responses, control signals and friction force are presented as a function of the friction models, control laws and compensation methods used.

2. SYSTEM MODEL

The mathematical model of the nonlinear system (1) was obtained by applying the Euler-Lagrange method and known expressions for Coulomb [1] and viscous friction (1), Stribeck (2) and the LuGre friction model (3) [2-4], where F_c is the Coulomb friction force, F_s is the maximum static friction force, F_v is the viscous friction, x is position, $\dot{x}$ velocity, v_s is Stribeck velocity, δ is a coefficient that depends on the type and scope of the model (δ=2 was taken in the paper), σ_0, σ_1 are respectively the coefficients of strength and damping of asperity fibers, σ_2 is the coefficient of viscous friction, z is a variable for the LuGre model, which refers to the amount of stretching of asperity fibers in the simulation model. In (5), the controlled system model is given with the LuGre friction model based on which the simulation was performed, a similar controlled system model was created for the Stribeck friction model.

$$F_{tr}(\dot{x},\theta) = F_c sgn(\dot{x}) + F_v \qquad F_v = \sigma_2 \dot{x} \tag{1}$$

$$F_{tr}(\dot{x},\theta) = \left[F_c + (F_s - F_c)e^{-\left(\frac{|\dot{x}|}{|v|_s}\right)^{\delta}}\right] sgn(\dot{x}) + \sigma_2 \dot{x}, \tag{2}$$

$$g(\dot{x}) = F_c + (F_s - F_c)e^{-\left(\frac{|\dot{x}|}{|v|_s}\right)^{\delta}}, \delta = 2 \qquad \frac{dz}{dt} = \dot{x} - \frac{|\dot{x}|}{g(\dot{x})} z$$

$$F_{tr}(\dot{x},\theta) = \sigma_0 z + \sigma_1 \frac{dz}{dt} + \sigma_2 \dot{x}. \tag{3}$$

The system model is given in the general form (4), x is the position (linear or angular), F_{tr} is the friction force, which depends on the speed, $\dot{x}$ and the parameters Θ describing the friction model used, W refers to the mass or inertia, k_m is the motor amplification coefficient.

$$\begin{bmatrix} \dot{x} \\ \ddot{x} \end{bmatrix} = \begin{bmatrix} \dot{x} \\ -W^{-1} F_{tr}(\dot{x},\theta) \end{bmatrix} + \begin{bmatrix} 0 \\ W^{-1} k_m \end{bmatrix} u. \tag{4}$$

The simulation models are based on Fig. 1, where the controller depends on the PID simulation [5-7], the SMC controller [8, 9], with and without set point compensation, the TS LQR controller [9], and the control object is a DC motor and the friction model is Stribeck or LuGre.

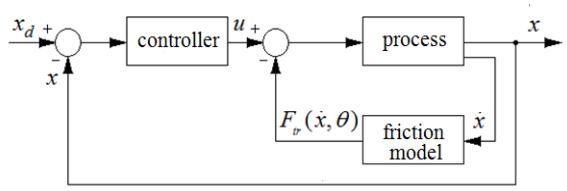

Figure 1. Block diagram of the control object and the controller

The control object and the friction model are given by equation (5), in which the variables are given in the following order: x_1=x position, x_2=v velocity, x_3=i_a rotor current, x_4=z internal variable describing the elastic deformation of

the asperity fibres according to the LuGre friction model:

$$\begin{aligned} \dot{x}_1 &= x_2 \\ \dot{x}_2 &= -\sigma_1 (x_2 - \frac{|x_2|}{g(x_2)} x_4) - \sigma_2 x_2 - \sigma_0 x_4 + k_m x_3 \\ \dot{x}_3 &= -a x_2 - b x_3 + c u \\ \dot{x}_4 &= x_2 - \frac{|x_2|}{g(x_2)} x_4 \end{aligned} \tag{5}$$

$$g(x_2) = F_c + (F_s - F_c) e^{-(\frac{x_2}{v_s})^2}.$$

The analysis of the effect of friction was performed on the basis of simulations made using a system simulation model and a friction model with different control laws. First, a simulation was carried out with the PID controller, the Stribeck model and the LuGre model, without and with pre-filtering of the setpoint.

3. ANALYSIS OF THE INFLUENCE OF FRICTION FORCE

We use a classical PID controller to control the position x (either linear or angular),x_d is the setpoint of the position. The parameters of the PID controller were chosen to show the influence of friction and the model used on the quality of the control. The friction models Stribeck and LuGre were used and the controlled system model (5) with the parameters given in the Table 1 partly taken from [3]. Figures 2 and 3 show the response of the position to the step signal when using the Stribeck and LuGre models, with the classic PID (6) used as the controller, the setpoint is shown in blue and the achieved position value in red colour. Response according to Fig. 2 is similar to the response without the friction model, since the Stribeck model provides the response at low speeds. In Fig. 3 we can see that due to the transition from the static friction region to the dynamic friction region, there is a permanent oscillation around the set value (error at steady state), which leads to the occurrence of limit cycles which are not seen in Fig. 2. This phenomenon and the dynamics are described by the LuGre model, in contrast to the Stribeck model, which does not describe them.

Table 1. Parameters of controlled system

Parameter	Value
σ_0	10^4 *N/m*
σ_1	100 *Ns/m*
σ_2	4 *Ns/m*
F_c	10 *N*
F_s	15 *N*
v_s	0.001*m/s*
Δ	2
Ra	4.58 *Ω*
La	0.0281 *H*
Ke	1.25 Vs/rad
Km	1.25 *Nm/A*

$$u = k_p (e(t) + \frac{1}{T_i} \int e(t) dt + T_d \frac{de(t)}{dt}) \tag{6}$$

$$e = x_1 - x_d$$

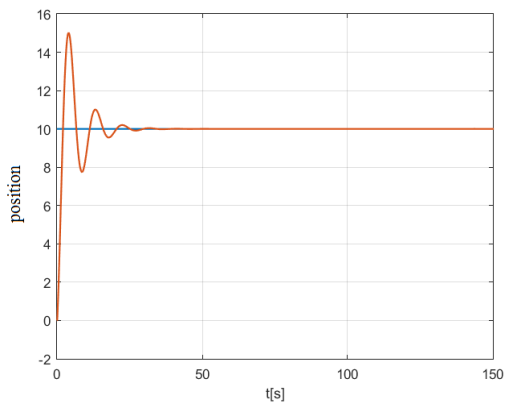

Figure 2. Response of the position when using the Stribeck model and the classic PID controller

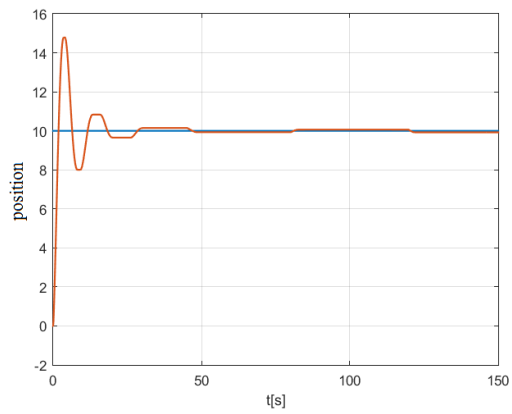

Figure 3. Response of the position when using the LuGre model and the classic PID controller

The use of a compensator (pre-filter) of the set value or simply the use of a ramp of the set value reduces the jump in the position response, it can even be completely eliminated, but the effect of the limit cycles increases.

Figures 4 and 5 show the friction force and the control signal when using a classic PID controller without compensation of the position setpoint and the LuGre friction model, where the oscillation of both the friction force and the control signal is clearly visible. The control signal must oscillate in order to maintain the position response.

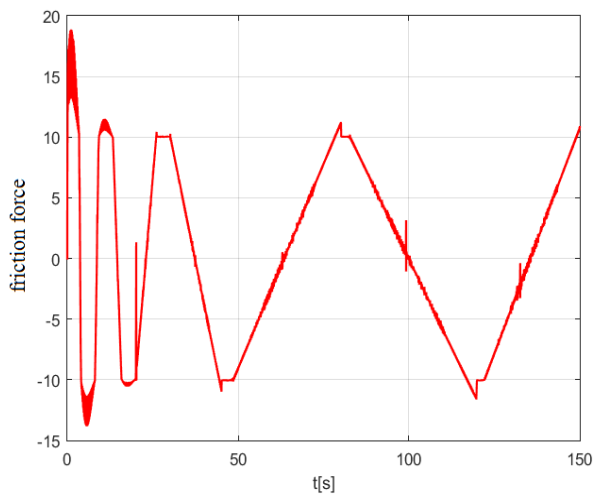

Figure 4. Friction force when using the Lugre model and the classic PID controller

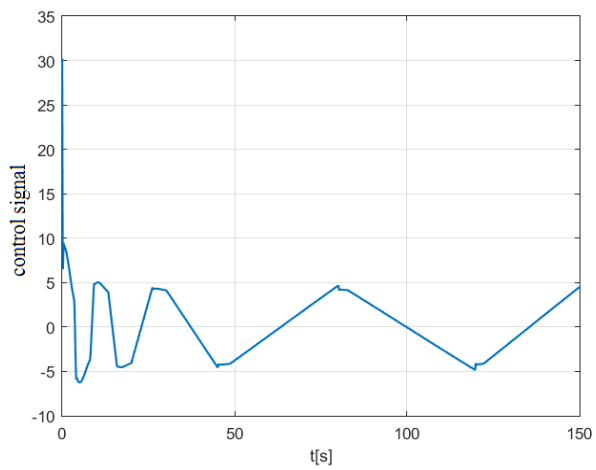

Figure 5. Control signal when using the Lugre model and the classic PID controller

In the further analysis, we used the SMC controller with exponential reaching law (7), Stribeck and LuGre friction model. The sliding surface s is given by (8), where e is the deviation error of the current value $x=x_1$ (the difference of the position from the system model, x_1 (5) and the set value of the position, x_d (9)). By replacing the corresponding equations from (5) and arranging the expressions, the control law of the SMC controller is obtained in the form of (10), where the expressions for T_f and X_d are given as (11) and (12) respectively.

$$\dot{s} = -k_d s - k\, sgn(s(x)), \tag{7}$$

$$s = \left(\frac{d}{dt} + \lambda\right)^{n-1} e, \tag{8}$$

$$e = x_1 - x_d, \tag{9}$$

$$u = \frac{1}{c}(bx_3 + 2\lambda T_f + (a-\lambda)x_2 + \\ + X_d - k_d s - k\,\mathrm{sgn}(s)), \tag{10}$$

$$T_f = \sigma_1\left(x_2 - \frac{|x_2|}{g(x_2)}x_4\right) + \sigma_2 x_2 + \sigma_0 x_4, \tag{11}$$

$$X_d = \dddot{x}_d + 2\lambda\ddot{x}_d + \lambda\dot{x}_d. \tag{12}$$

A very fast response, similar to an aperiodic response without jumps, is observed for both applied models, although the response is faster when the LuGre model is applied. Chattering is observed in the control signals in both cases, which could be reduced by using the function $tg(s)$ instead of $sgn(s)$. Figures 6 and 9 show that the friction forces are fully compensated after a few seconds, they do not have a pronounced oscillatory character as when with a PID controller, the setpoint is shown in blue and the achieved position value in red colour. Figure 7 shows the friction force when using the Stribeck model. It can be seen that, in contrast to the PID control law, the friction force does not have a pronounced occurrence of oscillations. Figure 8 shows the control signal when the Stribeck model is applied, where chattering is noticeable.

The control error is almost completely absent, the steady-state error is reduced to almost zero and the limit cycles are eliminated. All this is reflected in the use of robust nonlinear controllers such as the SMC. An additional setpoint compensator is not required. Figure 10 shows the friction force when the LuGre model is applied. In contrast to

the PID control law, figure shows that the friction force has no oscillations. Figure 11 shows the control signal when using the LuGre model, where chattering is also noticeable.

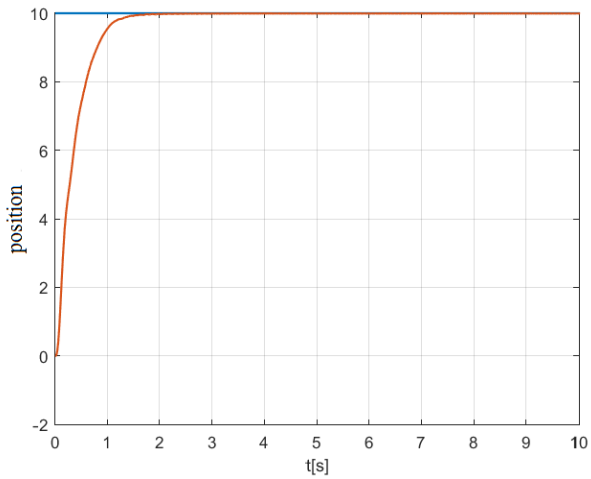

Figure 6. Response of the position when using the Stribeck model and the SMC controller

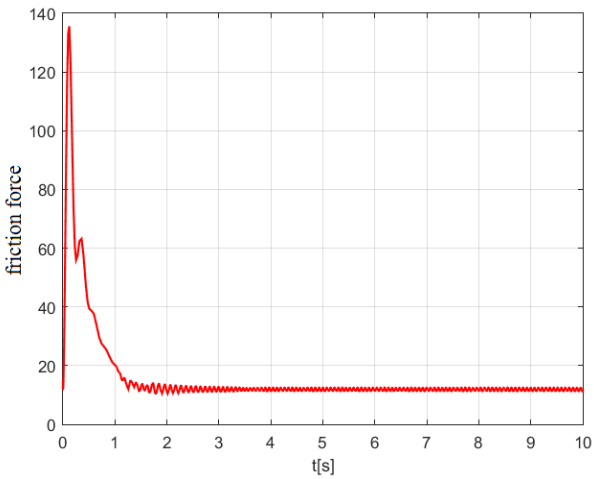

Figure 7. Friction force when using the Stribeck model and the SMC controller

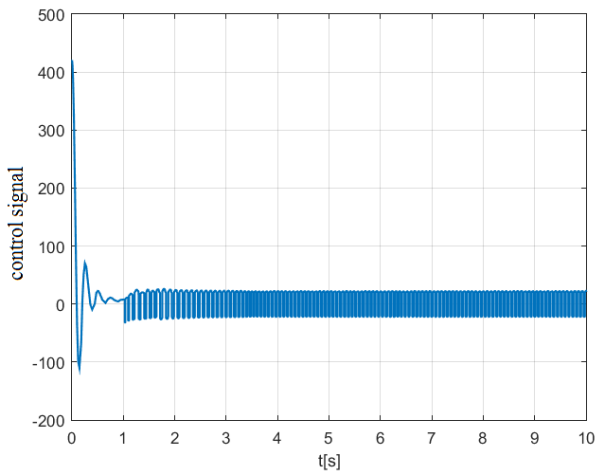

Figure 8. Control signal when using the Stribeck model and the SMC controller

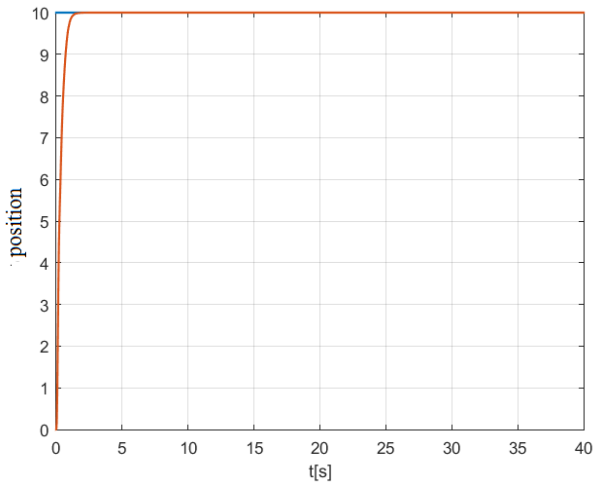

Figure 9. Response of the position when using the LuGre model and the SMC controller

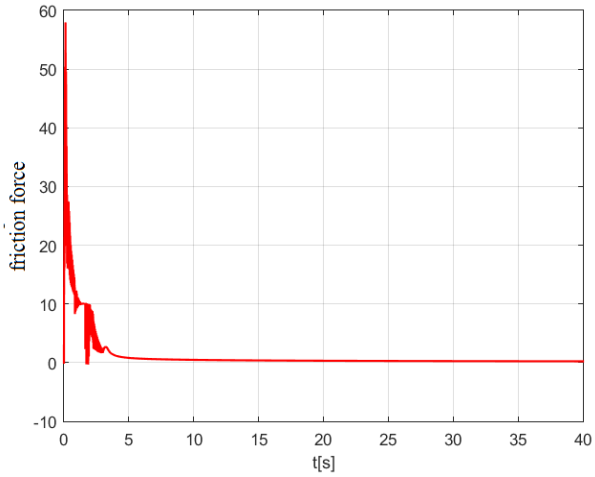

Figure 10. Friction force when using the Lugre model and the SMC controller

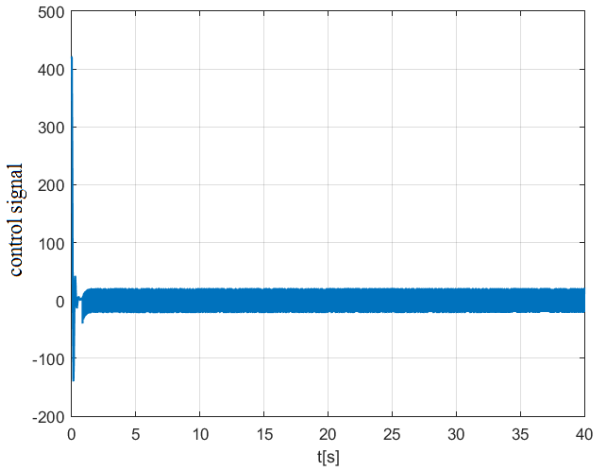

Figure 11. Control signal when using the LuGre model and the SMC controller

4. TAKAGI-SUGENO LQR CONTROL

The analysis of the influence of the friction force and its compensation was performed by modelling the nonlinear system (5) using the TS fuzzy system, which is expressed in the form of several local linear dynamic systems of the form (13) with *m* rules (R_1-R_m). An approach based on local approximation in fuzzy space was used by replacing the nonlinear terms in (5) with suitably chosen linear terms, which in the case of system 1 (5) reduces the rules to the state variable x_2, since the nonlinearities accordingly appear in the form of an exponential function and an absolute value [3]. The membership functions $\mu_{Pij}(x_i)$ of the fuzzy sets P_{10} ,...,P_{nm} are suitably selected functions of the triangular or Gaussian type.

The activation degree and the fuzzy basis function *j=1,...,m* of this rule is given by the expression (14), where the nonlinear system (5) is approximated by the TS fuzzy system (15) and the control law is generated using the parallel distributed control (PDC), replacing the linear matrix inequality (LMI) method to determine the stability of the system thus constructed by the LQR method.

$$R_j: IF\, x_1 \text{is in the area of } P_{1j} \text{and } \ldots$$
$$\text{and } x_n \text{is in the area of } P_{nj}$$

$$THEN\ \dot{x}_i = A_i x + B_i u \tag{13}$$

$$\mu_j(x) = \prod_{i=1}^{n} \mu_{Pij}(x_i)$$
$$\xi_j = \frac{\mu_j(x)}{\sum_{j=1}^{m} \mu_j(x)} \tag{14}$$

$$\dot{x}(t) = \frac{\sum_{j=1}^{m} \mu_j(x(t))(A_j x(t) + B_j u(t))}{\sum_{j=1}^{m} \mu_j(x(t))} =$$
$$= \sum_{j=1}^{m} \xi_j(x(t))\,(A_j x(t) + B_j u(t)). \tag{15}$$

For each individual rule of the TS fuzzy controller, control is designed on the basis of a specific performance index based on the *Q* and *R* matrices. For this purpose, the *lqr* command is used in MATLAB, where the *Q* and *R* matrices are selected by trial and error. The control law was generated by determining the gain matrix k_j for each individual rule (13), which was obtained from the linear quadratic optimization problem (16) and for each individual linear system based on the fuzzy model (5).

$$J = \int_{t_0}^{t_f} (x^T Q x + u^T R u) dt, \tag{16}$$

$$u = -\left[\sum_{j=1}^{m} \xi_j\,(t) k_j\right] x(t). \tag{17}$$

The total control signal is obtained as the sum of the product of the fuzzy basis function and the local control signals obtained within the if-then rules of the fuzzy controller of the obtained PDC control (17). Based on the obtained control laws $u_j(t)$, the TS controller is designed. Using the local TS approximation, the model (5) for velocities around zero reduces to (18), which is exactly one of the rules for the TS model for low velocities, i.e. velocities close to zero.

$$\begin{aligned} \dot{x}_1 &= x_2 \\ \dot{x}_2 &= -(\sigma_1 + \sigma_2) x_2 + k_m x_3 - \sigma_0 x_4 \\ \dot{x}_3 &= -a x_2 - b x_3 + c u \\ \dot{x}_4 &= x_2. \end{aligned} \tag{18}$$

A similar law was found in [10, 11]. The parts of the rules for velocities around Stribeck are derived in a similar way.

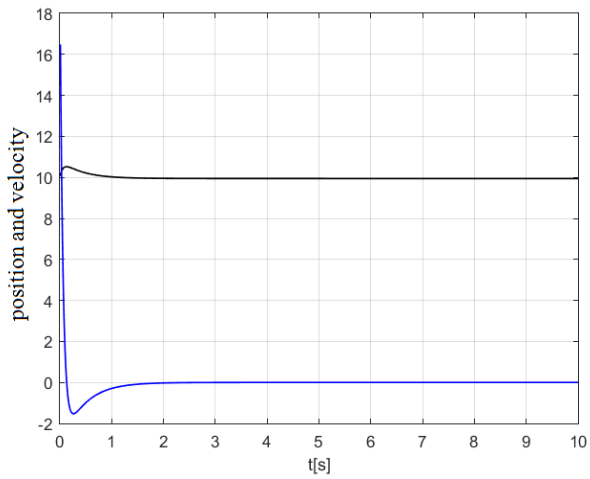

Figure 12. Control signal when using the LuGre model and the TS LQR controller

The simulation was done using the 4*th* order Runge-Kuta method, for which a routine was written in MATLAB.

Figure 12 shows the position response and the speed of the position change when using the TS LQR controller. It can be observed that the friction forces are fully compensated after one second, which is a consequence of using the TS LQR controller and approximating the nonlinear friction force model by a linear one.

5. CONCLUSION

The simulations carried out on the basis of Stribeck and LuGre friction model show that the LuGre model describes the friction of mechanical systems much better than Stribeck model. Therefore, the LuGre model is regularly used in industrial friction compensation methods and in the identification of friction parameters. All newer thyristor controllers have an integrated friction compensation option. Based on the simulation analysis during position control when using the PID controller, a step in the position response as well as an oscillating behaviour of the friction force and the control variables is observed. The position pre-filter reduces the jump, but increases the oscillatory force of the friction force and the control variables. In the simulation with the SMC controller, good friction compensation was achieved and the error in the steady state of the position was eliminated, and chattering in the control signal was observed as the only drawback.

Significantly better position response in terms of speed and overshoot was obtained in the simulation with the TSLQR controller, where the linearization of the nonlinear system was performed with the fuzzy model. The proposed controller was obtained by determining the gain matrix for each individual fuzzy rule using the LQR theory. The proposed controller was obtained by determining the gain matrix for each fuzzy rule using LQR theory. It remains to be analysed in future works on a real mechanical system with a TSLQR controller and a LuGre type fuzzy friction model, without and with a friction force compensation based on this model.

ACKNOWLEDGEMENT

This work was supported by the Ministry of Science, Technological Development and Innovation of the Republic of Serbia [grant number 451-03-137/2025-03/200102 and 451-03-137/2025-03/200109].

REFERENCES

[1] C.A. Coulomb: *Th´eorie des machines simples*, M´emoires de Math´ematiqueet de Physique de l'Academie ds Sciences, 1821.

[2] H. Olsson, K. J. Astroem, C. Canudas de Wit, P. Lischinsky: A new model for control of systems with friction, IEEE Trans. on Automatic Control., Vol. 40, No. 3, pp. 419- 425, 1995.

[3] D.D. Rizos, S.D. Fassois: Friction identification based upon LuGre and Maxwell slip models, IEEE Transaction on Control System Technology, Vol. 7, No. 1, pp. 153-160, 2008.

[4] K. J. Astrom, T. Hagglund: The future of PID control, Control Engineering Practice, Vol. 9, No. 11, pp. 1163-1175, 2001.

[5] B. Armstrong, B. Amin: PID Control in the presence of static friction: A comparison of algebraic and describing function analysis, Automatica, Vol. 32, No. 5, pp. 679-692, 1996.

[6] F. Cameron, D. Seborg: A self-tuning controller with a PIDstructure, International Journal of Control, Vol. 38, No. 2, pp. 401-407, 1983.

[7] V.I. Utkin: Variable structure systems with sliding modes, IEEE Transactions on Automatic Control, Vol. 22, No 2, pp. 212-222, 1977.

[8] W. Gao, J.C. Hing: Variable structure control of nonlinear system, A new approach, IEEE Trans, Ind. Elec., Vol.40, No. 1, pp. 45-55, 1993.

[9] J.H. Lilly: Fuzzy Control and Identification, John Wiley & Sons, 2010.

[10] K. Tanaka, H. Wang: Fuzzy control design system and analysis: A linear matrix inequality approach, John Wiley & Sons, Inc., 2004.

[11] D. G. Luenberger, Y. Ye: Linear and Nonlinear Programming, Reading, MA, Addison-Wesley, 1984.

Society of Production Engineering

ICPES 2025

40th INTERNATIONAL CONFERENCE ON PRODUCTION ENGINEERING - SERBIA 2025

DOI: 10.46793/ICPES25.091R

University of Nis Faculty of Mechanical Engineering

Nis, Serbia, 18 - 19th September 2025

APPLICATION OF RANDOM FOREST REGRESSION FOR PREDICTION OF SURFACE ROUGHNESS IN FIBER LASER CUTTING

Dragan RODIĆ*, Milenko SEKULIĆ, Borislav SAVKOVIĆ, Anđelko ALEKSIĆ, Aleksandra KOSANOVIĆ
Orcid: 0000-0001-9777-9185; **Orcid:** 0000-0002-0155-9194; **Orcid:** 0000-0003-4134-9682; **Orcid:** 0009-0003-5231-0940;
Faculty of Technical Sciences, University of Novi Sad, Novi Sad, Serbia
*Corresponding author: rodicdr@uns.ac.rs

Abstract: *Accurate prediction of surface roughness (Ra) in laser cutting is essential for quality control and process optimisation. This study presents a Random Forest Regression (RFR) model for the prediction of Ra in fibre laser cutting of EN 10130 steel sheets. The model was trained using 14 experimental samples obtained from a Box-Behnken design with cutting speed, abrasive concentration and gas pressure as input parameters. Three additional samples were used for testing. The RFR model was implemented in MATLAB with 500 regression trees. On the test set, it achieved an RMSE of 0.204 µm and an R^2 of 0.55, with an average absolute error of 2.11%. The average error across all 17 samples remained below 10%. These results confirm that Random Forest is a reliable and interpretable method for modelling surface roughness in laser cutting, especially when working with limited and non-linear experimental data.*

Keywords: *Surface Roughness, Laser Cutting, Random Forest Regression, Machine Learning, Predictive Modeling.*

1. INTRODUCTION

The Laser processing has become one of the most versatile and widely used techniques in modern manufacturing, as it can process a wide range of materials with high precision and flexibility. Despite its sophistication, modelling and predicting the outcomes of laser processes remains a challenge due to the highly nonlinear and multivariate nature of light–matter interactions [1]. In recent years, machine learning (ML) has emerged as a powerful tool for modelling such complex interactions and offers a machine learning-based alternative to traditional physics-based approaches [2].

Various applications of ML in laser processing have shown promising results, especially in the prediction of surface quality parameters such as surface roughness, kerf width and heat-affected zones. For example, deep learning models have shown their potential for both numerical prediction and visual simulation of laser-cut surfaces, improving understanding and process monitoring [1]. Similarly, random forest based models have been successfully used to predict groove geometry and quality in circular laser grooving processes, providing valuable

insights into the most influential process parameters [3].

Surface roughness (Ra), one of the most important quality indicators in laser cutting, has been the subject of numerous studies. Image-based quantification of roughness using neural networks has been investigated as a fast, non-contact alternative to conventional profilometry.

However, validation for different material types is still required for industrial use [4]. Predictive modelling has also been applied in the context of functional laser surface texturing (LST), where surface roughness and topography are closely linked to functional properties such as wettability and biocompatibility [5].

Several research efforts have focused on improving the architecture and optimisation strategies of machine learning models, in particular artificial neural networks (ANNs), to obtain more accurate predictions of surface quality. It has been shown that the optimisation of ANN hyper-parameters using Taguchi methods can significantly improve the performance of roughness prediction models for thermoplastic sheets [6]. In addition, hybrid and ensemble approaches — such as combining neural networks with optimisation algorithms (e.g. HWO, PSO) have shown higher accuracy in predicting kerf deviations in CO_2 laser cutting of polymer materials [1].

In the context of metal matrix composites, ML algorithms such as ANN and k-nearest neighbours (KNN) have been used to improve surface finish in pulsed CO_2 laser cutting, with KNN showing slightly better accuracy than ANN [7]. Similarly, ANN and other classical ML algorithms have been shown to be effective in predicting surface roughness in diamond machining of both brittle and ductile materials, proving their robustness even when working with small data sets [3].

In addition to surface roughness, machine learning has also been used to predict several quality indicators, including kerf waviness and heat-affected zone (HAZ), as demonstrated by the successful application of ELM and Random Forest models in laser cutting of silicon steel [8]. These studies highlight the benefits of ML in multi-response modelling, where complex interactions between process parameters and outcome quality need to be captured simultaneously.

Overall, these efforts emphasise the growing adoption of machine learning in laser-based manufacturing, with a trend toward interpretable, accurate, and data-efficient models. Building on this foundation, the present study investigates the use of Random Forest Regression for predicting surface roughness in fibre laser cutting of EN 10130 steel. Unlike many previous studies that rely on neural networks or complex hybrid approaches, this work evaluates the capability of random forests as a standalone method, particularly in scenarios with limited experimental data. The model is trained on a subset of experimental results and tested on independent samples to assess its generalisation ability. Predictive performance is reported using RMSE and R^2, while the percentage error is analysed to reflect the practical accuracy required in industrial applications.

2. METHODOLOGY AND METHODS

Random Forest (RF) is a non-parametric ensemble learning technique introduced by Breiman [9], which constructs multiple decision trees and aggregates their predictions to enhance accuracy and reduce overfitting. This (RF) is a non-parametric ensemble learning technique that constructs multiple decision trees and aggregates their predictions to enhance accuracy and reduce overfitting. In this study, RF was selected due to its capability to:

- Model nonlinear relationships without requiring prior assumptions,
- Provide internal estimates of feature importance, and

- Demonstrate strong generalization performance on small datasets.

The experimental dataset consisted of 17 samples obtained through a Box-Behnken design, with three input parameters:

- Cutting speed (v) [m/min],
- Laser power (Pw) [% of machine capacity],
- Assist gas pressure (P) [bar].

The target output was surface roughness (Ra), expressed in micrometers (µm), and evaluated using a Mitutoyo Surftest SJ-210 profilometer. The laser-cut edge typically consists of three zones: the entry zone, a smooth central zone, and a rough bottom zone. Particular attention was given to the rough zone, as its width is a sensitive indicator of cut quality and process stability.

The overall workflow of the modeling process is illustrated in Figure 2. The procedure began with data preparation, where 17 experimental samples were characterized by three primary process parameters: cutting speed (v), laser power (Pw), and assist gas pressure (P). To enhance model expressiveness and capture potential nonlinear interactions, two engineered features were introduced: the ratio of cutting speed to pressure (v/P), representing material removal efficiency, and the product of power and pressure (Pw·P), reflecting the combined thermal and mechanical influence on melt expulsion. The dataset was then split into a training set of 14 samples and a test set consisting of samples No. 4, 7, and 12. A Random Forest Regression model was trained using the training data, employing 500 decision trees with fixed maximum depth and bootstrap sampling. Once trained, the model was applied to predict surface roughness (Ra) for the test samples. Performance metrics included root mean square error (RMSE), coefficient of determination (R^2), and percentage error. Additionally, variable importance analysis was conducted to determine the relative influence of each input feature on the prediction outcome.

In addition to the original process parameters, two engineered features (v/P and Pw·P) were included to capture potential interactions and nonlinear effects that may influence surface roughness. Two additional features were engineered to enrich the model:

- the ratio of cutting speed to gas pressure (v/P), and
- the product of laser power and pressure (Pw·P).

All features were used without normalization, as Random Forest models are invariant to scaling. The overall modeling procedure is summarized in Figure 1. The workflow includes data preprocessing, feature engineering, model training using Random Forest Regression, and evaluation using three held-out test samples.

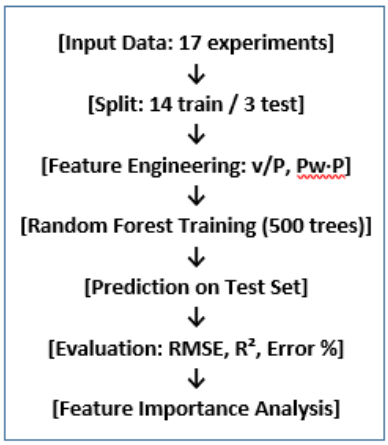

Figure 1. Workflow of the RFR modeling process for predicting Ra in laser cutting.

Model training was performed on the 14-sample training subset. Predictive performance was evaluated on the remaining 3 test samples by calculating:

- Root Mean Square Error (RMSE) – indicating the average deviation between predicted and actual values,
- Coefficient of Determination (R^2) – measuring the proportion of output variance captured by the model,

- Absolute percentage error (APE) – used to interpret prediction accuracy from an engineering standpoint.

Table 1. Experimental and Random Forest predicted Ra for the Box–Behnken design

No.	Input factors			Output		Error
	v [m/min]	Pw [%]	P [bar]	Ra [µm]	RFG	E [%]
1.	0.90	80.00	1.10	3.151	2.943	6.60%
2.	1.30	80.00	1.10	3.994	3.613	9.52%
3.	0.90	88.00	1.10	2.541	2.467	2.91%
4. t	1.30	88.00	1.10	2.951	3.007	1.90%
5.	0.90	84.00	1.00	2.399	2.450	2.13%
6.	1.30	84.00	1.00	2.585	2.815	8.89%
7. t	0.90	84.00	1.20	2.342	2.386	1.88%
8.	1.30	84.00	1.20	3.320	3.054	8.01%
9.	1.10	80.00	1.00	2.493	2.687	7.78%
10.	1.10	88.00	1.00	2.787	2.596	6.86%
11.	1.10	80.00	1.20	2.690	2.692	0.07%
12.t	1.10	88.00	1.20	2.269	2.327	2.56%
13.	1.10	84.00	1.10	1.964	2.087	6.27%
14.	1.10	84.00	1.10	2.025	2.087	3.06%
15.	1.10	84.00	1.10	2.159	2.087	3.33%
16.	1.10	84.00	1.10	2.188	2.087	4.61%
17.	1.10	84.00	1.10	2.099	2.087	0.57%

In addition, predictions were generated for all 17 samples to assess the model's overall behavior, confirming consistent accuracy with individual errors remaining below 10%. To further interpret the model, a feature importance analysis was conducted using the *predictorImportance* method available in MATLAB's *TreeBagger* implementation.

This technique quantifies the relative contribution of each input feature to the model's predictive performance by aggregating the reduction in prediction error across all decision splits involving that feature. The resulting scores provide insight into which parameters most strongly influence surface roughness prediction.

3. RESULTS AND DISCUSSION

Random Forest Regression (RFR) has proven to be an effective method for modelling complex nonlinear relationships in engineering applications, especially when working with limited data sets. In this study, an RFR model was trained using 14 experimental samples obtained from a Box-Behnken design and applied to fibre laser cutting of EN 10130 steel. The experiments varied three process parameters: Cutting speed (v), laser power (Pw) and auxiliary gas pressure (P). The model was tested on three unseen data points (samples 4, 7 and 12).

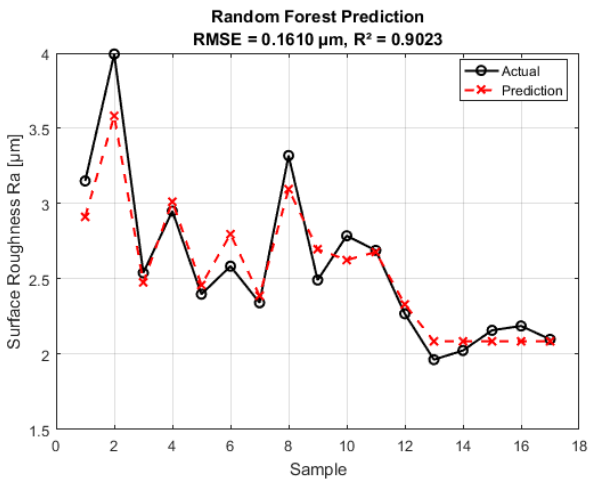

Figure 2. Random Forest prediction of Ra for all 17 samples (RMSE = 0.1610 µm, R^2 = 0.9023).

The predictions for all 17 samples are shown in Figure 2 and show good agreement between the actual and predicted surface roughness (Ra) values. The model achieved a Root Mean Square Error (RMSE) of 0.1610 µm

and a coefficient of determination (R^2) of 0.9023, which means that more than 90% of the variance in Ra is explained by the model. This high degree of accuracy confirms the model's ability to generalise well across the entire data set.

To further evaluate robustness, predictions were made for a hold-out test set that was not used in training. Figure 3 illustrates the results for these test patterns with an RMSE of 0.2044 µm and an R^2 of 0.5532. Although the R^2 value is lower due to the small number of test points, all prediction errors remained below 10%, which is considered acceptable for technical applications. The drop in performance in the test series can be attributed to the scarcity of data, but the model still shows reasonable predictive power and generalisation ability.

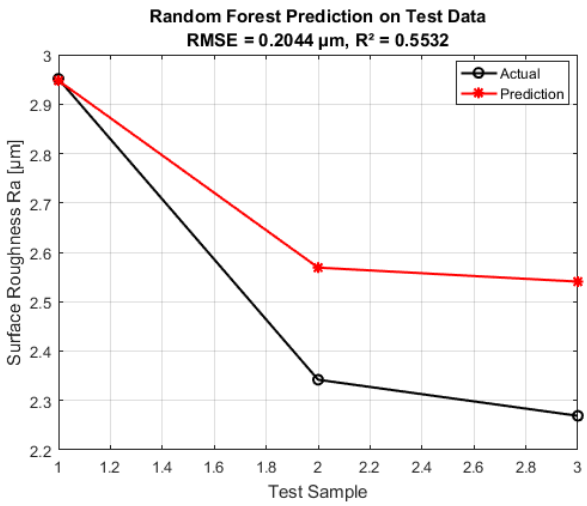

Figure 3. Prediction on hold-out test data (samples 4, 7, 12) (RMSE = 0.2044 µm, R^2 = 0.5532).

Overall, these results confirm that Random Forest is a suitable method for the prediction of surface roughness in laser cutting, providing high accuracy and robustness even with a small number of training samples.

In order to interpret the behaviour of the model and evaluate the contribution of the individual input parameters, a manual estimate of the significance of the features was made. Since the *TreeBagger* object in MATLAB does not directly support *predictorImportance*, a user-defined method was used. This method calculates the frequency and depth of use of each predictor in all decision trees, followed by normalisation.

The results are shown in Figure 4. Cutting speed (v) proved to be the most influential parameter with a normalised importance value of 0.41. This confirms the key role of cutting speed in determining surface quality, as higher speeds often lead to increased roughness due to insufficient interaction time between the laser beam and the material. If the speed is too high, the energy input per unit length is reduced, resulting in incomplete melting, unstable melt flow and irregularities on the cut surface. Conversely, lower speeds can lead to overheating and dross formation, but generally produce smoother surfaces due to a more stable melt output.

The second most important feature was an interaction term or constructed feature (e.g. Pw–P) with a normalised importance of 0.38, indicating that non-linear relationships between laser power and gas pressure were effectively captured by the model. This interaction reflects the coupled influence of energy input (through laser power) and melt removal efficiency (facilitated by assist gas pressure). For example, higher laser power can increase the volume of molten material, which requires sufficient gas pressure to evacuate it effectively. If these parameters are not properly balanced, the melt pool may solidify unevenly, increasing surface roughness.

The assist gas pressure (P) alone showed the smallest contribution of 0.20, indicating that its isolated effect on Ra is less pronounced. Whilst the assist gas plays a crucial role in removing molten material and preventing oxidation at the cut edge, its influence only becomes more apparent when combined with other factors, particularly cutting speed and laser power. In the area tested, the pressure fluctuations alone may not have been sufficient to produce a strong

direct effect on roughness, but they still contribute indirectly through their interaction with energy input and material flow dynamics.

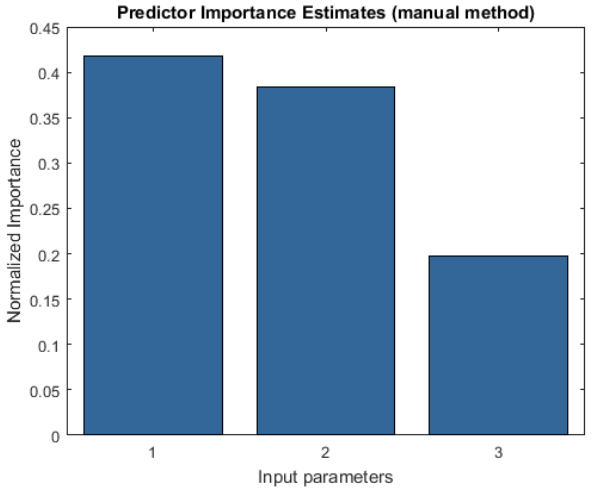

Figure 4. Normalized importance of input parameters in the Random Forest model, where 1 = cutting speed (v), 2 = laser power (Pw), and 3 = assist gas pressure (P).

To better assess the performance of the proposed random forest regression model, a comparison was made with a previously developed hybrid HRSML model [10] that combined response surface methodology and random forest. In the earlier study, the hybrid model achieved an RMSE of 0.2637 µm and an R^2 of 0.8272. In contrast, the stand-alone Random Forest model in the current study achieved better accuracy with an RMSE of 0.1610 µm and an R^2 of 0.9023.

This This result underlines the inherent robustness and adaptability of the Random Forest algorithm, even when used without hybridisation or prior regression shaping. The improved performance can be attributed to several key properties of random forests. First, the ensemble structure of the algorithm, which is based on a bootstrap aggregation of decision trees, enables the effective modelling of complex nonlinear relationships and high-level interactions between input features that are often difficult to capture with purely parametric approaches such as RSM. Second, Random Forest is inherently resistant to overfitting, especially when the number of trees is sufficiently large and the tree depth is appropriately constrained, which is critical when working with small data sets typically encountered in experimental laser processing studies.

In addition, the model's ability to internally estimate the importance of features and handle collinearity without explicit variable selection makes it particularly well suited to multi-parameter manufacturing problems where the interactions between inputs are not always intuitive or easily expressed analytically. Unlike hybrid models, that require two-stage modelling strategies (first fitting a regression model and then correcting the residuals with machine learning), the Random Forest approach learns directly from the raw data and optimises performance holistically. This not only simplifies implementation, but also improves generalisability by avoiding potential error propagation between modelling stages.

The findings suggest that, under conditions of well-structured yet limited data, Random Forest regression alone can offer a high level of accuracy and interpretability for surface roughness prediction in laser cutting. This makes it a valuable modeling option for industrial applications where rapid deployment, transparency, and robust performance are essential.

4. CONCLUSION

This study demonstrates the effectiveness of Random Forest Regression (RFR) in predicting surface roughness (Ra) in fibre laser cutting of EN 10130 steel. Using a dataset of 17 experimental samples and three key process parameters cutting speed, laser power and assist gas pressure the model was trained on 14 samples and tested on 3. All prediction errors remained below 10 %, confirming the robustness of the model even in data-limited scenarios.

Compared to a previously developed hybrid HRSML model, the stand-alone Random Forest Regression (RFR) model demonstrated superior predictive accuracy (RMSE = 0.1610 µm, R^2 = 0.9023), confirming its robustness even without additional regression frameworks. Feature importance analysis revealed that cutting speed was the most influential factor affecting Ra, followed by the interaction between laser power and gas pressure, while gas pressure alone had the smallest individual contribution. Despite its strong performance and ability to model complex nonlinear relationships, a potential limitation of RFR is the lack of an explicit mathematical model, which may reduce interpretability in analytical or optimization contexts where explicit equations are required.

The results suggest that RFR is a powerful tool for modelling complex processes. Its ability to generalise well and provide insights into the relevance of parameters makes it particularly suitable for quality control and process optimisation in laser-based production environments.

ACKNOWLEDGEMENT

This research has been supported by the Ministry of Science, Technological Development and Innovation (Contract No. 451-03-137/2025-03/200156) and the Faculty of Technical Sciences, University of Novi Sad through project “Scientific and Artistic Research Work of Researchers in Teaching and Associate Positions at the Faculty of Technical Sciences, University of Novi Sad 2025” (No. 01-50/295).

REFERENCES

[1] A. F. Courtier, M. McDonnell, M. Praeger, J. A. Grant-Jacob, C. Codemard, P. Harrison, et al.: Modelling of fibre laser cutting via deep learning, Optics Express, vol. 29, pp. 36487-36502, 2021.

[2] B. Mills and J. A. Grant-Jacob: Lasers that learn: The interface of laser machining and machine learning, IET Optoelectronics, vol. 15, pp. 207-224, 2021.

[3] N. E. Sizemore, M. L. Nogueira, N. P. Greis, and M. A. Davies: Application of machine learning to the prediction of surface roughness in diamond machining, Procedia Manufacturing, vol. 48, pp. 1029-1040, 2020.

[4] N. Levichev, A. T. García, M. Kardan, D. Cattrysse, and J. R. Duflou: Experimental validation of a machine learning algorithm for roughness quantification in laser cutting, Procedia CIRP, vol. 113, pp. 564-569, 2022.

[5] T. Steege, G. Bernard, P. Darm, T. Kunze, and A. F. Lasagni, "Prediction of surface roughness in functional laser surface texturing utilizing machine learning," in Photonics, 2023, p. 361.

[6] J. D. Kechagias, A. Tsiolikas, M. Petousis, K. Ninikas, N. Vidakis, and L. Tzounis: A robust methodology for optimizing the topology and the learning parameters of an ANN for accurate predictions of laser-cut edges surface roughness, Simulation Modelling Practice and Theory, vol. 114, p. 102414, 2022.

[7] M. Arunadevi, S. Saravanan, G. Mahesh, and S. Chethan: Machine Learning Based Surface Finish Prediction and Optimization of Process Parameters in Pulsed CO2 Laser Cutting of Particle (TiC) Reinforced Al6061 Composite Using KNN & ANN, Journal of The Institution of Engineers (India): Series D, pp. 1-10, 2024.

[8] T. H. Nguyen, C.-K. Lin, P.-C. Tung, C. Nguyen-Van, and J.-R. Ho: An extreme learning machine for predicting kerf waviness and heat affected zone in pulsed laser cutting of thin non-oriented silicon steel, Optics and Lasers in Engineering, vol. 134, p. 106244, 2020.

[9] L. Breiman: Random forests, Machine learning, vol. 45, pp. 5-32, 2001.

[10] D. Rodić, M. Sekulić, B. Savković, M. Madić, and M. Trifunović: Integration of RSM and Machine Learning for Accurate Prediction of Surface Roughness in Laser Processing, Applied Sciences, vol. 15, p. 7064, 2025.

Society of Production Engineering

ICPES 2025

40th INTERNATIONAL CONFERENCE ON PRODUCTION ENGINEERING - SERBIA 2025

DOI: 10.46793/ICPES25.099K

University of Nis Faculty of Mechanical Engineering

Nis, Serbia, 18 - 19th September 2025

INFLUENCE OF COOLING FLUID TYPE ON THE TEMPERATURE OF HIGH SPEED MOTORIZED SPINDLE

Miloš KNEŽEV[1,*], Cvijetin MLAĐENOVIĆ[1], Dejan MARINKOVIĆ[1], Aco ANTIĆ[1], Aleksandar ŽIVKOVIĆ[1]

Orcid: 0000-0003-0125-9383; **Orcid:** 0000-0001-5480-6673; **Orcid:** 0000-0001-7778-5879; **Orcid:** 0000-0002-8520-762X; **Orcid:** 0000-0003-2274-4927;

[1]University of Novi Sad, Faculty of Technical Sciences, Novi Sad, Serbia

*Corresponding author: knezev@uns.ac.rs

Abstract: *Modern machine tools are expected to deliver significantly higher productivity while minimizing production costs. This requirement has led to the widespread adoption of high-speed machining and the integration of motorized spindles. However, operating at high rotational speeds results in substantial heat generation, which can cause unexpected failures. Therefore, understanding and predicting the thermal behavior of motorized spindles is essential for ensuring operational stability and extending component life. Key sources of heat in motorized spindles include electrical losses within the motor and friction within angular contact ball bearings. To maintain thermal balance, several cooling methods are commonly employed, such as a cooling jacket around the stator, oil mist lubrication, and forced air convection. This paper focuses on the influence of cooling fluid type on the temperature of angular contact ball bearings in a motorized spindle. The cooling system includes a stator cooling jacket, which plays a key role in heat dissipation. A two-dimensional finite element thermal model is developed to simulate heat generation and transfer mechanisms within the spindle assembly. The analysis focuses on temperature distribution in the front and rear bearing regions under two cooling fluid. he simulation results demonstrate noticeable differences in thermal response depending on the coolant type, offering insight into optimal cooling strategies. Water-based cooling shows higher thermal conductivity and efficiency, while oil provides better lubrication and damping characteristics. The study highlights the importance of selecting the appropriate coolant in accordance with spindle design and application requirements. These findings contribute to the ongoing development of more efficient and thermally stable motorized spindle systems for advanced manufacturing.*

Keywords: *Motorized spindle, angular contact bearings, thermal analysis, cooling fluid, finite element method*

1. INTRODUCTION

Machining continues to play a key role in modern manufacturing across a wide range of industries. The majority of metal components undergo some form of machining during their production cycle. As a result, advancements in machining technologies can significantly influence both production efficiency and overall manufacturing costs. [1] High-speed machining, in particular, has gained considerable attention due to its ability to enhance productivity while simultaneously lowering production expenses. However, increasing spindle speed also leads to negative

effects such as noise, vibration (chatter), and heat generation within the spindle system. [2]

During high-speed machining, the excessive heat causes uneven thermal expansion in different machine components, resulting not only in increased friction and wear of the spindle but also in larger machining tolerances. [3] Although high-speed spindles are relatively new technology, numerous studies have addressed various aspects of spindle systems through different analytical and experimental methods.

The dimensional accuracy and surface quality of the machined workpiece largely depend on the thermal, dynamic, and other characteristics of the machine tool spindle system. High-speed spindles are known to experience reliability issues and sudden failures, which are primarily caused by thermal loads. [4] The authors developed a mathematical model to predict bearing temperatures influenced by heat generated in the motor due to electrical losses. A thermal model of the spindle was created using the finite element method, selected for its capability to effectively integrate heat conduction with complex geometries and physical conditions.

The study also showed that decreasing the fluid flow in the cooling jacket results in higher bearing temperatures, emphasizing the significance of efficient cooling.[5]. Statistics indicate that thermal errors can account for up to 60 - 70% of the total geometric errors in a workpiece. [6] Studies, [7] have demonstrated that thermal deformation in numerical control (NC) lathes can reach values as high as 80 µm at spindle speeds of 2000 rpm, while CNC machining centers may experience thermal errors up to 50 µm at 8000 rpm—levels that are clearly unacceptable for precision machining.

Given these findings, investigating the thermal behavior of spindles is crucial to minimizing their impact on the dimensional accuracy of machine tools.

2. HIGH SPEED MOTORIZED SPINDLE

High speed motorized spindles are key elements in modern machining centers, capable of reaching very high rotational speeds—often tens of thousands of revolutions per minute—which enable faster material removal, improved surface finish, and enhanced machining accuracy.

Compared to conventional spindles, motorized spindles integrate the motor directly into the spindle shaft, eliminating power transmission components such as gears and belts. This design reduces vibrations, improves rotational balance, and allows for precise control of acceleration and deceleration. However, the high-speed operation and significant heat generated by the built-in motor place considerable thermal and mechanical stress on spindle components, pushing them to their operational limits [8]. A schematic of a typical high-speed spindle is shown in Fig. 1.

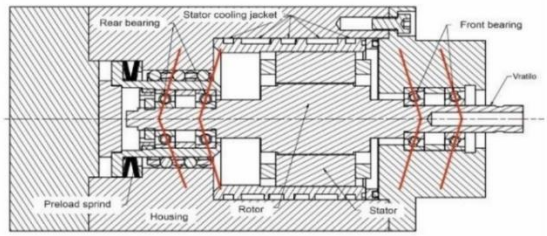

Figure 1. Scheme of high speed spindle

Manufacturers state that high-speed spindles are equipped with efficient liquid cooling systems. Cooling jackets are installed both around the front bearing area and surrounding the spindle, motor, and stator to reduce temperature rises caused by bearing friction and motor losses. By controlling heat generation during operation, the spindle's performance is enhanced, resulting in higher productivity and improved machining quality. The spindle achieves its maximum rated performance within an optimal coolant temperature range of 20 °C to 25 °C. Actual performance, however, varies depending on the coolant temperature and the type of cooling medium used. [9]

3. FINITE ELEMENT MODEL OF MOTORIZED SPINDLE

This paper presents a finite element model analysis of a motorized spindle, emphasizing the role of the cooling jacket and how the flow of different cooling fluids influences the spindle's temperature distribution. The geometry of the spiral cooling jacket surrounding the stator surface of the motorized spindle is illustrated in figure 2.

Figure 2. Schematic geometry of the spiral cooling jacket

Specialized commercial software was employed to develop the 2D surface model of the motorized spindle and perform the detailed thermal analysis. The electric motor inside the spindle acts as a significant heat generator. Most motorized spindles use AC induction motors, with the effective input power of the motor. The heat generated by the motor, which contributes significantly to the spindle's thermal load, can be estimated using the following relation:

$$Q_m = U \cdot I \cdot \cos\varphi - T \cdot \omega \quad (1)$$

In this context, U represents the input voltage, while I denotes the current in each phase. The phase angle φ between voltage and current determines the ratio of real (effective) power to apparent power. The effective electrical input power is partly transformed into mechanical output, while the remainder is lost—primarily in the form of heat.

Where: Q_{motor} is the heat generated by the motor [W], U is the input voltage [V], I is the current [A], ϕ is the phase angle [rad], T is the torque [Nm], ω is the angular velocity [rad/s], calculated as $\omega = \frac{2\pi n}{60}$, where n is the otational speed in revolutions per minute (rpm).

In tabele 1 has been given motor input parameters.

Table 1. Motor input parameters

Exp no.	Voltage [V]	Freqfency [Hz]	Current [A]	Power [kW]	efficiency
1	220	1500	12.3	3	0.88

The main contributors to thermal deformation in the spindle system are the heat generated by the motor and the spindle bearings. Heat removal is primarily managed through forced convection in the cooling channels and by airflow around the spindle housing. This analysis focuses on the impact of different cooling fluids on the temperature distribution within the cooling jacket. The forced convection within the stator cooling channels is characterized by a convective heat transfer coefficient, which is estimated using the following equation:

$$h_v = \frac{N_u \cdot k}{l_t} \quad (2)$$

where *Nu* is Nusselt number, *k* is the thermal conductivity of the fluid, lt channel length.

$$N_u = 0{,}012\left(R_e^{0,87} - 280\right)P_r^{0,4}\left[1 + \left(\frac{D}{L}\right)^{\frac{2}{3}}\right]\left(\frac{P_r}{P_{rw}}\right)^{0,11} \quad (3)$$

$$R_e = \frac{V \cdot D}{\nu} \quad (4)$$

$$V = \frac{Q}{A} = \frac{Q}{h \cdot b} \quad (5)$$

Re is Reynolds number, and *Pr* is Prandtl number (0.7 < *Pr* < 100) of the coolant, D/L is ratio of diameter to length of the tube or channel (geometrical factor), γ is the kinematic viscosity of the fluid, and Pr/Prw≈1 for water, **V** is mean flow velocity, **ν is** kinematic viscosity, **Q** is volumetric flow rate, A is cross-sectional area through which the

fluid flows, h and b are for a rectangular cross-section.

Heat conduction between the stator, cooling jacket, and spindle housing was calculated and modelled using a thermal resistance network approach. This network defines the conductive and convective resistances among the stator, cooling jacket, and housing components. To simplify the analysis, thermal resistances at each interface were individually calculated, allowing for a more manageable formulation of the heat transfer equations.

$$R = \frac{\ln\left(\frac{R_O}{R_i}\right)}{2 \cdot \pi \cdot l \cdot k} \quad (6)$$

Where R_o is outer radius, R_i, is inner radius of considered element, l is element length, and k is the thermal conductivity of material. On the figure 3 conduction network has been presented and R_{kkh} is conduction resistance between cooling jacket and housing, where cooling jacket have been considered as cylinder, while R_{skh} is conduction resistance among cooling jacket and stator.

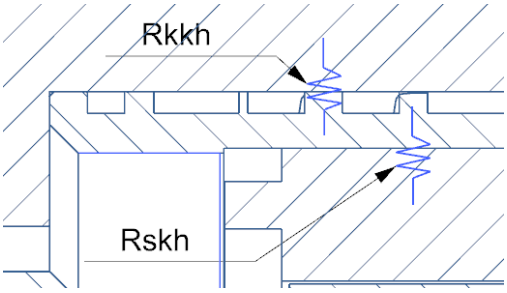

Figure 3. Radial conduction between stator/cooling and jacket/housing

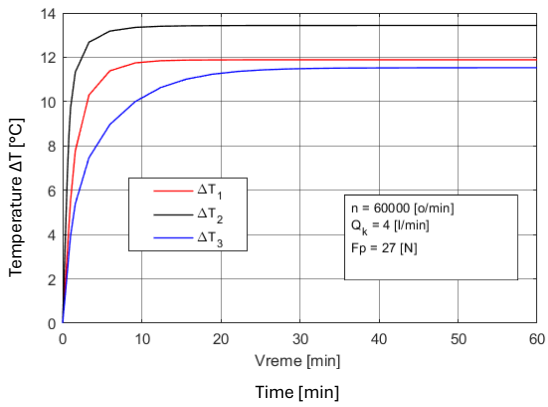

Figure 4. Temperature increase during oil cooling

A free convection coefficient of 12 W/mK is assumed for the ambient air surrounding stationary components such as the spindle housing. The primary objective of this analysis is to develop a mathematical model of the stator cooling jacket and investigate how the type of cooling fluid specifically water and oil, affects the thermal behaviour of the motorized spindle. To isolate this effect, all other heat sources, modes of convection, and radiation are held constant throughout the analysis. Given that spindle bearings are critical to machine performance and reliability, the results focus on their temperature response.

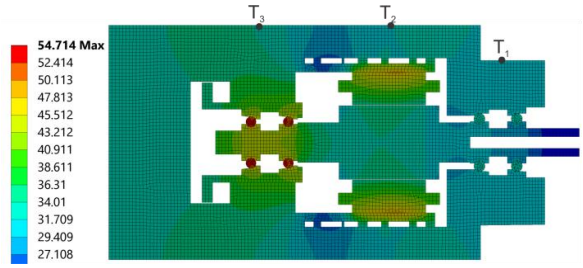

Figure 5. Steady-state temperature distribution at n=60,000 rpm with spindle housing cooled by oil.

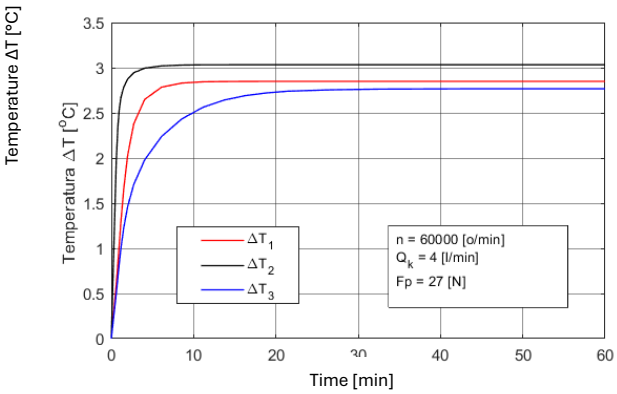

Figure 6. Temperature increase during water cooling

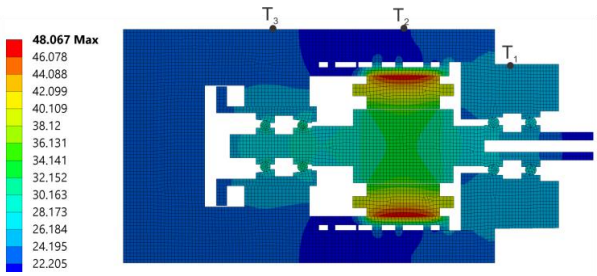

Figure 7. Steady-state temperature distribution at n=60,000 rpm with spindle housing cooled by water

4. CONCLUSION

When the housing is cooled with oil, the heat generated in the electric motor and bearings is distributed almost evenly between the housing and the spindle, with a slightly larger portion of the heat directed toward the rear bearing via the spindle. Smaller amount is transferred through the housing toward the front bearing (Figure 4 and 5).

However, with water cooling, the temperature difference between the housing and the spindle is significantly greater (Figure 6 and 7). In this case, a larger portion of the motor-generated heat is carried through the spindle toward the front bearing, while temperatures along the housing remain relatively uniform. This indicates that the heat is distributed almost equally through the housing toward both the front and rear bearings. In conclusion, the developed computational model serves as an effective engineering tool for analysing the thermal behaviour of motorized spindles. Its straightforward structure, based on a thermal resistance network, allows for quick and sufficiently accurate prediction of temperature distribution within key system components.

Moreover, the model facilitates comparison of different cooling fluids, which is essential for optimizing the cooling system during the early stages of design. This approach not only enhances the reliability and operational precision of the spindle but also reduces the risk of thermally induced damage to bearings and other sensitive parts.

ACKNOWLEDGEMENT

This research has been supported by the Department of Production Engineering, Faculty of Technical Sciences, University of Novi Sad through project “The future of production engineering)”.

REFERENCES

[1] A. Zahedi and M. R. Movahhedy, “Thermo-mechanical modeling of high speed spindles,” *Sci. Iran.*, vol. 19, no. 2, pp. 282–293, Apr. 2012, doi: 10.1016/j.scient.2012.01.004.

[2] K. J. H. Al-Shareef and J. A. Brandon, “On the effects of variations in the design parameters on the dynamic performance of machine tool spindle-bearing systems,” *Int. J. Mach. Tools Manuf.*, vol. 30, no. 3, pp. 431–445, Jan. 1990, doi: 10.1016/0890-6955(90)90187-N.

[3] C. H. Chien and J. Y. Jang, “3-D numerical and experimental analysis of a built-in motorized high-speed spindle with helical water cooling channel,” *Appl. Therm. Eng.*, vol. 28, no. 17–18, pp. 2327–2336, Dec. 2008, doi: 10.1016/j.applthermaleng.2008.01.015.

[4] H. Li and Y. C. Shin, “Integrated Dynamic Thermo-Mechanical Modeling of High Speed Spindles, Part 1: Model Development,” *J. Manuf. Sci. Eng.*, vol. 126, no. 1, pp. 148–158, Feb. 2004, doi: 10.1115/1.1644545.

[5] M. Knežev, M. Zeljković, C. Mlađenović, H. Smajić, A. Stekolschik, and A. Živković, “Effect of various fluid flow on temperature of an angular contact ball bearings in motorized spindle,” 2021, no. May.

[6] R. Ramesh, M. A. Mannan, and A. N. Poo, “Error compensation in machine tools- a review. Part II: Thermal errors,” *Int. J. Mach. Tools Manuf.*, vol. 40, no. 9, pp. 1257–1284, 2000, doi: 10.1016/S0890-6955(00)00010-9.

[7] K. Liu, Y. Liu, M. Sun, X. Li, and Y. Wu, “Spindle axial thermal growth modeling and compensation on CNC turning machines,” *Int. J. Adv. Manuf. Technol.*, vol. 87, no. 5–8, pp. 2285–2292, Nov. 2016, doi: 10.1007/s00170-016-8593-5.

Society of Production Engineering

ICPES 2025

40th INTERNATIONAL CONFERENCE ON PRODUCTION ENGINEERING - SERBIA 2025

DOI: 10.46793/ICPES25.104B

University of Nis Faculty of Mechanical Engineering

Nis, Serbia, 18 - 19th September 2025

MULTILAYER LASER CUTTING OF STEEL PLATES

Jelena BARALIĆ[1]*, Bogdan NEDIĆ[2]

Orcid: 0000-0002-8023-7942; **Orcid:** 0000-0002-4236-3833

[1] Faculty of Technical Sciences Čačak, University of Kragujevac, Čačak, Serbia

[2] Faculty of Engineering, University of Kragujevac, Kragujevac, Serbia

*Corresponding author: jelena.baralic@ftn.kg.ac.rs

Abstract: *A laser is a monochromatic, coherent, convergent beam of electromagnetic radiation with wavelengths from ultraviolet to infrared. Almost all types of materials can be machined with a laser. The laser beam has a very high energy density. In laser cutting, a laser beam is used as a tool, under the influence of which the machined material melts and evaporates. In this way, a precise cut is created with minimal mechanical stress. During laser cutting of material, a heat affected zone is created right next to the cut. For simultaneous cutting of multiple layers of sheet metal - where several sheets are stacked and cut at the same time - laser cutting offers a flexible alternative to traditional punching or mechanical cutting. This is particularly important in the production of parts of small series, complex geometries and from materials that are difficult to process with conventional machining processes. This paper presents the results of research on the possibility of multilayer laser cutting of steel plates. The influence of the traverse speed and number of plates was analyzed. One, two and three plates with a thickness of 4 mm, from S355J2+N (Č0563), were cut with the recommended traverse speed and the traverse speed higher and lower than the recommended values. The width of the cut and the roughness of the machined surface were analyzed, as well as the possibility of cutting through all layers.*

Keywords: *laser beam cutting, multilayer, cutting width, surface roughness.*

1. INTRODUCTION

Unconventional machining methods use electrical, chemical, light, magnetic, nuclear and other forms of energy for machining of materials. This energy is directly supplied to the process - the cutting zone.

Laser is the abbreviation of light amplification by stimulated emission of radiation. A highly collimated, monochromatic and coherent light beam is generated and focused to a small spot [1]. In this way, a very high energy density is achieved (10^6 W/mm^2). Laser gas, which is most often a mixture of oxygen and nitrogen, is supplied to the cutting head and surrounds the laser beam and the

cutting zone during cutting. The laser beam is focused on the workpiece, which is heated, melted and partially vaporized, thus cutting the material. The molten material formed during the cutting process is removed from the cutting zone by the laser gas. Figure 1 shows the principle of laser operation.

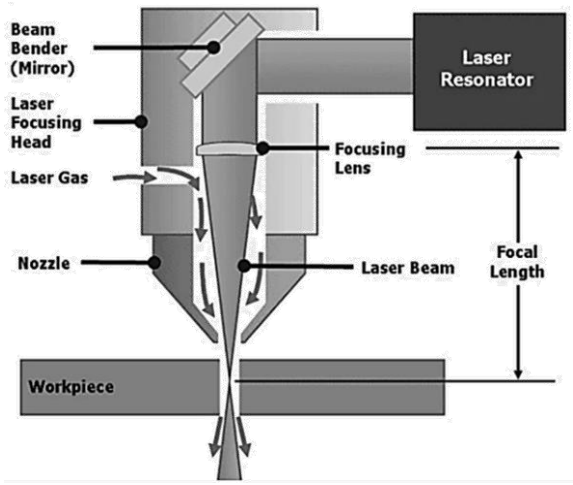

Figure 1. The working principle of the laser [2]

During laser beam cutting, part of the laser beam is reflected from the surface of the workpiece. The remaining part of the energy of the laser beam is absorbed and thus the material of the workpiece is heated. When the material is heated enough, it begins to melt and vaporization occurs, Figure 2.

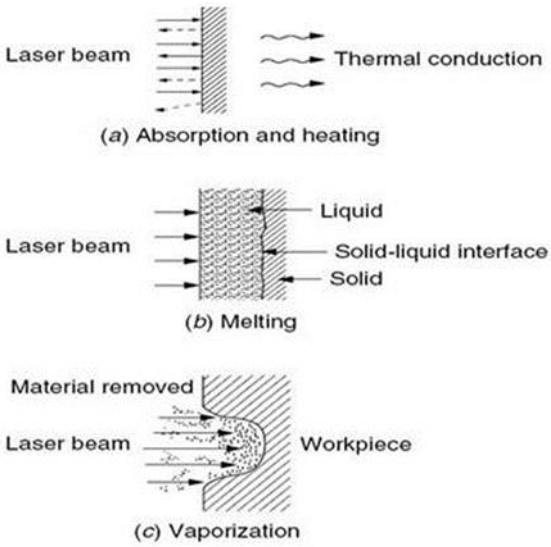

Figure 2. Physical processes that take place during laser beam machining [1]

Multilayer laser cutting

Today, the laser is most often used for cutting almost all types of materials according to predefined contours. In order to achieve higher productivity of the cutting process, more and more attention is paid to simultaneous cutting of several layers of material. Multiple layers of steel can be laser cut, but there are limitations depending on the thickness and type of steel. In principle, it is possible to cut multiple layers if they are well attached and if the maximum power of the laser is sufficient to cut through the total thickness of the material. The most common problems that occur during multi-layer laser cutting of steel are:

- Deformation of the material due to heating, which is especially pronounced when cutting thin sheets or cutting complex contours,
- Fusion of layers of material to be cut and
- Change in the microstructure of the processed material - appearance of heat affected zone [2].

All parameters of the laser cutting process, like power, speed, laser gas pressure, and focal position affect the possibility of cutting multiple layers of material. In practice, it is easiest to set the traverse speed. Higher traverse speeds reduce kerf width and surface roughness but may cause incomplete cuts if traverse speed is too fast. Slower traverse speeds improve edge quality but increase thermal load and cycle time.

Fiber lasers

Fiber lasers use an optical fiber as an optical resonator. Optical fiber gives the name to this type of laser. The laser beam is obtained in an optical fiber whose core is enriched with some of the rare chemical elements such as ytterbium (Yb), erbium (Er), tyllium (Tm), neodymium (Nd), dispersion (Dy), holmium (Ho), praseodymium (Pr). The optical core of the optical fiber is the active material of the laser. By illuminating the core, ions are excited, that

is, stimulated emission of light by excited ions of the elements of the core.

Fiber lasers are increasingly used for metal cutting due to the higher efficiency of energy absorption on metal surfaces, higher cutting speeds and lower operating costs compared to CO2 lasers. Fiber lasers can cut materials up to five times faster and consume approximately 50% less energy [3]. Their streamlined design with fewer moving parts reduces maintenance costs and downtime. Figure 3 shows the working principle of the fiber laser.

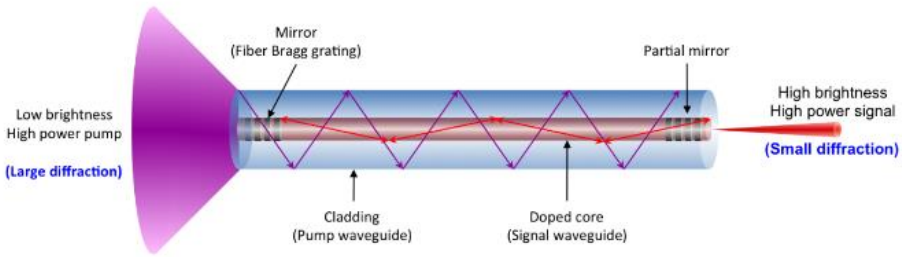

Figure 3. Schematic diagram of fibre laser [4]

The high-power pump light flows through an optical fiber consisting of two main components: a core and a cladding. The core is made of silicon glass and provides a path for the light. This core is covered by an mantle. When light reaches the mantle, it is all reflected back into the core. After that, the light reaches the doped core.

2. EXPERIMENTAL RESEARCH

The goal of the experiment realized within this paper was to analyze the possibility of laser cutting of multiple layers of material. The tests were performed on a TruLaser 3040 laser cutting machine from the Trumpf company at the "Wacker Neuson" company in Kragujevac. This type of laser is characterized by high flexibility and economy, as well as excellent quality. Figure 4 shows the company's laser machine.

Figure 4. Trumpf TruLaser 3040 laser

The power of the machine is 6 KW. For the purposes of the experiment, plates with a thickness of 4 mm, material marked S355J2+N (Č0563) were used. The characteristics of material are given in table 1.

The recommended values of the parameters of the laser cutting process have been adopted. The parameter that was varied during the experiment is the traverse speed. The cut samples are 40x40 mm tiles.

In the experiment, four tile samples were cut on one, two and three layers of material. In these experiments, the plates-layers are tightly joined, with no gap between them.

After laser cutting, the quality of the cut was investigated, the width of the cut and the surface roughness were measured.

For analyzing the possibility of cutting multiple layers of material using a laser in order to achieve savings in laser operation time and material savings, three experiments were performed. The first experiment involves cutting a sample of 40x40 mm tiles on one layer of 4 mm thick material. Four tiles were cut at different traverse speeds, while the other parameters were unchanged and kept as recommended. The second experiment involves cutting a tile of the same dimensions from two layers of material, while in the third, cutting was done from three layers of material, Figure 5.

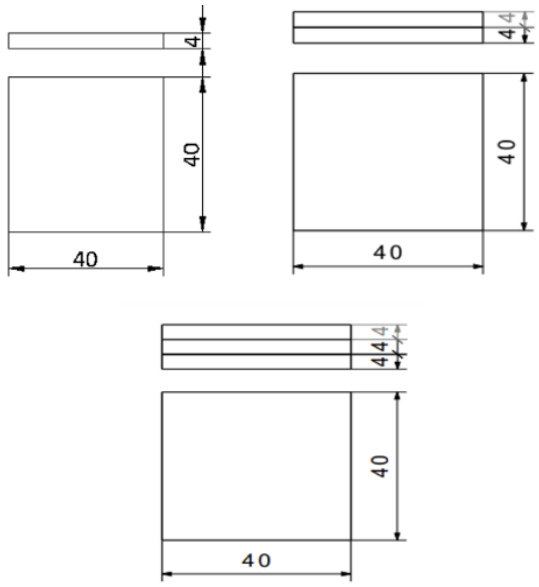

Figure 5. Samples for the first, second and third experiment

With the help of the Trutops software, the input parameters for cutting the material were set and only the traverse speed was varied.

Table 1. Material properties

Material designation	Chemical composition				Mechanical properties
	C %	Mn %	Si %	P, S %	R_e, N/mm^2
S355 J2+N (Č0563)	≤ 0.22	≤ 1.60	0.55	≤ 0.035	≥ 355

Table 2 provides data on the conditions for cutting the tiles and marking the samples. Traverse speed is expressed in % in relation to the recommended value. The pressure of the working gas (mixture of nitrogen and oxygen) was 0.7 bar.

Table 2. Traverse speed and laser power in experiments

Exp. No.	No of layers	Sam. No.	Thic. [mm]	P [KW]	Rec. traverse speed [mm/min]	Traverse speed [%]
E1	**1**	11	4	~3.2	3300	85%
		12	4			100%
		13	4			110%
		14	4			120%
E2	**2**	21	8	~4.6	2830	85%
		22	8			100%
		23	8			110%
		24	8			120%
E3	**3**	31	12	~6	2050	85%
		32	12			100%
		33	12			110%
		34	12			120%

3. RESULTS AND DISCUSSION

First experiment - Figure 6 shows sample number 11 from the upper and lower side and cut surface. One layer was cut, with a speed of 85% of the recommended one. The plate has been cut successfully. No burr was observed from the bottom side.

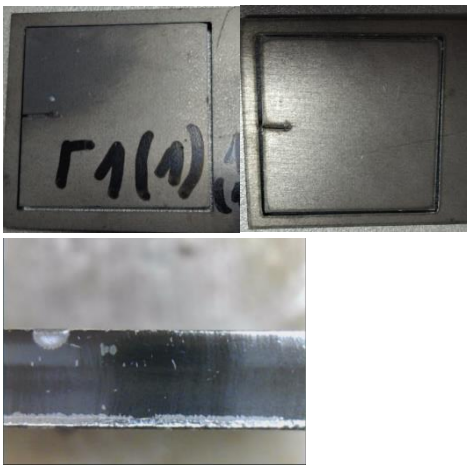

Figure 6. Sample 11, the upper and bottom side and the cut surface

Figure 7 shows sample number 12, the top and bottom side and the cut surface. One layer of steel was cut with 100% of the recommended traverse speed. The plate has been cut successfully. No burr was observed from the bottom side.

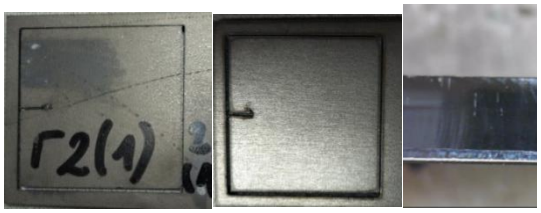

Figure 7. Sample 12, the upper and bottom side and the cut surface

Figure 8 shows sample number 14 from the top and bottom side. One layer was cut with a speed of 120% of the recommended traverse speed value. Due to the high travers speed and the impossibility of removing the molten material, the sample was not successfully cut on the lower side, the molten material was retained. The plate was not separated, so there was no measurement of the cut surface topography.

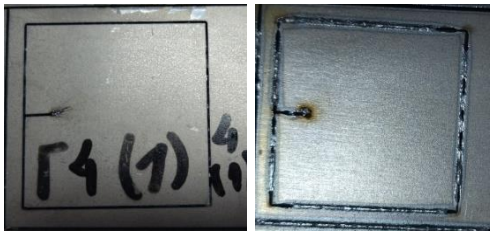

Figure 8. Sample 14, the upper and bottom side

Figure 9 shows sample number 21 from the top and bottom side, as well as the cut surface. Two layers of material were cut with a traverse speed of 85% of the recommended value. Cutting was successfully performed on the top and bottom of both tiles. The appearance of burr on the lower plate can be observed.

Figure 9. Sample 21, the upper and bottom side and the cut surfaces

Figure 10 shows sample number 24 from the top and bottom side. Two layers were cut with a traverse speed of 120% of the recommended one. At this speed, there was no cutting of the layers, but partial cutting and melting of part of the material. Also, it can be seen from the bottom side a large retention and deposition of molten material. In this case, it was not possible to separate the samples from the plate, so the surface topography was not measured.

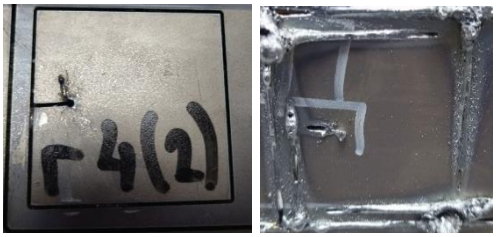

Figure 10. Sample 24, the upper and bottom side

Figure 11 shows sample number 31 from the top and bottom side, as well as the cut surfaces of the top layer and the bottom two layers. The cutting of the samples was done with a traverse speed of 85% of the recommended one. All three layers were cut, however, the samples of the second and third layers were joined, and it was not possible to separate them.

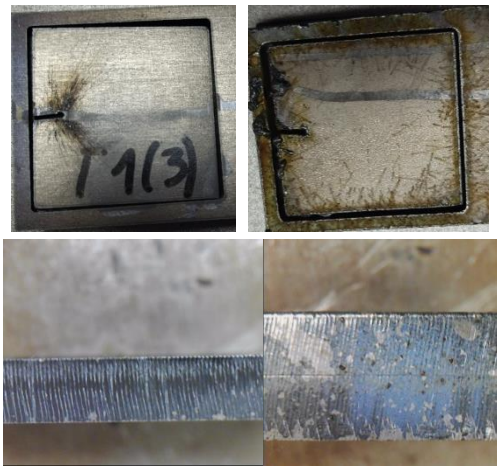

Figure 11. Sample 31 from the upper and bottom sides as well as the cut surface of the upper separated layer and the cut surface of the merged middle and bottom layers

Figure 12 shows sample number 32 from the top and bottom side. Three layers of material were cut with the recommended traverse speed (100%). As in the previous case, all three layers were cut, but there was also a merging of the second and third layers, which could not be separated.

Figure 12. Sample 32 from the upper and bottom sides as well as the cut surface of the upper separated layer and the cut surface of the merged middle and bottom layers

Figure 13 shows sample number 34 from the top and bottom side. Three layers were cut at the same time with a traverse speed of 120% of the recommended value. At this traverse speed, not a single layer was cut. The cutting is partially done, but not completely. Due to the high traverse speed, the working gas did not successfully carry away the molten material, instead, it cooled quickly and remained trapped and deposited between the layers. No layer could be removed.

Figure 13. Sample 34 from the upper and bottom side

The width of the cut of the samples was measured from the upper side of the upper layer and the lower side of the lower layer. The measurement was performed on a tool microscope. The surface roughness was measured using the device ISR - C002, INSIZE. The measuring device is placed on the base of the Talisurf-6 measuring system. The surface roughness parameters were measured at a distance of 1 mm from the upper surface. Table 3 shows the measurement results.

Table 3. The width of the cut and the roughness of the machined surface

Sample No	Width of cut		Roughness	
	Upper side mm	Bottom side Mm	Ra (µm)	Rmax (µm)
11	0.507	0.809	1.757	9.533
12	0.511	0.891	2.207	13.435
13	0.537	0.931	2.148	40.304
14	0.524	1.499	-	-
21	1.128	0.808	2.943	17.485
	0.045	0.08	2.298	18.176
22	0.016	0.495	1.060	7.458
	0.405	0.636	2.592	19.016
23	0.708	0.722	4.555	19.164
	0.44	-	-	-
24	0.143	-	-	-
	-	-	-	-
31	0.798	0.81	10.718	67.173
	0.131	0.407	-	-
32	0.61	0.74	6.925	43.218
	1.668	1.011	7.165	35.562
33	0.911	0.801	6.925	43.218
	0.789	-	-	-
34	-	-	-	-

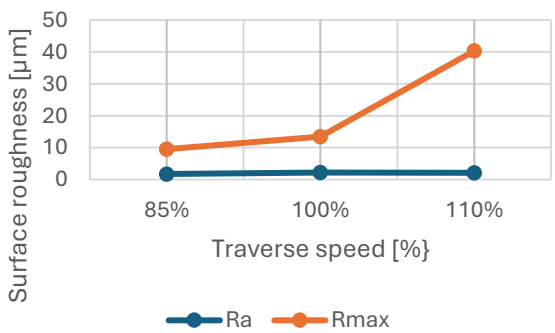

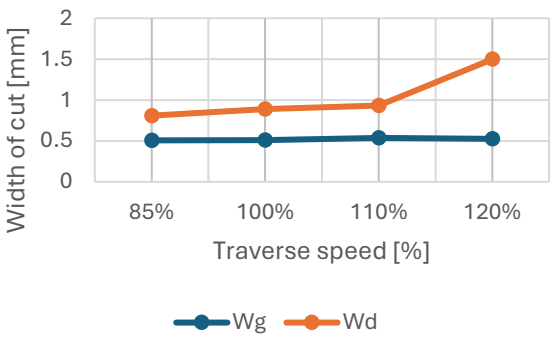

Figure 14. Diagrams of the roughness of the machined surface and the width of the cut depending on the traverse speed

Based on the results shown in table 3, the diagrams of the change in the roughness of the machined surface and the width of the cut depending on the traverse speed are shown, figure 14. The diagrams are given only for cutting one layer of material.

4. CONCLUSION

When cutting one layer of material, samples were cut during laser cutting with values of 85%, 100% and 110% of the recommended traverse speed value. Only when cutting with a traverse speed of 120% of the recommended one, complete cutting of the material did not occur. When cutting two layers of material, both layers were completely cut when cutting with a traverse speed of 85% and 100% of the recommended traverse speed value, for the total thickness of the material. When cutting with 110% of the recommended traverse speed, the upper layer of material is completely cut, but the lower layer is not. High melt retention was observed when cutting at 120% of the recommended traverse speed, so the layers remained uncut. When cutting three layers of material with 85% and 100% of the recommended traverse speed the layers are completely cut, but the bottom two layers remain merged. By cutting three layers with 110% of the recommended traverse speed, only the top layer is completely cut, while when processing with 120% traverse speed, no layer is completely cut.

Based on the conducted experiments, it is observed that when cutting multiple layers with a laser, the traverse speed should be chosen carefully. In the experiment, the recommended traverse speed values were chosen based on the machine manufacturer's literature for the total thickness of the material being cut. When cutting three layers of material during processing with 85% and 100% traverse speed, the middle and bottom layers were merged. It can be concluded that when cutting thicker layers of material, lower traverse speed values should be adopted than those recommended for the total thickness of the material.

The analysis of the effect of traverse speed on the roughness of the machined surface and the width of the cut was done only for cutting one layer of material, because only in this case the material was completely cut for all values of traverse speed. From the diagram, it can be seen that with the increase in traverse speed, the roughness of the machined surface increases and the width of the cut increases.
It is necessary to carry out more detailed research on the influence of number and thickness of layers and traverse speed on the width of the cut and the roughness of the machined surface in order to be able to present more detailed conclusions.

ACKNOWLEDGEMENT

This study was supported by the Ministry of Science, Technological Development and Innovation of the Republic of Serbia, and these results are parts of the Grant No. 451-03-136/2025-03/200132, with University of Kragujevac - Faculty of Technical Sciences Čačak.

REFERENCES

[1] H. El-Hofy: Advanced Machining Processes Nontraditional and Hybrid Machining, Hassan McGraw-Hill, New York, 2005.

[2] 2D Laser Cutting: Process, Capabilities, & Benefits, available at: https://www.tdmfabrication.com/blog/2d-laser-cutting, accessed:15.08.2025.
[3] High-Speed Laser Cutting Optimization for Multi-Layered Sheet Metal Assemblies, available at: https://www.anebon.com/news/high-speed-laser-cutting-optimization-for-multi-layered-sheet-metal-assemblies/, accessed: 10.08.2025.
[4] Fibre Lasers – Working Principles, Applications & More, available at: https://fractory.com/fibre-lasers-explained/0208, accessed: 02.08.2025.
[5] Šta su fiber laseri ?, available at: https://chitech.rs/sta-su-fiber-laseri/, accessed: 01.08.2025.
[6] D. Milikić, Nekonvencionalni postupci obrade - priručnik za studije i praksu, Fakultet tehničkih nauka, Novi Sad, 2002.
[7] M. Madić, Matematičko modeliranje i optimizacija procesa laserskog sečenja primenom metoda veštačke inteligencije, Doktorska disertacija, Univerzitet u Nišu, Mašinski fakultet, Niš, 2013.
[8] N. Dodd, E. Ballantyne, G. Heron, R. Goodall: Multi-layer laser cutting of electrical steel sheets applied to electric machine laminations, PLoS ONE, Vol. 18, No. 7, (13), 2023.
[9] M. Alsaadawy, M. Dewidar, A. Said, I. Maher, T. A. Shehabeldeen: A comprehensive review of studying the influence of laser cutting parameters on surface and kerf quality of metals, The International Journal of Advanced Manufacturing Technology, Vol. 130, pp. 1039-1074, 2024.

Society of Production Engineering

ICPES 2025

40th INTERNATIONAL CONFERENCE ON PRODUCTION ENGINEERING - SERBIA 2025

DOI: 10.46793/ICPES25.112I

University of Nis Faculty of Mechanical Engineering

Nis, Serbia, 18 - 19th September 2025

QUANTITATIVE ANALYSIS OF TOOL WEAR IN DEEP HOLE DRILLING

Milan IVKOVIĆ[1], Strahinja ĐUROVIĆ[2], Bogdan ŽIVKOVIĆ[1], Stefan ĐURIĆ[1], Aleksandar ĐORĐEVIĆ[1], Goran DEVEDŽIĆ[1], Suzana PETROVIĆ SAVIĆ[1]*

Orcid: 0000-0001-5176-5837; **Orcid:** 0000-0002-6589-5883; **Orcid:** 0000-0002-5629-6221;

[1]Faculty of Engineering University of Kragujevac, Kragujevac, Serbia

[2] Faculty of Technical Sciences, University of Pristina in Kosovska Mitrovica, Kosovska Mitrovica, Serbia

*Corresponding author: petrovic.suzana@gmail.com

Abstract: *This paper presents an experimental procedure for the automatic detection and quantitative evaluation of surface wear on drills used in deep hole drilling processes. The analysis was based on images of the cutting edge captured by an industrial camera under controlled conditions, with a particular focus on the curved edge segment, which is especially prone to wear. A custom image processing algorithm was developed within the MATLAB programming environment, employing a multi-stage approach—preprocessing, surface condition classification, and distance analysis of worn zones from the curved edge—to calculate VB_mean as an indicator of wear severity. The algorithm successfully distinguishes between healthy regions, grinding marks, mechanical damage, and active wear, significantly reducing the risk of misinterpretation. Quantitative analysis performed on a dataset of 50 samples demonstrated repeatability of the results and potential for further industrial application. The observed wear patterns may serve as a basis for optimizing process parameters and implementing predictive maintenance strategies. The proposed methodology represents a step toward automated tool condition monitoring under demanding machining conditions, with the potential for integration into broader technical diagnostics systems.*

Keywords: *deep drilling, tool wear, image processing.*

1. INTRODUCTION

In modern manufacturing processes, deep hole drilling holds a significant place, particularly in industries with strict demands for precision, reliability, and surface quality—such as aerospace, energy, and precision engineering. The technologies used for this type of machining enable efficient material removal at considerable depths, but also subject the tool to substantial mechanical and thermal loads. During operation, the cutting edge of the drill is exposed to complex stress mechanisms—a combination of friction, elevated temperatures, and abrasion. As a result, cutting edge wear occurs, which directly affects process stability, surface quality, and the overall tool life. Recognizing and analysing these changes is essential for process optimization and timely tool replacement [1,2].

Most commonly in practice, wear monitoring is accomplished through visual observation or manual measurements, which, apart from being time-consuming, are also prone to

subjective interpretation. As even small deviations from the tool geometry can lead to significant errors in dimensional accuracy, surface roughness, and tolerance generation, it becomes obvious that the need is for an objective and precise quantitative evaluation method. Automation of the process enables the rapid analysis of a large number of samples and offers opportunities for integration in industrial monitoring systems [3-5].

In this study, we focused on the analysis of the surface condition of drills used in deep hole drilling processes based on images acquired by an industrial camera. Our target was the development of an experimental algorithm for automatic detection, and quantification of wear zones, with particular emphasis on calculating the parameter VB_mean—the average wear width along the curved cutting edge of the tool.ool.

The algorithm was designed to identify different types of surface changes—healthy regions, wear zones, grinding marks, and potential damage—using multi-channel binary segmentation. Additionally, we introduced a calibration feature based on a 1 mm reference marker, allowing the results to be expressed in real-world units rather than pixels. This enabled quantitative comparison across different samples and facilitated the interpretation of results in a practical context.

This approach not only contributes to a deeper understanding of wear processes under deep drilling conditions, but also paves the way for further improvement of tool condition monitoring methods in industrial environments.

2. MATERIALS AND METHODS

2.1 Experimental setup

For this experimental analysis, we examined drills that had been exposed to actual working conditions during industrial use. The machining was carried out on a TBT T30-2-500 horizontal deep hole drilling machine (TBT Tiefbohrtechnik GmbH+Co). Thanks to its high positioning accuracy, rigid construction, and efficient internal coolant system, this machine enables reliable execution of deep drilling processes (up to 500 mm depth) within a diameter range of 4 to 30 mm, at spindle speeds ranging from 550 to 6400 rpm, feed rates from 35 to 320 mm/min, and coolant pressures up to 80 bar.

The experimental setup involved horizontal fixation of the drill using a precision prism, with simultaneous image acquisition from two cameras: an industrial camera (48 MP FHD Camera V8, C-mount lens, optical zoom 8×–100×) equipped with side-mounted ring lighting, and a front-facing Vividia 2.0 MP handheld USB digital microscope. This configuration enabled high-resolution imaging of the curved cutting edges, providing sufficient detail for subsequent image processing and quantitative wear analysis (Fig.1).

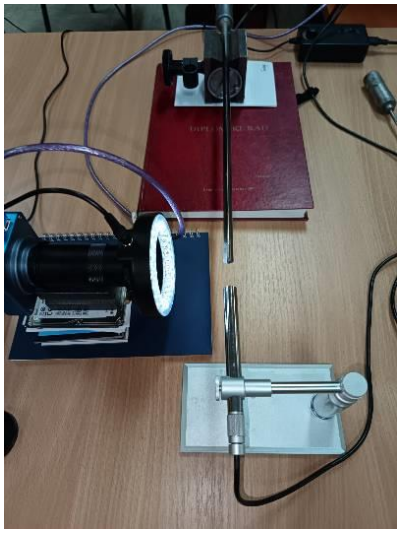

Figure 1. Experimental setup for visual analysis of drill wear

This configuration enables simultaneous observation of both the lateral surface and the tool's tip (Fig. 2), providing comprehensive visual information about the condition of the cutting edge. The lighting system was optimized to eliminate shadows and reflections, while image acquisition was performed via a computer under controlled, vibration-free conditions.

All images were captured at a constant distance and fixed orientation of the camera

relative to the tool, using a stable laboratory platform.

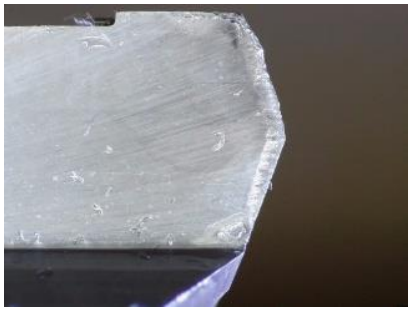

a)

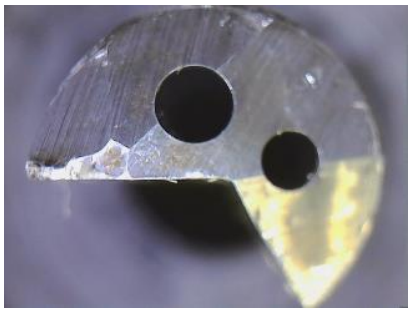

b)

Figure 2. Representative images of tool wear captured from two angles: (a) side view, (b) frontal view captured with a microscope camera

2.2 Algorithm for tool wear detection

A custom - developed algorithm, implemented in the MATLAB environment, was applied for image processing of the tool edges, enabling automatic detection and visual representation of wear [6,7]. The algorithm performs segmentation of the tool geometry, identification of worn areas, and calculation of the average wear width (VB_mean) along the curved cutting edge.

The algorithm structure is organized into three logical stages (Fig. 3):

1. The preprocessing phase includes importing the input image and preparing it for further analysis. The image is first converted to grayscale (Fig.4a), followed by local contrast enhancement using the CLAHE (Contrast Limited Adaptive Histogram Equalization) (Fig.4b) method with parameters: tile grid size 8×8 and clip limit 0.01. Gaussian filtering (σ = 0.8) is then applied to reduce noise. To enhance the visualization of surface texture, a so-called relief map is extracted based on local contrast variations;

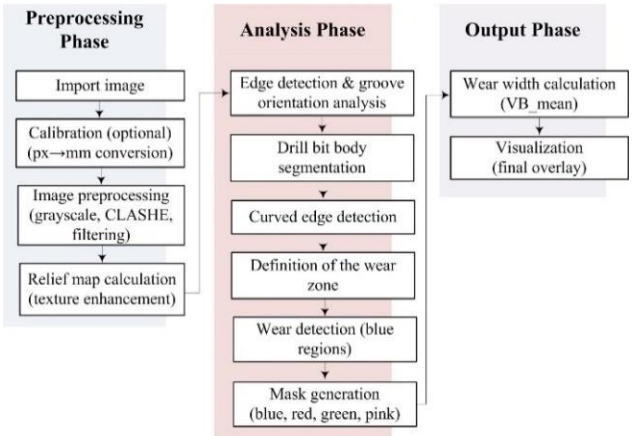

Figure 3. Tool wear detection algorithm

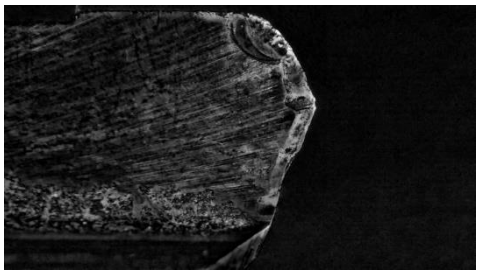

a)

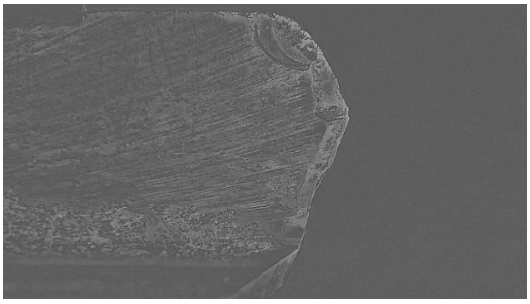

b)

Figure 4. Preprocessing phase: a) Grayscale image, and b) Local contrast enhancement

2. The analytical phase involves segmentation of the drill body and extraction of the curved edge on the frontal surface. Wear regions (blue zones) are identified using a robust threshold defined by the median and robust standard deviation (k = 0.5). Simultaneously, an analysis of groove orientation is performed to detect grinding marks (green regions) and mechanical damage that deviates from the dominant direction (red regions);

3. The results phase includes quantitative evaluation of wear. The VB_mean parameter is calculated as the median distance of the detected blue regions from the curved cutting edge. The result is presented as a colour map (Fig.5) allowing for intuitive visualization of the tool condition.

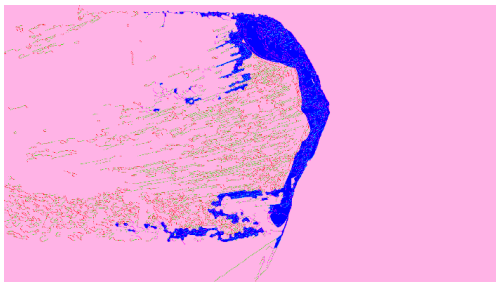

Figure 5. Drill condition map (pink - healthy surface, blue - wear, green - grinding marks, red - damage)

The analysis was conducted on a dataset of 50 images obtained under controlled laboratory conditions. The applied calibration, based on a 1 mm reference marker, enabled the conversion from pixels to millimetres and provided an approximate metric interpretation of the results.

3. RESULTS

The experimental algorithm was applied to a sample of 50 tool images with the aim of quantitatively and visually assessing tool wear. The key processing stages—preprocessing, surface classification, and extraction of relevant regions—were presented in the previous section (Fig. 4 and Fig. 5). Based on the extracted blue regions (identified as wear) and their distance from the curved edge, the average wear width (VB_mean) was calculated.

For the representative example, the average wear width was determined to be VB_mean = 90 px (approximately 109.51 px = 1 mm).

VB_mean is a simple yet effective quantitative parameter for defining the intensity of wear along the active cutting tool edge. Its use offers a handy opportunity for comparison of images regularly without actual measurement, and it reduces subjective error significantly.

Additionally, the local distribution of the shown worn areas also testifies to local loading—dominant in this case in the upper right portion of the edge (Fig. 5). It is a result of faulty cutting conditions, tool geometry, or poor heat removal during the drilling process. The visual examination of the classified image also facilitates the identification of other potentially harmful features, including grinding marks (potentially indicating prior sharpening) and localized damage (also in need of analysis). Through this, the output from the algorithm contributes to further knowledge about the condition of the tool, enabling not only evaluation of current wear but also potential classification of samples by level of degradation.

4. DISCUSSION AND CONCLUSION

The obtained results demonstrate that the developed algorithm effectively detected and quantified surface wear on the tool. Metrics such as VB_mean enabled objective comparison between samples, confirming the applicability of the method in the context of automated tool condition analysis. In the representative example (Fig. 5), a tendency toward localized wear was observed in the upper right area of the curved edge. Although currently illustrative, this pattern may indicate an asymmetric distribution of load and thermal flow during the machining process. Such wear patterns are consistent with known wear mechanisms in deep hole drilling, particularly when working with difficult-to-machine materials under pronounced thermomechanical stress [1,5,8].

While this study focuses on image-based analysis of tool wear under controlled laboratory conditions, these findings are complementary to existing industrial approaches, where real-time process data and machine learning models have been employed to predict tool wear during CFRP drilling [8]. Integrating image-based

diagnostics with in-process monitoring can provide a comprehensive framework for predictive maintenance in drilling operations. Building on advances in Python-based image analysis for drilling damage assessment [7], the proposed algorithm extends these capabilities by automatically distinguishing between different types of surface changes — wear, grinding marks, and damage — which significantly improves diagnostic accuracy. This prevents misinterpretation of traces from previous interventions (e.g., sharpening) as active wear, thereby increasing the reliability of tool condition evaluation. Such capability is particularly valuable in the context of ongoing research on optimizing drilling methods and tool design, where accurate surface characterization is essential for understanding wear mechanisms and improving process performance.

Compared to conventional inspection methods (visual assessment, manual measurements), the digital approach offers a higher degree of repeatability, eliminates subjective error, and enables potential integration into predictive maintenance systems. Particularly noteworthy are the results related to the precise detection of the VB_mean line, which not only quantifies the degree of wear but can also serve as an input parameter for predictive models of the tool's remaining useful life [7,8].

In conclusion, this study presents the development of an experimental procedure for visual and quantitative evaluation of drill wear in deep hole drilling, based on industrial camera imaging and image processing techniques. The algorithm enabled automatic identification of wear zones along the curved cutting edge and calculation of VB_mean as a relevant wear parameter. This approach provides reliable wear mapping and contributes to a deeper understanding of tool behaviour during operation.

Future research will focus on analysing a larger number of samples, correlating results with operational parameters, and integrating the method into predictive maintenance systems under real industrial conditions.

ACKNOWLEDGEMENT

This paper is the result of research conducted under the author's contract No. 451-03-137/2025-03/200107, dated February 4, 2025. The authors would also like to acknowledge the support of Zastava Arms AD, Kragujevac, for providing the material samples used for imaging and analysis in this study.

REFERENCES

[1] X. Li, C. Zhai, W. He, Y. Lu, B. Zhang: Experimental Investigation of Tool Wear and Machining Quality of BTA Deep-Hole Drilling in Low-Carbon Alloy Steel SA-5083, Materials, Vol. 16, pp. 6686, 2023.

[2] X. Li, C. Zhai, C. Eang, R. Wu, C. Zang, S. Zhang, B. Guo, Y. Su: Experimental Investigation and Modeling of Surface Roughness in BTA Deep Hole Drilling with Vibration Assisted, Materials, Vol. 18, pp. 56, 2025.

[3] R. Munaro, A. Attanasio, A. Del Prete: Tool Wear Monitoring with Artificial Intelligence Methods: A Review, Journal of manufacturing and materials processing, Vol. 7, pp. 129, 2023.

[4] J. Bharani Chandar, L. Nagarajan, M. Siva Kumar: RECENT RESEARCH PROGRESS IN DEEP HOLE DRILLING PROCESS: A REVIEW, Surface Review and Letters, Vol. 28, No. 11, pp. 2130003, 2021.

[5] D. Fandiñoa, V. Guski, R. Wegert, S. Schmauder, H.-C. Möhringb: Numerical Investigations on Single Lip Deep Hole Drilling, Procedia CIRP, Vol. 102, pp. 132-137, 2021.

[6] T. Chunlei, C. Yan, C. Tian, Y. Tianlong: The application and optimization of rolling processing technology in improving the efficiency of deep hole processing, Advances in Mechanical Engineering, Vol. 16, No. 12, pp.1-17, 2024.

[7] R.D.F. Sousa Costa, M.L.S. Barbosa, F.G.A. Silva, T.E.F. Silva, A. M.P. de Jesus, F.J.G. Silva, L.M.P. Durão, J.M.R.S. Tavares: Image Analysis Techniques Applied in the Drilling of a Carbon Fibre Reinforced Polymer and Aluminium Multi-Material to Assess the

Delamination Damage, Processes, Vol. 12, pp. 1258, 2024.

[8] C. Domínguez-Monferrer, J. Fern´andez-P´erez, R. De Santos, M.H. Migu´elez, J.L. Cantero: Machine learning approach in non-intrusive monitoring of tool wear evolution in massive CFRP automatic drilling processes in the aircraft industry, Journal of Manufacturing Systems, Vol. 65, pp. 622-639, 2022.

Session 2:

Metal forming and joining technologies

Society of Production Engineering

ICPES 2025

40th INTERNATIONAL CONFERENCE ON PRODUCTION ENGINEERING - SERBIA 2025

DOI: 10.46793/ICPES25.119M

University of Nis Faculty of Mechanical Engineering

Nis, Serbia, 18 - 19th September 2025

DETERMINATION OF THE FLOW CURVE OF ALZN5MG3 ALLOY USING THE MODIFIED RASTEGAEV TEST

Mladomir MILUTINOVIĆ[1*], Dejan MOVRIN[1], Milica PANIĆ[1], Marko VILOTIĆ[1], Nemanja PRODANOVIĆ[1]

Orcid: 0000-0002-3828-8500; **Orcid:** 0000-0001-7812-0713; **Orcid:** 0009-0008-5548-6382; **Orcid:** 0000-0002-1945-0007;

[1]Faculty of technical sciences, Novi Sad, Serbia

*Corresponding author: mladomil@uns.ac.rs

Abstract: *The application of a modified Rastegaev test for determining flow curves is presented in this paper, as these curves are essential for accurate modeling and simulation of metal forming processes. First, a comprehensive overview of conventional flow curve determination methods is provided, including tensile, compression and tensile testing techniques. The modified Rastegaev test is then described in detail, with particular emphasis on its ability to evaluate material behavior across a wide range of plastic strains.*

The experimental part focuses on characterizing the flow behavior of an AlZn5Mg3 aluminum alloy using the modified Rastegaev test. The resulting data were used to construct the flow curve of the tested alloy, which was subsequently approximated using the Ludwik equation.

Keywords: *flow curve, modiefied Rastegaev test, Ludwik equation, Hollomon equation*

1. INTRODUCTION

Reliable flow curve data is indispensable for the design, simulation, and optimization of metal forming processes. By quantifying the relationship between stress and plastic strain, flow curves provide the necessary input for accurately predicting material behavior under different loading conditions. Traditionally, flow curves have been obtained through conventional testing methods such as tensile, compression, and torsion tests [1]. While these approaches are widely used, each of them has certain limitations, particularly in their ability to cover a wide range of plastic strains or to reproduce the complex stress states encountered in industrial forming operations. As a result, there is a continued need for alternative testing techniques that can extend the applicability and accuracy of flow curve determination [2, 3].

One such approach is the Rastegaev test [4], originally designed to account for the effects of inhomogeneous deformation in compression testing. In a standard compression test, friction between the specimen and the tool surfaces often leads to inhomogeneous deformation, barrelling of the specimen, and deviations in the measured stress–strain response. These

effects restrict the accuracy of the derived flow curve, particularly at higher plastic strains. To address this problem, Rastegaev [4] proposed a modified specimen geometry that significantly reduces frictional influences. The conventional Rastegaev specimen (Fig. 1a) is a cylindrical sample with cylindrical recesses on its surfaces. These recesses are filled with lubricant (Fig.1b) prior to testing to minimize friction and prevent the extreme barreling (a bulging shape) typical of standard upsetting tests. Building on this concept, the Rastegaev test allows the determination of flow curves over an extended range of plastic strains ($\varphi_{max} \approx 1.4$) [5], making it especially suitable for materials used in large plastic deformation processes such as bulk metal forming

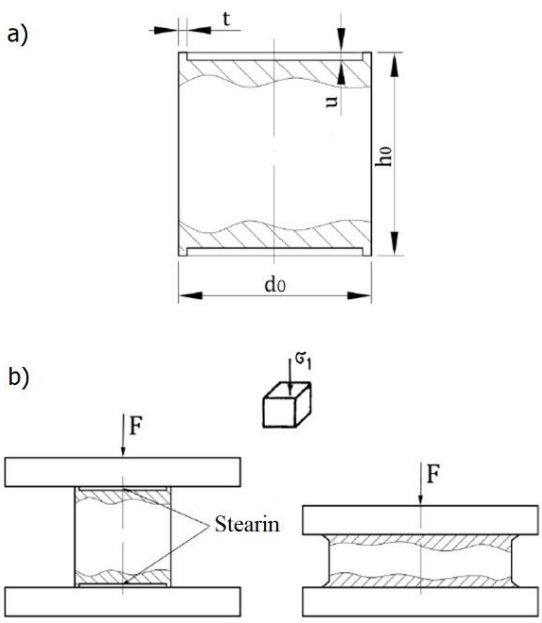

Figure 1. Conventional Rastegaev specimen (a) and corresponding testing procedure (b)

In addition to specimens with cylindrical recesses, the Rastegaev test can also be performed using specimens with different geometrical features (Fig. 2). Although these specimens are less commonly used in practice due to manufacturing challenges, they offer certain advantages. In particular, specimens with conical recesses exhibit greater stability during testing, allowing better control of the deformation pattern at large strains and enabling the determination of flow curves over a wider range of plastic strains ($\varphi_{max} \approx 2$) [6].

In this work, the modified Rastegaev test is applied to an AlZn5Mg3 aluminum alloy. The experimental results were used to construct the material's flow curve, which was subsequently analyzed and approximated using the Ludwik empirical equation, also known as the power-law hardening model. The study aims to demonstrate the effectiveness of the modified Rastegaev test in determining flow behavior and to provide insight into its advantages compared to conventional testing techniques.

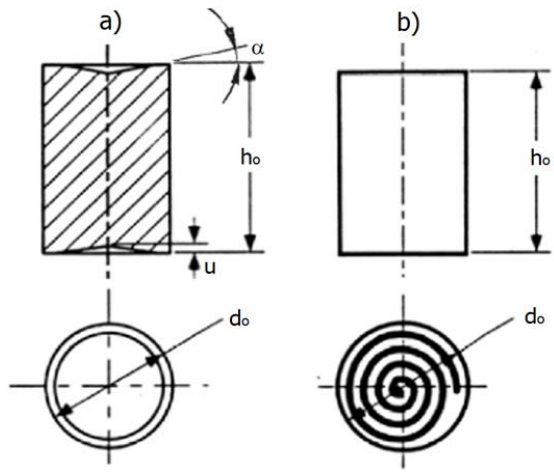

Figure 2. Specimens for the modified Rastegaev test: (a) with conical recesses and (b) with spiral grooves

2. MATERIAL AND EXPERIMENT

The modified Rastegaev test was performed using cylindrical specimens with conical recesses (Fig.3), made from AlZn5Mg3 aluminum alloy. Three specimens were prepared for the purposes of experimental testing [7].

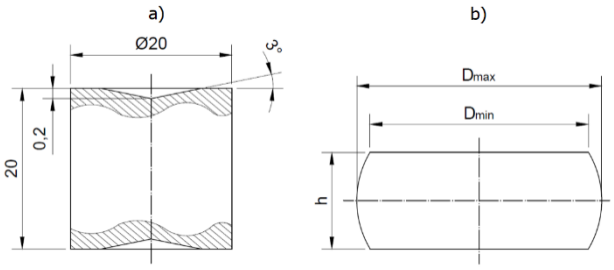

Figure 3. Specimens before and after compression

The upsetting tests were carried out in multiple stages (specimens 1 and 2) on a Sack &

Kiesselbach 630 t hydraulic press using flat plates (Fig.4), with each stage corresponding to a 10% reduction in height. After each stage, the sample's height (*h*), as well as its maximum (D_{max}) and minimum diameter (D_{min}), were measured. The third specimen was compressed in a continuous (single-stage) manner. Fig.5 shows the load (*F*) plotted as a function of die stroke (*s*) for all three specimens. The comparison of specimens before and after compression (Fig.6) shows minimal barreling, indicating effective suppression of frictional effects and deformation under near-uniaxial stress conditions. It should be noted that visible cracks were observed in specimen 3, most likely resulting from lubricant layer failure under high contact pressures. This can be attributed to the experimental procedure—unlike the first two specimens, where the lubricant layer was renewed after each deformation stage, specimen 3 (due to continuous upsetting) was lubricated only at the beginning of the process.

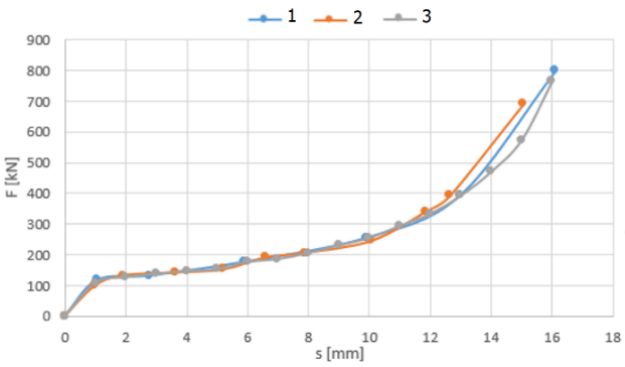

Figure 4. Load –stroke diagram

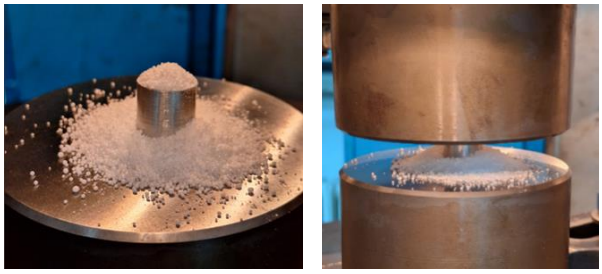

Figure 5. Preparation (lubrication) of a specimen (left), and upsetting with flat plates (right)

Figure 6. Specimens before and after compression

3. EXPERIMENTAL RESULTS

True stress (*K*) and true strain (φ) necessary for obtaining the flow curve, were determined using the following equations:

$$K = \frac{F}{A}, \quad \varphi = \ln\frac{h_o}{h} \tag{1}$$

where the average diameter (*D*) and cross-sectional area (*A*) are calculated as follows:

$$D = \frac{D_{max} - D_{min}}{2}, \quad A = \frac{D^2 \cdot \pi}{4} \tag{2}$$

Since the third specimen was upset continuously, D_{min}, D_{max}, and *h* could not be measured. Therefore, the average diameter (*D*) was calculated based on volume constancy ($V_o = V$), while the height (*h*) was determined as the difference between the initial specimen height and the achieved stroke (*s*).

$$D = D_o\sqrt{\frac{h_o}{h}}, \quad h = h_o - s \tag{3}$$

Figure 7. presents the flow curves derived from the experimental results.

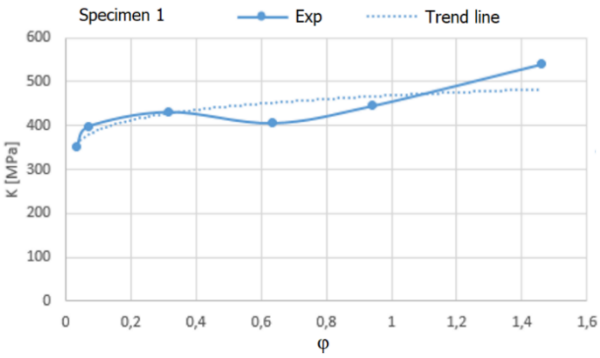

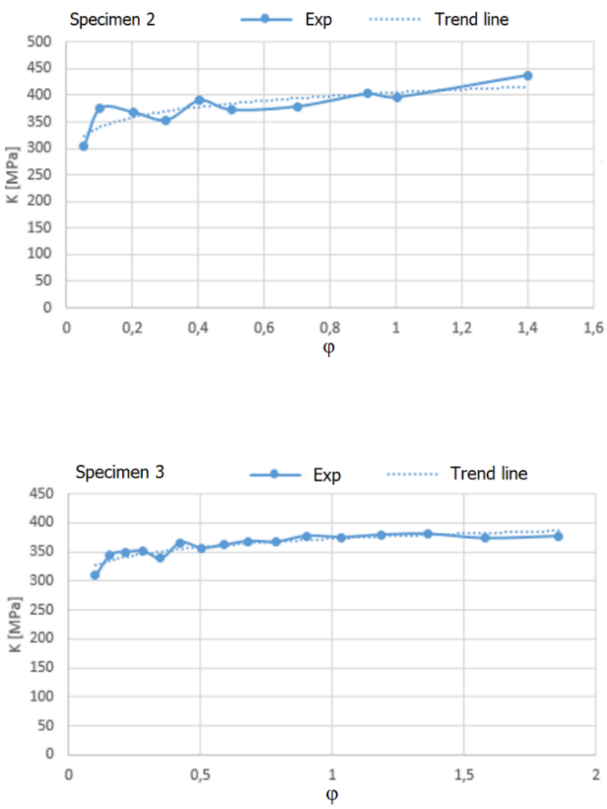

Figure 7. Flow curves determined experimentally

Analytical flow curves for all three specimens were obtained by approximation using the Ludwik equation (5)

$$K = K_o + C \cdot \varphi^n \tag{4}$$

where:

K_o – yield stress

C, n - material-dependent constants

The analytical forms of the Ludwik flow curve equations for all three specimens are given in Eq.6, with the corresponding graphs shown in Fig. 7:

$$K_{(1)} = 260 + 223.13 \cdot \varphi^{0.24}$$
$$K_{(2)} = 260 + 145.95 \cdot \varphi^{0.268}$$
$$K_{(3)} = 260 + +113.35 \cdot \varphi^{0.209} \tag{7}$$

The yield stress (K_o) for aluminum AlZn5Mg3 is 260 MPa [7].

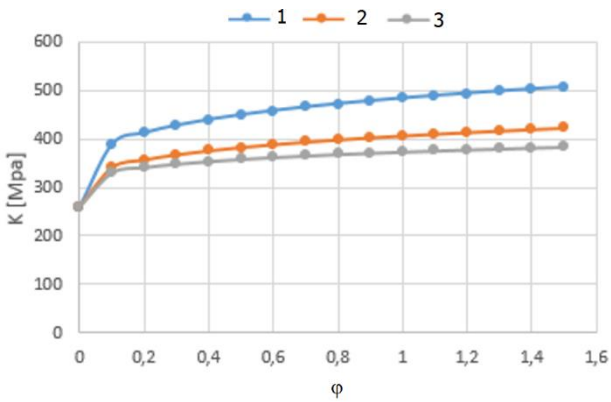

Figure 8. Flow curves approximated using Ludwik's equations

4. CONCLUSION

The study demonstrated the effectiveness of the modified Rastegaev test, which employs cylindrical specimens with conical recesses, in determining the flow curve of the AlZn5Mg3 aluminum alloy. Compared to the conventional Rastegaev test using cylindrical specimens with cylindrical recesses, this modification further reduces frictional effects, allowing accurate characterization of material behavior over a wide range of plastic strains. Results from the tests indicate that large plastic strains (φ=1.4–1.6) can be achieved without notable process instability or barreling, demonstrating the method's robustness and reliability. This stability under high deformation conditions highlights its suitability for its for accurate flow curve determination and its potential for advanced metal forming applications.

ACKNOWLEDGEMENT

This research has been supported by the Ministry of Science, Technological Development and Innovation (Contract No. 451-03-137/2025-03/200156) and the Faculty of Technical Sciences, University of Novi Sad through project "Scientific and Artistic Research Work of Researchers in Teaching and Associate Positions at the Faculty of Technical Sciences, University of Novi Sad 2025" (No. 01-50/295).

REFERENCES

[1] M. Plačnik, D. Vilotić: *Tehnologija plastičnog deformisanja*, Fakultet tehničkih nauka, Novi Sad, 2003.

[2] V. Vujović: *Deformabilnost*. Monografija, Fakultet tehničkih nauka, Novi Sad; 1992.

[3] M. Schmiedt, R. Schneider, J. Jung, W. Rimkus, A.kK.M. De Silva: Flow Curve Approximation of High-Strength Aluminium Alloys in Heat-Assisted Forming Processes. Production Engineering, Vol. 18, pp. 1–12, 2024.

[4] K. Pöhlandt: Determining the Flow Curves and the Anisotropy Properties of Metals through the Rastegaev Compression Test. Draht, Vol 42, pp. 247–252, 1991.

[5] M.V Rastegaev: *A New Method of Homogeneous Compression of Specimens for Determining Flow Stress and the Coefficient of Internal Friction*. Zavod. Lab. 6, 1939.

[6] V. Mandić: *Fizičko i numeričko modeliranje procesa obrade deformisanjem*. Fakultet inženjerskih nauka u Kragujevcu, 2012.

[7] N. Prodanović: Određivanje krive tečenja primenom modifikovanog rastegaev testa. Diplomski rad. Fakultet tehničkih nauka, novi Sad, 2024.

Society of Production Engineering

ICPES 2025

40th INTERNATIONAL CONFERENCE ON PRODUCTION ENGINEERING - SERBIA 2025

DOI: 10.46793/ICPES25.124J

University of Nis Faculty of Mechanical Engineering

Nis, Serbia, 18 - 19th September 2025

MODELING DEFORMATION FORCE IN OPEN DIES USING NEURAL NETWORKS

Mileta JANJIĆ[1]
Orcid: 000-0001-8403-2744
[1]University of Montenegro – Faculty of Mechanical Engineering, Podgorica, Montenegro
*Corresponding author: mileta@ucg.ac.me

Abstract: *The paper presents a study of deformation in open dies of the aluminum alloy AlMgSi0.5. A part of the research focused on modeling the deformation force during the process is provided. The investigation was conducted according to an experimental plan, adopting a full multi-factorial orthogonal plan with repetition at the central point. The input factors were the geometric parameters of the die and the workpiece, as well as the temperature. Deformation forces were recorded at each point of the plan, and modeling was performed. The modeling was carried out in MATLAB using a Feedforward Neural Network (FNN), with the Deep Learning Toolbox. The obtained model values show a high degree of correlation with the experimentally measured deformation forces.*

Keywords: *Bulk Metal Forming, Open Die, Deformation Force, Neural Networks, Modelling*

1. INTRODUCTION

In the metal processing industry, production conditions have recently changed and become increasingly demanding. This is reflected in the need to produce metal components with minimal consumption of materials, energy, and production time. These requirements are driven by global trends characterized by energy and raw material crises. This is particularly evident in metal forming processes, due to their extensive industrial application. Within metal forming, bulk forming — especially in open-die forging — stands out due to its complexity [1,2].

The main reason for the widespread use of open-die forging lies in its ability to produce workpieces of various shapes with favorable mechanical properties. This is achieved through a favorable stress state within the workpiece during processing, particularly in the final stage, where compressive stress components dominate. On the other hand, the development of materials and tooling technologies, as well as the ability to apply the process at high temperatures and deformation rates, are

additional reasons for the broad application of open-die forming [2,3,4].

For the cost-effective design of bulk forming in open dies, it is essential to understand all relevant parameters that influence the forming process, in order to determine the key mechanical process parameters such as forming force. For this purpose, engineering methods are used, as well as numerical modeling techniques, such as the Finite Element Method (FEM), through the use of advanced software packages. In addition, modeling results obtained by other methods can also be utilized. By applying such model-based results to specific forming cases, it is possible to avoid complex numerical simulations or to use them for validation purposes [5,6].

This paper presents a modeling approach based on Artificial Intelligence (AI), using Artificial Neural Networks (ANN), for bulk forming in open dies. This method is well-suited for modeling complex nonlinear relationships, where conventional methods are often insufficiently effective [7].

2. EXPERIMENTAL RESEARCH

The bulk forming process in open dies was investigated for a family of stepped axisymmetric parts. Two height levels were adopted on the upper side and one height level on the lower side of the die parting plane (Figure 1.) [6].

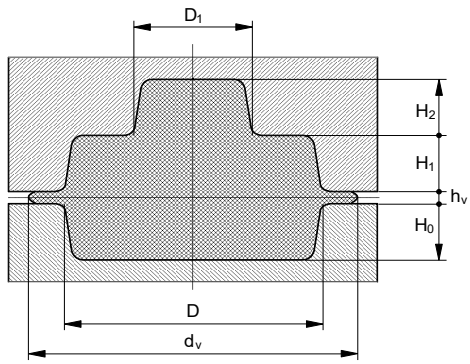

Figure 1. Stepped axisymmetric part

The following zones exist in the meridional cross-section of the workpiece:

1. bottom die zone (H_0),
2. flange zone (hv),
3. first level of the upper die zone (H_1) and
4. second level of the upper die zone (H_2).

The research is conducted under laboratory conditions, adjusted to closely resemble real (production) conditions present in an actual industrial environment. The following conditions for investigating the deformation force are adopted:

1. The tested material is the aluminum alloy AlMgSi0.5, which is very commonly used in bulk forming processes, especially in extrusion and open-die forging. The chemical composition of the experimental material is given in Table 1.

Table 1. Chemical Composition of the Material

AlMgSi0,5	Fe%	Si%	Ti%	Cu%	Zn%
	0.207	0.477	0.01	0.09	0.068
	V%	Cr%	Mn%	Mg%	Ni%
	0.004	0.01	0.1	0.493	0.02

2. The testing is conducted at the hot working temperatures of the mentioned alloy, i.e., within the range t=(420÷460) ^{o}C.
3. The deformation is performed at a constant deformation rate: v=2 mm/s.
4. The process is carried out with lubrication using graphite grease, which is also applied under production conditions.

2.3 Experimental plan

The experimental plan is based on preliminary research, and the input factors have been adopted according to which the dependence of the working force will be determined.

A full multi-factor orthogonal experimental plan with factors varied at two levels is

adopted, including four repetitions at the central point of the plan (n_o = 4).

The input variables (independent variables – factors) include the geometric factors of the die (Figure 1.) and the workpiece, as well as the working temperature. The input factors considered are:

- The geometric factors of the die, expressed as dimensionless ratios of characteristic die dimensions to the base diameter of the die D, to ensure generality of the results:

$$X_1=H_1/D,\ X_2=H_2/D,\ X_3=D_1/D \quad (1)$$

where:

H_1 - height of the first level of the upper die,

H_2 - height of the sec. level of the upper die,

D_1 - diameter of the sec. lev. of the upper die,

D - base diameter of the die.

- The geometric factor of the workpiece is the ratio of the initial diameter of the workpiece to the base diameter of the die:

$$X_4=d_0/D \quad (2)$$

where:

d_0 - workpiece diameter.

- The temperature factor is considered in hot working and represents the working temperature in degrees Celsius:

$$X_5=T\ [°C] \quad (3)$$

The number of points for k factors with n_o repetitions at the central point is:

$$N=2k+n_0. \quad (4)$$

2.4 Experimental plan matrix

The experimental plan matrix for the full 5-factor plan is given in Table 2.

Table 2. Plan matrix

Plan:				Points	Input factors					Output
					X_1	X_2	X_3	...	X_5	
2^5	...	2^3	2^2	1	-1	-1	-1	...	-1	Y_1
				2	+1	-1	-1	...	-1	Y_2
				3	-1	+1	-1	...	-1	Y_3
				4	+1	+1	-1	...	-1	Y_4
				5	-1	-1	+1	...	-1	Y_5
				6	+1	-1	+1	...	-1	Y_6
				7	-1	+1	+1	...	-1	Y_7
				8	+1	+1	+1	...	-1	Y_8
				⋮	⋮	⋮	⋮	⋮	⋮	⋮
				2^5=32	+1	+1	+1	...	+1	Y_{32}
Central points				2^k+1=33	0	0	0	...	0	Y_{33}
				2^k+2=34	0	0	0	...	0	Y_{34}
				2^k+3=35	0	0	0	...	0	Y_{35}
				2^k+4=36	0	0	0	...	0	Y_{36}

The adopted levels of variation of the input factors are given in Table 3.

Table 3. Levels of Variation of Input Factors in the Experimental plan

Input factors	lower level	Middle level	Upper level
X_1	0.175	0.250	0.357
X_2	0.150	0.250	0.417
X_3	0.417	0.500	0.600
X_4	0.757	0.839	0.908
X_5 [°C]	420	440	460

The following values of other dimensions of the workpiece and the die are adopted (Figure 1.):

- Base diameter of the die: D=40 mm;
- Height of the flange: h_v= 1 mm;
- Diameter of the flange: dv=50 mm;
- Height of the bottom die: H_0=10 mm.

The heights of the workpieces are determined based on the dimensions of the die

and the diameter of the workpiece, in order to enable variations of the input factors (Table 3.), and the number of workpieces is determined according to the points of the plan matrix (Table 4).

Table 4. Dimensions and Numbers of Workpieces

Workpiece diematar d_0 [mm]	No	Height h_0 [mm]	No of workpieces
30.28	1	34.42	2
	2	36.33	2
	3	37.07	2
	4	42.18	2
	5	46.21	2
	6	48.12	2
	7	48.86	2
	8	53.97	2
33.56	9	33.94	4
36.30	1	23.95	2
	2	25.28	2
	3	25.80	2
	4	29.35	2
	5	32.16	2
	6	33.49	2
	7	34.00	2
	8	37.56	2

2.5 Experimental Equipment

For deformation, a static testing machine with a hydraulic drive, type R100, of Russian manufacture was used, capable of performing tensile and compressive tests (Figure 2.). The maximum load capacity of the press is 1 MN, and the maximum deformation rate is v=2 mm/s.

Measurements during the stated experimental investigations were conducted using the measurement system shown in Figure 3.

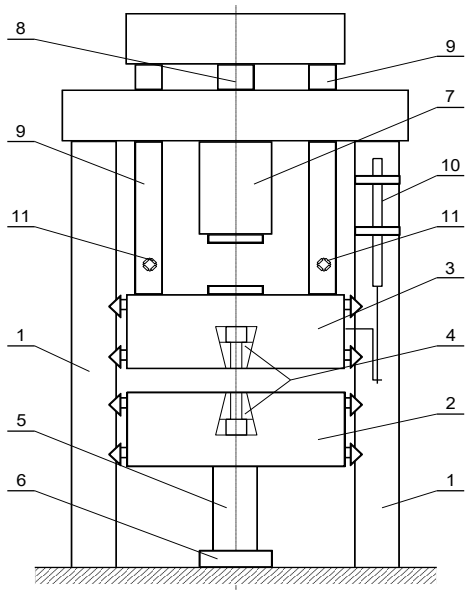

Figure 2. Hydraulic press: 10 – inductive displacement sensor, 11 – force sensors.

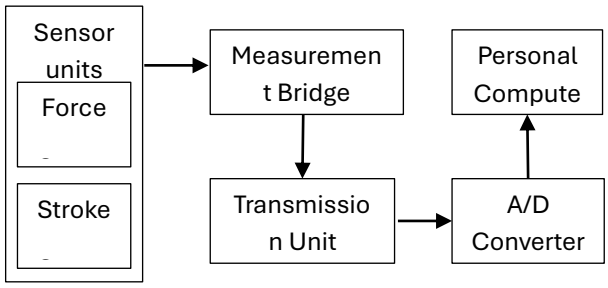

Figure 3. Information measurement system

Strain gauge sensors of type HBM 6/120LY11, connected in a full Wheatstone bridge, were used as force sensors, while an inductive displacement sensor of type HBM W 200K was used for displacement measurement. The signals from the sensor units were amplified using a digital six-channel measuring bridge of type HBM KWS.637.D4. The analog output signal from the bridge was transmitted via a transmission unit to an AD/DA card of type DT 2801-A, converted to digital form, and stored on a personal computer with installed GLOBAL-LAB data acquisition software. Temperature control was performed using a

digital thermometer for measuring the temperature on the surface of hard materials, type DT IM Dalmacija. The thermometer uses a tactile probe based on a thermocouple.

2.6 Measurement of deformation force during the deformation process

As part of the experimental research, measurements of the deformation force during bulk deformation in open dies were performed according to the experimental plan. The order of execution of the experimental points from the plan matrix was randomized. Lubrication was done by manually applying a layer of graphite grease onto the working surfaces of the tools. To achieve isothermal deformation, the deformation tools were heated together with the workpieces.

After heating in the furnace, the deformation tool assembly, together with the workpiece, was placed on the press. After starting the information measurement system for force measurement as a function of displacement, the press was put into operation. The deformation of the workpieces was carried out in a single stroke, and the process was stopped upon reaching the final dimensions. The final dimensions were ensured by a steel ring whose thickness corresponds to the required flange height.

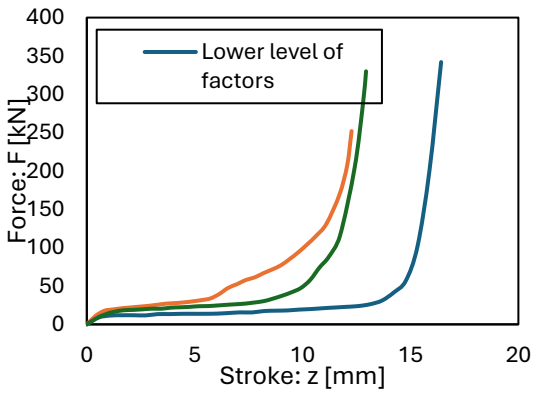

Figure 4. Forces for the lower, middle, and upper factor levels

Upon stopping the press stroke, the measurement process with the information measurement system was also stopped, and the force signals from the strain gauge sensors on both supporting columns of the upper press table, as well as from the inductive displacement sensor, were recorded on the computer's hard drive.

In this way, the force variations as a function of displacement were obtained at all points of the experimental plan. Figure 4. shows the deformation forces for the lower, middle, and upper levels of variation of the input factors.

3. MODELING OF DEFORMATION FORCE USING NEURAL NETWORKS

The modeling of the deformation process in open dies was carried out in Matlab version 24.2.0. The Deep Learning Toolbox was used for fitting via a Feedforward Neural Network (FNN), which represents a standard multilayer network. Launching this application activates a very efficient GUI where modeling can be performed in a relatively simple way.

First, it is necessary to prepare the input and output data. The output data must be in the form of a matrix with a certain number of rows and columns equal to the number of points in the experimental plan. It was chosen to be a matrix of dimension Y[101,36]. Since the displacement differs for individual points of the plan, displacement normalization must be performed. This is achieved using the expression:

$$Z_{norm}=(z-z_{min})/(z_{max}-z_{min}) \quad (5)$$

This ensures that the value of the normalized displacement ranges from 0 at the start of deformation to 1, which corresponds to the maximum displacement value at the end of the deformation process. For each value of the normalized displacement, the corresponding force values for individual points of the plan are entered, thus obtaining a normalized matrix of output values.

The input data are prepared to have 5 rows, corresponding to the number of input factors, and 36 columns, corresponding to the number of points in the plan matrix, so the matrix has dimensions X[5,36]. Each column contains the

values of the input factors for a specific point of the plan.

After entering the data, the structure of the neural network is selected (Figure 5.).

The structure of the neural network for modeling the deformation force consists of:

1. Input layer with 5 input features, corresponding to the input factors,
2. Hidden layer with 10 neurons, using a sigmoid activation function (wave-like symbol),
3. Output layer with 100 neurons, using a linear activation function (straight-line symbol).

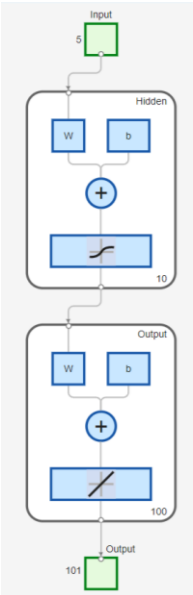

Figure 5. Neural network structure

So, this is a classic "function fitting" regression network, which is used to learn the relationship between multiple inputs and a complex vector output. The neural network is created using the command:

net = fitnet(hiddenLayerSize,trainFcn); (6)

and trained using the command:

[net,tr] = train(net,x,t); (7)

This yields a function that models the deformation force in all points of the experimental plan of the form:

y = net(x); (8)

This applies throughout the entire hypercube space, and likely within a certain domain outside of that space as well.

Figure 6. shows the modeled values of the deformation force for the lower, middle, and upper levels of the input factors. Figures 7. through 9. present comparative values of the experimentally obtained deformation force and those modeled using neural networks.

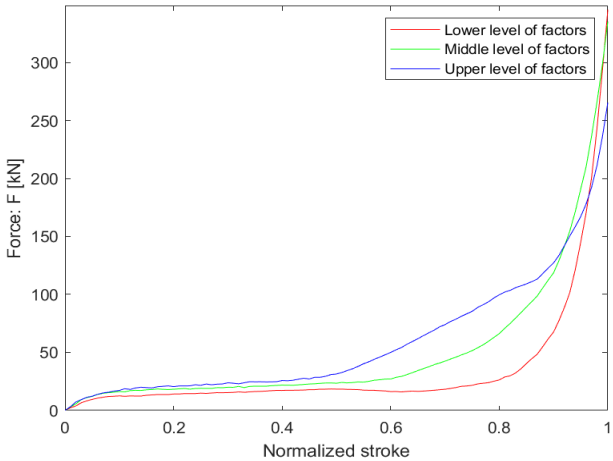

Figure 6. Modeled force values for the lower, middle, and upper factor levels

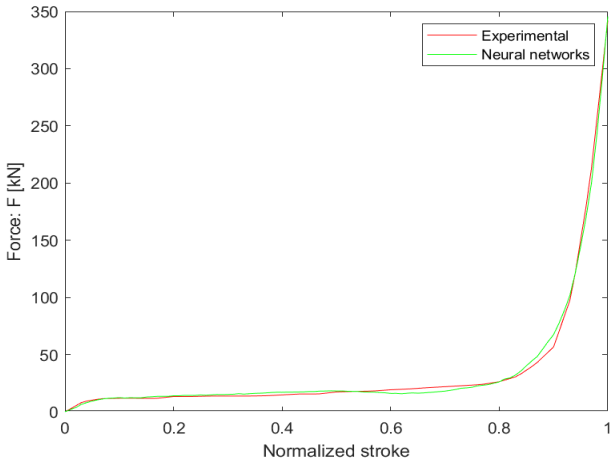

Figure 7. Experimental and modeled force values for the lower factor level

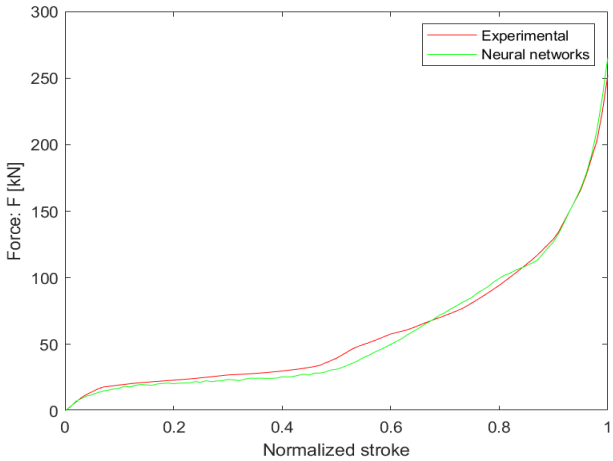

Figure 8. Experimental and modeled force values for the upper factor level

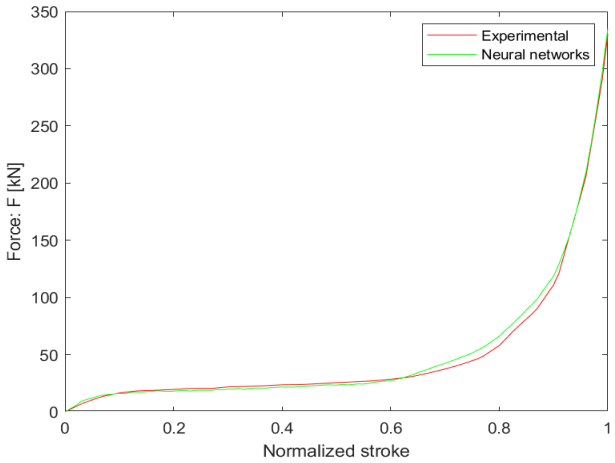

Figure 9. Experimental and modeled force values for the middle factor level

4. ANALYSIS OF RESULTS

From the figures, a good match between the experimental and modeled values can be concluded. The Deep Learning Toolbox enables analysis of modeling performance.

Figure 10. shows the results of training the neural network in MATLAB for modeling the deformation force in open dies in the form of the standard plotregression graph that MATLAB generates for assessing the quality of the network. The figure shows a high degree of model correlation (>95), which means the model closely follows the training data, generalizes the problem well, and is not overfitted.

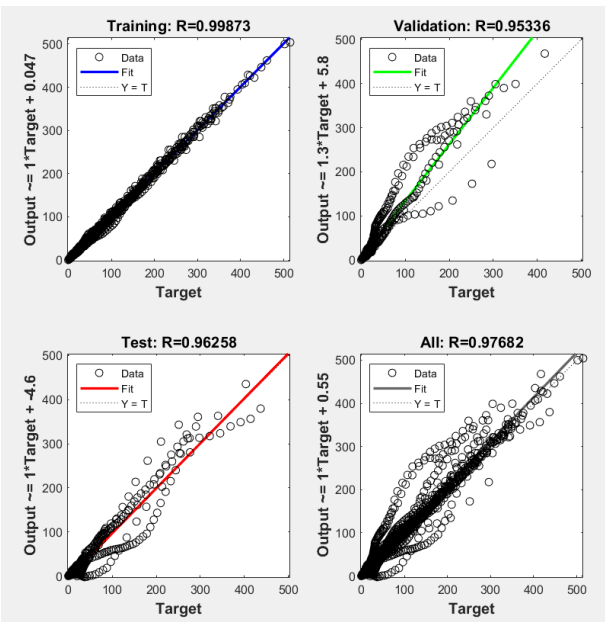

Figure 10. Neural network training results

It can be stated that a very successful model was obtained using a neural network for the compression deformation force in open dies. The network can be successfully used to predict compression results without the need for complex simulations, such as the finite element method.

5. CONCLUSION

Neural networks can be successfully used for modeling the deformation force during bulk deformation in open dies. This is demonstrated in the paper through the example of modeling the deformation force in the deformation of the aluminum alloy AlMgSi0.5 in open dies.

Deformation forces were recorded at each point of the full multi-factor orthogonal plan with repetition at the central point. The input factors adopted were geometric factors of the die and billet, given as relative ratios, and the hot working temperature. The modeling of the dependence of the deformation force on the working stroke was performed using a Feedforward Neural Network (FNN) in Matlab, utilizing the Deep Learning Toolbox.

A good agreement between experimental and modeled values was obtained, with a high degree of model correlation (>95), indicating that the modeled values are adequate. Thus, it can be concluded that the network can be successfully used to predict compression results under given conditions, without the need for complex numerical simulations.

REFERENCES

[1] F. Chao, L. Weike, C. Xianhui, D. Yunlai, W. Jun, X. Yi: A Study on Forging Process of New Aluminum Alloy, Journal of Physics Conference Series, Vol. 2194, No. 1:012016, pp. 1-6, 2022.

[2] E. Kavehand all: Severe plastic deformation for producing superfunctional ultrafine-grained and heterostructured materials: An interdisciplinary review, Journal of Alloys and Compounds, Vol. 1002, No. 174667, 2024.

[3] A. Evstifeev, A. Mavlyutov, A. Voropaev, D. Volosevich: Optimization of Strength and Plasticity in Layered Aluminum Composites

Through High-Pressure Torsion Treatment, Metals, Vol 14, No. 12, 2024.

[4] J. Lv, Z. Jing-Hua, V. A. Yardley, S. Zhusheng, L. Jianguo: A Review of Microstructural Evolution and Modelling of Aluminium Alloys under Hot Forming Conditions, Metals, Vol. 10, No. 11 2020.

[5] P. Thi-Ha-Linh, L. The-Thanh, N. Duc-Toan: A Study Utilizing Numerical Simulation and Experimental Analysis to Predict and Optimize Flange-Forming Force in Open-Die Forging of C45 Billet Tubes, Applied Sciences, Vol. 13, No. 16, 2023.

[6] M. Janjić: (2008) Stress Deformation Parameter Investigation in the Processes of the Bulk Metal Forming, Monograph, Faculty of Mechanicall Engineering, University of Montenegro, Podgorica, 2008.

[7] A. Jenab, A. Karimi Taheri, and K. Jenab: The Use of ANN to Predict the Hot Deformation Behavior of AA7075 at Low Strain Rates, Journal of Materials Engineering and Performance, Vol. 22, No. 3, 2013.

Society of Production Engineering

ICPES 2025

40th INTERNATIONAL CONFERENCE ON PRODUCTION ENGINEERING - SERBIA 2025

DOI: 10.46793/ICPES25.132W

University of Nis Faculty of Mechanical Engineering

Nis, Serbia, 18 - 19th September 2025

THERMOMECHANICAL PROCESSING OF NEAR BETA TITANIUM ALLOYS

Fernando WARCHOMICKA[1*], Esmaeil SHAHRYARI[1], Ricardo HENRIQUE BUZOLIN[1], Franz FERRAZ MILLER BRANCO[1], Cecilia POLETTI[1]

Orcid: 0000-0002-4909-8657; **Orcid:** 0000-0002-3955-6917;
Orcid: 0000-0002-0641-9545; **Orcid:** 0000-0002-4776-920X;

[1]Institute of Materials Science, Joining and Forming, Graz University of Technology, Austria,
*Corresponding author: fernando.warchomicka@tugraz.at

Abstract: *Near beta titanium alloys are promising materials for structural applications due to their high specific strength, good hardenability and fatigue resistance. The high performance of these alloys mainly depends on the type of microstructure, which can be engineered through thermomechanical processing. Based on the assumption that the beta stabilising elements affect the phase transformation and plastic deformation, this work aims to describe the deformation behaviour and subsequent microstructural changes by thermal activation in titanium alloys with different Mo equivalent. Hot compression tests of selected near beta titanium alloys (Ti-55531, Ti17 and Ti-xMo) were carried out in the beta and alpha+beta fields over a wide range of temperature, strain, and strain rate. The characterisation of the microstructural features after hot deformation was carried out by scanning electron microscopy images and electron backscatter diffraction measurements. This contributes to the analysis of the effect of deformation on the dynamic recovery followed by continuous dynamic recrystallisation in the beta field, and on the globularisation of the alpha phase in the alpha+beta field. The development and improvement of microstructure-based mesoscale models for near beta titanium alloys describe the behaviour of the material under plastic deformation, restoration, and phase transformation.*

Keywords: *Titanium alloys, hot deformation, metallography, modelling, restoration mechanisms*

1. INTRODUCTION

The evolution of engineering materials is giving us opportunities for innovation in the mechanical design and the substitution of conventional materials in different application fields. Titanium alloys are highly attractive materials for various applications, including aerospace, process engineering, automotive, medical, and sports industries, due to their high specific strength, stiffness, good corrosion, and creep resistance [1,2]. The use of β and near β titanium alloys has become increasingly common for structural components, particularly in aerospace and biomedical applications. These alloys (metastable β, and β -rich alloys) by high ductility due to their body-

centered cubic structure, superior fatigue resistance, and a wide range of strength-to-weight ratios. Near β alloys also exhibit relatively good workability due to their lower beta-transus temperature (T_β) compared to typical α + β alloys.

Thermomechanical processing is essential for these materials, as it enables the production of near-net shapes and the optimization of mechanical properties through microstructure control. The microstructural evolution of titanium alloys during processing depends on the deformation window. Parameters such as the initial microstructure, deformation temperature, soaking time before deformation, strain rate, and total strain influence both the material's flow behavior and the morphology of the phases present. Subsequent annealing and ageing treatments can further improve toughness [1,3]

The hot deformation of near β alloys titanium alloys has been widely studied. The restoration mechanisms that occur during deformation are influenced by temperature, strain rate, and phase volume fraction,[3] as well as by the distribution of the α phase and the stacking fault energy of both phases. In titanium alloys, dynamic recovery of the beta phase is the dominant mechanism during deformation near the T_β, as shown for different alloys through metallographic observations [4,5] and flow stress analysis [6]. As in other high–stacking-fault-energy materials, such as α-iron[7] and aluminum alloys,[8] continuous dynamic recrystallization (cDRX)[8] and geometric dynamic recrystallization (gDRX) are expected to occur at large strains.[9]. cDRX involves the progressive and continuous development of misorientation within low-angle grain boundaries (LAGBs) through lattice rotation, transforming them into high-angle grain boundaries (HAGBs), while gDRX takes place at low strain rates and large strains. This mechanism occurs by the pinching off of prior β HAGBs, forming new grains that are similar in size to the subgrains. The identification of this mechanism can be challenging and the use of in-situ water quenching immediately after the deformation can help to suppress static recrystallization (SRX) or avoid a misinterpretation of the microstructure [10].

Accurate microstructural characterization and a clear understanding of the active mechanisms and kinetics during deformation are essential for developing robust models to predict microstructure evolution during industrial processing.

This work summarizes the authors' findings on the hot deformation behavior of near-β titanium alloys and the resulting microstructures. Further details can be found in references [11-18].

2. METHODOLOGY

This work comprises the study of different near β alloys, as described in the Table 1. The alloys present different beta-transus temperature (T_β).

Table 1. Studied alloys by thermomechanical process.

Alloy	T_β
Ti-10V-2Fe-3Al	810 °C
Ti–5Al–5Mo–5V–3Cr–1Zr	803 °C [11]
Ti–5Al–5Mo–5V–3Cr	850°C [16]
Ti-17	865°C [15]
Ti-15 Mo	730°C [18]
Ti-18 Mo	712 °C

Hot compression tests were carried out using a Gleeble®3800 servo hydraulic system machine (Figure 1) at constant strain rates up to 10 s^{-1} at temperatures in the range of Tβ± 100°C, and true strain up to 0.7. The specimens were heated to the compression temperature at a heating rate of 5K/s and were held at the deformation temperature to reach the equilibrium of α phase below the T_β, and a full β transformation into the β field above Tβ. Immediately after hot compression, the samples were in-situ water-quenched to room temperature, keeping the microstructure for further microscopic analyses. All the

experiments were carried out in an Argon atmosphere to prevent oxidation and formation of alpha case of the specimens.

For metallographic observations, samples were hot mounted in PolyFast (Struers) resin, followed by sequential grinding with SiC papers and final polishing using a 5:1 mixture of colloidal silica (OP-S, Struers) and hydrogen peroxide.

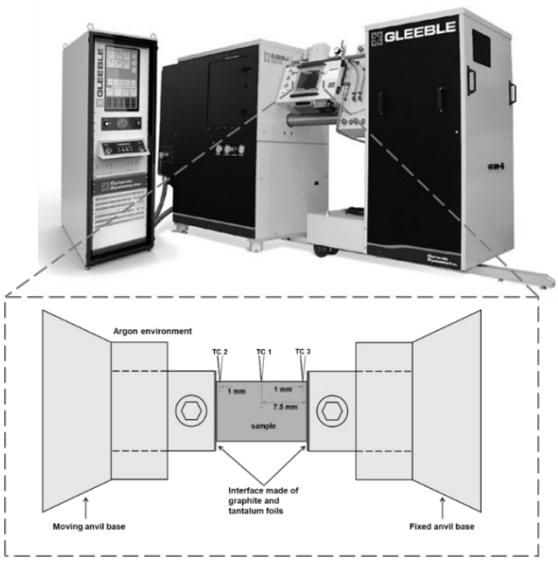

Figure 1. Testing machine Gleeble® 3800 and a scheme of the sample positioned for compression tests.

Electron backscatter diffraction (EBSD) measurements and scanning electron microscopy (SEM) images were used to characterise the microstructure of the deformed samples in the β phase and α+β phase regions, respectively. A TESCAN Mira3 field emission gun scanning electron microscope (FEG-SEM) equipped with an EDAX-Ametek Hikari EBSD camera and APEX V2.5.1001 software was used for the measurements. EBSD measurements were conducted with different step sizes depending on the initial beta grain size.

3. RESULTS AND DISCUSSION

3.1 Flow behaviour

The flow stress is strongly influenced by both temperature and strain rate. In the β region, deformation behavior varies with chemical composition. Alloys such as Ti-10-2-3 and Ti-5-5-5-3-1 exhibit an initial sharp peak—indicative of discontinuous yielding—followed by a steady-state regime, whereas Ti–xMo alloys show strain hardening before reaching steady state (Figure 2). Ti-17 alloys predominantly display steady-state behavior.

In the α + β region, deformation typically results in flow softening as strain increases. The rate of softening is affected by the strain rate and the initial morphology of the α phase. For example, in Ti-17 with an initial lamellar microstructure, increased strain rates lead to more pronounced softening, as shown in Figure 3 [15].

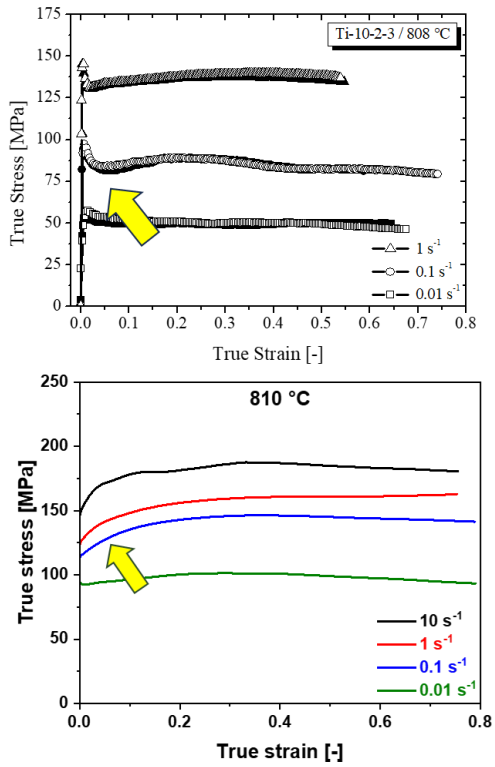

Figure 2. Example of flow curves of Ti-10-2-3 (above) and Ti-15Mo [18] (below) in the β-phase region at various strain rates. Arrows indicate the discountinuous yielding and the strain hardening.

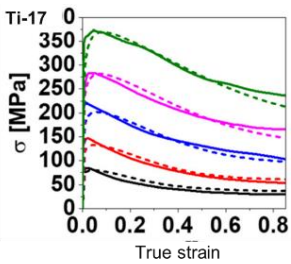

Figure 3. Example of flow curves of Ti-17 in the α+β-phase region at various strain rates [15].

3.2 Deformation in the β region

Figures 4 and 5 show an example of the microstructure of Ti-18Mo deformed in the β region. During deformation of near-β alloys, changes in the misorientation are observed alongside the development of substructures. Dynamic recovery (DRV) is the dominant restoration mechanism, but its activity varies among grains due to differences in initial crystallographic orientations, leading to heterogeneous subgrain formation. In addition to DRV, fine new grains form via continuous (cDRX) and geometric dynamic recrystallization (gDRX), particularly near prior grain boundaries in all the studied materials.

With increasing temperature at a constant strain rate, subgrain size increases, as illustrated in Figure 4. At higher strain rates, deformation bands appear, and both the fraction of DRV and the subgrain size decrease (Figure 5) [18]. Quantification of DRV and DRX in Ti–xMo alloys shows that both fractions decrease with increasing strain rate and decreasing temperature. Only very small amounts of DRX were observed—up to approximately 2% at the highest temperature and lowest strain rate for Ti-15Mo [18]

3.3 Deformation in the α+β region

The final microstructure obtained during deformation in the α+β region is influenced by both the initial microstructure and the strain rate, as illustrated in Figures 6 and 7 for Ti-10Al-2Fe-3Al and Ti-15Mo, respectively.

For partially fragmented starting microstructures (Figure 6), deformation primarily causes rotation of the α grains perpendicular to the applied load. As strain increases, the elongated α grains begin to fragment and gradually transform into a globularized microstructure. At higher strain rates, the α grains become thinner and the volume fraction of globular α grains decreases.

When the initial microstructure is lamellar (Figure 7), the transition toward a globular morphology proceeds through several stages [15], including diffusion-controlled processes, kinking, and fragmentation of the α lamellae. This mechanism is more evident at low strain rates and higher α-phase fractions. Near the T_β temperature, globularization of the α phase occurs more rapidly and additionally promotes continuous dynamic recrystallization (cDRX) at higher strains.

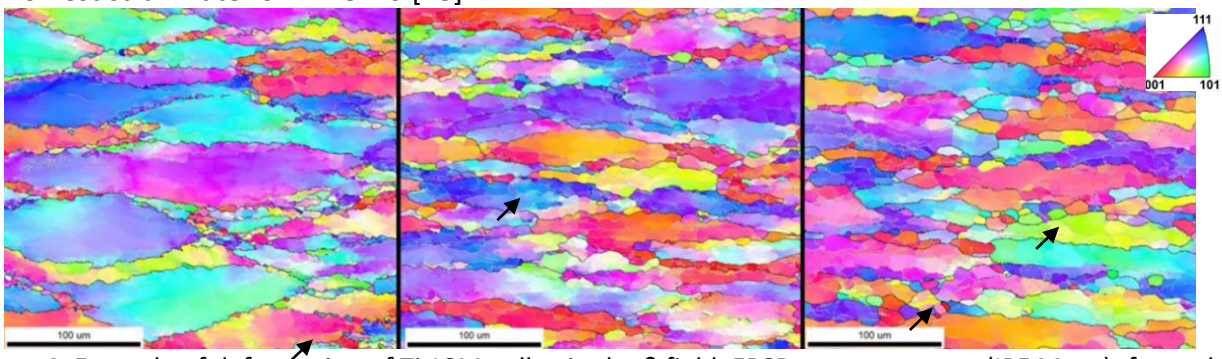

Figure 4. Example of deformation of Ti 18Mo alloy in the β field. EBSD measurements (IPF Maps)of samples deformed at 0.01s^{-1} and 0.7 of true strain at 810°C (left), 860°C (center) and 910°C (right). Black arrows show the formation of new grains. Deformation axis is vertical.

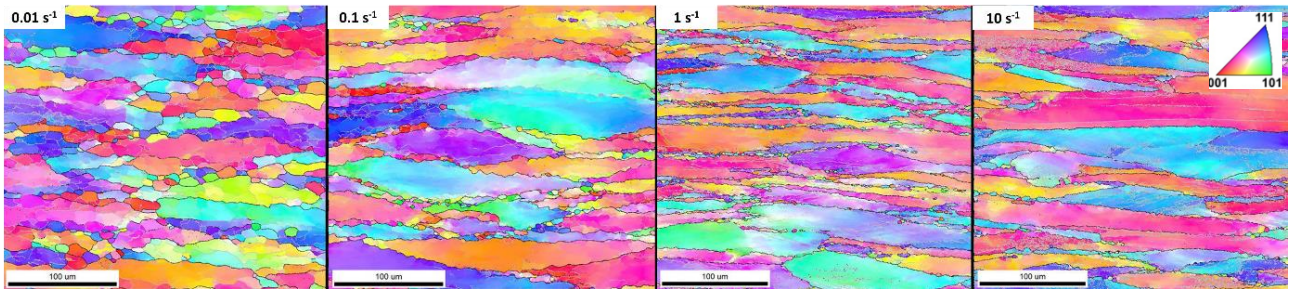

Figure 5. Example of deformation of Ti 18Mo alloy in the β field. EBSD measurements (IPF Maps) of samples deformed at 910°C at different strain rates. Deformation axis is vertical.

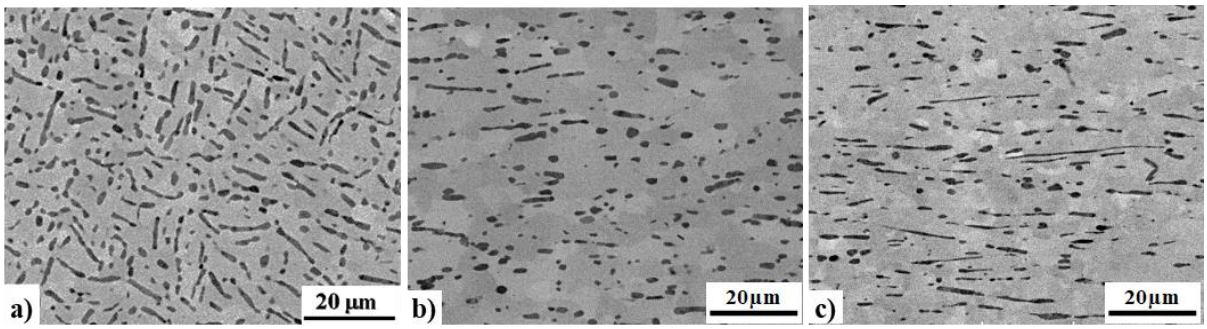

Figure 6. Example of deformation at 768°C of a partial globularized initial microstructure in Ti-10V-2Fe-3Al alloy: a) Initial microstructure without deformation, b) Deformed at 0.01s-1 and 0.7 true strain, and c) Deformed at 1s-1 and 0.7 true strain. Deformation axis is vertical.

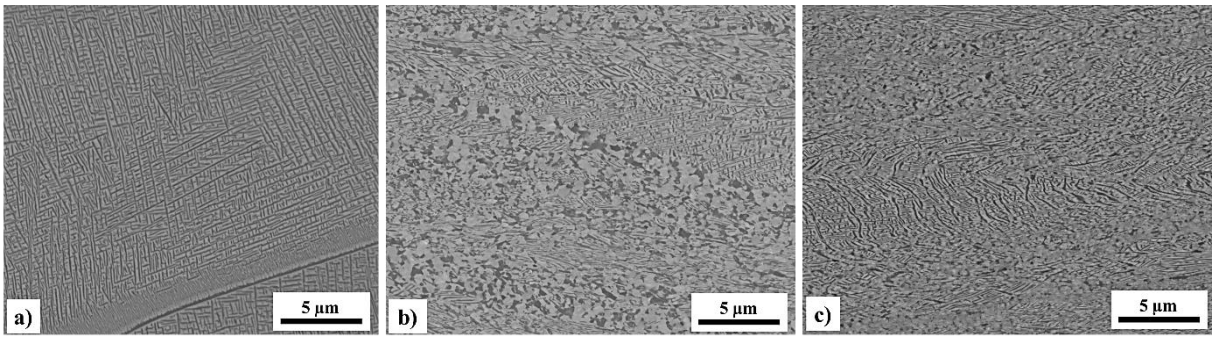

Figure 7. Example of deformation at 610°C of a fine lamellae initial microstructure in Ti-15Mo alloy: a) Initial microstructure without deformation, b) Deformed at $0.01s^{-1}$ and 0.7 true strain, and c) Deformed at $1s^{-1}$ and 0.7 true strain. Deformation axis is vertical.

3.4 Strategy for modelling and simulation of the microstructure

Physically based models are developed for predicting the microstructure evolution and the flow stress of near beta titanium alloys. The models are able to predict microstructural features such as grain size, subgrain size, boundary misorientation and dislocation densities evolution during deformation. For that, the models require a broad array of parameters that fall generally into three categories: initial microstructure inputs, fixed material constants (often derived from literature), and fitted parameters that govern the kinetics of the various deformation and restoration mechanisms (DRV, CDRX, globularization, etc.). SEM and EBSD analyses are typically used to quantify and provide the initial microstructural inputs. Constitutive equations are commonly applied to fit the flow stress as a function of processing parameters such as temperature, strain, and strain rate (see Figures 2 and 3). Examples of model predictions and experimental validation can be found in the works of Miller et al. and Buzolin et al. for the titanium alloys Ti-5-5-5-3 and Ti-17 [14–17], as well as for the α+β alloy Ti-6Al-4V [19].

4. CONCLUSION

Thermomechanical processes can be simulated and characterized by combining Gleeble testing machine—which provides flow stresses and a frozen microstructure—with scanning electron microscopy equipped with an EBSD detector. EBSD analysis is particularly valuable for identifying the dominant restoration mechanisms and quantifying subgrain size, grain size, and the fractions of recovered and recrystallized microstructures.

In this work, we summarized results for near-β titanium alloys. The main conclusions are as follows:

• Temperature and strain rate significantly influence the heterogeneity of the microstructure during deformation.

• During deformation in the β region, the flow stress depends on temperature, strain rate, and the content of β-stabilizing elements. Alloying elements can lead to either discontinuous yielding or strain hardening before the steady-state regime is reached. Dynamic recovery (DRV) is the primary restoration mechanism, followed by continuous dynamic recrystallization (cDRX) and geometric dynamic recrystallization (gDRX).

• In the α + β region, deformation generally leads to flow softening, with the softening rate affected by strain rate and the initial α-phase morphology. Dynamic globularization is observed in initial lamellae microstructure.

• Modelling and simulation are essential for optimizing thermomechanical processing of titanium alloys to achieve tailored microstructures and mechanical properties.

ACKNOWLEDGEMENTS

The authors carried out this work supported by the Austrian Science Fund (FWF) joint project (I5818–N, Deformation-phases-strength interaction in β-Ti alloys), and Czech Science Foundation (GACR), project no. 22–21151K, and and D-1303000107/CD-Laboratory for Design of High-Performance Alloys by Thermomechanical Processing from Christian Doppler Forschungsgesellschaft.

REFERENCES

[1] G. Lütjering, J.C. Williams, Titanium, Springer Berlin Heidelberg, Berlin, Heidelberg, 2007. https://doi.org/10.1007/978-3-540-73036-1.

[2] M. Peters and C. Leyens: Titan und Titanlegierungen, Wiley-VCH, Köln, 2002, pp. 139–61.

[3] I. Weiss, S. L. Semiatin: Thermomechanical Processing of Beta Titanium Alloys: An Overview, Mater. Sci. Eng. A, 1998, vol. 243, pp. 46-65. doi:10.1016/S0921-5093(97)00783-1.

[4] T. Furuhara, Y. Toji, and T. Maki: in Ti-2003: Science and Technology, G. Luetjering and J. Albrecht, eds., Wiley-VCH, Weinheim, 2004, pp. 1219–26.

[5] D.G. Robertson, H. B. McShane: Isothermal hot deformation behaviour of metastable β titanium alloy Ti-10V-2Fe-3Al, Mater. Sci. Technol., 1997, vol. 13, pp. 575-583.

[6] D.G. Robertson, H. B. McShane: Analysis of high temperature flow stress of titanium alloys IMI 550 and Ti-10V-2Fe-3Al during isothermal forging, Mater. Sci. Technol., 1998, vol. 14, pp. 339-345. https://doi.org/10.1179/mst.1998.14.4.33

[7] G. Glover, C. M. Sellars: Recovery and recrystallization during high temperature deformation of α-iron, Metall. Trans., 1973, vol. 4, pp. 765-775

[8] S. Gourdet, F. Montheillet: An experimental study of the recrystallization mechanism during hot deformation of aluminium, Mater. Sci. Eng. A, 2000, vol. 283, pp. 274-288

[9] M. E. Kassner, S. R. Barrabes: New developments in geometric dynamic recrystallization, Mater. Sci. Eng. A, 2005, vol. 410-411, pp. 152-155.

[10] F. Warchomicka, D. Canelo-Yubero, E. Zehetner, G. Requena, A. Stark, C. Poletti, In-Situ Synchrotron X-Ray Diffraction of Ti-6Al-4V During Thermomechanical Treatment in the Beta Field, Metals (Basel). 9 (2019) 862. https://doi.org/10.3390/met9080862.

[11] F. Warchomicka, C. Poletti, M. Stockinger, Study of the hot deformation behaviour in Ti 5Al–5Mo–5V–3Cr–1Zr, Mater. Sci. Eng. A. 528 (2011) 8277–8285. https://doi.org/10.1016/j.msea.2011.07.068

[12] M. Dikovits, C. Poletti, F. Warchomicka, Deformation Mechanisms in the Near-β Titanium Alloy Ti-55531, Metall. Mater. Trans. A. 45 (2014) 1586–1596. https://doi.org/10.1007/s11661-013-2073-4.

[13] C. Poletti, L. Germain, F. Warchomicka, M. Dikovits, S. Mitsche, Unified description of the softening behavior of beta-metastable and alpha+beta titanium alloys during hot deformation, Mater. Sci. Eng. A. 651 (2016) 280–290. https://doi.org/10.1016/j.msea.2015.10.109.

[14] R.H. Buzolin, D. Canelo-Yubero, F. Warchomicka, M. Lasnik, A. Krumphals, M.C. Poletti, Refinement of the Ti-17 microstructure after hot deformation: Coupled mesoscale model, Mater. Sci. Eng. A. (2020) 140268. https://doi.org/https://doi.org/10.1016/j.msea.2020.140268.

[15] R.H. Buzolin, M. Lasnik, A. Krumphals, M.C. Poletti, Hot deformation and dynamic α globularization of a Ti-17 alloy: Consistent physical model, Mater. Des. 197 (2021) 109266. https://doi.org/https://doi.org/10.1016/j.matdes.2020.109266

[16] R.H. Buzolin, M. Lasnik, A. Krumphals, M.C. Poletti, A dislocation-based model for the microstructure evolution and the flow stress of a Ti5553 alloy, Int. J. Plast. 136 (2021). https://doi.org/10.1016/j.ijplas.2020.102862

[17] F. Miller Branco Ferraz, ., A comprehensive mean-field approach to simulate the microstructure during the hot forming of Ti-17. Materials Science & Engineering A 903 (2024) 146645- https://doi.org/10.1016/j.msea.2024.146645

[18] E. Shahryari et al., "Heterogeneous dynamic restoration of Ti–15Mo alloy during hot compression" Journal of Materials Research and Technology 33 (2024) 7656–7667 https://doi.org/10.1016/j.jmrt.2024.11.089

[19] Miller Branco Ferraz F., Buzolin R.H., Warchomicka F., Terrazas-Monje T., Ebenbauer S., Leitner T., Krumphals A., Poletti M.C., Effects of recovery and phase transformation on the recrystallization kinetics of Ti-6Al-4V during β-processing, 2025, Mater. Sci. Eng. A, 922, 147628. DOI: 10.1016/j.msea.2024.147628.

Society of Production Engineering

ICPES 2025

40th INTERNATIONAL CONFERENCE ON PRODUCTION ENGINEERING - SERBIA 2025

DOI: 10.46793/ICPES25.139M

University of Nis Faculty of Mechanical Engineering

Nis, Serbia, 18 - 19th September 2025

CRITERIA FOR SELECTING GEAR MANUFACTURING METHODS

Aleksandar MILTENOVIĆ[1], Damjan RANGELOV[1], Marko PERIĆ[1], Lazar STOJANOVIĆ[1]
Orcid: 0000-0002-1453-2548; **Orcid:** 0000-0003-3071-893X;
[1]Faculty of Mechanical Engineering, University of Niš, Niš, Serbia
*Corresponding author: aleksandar.miltenovic@masfak.ni.ac.rs

Abstract: *Gear can be produced on many processes, such as conventional ones like traditional machining (hobbing, shaping, milling) and forming methods (casting, forging, molding) to modern techniques like additive manufacturing. Selecting an optimal gear production method is a complex multi-criteria decision that significantly impacts the gear's quality, performance, cost, and production efficiency. The topic of this paper is a discussion of the key selection criteria for gear manufacturing methods in light of current needs and technological advancements. These criteria include the gear material, geometry and type of gear, required precision and quality level, production volume, cost, gear size, load carrying capacity, and lead time. For each criterion, brief academic explanations are provided to illustrate how it influences the choice of manufacturing process. The goal is to provide an overview for engineers responsible for developing machines with gears.*

Keywords: *gears, manufacturing, machining, forming, unconventional manufacturing*

1. INTRODUCTION

Gears are critical mechanical components used to transmit motion and torque, and they can be manufactured by numerous methods. No single manufacturing process is ideal for all gear types or applications and the optimal method depends on a combination of factors.

Important criteria include the gear's material, its geometry (type and complexity), the precision or requested tolerances, expected production volume, economic cost, physical size of the gear, desired performance (e.g. load carrying capacity, noise level, environmental resistance), and allowable lead time for production. Each of these factors can strongly influence which manufacturing process is most suitable. For instance, producing high-precision steel gears in low quantities requires different methods than mass-producing inexpensive plastic gears, which are less reliable. All the manufacturing technologies with additional information are given in Table 1.

2. MATERIAL CONSIDERATIONS

The gear material fundamentally narrows the possible manufacturing processes. In some cases, gear must be produced with a special material, as specified in standards, such as in the case of worm gears, which are made primarily from special bronze (Fig. 2).

Metallic gears are typically produced by machining or metal-forming processes, whereas plastic gears are often injection

molded or machined from plastic stock. Material properties like strength, hardness, and melting point can determine suitable methods. For instance, high-strength steels can handle heavy loads and are preferred in high-stress, high-precision gears. Steel and other metals can be forged or machined to achieve the required properties and accuracy; indeed, forged steel gears benefit from a grain flow that imparts superior fatigue strength. In contrast, plastics are used in less demanding applications and offer advantages such as light weight and self-lubrication, but they cannot be forged or cast in the same manner as metals. Instead, injection molding is the go-to high-volume process for plastic gears.

Metals can be machined to very high accuracy or ground after heat treatment for precision, and they can also be cast or sintered (powder metallurgy) for near-net shapes. Harder metals may be difficult to machine and might favor processes like precision forging or require annealing steps. Plastics, on the other hand, can be molded in complex shapes efficiently; however, not all plastics mold easily (Fig. 1).

Table 1. Overview of manufacturing methods for gears

Method		Characteristics	Advantages	Disadvantages
Conventional	**Milling**	Cutting involute profile with a cutter	Simple, widely available equipment	Limited accuracy, lower productivity
	Gear hobbing	Continuous cutting	High productivity	Special equipment
	Shaping	Cutting teeth with a gear shaper	Suitable for internal gears	Slow process, noisy
	Gear grinding	Fine finishing of tooth flanks	High accuracy and surface quality	Expensive, slow process
	Broaching	Cutting internal gears with a special tool	Fast for serial production	Rough finishing, low accuracy
	Saw cutting	Cutting simple gears	Simple, low-cost	Rough finishing, low accuracy
Unconventional	**Electrical Discharge Machining (EDM)**	Wire or die-sinking shaping of gear teeth	High precision, complex shapes	Slow, high energy consumption
	Laser cutting and machining	Cutting gears with laser	Fast prototyping	Limited for thick materials
	Chemical etching	Chemical removal of material	For micro-gears, thin metals	Limited to thin materials
	Ultrasonic machining	Abrasive shaping with ultrasonic vibrations	Hard materials machining	Slow, requires special equipment
	Hydroforming	Shaping thin-walled gears by fluid pressure	Good material structure, thin walls	Limited to specific applications
	Plastic deformation (forging, rolling)	Forging or rolling teeth	High gear strength	Expensive equipment
	Sintering (Powder metallurgy)	Pressing metal powder in a die and sintering	Low unit cost for mass produc., good repeat.	Small size only
	Additive manufa-cturing (3D printing)	SLS, SLA, FDM prototyping	Fast prototyping, complex shapes	Low strength (plastic), accuracy
plastic gears	**Injection molding**	Flexible, no expensive molds	High productivity, low cost in mass product.	Expensive molds, lower precision
	CNC milling	Machining plastic gears on CNC machines	Flexible, no expensive molds	Higher cost per unit, slow product.
	Extrusion and cutting	Extrusion of plastic profiles, gear cutting	Simple for basic shapes	Limited shaping, lower precision

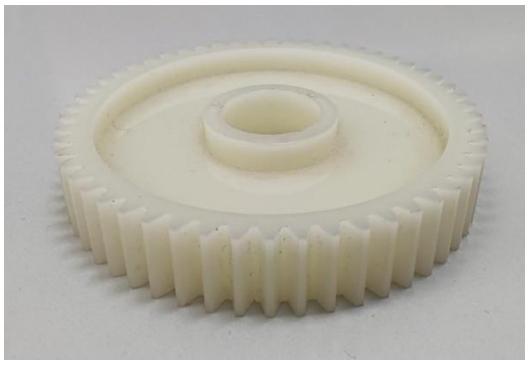

Figure 1. Plastic gear made by inject molding

3. GEAR GEOMETRY AND COMPLEXITY

The gear geometry – including tooth profile, helix angle, and overall shape (spur, helical, bevel, worm, internal gear, etc.) – strongly influences which processes are feasible. For example, spur gears with external teeth are relatively straightforward to manufacture; they can be cut by standard hobbing or milling with relative ease. Helical gears, however, require precise control of the helix angle and typically need specialized hobbing or 5-axis machining. Bevel gears and worm gears often cannot be made by the same equipment used for spur/helical gears and they demand dedicated gear cutting machines (Gleason cutting for bevel gears, thread grinding for worms - Fig. 2).

Figure 2. Worm gear set with center distance 30 mm in which worm gear is made from bronze

Gears with internal tooth geometry pose additional complexity. Traditional hobbing machines can cut external spur and helical teeth efficiently but cannot cut internal gears. In such cases, processes like gear shaping or broaching are required – a gear shaper uses a cutter that reciprocates to form teeth and can create internal gears or other profiles that hobbing cannot handle. This means that if a design calls for an internal gear or a cluster gear arrangement, the manufacturing method must be one that supports internal geometry (shaping, broaching, or possibly additive manufacturing), whereas simple external gears give more flexibility in method (hobbing, milling, etc.). Likewise, very fine-pitch gears or non-standard tooth profiles might necessitate wire EDM or additive manufacturing.

4. REQUIRED PRECISION AND QUALITY

Gears are classified by quality grades (ISO standard), which specify tolerances on tooth dimensions, runout, surface finish, etc. The required precision level is directly tied to the capabilities of the manufacturing method. If a gear must have very tight tolerances, the manufacturing process must either inherently achieve precision or include finishing steps.

Machining processes, especially with CNC, can achieve very tight tolerances on gear tooth geometry – gear hobbing or shaping followed by gear grinding is commonly used for high-precision metal gears. Grinding or lapping as a post-process can correct small deviations from heat treatment or prior processes. In contrast, injection molding of plastic gears yields comparatively looser tolerances due to material shrinkage and mold limitations; these gears are usually for moderate precision needs where some inaccuracy is acceptable. Machined plastic gears, however, can be cut with finer tolerances and less variability.

Powder metallurgy can produce gears with minimal post-processing, but shrinkage in sintering and porosity mean such gears usually achieve only modest precision and often need sizing or surface finishing. Stamping/blanking sheet metal can rapidly create gear forms, but the process is generally limited to thin gears with relatively coarse tolerances and may produce burrs or distortion that affect precision.

5. COST AND PRODUCTION VOLUME

The number of gears to be produced is one of the most decisive factors in process selection. Some manufacturing methods have high fixed costs but low per-unit costs, making them economical only when producing large volumes. Injection molding exemplifies a high-volume method. It requires an mold tool and setup, but once the mold is made, thousands of plastic gears can be produced very cheaply and quickly.

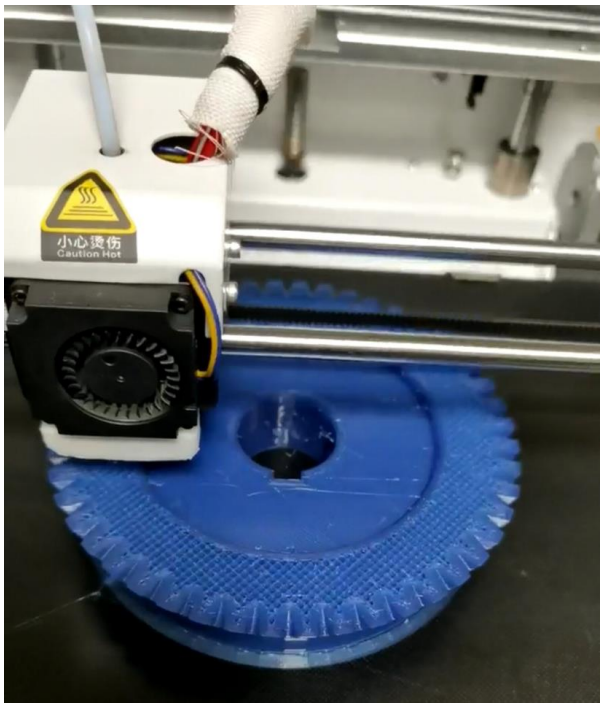

Figure 3. FDM 3D printing of bevel gear

Machining is generally more expensive per part due to longer cycle times and material waste, but it is "economical for small runs or prototypes" when avoiding fixed costs. Also, 3D printing (Fig. 3) can produce one-off gears or very low volumes quickly; although each printed part's cost would be unacceptable for mass production, it can be justified for prototyping. Blanking/stamping is in between – the dies are costly, but once made, stamping out sheet-metal gears is extremely fast. In summary, the expected production volume funnels the choice: high-volume projects favor methods like injection molding, die casting, forging, or sintering that spread costs over many units. Low-volume or one-off production leans toward machining or possibly additive manufacturing despite higher unit costs, because those avoid large initial investments and can adapt quickly to design changes. A careful economic analysis is often performed to compare the total cost for the anticipated quantity under different processes, ensuring the chosen method aligns with the project's volume and budget constraints.

Additionally, labor costs must be taken into account. For instance, precision CNC machining and grinding produce excellent gears but are labor- and time-intensive, thereby driving up the costs of each part.

Cost is also affected by material utilization. Machining operations are wasteful by nature – a large portion of expensive metal might end up as chips, which is material cost lost.

6. GEAR SIZE AND SCALE

The physical size of the gear has a major impact on manufacturing method viability. Very large diameter gears (gears in heavy industrial equipment – Fig. 4, wind turbines, or large machinery measuring on the order of 1–4 m in diameter) are impractical to produce with certain methods.

Figure 4. Industrial gear with 3,5 m diameter used in copper mining industry

Hobbing or grinding extremely large gears is technically possible but requires specialized oversized machines and becomes time-consuming. In such cases, casting is often the preferred method to create the gear blank or

even the rough gear teeth, because pouring molten metal can fill a large gear shape more easily than trying to cut it from a solid billet.

For moderate-size metal gears in that range or smaller, forging can produce a strong near-net shape which might then be machined to final precision. Small gears, on the other hand (millimeters to a few centimeters in size), can be produced by methods that might not suit large gears. Powder metallurgy is commonly used for small gears. Very small metallic or plastic gears can also be made by precision stamping or fine blanking if they are flat, or by micro-molding for plastics. For production of tiny gears - microgears should be used chemical etching.

7. MECHANICAL PROPERTIES

The operational demands on the gear (torque, speed, fatigue, shock, temperature, etc.) are important criteria for method selection. If a gear must handle very high loads or operate in critical, high-stress conditions, this usually dictates using a strong metal and a process that optimizes mechanical properties.

Forging is often chosen for such applications because forged metal has a refined grain flow and superior fatigue strength. On the other hand, casting generally yields lower strength due to potential porosity.

Powder metal gears are typically not as strong as wrought or forged gears because residual porosity and sintered microstructure limit their fatigue performance. Similarly, plastic gears have much lower load capacity and temperature resistance than metal gears; they are chosen for light-duty applications or where their self-lubricating and noise-damping qualities are advantageous.

Mechanical performance is not just about strength – wear and scuffing resistance, friction, and noise are also key. Hardened steel gears with smooth finish will wear slowly, but they may be noisier in operation. Plastic gears run quieter and do not require lubrication in many cases, which is a reason they are used. However, plastics can creep over time and are sensitive to temperature and chemicals.

Heat treatment is another aspect: metal gears often undergo processes like carburizing, nitriding, or induction hardening after initial machining to improve wear and fatigue performance. This introduces another manufacturing consideration – some methods like forging already involve high-temperature deformation which can enhance properties, whereas machining just shapes the metal and then relies on separate heat treatments to harden it. The required surface hardness and core toughness will therefore influence whether a gear is, say, machined then casehardened, or forged then minimally machined, etc. If surface finish and contact fatigue are critical, a final grinding or honing may be introduce as final step.

8. LEAD TIME AND FLEXIBILITY

The urgency of production and flexibility in design changes also influence the process selection. Some methods entail substantial lead times, chiefly due to tooling fabrication. Injection molding requires designing and manufacturing a precision mold, similiary to sintering, which can take weeks to months. Die casting or forging dies similarly involve time-consuming tooling production. If a project cannot afford this upfront time, such methods are not practical. By contrast, CNC machining and 3D printing have much shorter lead times. A CNC-machined gear only requires a CAD model and programming, allowing a part to be made in hours or days.

9. CONCLUSION

Selecting a gear manufacturing method is a multi-factor optimization problem, requiring a holistic look at design requirements, material capabilities, and economic factors. The paper discusses the criteria based on which the appropriate manufacturing technology is selected, such as material, cost, precision,

quality, gear size, mechanical properties, and lead time. In the paper, an overview of manufacturing technologies that are of interest to engineers responsible for developing machines with gears is given.

REFERENCES

[1] N. Harrison, “Gear Manufacturing 101: A Guide on the Gear Production Processes,” RapidDirect Blog, May 6, 2022
[2] Bartosch, “The Difference Between Injection Molded Plastic Gears and Machined Plastic Gears,” Intech Power (Blog), Dec. 27, 2022.
[3] “A Deep Dive into Custom Gear Manufacturing,” Gear Technology India, Gear Technology India Magazine, 2023.
[4] W. P. Crosher, “Gear Accuracy vs. Manufacturing Costs,” Gear Solutions, Aug. 10, 2013.
[5] D. McClements, "CNC Machining vs. Plastic Injection Molding: Differences and Comparison," Xometry, Sep. 12, 2022.

Society of Production Engineering

ICPES 2025

40th INTERNATIONAL CONFERENCE ON PRODUCTION ENGINEERING - SERBIA 2025

DOI: 10.46793/ICPES25.145W

University of Nis Faculty of Mechanical Engineering

Nis, Serbia, 18 - 19th September 2025

HYDROGEN EMBRITTLEMENT OF RECYCLED PRESSURE VESSEL STEEL P460NL

Tobias Walder[1], Fabian BOBNER[1], Thomas STAUBMANN[1], Hamdi ELSAYED[1], Fernando WARCHOMICKA[1], Rudolf VALLANT[1], Sveto CVETKOVSKI[2]

Orcid: 0009-0007-4386-3091; **Orcid:** 0009-0003-2627-3752; **Orcid:** 0009-0002-8833-7638; **Orcid:** 0009-0004-4061-5533; **Orcid:** 0000-0002-4909-8657; **Orcid:**0000-0002-2450-7119; **Orcid:** 0000-0002-5609-9201;

[1]Graz University of Technology, Institut of Materials Science, Joining and Forming, Graz, Austria

[2]Ss. Cyril and Methodius University in Skopje (UKIM) Faculty of Technology and Metallurgy

*Corresponding author: rudolf.vallant@tugraz.at

Abstract: *Hydrogen embrittlement (HE) presents a critical challenge to the structural integrity of pressure vessels, especially those manufactured from recycled steel. This study explores the susceptibility of recycled P460 NL1 pressure vessel steel to hydrogen induced degradation. A comprehensive approach is employed, combining Slow Strain Rate Testing (SSRT) under electrochemical hydrogen charging, metallographic analysis, and Thermal Desorption Spectroscopy (TDS), to investigate the influence of microstructural characteristics on mechanical performance and hydrogen uptake. Both base metal and welded specimens are examined to assess the effects of welding on hydrogen behavior. Additionally, detailed microstructural investigations are carried out to evaluate the role of non-metallic inclusions, specifically their number, size, and morphology in the embrittlement mechanisms of both recycled and conventionally produced steels.This study aims to elucidate the relationship between hydrogen absorption, inclusions, and microstructural features in recycled steels, which are increasingly utilized in sustainable engineering applications. The findings are expected to enhance the understanding of embrittlement mechanisms in recycled steels and support the development of effective mitigation strategies against hydrogen-related failures.*

Key words: *P460NL1, HE, Electrochemical hydrogen charging, SSRT, TDS*

1. INTRODUCTION

From the point of The European Green Deal [1] steel producers face two issues, which are -

- Increasing the recycling share to reduce CO_2 emissions, i.e. use up to 100% scrap [2]
- higher hydrogen load on steel infrastructure, like tubes or vessels for energy supply, i.e. transport and production of hydrogen (gas or liquid solutions) [3,4]

In difference to conventional steel making from ore (Blast furnace and Linz-Donawitz Oxygen converter / BOF) the recycled steel is produced from scrap, remelted in the Electric Arc Furnace (EAF), where also the metallurgical deoxidation is performed,

afterwards going directly to the continuous casting and the hot-rolling mill for producing sheets. By this recycling procedure the CO_2-emission is reduced from 2.3 t (BOF) to 0.7 t (EAF) per ton raw steel. [5]

A higher susceptibility for Hydrogen Embrittlement (HE) or more specific Hydrogen Assisted Cracking (HAC) due to the higher amount of Non-Metallic-Inclusions (NMI) of a Recycled Steel (RSt) in comparison to Conventional Steel (CSt) should be expectable. Here especially sulfide inclusions (MnS) are to be mentioned, as they form segregation sites for hydrogen and can induce cracks. [6,7]

The H- absorption depends on the microstructural features of the steel, such as grain size, grain boundaries, dislocations, interstitial lattice sites, defects etc., which also depends on the production processes. HAC refers to the loss of ductility in metals caused by hydrogen absorption into the crystal lattice. The diffusion and concentration of atomic hydrogen around zones of high triaxiality promote local embrittlement mechanisms [8] Transport of hydrogen through the metal is determined by diffusion between interstitial lattice sites and trapping of hydrogen at microstructural sites such as grain boundaries, dislocations, carbides, inclusions and precipitate particles. [9]

2. EXPERIMENTAL

The investigated Recycled Steel (RSt) and the Conventional Steel (CSt) examined for comparison purposes, both specified as P460NL1, are weldable fine grain steel sheets of 12 mm thickness. According to manufacturer's data they fulfill the european standard EN 10028-3 with regards to chemical composition and mechanical properties. To note that the RSt has too high N-content and is normalized rolled and the CSt in contrast is normalised rolled and tempered - s. [10]

Table 1. Chemical composition and mechanical properties of Recycled Steel (RSt) vs. Conventional Steel (CSt) P460NL1 acc. to manufacturers data and compared to EN 10028-3 (Nb, Ti, V analysed by IMAT OES Spectrolab 2.3).

wt.%	C	Si	Mn	P	S	Al_{total}	N	Cr	Cu	Ni	Mo	Nb	Ti	V	EV1	CEV
RSt	0.16	0.25	1.22	0.016	0.005	0.055	0.08	0.07	0.3	0.25	0.1	0.038	0.003	0.059	0.100	0.427
CSt	0.17	0.43	1.57	0.011	0.001	0.031	0.011	0.04	0.17	0.49	0.01	0.03	0.003	0.09	0.123	0.504
EN 10028-3	≤0.20	≤0.60	1.10-1.70	≤0.025	≤0.008	≥0.020	≤0.025	≤0.30	≤0.30	≤0.80	≤0.10	≤0.05	<0.03	≤0.20	≤0.22	≤0.53

EV1: V+Ti+Nb CEV = C + Mn/6 + (Cr+Mo+V)/5 + (Ni+Cu/15)

	R_{eH} (MPa)	R_m (MPa)	A_5 %	ISO-V(-20) J [2)]
RSt	512	627	29	144 (-20°C)
CSt [1)]	537	639	24	119 (-50°C)
EN 10028-3	≥460	570-730	≥16	≥35 (-20°C)

[1)] normalised & tempered [2)] transverse

The electrochemical H-charging without mechanical load was performed on 4-edged samples 5x5x24mm^3 from the 12mm sheets for 1, 4, 8, 12 and 24 hours at approx. -3mA/cm^2 cathodic current density in a 3.5% NaCl solution at room temperature, adding 1g/l thiourea as a H-recombination poison. Afterwards the samples were cooled in liquid nitrogen and the TDA measurements performed.

The electrochemical H-charging with mechanical load was performed on tensile samples A5 x 25 acc. to standard DIN 50125, cutted out in the sheets rolling direction for Slow Strain Rate Tests (SSRT) acc. to ASTM G129-21 with a strain rate of 10^{-5}/s. The SSRT were performed in air and with electrochemical H-charging conditions as explained above.

Submerged Arc Welding (SAW) without preheating was performed on the RSt and subsequently A5 x 25 tensile specimens manufactured, which include the weld and investigated in SSRT as explained above. The welding parameters are shown in Table 2.

Table 2. Welding parameters of Tandem SAW procedure of the RSt on 12mm sheet without preheating - V-joint outer and inner pass.

Welding wire	Welding flux	1st pass - outer pass 2nd pass - inner pass	Heat Input, kJ/cm
EMS 2 Mo, Ø 4 mm	BB 24	Wire 1: 630 A, 30V, 1m/min Wire 2: 650 A, 33V, 1m/min	24 kJ/cm (11 + 13)

After the SSRT fracture pieces were cooled in liquid nitrogen and subsequently the H-uptake determined in a Thermal Desorption Analysis (TDA) device *Bruker Galileio G8* with a detection limit (DL) of 0.01 wppm.

3. RESULTS

Microstructure of base materials, weld and inclusion analyses

In Light Optical Microscope (LOM) the Nital etched longitudinal section of the RSt show banded structures of Ferrite (77%) and Pearlite (23%). The width of the bands is approx. 10 µm for the Pearlite and 30 µm for the Ferrite. In contrast the CSt is in tempered condition and show finer and less pronounced banded structure, whereby the Pearlite bands are partially dissolved in forming carbides. The microstructure of the SAW weld, performed just on the RSt, consists mainly of Acicular Ferrite (AF), Bainite (B) and Grain Boundary Ferrite (GBF) and is thus completely different to the RSt base material microstructure - s. Figure 1.

Figure 1. LOM microstructures in longitudinal sections / RSt normalized rolled (top left), CSt normalized rolled and tempered (top right) and the SAW weld of RSt (RStw).

The Vickers hardness measurements on a longitudinal section of a tested RSt tensile sample (RStw) revealed slightly elevated hardness levels of 250 HV1 in the welded area, compared to 230 HV1 in the RSt base material, thus representing an even-matched welding - s. Figure 2.

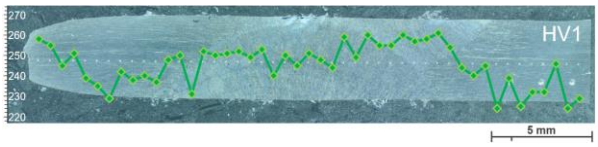

Figure 2. Hardness HV1 on a longitudinal section of a RStw tensile specimen - containing the even-matched SAW welding.

The number of non-metallic inclusions (NMIs) larger than 6µm^2 and based on the standard EN 10247, in the RSt is about three times higher than in the CSt. This means, 60-100 vs. 20-30 NMIs per mm^2. Generally, the same types of inclusions were found in both steels, i.e. CaS, AlMgO and AlO - s. Figure 3. To note that in the CSt additionally MnS-inclusions were detected. Furthermore, incompletely molten metallic inclusions (MI) of NbTi-type (micro-alloying elements) were detected in the RSt and in the CSt, too. It cannot be ruled out that further inclusions may be present, which would require more detailed and extensive analyses.

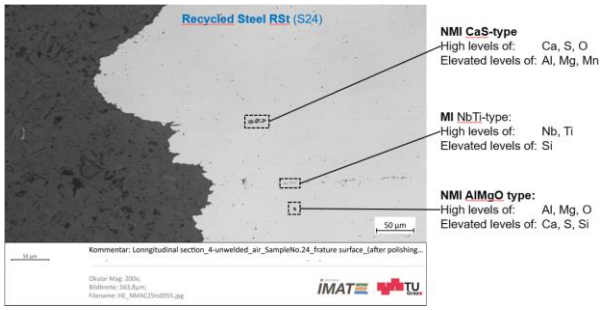

Figure 3. Types of selected NMIs in RSt in a tested tensile sample, close to the fracture (longitudinal section).

Hydrogen uptake without mechanical loading and electrochemical polarization

To assess the potential H-uptake of the investigated steels, individual specimens were subjected to charging, as described in the experimental section. The corresponding results indicate a significantly higher H-uptake of the CSt-sample after 24 hours of exposure, compared to the RSt. The latter reaches the H-saturation already after approx. 12 hours and shows a max. H-content of 0.34 wppm. In contrast the CSt has faster H-uptake and reach a value of 0.67 wppm after 24 hours - presented in Figure, left.

The polarization tests show distinct differences as well. This means, the RSt has a higher Open Circuit Potential (OCP) of -0.67 V and is therefore more noble than the CSt exhibiting an OCP of -0.70 V vs. Ag/AgCl reference electrode. The corrosion rate evaluation using the Tafel method result in 1.8 µm/year for the RSt vs. 4.8 µm/year for the CSt. The cathodic branch of the RSt is larger and reach a sharp increase of H_2-formation at approx. -0.95 vs. -0.85V for the CSt - s. Figure 4, right.

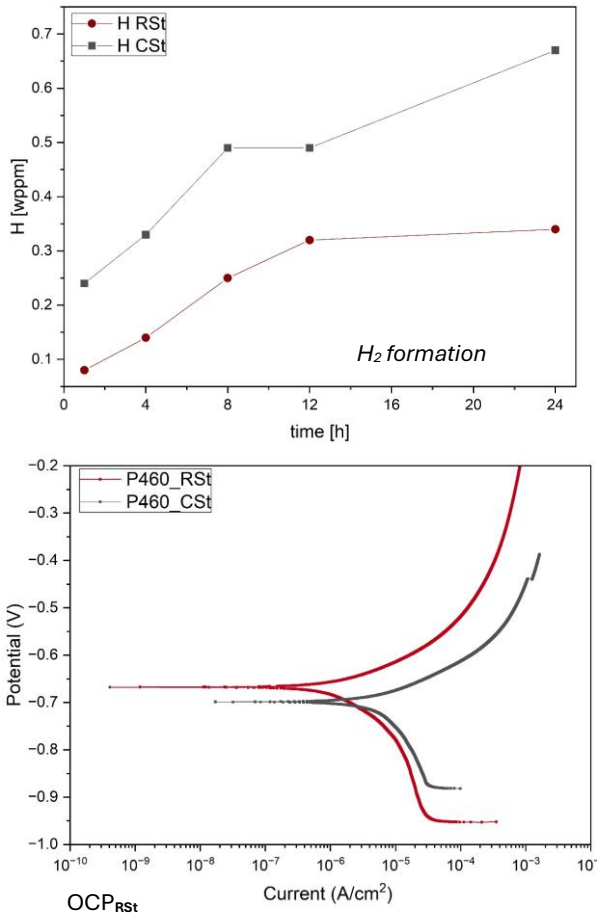

Figure 4. H-uptake in electrochemical charging (left) and polarisation curve (right) in 3.5% NaCl and 1g/L Thiourea solution vs Ag/AgCl reference electrode.

REFERENCES

[1] F. Umbach: The European Green Deal faces huge challenges; Energy Transition, February

10; 2020. https://www.gisreportsonline.com/r/european-green-deal/

[2] L. Yang et al.: Life cycle carbon footprint of electric arc furnace steelmaking processes under different smelting modes in China; Sustainable Materials and Technologies; Volume 35, April 2023. https://doi.org/10.1016/j.susmat.2022.e00564

[3] Vallourec Expands its Range of Qualified Materials for Hydrogen Service, 02/27/2023; https://www.vallourec.com/en/all-news/group-2023-qualified-materials-for-hydrogen-service

[4] Sandvik to acquire the tube engineering solutions company Gerling GmbH, 2021 https://www.home.sandvik/en/news-and-media/news/2021/11/sandvik-to-acquire-the-tube-engineering-solutions-company-gerling-gmbh/

[5] F. Passaro: A Green Future for Steel, Climate Bonds Initiative 2022; www.climatebonds.net

[6] M. Elboujdaini & R. W. Revie: Metallurgical factors in stress corrosion cracking (SCC) and hydrogen-induced cracking (HIC), J Solid State Electrochem 13:1091–1099 (2009); DOI 10.1007/s10008-009-0799-0

[7] Z. Szklarska-śmialowska, E. Lunarska: The effect of sulfide inclusions on the susceptibility of steels to pitting, stress corrosion cracking and hydrogen embrittlement; Materials and Corrosion, Volume 32, Issue 11, 478-485 (1981); https://doi.org/10.1002/maco.19810321103

[8] N. Shikomba et al.: Resistance of welded low-alloyed pressure vessel and pipeline steels in gaseous hydrogen; Welding in the World, May 2025. https://doi.org/10.1007/s40194-025-02074-7

[9] A. Turnbull ed.: Proceedings of Conference *Hydrogen Transport and Cracking in Metals*, 1995; ISBN 0-901716-67-7; pp. 4, 130.

[10] G.T. Park, S.U. Koh, H.G. Jung, K.Y. Kim, Effect of microstructure on the hydrogen trapping efficiency and hydrogen induced cracking of linepipe steel, Corros. Sci. 50 (2008) 1865–1871, https://doi.org/10.1016/j.corsci.2008.03.007

[11] D. Brooksbank and K. W. Andrews: Production and application of clean steels, J. Iron Steel Inst., 210 (1972), 246.

[12] A. Hamed et al.: Assessing the hydrogen embrittlement susceptibility of an existing L360NB natural gas pipeline steel for 100 % hydrogen transport; Corrosion Science 244 (2025) 112648. https://doi.org/10.1016/j.corsci.2024.112648

Society of Production Engineering

ICPES 2025

40th INTERNATIONAL CONFERENCE ON PRODUCTION ENGINEERING - SERBIA 2025

DOI: 10.46793/ICPES25.151Z

University of Nis
Faculty of Mechanical Engineering

Nis, Serbia, 18 - 19th September 2025

IMPACT OF GATING SYSTEM DESIGN ON MECHANICAL PROPERTIES OF ALUMINIUM SAND CASTINGS

Marko ZAGORIČNIK[1], Lazar KOVAČEVIĆ[1], Vladimir TEREK[1], Zoran BOBIĆ[1], Pal TEREK[1]
Orcid: 0000-0003-0798-456X; **Orcid:** 0000-0002-0843-4984; **Orcid:** 0000-0001-9994-6039;
[1]University of Novi Sad, Faculty of Technical Sciences, Serbia,
*Corresponding author: zagoricnik@uns.ac.rs

Abstract: *Aluminium alloys are extensively employed across modern industries, appreciated for their advantageous combination of low weight, corrosion resistance, strength, and ductility. Nonetheless, casting defects—including inclusions, porosity, hydrogen absorption, and particularly bifilms—can significantly compromise the mechanical properties of cast components. The present investigation centres on bifilm-related defects, which originate from the oxidation behaviour of aluminium alloys. Upon exposure to air, a thin oxide layer instantly forms on the molten metal surface. When disrupted, this film is immediately replaced by a new one, and such layers can become entrained within the melt during various stages of processing. Once inside the liquid metal, these oxide films retain their structural integrity due to their inert nature, remaining as compacted and folded entities that do not dissolve or disperse. Their presence has a pronounced negative impact on mechanical properties and can result in internal discontinuities that reduce mechanical properties and manifest as leak paths after machining. While bifilms can be introduced during melting, charging, or refining, the pouring phase presents a critical opportunity for their entrapment. Thus, the design of the gating system becomes essential. In this preliminary study, the role of flow dynamics during mould filling was examined by comparing two distinctly configured gating systems in sand casting of aluminium alloy: a top-gated setup promoting turbulent flow, and a bottom-gated arrangement intended to minimize flow disturbance. Advanced simulation using Magmasoft software confirmed the expected flow behaviours, illustrating greater splashing and air entrapment in the top-gated configuration. Following casting, samples were machined and subjected to tensile testing. Results demonstrated a statistically significant increase in ultimate tensile strength for specimens produced via the bottom-gated system. This exploratory experiment lays the groundwork for continued investigations into bifilm mitigation through optimized gating design.*
Keywords: *Bifilms, casting, entrainment, aluminium alloy, gating systems*

1. INTRODUCTION

Many liquid metals are not actually pure liquid. Most of them contain floating solid phases that can reduce the mechanical properties of castings. Much evidence applies to aluminium and its alloys, where research has been focused, but steels and nickel alloys also may suffer from these defects [1]. Additionally, aluminium alloys are especially vulnerable to entrainment, a process in which the thin oxide layer on the surface of the melt enters the liquid and folds in on itself,

remaining crumpled during the solidification, and acting as a crack during exploitation. Prof. Cambell has made significant research in this field [2,3] highlighting the effect of entrainment defects on castings.

How does entrainment happen? When a molten metal is poured, its surface area increases as it flows. Due to the high reactivity of aluminium alloys oxides immediately form on the newly available surface. If the surface ever contracts, the oxide layers cannot merge like surface of the molten metal, and they crumple and fold on themselves. Similarly, if the melt splashes, droplets oxidise in the air and when they fall back to the melt they introduce the oxides to the bulk. Poor gating system design causes the melt to flow uncontrollably: swirling, splashing, eroding the mould, and trapping air as it flows. This process introduces large amounts of surface oxides and sand inclusions into the casting. Due to the similar density of its oxides compared to the liquid aluminium, these inclusions float up very slowly and often remain in the castings. Careful design of filling systems can minimize turbulence and splashing, greatly reducing the entrainment defects [2,3].

Previous research on bifilms, conducted on Al-Si-Mg alloys yielded results that indicate the negative effect of bifilms on the scatter of mechanical properties of castings. These experiments compared different gating systems which were designed to promote or reduce the creation and entrainment of surface oxides [4,5]. Another research, on Cu-Al alloy [6] also designed an experiment that compared the effects of different gating systems on bifilm creation. The results have shown similar trends. Another research on Al-Cu alloy [7], compared the tensile properties of top gated, and tilt poured specimens, and indicated that the increased bifilm generation in the top gated system was responsible for the scatter of mechanical properties.

This paper is a fundamental testing of an experimental setup and serves as a replication study for similar previous work [4,5,6,7]. Unlike prior studies that used more robust gating systems, this experiment utilized a detailed, and more efficient design to optimize metal utilization. This study focused on establishing a reliable methodology for investigating the effects of bifilms in highly reactive (oxidizing) aluminium alloys.

2. MATERIALS AND METHODS

In this study, Al-Si alloy was used to produce standard tensile strength test pieces using two different filling system designs, namely one bottom gated and one top gated. To make the moulding easier, the test pieces were cast as cylindrical bars with diameter of 20 mm. Multiple bars were cast simultaneously so that the results can be averaged. Both filling systems included the same spacing and position of the test pieces in the mould, to minimize the difference in cooling conditions in the mould.

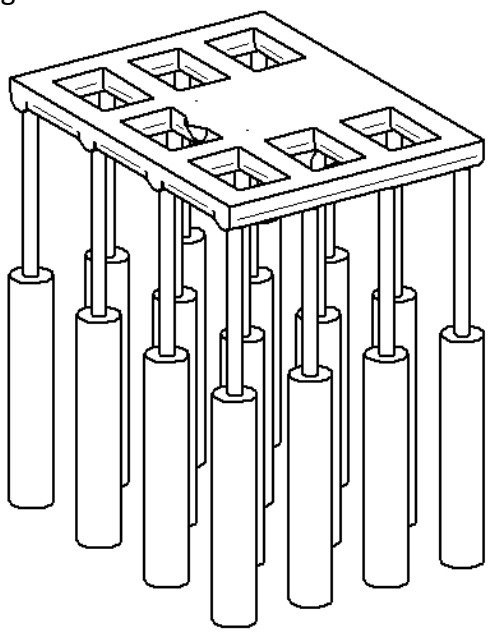

Figure **1.** CAD drawing of the top gated system

The experimental design of top gated system is given in Fig. 1. The chosen geometry is a representative of widespread methoding practice in foundries that prioritize minimal expenditures and prefer quick and simple solutions. This design has a hemispherical oval

pouring basin that is easy to produce but is not particularly successful at controlling melt flow pattern. Its small volume provides too short reaction time window for the operator to keep the liquid level stable. The pouring basin simply extends into the runners. The runners are a square grid that redirects the flow towards the castings. Its design is very primitive, without any reduction in cross section, to represent the bare minimum that serves the purpose. As the gates branch down from the runner, again without tapering, they provide relatively large vertical fall into the casting (200 mm). This unrestricted fall causes the melt to hit the bottom at a great velocity and hopefully create a significant splashing (see Fig. 2). As the pouring continues, the liquid level in the casting rises, reducing the height of the fall. This type of filling system creates a temperature gradient, placing the hottest section on the top of the casting, which is an advantage of the top gated system. Solidification of the casting is directional and occurs from the bottom-up, promoting better feeding.

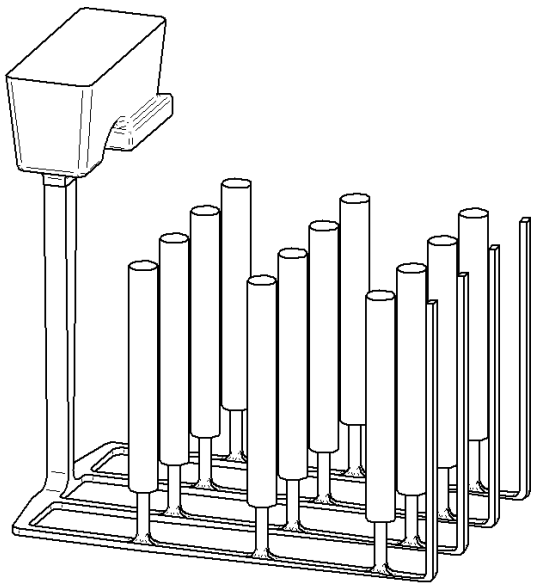

Figure 2. CAD drawing of the bottom gated system

The experimental design of top gated system is given in Fig. 2. The chosen geometry should provide a quiescent filling of the mould cavity, carefully avoiding air entrapment, high turbulence, and high melt velocity when entering the casting. The design begins with a carefully designed pouring basin. The well has an undercut, which reduces turbulence and splashing when the initial melt hits its bottom. Once the initial turbulence has settled, and the level of melt slowly rises in the filling well, it climbs over the rounded step, towards the sprue. The sprue is plugged with a ceramic stopper before the start of the pour to prevent rogue droplets and the very surface of the rising melt from entering. These contain the most oxides. Once the melt reaches about 60% of the pouring basin height the stopper is removed, and the melt starts flowing into the sprue, without turbulence, and containing a minimal number of oxides. The operator must keep pouring at a constant rate, so that the liquid level never drops too low, or overflows. This is achieved by making the pouring basin large enough to account for human reaction time, which is approximately one second. Increasing the pouring basin obviously reduces the effective yield of the casting, slightly increasing the cost of production due to recycling of the larger gating system. On the other hand, producing better castings, with fewer defective parts, and more consistent mechanical properties is economically beneficial, so the cost of the gating system should be net positive. The sprue is tapered, so that it follows the reducing cross section of the falling metal stream, preventing the stream from pulling air out of the mould and eroding the sand. The sprue and runner entrance are rounded, to reduce turbulence caused by the melt turning sharp corners. The runner branches into rows, which extend into the mould and connect to the gates. The cross section of the runner branches decreases after each gate, to accommodate the volume loss that goes into the casting. The runner ends in a vertical runner extension designed to catch the first melt that entered the gating system which contains the most oxides and possible inclusions. The vertical extension also provides backwards pressure into the runner, ensuring that melt velocity at the gates does not exceed critical value of 0.5 m/s, above

which surface turbulence and splashing can occur. The gates are simple vertical tubes, extending from the runner into the casting. Their cross section is large enough to ensure the melt velocity is below above-mentioned critical value. The filling rate of the test pieces should be fast enough to prevent oxide laps from forming, so the part should be filled in the shortest time possible, while avoiding the creation of bifilms. This orientation of the filling system creates a thermal gradient in which the bottom of the casting is the hottest part, since the melt enters from there. This creates less optimal solidifying conditions, since there is no feeding of the part. Regardless of this, most of the part is going to be machined away, and its ends will only be used to hold onto while preforming tensile tests, so this should have minimal impact. Due to the small diameter of the part, and low shrinkage of the used alloy, no feeding of the castings is necessary.

The mould was made from quartz sand bonded with bentonite clay, with 5% moisture. The greensand mixture was carefully prepared and mixed, ensuring a homogenous mixture for both moulds, to remove mould variation interfering with the castings. The modelling set was a mixture of aluminium, and 3D printed parts. The mould was made using pneumatic, and hand tools. Fine parts of the gating system were closely inspected, the mould was cleaned of loose sand using compressed air, assembled, and covered to prevent loose sand or dust from entering before the pour. The ambient temperature at the time of pouring was around 30°C. The moulding was completed in around 1h before the pouring.

Table 1. Alloy chemical composition

Si (%)	Fe (%)	Mg (%)	Cu (%)	Zn (%)
7.55	1.39	1.34	0.97	0.71
Sn (%)	**Pb (%)**	**Mn (%)**	**Ti (%)**	**Al (%)**
0.50	0.26	0.21	0.05	Balance

The chemical composition of the used Al-Si alloy is given in Table 1. The alloy was heated to 700°C and held at the casting temperature for 4 hours. Temperature was measured before each pour. The slag was removed several times while holding and a final time immediately before pouring. Due to the low volume of the furnace, the two gating configurations could not be poured from the same batch. They were cast in two consecutive days, carefully replicating the same steps while melting, moulding, and pouring. After cooling, the moulds were broken, the gating systems were removed, and test pieces were machined to precise measurements shown in Fig. 3, and within dimension tolerances specified by [8].

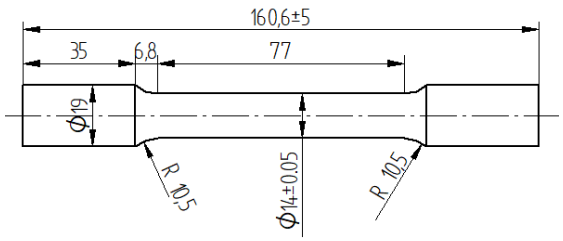

Figure 3. Technical drawing of a test piece

Machined test pieces were subjected to tensile strength testing on a VEB ZDM 5/91 Fmax 5kN at room temperature, according to the standard procedure [8]. During testing, some test pieces broke at the radius, making them invalid, so they were excluded from the results. A total of 14 top gated, and 8 bottom gated specimens were successfully tested.

3. NUMERICAL VERIFICATION OF GATING SYSTEMS

Both filling systems were examined using computer simulations in MAGMASOFT 5.4.1. The gating systems was modelled in Siemens Solid Edge 2023 and imported into MAGMASOFT 5.4.1. Corresponding materials were assigned to the parts of the assembly, and a mesh was generated. The density of the mesh was selected so that the smallest cross sections have at least 8×8 cells, and radii are well represented. High mesh quality is crucial in getting a good result of a numerical

simulation. Parameters such as type of mould, mould temperature, initial melt temperature, and pouring rate were defined to match actual future experiment values. The simulation provided results that showed the melt behaviour, most importantly its velocity, and the progress of melt free surface during the mould filling. The differences in the filling systems are shown in Figs. 4 and 5. As intended, the top gated system has a major flaw, the slow movement of the melt in the runner, followed by a chaotic waterfall-like splashing into the part cavities.

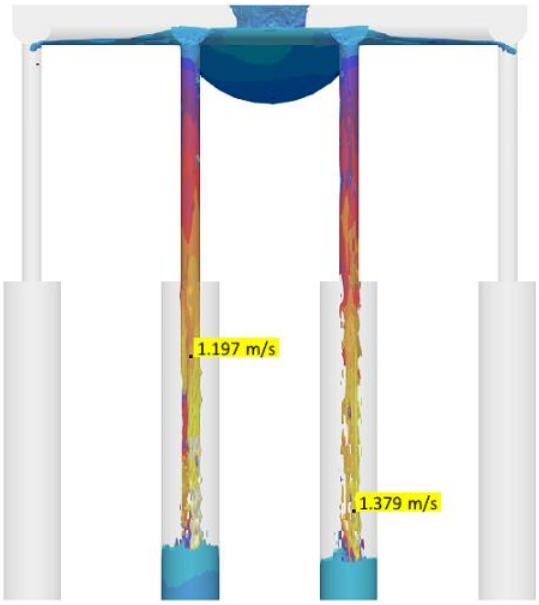

Figure 4. A side view of the top gated system, with velocity shown in colour (warmer colours represent higher velocity). Two points were picked to show melt velocity.

The melt velocity reaches 1.4 m/s and the stream breaks apart into individual droplets, before hitting the bottom of the mould. In contrast, the bottom gated system shows a gentle filling of the part, reaching only around 0.2 m/s when entering the test piece. The melt velocity in the sprue and runner is high, but this cannot be avoided due to the height of the castings. High melt velocity is not that detrimental when contained by a properly designed gating system and does not cause significant surface turbulence. The only turbulent part of flow in the bottom gated system is in the very beginning, while the sprue and runner are not yet completely filled with the melt. That is why the vertical runner extension is an important part of the gating system, since it catches the “dirty” melt that has the bifilms that were created while proper filling conditions were being established.

The simulation results can only be confirmed by actual experiments. They can be used only as a rough prediction of the actual test and cannot be trusted completely.

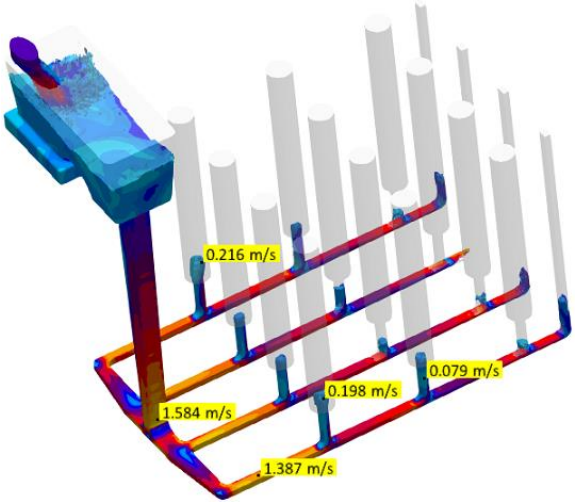

Figure 5. Isometric view of the bottom gated system, with velocity represented in colour. Several points were chosen to show velocity in certain areas.

4. RESULTS AND DISCUSSION

While pouring, several observations were made:

- Pouring time: the bottom gated system took less time to fill, around 4 seconds compared to 8, despite their similar mass (4,1 kg and 4.7 respectively). These pouring times align with the simulation results. The yield of both gating systems is similar: Top gated 46% and Bottom gated 41%, which further confirms that a much shorter pouring time can be achieved without compromising yield.
- Filling pattern: the top gated test pieces were filled one by one, with the pieces closest to the pouring cup being filled first. The splashing of the melt into the test pieces could be heard from the mould, and air from the cavity was

escaping through the gates. The bottom gated test pieces were all filled at the same time and the same rate. Due to the quality of the pouring basing, the bottom gated system was easier to pour.

- Casting difficulty: The top gated system was more difficult to pour, the pouring cup was close to overfilling, while the runners were half empty. This drastically extended the pouring time.

Due to a mistake which was later determined, the runner was 3D printed with 30% less height than required. This caused the last row of the bottom gated casting to be scrapped, since the melt froze in the runner before they were completely filled. These errors must be prevented in future research.

The results of tensile testing are shown in Table 2. Statistical analysis was performed using JMP Pro 14 (SAS Institute Inc.). Both top and bottom gated data was successfully tested for normality. Mean values, standard deviation, and 95% confidence intervals were calculated. The mean tensile strength and 95% confidence intervals of the specimens are shown in Fig. 6. The confidence intervals do not overlap, which shows a statistically significant difference in the results. A two tailed t-test was performed, and the resulting p-value was determined to be 0.00195. There is a statistically significant improvement in ultimate tensile strength of the bottom gated specimens, compared to top gated specimens.

Table 2. Tensile testing results

TG(MPa)	BG(MPa)
130.9	140.8
112.2	151.3
128.7	124.0
116.6	147.8
135.7	143.1
129.6	134.8
112.1	145.3
110.5	134.8
132.5	
127.4	
140.2	
135.1	
101.9	
128.7	

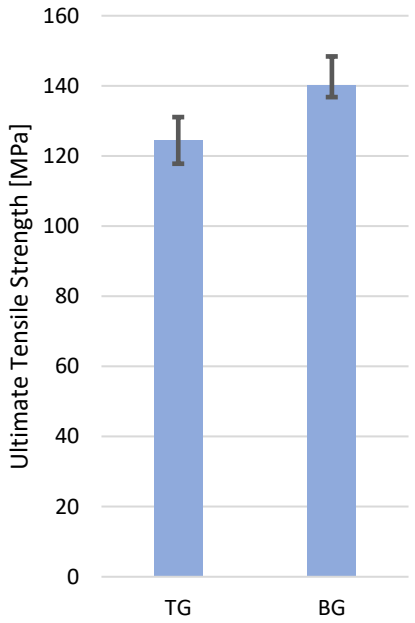

Figure 6. Comparison of top gated (TG) and bottom gated (BG) ultimate tensile strength with their respective confidence intervals. Eror bars represent 95% confidence intervals

This increase of mechanical properties is attributed to the lack of bifilms in the bottom gated test pieces.

Although mechanical properties could be affected by many factors, such as grain size, chemical composition, sand inclusions, microstructure, the experiment was designed to keep any variation of these factors to a minimum. Another important difference in the results is a narrower deviation of ultimate tensile strength in bottom gated specimens (8.8MPa compared to 11.5MPa).

Similar trends were reported by [7]. This also points to a lower presence of bifilms due to their impact on tensile strength, and result scatter. When subjected to tensile strain, bifilms act as initial cracks, and propagate cracks easier than sound test pieces. Depending on number of bifilms and their size, some test pieces fail at much lower strain, causing a greater scattering of results. In [4],[5], similar results were achieved on different Al-Si-Mg alloys, pointing to the detrimental effects of bifilms. In [6], a drop in

Ultimate tensile strength, and reliability in top gated castings was found in a Cu-Al alloy. In [7], entrained surface films were found to be responsible for much of the scatter in the mechanical properties and impaired the reliability of casting in an Al-Cu alloy.

5. CONCLUSION

- The bottom gated configuration proved to be easier to pour than top gated. A shorter pouring time, better filling pattern, and less splashing was observed in the bottom gated configuration.
- Tensile strength testing provided results which indicate that the bottom gated configuration yields statistically higher mechanical properties, with less spread.
- The experimental results point to the negative influence of bifilms on mechanical properties of castings.
- The experiment proved the methodology to be valid in determining detrimental effects of bifilms.
- Another iteration of the experiment, with both configurations being cast from the same batch, or connected in a branching gating system might provide even more convincing results on the negative effects of bifilms.
- Further studies, on aluminium alloys without magnesium are recommended.

ACKNOWLEDGMENTS

Authors would like to thank MAGMA Giessereitechnologie GmbH, Germany for their generous support through donation of their software MAGMASOFT 5.4.1.

REFERENCES

[1] M. Caturla, J. Jiang, E. Louis, J. Molina: Some Issues in Liquid Metals Research, Metals, Vol 5, No. 4, pp. 2128-2133, 2015

[2] J. Campbell: *Complete casting handbook: metal casting processes, techniques and design*, Elsevier, Oxford, 2015

[3] J. Campbell: Entrainment defects, Materials Science and Technology, Vol 22, No 2, pp. 127-145, 2006.

[4] G. Eisaabadi B, P. Davami, S.K. Kim, N. Varahram, Y.O. Yoon, G.Y. Yeom: Effect of oxide films, inclusions and Fe on reproducibility of tensile properties in cast Al–Si–Mg alloys: Statistical and image analysis, Materials Science and Engineering: A, Vol. 558, pp. 134-143, 2012.

[5] N. Green, J. Campbell: Statistical distributions of fracture strengths of cast Al-7Si-Mg alloy, Materials Science and Engineering, Vol 173, pp. 261-266, 1993.

[6] X.-Y. Zhao, Z.-L. Ning, F.-Y. Cao, S.-G. Liu, Y.-J. Huang, J.-S. Liu, and J.-F. Sun: Effect of double oxide film defects on mechanical properties of as-cast C95800 alloy, Acta Metallurgica Sinica (English Letters), Vol. 30, No. 6, pp. 541–549, 2017.

[7] J. Mi, R. A. Harding, J. Campbell: Effects of the entrained surface film on the reliability of castings, Metallurgical and Materials Transactions A, vol. 35, No 9 pp. 2893–2902, 2004.

[8] ISO 6892-1, Metallic materials – Tensile testing – Part 1: Methid of a test at room temperature, 2019.

Society of Production Engineering

ICPES 2025

40th INTERNATIONAL CONFERENCE ON PRODUCTION ENGINEERING - SERBIA 2025

DOI: 10.46793/ICPES25.158M

University of Nis Faculty of Mechanical Engineering

Nis, Serbia, 18 - 19th September 2025

ANALYSIS OF THE PREFORMING STAGE IN THE CLOSED-DIE HOT FORGING PROCESS

Mihajlo MILOJKOVIĆ[1]*, Saša S. RANĐELOVIĆ[1]

Orcid: 0000-0002-2334-8929

[1]Faculty of Mechanical Engineering, University of Niš, Serbia

*Corresponding author: mihajlomilojkovicwp.4@gmail.com

Abstract: *Closed die hot forging is the most frequently used forging method for industrial manufacturing of complex parts. When it comes to complex parts, an optimised preforming stage is crucial to achieve for precise finished products. Because it is consisted of multiple sequences, there is significant room for enhancement and innovation in industry settings. This article goes through multiple advanced ideas and papers that tackle this problem and analyses their further implementation in conventional settings. Additionally, it examines the optimisation of preforming on an industry case study with a specific product and reviews the future scope of implementing new-age methods for easier and precise optimisation.*

Keywords: *Closed-die hot forging, preforming, billet, optimisation, industrial case study, experimental study, multi-stage hot forging.*

1. INTRODUCTION

Forging refers to the method by which metal undergoes plastic deformation through the application of heat and pressure. The process can be performed at various temperatures, leading to different types of forging: cold, warm and hot forging. For future referencing, in this article the main type of forging that will be discussed is hot forging. Hot forging includes shaping metal at raised temperatures, usually between 700°C and 1,200°C. The metal is heated to provide flexibility and make it more pliable. Components produced through the forging process, referred to as "forgings," exhibit enhanced structural integrity, impact strength, fracture toughness, fatigue endurance and uniformity, with very high dimensional accuracy. The significant versatility of this process is evident in its ability to produce forgings from a wide range of metal materials, including steel, aluminium, titanium, and various alloys, in nearly any size and shape. A forging process is considered successful when the die cavity is entirely filled and the stress within the workpiece remains below the ultimate stress associated with the material of the workpiece, all while utilising the least amount of force. Finite Element (FE) simulations are frequently used in the design of forging sequences, as they serve as an excellent resource for identifying and evaluating quality parameters such as form filling, folds, forming forces, and temperature profiles. Complex geometries in forgings are

created through multi-stage processes. In these instances, it is crucial to identify the optimal design for the multi-stage process that minimises the number of forging steps.

1.1. CLOSED-DIE FORGING

In closed die forging, often referred to as impression die forging, the die exerts pressure on the material via the interface, leading to the formation of a cavity shaped component. A standard configuration of closed die forging is illustrated in Figure 1.

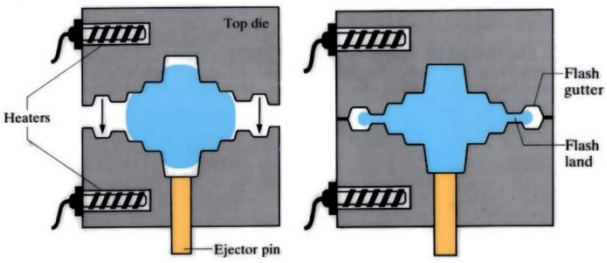

Figure 1. Schematic arrangement of the closed die hot forging process

The parameters for input and output, as well as their interconnections, must be examined in relation to their impact on product quality to enhance process efficiency.

1.2. Multi-stage CDHF

Practical industrial forging typically includes several stages. The quantity of these stages is determined by the complexity of the geometry, the characteristics of the metal flow and the desired precision of the component. These stages can be divided into three main categories that differ in design and complexity, but all play an important role in the process's success and the quality of the final product.

- Upsetting
- Preforming
- Finishing

These stages can consist of multiple sequences. A categorized view of a full forging cycle including these stages is displayed in Figure 2 [1].

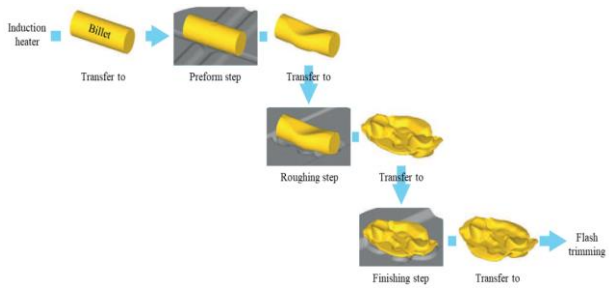

Figure 2. Forming stages in the hot forging process

2. OPTIMISATION METHODS

As previously mentioned, the upsetting and preforming steps in CDHF are crucial for achieving and maximising the efficiency of total die coverage during forging. The upsetting is typically planned and developed by forging engineers, relying primarily on their experience and iterative trial-and-error design process. In industrial practice, once engineers receive the necessary product documentation, the design process begins with drafting the billet's shape and dimensions in relation to the final product, taking into account its overall geometry, volume, and mass. Next in line is a series of tests to see if some changes to the initial values of the billet improve the process parameters and optimise it. Finally, the definitive billet parameters are adopted and the process goes into its ensuing stages. Some articles tackle this initial process with the help of optimising software and FEM analysis and will be discussed in the upcoming subsections.

2.1. Different billet optimisation methods

Mangshetty et al. [2] applied FEM in ANSYS, coupled with optimisation algorithms, to analyse how billet height-to-diameter ratios affect metal flow, strain distribution, and die loading in aluminium MMCs. Their results showed that optimised ratios could reduce forging loads by nearly 10 kN, however the framework was limited to a 2D simulation with simplified frictional and thermal conditions, excluding aspects such as die life or multi-stage sequences. Soranansri et al. [1]

extended billet optimisation into a full process design by combining billet geometry selection with hot forging die design and experimental validation for biomedical prostheses. Their study confirmed that billet geometry of Ø36 × 99 mm improved material utilisation by over 260% and ensured defect-free die filling, with the mass ratio factor identified as a key sizing parameter, although the work was restricted to AISI 316L and did not assess scalability or die wear. Han et al. [3] introduced a data-driven methodology by generating NURBS-based preform geometries and training CNNs on FEM-derived microstructural data, achieving up to 19.64% grain size refinement and 40% load reduction in IN718 forging. Despite these advances, the approach relied on computationally expensive datasets, image-based CNN training with limited interpretability, and validation only on a single superalloy. Collectively, these works demonstrate that billet optimisation through FEM, experimental validation, and machine learning can improve forging efficiency and accuracy, but they remain highly material-specific and computationally demanding, limiting their broader industrial implementation.

2.2. Preforming optimisation

Claus et al. [4] proposed an automated forging sequence design method integrating ANN-based shape classification, a complexity scoring model, fuzzy logic for stage determination, and a point-shift algorithm to generate preforms directly from STL geometries. FEM simulations verified that the approach could provide viable forging sequences with satisfactory filling in under one hour, but the outputs were only approximate, misclassifications occurred, and crucial geometric features like draft angles and fillets were excluded. Aybar et al. [5] analysed four forging process routes for a torque rod housing using FEM and experimental validation, demonstrating that preforming stages (including upsetting and shaft crushing) were essential to achieve full die filling, minimise burr formation, and halve die stresses compared to single-step forging. However, their reliance on conventional volumetric distribution graphs restricted the designs sophistication and applicability. Huang et al. [6] conducted a multi-objective optimisation of preforming dies for I-shaped forgings with DEFORM-2D, comparing linear and arc-shaped transitions between web and wing. They found that a linear angle of 53.5° and arc radius of 66 mm reduced loads by up to 76% and improved wear distribution, although the use of 2D models and simplified design variables limited industrial use. Movrin et al. [7] applied the finite volume method to optimise wheel hubs and sockets, testing process variants to balance die filling, contact pressure, and stage reduction. Their optimised approach achieved pressures below 1100 MPa and defect-free production trials, although the simulations used simple friction and heat transfer assumptions and overlooked long-term tool fatigue. Taken together, these studies illustrate how AI-based automation, FE modelling, and experimental validation converge to show that preforming remains very important for reducing forging loads, ensuring material flow, and extending die life. However, for robust industrial adoption, progress is required in realistic thermo-mechanical modelling and wider material coverage.

3. INDUSTRY CASE STUDY

This paper has, to this point, presented the basics of forging and intricacies of closed die hot forging. A number of articles were covered that show the importance of billet shape/dimension and preforming design optimisation. The integral nature of preforming in a multi-stage process will be presented with a industrial case study. The study is based on the forging process optimisation of a drawhook that is used in the railway industry. The hook is made in the ˝Ming˝ production plant [8], which is

specialised in machining and forging. In Figure 3 the hooks dimensions are presented.

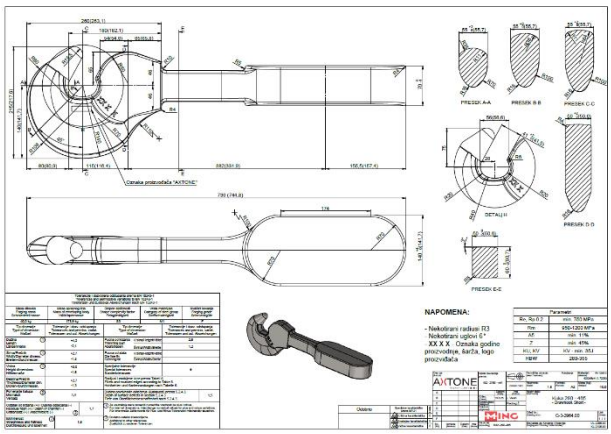

Figure 3. Drawhook technical drawing

From the shape of the hook it can be assumed that the preforming stage will be complex, because optimal mass redistribution cannot be achieved with one step of preforming. The mass of the hook is 41kg. In an industrial setting the flow of the whole forging process is mainly dictated by engineering experience and trial by error design. Firstly, the mass of the finished product is increased by 20% - an optimal initial increase that accounts for the mass that is lost in the flash of the forging and also in the trimming process after forging. This percentual increase is obtained through experience. By analysing the shape of the hook it is determined that the optimal shape of the billet is cylindrical. From the dimensions of the hook, the presumed length of the cylindrical billet is 505 mm and it will later be tested and optimised. In corelation to the length, the presumed diameter of the billet is 110 mm. After establishing the initial dimensions of the billet, initial testing of the billet is required to examine if it meets dimensional requirements.

The FEM analysis is done in the FORGE programme developed by Transvalor. The initial idea is that for this forging process two preforming steps are required with one finishing step. Preforming is conducted using a basic upsetting die on different parts of the cylinder. The first step of preforming is presented in Figure 4.

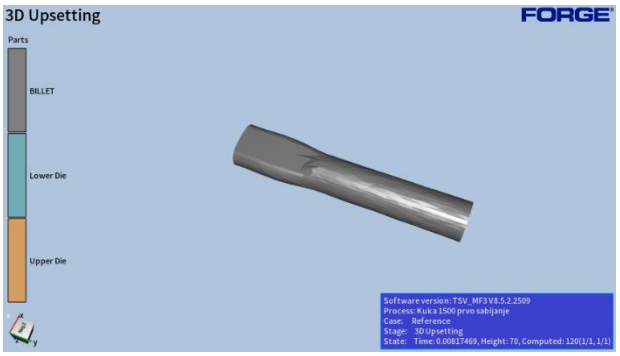

Figure 4. The first step of preforming – free upsetting on one end of the cylinder

The next step of preforming is done in a similar fashion to the first, but in a different plane to secure the complex geometry and shape on opposite ends of the hook. The second preforming step is provided on Figure 5.

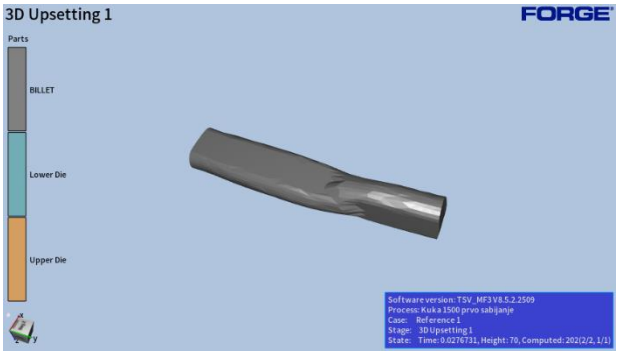

Figure 5. Second preforming step – flattening of the cylinder in a different plane

The finishing step of forming is done in a specially designed die made using a numerical mill. Bottom and top dies are presented in Fig. 6 and 7.

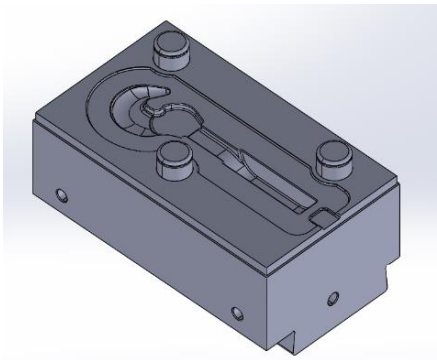

Figure 6. Bottom die design in SolidWorks

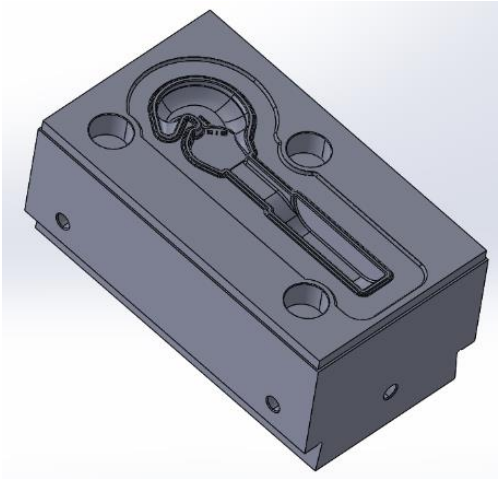

Figure 7. Top die design in SolidWorks

After the simulation of the finishing step, it is concluded that the die filling is not optimal. Finishing geometry is not ensured because the mass redistribution is not properly achieved in the preforming stage. Because of the underfill, the rounded edges are not made and also there are surface impurities. The finished part after the finishing stage is shown in Figure 8.

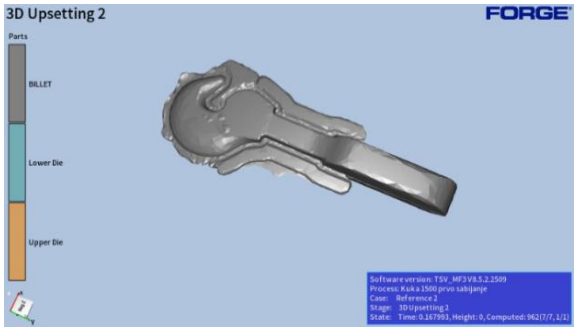

Figure 8. Finished part after the finishing step

Even though the forging is not optimal, the process is verified in industrial conditions to determine validity of the FEM simulation and results. Simulation results and results of the industrial trial is compatible. Compatibility insures that, after the process is optimised in the simulator, changes are applicable in real life.

The first changes to the process are started with the billet. The length is shortened to 490 mm and the diameter is increased to 120 mm. This change is determined by engineering experience. Preforming is more complex, with 5 preforming steps to ensure the most optimal mass redistribution and later on metal flow. Preforming is also done by free upsetting different areas of the cylindrical billet. This change in the number of steps is based on trial and error and by watching different parts of the hook in different planes. The optimised version of preforming is shown in Figure 9.

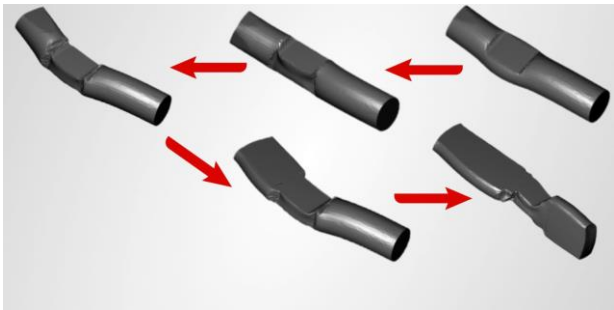

Figure 9. The five steps of preforming

From the pictures of the optimised preforming stage, it can be determined that the new preform more closely resembles the finished part, so the final dimensions and tolerances are easily made in the finishing step. The first preforming concept is more simple and was the first trial because it is more economically justified, but because the process is not optimal the second preforming version is the only applicable version. The finishing step is presented in Figure 10.

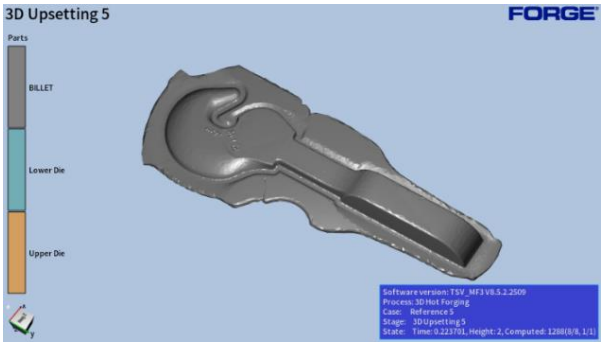

Figure 10. The finishing step of forging

When the finishing stages of the two concepts are compared, there is a major difference in flash formation, the dimensional tolerances are justified and rounded edges and angles are obtained.

The final process parameters are:

- Temperature of 200 °C on the bottom and top dies
- Force of the die is 160 kJ
- Including preforming and finishing stages – 10 steps of the process

- Temperature of the billet is 1050 °C
- Material of the billet is 42CrMo4

After the forging process, the forged hook is trimmed and the flash is removed. In industrial settings, problems that are being faced in forging products are resolved mostly like the sequence that was presented here. Because of the volume of demand for forged parts at industrial plants like ,,Ming˝, this is still the main way and frequently the most effective way of tackling these problems.

4. CONCLUSION

Using the industry case study as an overview of the workflow that is usually applied in industrial settings, it can be concluded that there is much room for optimisation. Some of the presented algorithms and neural networks/machine learning ideas for optimisation can be utilised and implemented on the industrial level, making the trial and error method and optimisation based on experience obsolete. The sheer volume of production at plants complicates the implementation of these ideas and methods, but these ideas are the future of optimised and efficient forging. Plants that have big databases of production parts, faced problems and their solutions are the perfect starting place for developing and broadening these algorithms/networks. Future work will focus on implementing these ideas in a product of industrial plants.

ACKNOWLEDGEMENT

I would like to express my sincere gratitude to Prof. dr Saša Ranđelović, whose guidance and expertise were invaluable throughout this study. I am also grateful to ,"MING" production plant for providing the access and facilities necessary for this work.

REFERENCES

[1] P. Soranansri, T. Rojhirunsakool, T. Nithipratheep, C. Ngaouwnthong, K. Boonpradit, C. Treevisootand, W. Srithong, P. Chuchuay, K. Sirivedin: *Hot Forging Process Design and Initial Billet Size Optimization for Manufacturing of the Talar Body Prosthesis by Finite Element Modeling*, Applied Science and Engineering Progress, Volume 15, 2021.

[2] S. Mangshetty, S. Balgar: *Billet shape optimization for minimum forging load using FEM analysis*, International Journal of Engineering Research and Development, Volume 3, Issue 3 (August 2012), PP. 11-16.

[3] B. Han, K. Kim, J. Park, S. Hwang, J. Kim, N. Kim: *Preform design to reduce forging load and grain size simultaneously in disk forging of IN718*, Journal of Materials Research and Technology 31, pp. 1644–1654, 2024.

[4] Y. Hedicke-Claus, M. Kriwall, M. Stonis, B.A. Behrens: *Automated design of multi-stage forging sequences for die forging*, Production Engineering, Vol. 17, pp. 689–701, 2023.

[5] E. Aybar, I. Kılınç: *The Effect of Pre-Forming on The Forged Part in the Hot Forging Process*, in: 3rd International Conference on Design, Research and Development, 13-15.12.2023, Istanbul, Turkey, pp. 264-275

[6] L. Huang, Q. Zhong: *Analysis and optimal design of forging preforming for I shaped forgings*, Journal of Physics: Conference Series 2842, 2024.

[7] D. Movrin, M. Plančak, D. Vilotić, M. Milutinović, P. Skakun, O. Lužanin, I. Trbojević: *Optimisation and design of multistage hot forging processes by numerical simulation and experimental verification*, Journal for Technology of Plasticity, Vol. 35, 2010.

[8] MING doo – Company for Manufacturing, Engineering, Forging, and Machining, https://mingbgd.co

Session 3:

Materials and surface engineering and tribology

Society of Production Engineering

ICPES 2025

40th INTERNATIONAL CONFERENCE ON PRODUCTION ENGINEERING - SERBIA 2025

DOI: 10.46793/ICPES25.165P

University of Nis Faculty of Mechanical Engineering

Nis, Serbia, 18 - 19th September 2025

EFFECT OF THE MAXIMUM TEMPERATURE ON THE HARDNESS AT THE HEAT AFFECTED ZONE OF THREE DIFFERENT CARBON STEELS AFTER A SLOW COOLING

Nima POURSALIMI[1], Juan Carlos FERRERO-TABERNER[1], Lorenzo SOLANO-GARCÍA[*2], Norberto FEITO-SÁNCHEZ[3], Miguel Ángel PÉREZ-PUIG[4], Fidel SALAS-VICENTE[4]

Orcid: 0009-0008-8339-5015; **Orcid:** …;**Orcid:** 0000-0003-0535-314X
Orcid: 0000-0001-7330-6404; **Orcid:** 0000-0001-9343-9888; **Orcid:** 0000-0003-0834-4425

[1]Universitat Politècnica de València, Spain
[2]Institute of Design and Manufacturing, Universitat Politècnica de València, Spain
[3]Institute of Mechanical and Biomechanical Engineering-I2MB, Universitat Politècnica de València, Spain
[4]Institute of Materials Technology, Universitat Politècnica de València, Spain
*Coresponding author: lsolano@mcm.upv.es

Abstract: *The welding of carbon steels causes microstructural changes at the heat affected zone that modify the behaviour of the material during its in-service life. Usually these changes are associated with an increase in the hardness and a loss of tenacity that, despite being within an acceptable range, should be considered and predicted when the weld is part of a highly demanding application. Unfortunately, the common Continuous Cooling Transformation (CCT) diagrams employed for heat treatments are not always a reliable data source as the heat cycle in welding is different from that of a quench, with higher temperatures and no soaking time. This implies that hardness at the heat affected zone (HAZ) will not depend only on the cooling rate but also on the heating rate and the maximum temperature at each point of the HAZ, parameters that control the transformation of perlite to austenite and the homogenization of austenite.*

This paper studies the effect of the maximum temperature at each point of the HAZ on the hardness of three different steels (S355, C45 and S700MC) when a relatively slow cooling rate is assured. This has been done by heating different samples inside a furnace till the selected maximum temperatures are reached and immediately cooling them under an air flow. The results show that once a certain temperature is reached, a transition from low to high hardness takes place. This transition is related to grain coarsening and the end of the austenization process, although, when compared to an oil quench, other changes like the apparition of Widmanstätten microstructures are also present.

Keywords: *Welding, steel, heat affected zone, hardening, overheating, CCT diagram, Widmanstätten.*

1. INTRODUCTION

In welding, the heat affected zone (HAZ) is the part of the base material that does not melt but whose microstructure changes as a result of being subjected to a thermal cycle. Each point of the HAZ, that surrounds the weld bead, experiments a different thermal cycle

depending on the distance to the fusion line, where the material reaches the melting point. The closer to the fusion line, the higher the peak temperature reached by the material, the more intense the thermal cycle and, as a consequence, the greater the changes in the microstructure.

This gradual variation of the microstructure of the HAZ from the fusion line to the unaltered base metal is associated with a corresponding variation of properties. Actually, in carbon steels, those variations are not exactly gradual, as a quantitative leap is observed when the material reaches a temperature that leads to austenization. When this happens, and it's inevitable near the fusion line, the material can quench under a fast cooling and undesirable, very hard and fragile metallurgical phases can appear. The control of hardness at the HAZ is of paramount importance and one of the main control parameters that welding standards include, stablishing thresholds that must not be surpassed.

When necessary, a first prediction of the hardness a material can reach at the HAZ is possible taking into account the carbon content[1], using the equations like the Yurioka equation [2] or, still better, the common continuous cooling transformation (CCT) diagrams that take into account the cooling rate. Unfortunately, CCT diagrams are build for a thermal cycle where a low austenization temperature is reached and maintained for a certain period of time until complete austenization is achieved.

The welding thermal cycles differ from the ones associated with the CCT diagrams as there is no soaking time and higher temperatures are reached. The absence of a soaking time means time must be compensated with higher temperatures and that complete austenization is not achieved at the expected temperature[3],[4]. Furthermore, the total heat input to the material also depends on the heating rate. On the other hand, the high peak temperatures reached at some point of the HAZ imply a severe grain coarsening and a change in the behaviour of the material during cooling, including the possible apparition of Widmanstätten microstructures [5].

Although the effects the heating rate and peak temperature has been taken into account for multiple steels in [4], the data is only available for cooling rates over the critical one and, thus, not applicable to welding.

This lack of means to predict the exact nature of the microstructure at the HAZ after welding is usually not so important, but for high demanding applications, knowing the exact properties of the weld can be necessary. This is also important for finite elements simulations, as the mechanical behaviour of the material is not that of the original base metal.

This paper presents the results of a research designed to reproduce the thermal cycles at the HAZ at different distances to the fusion line on three different carbon steels to study the effect of the peak temperature on the hardness of the material.

2. MATERIALS AND METHODS

2.1. Materials

In order to study the influence of the peak temperature at different points of the HAZ on the hardness of welded carbon steels, three different steels were selected: S355, C45 and S700MC. All of them were available in plates of 3 mm thickness

S355 (EN 10025-2) is a mild structural steel commonly used in construction and engineering thanks to its good weldability and machinability. Due to its low carbon content, no hard structures are expected at the HAZ after welding under usual welding conditions. Its composition and mechanical properties can be seen in tables 1 and 2.

Table 1. Percentages (%) of main alloy elements for S355 steel

C	Si	Mn	Cu	C_{eq}
0.078	0.4	1.0	0.3	0.39

Table 2. Properties of the S355 steel plate

σ_u (MPa)	σ_Y (MPa)	A_L (%)	Hardness(HV)

560	452	29	180

C45 steel (EN 683-1) is a medium carbon steel usually selected for the manufacturing of shafts and other mechanical parts thanks to its good toughness, strength and wear resistance. C45 steel has a low weldability due to its high carbon content. So, preheating, an hydrogen back out treatment or a post-weld heat treatment is more than advisable. Its composition and mechanical properties can be seen in tables 3 and 4.

Table 3. Percentages (%) of main alloy elements for C45 steel

C	Si	Mn
0.478	0.24	0.79

Table 4. Properties of the C45 steel plate (as receibed)

σ_u (MPa)	σ_Y (MPa)	A_L (%)	Hardness(HV)
792	498	19.5	201

S700MC steel (EN 10149-2) is a structural high-strength low-alloy (HSLA) steel whose properties are mainly based on its small grain size thanks to a thermomechanical treatment. This steel has good weldability due to its low carbon content, but the heat input leads to a loss of properties at the HAZ due to grain coarsening. Tables 5 and 6 show its composition and mechanical properties.

Table 5. Percentages (%) of main alloy elements for S700MC steel

C	Mn	Si	Cr	Nb	V	Ti
0.06	1.86	0.026	0.03	0.07	0.0055	0.124

Table 6. Properties of the S700MC steel plate

σ_u (MPa)	σ_Y (MPa)	A_L (%)	Hardness (HV)
792	740	18.5	302

2.2. Samples preparation

For each steel, a pack of 10 mm width samples was cut from plates of 3 mm thickness. A hole of 0,9 mm diameter was drilled on each of the samples to insert the edge of a thermocouple.

These samples were heated to different peak temperatures, from 850 to 1250 °C, inside a furnace set at 50 °C over the peak temperature. The achieved heating rate was slower than the heating rate of the material during welding, but allowed the extraction of the samples from inside the furnace at the desired temperature. A higher heating rate would have been too fast to accurately determine the moment of extraction and manually remove the samples.

Once outside the furnace, the samples were inmediately cooled under air flow with the aid of two air blowers at a distance of 25 cm.

Once cold, a piece of the sample near the thermocouple hole was cut and prepared for metallography and hardness measurement.

2.3. Metallography preparation and hardness meaurement

After cut, a small piece of each treated samples was grinded using silicon carbide grinding paper, grit #220 and #500, and polished with 3 micron diamond paste. Subsequently, the samples where etched using Nital-3 (3% nitric acid in ethanol) during 6 to 10 seconds.

Hardness measurements were done using a load of 0.5 kg in a Innovatest 400 Vickers microhardness meter. 5 measurements were taken for each sample. The dimensions of the footprints were measured using the ImageJ software.

3. RESULTS

Figure 1 shows the heating curves of one sample compared with the measured heating curve of an actual welding process. As commented above, the heating rate inside the furnace was a lot lower, but it's impossible to manually accurately stop the heating process

with a heating rate over 150 °C/s, which is the real one.

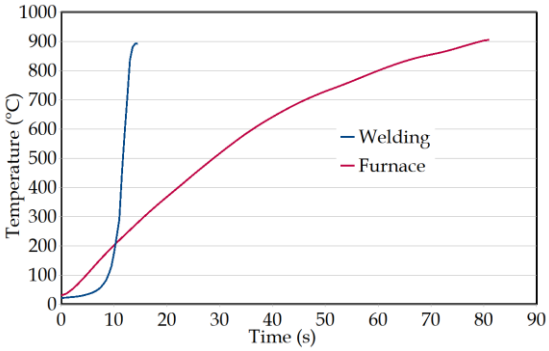

Figure 1. Heating rates in a real weld and inside a furnace

Although this represents an important difference between the two heating processes[4], in practice it only means the microstructure obtained at the furnace will correspond to a point slightly nearer to the fusion line than expected due to the greater heat input.

Regarding the cooling rate, figure **2** shows how it was more accurately reproduced.

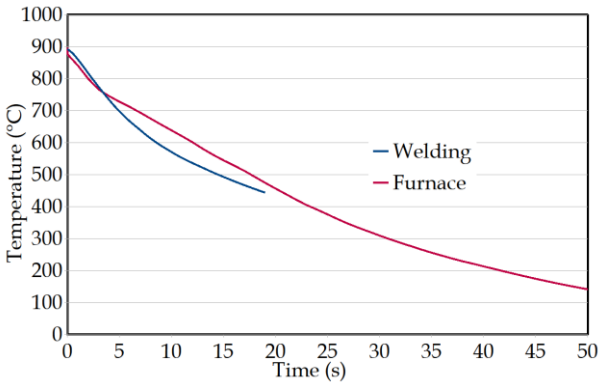

Figure 2. Cooling rates in a real weld and inside a furnace

The evolution of hardness with the peak temperature for S355 steel is presented in figure 3. As can be seen, hardness is always low regardless of the peak temperature, as expected due to the low carbon content of this steel.

Nevertheless, while for low peak temperatures there is a softening of the material when a peak temperature of 1100 °C is reached, hardness experiments a sudden increase from 160 to more than 200 HV. This change can be associated with the overheating of the sample, that leads to grain coarsening and the apparition of Widmanstätten ferrite, as can be seen in figure 4.

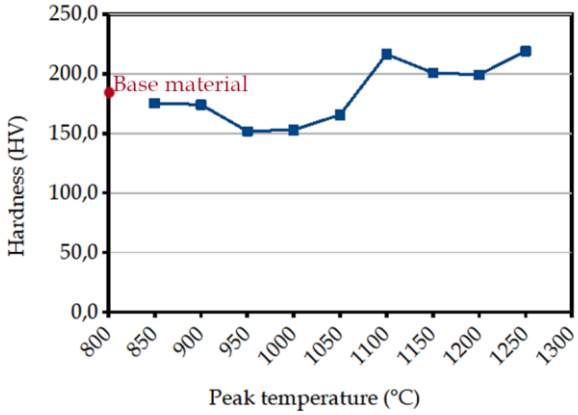

Figure 3. Relationship between hardness and peak temperature for S355 steel

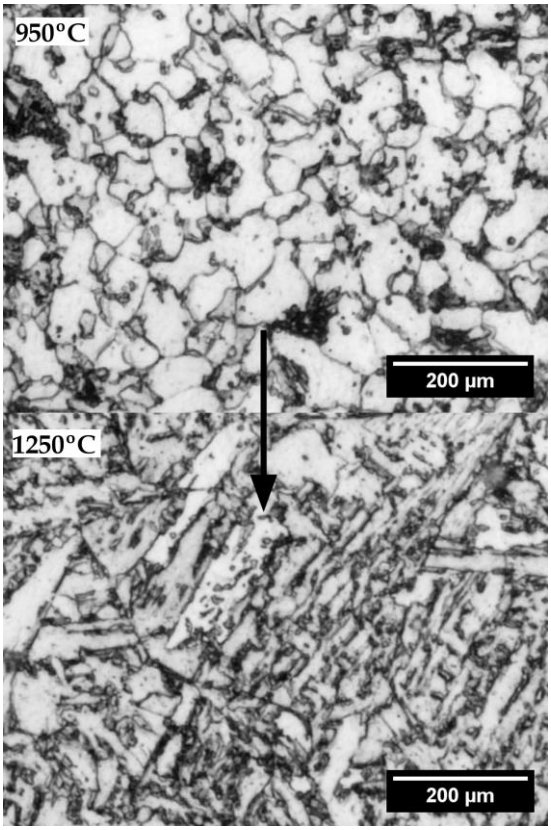

Figure 4. Microstructure of S355 steel when heated to low and high austenizing temperatures.

C45 steel hardness (figure **5**) shows a more marked transition that begins at a peak temperature of 1000 °C and is associated with the apparition of martensite once the complete (or almost) austenization is achieved.

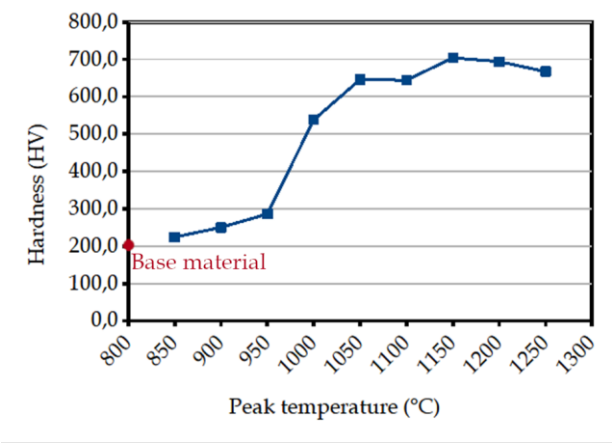

Figure 5. Relationship between hardness and peak temperature for C45 steel

This hardness increment can't be predicted by the CCT diagram of the steel, that predicts mainly fine pearlite and bainite for the used cooling rate, but is somehow expected because a higher peak temperature leads to a displacement of the CCT curves to the right [8], [9] and to a higher level of austenization. Also, this seems to shift the martensite start temperature to higher values [6], [7], all favouring harder microstructures.

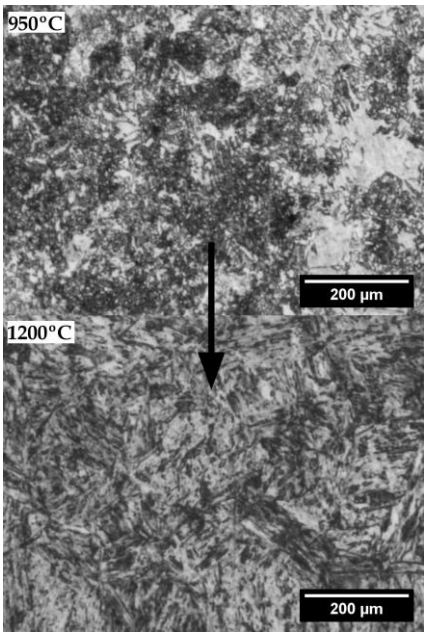

Figure 6. Microstructure of C45 steel when heated to low and high austenizing temperatures.

The change in the microstructure can be seen in figure 6. At 950 °C some martensite is present (white area). Its quantity rises as the peak temperature increases until all the microstruc ture is martensitic, except for a very small percentage of allotriomorphic and Widmanstätten ferrite not visible in the figure.

Figure 7 shows the hardness of the samples of the S700MC steel. As this steel obtains its high mechanical properties from its fine grain, the grain growth associated with the heat input leads to recrystallization, grain growth and a hardness decrease in all the tested samples with respect to the initial state of the samples.

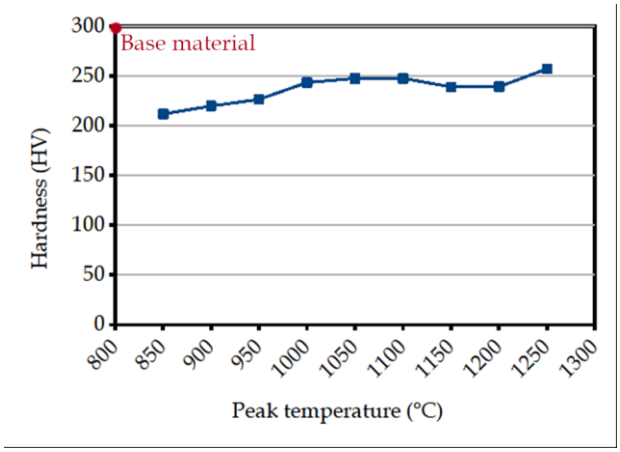

Figure 7. Relationship between hardness and peak temperature for S700MC steel

In this case the graph shows a slow but constant hardness increment as the peak temperature is increased, without a detectable abrupt leap at a concrete temperature. This evolution is similar to the one found after 1 hour annealings at different temperatures [10]. In contrast, there is a notable change in the microstructure (see figure **8**) when the peak temperature reaches 1200 °C. just at that temperature the microstructure changes from small equiaxial grains to more irregular bainitic-ferritic coarse grains with Widmanstätten shape.

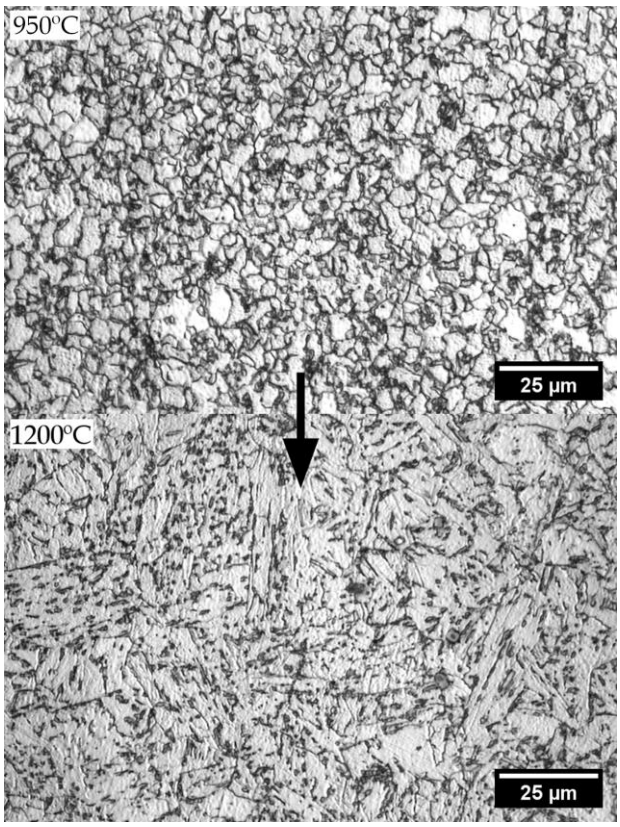

Figure 8. Microstructure of S700MC steel when heated to low and high austenizing temperatures.

4. CONCLUSION

All three tested steels have shown an increase in hardness as the peak temperature increases that is impossible to predict looking at the CCT diagrams of the steels. This confirms the difficulties of predicting the microstructure and properties of the HAZ in a welded joint with data from common heat treatments.

In the two common carbon steels, S355 and C45, hardness experiments a fast growth once a threshold temperature is reached. This transition is associated with grain growth and a change in the microstructure transformation during cooling to Widmanstätten ferrite in the first case and to martensite in the second.

The thermomechanical S700MC steel shows a small gradual rise in hardness with the peak temperature. Although in this case hardness does not experiment sudden leap, there is a sudden change from a fine to a coarse microstructure between 1150 and 1200 °C.

ACKNOWLEDGEMENT

The authors are grateful for the financial support provided by the Conselleria de Educación, Universidades y Empleo of the Generalitat Valenciana through the “Programa para la promoción de la investigación científica, el desarrollo tecnológico y la innovación en la Comunitat Valenciana” (CIGE/2023/153).

REFERENCES

[1] J. L. lamont W. Crafts, *Hardenability and steel selection*. 1949.

[2] N. Yurioka, “Prediction of HAZ hardness of transformable steels,” *Met. Constr.*, no. 217, 1987.

[3] Q. Yuan *et al.*, “Effects of rapid heating on the phase transformation and grain refinement of a low-carbon mciroalloyed steel,” *J. Mater. Res. Technol.*, vol. 23, pp. 3756–3771, Mar. 2023, doi: 10.1016/j.jmrt.2023.02.018.

[4] A. Rose, *Atlas der Wärmebehandlung der Stähle*. Düsseldorf, 1961.

[5] D. Séférian, *The metallurgy of welding*. New York, 1962.

[6] C. Celada-Casero, J. Sietsma, and M. J. Santofimia, “The role of the austenite grain size in the martensitic transformation in low carbon steels,” *Mater. Des.*, vol. 167, p. 107625, Apr. 2019, doi: 10.1016/j.matdes.2019.107625.

[7] S.-J. Lee and K.-S. Park, “Prediction of Martensite Start Temperature in Alloy Steels with Different Grain Sizes,” *Metall. Mater. Trans. A*, vol. 44, no. 8, pp. 3423–3427, Aug. 2013, doi: 10.1007/s11661-013-1798-4.

[8] A. Matsuzaki and H. K. D. H. Bhadeshia, “Effect of austenite grain size and bainite morphology on overall kinetics of bainite transformation in steels,” *Mater. Sci. Technol.*, vol. 15, no. 5, pp. 518–522, May 1999, doi: 10.1179/026708399101506210.

[9] Z. Babasafari *et al.*, “Effects of austenizing temperature, cooling rate and isothermal temperature on overall phase transformation characteristics in high carbon steel,” *J. Mater. Res. Technol.*, vol. 9, no. 6, pp. 15286–15297, Nov. 2020, doi: 10.1016/j.jmrt.2020.10.071.

[10] G. J., "Effect of heat treatments on the mechanical properties of thermomechanically treated steel," *Mach. Technol. Mater.*, no. 12, 2013.

Society of Production Engineering

ICPES 2025

40th INTERNATIONAL CONFERENCE ON PRODUCTION ENGINEERING - SERBIA 2025

DOI: 10.46793/ICPES25.172B

University of Nis Faculty of Mechanical Engineering

Nis, Serbia, 18 - 19th September 2025

NANOCORROSION EFFECT ON NITI ARCHWIRE EXPOSED TO VARIOUS MOUTHWASHES

Zoran BOBIĆ[1*], Lazar KOVAČEVIĆ[1], Vladimir TEREK[1], Marko ZAGORIČNIK[1], Sanja KOJIĆ[1], Goran STOJANOVIĆ[1], Bojan PETROVIĆ[2], Pal TEREK[1]

Orcid:0000-0002-0843-4984; **Orcid:**0000-0002-4087-4373; **Orcid:**0000-0002-4764-3172; **Orcid:** 0000-0002-4092-9733; **Orcid:** 0000-0003-2098-189X; **Orcid:** 0000-0002-3575-3921; **Orcid:** 0000-0001-9994-6039;

[1]University of Novi Sad, Faculty of Technical Sciences, Novi Sad, Serbia

[2]University of Novi Sad, Faculty of Medicine, Novi Sad, Serbia

* Corresponding author: zoranbobic@uns.ac.rs

Abstract: *Nitinol is widely used for orthodontic archwires due to its favourable mechanical properties and corrosion resistance. To maintain oral hygiene and prevent dental plaque, orthodontic patients are advised to use commercially available mouthwashes, many of which contain chlorine- or fluorine-based compounds. These compounds can interact with the surface oxide layer of NiTi alloy, potentially leading to its degradation and the release of toxic nickel ions into the surrounding biological environment. The detrimental effects of chlorine- and fluorine-containing media on NiTi are well-known. However, due to the typically low intensity of the corrosion processes, the characterization of surface corrosion effects in such environments remains a great challenge. In this study, non-electrochemical corrosion tests were conducted on NiTi archwires exposed to artificial saliva and several commercially available mouthwashes to quantify nanometric changes in surface topography. Corrosion effects were evaluated using atomic force microscopy (AFM) in contact mode, with measurements taken at predefined surface locations before and after the corrosion tests. The topographical changes were evaluated using surface roughness parameters: Sa, Ssk, Sdr, and S10z. The analysis revealed that mouthwashes containing chlorine compounds resulted in both material loss and gain on the surface, while fluorine-based mouthwashes caused only material loss. In contrast, samples exposed to artificial saliva exhibited no significant topographical changes. The analytical approach developed in this study proves effective for identifying and distinguishing types of nanoscale surface alterations associated with corrosion. The observed material gain in chlorine-containing mouthwashes is likely due to surface reoxidation, a phenomenon not present in fluorine-containing solutions.*

Keywords: *NiTi, Corrosion, Mouthwashes, Artificial Saliva, AFM, Nano topography*

1. INTRODUCTION

Nickel–titanium (NiTi) alloy is a biomaterial widely used in dental orthodontic applications. During orthodontic treatment, practitioners often recommend that patients use various mouthwashes to prevent caries and protect dental enamel [1]. As a result, NiTi wires are exposed to different oral environments that may lead to corrosion and the release of metal ions into the body. The release of these ions can have adverse biological effects, depending on the ion species and their concentrations [2].

Corrosion resistance is a critical property of biomaterials, as it directly influences their biocompatibility. It has been shown that nickel ion release, caused by corrosion processes, can lead to allergenicity, toxicity, and even carcinogenicity [1,2]

Evaluating the corrosion behavior of NiTi alloys under conditions similar to those in the human oral cavity remains a significant characterization challenge. Many studies [3–6] avoid the complexities of characterizing nanostructures and nanoscale surface changes by employing accelerated corrosion tests. However, such tests do not accurately replicate real clinical conditions.

Therefore, the aim of this work was to perform non-accelerated corrosion tests on NiTi wires in various corrosive media and to characterize and quantify the resulting topographical changes. To achieve this, atomic force microscopy (AFM) measurements were conducted before and after the corrosion tests.

2. EXPERIMENTAL

The corrosion performance of NiTi orthodontic wires (Dentaurum, Germany) was evaluated in this study. Four prismatic specimens were prepared from the as-received wire. Prior to the corrosion tests, six scan locations were marked on each specimen. To facilitate the relocation of the same areas after corrosion testing, the scan sites were identified by making small scratches on the specimen surface. Returning to the same locations after testing allows for the characterization of nano-topographic changes induced by corrosion with a relatively low number of measurements. In contrast, detecting such changes through randomly selected areas would require a significantly larger number of measurements, both before and after corrosion. Each specimen was exposed to one of four selected corrosive media (artificial saliva or commercial mouthwash).

Corrosion was characterized by analyzing changes in surface topography. For this purpose, each specimen was examined at six predefined locations before and after the corrosion test using atomic force microscopy (AFM; CP-II di, Veeco). AFM measurements were conducted in contact mode using a symmetrically etched silicon nitride tip. The scanning parameters were as follows: fast scanning direction along the X-axis, scanning area of 100 × 100 µm, setpoint of 225 nN, scanning rate of 0.5 Hz, and gain of 0.5.

Table 1. Sample denotation

Sample	Corrosive medium
Sample 1	Artificial Saliva
Sample 2	Aquafresh® Mouthwash
Sample 3	Eludril® Mouthwash
Sample 4	Listerine® Mouthwash

To enable accurate repositioning of the probe after the corrosion test, a specific procedure was developed. Before and after testing, the probe was positioned relative to the specimen using a predefined probe elevation to maintain consistency in the probe/sample alignment. However, during the approach of the probe to the sample surface, deviations from the ideal path were occasionally observed. These deviations may lead to slight mismatches in scanning location before and after corrosion exposure. Therefore, the exact probe path was determined both before and after the corrosion test. Based on differences in probe trajectories and specimen height variations, probe position corrections were calculated. However, even this procedure could not guarantee precise repositioning of the probe at identical locations following corrosion exposure. To address this, 80 × 80 µm and 10 × 10 µm sub-areas were extracted from the original 100 × 100 µm scanned regions. The effects of corrosion were evaluated within these extracted areas.

Topographic image analysis was conducted using SPIP software (Image Metrology), which was used to extract the 80 × 80 µm and 10 × 10 µm regions and calculate surface roughness parameters. All quantitative parameters obtained from the AFM measurements were first subjected to a normality test (Anderson–Darling test, $p > 0.05$), followed by a paired t-

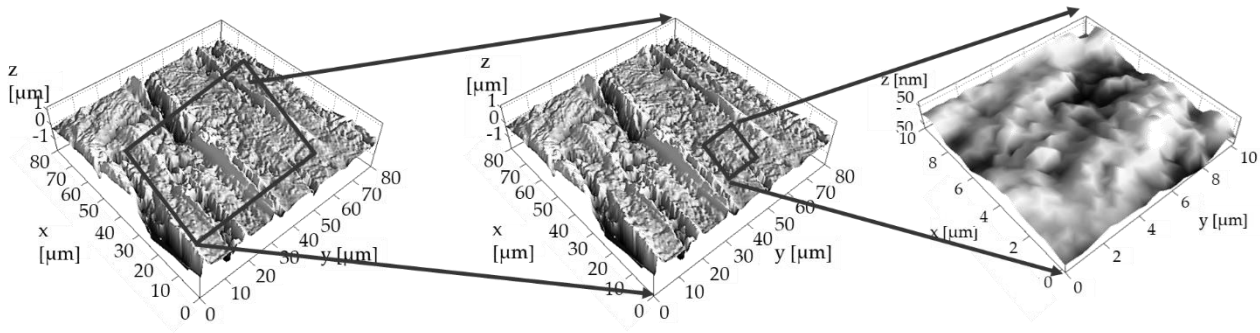

Figure 1. Characteristic surface topography image of NiTi with the marked location used for evaluating corrosion effects.

test. Statistical analyses were performed using Minitab 16 software at a significance level of 5%. test. Statistical analyses were performed using Minitab 16 software at a significance level of 5%.

3. RESULTS

Representative topography images of NiTi surface before corrosion test are presented in Figure 1. The NiTi surface exhibits characteristic parallel grooves with smooth areas between them, a pattern resulting from the manufacturing process.

Representative AFM topography images of Sample 3 before and after the corrosion test are presented in Figure 2. A comparison of these two images reveals slight nano scale changes in surface topography following the corrosion test.

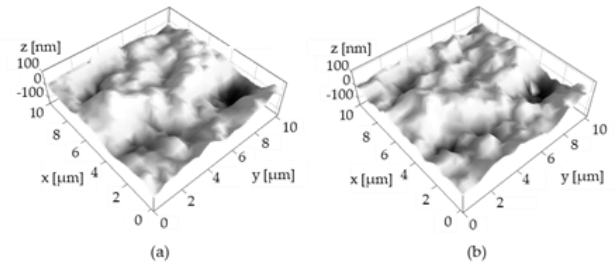

Figure 2. Representative AFM topography images of Sample 3: (a) before and (b) after the corrosion test.

Figures 3 and 4 present the calculated surface roughness parameters over a 10 µm × 10 µm area, both before and after corrosion testing. Prior to corrosion, all samples showed Sa values between 10–30 nm and S10z values ranging from 80–180 nm, indicative of a nearly polished surface state (Figure 2). Following the corrosion test, slight changes in Sa and S10z were observed, with statistically significant differences detected in Samples 2, 3, and 5.

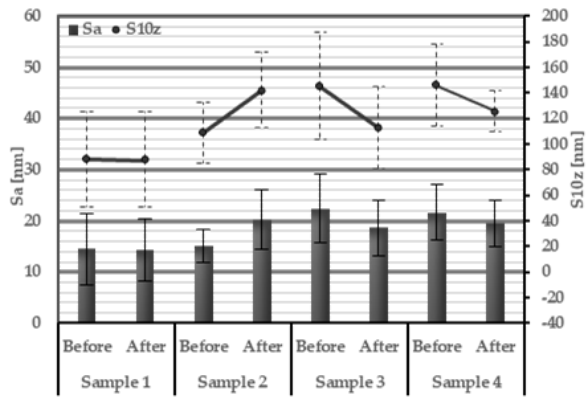

Figure 3. Surface roughness parameters Sa and S10z before and after the corrosion test.

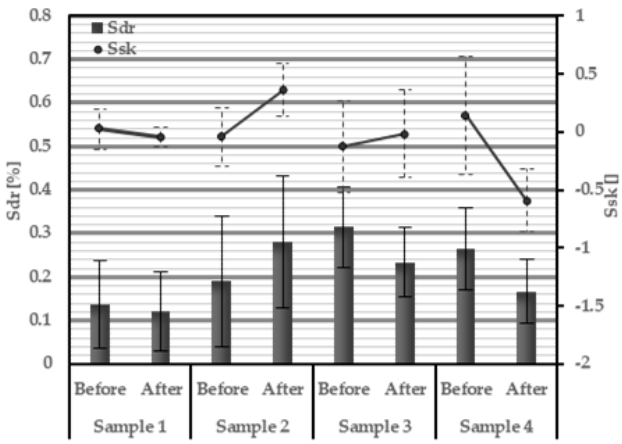

Figure 4. Surface roughness parameters Sdr and Ssk before and after corrosion test

Figure 3 shows the results for the Sdr and Ssk parameters. Before corrosion, the Ssk values were low, indicating a uniform surface without prominent protrusions or grooves. Similarly, the Sdr values were close to zero, reflecting a relatively flat surface with minimal deviation

from an ideal smooth profile, i.e., minimal surface protrusions or pits. After corrosion testing, changes in both Ssk and Sdr were observed. These changes were statistically significant for Sample 2 and 4 with respect to the Ssk parameter, and for Samples 2, 3, and 4 with respect to the Sdr parameter.

4. DISCUSSION

The changes observed in surface topography over 10 × 10 µm areas for samples treated with mouthwashes (Samples 2, 3, and 4) indicate that the corrosion processes induced nanoscale alterations. These findings confirm that the corrosion effects were of very low intensity and could only be statistically discerned in regions with low initial surface roughness. In this study, such regions were identified exclusively within surface segments of 10 × 10 µm.

The results of statistical analysis revealed that samples exposed to the investigated mouthwashes (Samples 2, 3, and 4) exhibited statistically significant changes in nearly all analyzed surface roughness parameters. These, observed changes are consistent with findings from previous studies where it was shown that the presence of fluoride and chloride ions leads to reduced corrosion resistance [1,4,5,7–10], change in surface morphology [1,5,7,8,10], and increased nickel ion release from NiTi alloys [9,11–14].

To determine whether the corrosion caused by specific media led to material loss, gain, or both, it was necessary to assess the changes relative to the surface mean plane. In this study, a methodology was developed for evaluating material gain or loss by analyzing the combined changes in various surface roughness parameters. The underlying logic behind the developed methodology is explained on an exemplary surface and graphically presented in Figure 5. The initial surface was approximated by a sinusoidal profile with minor peaks and valleys distributed around the mean plane (Figure 5a). The possible effects of corrosion and the locations of their manifestation on the initial profile are schematically represented by symbols given in Figure 5b. After incorporating these transformations, a profile model is obtained. It contains all the changes that may occur on the initial profile (Figure 5c). By analyzing the formulas used to calculate them, the change in each surface roughness parameter (Sa, Sdr, Ssk) can be correlated with a specific dominant corrosion effect, i.e., material gain or loss relative to the mean profile plane. Through an elimination-based approach, effects that produce contradictory trends in the roughness parameters can be excluded. This enables the identification of the predominant corrosion mechanism acting on each sample.

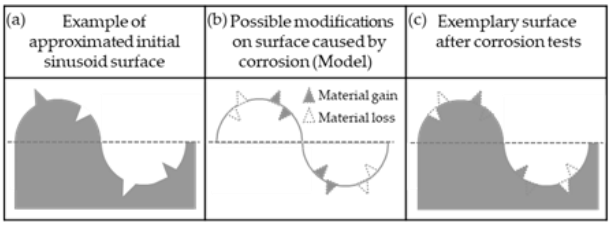

Figure 5. Graphical presentation of the analysis performed for detection of corrosion effects on surface topography: (a) approximated initial profile (before treatment); (b) possible corrosion effects and their locations; (c) profile of exemplary surface after corrosion.

The analysis begins with the evaluation of changes in the Sa parameter, as illustrated in Figure 6. An increase in Sa, as observed for Sample 2, may result from either material gain above the mean plane and/or material loss below it. All other potential effects would lead to a reduction in Sa and are therefore considered non-dominant. Conversely, the decrease in Sa observed for Sample 3 suggests the presence of material loss above and/or material gain beneath the mean plane. Sample 4 did not exhibit a detectable change in the Sa parameter, which means that in this medium all corrosion effects can be present on the surface.

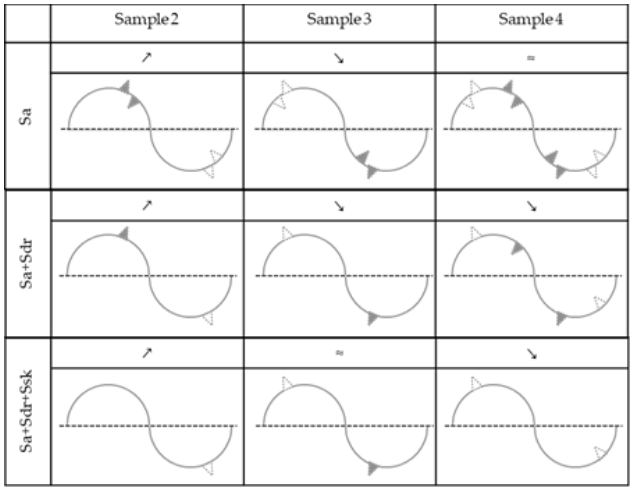

Figure 6. Determining the main corrosion effects. The empty triangle (material loss) vs. the full triangle (material gain). The statistical results are indicated by the following symbols: ≈, ↗, ↙. These symbols represent: insignificant difference, significant increase, and significant decrease in parameters.

The Sdr parameter for Sample 2 also increased following the corrosion test, implying that effects which would reduce the developed surface area can be excluded as dominant mechanisms. The concurrent increase in both Sa and Sdr values in Sample 2 is thus consistent with corrosion-induced material gain above the mean plane and/or material loss beneath it. A similar analytical approach was applied to Samples 3 and 4, and the findings are also presented in Figure 6.

The analysis of corrosion-induced changes in the Ssk parameter is inherently more complex. It is well established that high positive Ssk values indicate a surface dominated by peaks above the mean plane, and vice versa [42]. However, due to the high sensitivity of this parameter, its variations cannot be directly or clearly linked to a specific corrosion mechanism. For instance, significant changes in Ssk may result from relatively low-intensity alterations at peaks or valleys located far from the mean plane. Conversely, high-intensity changes in the surface topography may shift the position of the mean plane relative to otherwise unchanged features, thereby amplifying the apparent prominence of a large number of peaks or valleys. Nonetheless, it was possible to discern a previous effect by observing a change in Sa parameter. It can be reasonably proposed that a significant change will inevitably lead to a repositioning of the mean plane . Consequently, in the event of a substantial change in the Ssk parameter, it is possible to deduce whether this change is primarily the result of mean plane repositioning or a consequence of low-intensity, localized corrosion effects on the surface profile.

For Sample 2, an increase in both Sa and Ssk was observed. In consideration of the preceding analysis, it can be determined that the corrosion resulted in material loss on the surface. Furthermore, it can be deduced that all other possible effects are negligible. A similar analysis was performed, and it was determined that a dominant corrosion effect was present for all of the investigated media. The results of this analysis are presented in Figure 13. The analysis revealed that treatments with fluoride-containing media, namely Aquafresh® (Sample 2) and Listerine® (Sample 4), caused material loss, while fluoride-containing Eludril® (Sample 3) caused both material loss above the mean plane and/or material gain beneath the mean plane.

5. CONSLUSION

This investigation evaluated the topographic changes of NiTi alloy archwires exposed to artificial saliva and fluorine- and chlorine-containing mouthwashes. The following conclusions can be drawn from the results obtained:

- The sample exposed to artificial saliva did not display statistically significant changes in any surface roughness parameter.
- A new analysis method was developed to identify material gain or loss based on surface roughness parameters. It revealed that fluoride mouthwashes (Aquafresh® and Listerine®) cause material loss, while chlorine mouthwashes (Eludril®) can cause both gain and loss.

REFERENCES

[1] N. Schiff, B. Grosgogeat, M. Lissac, F. Dalard, M." Ele Lissac, F. Dalard, Influence of fluoridated mouthwashes on corrosion resistance of orthodontics wires, Biomaterials. 25 (2004) 4535–4542. https://doi.org/10.1016/j.biomaterials.2003.11.042.

[2] R. Köster, D. Vieluf, M. Kiehn, M. Sommerauer, J. Kahler, S. Baldus, T. Meinertz, C.W. Hamm, Nickel and molybdenum contact allergies in patients with coronary in-stent restenosis, Lancet. 356 (2000) 1895–1897. https://doi.org/10.1016/S0140-6736(00)03262-1.

[3] X. Li, J. Wang, E. Han, W. Ke, Influence of fluoride and chloride on corrosion behavior of NiTi orthodontic wires, Acta Biomater. 3 (2007) 807–815. https://doi.org/10.1016/j.actbio.2007.02.002.

[4] H.H. Huang, T.H. Lee, T.K. Huang, S.Y. Lin, L.K. Chen, M.Y. Chou, Corrosion resistance of different nickel-titanium archwires in acidic fluoride-containing artificial saliva, Angle Orthod. 80 (2010) 547–553. https://doi.org/10.2319/042909-235.1.

[5] P. Osak, B. Łosiewicz, EIS Study on Interfacial Properties of Passivated Nitinol Orthodontic Wire in Saliva Modified with Eludril® Mouthwash, Prot. Met. Phys. Chem. Surfaces. 54 (2018) 680–688. https://doi.org/10.1134/S2070205118040226.

[6] G. Perinetti, L. Contardo, M. Ceschi, F. Antoniolli, L. Franchi, T. Baccetti, R. Di Lenarda, Surface corrosion and fracture resistance of two nickel-titanium-based archwires induced by fluoride, pH, and thermocycling. An in vitro comparative study, Eur. J. Orthod. 34 (2012) 1–9. https://doi.org/10.1093/ejo/cjq093.

[7] X. Li, J. Wang, E. hou Han, W. Ke, E. hou Han, W. Ke, E. hou Han, W. Ke, Influence of fluoride and chloride on corrosion behavior of NiTi orthodontic wires, Acta Biomater. 3 (2007) 807–815. https://doi.org/10.1016/j.actbio.2007.02.002.

[8] E.J. Kassab, J.P. Gomes, Assessment of nickel titanium and beta titanium corrosion resistance behavior in fluoride and chloride environments, Angle Orthod. 83 (2013) 864–869. https://doi.org/10.2319/091712-740.1.

[9] N. Schiff, M. Boinet, L. Morgon, M. Lissac, F. Dalard, B. Grosgogeat, Galvanic corrosion between orthodontic wires and brackets in fluoride mouthwashes, Eur. J. Orthod. 28 (2006) 298–304. https://doi.org/10.1093/ejo/cji102.

[10] S. Kožuh, L. Vrsalović, M. Gojić, S. Gudić, B. Kosec, Comparison of the corrosion behavior and surface morphology of niti alloy and stainless steels in sodium chloride solution, J. Min. Metall. Sect. B Metall. 52 (2016) 53–61. https://doi.org/10.2298/JMMB150129003K.

[11] C.M. Ogawa, K. Faltin, F.A. Maeda, C.L.F.F. Ortolani, R.O. Guaré, C.A.B.B. Cardoso, A.L.F.F. Costa, In vivo assessment of the corrosion of nickel–titanium orthodontic archwires by using scanning electron microscopy and atomic force microscopy, Microsc. Res. Tech. 83 (2020) 928–936. https://doi.org/10.1002/jemt.23486.

[12] E.O. Nasakina, M.A. Sudarchikova, K. V. Sergienko, S. V. Konushkin, M.A. Sevost'Yanov, Ion release and surface characterization of nanostructured nitinol during long-term testing, Nanomaterials. 9 (2019). https://doi.org/10.3390/nano9111569.

[13] P. Močnik, T. Kosec, J. Kovač, M. Bizjak, The effect of pH, fluoride and tribocorrosion on the surface properties of dental archwires, Mater. Sci. Eng. C. 78 (2017) 682–689. https://doi.org/10.1016/j.msec.2017.04.050.

[14] A. Mirhashemi, S. Jahangiri, M. Kharrazifard, Release of nickel and chromium ions from orthodontic wires following the use of teeth whitening mouthwashes, Prog. Orthod. 19 (2018) 4. https://doi.org/10.1186/s40510-018-0203-7.

Society of Production Engineering

ICPES 2025

40th INTERNATIONAL CONFERENCE ON PRODUCTION ENGINEERING - SERBIA 2025

DOI: 10.46793/ICPES25.178D

University of Nis
Faculty of Mechanical Engineering

Nis, Serbia, 18 - 19th September 2025

A COMPARATIVE STUDY ON THE TRIBOLOGICAL BEHAVIOR OF NEW AND USED 10W-40 ENGINE OIL APPLIED IN GASOLINE AND DIESEL ENGINES

Dragan DZUNIC[1], Vladimir KOCOVIC[1], Zivana JOVANOVIC PESIC[1, *], Slobodan MITROVIC[1], Milan ERIC[1]

Orcid: 0000-0002-1914-1298; **Orcid:** 0000-0002-1373-0040; **Orcid:** 0000-0001-8691-4863;

[1] University of Kragujevac, Faculty of Engineering, Kragujevac, Republic of Serbia

*Corresponding author: zixi90@gmail.com

Abstract: *This study presents a comparative analysis of the tribological behaviour of new and used SAE 10W-40 engine oil, collected from gasoline and diesel passenger car engines and tested under cold-start conditions. The investigation examined the influence of oil aging and engine type on viscosity, friction, and wear. Block-on-disc experiments were performed using aluminium (EN AW-6060) against hardened steel (EN 25CrMo4) following ASTM G77 procedures. The results showed that used oils exhibited lower coefficients of friction and smaller wear scars compared to new oil. The diesel-derived sample achieved the best performance, with the lowest steady-state friction and wear volume, likely due to degradation products and fuel residues that enhanced boundary lubrication. Although used oils displayed improved short-term tribological behaviour, their long-term performance in actual engines is limited by oxidation, contamination, and corrosiveness. These findings provide insights into lubricant degradation and may support the optimization of oil-change intervals and the development of improved multigrade oils.*

Keywords: *Tribology, engine oil, Cold-start conditions, Wear scar analysis, Gasoline and diesel engines*

1. INTRODUCTION

The application of aluminium in internal combustion engine construction has become increasingly widespread, particularly in the manufacture of sliding bearings, pistons, and connecting rods. This material offers several advantages, including low specific weight, high corrosion resistance, favorable thermal conductivity, recyclability, and a measurable contribution to improved fuel economy. Nevertheless, its relatively limited wear resistance and certain mechanical constraints necessitate careful consideration of surface protection, with engine oil quality playing a decisive role in ensuring reliability and durability [1].

The performance of engine oil exerts a profound and multifaceted influence on the wear behaviour of aluminium surfaces. Wear represents one of the principal mechanisms of material degradation in engine blocks, and its progression is governed by several factors: the presence of hard particles and chemical

contaminants in cooling and lubricating fluids promotes abrasive and corrosive wear; exposure to high-temperature gases contributes to erosive wear; frictional interaction between the cylinder wall and piston rings may induce adhesive wear even under lubricated conditions; and material fatigue further accelerates deterioration. High-quality engine oils mitigate these effects by reducing friction, maintaining optimal viscosity, and incorporating additive packages designed to protect aluminium components against wear and corrosion [2,3].

The SAE 10W-40 multigrade engine oil is among the most commonly applied lubricants in passenger car engines, primarily due to its capacity to maintain reliable performance across a wide range of operating temperatures. The “10W” designation reflects its ability to ensure adequate fluidity and lubrication during cold starts, whereas the “40” grade denotes sufficient viscosity retention at elevated thermal and mechanical loads. Such versatility enables 10W-40 oils to provide both start-up protection and long-term durability under diverse service conditions. Their formulations typically combine refined base oils with advanced additive packages, which collectively enhance viscosity stability, reduce friction and wear, and safeguard components from corrosion and deposit formation. Furthermore, recent studies have demonstrated that the incorporation of graphene–cellulose nanocomposites into 10W-40 oil can further improve its thermophysical and tribological performance, yielding a lower coefficient of friction and superior wear resistance, thereby extending the protective capabilities of this lubricant [4].

During service, engine oil inevitably undergoes degradation as a consequence of prolonged exposure to elevated temperatures, mechanical stresses, and by-products of fuel combustion. These processes manifest through visible changes such as darkening of the oil, loss of transparency, and the development of an unpleasant odour, which are commonly recognized as the first signs of oil aging and contamination. Among the resulting alterations, variations in kinematic viscosity are of particular importance. A reduction in viscosity leads to decreased oil pressure and insufficient film strength, thereby increasing friction and accelerating the wear of critical engine components such as piston rings and bearings. Conversely, an excessive rise in viscosity compromises oil circulation and impedes the stable formation of a lubricating film at tribological contact surfaces [5–7].

Recycling of used engine oils is an essential strategy for sustainable resource utilization, environmental protection, and the mitigation of ecological hazards arising from toxic compounds contained in spent lubricants. The recycling of SAE 10W-40 engine oil poses particular challenges due to its complex chemical composition and the accumulation of contaminants during engine operation. Additive packages and chemical constituents undergo significant transformations under thermal and mechanical stress, generating harmful by-products that require advanced refining or re-refining technologies. Recent industrial advances, such as the development of Quartz EV3R 10W-40 by Total Energies, have demonstrated the feasibility of producing high-performance lubricants entirely from re-refined base oils, achieving up to a 46% reduction in wear and a 20% improvement in piston cleanliness compared to conventional oils [8]. Complementary academic studies have also provided promising results: Jurny et al. reported that solvent extraction using N-methyl-2-pyrrolidone enabled the recovery of approximately 10 L of reusable base oil from 25 L of used lubricant, thereby significantly reducing dependence on virgin crude oil for base stock production [9].

In this study, a comparative tribological analysis was carried out on new and used SAE 10W-40 engine oil after operation in gasoline and diesel passenger car engines. The investigation was performed under cold-start conditions, with the objective of assessing how oil aging and engine type influence viscosity changes, frictional response, and wear

protection. By examining both new and used oils, the study highlights the degradation mechanisms of 10W-40 under distinct combustion regimes and start-up stresses, thereby providing valuable insight into lubricant performance in real-world applications.

2. MATERIALS AND METHOD

This study investigated the tribological performance of SAE 10W-40 multigrade engine oil in both new and used conditions. New oil was tested as a reference to establish its baseline tribological properties, while used oil samples were collected after extended operation in gasoline and diesel passenger car engines. In service, the oil undergoes significant physicochemical changes, including variations in viscosity, darkening of colour, and accumulation of combustion by-products, all of which can directly influence its lubricating efficiency. The 10W-40 grade was selected because of its widespread application in passenger cars, providing adequate lubrication at low temperatures ("10W") while maintaining sufficient viscosity at elevated thermal and mechanical loads ("40").

Experimental testing was carried out using a TPD-95 block-on-disc tribometer, equipped with computer-controlled precision to ensure stable and repeatable operating conditions, in accordance with the ASTM G77 standard. In this configuration, an aluminium block (EN AW-6060 alloy) was pressed against a rotating hardened steel disc (EN 25CrMo4, 60–64 HRC, ground finish, Ø 35 mm), effectively replicating sliding contact conditions representative of real engine components. The aluminium blocks were prepared following a standardized surface treatment: sequential grinding at 500 rpm for 1 minute per side using progressively finer silicon carbide abrasive papers (P600, P1200, and P2000). This preparation ensured uniform surface conditions across all samples, which is essential for experimental reliability.

The tribological tests were performed under identical operating parameters: a normal load of 20 daN, a sliding speed of 0.5 m/s, and a total sliding duration of 600 seconds. Continuous lubrication during testing was provided by a reservoir system (30 ml capacity), ensuring a stable supply of oil at the contact interface. Under these conditions, three sets of experiments were defined: new 10W-40 oil, used 10W-40 oil collected from a gasoline engine, and used 10W-40 oil collected from a diesel engine.

The volume of worn material was calculated analytically using the following expression:

$$V = \left(\frac{306.25}{2} \cdot 2arcsin\left(\frac{b}{35}\right) - \frac{\sqrt{306.25 - \frac{b^2}{4}} \cdot b}{2} \right) \cdot 6.35 \quad (1)$$

where b is the width of the wear mark (mm), 306.25 is the square of the disc radius, and 6.35 mm represents the block width. This equation accounts for the geometry of the block-on-disc contact and enables accurate estimation of volumetric wear based on the measured scar dimensions.

3. RESULTS AND DISCUSION

Figure 1 shows the variation of the coefficient of friction (μ) as a function of sliding distance for new SAE 10W-40 oil, as well as for used oil collected from diesel and gasoline engines.

At the beginning of the test, all samples exhibited relatively high friction values due to the absence of a fully established lubricating film. For the new 10W-40 oil (AL-10W-40-N), the coefficient of friction started at approximately 0.05–0.055 and gradually decreased to a stable level of around 0.02 after about 100 m of sliding. This behaviour reflects the running-in process, during which the oil film progressively formed and stabilized the contact conditions.

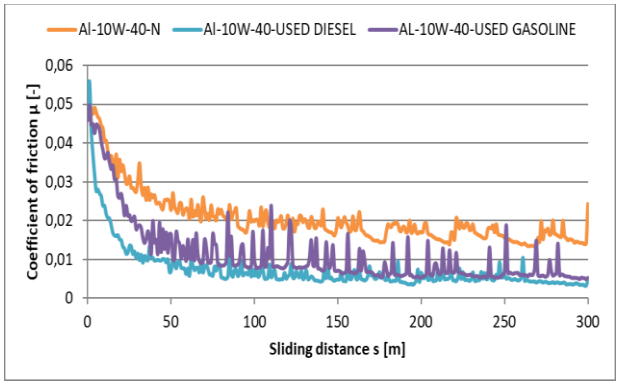

Figure 1. Coefficient of friction versus sliding distance for new and used SAE 10W-40 engine oils

In contrast, the used oil samples demonstrated improved frictional behaviour. The oil collected from the diesel engine (AL-10W-40-USED DIESEL) exhibited the lowest steady-state friction, stabilizing below 0.01 after the initial running-in stage. This may be attributed to chemical and physical changes in the oil during operation, including the presence of degradation products and fuel residues, which could enhance boundary lubrication properties under the given test conditions.

The used gasoline engine oil (AL-10W-40-USED GASOLINE) showed intermediate behaviour. While the initial friction values were comparable to those of the new oil, the coefficient of friction decreased more rapidly and reached values close to those of the used diesel oil. However, the curve exhibited more pronounced fluctuations, which may indicate less stable lubricating film formation, possibly due to differences in contamination mechanisms between gasoline and diesel combustion.

Table 1 presents the average wear scar width and the corresponding calculated wear volume for aluminium samples lubricated with new and used SAE 10W-40 engine oils. The values represent the mean of multiple measurements for each test group, ensuring statistical reliability.

The results indicate a consistent trend of reduced wear in the presence of used engine oils compared to new oil. The new 10W-40 oil produced the largest average wear scar (2.643 mm) and the highest wear volume (0.559 mm³), reflecting the oil's baseline tribological behaviour in the absence of degradation products. In contrast, the used oils exhibited smaller wear scars and correspondingly lower wear volumes, with 2.300 mm (0.368 mm³) for the gasoline engine sample and 2.000 mm (0.242 mm³) for the diesel engine sample.

Table 1. Average wear scar width and wear volume of aluminium samples lubricated with SAE 10W-40 engine oils

Sample	Wear scar width, b (mm)	Wear volume (mm^3)
AL-10W-40-N (New Oil)	2.643	0.559
AL-10W-40-USED GASOLINE	2.300	0.368
AL-10W-40-USED DIESEL	2.000	0.242

The reduced wear observed with used oils can be attributed to chemical and physical transformations occurring during engine operation. Degradation products, fuel residues, and oxidized compounds may act as additional boundary lubricants, temporarily improving the oil's ability to form protective films on aluminium surfaces. Among the tested samples, the diesel-derived oil showed the lowest wear scar and wear volume, which is consistent with its lower steady-state coefficient of friction (Figure 1), suggesting more stable boundary film formation under the applied test conditions.

Nevertheless, it must be emphasized that although used oils may demonstrate improved short-term tribological behaviour in laboratory block-on-disc testing, their long-term protective performance in actual engine operation is adversely affected by oxidation, contamination, and increased corrosiveness. This dual effect highlights the necessity of carefully balancing lubricant degradation and protective efficiency when evaluating oil performance in real applications.

4. CONCLUSION

This study investigated the tribological behaviour of new and used SAE 10W-40 engine oil, with samples obtained from both gasoline

and diesel passenger car engines and tested under cold-start conditions. The findings highlight the influence of oil degradation and engine type on viscosity, frictional behaviour, and wear protection.

The results demonstrated that used oils exhibited lower coefficients of friction and reduced wear scar dimensions compared to new oil. The diesel-derived oil, in particular, achieved the lowest steady-state friction values and the smallest wear volume, suggesting the formation of a more stable boundary film. This behaviour is most likely associated with the presence of degradation products and fuel-derived compounds that temporarily enhance lubrication under boundary contact conditions.

However, despite these short-term improvements observed in laboratory testing, it must be emphasized that prolonged use of aged oils in engines is not beneficial. Chemical degradation, contamination, and increased corrosiveness compromise the long-term protective performance of lubricants. The insights gained from this comparative study contribute to a deeper understanding of oil degradation mechanisms and may support the optimization of oil-change intervals, lubricant formulation strategies, and improved protection of aluminium-based engine components.

ACKNOWLEDGEMENT

This paper is the result of research conducted under the author's contract No. 451-03-137/2025-03/200107, dated February 4, 2025, and supported by the Ministry of Science, Technological Development and Innovation, Republic of Serbia.

REFERENCES

[1] Z. Aleš, J. Pavlů, J. Svobodová, M. Kučera, M. Hromasová, M. Pexa: Impact of contaminants in motor oil on the wear of aluminum parts of the internal combustion engine, Manufacturing Technology, Vol. 17, No. 5, pp. 647-652, 2017.

[2] M.S. Kaiser, S. Dutta: Wear behavior of commercial aluminium engine block and piston under dry sliding condition, International Journal of Materials and Metallurgical Engineering, Vol. 8, No. 8, pp. 860-865, 2014.

[3] S. Rațiu, A. Josan, V. Alexa, V.G. Cioată, I. Kiss: Impact of contaminants on engine oil: A review, Journal of Physics: Conference Series, Vol. 1781, p. 012051, 2021.

[4] J.G. Alotaibi, et al.: Enhancing engine oil performance with graphene-cellulose nanoparticles: insights into thermophysical properties and tribological behavior, Frontiers in Materials, Vol. 12, p. 1549117, 2025.

[5] K. Sakamoto, F. Mizutani, M. Shimomura, K. Yama, T. Matsunaga, S.-S. Lee: Evaluation of engine oil degradation based on viscosity and transmitted light intensity measurements, Sensors and Actuators A: Physical, Vol. 361, p. 114597, 2023.

[6] R. Smigins, K. Amatnieks, A. Birkavs, K. Górski, S. Kryshtopa: Studies on engine oil degradation characteristics in a field test with passenger cars, Energies, Vol. 16, p. 7955, 2023.

[7] Y.N. Bezborodov, N.N. Lysyannikova, E.G. Kravcova: Results of the study of anti-wear properties of the exhaust motor oil, Procedia Engineering, Vol. 150, pp. 654-660, 2016.

[8] Total Energies Lubrifiants, Stellantis: Quartz EV3R 10W-40 – a 100% re-refined engine lubricant with reduced wear and improved cleanliness, 2024

[9] M. Jurny, M. Elbourawi, E. Zorgani: Recycling of used engine oil using extraction by single solvent, American Journal of Chemical Engineering, Vol. 11, No. 2, pp. 33-38, 2023.

Society of Production Engineering

ICPES 2025

40. INTERNATIONAL CONFERENCE ON PRODUCTION ENGINEERING - SERBIA 2025

DOI: 10.46793/ICPES25.183P

University of Nis Faculty of Mechanical Engineering

Nis, Serbia, 18 – 19th September 2025

ASSESSMENT OF MEASUREMENT UNCERTAINTY IN MECHANICAL MATERIAL TESTING – THEORETICAL FRAMEWORK AND PRACTICAL APPLICATION

Dušan PETKOVIĆ[1]*, Predrag JANKOVIĆ[1]
Orcid: 0000-0002-1871-7144; **Orcid:** 0000-0001-9951-4500;
[1]University of Niš, Faculty of Mechanical Engineering, Niš, Serbia
*Corresponding author: dusan.petkovic@masfak.ni.ac.rs

Abstract: *This professional paper addresses a fundamental aspect of metrological quality assurance in mechanical material testing: the assessment of measurement uncertainty. Starting from the importance of reliable measurement results for industry, research, and development, the paper thoroughly elaborates on the theoretical framework of measurement uncertainty in accordance with international standards, primarily the GUM (Guide to the Expression of Uncertainty in Measurement) document. Special emphasis is placed on the clear distinction between measurement error and measurement uncertainty, as well as on different evaluation methods (Type A and Type B). General sources of uncertainty characteristic of mechanical testing are discussed, including the influence of equipment, the material/specimen itself, environmental conditions, and human factors.*

The methodology for assessing measurement uncertainty is presented step-by-step, from defining the measurement model and identifying input quantities, through calculating standard and combined uncertainty, to determining expanded uncertainty. The practical application of this methodology is demonstrated through a specific example of hardness determination by Rockwell method. For this example, key sources of uncertainty are analysed, and guidelines for their quantification are provided.

Keywords: *Mechanical material testing, Measurement uncertainty, Hardness determination, Product quality.*

1. INTRODUCTION

Measurement uncertainty represents a quantitative estimate of the quality of a measurement result. Unlike measurement error, which denotes the difference between the measured and the "true" value (usually unknowable in practice), uncertainty expresses the level of confidence that the measured result is close to the actual value. In other words, uncertainty does not claim to correct the result but rather describes the range within which the true value is reasonably expected to lie. This distinction between error and uncertainty is essential for proper interpretation of results, particularly in mechanical material testing, where results are often used for safety-critical decisions.

The international reference document for the assessment of measurement uncertainty is

the Guide to the Expression of Uncertainty in Measurement (GUM), first published by ISO, IEC, and other organizations in 1993. The GUM establishes a systematic and harmonized methodology for evaluating and expressing uncertainty, making measurement results comparable across laboratories and countries. In addition to the GUM, specific standards are relevant for mechanical testing, such as ISO 6508 for Rockwell hardness testing or ISO 6892 for tensile testing, which provide both testing procedures and indications of relevant sources of uncertainty. Together, these standards ensure that both the test execution and the evaluation of its reliability follow internationally recognized best practices.

The GUM distinguishes two basic approaches to evaluating uncertainty: Type A, based on statistical analysis of repeated observations, and Type B, based on other sources of information such as instrument specifications, calibration certificates, or literature data. Type A evaluation allows the quantification of variability through repeatability and reproducibility studies, making it particularly useful in routine laboratory conditions. Type B evaluation, on the other hand, enables the incorporation of knowledge about systematic influences or limitations of the measurement system, even when repeated measurements are not available. In most practical cases, both approaches are combined, ensuring a comprehensive picture of the uncertainty budget.

Mechanical material testing is characterized by a wide range of potential uncertainty sources. Equipment-related sources include instrument calibration, resolution, and stability of applied forces or displacements. Material-related sources stem from the specimen itself, such as inhomogeneity, anisotropy, or preparation quality. Environmental factors, including temperature and humidity, may significantly influence results, particularly in sensitive tests. Finally, human factors, such as operator skill or the application of testing procedure, cannot be neglected, especially in semi-automated or manually controlled tests. Identifying and quantifying each of these contributions is the foundation of a systematic uncertainty analysis.

2. METHODOLOGY FOR ASSESSING MEASUREMENT UNCERTAINTY

The first step in assessing measurement uncertainty is to define the measurement model, i.e., the mathematical relationship that links the measurand (the quantity to be determined) with the input quantities that influence the result. For example, in Rockwell hardness testing, the model incorporates applied force, indenter geometry, depth measurement, and material response. According to the GUM, all sources of variability should be expressed as input quantities, each with an associated probability distribution. A well-defined measurement model ensures traceability and transparency, making subsequent calculations consistent and reproducible.

Once the measurement model is established, the next step is to identify all relevant input quantities and assign uncertainty values to each. Input uncertainties can originate from different sources: calibration data, instrument resolution, repeatability tests, environmental monitoring, or published literature. Depending on the available information, the uncertainty of each input quantity is evaluated either using the Type A method (statistical analysis of repeated measurements) or the Type B method (data from certificates, manufacturer specifications, expert judgment). Assigning an appropriate probability distribution (normal, rectangular, triangular, etc.) to each input is crucial for realistic propagation of uncertainty.

Each input uncertainty is expressed as a standard uncertainty, usually corresponding to a 1-sigma coverage (approximately 68% confidence level). The propagation of these uncertainties through the measurement model can be performed analytically (using sensitivity coefficients derived from partial derivatives) or numerically (e.g., Monte Carlo simulations). The result is the combined standard

uncertainty, which represents the overall uncertainty of the measurand at the standard level of confidence. This step highlights how different sources contribute to the final result and prevents overlooking dominant factors.

For practical engineering and quality assurance purposes, uncertainty is usually expressed as an expanded uncertainty, which corresponds to a higher confidence level (typically 95%). This is achieved by multiplying the combined standard uncertainty by a coverage factor k, most commonly k = 2.

3. MEASUREMENT UNCERTAINTY OF MEASURED ROCKWELL HARDNESS – ASSESMENT EXAMPLE

Measurement uncertainty analysis is a useful tool to help determine sources of error and to understand differences in test results. Most product specifications have tolerances that have been developed over the past years based mainly on the requirements of the product but also, in part, on the performance of the machine used to make the hardness measurement. These tolerances therefore incorporate a contribution due to the uncertainty of the hardness measurement and it would be inappropriate to make any further allowance for this uncertainty by, for example, reducing the specified tolerance by the estimated uncertainty of the hardness measurement. In other words, where a product specification states that the hardness of an item shall be higher or lower than a certain value, this should be interpreted as simply specifying that the calculated hardness value(s) shall meet this requirement, unless specifically stated otherwise in the product standard. However, there might be special circumstances where reducing the tolerance by the measurement uncertainty is appropriate. This should only be done by agreement of the parties involved [SRPS 6508 2024].

The approach for determining uncertainty presented in this study considers only those uncertainties associated with the overall measurement performance of the hardness testing machine with respect to the hardness reference blocks (abbreviated as CRM). “CRM” stands for “certified reference material” (in hardness testing standards, certified reference material is referred to as a hardness reference block, i.e. a piece of material with a certified value and associated uncertainty). These performance uncertainties reflect the combined effect to all the separate uncertainties. Because of this approach, it is important that the individual machine components are operating within the tolerances. It is strongly recommended that this procedure is applied for a maximum of one year after the successful passing of a verification and calibration.

3.1 Procedure of calculation

The measurement uncertainty of the measured hardness values was derived according to the procedure defined in the standard SRPS EN ISO 6508-1:2024 based on the indirect calibration of the device, point 9 and Annex G [SRPS 6508]. This procedure calculates an expanded uncertainty U, associated with the measured hardness value. The approach to this calculation is given in Table 1 together with details of the symbols used. In this procedure, several uncorrelated standard uncertainty sources are combined by the Root-Sum Square (RSS) method and then multiplied by the coverage factor k = 2. The uncertainty contribution from a systematic source is then added arithmetically to this value.

Bias of the machine

The bias, b, of a hardness testing machine (also termed “error”) is derived from the difference between — the certified calibration value of the hardness reference block, and

— the mean hardness value of the five indentations made in the hardness reference block during calibration of the hardness testing machine and can be implemented in different ways into the determination of uncertainty.

Table 1. Calculation procedure

Test method		**HRB**					**HRC**				
Hardness of CRM HCRM		83,1					55,6				
Machine display resolution δms		0,5					0,5				
Data from Calibration certificate*	X CRM	96.66					45.42				
	b	1.76					0.92				
	U*HTM	0.56					0.48				
Measured uncertainty (from Calibration certificate) of machine UHTM = U*HTM /2		0.28					0.24				
Measured values		H1	H2	H3	H4	H5	H1	H2	H3	H4	H5
		85	84	84.5	84.5	84	56.5	57	57	57	56.5
$\bar{H} = \frac{H1 + H2 + H3 + H4 + H5}{5}$		84.4					56.8				
$S_H = \sqrt{\frac{1}{n-1}\sum_{i=1}^{n}(H_i - \bar{H})^2}$		0.42					0.27				
Bias $\boldsymbol{b} = \bar{H} - H_{CRM}$		1.3					1.2				
		(10-45] ± 4 HRB (45-80] ± 3 HRB (80-100] ± 2 HRB					± 1,5 HRC				
Bias ***b*** acceptable?		Yes (1.3 < 2)					Yes (1.2 < 1.5)				
Rrepeatability range $r = Hn - H1$ ***(Whichever is greater)***		H2-H1=-1					H2-H1=0.5				
		H3-H1=-0.5					H3-H1=0.5				
		H4-H1=-0.5					H4-H1=0.5				
		H5-H1=-1					H5-H1=0				
Maximum permissible repeat ability range, *r*, of the testing machine ***(Whichever is greater)***		$\leq \mathbf{0,04}(\mathbf{130} - \bar{H}) = 1{,}824$					$\leq \mathbf{0,02}(\mathbf{100} - \bar{\mathrm{H}})$=0,884 ≤0,89				
		-					**0,8 HRC**				
r acceptable?		Yes (1 < 1.824)					Yes (0.5 < 0.89)				
$\boldsymbol{U_H = 1{,}14 * S_H}$		0.48					0,31				
$\boldsymbol{U_{ms} = \delta_{ms}/sqrt(2*3)}$		0.20					0.20				
Determination of the corrected expanded uncertainty $\boldsymbol{U = 2\sqrt{U_H^2 + U_{ms}^2 + U_{HTM}^2}}$		1.2					0.9				
Measurement result with modified hardness $\boldsymbol{H} = (\bar{H} - b) \pm U$		(84.4 - 1.3) ± 1.2 83.1 ± 1.2					(55.8 - 1.2) ± 0.9 54.6 ± 0.9				
Measurement result with modified uncertainty $\boldsymbol{H_U} = \bar{H} \pm (U + \lvert b \rvert)$		84.4 ± (1.2 +1.3) 84.4 ± 2.5					55.8 ± (0.9 + 1.2) 55.8 ± 2.1				

4. CONCLUSION

The determination of measurement uncertainty in Rockwell hardness testing is a critical aspect of ensuring the reliability and traceability of hardness results in material testing. This paper has presented the theoretical framework of measurement uncertainty, emphasizing its role in quantifying the confidence level of test outcomes. Through a detailed description of the procedure for evaluating uncertainty in Rockwell hardness measurements, it has been demonstrated that a systematic approach, incorporating all relevant sources of variability, can significantly enhance the credibility of the testing process. By applying established metrological principles and uncertainty estimation methods, laboratories can ensure compliance with international standards and improve decision-making based on hardness values. Ultimately, understanding and managing measurement uncertainty is essential for maintaining quality control and supporting the integrity of mechanical property evaluations in industrial applications.

The results and methodology presented in this study provide a practical framework for laboratories and quality control departments aiming to improve the reliability of Rockwell hardness testing. By identifying and quantifying individual sources of uncertainty—such as instrument precision, operator variability, and environmental conditions, this approach enables targeted improvements in the measurement process.

ACKNOWLEDGEMENT

This research was financially supported by the Ministry of Science, Technological Development and Innovation of the Republic of Serbia (Contract No. 451-03-137/2025-03/200109).

REFERENCES

[1] SRPS EN ISO 6508-1:2024, *Метални материјали – Испитивање тврдоће по Роквелу – Део 1: Метода испитивања*, 2024. ISO/IEC

[2] Guide 98-3:2008, Uncertainty of measurement — Part 3: Guide to the expression of uncertainty in measurement (GUM: 1995).

[3] ASTM E18, Standard Test Methods for Rockwell Hardness of Metallic Materials.

[4] Guide E.U.R.A.M.E.T. cg-16, Guidelines on the Estimation of Uncertainty in Hardness Measurements. [ht t p:// www .euramet .org].

[5] Gabauer W., Manual of Codes of Practice for the Determination of Uncertainties in Mechanical Tests on Metallic Materials, The Estimation of Uncertainties in Hardness Measurements, Project, No. SMT4-CT97-2165, UNCERT COP 14: 2000.

[6] Polzin T., Schwenk D. Method for uncertainty determination of hardness testing; PC file for the determination, Materialprüfung, 44 (2002) 3, pp. 64–71.

Session 4:

Process planning and production control, logistics and optimization

Society of Production Engineering

ICPES 2025

40th INTERNATIONAL CONFERENCE ON PRODUCTION ENGINEERING - SERBIA 2025

DOI: 10.46793/ICPES25.189GM

University of Nis Faculty of Mechanical Engineering

Nis, Serbia, 18 - 19th September 2025

DEEP LEARNING TECHNIQUES FOR DEFECT DETECTION IN AUTOMATED QUALITY CONTROL SYSTEMS

A. Gandhi MANIKANDAN[1*], V. SANDHIYA[1], P. HARINE[1], R. AJAY DHISONE[1], M. SATHYAPRAKASH[1].

…; Orcid: 0009-0004-7979-2721; **Orcid:** 0009-0006-7509-9254; **…..; …..**

[1]SRM TRP Engineering College, Trichy, Tamilnadu, India - 621105

*Corresponding author: nagadeepan.a@gmail.com

Abstract: *Automated quality control (AQC) systems have transformed modern manufacturing by enabling high-speed, consistent, and cost-efficient inspection of products. However, traditional image processing techniques often fail to detect subtle, non-conforming defects due to limitations in adaptability and generalization. This paper explores the integration of deep learning (DL) techniques—particularly convolutional neural networks (CNNs), autoencoders, and vision transformers—for enhancing defect detection accuracy in AQC environments. A comprehensive methodology is presented where training datasets are augmented using synthetic defect generation, followed by supervised and unsupervised learning approaches for feature extraction and classification. The research evaluates various model architectures using metrics such as accuracy, precision, recall, and inference time on datasets collected from electronic component inspection and surface defect analysis in metal casting. The results demonstrate that DL models significantly outperform conventional rule-based systems, particularly in detecting micro-defects and anomalies in complex textures. Moreover, the incorporation of transfer learning and model pruning techniques further reduces computational overhead, making the deployment feasible in real-time production lines. This study concludes with an outline of implementation challenges, including data imbalance, hardware constraints, and model interpretability, and proposes potential directions for future research in intelligent adaptive inspection systems. The findings aim to contribute toward the development of robust, scalable, and intelligent quality control frameworks aligned with Industry 4.0 principles.*

Keywords: *deep learning, defect detection, automated quality control, convolutional neural networks, computer vision, real-time inspection, Industry 4.0*

1. INTRODUCTION

The rise of Industry 4.0 has necessitated a paradigm shift in manufacturing processes, with a strong emphasis on automation, interconnectedness, and intelligent systems. Automated Quality Control (AQC) is a critical component of this transformation, moving away from manual and error-prone inspection methods to fast, reliable, and objective systems. Traditional AQC systems often rely on classical computer vision

techniques, such as thresholding, edge detection, and feature matching [1,2]. While effective for simple, well-defined defects, these methods struggle with complex, textured surfaces and subtle, non-conforming anomalies. They lack the adaptability and generalization capabilities required to handle the wide variety of defects that can occur in real-world production environments.

This paper addresses the limitations of conventional AQC systems by proposing the integration of advanced deep learning (DL) techniques for defect detection. DL models, particularly those based on neural networks, have demonstrated state-of-the-art performance in complex image recognition tasks, making them ideal candidates for enhancing the accuracy and robustness of AQC. This study focuses on three key DL architectures: Convolutional Neural Networks (CNNs), Autoencoders, and Vision Transformers (ViTs). We present a comprehensive methodology for dataset preparation, model training, and performance evaluation, and discuss the results of their application to real-world manufacturing datasets. The ultimate goal is to contribute to the development of intelligent quality control frameworks that are scalable and aligned with the principles of Industry 4.0.

2. METHODOLOGY

Our methodology is structured to provide a robust and systematic approach to deep learning-based defect detection. The process begins with dataset acquisition, followed by data augmentation, model selection and training, and finally, performance evaluation.

2.1 Dataset Preparation

We utilized two distinct datasets to evaluate the models: one consisting of electronic components and another comprising images of metal castings. The electronic component dataset includes various micro-defects such as solder bridges, missing components, and cracks. The metal casting dataset contains surface anomalies like pores, cracks, and scratches. To address the typical data imbalance problem where defect samples are rare, we employed data augmentation techniques. These included standard image transformations (rotation, scaling, flipping) as well as more advanced methods like synthetic defect generation using Generative Adversarial Networks (GANs) or image manipulation techniques to create realistic defect examples.

Model Architectures and Training

Three primary deep learning architectures were chosen for this study:

1. Convolutional Neural Networks (CNNs): CNNs, such as VGGNet, ResNet, and YOLO, are well-suited for feature extraction from images. We trained several CNN models in a supervised manner, where each image was labeled as either “defective” or “non-defective,” or with specific defect types.

1. Autoencoders:
   a) For unsupervised learning, we used a standard autoencoder and a variational autoencoder (VAE) [3]. These models are trained to reconstruct normal, non-defective images. Defects are identified by a high reconstruction error, as the model struggles to reproduce features it has not been trained on. This approach is particularly useful in scenarios with very few defect samples.
2. Vision Transformers (ViTs):
   a) ViTs represent a more recent approach, adapted from natural language processing. They process images as sequences of patches and use a self-attention mechanism to

learn global dependencies [4]. We fine-tuned a pre-trained ViT model for the defect classification task, which leverages the benefits of transfer learning.

Model Evaluation :

To rigorously assess the effectiveness of each deep learning architecture deployed in this study, a comprehensive evaluation framework was employed. The models were benchmarked using a suite of standard classification metrics—accuracy, precision, recall, and F1-score—which collectively provide a multidimensional view of performance across both balanced and imbalanced datasets.

Accuracy reflects the overall correctness of the model's predictions, offering a general measure of performance.

Precision quantifies the proportion of true positive predictions among all positive predictions, which is critical in minimizing false alarms in defect detection.

Recall measures the model's ability to identify all actual defect instances, ensuring that no defective item escapes detection.

F1-score, the harmonic mean of precision and recall, balances the trade-off between false positives and false negatives, making it particularly valuable in quality control contexts where both types of errors carry operational consequences.

In addition to these classification metrics, inference time—defined as the time required for the model to process and classify a single image—was measured to evaluate the feasibility of real-time deployment. This metric is especially pertinent in high-throughput manufacturing environments where latency can directly impact production efficiency and decision-making speed.

All performance metrics were computed on a separate, unseen test dataset that was not used during training or validation. This approach ensures that the evaluation reflects the model's generalization capability, i.e., its ability to perform reliably on new, previously unencountered data. Such validation is essential for industrial applications, where models must maintain robustness across varying lighting conditions, surface textures, and defect types.

3. RESULT AND DISCUSSION :

The empirical findings of this study affirm the superior performance of deep learning models over traditional image processing techniques in the domain of automated quality control (AQC). By leveraging hierarchical feature extraction and nonlinear representation learning, deep neural networks—particularly Convolutional Neural Networks (CNNs), autoencoders, and Vision Transformers (ViTs)—demonstrated a remarkable ability to detect subtle and complex defect patterns that conventional algorithms often fail to capture.

3.1 Electronic Component Inspection

In the task of inspecting electronic components, the ResNet-50 architecture emerged as a high-performing model, achieving an outstanding accuracy of 98.5% and precision of 97.2%. These metrics represent a substantial leap over traditional methods such as Canny edge detection, which yielded only 85.1% accuracy, highlighting the limitations of rule-based feature extraction in handling nuanced defect morphologies.

The Vision Transformer (ViT), enhanced through transfer learning, exhibited

exceptional proficiency in identifying texture-based anomalies. Its global attention mechanism enabled the model to capture long-range dependencies and contextual cues, making it particularly effective in scenarios where defect patterns are spatially dispersed or irregular.

3.2 Metal Casting Surface Analysis

For surface defect detection in metal casting applications, an unsupervised autoencoder model was employed. Trained exclusively on defect-free samples, the autoencoder learned a compact representation of normal surface textures. During inference, deviations from this learned manifold were flagged as anomalies. This approach yielded a recall rate of 95.8%, underscoring its efficacy in identifying rare or previously unseen defects without requiring extensive labeled datasets.

Such anomaly detection frameworks are especially valuable in industrial contexts where defect occurrences are infrequent, and the cost or feasibility of collecting large-scale annotated data is prohibitive.

4. IMPLEMENTATION CHALLENGES

Despite the promising performance of deep learning-based AQC systems, several practical and infrastructural challenges must be addressed to facilitate their widespread adoption in manufacturing environments.

4.1 Data Imbalance and Scarcity

One of the most pressing issues is the imbalance and scarcity of real-world defect data. In many industrial settings, defective samples constitute a small fraction of the overall production output, leading to skewed datasets that hinder model generalization. While synthetic data generation techniques—such as image augmentation, GAN-based synthesis, and simulation-driven rendering—offer partial remedies, they often fall short in replicating the full spectrum of defect variability encountered in practice.

Future research should explore domain adaptation, few-shot learning, and active learning strategies to enhance model robustness under data-constrained conditions.

4.2 Hardware and Computational Constraints

The deployment of deep learning models for real-time quality control necessitates high-throughput inference capabilities, which in turn require specialized hardware such as Graphics Processing Units (GPUs) or edge AI accelerators. For small and medium-sized enterprises (SMEs), the financial and infrastructural investment needed to support such hardware can be prohibitive.

Efforts toward model compression, quantization, and efficient architecture design (e.g., MobileNet, EfficientNet) are essential to enable cost-effective deployment without compromising performance. Additionally, cloud-based inference and federated learning frameworks may offer scalable alternatives for resource-limited settings.

5. CONCLUSION

This study has demonstrated the substantial promise of deep learning techniques—namely Convolutional Neural Networks (CNNs), autoencoders, and Vision Transformers—in reshaping automated quality control systems across

diverse industrial applications. These models not only surpass traditional image processing methods in terms of defect detection accuracy and robustness, but also offer adaptive learning capabilities that are critical for dynamic manufacturing environments.

By incorporating strategies such as transfer learning and model pruning, the proposed frameworks achieve both high performance and computational efficiency, making them suitable for real-time deployment. The success of unsupervised approaches, particularly in scenarios with limited defect data, further underscores the versatility of deep learning in addressing practical constraints faced by manufacturers.

Looking forward, the evolution of intelligent quality control systems will depend on several key research directions: the development of advanced data augmentation techniques to mitigate data imbalance; the design of hybrid architectures that synergize the strengths of multiple models; and the integration of explainable AI (XAI) to enhance transparency, trust, and regulatory compliance.

ACKNOWLEDGEMENT

This research was supported by the SRM TRP Engineering College. We extend our gratitude to our colleagues for their valuable feedback and assistance.

REFERENCES

[1] H. Czichos, D. Klaffke, E. Santner, M. Woydt: Advances in tribology: the materials point of view, Wear, Vol. 190, No. 2, pp. 155-161, 1995.

[2] D. P. Kingma and M. Welling: Auto-Encoding Variational Bayes, in: International Conference on Learning Representations, 2014.

[3] A. Dosovitskiy, L. Beyer, A. Kolesnikov, D. Weissenborn, X. Zhai, T. Unterthiner, M. Dehghani, M. Minderer, G. Heigold, S. Gelly, J. Uszkoreit, N. Houlsby: An Image is Worth 16x16 Words: Transformers for Image Recognition at Scale, in: International Conference on Learning Representations, 2021.

Society of Production Engineering

ICPES 2025

40th INTERNATIONAL CONFERENCE ON PRODUCTION ENGINEERING - SERBIA 2025

DOI: 10.46793/ICPES25.194N

University of Nis Faculty of Mechanical Engineering

Nis, Serbia, 18 - 19th September 2025

MULTI-CRITERIA OPTIMIZATION OF CO_2 LASER CUTTING OF METALS USING HYBRID AHP–TOPSIS APPROACH

A. Nagadeepan[1], M. Pranav[2], P. Santhosh[3], S. SivaShankaran[4], V. Senthilkumar[5]

Orcid: 0000-0002-7442-2658; **Orcid:** 0000-0003-1673-3180;

[1]SRM TRP Engineering College, Trichy, Tamilnadu, India - 621105

*Corresponding author: nagadeepan.a@gmail.com

Abstract: *The non-linear effects of the laser cutting process parameters and their interactions on the cut quality for ferrous and non-ferrous metals were difficult to predict. It is vital and complex to find the optimum process condition for a specific application and requires evaluation of a number of competing and distinct process performance characteristics. Various Multi Criterion Decision-Making (MCDM) techniques which are simple and logical are available to aid the selection of optimal combination of cutting parameters in the modern manufacturing processes. The laser cutting is one modern manufacturing process which is capable of cutting complex shapes in almost all the engineering materials and requires a variety of parameters and performance characteristics. To predict the non-linear effects in laser cutting, box-behnken design with three process parameters laser beam power, cutting speed and gas pressure was employed to design the experiments. The analytic hierarchy process (AHP) is used to predict the weightage among the responses and then technique for order of preference by similarity to ideal solution (TOPSIS) is used to optimize the process parameters associated with laser cutting of ferrous and non-ferrous alloys.*

Keywords: *CO_2 laser cutting process, AHP, TOPSIS, MCDM, Boxbehnken, Aluminium 8011 alloy*

1. INTRODUCTION

Laser cutting has become a contemporary industrial staple owing to its ability to generate sophisticated geometries with high accuracy, minimum heat affected zones and a decreased requirement for additional finishing. It is used in the shipbuilding, automobile, aerospace and medical device sectors where efficiency and cut quality are crucial. when these benefits are considered, laser cutting is intrinsically complicated due to the nonlinear interactions of many process variables, including laser power, cutting speed, and assist gas pressure, which affect material removal rate (MRR), kerf width (Kw) and surface roughness (Ra). It is difficult to achieve an optimal equilibrium among these responses since advances in one may compromise another. Recent studies demonstrate significant advancements in laser-based machining optimization, decision-making approaches, and process modeling. Using principal component analysis and orthogonal arrays to optimize Nd:YAG laser cutting of nickel-based superalloy sheets from several angles has been proven to be a fundamental

method for increasing machining precision [1]. Experiments on fiber and CO_2 laser settings highlight the importance of parameter sensitivity and show significant impacts on the quality of the cut surface for stainless steels [2]. Gears and cutting fluids have been chosen using hybrid multi-criteria decision-making MCDM frameworks like AHP-MARCOS [3] while multi-attribute decision-making techniques have becoming more popular in additive manufacturing applications [4]. The optimization of machining parameters is a common application for evolutionary algorithms which provide reliable solutions for intricate industrial systems [5]. Further improving performance prediction and optimization are intelligent decision models designed for non-traditional machining processes [6]. ANFIS models adjusted by genetic algorithms have proven to be accurate in predicting kerf width for laser machining of titanium alloys [7]. The application of the Analytical Hierarchy Process in advanced manufacturing is further supported by its ongoing development as a decision-support tool [8]. The effectiveness of fuzzy AHP-based MCDM techniques for multi-objective optimization has been demonstrated in recent work on laser cutting polyethylene [9] and thorough evaluations of Nd:YAG and CO_2 laser drilling of fiber-reinforced composites [10] have also been conducted. Heat influence modeling is emphasized in parameter optimization studies for sheet metal laser cutting [11] and multi-criteria decision analysis is becoming more and more common in sustainable manufacturing practices [12]. Due to its ability to facilitate remote optimization and decision support cloud-edge collaborative manufacturing has become a significant paradigm [13]. Research on GFRP fiber laser cutting demonstrates that multi-objective optimization is a successful method for improving quality [14]. Reconfigurable manufacturing system metrics can be prioritized using hybrid fuzzy AHP–TOPSIS frameworks, which facilitate adaptive production planning [15].

Standard optimization methods usually focus on a single performance measure which might not be enough in industrial settings where quality, accuracy and efficiency all need to be improved at the same time. TOPSIS evaluates process options by assessing how closely they resemble the ideal solution and the Analytic Hierarchy Process offers a methodical framework for allocating weights to performance measures based on expert opinion. A hybrid decision making model that combines TOPSIS and AHP allows for efficient trade off analysis in multi response optimization.

The effects of laser power (0.32kW, 0.33kW, 0.34 kW), cutting speed (0.20m/min, 0.21m/min, 0.22 m/min) and gas pressure (0.70bar, 0.80bar, 0.90 bar) on Ra, Kw and MRR during CO_2 laser cutting of Al 8011 alloy were effectively investigated in this work using the Box–Behnken Design (BBD). By using this hybrid framework, the study seeks to provide companies a generalizable decision support tool that will allow for the methodical improvement of CO_2 laser cutting procedures for increased precision, reliability and efficiency.

2. METHODOLOGY

2.1. Experimental Design

The Box–Behnken Design (BBD) was chosen to model the interaction effects of three process parameters: laser power, cutting speed, and gas pressure, each at three levels (low, medium, high). This design generated 17 experimental trials, ensuring efficient quadratic modeling while minimizing the number of runs compared to a full factorial design.

2.2. Input Parameters and Levels

The quality and efficiency of the CO_2 laser cutting process are strongly governed by three primary parameters: laser power, cutting speed, and assist gas pressure. These parameters were selected due to their direct influence on heat input, material melting/vaporization, and molten material removal efficiency, respectively. Each

parameter was studied at three levels (low, medium, high) to capture nonlinear interactions and second-order effects while maintaining an efficient experimental design.

Table 1. Parameters and its levels

Parameter	Level 1	Level 2	Level 3
Power (kW)	0.32	0.33	0.34
Speed (m/min)	0.2	0.21	0.22
Pressure (bar)	0.7	0.8	0.9

2.3. Response Measurements

To evaluate the effect of process parameters on CO_2 laser cutting performance, three key responses were considered: surface roughness (Ra), kerf width (Kw), and material removal rate (MRR). These responses capture the balance between cut quality and productivity, which is crucial for industrial adoption.

Surface Roughness (Ra, µm): Measured using a contact profilometer with a cutoff length of 0.8 mm. For accuracy, three readings were taken at different locations on each specimen, and the mean value was reported. Lower Ra values indicate smoother surfaces and superior cut quality.

Kerf Width (Kw, mm): Determined using an optical microscope (10× magnification) across multiple cross-sections of the cut. Consistent and minimal kerf width reflects high dimensional accuracy and efficient energy utilization during cutting.

Material Removal Rate (MRR, mm^3/s): Computed from the relationship between material thickness, kerf width, and cutting speed. MRR quantifies process productivity, with higher values corresponding to faster and more efficient cutting.

The Box–Behnken Design (BBD) was employed to generate 17 experimental trials, ensuring an efficient exploration of parameter effects while minimizing experimental runs compared to a full factorial design. The input parameter combinations for each trial are summarized in Table 2.

Table 2. Experimental Trial Matrix (Input Parameters)

Expt. No.	Power (kW)	Speed (m/min)	Pressure (bar)
1	3.3	2.2	0.7
2	3.3	2	0.9
3	3.3	2.1	0.8
4	3.4	2.1	0.9
5	3.2	2.1	0.7
6	3.3	2.1	0.8
7	3.3	2.1	0.8
8	3.4	2	0.8
9	3.2	2.2	0.8
10	3.2	2.1	0.9
11	3.3	2.2	0.9
12	3.3	2.1	0.8
13	3.3	2	0.7
14	3.4	2.2	0.8
15	3.2	2	0.8
16	3.3	2.1	0.8
17	3.4	2.1	0.7

Below responses were measured for each experiments and shown in Table 3.

Table 3. Experimental results.

Expt.	Ra (µm)	Kw	MRR
1	1.95	0.26	8.4
2	2.6	0.24	9.2
3	2.2	0.27	8.9
4	2.55	0.25	10.2
5	2.1	0.28	8
6	2.25	0.27	8.8
7	2.18	0.27	8.9
8	2.65	0.26	10
9	1.9	0.29	7.9
10	2.4	0.25	8.5
11	2.15	0.23	8.6
12	2.22	0.27	8.8
13	2.55	0.3	9
14	2.05	0.26	9.5
15	2.7	0.31	8.3
16	2.2	0.27	8.9
17	2.35	0.28	9.8

3. RESULTS AND DISCUSSIONS

3.1 AHP Weight Distribution

The Analytic Hierarchy Process (AHP) provided a structured way to assign importance to the selected responses. The results confirmed that industry places the highest priority on surface quality since it directly affects post-processing and functional performance of components. Thus, surface roughness (Ra) received the highest weight (0.45), followed by kerf width (Kw) at 0.35, as it governs dimensional accuracy and tolerance control. The material removal rate (MRR) was given a lower weight (0.20), reflecting the industrial preference to sacrifice productivity if necessary in order to maintain cut quality. Consistency Ratio (CR) was verified to be below 0.1, confirming reliable judgments. This weight distribution ensured that the optimization framework emphasized precision and consistency rather than throughput alone.

3.2 TOPSIS Rankings

The Technique for Order of Preference by Similarity to Ideal Solution (TOPSIS) was then applied to rank the experimental runs based on their closeness to the ideal solution (minimum Ra, minimum Kw and maximum MRR).
Experimental results were normalized to eliminate scale effects. Weighted values were obtained using AHP-derived weights.
Ideal solution: minimum Ra, minimum Kw, maximum MRR. Negative-ideal solution: maximum Ra, maximum Kw, minimum MRR.
Euclidean distances were computed from each solution. Closeness Coefficient (CCi) was calculated as:

$$CC = \frac{S^{+}}{S^{+} + S^{-}}$$

Runs with very high power or low speed, while improving MRR, tended to worsen Ra and Kw due to excess heat input, whereas overly high speeds reduced MRR considerably. The hybrid AHP–TOPSIS approach effectively identified a balanced parameter window that maximized both cut quality and efficiency.

Table 4. TOPSIS results

Run	S^{+}	S^{-}	CCi	Rank
1	0.0107	0.0137	0.561	6
2	0.0157	0.0094	0.375	12
3	0.012	0.012	0.5	9
4	0.019	0.0065	0.255	14
5	0.0077	0.0171	0.689	3
6	0.012	0.012	0.5	11
7	0.0231	0.0026	0.1	17
8	0.0218	0.004	0.155	16
9	0.0059	0.0201	0.773	1
10	0.0079	0.0164	0.675	4
11	0.0093	0.0157	0.629	5
12	0.012	0.012	0.5	10
13	0.0181	0.006	0.248	15
14	0.0157	0.0093	0.371	13
15	0.0093	0.0157	0.629	5
16	0.012	0.012	0.5	8
17	0.0217	0.0042	0.161	16

The TOPSIS results provided valuable insights into the trade-offs between quality and productivity in CO_2 laser cutting. Run 9 (3.2 kW power, 2.2 m/min cutting speed, and 0.80 bar gas pressure) achieved the highest closeness coefficient (0.773), making it the most desirable parameter setting. This condition offered a smoother surface finish and narrower kerf without sacrificing material removal efficiency, confirming its suitability for precision applications. Runs 5, 10, and 11 also ranked highly, indicating that slightly lower power combined with medium to high speeds and balanced pressure levels can deliver competitive performance.

In contrast, the lowest-ranked runs (7, 8, 13, and 14) showed poor optimization scores due to unfavorable trade-offs. These settings either produced rough surfaces with excessive kerf widening at higher power levels, or compromised productivity at very low cutting speeds. This highlights the sensitivity of the process to parameter imbalance—particularly the role of power, which, if excessive, introduces thermal defects, while insufficient power leads to incomplete cutting.

Overall, the results emphasize that the hybrid AHP–TOPSIS framework is capable of

systematically identifying optimal process windows in multi-objective scenarios. Instead of relying on single-response optimization, this method ensured that both quality and productivity requirements were met, offering a practical decision-support tool for industries where precision cutting of metals is critical.

4. CONCLUSION

This study successfully applied a hybrid AHP–TOPSIS multi-criteria decision-making framework to optimize CO_2 laser cutting parameters for metals. The following key conclusions were drawn:

Weight Prioritization – The Analytic Hierarchy Process (AHP) confirmed that industrial preference strongly favors surface quality, with surface roughness (Ra, 0.45) and kerf width (Kw, 0.35) outweighing material removal rate (MRR, 0.20). This ensures optimization focuses on precision rather than throughput alone.

Optimal Process Window – TOPSIS analysis identified the optimal parameter combination as 3.2 kW laser power, 2.2 m/min cutting speed, and 0.80 bar assist gas pressure, corresponding to Run 9, with the highest closeness coefficient (0.773). This setting provided the best trade-off between Ra, Kw, and MRR.

Trade-Off Behavior – Excessive laser power and very low speeds led to thermal damage, higher roughness, and kerf widening, while overly high speeds reduced MRR drastically. Balanced parameter selection is therefore essential for maintaining both cut quality and productivity.

Methodological Superiority – The hybrid AHP–TOPSIS approach proved more robust than single-objective optimization, as it systematically addressed conflicting criteria and offered clear decision-making guidance for complex manufacturing environments.

Industrial Relevance – The findings demonstrate that multi-objective optimization frameworks can significantly improve the reliability, consistency, and efficiency of CO_2 laser cutting. This contributes directly to reduced post-processing, lower production costs, and enhanced dimensional accuracy in real-world applications.

In summary, the proposed hybrid MCDM methodology provides a generalizable, industry-ready decision-support tool for optimizing advanced laser-based manufacturing processes, with potential for application across diverse materials and cutting environments.

REFERENCES

[1] A. K. Dubey, V. Yadava: Multi-objective optimization of Nd:YAG laser cutting of nickel-based superalloy sheet using orthogonal array with principal component analysis, Optics and Lasers in Engineering, Vol. 46, No. 2, pp. 124–132, 2008. https://doi.org/10.1016/j.optlaseng.2007.08.011

[2] Ł. Bohdal, D. Schmidtke: Effect of fiber and CO_2 lasers parameters on the cut surface quality of RVS 1.4301 stainless steel, Journal of Mechanical Engineering and Sciences, Vol. 16, No. 2, pp. 8862–8872, 2022. https://doi.org/10.15282/jmes.16.2.2022.05.0701

[3] B. Varghese, P. Karande: AHP-MARCOS, a hybrid model for selecting gears and cutting fluids, Materials Today: Proceedings, Vol. 52, pp. 1397–1405, 2022. https://doi.org/10.1016/j.matpr.2021.11.142

[4] Y. Qin, Q. Qi, P. Shi, S. Lou, P. J. Scott, X. Jiang: Multi-attribute decision-making methods in additive manufacturing: the state of the art, Processes, Vol. 11, No. 2, p. 497, 2023. https://doi.org/10.3390/pr11020497

[5] N. A. Zolpakar, M. F. Yasak, S. Pathak: A review: use of evolutionary algorithm for optimisation of machining parameters, The International Journal of Advanced Manufacturing Technology, Vol. 115, No. 1, pp. 31–47, 2021. https://doi.org/10.1007/s00170-021-07155-7

[6] S. Chakraborty, V. Kumar: Development of an intelligent decision model for non-traditional machining processes, Decision Making: Applications in Management and Engineering, Vol. 4, No. 1, pp. 194–214, 2021. https://doi.org/10.31181/dmame2104194c

[7] M. Ji, T. Muthuramalingam, D. Saravanakumar, R. Machnik, N. E. Karkalos, P. Karmiris-Obratański: Prediction and optimization of kerf width in laser beam machining of titanium

alloy using genetic algorithm tuned adaptive neuro-fuzzy inference system, The International Journal of Advanced Manufacturing Technology, Vol. 132, No. 11, pp. 5873–5893, 2024. https://doi.org/10.1007/s00170-024-13681-x

[8] M. Tavana, M. Soltanifar, F. J. Santos-Arteaga: Analytical hierarchy process: Revolution and evolution, Annals of Operations Research, Vol. 326, No. 2, pp. 879–907, 2023. https://doi.org/10.1007/s10479-021-04432-2

[9] G. Basar, O. Der: Multi-objective optimization of process parameters for laser cutting polyethylene using fuzzy AHP-based MCDM methods, Proceedings of the Institution of Mechanical Engineers, Part E: Journal of Process Mechanical Engineering, 2025, Article ID: 09544089251319202. https://doi.org/10.1177/09544089251319202

[10] Y. K. Mishra, S. Mishra: A comprehensive review on Nd:YAG and CO_2 laser drilling of fiber-reinforced composites: mechanisms, defects, and optimization, Engineering Research Express, 2025. 10.1088/2631-8695/addb9a

[11] Y. Wang, X. Liao, J. Lu, J. Ma: Optimization method of sheet metal laser cutting process parameters under heat influence, Machines, Vol. 12, No. 3, p. 206, 2024. https://doi.org/10.3390/machines12030206

[12] A. Jamwal, R. Agrawal, M. Sharma, V. Kumar: Review on multi-criteria decision analysis in sustainable manufacturing decision making, International Journal of Sustainable Engineering, Vol. 14, No. 3, pp. 202–225, 2021. https://doi.org/10.1080/19397038.2020.1866708

[13] L. Guo, Y. He, C. Wan, Y. Li, L. Luo: From cloud manufacturing to cloud–edge collaborative manufacturing, Robotics and Computer-Integrated Manufacturing, Vol. 90, p. 102790, 2024. https://doi.org/10.1016/j.rcim.2024.102790

[14] S. Huang, Z. Fu, C. Liu, J. Li: Multi-objective optimization of fiber laser cutting quality characteristics of glass fiber reinforced plastic (GFRP) materials, Optics & Laser Technology, Vol. 167, p. 109720, 2023. https://doi.org/10.1016/j.optlastec.2023.109720

[15] R. Pansare, G. Yadav, M. R. Nagare: A hybrid framework to prioritize the performance metrics of reconfigurable manufacturing system (RMS) using fuzzy AHP–TOPSIS method, The International Journal of Advanced Manufacturing Technology, Vol. 124, No. 3, pp. 863–885, 202 https://doi.org/10.1007/s00170-022-10440-8

Society of Production Engineering

ICPES 2025

40. INTERNATIONAL CONFERENCE ON PRODUCTION ENGINEERING - SERBIA 2025

DOI: 10.46793/ICPES25.200C

University of Nis
Faculty of Mechanical Engineering

Nis, Serbia, 18 - 19. September 2025

INFORMATION SYSTEMS IN THE FUNCTION OF BUSINESS LOGISTICS

Srećko ĆURČIĆ, Dejan Ž. VELJKOVIĆ*
Orcid: 0000-0002-6632-293X; **Orcid:** 0009-0009-3773-9080
[1] University of Kragujevac, Faculty of Technical Science Čačak, Serbia,
*Corresponding author: srecko.curcic@ftn.kg.ac.rs

Abstract: *Today's world is globalized and dependent on the security and timeliness of supply, which is made possible by a high-quality logistics organization. Additional importance to logistics is given by the trend of moving production to areas with lower production costs, whereby the key competitive advantage becomes: quality and costs within the supply chain, in which logistics is one of the most important links. The global market is characterized by constant competition from large companies that want the best possible positions on the market. Companies have to conquer the market by winning over consumers. Therefore, various methods and techniques are applied in order to increase flexibility, reduce costs, and thus the price of the product, while the quality of the product must be at a certain (required) level. Therefore, consumers must be satisfied in terms of performance, design, quality, price and delivery time of the product. One of the current solutions is the lean approach, which is increasingly being applied both in production and service organizations. The aim of this paper is to familiarize with the basic concepts related to logistics services as activities of companies related to product delivery and customer service. In today's market, which is characterized by the competitiveness of products, a suitable logistics service can ensure adequate market share of products and companies, i.e. retention of existing and acquisition of new customers.*

Key words*: Information systems, logistics, customers.*

1. INTRODUCTION

Logistics, thanks to a practical approach to the problem of optimization and organization of cargo movement and information, financial and service flows, ensures the achievement of greater user satisfaction, increased efficiency with reduced costs and obtaining additional value as a basic competitive advantage.

The creation of the basis for designing a new logistics concept solution that contains a plan for connecting the economic, transit and supply functions of the region basically coincides and is linked to the process of development of logistics centers (LC) which imply the concentration, coordination and rationalization of the flow of goods [1]. Logistics centers as an idea and a real form have existed for many years. However, their function, structure and goals of establishment and development have had various roots over time and acquired various forms, with different names and functions, both in terminological and technological terms.

Many companies have yet to take full advantage of digitalization and the application

of new technologies in their supply chains. In today's digital environment, the effective application of new technologies is and will be increasingly essential to make the logistics sector more sustainable, efficient and able to meet the expected growth in cargo demand.

Next-generation robotics, artificial intelligence, automation, blockchain technologies, big data analytics, and sensor applications are just some of the technologies that businesses must consider integrating into their operations and supply chain strategies today [2]. It is vital for companies in the logistics industry to digitize processes to meet increasing demand by increasing efficiency, flexibility and personalizing the customer experience. Therefore, technological neutrality and interoperability must be important parameters when drafting laws and creating new systems supported by research and innovation.

2. LOGISTICS CONCEPT OF THE MODERN ENTERPRISE

A high level of effectiveness and efficiency in any modern logistics center cannot be achieved or imagined without a modern logistics information and communication system.

The information system collects data, processes it, stores, analyzes and distributes information for specific purposes. CBIS (Computer-Based Information System) is an information system that uses computer technology [2]. For the information management process, it is necessary to have a developed research system for collecting, sorting, processing, analyzing, evaluating, storing, storing, distributing, using and applying information.

The information system helps the management in making timely rational decisions on the basis of which some action is taken. Information plays a key role in the decision-making process, so based on this, it can be concluded that the information system can be defined as a network of interconnected components that function together in the process of selecting, processing, storing and sending information, with the aim of helping with decision-making, coordination and control in the organization.

Based on the system approach, an information system can be defined as an organized set of methods, processes and operations for collecting, storing, processing, transmitting and distributing data within an organization, including the equipment used for all of these and the people who carry out these activities. The information system can also be a management information system, which ensures the transfer, storage and processing of data and information necessary for management.

Telematics, as an important development part of the logistics center that receives and stores information with the help of telecommunications devices, represents the link between modern information technologies and the latest achievements in the field of telecommunications. The concept of telematics is related to the system in which all the information that is created by combining transport units, computing, information technology, wireless telecommunications and satellite systems for global positioning flows. There are a number of different telematics systems. Each of these systems represents a different combination of three basic factors: hardware components, data transfer parts and management software. Telematics systems can be divided according to their independence from other systems into independent, dependent and conditionally dependent on auxiliary systems, such as e.g. global positioning systems (GPS), mobile phone networks (GPRS), navigation software, digital maps, routing software (optimization of the movement path) [2].

The optimization of the mentioned flows is conditioned by good logistical support, which ensures satisfactory services for users, through system interoperability, which is defined as the ability of individual systems to function together and successfully fulfill the set goals through the realization of adequate decisions.

Making timely and adequate business decisions requires concise, accurate and relevant information, as key factors in the quality and functionality of customer and logistics services. The collection of data important for the interoperability of the system requires a proactive process that can be realized through wireless sensor networks. Processes related to data processing into relevant information and their routing to the appropriate information logistics system should enable the achievement of economic efficiency, operational readiness, suitability and reliability of logistics and e-logistics systems [1].

The basic task of the information flows created in this way is the transfer and use of information in real time at all locations of the flow of material content through supply networks.

Fast, high-quality, timely and efficient transport services are realized by the integration of technical, human, financial and information-communication resources in traffic and transport. The application of intelligent transport systems conditions changes in the concepts of information and communication systems, imbued with logistical flows related to making business decisions. The importance of the representation of logistics flows in an intelligent form is the basis of the satisfaction of logistics services to the user, through autonomous cooperatives, crucial in conquering the service market and achieving added value as a basic competitive advantage [1].

2.1 Development of green logistics

The situation in the world is currently such that the achievement of green logistics is still far away. An exception is reversible distribution, which has opened up new market opportunities related to waste disposal and recycling. And that is certainly a significant step, but still only a secondary contribution of logistics to environmental protection, while the direct impact is still on the sidelines.

The marginalization of the immediate impact of logistics on the environment is largely due to the often hard-to-see consequences, unlike some other types of industry. As environmental polluters come under increasing pressure from the public, the question is not whether logistics will have to show its greener face, but only when and how. In this sense, the following approaches are generally available to companies whose operations significantly depend on the implementation of logistics processes or logistics companies [2]:

- Top-down approach, when the initiative comes from the government through legal regulations.
- Bottom-up approach, when interest in the environment comes from the industry itself.
- A combination of the previous two approaches, which is usually realized through a certificate.

The first way involves the application of legal repression and is therefore very unpopular. State regulations and interventions more and more directly affect environmental polluters. In this sense, it is necessary to do a cost-benefit analysis, including the costs of removing the damage caused by poor environmental management, and keep in mind that prevention is always better and cheaper than correction.

In the European Union, there is a growing interest in charging the costs of environmental pollution, although this will inevitably lead to an increase in the price of transport services. Although the first principle seems to be the only possible way, the bottom-up approach has its advantages. This approach to solving environmental problems is very popular with manufacturers when business interests coincide with the interests of environmental protection. Namely, due to the great publicity given to ecology, many companies have seen this as their business opportunity. According to research in the USA, 75% of users claim that when choosing a manufacturer, they take into account the ecological reputation, and even 80% are ready to pay more for green products [5]. The third, and perhaps the best approach, is a compromise of the previous two. The practice of introducing standards and obtaining certificates has proven to be very good. If a company meets certain standards in

environmental protection, it receives proof of this in return - a Certificate, which it later uses in marketing activities. As an incentive to this approach, the state can request that the companies it cooperates with have a certified environmental protection quality system. It can have a big initial impact if you consider that the state is often the biggest buyer of goods and services.

Environmental protection is one of the most important and common topics of today's modern society. Efforts undertaken with the aim of permanent integration of logistics activities into the concept of environmental protection should be placed in that context. This is all the more important if we bear in mind that transport, as an integral part of logistics, is a significant source of pollution. Logistics - Environmental supply chains both in terms of exhaust gas emissions and noise.

By sublimating models and trends in the world in the field of logistics development as a friend of the environment, it is assumed that in the near future this topic will deserve the attention it undoubtedly deserves. The principle of combining regulations and stimulating logistics to become more environmentally friendly is probably the best path towards green logistics, which for now in the world is just a nice unfulfilled wish.

2.2 Blockchain in logistics

Blockchain, invented by Satoshi Nakamoto, is a distributed database technology that records digital information with transparency, security and operates without a controlling central authority. Originally developed as an accounting method for the virtual currency Bitcoin, the technology is primarily used to verify transactions within digital currencies, code and insert virtually any document into the blockchain. In this way, an indelible record is created that cannot be changed. The authenticity of records can be verified by the entire community using the blockchain, instead of a single centralized authority.

Blockchain makes logistics more efficient and transparent. Blockchain's ability to act as a ledger makes it the perfect technology to facilitate shipment tracking, global contracts and payment processing throughout the logistics industry.

Blockchain offers an end-to-end solution for companies that want to run a more flexible, organized and efficient business.

It is a system that documents all changes and records in real time, which can help logistics companies become more efficient through a public ledger/data system that records the movements of each shipping container. Armed with that data, companies can implement more optimal routes and eliminate unnecessary steps in the delivery process.

Distributed and decentralized ledgers also reduce bottlenecks and administrative errors. Using smart contracts, traders no longer need brokerage houses, lawyers or third parties to complete tasks.

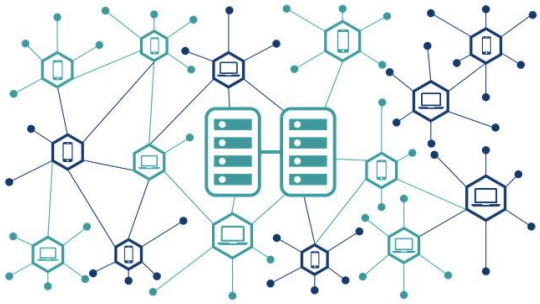

Figure 5. Blockchain in logistics [3]

Smart contracts allow retailers and logistics companies to enter into binding agreements that terminate immediately if all agreed terms are not met. These ledger-based contracts increase transparency and profitability, reducing lead times and costly errors.

2.3 Automation in logistics

Automation or automatic control in logistics refers to the use of control systems, machines or software to improve business efficiency. It usually refers to processes that must be performed in a warehouse or distribution center and that result in minimal human intervention. In fact, along the supply chain (procurement, distribution, customer service, reverse logistics ...) there are many processes that could be automated. For example, Stock Logistic has warehousing and distribution services, both for dry and refrigerated cargo, for any type of industry [7].

The main advantages of logistics automation [8] are:

Access to loading and analyzing data in real time, which enables the launch of reports, which can contribute to making more correct business decisions.

Reduction of errors that cause large costs, because e.g. when entering data manually, there are often numerous errors that result in increased shipping costs.

Organizational control. Systems are usually flexible enough to adapt to the company's business rules and, at the same time, powerful enough to force all users, both internal and external, to follow policies that ensure efficient and profitable delivery.

Customer service, which includes real-time cargo tracking, automatic pickup, adequate insurance and cargo accounting by incorporating it into the order specification.

Scalability and speed, as the system's ability to adapt to increased workload as easily as possible. The software enables easy entry into the system and management with greater adaptability, for example storage. In addition, all freight invoices can be combined into one weekly invoice, regardless of how many shipments we have at each location.

Logistics automation, however, also has several disadvantages, such as a lack of flexibility, both in processes and in process changes. In other words, the possibility of standardizing certain processes in order to execute them more efficiently in an automated system is debatable.

Taking into account the large number of participants in the supply chain consisting of: suppliers, manufacturers, buyers, distributors, etc., the behavior of all of them can be a kind of trap, because they are reluctant to include the necessary and mandatory technological solutions for automation.

The time frame is another element that is often cited against them. Namely, the implementation of an automated system can take an average of 10 years, which together with start-up costs, sometimes results in a return on investment that companies consider low.

3. SOFTWARE FOR LOGISTICS PROCESSES

3.1 MES (Manufacturing Execution System)

Manufacturing management software (MES) is an information system that connects, monitors and controls complex production processes and data flows in an enterprise. The main goal of MES is to ensure efficient running of production operations and improve production performance. MES collects data on raw materials, semi-finished products, products, performance, traceability, material management and work in progress and other activities in the company. This data enables all decision makers to monitor, organize the shop floor and optimize the production process. The advantages of this software are that [4]:

- Enables full control over the production process.
- Eliminates activities that do not create added value.
- Proactively and systematically standardizes and implements processes over locations.
- Enables efficient management of inventory and commodity flows in real time. • Enables real-time traceability and control in the manufacturing supply chain.
- Accelerates analysis of the causes of production downtime and problem solving.

- Continually affects the improvement of product quality.
- Assists in data-driven strategic and operational planning.
- Shortens the production cycle time.
- Increases utilization of machines and equipment.
- Reduces production costs.
- It has a modular character.
- Is the so-called "Tailor made", fully adaptable to user processes.

3.2 Business software (ERP) for production

PANTHEON Manufacture is a program for managing production, which comprehensively and effectively manages processes in the company. The program monitors and optimizes the entire product path, starting from raw materials, semi-finished products and ending with the final product. The program is practically a business-information system that connects and improves all aspects of business so that production, business processes and employees act as a single system [5].

Wholesale is a business model in which products and services are sold in larger quantities to traders, distributors or other business entities who further sell those products to end consumers. Wholesale usually involves the sale of products in larger packages, at lower prices per unit, and is usually done between business entities rather than between business entities and individuals.

Retailers and distributors can buy larger quantities of products at lower prices, which gives them the opportunity for a higher margin on further sales. Also, wholesale is associated with a higher degree of efficiency in the supply chain, transport and storage costs are lower, and inventory monitoring is facilitated.

In wholesale, special business processes and tools are often used to manage sales, procurement, inventory and finances. ERP business software for wholesalers provides comprehensive solutions for managing wholesale operations, including order tracking, inventory management, sales tracking and financial reporting.

There are numerous advantages of using an ERP business system, of which the most important for wholesale are: integration of business processes, inventory tracking, sales and ordering management, financial management, analytics and reporting.

Wholesale business software enables the integration of various business functions and processes within the wholesale business environment, which includes management of procurement, sales, inventory, logistics, finance and all other essential sectors. The integrated system enables significantly better coordination and communication between different services, which results in greater efficiency, while reducing operational errors.

Wholesale involves tracking large quantities of products, which are often located in different locations. ERP business software for wholesale enables tracking of inventory, flow of goods, management of batches or batches of products, along with optimization of inventory management. Thanks to this, the frequency of occurrence of shortages or excess stock is reduced, inventory accuracy is improved and thus product availability is ensured at the right time.

ERP software for wholesale enables wholesale companies to track sales, manage orders and automate processes from the moment of purchase order creation to product delivery, which includes customer tracking, pricing policy management, purchase order processing, warehouse and logistics management, all the way to generating sales reports. At the same time, effective sales management significantly contributes to improving service and increasing customer satisfaction.

Also, ERP software has financial modules that enable monitoring of financial data, bookkeeping, payment management as well as generation of financial reports and analysis. This is crucial for wholesale as it allows tracking of costs, revenue, margins and profitability. Also, the ERP system facilitates financial reporting, tax monitoring and compliance with other legal regulations.

In addition, ERP software for wholesale has the ability to generate reports and analyze data that are crucial for making data-driven business decisions. Wholesale relies on timely information about sales, inventory, demand trends and financial condition. ERP systems also often include advanced analytics and reporting tools that provide access to relevant data in real time, helping management make timely business decisions and identify areas for business optimization. Choosing the right business software for wholesale allows you to save working time through the automation of business processes, the availability of quality information in appropriate reports and overviews, which all together results in more optimal financial management and timely decision-making. At the same time, they can easily monitor the stock of goods, the efficiency of the employees' work, improve and modernize the business.

3.3 Zeo Route Planning Software

Software for planning the path (route), such as e.g. "Zeo route planner" applications are very useful tools for the logistics industry, which provide a systematic approach to business rationalization. In applications of this type, route optimization is performed, significantly facilitating the work of transport companies, which helps companies around the world in planning and optimizing logistics.

By using software for route planning, thanks to the calculation of the most efficient routes, travel time is shortened, fuel costs are minimized, resources are optimized, daily work is simplified, deliveries are ensured on time, and final performance is improved [6].

The option of automatic assignment of deliveries removes many doubts about the planning of delivery logistics, taking into account factors such as the availability and location of the driver. In this way, deliveries are optimally distributed among drivers, which, while reducing manual workload, ensures that every time a delivery is efficiently assigned, increasing the productivity of the entire transport fleet and minimizing delays.

The application of route planning applications also empowers drivers. They have the appropriate real-time data, navigation aids and necessary communication tools. This not only improves their individual efficiency, but also encourages collaboration and creates an informed work environment. Drivers equipped with the right software tools can more easily manage challenges, leading to improved delivery times, greater customer satisfaction and an overall positive contribution to the company's operational efficiency.

The integration of real-time data and navigation tools enables logistics companies to make timely decisions on the fly, whether it's adjusting to traffic conditions, rerouting due to unforeseen circumstances, or optimizing delivery schedules in real-time. Software of this type helps companies reduce operating costs, improve route efficiency and increase the ability to take advantage of business growth opportunities.

By capturing delivery confirmations (proofs) containing photos, customer signatures and notes, companies can verify and accurately communicate the status of each delivery, which contributes to greater customer satisfaction, reduces the possibility of disputes, contributes to trust and consequently loyalty and repeat business.

Route planning software provides accurate real-time ETAs, and estimated time of arrival is known to be a key factor in meeting customer expectations. By sending notifications to customers about the status of their shipments, companies improve the overall customer experience. Providing realistic ETAs contributes to increasing customer satisfaction, loyalty and the number of positive reviews, which in turn increases the logistics company's chances for sustainable growth.

Route planner apps simplify the complex process of shopping search and management. They contain software tools that enable logistics companies to efficiently locate and organize inventory. In addition to shortening the time for performing these tasks, the application also contributes to precise and simple route planning. The result is a

significantly more efficient supply chain, lower operating costs and improved ability to manage logistics operations.

3.4 Inventory management software

Inventory management software, such as AB Soft business information system, have several applications that deal with the issue of inventory management in different ways. The main application usually monitors all changes in warehouses of goods, materials and finished products and processes them in an accounting manner (the ROK application in the case of the AB Soft system). The second monitors the state of consumables and tools, in stock and in use, also with the transfer of data to financial accounting and optionally to operational accounting (MAT application in the case of the AB Soft system).

The third one monitors stocks and changes in packaging records (EVA application in the AB Soft environment). Unlike these applications that also have an accounting component (except for EVE), which connects them to bookkeeping, the software also contains an application that is not intended for bookkeeping purposes, but is primarily intended for storekeepers, for keeping stock records without the influence of bookkeeping changes (the MAGIC application in the AB Soft environment). This application is intended for running the business of one or more warehouses.

In the warehouses, the stock list of items and all changes are monitored: receipts, transfer notes, dispatch notes, requirements and documents of other types. Each document is printed in the appropriate form and remembered with all elements, so that it can always be viewed and printed again. Stock lists are tracked by warehouses or in detail, by places in warehouses with tracking of additional characteristics of items such as shelf life or lot number. By adding barcode readers or mobile android devices and setting certain functionalities on them, work in the warehouse and postings in the application itself are significantly accelerated.

The application uses the code books of programs for material bookkeeping or goods material bookkeeping (MAT or ROK in the AB Soft environment) and during posting it can send posting orders to these programs. In this way, the business system can be organized so that storekeepers using this application monitor cards and stock lists in the warehouses they are in charge of without affecting accounting changes, but also that at the same time each change is forwarded to accounting programs, where accounting is processed. In addition to standard warehouse reports such as stock lists, cards, periodic changes and the like, this application (MAGIC in the AB Soft environment) has special reports that compare the conditions and changes made in the warehouse and accounting applications.

3.5 Software for complaints and customer support - After Sales Service

One of the parameters used to measure the company's success is the base of loyal and satisfied clients. The first impression is the most important, then the user gets an image of the company and later, on the basis of that formed opinion, he decides whether he will consider the company in question again and give him the honor of cooperating again. Once trust is established, the relationship must be nurtured with a touch of subtlety and kindness, as daily challenges pile up and time runs out.

The basic principle that must be implemented in the company statute as well as in the core of every employee is user satisfaction through the efficiency of resolving complaints. In order to understand the needs, target groups and key products, the company should organize a series of initial meetings with the user, and at the same time it must research the market in order to identify the main competitors. Based on the final and complete information, a plan of activities and methods of access to end users are presented. Quality claims and customer support software must offer:

- Accepting calls and calling users, "call me back" option

• Exchange of messages via Email, Online Chat, SMS, social networks, ticketing system • Complaints (complaint processing, monitoring of legal deadlines, resolution)

• Organization of logistics, receiving orders and tracking the status of shipments

• Surveys, market and public opinion research

• Call recording, overview of campaigns and orders

• Creation of sales base, Loyalty program, Tele-marketing.

After a certain period of time, a summary of what has been done is made, based on the collected information, the process and additional activities are adjusted in order to complete and create a comprehensive service that should result in an increase in end-user satisfaction and a new way of identifying and positioning the company on the market.

4. CONCLUSION

The quality of goods and goods transportation is one of the most important factors for ensuring adequate intensity and dynamics of demand and volume of transportation. The tariff system of transport companies should be constantly modernized, while the responsibility for the maintenance, modernization and construction of infrastructure should be assumed by the states. There are many factors that affect logistics, such as globalization, various demographic changes, technological innovations, political instability, but also everyday events. What stands out from the social trends is primarily the fact that there is more and more population, the population is getting older and with these elements we get new demands that turn out to be in the logistics sector. Of course, the well-known reasons for the delay in the application of new technologies based on logistic principles, at least those from the nineties, are behind us. In addition to eliminating the shortcomings of strategic transport documents at the national level, improving the utilization of storage capacities, developing the RTC network, redirecting goods flows to water transport, harmonizing with EU regulations, etc., it is necessary for the state to create a clear policy and strategy aimed at rationalizing and optimizing the distribution and transport of goods, which ultimately leads to the formation and development of logistics centers and intermodalism.

ACKNOWLEDGEMENT

This study was supported by the Ministry of Science, Technological Development and Innovation of the Republic of Serbia, and these results are parts of the Grant No. 451-03-136/2025-03/200132 with University of Kragujevac - Faculty of Technical Sciences Čačak.

REFERENCES

[1] S. Ćurčić, T. Pantelić: *Logistički sistemi*, Tehnički fakultet, Čačak, 2005.

[2] D. Regodić: *Logistika*, Fakultet za informatiku i menadžment, Univerzitet Singidunum, Beograd, 2014.

[3] https://builtin.com/2020

[4] K. Terauchi, M. Suezaki, H. Ishibashi, N. Takahashi, A. Nabeshima, S. Hayashi: Use of smarter distribution for global logistics service: High added value service achieved through integration of procurement, logistics, and information, Hitachi Review, vol. 64, 2015.

[5] J. Macaulay, B. Lauren, G. Chung. "Internet of things in logistics: A collaborative report by DHL and Cisco on implications and use cases for the logistics industry." *DHL Trend Research and Cisco Consulting Services*: pp. 439-449, 2015.

[6] W. M. Feld: *Lean Manufacturing: Tools, Techniques and How to Use Them*, The St. Lucie Press/APICS Series on Resource Management, Boca Raton, Florida, 2001.

[7] The automation process in the logistics sector, available at: https://www.stocklogistic.com/en/logistics/the-automation-process-in-the-logistics-sector/, accessed: 19.07.2024.

[8] https://www.stocklogistic.com/en/the-automation-process-in-the-logistics-sector)/pregledano dana 19.07.2024

Society of Production Engineering

ICPES 2025

40th INTERNATIONAL CONFERENCE ON PRODUCTION ENGINEERING - SERBIA 2025

DOI: 10.46793/ICPES25.211C

University of Nis Faculty of Mechanical Engineering

Nis, Serbia, 18 - 19th September 2025

DEFINING PRODUCTION LOGISTICS FOR INDUSTRY 4.0

Srećko ĆURČIĆ[1]

Orcid: 0000-0002-6632-293X

[1]Department of Mechatronics, University of Kragujevac, Faculty of Technical Sciences Čačak, Serbija

*Corresponding author: srecko.curcic@ftn.kg.ac.rs

Abstract: *This paper defines the production logistics of the company INMOLD Group Požega, Serbia, where the basic segments of production logistics used by this company are listed. Possible improvements in production logistics should enable, in some processes, the introduction of Industry 4.0 with certain segments of the new industrial revolution. The goal of the work is to explain, through analysis, how the production logistics of a plant works, where an idea and an agreement with customers create a product that represents an automated process on the market.*

Keywords: production logistics; industry 4.0; QR code

1. INTRODUCTION

Differentiating the logistics system involves observing subsystems, their interactions, the structure of technological production elements, processes, and activities, environmental impacts, and critical logistics capabilities. These elements represent relevant constraints in the functioning of enterprises characterized by multi-phase and multi-directional transformation processes, from material procurement through production material flows to consumption.

The goal is to identify key elements that achieve spatial, quantitative, temporal, and assortment alignment of production and consumption demands [1].

To understand the logistics of a company, it is necessary to use a systemic and process-oriented approach in analyzing the company, as the company, as a logistics system, is a complex, unified entity comprising multiple interactive processes.

For implementing the interface within a company, the following functions are defined [2]:

- Technical, informational, and managerial functions that support:
- Technical resources (components of production, transportation, and storage) connected to material flows.
- Information system, in terms of data and information collection, storage, transfer, processing, and distribution.
- Business processes, particularly their economic components, which facilitate planning, evaluation, decision-making, control, and monitoring of business operations.

Considering the pressure of innovation and the needs of new generations, companies have taken measures over the years to outsmart their competitors and maintain a leading position in a game where the sky is the limit. To better track the outcomes of improved, faster, and more efficient company measures, humanity has created segments of revolutionary epochs. Today, in production systems, we are living through the fourth industrial revolution, better known as Industry 4.0 [2].

Syber-physical systems, as the foundation of Industry 4.0, utilize modern management software systems equipped with internet addresses for connectivity and addressing through the Internet of Things (IoT). With such technologies, products and production resources become networked and capable of "communicating," enabling new production methods and real-time optimization. The combination of advancements in five core technologies supporting the growth of Industry 4.0 will open new opportunities in this field. Specifically, the technologies present in today's smart factories driving this industry are primarily IoT solutions, artificial intelligence, interfaces, advanced robotics, and 3D printing [3]. In practice, smart factories are now equipped with advanced sensors, embedded software, and robotics that collect and analyze data, enabling better decision-making. Additionally, these solutions reach their full potential when production operation data is combined with operational data from ERP systems, supply chains, customer service, and other enterprise systems. This integration leads to entirely new levels of analysis and insights from previously isolated information.

1.1. Flexible customer orientation

When discussing customer orientation, where client demands frequently shift under the influence of market trends, flexibility represents a significant competitive advantage. For such a company, it is crucial to achieve the ability to individually adapt products and production volumes to meet customer preferences. In this context, numerous solutions enable this type of flexibility, such as automated order handling, flexible manufacturing systems, adaptive logistics, and more.

1.2. Operational excellence

Within the framework of operational excellence, emphasis should be placed on increasing productivity through continuous and dynamic optimization of all processes along the value chain to achieve efficiency aligned with customer demands. This is particularly crucial during periods of technological transition. Technologies supporting such changes are predominantly based on automated real-time production management and process control, improving employee productivity, and synchronizing product design with manufacturing.

1.3. Environment, Safety, and Health

To foster human values and implement a corporate culture that promotes a healthy working environment during the transition to Industry 4.0, solutions tailored to HR activities should be sought. These solutions should focus on improving workplace ergonomics and safety, as well as reducing resource and energy consumption.

1.4. People

According to data from the Education Commission, it is projected that by 2030, more than half of nearly two billion young people worldwide will lack the skills or qualifications necessary to participate in the evolving global workforce. In practical terms, this means that over 50% of tomorrow's human capital may potentially be unprepared to acquire the skills required for future job roles. Therefore, companies must find ways to develop their employees through education and training, preparing them for the demands of the new industrial revolution.

1.5. Solutions

The previously mentioned segments can have varying interpretations and levels of elaboration depending on the industry, down to the level of specific activities. There are four key foundations for implementing technological transformation towards Industry 4.0, consisting of:

Aligned IT/Cloud Platforms: Establishing robust and scalable IT and cloud infrastructures that support data storage, processing, and analysis across the organization.

Machine-to-Cloud Communication: Enabling seamless interaction between machines and cloud platforms to collect, exchange, and process data in real-time, facilitating predictive maintenance, monitoring, and optimization.

Operational Model for Comprehensive Alignment: Designing an operational framework that ensures the synchronization of processes, technologies, and human resources to align with the strategic goals of Industry 4.0 transformation.

Potential Partnerships for Additional Capabilities: Collaborating with external partners, such as technology providers, startups, and academic institutions, to leverage expertise, accelerate innovation, and explore new opportunities.

These pillars are essential for successfully navigating the transition to Industry 4.0 and unlocking its full potential for enhanced productivity and competitiveness. [4].

Figure 1. Basic Elements of Industry 4.0 [4]

Some of the most important technologies (there are 40 in total) involved in the concept of Industry 4.0 include:

Cyber-Physical Systems (CPS): Systems that integrate physical processes with computational ones, enabling real-time monitoring and control.

Radio Frequency Identification (RFID): Technology used for tracking and identifying objects via radio waves.

Near Field Communication (NFC): Short-range communication technology for secure data exchange between devices.

Digital Product Memory (DPM): Embedding digital information within physical products for enhanced traceability and lifecycle management.

Smart Machining: Advanced manufacturing processes integrating intelligence and automation.

M2M (Machine-to-Machine Communication): Enabling direct communication between devices for process efficiency.

MMI (Man-Machine Interaction): Interfaces allowing intuitive and efficient interaction between humans and machines.

Augmented Reality (AR): Overlaying digital content on the real world to assist in tasks such as maintenance and training.

Virtual Reality (VR): Fully immersive simulations for design, testing, and training.

QR Code: Quick-response codes for easy access to product information or processes.

Digital Twin: Virtual replicas of physical systems for real-time monitoring, simulation, and optimization.

Unified Architecture (OPC-UA): A communication standard ensuring interoperability between systems.

Internet of Things (IoT): Connecting devices to collect and exchange data.

Industrial Internet of Things (IoT): A specialized branch of IoT focused on industrial applications.

Cloud Computing: Platforms for scalable storage, processing, and accessibility of data.

Big Data: Managing and analyzing vast amounts of data to gain actionable insights.

2. PRODUCTION LOGISTICS OF THE INMOLD GROUP

In this chapter, the production logistics of Inmold Group is described, with proposals for improvement in certain key production

sequences through Industry 4.0 or its latest technologies.

2.1. Preparation for Production

One of the key activities within a company's production function, alongside determining the optimal production type and creating various production plans, is the activity of production preparation. This activity is undertaken prior to the technological process itself, with the goal of ensuring smooth and uninterrupted production without delays or issues.

The technical preparation of production includes the following activities: determining the production program, preparing materials, preparing tools and equipment, preparing the workplace, and preparing the technological process [2].

As part of determining the production program, the product assortment is defined, the optimal type of production is determined, and the product is designed.

As part of material preparation, the following tasks are performed: selection of materials, definition of material nomenclature, determination of material standards, and ensuring compliance with appropriate material standards.

The preparation of tools and equipment includes the preparation of machines and tools, which involves: selecting and systematizing tools, ensuring tool availability, and maintaining tool records.

To ensure the workplace is ready for the production process, it is necessary to define tasks and duties, organize the workplace layout, and determine the method of workplace servicing. Depending on the servicing system, workplaces can be classified as stable or unstable.

The preparation of the technological process includes selecting the technological procedure and detailing the technological process.

Operational preparation of production includes activities such as creating the operational production plan, scheduling and timing the work operations, and issuing operational documentation. The most important documents in this process are the work order, work schedule, operation list, material requisition, return slip, and similar [5].

To ensure the workplace is prepared for the production process, it is necessary to define tasks and responsibilities, organize the workspace, and determine the method of workplace servicing. Depending on the servicing system, workplaces can be categorized as stable or unstable.

The preparation of the technological process includes selecting the technological procedure and detailing the technological process.

Operational preparation of production encompasses activities such as creating the operational production plan, scheduling and timing work operations, and issuing operational documentation. Key documents in this process include the work order, work schedule, operation list, material requisition, return slip, and similar [2].

2.2. Proposal for Improvement

Due to the high workload and certain "tightening" of deadlines in robot production, there are specific shortcomings in production preparation and organization. When one sector completes its task, such as the painting department waiting for the construction to finish welding, delays occur. Similarly, materials need to arrive at the company on time, and the electrical assembly must complete its tasks before programmers can test the robot and proceed with the remaining steps. The described issues, such as a lack of communication and awareness between departments, often lead to delays and missed deadlines. To address the described issues and improve coordination within Inmold Group, introducing digital enhancements is a crucial step. Digital solutions can streamline communication, optimize workflows, and reduce delays, ensuring smoother production processes and better adherence to deadlines. Analyzing the problem leads to the idea or need for an application accessible to the entire sector, providing critical information about current tasks, their deadlines, and the

individuals responsible. Most importantly, the application ensures the entire team is notified when a task is completed so that the next steps can be initiated immediately, avoiding wasted time. One interface of this application is illustrated in Fig. 2.

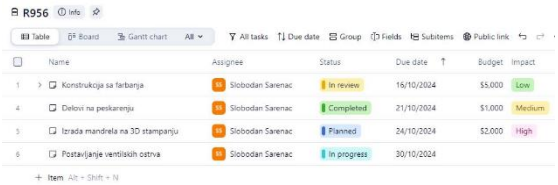

Figure 2. Application Excerpt for Organization, [2]

From Fig. 2, in the top-left corner, we can see which project is currently being worked on. The display shows the active tasks that need to be completed within the specified deadlines. Additionally, it provides information on the person or team responsible for the project, along with the urgency level and allocated budget.

An example of a well-organized project would look like this: After the robot's electrical installation, as well as the installation of all actuators, valves, and other components, software testing of the robot follows. The programming department needs to be informed that the assembly department is nearing the end of its task. This is the key purpose of this application. The software starts being prepared, and as soon as the assembly is completed, the programmers take over their part of the work, ensuring there are no delays.

Advantages: time savings, better-informed personnel about project activities, improved organization, and faster project completion.
Disadvantages: training for use, cost, as this requires everyone to have a company phone, and the application itself is not inexpensive.

2.3. Production Flow

The selection of materials should enable achieving optimal results in production. Therefore, special attention should be given to the quality of materials and their cost. The quality of the material directly affects the quality of the product, while low-quality materials increase the likelihood of breakage and defects during production. The cost of materials impacts the final product's price and the overall financial performance. Additionally, when selecting materials, consideration should be given to the possibility of substituting materials with alternatives. Optimal inventory levels should ensure production continuity while minimizing procurement and storage costs. This issue is addressed not only by the production function but also by the procurement function within the company. Material records must be up-to-date to provide information on both the required and available materials, thereby ensuring production continuity as well. [2]

Workstation preparation includes: defining tasks and responsibilities, organizing the workspace, and establishing the procedure for servicing the workstation.

The process of identifying material requirements

Production planning begins at the production planning level. Management at Inmold regularly analyzes market trends, sales, and demand history. Based on this data, production batches and quantities are planned, enabling efficient inventory management.

Once the production plan is approved, the next step is the preparation of documentation that serves as the basis for material requirements. This documentation includes:

- Bill of Materials (BOM): This document contains all the necessary materials and components required for the production of a specific product. The BOM specifies the types of materials, quantities, and specifications.
- Production Schedule: This document determines the timing and sequence of production. It provides information on when specific materials will be needed.

Once the planning is complete, the production manager initiates a material requisition. This requisition includes:

- Product Identification: Each order is assigned a unique identification number.
- Required Date: Specifies when the corresponding material is needed in the production process.

- Tracking Codes: QR codes (Quick Response codes) are included to facilitate easier tracking and management of materials.

Material requisitions go through an approval process. This process includes:

- Availability Check: The logistics team verifies whether the requested materials are available in the warehouse or if an order needs to be placed with suppliers.
- Financial Approvals: Depending on the value of the requisition, financial approval may also be required.

If material requisitions cannot be fulfilled from the warehouse, the logistics team contacts suppliers. Key aspects of this process include:

- **Creation of Purchase Order:** Based on the approved requisition, the logistics team creates a purchase order containing all necessary information about the materials, quantities, and delivery deadlines.
- Communication and Negotiations: During this step, the logistics team negotiates with suppliers regarding prices, delivery terms, and material quality.

Delivery Tracking: Once purchase orders are signed, the logistics team actively monitors the delivery status. They communicate with suppliers to ensure that deliveries arrive on time and in the specified quantities.

Receiving and Storing Materials

When materials arrive at the factory, the receiving process includes:

- Quality Control: The receiving team inspects the quality and quantity of each delivery. They compare the delivered materials with the purchase order and accompanying documents.
- QR Code Scanning: All received materials are scanned and entered into the inventory management system. This allows for real-time tracking and inventory management.

Storage: After receipt, materials are stored following standardized procedures. The Warehouse Management System (WMS) optimizes warehouse layout, ensuring that materials are easily accessible for production.

Material Issuance: When the production process begins, materials need to be issued.

- Issuance Request: The production manager generates a material issuance request, containing information about the required materials and quantities.
- System Update: Once the materials are issued, the system is automatically updated to reduce the available inventory in the warehouse.

Material Tracking During Production: Throughout the production process, all materials are monitored. This includes:

- Consumption Recording: The system tracks how much material is used in each production batch, aiding in planning for future requirements.

Data Analysis: After production is completed, consumption data is analyzed to identify the causes of any deviations from the planned quantities.

The material requisition management system at Inmold is a comprehensive process that ensures efficiency at every stage, from planning to production. Robust documentation, active management, and technology integration enable the company to maintain high standards of quality and productivity. In this dynamic industry, Inmold continually adapts to changes in demand and market conditions, securing its position as a leader in plastic container manufacturing.

Energy Consumption Monitoring

It includes real-time monitoring of energy consumption and comparison with periodically archived data.

Energy Efficiency: The goal is to use less energy to perform the same task, reducing waste and improving operational sustainability.

Energy consumption data is processed and used for:

- Reporting: Providing detailed energy consumption data, both historical and real-time, along with reports on energy efficiency.
- Real-Time Visualization: Displaying real-time consumption information allows users to see the immediate impact of their processes on efficiency, enabling better monitoring and management.

The production processes of robots demand significant energy consumption. A key issue arises from reactive energy generated by

braking resistance, which is used to stabilize operation and reduce the energy required for starting and subsequently operating the main axis. This axis consumes substantial energy as it bears the heaviest components and performs numerous operations under heavy load.

The challenge lies in the fact that the high energy required to start the axis is only necessary during the initial few cycles until the robot gains significant speed and utilizes its reactive energy effectively. After this phase, high energy is no longer needed.

This is where Industry 4.0 and efficient energy monitoring methods can be highly beneficial.

In addition to the high-quality products, particularly IML robots, Inmold also excels in marketing. A key component of this is a well-designed website, which gives customers the impression that the company is serious and professional in its domain. The website serves as a platform to showcase the company's portfolio effectively.

2.4. Proposal for Improvement

We must consider that effective storage can be enhanced by introducing innovations and implementing Industry 4.0 through the use of QR codes. QR codes have significant applications in manufacturing, especially in the context of Industry 4.0. They enable efficient tracking of products throughout the entire production process.

Application of QR Codes in Manufacturing

Product Identification:

Each product can have a unique QR code containing key information such as:

- Manufacturer Details: Information about the producer or brand.
- Production Date: The date when the product was manufactured.
- Ingredients/Components: A breakdown of materials or components used in the product.
- Additional Details: Other relevant data, such as batch numbers, serial numbers, or certifications.

Benefits:

- Inventory Management: Simplifies stock tracking and helps ensure proper rotation of inventory.
- Product Identification: Enables quick and accurate identification of products during production, storage, and distribution.
- Traceability: Provides end-to-end visibility across the supply chain, making it easier to track the product's journey.
- Consumer Transparency: Offers customers easy access to product details, enhancing trust and satisfaction.

This application of QR codes improves efficiency in managing inventory, quality control, and product traceability while meeting modern manufacturing standards.

2.5. Process Tracking:

QR codes can be utilized at every stage of production, enabling comprehensive tracking of a product's progress. By using QR codes for process tracking, manufacturers can ensure transparency, maintain high-quality standards, and streamline their operations.

Integration with IoT Devices:

In Industry 4.0, QR codes can be connected to the Internet of Things (IoT) to automate processes and enhance efficiency. This integration bridges the gap between physical assets and digital systems, enabling seamless automation and smart factory operations.

Quality and Control:

QR codes can store detailed instructions on quality requirements and standards, allowing workers to quickly verify specifications by scanning the code.

Logistics and Distribution:

In logistics, QR codes can streamline product distribution by providing detailed information about storage locations and transportation routes.

Data Analysis:

Collected production data can be analyzed to improve processes and optimize operations. QR codes facilitate the easy and rapid collection of real-time data, enabling informed decision-making.

The use of QR codes in manufacturing represents an important step toward

digitalization and efficiency improvement, which is essential for the successful implementation of the Industry 4.0 concept.

Goal: Optimize storage processes, accelerate inventory management, and reduce errors in inventory control at Inmold.

Creating Unique QR Codes for All Materials

Description: For each material in the warehouse, create a unique QR code containing the following information: Material name, Code, Quantity,Product description, Expiry date, Supplier.

Feasibility: QR codes can be easily generated using widely available software and printed using standard label printers, making the implementation straightforward and cost-effective.

Installation of QR Code Scanners

Description: Equip warehouse workers with portable QR code scanners or mobile devices with scanning capabilities.

Advantage: This setup allows for quick and efficient scanning of QR codes during material receiving, storage, and issuance processes.

Inventory Management System (IMS)

Description: Develop a software system connected to a materials database. When a QR code is scanned, the system automatically updates inventory levels, tracks the status of each material, and generates reports.

Advantage: Provides real-time inventory data, reducing the risk of shortages or overstocking.

2.6. Employee Training Program

Description: Conduct training sessions for employees on how to use the new scanning and inventory management system.

Advantage: Familiarizing workers with new technologies enhances their efficiency and reduces potential errors.

2.7. Data Analysis

Description: We will track data on material movement within the warehouse, including the time taken to transition between different stages (receiving, storage, and issuing).

Advantage: Data analysis can uncover patterns and help optimize warehouse processes.

2.8. Periodic Maintenance and Updates

Description: Establish a system for regular maintenance and updates of QR codes and software to ensure all data remains accurate and up-to-date.

Advantage: This will prevent issues caused by outdated or inadequate information in the system.

The introduction of QR codes into the material storage process at Inmold Požega represents an innovative solution that will enhance the efficiency and accuracy of inventory management. This system will help reduce errors, accelerate the inventory process, and provide better insight into stock levels, which will have a positive impact on the company's overall operations.

3. CONCLUSION

Based on the previous considerations, several conclusions can be drawn. First and foremost, logistics elements are present in all parts of the business process, particularly in production. A special focus of this work is on production logistics, where particular attention is given to procurement, material control, and production preparation. The efficiency of the production process is ensured through management, quality, and support from information technologies.

This paper presents the production logistics of INMOLD Group in Požega, focusing on the key segments that make up this dynamic and complex field. By analyzing the process from idea to product realization, we have established that production logistics plays a crucial role in optimizing operations and increasing the company’s competitiveness.

The application of Industry 4.0 concepts, such as automation and digitalization, has proven to be highly significant in addressing existing issues in logistics. The introduction of new technologies, such as the IML robot, not only improves production processes but also reduces the time required for manufacturing,

thereby enhancing the company's responsiveness to market demands.

Through the analysis of each segment of logistics, specific challenges have been identified, and solutions have been proposed that rely on innovation and technological advancements. These solutions not only optimize current processes but also prepare the company for future challenges in an increasingly competitive business environment.

We conclude that production logistics is not only the foundation for the company's operations but also a dynamic tool that can support its growth and development. Without adequate production logistics, companies risk losing their competitive advantages. Therefore, strategically focusing on optimizing production logistics, along with the integration of new technologies, is a key step toward successful business operations in the future.

ACKNOWLEDGEMENT

This study was supported by the Ministry of Science, Technological Development and Innovation of the Republic of Serbia, and these results are parts of the Grant No. 451-03-136/2025-03/ 200132 with University of Kragujevac - Faculty of Technical Sciences Čačak

REFERENCES

[1] Dušan Regodić , Automatizacija i proizvodni sistemi , Singidunum, 2011.

[2] INMOLD GROUP: IML roboti i karakteristike, Elaborat: INMOLD GROUP Požega, 2019.

[3] Nenad Stajić: Industrija 4.0 kao poslovno okruženje, Ekonomski fakultet Beograd, EKONOMSKE IDEJE I PRAKSA | BROJ 39 | DECEMBAR 2020.

[4] Industrija 4.0 kao poslovno okruženje, Ekonomski fakultet Beograd, 2016.

[5] "Logistics and Supply Chain Management" by Martin Christopher , 1992.

Society of Production Engineering

ICPES 2025

40th INTERNATIONAL CONFERENCE ON PRODUCTION ENGINEERING - SERBIA 2025

DOI: 10.46793/ICPES25.221S

University of Nis Faculty of Mechanical Engineering

Nis, Serbia, 18 - 19th September 2025

APPLICATION OF THE MATHEMATICAL CONVOLUTION OPERATOR IN THE OPTIMIZATION OF RESOURCE PLANNING AND SCHEDULING

Aleksandar STANKOVIĆ[1,] *, Milica MILUNOVIĆ[1], Goran PETROVIĆ[1]

Orcid: 0000-0001-8841-1258; **Orcid:** 0000-0001-8841-1258; **Orcid:** 0000-0002-3562-9576

[1]University of Niš, Faculty of Mechanical Engineering in Niš, Serbia,

*Corresponding author: aleksandar.stankovic@masfak.ni.ac.rs

Abstract: *This paper explores the application of the mathematical operator convolution in the context of resource planning and scheduling problems in industrial processes. Convolution is used as a tool for modelling the interactions between different operations and resources, while taking into account time dependencies and system capacities. It is applied in the context of resource planning and scheduling problems in industrial processes to model the combined probability distributions of the durations of individual operations. Mathematically, convolution enables the calculation of the overall impact of available resources on task execution over time, through the integration or summation of corresponding functions that describe operations and resource capacities. The advantage of applying the convolution operator in the context of summing operation execution times lies in its ability to accurately model the combined probability distribution of total process durations, taking into account the variability and uncertainty of individual operation times. This approach shows that applying convolution in resource planning and scheduling leads to more efficient schedules, with significant improvements in overall productivity and reductions in operational costs compared to traditional methods. The results confirm the potential of convolution as a mathematical tool for solving complex optimization problems in industrial and manufacturing systems.*

Keywords: *Planning and scheduling of resources, convolution, optimization.*

1. INTRODUCTION

Efficient resource planning and scheduling represent fundamental challenges in industrial and manufacturing systems, directly impacting productivity, cost-efficiency, and competitiveness. Traditional approaches to scheduling often rely on deterministic or heuristic models that may not sufficiently capture the dynamic and uncertain nature of real-world production environments. These methods typically assume fixed processing times and static resource availability, which can lead to suboptimal performance when faced with variability in task durations, machine reliability, or workforce capacity.

In recent years, researchers have increasingly explored advanced mathematical and computational tools to address these challenges. Among these tools, the convolution operator, widely used in fields such as signal processing, probability theory, and control

systems, presents a promising yet underutilized technique in the domain of production planning. Convolution allows for the aggregation of multiple time-dependent functions, enabling the modeling of complex interactions between tasks and resources over time.

Convolution is a mathematical operator in probability and statistics, widely used for deriving the distribution of the sum of independent random variables. In the papers [1] and [2] present the discrete and continuous forms of convolution, while [3] and [4] formalize its mathematical properties. [5] provide exact methods for discrete convolution, and [6] introduce a probability programming language, a computational tool for symbolic and numerical manipulation of probability distributions. In the paper [7] develops a computer-based method for calculating convolutions of statistical distributions, [8] explores normal approximation without standard tables, and [9] extend convolution analysis to the distribution of products of continuous random variables.

This paper proposes the application of the convolution operator as a method for modeling and optimizing resource allocation and scheduling. By interpreting operation times and resource capacities as functions that can be convolved, it becomes possible to represent cumulative effects and dependencies more accurately than through traditional additive models. This approach is particularly useful in environments characterized by uncertainty and variability, as it enables the computation of combined probability distributions for process durations.

The goal of this research is to demonstrate how the mathematical properties of convolution can be applied to generate more reliable and efficient schedules. Through illustrative examples and comparative analysis, the study shows that convolution-based modeling leads to improved utilization of resources, reduced idle times, and lower overall operational costs.

The remainder of the paper is structured as follows: Section 2 provides a theoretical background on convolution and its mathematical foundations. Section 3 presents the methodology for modeling scheduling problems using mathematical convolution, with a focus on stochastic processing times and a practical case study. Finally, Section 4 concludes the paper and suggests directions for future research.

2. THEORETICAL BACKGROUND

The convolution operator is a well-established concept in fields such as signal processing, control theory, and probability. Its strength lies in the ability to describe how two functions interact over time, especially when modelling cumulative effects. Convolution is defined as the integral (or summation in the discrete case) of the product of two functions, where one of the functions is reflected with respect to the origin and shifted along the time axis. For continuous functions $f(t)$ and $g(t)$, convolution is defined as [7]:

$$(f * \mathrm{g})(t) = \int_{-\infty}^{\infty} f(\tau) g(t-\tau)\, d\tau \qquad (1)$$

In its discrete form, which is more applicable to digital and computational models such as production scheduling, convolution is expressed as [10]:

$$(f * \mathrm{g})[n] = \sum_{k=-\infty}^{\infty} f[k] g[n-k] \qquad (2)$$

In probability theory, convolution is used to determine the probability distribution of the sum of two independent random variables. If X and Y are independent random variables with probability density functions f_X and f_Y, then the distribution of the variable $Z = X + Y$ corresponds to the convolution of f_X and f_Y. This property is particularly useful for modeling the total duration of a process composed of multiple operations with variable processing times.

Example 1. *Continuous convolution*: Continuous convolution uses an integral to calculate the overlap of two functions in a continuous domain, which is useful in signal analysis, systems with continuous data, and in

modeling probability density functions. Below is a concrete example of continuous convolution with two functions defined in a continuous time domain.:

$$f(t) = \begin{cases} 1, & 0 \leq \mathrm{t} \leq 2 \\ 0, & \end{cases} \tag{3}$$

$$g(t) = e^{-t}u(t) \tag{4}$$

where $u(t)$ is the unit step function, defined as:

$$u(t) = \begin{cases} 1, & t \geq 0 \\ 0, & t < 0 \end{cases} \tag{5}$$

The main goal is to calculate the convolution of random variables by applying the equation (1). By summing two independent functions, represented by equations (3) and (4), and applying continuous convolution, the total value of the function$(f * \mathrm{g})(t)$ is obtained in the following form:

$$(f * \mathrm{g})(t) = \begin{cases} (e^2 - 1)e^{-t} & t \geq 0 \\ 0, & t < 0 \end{cases} \tag{6}$$

Example 2. *Discrete Convolution*: It is applied to discrete data sequences and is calculated as the sum of the products of the elements of two sequences. Below is an example of discrete convolution with two discrete functions defined over the set of integers:

$$f[n] = \begin{pmatrix} 0 & 1 & 2 \\ 1 & 2 & 1 \end{pmatrix} \tag{7}$$

$$g[n] = \begin{pmatrix} 0 & 1 & 2 \\ 1 & 1 & 1 \end{pmatrix} \tag{8}$$

Since $f[n]$ and $g[n]$ are functions defined for a finite number of values, the summation is performed only over the range where the functions overlap. The calculation procedure using discrete convolution for different values of n is presented below:

$$\text{For } n = 0\text{: valid } (f * \mathrm{g})[0] = f[0] \cdot g[0] = (1) \cdot (1) = 1 \tag{9}$$

$$\text{for } n = 1\text{: valid } (f * \mathrm{g})[1] = f[0] \cdot g[1] + f[1] \cdot g[0] = (1) \cdot (1) + (2) \cdot (1) = 3 \tag{10}$$

$$\vdots$$

$$\text{for } n = 4\text{: valid } (f * \mathrm{g})[4] = f[2] \cdot g[2] = (1) \cdot (1) = 1 \tag{11}$$

By summing two discrete functions defined on the set of integers and applying discrete convolution, the sum is obtained in the following form:

$$(f * \mathrm{g})[n] = \begin{pmatrix} 0 & 1 & 2 & 3 & 4 \\ 1 & 3 & 4 & 3 & 1 \end{pmatrix} \tag{12}$$

In the context of industrial planning and scheduling, conventional approaches often rely on deterministic parameters, assuming that processing times and resource availability are known and fixed in advance. While such models simplify analysis, they fail to accurately capture the stochastic and dynamic nature of real-world production systems. In practice, processing times are frequently subject to variability due to machine breakdowns, operator performance, supply delays, or changes in batch size.

As a result, modern planning and scheduling approaches increasingly incorporate uncertainty modeling, using probability-based methods, fuzzy logic, and robust optimization [11], [12], [13]. However, these approaches often require complex formulations and significant computational resources. In contrast, convolution offers a mathematically elegant and computationally efficient way to aggregate uncertain or time-dependent inputs.

In scheduling applications, convolution can be used to: Model the cumulative effect of successive operations on a single resource, Determine the distribution of total completion time for a set of tasks, Analyze how resource capacity interacts with overlapping or dependent tasks, Capture both temporal dependencies and resource-sharing dynamics through function-based modeling.

This theoretical foundation provides the basis for the methodology proposed in this paper, in which convolution is applied as a tool for modeling and optimizing resource allocation in production systems. By incorporating convolution into planning models, it is possible to obtain more realistic performance estimates, account for uncertainty, and enable more adaptive and efficient production scheduling.

3. MATHEMATICAL CONVOLUTION MODELS FOR STOCHASTIC RESOURCE PLANNING AND SCHEDULING – CASE STUDY

In this section, we present the proposed methodology for applying the convolution operator to optimize resource planning and scheduling in industrial systems. The core idea is to model operations and resource availability as time-dependent functions, whose convolution reflects the cumulative impact of their interaction over time. This approach enables a more realistic representation of variability and dependencies in the production process.

We consider a production environment where multiple operations must be assigned to available resources (e.g., machines, workstations), each with specific capacity constraints. Each operation is characterized by a probabilistic or uncertain processing time, and the objective is to generate a schedule that minimizes total makespan or idle time C_{max}, while respecting capacity limits and operational sequences. Traditional scheduling methods aggregate processing times linearly, which does not account for time overlaps, waiting periods, or variability. To address this, we introduce convolution as a modelling tool that captures how tasks and resources interact over time. In this section, a discrete convolution approach is applied to calculate the overall process completion time defined as the objective function $Z = C_{max}$.

Specifically, the total duration of two independent operations with discrete probability distributions is considered.

Step 1: The first step involves defining the independent random variables X and Y, where:

- X denotes the processing time of the first operation with probability distribution $P(X)$,
- Y denotes the processing time of the second operation with distribution $P(Y)$,

For two discrete random variables X and Y, the probability distribution of their sum $Z = X + Y$ is computed using the discrete convolution formula [10]:

$$\mathrm{P}(Z = z) = \sum_k P(X = n)P(Y = z - n) \qquad (13)$$

Here, $P(Z = z)$ represents the probability that the total duration Z takes the value z, calculated as the sum of the products of all valid combinations $X = k$ and $Y = z - kY$.

This case study demonstrates the application of discrete convolution in determining the probability distribution of the total duration of two consecutive production operations. Operations O_1 and O_2 are assumed to have variable durations due to process uncertainties, which are modeled as two independent discrete random variables X and Y.

The probability functions of these variables are based on empirical data. Let the following discrete probability distributions be defined for X and Y. For variable X (operation O_1), the discrete values and their probabilities presented in table 1 and figure 1.

Table 1. Probability Function of Operation O_1 Duration Modeled by Random Variable X

$X[min]$	6.6	6.8	7.0	7.2	7.4	7.6
$P_x(x)$	0.04	0.13	0.22	0.04	0.17	0.17
$X[min]$	7.8	8.0	8.2	8.4		
$P_x(x)$	0.04	0.08	0.04	0.04		

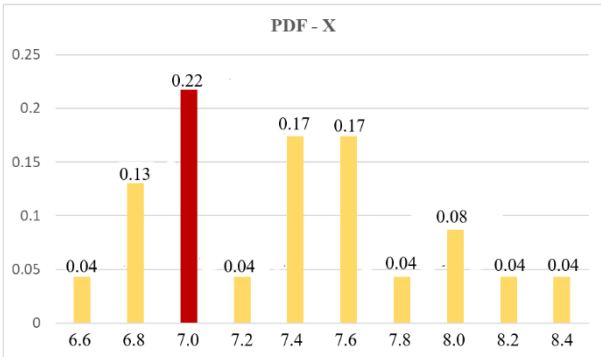

Figure 1. Discrete Probability Distribution of Variable X (Operation O1)

Similarly, for variable Y (operation O_2) presented in tabele 2 and figure 2:

Table 2. Probability Mass Function of Operation O_2 Duration Modeled by Random Variable Y

$Y[min]$	10.6	10.8	11	11.2	11.4	11.6
$P_y(y)$	0.09	0.24	0.14	0.09	0.04	0.14
$Y[min]$	11.8	12	12.2	12.4		
$P_y(y)$	0.04	0.04	0.04	0.09		

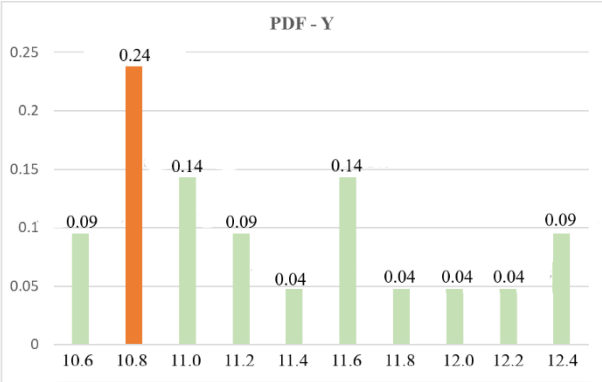

Figure 2. Discrete Probability Distribution of Variable Y (Operation O_2)

$$P_Z(17,2) = P_X(6,6) \cdot P_Y(10,6) = 0{,}0434 \cdot 0{,}09523 = 0{,}0041 \quad (14)$$

$$P_Z(17,4) = P_X(6,6) \cdot P_Y(10,8) + P_X(6,8) \cdot P_Y(10,6) = 0{,}0434 \cdot 0{,}24 + 0.13 \cdot 0{,}095 = 0{,}0228 \quad (15)$$

This procedure is repeated for all values of $z \in Z$ to obtain the complete probability distribution for the total duration $Z = X + Y$.

$$P_Z(20,8) = 0{,}0041 \quad (16)$$

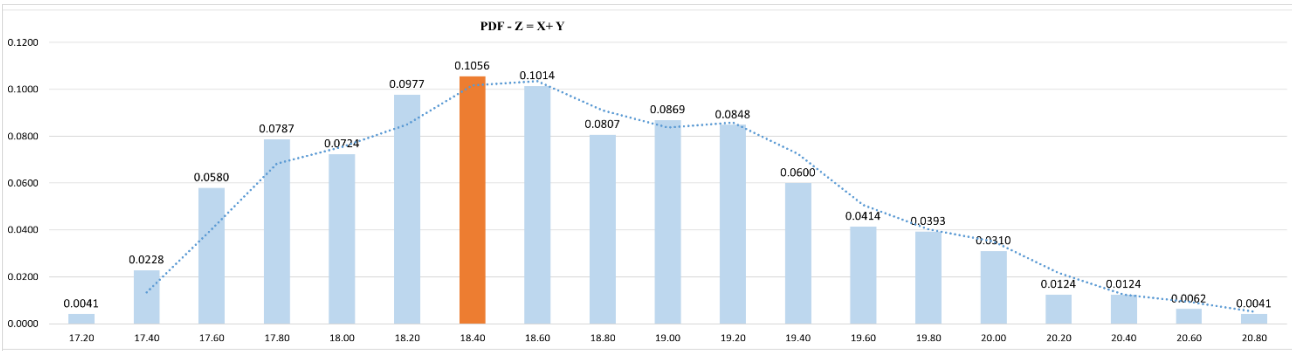

Figure 3. Probability distribution of the objective function $Z = stochCt_{max}$ obtained by applying the discrete convolution operator in the scheduling example.

Step 2: Applying the Discrete Convolution

Operator: The discrete convolution operator is now used to determine the probability distribution of the sum of the two random variables. According to Equation (13), the probability for each possible value of Z is obtained by summing all valid products of $P(X = n)$ and $P(Y = z - n)$, over all values n for which both terms exist. The set of possible values for the variable Z is given by. To compute $P(Z = 17.2)$, for instance, all valid combinations of values $n \in X$ such that $17.2 - n \in Y$ are evaluated. The calculation is performed as follows:

Table 3. Discrete Probability Distribution of Variable Z=X+Y

$Z[min]$	17.2	17.4	17.6	17.8	18.0	18.2
$P_z(Z)$	0.0041	0.0228	0.0580	0.0787	0.0724	0.0977
$Z[min]$	18.4	18.6	18.8	19.0	19.2	19.4
$P_z(Z)$	0.1056	0.1014	0.0807	0.0869	0.0848	0.0600
$Z[min]$	19.6	19.8	20.0	20.2	20.4	20.60
$P_z(Z)$	0.0414	0.0393	0.0310	0.0124	0,0124	0.0062
$Z[min]$	20.80					
$P_z(Z)$	0.0041					

A graphical representation of the objective function $Z = stochCt_{max}$, obtained through the discrete convolution of two independent processing time distributions, is shown in Figure 3.

The graph provides insight into the most likely outcomes and the spread of potential values, which is crucial for robust production planning under uncertainty.

4. CONCLUSION

The implementation of discrete convolution in the calculation of the stochastic objective function $Z = stochCt_{max}$, enables a comprehensive representation of uncertainty in production scheduling. Unlike traditional deterministic approaches that rely solely on average or fixed values, this method considers the full range of possible processing times for each operation, modeled through discrete probability distributions. By convolving these distributions, we obtain a new distribution for the total completion time, which reflects all potential outcomes and their likelihoods. This probabilistic perspective is particularly useful in complex and dynamic production environments, where variability and uncertainty are inherent to the process. The resulting stochastic function Z allows decision-makers to evaluate not only the expected value of the completion time but also the risks associated with delays and the probability of meeting deadlines. Such insights are critical for robust scheduling, capacity planning, and resource allocation, especially in scenarios with high variability or limited buffer times.

In summary, discrete convolution serves as a powerful analytical tool that bridges the gap between theoretical scheduling models and real-world production challenges, offering more resilient and informed planning strategies.

ACKNOWLEDGEMENT

This research was financially supported by the Ministry of Science, Technological Development and Innovation of the Republic of Serbia (Contract No. 451-03-136/2025-03/200109).

REFERENCES

[1] Ross, S. M. (2002). *A first course in probability* (6th ed.). Prentice Hall.

[2] Grinstead, C. M., & Snell, J. L. (1997). *Introduction to probability* (2nd rev. ed.). American Mathematical Society.

[3] Hogg, R. V., & Craig, A. T. (1995). *Mathematical statistics* (5th ed.). Prentice Hall.

[4] Parzen, E. (1960). *Modern probability theory and its applications*. John Wiley & Sons.

[5] Woodward, J. A., & Palmer, C. G. S. (1997). On the exact convolution of discrete random variables. *Applied Mathematics and Computation, 83*(1), 69–77.

[6] Glen, A., Evans, D., & Leemis, L. (2001). A probability programming language. *The American Statistician, 55*(2), 156–166.

[7] Jones, T. A. (1977). A computer method to calculate the convolution of statistical distributions. *Mathematical Geology, 9*(6), 635–647.

[8] Thompson, P. (2000). Getting normal probability approximations without using normal tables. *The College Mathematics Journal, 31*(1), 51–54.

[9] Glen, A., Leemis, L., & Drew, J. (2004). Computing the distribution of the product of two continuous random variables. *Computational Statistics & Data Analysis, 44*(3), 451–464.

[10] Evans, D. L., & Leemis, L. M. (2004). Algorithms for computing the distributions of sums of discrete random variables. Mathematical and Computer Modelling, 0, 1-10. https://doi.org/10.1016/j.mcm.2004.03.002.

[11] Stanković, A., Petrović, G., Turudija, R., Marković, D., & Ćojbašić, Ž. (2025). Hybrid machine learning approach for parallel machine scheduling under uncertainty. Expert Systems with Applications, 279, 127427. https://doi.org/10.1016/j.eswa.2024.127427

[12] Stanković, A., & Petrović, G. (2025). Priority decision rules with a fuzzy MCDM approach for solving flexible job shop problem: A real case study of optimizing manufacturing. Acta Polytechnica Hungarica, 22(1), 143–162. https://doi.org/10.12700/APH.22.1.2025.143.

[13] Stanković, A., Petrović, G., Marković, D., & Ćojbašić, Ž. (2022). Solving flexible job shop scheduling problem with transportation time

based on neuro-fuzzy suggested metaheuristics. Acta Polytechnica Hungarica, 19(4), 209–227. https://doi.org/10.12700/APH.19.4.2022.209.

Society of Production Engineering

ICPES 2025

40th INTERNATIONAL CONFERENCE ON PRODUCTION ENGINEERING - SERBIA 2025

DOI: 10.46793/ICPES25.228M

University of Nis Faculty of Mechanical Engineering

Nis, Serbia, 18 - 19th September 2025

BLOCKCHAIN APPLICATION IN SUPPLY CHAIN MANAGEMENT

Miodrag MANIĆ[1*], Nikola VITKOVIĆ[1], Zorana STANKOVIĆ[1], Vladimir MITROVIĆ [1]

Orcid: 0000-0002-7892-5957; **Orcid:** 0000-0001-6956-8540; **Orcid:** 0000-0001-8974-3916; **Orcid:** 0009-0007-9400-5177;

[1]University of Niš, Faculty of Mechanical Engineering in Niš, Serbia,

*Corresponding author:miodrag.manic@masfak.ni.ac.rs

Abstract: *The use of blockchain technology in various areas of industry and society has gained noteworthy interest over the last few years. Supply chain management is no exception from this trend. The most common terms between blockchain and supply chain are, among others, data transparency, traceability, immutability, security, and a collaborative multi-peer environment. These imply the possible suitability of blockchain adoption for supply chain applications. This paper aims to explore how blockchain can enhance the efficiency of the supply chain by addressing the common steps of the supply chain process. In addition, real-world case studies of blockchain adoption for the supply chain were examined.*

Keywords: *blockchain technology, supply chain management, data bases, case studies*

1. INTRODUCTION

Blockchain technology is increasingly being explored for its potential use across various industry areas and processes they are built upon. The application of blockchain, while not limited to, can be found in finance, healthcare, energy, supply chain, transportation, internet of things (IoT), resource management and others [1]. The specific aim of this paper is to explore the advantages of block-chain in supply chain management (SCM), and how does the technology relate to transparency, traceability and security within supply chain. To understand the value blockchain can bring to SCM, it is essential to know what blockchain tech-neology is. At the broader level, blockchain of is one of the governing technologies behind the concept of Web3, with both blockchain and Web3 being terms that have gained significant attention over the last decades. Their importance lies in the ability to transform conventional processes, redefining how people, businesses, and organizations interact. At its core, Web3 is built around the idea of decentralization, ensuring that no single entity has the monopoly on data, identic-ty, or processes. Blockchain technology serves as the underlying mechanism that enables this decentralization.

To answer the question why decentralization of Web3 is important, how does blockchain conveys this idea, and how

does it all come together in business application such as SCM, the one can start by analysing some major differences between Web3 and its predecessor, Web 2.0 [2]. A key distinction between Web3 and Web 2.0 is the shift from centralized control, where data and processes are managed by companies or authorities, to a decentralized model, where users re-tain ownership of their data. The centralized design of Web 2.0 implied that control was at the hands of the individuals or groups of individuals, such as companies or authorities. This arrangement of data ownership led to major issues with privacy and trust concerning the usage of private data. On the other hand, Web3 promotes ownership of the data by users, who also decide how their own data can be used. Even further, trust is not handed to a particular organization, instead, it is distributed among network participants, who can arrange a mutual agreement on data manipulation through a consensus mechanism on the network.

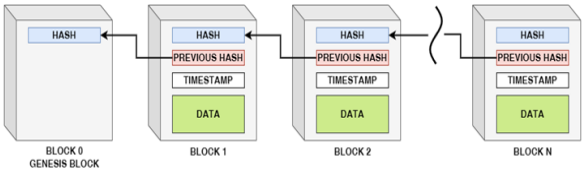

Figure 1. Blockchain structure. Genesis block is the initial block in the chain.

This decentralization can be achieved through blockchain, a form of distributed ledger technology (DLT), which is a technology that distributes data (also referred by records or transactions) at many locations of decentralized network, keeping the same digital copy of the record at each location [3]. DLT can be per-ceived as an option for data storage, which traditionally has been the role of databases. Table 1 summarizes the key differences between DLT and databases, emphasizing that databases support the aspects of centralization, while distributed ledgers oppose it by design. Blockchain utilizes this decentralized approach by grouping records into chronologically linked blocks.

Table 1. Main differences between databases (DB) and distributed ledgers (DL)

Aspect	Database (DB)	Distributed Ledger (DL)
Control / Ownership	Centralized-managed by a single authority or organization	Decentralized-multiple participants share control.
Data Management	Single entity can read, write, update, and delete records.	Each participant maintains a copy; data changes require consensus.
Consensus Mechanism	Not required — trust in central administrator.	Required — participants agree on the state of the ledger (e.g., Proof of Work, Proof of Stake).
Data Immutability	Data can be updated or deleted.	Data is immutable — once written, records cannot be altered.
Transparency	Access limited to authorized users.	Often transparent — all participants can verify transactions.
Data Validation	Central administrator validates data.	Validation done collectively by network participants.

New records must be approved by every peer on the network through a consensus mechanism. When new record is added to blockchain, timestamp is added, cryptographic hash is made for that block, and previous block is linked to it. Figure 1 shows the basic structure of blockchain. Changing the block implies changing the hash of all blocks starting from the one being changed, which requires extremely excessive computing power. This design of blockchain implies security, transparency, traceability, immutability and trustworthiness of records, as no individual can tamper with it on their own. Consequently, trustworthiness is not only relatable to records, it is also introduced within the peers on the network, as every peer

in-volved has the ability to individually view and verify records.

2. BLOCKCHAIN IN SUPPLY CHAIN MANAGEMENT

The very native way to understand how blockchain can be applied to SCM is to view both from their common ground, that is the chain they are referring to. The chain components in SCM refer to every single entity or process that either trans-forms goods towards their final form or conveys various customer services.

The blockchain, representing the linked (and ordered) chain (or list) of data blocks, as depicted in Fig. 1, can be used to trace this entire process in SCM, from start to finish, step by step. The authors in [4] state that end-to-end traceability of the product is achieved by recording relevant information within each block about the product's nature, quality, quantity, ownership, and location. This further implies that the successful implementation of blockchain in SCM must provide answers to some important questions about the product's status at each step of the supply chain. Figure 2 gives an overview of some of these questions, in the example of the farm-to-fork principle mentioned for the agri-food sector. Of course, most of these questions can be generalized for SCM in other sectors as well.

Example, a food company uses blockchain to track the journey of mangoes from farm to supermarket. There are the steps:

1. **Farmer** records the harvest details (date, location, batch ID) on the blockchain.
2. **Transporter** adds data about shipment temperature and route.
3. **Processor** logs packaging and quality inspection results.
4. **Distributor** updates storage and delivery records.
5. **Retailer** scans the product QR code to verify the entire history.
6. **Customer** can trace the origin and freshness via the blockchain record.

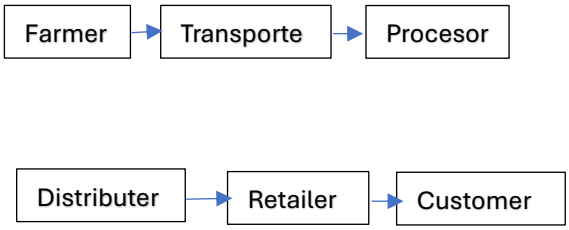

Figure 2. Blockchain Ledger (Shared, Immutable, Transparent)

Each block in the blockchain contains:

- Timestamp
- Participant ID
- Product data (e.g., batch no., temperature, location)
- Digital signature for validation

Benefits for all are:

- Traceability of products in real-time
- Reduced fraud and counterfeit goods
- Faster recalls in case of contamination
- Increased trust among all participants

In order for blockchain to be able to address these questions of SCM, some important aspects of its implementation and implications have to be considered. Authors in [5] point out that productive and reliable blockchain network in SCM relies on adequate tracking system for products. A tracking system, in case of blockchain technology, is essentially an IoT system that enables the product to be verified by its identity and location (e.g., RFID and GPS tags, QR codes), and by its property (e.g., biochemical condition). This verification is done by sensors that scan the product for its identity, sense physical properties of the product and gather information about environmental conditions (e.g., storage temperature and humidity, shakings during handling and transportation). The capabilities of the blockchain technology are further facilitated by direct implementation of data obtained from the tracking system into the blockchain's self-executing smart contracts, a code that includes terms of agreement, which automatically run when coded conditions are met. The real-time data obtained from IoT system can be used to drive instant actions based on the specific values. For instance,

payment procedure can be initiated as soon as the predetermined conditions are met, without the need to involve intermediaries such as banks or administration. One of the examples of automatic execution of smart contracts is when delivery status of the product is confirmed by its RFID tag, GPS tag or QR code at delivery location. Even further, if the delivery deadline has been exceeded or handling procedures weren't respected, a penalty clause coded directly within the terms of agreem ent can be executed. Smart contracts can also act as an alert system that notifies all interested entities in case of undesired condition, such as temperature being out of range during storage. This process on blockchain network eliminates the involvement of intermediaries, reducing time and cost of the administrative and billing procedures.

Another benefit of having sensory data recorded on blockchain and being used in automated smart contracts is that the trust between businesses and consumers can be solidified, on the basis that fraud occurrences can be prevented, and authenticity and ethical sourcing can be verified at each stage. Of course, this is backed up with data on blockchain network being immutable, transparent and traceable. The end consumers may appreciate knowing detailed information about the origin, production process, storage conditions and distribution of the product. Another critical benefit of traceability in SCM is the case when the product can be contaminated, as is the case with food and beverages in agri-food and HoReCa (hotels, restaurants, catering) sectors, or with medications in pharmaceutical industry. Blockchain can help in tracking the origin and distribution of the product, making it more feasible to do necessary recalls, minimizing the health risk and optimizing time and cost resources [6][7].

The discussion in this section analyzed the possibilities of blockchain by using food supply chain as an example, but the entire concept can be generalized to other domains (e.g., manufacturing, pharmaceutical, HoRECa), with having in mind the expected specifics of the particular domain. The following section backs up theoretical part of this discussion by exploring two case studies from agri-food sector that represent successful cases of blockchain implementation in this field.

3. CONCLUSION

The integration of blockchain technology into supply chain process was ana-lysed by looking at how blockchain can help at every step of the supply chain. Benefits of the system can be found in transparency, traceability and security of the data that improve trust with customers and stakeholders, process automation using smart contracts and more efficient reaction in case of fraudulent or contam-inated products. Emphasis is also placed on IoT systems that should support blockchain implementation. Presented case studies showcased that blockchain can be successfully implemented in supply chain applications for both large corporates on one side, and small and medium enterprises on other side. Discussion about ethical aspect of blockchain reveals that there is an initiative to drive the technology towards responsible usage, and that certain ethical subject have al-ready been addressed. The very recently systematized Ethical Guidelines for Blockchain Systems can serve as general guide for blockchain systems in supply chain applications, as well as in other domains.

REFERENCES

[1] Abou Jaoude, J., & Saade, R. G. (2019). Blockchain applications–usage in different domains. Ieee Access, 7, 45360-45381.

[2] Buldas, A., Draheim, D., Gault, M. and Saarepera, M., 2022, November. Towards a foundation of Web3. In International Conference on Future Data and Security Engineering (pp. 3-18). Singapore: Springer Nature Singapore.

[3] Liu, X., Farahani, B., Firouzi, F. (2020). Distributed Ledger Technology. In: Firouzi, F.,

Chakrabarty, K., Nassif, S. (eds) Intelligent Internet of Things. Springer, Cham. https://doi.org/10.1007/978-3-030-30367-9_8

[4] Saberi, S., Kouhizadeh, M., Sarkis, J. and Shen, L., 2019. Blockchain technology and its relationships to sustainable supply chain management. International journal of production research, 57(7), pp.2117-2135.

[5] Azzi, R., Chamoun, R.K. and Sokhn, M., 2019. The power of a blockchain-based supply chain. Computers & industrial engineering, 135, pp.582-592.

[6] Ellahi, R.M., Wood, L.C., Bekhit, A.E.D.A.: Blockchain-based frameworks for food traceability: a systematic review. Foods, 12(16), p.3026 (2023).

[7] Garcia-Torres, S., Albareda, L., Rey-Garcia, M., Seuring, S.: Traceability for sustainability–literature review and conceptual framework. Supply Chain Management: An International Journal, 24(1), pp.85-106 (2019).

Session 5:

Artificial intelligence in manufacturing

Society of Production Engineering

ICPES 2025

40th INTERNATIONAL CONFERENCE ON PRODUCTION ENGINEERING - SERBIA 2025

DOI: 10.46793/ICPES25.234U

University of Nis Faculty of Mechanical Engineering

Nis, Serbia, 18 - 19th September 2025

ARTIFICIAL INTELLIGENCE AND CNC MANUFACTURING

Milica UTVIC[1*], Bojan STOJCETOVIC[1], Milan MISIC[1], Aleksandar SKULIC[1], A. Kokic ARSIC[1], Martina PETKOVIC[1], Strahinja DJUROVIC[1]

Orcid: 0009-0004-9127-6340; **Orcid:** 0000-0001-7418-6985; **Orcid:** 0000-0002-9695-7776; **Orcid:** 0000-0002-5332-3087; **Orcid:** 0009-0004-6310-6379; **Orcid:** 0000-0003-3210-3250; **Orcid:** 0000-0003-3971-7984;

[1]Kosovo and Metohija Academy of Applied Studies, Leposavić, Republic of Serbia *Corresponding author: milica.utvic@akademijakm.edu.rs

Abstract: *The integration of artificial intelligence into CNC (Computer Numerical Control) manufacturing is one of the key development directions within the concept of Industry 4.0. Modern manufacturing systems increasingly rely on intelligent algorithms that enable dynamic process adaptation, increased precision, cost reduction and better quality control. This paper analyzes the application of artificial intelligence in the field of CNC manufacturing, with a focus on machine learning, predictive maintenance, optimization of cutting parameters, and automation of the programming process. Special attention is paid to the possibilities offered by systems based on real-time data, as well as the integration of sensor and diagnostic technologies to improve the reliability and productivity of the manufacturing system. Based on theoretical and empirical analysis, the aim of the paper is to point out the prospects for the transformation of traditional CNC production into intelligent and self-adaptive production systems of the future, as well as a general overview of the situation in Serbia when it comes to this topic.*

Keywords: *artificial intelligence, CNC manufacturing, machine learning, Industry 4.0, automation, predictive maintenance.*

1. INTRODUCTION

The modern era is characterized by the accelerated digitalization of production processes, aimed at achieving greater efficiency, flexibility and adaptability to an increasingly demanding market. Within the concept of Industry 4.0, which involves the integration of intelligent technologies into all segments of industrial production, a special place is occupied by the application of artificial intelligence in the management of machine processes. With the advent of Industry 4.0, CNC machines are no longer isolated systems, but become part of intelligent networks in which artificial intelligence plays a key role in automation, adaptive control and predictive maintenance of production [1]. One area in which the impact of these technologies is particularly pronounced is CNC (Computer Numerical Control) production, as the foundation of modern machining.

CNC technologies enable automated control of machine tools based on digitally defined parameters, thereby ensuring high precision, reliability and reproducibility in material processing. However, with the introduction of artificial intelligence, CNC production is moving to a new technological level — from traditional

automation to an intelligent and self-managing system. Thanks to machine learning algorithms, neural networks and real-time data processing, AI allows CNC machines to analyze operating conditions themselves, optimize processing parameters, predict failures and adapt to new requirements without human intervention.

2. THEORETICAL FRAMEWORK

2.1. Development of CNC technologies

CNC is a computer-controlled machine tool technology that has significantly improved the precision, reproducibility, and automation of manufacturing processes over the decades. In addition, CNC systems are an essential part of modern manufacturing technology, enabling high accuracy, repeatability, and control over complex machining processes [2]. Unlike traditional hand-operated machines, CNC machines perform tasks according to digital instructions, usually written in G-code. The application of CNC technology has enabled the production of complex geometric shapes with minimal deviation, which is essential in industries such as the automotive, aerospace, medical, and precision engineering industries.

The development of CNC technology has enabled the introduction of intelligent control systems that increase the precision and automation of manufacturing processes in the mechanical engineering industry [3].

The evolution of CNC systems from pneumatic and electromechanical controls to computerized systems has also followed the growth of market needs for greater flexibility and faster adaptation to serial and individual production. In the last decade, the development of the Internet of Things (IoT), cloud technologies and sensor networks has laid the foundation for further digital transformation of production in the direction of so-called smart factories.

2.2. The foundation of artificial intelligence

Artificial intelligence represents the ability of computer systems to simulate the processes of human intelligence, such as learning, reasoning, decision-making and adapting to new conditions. Artificial intelligence-based approaches allow CNC processing systems to dynamically adjust cutting parameters, optimize tool trajectories and anticipate maintenance needs, significantly improving production efficiency [4]. Within the framework of technical disciplines, machine learning (ML) is of special importance, as a subdiscipline of AI, which allows systems to recognise forms from large amounts of data and automatically improve their performance. Typical applications of AI in industry include intelligent process control, anomaly detection, predictive diagnostics, visual inspection of products and optimization of production parameters. The combination of AI with sensory and Big Data systems enables the implementation of advanced concepts such as self-sustaining production systems and adaptive production cells.

3. PREDICTIVE ANALYTICSAND QUALITY MANAGEMET IN CNC MANUFACTURING SUPPORTED BY AI

The integration of artificial intelligence into CNC manufacturing is one of the most important steps towards realizing the concept of a smart factory and improving the competitiveness of modern industrial systems. The introduction of AI technologies into the control of CNC machines enables automatic adaptation and optimization of the machining process, which results in improved product quality, reduced costs and reduced production time. The application of artificial intelligence in the quality management of CNC manufacturing contributes to the reduction of errors, increased precision and optimization of the control process in real time [5]. On the other hand, machine learning, as a subdiscipline of artificial intelligence, provides the opportunity to develop algorithms that, based on large data sets, can recognize patterns and predict system behavior. In CNC manufacturing, these algorithms analyze data obtained from sensors that monitor parameters such as cutting speed

and force, tool temperature, vibration and other factors that affect the quality and efficiency of the process. Based on this information, the system can automatically adjust cutting parameters in real time, thereby achieving optimal productivity and reducing tool wear.

One of the most important applications of AI in CNC systems is predictive maintenance. Instead of routine or reactive maintenance, AI allows monitoring the condition of machines in real time and predicting potential failures before they occur. This approach significantly reduces downtime, increases reliability and extends the life of equipment, which represents significant financial and operational benefits for manufacturing companies.

In addition, traditional CNC machine programming requires expertise and time to create precise instructions in the form of G-code. With the introduction of AI, systems are being developed that can automatically generate and optimize G-code based on CAD models, thereby reducing production setup time and reducing the possibility of human error. These systems can also adjust programs according to changes in material, operating conditions or quality requirements.

3.1.AI-powered quality control

The integration of intelligent systems into CNC manufacturing enables adaptive process control and real-time decision-making, which is the essence of the digital factory concept [6]. On the other hand, the integration of AI into quality control systems allows the use of sensor data, images, and video for automatic detection of defects and deviations. Machine learning and computer vision algorithms enable fast and precise inspection of parts, which increases the reliability of control and reduces the need for manual inspection. Within the framework of the Industry 4.0 concept, CNC machines are becoming intelligent systems that use real-time data to optimize production processes and improve product quality [7].

4. ADVANTAGES AND CHALLENGES OF IMPLEMENTING ARTIFICIAL INTELLIGENCE IN CNC PRODUCTION

4.1 Advantages of applying artificial intelligence

Machine learning, as one of the key areas of artificial intelligence, allows systems to independently improve their performance based on data, which is of great importance for the automation of CNC manufacturing processes. [8] The application of artificial intelligence in CNC manufacturing brings a number of significant advantages that affect the improvement of productivity, quality and cost-effectiveness of manufacturing systems. The main advantages include: increased efficiency and accuracy, preventive and predictive maintenance, reduction of human error, flexibility of production, but also improvement of product quality.

Integrated inspection and quality control systems based on AI provide high accuracy in defect detection, thereby reducing the number of rejected parts and increasing end-user satisfaction.

4.2 Challenges of applying artificial intelligence

Despite its many advantages, the implementation of AI in CNC manufacturing also faces a number of challenges that may slow down or hinder its widespread application:

high costs of implementation and maintenance, technical complexity and integration, dependence on data quality and quantity, data security and protection, resistance to change, and personnel training.

Overall, although the application of artificial intelligence in CNC manufacturing carries significant potential for improving production capacities, its successful development and implementation depend on careful management of technological, organizational, and financial aspects.

5. EXAMPLES FROM PRACTICE IN THE REPUBLIC OF SERBIA

Although the application of artificial intelligence in CNC manufacturing in Serbia is still in its early stages, there are significant developments and concrete examples that indicate the growing interest and potential for digital transformation of the industry. The digitalization of production in domestic factories increasingly includes the application of automation and intelligent systems as a prerequisite for increasing efficiency and competitiveness [9]. The main challenges are focused on the modernization of the existing production base and the integration of intelligent systems into traditional production processes.

The Serbian automotive industry, with a large number of suppliers and small and medium-sized enterprises, has started to apply elements of AI in CNC manufacturing to improve quality and efficiency. Companies such as MK Grupa and Magna Petrovac are introducing machine condition monitoring systems based on sensors and software solutions that use elements of machine learning for predictive maintenance.

Some machine shops and factories in the Republic of Serbia, such as Potisje from Subotica and VISS Masina from Niš, are collaborating with technological faculties to develop AI models for optimizing metalworking processes. Within these projects, AI is used for automatic analysis of vibrations and heat during the operation of CNC machines in order to improve maintenance planning and reduce the risk of failures.

Technology incubators in Belgrade and Novi Sad, such as Startit Center and ICT HUB, support the development of startups working on integrating AI into industrial production systems, including CNC equipment. These projects include the development of software for intelligent quality control and automated programming, which is an innovative approach that is gradually being applied in practice.

In addition, industrial incubators play a key role in supporting innovation and digital transformation of small and medium-sized enterprises in Serbia, thereby improving competitiveness in the modern market [10].

Although Serbia is in a phase of gradual digitalization, these examples indicate a positive trend in the adoption of modern technologies. Additional efforts are needed in the areas of education, financing and infrastructure to fully exploit the benefits that AI brings to CNC manufacturing.

6. THE FUTURE OF AI APPLICATIONS IN CNC PRODUCTION

Given the increasingly intensive digitalization of industry and global trends in the application of artificial intelligence in production processes, the Republic of Serbia is facing significant challenges and opportunities in the field of CNC production. In order to achieve a competitive position in the European and global markets, it is necessary to direct development towards several key directions, namely: strengthening scientific research and development infrastructure, encouraging digital transformation in enterprises, human resource development and education, but also improving infrastructure and digital security. Overall, focusing on these development directions will enable Serbia to build a sustainable and competitive industrial sector based on the most modern technologies, which will contribute to economic growth and improving the quality of production.

7. CONCLUSION

The integration of artificial intelligence into CNC manufacturing is a key step towards the digital transformation of industrial processes in accordance with the principles of Industry 4.0. The application of AI technologies allows for a significant increase in efficiency, precision and flexibility of production, as well as a reduction in maintenance costs and improvement of product quality. Machine learning and predictive maintenance contribute to greater reliability and continuity of CNC machines, while automation of programming and quality

control reduces human errors and speeds up production cycles. However, the successful implementation of AI in manufacturing systems requires overcoming numerous challenges, such as high implementation costs, technical complexity of integration, the need for adequate infrastructure, and the development of qualified personnel. In the Republic of Serbia, progress in this domain depends on strong cooperation between academic institutions, industry and state institutions, as well as systemic measures that encourage digitalization and innovation.

The future of CNC manufacturing in Serbia is closely linked to the adoption and further development of artificial intelligence, which will enable the creation of intelligent and self-adaptive production systems. With this approach, the domestic industry can strengthen its competitiveness in the global market and contribute to economic growth based on knowledge and technologies.

REFERENCES

[1] N. Tomić: CNC technologies and process management. Belgrade: Faculty of Mechanical Engineering, 2019, p. 45.

[2] S. Kalpakjian and S. R. Schmid, *Manufacturing Engineering and Technology*, 7th ed., Boston: Pearson Education, 2013, str. 842.

[3] N. Stojanović and Z. Marković, CNC technologies in modern mechanical engineering, Novi Sad: Faculty of Technology, 2018, p. 75.

[4] Y. Zhang, L. Wang, and J. Zhou, "AI-driven optimization in CNC machining: A review," *Journal of Manufacturing Systems*, vol. 62, pp. 325-340, 2022, стр. 330.

[5] T. Milićević, Quality Management in CNC Production Using Artificial Intelligence (Master's Thesis). University of Niš, Faculty of Mechanical Engineering, 2022, p. 63.

[6] M. Grujić, Intelligent Production Systems, Belgrade: University of Belgrade, Faculty of Mechanical Engineering, 2020, p. 98.

[7] D. Jovanović, Industry 4.0 – digital transformation of production. Belgrade: Faculty of Mechanical Engineering, University of Belgrade, 2019, p. 139.

[8] M. Milošević, Fundamentals of Artificial Intelligence and Machine Learning, Novi Sad: Technical Book Publishing House, 2018, p. 120.

[9] D. Perić, Application of automation in modern production in Proceedings, Belgrade: Institute for Automation and Production Systems, 2018.

[10] M. Savić, "Industrial incubators as a support for innovation in Serbia," Proceedings of the Faculty of Economics, vol. 45, no. 3, pp. 112–125, 2019, p. 118.

Society of Production Engineering

ICPES 2025

40th INTERNATIONAL CONFERENCE ON PRODUCTION ENGINEERING - SERBIA 2025

DOI: 10.46793/ICPES25.239T

University of Nis
Faculty of Mechanical Engineering

Nis, Serbia, 18 - 19th September 2025

USE OF GENERATIVE AI IN THE CROATIAN MANUFACTURING INDUSTRY

Maja TRSTENJAK[1*], Biljana CVETIĆ[2], Vanina MACOWSKI DURSKI SILVA[3], Bernhard AXMANN[4],
Orcid: 0000-0002-6157-3940; **Orcid:** 0000-0002-2398-4327;
Orcid: 0000-0002-8869-3272; **Orcid:** 0000-0002-0190-6547;
[1] Faculty of Mechanical Engineering and Naval Architecture, University of Zagreb, Ivana Lučića 5, 10 000 Zagreb, Croatia
[2] Faculty of Organizational Sciences, University of Belgrade, Jove Ilića 154, 11 000 Belgrade, Serbia
[3] Federal University of Santa Catarina, R. Eng. Agronômico Andrei Cristian Ferreira, s/n - Trindade, Florianópolis - SC, 88040-900, Brazil
[4] The Technical University Ingolstadt of Applied Sciences, Esplanade 10, 85049 Ingolstadt, Germany
*Corresponding author: maja.trstenjak@fsb.unizg.hr

Abstract: *As global manufacturing shifts toward the principles of Industry 5.0, emphasizing human-centricity, sustainability, and resilience, Generative Artificial Intelligence (GenAI) has emerged as a key enabler of next-generation industrial systems. While international research highlights the potential of GenAI tools to optimize workflows, enhance decision-making, and foster collaboration between humans and machines, the practical application of these technologies in the Croatian manufacturing industry remains underexplored. This study seeks to address that gap by examining the current state, usage patterns, and future potential of GenAI adoption among professionals in Croatian manufacturing companies.*
A structured online survey was distributed to 682 manufacturing professionals across Croatia, yielding 33 complete responses. The questionnaire gathered data on demographics, company characteristics, and the use of GenAI in general applications (e.g., ChatGPT, DALL·E), office productivity tools (e.g., Microsoft Copilot, Google Gemini), and automation systems. The results reveal that while awareness of GenAI is relatively high, actual usage is still low. Text-based tools are the most widely used, primarily for content generation and operational support. Use of AI-enhanced office tools and automation platforms is less common, and the intensity of usage varies significantly across respondents. Despite the modest adoption levels, the study finds strong interest in expanding the use of GenAI technologies: 85% of respondents indicated they plan to increase usage in the near future. However, challenges such as limited infrastructure, lack of training, and inconsistent integration across workflows remain prevalent. The findings underscore the need for targeted policy support, investment in digital infrastructure, and cross-sector collaboration to unlock the full potential of GENAI in the Croatian manufacturing sector. This research provides a valuable empirical foundation for future studies and strategic initiatives aimed at fostering sustainable, intelligent, and human-centered manufacturing systems in Croatia, in line with the broader goals of Industry 5.0.

Keywords: *Industry 5.0, Generative AI, artificial intelligence, manufacturing*

1. INTRODUCTION

The rapid development of artificial intelligence (AI), and particularly Generative AI (GenAI), is redefining the future of manufacturing worldwide [1]. As industries move from the automation-driven paradigm of Industry 4.0 toward the human-centric and sustainable vision of Industry 5.0, the role of AI technologies is expanding beyond process optimization into the realms of creativity, personalization, collaboration, and resilience [2]. Among these technologies, GenAI stands out for its capacity to generate new content, simulate scenarios, support decision-making, and facilitate intuitive human-machine interaction, making it a key enabler of next-generation manufacturing systems.

Globally, recent studies have explored how GenAI can contribute to the sustainability goals of Industry 5.0, including energy efficiency, predictive maintenance, digital twin enhancement, and user-focused design [3]. Research has demonstrated that GenAI-powered systems can optimize resource use, support ethical governance, and enable proactive problem-solving by generating synthetic data, guiding adaptive planning, and improving the interaction between humans and machines. Integrations such as GenAI-based chatbots, explainable AI in fault diagnostics, and hybrid models for additive manufacturing are reshaping industrial ecosystems across sectors—from large-scale production to small, experimental factories.

Despite the growing global momentum, the use of generative AI in the Croatian manufacturing industry remains underexplored, both in terms of academic research and practical application. Croatian manufacturing firms, many of which are small or medium-sized enterprises (SMEs), face unique challenges and opportunities in digital transformation [4]. These include limited resources for AI experimentation, fragmented data infrastructures, and a need to balance productivity with the well-being of workers and environmental responsibility. Understanding how GenAI can be meaningfully implemented in this context is essential for aligning Croatia's industrial development with European Union strategic goals and broader Industry 5.0 ambitions.

This paper aims to address this gap by investigating the current state, challenges, and potentials of generative AI adoption in Croatian manufacturing.

2. RELATED WORK

The emergence of Industry 5.0 has redefined the role of technology in manufacturing by shifting the focus from efficiency alone to a balanced emphasis on human-centricity, sustainability, and resilience. Within this evolving framework, Generative Artificial Intelligence (GenAI) has emerged as a transformative enabler, offering substantial potential to reshape the manufacturing landscape, including in Croatia. This literature review synthesizes key insights from recent academic contributions that explore GenAI's integration across various industrial functions and its alignment with Industry 5.0 principles.

A growing body of work positions GenAI as central to achieving sustainability goals in Industry 5.0. One foundational study develops a strategic roadmap that identifies ten key GenAI functions contributing to data-driven decision-making, operational resilience, and sustainable innovation. Crucially, the authors emphasize that while these functions are individually impactful, their synergistic application provides enhanced benefits when deployed in a structured sequence [3].

The integration of GenAI with digital twin (DT) technology has also been recognized as a critical area of innovation, particularly in predictive maintenance and fault diagnostics. GenAI enhances DTs by generating synthetic data, enabling real-time simulations, and improving anomaly detection, thus addressing key limitations such as data

scarcity. These contributions align strongly with Industry 5.0 by incorporating explainable AI (XAI) and edge computing for enhanced transparency and real-time responsiveness [5].

In the domain of adaptive social manufacturing, researchers have proposed frameworks that link GenAI functions to specific sustainability dimensions. Through a combination of content analysis and system dynamics modeling, these studies show that GenAI can promote inclusivity, ethical governance, and efficient resource use—core tenets of human-centric industrial design. Importantly, this work recognizes the need for balanced implementation that honors both technological and societal objectives [6].

Further exploring specific tools, several publications examine the impact of well-known GenAI models such as ChatGPT and DALL·E on production optimization, supply chain management, and customer engagement. These tools demonstrate tangible benefits in operational efficiency and responsiveness but also bring challenges related to data privacy, bias, and interoperability, suggesting a need for thoughtful integration strategies [7].

Other studies focus on GAI's accelerative role in bridging Industry 4.0 and Industry 5.0, particularly through four key dimensions: smart manufacturing, smart working, smart products/services, and smart supply chains. These works underline GAI's capacity to enhance mass customization, human-machine collaboration, and real-time logistics, though they also call for further domain-specific research on organizational impacts and system integration [2].

From a user interface perspective, the application of customized GenAI chatbots has proven valuable in human-machine interaction (HMI). By facilitating real-time data access and predictive troubleshooting via natural language interfaces, these tools exemplify the user-friendly, intuitive interaction environments envisioned in Industry 5.0. Such systems also support enhanced machine learning model training and autonomous decision-making, reinforcing the shift toward operator empowerment [8].

The concept of parallel manufacturing, introduced through the DeFACT framework, extends GenAI's application to decentralized collaborative production. Incorporating digital, robotic, and human workers, the model relies on blockchain, scenario engineering, and GAI to support trust, adaptability, and customization, even in low-trust environments [9].

In the area of additive manufacturing (AM), Hybrid Additive Manufacturing (HAM) envisions a cyber-physical-social system where GenAI contributes to the digital training and behavioral modeling of intelligent products. This new paradigm expands AM's scope beyond material creation to include socially responsive and adaptive entities, underscoring GenAI's potential in future-ready design systems [10].

On a broader scale, frameworks such as AIDAF (Adaptive Integrated Digital Architecture Framework) demonstrate how GenAI can be integrated into enterprise architecture, particularly in healthcare and manufacturing. These systems aim to support cost reduction, strategic decision-making, and open, collaborative platforms, such as the proposed DSA&OHP2030 initiative, that align with Society 5.0 and Industry 5.0 visions [11].

Concrete implementations of GAI-enhanced systems in manufacturing environments further validate the technology's real-world potential. For instance, one study documents the deployment of a robotic cell and voice assistant, resulting in significant cycle time reduction and improved worker well-being, demonstrating that GenAI-driven solutions can effectively support safer and more satisfying work environments [12].

Moreover, the design of GPT-powered industrial bots for small factories illustrates how generative AI can monitor worker well-being and optimize operations in a personalized and context-sensitive manner. These tools not only assist in fault detection

and root cause analysis but also offer environment-specific recommendations to operators, reinforcing I5.0's human-centered philosophy [13].

The integration of AIGC (AI-Generated Content) within Product Lifecycle Management (PLM) is also gaining traction. One reviewed study introduces a human-in-the-loop framework that embeds AIGC across the manufacturing lifecycle while addressing current technological and ethical challenges, laying a foundation for more collaborative and resilient production systems [14].

AI-DT integration continues to be a focus area, with frameworks that leverage predictive analytics and scenario simulations to support autonomous decision-making and system adaptability. These models are essential for establishing global standards and ensuring scalability in future industrial ecosystems [15]. The importance of human-centric equipment health monitoring (EHM) is emphasized in studies that incorporate user needs into advanced model architectures, such as EDA-CGANs and knowledge distillation techniques. By incorporating XAI for interpretability, these approaches align technical innovation with operator expectations and safety, a defining characteristic of Industry 5.0 [16].

Finally, a comprehensive vision for human-robot collaboration (HRC) stresses the development of cobots that are context-aware, socially intelligent, and capable of balancing safety with performance. This interdisciplinary perspective underscores the role of GAI as a catalyst for enabling dynamic and personalized interaction between humans and machines [17].

3. METHODOLOGY

The research was conducted to gain insights into how generative artificial intelligence (GenAI) tools and AI-powered office solutions are being utilized within the Croatian manufacturing sector. A structured, multi-phase methodology was employed, with the primary data collection instrument being a detailed questionnaire developed specifically for professionals working in manufacturing environments.

The survey instrument consisted of 19 questions, divided into four thematic sections. The first section collected demographic and professional background information, such as respondents' gender, job role, industry segment, years of experience, and the size of their company. The second section explored the use of general-purpose GAI tools—such as ChatGPT and DALL·E—in work-related contexts. The third part addressed the adoption of generative AI features integrated into commonly used office software, including tools like Microsoft Copilot and Google Gemini. The final section captured broader trends in automation and digital technology adoption at the organizational level.

Prior to broad distribution, the questionnaire was piloted with a small number of manufacturing professionals to test the clarity and relevance of the questions. Based on the pilot feedback, minor adjustments were made to ensure the survey would be both accessible and meaningful. To accommodate the target group, the final version was translated into Croatian.

The finalized survey was distributed via email to 682 professionals employed in Croatian manufacturing companies. From this outreach, 33 completed responses were received, resulting in a response rate of roughly 4.8%. Despite the relatively limited sample size, the data gathered offers an important first look at how GenAI technologies are entering the manufacturing workspace in Croatia—highlighting early use cases, benefits, and practical limitations encountered during adoption.

4. RESULTS

The study gathered responses from a total of 33 professionals working in the Croatian manufacturing industry. The majority of respondents were male (91%), with only 9% identifying as female. Respondents

represented a diverse range of industry sectors, including metal processing, food and beverage, printing, tourism-related manufacturing, and service industries. Companies of all sizes were represented: 35,3% of participants worked in small enterprises (1–50 employees), 23,5% in medium-sized firms (51–250), and another 29,4% in large companies (251–1000).

Most participants had significant industry experience, with 58,8% reporting more than 10 years in the field. Job roles varied and included operations managers, production directors, procurement officers, and mid-level management positions, offering insights from different decision-making and operational layers within manufacturing firms.

When asked about the purpose of using general generative AI tools (e.g., ChatGPT, DALL·E), a strong preference for text-based tools was observed. Approximately two-thirds of respondents used tools like ChatGPT for content generation and query-based support. A small number indicated using image-based tools, while others reported no use of general GenAI tools.

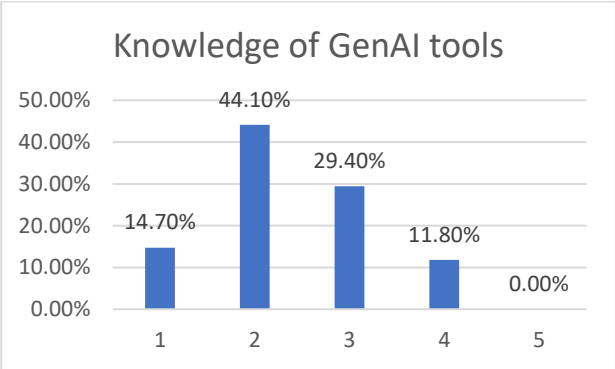

Figure 1. Assessment of knowledge about working with general generative AI tools

In terms of intensity of use, responses were widely distributed. About 20,6% respondents rated their usage as moderate (level 3 on a 5-point scale), while 70,6% reported low to minimal use (levels 1–2). Only a few respondents reported high or very high intensity of use (8,8%).

Satisfaction with GenAI tools also showed variation. While 44,1% respondents expressed moderate satisfaction, 14,7% reported very high satisfaction, and 17,6% expressed low satisfaction.

Notably, 85,3% stated that they plan to increase their use of generative AI tools in the future, indicating strong perceived value and interest in broader adoption.

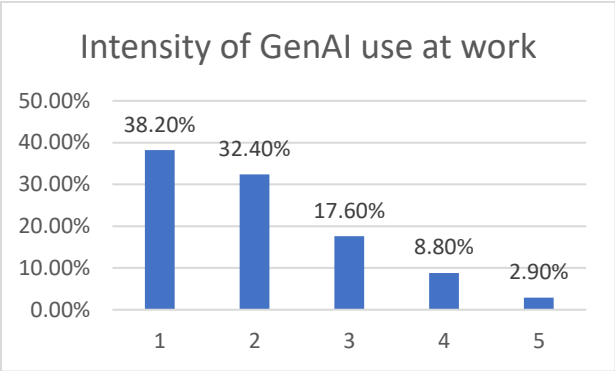

Figure 2. Intensity of use of special office generative artificial intelligence at work

Regarding AI-enhanced office tools such as Microsoft Copilot or Google Gemini, the most common uses were for document summarization (50%) and email writing (38,2%). However, usage was less widespread than general-purpose GenAI tools. Many respondents either did not use these tools or used them at a low intensity.

As with general GenAI tools, satisfaction levels for office AI tools were mixed, with most respondents expressing moderate satisfaction, while a smaller portion were highly satisfied or dissatisfied.

Participants also reported on their use of automation technologies within their organizations. Common applications included order processing (26,5%), inventory management (26,5%), document handling (44,1%), and warehouse operations (26,5%). However, 38,2% respondents indicated no use of automation tools, highlighting a gap in broader digital transformation efforts among certain firms.

The intensity of automation tool use varied, with the largest share reporting minimal or low usage, suggesting that automation adoption is still in its early stages in parts of the Croatian manufacturing sector.

5. DISCUSSION

The results of this study offer an important early insight into the application of Generative AI (GenAI) technologies in the Croatian manufacturing industry, particularly within the broader transition toward Industry 5.0. While global literature increasingly recognizes the transformative role of GenAI—from enhancing digital twins and predictive maintenance to enabling human-machine collaboration—the findings from this survey show that Croatia is still in the early stages of practical adoption.

First, the survey responses reveal that a majority of manufacturing professionals are aware of and have experimented with GenAI tools, particularly text-based platforms like ChatGPT, which are used primarily for information retrieval and content generation. However, the intensity of use remains modest, with most respondents reporting low to moderate engagement. This suggests that while there is interest and awareness, full integration into daily workflows has not yet been achieved. Still, the high percentage of respondents who plan to increase their use of GenAI in the future (85%) reflects strong latent potential and openness to technological innovation.

Interestingly, the adoption of generative AI features embedded in office tools—such as Microsoft Copilot or Google Gemini—is less widespread, indicating that enterprise-level AI deployments may face barriers such as software availability, digital infrastructure limitations, or lack of internal training and support. Similar patterns were observed with automation tools, which remain underutilized across the surveyed companies. While some respondents reported the use of tools for document management, inventory control, and order processing, a significant number of professionals (over one-third) indicated no current use of automation technologies. These results echo concerns noted in the introduction, such as resource limitations, fragmented IT ecosystems, and a cautious organizational culture—factors that may slow the pace of digital transformation in Croatian manufacturing SMEs.

Another important aspect is the human-centric dimension. Most respondents occupy middle or upper management positions with extensive professional experience, making them key actors in shaping technological strategies. Their moderate satisfaction levels suggest that existing GenAI tools are not yet fully aligned with local workflows or expectations, pointing to the need for more tailored, context-sensitive AI solutions. Furthermore, low reported use of GenAI for creative or collaborative tasks may indicate a lingering perception of AI as a support tool rather than a co-creative partner—an issue that resonates with broader debates in Industry 5.0 literature.

Finally, it is worth noting that although the survey had a limited sample size (33 respondents), the diversity in company sizes and industry segments adds depth to the findings. The trends identified in this research highlight the need for targeted policy support, cross-sector education, and structured investment in digital infrastructure to ensure the Croatian manufacturing sector can fully leverage the potential of generative AI technologies.

6. CONCLUSION

This study represents one of the first empirical investigations into the use of generative artificial intelligence within the Croatian manufacturing industry. While adoption levels remain in their early phases, the findings reveal a clear interest in and openness to expanding the use of GenAI tools among industry professionals. Text-based generative AI applications—such as ChatGPT—are the most commonly used, while more advanced or embedded tools,

including office AI features and automation systems, are still emerging.

The survey confirms several core challenges facing Croatian manufacturers: a lack of infrastructure, limited use of automation, and uneven digital maturity across enterprises. At the same time, it highlights substantial to support this evolution, several recommendations emerge:

- Education and training initiatives should be introduced to improve GAI literacy and implementation skills at all organizational levels.
- Public policy and funding should prioritize small and medium-sized enterprises, helping them overcome financial and technological entry barriers.
- Collaborative projects involving universities, technology providers, and manufacturers can serve as innovation testbeds for Croatian-made GAI applications tailored to local industry needs.

Future research should extend this pilot study by including larger samples, qualitative interviews, and longitudinal tracking to evaluate the evolving role of generative AI in Croatian industry. Doing so will help ensure that the country not only follows global trends but also actively shapes the development of a sustainable, innovative, and human-centered industrial ecosystem.

REFERENCES

[1] K. P. Agrawal, "Towards Adoption of Generative AI in Organizational Settings," *J. Comput. Inf. Syst.*, vol. 64, no. 5, pp. 636–651, Sep. 2024, doi: 10.1080/08874417.2023.2240744.

[2] P. Boareto, A. Szejka, E. Loures, F. Deschamps, and E. Santos, "Accelerating Industry 4.0 and 5.0: The Potential of Generative Artificial Intelligence," presented at the INNOVATIVE INTELLIGENT INDUSTRIAL PRODUCTION AND LOGISTICS, IN4PL 2024, PT I, M. Dassisti, K. Madani, and H. Panetto, Eds., 2025, pp. 456–472. doi: 10.1007/978-3-031-80760-2_29.

[3] M. Ghobakhloo, M. Fathi, M. Iranmanesh, M. Vilkas, A. Grybauskas, and A. Amran, "Generative artificial intelligence in manufacturing: opportunities for actualizing Industry 5.0 sustainability goals," *JOURNAL OF MANUFACTURING TECHNOLOGY MANAGEMENT*, vol. 35, no. 9, pp. 94–121, May 2024, doi: 10.1108/JMTM-12-2023-0530.

[4] M. Mustapić, M. Trstenjak, P. Gregurić, and T. Opetuk, "Implementation and Use of Digital, Green and Sustainable Technologies in Internal and External Transport of Manufacturing Companies," *Sustainability*, vol. 15, no. 12, Art. no. 12, Jan. 2023, doi: 10.3390/su15129557.

[5] E. Mikolajewska, D. Mikolajewski, T. Mikolajczyk, and T. Paczkowski, "Generative AI in AI-Based Digital Twins for Fault Diagnosis for Predictive Maintenance in Industry 4.0/5.0," *APPLIED SCIENCES-BASEL*, vol. 15, no. 6, Mar. 2025, doi: 10.3390/app15063166.

[6] P. Jourabchi Amirkhizi, S. Pedrammehr, S. Pakzad, and A. Shahhoseini, "Generative Artificial Intelligence in Adaptive Social Manufacturing: A Pathway to Achieving Industry 5.0 Sustainability Goals," *Processes*, vol. 13, no. 4, Art. no. 4, Apr. 2025, doi: 10.3390/pr13041174.

[7] S. Sai, R. Sai, and V. Chamola, "Generative AI for Industry 5.0: Analyzing the Impact of ChatGPT, DALLE, and Other Models," *IEEE Open Journal of the Communications Society*, vol. 6, pp. 3056–3066, 2025, doi: 10.1109/OJCOMS.2024.3400161.

[8] K. S. Kiangala and Z. Wang, "An experimental hybrid customized AI and generative AI chatbot human machine interface to improve a factory troubleshooting downtime in the context of Industry 5.0," *Int J Adv Manuf Technol*, vol. 132, no. 5, pp. 2715–2733, May 2024, doi: 10.1007/s00170-024-13492-0.

[9] J. Yang, Y. Wang, X. Wang, X. Wang, X. Wang, and F.-Y. Wang, "Generative AI Empowering Parallel Manufacturing: Building a '6S' Collaborative Production Ecology for Manufacturing 5.0," *IEEE Transactions on*

Systems, Man, and Cybernetics: Systems, pp. 1–15, 2024, doi: 10.1109/TSMC.2024.3349555.

[10] V. Terziyan and O. Kaikova, "Hybrid Additive Manufacturing: A Convergence of Physical, Digital, and Social Realms Driven by Generative AI," presented at the ADVANCES AND TRENDS IN ARTIFICIAL INTELLIGENCE: THEORY AND APPLICATIONS, IEA-AIE 2024, H. Fujita, R. Cimler, A. Hernandez-Matamoros, and M. Ali, Eds., 2024, pp. 427–441. doi: 10.1007/978-981-97-4677-4_35.

[11] Y. Masuda *et al.*, "Vision Paper for Enabling Generative AI Digital Platform Using AIDAF in Healthcare and Manufacturing Industry," in *Human Centred Intelligent Systems*, A. Zimmermann, R. Schmidt, L. C. Jain, and R. J. Howlett, Eds., Singapore: Springer Nature, 2025, pp. 177–190. doi: 10.1007/978-981-97-8598-8_16.

[12] "Redefining Human-Machine Collaboration: Industry 5.0 to Improve Safety and Efficiency | IEEE Latin America Transactions." Accessed: Jul. 29, 2025. [Online]. Available: https://latamt.ieeer9.org/index.php/transactions/article/view/9412

[13] H. Wang, M. Liu, and W. Shen, "Industrial-generative pre-trained transformer for intelligent manufacturing systems," *IET Collab. Intell. Manufact.*, vol. 5, no. 2, p. e12078, Jun. 2023, doi: 10.1049/cim2.12078.

[14] J. Leng *et al.*, "AIGC-empowered smart manufacturing: Prospects and challenges," *Robotics and Computer-Integrated Manufacturing*, vol. 97, p. 103076, Feb. 2026, doi: 10.1016/j.rcim.2025.103076.

[15] "From Simulation to Autonomy: Reviews of the Integration of Artificial Intelligence and Digital Twins | International Journal of Precision Engineering and Manufacturing-Green Technology." Accessed: Jul. 29, 2025. [Online]. Available: https://link.springer.com/article/10.1007/s40684-025-00750-z

[16] J.-F. Dang, T.-L. Chen, and H.-Y. Huang, "The human-centric framework integrating knowledge distillation architecture with fine-tuning mechanism for equipment health monitoring," *Advanced Engineering Informatics*, vol. 65, p. 103167, May 2025, doi: 10.1016/j.aei.2025.103167.

[17] N. Berx, W. Decré, J. De Schutter, and L. Pintelon, "A harmonious synergy between robotic performance and well-being in human-robot collaboration: A vision and key recommendations," *Annual Reviews in Control*, vol. 59, p. 100984, Jan. 2025, doi: 10.1016/j.arcontrol.2024.100984.

Society of Production Engineering

ICPES 2025

40th INTERNATIONAL CONFERENCE ON PRODUCTION ENGINEERING - SERBIA 2025

DOI: 10.46793/ICPES25.247B

University of Nis Faculty of Mechanical Engineering

Nis, Serbia, September 18 – 19, 2025

DYNAMIC FLEXIBLE JOB SHOP SCHEDULING PROBLEM BASED ON GENETIC ALGORITHM

Katarina BRENJO[1,] *, Aleksandar JOKIĆ[1], Milica PETROVIĆ[1]
Orcid: 0000-0001-8854-8246; **Orcid:** 0000-0002-7417-4244; **Orcid:** 0000-0002-4950-6518;
[1]University of Belgrade – Faculty of Mechanical Engineering, Belgrade, Serbia
*Corresponding author: kbrenjo@mas.bg.ac.rs

Abstract: *The increasing frequency and sophistication of cyber-attacks on manufacturing systems demand that scheduling frameworks evolve to include cybersecurity considerations. The integration of dynamic and cybersecurity-related factors into the flexible job shop scheduling problem modelling is essential to better reflect real-world manufacturing conditions. This paper addresses the flexible job shop scheduling problem in a dynamic manufacturing environment, affected by three unexpected disturbances: the arrival of new jobs into the manufacturing system, job cancellations, and machine tool breakdowns. Particularly, some of these disturbances are caused by cyber-attacks targeting manufacturing systems, increasing risks to production and operational reliability. These disturbances have a significant impact on manufacturing efficiency, affecting delivery deadlines, resource utilization, and overall processing time. In this research paper, a genetic algorithm is applied as a robust artificial intelligence technique suitable for solving NP-hard combinatorial problems such as the dynamic flexible job shop scheduling problem. The algorithm facilitates real-time adjustment through rescheduling mechanisms, aiming to achieve a specified optimization objective – minimizing the total processing time (makespan). The proposed method is implemented in the MATLAB® environment and validated through simulations using relevant benchmark problems. Experimental results demonstrate that the proposed methodology significantly improves adaptability and performance in dynamic manufacturing environments, while maintaining high efficiency despite sudden interruptions. Overall, the proposed approach advances intelligent and adaptive real-time rescheduling in a flexible job shop environment, supporting the Industry 4.0 concept by enhancing the flexibility, efficiency, and performance of intelligent manufacturing systems that can withstand both disturbances and emerging cyber threats.*

Keywords: *dynamic flexible job shop scheduling, genetic algorithm, rescheduling, manufacturing systems, optimization, disturbances, cyber-attack.*

1. INTRODUCTION

In the era of Industry 4.0, manufacturing systems are transforming into intelligent, self-organizing, and data-driven environments that integrate both physical operations and decision-making processes. Within this context, the scheduling of operations plays a critical role in enabling flexibility, efficiency, and responsiveness to dynamic and unpredictable conditions [1]. While these developments improve efficiency and flexibility, they also expose manufacturing environments to a wide

range of disturbances, including those caused by cyber-attacks [2]. These disturbances can result in severe consequences, posing significant challenges to traditional scheduling approaches.

The Flexible Job Shop Scheduling Problem (FJSSP) is a well-known NP-hard combinatorial optimization problem that extends the classical Job Shop Scheduling Problem (JSSP) by allowing operations to be performed on one of several alternative machine tools. This flexibility provides a more realistic representation of manufacturing environments, but it also significantly increases computational complexity. When such scheduling problems occur in dynamic environments, where the system is affected by unplanned events, it becomes the Dynamic Flexible Job Shop Scheduling Problem (DFJSSP) [3]. Unlike static models, the DFJSSP better reflects real-world manufacturing conditions by incorporating the need for rescheduling in response to unexpected changes.

This research paper addresses the DFJSSP in the presence of three types of disturbances: (i) the arrival of new jobs [4], (ii) the cancellation of existing jobs [5], and (iii) machine breakdowns [6]. Notably, some of these disturbances represent a direct consequence of cyber-attacks targeting manufacturing systems.

To respond effectively to these challenges, a scheduling approach based on Genetic Algorithms (GA) is proposed [7]. The GA-based approach enables real-time adaptation through dynamic rescheduling, taking into account the current state of the manufacturing system. The algorithm is designed to minimize total processing time (makespan) [8].

Previous studies have demonstrated the effectiveness of GA in addressing key disturbances in manufacturing systems. For instance, [7] developed a modular GA-based framework for dynamic adaptation that supports both regeneration and modification of populations following disruptions, such as machine tool breakdowns and job cancellations, thereby facilitating the effective continuation of the search process. Similarly, the authors of [9] applied GA to dynamic job-shop scheduling with continuous arrival of new jobs, optimizing multiple objective functions and outperforming priority rule-based approaches under both deterministic and stochastic conditions. The research in [10] extended GA applications to real-time rescheduling by considering critical disturbances, such as machine failures, new job arrivals, and job cancellations, thereby enabling the rapid generation of new optimal schedules without reevaluating completed operations. In addition, [11] introduced a novel GA designed to handle machine tool breakdowns, achieving significant reductions in makespan compared to conventional methods by efficiently managing interruptions without deferring operations. Furthermore, [12] proposed an improved GA combined with a rolling scheduling strategy and specialized mutation operators, demonstrating enhanced local search capabilities and objective function performance when handling new job arrivals and machine downtimes in dynamic environments. These contributions highlight the suitability and flexibility of GA-based methods for robust and adaptive scheduling in complex manufacturing environments characterized by high levels of uncertainty and disturbance occurrence.

The developed methodology is implemented in the MATLAB® environment, which supports the representation of alternative process plans, the management of dynamic constraints, and the visualization through Gantt charts.

This paper is organized as follows: Section 2 formulates the DFJSSP and defines the associated constraints and objectives. Section 3 presents the proposed GA-based solution methodology. Section 4 provides the experimental evaluation and simulation results discussion. Section 5 concludes the research paper outline. Section 6 provides essential directions and insightful suggestions for future research.

2. DFJSSP FORMULATION

The flexibility of manufacturing processes is a fundamental requirement for efficient and adaptive manufacturing systems, encompassing various dimensions such as machine tool flexibility, tool flexibility, tool orientation flexibility, and process flexibility. This research paper focuses on three key types of flexibility: (i) machine tool flexibility, where a single operation can be performed on multiple alternative machine tools; (ii) process plan flexibility, which refers to the possibility of processing a job in different ways; and (iii) operation sequence flexibility, which represents the ability to change the order of operations during the optimization of manufacturing processes.

According to the mathematical model developed in [13], three alternative manufacturing process plans are generated for each job, based on the criterion of minimizing total production time, taking into account both the processing time of operations and the transportation time between alternative machine tools. The resulting process plans represent one of the key input parameters for the scheduling process, where the final assignment and sequencing of operations are subject to further optimization.

To determine the optimal scheduling plan, this study considers makespan as the objective function. The mathematical formulation of minimizing makespan is defined as:

$$obj = \max(c_{ij}), \left(c_{ij} \in T_d(s_{ij}, c_{ij})\right), \quad (1)$$

where: c_{ij} – the completion time of operation O_{ij}; s_{ij} – the start time of operation O_{ij}; T_d – the set of start times and completion times of all operations of all jobs.

Examples of selected alternative manufacturing process networks for processing four jobs are presented in Figure 1, while Figure 2 illustrates a job-shop scheduling problem.

A set of operations is determined for each job, along with a specified sequence of these operations on machine tools. The processing time for each operation on the corresponding machines is also specified. For instance, to process jobs 1 and 2, three operations are required for each; job 3 requires four operations, while job 4 requires two operations. Based on the information provided by the alternative manufacturing process networks, an initial scheduling plan is generated before any potential disturbance. Subsequently, an optimal rescheduling plan is developed following each of the three mentioned disturbances (Figures 3, 4, and 5).

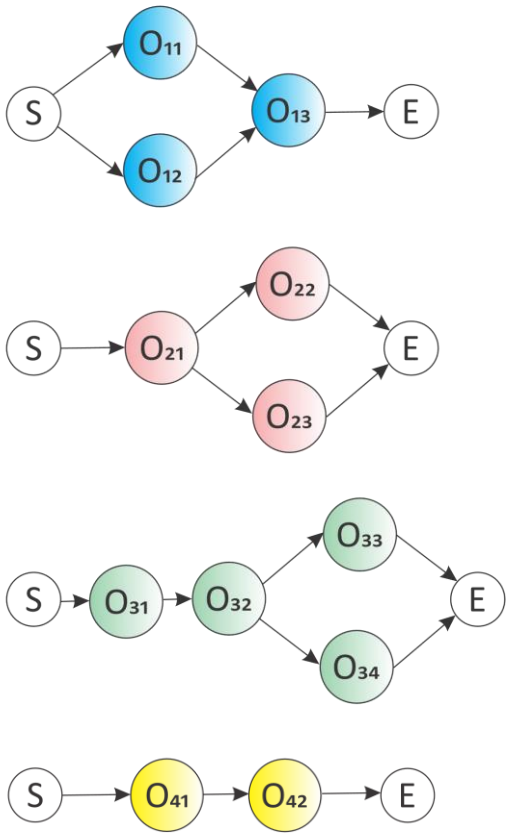

Figure 1. Alternative manufacturing process plans

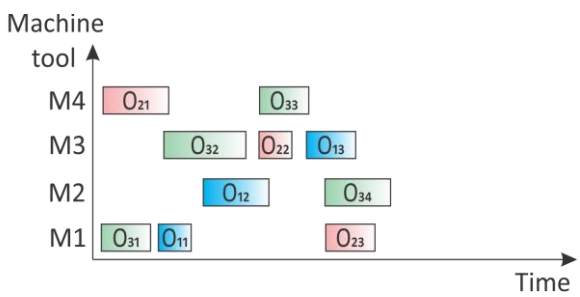

Figure 2. Gantt chart of job shop schedule

The arrival of a new job implies the need to modify the order of existing operations after the arrival time, while also considering operations required for processing the new job (Figure 3). The updated scheduling plan, also referred to as the rescheduling plan, can be utilized to enhance the overall performance of the manufacturing system in processing new jobs while simultaneously meeting the deadlines for all jobs within the system.

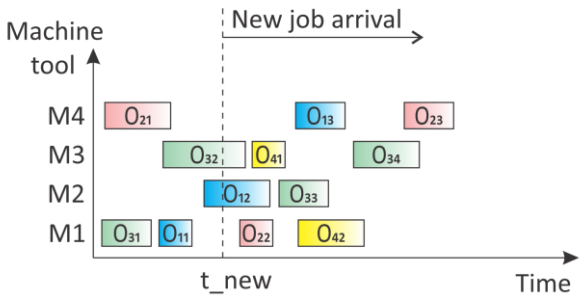

Figure 3. Rescheduling due to the arrival of a new job 4 in the system

Job cancellation represents a disturbance that requires the termination of processing for a specific job. Therefore, after the cancellation, rescheduling is performed for the remaining jobs, excluding all remaining scheduled operations of the canceled job (Figure 4).

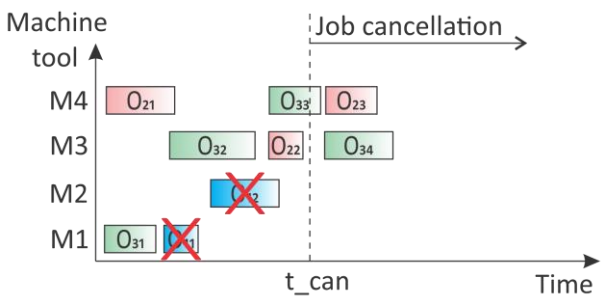

Figure 4. Rescheduling due to the cancellation of job 1

A machine tool breakdown results in the rescheduling of all ongoing operations that were not completed at the moment of failure and were assigned to the failed machine tool. Modeling approaches for handling such disturbances typically assume that all incomplete operations are reassigned to alternative machine tools suitable for continuing the processing of the corresponding job (Figure 5).

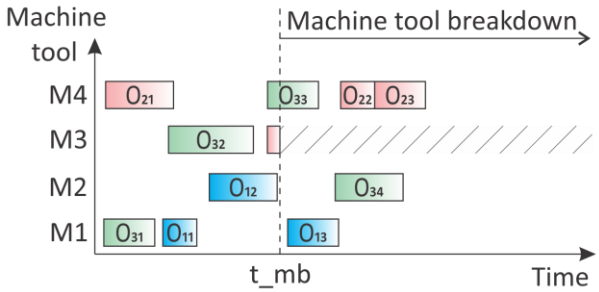

Figure 5. Rescheduling due to the breakdown of machine tool M3

The following assumptions are taken into account during the rescheduling processes illustrated in Figures 3, 4, and 5:

- The time required for rescheduling is considered to have no substantial impact, and processing of all jobs on all machine tools resumes immediately after the rescheduling is completed.
- If an operation was in progress at the moment a disturbance occurred, it continues on the same machine tool; in the case of a machine breakdown, the operation is reassigned to an alternative machine tool on which it can be processed.
- At any given moment, each machine tool can process only one operation of a single job.
- Jobs are available for processing starting from time $t_0 = 0$ in the initial scheduling plan, and from time $t = r_i$ after a disturbance occurs, where r_i represents the release time – the earliest moment when the next operation of job i can initiate.
- Different operations of the same job cannot be processed simultaneously.
- Once an operation on a machine tool is completed, the job is immediately transferred to the machine where the next operation is scheduled, considering also the transportation time between machines.
- The setup time of the machine tool, as well as other production resources for the subsequent operation is not taken into account in DFJSSP.
- The duration of the machine tool breakdown is unknown. Therefore, all operations that were scheduled to be processed on the failed machine tool must be reassigned to alternative machines during rescheduling.

2.1 The mathematical model of the DFJSSP

The mathematical model of the dynamic flexible job shop scheduling problem, presented below, is based on the research outlined in studies [14, 15].

List of symbols:

N – number of jobs $i = 1, \dots, N$;

M – number of machine tools, $m = 1, \dots, M$;

O_{ijk}^{m} – the k-th operation of the j-th alternative manufacturing process of job i executed on machine tool m;

r_i – release time for job i is the earliest time when the next operation of job i can start after the disturbance occurs;

r_m – release time for machine m is the earliest time when the next operation can start on machine tool m after the disturbance occurs;

t_{new} – new job arrival time;

t_{can} – job cancellation time;

t_{mb} – machine tool breakdown time;

t_d – time of disturbance occurrence (in general);

s_{ijk}^{m} – start time of the operation O_{ijk}^{m};

c_{ijk}^{m} – completion time of the operation O_{ijk}^{m};

z_{ijk}^{m} – a binary variable that takes the value 1 if the machine tool assigned to perform O_{ijk}^{m} remains unchanged, and 0 otherwise.

2.2 New job arrival and job cancellation

From the moment the disturbance occurs, it is necessary to reschedule the interrupted operations. Operations that were completed prior to the occurrence of the disturbance, as well as those that were performed at that moment, are excluded from the rescheduling process. In the case of the arrival of a new job (Figure 3), the completed operations O_{11}, O_{21} and O_{31} ($c_{ijk}^{m} \leq t_{new}$), as well as the operations in progress at the time O_{12} and O_{32} ($s_{ijk}^{m} < t_{new} < c_{ijk}^{m}$), are excluded from the rescheduling process. In the case of job cancellation (Figure 4), the following operations are not considered during rescheduling: O_{11}, O_{12}, O_{21}, O_{22}, O_{31}, and O_{32} ($c_{ijk}^{m} \leq t_{can}$), as well as operation O_{33} ($s_{ijk}^{m} < t_{can} < c_{ijk}^{m}$), which was performing at the time of cancellation. The remaining operations are included in the rescheduling ($s_{ijk}^{m} > t_d$, where $t_d = t_{new}$ in the case of a new job arrival, and $t_d = t_{can}$ in the case of job cancellation).

The release time r_i is calculated based on the general equation (2):

$$r_i = c_{ijk}^{m} \times z_{ijk}^{m} + t_d \times \left(1 - z_{ijk}^{m}\right). \tag{2}$$

In the case where an operation of a job was in progress at the time t_d, and the machine tool on which the operation was being performed remains unchanged (i.e., $z_{ijk}^{m} = 1$), the equation (2) takes the following form, given by the equation (3):

$$r_i = c_{ijk}^{m} = \\ = \left\{ s_{ijk}^{m} + t_{ijk}^{m} \,\middle|\, s_{ijk}^{m} < t_d < c_{ijk}^{m} \right\}. \tag{3}$$

On the other hand, if the operation was completed prior to the occurrence of the disturbance, assuming $z_{ijk}^{m} = 0$ (indicating that it is unknown whether the machine tool on which the next operation will be performed will change), the earliest possible start time r_i of the next operation of the job after t_d is calculated according to equation (4):

$$r_i = t_d = \\ = \max\left(\left\{ c_{ijk}^{m} \,\middle|\, c_{ijk}^{m} < t_d \right\}, t_d \right) \tag{4}$$

It is necessary to determine the state of the machine tools at the moment t_d, that is, whether an operation is being performed on the machine at that moment or is the machine available. The earliest possible start time of the next operation O_{ijk}^{m} on machine m after the disturbance occur is calculated using the following expression (5):

$$r_m = c_{ijk}^{m} \times z_{ijk}^{m} + t_d \times \left(1 - z_{ijk}^{m}\right). \tag{5}$$

At the moment the disturbance occurred, if the operation was being performed on machine tool m, it is assumed that $z_{ijk}^{m} = 1$, which indicates that the operation continues on the same machine tool, and equation (5) reduces to expression (6):

$$r_m = c_{ijk}^{m} = \\ = \left\{ s_{ijk}^{m} + t_{ijk}^{m} \,\middle|\, s_{ijk}^{m} < t_d < c_{ijk}^{m} \right\}. \tag{6}$$

If the operation O_{ijk}^{m} was completed prior to the arrival of the new job in the system, it is

assumed that $z_{ijk}^{m} = 0$ (indicating that it is unknown whether the next operation of the job i will be performed on the same machine tool), and equation (5) reduces to expression (7):

$$r_m = t_d = \\ = \max\left(\left\{c_{ijk}^{m} \middle| c_{ijk}^{m} < t_d\right\}, t_d\right). \quad (7)$$

2.3 Machine breakdown

In the case of a machine tool breakdown (Figure 5), the completed operations O_{11}, O_{12}, O_{21}, O_{31}, and O_{32}, are excluded from rescheduling, as well as operation O_{33}, which was in progress on a machine unaffected by the failure. On the other hand, operation O_{22}, which was being processed on the failed machine, must be reassigned to an alternative machine tool. The earliest possible start time of the next operation of job i after the occurrence of the disturbance can be calculated using the equation (8):

$$r_i = c_{ijk}^{m} \times z_{ijk}^{m} + t_{mb} \times \left(1 - z_{ijk}^{m}\right), \\ m \neq r; \quad (8)$$

r represents the machine tool that has failed.

If $m \neq r$, two possible cases arise. The first case occurs when operation O_{ijk}^{m} was performing at the moment of the failure of another machine tool, in which case $z_{ijk}^{m} = 1$, i.e., the operation continues to be performed on machine m, and the equation (8) reduces to the equation (9):

$$r_i = c_{ijk}^{m} = \\ = \left\{s_{ijk}^{m} + t_{ijk}^{m} \middle| s_{ijk}^{m} < t_{mb} < c_{ijk}^{m}\right\}. \quad (9)$$

The second case applies when operation O_{ijk}^{m} was completed before the failure of the other machine tool, in which case $z_{ijk}^{m} = 0$, since it is unknown whether the next operation of job i will be performed on the same machine m as the previous one, as presented in the equation (10):

$$r_i = t_{mb} = \\ = \max\left(\left\{c_{ijk}^{m} \middle| c_{ijk}^{m} < t_{mb}\right\}, t_{mb}\right), i \in N. \quad (10)$$

If $m = r$ and $s_{ijk}^{m} < t_{mb} < c_{ijk}^{m}$, this indicates that the machine tool on which the operation O_{ijk}^{m} was in progress has failed. The interrupted operation is transferred to a different machine tool for further processing, in which case $z_{ijk}^{m} = 0$, i.e., O_{ijk}^{m} will continue to be processed on alternative machine m, and equation (8) is replaced by equation (11):

$$r_i = t_{mb} \quad (11)$$

Following the previous evaluation of the time when processing of job i can be resumed – r_i, the time at which the machine tool m can resume processing the job – r_m, is calculated according to expression (12):

$$r_m = c_{ijk}^{m} \times z_{ijk}^{m} + t_{mb} \times \left(1 - z_{ijk}^{m}\right), m \neq r. \quad (12)$$

3. GENETIC ALGORITHM-BASED SOLUTION METHODOLOGY

A biologically inspired optimization method based on Genetic Algorithms (GA) is applied to obtain an optimal scheduling plan in accordance with the defined mathematical model. Each individual (chromosome) in the population consists of a primary substring, representing the operation sequence, and a secondary substring, encoding selected alternative manufacturing process plans. The initial population is generated based on the number of jobs and operations, while the fitness function is evaluated using the mathematical model for optimization defined in equation (1).

The algorithm then iteratively performs the core steps of selection (via roulette wheel), crossover, and mutation, applying operators to both substrings to generate new solutions. This process allows the algorithm to explore a wide solution space, maintain diversity, and converge toward optimal or near-optimal schedules. A detailed implementation procedure of the GA is provided in [16].

When a disturbance occurs, the GA generates an optimal rescheduling plan by repeating the same evolutionary steps, incorporating new jobs, excluding cancelled ones, or considering machine tool breakdowns. In this process, the initial population is generated to reflect the number of jobs remaining to be processed and the current state of the manufacturing system.

4. EXPERIMENTAL VERIFICATION AND DISCUSSION

To verify the mathematical models for the Dynamic Flexible Job Shop Scheduling Problem (DFJSSP), considering three types of disturbances, three experiments were conducted using 24 problems of varying complexity, which encompassed 18 benchmark jobs, as comprehensively presented in [17]. The networks of alternative manufacturing processes for all jobs included in the experiments were also adopted from this reference.

A genetic algorithm was used for both scheduling and rescheduling optimization, with the objective function makespan. The following genetic algorithm parameters were adopted for the initial scheduling phase: a population size of 120, a maximum number of generations set to 100, a crossover probability of pc = 0.6, and a mutation probability of p_m = 0.2. For the rescheduling phase, the parameters were adjusted to a population size of 100, with a maximum number of generations set to 80, while keeping the crossover and mutation probabilities unchanged. The proposed method and the corresponding experiments are implemented and tested in the MATLAB® environment. Experiment 1 addresses the scheduling problem labeled as Problem 21, focusing on the arrival of three new jobs at 30s. Experiment 2 involves scheduling for Problem 23 and analyzing the case of three jobs with cancellations occurring at 50s. Experiment 3 corresponds to Problem 22 and analyzes the breakdown of two machine tools that occurs at 40s.

The scheduling problems differ in terms of the number of jobs and the number of operations. For each job, three alternative process plans were generated and used during the scheduling optimization.

4.1 Arrival of new jobs

The scheduling of selected manufacturing processes for the initial set of jobs (2-3-5-6-7-9-10-11-13-14-16-18 – Problem 21) proceed without disturbance until the arrival of new jobs: 12, 15, and 17 into the manufacturing system at time $t_{new} = 30s$, at which point the rescheduling of the remaining operations is performed. In the first phase, prior to the arrival of the new jobs, a genetic algorithm generates the initial scheduling plan for the twelve jobs. After the arrival of the three new jobs, a new primary substring is formed, containing all unfinished operations of the initial jobs, as well as all operations of the new jobs, along with a new secondary substring that, compared to the initial one, also includes genes with information on the selected alternative manufacturing processes for the new jobs.

If the machine tool on which the first operation of a new job should begin is available at time $t_{new} = 30s$, processing starts immediately. Otherwise, the operation waits until the current processing is completed. For all operations that are yet to start, the earliest possible start time is the sum of the arrival time of the new jobs and the transportation time from the previous machine tool (if the previous and following operations are performed on different machines; otherwise, transportation time is disregarded). Operations that are in progress continue until completion. Afterward, according to the selected manufacturing process, the next operation either immediately starts on the same machine tool or the job is transferred to a different machine. In this way, the second phase of the algorithm performs rescheduling based on the new situation.

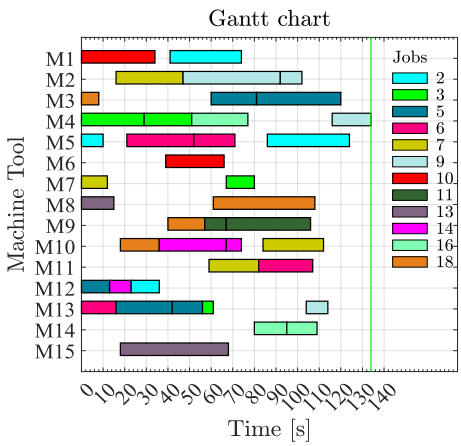

Figure 6. Problem 21 initial scheduling (*makespan* = 134s)

Figure 6 illustrates the Gantt chart representing the initial, optimal scheduling plan before the arrival of the new jobs, with a total processing time (makespan) of 134 seconds for all 12 jobs.

After the arrival of jobs 12, 15, and 17 at time $t_{new} = 30s$ and the following rescheduling, a new rescheduled plan is generated (Figure 7). It is observed that in this case, the makespan was 149s, indicating an increase in the total processing time due to the dynamic disturbance. Although the completion time is longer, the proposed approach successfully maintains the stability and functionality of the manufacturing system despite the disturbance caused by the arrival of new jobs.

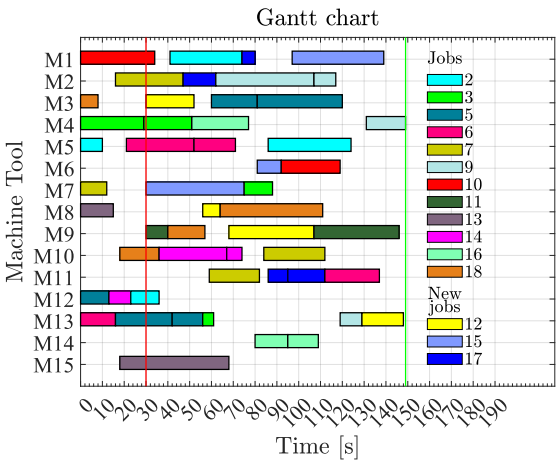

Figure 7. Rescheduling after arrival of new jobs 12, 15, and 17 at $t_{new} = 30s$ (*makespan* = 149s)

4.2 Job cancellations

The scheduling of selected manufacturing processes for the initial set of jobs (1-4-5-6-7-8-9-11-12-13-14-15-16-17-18 – Problem 23) proceed without disturbance until the cancellation of certain jobs: 1, 7, and 17 in the manufacturing system at time $t_{can} = 50s$, at which point the rescheduling of the remaining operations is performed. In the first phase, before the cancellation event, a genetic algorithm generates an initial scheduling plan with selected alternative manufacturing processes for all fifteen jobs. After the cancellation of the three jobs, a new primary substring is generated containing all unfinished operations of the jobs remaining in the system, excluding all remaining operations of the cancelled jobs, as well as a new secondary substring which, compared to the initial one, excludes as many elements (genes) as there are jobs that stop processing from the cancellation time onward.

Operations that have been completed before time $t_{can} = 50s$ remain fixed and are not subject to rescheduling. Operations that are in progress at the time of cancellation continue until completion if they belong to jobs that were not cancelled, while those belonging to cancelled jobs are interrupted immediately at that moment t_{can}. All operations of the cancelled jobs, whether in progress or not yet started, are removed from the rescheduling plan. For all remaining operations that have not yet begun, the earliest possible start time is set to the cancellation time t_{can} plus transportation time from the previous machine (if the machine tool is different). The second phase of the algorithm performs rescheduling based on this updated set of twelve jobs.

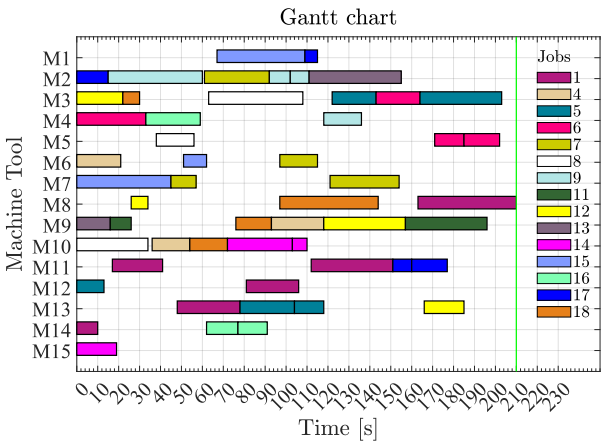

Figure 8. Problem 23 initial scheduling (*makespan* = 210s)

Figure 8 shows the Gantt chart representing the initial, optimal scheduling plan before the cancellation of jobs, with a total processing time (makespan) of 210s for all fifteen jobs. After the cancellation of jobs 1, 7, and 17 at time $t_{can} = 50s$ and the following rescheduling, a new rescheduled plan is formed (Figure 9).

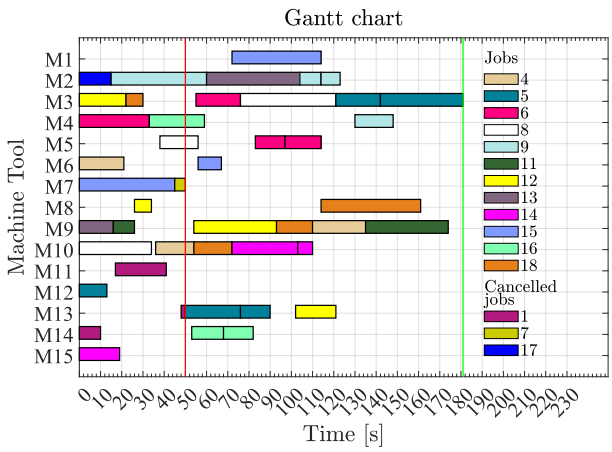

Figure 9. Rescheduling after cancellation of jobs 1, 7, and 17 at $t_{can} = 50s$ (*makespan* = 181s)

It is observed that in this case, the makespan was reduced to 181s, reflecting the removal of processing due to job cancellations. The proposed approach effectively adapts to dynamic changes and maintains operational efficiency within the manufacturing system, despite disturbances caused by job cancellations.

4.3 Machine tool breakdowns

The scheduling of the selected manufacturing processes for the initial set of jobs (2-3-4-5-6-8-9-10-11-12-13-14-16-17-18 – Problem 22) proceed without disturbance until the breakdown of machine tools M6 and M11 at time $t_{mb} = 40s$,at which point the rescheduling of the remaining operations is performed. In the first phase, prior to the breakdown event, a genetic algorithm generates an initial scheduling plan that selects alternative manufacturing processes for all fifteen jobs. After the machine tool breakdowns, all operations assigned to the broken machine that are still in progress are interrupted. Operations that were completed before t_{mb} remain fixed and are excluded from rescheduling. Operations that were in progress on the broken machine tools at t_{mb} are halted and rescheduled from the beginning, considering alternative manufacturing processes that exclude the broken machines. Operations that were in progress on machine tools that remain functional at the moment the disturbance occurs, continue processing according to the initial plan until completion.

A new primary substring is generated, containing the unfinished operations of all jobs, including those interrupted due to the breakdown, with updated processing routes that exclude the failed machine tools. A new secondary substring is also generated, including the updated selection of alternative manufacturing processes for the affected jobs. For all remaining operations yet to start, the earliest possible start time is set to the machine breakdown time t_{mb} plus the transportation time from the previous machine if the operation is not performed on the same machine tool. The second phase of the algorithm performs rescheduling based on this updated set of operations and manufacturing routes, adapting to the constraints imposed by the machine breakdown.

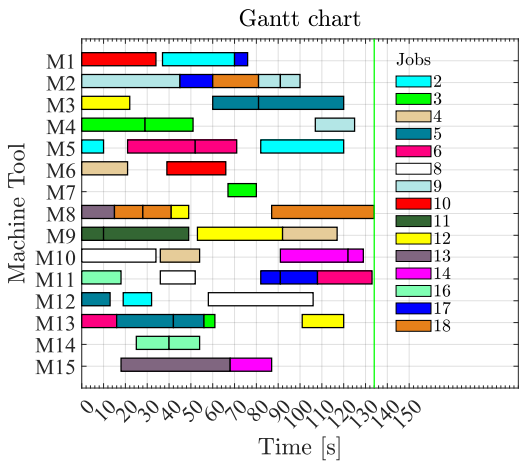

Figure 10. Problem 22 initial scheduling (*makespan* = 134s)

After the breakdowns at $t_{mb} = 40s$ and the following rescheduling, a new rescheduling plan is formed and shown in Figure 11.

Figure 10 shows the Gantt chart representing the initial, optimal scheduling plan before the machine tool breakdowns, with a total processing time (makespan) of 134s for all fifteen jobs.

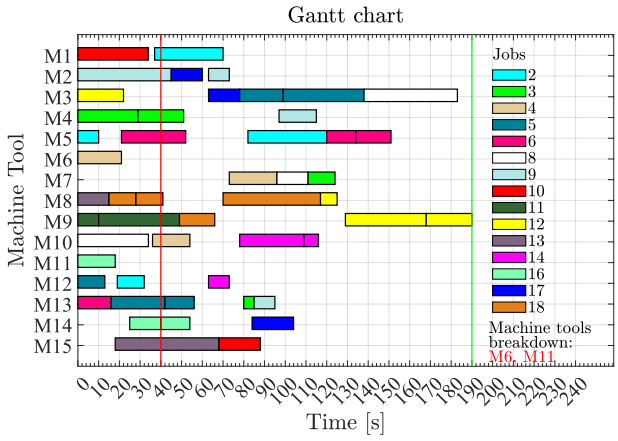

Figure 11. Rescheduling after machine tools M6 and M11 breakdown at $t_{mb} = 40s$ (*makespan* = 190s)

The results show that the makespan increased to 190s, indicating an extension of the total processing time due to the disturbance caused by the machine breakdowns. Despite the increase in the makespan, the proposed approach effectively maintains the stability and functionality of the manufacturing system by dynamically adapting the scheduling to the changed conditions.

5. CONCLUSION

This paper has presented a comprehensive approach to the Dynamic Flexible Job Shop Scheduling Problem (DFJSSP) under the influence of three types of disturbances: the arrival of new jobs, job cancellations, and machine tool breakdowns. Importantly, these disturbances are considered not only as typical dynamic events but also as potential consequences of cyber-attacks targeting manufacturing systems, which highlights the growing cybersecurity risks within modern production environments.

A genetic algorithm-based methodology was developed and implemented in the MATLAB® environment, enabling effective real-time rescheduling that minimizes total processing time (makespan). The experimental evaluation was performed on benchmark problems, demonstrating that the proposed approach maintains high scheduling efficiency and adaptability despite the presence of dynamic and cyber-induced disturbances. The results validate that the methodology can successfully manage and reduce the negative impact of such disturbances on production performance, thus supporting the Industry 4.0 concept of intelligent, flexible, and secure manufacturing systems.

In particular, three separate experiments were carried out to evaluate the rescheduling capabilities of the proposed solution under different types of disturbances. The first experiment analyzed the arrival of three new jobs into the system, requiring the integration of their operations into the existing schedule. The second experiment examined the cancellation of three jobs, focusing on the adaptation of the schedule by removing unfinished operations and redistributing available resources. The third experiment addressed the breakdown of two machine tools, requiring the reassignment of operations that were either ongoing or planned for the failed machines to alternative machines. Across all three cases, the genetic algorithm successfully adjusted the scheduling plans, demonstrating resilience, efficiency, and robustness in dynamically changing environments that could originate from or be aggravated by coordinated cyber-attacks. This research opens numerous paths for further investigation to improve the robustness and applicability of DFJSS in cybersecurity-aware manufacturing environments. First, future studies could incorporate the explicit modeling of machine tool downtime, including the waiting time until the failure is resolved and the machine becomes available again. This would provide a more realistic representation of manufacturing disturbances, enabling more precise rescheduling strategies.

Moreover, the simultaneous occurrence of multiple disturbances, possibly caused or aggravated by coordinated cyber-attacks, within the same manufacturing system poses complex rescheduling challenges. Future research could focus on developing integrated rescheduling frameworks that consider all such disturbances together, improving the system's resilience to sequential disturbances.

In terms of optimization approaches, it is valuable to explore and compare alternative metaheuristic algorithms (e.g., Ant Colony Optimization, Particle Swarm Optimization, or hybrid methods) for dynamic scheduling problems, to evaluate their relative performance, convergence behavior, and adaptability under dynamic and cybersecurity-related disturbances.

ACKNOWLEDGEMENT

This research was supported by the Science Fund of the Republic of Serbia, Grant No. 17801, Cybersecurity of Motion Control Systems in Industry 4.0 - MCSecurity, as well as by the Ministry of Science, Technological Development, and Innovations of the Serbian Government under Contract No. 451-03-137/2025-03/200105.

REFERENCES

[1] D. A., Rossit, F., Tohmé, and M. Frutos, "Industry 4.0: smart scheduling", *International Journal of Production Research*, vol. 57, pp. 3802-3813, 2019.

[2] A. B. Avila, A. Zarreh, C. Saygin, H. D. Wan, and Y. Lee, "Evaluation of Dynamic Scheduling Policies against Cyber-attacks on an Open-Shop Manufacturing System using Simulation", *International Journal of Multidisciplinary and Current Research*, vol. 9, 2021.

[3] X. N. Shen, and X. Yao, "Mathematical modeling and multi-objective evolutionary algorithms applied to dynamic flexible job shop scheduling problems", *Information Sciences*, vol. 298, pp. 198-224, 2015.

[4] K.B. Ali, S. Bechikh, A. Louati, H. Louati, and E. Kariri, "Dynamic Job Shop Scheduling Problem with New Job Arrivals using Hybrid Genetic Algorithm", *IEEE Access*, vol. 12, pp. 85338-85354, 2024.

[5] N. Zhu, G. Gong, D. Lu, D. Huang, N. Peng, and H. Qi, "An effective reformative memetic algorithm for distributed flexible job-shop scheduling problem with order cancellation", *Expert Systems with Applications*, vol. 237, p. 121205, 2024.

[6] N. Al-Hinai, and T. Y. Elmekkawy, "Robust and stable flexible job shop scheduling with random machine breakdowns using a hybrid genetic algorithm", *International Journal of Production Economics*, vol. 132, pp. 279–291, 2011.

[7] A. Madureira, "A Genetic Approach for Dynamic Job-Shop Scheduling Problems", *MIC'2001 - 4th Metaheuristics International Conference*, no. March. pp. 41–46, 2001.

[8] N. Kundakcı, and O. Kulak, "Hybrid genetic algorithms for minimizing makespan in dynamic job shop scheduling problem", *Computers* and *Industrial Engineering,* vol. 96, pp. 31–51, June. 2016.

[9] Y. M. Wang, H. L. Yin, and K. Da Qin, "A novel genetic algorithm for flexible job shop scheduling problems with machine disruptions", *The International Journal of Advanced Manufacturing Technology*, vol. 68, no. 5–8, pp. 1317–1326, 2013.

[10] S. Lin, E. Goodman, and W. Punch, "A Genetic Algorithm Approach to Dynamic Job Shop Scheduling Problem", *ICGA,* pp. 481–488, 1997.

[11] A. K. Jain and H. A. Elmaraghy, "Production scheduling/rescheduling in flexible manufacturing", *International Journal of Production Research*, vol. 35, no. 1, pp. 281–309, 1997.

[12] L. Yin, L. Gao, X. Li, and H. Xia, "An improved genetic algorithm with rolling window technology for dynamic integrated process planning and scheduling problem", *IEEE 21st International Conference on Computer Supported Cooperative Work in Design (CSCWD)*, pp. 414–419, 2017.

[13] M. Petrović, N. Vuković, M. Mitić, and Z. Miljković, "Integration of process planning and scheduling using chaotic particle swarm optimization algorithm", *Expert Systems with Applications*, vol. 64, pp. 569-588, 2016.

[14] S. Lv, and L. Qiao, "Process planning and scheduling integration with optimal rescheduling strategies", *International Journal of Computer Integrated Manufacturing*, vol. 27, no. 7, pp. 638–655, 2014.

[15] H. Xia, X. Li, and L. Gao, "A hybrid genetic algorithm with variable neighborhood search for dynamic integrated process planning and scheduling", *Computers & Industrial Engineering*, vol. 102, pp. 99–112, 2016.

[16] Miljković, K., Petrović, M., Babić, B., Dynamic integrated process planning and scheduling

based on genetic algorithms, Technical solution, 2021.

[17] M. M. Petrović, "Design of intelligent manufacturing systems by using artificial intelligence", Ph.D. dissertation, University of Belgrade-Faculty of Mechanical Engineering, Belgrade, Serbia, 2016.

Society of Production Engineering

ICPES 2025

40th INTERNATIONAL CONFERENCE ON PRODUCTION ENGINEERING - SERBIA 2025

DOI: 10.46793/ICPES25.259T

University of Nis Faculty of Mechanical Engineering

Nis, Serbia, 18 - 19th September 2025

RECENT ADVANCES IN ARTIFICIAL INTELIGENCE AND MACHINE LEARNING FOR PROCESS OPTIMIZATION IN TURNING

Aleksandar TRAJKOVIĆ[1]*, Miloš MADIĆ[2]

Orcid: 0009-0006-1390-8167; **Orcid:** 0000-0002-2310-2590;

[1]University of Niš, Faculty of Mechanical Engineering, Niš, Serbia

*Corresponding author: aleksandar.trajkovic@masfak.ni.ac.rs

Abstract: *The integration of artificial intelligence (AI) and machine learning (ML) into turning is transforming traditional manufacturing into a highly adaptive, data driven process. This review examines five key application areas, tool wear prediction, cutting force estimation, surface quality, energy consumption modeling and productivity optimization, highlighting the shift from static, empirical approaches to dynamic, hybrid frameworks that blend physics-based models with data driven algorithms. Advances in sensing technologies, digital twin platforms, and edge cloud integration now enable real time monitoring and multi objective optimization, enhancing both efficiency and sustainability. The analysis identifies multi modal data fusion, online adaptive learning, cross domain model transfer, and life cycle integrated decision making as emerging trends poised to drive the next generation of intelligent, sustainable, and self-optimizing turning systems.*

Keywords: *Turning, Artificial Intelligence, Machine Learning, Hybrid modeling, Predictive manufacturing*

1. INTRODUCTION

Turning is one of the oldest and most fundamental machining processes, traditionally employed to remove excess material from a rotating workpiece in the form of chips. Due to its versatility, ability to achieve high dimensional accuracy, and capability to produce a wide range of cylindrical geometries, turning has remained a cornerstone of modern manufacturing technologies. Its efficiency in the production of cylindrical components, combined with the potential to deliver superior surface quality under both conventional and advanced cooling/lubrication conditions, makes it a preferred method for achieving precise dimensional tolerances and functional surface integrity in high performance applications [1]. Industrial demand for components that can

be most efficiently produced by turning, such as shafts, bushings, and precision cylindrical parts, has solidified its role as a primary metal cutting process in various sectors, including automotive, aerospace, and energy [2].

In a typical turning operation, the workpiece is held and rotated by the spindle while a single point cutting tool removes material by traversing parallel (Z axis) or perpendicular (X axis) to the axis of rotation [3]. Critical process parameters, such as cutting speed, feed rate, and depth of cut, directly influence machining efficiency, surface finish, tool wear, and overall productivity. These parameters must be carefully selected and optimized according to material properties, cutting tool characteristics, and required tolerances to achieve an effective balance between productivity and quality [4], [5]. Improper selection of these parameters can lead to excessive tool wear, poor surface integrity, and reduced material removal rate, ultimately increasing production costs.

Beyond its traditional role, turning has undergone continuous technological advancements, integrating high performance cutting tools, computer aided design and manufacturing (CAD/CAM) systems, and real time process monitoring. The introduction of coated carbide, cermet, and ceramic tools has extended cutting tool life while enabling higher cutting speeds and feeds, thereby improving overall process efficiency [6]. Additionally, the integration of advanced CNC control systems has enabled the implementation of adaptive control strategies, allowing for real time adjustment of cutting parameters in response to tool wear or varying workpiece conditions.

Artificial Intelligence (AI) refers to the ability of computer systems to perform tasks that typically require human cognitive functions, such as perception, reasoning, learning, and problem solving. It encompasses a wide range of subfields, including natural language processing, computer vision, and robotics, each aimed at enabling machines to make informed decisions and adapt to changing conditions. Machine Learning (ML), a subset of AI, focuses specifically on algorithms that learn patterns from data to improve their performance over time without explicit reprogramming [7]. These algorithms range from simple linear regression models to complex deep learning architectures capable of processing high dimensional datasets.

In the context of manufacturing, both AI and ML rely heavily on data collected from a wide variety of sources. Typical industrial data streams originate from sensors monitoring temperature, vibration, acoustic emission, cutting forces, and other process variables, as well as from control systems, computer aided manufacturing (CAM) platforms, and enterprise resource planning (ERP) databases[8]. The quality and structure of this data directly influences model accuracy, making preprocessing steps, such as noise reduction, normalization, and feature extraction, essential [9]. Properly processed data enables predictive analytics for tasks like process optimization, tool condition monitoring, and quality assurance, transforming raw measurements into actionable intelligence that supports autonomous and adaptive manufacturing systems.

The evolution of turning from a conventional metal cutting operation to an intelligent, data driven process reflects the broader transformation occurring in manufacturing under the influence of Industry 4.0 technologies. While fundamental knowledge of process kinematics, material behavior, and parameter optimization remains critical, the integration of AI and ML offers opportunities for enhancing precision, productivity, and adaptability. By leveraging multi source sensor data, advanced algorithms can accurately predict process outcomes, detect anomalies, and adapt control strategies in real time, thereby minimizing waste and maximizing efficiency [10]. This convergence of traditional machining expertise with computational intelligence establishes a foundation for developing robust, autonomous turning

systems capable of meeting the growing demands for high quality, cost effective, and sustainable manufacturing. Against this backdrop, the present work aims to explore and advance AI and ML based approaches for turning process optimization.

2. APPLICATION OF AI AND ML IN TURNING MACHINING

2.1 Tool wear prediction

Tool wear prediction remains a central challenge in modern turning, directly affecting dimensional accuracy, surface integrity, tool life, and costs. In practical manufacturing environments, researchers are increasingly combining AI techniques with multi sensor monitoring systems to capture and anticipate wear progression as it unfolds on the shop floor. Such approaches often employ vibration, acoustic emission, spindle power, and cutting force signals, which are processed through advanced signal analysis methods and fed into machine learning models for accurate wear estimation [11]. By correlating sensor features with the actual wear state, researchers have demonstrated that AI driven methods can significantly outperform conventional threshold-based monitoring strategies in both prediction accuracy and adaptability to changing cutting conditions.

In addition to data driven models, hybrid approaches have been developed, combining physics-based wear models with AI algorithms to leverage the strengths of both domains [12]. These methods benefit from the interpretability of mechanistic models while gaining the flexibility of ML to adapt to complex and nonlinear wear patterns. Studies have shown that the fusion of physical insights with advanced regression or classification models enables a more robust prediction framework, particularly under variable machining parameters. Furthermore, the adoption of deep learning architectures, such as convolutional neural networks and recurrent neural networks, has enabled automatic feature extraction from raw signal data, reducing the reliance on manual feature engineering and improving generalization to unseen machining scenarios [13].

Another emerging direction is the utilization of cloud based and digital twin systems for tool wear prediction. By integrating sensor data into a virtual replica of the machining process, digital twins can continuously update the tool wear model based on real time inputs, thereby allowing adaptive process control [14]. This integration not only supports predictive maintenance but also enables optimization of cutting parameters to prolong tool life.

Some implementations have used streamlined neural architectures, such as pruned convolutional networks or compact gradient boosted ensembles, embedded directly into CNC controllers. These designs process sensor data locally, delivering wear state updates within milliseconds, and avoid the bandwidth load of constant cloud communication [15].

2.2 Cutting force

Cutting force prediction plays a decisive role in maintaining process stability and achieving consistent productivity. A growing body of work now explores hybrid AI models that merge physical process knowledge with adaptive learning strategies, enabling force estimation to remain accurate even under fluctuating machining conditions. One notable approach integrates mechanistic force models derived from cutting mechanics with data driven adjustment layers, producing hybrid systems that substantially improve prediction accuracy across variable machining regimes. This synergy supports robust predictions even when tool geometry, material properties, or machining conditions deviate from nominal parameters, providing flexibility without sacrificing interpretability [16].

Beyond hybrid frameworks, purely data driven methods have demonstrated exceptional adaptability and precision, particularly through deep learning. Multi-layer neural networks, including convolutional and recurrent architectures, have become

especially adept at modeling the nonlinear, time dependent behavior of cutting forces. These models leverage large sensor datasets, captured from vibration, spindle load, acoustic emissions, or torque signals, to learn complex patterns that standard regression models struggle to detect. Their increasing accuracy and real time applicability mark them as critical tools for modern, intelligent machining systems [17].

Some studies have explored pairing live force measurements with virtual machining environments that update in real time. This approach allows the simulation to mirror the evolving cutting process, enabling immediate adjustments to feed rate or spindle speed when force spikes are predicted. This setup enables predictive control strategies such as adaptive feed rate optimization and proactive tool path adjustment, helping to minimize undesired force spikes and mitigate chatter. Cloud integration also offers scalable computational support and facilitates cross machine learning adaptations, ultimately helping to standardize performance across diverse setups [18].

At the same time, there's growing interest in low latency, on edge inference solutions. Lightweight AI models, such as pruned neural networks or compact ensemble learners, are being optimized for real time deployment directly on CNC controllers. These solutions address the imperative for fast, reliable cutting force feedback without overloading communication channels or cloud infrastructure, paving the way for closed loop control even in resource constrained environments [19].

2.3 Surface quality prediction

Surface quality, commonly expressed through roughness parameters, remains a defining factor in part performance, influencing everything from assembly precision to service life. Increasingly, AI driven predictive models are being used to process real time sensor data, enabling proactive adjustments that keep surface finish within tight specification limits. By extracting features from spindle power, acoustic emissions, and vibration signals, these models can forecast surface roughness with noteworthy accuracy, enabling immediate on the fly adjustments to maintain desired finish standards [20].

Hybrid modeling approaches, integrating mechanistic surface generation models with machine learning corrections, have proven particularly robust. Mechanistic models capture the foundational physics of tool–workpiece interaction, while the data driven layer compensates for complex, real world non idealities such as tool vibration, material heterogeneity, and tool wear. This dual layer strategy enhances reliability across varied cutting conditions without sacrificing model interpretability [21].

Researchers have tested edge optimized predictors, including MobileNet style convolutional models and reduced tree ensembles, which can run on embedded controllers. This setup enables the control system to adjust spindle speed or feed rate almost instantly when the forecasted surface finish begins to drift. This enables real time roughness prediction and closed loop adjustment of feed rates or spindle speeds, all with minimal latency and without reliance on cloud back ends [22].

Certain research groups are experimenting with virtual process replicas that continuously incorporate live surface finish measurements. These replicas can forecast how surface quality will evolve if current parameters are maintained, helping engineers intervene before defects occur. By pairing live sensor streams with virtual replicas of the machining process, predictive roughness models can self-update continuously, adapting to tool wear progression, changes in material behavior, or shifts in ambient conditions. This enables not only predictive quality control but also long-term process optimization across tool life and across multiple machines [23].

Finally, a practical direction gaining traction is the use of transfer learning or few shot adaptations for surface quality models. Pretrained models, developed on datasets

from one material or machine, can be swiftly adapted to new setups using minimal new data, significantly reducing the cost of model deployment in varied production environments [24].

2.4 Energy consumption prediction

In the drive toward sustainable manufacturing, predicting and optimizing energy consumption in CNC turning has gained strategic importance. Recent studies show that targeting specific cutting energy through parameter optimization can yield significant efficiency gains without sacrificing throughput or part quality. These approaches often involve fine tuning of machining parameters, such as cutting speed, feed rate, and depth of cut, using advanced optimization algorithms to minimize energy use without compromising productivity or quality [25].

Artificial intelligence techniques, particularly artificial neural networks (ANNs), have emerged as powerful tools for modeling and predicting energy consumption under varying cutting conditions. By leveraging multi sensor inputs and historical machining data, these models can capture the nonlinear relationships between process parameters and energy demand, enabling real time adjustments for optimal efficiency. Hybrid frameworks that combine ANN prediction with control and monitoring systems allow for dynamic recalibration of parameters during turning operations [26].

Sustainability focused studies further extend prediction models by incorporating specific cutting energy into multi objective optimization. This approach simultaneously targets energy efficiency, tool wear reduction, and overall process sustainability, particularly when using advanced techniques like minimum quantity lubrication (MQL). By integrating such lubrication strategies into predictive models, researchers have achieved significant reductions in energy usage alongside improvements in surface quality and tool life [27].

The inclusion of environmentally friendly lubricants, such as vegetable based MQL fluids, adds an ecological dimension to energy consumption optimization. In such cases, ANN based multi objective optimization frameworks can balance surface roughness, energy consumption, carbon emissions, and machining cost, providing a comprehensive decision-making tool for sustainable CNC turning [28].

Finally, recent advancements also highlight the role of material specific and process specific studies in energy consumption modeling. Tailored models that account for unique properties of workpiece materials, cutting tools, and machining setups can further enhance prediction accuracy, enabling a transition toward fully adaptive, sustainable, and energy aware manufacturing systems [29].

2.5 Productivity

Maximizing productivity in turning, whether measured as MRR, parts per hour, or effective throughput, remains a priority for competitive manufacturing. New AI driven modeling approaches are proving valuable in mapping the complex relationships between cutting parameters and real-world output, allowing for informed, high impact adjustments. By utilizing operational data streams, such as spindle power, feed rate, and machining cycles, these models can predict productivity with high fidelity, enabling proactive adjustments to maximize output without compromising quality [30].

Hybrid modeling approaches that combine mechanistic productivity estimators with data driven optimization layers show considerable promise. The mechanistic models provide baseline output estimates grounded in tool workpiece geometry and cutting mechanics, while machine learning corrections account for real world inefficiencies, like operator intervention, tool wear, or thermal deflection. This fosters a resilient productivity forecast that adapts to dynamic shop floor conditions [31].

Advanced optimization frameworks further elevate productivity prediction by integrating multi objective considerations. For

example, productivity models are now designed to simultaneously balance output rate, energy consumption, and surface quality. These systems typically employ evolutionary algorithms, ANN based controllers, or reinforcement learning agents to discover optimal operating points that satisfy multiple production goals concurrently offering a comprehensive toolkit for sustainable, high efficiency machining [32].

Moreover, the rise of digital twin platforms and real time simulation has enhanced productivity modeling capabilities. By continuously integrating live sensor data into virtual replicas of the machining process, these systems can simulate "what if" scenarios in real time testing parameter shifts or tooling changes before committing them to actual production. This enables adaptive control strategies that autonomously enhance throughput while maintaining part quality and tool life [33].,

3. FUTURE DIRECTIONS

The evolution of AI and ML in turning will increasingly center on multi modal sensor fusion, combining acoustic, vibration, force, temperature, and vision data into unified process models. This integration will strengthen multi objective optimization, balancing quality, throughput, energy consumption, and tool life in real time. Online adaptive learning will replace static deployments, enabling continuous recalibration as tools wear, materials vary, and environmental conditions change. Transfer learning will reduce the cost and time of implementation across diverse machines and materials. On the sustainability front, integrating life cycle assessment (LCA) into optimization frameworks will make environmental impact a standard decision-making parameter. The convergence of digital twins with hybrid edge–cloud architectures will support distributed, predictive, and self-optimizing manufacturing networks, aligning with Industry 4.0 and paving the way toward Industry 5.0.

4. CONCLUSION

This review demonstrates that AI and ML based approaches, particularly hybrid models, are redefining predictive modeling in turning. Advances in tool wear, cutting force, and surface quality prediction are enabling real time control, while machining time models are closing the gap between CAM estimates and shop floor realities. Energy consumption modeling now integrates sustainability goals, and productivity optimization is evolving into a multi objective discipline. Collectively, these developments signal a transition toward intelligent, connected, and environmentally responsible machining systems, where adaptive algorithms, real time feedback, and digital twins converge to deliver high performance, resilient manufacturing in dynamic industrial environments.

ACKNOWLEDGEMENT

This research was financially supported by the Ministry of Science, Technological Development and Innovation of the Republic of Serbia (Contract No. 451 03 137/2025 03/200109).

REFERENCES

[1] N. Jouini, J. A. Ghani, S. Yaqoob, and A. Z. Juri, Optimized Machining Parameters for High Speed Turning Process: A Comparative Study of Dry and Cryo+MQL Techniques, Processes, Vol. 13, No. 3, 2025, doi: 10.3390/pr13030739.

[2] W. Li, Advanced Manufacturing and Precision Machining, Applied Sciences, Vol. 14, No. 24, 2024, doi: 10.3390/app142411642.

[3] Z. Haitao, G. Jingfeng, T. Yongbo, Z. Shuixiang, and Y. Xiaoxi, An analysis of compensation for radial thermal errors of a turning center with a three axis feed system, Sci Rep, Vol. 15, No. 1, p. 23345, 2025, doi: 10.1038/s41598 025 05804 5.

[4] M. S. Surya, Optimization of machining parameters while turning AISI316 stainless steel using response surface methodology, Sci Rep, Vol. 14, No. 1, p. 30083, 2024, doi: 10.1038/s41598 024 78657 z.

[5] J. V Abellán Nebot, C. Vila Pastor, and H. R. Siller, A Review of the Factors Influencing Surface Roughness in Machining and Their Impact on

Sustainability, Sustainability, Vol. 16, No. 5, 2024, doi: 10.3390/su16051917.

[6] V. F. C. Sousa and F. J. G. Silva, Recent Advances in Turning Processes Using Coated Tools—A Comprehensive Review, Metals (Basel), Vol. 10, No. 2, 2020, doi: 10.3390/met10020170.

[7] R. X. Gao, J. Krüger, M. Merklein, H. C. Möhring, and J. Váncza, Artificial Intelligence in manufacturing: State of the art, perspectives, and future directions, CIRP Annals, Vol. 73, No. 2, pp. 723–749, 2024.

[8] S. J. Plathottam, A. Rzonca, R. Lakhnori, and C. O. Iloeje, A review of artificial intelligence applications in manufacturing operations, J Adv Manuf Process, Vol. 5, No. 3, p. e10159, 2023, doi: https://doi.org/10.1002/amp2.10159.

[9] A. Presciuttini, A. Cantini, F. Costa, and A. Portioli Staudacher, Machine learning applications on IoT data in manufacturing operations and their interpretability implications: A systematic literature review, J Manuf Syst, Vol. 74, pp. 477–486, 2024, doi: https://doi.org/10.1016/j.jmsy.2024.04.012.

[10] M. S. Ahmmed, S. P. Isanaka, and F. Liou, Promoting Synergies to Improve Manufacturing Efficiency in Industrial Material Processing: A Systematic Review of Industry 4.0 and AI, Machines, Vol. 12, No. 10, 2024, doi: 10.3390/machines12100681.

[11] Z. Che, C. Peng, J. Wang, R. Zhang, C. Wang, and X. Sun, KAN Based Tool Wear Modeling with Adaptive Complexity and Symbolic Interpretability in CNC Turning Processes, Applied Sciences, Vol. 15, No. 14, 2025, doi: 10.3390/app15148035.

[12] T. Namboodri and C. Felhő, AI FOR QUALITY OPTIMIZATION IN TURNING: A SHORT REVIEW., MM Science Journal, 2025.

[13] L. Colantonio, L. Equeter, P. Dehombreux, and F. Ducobu, Explainable AI for tool condition monitoring using Explainable Boosting Machine, Procedia CIRP, Vol. 133, pp. 138–143, 2025, doi: https://doi.org/10.1016/j.procir.2025.02.025.

[14] S. C. S and A. Ramesh, Digital twin enabled surface quality prediction and optimization in dry turning of Ti6Al4V using ANFIS and genetic algorithm, Journal of King Saud University – Engineering Sciences, Vol. 37, No. 5, p. 17, 2025, doi: 10.1007/s44444 025 00030 w.

[15] M. Kodrič, J. Korbar, M. Pogačar, and G. Čepon, Development of a resource efficient real time vibration based tool condition monitoring system using PVDF accelerometers, Measurement, Vol. 251, p. 117183, 2025, doi: https://doi.org/10.1016/j.measurement.2025.117183.

[16] A. Suárez, F. Veiga, X. Sandua, P. J. Rivero, L. N. L. de Lacalle, and A. Wretland, Machinability of Waspaloy: an investigation of cutting forces and tool wear in turning, The International Journal of Advanced Manufacturing Technology, Vol. 139, No. 5, pp. 3159–3172, 2025, doi: 10.1007/s00170 025 15983 0.

[17] M. Liu, H. Xie, W. Pan, S. Ding, and G. Li, Prediction of cutting force via machine learning: state of the art, challenges and potentials, J Intell Manuf, Vol. 36, No. 2, pp. 703–764, 2025, doi: 10.1007/s10845 023 02260 8.

[18] M. Mirzabagherian, S. Amini, and M. Bayat, Investigation of the effects of ultrasonic assisted face turning with CO2 cooling on cutting forces, residual stress, and surface quality, International Journal of Lightweight Materials and Manufacture, Vol. 8, No. 5, pp. 551–561, 2025, doi: https://doi.org/10.1016/j.ijlmm.2025.04.003.

[19] J. Stanojković, M. Madić, M. Trifunović, P. Janković, and D. Petković, A NOVEL APPROACH TO PREDICTING THE CUTTING FORCE IN TURNING USING DIMENSIONAL ANALYSIS, Facta Universitatis, Series: Mechanical Engineering, 2025.

[20] A. T. Abbas, N. Sharma, K. F. Alqosaibi, M. A. Abbas, R. C. Sharma, and A. Elkaseer, Investigation of Surface Quality and Productivity in Precision Hard Turning of AISI 4340 Steel Using Integrated Approach of ML

MOORA PSO, Processes, Vol. 13, No. 4, 2025, doi: 10.3390/pr13041156.

[21] T. Namboodri and C. Felhő, AI FOR QUALITY OPTIMIZATION IN TURNING: A SHORT REVIEW., MM Science Journal, 2025.

[22] T. Namboodri and C. Felhő, AI FOR QUALITY OPTIMIZATION IN TURNING: A SHORT REVIEW., MM Science Journal, 2025.

[23] J. H. Ko and C. Yin, A review of artificial intelligence application for machining surface quality prediction: from key factors to model development, J Intell Manuf, 2025, doi: 10.1007/s10845 025 02571 y.

[24] Y. Zhu, T. Österlind, A. Rashid, and A. Archenti, Data driven approaches for surface quality monitoring and prediction based on heterogeneous multi channel signal fusion in hard part machining, Eng Appl Artif Intell, Vol. 160, p. 111865, 2025, doi: https://doi.org/10.1016/j.engappai.2025.111865.

[25] K. Noor, M. A. Siddiqui, and A. I. Syed, Optimization of specific energy consumption in CNC turning of a hardened alloy steel roll at low cutting speeds, Journal of Engineering, Design and Technology, Vol. 23, No. 2, pp. 368–385, 2025.

[26] B. F. Abaza and V. Gheorghita, Artificial Neural Network Framework for Hybrid Control and Monitoring in Turning Operations, Applied Sciences, Vol. 15, No. 7, 2025, doi: 10.3390/app15073499.

[27] R. S. Revuru, K. T. Sanjay, B. Srinu, and P. V. Krishna, Evaluation of optimum process parameters based on specific cutting energy in turning for sustainability, The International Journal of Advanced Manufacturing Technology, Vol. 136, No. 10, pp. 4569–4579, 2025, doi: 10.1007/s00170 025 15068 y.

[28] T. Hakmi, H. Abderazek, Y. F. Yapan, A. Hamdi, and A. Uysal, Enhancing sustainability in CNC turning of POM C polymer using MQL with vegetable based lubricant: machine learning and metaheuristic optimization approaches, The International Journal of Advanced Manufacturing Technology, Vol. 139, No. 3, pp. 1661–1684, 2025, doi: 10.1007/s00170 025 15962 5.

[29] M. A. Khan, R. Ahmad, S. H. I. Jaffery, S. I. Butt, M. S. Khan, and D. Zahid, Sustainability analysis of tool wear, energy efficiency, surface quality, and energy during dry, MQL, and wet turning of Inconel 718, International Journal of Sustainable Energy, Vol. 44, No. 1, p. 2515447, Dec. 2025, doi: 10.1080/14786451.2025.2515447.

[30] A. T. Abbas, N. Sharma, K. F. Alqosaibi, M. A. Abbas, R. C. Sharma, and A. Elkaseer, Investigation of Surface Quality and Productivity in Precision Hard Turning of AISI 4340 Steel Using Integrated Approach of ML MOORA PSO, Processes, Vol. 13, No. 4, 2025, doi: 10.3390/pr13041156.

[31] A. Ginting, R. A. Sidabutar, F. D. Pranata, K. Syam, S. Situmorang, and T. Fikriawan, Productivity improvement in hard turning of AISI 4340 with response surface methodology and machine learning, International Journal of Machining and Machinability of Materials, Vol. 27, No. 1, pp. 85–103, Jan. 2025, doi: 10.1504/IJMMM.2025.145073.

[32] M. M. Nasr and S. Anwar, Developing an intelligent approach based on ANFIS and advanced NSGA III for improving the turning performance of additively manufactured γ TiAl alloy, The International Journal of Advanced Manufacturing Technology, Vol. 137, No. 7, pp. 3333–3358, 2025, doi: 10.1007/s00170 025 15366 5.

[33] K. Ramesha et al., ANN and machine learning based predictions of MRR in AWSJ machining of CFRP composites, Sci Rep, Vol. 15, No. 1, p. 14218, 2025.

Session 6:

Machine tools and automation, flexible technological systems

Society of Production Engineering

ICPES 2025

40th INTERNATIONAL CONFERENCE ON PRODUCTION ENGINEERING - SERBIA 2025

DOI: 10.46793/ICPES25.270M

University of Nis
Faculty of Mechanical Engineering

Nis, Serbia, 18 - 19th September 2025

DEVELOPMENT OF A 2-AXIS SCARA ROBOT MOTION CONTROLLER BASED ON MCU

Bogdan MOMCILOVIC[1*], Nikola SLAVKOVIC[2]
Orcid: 0009-0000-4017-5399; **Orcid:** 0000-0003-1147-284X;
[1]University of Belgrade, Faculty of Mechanical Engineering, Serbia
*Corresponding author: bmomcilovic@mas.bg.ac.rs

Abstract: *The robot systems are designed and developed in such a way that they can successfully realize the specified task. Robot control systems must enable control of robot movement and all other activities necessary for completing the programmed tasks. One of the most important parts of any robot is its motion, and precise control in real-time. This paper proposes the development of a robot motion controller based on the MIKROE MINI-M4 development board with the STM32F415RG microcontroller. Research related to the field of motion controller development presented in this paper includes the realization of interpolation tasks in joint coordinates (PTP control) and interpolation of linear path segments in world coordinates (CP control). To perform these tasks, a mathematical model of interpolation in joint and world coordinates of a two-axis robot with non-trivial kinematics is introduced. The interpolator model is developed so that the joints' or the end-effector's velocities have a trapezoidal profile. To achieve the required trapezoidal velocity profile, synchronized control sequences are generated as a series of pulses with appropriate frequencies for each axis. As a verification, before implementing the mathematical model into the motion controller, simulations of the mathematical model itself and the robot's motion in the joint and world coordinates are performed in the MATLAB environment. The motion controller is implemented on the aforementioned development board with a microcontroller (MCU) using the MIKROC programming environment. The series of pulses with appropriate frequencies is tested on an oscilloscope as the first verification method of the realized motion controller. Reference points of movement defined in joint or world coordinates are obtained by interpreting the program in the MATLAB environment and transferred via serial communication to the MCU with integrated motion control using the MIKROE EasyPIC V7 development board. Experimental verification of the developed motion controller was performed by laser engraving the programmed trajectory of the robot end-effector according to the desired PTP or CP motion control.*

Keywords: *industrial robot, motion controller, non-trivial kinematics, interpolator, MCU*

1. INTRODUCTION

The use of robots in packaging represents a significant technological advancement, evolving from rudimentary mechanized systems to sophisticated, intelligent automation. Over the years, robots have become integral to the packaging process, known for their precision, efficiency, and versatility [1]. In the assembly line of any industry, the SCARA robot is commonly seen. It is generally used for pick and place tasks, but it has a wide range of applications. Hiroshi Makino developed the first SCARA (Selective

Compliance Assembly Robot Arm) robotic arm in Japan in 1979 [2].

Robot systems are developed to ensure they can efficiently accomplish the desired tasks. The robot control systems have to facilitate the control of both movement and any other auxiliary activities essential for executing the programmed tasks. Among the key components of a robot, its ability to move with precision and the need for real-time control is of utmost importance. The robot controller plays a crucial role in ensuring accuracy and directly affects the speed of the robot's movement. A need common to many robot applications is the accurate following of a specific path by the end-effector of the robot, which translates to accurately positioning the individual links that constitute the robot. The individual links are driven by joint actuators, which are rotary electric motors. In other words, the motion of the joint produced by the actuators determines the position and orientation of the end-effector at any time [3, 4]. In recent years, studies have focused on improving robot controllers in both hardware and software. The software includes algorithms that perform kinematics calculations, trajectory planning, and communication, while the hardware platform refers to the hardware circuit [5].

With the advancement of microcontroller (MCU) technology, it is now feasible to implement motion control systems using low-cost, high-performance MCUs that can meet the speed and precision requirements of robot mechanisms. Microcontrollers are well-suited for controlling robotic arms because they are relatively inexpensive, easy to program, and can be used to implement complex control algorithms. Additionally, microcontrollers can be used to interface with a variety of sensors and actuators, which makes them ideal for controlling robotic arms in a variety of different environments [6].

A standard commercial industrial robot usually does not enable open access to its control system. It presents a kind of box where the user cannot change the robot program. An open control system is required for verification of custom control algorithms in the laboratory and for the students' education. It should allow easy modification of the control structure, the ability to add axes, the possibility of connection of additional components, and integrate it into the control structure and monitoring functionalities from a high-level robotic controller to low-level control of servo drives [7].

This paper proposes the development of an open-source robot motion controller based on the MIKROE MINI-M4 development board, featuring the STM32F415RG microcontroller, for, in this development phase, a 2-axis SCARA robot with non-trivial kinematics. The controller is designed to realize interpolation tasks in joint coordinates (PTP control) and interpolate linear path segments in world coordinates (CP control).

2. OUTLINE OF THE CONCEPT

The paper presents the developed MCU-based motion controller of the 2-axis SCARA robot. Fig. 1 shows the developed system, including software and hardware integration with the realized prototype of the industrial SCARA-type robot.

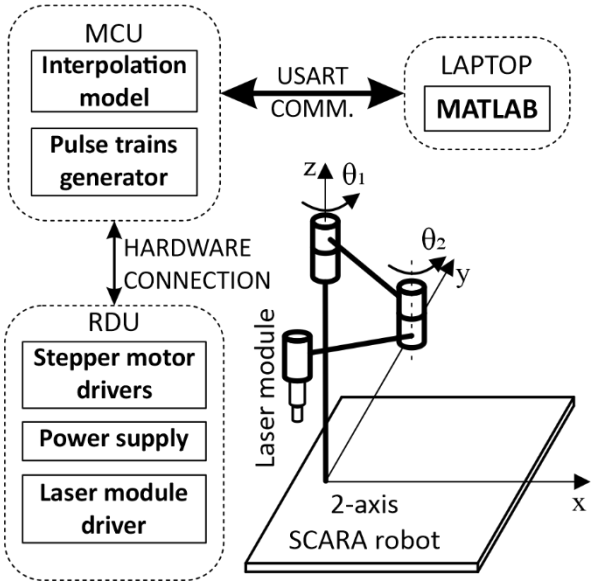

Figure 1. Outline of the concept

The communication with the robot is allowed through the achieved serial (USART) communication between MATLAB and the MCU. The reference points of movement

defined in joint or world coordinates are obtained by interpreting the program in the MATLAB environment. The interpreted data are transferred via serial communication to the MCU.

After obtaining the necessary data, the MCU, with an implemented interpolation model and motion control module, generates pulse trains to control the robot's stepper motors. To verify the developed system and the accuracy of the movements, a laser module is used as the end-effector of the robot to engrave the given trajectory. To move the robot, the neccesary hardware connections with robot drive unit (RDU) are performed.

3. INTERPOLATION MODEL

Path planning is one of the essential problems in robotics. The task of robot motion is defined by the path along which the robot, or end-effector, must move. The path can be represented by a geometric curve or a sequence of positions in joint or world coordinates. The problem of trajectory planning involves determining the desired reference joint or world coordinates as a function of time for the control system so that the robot follows the desired path.

3.1 PTP motion planning

In this paper, for the PTP motion planning, a linear trajectory with parabolic transitions is used, which enables synchronous PTP motion with a trapezoidal profile of joints' velocities, $\dot{\theta}_1$ and $\dot{\theta}_2$ [8]. For a given initial and final positions, q_0 and q_f, the motion duration t_f, as well as the acceleration time t_a, the segments of the polynomial trajectory can be generated as (1).

$$q(t)=\begin{cases} q_0+\frac{1}{2}\cdot\ddot{q}\cdot t^2, 0\le t\le t_a \\ q_0+\ddot{q}\cdot t_a\cdot\left(t-\frac{t_a}{2}\right), t_a<t\le t_{fa} \\ q_f-\frac{1}{2}\cdot\ddot{q}\cdot(t_f-t)^2, t_{fa}<t\le t_f \end{cases}$$

$$\dot{q}(t)=\begin{cases} \ddot{q}\cdot t, 0\le t\le t_a \\ \ddot{q}\cdot t_a, t_a<t\le t_{fa} \\ \ddot{q}\cdot(t_f-t), t_{fa}<t\le t_f \end{cases} \quad (1)$$

$$\ddot{q}(t)=\begin{cases} \ddot{q}, 0\le t\le t_a \\ 0, t_a<t\le t_{fa} \\ -\ddot{q}, t_{fa}<t\le t_f \end{cases}$$

$$t_{fa}=t_f-t_a$$

For the 2-DOF planar manipulator, the function $q(t)$ is defined as $q(t)=[\theta_1(t),\theta_2(t)]^T$. To realize the control of the stepper motors, the previous equations need to be defined in the discrete domain with the interpolation period T.

The time functions of acceleration, velocitiy and position from equation (1) could be expressed as $\ddot{\theta}_i(k\cdot T)$, $\dot{\theta}_i(k\cdot T)$ and $\theta_i(k\cdot T)$, for $i=1,2$. Since the interpolation period T and the motion duration $t=t_f$ are known, the interpolation period T can be excluded from the argument, so the trajectory segments in discrete domain are generated as (2):

$$\ddot{\theta}_i(k)=\begin{cases} \ddot{\theta}_{i\max}, k=0,...,n_a-1 \\ 0, k=n_a,...,(n-n_a)-1 \\ -\ddot{\theta}_{i\max}, k=(n-n_a),...,n-1 \end{cases}$$

$$\dot{\theta}_i(k+1)=\dot{\theta}_i(k)+\ddot{\theta}_i(k)\cdot T \quad (2)$$

$$k=0,...,n-1$$

$$\theta_i(k+1)=\theta_i(k)+\dot{\theta}_i(k)\cdot T+\frac{1}{2}\cdot\ddot{\theta}_i(k)\cdot T^2$$

$$k=0,...,n-1$$

where $n=div(t_f/T)$, $n_a=div(t_a/T)$, and $div()$ represents the integer division operator. Maximum joint velocities and accelerations are calculated using (3):

$$\dot{\theta}_{1m} = \frac{\Delta\theta_1}{(n-n_a)\cdot T} \quad \dot{\theta}_{2m} = \frac{\Delta\theta_2}{(n-n_a)\cdot T}$$
$$\ddot{\theta}_{1\max} = \frac{\dot{\theta}_{1m}}{n_a \cdot T} \quad \ddot{\theta}_{2\max} = \frac{\dot{\theta}_{2m}}{n_a \cdot T} \tag{3}$$

where $\Delta\theta_1 = \theta_{1f} - \theta_{10}$, and $\Delta\theta_2 = \theta_{2f} - \theta_{20}$.

3.2 CP motion planning

Within this paper, the case of trajectory planning for rectilinear path segments using a parametric description [8, 9] was considered. The parametric description of the straight-line path segment connecting points P_i and P_f, Fig.2, can be expressed as (4):

$$\boldsymbol{p}(s) = \boldsymbol{p}_i + \frac{s}{|\boldsymbol{p}_f - \boldsymbol{p}_i|}\cdot(\boldsymbol{p}_f - \boldsymbol{p}_i)$$
$$\boldsymbol{p}(0) = \boldsymbol{p}_i = [x_0, y_0, 0]^T \tag{4}$$
$$\boldsymbol{p}(|\boldsymbol{p}_f - \boldsymbol{p}_i|) = \boldsymbol{p}_f = [x_f, y_f, 0]^T$$

where s represents the curvilinear coordinate, which determines the distance between the point P in relation to the initial position P_i.

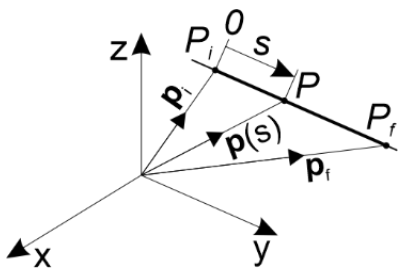

Figure 2. Parametric description of the straight-line

For a given initial and final positions, $\boldsymbol{p}_i$ and $\boldsymbol{p}_f$, the motion duration t_f, as well as the acceleration time t_a, the first and second derivatives of the curvilinear coordinate s are calculated as (5):

$$\dot{s} = \frac{\Delta s}{t_f - t_a}$$
$$\ddot{s} = \frac{\dot{s}}{t_a} \tag{5}$$
$$\Delta s = |\boldsymbol{p}_f - \boldsymbol{p}_i|$$

The rectilinear path segments are now calculated as (6):

$$\ddot{s}(t) = \begin{cases} \ddot{s}, 0 \le t \le t_a \\ 0, t_a < t \le t_{fa} \\ -\ddot{s}, t_{fa} < t \le t_f \end{cases}$$
$$\dot{s}(t) = \begin{cases} \ddot{s}\cdot t, 0 \le t \le t_a \\ \dot{s}, t_a < t \le t_{fa} \\ -\ddot{s}\cdot(t_f - t), t_{fa} < t \le t_f \end{cases} \tag{6}$$
$$s(t) = \begin{cases} \frac{1}{2}\cdot\ddot{s}\cdot t^2, 0 \le t \le t_a \\ \dot{s}\cdot\left(t - \frac{t_a}{2}\right), t_a < t \le t_{fa} \\ -\frac{1}{2}\cdot\ddot{s}\cdot(t_f - t)^2, t_{fa} < t \le t_f \end{cases}$$

For the known interpolation period T and the motion duration $t = t_f$, the trajectory in the discrete domain can be expressed as (7):

$$\ddot{s}(k) = \begin{cases} \ddot{s}, k = 0, ..., n_a - 1 \\ 0, k = n_a, ..., (n - n_a) - 1 \\ -\ddot{s}, k = (n - n_a), ..., n - 1 \end{cases}$$
$$\dot{s}(k+1) = \dot{s}(k) + \ddot{s}(k)\cdot T$$
$$k = 0, ..., n-1 \tag{7}$$
$$s(k+1) = s(k) + \dot{s}(k)\cdot T + \frac{1}{2}\cdot\ddot{s}(k)\cdot T^2$$
$$k = 0, ..., n-1$$

Based on the previously calculated and equation (4), as well as the first and second derivatives of equation (4), the end-effector's acceleration $\ddot{\boldsymbol{p}}_e$, velocity $\dot{\boldsymbol{p}}_e$ and position $\boldsymbol{p}_e$ in the world coordinates are determined as (8) for $k = 0,1, \dots, n-1$:

$$\ddot{\boldsymbol{p}}_e(k)=\begin{bmatrix}\ddot{x}_e(k)\\ \ddot{y}_e(k)\\ 0\end{bmatrix}=\ddot{s}(k)\cdot\frac{(\boldsymbol{p}_f-\boldsymbol{p}_i)}{|\boldsymbol{p}_f-\boldsymbol{p}_i|}$$

$$\dot{\boldsymbol{p}}_e(k)=\begin{bmatrix}\dot{x}_e(k)\\ \dot{y}_e(k)\\ 0\end{bmatrix}=\dot{s}(k)\cdot\frac{(\boldsymbol{p}_f-\boldsymbol{p}_i)}{|\boldsymbol{p}_f-\boldsymbol{p}_i|} \qquad (8)$$

$$\boldsymbol{p}_e(k)=\begin{bmatrix}x_e(k)\\ y_e(k)\\ 0\end{bmatrix}=\boldsymbol{p}_i+s(k)\cdot\frac{(\boldsymbol{p}_f-\boldsymbol{p}_i)}{|\boldsymbol{p}_f-\boldsymbol{p}_i|}$$

For the control software realization, the 2-DOF manipulator's joint coordinates, $\theta_1(k)$ and $\theta_2(k)$, are determined based on the calculated position of the end-effector $\boldsymbol{p}_e(k)$ using the inverse kinematics equations (9) for SCARA type robot:

$$\begin{gathered}c\theta_2=\frac{x_e^{\,2}(k)+y_e^{\,2}(k)-a_1^{\,2}-a_2^{\,2}}{2\cdot a_1\cdot a_2}\\ s\theta_2=-\sqrt{1-c^2\theta_2}\\ \theta_2(k)=A\tan 2\left(s\theta_2,c\theta_2\right)\\ \alpha=A\tan 2\left(y_e(k),x_e(k)\right)\\ \beta=A\tan 2\left(a_2\cdot s\theta_2,a_1+a_2\cdot c\theta_2\right)\\ \theta_1(k)=\alpha-\beta\end{gathered} \qquad (9)$$

where a_1 and a_2 represent the lengths of the robot's segments. The inversion of the Jacobian matrix J^{-1} could be used to determine the velocities and accelerations in joint coordinates.

4. MOTION CONTROL DEVELOPMENT

The development concept of an MCU-based motion controller presented in this paper consists of three parts: 1) software implementation of the interpolation model, 2) routine development for generating pulse trains, and 3) hardware connection of the MCU to a prototype of the industrial SCARA-type robot.

4.1 Software implementation

For programming the selected STM32F415RG microcontroller mikroC PRO for ARM compiler was used. The environment of the compiler enabled writing, compiling, and debuging the code.

The presented interpolation model for the joint and world coordinates trajectory planning is implemented in the form of routines that are executed depending on the desired motion of the robot (PTP or CP mode). In order to control the motion of a stepper motors driven robot, it is necessary to convert the calculated values of the joint coordinates into the appropriate number of pulses.

Given that the trajectory is divided into segments according to the interpolation period T and the number of segments is known, the joint coordinate's change is calculated relative to the previous segment, for each current segment. For the PTP mode, this change is calculated using (11), according to (2):

$$\Delta\theta_i(k)=\dot{\theta}_i(k-1)\cdot T+\frac{1}{2}\cdot\ddot{\theta}_i(k-1)\cdot T^2 \qquad (11)$$

while for the CP mode, this change is calculated using (12), according to (9):

$$\Delta\theta_i(k)=\theta_i(k)-\theta_i(k-1) \qquad (12)$$

The joint coordinates' changes (11) and (12) are converted into the corresponding number of pulses based on the angular resolution of each robot axis. The angular resolution of the robot axis φ_k is calculated based on the hardware characteristic of the stepper motor α_k, the set microstep on the stepper motor driver ms, and the joint's gear ratio i_p using (13):

$$\varphi_k=\frac{\alpha_k}{ms\cdot i_p} \qquad (13)$$

The corresponding number of steps $k_{k,i}$ is now obtained based on equation (14), noting that the angular resolutions of the individual axis $\varphi_{k,i}$ do not have to be equal.

$$k_{k,i}(k)=\frac{\Delta\theta_i(k)}{\phi_{k,i}} \qquad (14)$$

Based on the calculated number of steps $k_{k,i}$ and the known interpolation period T, the one pulse duration T_{imp} is calculated, while the

high-level duration T_h is known in advance, Fig.3.

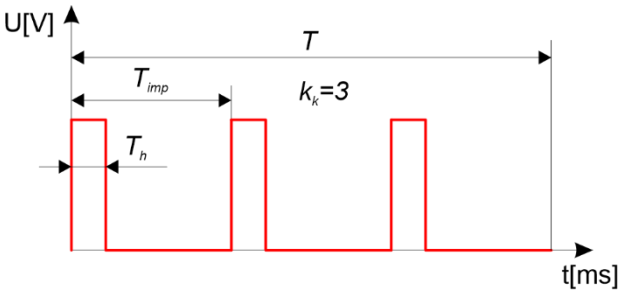

Figure 3. Pulse train characteristics

4.2 Pulse trains generation

To create a routine that generates pulse trains in real time on the selected MCU, a timer is used, which counts clock cycles to measure time intervals.

```
routine: timer_interrupt()
        On every microsecond
            DO:
                micros_count++;
routine: pulse_train()
        while (micros_count <= T)
            DO:
                updatePortAState();
                updatePortBState();
                switchPortsStates();
routine: updatePortA(B)State();
        if (micros_count <= T_h)
            DO:
                PortAState = 1;
                (PortBState = 1;)
        elif (micros_count <= T_impA(B) - T_h)
            DO:
                PortAState = 0;
                (PortBState = 0;)
routine: switchPortsStates();
        Update state of the physical pin
            DO:
                GPIO_A = PortAState;
                GPIO_B = PortBState;
```

Figure 4. The algorithm for pulse trains generation

The task of the developed routine is to perform a synchronous update of the corresponding ports' states on the MCU, defined as outputs. The algorithm for making such a routine is shown in Fig. 4.

The pulse trains generated in this way are tested on a 2-channel oscilloscope as the first verification method of the realized motion controller, Fig 5.

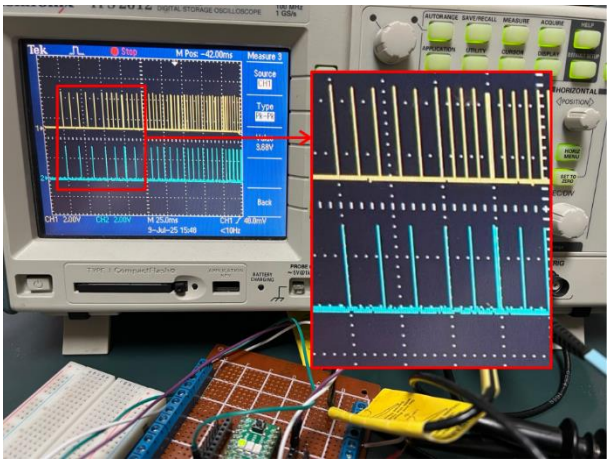

Figure 5. Oscilloscope verification

The oscilloscope display confirmed the synchronous generation of the control sequence in real time, based on the calculated number of pulses for each path segment, as well as the one pulse duration T_{imp}.

4.3 Hardware connection

To realize the motion controller of the 2-axis SCARA robot, the hardware connection of the MCU with the necessary electronic components is performed. The connection between all the components used to prove the presented concept is shown in Fig. 6.

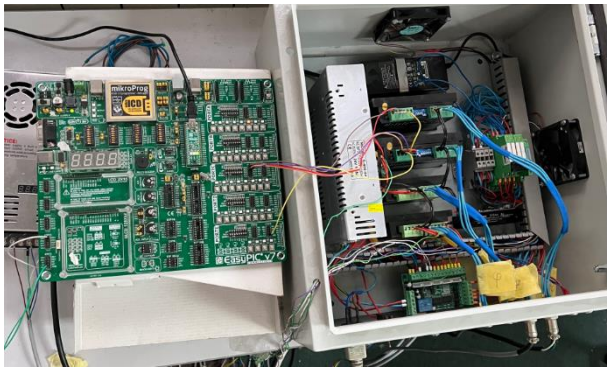

Figure 6. Hardware connection of the components

To achieve the communication and data exchange between MATLAB and MCU, the MIKROE MINI-M4 development board with the STM32F415RG microcontroller is placed on the MIKROE EasyPIC V7 development board, which provides the necessary peripherals. In this case, a laser module is used as an end-effector of the robot. The laser module provides engraving of

the robot's toolpath. The remaining components represent the standard elements for controlling the robot, which uses stepper motors for drives.

5. EXPERIMENTAL VERIFICATION

The developed MCU-based 2-axis SCARA robot motion controller is verified through several experiments. To verify the accuracy of the positioning and the robot's tooltip movement according to the given trajectory, the laser module is used as the robot's end-effector.

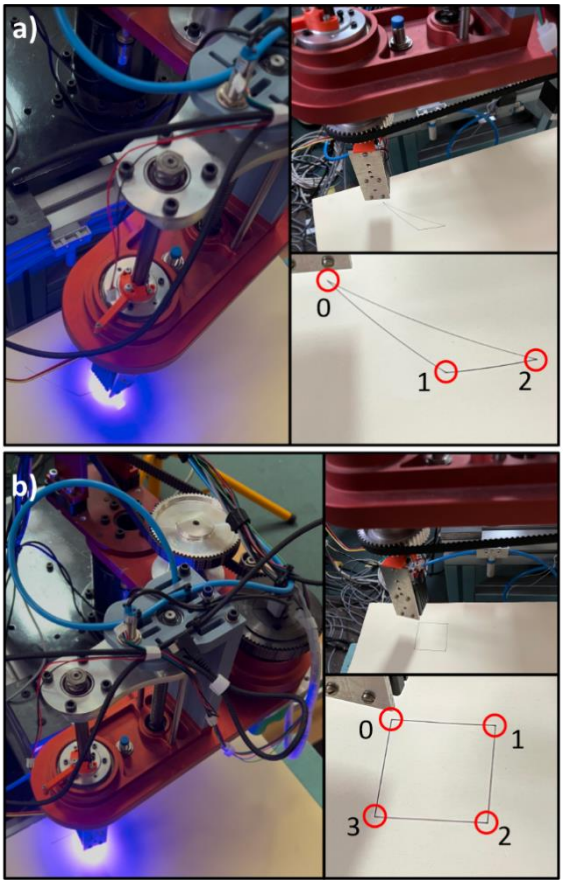

Figure 7. Experimental verification

The developed motion controller is tested with the desired trajectories in PTP or CP motion mode. In both cases, the trajectory consists of several positions defined in the joint (PTP mode) or world (CP mode) coordinates. The given acceleration time is $t_a = 0.5s$, time of the robot movement between two positions is $t_f = 5s$, the high-level duration is $T_h = 250us$, and interpolation period is $T = 50ms$.

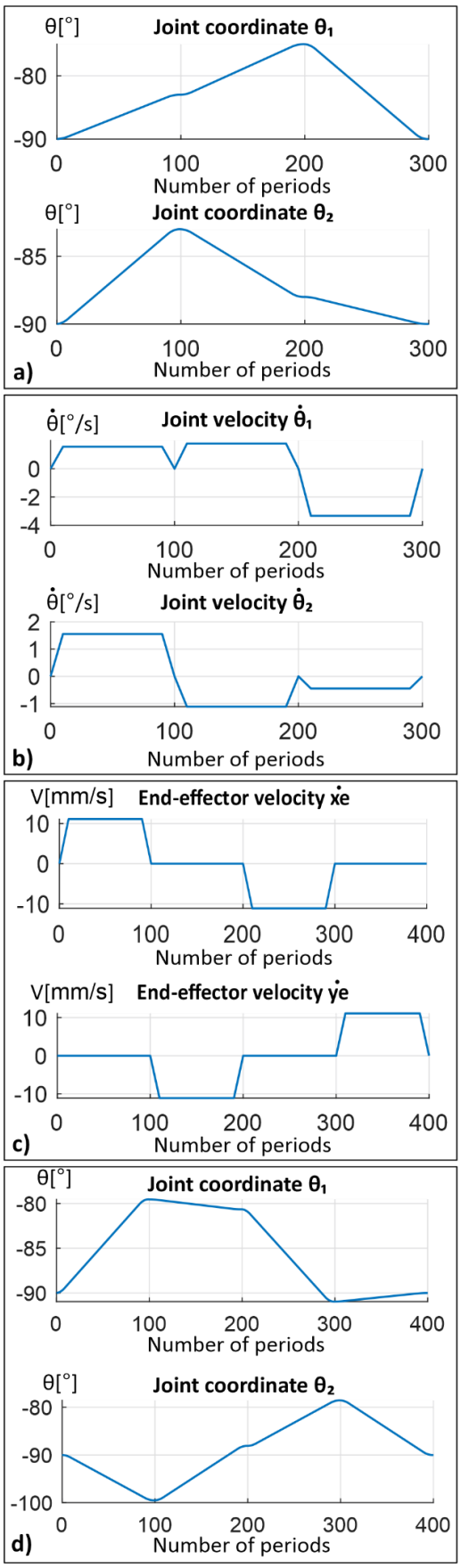

Figure 8. Interpolation results for PTP and CP mode

The engraved trajectory of the robot's toolpath as the result of the defined robot's

movement in PTP motion mode with defined positions 0-1-2-0, is shown in Fig. 7a. According to the defined interpolation model, the robot's toolpath between two positions (0-1, 1-2 or 2-0) represents a part of the arc obtained as a result of synchronous movement of the two axes. In this case, the robot positions are defined in the joint coordinates.

The engraved trajectory of the robot's toolpath, as the result of the defined robot's movement in CP motion mode with defined positions 0-1-2-3-0, is shown in Fig. 7b. In this case, the robot positions are defined in the world coordinates, and the robot's toolpath between two positions is a straight line.

Based on the interpolation model and the set parameters of the robot motion in PTP mode, Fig. 8a shows the joint coordinates dependence of the interpolation periods, and Fig. 8b shows the joint velocities dependence of the interpolation periods. Defined robot positions in the joint coordinates are: [0(-90°, -90°), 1(-83°, -83°), 2(-75°, -88°), 0(-90°,90°)].

For CP motion mode, Fig. 8c shows the end effector velocity dependence of the interpolation periods, and Fig. 8d shows the joint coordinates dependence of the interpolation periods for the given motion in CP mode. Defined robot positions in the world coordinates are: [0(-275mm, -275mm), 1(-225mm, -275mm), 2(-225mm, -325mm), 3(-275mm, -325mm), 0(-275mm, -275mm)].

6. CONCLUSION

This paper presents the development of the MCU-based motion controller for the 2-axis SCARA robot with non-trivial kinematics. To achieve this, the interpolation model is implemented on the MCU as routines supporting both point-to-point (PTP) and continuous path (CP) robot control. The presented concept is validated through several experiments, and the end-effector trajectories are obtained via laser engraving.

By measuring the physical distance between reference points on the obtained trajectories, it can be concluded that the robot moves precisely, according to the given coordinates. Furthermore, the measured time for the robot's movements corresponds to the programmed movement time.

Future research will focus on enhancing the interpolation model for circular path segments and developing methods for planning the orientation of the end-effector.

ACKNOWLEDGEMENT

This research was supported by the Ministry of Science, Technological Development and Innovations of the Serbian Government under the contract No. 451-03-137/2025-03/ 200105.

REFERENCES

[1] Riyan Vikas Patel, 2024, Opportunities and Challenges for Adoption of Robotics in Packaging Industry: A Review, IOSR Journal of Engineering, Vol. 14, and Issue 1, pp. 32-38.

[2] Tay, See Han, Wai Heng Choong, and Hou Pin Yoong. "A review of SCARA robot control system." 2022 IEEE International Conference on Artificial Intelligence in Engineering and Technology (IICAIET). IEEE, 2022.

[3] Mustafa, Mustafa M., and Ibrahim Hamarash. "Microcontroller-based motion control for DC motor driven robot link." 2019 International Aegean Conference on Electrical Machines and Power Electronics (ACEMP) & 2019 International Conference on Optimization of Electrical and Electronic Equipment (OPTIM). IEEE, 2019.

[4] Gopal, Madan. Control systems: principles and design. McGraw-Hill Science, Engineering & Mathematics, 2008.

[5] Cong, V. D. (2021). Industrial Robot Arm Controller Based on Programmable System-on-Chip Device. FME Transactions, 49(4).

[6] Rahulraj Mahan, Aarti Patil, Jyoti Kedar, 2024, Movementable Robotic Arm Using MicroController, International Journal of Enhanced Research in Management & Computer Applications, Vol. 13, Issue 4, pp. 654-659.

[7] Robert UVEGES, Frantisek DUROVSKY, David LINDR, OPEN ROBOTIC CONTROLLERS, Acta

Electrotechnica et Informatica, Vol. 16, No. 3, 2016, pp. 8–13.

[8] D. Milutinović, Industrijski roboti, Univerzitet u Beogradu - Mašinski fakultet, 2024.

[9] L. Sciavicco, B. Siciliano, Modelling and control of robot manipulators, Springer Science and Business Media,2012.

Society of Production Engineering

ICPES 2025

40th INTERNATIONAL CONFERENCE ON PRODUCTION ENGINEERING - SERBIA 2025

DOI: 10.46793/ICPES25.279P

University of Nis Faculty of Mechanical Engineering

Nis, Serbia, 18 - 19th September 2025

HOW THE LOLA 8A COMPUTER WAS MADE — A REVERSE ENGINEERING STUDY

Stevan PAROJČIĆ[1], Dragan PAVLOVIĆ[1]*

Orcid: 0000-0003-2299-0579

[1] Lola Institute, Kneza Višeslava 70A, 11030 Belgrade, Serbia

*Corresponding author: pavlovic.dragan74@gmail.com

Abstract: *This paper presents the reconstruction process of the domestic microcomputer Lola 8A, originally developed in the early 1980s at the "Ivo Lola Ribar" Institute. Through reverse engineering, the original device hardware was analyzed, its functional units mapped, and a working replica of the computer system was built using modern tools and replacement components. Special emphasis was placed on preserving the original architecture, the behavior of the software environment, and compatibility with peripheral units. The process involved creating a new motherboard and reviving the ROM environment by implementing a BASIC interpreter, a monitor program, and a mini-assembler. The device was successfully tested using controlled environments and original applications, although very few of the latter have survived. This project not only reconstructed a significant example of domestic technological heritage but also laid the foundation for educational use, museum exhibits, and the development of modernized platforms based on open hardware principles.*

Keywords: *Lola 8A, Reverse Engineering, Intel 8085 Microprocessor, BASIC Interpreter, Digital Technological Heritage, Retro Computers.*

1. INTRODUCTION

At a time when microcomputers were beginning to conquer the world, the 'Ivo Lola Ribar' factory from Železnik made a significant leap forward — in the early 1980s, it started developing its computer system, the Lola 8. This device represented one of the first attempts in the former Yugoslavia to construct a functional, affordable, and technically competitive microcomputer, intended for a broad range of users, from educational institutions and industrial automation to household use as a home computer.

Unlike domestically produced computers such as the Pecom, the Lola 8A gives the impression of significantly more robust and reliable construction, both in terms of component selection and overall design approach. Architecturally and structurally, its quality and integration logic resemble higher-tier Western systems such as the BBC Model B or Apple II, featuring an efficient switched-mode power supply, a compact enclosure, and a high-quality keyboard, marking a substantial advancement over domestic standards of that time. Lola 8a represents one of the brightest achievements of the domestic industrial electronics of that period.

Motivated by the technical significance of this computer and its place within the domestic technological heritage, Author (1) conducted a complete reconstruction of the Lola 8A computer in 2023 using reverse engineering. Author (2) also participated in the project, providing additional analytical and technical support.

This endeavor encompassed the physical and functional analysis of the remaining operational device, the development of a new motherboard, the replacement of obsolete components, as well as the revitalization of the software environment. The ultimate goal was multifaceted: functional replication, process documentation, educational demonstration, and a contribution to the preservation of domestic engineering heritage, with genuine potential for future applications.

2. THE ORIGINAL LOLA 8A COMPUTER — A TECHNICAL REVIEW

The Lola 8A computer, developed in the early 1980s within the 'Ivo Lola Ribar' Institute, represented one of the first domestic attempts to create a microcomputer system intended for industrial and educational applications. Radovan Novaković authored the hardware design, while Nela Ristanović developed the software part [1].

The Lola 8A was developed as a derivative model of systems based on the Intel 8085 microprocessor, which was primarily used at the Institute for industrial CNC machines and robotics [2]. The Intel 8085, operating at a clock speed of 5 MHz, provided essential control and logical functions in real time. The memory configuration included 6 KB of static RAM (type 6264), with the possibility of expansion up to 38 KB, which at the time represented a considerable investment due to the high cost of memory. The ROM memory totaled 12 KB, expandable to 16 KB, and contained a built-in BASIC interpreter, allowing for direct programming without the need for external tools.

In the domain of video subsystems, the advanced HD46505SP video controller (also known as the CRTC – Cathode Ray Tube Controller) was used, providing a graphical resolution of 75×80 pixels and a text mode of 40×25 characters. This chip was comparable to those used in computers such as the BBC Micro and Amstrad CPC, placing the Lola 8A among the more powerful graphics platforms of domestic production.

The audio subsystem was based on the popular AY-3-8910 chip, which enabled three independent tones across an eight-octave range and was widely used in the microcomputer industry of the time. However, this chip has become increasingly difficult to source in recent years.

The computer featured a 48-key alphanumeric keyboard, and all subsystems—from power supply to peripheral units—were housed in a compact, integrated enclosure with switched-mode power supply, representing an advanced design decision compared to the then-dominant solutions relying on bulky transformers.

Table 1. *Detailed Overview of Lola 8A Computer Specifications*

Component	Specification
Processor (CPU)	Intel 8085A @ 4.9 MHz
Random Access Memory (RAM)	16 KB (expandable up 32 KB)
ROM	12 kB, expandable to 16 kB, with BASIC interpreter
Video controller	HD46505SP(CRTC), graphics 75 x 80 pixels, text 40 x 25 characters
Audio chip	AY-3-8910, three tones, eight octave range
Keyboard	Alphanumeric, 48 buttons
Housing	Compact, integrated with switching power supply
Extensions	64-pin EURO connector (A/D, I/O, serial interfaces)
Intended	Industry, CNC systems, education

3. REVERSE ENGINEERING PROCESS

For expansion purposes, the system featured a 64-pin EURO connector, which allowed for the connection of additional modules such as A/D converters, I/O units, and serial/communication interfaces. Among other notable components were the SAB8226 used as a buffer chip—a relatively rare element today—and a large number of standard TTL integrated circuits. Notably, the ULA (Uncommitted Logic Array), which was commonly used in many computers of that era, was not implemented, simplifying servicing and enabling easier replacement of individual components. A detailed overview of the Lola 8A computer specifications is presented in Table 1.

Reverse engineering represents a methodological approach to the analysis and reconstruction of an existing device or system to understand its structure, functionality, and mode of operation, especially in cases where the original technical documentation is unavailable or incomplete.

There is very little information in the literature regarding the mentioned computer. In the context of reconstructing the "Lola 8a" computer, this process was essential for identifying components, mapping interconnections, and enabling future replication of the system.

Given that the Lola Institute possesses the original version of the Lola8a computer, the first step in the process was a physical inspection and analysis of the device. This included careful disassembly and identification of all components, with special attention given to preserving the original connections and traces on the printed circuit board (PCB). Based on visual inspection and the layout of elements, a preliminary schematic of interconnections was created using the KiCad 7.0 software [3]. A detailed list of problematic connections was also compiled, after which testing began.

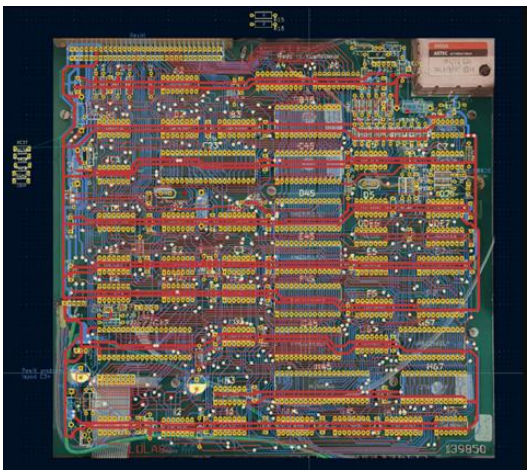

Figure 1. Connection diagram in KiCad 7.0 software package

During the process, the following tools and methods were used:

Logic analyzer – utilized for monitoring digital signals, detecting errors, and analyzing communication protocols between digital components such as chips.

Oscilloscope – used to measure both analog and digital voltages. Particularly useful for verifying clock signals and bus activity, as well as for checking the operation of chips and other elements.

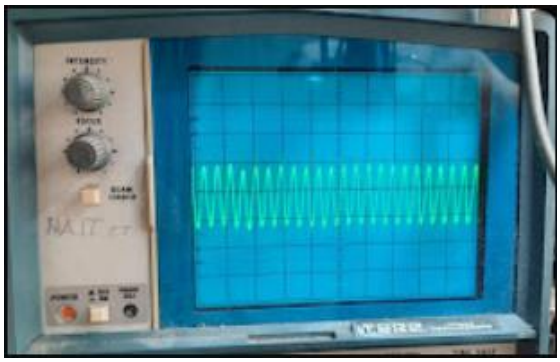

Figure 2. Verification of the operation of elements with the help of an oscilloscope

Micro-analysis – used for detailed visualization of traces and connections on the printed circuit board (PCB), identification of components with unclear markings, as well as for analyzing internal layers in multilayer boards without causing physical damage.

Numerous challenges hindered the reverse engineering process for the computer:

Lack of detailed technical documentation – the analysis required a deductive approach,

relying on scarce information from the available manual for the Lola 8a computer and comparisons with architecturally similar systems.

Inactive or damaged chips – dynamic testing during operation was not possible, so the chips were subjected to static analysis of pins, current paths, and logical connections in order to determine their function and potential interactions within the hardware architecture.

The search for original components – involved an extensive investigation through old electronic devices of a compatible generation, followed by careful disassembly and testing of preserved and functional parts.

Sourcing replacement parts – particularly for specific components that are no longer in production, which required searching for functional equivalents. However, some elements had to be repurposed from old computers, such as the 7404 inverter.

All steps were carefully documented—including photographs, schematics, measurements, and notes—to facilitate future reconstruction of the device and support the education of other researchers and enthusiasts. This approach not only contributes to the transparency of the work but also serves as a foundation for the potential creation of a functional replica of the Lola 8a.

4. DEVICE RECONSTRUCTION AND TESTING

The reconstruction process of the Lola8a computer required a careful combination of engineering expertise, research, and enthusiasm. At this stage of the project, the focus was on the precise reconstruction of the hardware assembly, revitalization of the software part, and thorough detail functionality testing to achieve a faithful replica of the original system.

The initial step involved designing a new motherboard using the KiCad 7.0 software for PCB layout. Photographs and manually recorded layouts from the original Lola8a device served as references. After finalizing the design, the board was manufactured by JLC PCB. Component soldering was carried out carefully and manually, with special emphasis on preserving the original system logic. Components that are no longer available were replaced with modern equivalents, following prior compatibility testing.

Alongside the physical reconstruction, the revival of the software component was carried out.

As a brief overview of the Lola ROM, in addition to BASIC, both a monitor program and a mini-assembler were implemented, enabling easier manipulation and correction of machine programs. Embedding monitor and assembler programs into the computer's ROM had not been practiced until now, although similar implementations were observed in Acorn's BBC system. It should be noted that it is not possible to run both the assembler and BASIC simultaneously; the system operates in one of the modes—either monitor or BASIC [4].

The keyboard and monitor are connected using converter units that translate signals into a format compatible with modern devices, while preserving the logic of the original interaction. The computer replica has been successfully integrated with several original peripheral components, including period-specific keyboards, CRT monitors, and external storage (cassette tapes). Through a series of adapters and electronic interfaces, communication between the replica and these units was enabled without compromising functionality.

The final stage of the project involved intensive system testing under controlled conditions. Test programs were executed, including examples written in the BASIC language, to verify input/output functionality. Industrial applications that were once used on Lola8a systems, where available, were run in an emulated environment due to the lack of additional original hardware. The only preserved game operated flawlessly. Results demonstrated a high level of accuracy and reliability compared to the original system. The computer's stability was tested through continuous operation for more than 48 hours without errors, confirming the quality of the reconstructed system.

Figure 3. Testing the Lola8a device

To verify the functionality of the developed software environment for the Lola 8a replica, basic real-time system tests were conducted. The testing focused on confirming proper initialization of hardware resources, execution of basic instructions, and operation of input-output (I/O) modules.

The entire process has been thoroughly documented through technical reports, reconstruction photographs, video demonstrations of the system's operation, as well as a digital archive of software components. This ensures the project's lasting value for future research, educational purposes, and the preservation of domestic technological heritage.

5. CONCLUSION

By implementing a replica of the Lola 8a computer, a significant example of domestic digital technology from the mid-1980s was successfully reconstructed. The project encompassed the entire process of reverse engineering, identification of hardware functional units, and the development of new technical documentation.

The result holds multifaceted value: as an educational tool for studying the fundamentals of digital systems, as an exhibit for museum and academic presentations, and as a foundation for the development of modernized versions based on FPGA technology or open-source hardware.

Potential applications include data acquisition, control of basic CNC systems, and development of mini educational platforms ('Mini Lola'), thereby positioning the project within the domain of contemporary technical practice.

The expertise acquired during the project is readily applicable to tasks involving the restoration, analysis, and interpretation of vintage computer systems.

ACKNOWLEDGEMENT

The authors gratefully acknowledge the financial support of the Ministry of Science, Technological Development and Innovation of the Republic of Serbia (Grant No. 451-03-136/2025-03/ 200066).

REFERENCES

[1] Dejan Ristanović, Home Computers Made in Serbia (PDF, original in Serbian).

[2] LOLA Computer Factory, LOLA8A User and Programming Manual, Belgrade, 1986 (original in Serbian).

[3] Lola8a blog, available at: https://lola8a.blogspot.com/, accessed: 08.07.2025.

[4] Computer World, Our Test: Lola 8A at Home and in School, September 1987 (original in Serbian).

Society of Production Engineering

ICPES 2025

40th INTERNATIONAL CONFERENCE ON PRODUCTION ENGINEERING - SERBIA 2025

DOI: 10.46793/ICPES25.285M

University of Nis Faculty of Mechanical Engineering

Nis, Serbia, 18 - 19th September 2025

EXPLAINABLE ARTIFICIAL INTELLIGENCE IN INDUSTRIAL AUTOMATION AND ROBOTICS: STATE, PROSPECTS AND A CASE-STUDY

Nemanja MARKOVIĆ[1], Emilija ĆOJBAŠIĆ[2], Dejan RANČIĆ[2], Nedeljko DUČIĆ[3], Žarko ĆOJBAŠIĆ[1,*]

Orcid: 0000-0002-9445-7700; ...; **Orcid:** 0009-0001-3071-5897;

[1]Faculty of Mechanical Engineering, University of Niš, Niš, Serbia

[2]Faculty of Electronic Engineering, University of Niš, Niš, Serbia

[2]Faculty of Technical Sciences, University of Kragujevac, Čačak, Serbia

*Corresponding author: zcojba@ni.ac.rs

Abstract: *The integration of Artificial Intelligence (AI) into industrial automation and robotics has led to considerable improvements in adaptability, efficiency, and decision-making, allowing industrial control and robotics to respond to new challenges and demands in industrial setting. However, the non-transparent nature of many AI solutions poses significant challenges in safety-critical industrial environments where transparency, trust, and reliability are essential. Explainable Artificial Intelligence (XAI) addresses these concerns by providing insights into the inner workings of AI-driven systems. This paper briefly reviews the current landscape of XAI applications in industrial automation and robotics, highlighting key methods and limitations. It categorizes state-of-the-art approaches applicable to industrial control, fault detection, predictive maintenance, and human-robot interaction. Special attention is given to XAI methods based on Adaptive Neuro-Fuzzy Inference Systems (ANFIS), while a XAI in industrial automation case study is also presented. Finally, future research directions are outlined, aimed at integrating XAI more seamlessly with autonomous systems, fostering safer, more transparent, and user-aligned intelligent automation solutions.*

Keywords: *Explainable Artificial Intelligence (XAI), Industrial Automation, Robotics, Intelligent Control Systems, Trustworthy Artificial Intelligence, Adaptive Neuro-Fuzzy Inference Systems (ANFIS)*

1. INTRODUCTION

Artificial Intelligence (AI) has become deeply integrated into modern life, delivering high performance across sectors such as healthcare, finance, and transportation, but often through complex and opaque models like deep neural networks. As these advanced AI models function as "black boxes", Explainable AI (XAI) [1][2] has emerged to enhance transparency and interpretability, providing insights into how AI systems make decisions and fostering trust among users [3][4][5]. The core motivation for XAI lies in the need for responsibility, ethical use, and user confidence in critical applications, where understanding and justifying AI decisions is essential to ensure confidence, safety, and informed decision-making [6][7][8].

Explainable Artificial Intelligence (XAI) is also crucial for building trust and facilitating the adoption of AI systems in Industry 4.0 and 5.0, as it provides human-understandable explanations for decisions made by complex models used in automation and manufacturing

processes [1][2]. By enhancing transparency and interpretability, XAI supports smarter, safer, and more accountable industrial operations, enabling better integration of AI in high-stakes applications such as predictive maintenance, quality control, and smart manufacturing. In the context of Industry 4.0 and 5.0, XAI is also becoming increasingly essential for industrial robotics [9][10] because it enhances transparency, trust, and accountability in AI-driven robotic systems, which is critical for ensuring safety and facilitating broader adoption in dynamic and safety-critical environments.

2. BRIEF CLASSIFICATION OF EXISTING XAI METHODS

Adopting high-stakes industry applications requires a number of current research initiatives towards responsible or human-centric XAI based systems in industrial automation and robotics.

XAI approaches can be categorized based on their characteristics, such as whether they are specific to a model or model-agnostic, whether they provide local or global explanations, and whether they are applied before, during, or after model training, including visualization, textual explanations and surrogate-based methods, etc. Fig. 1 categorises XAI methods in one possible way, focusing on XAI applications in industrial automation and robotics.

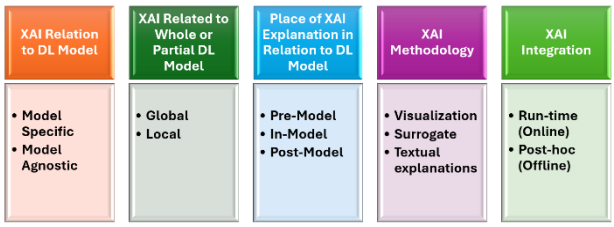

Figure 1. Taxonomy of XAI approaches [13][2][6]

The most common XAI methods include SHAP, LIME, feature importance, decision trees, partial dependency plots, and visualization techniques such as activation maps [3][4][5][6]. For example, SHAP (SHapley Additive exPlanations) provides data-driven insights by assigning each feature an importance value based on game theory, while LIME (Local Interpretable Model-agnostic Explanations) generates local approximations of complex models to explain individual predictions.

2.1 XAI in Industrial Control and Robotics based on ANFIS

The Adaptive Network-based Fuzzy Inference System (ANFIS) offers a modelling approach that yields transparent and interpretable reasoning, though it typically handles data with significantly lower dimensionality compared to deep learning (DL) models. One of the proposed promising approaches to building XAI systems assumes that DL and ANFIS approaches are united to benefit from high-dimensionality capability of DL and interpretability of ANFIS systems.

Combining CNN deep learning computer vision models with ANFIS in industrial automation and robotics potentially [11][12]:

- Enhances system transparency and trustworthiness through explainable AI,
- Improves interpretability of deep learning models in industrial computer vision,
- Provides guidance for next DL applications in industrial automation and robotics.

ANFIS based XAI can be implemented by interconnecting Deep Learning (DL), black box model, with ANFIS, as an interpretable model, in series or in parallel connection [11][12][13].

2. CASE STUDY – AN APPLICATION OF XAI IN INDUSTRIAL CONTROL AND ROBOTICS

In our previous paper [13] a XAI approach for industrial automation has been considered, based on ANFIS. The considered XAI approach has been applied to industrial automation in the food industry, namely to the deep learning-based system for grading of apples and defective apples detection on a robotic fruit sorting and packaging line.

In the industrial setup, the proposed approach was implemented on a Siemens SIMATIC S7-1500 PLC equipped with a Siemens TM NPU artificial intelligence module,

integrated with a Basler 2 MP 25 FPS camera, and tested using an experimental setup that includes a FlexLink conveyor and a Mitsubishi RV-2SDB industrial robot. Alternative setup based on the NVIDIA Jetson Xavier NX series has also been considered. In our previous approach, computer vision related deep learning model takes input and produces some features of the apples, which can be called decisions (namely size, roundness, bruising, color). These decisions (output of deep learning model) are used as input in ANFIS model. The role of ANFIS model is to find rules which are responsible for deep learning model to take decisions by classifying apples in quality classes (Fig. 2).

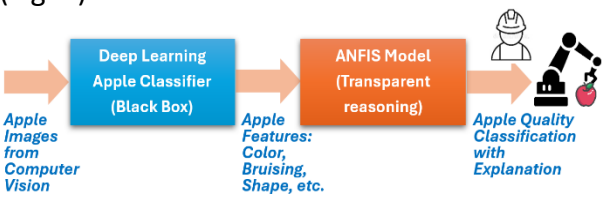

Figure 2. XAI based on cascade connection of DL and ANFIS [13]

Here, two alternative approaches [13][14] are considered for the same problem. Namely, SHAP and LIME methods, briefly defined in Section 2, have been implemented to obtain XAI solution to considered industrial problem in an industrial automation/robotic setup. Both methods have been implemented using Python.

SHAP method analyzed the input image to determine the influence of each region on the DL model's class prediction. The image was resized and normalized to expected input format, while a masker hid or blurred pixels estimating their contribution. SHAP explainer was initialized with the prediction function and masker, converting images into class probabilities. SHAP values were then computed, indicating each image segment's contribution to class probabilities. Fig. 3 shows SHAP results for several classes, displaying the original image with color-coded regions: red regions indicate pixels that increase class probability, while blue reflect negative contributions that lower it.

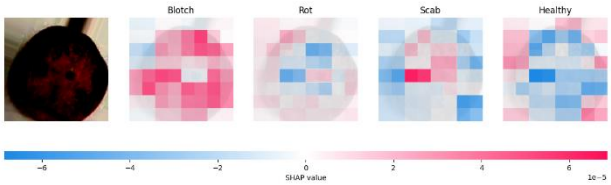

Figure 3. SHAP results for several classes

LIME method used local linear approximations to explain model decision for a specific sample. It generated perturbations of the original image to observe how the model responded to input changes. A local linear model was then trained to approximate the behaviour of the original model near the sample. Modified versions of the input, along with the predictions of the original model, served as training data for this local model. LIME explainer produces a mask highlighting pixel areas that contribute most to the class prediction. Fig. 4 shows the original image overlaid with mask, emphasizing the most influential regions. Yellow-highlighted areas indicate the parts of the model that most influenced the final decision.

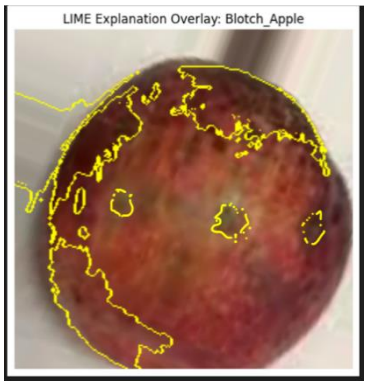

Figure 4. LIME explanation

In presented results, both SHAP an LIME demonstrated a promising potential for interpreting model predictions in the observed case, especially for lower-grade apple classes with visible skin defects, such as lesions, blotches or rot. Possible future extension of results might include combination of SHAP with ANFIS or Large Language Models (LLM) to provide hybrid XAI methods offering better understanding of SHAP explanations. Also, complementary strengths of SHAP and LIME suggest potential for hybrid use in real-time industrial applications.

3. CONCLUSIONS AND FUTURE RESEARCH DIRECTIONS

The current state of XAI in industrial automation and robotics reflects a growing need for integration of explainability in AI solutions. XAI development remains challenged by the difficult trade-off between model transparency and performance, the lack of standardized evaluation methods, and the need for context-aware, real-time, and human-centred solutions to ensure trust, safety, and adoption in critical applications [5][6][2].

Main research directions in Explainable Artificial Intelligence (XAI) for industrial automation and robotics can be summarized as:

- Development of novel hybrid XAI systems combining deep learning and interpretable rules and LLMs for accurate and easily understandable explainable industrial automation and industrial robotics.
- Emphasis on real-time explainability for safety-critical robotic systems in dynamic industrial environments.
- Research on human-centered XAI interfaces to build trust and support collaboration in industrial settings.
- Improvement of surrogate and post-hoc methods to explain common black-box AI models without sacrificing performance.
- Development of standardized XAI metrics to evaluate interpretability, usability, and trust in industrial applications.

The prospects of XAI in industrial automation and robotics lie in developing transparent, human-centric systems that balance interpretability with high-performance enabling safer, more trustworthy intelligent operations [6][10][2].

ACKNOWLEDGEMENT

This work has been supported by the Ministry of Science, Technological Development and Innovation of the Republic of Serbia [Grant Numbers: 451-03-137/2025-03/200109, 451-03-137/2025-03/200102 and 451-03-136/2025-03/200132].

REFERENCES

[1] Trivedi, C., et al, (2024). Explainable AI for Industry 5.0: Vision, Architecture, and Potential Directions. *IEEE Open Journal of Industry Applications*, DOI 10.1109/OJIA.2024.3399057.

[2] Ahmed, I., Jeon, G. and Piccialli, F. (2022), From artificial intelligence to explainable artificial intelligence in industry 4.0: a survey on what, how, and where. *IEEE Transactions on Industrial Informatics*, 18(8), pp.5031-5042.

[3] Saranya, A. and Subhashini, R., (2023). A systematic review of Explainable Artificial Intelligence models and applications: Recent developments and future trends, *Decision Analytics Journal*, 7, 100230.

[4] Chamola, V., Hassija, V., Sulthana, A.R., Ghosh, D., Dhingra, D. and Sikdar, B., (2023). A review of trustworthy and explainable artificial intelligence (XAI). *IEEE Access*, DOI: 10.1109/ACCESS.2023. 3294569.

[5] Longo, L. et al (2024). Explainable Artificial Intelligence (XAI) 2.0: A manifesto of open challenges and interdisciplinary research directions, *Information Fusion*, 106, p.102301, DOI: 10.1016/j.inffus.2024.102301.

[6] Kalasampath, K., Spoorthi, K.N., Sajeev, S., Kuppa, S.S., Ajay, K. and Angulakshmi, M., (2025). A Literature review on applications of explainable artificial intelligence (XAI). *IEEE Access*, DOI: 10.1109/ACCESS.2025.3546681.

[7] Saranya, A. and Subhashini, R., (2023). A systematic review of Explainable Artificial Intelligence models and applications: Recent developments and future trends, *Decision analytics journal*, 7, p.100230, https://doi.org/10.1016/j.dajour.2023.100230.

[8] Chamola, V., Hassija, V., Sulthana, A.R., Ghosh, D., Dhingra, D. and Sikdar, B., (2023). A review of trustworthy and explainable artificial intelligence (XAI), *IEEE Access*, Vol. 11, 78995, DOI: 10.1109/ACCESS.2023.3294569.

[9] Sakai, T. and Nagai, T., 2022. Explainable autonomous robots: a survey and perspective. *Advanced Robotics*, 36(5-6), pp.219-238.

[10] Sobrín-Hidalgo, D., Guerrero-Higueras, Á.M. and Matellán-Olivera, V., (2025). Generating Explana-tions for Autonomous Robots: a Systematic Review. *IEEE Access*, DOI: 10.48550/arXiv.2412.18516

[11] Hitendra G. (2021), *A Way Towards Explainable AI Using Neuro-Fuzzy System*, 2021 5th IEEE International Conference on Information Systems and Computer Networks (ISCON), India.

[12] Ismail, M., Shang, C., Shen, Q. (2022). Towards a Framework for Interpretation of CNN Results with ANFIS. In: Jansen, T., Jensen, R., Mac Parthaláin, N., Lin, CM. (eds), *Advances in Intelligent Systems and Computing*, vol 1409.

[13] Marković, N., Milošević, M., Ćirić, I., Ćojbašić, E. and Ivačko, N. (2024), *ANFIS Based Explainable AI Approach for Industrial Automation in the Food Industry*, Proceedings of the ICIST 2024.

[14] Chiu, M.C. and Yang, L.S., (2024). Integrating explainable AI and depth cameras to achieve automation in grasping Operations: A case study of shoe company. *Advanced Engineering Informatics*, 62, p.102

Society of Production Engineering

ICPES 2025

40th INTERNATIONAL CONFERENCE ON PRODUCTION ENGINEERING - SERBIA 2025

DOI: 10.46793/ICPES25.290D

University of Nis
Faculty of Mechanical Engineering

Nis, Serbia, 18 - 19th September 2025

FROM MODULAR LEGACY TO OPEN INNOVATION: EVOLUTION OF THE LOLA CNC SYSTEM ARCHITECTURE

Zoran DIMIĆ[1]*, Andrija DEVIĆ[1], Saša ŽIVANOVIĆ[2], Aleksa KROŠNJAR[1], Stevan PAROJČIĆ[1], Dragan PAVLOVIĆ[1]
Orcid: 0000-0002-1496-4981; **Orcid: Orcid:** 0000-0003-4950-8203;
Orcid: 0000-0003-2299-0570
[1]LOLA INSTITUT, Belgrade, Serbia
[2]University of Belgrade, Faculty of Mechanical Engineering, Serbia
*Corresponding author: zoran.dimic@li.rs

Abstract: *This paper provides a comprehensive overview of the development, technical architecture, and practical applications of the* LOLA 30 CNC *system, a landmark achievement in domestic industrial innovation in the field of numerical control. Developed in the early 1980s by the* LOLA Institute*, the system is examined within its historical context, with particular attention to its architectural features and its broader impact on industrial autonomy and engineering education. Special emphasis is placed on its modular design, integration with the* PA512 *programmable logic controller, and representative use cases. The paper also presents a comparative analysis between the LOLA 30 CNC and the modern* LOLA ROSA CNC system*, which is based on open-architecture hardware and software. Key technological advancements of the new system, particularly in terms of reconfigurability and distributability, are highlighted.*

Keywords: *LOLA 30 CNC, numerical control, modular architecture, domestic CNC system, PA512, LinuxCNC, industrial automation, retrofitting, digital twin.*

1. INTRODUCTION

The development of computer numerical control (CNC) systems has played a pivotal role in modernizing manufacturing technologies, particularly in the context of industrial autonomy and engineering education. Among the most notable domestic contributions to this field is the LOLA 30 CNC system, developed in 1983 by the LOLA Institute in Belgrade. As one of the earliest domestic CNC solutions in the former Yugoslavia, the LOLA 30 system was implemented on over 50 machine tools and became a cornerstone of local innovation in control systems and modular design [1].

This paper provides a historical and technical overview of the LOLA 30 system (Figure 1), examining its architectural features, integration with the PA512 programmable logic controller (PLC), and its broader impact on industrial development and academic training. The system's modularity, support for up to five axes, and analog spindle interface positioned it as a versatile platform for various machine tool configurations [1]. In parallel, the paper

examines the evolution toward modern open-architecture CNC systems.

2. FROM CLOSED MODULARITY TO OPEN

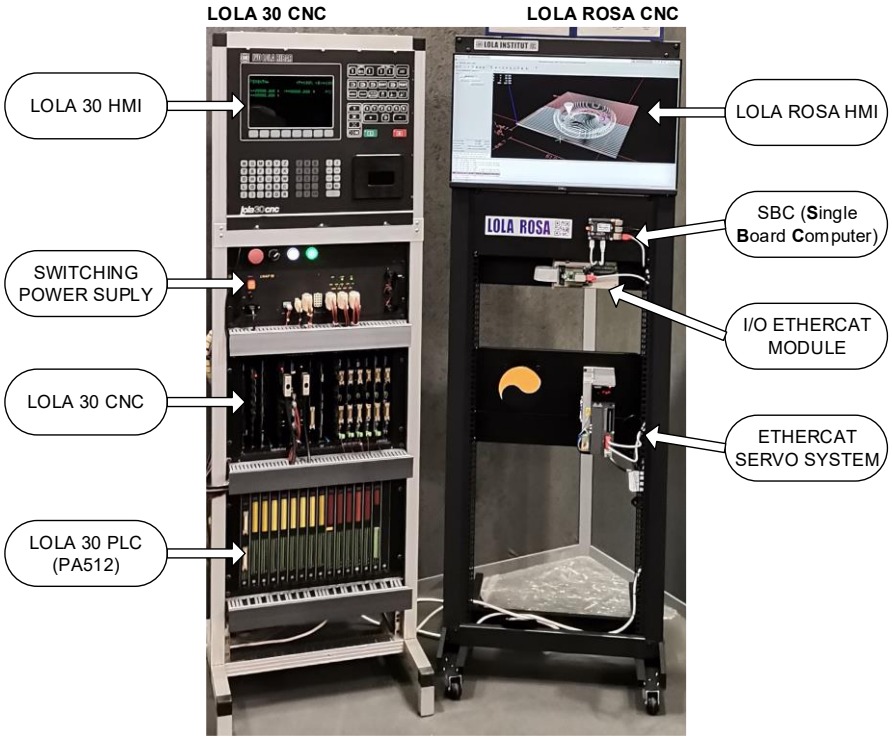

Figure 1. LOLA 30 CNC vs LOLA ROSA

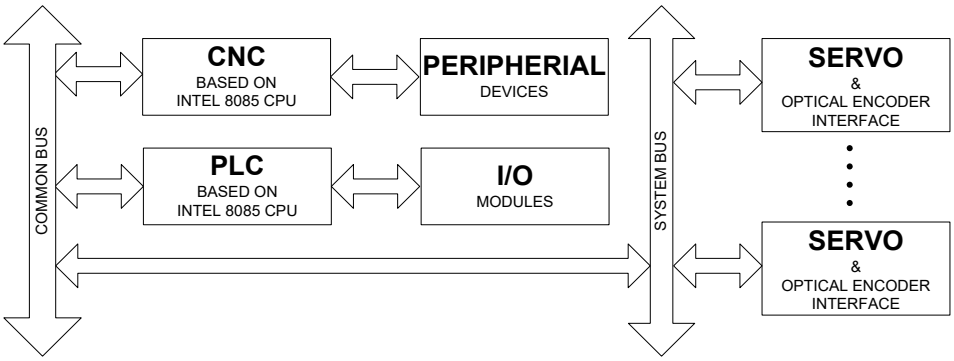

Figure 2. Simplified structure diagram of LOLA 30 CNC

New CNC systems, as LOLA ROSA CNC (Figure 1), offer enhanced reconfigurability, distributability, and integration with CAD/CAM environments, enabling virtual commissioning and digital twin applications [2,3]. A comparative analysis highlights the technological shift from proprietary to open, flexible control architectures.

By situating the LOLA 30 within the broader trajectory of CNC development, from early numerical control to contemporary cyber-physical systems, this study underscores the significance of domestic innovation in shaping Serbia's industrial and educational landscape.

RECONFIGURABILITY

The development of CNC systems in Serbia during the 1980s marked a pivotal step toward industrial autonomy and technological self-reliance. Within this context, the LOLA 30 CNC system emerged as one of the most significant domestic innovations in machine tool control. Deployed on more than 50 installations, it laid the foundation for modular control system design in the former Yugoslavia.

Technically, the LOLA 30 system was based on a closed modular architecture, supporting up to six control axes and featuring an analog

spindle interface (Figure 2). It was tightly coupled with the PA512 programmable logic controller, which handled machine-level logic and interfacing. Operating modes, including Auto, MDI, Edit, Test, Jog, and Reference Point, were selected through a physical keyboard, which functioned as one of the peripheral devices. Both the CNC and PLC control architectures are built upon the Intel 8085 microprocessor. Although reliable, the system's closed design limited adaptability and long-term scalability.

Recent developments at the LOLA Institute led to the creation of modern CNC systems built on open architecture, especially leveraging the LinuxCNC platform. These systems represent a paradigm shift toward reconfigurable, distributed, and interoperable architectures, with seamless CAD/CAM integration, STEP-NC support, and digital twin functionality [2,3,7,8].

In contrast to its predecessor, the modern LOLA ROSA CNC system (Figure 3) utilizes a standard industrial SBC (**S**ingle **B**oard **C**omputer) with EtherCAT-based analog/digital I/O modules [6]. Real-time performance is ensured through real-time operating system and LinuxCNC open architecture software, which supports interpolation, multi-axis motion, and flexible kinematic configurations. Such systems have been deployed in projects like the LOLA HBG 80 V3 [2], a retrofitted horizontal machining center with a virtual machine model and possible STEP-NC compatibility. The shift from the LOLA 30 to its open-architecture successors is not merely a technical upgrade; it signals a strategic evolution in control system philosophy, one aligned with Industry 4.0 principles, as shown in Table 1.

Table 1. Comparative Analysis: LOLA 30 CNC vs. Modern LOLA CNC System

Feature	LOLA 30 CNC (1983)	Modern LOLA CNC (LinuxCNC-based)
Architecture	Closed, modular	Open, reconfigurable, and distributed
Control Axes	Up to 6 axes	3–6+ axes, depending on configuration
Spindle Interface	Analog only	Analog and digital (PWM, VFD, etc.)
PLC Integration	PA512 (proprietary)	Soft PLC or external PLC (Modbus, EtherCAT)
Software	Proprietary, fixed configuration	Open-source, fully configurable
User Interface	Hardware keyboard and fixed panel	Custom GUI, virtual HMI, touchscreen optional
Programming Support	ISO G-code (limited)	G-code, user-defined macro support, possible use of STEP-NC
CAD/CAM Integration	Minimal or manual	Full integration (e.g., PTC Creo, STEP-NC)
Digital Twin Support	Not supported	Supported (real-time simulation and virtual commissioning)
Kinematics Support	Fixed kinematics	Flexible: Cartesian, SCARA, Delta, hybrid systems
Hardware Platform	Custom-built controller hardware	Industrial PC with standard I/O expansion
Adaptability/Retrofitting	Limited	Highly adaptable to various machine types
Educational Use	Limited (industrial focus)	Strong: supports simulation, training, and R&D environments

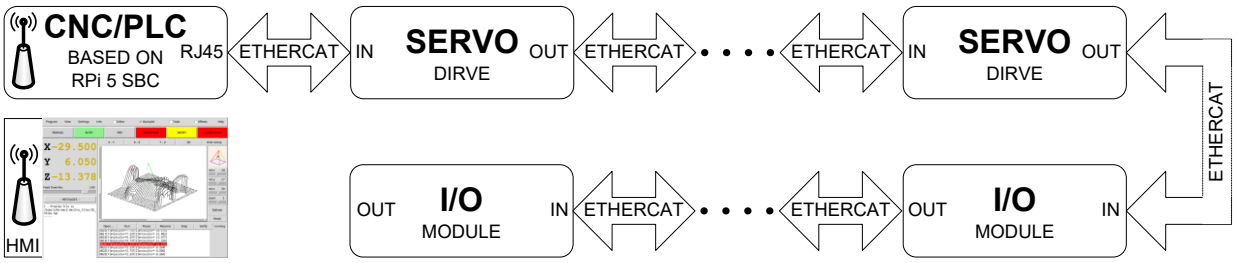

Figure 3. Simplified structure diagram of LOLA ROSA

3. SOFTWARE ARCHITECTURE AND DIGITAL INTEGRATION

The modern LOLA CNC systems are powered by LinuxCNC, an open-source real-time control platform derived from the NIST EMC2 initiative. The architecture provides deterministic motion control, with a real-time core managed via the Real-Time Application Programming Interface (RTAPI) and the Hardware Abstraction Layer (HAL). Motion planning, G-code interpretation, and kinematics configuration are modular and highly adaptable.

The system's reconfigurability is one of its defining advantages. Machine kinematics, tool changers, safety routines, spindle interfaces, and I/O mappings are all defined through text-based configuration files. All of this makes the architecture especially suitable for retrofitting diverse machine types, ranging from 3-axis mills to custom multi-axis platforms and woodworking centers [3].

Integration capabilities include:

- G-code and STEP-NC programming, supporting semantic and feature-based process planning [4],
- Modbus/EtherCAT protocols for external PLC and real-time I/O extensions,
- Digital twin environments, including ROS, Siemens NX, and custom-built virtual models.

LOLA's latest control systems feature custom-developed user interfaces, a virtual HMI that mimics the physical panel, and full synchronization with CAD/CAM and simulation environments, such as PTC Creo and STEP-NC Machine. For example, the LOLA HBG 80 V3, BACCI MX6, EMCO F1 [2,3,7,8] etc., incorporates digital twins for toolpath simulation, process monitoring, and virtual program validation [2,7].

By combining open-source control, semantic interoperability, and virtual feedback loops, the modern LOLA CNC architecture, built around EtherCAT communication capabilities, offers a robust solution tailored for demanding industrial environments. Its reconfigurable structure enables rapid adaptation to diverse machining tasks and evolving production needs, while its distributed design ensures seamless integration of modular components across decentralized systems. Additionally, the architecture provides a flexible platform for engineering education and applied research.

4. CONCLUSION

The trajectory of CNC development at the LOLA Institute reveals a compelling fusion of technological heritage and forward-looking innovation.

The original LOLA 30 system provided a resilient, modular platform during a time of domestic industrial consolidation. Though constrained by its closed architecture, it fostered technical expertise and served as a national milestone in automated control.

By contrast, the modern LOLA CNC systems based on open platforms like LinuxCNC reflect Serbia's alignment with global cyber-physical manufacturing trends. These systems support a broad range of applications, from conventional machining to hybrid digital twins, and integrate tools like STEP-NC, ROS, and CAD/CAM environments with ease.

More than a generational shift in technology, the evolution from LOLA 30 to its open successor embodies a new philosophy:

one that values openness, adaptability, and knowledge-sharing. These CNC platforms continue to serve as bridges between industry and academia, theory and practice, legacy and innovation.

As Serbia pursues its industrial transformation, initiatives like LOLA CNC underscore the significance of local engineering achievements and their potential to make a meaningful contribution to the global manufacturing ecosystem.

ACKNOWLEDGEMENT

The paper is part of the research conducted within projects supported by the Ministry of Science and Technological Development of the Republic of Serbia, under contract no. 451-03-137/2025-03/200105 for 2025, and by contract no. 451-03-136/2025-03/ 200066 for 2025.

REFERENCES

[1] LOLA Institute. LOLA 30 CNC – Control Systems Overview. Available at: https://www.li.rs/en/machine-tools/machine-tool-control-systems/lola-cnc-systems/lola-30-cnc, accessed: 11.07.2025.

[2] S. Živanović, Z. Dimić, N. Vorkapić, B. Kokotovic, N. Slavkovic, Virtual Horizontal Machining Center LOLA HBG 80 for Program Verification and Monitoring, FME Transactions, Vol. 49, No.3, pp. 696–703, 2021.

[3] Rakić, S. Živanović, Z. Dimić, M. Knežević, Digital Twin Control of Multi-Axis Wood CNC Machining Center Based on LinuxCNC. BioResources, Vol.16, No.1, pp. 1115–113, 2021.

[4] K. Latif, W.F. Lu, B. Song, A review of G code, STEP, STEP-NC, and open architecture control technologies, International Journal of Advanced Manufacturing Technology, Vol.114, pp.2549–2566, 2021.

[5] LinuxCNC Documentation Project. LinuxCNC *User Manual and Developer Resources*. Available at: https://linuxcnc.org/docs/, accessed: 11.07.2025.

[6] K. Erwinski, G. Karasek, S. Živanović, Z. Dimic, N. Slavkovic, Real-time control of a KEOPS-DELTA parallel kinematics machine using LinuxCNC and ETHERCAT, in: *Proceedings of the 43rd JUPITER conference, 39th symposium NC-Robots-FTS,* 04-05.10.2022, University of Belgrade, Faculty of Mechanical Engineering Belgrade, Serbia, pp. 3.47-3.54.

[7] Dimić, S. Živanović, D. Pavlović, M. Furtula, M. Djurković, A. Rakić, B. Kokotović, Reconfigurable open architecture control system with integrated digital twin for 3-axis woodworking milling machine ,Wood Material Science & Engineering Vol. 19, No.6, 2024.

[8] Z. Dimić, S.Živanović, J. Vidaković, A. Dević, Reconfigurable control system for machine tools with a switchable kinematic and variable execution flow of the kinematic algorithm, in: *Proceedings of the 17th International Conference on Accomplishments in Mechanical and Industrial Engineering DEMI 2025,* 29-30.05.2025, University of Banja Luka, Faculty of Mechanical Engineering, pp. 95-100

Society of Production Engineering

ICPES 2025

40th INTERNATIONAL CONFERENCE ON PRODUCTION ENGINEERING - SERBIA 2025

DOI: 10.46793/ICPES25.295B

University of Nis Faculty of Mechanical Engineering

Nis, Serbia, 18 - 19th September 2025

MATHEMATICAL MODEL OF PNEUMATIC CARTESIAN ROBOT

Vladislav BLAGOJEVIĆ[1*], Saša S. RANĐELOVIĆ[1], Srđan MLADENOVIĆ[1]
Orcid: 0000-0003-2722-0831; **Orcid:** 0000-0002-2334-8929; **Orcid:** 0000-0002-2499-9870;
[1]Faculty of Mechanical Engineering, Niš, Serbia
*Corresponding author: vladislav.blagojevic@masfak.ni.ac.rs

Abstract: *This paper presents the development of a mathematical model for a robot with a Cartesian structure, commonly used in industrial and automation systems due to its simplicity, accuracy, and ease of control. The robot's mechanical design is based on three linear, orthogonal axes (X, Y, and Z), allowing straightforward positioning in three-dimensional space. The study focuses on the formulation of the kinematic and dynamic models necessary for precise control and trajectory planning. The dynamic model is derived using Newton-Euler methodology. Special attention is given to the structural configuration and the movement constraints imposed by the linear pneumatic actuators (three rodless cylinders, one cylinder with a piston rod on one side and a gripper). The resulting model provides a clear mathematical framework for understanding the behaviour of the Cartesian robot under various operating conditions. This work lays the foundation for future implementation of control algorithms and integration into automated systems, and it serves as a reference for the design and analysis of similar robotic platforms.*

Keywords: *Cartesian structure, Robot, Pneumatic, Mathematical Model.*

1. INTRODUCTION

A pneumatic Cartesian robot is a type of robotic system that moves along three linear axes — X, Y, and Z — using pneumatic cylinders powered by compressed air, figure 1. Unlike traditional electric-driven robots, pneumatic Cartesian robots rely on air pressure to create motion, offering a fast and simple solution for many industrial tasks [1].

The construction of these robots is based on a straightforward mechanical structure: each axis is equipped with a pneumatic actuator that allows movement in a straight line. The frame, often made of aluminium or steel, provides rigidity and precision to the system. Pneumatic valves control the flow of air, enabling the robot to extend or retract actuators at high speeds. Movement is usually directed through a basic control system, sometimes integrated with sensors to improve position accuracy.

One of the main advantages of pneumatic Cartesian robots is their speed. Because air-powered actuators can respond almost instantly, these robots are ideal for high-cycle applications such as picking and placing parts, sorting small objects, or moving lightweight products on assembly lines. Their design is also relatively cost-effective, both in terms of initial investment and maintenance, making them a popular choice in industries that prioritize quick operation and simple automation [2,3].

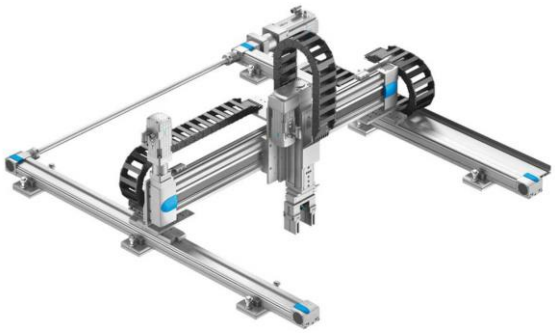

Figure 1. Pneumatic Cartesian robot

However, pneumatic systems have limitations, especially regarding precision and energy efficiency. Since air is compressible, fine control of motion is harder to achieve compared to electric-driven robots. This can lead to variability in positioning, which is not suitable for tasks requiring high accuracy. In order to better control the robot, it is very important to have a good mathematical model.

Despite these challenges, pneumatic Cartesian robots excel in environments where speed, reliability, and simplicity are more critical than pinpoint accuracy [3]. They are commonly used in packaging, food processing, laboratory automation, and light manufacturing. With proper design and integration, these robots can greatly enhance productivity while keeping system complexity and costs low.

2. ARCHITECTURE OF A PNEUMATIC CARTESIAN ROBOT

The architecture of a pneumatic Cartesian robot refers to its mechanical structure, motion system, and control components, all working together to achieve linear movement along three perpendicular axes (X, Y, and Z) using compressed air as the power source, figure 2. This type of robot is designed for straightforward, fast, and reliable handling of tasks in industrial automation.

The robot's frame is typically built from aluminium profiles or steel beams to provide rigidity and support for all moving parts. The frame is laid out in a rectangular, gantry-like structure, ensuring stability during fast linear movements.

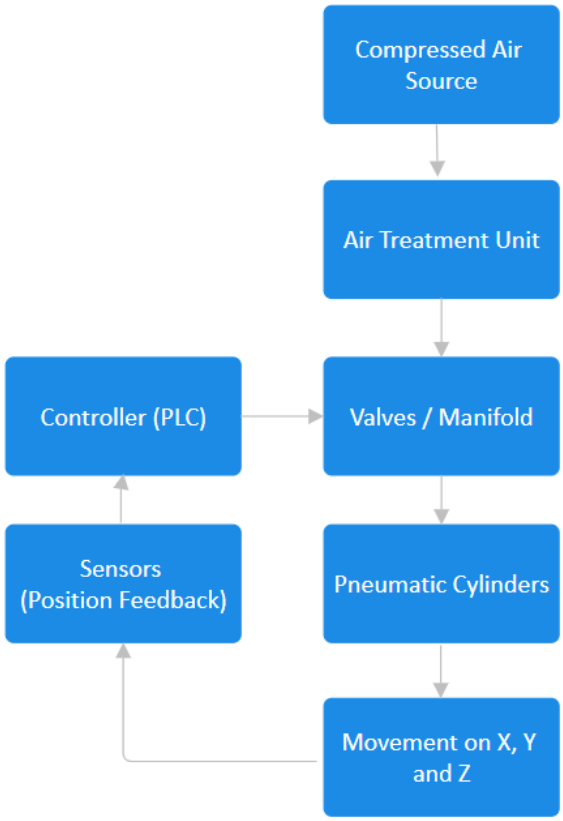

Figure 2. The architecture of a pneumatic Cartesian robot

Each axis is equipped with linear guides or sliding rails. These rails keep the motion aligned and reduce friction, allowing the pneumatic actuators to move the load precisely and smoothly.

The movement along each axis (X, Y, Z) is driven by pneumatic linear actuators. When compressed air is introduced into the cylinder, it pushes or pulls the piston, causing linear displacement.

The system needs a compressed air source that delivers clean, dry air at controlled pressures. Air treatment units are often used to ensure reliable actuator performance.

Proportional control valves manage airflow into and out of the cylinders. Those valves are commonly used to switch air direction based on control signals.

The robot may be controlled by a Programmable Logic Controller (PLC) or a dedicated pneumatic controller. This unit sends

signals to the proportional valves to control actuator movement.

Sensors are placed along the axes to detect the position of moving parts, ensuring safe and accurate operation.

The end of the robot usually carries a simple gripper, suction cup, or another tool adapted to the specific task. Pneumatic actuators often power these tools as well.

Emergency stops, pressure monitors, and safety barriers are incorporated to protect operators and equipment.

Flexible energy chains organize and protect the pneumatic tubes and sensor wires as the robot moves along different paths.

4. MATHEMATIC MODEL OF PNEUMATIC CARTESIAN ROBOT

A pneumatic cartesian robot consists of three rodless cylinders, one cylinder with a piston rod on one side and a gripper on the end, figure 3.

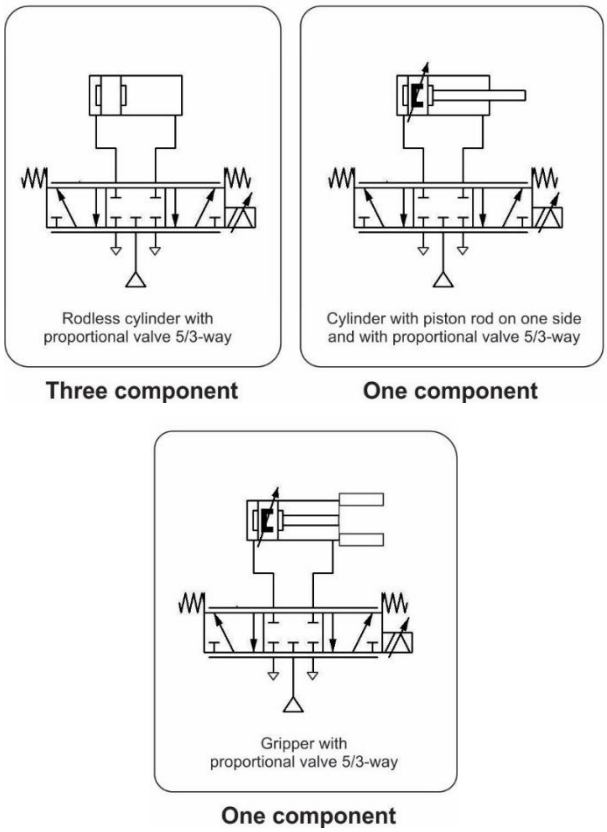

Figure 3. Pneumatic Cartesian robot

The dynamic equation of each rodless cylinders can be best represented by the motion equation (1):

$$(M_L + M_P)\ddot{xp} + \beta\dot{xp} + F_f + F_L == (P_1 - P_2)A \quad (1)$$

where: M_L - the mass of external parts connected to the cylinder rod, M_P - the piston and rod assembly mass, *xp* - the piston position in *x* or *y* or *z* direction (coordinate axis), *β* - the viscous friction coefficient, F_f - the Coulomb friction force, F_L - the external force, P_1 and P_2 - the absolute pressures in the cylinder's chambers, *A* - the piston effective area.

The dynamic equation of cylinder with a piston rod on one side and gripper with two fingesrs can be best represented by the motion equation (2):

$$\begin{aligned}(M_L + M_P)\ddot{xp} + \beta\dot{xp} + F_f + F_L = \\ = P_1A_1 - P_2A_2\end{aligned} \quad (2)$$

where: A_1 and A_2 - the piston effective areas on the left and right sides of cylinders.

Dynamics of the pressure change in thepneumatic cylinder chambers can be represented by (3):

$$\begin{aligned} W &= \frac{RT}{V_{0i} + A_i\left(\frac{1}{2}L \pm x\right)} \\ ALFA &= \alpha_{in}\dot{m}_{in} - \alpha_{out}\dot{m}_{out} \\ \dot{P}_i &= W[ALFA \pm \alpha P_i A_i \dot{x}] \end{aligned} \quad (3)$$

where: *R* - the ideal gas constant, *T* - temperatures, $\dot{m}_{in}$ and $\dot{m}_{out}$ - the mass flows entering and leaving the chamber, respectively, α, α_{in}, α_{out}- the coefficients taking the values between 1 and *κ*, depending on the heat transfer process [4], *L* - the piston stroke, *i*=1, 2 the cylinder chambers index, V_{0i} - the inactive cylinder volumes. In this form the pressure equation change accounts for the different heat transfer processes of the charging and discharging processes, air compression or expansion during the piston motion, the difference in effective areas on the opposite sides of the piston and the inactive volumes at the ends of stroke.

The first term in equation (3) represents the effect on pressure of the gas flow in or out of the chamber while the second term of the

equation accounts for the effect of piston motion [4,5].

Each of the cylinders, as well as the gripper, is controlled by proportional 5/3 valves with electromagnetic activation.

In order to simplify the problem of designing the mathematical model of the valve, it is assumed that the movements of the valve armature and the piston are small and that it is a static problem.The displacement of the piston of the proportional valve depending on the activating current signal can be described as:

$$\boldsymbol{x_v} = K_1 u \tag{4}$$

where: K_1 – valve coefficient and u - a current control signal from PLC. Depending on the size of the control signal, the piston of the proportional valve moves to one side or the other, thus changing the active orifice area of the valve.

Mass flow through proportional valve orifice can be represented by:

$$U = c_f A_v C_1 \frac{P_{up}}{\sqrt{T}} \tag{5}$$

$$J = \frac{P_{down}}{P_{up}} \tag{6}$$

$$\dot{m}_v = \begin{cases} UC_1, & J \leq 0{,}528 \\ UC_2 J^{1/k} \sqrt{1 - J^{\frac{k-1}{k}}}, & J > 0{,}528 \end{cases} \tag{7}$$

where: $\dot{m}_v$- the mass flow through proportional valve orifice, $\boldsymbol{c_f}$ - nondimensional coefficient, P_{up} and P_{down} - are upstream and downstream pressure in valve, A_v – represents active orifice area of the valve and its value depends on the magnitude of the valve activation signal. The dependence of the active orifice area of the valve on the activation signal is explained in detail in the paper [5].

Constants C_1 and C_2 are depending of fluid, in our case it is compressed air ($k = 1{,}4$) and $C_1 = 0{,}040418$ and $C_2 = 0{,}156174$**,** [5].

5. CONCLUSION

This study presented the development of a mathematical model for a Cartesian-structure robot, focusing on the analytical formulation of its kinematic and dynamic characteristics. The model provides a structured framework for understanding the system's motion behavior and serves as a foundation for future analysis and optimization. Although no simulations were conducted within the scope of this paper, the derived equations and theoretical framework can be directly applied in computational environments to evaluate performance under various operational scenarios. Future work will involve validating the model through numerical simulations and experimental testing to confirm its accuracy and applicability in real-world robotic systems.

ACKNOWLEDGEMENT

This research was financially supported by the Ministry of Science, Technological Development and Innovation of the Republic of Serbia (Contract No. 451-03-137/2025-03/2001009).

REFERENCES

[1] T. Yoshikawa: *Foundations of Robotics, Analysis and Control*, MIT press, 1990.

[2] T. Bajd, M. Mihelj, J. Lenarčič, A. Stanovnik, M. Munih: *Robotics*, Heidelberg: Springer, 2010.

[3] J. J. Craig: *Introduction to Robotics, Mechanics and Control*. New Jersey: Pearson Education, Inc., 2005.

[4] E. Richer, Y. Hurmuzlu: *A high performance pneumatic force actuator system part 1 – Nonlinear mathematical model*, ASME Journal of Dynamic Systems Measurement and Control, 122 Vol. 3, pp. 416-425, 2000.

[5] V. Blagojević, M. Stojiljković: Mathematical and simulink model of the pneumatic system with bridging of the dual action cylinder chambers, FACTA UNIVERSITATIS: Series Mechanical Engineering, Vol. 5, No. 1, pp. 23-31, 2007.

Session 7:

CAx and smart technologies

Society of Production Engineering

ICPES 2025

40th INTERNATIONAL CONFERENCE ON PRODUCTION ENGINEERING - SERBIA 2025

DOI: 10.46793/ICPES25.300Z

University of Nis Faculty of Mechanical Engineering

Nis, Serbia, 18 - 19th September 2025

PROGRAMMING AND VERIFICATION OF MILLING OPERATIONS FOR CNC MACHINES WITH HORIZONTAL ROTARY AXIS

Sasa ZIVANOVIC[1]*, Julija MALETIC[2], Nikola VORKAPIC[1], Nikola SLAVKOVIC[1], Zoran DIMIC[2], Radovan PUZOVIC[1]

Orcid: 0000-0003-4950-8203; **Orcid:** 0000-0002-4465-7552; **Orcid:** 0000-0001-5081-4828; **Orcid:** 0000-0003-1147-284X; **Orcid:** 0000-0002-1496-4981; **Orcid:** 0000-0003-0552-5247

[1] University of Belgrade, Faculty of Mechanical Engineering, Serbia

[2]LOLA Institute, Serbia

*Corresponding author: szivanovic@mas.bg.ac.rs

Abstract: *The paper analyses the programming of CNC milling machines with horizontal rotary axis. These are usually machines for rapid prototyping of rotating symmetrical and/or asymmetrical parts. The paper analyses the available programming software, which can be one of the standard CAD/CAM systems or a specialized CAM system. In addition to the analysis of the programming method procedure, the verification of the program by simulating the removal of material and simulating the operation of a virtual machine according to a given program was also considered. Verification of programming methods was realized by machining several characteristic parts, on developed 3-axis desktop CNC milling machine - Multiprodesk, that has two translational and one horizontal rotary axis.*

Keywords: *programming, simulation, verification, rotary machining*

1. INTRODUCTION

The complexity of the model of a part is directly related to the complexity of the milling machine that needs to be chosen for the machining process [1]. When it is necessary to implement machining of rotary primarily asymmetrical parts, machining with at least one rotating axis on the machine is necessary, so that machining is possible in one clamping.

The paper discusses the programming and verification of programs for CNC machine tools that have a horizontal rotary axis [2], Fig.1. These CNC machine tools can be:

- 3-axis with two translational axes and one horizontal rotary axis,
- 4-axis with three translational axes and an integrated or additional horizontal rotary axis and,
- 5-axis with three translational axes and an integrated or additional two-axis rotary table.

The type of machine whose programming is considered in this paper belongs to the class of CNC machines for rapid prototyping by milling, where one horizontal rotary axis is used for machining. These machines can be 3-axis, with two translational and one rotary axis (Fig.1a) or

4-axis with three translational and one rotary axis (Fig. 1b). This kind of machining is also possible with a 5-axis machine (Fig.1c) where the rotary axes can be positioned so that one of the rotary axes is horizontal.

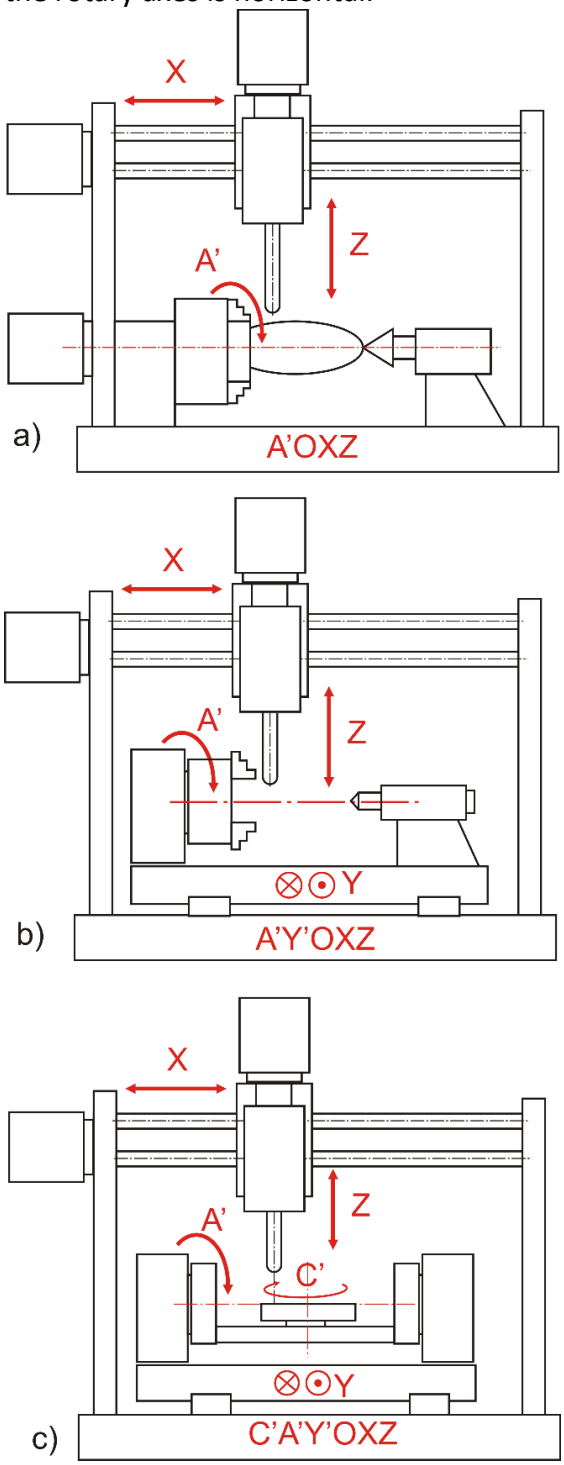

Figure 1. CNC machines with horizontal rotary axis [2]

The structure of the machine from Fig.1a is A'OXZ and has a horizontal rotary axis A' on which the workpiece is mounted, and the tool is carried by two translational axes Z and X. This machine was developed, as an educational machine – Multiprodesk (Fig.2) and this paper considers an adequate system for its programming.

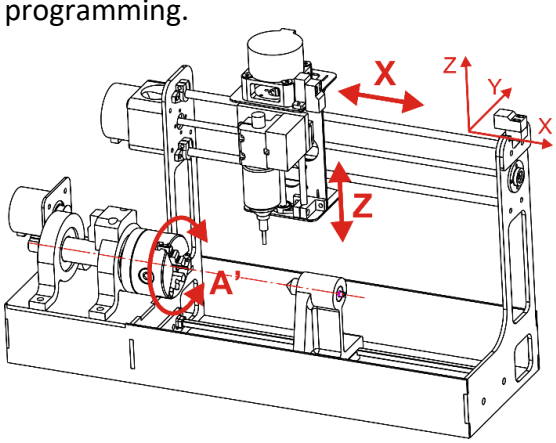

Figure 2. Multiprodesk - CNC machine with kinematic structure A'OXZ [3]

The structure of the machine from Fig.1b is A'Y'OXZ and also have a horizontal rotary axis A' and translatory Y' axis on a workpiece side. This machine is also developed, as an industrial prototype LOLA VMC 4 (Fig.3).

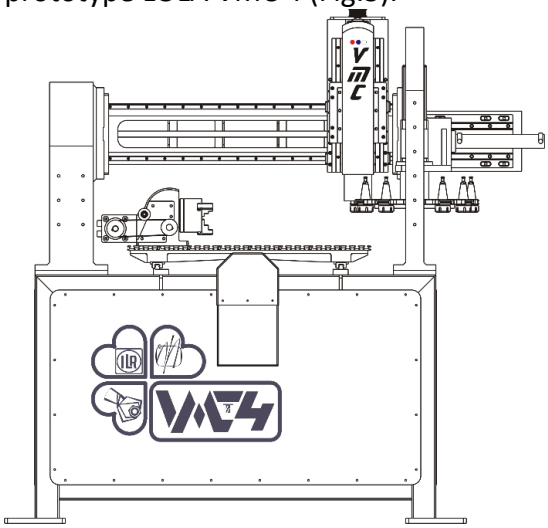

Figure 3. LOLA VMC4 - CNC machine with kinematic structure A'Y'OXZ

And the last machine in the considered class is a plan for future development, and in relation to the basic structure, it would have a two-axis rotary table. Its planned structure is C'A'Y'OXZ (Fig.1c) and it is possible to plan machining with a horizontal rotary axis. This kind of machining is possible when axis A' occupies a position such that axis C' is rotating around the horizontal axis.

1.1 Programming methodology

Available standard CAD/CAM systems, as well as specialized CAM software, can be used as a programming system for machine tools with a horizontal rotary axis [4,5].

Depending on the model format and the CAD system used for model preparation, the choice of programming system also depends. If we are talking about a machine for rapid prototyping, then most often it is a model in STL format, so the choice of specialized CAM systems that can work on the basis of such models is common. In this work, the developed educational 3-axis machine for rapid prototyping - Multiprodesk [4] will be used to verify the environment for programming such class of machines.

1.2 Programming based on CAD/CAM system

The system for programming CNC rotary machining using the CAD/CAM system [6] is shown in Fig.4.

It is possible to exchange geometric workpiece models with other CAD systems and generate toolpath.

Toolpath verification is possible by simulating moving tools along the tool path, material removal simulating, and simulating the working of virtual machine according to the given program in CLF format [1].

Tool path programming was performed using PTC Creo Parametric CAD/CAM software, resulting in a CL file containing the tool path. The toolpath defined in this way contains data on the position and orientation of the tool during machining in relation to the coordinate system of the workpiece and as such cannot be used directly on the machine, but must be postprocessed in order to obtain G-code were defined necessary movements of the axes of the machine tool. Program verification is also performed after postprocessing based on G-code in the Vericut environment.

The basic part of the system consists of developed and implemented postprocessor, without using the postprocessor generator from CAD/CAM system.

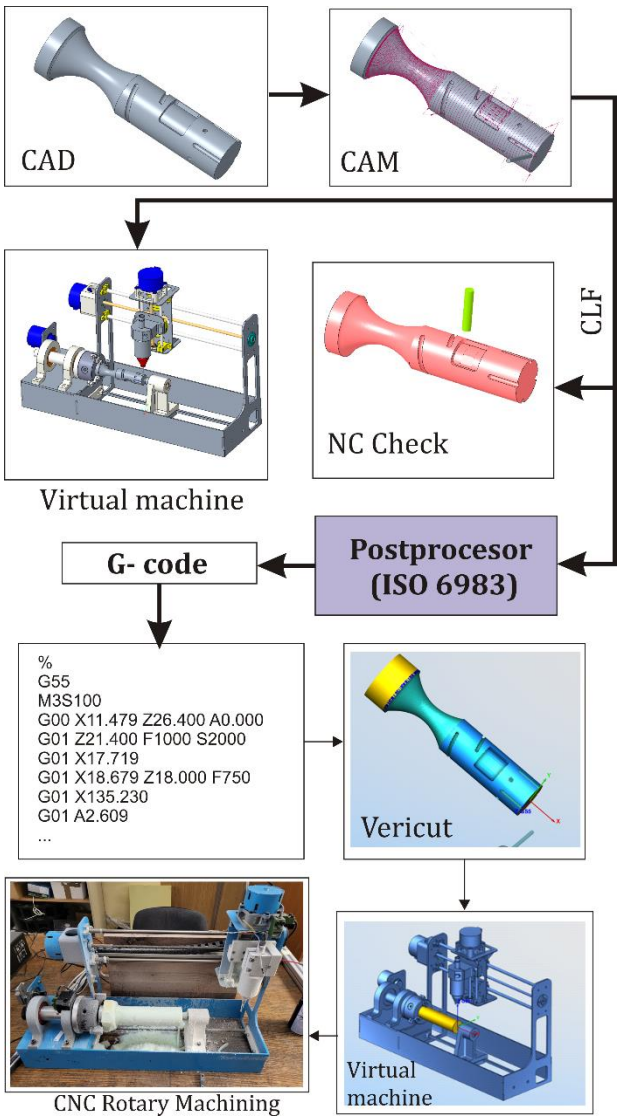

Figure 4. Programming based CAD/CAM system

The developed postprocessor is modified version of the software developed in [7]. The developed post-processing software has been modified using the kinematic equations describing the structure of the considered four-axis machine with horizontal rotary axis. The kinematic equations used within this software are derived based on the solution of the inverse kinematic problem, shown in [8] and [9].

1.3 Programming based on specialized CAM

As a system for programming the 3-axis CNC machine tools with two translatory and one horizontal rotary axis, considering that the machine is planned for rapid prototyping of soft materials, recommended by specialized CAM software packages which have the possibility of

programming machining with rotary axis (Rotary Machining).

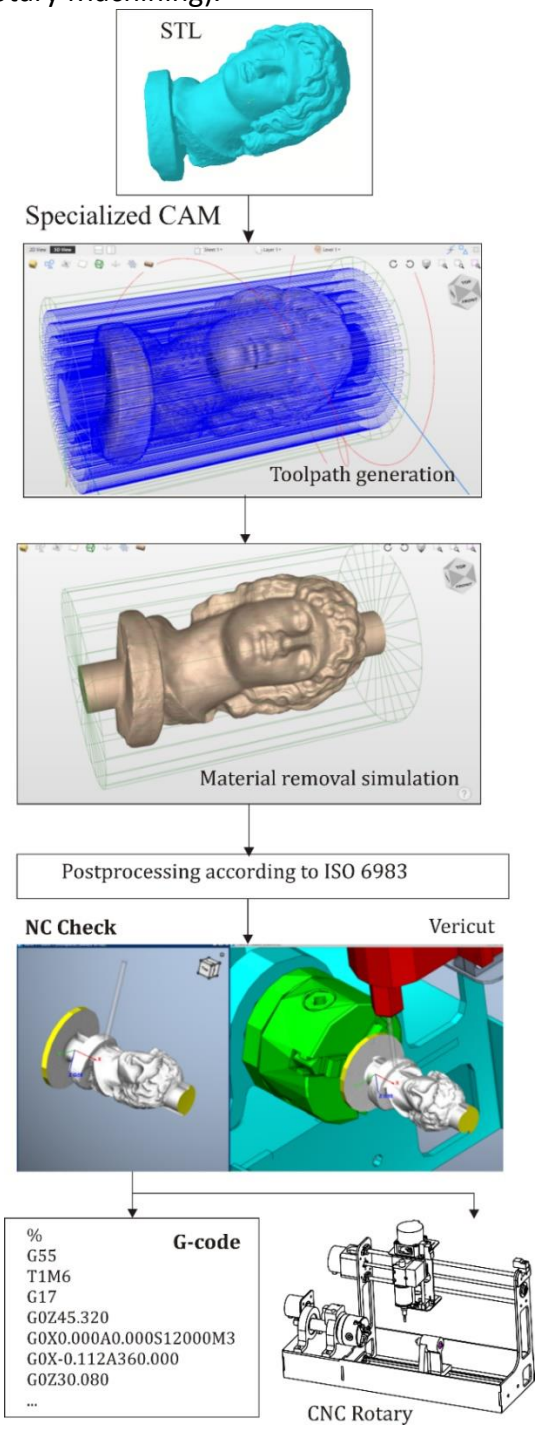

Figure 5. Programming based on STL model in Vectric Aspire environment

For rapid prototyping, models are mostly in STL or OBJ format. The paper analyzes the application of the software Vectric Aspire and DeskProto, which can be used for programming machine with a rotary axis.

An example of programming method based on specialized CAM software Vectric Aspire is given in Fig.5 with rotary machining option.

Programming includes the following stages: (1) defining job setup (single sided, double sided and rotary); (2) defining rawpiece dimensions; (3) define rotary axis; (4) loading of STL file and setting orientation and model size; (5) defining material setup - diameter, zero point; (6) selection toolpath operation (3D roughing, 3D finishing, etc.); (7) define parameters (tool, strategy, machining allowance, ...);

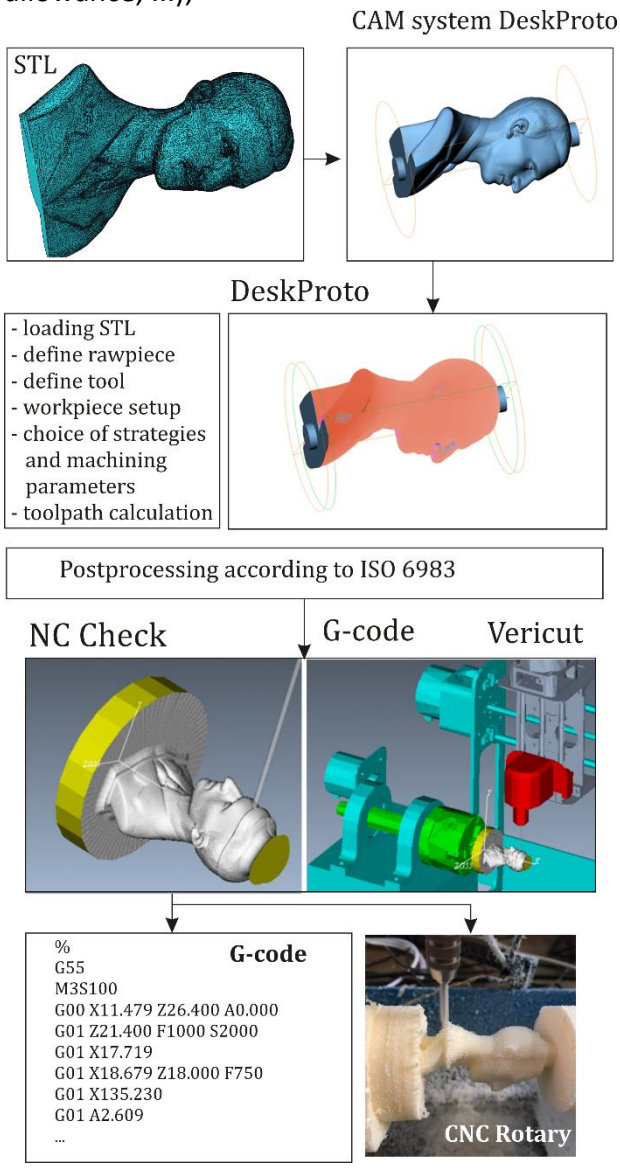

Figure 6. Programming based on STL model in DeskProto environment

(8) calculating toolpath; (9) previewing toolpaths - material removal simulation; (10) saving toolpaths in G-code using appropriate postprocessor for rotary machining; (11) NC Check in Vericut software environment using material removal simulation and machine simulation.

The second example of programming method based on specialized CAM software DeskProto is given in Fig.6 with rotary machining option.

DeskProto is a specialized CAM programming software that can load STL files, with the possibility of rotary machining, which can be either continuous or indexed rotation, with application of different machining strategies. Programming in the DeskProto environment is very intuitive and enables quick and efficient obtaining of G-code. The description of the programming procedure can be described in several stages: (1) selection of machine and type of milling (here machine with rotary axis and rotary machining); (2) loading model in STL format with the selection of the axis of rotation; (3) selection of tools, machining mode and strategy, depth per pass for pre-machining and machining allowance for finishing; (4) toolpath generation and display and (5) generation G- code.

2. EXPERIMENTAL VERIFICATION

Experimental verification of the programming methods was performed on a desktop 3-axis CNC machine tool with two translatory and one rotary axis, with a kinematic structure of A'OXZ.

Figure 7. Example machining workpiece which is programmed using CAD/CAM system

The machining shown in this chapter is in fact a test of the considered programming methods on the machine, on selected examples. The first example used CAD/CAM system for machining some trial part for rotary machining, Fig.7.

The remaining two examples considered a verification of programming based on specialized CAM software packages, Figs. 8 and 9.

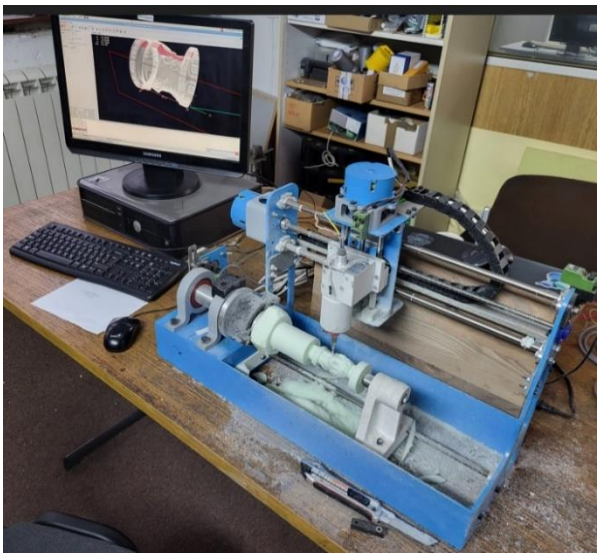

Figure 8. Example machining workpiece which is programmed using Vectric Aspire

The machined parts verified the considered programming methods. Correct positioning, determination of the zero point was achieved, the machining was without collisions and without errors.

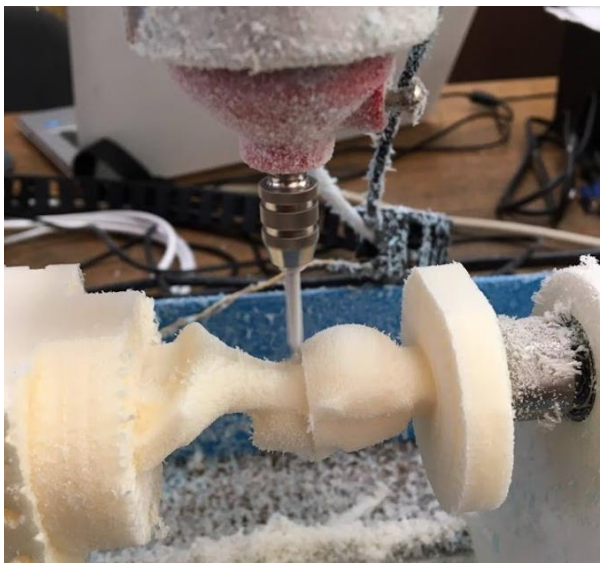

Figure 9. Example machining workpiece which is programmed using DeskProto

3. CONCLUSION

The paper presents programming methods and testing of a 3-axis CNC machine tool with two translational and one rotary axis (Multiprodesk-mill), with kinematic structure A'OXZ. Experimental verification of considered programming methods was carried out on the desktop variant of the machine, while in the coming period, testing of the operation of the rotary axis is also planned on the industrial variant of the LOLA VMC4 machine.

The considered programming methods for rotary machining on 3-axis CNC machine tool with two translatory and one rotary axis follows current trends such as: (i) adaptation to the specific needs of certain branches of industry, by introducing reconfigurable and adaptable machine tools; (ii) open architecture contol system based on LinuxCNC; (iii) application of the developed machine and programming methods in education and research; (iv) consideration of new methods in CNC programming; (v) adoption of digitization and virtualization for program verification to improve industrial production within the framework of the Industry 4.0 paradigm

ACKNOWLEDGEMENT

The paper is a part of the research done within the projects that was supported by the Ministry of Science, Technological Development and Innovation of the Republic of Serbia by contract no. 451-03-137/2025-03/200105 dated 4 February 2025.

REFERENCES

[1] A. M. Joshi, Computer aided process planning for multi-axis CNC machining using feature free polygonal CAD models, Graduate Theses and Dissertations, 2015, available at: https://lib.dr.iastate.edu/etd/14844, accessed: 24.04.2005.

[2] S. Zivanovic, N. Slavkovic, New generation of machine tools and robots, University of Belgrade, Faculty of Mechanical Engineering, ISBN 978-86-6060-210-9, 2025. (In Serbian)

[3] S. Živanović,, N. Vorkapić, N. Slavković, Z. Dimić, J. Vidaković, Multifunctional and reconfigurable machine tool for rapid prototyping by milling, laser processing, and additive manufacturing using cylindrical coordinates, patent no. 1805, type of patent: small patent. Publication: Intellectual Property Gazette: 3/2024, recognized by: Intellectual Property Office of the Republic of Serbia.

[4] N. Vorkapić, S. Živanović, Z. Dimić, Development of an educational 3-axis CNC machine tool for rapid prototyping with two translational and one rotary axis, TEHNIKA, Vol. 68, No. 6, pp.725-732, 2020. (in Serbian)

[5] N. Vorkapić, S. Živanović, B. Kokotović, N. Slavković, Z. Dimić, Programming of 3-axis CNC milling machines with two translatory and one rotary axes, in: Proceedings of th 42. JUPITER Conference, 06-07. 10.2020, Belgrade, Serbia, pp. 3.122-3.128. (in Serbian)

[6] S. Zivanovic, G. Vasilic, Z. Dimic, N. Vorkapic, B.Kokotovic, N. Slavkovic, Programming methods and program verification for 3-axis reconfigurable hybrid kinematics machine, in: Proceedings of the 16th International Conference on Accomplishments in Mechanical and Industrial Engineering DEMI 2023, University of Banja Luka, Faculty of Mechanical Engineering, 01-02. 06. 2023, Banjaluka, Republic of Srpska, pp. 136-143.

[7] J. Maletić, S. Živanović, Verification of inverse kinematic equations for a five-axis machine tool with a spindle tilting configuration, Advanced Technologies & Materials, Vol. 47, No. 1, pp. 33-38, 2021.

[8] R.S. Lee, C. -H. She, Developing a postprocessor for three types of five-axis machine tools, International Journal of Advanced Manufacturing Technology, Vol.13, pp. 658–665, 1997.

[9] M.A. Chu, C.V. Nguyen, H.M Nguyen, E. Lj. Bohez, Transformation of CAM data for 5-axis CNC machine Spinner U5-620, International Journal of Mechanical Engineering and Robotics Research, Vol.9, No.2, 2020.

Society of Production Engineering

ICPES 2025

40th INTERNATIONAL CONFERENCE ON PRODUCTION ENGINEERING - SERBIA 2025

DOI: 10.46793/ICPES25.307V

University of Nis Faculty of Mechanical Engineering

Nis, Serbia, 18 - 19th September 2025

CNC SIMULATOR BASED ON LINUXCNC CONTROL AND PROGRAMMING SYSTEM

Goran VASILIĆ[1,*], Milan MILUTINOVIĆ[1], Saša ŽIVANOVIĆ[2], Zoran DIMIĆ[3]

Orcid: 0000-0003-0465-192X; **Orcid:** 0000-0003-4950-8203; **Orcid:** 0000-0002-1496-4981;

[1]The Academy of Applied Studies Polytechnic, Belgrade, Serbia

[2] University of Belgrade, Faculty of Mechanical Engineering, Serbia

[3] LOLA Institute, Belgrade, Serbia

*Corresponding author: goran.v.vasilic@gmail.com

Abstract: *This work presents a CNC simulator that was created based on the need to design and form a working environment within which training of operators and programmers of CNC machines will be carried out in an economically profitable way. The CNC simulator is based on a Raspberry PI 5 microcomputer and LinuxCNC open-source software system intended for control and programming of CNC machines and industrial robots. The LinuxCNC software system was configured according to the set requirements and current needs. With the control system configured in this way, two working environments were formed that are currently used in the realization of laboratory exercises of the teaching process of the higher education institution. In the framework of the paper, the created working environments are described, and in the conclusion, the observations obtained by analyzing the results achieved using the CNC simulator are presented.*

Keywords: *LinuxCNC, Raspberry PI, CNC machine programming, Virtual CNC machine, Complex CNC machine*

1. INTRODUCTION

With the rapid development of the industry, the need for CNC machine operators and programmers is increasing. Training for the operation and programming of CNC machines, in addition to the theoretical part, also includes practical work in which the acquired theoretical knowledge is applied. Regardless of whether the training of personnel is carried out within the production plant or within institutions that have personnel qualified to conduct training, the following problems arise: i) the need for CNC machines intended only for training, ii) the risk of injury during training, iii) the possibility of causing significant damage to the equipment, etc. Following the example of well-known brands such as HAAS and FANUC (Figure 1), the authors of this paper have developed their educational simulator, which they have called “CNC EduSim”.

Figure 1. CNC simulator: a) HAAS [1], b) FANUC [2]

The developed and built CNC EduSim simulator, in addition to being significantly more affordable, also has features that branded simulators do not have, which will be discussed in the following text.

2. DESCRIPTION OF THE EDUCATIONAL SIMULATOR

During the development of CNC EduSim, a prototype simulator was first built. The goal was to create a simulator with minimal investment, based on which the justification for further development and construction of a larger number of simulators would be established. After testing the built prototype, it was determined that the simulator can be used for educational purposes and that it fully meets all needs.

On the built prototype of the simulator, certain defects were observed that disturbed comfortable work. Also, when working on the prototype, one did not fully get the impression that one was working on the control unit of a CNC machine. After removing the defects and redesigning the housing, several simulators were built, which are shown in Figure 2.

Figure 2. CNC EduSim simulators built

The developed and built CNC simulators are primarily intended for the training of operators and programmers of CNC machines. For this reason, during the development, care was taken to ensure that CNC EduSIM meets the set requirements, such as:

· to look like commercial simulators or the control panel of an industrial CNC machine,

· to have external connections that improve the functionality of the simulator,

· that it can be used for training operators and programmers for CNC machines of different purposes and structures (CNC lathes, three-axis CNC milling machines, multi-axis CNC milling machines, CNC wire-cutting machines ...),

· to be able to simulate tool movements based on G-code programs that are manually written or generated using one of the available CAD/CAM software systems,

· to be able to simulate tool movement based on parametric G-code programs,

· to be able to simulate the operation of a CNC virtual machine during the machining process, which is driven by identical control signals as the real machine,

· that it can be easily adapted to new requirements.

The developed CNC EduSim (Figure 3) consists of a touch screen, an alphanumeric keyboard, and a series of switches and ports.

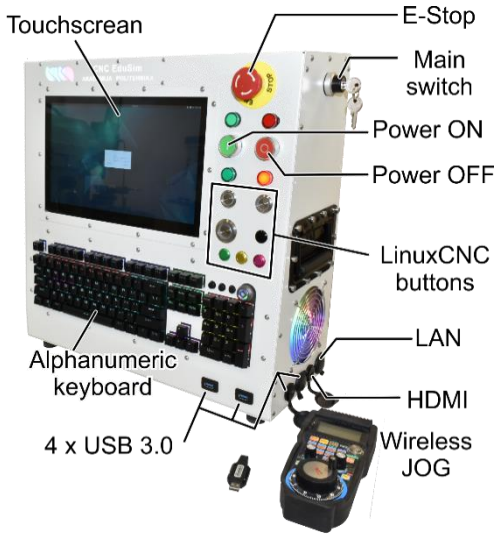

Figure 3. CNC EduSim - switches, buttons, and ports

Buttons and switches are divided into two groups. The first group consists of buttons and switches that provide power to the simulator, as well as turning it on and off. By turning on the simulator, the LinuxCNC software control system for CNC machines is started [3]. The second group consists of keys that facilitate work in the LinuxCNC software control system and are intended for starting, pausing and stopping the loaded G-code program, for initializing the machine, software turning on and off the machine (Machine ON/OFF).

CNC EduSim has a total of four USB-3.0 ports designed to transfer the G-code of the program

from the USB memory to the simulator and vice versa. Also, USB-3.0 ports are used to connect peripheral hardware (computer mouse, handwheel-JOG, etc.) to the simulator. In addition to the USB-3.0 port, CNC EduSim has an HDMI port for an additional monitor or projector, as well as a LAN port for connecting the simulator to the Internet.

The above components were used in order to fully utilize the capabilities of the Raspberry Pi-5 microcomputer [4]. All components shown in Figure 3 (switches, buttons, connectors, monitor and keyboard) are connected to the microcomputer RaspberryPi-5 (RPI-5) directly or through other electrical components such as relays and USB 3.2 HUB HAT (Figure 4). Also, LinuxCNC 2.9.4 Raspberry Pi5 Debian operating system [5] is installed on the RPI-5, which represents the control and programming system of CNC EduSim.

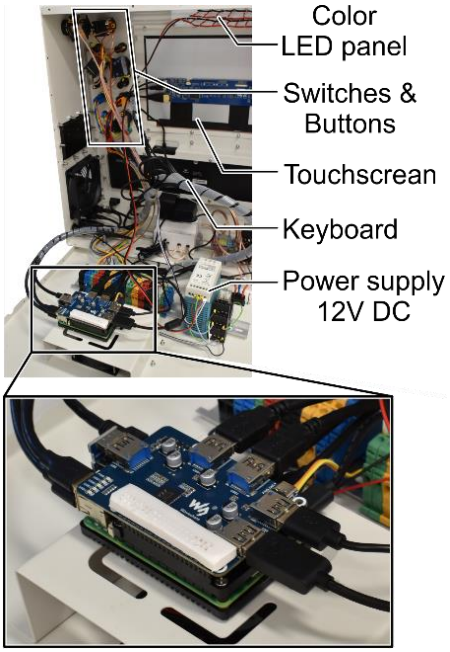

Figure 4. Raspberry Pi 5 + USB 3.2 HUB HAT

2.1 Linuxcnc control and programming system

The main advantage of LinuxCNC compared to other control systems is that it has an open architecture system that can be freely accessed and configured according to one's own needs. Therefore, LinuxCNC can be used for:

control of CNC machines intended for conventional machining (turning, milling, grinding),

control of CNC machines intended for non-conventional machining methods (plasma cutting, laser cutting, wire cutting),

control of industrial robots with serial, parallel and hybrid kinematics.

Taking into account the set requirements for CNC EduSim and the previous experiences of the author [6-8], the LinuxCNC software control system has emerged as a solution that will meet all current and future requirements.

2.2 Working environment for education on cnc edusim simulators

Considering that the CNC EduSim simulators are intended for the education of both programmers and operators of CNC machines, two working environments have been prepared for their use.

The working environment for training CNC machine programmers is shown in Figure 5. The working environment includes a sufficient number of CNC EduSim simulators, which will ensure smooth, comfortable and independent work for each training participant. Also, the working environment includes a simulator for a qualified demonstrator who conducts training. As shown in Figure 5, during the training the demonstrator uses the previously mentioned simulator prototype, while the course participants use improved and redesigned versions of the simulator.

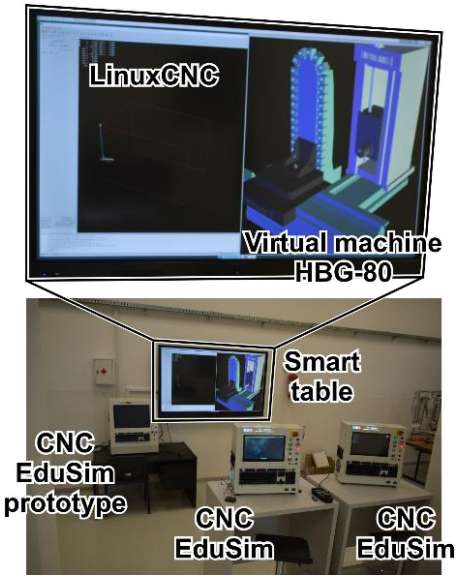

Figure 5. A working environment for training

CNC machine programmers on CNC EduSim. Apart from the primary goal that the participants of the training acquire the knowledge necessary for successful programming of CNC machines, a secondary goal was also imposed during the formation of the working environment. As the need for the training participants to get a feel for the operation of the CNC machine during the execution of the prepared G-code program was highlighted, the secondary goal of the training was also defined. In order to successfully achieve the secondary goal, using the capabilities of the LinuxCNC software control and programming system, a virtual machine is configured in the Python 3D graphics environment on each CNC EduSim simulator. Figure 5 shows a virtual LOLA HBG-80 CNC milling machine, which represents a Digital Twin machine, i.e. a virtual machine that, according to the loaded G-code program, fully simulates the operation of a real machine [9]. In addition to training CNC milling machine programmers, CNC EduSim simulators are configured so that they can also be used to train CNC lathe programmers. Examples of tool motion simulation according to G-code programs prepared for a CNC lathe are shown in Figure 6.

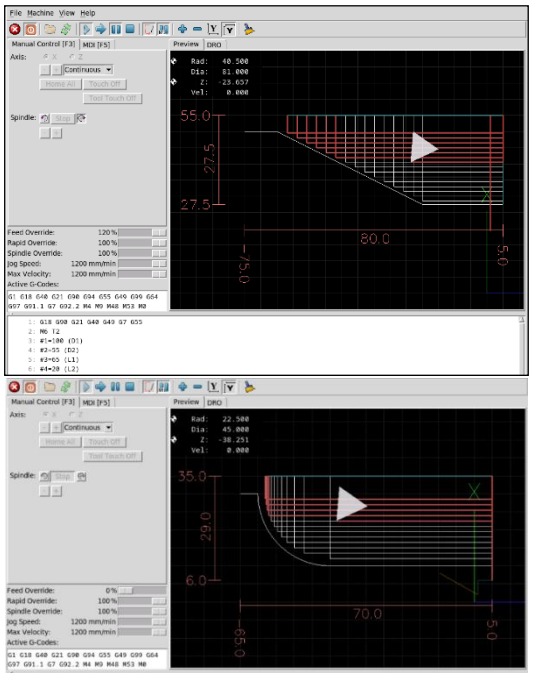

Figure 6. CNC EduSim – tool path simulation according to G-code programs prepared for CNC lathe [10]

As mentioned, CNC EduSim simulators are also intended for the training of CNC machine operators, and in accordance with that, a trial working environment was formed (Figure 7).

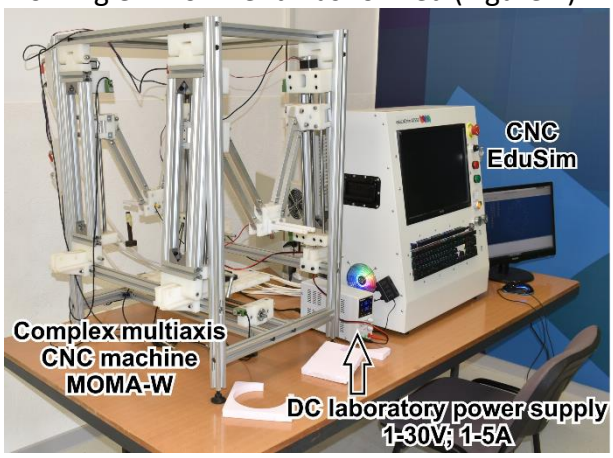

Figure 7. Work environment for training CNC operators

The working environment from Figure 7 consists of a CNC EduSim simulator, a laboratory power supply and a complex multi-axis machine tool MOMA-W, which is also the subject of current research by the author of this paper. The complex machine MOMA-W [11] is intended for cutting foam materials with a red-hot wire. The MOMA-W machine tool consists of two independent parallel mechanisms connected to each other by a wire. Each of the mechanisms used has two degrees of freedom, and the movements of the platforms of the mechanisms ensure translational movements of the wire (tool) in two directions as well as rotational movements around two axes. The mechanism of the MOMA-W machine tool has extremely complex kinematics. Also, the mechanism of the MOMA-W machine tool cannot be characterized either as a mechanism with parallel kinematics or as a mechanism with hybrid kinematics, and for this reason the mechanism is characterized as a complex mechanism, which is where the name of the machine comes from. The wire that connects the platforms of the used mechanisms and is used to cut the foam materials is heated by the laboratory power supply, and the entire environment is intended for training operators to work on WEDM (Wire Electrical Discharge Machining) CNC machines. According to the

dimensions, the complex machine tool MOMA-W can be characterized as a table machine that can be used not only for education but also for research purposes.

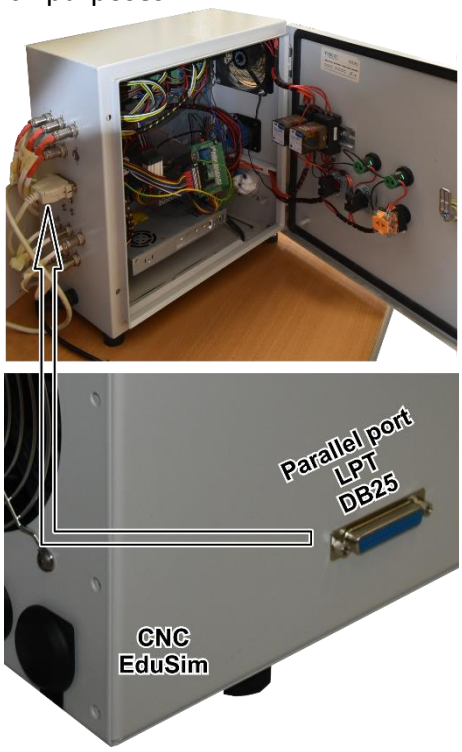

Figure 8. Electro-energetic system of the complex multi-axis machine tool MOMA-W

In addition to the equipment shown in Figure 7, the working environment also includes the electro-energetic part of the control system, which is connected to the CNC EduSim simulator via a parallel port (Figure 8).

The electrical subsystem contains stepper motor drivers (5 X TB6600), appropriate power supplies (12V-DC, 24V-DC), components used for automation realisation (switches, buttons, relays, etc.) and external connections for stepper motors and drive axle sensors. The electric-energy subsystem was developed and built so that, in addition to controlling a complex machine, the MOMA-W tool can also be used for other desktop machines that have a maximum of five drive axes. In other words, the electro-energetic subsystem can be used to control five-axis CNC machines as well as five-axis industrial robots whose motors and sensors are compatible with the aforementioned electrical components.

Figure 9 shows a gear made on a complex multi-axis MOMA-W machine. By creating gears, but also other parts of simple or complex geometry, where G-code programs written by hand, generated using available CAD/CAM systems and parametric programs [11] were used, it was confirmed that the created environment fully meets all the needs for successful training of CNC machine operators.

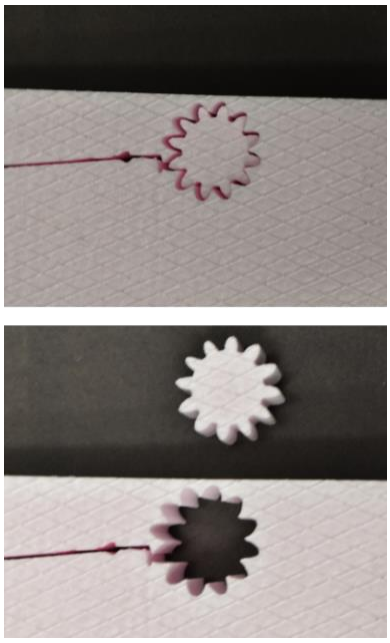

Figure 9. Gear made on a complex multi-axis machine MOMA-W

2.3. Forthcoming improvements of cnc edusim and formed working environments

As already mentioned, LinuxCNC is an open architecture software system and can be modified and adapted to current needs. LinuxCNC has predefined graphical interfaces (Axis, Mini, TkLinuxCNC) through which CNC machines and all peripheral equipment are managed. The predefined interfaces fully support all the functions that control units of branded CNC machines have, such as initializing the machine, zeroing the workpiece, loading, starting and stopping the program, Manual Data Input-MDI, tool change, turning on and off the cooling and lubrication system, etc. The disadvantage of the LinuxCNC software system is that the graphical environments mentioned do not resemble the graphical interface of any

branded CNC machine, so during training it's not possible to get full feeling that you are working on a specific CNC machine. In order to eliminate this shortcoming, one of the directions for further improvements is the creation of appropriate graphical interfaces like the QtDragon interface is (Figure 10) [12].

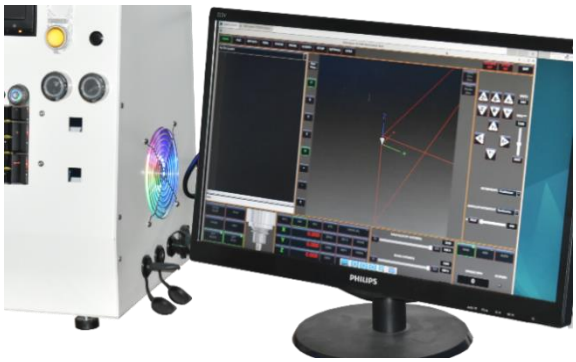

Figure 10. LinuxCNC QtDragon graphical user interface

Another direction of improvement relates to the development and construction of desktop educational CNC machines in order to improve the education of CNC operators. In the first step, the CNC machines that each production plant owns, i.e. a CNC lathe and a three-axis CNC milling machine, would be built. With the mentioned CNC desktop machines, during the CNC operator training, it would be possible to master all the necessary procedures that are performed before, during and after the machining process on a specific CNC machine. This primarily refers to basing and clamping the preparation, defining the coordinate system of the workpiece, tool measuring, loading and starting the prepared program, finishing the part, measuring and controlling the manufactured part, etc. The next steps would be: development and construction of a four-axis CNC milling machine, development and construction of a five-axis CNC milling machine, development and construction of a four-axis lathe (XYZC).

3. CONCLUSION

Based on the many years of work experience of the author of this paper and on the basis of the perceived opportunities for improving teaching processes at the Faculty of Mechanical Engineering of Belgrade University and the Academy of Applied Studies Polytechnic, also in Belgrade, the initial idea for the construction of a CNC simulator appeared. After defining the goals and expected outcomes of using the CNC EduSim simulator, one simulator prototype was first built, and then five more fully functional simulators. The prototype and three more redesigned CNC EduSim simulators are located in the laboratory for CNC technologies and conventional machining in Zemun. Two redesigned simulators are located in the Požarevac, where the Academy of Applied Studies Polytechnic also has its own classrooms. CNC EduSIM simulators are widely used for the implementation of exercises in the following subjects: CNC machine programming, Computer aided design CAM, parametric programming of CNC machines, programming of CNC systems I and programming of CNC systems II. Also, to an increasing extent, CNC EduSim simulators are used when preparing final papers for basic and master applied studies. With the goals achieved so far and the results achieved, the assessment is that the built CNC EduSim simulators fully met expectations. In terms of education, comparing the knowledge of students from the period when simulators were not used with the acquired knowledge of students who worked on the CNC EduSim simulator, a significant difference is observed, which justifies the construction of the simulator. After the implementation of the described improvements, the plan is to commercialize the CNC EduSim simulators and offer them to secondary and vocational schools at an affordable price.

In addition to educational purposes, CNC EduSim is also used in the scientific research work of the author of this paper. Primarily, the CNC EduSim simulator is used to configure the control system of CNC machines of various configurations with an emphasis on machines with parallel and hybrid kinematics. Further research work will be directed towards the development of reconfigurable control for a specific group of CNC machines, and the results

will be published in appropriate scientific journals and conferences.

ACKNOWLEDGEMENT

The work is the result of research supported by the Academy of Applied Studies Polytechnic by decisions of the Academy Board 26/40 of 20. XI 2023 and 24/03 of 26.II 2024.

The paper is part of the research conducted within projects supported by the Ministry of Science and Technological Development of the Republic of Serbia, under contract no. 451-03-137/2025-03/200105 for 2025, and by contract no. 451-03-136/2025-03/ 200066 for 2025.

REFERENCES

[1] HAAS Control Simulator, available at: https://www.haascnc.com/machines/desktop-machines/control-simulator.html#gsc.tab=0, accessed: 07.07.2025.

[2] FANUC CNC simulator & CNC machining simulator, available at: https://www.fanucamerica.com/products/cnc/fanuc-simulators/cnc-simulator, accessed: 07.07. 2025.

[3] LinuxCNC, available at: https://www.linuxcnc.org/docs/html/user/user-intro.html, accessed: 07.07.2025.

[4] Raspberry Pi Compute Module 5, A rapsberry Pi for deeply embedded applications, available at: https://datasheets.raspberrypi.com/cm5/cm5-datasheet.pdf, accessed: 07.07.2025.

[5] LinuxCNC 2.9.4 Raspberry Pi 5 OS based on Debian Bookworm LinuxCNC, available at: https://linuxcnc.org/downloads/, accessed: 07.07.2025

[6] M. Milutinović, G. Vasilić, S. Živanović, B. Kokotović, Z. Dimić, N. Slavković: The International Journal of Advanced Manufacturing Technology: Calculation Of Wheel Path For 3+2-Axis Grinding Of Brazed Carbide Profile Mill Cutters For Wood And Plastic, February 2024, Vol. 130, No.7-8, DOI:10.1007/s00170-024-12992-3

[7] G. Vasilić, S. Živanović, B. Kokotović, Z. Dimić: Journal of Mechanical Science and Technology: Configuring and Analysis Of A Class Of Generalized Reconfigurable 2-Axis Parallel Kinematic Machine, Vol.33, 2019. DOI: 10.1007/s12206-019-0636-z

[8] D. Milutinović, M. Glavonjić, S. Živanović, Z. Dimić, N. Slavković, in: *33rd Conference on Production Engineering of Serbia*, 16-17.06.2020, Belgrade, Serbia, pp.151-155.

[9] N. Vorkapić, S. Živanović, Z. Dimić, B. Kokotović, N. Slavković: FME Transactions: Virtual Horizontal Machining Center LOLA HBG 80 for Program Verification and Monitoring, Vol. 49, No. 3, pp. 696-703, 2021. DOI: 10.5937/fme2103696V

[10] G. Vasilić, S. Živanović, M. Milutinović: TEHNIKA, Union of Engineers and Technicians of Serbia: Parametric Programming Of CNC Lathes, Vol. 79, No. 6, pp. 699-706, 2024. DOI: 10.5937/tehnika2406699V

[11] G. Vasilić: *Conceptual Design Of One Class Of Complex Machine Tools,* PhD thesis, University of Belgrade Faculty of Mechanical Engineering, 2023. URL: NaRDuS

[12] QtDragon GUI, available at: https://linuxcnc.org/docs/html/gui/qtdragon.html, accessed: 07.07.2025

Society of Production Engineering

ICPES 2025

40th INTERNATIONAL CONFERENCE ON PRODUCTION ENGINEERING - SERBIA 2025

DOI: 10.46793/ICPES25.314V

University of Nis Faculty of Mechanical Engineering

Nis, Serbia, 18 - 19th September 2025

THE CONCEPT OF SMART INFORMATION SYSTEMS IN PRODUCTION ENGINEERING: A METAVERSE APPROACH

Nikola VITKOVIĆ[1], Miodrag MANIĆ[1], Milan MITKOVIĆ[2], Sven MARIČIĆ[3], Marek CHODNICKI[4], George VOSNIAKOS[5], Panorios BENARDOS[5], Emmanuel STATHATOS[5]

Orcid: 0000-0001-6956-8540; **Orcid:** 0000-0002-7892-5957; **Orcid:** 0000-0001-6644-3216; **Orcid:** 0000-0001-9471-5557; **Orcid:** 0000-0002-4484-8359

[1]Faculty of Mechanical Engineering, University of Niš, Serbia

[2]Faculty of Medicine, University of Niš, Serbia

[3]Juraj Dobrila University of Pula, Croatia

[4]Gdańsk University of Technology, Poland

[5]National Technical University of Athens, Greece

*Corresponding author: nikola.vitkovic@masfak.ni.ac.rs

Abstract: *The evolution of Industry 4.0 and Industry 5.0 has opened new pathways for integrating advanced digital ecosystems in production engineering. Among these, the Metaverse—a convergence of immersive XR technologies, real-time data, and collaborative virtual spaces—enables the development of Smart Information Systems (SIS) that enhance intelligence, adaptability, and interconnectivity. This paper explores how immersive, persistent digital layers support data-driven decision-making, digital twins, and human-machine interaction. By integrating XR, IoT, AI, and ERP systems, the Metaverse enables virtual prototyping, planning, and human-centered education. It also introduces an atomic knowledge approach, transforming tacit expertise into reusable, structured units embedded within SIS and Metaverse workflows. Technical architecture elements, including XR interfaces and cloud-edge integration, are outlined. Key challenges such as interoperability, privacy, latency, and scalability are addressed, alongside potential solutions and implementation pathways. This work proposes a foundational roadmap for resilient, human-centric, and intelligent production systems.*

Keywords: *Smart Information Systems, AI, ERP, Metaverse, XR, Virtual simulations, Workflow*

1. INTRODUCTION

The rapid evolution of digital technologies is transforming production engineering through the integration of Smart Information Systems (SIS), which include artificial intelligence (AI), the Industrial Internet of Things (IIoT), cloud computing, and big data analytics. These systems enable intelligent automation and data-driven decision-making, reshaping modern manufacturing. At the front of this change is the Industrial Metaverse, a virtual space where digital twins, extended reality (XR), cyber-physical systems, and human operators interact. This environment allows real-time engagement with digital representations of physical assets, facilitating

collaborative design, simulation, remote monitoring, and predictive maintenance.

The combination of SIS and the metaverse represents a shift toward more intuitive and intelligent production workflows. Integrating digital twins in immersive settings enhances situational awareness and enables virtual collaboration among geographically distributed teams. Nonetheless, challenges remain, including data interoperability, security, system scalability, and cognitive load. There is a need for effective frameworks to support real-world implementation. This paper explores how SIS can be embedded within metaverse architectures to advance production engineering. It offers an overview of enabling technologies, integration strategies, potential benefits, and the challenges ahead.

2. LITERATURE REVIEW

The transformation of production engineering through Smart Information Systems (SIS) is being accelerated by cyber-physical systems, the Industrial Internet of Things (IIoT), big data analytics, and artificial intelligence, hallmarks of Industry 4.0 and the emerging paradigm of Industry 5.0 [1, 2]. These SIS frameworks enable real-time monitoring, predictive maintenance, and adaptive decision-making in manufacturing environments. One of the key components of SIS is the digital twin (DT), which is a virtual replica of physical assets or systems that continuously mirrors real-time operational data. DTs enable simulation, optimization, and predictive control across the product lifecycle [3, 4]. While conventional DT implementations rely on 2D dashboards, recent advances are moving toward immersive representations using extended reality (XR) for more intuitive interaction and richer data engagement [5]. This evolution is converging into what is now termed the Industrial Metaverse: a persistent, shared digital environment where physical production systems, human operators, and digital twins co-exist and interact through immersive technologies [6, 7]. Leading manufacturing enterprises like BMW and Siemens have demonstrated the potential of this approach, using metaverse platforms like NVIDIA Omniverse for virtual factory planning, simulation, and collaborative design [8]. Recent frameworks such as Digital Twin Systems Engineering (DTSE) seek to systematize the integration of digital twins, AI, and human-centered design within the industrial metaverse [3]. DTSE emphasizes not only real-time feedback and adaptive control but also the importance of ergonomic and cognitive interaction in production environments. In this context, human-centric digital twins (HCDTs) emerge as a critical direction, integrating physiological data, motion capture, and wearable sensor data to assess worker ergonomics, safety, and productivity [1]. Furthermore, integration of IoT infrastructure is essential for scalable and responsive metaverse deployment. Studies suggest that metaverse platforms built for industrial use, must satisfy core attributes including immersion, interoperability, scalability, and real-time responsiveness, while also addressing cybersecurity and data governance concerns [9]. Systematic reviews on digital twins and smart manufacturing identify key challenges such as data standardization, model fidelity, real-time synchronization, and the need for robust simulation capabilities [4, 10]. Other studies emphasize that while individual components of the industrial metaverse such as XR training tools, AI-based predictive systems, and cloud-edge computing, are maturing, comprehensive integration into unified platforms remains limited [6, 7].

In summary, the current research establishes a strong foundation for SIS, digital twins, and immersive technologies as enablers of next-generation production systems. The Industrial Metaverse builds upon these pillars by offering a unified virtual-physical space for intelligent, human-in-the-loop manufacturing. However, further work is needed to develop interoperable architectures, standard protocols, and validated frameworks to fully realize this vision in industrial settings.

3. METHODOLOGY

This paper applies a conceptual and scenario-based methodology to demonstrate how atomic learning and immersive technologies can be integrated into Smart Information Systems (SIS) for production engineering. The approach is centered on modeling a real-world medical use case, specifically, the customization of internal plates and fixators, through the E-COOL platform and Metaverse-supported collaboration. A Workflow process model is used to map the interaction between physicians, engineers, and designers, highlighting how knowledge atoms are created, shared, and refined during design and manufacturing. The methodology focuses on the alignment of XR simulation environments with SIS logic, enabling the transformation of tacit and explicit knowledge into interoperable digital workflows. The proposed framework is evaluated through its ability to support personalized implant production while promoting collaborative decision-making in line with Industry 5.0 goals.

3.1 The Metaverse as a "Second World" Enabled by XR Technologies

The Metaverse can be understood as a persistent, immersive, and interactive "second world", an alternate digital layer that mirrors and extends the physical realm, where users, digital twins, and systems coexist in real time. This ecosystem enables realistic interactions with virtual assets that go beyond traditional representations, offering enhanced collaboration and simulation in shared virtual environments. At the core of this second world lies Extended Reality (XR), a combined term for immersive technologies including Virtual Reality (VR), Augmented Reality (AR), and Mixed Reality (MR). XR transforms flat dashboards into spatial, interactive environments: VR fully immerses the user in a synthetic space; AR overlays digital data on the real world; MR blends real and virtual objects in seamless coexistence. These modalities allow operators and engineers to engage intuitively with digital twins of production systems, supporting tasks such as training, remote diagnostics, virtual commissioning, and collaborative design. In industrial settings, XR-powered Metaverse spaces allow users to inhabit and manipulate live operational models, navigating through digital factories, simulating process flows, and diagnosing equipment performance virtually. These capabilities enable remote collaboration and real-time feedback, facilitating rapid response to disruptions and process variation. Recent studies highlight that XR in manufacturing enhances situational awareness, improves cognitive load management, and supports human-centric design principles by embedding users within the virtual production context [11]. Additionally, XR interfaces foster embodied interaction with digital twins, enabling spatial reasoning and shared decision-making among distributed teams [12]. By embedding SIS, AI analytics, and XR within the Metaverse, production engineering enters a new era of human-in-the-loop, immersive manufacturing systems. Rather than simply mirroring reality, this second world redefines the way data, systems, and people interact, spatially, continuously, and intuitively, in the spirit of Industry 5.0.

3.2 Manufacturing Workflows in Production Engineering

Manufacturing workflows denote the structured processes that convert raw materials into finished products. These workflows encompass design, prototyping, planning, production, maintenance, quality control, and logistics, coordinated across machines, systems, and human operators. In advanced production engineering, workflows have evolved into dynamic, data-driven, and adaptive sequences, enabled by Smart Information Systems (SIS) such as MES, ERP, AI analytics, IIoT sensors, and digital twins. Through these SIS integrations, production workflows now support real-time monitoring,

predictive maintenance, adaptive scheduling, and just-in-time manufacturing, minimizing downtime and enhancing efficiency. However, managing and visualizing these complex processes remains challenging due to the volume and heterogeneity of data, and the limitations of traditional 2D dashboards in conveying high-dimensional operational insights. To address these challenges, Extended Reality (XR) technologies are being integrated with digital twins to create immersive workflow experiences. XR-powered digital twins bring workflows into spatial contexts, allowing users to walk through factory layouts virtually, simulate assembly lines, and observe material flows in a single interactive environment [13]. For example, XR visual guidance in virtual assembly experiments has demonstrated over 50% reduction in task completion time and errors, underscoring XR's potential to enhance efficiency and reduce cognitive load [14]. By embedding manufacturing workflows within immersive XR environments, operators and engineers gain situational awareness, spatial reasoning, and real-time interaction with process data. This leads to more intuitive control interfaces, proactive decision-making, and collaborative optimization across teams, especially suited for Industry 5.0's human-centered production paradigms.

3.3 Metaverse Integration in Manufacturing Workflows

Integrating the Industrial Metaverse into manufacturing workflows fundamentally reimagines traditional production with immersive, real-time, and spatially rich environments. This integration is achieved by layering Smart Information Systems (SIS), including digital twins, AI analytics, IoT data, and XR interfaces, onto each operational phase. In design and process planning, engineers engage with a virtual 3D twin of the factory using VR to explore facility layouts, simulate production sequences, and test configuration scenarios. This immersive planning can accelerate decision-making, prevent costly rework, and optimize material utilization [15]. During production operations, the metaverse supports augmented reality (AR) interfaces for shop-floor personnel, delivering contextual overlays such as machine health metrics, task instructions, and safety warnings directly in the worker's field of view. This contextual layer boosts accuracy, reduces training time, and enhances situational awareness. For maintenance and quality assurance, mixed reality (MR) environments allow technicians and remote experts to interact with digital twins of equipment in real time. Stakeholders can diagnose faults, annotate repairs, and validate outcomes collaboratively in the same immersive virtual space, minimizing downtime and extending asset life [16]. Moreover, training and workforce development have been transformed. XR-enabled immersive simulations recreate real-world scenarios, transecting physical boundaries and enabling remote teams to train, collaborate, and innovate as avatars in a unified digital environment. A layered architecture model supports these integrations: real-time IoT telemetry feeds into a metaverse engine, which renders spatially coherent digital twins accessible via XR devices. Human operators (Meta-Operators) interface with this platform for seamless interaction across design, production, and maintenance phases [2].

These immersive integrations position the metaverse as more than a monitoring tool, yet it becomes an active, human-centered control layer overlaying physical workflows with spatial insight, collaboration, and intuitive decision support. Integrating SIS, XR, and immersive metaverse spaces thus offers a new paradigm for adaptive, efficient, and sustainable production systems in the era of Industry 5.0.

3.4 Enabling Tacit Knowledge in the Metaverse

Traditionally, tacit knowledge, the unspoken, experience-based know-how held

by skilled workers has been difficult to digitalize or transfer. The Metaverse, however, offers new opportunities to externalize and simulate this type of knowledge through immersive technologies. By capturing expert behaviors using motion tracking, gesture recording, and contextual voice interaction in XR environments, the Metaverse enables the encoding of skilled actions and decision-making processes. These recorded sessions can be replayed, adapted, and embedded in training scenarios or simulation workflows, allowing others to learn by virtually observing or interacting with expert avatars in situ. This approach facilitates not only knowledge retention as senior workers retire, but also knowledge scaling, as expertise can be delivered remotely and repeatedly. Furthermore, designers and engineers can embed tacit insights into virtual prototypes or collaborative spaces, enabling richer interdisciplinary co-creation. Thus, the Metaverse becomes a living knowledge environment, not only hosting data and processes but preserving and transmitting human skill, bridging the gap between explicit data and human intuition in production engineering.

3.5 The Atomic knowledge addition to Industrial SIS and Metaverse

Atomic knowledge refers to small, self-contained units of domain-specific expertise that can be modularly applied, reused, and shared across smart manufacturing systems. When integrated into Industrial Smart Information Systems (SIS) and the Industrial Metaverse, atomic knowledge serves as a dynamic bridge between data-driven automation and human-centric intelligence.

In traditional SIS, decision-making often relies on large data models or static expert rules. Atomic knowledge introduces small, adaptable knowledge artifacts, for example, how a specific implant geometry affects load distribution or how a material behaves under heat treatment. These atoms can be triggered by context (e.g., a CAD model, sensor reading, or user input) and embedded within digital twins, simulation environments, or XR interfaces in the Metaverse.

By incorporating atomic knowledge, the Metaverse becomes more than a visualization space. It evolves into an interactive learning environment, where engineers, physicians, and designers can retrieve, contribute, and validate domain insights in real time. These atoms also enable knowledge versioning, traceability, and AI-supported recommendation, essential for continuous improvement in complex manufacturing ecosystems. Thus, atomic knowledge enhances the adaptability, reusability, and personalization of SIS and XR workflows, empowering human-machine collaboration at the heart of Industry 5.0. The one approach for integration of novel atomic knowledge into existing educational material is presented in Figure 1.

This diagram illustrates a structured workflow for transforming initial educational materials into modular, atom-based course content. The process begins with the Material Analysis, conducted by educators (M1), to identify the fields and topics present in the input material. Based on the NEM definition (C1), the content is then organized in the Material Separation into Sections phase. This step uses domain-specific criteria such as science fields and topic aggregation methods to logically segment the material. Next, the Feature Extraction and Atom Definition stage identifies minimal learning units, termed "atoms", along with their representations and interrelations. This step is crucial for enabling personalized and adaptive learning structures. Supporting references guide the definition and representation of these atoms. In the final phase, Formation of the Courses, atoms are assembled into coherent course structures, guided by Novel Educational Methodology (NEM) [17] (C2) and informed by student needs (M2). The output is a logically structured, atomized curriculum that supports microlearning and facilitates flexible educational delivery. The framework enables a precise breakdown of complex educational

content into granular, reusable learning units, making it suitable for intelligent tutoring systems, e-learning platforms, and personalized learning environments. It reflects modern educational paradigms aligned with digital transformation and adaptive instruction.

To demonstrate the application of atomic learning within Smart Information Systems (SIS) and the Metaverse, the following medical use case is presented (Figure 2) and analysed.

This diagram extends the concept of atomic learning to the domain of biomedical product development and surgical planning. It outlines a workflow from Product Design to Simulations, including Material definition. These elements represent modular topics that can be taught, assessed, and reused independently.

They can be created, modified an reused by different skilled groups, like professors, engineers, scientist, and other which are interested in specific topic.

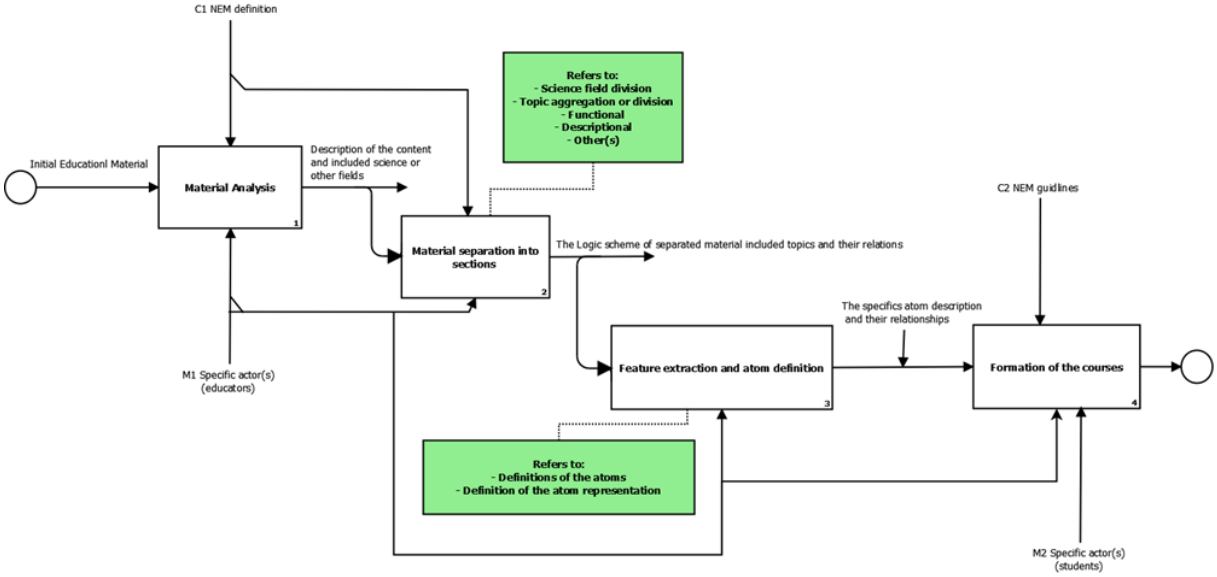

Figure 1. The SADT diagram for improvement of educational material by using atoms of knowledge

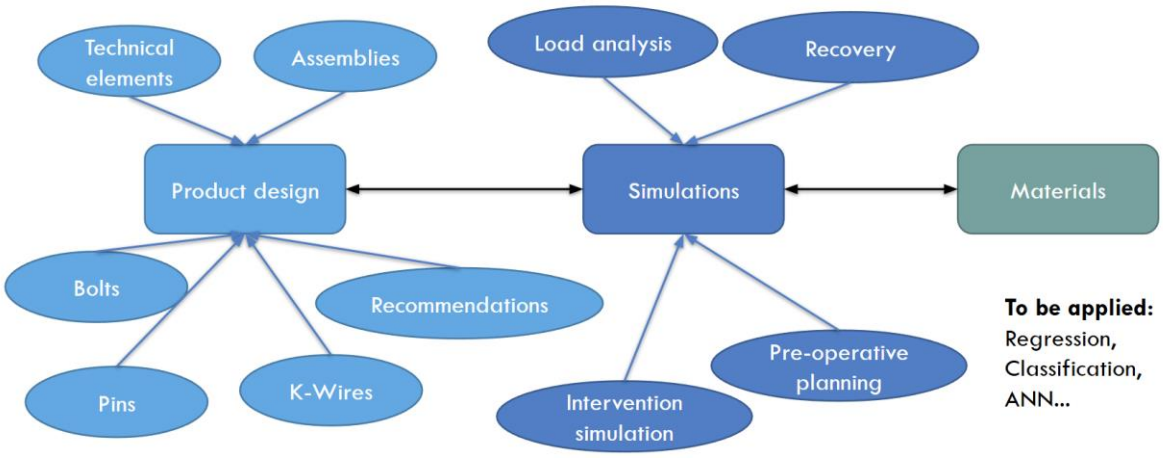

Figure 2. The Conceptual representation of the medical atoms in the specific domainsIn the

Simulation phase, atomic knowledge extends to Load Analysis, Recovery, Recommendations, Intervention Simulation, and Pre-operative Planning. Each simulation topic forms an atom that can be aligned with targeted educational objectives. For instance, one atom might focus on simulating the mechanical response of K-wires under stress, while another focuses on the recovery processes. The inclusion of AI techniques, such as regression, classification, and artificial neural networks (ANNs), highlights the potential for

intelligent tutoring systems to personalize content delivery and evaluation. These models can adapt learning paths based on individual performance or decision-making behavior in simulations. Overall, atomic learning enables a personalized, modular, and adaptive training approach that bridges engineering design and clinical applications, promoting effective learning in interdisciplinary medical education environments. To demonstrate the application of the aforementioned technologies, the following section presents a use case (Figure 3) on personalized implant production.

3.6 The personalised implant production proces

This diagram illustrates a comprehensive workflow for applying atomic learning and XR-based knowledge delivery in the development of personalized implants. The process begins with Patient Diagnostics and continues through the detection of the problem, leading to a need for a personalized implant.

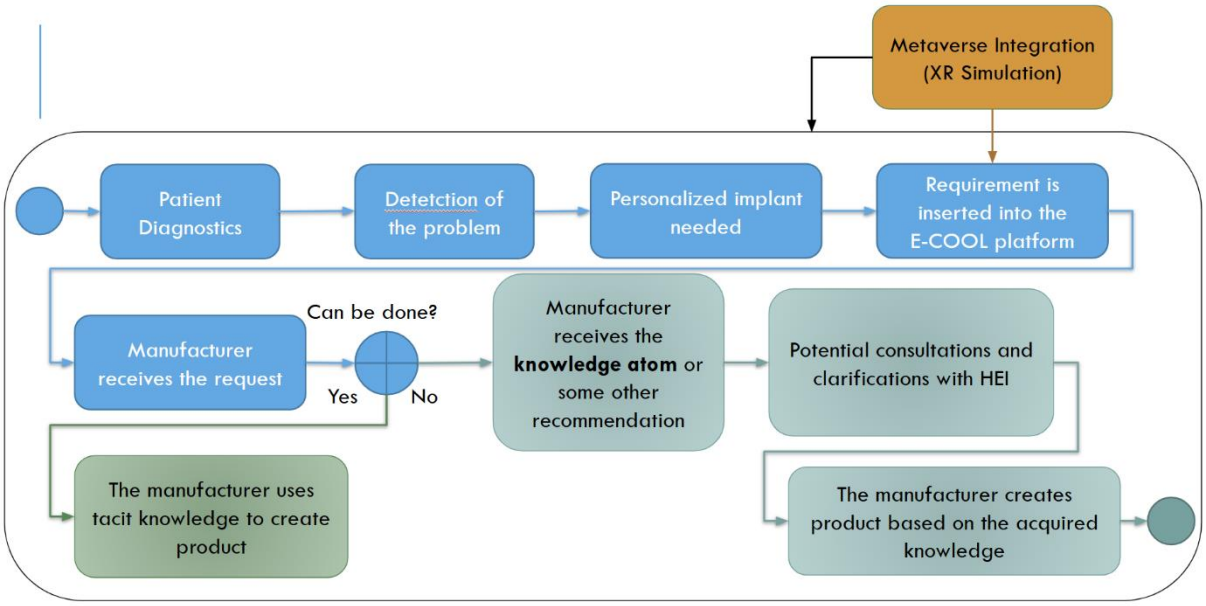

Figure 3. Comprehensive workflow for applying atomic learning and XR-based knowledge delivery in the development of personalized implants

The manufacturer receives the request, and the system checks whether the task can be fulfilled. If feasible, the manufacturer proceeds using tacit knowledge, practical, experience-based insights, to create the product. Alternatively, if additional information is needed, the manufacturer receives a knowledge atom or a structured recommendation. These atoms, representing minimal and reusable learning units, are informed by simulations and previous expert experience. To enable more visual approach, the integration of Metaverse (XR Simulation) is included. It supports immersive visualization, planning, and communication, enabling more informed decisions. If uncertainties remain, consultations with Higher Education Institutions (HEIs) help clarify the meaning or content of the knowledge atom. Ultimately, the manufacturer creates the product based on the acquired explicit or tacit knowledge. This workflow exemplifies how atomic learning, enhanced with XR and collaborative platforms, can enable responsive, knowledge-driven manufacturing tailored to individual medical needs, bridging diagnostics, design, education, and production in an intelligent healthcare ecosystem. The Workflow Swimline diagram, which describes the presented process, is shown in Figure 4.

This workflow diagram outlines a collaborative workflow among physicians, engineers, and designers in the development of personalized implants, leveraging both the E-COOL platform and Metaverse (XR Simulation) integration. The process starts in the Physician

lane, where a patient undergoes diagnostics. Upon detection of a problem, a personalized implant is identified as necessary and entered into the E-COOL platform. The process transitions to the Engineer, who receives the request and evaluates its feasibility through a decision node: "Can be produced?" If the answer is yes, the process continues using existing tacit knowledge. If not, the engineer accesses a knowledge atom or consults with higher education institutions (HEIs) for clarification. These consultations are essential for futher improvement of the process of creating different products.

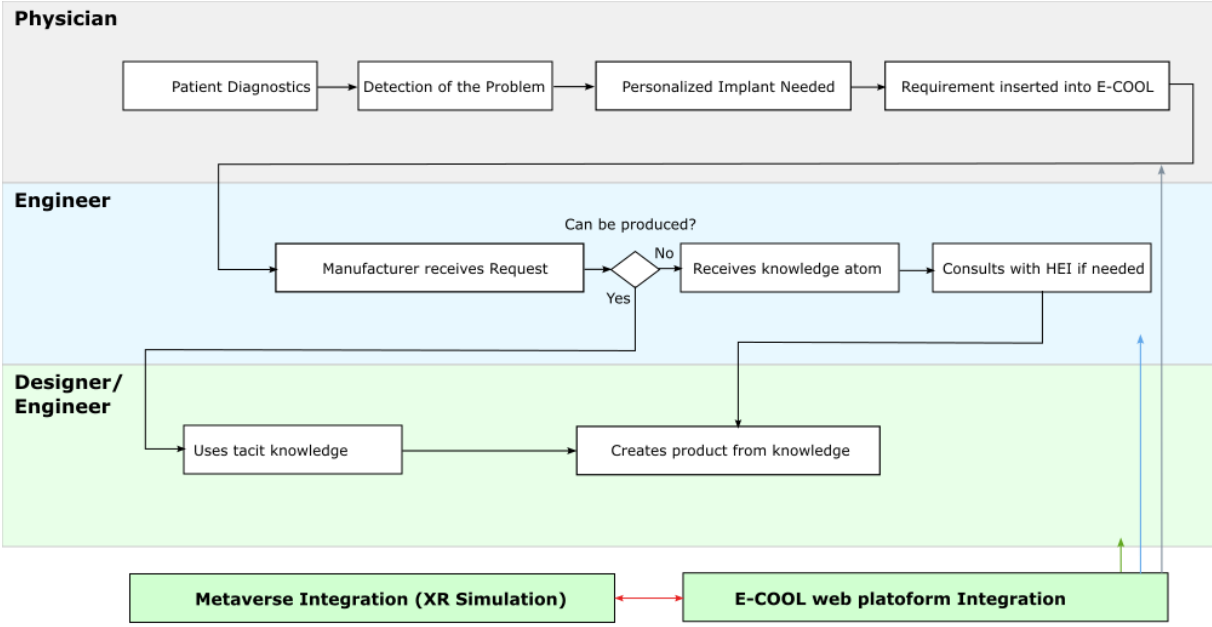

Figure 4. Comprehensive workflow for applying atomic learning and XR-based knowledge delivery in the development of personalized implants

In the Designer/Engineer lane, tacit knowledge and recommendations, obtained through XR simulation or expert consultation, are used to guide the design and manufacturing of the personalized product. The designer ultimately creates the product based on this accumulated knowledge. At the bottom, the Metaverse Integration (XR Simulation) and E-COOL platform serve as enabling infrastructures. XR provides immersive training, testing, and decision support, while E-COOL ensures traceability and centralized data handling. This framework enables efficient collaboration and knowledge transfer between disciplines, promoting precision, personalization, and intelligent manufacturing in healthcare innovation.

3.7 Example Scenario: Custom implant development using the Mitkovic-type internal fixator

In cases of complex tibial plateau fractures, presented in Figure 5, particularly those with unusual bone morphology, prior surgical alterations, or asymmetrical deformities, the standard Mitković internal fixator may require customization. Consider a patient with a severe lateral tibial plateau fracture and preexisting skeletal irregularities due to previous trauma. In this case, the orthopedic surgeon, following radiographic diagnostics and 3D CT reconstruction, determines that a standard fixator does not fit the lateral contour properly, risking improper stabilization and delayed healing.

Using the E-COOL platform, the physician initiates a request for a custom variant of the Mitković internal fixator. The request is reviewed by the engineering team, who perform feasibility analysis using digital twin simulations and finite element validation. If uncertainties arise regarding stress distribution or anatomical fit, the case is transferred to the

Metaverse platform, enabling immersive collaboration between the physician, engineers, and implant designers. Within this XR environment, they visualize the patient-specific anatomy, manipulate a 3D model of the fixator in real scale, and simulate the surgical procedure virtually. Using prior implant knowledge as well as new insights gathered during simulation, the system generates a refined "knowledge atom" to support the redesign. The design team applies reverse engineering on existing Mitković components, adapting the geometry to the patient's anatomy using CAD/CAM integration. Final prototypes are validated in the Metaverse environment before production. The output is a custom-fabricated, patient-specific internal fixator that conforms to Mitković's biomechanical principles while adapting to anatomical constraints, and is delivered with greater precision, collaboration, and reduced turnaround time.

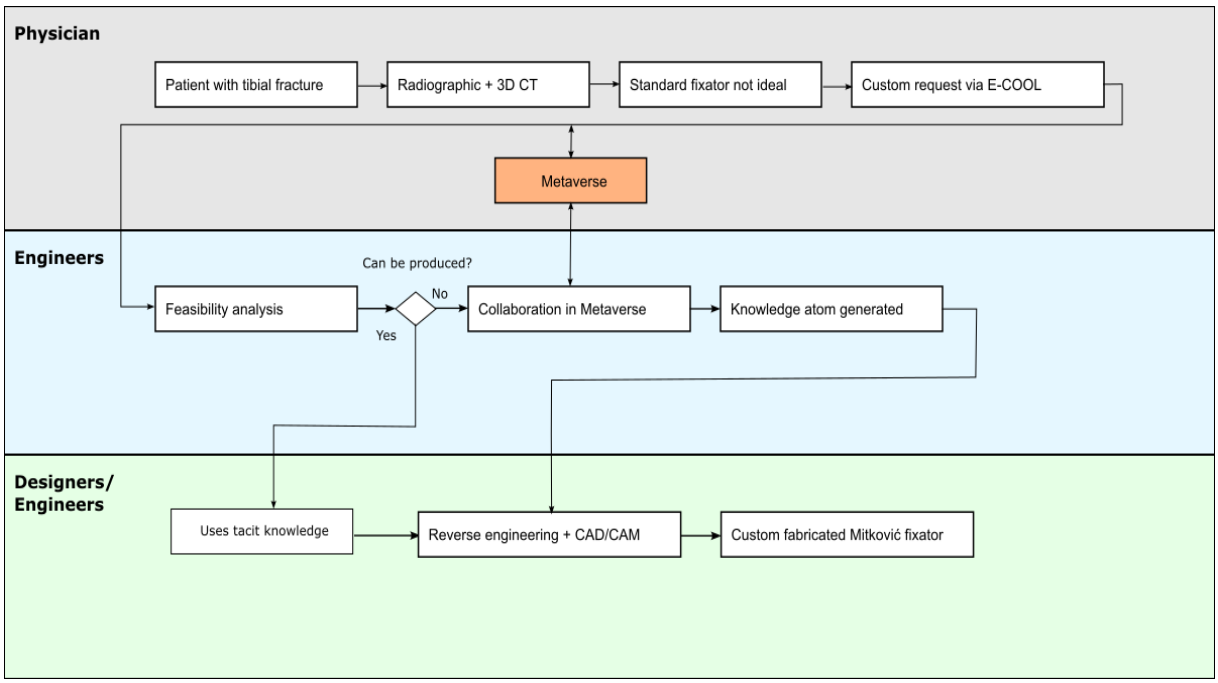

Figure 5. Workflow for Metaverse application in producing customized Mitkovic type internal fixators

4. CONCLUSION

This paper proposed a novel integration of Smart Information Systems (SIS), atomic learning, and Metaverse technologies to support collaborative, knowledge-driven production engineering. By conceptualizing the Metaverse as a shared digital environment, the framework enables engineers, designers, and physicians to interact in real time, simulate workflows, and contribute to a dynamic repository of atomic knowledge. The personalized implant use case, based on Mitković-type internal fixators, demonstrates how immersive technologies and modular knowledge units can transform traditional design and manufacturing processes. Knowledge atoms, generated during simulation and decision-making, enhance the system's adaptability and reusability across similar scenarios. This approach supports Industry 5.0 goals by aligning human expertise with digital intelligence and immersive collaboration. Future work will involve the formal structuring of atomic knowledge and practical validation across various domains. The proposed methodology represents a scalable foundation for building intelligent, human-centered production systems enhanced by extended reality and smart data integration. The possible applications are only limited by human imagination.

ACKNWOLEDGMENT

This work was supported by the European Union through the following Erasmus+ projects: "Collaborative e-platform for innovation and educational enhancement in medical engineering" – CALLME (Project Reference: 2022-1-RO01-KA220-HED-000087703), which focuses on enhancing education in medical engineering through the development of a collaborative digital platform and innovative teaching methodologies.
"Extended Reality for Machine Tool Training" – XMAN (Project Reference: 2023-1-PL01-KA220-VET-000162134), which aims to improve vocational education and training in manufacturing by integrating extended reality (XR) technologies into machine tool operation training.

REFERENCES

[1] Asad, U., Khan, M., Khalid, A., & Lughmani, W. A. (2023). Human-centric digital twins in industry: A comprehensive review of enabling technologies and implementation strategies. Sensors, 23(8), 3938. https://doi.org/10.3390/s23083938

[2] Fernández-Caramés, T. M., & Fraga-Lamas, P. (2024). Forging the industrial metaverse: Where Industry 5.0, XR, IIoT, edge computing and digital twins meet. IEEE Access, 12, 95778–95819. https://doi.org/10.1109/ACCESS.2024.3422109

[3] Zhang, S., Li, J., Shi, L., Ding, M., Nguyen, D. C., Chen, W., & Han, Z. (2024). Industrial metaverse: Enabling technologies, open problems, and future trends. arXiv preprint arXiv:2405.08542. https://arxiv.org/abs/2405.08542

[4] Nleya, S. M., Mahlatji, M. L., Chuma, J. M., & Adeola, S. O. (2024). Industrial metaverse: A comprehensive review, environmental impact and challenges. Applied Sciences, 14(13), 5736. https://doi.org/10.3390/app14135736

[5] Doolani, S. M., Wessels, C., Kanal, V., Sevastopoulos, C., Jaiswal, A., Nambiappan, H., & Makedon, F. (2020). A review of extended reality (XR) technologies for manufacturing training. Technologies, 8(4), 77. https://doi.org/10.3390/technologies8040077

[6] Cao, H., Söderlund, H., Derspeisse, M., & Johansson, B. (2023). Exploring the current applications and potential of extended reality for environmental sustainability in manufacturing. arXiv preprint arXiv:2312.17595. https://arxiv.org/abs/2312.17595

[7] Kour, R., Soni, A. K., Sharma, M., & Verma, R. (2025). Metaverse in industrial contexts – a comprehensive review. Frontiers in Virtual Reality. https://doi.org/10.3389/frvir.2025.1488926

[8] Siemens & NVIDIA. (2022). Siemens and NVIDIA partner to enable the industrial metaverse. Siemens Press Release. https://press.siemens.com/global/en/pressrelease/siemens-and-nvidia-announce-partnership-enable-industrial-metaverse

[9] Li, K., Cui, Y., Li, W., Lv, T., Yuan, X., Li, S., Ni, W., Simsek, M., & Dressler, F. (2022). When Internet of Things meets metaverse: Convergence of physical and cyber worlds. arXiv preprint arXiv:2208.13501. https://arxiv.org/abs/2208.13501

[10] Production digital twin: A systematic literature review of challenges. (2023). Computers in Industry, 149, 103850. https://doi.org/10.1016/j.compind.2023.103850

[11] Egbengwu, V., Garn, W., & Turner, C. J. (2025). Metaverse for manufacturing: Leveraging extended reality technology for human-centric production systems. Sustainability, 17(1), 280. https://doi.org/10.3390/su17010280

[12] Oppermann, L., Buchholz, F., & Uzun, Y. (2024). Industrial Metaverse? Human-Centred Design for Collaborative Remote Maintenance and Training Using XR-Technologies. In M. C. tom Dieck, T. Jung & Y.-S. Kim (Eds.), XR and Metaverse (pp. 195–209). Springer. DOI: 10.1007/978-3-031-50559-1_15.

[13] Chen, B., Macdonald, S., Attallah, M., Chapman, P., & Ghannam, R. (2025). A review of prototyping in XR: Linking Extended Reality to Digital Fabrication. arXiv preprint arXiv:2504.02998. https://arxiv.org/abs/2504.02998

[14] Pietschmann, L., Zuercher, P.-D., Bubík, E., Chen, Z., Pfister, H., & Bohné, T. (2023). Quantifying the impact of XR visual guidance on user performance using a large-scale virtual assembly experiment. arXiv preprint

arXiv:2308.03390. https://doi.org/10.48550/arXiv.2308.03390

[15] Miura, T., & Okabe, H. (2024). Leveraging the industrial metaverse for digital transformation: Realizing next-generation factories through simulation and immersive XR. EY Japan Insights. https://www.ey.com/en_jp/insights/technology/industrial-metaverse-unlocks-the-future-realizing-next-generation-factories-through-digital-transformation

[16] Tomaszewska, K. (2025). XR technology in manufacturing – Exploring practical applications, drivers, and barriers. Scientific Papers of Silesian University of Technology, Organization & Management Series, (217), 221–234. https://managementpapers.polsl.pl/wp-content/uploads/2025/04/217-TOMASZEWSKA.pdf

[17] Vitković, N., Mišić, D., Simonović, M., Banić, M., Miltenović, A., Mitić, J., & Milovanović, J. (2020). Novel educational methodology for personalized Massive Open Online Courses. In Proceedings of the 10th International Conference on Information Society and Technology (ICIST 2020) (Vol. 1, pp. 5–9). Kopaonik, Serbia. ISBN: 978-86-85525-24-7.

[18] Vitković, N., Trajanović, M., Barać, M., Trifunović, M., Stojković, J., Stan, S. D., & Pacurar, R. (2024). Novel approach for education in biomedical engineering based on atomic learning. In M. Trajanović, N. Filipović, & M. Zdravković (Eds.), Disruptive Information Technologies for a Smart Society: Proceedings of ICIST 2023 (Lecture Notes in Networks and Systems, Vol. 872, pp. 279–287). Cham: Springer Nature. https://doi.org/10.1007/978-3-031-50755-7_26

Society of Production Engineering

ICPES 2025

40th INTERNATIONAL CONFERENCE ON PRODUCTION ENGINEERING - SERBIA 2025

DOI: 10.46793/ICPES25.325S

University of Nis
Faculty of Mechanical Engineering

Nis, Serbia, 18 - 19th September 2025

RAPID PROTOTYPING OF A DEVICE FOR TESTING THE CONNECTION OF REINFORCED CONCRETE AND ANCHOR BOLT

Nikola ŠIBALIĆ[1]*, Marko MUMOVIĆ[1]
Orcid: 0009-0003-8908-2347; **Orcid:** 0000-0002-8911-2345;
[1]University of Montenegro, Faculty of Mechanical Engineering, Podgorica, Montenegro
*Corresponding author: nikola@ucg.ac.me

Abstract: *In this paper the prototype of the device for field testing of the connection between reinforced concrete and anchor bolt was developed. Anchor bolts are often used in construction and mechanical structures or equipment to fasten them to the base: concrete, stone or some other building material. The basic factors that are important for the safe functioning of anchor bolts are the condition of the base, the operating load, the influence of the environment and proper installation. That is why it is very important to carry out adequate testing of the connection between the anchor bolt and the base after their installation, because this is the only way to make sure that they will perform their critical role. The paper presents the original solution of the testing device, which will enable the testing of installed anchor bolts in a wide range. The device enables monitoring of the most important parameters related to the quality of the base in which they are installed, the quality of the installation and the quality of the anchor bolt. The initial solution of this device was given, which meets the current technical directives and was validated by the Finite Element Method (FEM), in order to check the capacity under the static load and determine potential stress concentrations. The model was optimized in several iterations, using the Topology Optimization method, in order to obtain a lightweight construction, and the obtained results were compared with the initial model. The models are made using additive technology Fused Filament Fabrication (FFF), with the application of Computer-Aided Design (CAD) and Computer-Aided Engineering (CAE). The device is ergonomically designed based on the operating load through the use of eco-friendly materials, optimization of mass and shape.*

Keywords: *Field testing device, Anchor bolts, CAD/CAE, Ergonomics, Topology optimization*

1. INTRODUCTION

Rapid prototyping includes a set of techniques that are used for the rapid formation of a physical model, which enables fast and economically efficient testing of the form and function of the product without the use of complex tools, which is most often achieved by some of the additive technologies [1,2]. The resulting prototype can be fully functional if its function is not too demanding.

Much more often, prototypes are partially functional because the materials used do not have the necessary properties to fulfill their function. Such prototypes are useful for experimental tests related to the geometry of

the prototype [3] for which there are a large number of formats [4]. The use of this approach significantly affects the production time and the price of the product [5]. The application of advanced CAD/CAE approaches such as Topology Optimization enables obtaining light structures [6-10]. The rapid prototyping method in this paper will refer to the development of a device for testing anchor bolts in field conditions. Anchor bolts are mechanical elements that provide a solid and reliable connection between the structure and the base, and they function on the mechanical principle of expansion using a taper.

For the proper functioning of the anchor bolts, it is necessary to choose a type that can respond to the given working conditions, proper assembly, as well as the quality of the base in which they are installed. That is why it is very important to perform a field test of the anchor bolts after their installation. The main process and reference quantities for this test are load force and anchor bolt displacement. Their measurement will be carried out through an integrated information measurement system that will contain reliable sensors, which can measure these quantities in a wide range of values, with high accuracy and repeatability.

The development of the initial prototype solution begins with the adoption of input parameters (type of anchor bolt, dimensions, geometric shape, expected load, examined spatial position and quality of the base), as well as output parameters that give a valid image of the behavior of the connection between the anchor bolt and reinforced concrete, i.e. the base (displacement and axial force). Based on the adopted parameters, dimensioning, design and technical drawings were carried out. When designing this device, particular care was taken with the ergonomics of the device, with the aim of improving comfort, safety, efficiency, easier handling and test performance.

2. INITIAL MODEL

The device consists of a support plate, on which there is a modified hydraulic cylinder that has a multipurpose role. A threaded spindle passes through it, at the upper end of which there are levers with a nut, through which the user applies a load that is transferred to the cylinder by means of a suitable rolling bearing, with the aim of transferring the axial load. At the lower end of the spindle is a receiving claw through which the load is transferred to the anchor bolt itself.

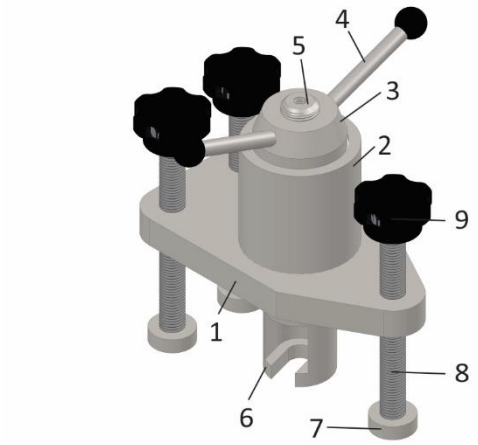

Figure 1. Initial model of the device for testing anchor bolts (1 - Support plate; 2 - Hydraulic cylinder; 3 - Nut; 4 - Lever; 5 - Threaded spindle; 6 - Claw; 7 - Pad; 8 - Support; 9 - Knob)

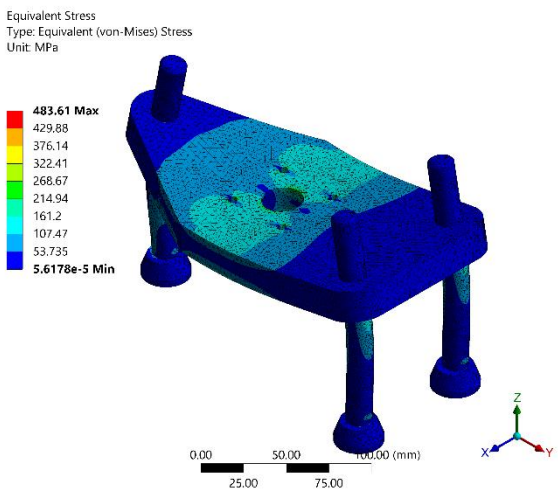

Figure 2. CAE analysis of the initial model

During loading operations, special attention was paid to the ergonomic and robust design, so the user can apply very large loads with little use of manual work. The mentioned components are supported on three adjustable supports, each of which has three degrees of freedom, so in this way it is ensured that the given load is uniaxial for different types of

foundations. The formed CAD model is shown in Figure 1.

A CAE analysis of the critical (stressed members) parts of the structure was performed using FEM (Figure 2).

Increased stress values occur only locally, and in the critical section the highest stress is $\sigma \approx 230$ *MPa*. The support plate will be made of aluminum alloy AA7075-T6, whose mechanical properties are $R_{p0.2}$=480 *MPa* and R_m=570 *MPa*, which gives a safety factor of about *S*=2.1.

The formed initial model was made predominantly using FFF additive technology and is shown in Figure 3.

Figure 3. The Iteration 1 of the prototype anchor bolt testing device

After the production of the Iteration 1, in addition to the over-dimensioning of the cylinder, support plate and its large mass (≈ 5.9 *kg*), poor ergonomics and unaesthetics, other defects were noticed. The structure has a large free movement when it is not under load, which is mainly due to the adopted axial ball bearing, which is separable and cannot be made fixed in a simple way. This bearing was chosen because it has the highest axial load capacity. The buckling support check was also performed according to Johnson's formula:

$$P_{cr} = \frac{\pi^2 EI}{(kL)^2}$$

Where: P_{cr} – critical load, E – Young's modulus for adopted material, I – area moment of inertia of the section, which for a circular area is $I = \frac{\pi}{2} r^4$, k – effective length factor, which for fixed support is k=0.65 and length of the support L=150 *mm*, and L_e=97.5 *mm* is an effective length of support. For adopted thread M16, the root diameter is 13.8 *mm*, and Young's modulus for the adopted A2 stainless steel is E=190 *GPa,* and yield strength is 640 *MPa*, where I=1780.27 mm^4, and cross sectional area is A=37.39 mm^2.

The critical load according to Johnson's formula is P_{cr}=23.52 *kN* per support, which means that there is no risk of their buckling.

3. TOPOLOGY OPTIMIZATION

In order to reduce the mass of the construction, Topology Optimization was applied to the most massive part, the support plate. The optimization criterion was the retention of stiffness with a mass reduction of 50%. A boundary condition related to the obtaining technology called extrusion is also set, because it allows us to obtain a geometry of constant cross-section in the plane of choice. The optimization result is shown in Figure 4.

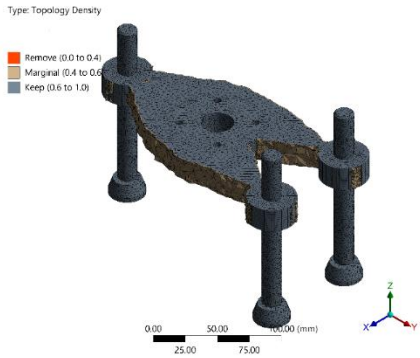

Figure 4. Support plate with supports of the Iteration 2 of the prototype

The resulting model was numerically tested using FEM, and the result of the numerical simulation is given in Figure 5.

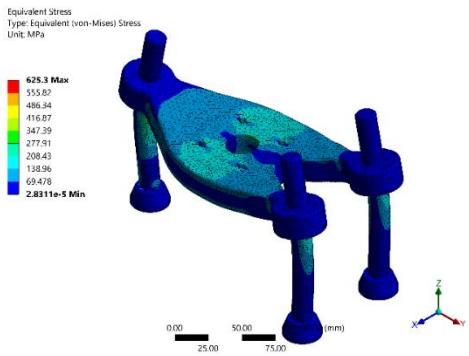

Figure 5. CAE analysis of Iteration 2.

Increased stress values occur only locally, and in the critical section the highest stress is $\sigma \approx 270$ *MPa*, which indicates that we still have a satisfactory level of safety of around S=1.9.

Since this cylinder is a pressure vessel and represents a critical element, its FEM analysis was performed. The surfaces exposed to pressure are shown in Figure 6, the fixed support is on the lower surface of the cylinder, and the results of this analysis are given in Figure 7.

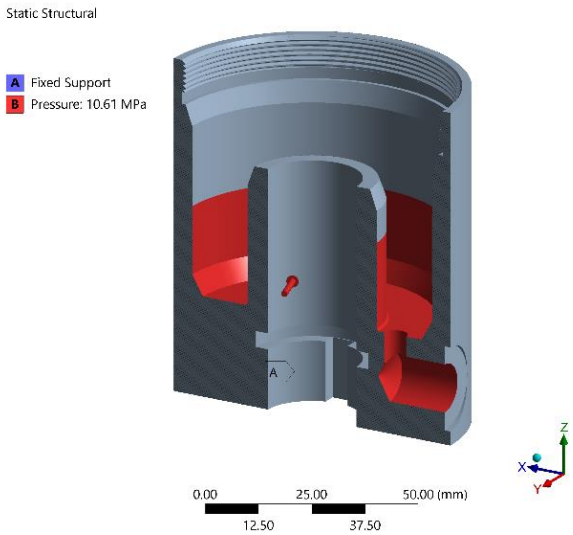

Figure 6. Surfaces exposed to pressure in a hydraulic cylinder

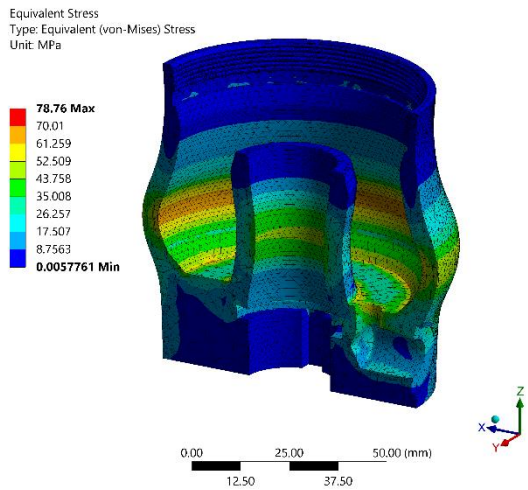

Figure 7. CAE analysis of a hydraulic cylinder

The maximum stress occurring in the material is far below the conventional yield stress for the selected AA7075-T6 alloy, which opens the possibility for further mass optimization. This was not pursued because the obtained result would not greatly affect the total mass of the structure, and would significantly complicate the technology.

The formed model of the Iteration 2 was made using FFF technology and is shown in Figure 8.

Figure 8. The Iteration 2 of the prototype anchor bolt testing device

By applying the Finite Element Method, the dimensions of the hydraulic cylinder were significantly reduced, and by using Topology Optimization, the support plate was improved. In addition to weight reduction, we also got a more aesthetic and better ergonomically adapted design. This shape gives it a characteristic and originality. The mass of the resulting construction is $\approx$4.4 *kg* without sensors.

When it comes to the free movement problem of the ball thrust bearing, it is overcome by using a four-point contact ball bearing which is a bearing adapted to the axial and radial load and by simply fixing it with a bushing on which it rests. This was not structurally possible to achieve with an ordinary axial ball bearing. The disadvantage of the newly chosen bearing is the reduced load capacity compared to the axial ball bearing.

4. INFORMATION MEASUREMENT SYSTEM

For the created prototype, an information measurement system was developed for this type of device through the application of modern electrical sensors in order to reduce measurement uncertainty and solve the problem of data transmission through the use of wireless transmission. The third iteration of the prototype with measuring elements, ergonomically adapted supports and handle is shown in Figure 9.

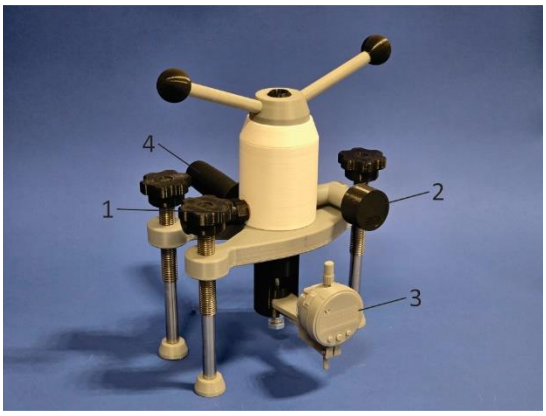

Figure 9. The third iteration of the prototype device for testing anchor bolts (1 - wireless pressure sensor; 2 - analog pressure gauge; 3 - wireless displacement sensor; 4 - handle for carrying the device)

The information measurement system consists of a pressure sensor that allows us to monitor the force value and a displacement sensor that is placed so that it touches the surface. Both sensors have the possibility of wireless data transmission, the acquisition of which is performed on a computer using a program obtained in *LabVIEW* software. Force and displacement were measured, and the results were obtained in graphic and *DATA* form. The diagrams obtained in this way are the force (*kN)* as a function of displacement (*mm*), and values of individual quantities in time (*s*).

The use of an information measurement system that uses wireless sensors offers a number of advantages for field testing which can be a very dynamic environment. It enables the elimination of power and communication cables, which simplifies installation and shortens testing time, especially in hard-to-reach and risky locations. The absence of cables also contributes to the ergonomics of this solution, as it reduces the risk of potential indirect injury to the operator or damage to the device during installation and testing.

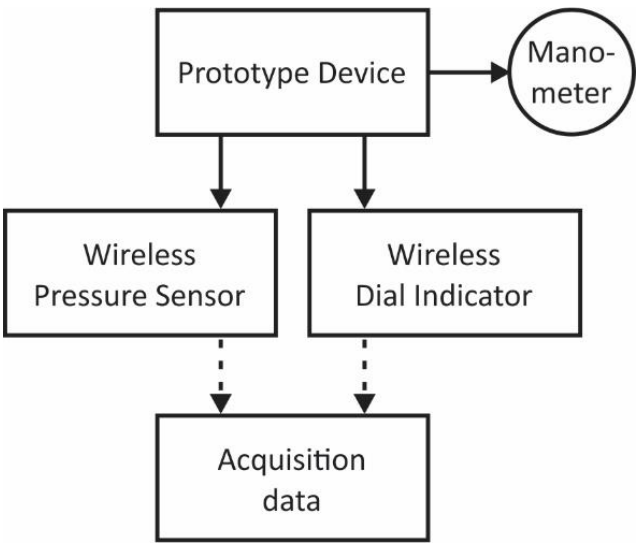

Figure 10. Block diagram of the information measurement system

5. CONCLUSION

The developed device for field testing of installed anchor bolts provides precise control of the tensioning force and movement of the anchor bolt, which enables a later assessment of the mechanical stability between the anchor bolt and the concrete (base). The optimized solution is ergonomically adapted using CAD/CAE tools, where the mass of the initial structure is reduced by 25%.

The developed prototype is current and applicable, especially when applied to test the connection of anchor bolt and concrete in an overhead position for a wide class of nominal diameters of the anchor bolt.

Application of the developed information measurement system enables more reliable measurement, simpler and safer work.

Future research will be related to the construction, which should provide an increase in the range of supports in order to test with the destruction of the material.

ACKNOWLEDGEMENT

This paper is the result of a project received from the Innovation Fund of Montenegro and the University of Montenegro - Faculty of Mechanical Engineering as part of the Proof of Concept program.

REFERENCES

[1] T. A. Yeshiwas, A. B. Tiruneh, M. A. Sisay: A review article on the assessment of additive manufacturing, *Sci: Mater Eng.* 20:85, 2025., doi.org/10.1186/s40712-025-0306-8.

[2] H. I. Medellín-Castillo, J. E. P. Torres: Rapid prototyping and manufacturing, *A review of current technologies: ASME Int. Mech. Eng. Congr. Expo. Proc.*, vol. 4, no. February, pp. 609–621, 2010., doi: 10.1115/IMECE2009-11750.

[3] S. Upcraft, R. Fletcher: The rapid prototyping technologies, *Assem. Autom.*, vol. 23, no. 4, pp. 318–330, 2003.

[4] T. S. Jones, R. C. Richey: Rapid prototyping methodology in action, *A developmental study: Educ. Technol. Res. Dev.*, vol. 48, no. 2, pp. 63–80, 2000., doi: 10.1007/BF02313401.

[5] M. Šibalić, N. Šibalić, M. Šekularac, A. Vujović: Process of Rapid Prototyping Using Wind Turbine as an Object of Experimental Research, *New Technologies, Development and Application V. NT 2022. Lecture Notes in Networks and Systems*, vol 472, Springer, 220–226, ISSN 2367-3370, 2022., doi.org/10.1007/978-3-031-05230-9_25.

[6] M. Mumović, N. Šibalić, A. Vujović, J. Šaković Jovanović: Topological Optimization of Vice Jaws Model for Pipe Clamping, *International Conference on Applied Sciences (ICAS 2022*), Bosnia and Herzegovina, Banja Luka 25-28 May 2022., *Journal of Physics: Conference Series* 2540 012027, 1–6, doi:10.1088/1742-6596/2540/1/012027.

[7] S. D. Slavov, M. I. Konsulova-Bakalova: An algorithm for topology optimization of gear reducer housing elements, *MATEC Web Conf.*, vol. 287, p. 01020, 2019., doi: 10.1051/matecconf/201928701020.

[8] J. Dvorakova, K. Dvorak: Topological Optimization of a Component Made by the FDM Method, *Int. J. Mech. Eng. Robot. Res.*, vol. 10, no. 2, pp. 67–71, 2021., doi: 10.18178/ijmerr.10.2.67-71.

[9] J. M. Mercado-Colmenero, M. A. Rubio-Paramio, M. Dolores La Rubia, D. Lozano-Arjona, C. Martin-Doñate: A numerical and experimental study of the compression uniaxial properties of PLA manufactured with FDM technology based on product specifications, *Int. J. Adv. Manuf. Technol.*, vol. 103, no. 5–8, pp. 1893–1909, 2019., doi: 10.1007/s00170-019-03626-0.

[10] X. P. Li, L. Y. Zhao, Z. Z. Liu: Topological Optimization of Continuum Structure based on ANSYS, *MATEC Web Conf.*, vol. 95, pp. 4–7, 2017., doi: 10.1051/matecconf/20179507020.

Society of Production Engineering

ICPES 2025

40th INTERNATIONAL CONFERENCE ON PRODUCTION ENGINEERING - SERBIA 2025

DOI: 10.46793/ICPES25.332K

University of Nis Faculty of Mechanical Engineering

Nis, Serbia, 18 - 19th September 2025

A BRIEF HISTORY OF CAD AND RELATED TECHNOLOGIES

Nikola KORUNOVIĆ[1]*, Miloš STOJKOVIĆ[1], Nikola VITKOVIĆ[1], Jovan ARANĐELOVIĆ[1]

Orcid: 0000-0002-9103-9300; **Orcid:** 0000-0001-9020-125X; **Orcid:** 0000-0001-6956-8540; **Orcid:** 0000-0001-9653-4119;

[1] University of Nis, Faculty of Mechanical Engineering, Serbia

*Corresponding author: nikola.korunovic@masfak.ni.ac.rs

Abstract: *Computer-Aided Design (CAD) evolved from its origins in late-1950s computer graphics to today's integrated digital-manufacturing environments. Initially used for simple 2D drafting, CAD advanced in the 1960s with the advent of 3D modeling, enabling the creation of complex surfaces and driving adoption in the automotive and aerospace industries. Subsequent breakthroughs—solid, feature-based and parametric modeling—spurred market growth but also delayed uptake of newer approaches like direct modeling, partly because established users favored familiar methods and partly because newer techniques remain under refinement. In recent years, CAD innovations have been absorbed into broader frameworks such as Computer-Integrated Manufacturing (CIM), Product Lifecycle Management (PLM) and digital manufacturing, all of which leverage emerging technologies: artificial intelligence, generative design, cloud computing, real-time simulation, augmented reality and virtual reality. Drawing on both literature and extensive practitioner experience, the paper offers a concise historical overview and outlines current CAD trends.*

Keywords: *Computer-Aided Design (CAD), 3D Modeling, Parametric Design, Direct Modeling, Product Lifecycle Management (PLM), Generative Design, Digital Manufacturing.*

1. INTRODUCTION

Computer-aided design (CAD) software has come a long way from automated drafting applications to highly integrated and versatile solutions. At the end of the 1950s, the progress of computer graphics facilitated the early use of CAD for graphical representation of geometrical figures and symbols. 2D CAD drafting programs emerged next, but the real CAD, in context of geometrical modeling, was born in the 60s with the invention of 3D modeling software. The key advance in 3D CAD was indisputably the possibility to create complex 3D surfaces.

3D modeling software was primarily developed and used in automotive and aerospace industry. Major breakthroughs that facilitated the creation of flexible CAD models and user-friendly CAD systems were the inventions of solid, feature-based and parametric 3D modeling. Those ideas had an enormous influence on the growth of CAD software market and industry applications. This, to an extent, slowed down the adoption of new concepts that emerged later, such as direct modeling. It may be argued that, aside from engineers being used to well-known ideas, the new ones have still not been perfected to a level that would allow them to take over the market.

The new inventions in CAD are finding their specific places in a broader concept of CIM, PLM, digital manufacturing etc. The mentioned

paradigms are related to integration and digitalization of the whole product lifecycle, which increasingly relies on new technologies such as artificial intelligence (AI), generative design, cloud computing, real-time simulation, augmented reality (AR), virtual reality (VR) and more.

This paper aims to bring a brief history of CAD systems, based on the available literature and the extensive experience of the authors in application, customization and teaching of CAD systems.

2. BRIEF HISTORY OF CAD

Geometric modeling in CAD programs has evolved through a series of stages during which the geometric presentation of physical objects and/or design concepts have been improved. This brief history of CAD is mainly related to geometrical modeling and organized according to decades and key breakthroughs.

2.1 The beginnings of CAD

The first software with CAD-like features was in fact CAM software PRONTO, developed in 1957 by Patrick Hanratty. The expression “Computer-aided design” was coined by Douglass Ross, a computer scientist who greatly contributed to development of computer graphics and invented numerical control language APT. Nevertheless, the title “father of CAD” is usually attributed to Ivan Sutherland who in 1963, within his PhD thesis at MIT, developed Sketchpad (Figure 1). Computer graphics based on wire models was invented at MIT at the beginning of the 1960s, but Sketchpad was the first software that utilized interactive graphics for engineering design and drafting, introducing CRT monitor and light pen as peripheral devices that will later be extensively used by various software [1].

Figure 1. Sketchpad user interface [2][1]

2.2 Early CAD systems and CAD related inventions in the 1960s

1960s were the era of in-house CAD systems, as the computers capable of CAD were very expensive and voluminous. In 1963, one of the first industrial CAD systems "DAC - 1" (Design Augmented by Computers) was created (General Motors and IBM). The other notable systems were CADD by McDonnel-Douglas (1966), PDGS by Ford (1967) and CADAM by Lockheed (1967), which were all basically 2D drafting applications [3].

During the 1960s, a series of inventions took place that were very important for CAD. The most prominent ones in the hardware area were the tablet, as a cheaper and more ergonomic alternative to light pen, improved graphical displays, dedicated graphics hardware, low-cost terminals and microcomputers. In the software department, the techniques for hidden line display and shading of isometric displays were very important for later CAD software development. New advances were also present in data management and application programming, which were specific to CAD [1]. During this period, it became obvious that CAD systems would be the future of engineering design, as they were already bringing great savings in

[1] SketchpadDissertation-Fig1-2.tif by Ivan Sutherland is licensed under Creative Commons Attribution-Share Alike 3.0 Unported license.

design efficiency and comfort, especially concerning repetitive activities.

2.3 1970s: commercial CAD systems and the beginning of 3D modeling

The 1970s saw the creation of the first commercial CAD software. The pioneers of CAD industry, formed in 1969, were Applicon (producing AGS) and Computervision (creator of CADDS). Soon after them, Auto-trol Technology, Calma and M&S Computing (Intergraph) were formed. They all used microcomputers and storage tube displays, as opposed to existing in-house systems that worked on mainframe computers and graphics terminals, which was an important step for commercial use of CAD software. Nevertheless, the early commercial software was still 2D and the companies were predominantly proprietary hardware producers that created software to raise their hardware sales [1]. Important place in CAD history is reserved for the software called Automated Drafting and Machining (ADAM), developed by Patrick Hanratty. Designed to function on every machine, it is still a basis for a large percentage of existing CAD software [4].

The 1970s are perhaps most important for the birth of the capable 3D modeling software, and it is when the key developments in evolution of geometric modeling took place. The early CAD systems were the emulation of 2D drafting, and the transition to 3D started by representing 3D geometry via wireframe models – points connected by lines, which are very limited in representing solid geometry [5]. The development of surface modeling methods was initiated by aircraft and automotive industries, to reduce the time and cost of design and manufacturing of typically complex sheet metal parts. The surfaces used in these industries are typically defined by several cross-sections or control points.

France and USA were the major centers where the underlying mathematics for 3D curves and surfaces used in CAD was developed. The first scientist to develop a mathematical approach to defining surfaces characteristic for the automotive industry was Paul de Casteljau in 1958 [6]. He was employed at Citroën that, aiming at keeping the competitive advantage, did not allow publishing of his work until 1974. In the meantime, other scientists developed alternative, largely similar, techniques for surface definition. Probably the best known of them is Pierre Bézier who, working for Renault, developed the well-known Bézier curves and surfaces [6], which by 1972 were used in the factory within the UNISURF application for 3D modeling and milling. UNISURF later became an important part of CATIA software. If the work of de Casteljau were published earlier, some of the credits for developing the mentioned theory would officially be his. Also important is the role of Steven A. Coons, at the time working at MIT, who developed the mathematics describing generalized surface segments, called Coons patches [7]. The underlying idea of Coons patches served as the basis for some of the most important surface definitions commonly used in CAD, like B-spline surfaces, non-uniform rational B-spline (NURB) surfaces, and others [8].

2.4 The invention and adoption of solid modeling

Mechanical CAD, of course, would not be as powerful as it is now without solid modeling [5]. Solid models are the only geometric models that are “aware” of both their boundaries and their volume, thus they allow for arbitrary operations to be performed on them. Research on solid modeling started independently in the end of 1960s and in the beginning of 1970s, in a significant number of research groups. Probably the most important of these was The CAD Group in Cambridge. In 1973 those groups met for the first time at PROLAMAT conference in Prague and started the discussion on the topic. Both B-Rep and Constructive Solid Geometry (CSG) model representation technologies were presented by different researchers [1]. Nevertheless, the appearance of the first usable solid modeling software had to wait for the technology to mature and the

computers to get more powerful. This started to happen at the end of the 1970s and became reality in the late 1980s. The first commercial solid modeler is often considered to be MAGI's SynthaVision, launched in 1972.

The explosion in the creation and use of quality CAD software happened in the 1980s. The enabling technologies, both software and hardware, were mature enough to enable rapid expansion of CAD programs offering solid modeling. The new 32-bit minicomputers and color raster technology emerged in the beginning of the 1980s. Later in the decade engineering workstations appeared. This was a very important change for designers: the price of a CAD seat became lower and software performance more predictable, because the resources became dedicated to specific designers. From 1981 to 1983 three important software packages capable of solid modeling were released: UniSolids by Unigraphics, CATIA V1 by Dassault Systèmes (as CADAM add-on) and I-DEAS by SDRC. In 1986 Intergraph launched I/EMS, the first software that combined B-REP solids, only NURBS (Non-rational B-splines) based geometric entities and object-oriented database. Personal computers appeared in the 1980s but did not become powerful enough to support solid modeling before the next decade.

2.5 The revolution: introduction of parametric, feature-based and associative modeling

The revolution in CAD came in 1987 with the release of Pro/ENGINEER by Parametric Technology Corporation (PTC), the first commercially available parametric and associative solid modeler. It also perfected the feature-based approach to modeling (Figure 2). The brain behind the software was dr Samuel P. Geisberg, Russian emigrant born in St. Petersburg by vocation professor of mathematics. The ease of making and promoting design changes in Pro/ENGINEER very quickly fascinated potential users, and the product rapidly took off, creating large profits and managing to be launched in two updated versions each year. Other software vendors were very quickly pushed to try and embed the same technology into their software. This was not easy, as Pro/ENGINEER was built for the new functionality from the core and the other software was not. Nevertheless, as the early versions of Pro/ENGINEER were not so complete and capable in some areas like surface modeling, drafting or engineering analysis, PTC was not taking a lot of seats from main players like CATIA, UniSolids or I-DEAS. Rather, Pro/ENGINEER commonly replaced installations of CADDS from Computervision, and it often appeared as the first solid modeling software in companies working in traditional way or using 2D CAD software.

Figure 2. A parametric feature-based model of pneumatic tire created in Pro/ENGINEER [9]

In the beginning of 1990s CAD software was run on UNIX workstations and major CAD software vendors were IBM-Dassault Systèmes, EDS (Electronic data systems) - Unigraphics, Parametric Technology Corporation and SDRC [3]. Eventually, they all offered parametric, feature-based solid modeling capability in their CAD software, with various levels of success. In the beginning, the others were behind Pro/ENGINEER in parametric modeling and associativity, but over time they caught up and started to offer some new original functionality like variational modeling.

As much as parametric design is advantageous, it requires the model to be history-based, i.e. that after each change model

features are rebuilt in the order in which they were built. Therefore, each model feature becomes dependent on some of the others, which it references. This is called parent/child relationships, and the ordered set of features is called history tree (Figure 3). If some of the parent features are deleted or changed, the model may fail to regenerate or unexpected changes may occur leading, in extreme cases, to the need for the whole model to be rebuilt. This is why history-based models must be carefully planned before creation. Some CAD vendors, especially SDRC, stated that using their programs helps avoid such occurrences. SDRC based its software on so-called "variational design", by which the model needn't be always fully constrained (Figure 4).

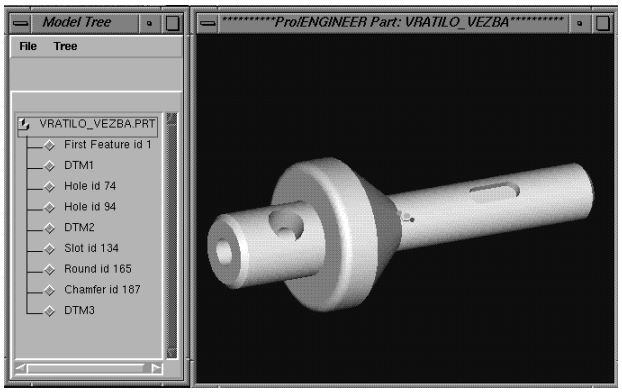

Figure 3. Solid model and history (model) tree in Pro/Engineer 20 (1999)

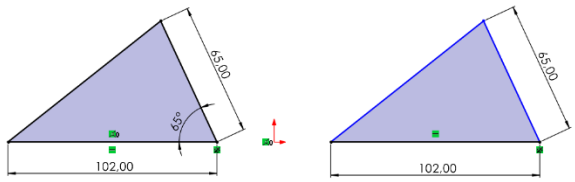

Figure 4. Fully and partially constrained sketches

2.6 Appearance of commercially available CAD kernels and mid-range CAD software

A geometry kernel provides the fundamental capabilities required to construct, modify, and evaluate both geometric entities and solid models. An important development took place at the end of the 1980s, when two solid stand-alone modeling kernels were released: ACIS by Three-Space Limited and Parasolid by Unigraphics. Together with later expansion of personal computers, this opened the door to so-called mid-range CAD solutions that appeared in the 1990s.

When, in the 1990s, both experienced companies and start-ups began offering mid-range solutions, these had the following characteristics: running only on MS Windows based PCs, using existing kernels and other component software technology, enabling design and leaving other functionality to be developed by third parties, and costing much less than high-end software. The trend started in the 1980s with AutoCAD by Autodesk, and at the time PCs were capable only of 2D CAD. After 32-bit Windows and Intel Pentium became available in 1994, solid modeling on PCs became feasible. Immediately after, in 1995, SolidWorks (Figure 5) became available and made a single most prominent appearance after Pro/ENGINEER. It generally offered only a part of Pro/ENGINEER's functionality, but it was created from the start as a native MS Windows application, with Windows-like user interface that in preceding years had become very popular with PC users. In the beginning, SolidWorks targeted new users of solid modeling software, transitioning from 2D CAD, and users of high-end CAD that did not need to pay for all the functionalities.

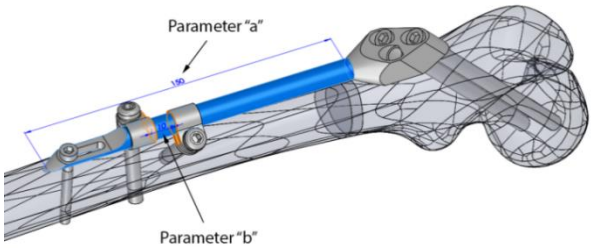

Figure 5. A model of orthopaedic fixator created in SolidWorks, with parameters used in structural optimization denoted [10]

Major software vendors, especially PTC, did not immediately see the great potential of mid-range solutions, treated them as low-end software and did not make a timely start in creating similar ones. Some have realized it earlier than others and tried to get on the train. Another mid-range software, very similar to SolidWorks, was created in 1996 by Intergraph and called Solid Edge. Autodesk entered this

market with Mechanical Desktop, which shortly became the mid-range solution sold in most copies. Although this software lacked the quality of SolidWorks and SolidEdge, it was probably the popularity and wide use of AutoCAD that pushed its sales. PTC tried to sale a stripped-down version of Pro/ENGINEER, a bit unfortunately called Pro/Junior, without much success. Whole situation ended with two big acquisitions in 1997, when Dassault Systèmes acquired SolidWorks and EDS-Unigraphics bought Solid Edge. In 1998, Dassault Systèmes released CATIA v5, which was naturally supported on Windows, and in 1999 Autodesk started shipping Inventor, which was based on ACIS kernel and a much better solution than Mechanical Desktop. Eventually, Dassault Systèmes acquired ACIS in 2000, which concluded a series of acquisitions that could only mean that the big players wanted to keep control on CAD market, by putting boundaries on mid-range software development and its target customers. To end the era of "big four" (Unigraphics, I-DEAS, CATIA and Pro/ENGEINEER) and the expansion of mid-range CAD, EDS (which became UGS) acquired SDRC in 2001. In subsequent years I-DEAS technology was built in EDS-Unigraphics, and it ceased to exist as an independent software solution. Since then, a list of major CAD software providers has not changed a lot, as any subsequent technological breakthroughs mainly resulted in the acquisition of smaller companies by big software vendors.

2.7 2000s: a calmer period, PDM and direct modeling

Most of the technologies that are still predominant in current CAD systems were established by the end of 1990s. In 2000s the focus shifted to making CAD software more user-friendly and to integrate it into PLM solutions with wider functionality.

The most important novelty related to geometrical modeling in CAD software was the reinvention of direct modeling. In 1992, Solid Designer by CoCreate introduced the concept of dynamic modeling by which no history tree was needed within a solid model, but the geometrical entities could directly be created and edited [11]. This was enabled by using solid modeling kernel ACIS by Spatial, which featured so-called "local operations". Nevertheless, direct modeling had to wait for quite a long time to become popular, i.e. until in 2007 a product called SpaceClaim was launched. The software offered direct modeling and editing of geometrical elements like surfaces and edges by moving, pulling, filling etc. (Figure 6).

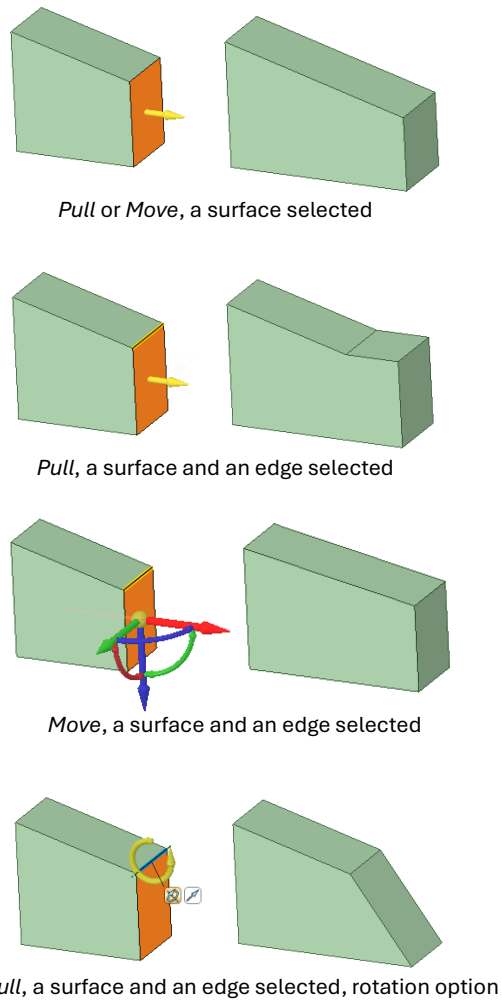

Figure 6. Results of application of pull and move operations in SpaceClaim, depending on geometry selection

SpaceClaim had practically the same functionality as Solid Designer, but the software was Windows-like, built from scratch and well marketed. It was also clearly stated that direct modeling was most useful in preparation of FEA models and CAM models. Moderate edits on existing models, especially if they do not contain model history records and/or were built

by someone else, were much easier using this technology. Bearing this in mind, it is no wonder that SpaceClaim was later acquired by FEA software vendor ANSYS and became its default solid modeler.

In the late 2000s, developers of feature-based CAD software were in a hurry to enable direct modeling in their products. In 2008, NX (ex-Unigraphics) and SolidEdge, both UGS products, started to offer a new tool named Synchronous Technology, while SolidWorks used Instant 3D technology. In the same year, direct modeling was included in CATIA V6, while in 2009 Autodesk started to offer Inventor Fusion Technology. Soon direct modeling became available in Pro/ENGINEER, who acquired CoCreate and built its direct modeling technology in its rebranded product Creo, namely in a specific version called Creo/Direct. As a result of direct modeling integration, some of the CAD solutions offered a new possibility, hybrid modeling, where direct editing operations are available in parallel to history-based modeling and often present in model tree as separate entries. Description and comparison of related technologies may, for example, be found in [12] or [13].

2.8 2010 – 2025: integration of the latest IT technologies into CAD systems, improved ease of use and teamwork

Arguably, there have not been any revolutionary discoveries in geometric modeling since 2010. Variational modeling is being further developed to better support history free CAD models, i.e. to try and establish efficient and robust geometry constraining methods in 3D, similar to the ones used in 2D sketching modules of CAD programs [13]. Considerable effort has been made to integrate the latest IT technologies into CAD systems, to make them more efficient, intuitive and user-friendly.

One of the current trends in CAD is the use of cloud-based systems, where computing resources — servers, storage, databases, networking, and software — are available on-demand over the Internet. For CAD, this brings advantages such as working anywhere from any device with internet connection; quick deployment – no installation and steep learning curve; fast access to new software features; easy tracking of changes; real-time collaborative editing; reuse of shared content; or data security and projects scalability [14]. The product that probably meets the previous criteria best and can be characterized as cloud native CAD is OnShape (Figure 7). It was launched in 2015 by the company of the same name, including two former SolidWorks CEOs, and then acquired in 2019 by PTC. One of the early promoters of cloud technology is also Autodesk's Fusion. According to our experience, it still functions better as a stand-alone application than as an in-browser CAD solution, but it strongly relies on could technology for wider functionality, such as data storage, collaboration or generative design. Autodesk Fusion is currently a common choice of smaller companies or individuals who require a solid set of design and manufacturing features for a moderate price.

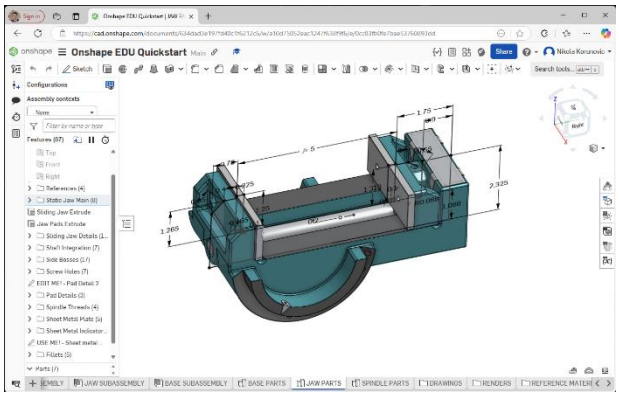

Figure 7. OnShape user interface, functional in arbitrary Web browser

Generative design is a process focused on exploring design possibilities. Generative design tools require the input of design objectives along with specifications such as performance or spatial needs, materials, manufacturing methods, and budget constraints. The software quickly produces design options by examining many variations of a solution. With each iteration, it assesses new concepts to identify successful and unsuccessful outcomes [15]. Based on continuous evaluation and design comparison,

iterative optimization is carried out until the recommended solutions are identified. In addition to topology optimization techniques, generative design uses optimization algorithms and AI. Enabling generative design in CAD software is currently an important priority for software vendors. Successful examples of generative design tools are Autodesk Fusion (Figure 8), PTC Creo, Siemens NX, Solid Edge or Dassault Systèmes CATIA.

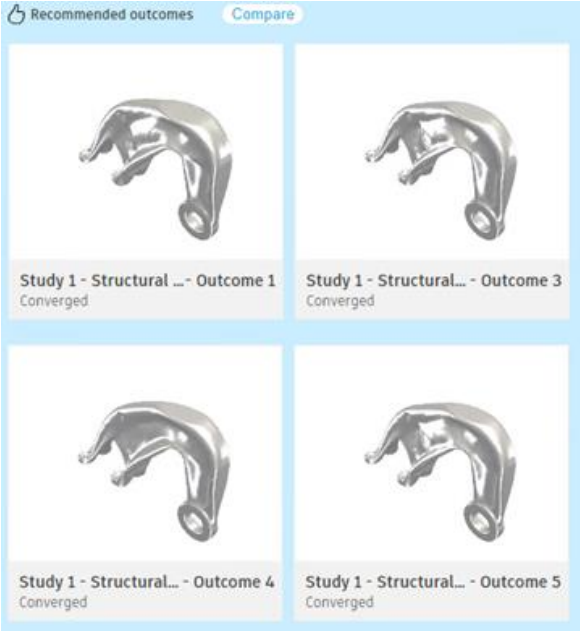

Figure 8. Outcomes of generative design study in Autodesk Fusion

Utilization of AI is currently a largest trend in software development, and it naturally finds its place in CAD. The application of AI in CAD is not a new idea. The potential of applying AI in intelligent design was recognized all the way back in 1965 by Mann [16] and later explored by many researchers and software vendors. The latest developments in AI have only accelerated its use and made it more common. One of the important applications of AI in CAD is within generative design. Current applications also include automated design generation, error detection and correction, personalized workflows, generation of CAD models from text prompts [17] or Building Information Modeling (BIM) [18].

Figure 9. Parametric CAD model created based on text prompt in Zoo Design Studio

For parametric CAD models, it is often advantageous for their sketches to be fully constrained—both dimensionally and geometrically. Such fully defined sketches make the resulting model more flexible and robust, permitting dimensional edits and error-free rebuilds. Zhou and Camba. [17] review multiple LLM (Large Language Models)-based systems that automate the generation of parametric sketches or complete partially drawn ones. All these systems accept text or vector sketch input, and some also process raster sketch images, substantially reducing the time required for sketch creation. Beyond 2D sketches, 3D CAD models can be produced from user text prompts (see Figure 9), hand-drawn sketches, point clouds, or a combination of these inputs.

According to Zhou and Camba, research in 2021–2022 was evenly divided between 2D

sketching and 3D modeling, but publications on 3D model generation have risen in 2023 and 2024, signaling a shift toward more intuitive parametric 3D modeling workflows.

Implicit modelling is an innovative technique for creating parametric 3D models (see Figure 10) in which a solid is described by a single mathematical function rather than by explicit topological elements (surfaces, curves, edges, etc.). In this method, the geometry of a body is captured as a signed distance field: points outside the boundary carry positive values, points inside carry negative values, and the surface itself is zero. This approach is particularly well suited to the complex shapes often required in additive manufacturing.

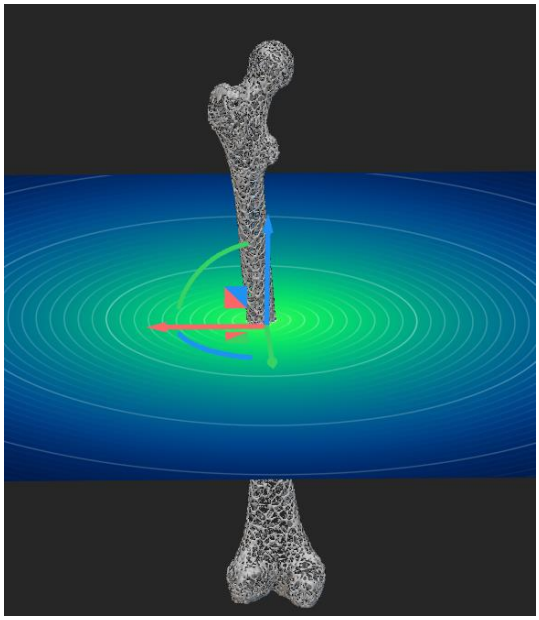

Figure 10. Implicit CAD model of bone made up of lattice structures with a field view in nTop

Real-time simulation is another useful tool that enables CAD modeling to be driven by mechanical behavior of a design. As the shape of the CAD model is changed by the designer, an optimized real-time FEA running in the background is updating the results on its deformation, stresses, strain or similar, helping get the right design early in the process. This is facilitated by the development of real-time simulation algorithms [19] as well as by increased performance of a typical CAD workstation.

Augmented reality (AR) and virtual reality (VR) devices enable a more realistic experience in CAD modeling, design exploration and presentation. That is why many vendors feature some of these technologies in their CAD software [20].

There are also a number of free and open-source CAD solutions available that have found their use among designers, usually for not so demanding modeling tasks. Examples include FreeCAD, based on a geometry kernel OpenCasCade, or Blender that is often used in modeling for rendering and animation.

3. ON INTEROPERABILITY AND UNIVERSAL FILE FORMATS

Each CAD program has its own native (natural, own) format, which precisely describes all geometric and non-geometric elements of the model. If the two programs do not use the same native format (which is often the case), data conversion must be performed.

Interoperability between different CAD software started in 1980 with the release of IGES (Initial Graphics Exchange Specification), vendor-neutral file format by U.S. National Bureau of Standards. It was initiated by United States Air Force (USAF) and based on Boeing data translation software. Other universal exchange programs that emerged over time, with the most prominent place belonging to STEP (STandard for the Exchange of Product model data).

There are currently two approaches to Product Data Exchange (PDX): geometric data exchange (GDE) and feature data exchange (FDE). In GDE the B-rep model is translated, from the native format of one to the native format of another CAD system. Feature data are lost, and the result is B-rep without features (dumb geometry). It is most often applied in practice. FDE - based on the model tree in one system, a model tree is created in another system, based on which the same geometry is created. It is not always possible and depends on the program version. Independent programs that are used for such translation tend to be expensive. One example of FDE translator is Proficiency by IT, which currently supports

mutual FDE between NX, SolidEdge, CATIA V5, SolidWorks, Creo and Inventor.

It may be argued that, during historical development of CAD software, vendors have most often chosen to disable FDE between their software and other software, excluding other programs of the same vendor. This was the way to bind customers to their solutions. Even now, this tends to be the case.

4. ON MODEL-BASED DEFINITION (MBD)

It was already mentioned that the possibility of automatic generation of 2D technical documentation or its complete avoidance was recognized very early, with the beginning of 3D modeling.

Today, there are two approaches to creating technical documentation based on 3D models: automated generation of technical documentation based on 3D models (technical drawings, components, expansion drawings...) and model-based definition (MBD) or digital product definition (DPD) (Figure 11) – use of 3D models and associated non-geometric data to define (specify) individual components or assemblies (without the need for technical drawings).

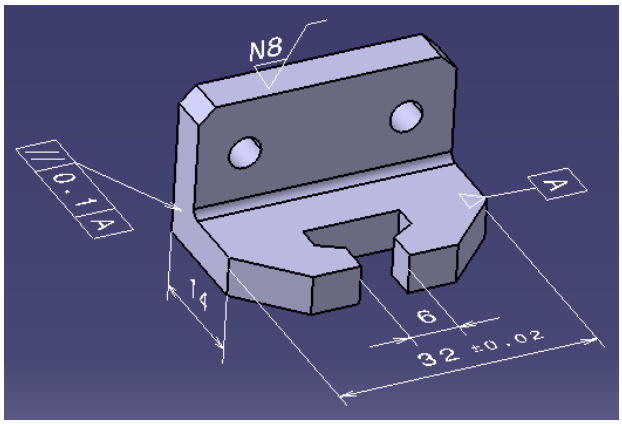

Figure 11. MBD in CATIA v5

5. CONCLUSION

A brief review of CAD development, from its beginnings to current state of the art, was given in previous chapters. It is too short to capture all the important events in history of CAD, but the effort of the authors was to capture the most important ones and name the key underlying technologies, giving at the same time their own views and sharing their own experience.

In our opinion, the key events in CAD development were:

1. Creation of sketchpad, the first software that utilized interactive graphics CRT monitor and light pen (1963)
2. Inventions of tablet improved graphical displays, dedicated graphics hardware, low-cost terminals and microcomputers (1960s)
3. Creation of techniques for hidden line display and shading (1960s)
4. Development of underlying mathematics for modeling curves and surfaces (late 1950s to late 1960s)
5. Appearance of commercial CAD software (1970s)
6. Birth of first 3D CAD software
7. Development of solid modeling (end of 1960s, 1970s)
8. Introduction of parametric, feature-based and associative modeling (1980s)
9. Appearance of geometric kernels as separate products (1980s)
10. Development of mid-range CAD solutions (1990s)
11. Introduction of direct modeling (1980s – 2000s)
12. Introduction of AI into CAD

In previous chapters it was also commented on how the developments in computer hardware influenced CAD software development. Today, new and fast evolving IT technologies like AI or cloud computing are having a great influence on CAD systems, leading to completely cloud-based CAD solutions, generative design enabled software, modeling in VR and others.

The competition between CAD software vendors has had both positive and negative influences on the development of CAD technology. On the one hand, the appearance of CAD-related inventions was very much accelerated by the appearance of smaller companies offering a lot of big system functionality for modest prices. On the other

hand, numerous acquisitions of smaller companies by big players were obviously achieved to take control of its fast-developing technology, slowing the overall improvement of CAD technology. David Weisberg wrote: "There is a phenomenon that takes place in the computer industry that is the reverse of the biological food chain. Except in this case, rather than the larger animals eating successively smaller animals the lower levels of the technology food chain absorb the capabilities of the higher levels. This phenomenon explains both the vast improvements we see in performance coupled with steadily reduced costs, particularly in regards to hardware" [1].

Following the fast and extensive evolution of CAD, we can only watch and hope for the next revolution.

ACKNOWLEDGEMENT

This research was financially supported by the Ministry of Science, Technological Development and Innovation of the Republic of Serbia (Contract No. 451-03-137/2025-03/200109)

REFERENCES

[1] Weisberg, D.E., History of CAD. History, 2022.
[2] Sutherland, I.E. Sketch pad a man-machine graphical communication system. in Proceedings of the SHARE design automation workshop. 1964.
[3] Tornincasa, S. and F. Di Monaco. The future and the evolution of CAD. in Proceedings of the 14th international research/expert conference: trends in the development of machinery and associated technology. 2010.
[4] Bi, Z. and X. Wang, Computer aided design and manufacturing. 2020: John Wiley & Sons.
[5] Stroud, I. and H. Nagy, Solid modelling and CAD systems: how to survive a CAD system. 2011: Springer Science & Business Media.
[6] Farin, G., Curves and surfaces for computer-aided geometric design: a practical guide. 2014: Elsevier.
[7] Coons, S.A., Surfaces for computer-aided design of space forms. 1967.
[8] Wikipedia_contributors. Steven Anson Coons. 2025 [cited 2025 22:09, March 11]; Available from: https://en.wikipedia.org/wiki/Steven_Anson_Coons.
[9] Trajanović, M., M. Stojković, and N. Korunović, Computer aided design of tires. Journal of Applied Engineering Science, 2005. 3(8): p. 19-32.
[10] Korunovic, N., et al., In silico optimization of femoral fixator position and configuration by parametric CAD model. Materials, 2019. 12(14): p. 2326.
[11] Fahlbusch, K.-P. and T.D. Roser, HP PE/SolidDesigner: dynamic modeling for three-dimensional computer-aided design. Hewlett-Packard Journal, 1995. 46(5): p. 6-13.
[12] Ushakov, D. Direct modeling–who and why needs it? A review of competitive technologies. in Isicad, Bricsys International Conference Moscow. 2011.
[13] Zou, Q. and H.-Y. Feng, Push-pull direct modeling of solid CAD models. Advances in Engineering Software, 2019. 127: p. 59-69.
[14] Aldayafleh, R., 8 Key Advantages of Cloud-Native CAD - Capital. 2024.
[15] Srivastava, J., Systematic Review of Difference Between Topology Optimization and Generative Design. IFAC-PapersOnLine, 2023. 56(2): p. 6561-6568.
[16] Mann, R., Coons,". Computer-Aided Design," McGraw-Hill Yearbook of Science and Technology McGraw-Hill Book Co., New York, 1965.
[17] Zhou, J. and J.D. Camba, The status, evolution, and future challenges of multimodal large language models (LLMs) in parametric CAD. Expert Systems with Applications, 2025: p. 127520.
[18] Sacks, R., et al. Automating design review with artificial intelligence and BIM: State of the art and research framework. in ASCE International Conference on Computing in Civil Engineering 2019. 2019. American Society of Civil Engineers Reston, VA.
[19] Marinkovic, D. and M. Zehn, Survey of Finite Element Method-Based Real-Time Simulations. Applied Sciences, 2019. 9(14): p. 2775.
[20] Hunde, B.R. and A.D. Woldeyohannes, Future prospects of computer-aided design (CAD)–A review from the perspective of artificial intelligence (AI), extended reality, and 3D printing. Results in Engineering, 2022. 14(100478): p. 1.

Society of Production Engineering

ICPES 2025

40. INTERNATIONAL CONFERENCE ON PRODUCTION ENGINEERING - SERBIA 2025

DOI: 10.46793/ICPES25.344S

University of Nis Faculty of Mechanical Engineering

Nis, Serbia, 18 - 19. September 2025

VIRTUAL REALITY ENVIRONMENT FOR TEACHING ASSEMBLY SEQUENCE ANALYSIS TO PRODUCTION ENGINEERING STUDENTS

Živojin SUVAJAC[1, *], Lazar MATIJAŠEVIĆ[1], Dušan NEDELJKOVIĆ[1], Živana JAKOVLJEVIĆ[1]

Orcid: 0009-0006-1667-2647; **Orcid:** 0000-0001-9153-0303; **Orcid:** 0000-0001-5909-4812; **Orcid:** 0000-0002-7878-2909;

[1]University of Belgrade – Faculty of Mechanical Engineering, Belgrade, Serbia

*Corresponding author: zsuvajac@mas.bg.ac.rs

Abstract: *Assembly sequence analysis represents the first step in assembly process design and plays a very important role in achieving optimal production time and cost, which is of great importance in large-scale and mass production. There are several different approaches to address this issue. As a rule, they start from the analysis of product components and their mutual liaisons (contacts, i.e., mates or joints), followed by generation of all feasible assembly sequences and, finally, selection of the optimal sequence according to appropriate criteria. However, mastering these tasks can be challenging for students who encounter them for the first time, and particularly when physical interaction with the product is limited. To facilitate and enhance students' understanding of these methods by making the learning process more intuitive and easier, while also assisting educators in effective teaching, the Virtual Reality (VR) technology can be used. This paper presents a VR-based learning workflow for teaching methods for assembly sequence analysis to production engineering students. The workflow contains predefined tasks that students follow in VR to achieve the intended learning outcomes without the need for significant manual effort. For this workflow several VR environments are developed. In addition to these environments, the paper presents the analysis of the students' experiences in their utilization.*

Keywords: *Assembly sequence analysis, Cut-set method, Bourjault method, VR technology, Production engineers' education*

1. INTRODUCTION

The assembly process represents the final and one of the most critical stages in manufacturing, during which individual components are joined to form a functional product. In addition to its direct influence on product performance and quality, assembly has a major impact on the overall efficiency and cost-effectiveness of production. In traditional industrial manufacturing, assembly-related activities account for approximately 20–30% of total production costs and between 40–60% of total production time [1]. These figures highlight the importance of assembly process

design, which becomes especially critical in large-scale and mass production.

The first step in assembly process design is assembly sequence analysis, which aims to determine the order in which parts should be assembled to form the final product. This analysis has three different approaches: finding all feasible sequences, finding all linear feasible sequences, and finding one feasible or one linear feasible sequence [2]. The first approach is the most complex, but it offers the greatest potential for the assembly process optimization. One of the first algorithms for generating all feasible assembly sequences was proposed by Bourjault [3]. Another notable approach in this field is the Cut-set method, introduced by Homem de Mello and Sanderson [4]. Despite being introduced many years ago, both methods are still actively used and studied, with ongoing research focused on enhancing their performance and integrating them into automated software tools. The Cut-set method has recently been applied in various contexts, including the generation of optimal disassembly sequences for End-of-Life products [5], the decomposition of complex assembly tasks in collaborative environments [6], and the identification of subassemblies within assembly planning [7]. Additionally, the core principles of the Bourjault method have inspired structured, question-based approaches aimed at analyzing disassembly paths and precedence relationships between components [8].

Considering their significance in defining assembly process steps and optimizing production performance, it is of great importance that future mechanical/production engineers acquire a deep understanding of these methods. Consequently, Bourjault and Cut-set methods are integrated into the curriculum of the Assembly Technology course at the Faculty of Mechanical Engineering, University of Belgrade. Due to their complexity, teaching these methods to production engineering students using traditional approaches brings about significant challenges primarily related to students' understanding of their principles. As a potential solution, we have developed a Virtual Reality (VR) based workflow to make these methods, as well as the whole assembly sequence analysis more accessible to students. The VR-based workflow and the initial results of its implementation are presented in this paper.

The remainder of the paper is structured as follows. In Section 2 we briefly introduce the methods used for assembly sequence analysis including Cut-set and Bourjault methods. Section 3 is related to the learning objectives and intended learning outcomes of the proposed workflow, whereas the workflow itself is presented in Section 4. Section 5 refers to students' experiences regarding the workflow utilization. Finally, Section 6 presents the conclusions of the paper.

2. ASSEMBLY SEQUENCE ANALYSIS METHODS DESCRIPTION

The starting point in assembly sequence analysis is the generation of Liaison Diagram. This diagram provides information about components of the product and shows the relations between them in a form of graph. In this graph, nodes represent the components of the product, while the liaisons (contacts, i.e., mates or joints) are shown as links labeled with numbers [2]. A Liaison Diagram for a simple exemplary product is shown in Fig. 1.

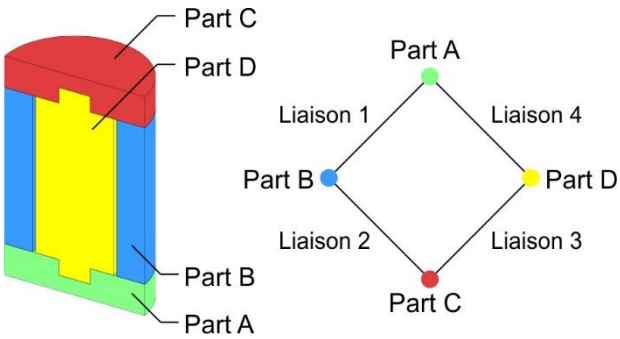

Figure 1. Simple product Liaison Diagram

There are certain assumptions on which the construction of the Liaison Diagram is based [9]:

1. Parts are rigid,
2. The liaison can be formed once and only once, and the relative position and orientation of the parts in the

(sub-)assembly cannot be changed once the assembly operation is finished.

The Liaison Diagram represents a starting point for the generation of all feasible sequences of product assembly. The following step is either Cut-set method or Bourjault method using which precedence questions are asked and answered in predefined manner to get the precedence relations which define the order in which parts must be assembled. Both methods (Cut-set and Bourjault) have the same objective and similar outputs and can be used according to the designer's preferences.

2.1 Cut-set method

Cut-set method assumes that disassembly sequences are the inverse of the possible assembly sequences. Therefore, the method evaluates whether each possible subassembly can be disassembled from the main assembly or another subassembly. During the evaluation the following precedence question is asked [9]:

From an assembled state, can subassembly S_j be disassembled from subassembly S_i?

It is important to note that a subassembly can consist of a single part [9]. There are three possible answers:

1. **Not applicable (N/A)** – the parts within set S_i or S_j do not form a connected subgraph, i.e., they are not physically connected.
2. **Yes** – The subassembly S_j can be physically disassembled from subassembly S_i. For example, based on Fig. 1, the subassembly S_j=(Part C, Part D) can be disassembled from the subassembly S_i=(Part A, Part B).
3. **No** – The subassembly S_j cannot be physically disassembled from subassembly S_i. For example, from Fig. 1, the subassembly S_j=(Part D) cannot be disassembled from the subassembly S_i=(Part A, Part B, Part C).

If the answer to the precedence question is **No**, the subassembly set S_i is recursively broken down by reassigning each of its components to a new subassembly S_j, while the remaining components form the new S_i. The precedence question is then repeated for each of these new combinations.

2.2 Bourjault method

Bourjault method determines the possibility of establishing each liaison at a given stage of assembly. The precedence question posed by this method is:

Can liaison i be established if liaisons from set B have previously been established?

This question is referred to as R-question and can be written in the form R(*i*; *B*). Similar to the Cut-set method, there are three possible answers to the question above [9]:

1. **Not applicable (N/A)** – The liaison *i* is automatically established by establishing liaisons from set *B*. For example, the answer to the question R(1; 2, 3, 4) for the assembly in Fig. 1 is **N/A** because liaison *i*=1 is automatically established by establishing liaisons from set *B*=(2, 3, 4).
2. **Yes** – The liaison *i* can be established even though the liaisons from set *B* have already been established. For example, for the assembly in Fig. 1, the answer to the question R(1; 2, 3) is **Yes** because the liaison *i*=1 can be established even though the liaisons from set *B*=(2, 3) have already been established.
3. **No** – The liaison *i* cannot be established if the liaisons from set *B* have already been established. For example, for the assembly in Fig. 1, the answer to the question R(1; 3, 4) is **No** because the liaison *i*=1 cannot be established if the liaisons from set *B*=(3, 4) have already been established.

If the answer to the R-question is N/A or No, the procedure continues by removing the liaisons from set *B* one by one and repeating the question. On the other hand, if the answer is Yes the procedure is stopped for the given liaison set *B*.

2.3 Precedence relations

The outputs of both methods (Cut-set and Bourjault), obtained by addressing the precedence question, are precedence relations. These relations define the order in which subassemblies should be assembled. They are derived from precedence questions for which the answer is **No** and can be expressed in the following form:

$$R(A;B) = NO \rightarrow A \geq B \quad (1)$$

where $A \geq B$ indicates that all liaisons from set A must be made before liaisons from set B [2].

2.4 Liaison Sequence Diagram

The Liaison Sequence Diagram provides a graphical representation of all feasible assembly sequences based on the precedence relations obtained from the Bourjault or Cut-set method. It represents a state diagram, where assembly states are depicted as tables and transitions between these states are illustrated with connecting lines. The number of cells in each table corresponds to the number of liaisons within the assembly. Empty cells indicate liaisons that have not yet been established, whereas filled denote liaisons that have already been completed [9]. Paths through this diagram, staring from the state in which all fields are empty (no liaison made) to the final state in which all fields are filled (all liaisons made) represent different assembly sequences. An example of Liaison Sequence Diagram is shown in Fig. 2.

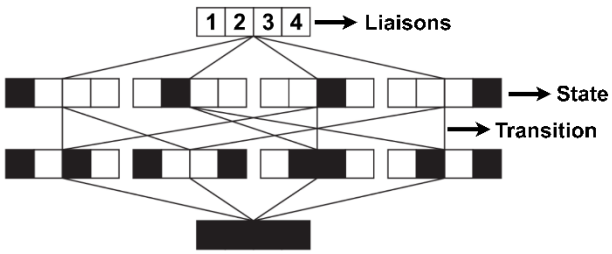

Figure 2. Simple product Liaison Sequence Diagram

When all feasible assembly sequences are generated and represented using the Liaison Sequence Diagram, following the predefined rules primarily related to Design-for-Assembly [10], the designer selects the most suitable assembly sequence to be implemented in assembly process. Learning workflow that will be presented in this paper intends to facilitate students' mastering and understanding of the described methods.

3. LEARNING OBJECTIVES AND OUTCOMES

The objectives of the VR-based learning workflow presented in this paper are to support the development of different types of knowledge, including factual knowledge – **F** (different approaches to assembly sequence design, key terminology, definitions and rules related to the Liaison Diagram, the Cut-set and Bourjault method, and the Liaison Sequence Diagram);

Table 1. ILOs with associated knowledge type (KT)

KT	ILO description
F	Capability to choose suitable technique for assembly sequence design – I1
F, P	Understanding the liaisons (mates and joints) between parts in the product – I2
F, P	Understanding physical constraints and relations between parts and subassemblies within product – I3
C	Understanding the influence of product design on assembly process – I4
C, P	Capability to define precedence of assembly operations within the process – I5
F, P	Capability to define all feasible assembly sequences for the selected product – I6
F, C	Capability to choose the most suitable assembly sequence – I7
P, M	Capability to apply VR tools to interact with virtual products and to extract useful information from a product by exploring it in virtual environment – I8
M	Capability to self-evaluate their own learning achievements – I9

conceptual knowledge – **C** (understanding the relations among key elements in the assembly sequence design, as well as the influence of the assembly sequence on the overall assembly process); procedural knowledge – **P** (understanding how to carry out certain tasks and procedures of assembly sequence design and to implement the corresponding methods); metacognitive knowledge – **M** (applying VR tools for solving assembly sequence design problem, as well as evaluating one's own

understanding of the methods and validating the results through virtual experimentation).

Each type of outlined knowledge helps students achieve specific Intended Learning Outcomes (ILOs) that are listed in Table 1. These ILOs define the expected results of the learning process in terms of students' performance.

4. WORKFLOW DESCRIPTION

The developed workflow for teaching and learning the assembly sequence analysis in VR environment consists of eight learning activities – tasks (T), as shown in Fig. 3.

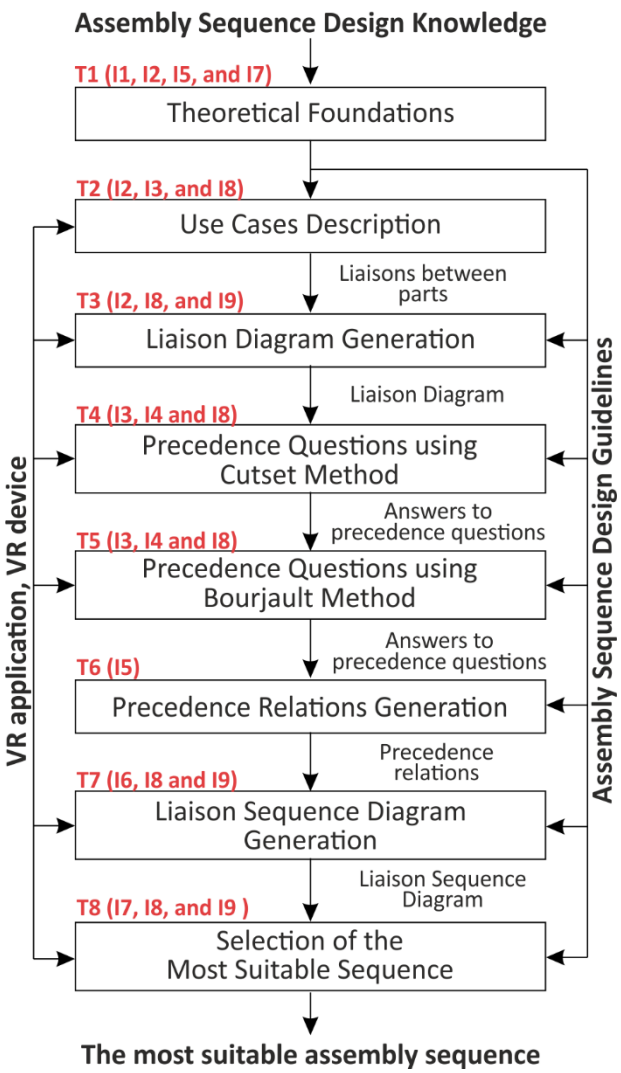

Figure 3. Learning activities within workflow

These tasks are designed to help students gain the intended knowledge and to achieve the ILOs – the ILOs achieved using certain task are presented in Fig. 3 in parentheses.

The development involved Unity3D v6000.0.3f1 as the main platform, SolidWorks for 3D modeling, and Oculus Rift S for immersive interaction. To prevent the collision between parts and to provide students with close to real-world experience and interaction between parts during assembling/ disassembling in VR, all parts within the model contain colliders. Since most of the parts in the selected use case are concave and some of them have complex form, creation of colliders was not a straightforward task. Unity's standard tools were not suitable for collider generation, and the open-source CoACD.unity library was used to create accurate mesh colliders and enable realistic physical interaction in VR. The details regarding this library can be found in [11].

For the workflow, we selected a step motor as the use case, providing a practical example of how the methods can be implemented in a realistic assembly scenario. The step motor is reduced to six parts/subassemblies labeled A–F, as shown in Fig. 4.

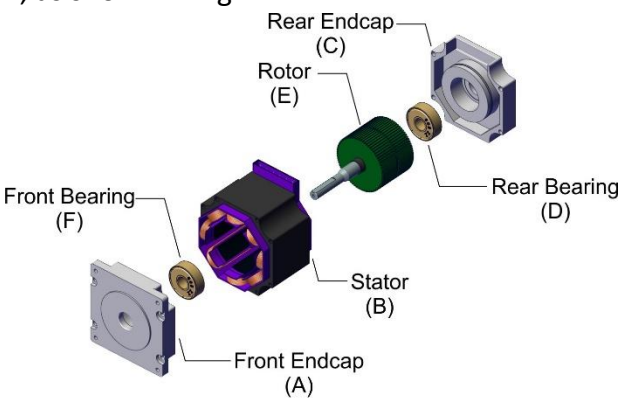

Figure 4. Exploded view of the step motor

Within T1 students are, in a traditional teaching manner, introduced to the fundamentals of assembly sequence design, including the advantages and shortcomings of identifying all feasible assembly sequences for designing assembly systems. This task focuses on mastering the theoretical concepts outlined in Section 2 and achieving I1, while simultaneously contributing to I2, I5, and I7.

In T2 students interact with a step motor assembly in a VR environment (Fig. 5). Through

this process, they explore the structure of the product and gain better insight into the physical relations between its parts. Also, students are provided with a technical drawing and a 3D exploded view of the step motor. Within this task, students obtain elements of I2, I3, and I8.

Based on the VR experience from T2, the technical drawing, the 3D exploded view, and cutaway VR model of the step motor that can be assembled and disassembled, students are expected to generate a Liaison Diagram. In VR environment, they construct the diagram by placing links on a virtual canvas, as shown in Fig. 6. After completing their Liaison Diagram, students have the option in VR to view the correct version of Liaison Diagram and compare it with their own. If students notice any discrepancies between their Liaison Diagram and the correct one, they can further explore the product to identify the cause of their mistake. This task contributes to ILOs I8 and I9, whereas I2 is fully achieved within T3.

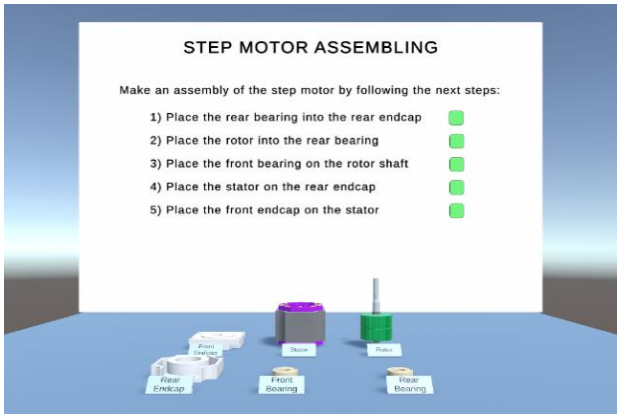

Figure 5. Interaction with the product in VR

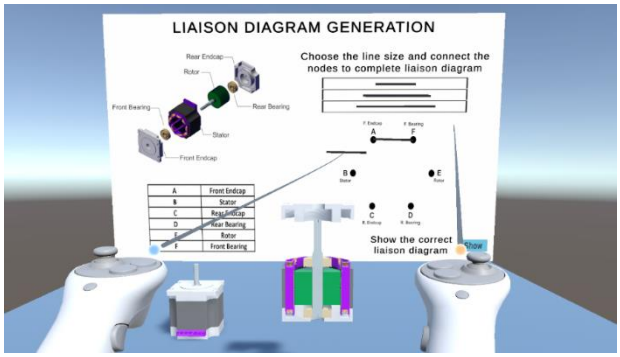

Figure 6. Liaison Diagram generation

In T4 students use the VR application to ask and answer precedence questions by applying the Cut-set method. The VR scene created for this task is shown in Fig. 7. The procedure for asking and answering precedence questions begins with defining the subassemblies S_i and S_j, which are generated using checkboxes on the central canvas (Fig. 8). Simultaneously, the nodes in the Liaison Diagram and the parts in the virtual product model that belong to subassembly S_j are automatically highlighted in red to visually distinguish between subassemblies S_i and S_j (Fig. 9).

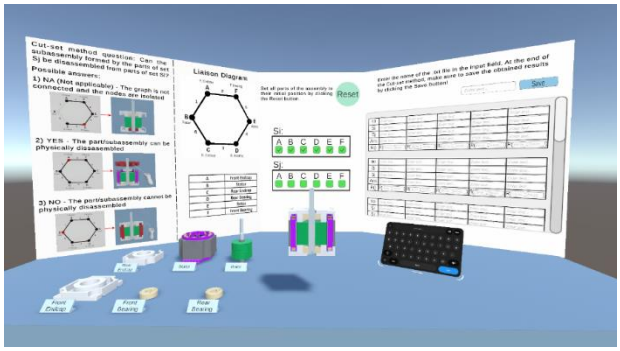

Figure 7. VR scene for Cut-set method

Figure 8. Checkboxes for generating subassemblies

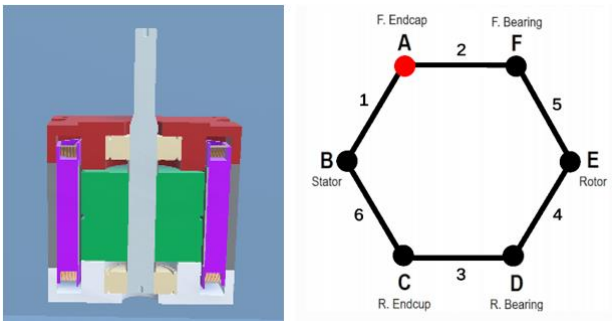

Figure 9. Automated highlighting of part and node

In the next step, students attempt to disassemble subassembly S_j from subassembly S_i on the virtual model of the product, to determine the answer to the precedence question defined by the Cut-set method (Fig. 10). The answers to the questions are entered into the table on the right canvas (Fig. 7) using a virtual keyboard and then stored in a .txt file. T4 contributes to I3, I4, and I8.

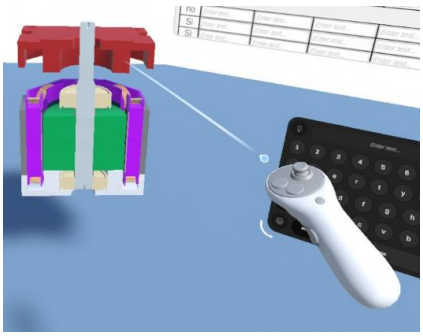

Figure 10. Disassembly trial

Task T5 refers to Bourjault method, and also contributes to I3, I4 and I8. In this task, students again use the VR application to ask and answer precedence questions, but this time by applying the Bourjault method. The VR scene related to this task is shown in Fig. 11.

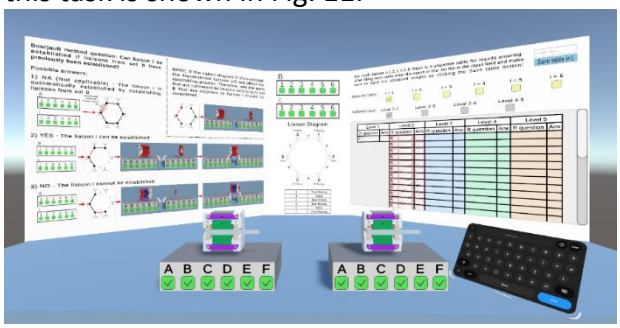

Figure 11. VR scene for Bourjault method

The procedure for asking and answering precedence questions begins with defining set *B* and liaison *i* from the R-question using checkboxes on the central canvas. This selection automatically generates corresponding Liaison Diagram in which liaisons that are not within set *B* are removed, and the liaison *i* is marked red; this is also displayed on the same canvas (Fig. 12).

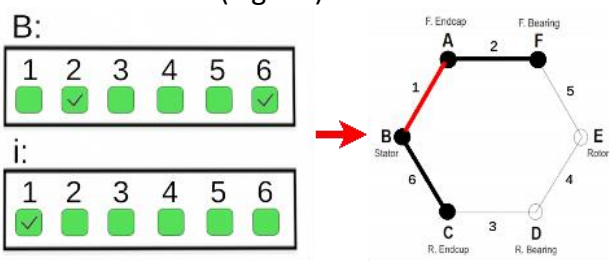

Figure 12. Checkboxes for defining set *B* and liaison *i* and corresponding Liaison Diagram

In front of the canvas, there are two instances of the step motor assembly. Each part of these assemblies can be activated or deactivated using the checkboxes located below them. Based on automatically generated Liaison Diagram, students activate/deactivate relevant parts and try to assemble these subassemblies (Fig. 13). Through this process, they derive the answer to the corresponding R-question. The parts between which the liaison *i* is established are highlighted in red.

Similarly to the Cut-set method, students enter their answers into a table on the right canvas (Fig. 11) using a virtual keyboard. Afterwards, these answers are saved in a .txt file for later assessment.

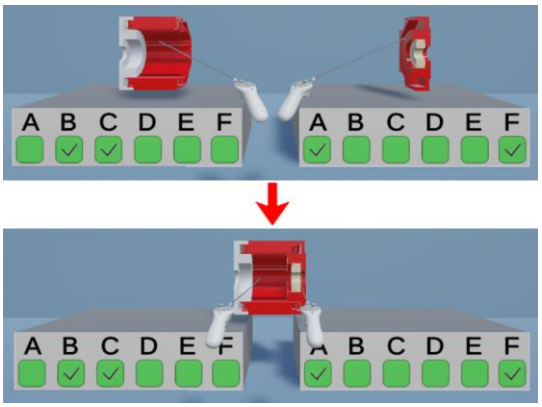

Figure 13. Assembly trial

To generate precedence relations in T6 students analyze the answers to the precedence questions obtained in tasks T4 and T5. These relations are generated separately for each method (Cut-set and Bourjault) and subsequently compared. In case of any differences between two sets of precedence relations, students should return to tasks T4 and T5 and try to discover their cause. During this task, students achieve I5.

Based on the precedence relations generated in task T6, within T7 students construct the Liaison Sequence Diagram for the step motor. After that, they immerse themselves in the VR environment to compare their diagram with a predefined reference version (Fig. 14). If they find differences between the diagrams, students should further explore the product, review its parts and connections, and try to understand where the error came from. In T7 students achieve I6, and this task contributes to I8 and I9.

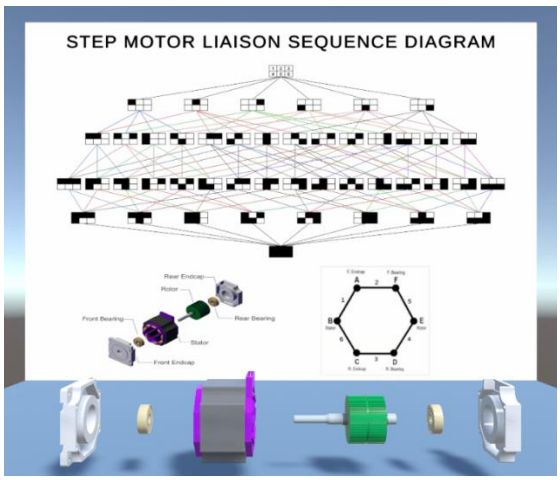

Figure 14. VR scene for Liaison Sequence Diagram analysis

As a final step, in T8 students test various selected assembly sequences in the VR environment shown in Fig. 14, and based on specific criteria (e.g., stability of subassemblies, the need for complex equipment, potential part damage) along with their own engineering reasoning, they select the most suitable assembly sequence. This is the final task in which I7, I8, and I9 are achieved.

5. STUDENTS EXPERIENCE

Despite the clearly defined rules of the methods used for assembly sequence analysis, and particularly for Cut-set and Bourjault methods, understanding their practical application can be challenging for students when a traditional teaching approach is used. This challenge becomes even greater if students do not have access to a physical model of the product, making the assembly sequence design more abstract and less intuitive. In some cases, even though a physical model of a product is available, certain factors including tight fits, size and weight of the product parts can complicate the product analysis and assembly/disassembly process. To address these challenges, the presented VR workflow offers meaningful support for learning and teaching the complex process of generating all feasible assembly sequences for a given product. The workflow enables students to better understand the subject matter and contributes to the learning outcomes through several interactive elements, such as:

1. Interaction with the product,
2. Easier engagement and improved understanding of the considered methods,
3. Easier Self-Evaluation.

Using the presented VR environment students interact with a 3D model of the step motor, freely assembling and disassembling it. The use of VR helps overcome some of the practical difficulties associated with real-world assembly that hinder students' concentration on mastering the assembly sequence design analysis techniques and direct their attention to alternative problems. These difficulties are related to applying relatively high forces due to tight fits (e.g., when mounting bearing) and the influence of the rotor's magnetic field when assembling other ferromagnetic parts. The seamless interaction with the product parts is very important for all steps in the process including generating the Liaison Diagram, asking and answering precedence questions, analysis of all feasible assembly sequences and selecting the most suitable one.

Specially designed VR scenes include features that simplify the learning process leading to easier engagement and improved understanding. These include the automatic generation of the Liaison Diagram using checkboxes for selecting either parts (Cut-set method) or liaisons (Bourjault method), red highlighting of parts creating liaison (Bourjault method) or the parts to be disassembled (Cut-set method), and structured tables for entering and reviewing precedence questions and answers for both methods.

The development of critical and self-critical thinking is one of the key objectives in engineering education. The presented workflow supports this process through student self-evaluation, particularly during the generation of the Liaison Diagram and the Liaison Sequence Diagram.

Students of the course in Assembly Technology at the University of Belgrade – Faculty of Mechanical Engineering had the opportunity to use the presented learning workflow within co-design lab in Erasmus+ XREN project ("Extended reality tools to

support learning activities in engineering"). Six students participated in the co-design lab.

Table 2. Excerpt of the results of students' survey (Avg – average grade on Likert scale, STD – Standard Deviation on Likert scale)

No	Question	Avg	STD
1.	Co-design lab helped me deepen my knowledge in the field	4.5	0.548
2.	Due to the co-design lab, I will remember more of what I have learned	4.33	0.816
3.	Co-design lab significantly improved my understanding of the subject content	4.33	0.516
4.	Co-design lab motivated me and made me commit myself more to the subject	4.17	0.983
5.	Co-design lab helped me figure out what is the most important in the subject	4.5	0.5483
6.	As a learning experience, the co-design lab was more productive than listening to a lecture	4.67	0.516
7.	As a learning experience, the co-design lab was more enjoyable than listening to a lecture	4	1.095
8.	The co-design lab should not be assigned to future classes	1.67 **(R)**	0.816
9.	The learning experience provided by the co-design lab was not worth the effort	1.5 **(R)**	0.837
10.	The co-design lab gave me stronger motivation to work hard at learning than listening to lectures does	4	0.894

Their experience has been surveyed, and positive results have been found. The questionnaire contained a total of 26 questions that were answered using a 5-point Likert scale:

1 - Strongly Disagree,
2 - Disagree,
3 - Neutral,
4 - Agree,
5 - Strongly Agree.

An excerpt of the results that refers to students' experience with new learning approach is presented in Table 2, in which questions 8 and 9 are reversed (control questions) - R. From this survey, it can be observed that this approach helped students to better understand the subject content and get better insight into its essence. Furthermore, students evaluated this approach as more productive and enjoyable than listening to a classical lecture. Overall satisfaction of students can be qualified as very positive. They also have an affirmative attitude regarding the inclusion of the developed approaches to future classes.

6. CONCLUSION

In this paper, we presented a VR-based workflow that provides an interactive and technologically enhanced approach to teaching and learning complex assembly sequence design methods. The integration of VR technology enables students to engage directly with virtual models, allowing them to explore product structure and gain a deeper understanding of the liaisons between product parts, precedence relations, and feasible assembly sequences. Moreover, the use of this technology facilitates the teaching and learning of procedures for implementation of complex Bourjault and Cut-set methods, particularly in situations where the physical product is not available to students and abstract reasoning becomes a barrier to understanding.

The opportunity for hands-on interaction in a virtual environment, combined with the encouragement of critical and self-critical thinking, makes this workflow a valuable support tool in engineering education. It also plays an important role in achieving the intended learning outcomes. The results of the students' survey show that they are highly satisfied with the learning outcomes obtained and that they prefer this way of teaching to classical lectures.

ACKNOWLEDGEMENT

This research was supported by the Ministry of Science, Technological Development and Innovations of the Serbian Government under the contract No. 451-03-137/2025-03/200105, by Erasmus+ Programme under the action of cooperation partnerships in school education (KA220HED), project "Extended reality tools to support learning activities in engineering" (XREN), as well as by the Science Fund of the Republic of Serbia, Grant No. 17801, Cybersecurity of Motion Control Systems in Industry 4.0 - MCSecurity.

REFERENCES

[1] M.V.A.R. Bahubalendruni, B.B. Biswal: A review on assembly sequence generation and its automation, Proceedings of the Institution of Mechanical Engineers, Part C: Journal of Mechanical Engineering Science, Vol. 230, No. 5, pp. 824-838, 2015.

[2] D.E. Whitney: *Mechanical Assemblies: Their Design, Manufacture, and Role in Production Development*, Oxford University Press, New York, 2004.

[3] A. Bourjault: *Contribution à une approche méthodologique de l'assemblage automatisé: élaboration automatique des séquences opératoires*, PhD thesis, Université de Franche-Comté, Besançon, France, 1984.

[4] H. De Mello, A.C. Sanderson: Automatic generation of mechanical assembly sequences, Carnegie Mellon University, Pittsburgh, Pennsylvania, 1988.

[5] B.M. Gunji, S.K. Pabba, I.R.S. Rajaram, P.S. Sorakayala, A. Dubey, B.B.V.L. Deepak, B.B. Biswal, M.V.A.R. Bahubalendruni: Optimal disassembly sequence generation and disposal of parts using stability graph cut-set method for End of Life product, Sadhana, Vol. 46, No. 21, pp. 1-15, 2021.

[6] H. Wang: Assembly Sequence Planning Algorithm in Collaborative Environment Based on Web, in: *Proceedings of the 11th International Conference on Computer Engineering and Networks*, 21-25.10.2021, Hechi, China, pp. 1266-1275.

[7] A.K. Gulivindala, M.V.A.R. Bahubalendruni, A.K. Inkulu, S.S.V.P. Varupala, K. Sankaranarayanasamy: A modified cut-set method for mechanical subassembly identification, Assembly Automation, Vol. 41, No. 6, pp. 659-680, 2021.

[8] F. De Fazio, C. Bakker, B. Flipsen, R. Balkenende: The Disassembly Map: A new Method to enhance design for product repairability, Journal of Cleaner Production, Vol.320, Art. no. 128552, 2021.

[9] D.F. Baldwin: Algorithmic methods and software tools for the generation of mechanical assembly sequences, MSc thesis, Massachusetts Institute of Technology, Cambridge, Massachusetts, 1990.

[10] G. Boothroyd, P. Dewhurst, W.A. Knight: *Product Design for Manufacture and Assembly*, CRC Press, Boca Raton, 2010.

[11] X. Wei, M. Liu, Z. Ling, H. Su: Approximate convex decomposition for 3D meshes with collision-aware concavity and tree search, ACM Transactions on Graphics (TOG), Vol. 41, No. 42, pp. 1-18, 2022.

Session 8:

Additive manufacturing technologies

Society of Production Engineering

ICPES 2025

40th INTERNATIONAL CONFERENCE ON PRODUCTION ENGINEERING - SERBIA 2025

DOI: 10.46793/ICPES25.355L

University of Nis Faculty of Mechanical Engineering

Nis, Serbia, 18 - 19th September 2025

OPTIMIZATION OF THE DELTA 3D PRINTER STRUCTURE

Natalija LAZAREVIĆ[1], Aleksandar LAZIĆ[1], Mihajlo POPOVIĆ[1]*, Miloš PJEVIĆ[1]

Orcid: 0000-0003-3607-9243; **Orcid:** 0000-0002-4454-8663

[1]Univ. of Belgrade, Faculty of Mechanical Engineering, Serbia

*Corresponding author: mpopovic@mas.bg.ac.rs

Abstract: *In recent years, additive manufacturing technologies have made significant progress in terms of structural solutions, printing parameters, materials, and software support. This paper presents the process of reconstructing and optimizing a damaged and non-functional Delta 3D printer, with the goal of making it suitable for use in an educational setting. A Delta 3D printer is a type of additive manufacturing system distinguished by its unique kinematic structure, where three vertical arms are arranged in a triangular base configuration and simultaneously control the printhead's position. This design enables high-speed operation, precise movement, and fabrication of models with significant height. This configuration is particularly advantageous in educational environments, as it illustrates the diversity of 3D printer mechanisms and underlying engineering principles. Using reverse engineering methods and modern additive manufacturing technologies – FFF (Fused Filament Fabrication) and SLA (Stereolithography), damaged and worn-out components were replaced and certain technical improvements were implemented. The reconstruction involved replacing key components and improving the printer's functionality and ease of use, making it more suitable for educational purposes. After the reconstruction, the device was successfully tested and is now capable of reliably producing functional models. The printer is operated using Marlin firmware and the Arduino.*

Keywords: *Delta 3D printer, Parallel Kinematic Mechanism, Additive technology, Reverse Engineering, Optimization*

1. INTRODUCTION

In recent years, additive manufacturing technologies have undergone significant advancements in design, materials, and printing parameters. Modern industry demands encourage the development of more efficient and precise 3D printers. Delta printers stand out among the available configurations, offering significantly high speeds, better surface quality, and greater build heights compared to conventional Cartesian printers. Due to these advantages and their unique geometry, delta printers are becoming increasingly interesting to development teams and researchers.

The goal of this project was to restore and upgrade a non-functional Delta 3D printer for the use in higher education facilities**.** The work was carried out primarily for educational purposes, aiming to provide students with hands-on experience in different configurations of additive manufacturing processes through laboratory exercises. The optimized printer now serves as a functional teaching tool within a course focused on 3D printing technologies.

Marlin firmware and *Arduino IDE* development environment were used to control the printer

According to the ASTM F2792-12a standard, there are seven categories of additive manufacturing processes. The printer discussed in this paper operates based on the Material Extrusion process, commonly known as FFF (*Fused Filament Fabrication*). This technology is based on the selective deposition of melted material onto the previous layer or the build plate through a heated nozzle. The FFF technology supports the use of various materials, such as PLA, PETG, ABS, ASA, and others.

During this project, materials used for printing were PLA, PLA+, and PETG, which do not release harmful emissions and require lower printing temperatures, making them suitable for hobbyist environments. One of the main limitations of the delta printer in question is the absence of an enclosed chamber, which is essential for using materials such as ABS and ASA.

1.1 Printer Configurations for FFF Technology

The main printer configurations used in FFF technology are Cartesian, Delta, Polar, and SCARA [2]. These configurations are illustrated in Figure 1.

Cartesian printers operate using a rectangular coordinate system, moving the extruder head along the X, Y, and Z axes. The linear motion and simple geometry make them the most widely used configuration on the market.

Delta printers move the extruder head using three pairs of rods whose synchronized motion ensures continuous parallelism between the extruder head and the builder plate. This configuration offers higher print speeds and supports the production of taller models.

Polar and SCARA configurations feature more complex kinematics, which require advanced motion control and complex software development. As a result, these systems are less commonly used compared to Cartesian and Delta printers.

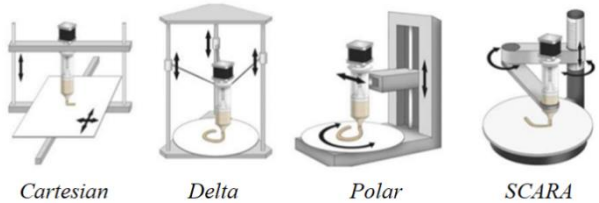

Figure 1. Different printer configurations for FFF technology [2]

Numerous studies highlight the advantages of the Delta configuration in FDM 3D printing. For instance, as shown in [3], Delta printers can achieve superior surface quality compared to Cartesian systems. As noted in [4], the RepRap project (Replicating Rapid Prototyper) is based on the concept of self-replicating machines, where a 'parent' printer can produce many of the components required to build a 'child' printer. As a result of this open-source approach, a wide range of hardware variations and individual adaptations has emerged.

1.2 Parallel mechanism in Additive Manufacturing Technologies

The Delta 3D printer is classified as a parallel kinematic mechanism. In such systems, the end effector (in this case, the extruder head) with *n* degrees of freedom is connected to the base through *n* independent kinematic chains, each containing an actuated joint [5].

The basic types of spatial parallel mechanisms include:

- mechanism with telescopic (variable-length) rods equipped with actuated prismatic joints,
- mechanisms with fixed-length rods equipped with actuated revolute joints at the base,
- mechanisms with fixed-length rods equipped with actuated prismatic joints at the base.

Different types of joints can be used in parallel kinematic mechanisms, including cylindrical, universal (Cardan), and spherical joints, as illustrated in Figure 2 in the listed order.

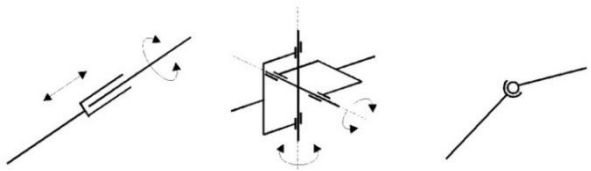

Figure 2. Different types of joints in parallel mechanisms

Various configurations of Delta Kossel printers are available on the market, which could feature spherical or universal joints, as illustrated in Figure 3. The configuration used in this study belongs to the third type of spatial parallel mechanisms. It contains fixed-length rods, spherical joints, and actuated prismatic joints.

Figure 3. Different types of joints in Delta printer variations

2. STRUCTURAL OPTIMIZATION OF A DELTA 3D PRINTER

At the beginning of the project, the Delta 3D printer was non-functional. The first step involved an analysis of the existing structure with the goal of identifying components that needed to be replaced, as well as parts of the system that could be functionally or aesthetically optimized. Reverse engineering was applied during the modeling of replacement parts, since technical documentation and compatible models for this version of the Delta printer were not available. Replacement components were manufactured using additive technologies, specifically the FFF (*Fused Filament Fabrication*) and SLA (*Stereolithography*) methods. The optimization process was iterative, with multiple technical solutions being evaluated in order to determine the most suitable option. The initial state of the printer at the beginning of the project is shown in Figure 4.

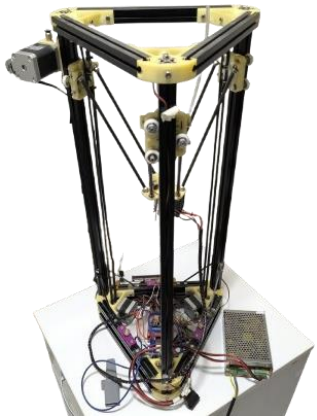

Figure 4. Initial condition of the Delta 3D printer

Following the successful reconstruction, all undertaken steps were categorized. The printer's condition before and after each step is presented below.

2.1 Replacement of Deteriorated Plastic Parts

In the initial phase, reverse engineering was applied to design replacement models for plastic components that had developed cracks and altered mechanical properties over time, such as increased brittleness, due to prolonged exposure to sunlight. The initial condition of the plastic parts can be seen in Figure 5. In Figure 5a, surface cracks in the material are visible. Figure 5b shows the breakage of a structural support element, where the screw is left exposed and lacks adequate support. In Figure 5c, surface discoloration is observed, indicating changes in mechanical properties of the material.

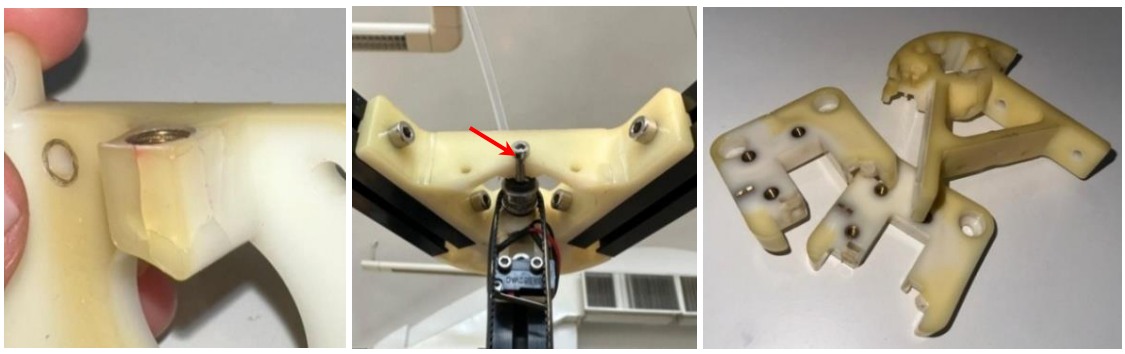

Figure 5. Deteriorated plastic parts: a) cracks, b) failure, c) surface discoloration

Figure 6 shows several replacement parts. The first picture provides a comparison between a worn-out component (left) and its replacement (right). The original part exhibits multiple cracks and a fracture near the screw hole, while the replacement part includes certain optimizations, such as the removal of redundant, non-functional surfaces and the addition of a brass threaded insert.

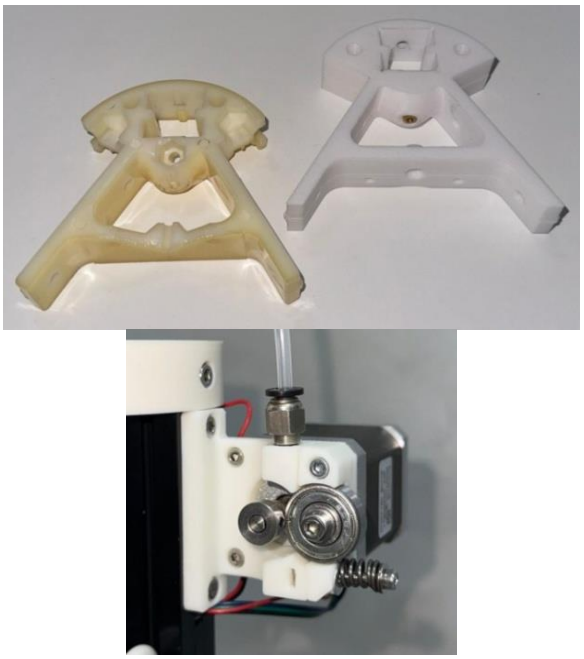

Figure 6. Replacement parts

Various materials were used to produce the structural support elements mounted on the upper frame of the printer, including ABS+, PLA Strong, and ASA. These materials were marked on the structure, as shown in Figure 7. The use of different materials enables a comparison of their behavior under real operating conditions, such as vibrations, mechanical loads, and other external factors over time. This further provides a basis for future studies focused on the long-term exploitation effects on mechanical properties and durability of different materials.

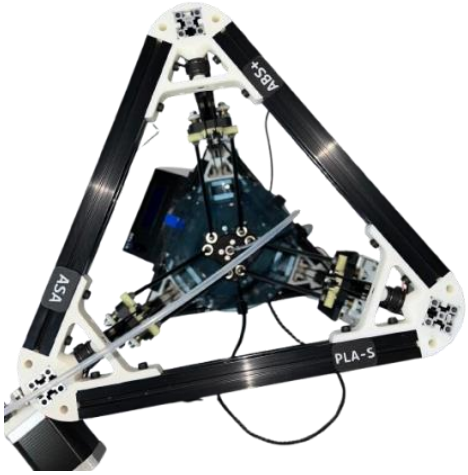

Figure 7. Marked materials for upper frame support elements

2.2 Replacement of the Extruder Head

The initial and final appearance of the extruder head is shown in Figure 8.

It was observed that the extruder head was deformed, with noticeable warping and a visible crack along the edge of the moving platform. Since the Delta printer configuration requires precise alignment between the extruder head and the print bed, addressing this issue was essential. Although the warping – caused by material degradation due to prolonged exposure to environmental conditions – contributed to the problem, the primary cause of the distorted geometry was the improper magnet installation.

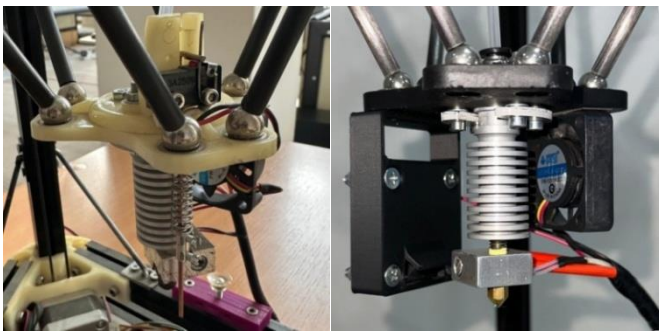

Figure 8. The initial and final appearance of the extruder head

As shown in Figure 9a, the magnets were unevenly positioned: on the left side, one magnet was pushed in too far, while on the right, the magnet wasn't inserted deeply enough. These magnets, together with the magnetic spheres on the rods, form spherical joints that directly affect the precision of the extruder's movement. Therefore, precise placement of the magnets is crucial for the system to function properly.

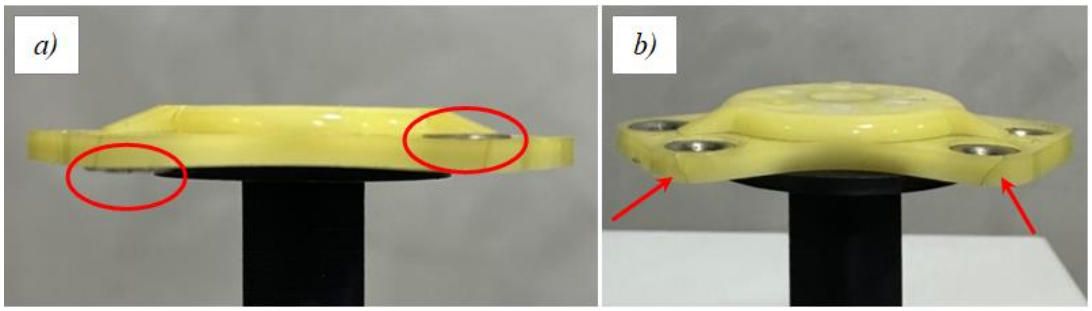

Figure 9. Deformed extruder head: a) improper magnet positioning, b) cracks

Figure 10 illustrates the iterative process of optimizing the moving platform. In the first step, by implementing reverse engineering, the original part (1) was replaced with an identical 3D-printed model (2), which was used to detect the issues. To resolve the issue with incorrect magnet positioning, small bases on the underside of the platform were added to act as physical stops during magnet installation (3), ensuring precise placement. Additionally, the number of screw holes for attaching the extruder was reduced to simplify assembly. FFF technology was used for the prototype stages, while SLA technology was applied for the final version (4) to achieve higher dimensional accuracy. In the final step (5), magnets were precisely installed into the designated recesses on the platform, ensuring proper geometry of the spherical joints and parallelism between the extruder head and the print bed.

Figure 10. Iterative optimization process of the moving platform

In the original configuration, the extruder head was equipped with a single fan used to cool the radiator. To improve print quality – particularly regarding layer formation and preventing material deformation caused by overheating – a second fan was added to cool the printed part. Accordingly, housing was designed for the new fan. The fan housing includes an air guide that directs the airflow toward the printing zone. Both fans are attached using magnets on the underside of the moving platform, allowing easy installation and removal without the need for additional tools. Figure 11 shows the fan housing with the

airflow direction highlighted to illustrate the effect of the air guide.

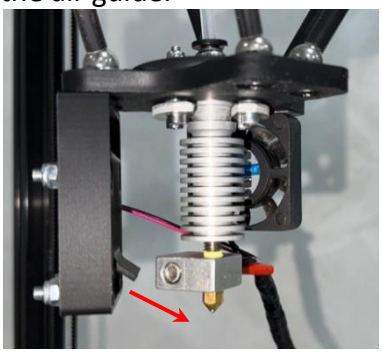

Figure 11. The new fan housing with an airflow guide

4.1 Bed Leveling System

Given the previously mentioned requirement to maintain parallelism between the extruder and the print bed, it was necessary to design an appropriate leveling system. Figure 12 shows the original (left) and improved (right) configuration of this system. Leveling is achieved at three points, evenly distributed at 120° intervals around the perimeter of the print bed. One pair of components was manufactured in a different colour to ensure consistent orientation during print bed assembly. This approach eliminates alignment errors caused by dimensional tolerances of individual 3D-printed components.

Figure 13 shows one of the leveling components, which consists of four main parts. The system is mounted on the printer frame using a base plate, with an integrated nut used for leveling. The height of the print bed is adjusted by rotating a knurled cylinder fixed to a screw, allowing the bed to be raised or lowered. A spring is added to eliminate backlash between the screw and the nut. The connection between the bed holder and the control cylinder is magnetic, allowing for quick and simple installation and removal of the print bed.

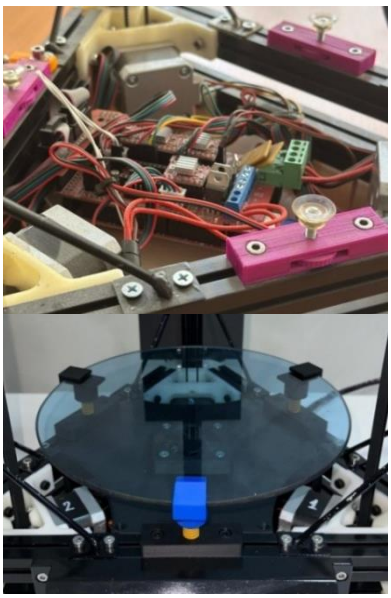

Figure 12. The original and improved bed leveling system

Figure 13. Bed leveling system component

The printer was originally equipped with an automatic bed leveling system that used an Allen key probe. However, it was overly complex and non-functional due to missing components. As a result, this system was fully replaced with manual leveling. The integration of an automatic bed leveling system remains a potential topic for future development and further optimization of the printer.

4.2 Electronic System Components

Initially, the printer did not have a dedicated storing space for the electronics, which could cause issues with isolating and organizing the components. To resolve this issue, an electronics housing was designed and constructed, consisting of two parts – a base and a top cover. The base features ventilation slots and is open toward the motors, allowing passive ventilation and improved airflow for

cooling. Additionally, a cooling fan was installed inside the top cover to provide active temperature regulation for both the electronic components and the motors. Figure 14 shows the original setup (left) and the designed housing parts.

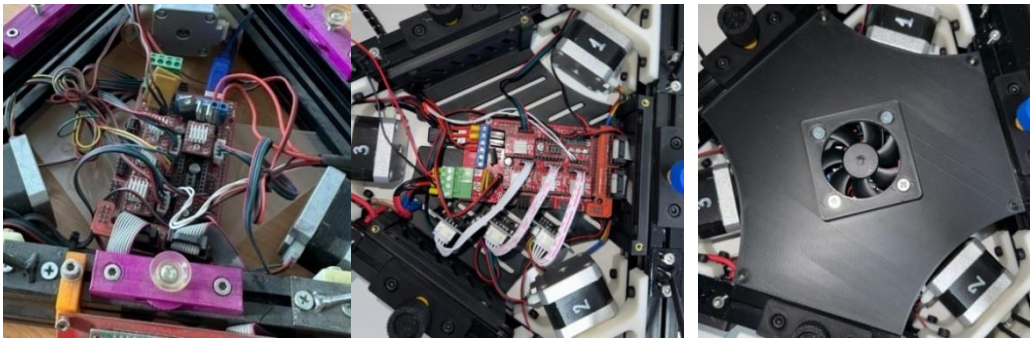

Figure 14. Original electronics setup and new housing parts

The original printer configuration did not include housings for components such as the power switch and power supply, which negatively impacted both safety and the printer's visual appeal. Thus, housings were designed for mounting these components directly onto the printer frame. All housings were produced using FFF technology. Figure 15 shows the original power switch (left) alongside the designed housings for the switch (center) and power supply (right).

Figure 15. The initial power switch and the designed power switch and power supply housings

4.3 Display Housing

In the original printer version, the display lacked proper protection. Its electronics were exposed to external factors, and the existing holders had cracks and provided insufficient support, allowing movements and bending of the screen during use. For these reasons, a new display housing was designed to provide mechanical protection for the electronic components, improve the device's appearance, and isolate the display from vibrations. The original screen and mounts are shown in Figure 16.

Figure 16. The initial appearance of the printer's display

The prototype version of the housing was made using FFF technology, while the final part was produced using SLA technology. Post-processing included support removal, varnishing, and painting of the 'DELTA' label. The housing at the end of the printing process (top), as well as the assembled final part (bottom), can be seen in Figure 17.

Figure 17. Housing after printing and final assembled part

4.4 Filament Holder

The printer came without a filament holder, which significantly complicated the printing process. The absence of the filament holder could lead to filament tangling or jamming on the spool, which could result in print failure or extruder damage. To ensure proper guidance and handling of the filament, a custom holder was designed and attached to the printer frame. The holder, shown in Figure 18, was produced using FFF technology.

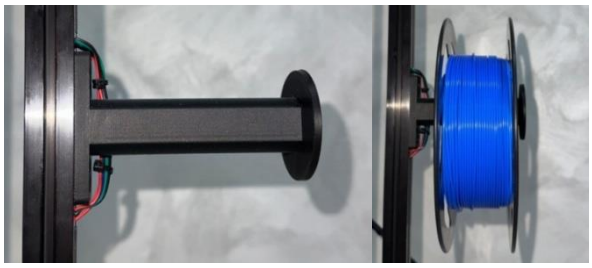

Figure 18. The designed filament holder

4.5 Additional Improvements

Mechanical stoppers were mounted on the printer frame to physically limit the movement of the extruder head in case of a system malfunction, preventing potential damage to the printer. Additionally, cable covers were added for aesthetic purposes, contributing to a cleaner appearance and improved wiring management. These components, shown in Figure 19, were also produced using FFF technology.

Figure 19. Mechanical stoppers (left) and cable covers (right)

5. CONCLUSION

Currently, additive manufacturing systems are rapidly evolving, with Cartesian configurations continuing to dominate the market. However, introducing delta systems into educational settings offers a valuable advantage. As a teaching tool, a delta printer allows students to gain knowledge not only in additive manufacturing technologies, but also in the field of mechanics and alternative motion geometries.

The goal of this project was to restore the functionality of an outdated Delta 3D printer and to optimize its systems and components. This objective was successfully achieved, resulting in improved reliability and precision of the device, while also leaving room for further upgrades. This project serves as a practical example of how an engineering approach can be effectively applied to solve technical challenges.

ACKNOWLEDGEMENT

The research work is funded by the Ministry of Science, Technological Development and Innovation of Republic of Serbia. Project Contract 451-03-137/2025-03/ 200105 from 04.02.2025.

REFERENCES

[1] ASTM F2792-12a: *Standard Terminology for Additive Manufacturing Technologies*, ASTM International, DOI: 10.1520/F2792-12A

[2] J. Sun, W. Zhou, L. Yan, D. Huang, and L. Lin: Extrusion-based food printing for digitalized food design and nutrition control. Journal of Food Engineering, Vol. 220, pp. 1–11, doi: 10.1016/j.jfoodeng.2017.02.028, 2018.

[3] Y. Zhuk, T. Klotchko: Comparison of 3D-printed parts' quality using printers with "CoreXY" and "Delta" kinematics, *Visnyk KPI. Series: Instrumentation Engineering*, Vol. 68(2), 2024.

[4] T. Gordelier, P. R. Thies, L. Johanning, L. Turner: Optimising the FDM additive manufacturing process to achieve maximum tensile strength, *Rapid Prototyping Journal*, Vol. 25(3), 2019.

[5] S. Živković: *Lecture Notes from the Course Machine Tools and Next-generation Robots*, University of Belgrade, Faculty of Mechanical Engineering, 2023/24.

Society of Production Engineering

ICPES 2025

40th INTERNATIONAL CONFERENCE ON PRODUCTION ENGINEERING - SERBIA 2025

DOI: 10.46793/ICPES25.364L

University of Nis Faculty of Mechanical Engineering

Nis, Serbia, 18 - 19th September 2025

IMPLEMENTATION AND OPTIMIZATION OF THE DELTA 3D PRINTER CONTROL SYSTEM

Aleksandar LAZIĆ[1], Natalija LAZAREVIĆ[1], Mihajlo POPOVIĆ[1]*, Miloš PJEVIĆ[1]

Orcid: 0000-0003-3607-9243; **Orcid:** 0000-0002-4454-8663

[1]University of Belgrade, Faculty of Mechanical Engineering, Serbia

*Corresponding author: mpopovic@mas.bg.ac.rs

Abstract: *This paper deals with the implementation of a control system for a Delta 3D printer, which was carried out to enable its use in educational applications. A detailed diagnostic was performed on essential hardware components of the Delta 3D printer, including the Arduino MEGA, RAMPS 1.4 board, stepper motors and their drivers, micro switches, display module, and other electronics. A customized version of the Marlin firmware, adapted for a Delta configuration, was then installed on the Arduino MEGA microcontroller. Key parameters such as build plate dimensions, print height, Delta radius, motor microstepping, and maximum motor speed and acceleration were configured. To optimize stepper motor performance, reference voltages were adjusted, and TL smoothers were installed to ensure stable and quieter operation. The final system evaluation included measuring motor voltage levels, verifying filament flow rates, checking the dimensional accuracy of printed parts, and validating the parameter setup. After hardware and firmware calibration, various slicing software tools available online were tested and compared. The aim of the analysis was to identify the most suitable slicing software for the optimized Delta system, as well as the optimal configuration of its parameters, in order to achieve the highest possible print quality.*

Keywords: *Delta 3D printer, Marlin firmware, Arduino, TL smoother, RAMPS 1.4, Slicer*

1. INTRODUCTION

Additive manufacturing technologies are experiencing rapid and continuous advancement, reflected in diverse design solutions, a wide range of available materials, and improved device performance. Among the available configurations, the Delta design stands out, utilizing parallel kinematics to achieve high speeds and increased print height. Aside from hobbyist and professional applications, the unique motion geometry and construction of Delta printers make them particularly interesting for educational purposes. For this reason, this project involved the complete hardware reconstruction and software customization of an outdated, non-functional Delta 3D printer, with the goal of integrating it into the university's curriculum. The project was carried out as part of an initiative to enhance practical education in additive technologies, where the optimized device is used for laboratory exercises and the development of practical skills in working with different 3D printer configurations.

The project employed *Marlin firmware* for hardware control, with the Arduino IDE development environment used for optimizing

the control code. An Arduino MEGA board was utilized to transmit the necessary control signals.

The implemented technology belongs to the material extrusion process, which, according to the ASTM F2792-12a standard, is one of the seven fundamental categories of additive manufacturing. This method, also known commercially as FFF (*Fused Filament Fabrication*), is based on the controlled deposition of molten material onto a build plate or previous layer through a nozzle [1]. This technology supports the use of various polymers, including PLA, PETG, ABS, ASA, and others.

1.1 An Overview of 3D Printer Configurations Used in FFF Technology

The fundamental 3D printer configurations used in FFF technology are Cartesian, Delta, Polar, and SCARA, shown in Figure 1 [2].

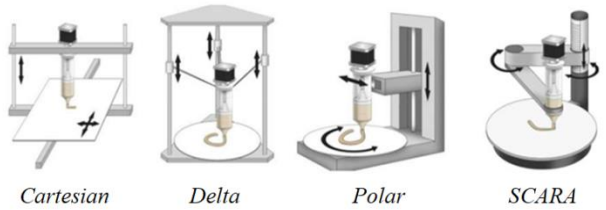

Figure 1. The fundamental 3D printer configurations for FFF technology

Cartesian printers operate based on a rectangular (Cartesian) coordinate system, where linear movement occurs along the mutually perpendicular X, Y, and Z axes. Their rectangular base and simple motion geometry make them easy to construct, which contributes to their widespread use in the market.

Delta configuration printers achieve extruder head movement through three synchronized pairs of rods. The extruder head remains parallel to the build plate at all times. Delta systems are characterized by higher printing speeds, greater build heights, smooth motion, and complex kinematics.

In polar configuration printers, printing is achieved through coordinated movement of the build platform and the extruder head. Typically, the build platform rotates while the extruder head moves along a radial path (spherical motion). A drawback of such systems is the complexity of the motion geometry, resulting in more complex control software. Platform rotation can cause dimensional inaccuracies in larger models and complicate the implementation of a heated build plate, which is essential for printing materials such as ABS.

SCARA (*Selective Compliance Articulated Robot Arm*) configuration printers control the extruder head using two jointed mechanical arms. This setup provides high flexibility and enables fast printing. However, due to the complexity of the motion mechanics, the control system development is challenging.

Many studies emphasize the advantages that Delta kinematics offer in 3D printing compared to traditional Cartesian configurations. In paper [3], it is indicated that the main advantage of delta kinematics is the high speed of the extruder head, enabled by the parallel motion of the platform connected through three pairs of rods. Paper [4] presents a performance comparison between Cartesian and Delta 3D printers. Similar observations can be found in paper [5], and both studies show that parts printed with Delta 3D printers exhibit smoother surfaces and higher overall print quality.

1.2 An Overview of Available Firmware

The two most commonly used firmware options for configuring 3D printers are Marlin and Klipper. **Klipper** is a newer, faster, and more modern firmware solution for 3D printers, offering a wide range of advanced features and a high customization potential. In contrast, **Marlin** is the most widely adopted and traditional firmware, known for its stability, broad hardware compatibility, and strong support from 3D printer manufacturers. While it may be less flexible in some advanced use cases, it remains the standard in many commercial and hobbyist 3D printing setups. Marlin firmware was used in this project, and its customization is presented later in the paper.

1.3 Comparative Analysis of Available Delta Configuration Printers

Additive technologies have become a crucial step in the product development process. Delta 3D printers have undergone significant development and optimization. From devices originally intended solely for hobbyists, they have evolved into professional machines tailored to the needs of industry today.

The first commercial Delta 3D printer was introduced in 2012, marking the start of this printing technology's development. Initially popular for hobby use due to its speed and precision, early models such as the *Anycubic Kossel* and *Monoprice MP Delta* were limited by factors including small build volume, restricted material compatibility, and manual calibration requirements, which reduced their suitability for professional and industrial applications. Advancements in motion mechanics, software solutions, and material compatibility have transformed Delta printers from hobbyist tools into professional systems. Modern Delta printers offer larger build volumes, higher speed and precision, as well as automated bed leveling. Additionally, current models support a broader range of materials, including engineering plastics, composites, metals, and ceramics.

Models such as *FLSUN V400* and *FLSUN S1*, equipped with a temperature-controlled chamber, represent examples of new generation Delta printers successfully used in industry as well as in advanced research and educational institutions. However, as noted in [6], perhaps the primary reason why Delta printers are still predominantly used for hobbyist applications is their limited print accuracy compared to Cartesian systems, due to the relatively lower positioning precision of the extruder head. Cartesian printers have demonstrated smaller deviations from the original CAD models [4].

Table 1 presents a comparison of key characteristics between an earlier-generation Delta 3D printer, the *Anycubic Kossel Plus*, and a modern model, the *FLSUN S1 PRO.*

Table 1. Performance comparison between earlier-generation and modern Delta 3D printers

characteristic	Anycubic Kossel Plus	FLSUN S1 PRO
max. print speed	up to ~150 mm/s	up to ~1200 mm/s
max. print acceleration	up to ~3000 mm/s^2	up to ~40 000 mm/s^2
chamber	no	yes
max. extruder temp.	260°C	350°C
print bed temp.	110°C	120°C
build volume	Ø230 x 300 mm	Ø320 x 430 mm
dimensions	△380 x 680 mm	550 x 595 x 1030 mm
weight	~7 kg	41 kg
positional accuracy	X/Y axis: 0.0125 mm	X/Y axis: 0.0125 mm
	Z axis: 0.0025 mm	Z axis: 0.0004 mm
price range	$150 – 200	$1 000 – 2 000

The Cartesian Bambu Lab P1 series, priced below $1 000, is comparable in terms of available features to professional Delta printers such as the FLSUN S1 Pro. While the FLSUN S1 Pro is more advanced and professional, both systems include a wide array of features: touchscreen interface, integrated monitoring camera, filament presence and run-out detection, filament tangle and clog detection, vibration compensation, debris and spaghetti detection, automatic shutdown, power-loss recovery, first-layer inspection, and smart zone heating. In contrast, most Delta printers priced

below $1 000 typically lack this level of advancement.

2. SOFTWARE OPTIMISATION OF DELTA 3D PRINTER

A detailed diagnostic was performed on the Delta 3D printer. The stepper drivers, motors, micro switches, RAMPS 1.4 board, Arduino MEGA, and display were tested for functionality. Faulty components were identified and replaced.

During the testing phase, several parts were printed, revealing poor surface quality characterized by a ripple effect. This issue was resolved by adding TL smoothers – electronic modules that reduce vibration and noise in stepper motors. This resulted in stable and quieter operation, and improved print quality.

Figure 2 shows the printed parts before and after the installation of TL smoothers. The improvement highlights the importance of proper hardware–software alignment in achieving high print quality.

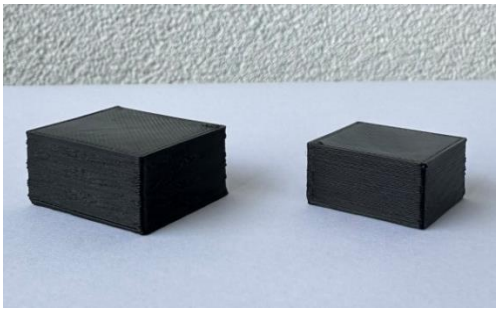

Figure 2. Surface quality before and after adding TL smoothers

A cooling fan was also added to improve airflow over the electronics and ensure thermal regulation of both the electronic components and the stepper motors.

As mentioned, the deployed control software was Marlin, which is an open-source firmware that, when combined with the Arduino Mega board, offers extensive configuration flexibility. Marlin allows users to customize the printer to their specific needs by adjusting parameters such as build volume, maximum speed and acceleration, filament sensor settings, and more. It was necessary to adjust the parameters in Marlin firmware to suit the parallel kinematics of the Delta configuration and the available components of the printer.

In the initial setup phase, it was necessary to define the type of control board using the function **#define MOTHERBOARD BOARD_RAMPS_14_EFB**, where E stands for extruder, F for fan, and B for heated bed. This configuration provides the necessary positions for implementing the part cooling and bed heating.

The next step involves defining the type of drivers. Using the directives **#define X_DRIVER_TYPE A4988**, **#define Y_DRIVER_TYPE A4988**, **#define Z_DRIVER_TYPE A4988**, and **#define E0_DRIVER_TYPE A4988,** all four stepper motors were defined, where the first three are used for positioning the extruder head along the X, Y and Z axes, while the fourth controls filament feeding.

The directive **#define TEMP_SENSOR_0 7** was used for specifying the temperature sensor type, which will enable precise temperature regulation of the extruder head. Since the printer does not include a heated bed, this was indicated by the function **#define TEMP_SENSOR_BED 0**, where 0 denotes the absence of a bed heating system.

The build volume is defined by the base radius and height, using the following lines of code: **#define DELTA_PRINTABLE_RADIUS 87** and **#define DELTA_HEIGHT 260**. To ensure accurate positioning it is necessary to define the rod length, which is done with the function **#define DELTA_DIAGONAL_ROD 210**. This means that the value of rod length is set at 210 mm. The key design dimensions of the Delta printer are shown in Figure 3. Due to positional tolerances, manual assembly cannot guarantee perfect horizontal alignment among all three micro switches, which together define the extruder's home position.

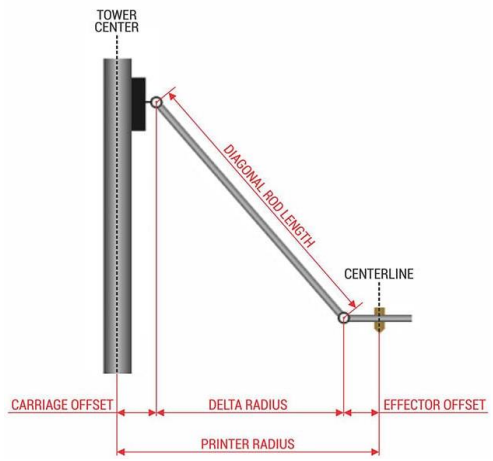

Figure 3. Key dimensions of the Delta printer

This is compensated by using the function **#define DELTA_ENDSTOP_ADJ { 0.0, 0.0, 0.0 }**, where corrected values for X, Y, and Z towers can be inputted in the brackets, respectively.

One of the key factors in maintaining the ideal parallelism between the extruder head and the print bed is a parameter known as the delta radius, which was defined using the directive **#define DELTA_RADIUS 105**, setting its value to 105 mm. The delta radius represents the horizontal distance between the centers of spherical joints located at rod ends, when the extruder head is positioned at the center of the build area. This is illustrated in Figure 3.

Due to angular tolerances, the towers of a Delta printer might not be positioned in the ideal configuration of exactly 120° between each tower, but could be slightly rotated with respect to one another. This can be corrected by implementing the function **#define DELTA_TOWER_ANGLE_TRIM { 0.0, 0.0, 0.0 }**, which allows the precise angular adjustment of the towers. The values in the brackets correspond to the angular corrections for the X, Y and Z towers, respectively.

The following lines of code are used for defining the home position, which in Delta configurations represents the maximum position of the printer's towers. These lines specify the pin to which each micro switch is connected for the respective towers. When a micro switch is triggered, the system recognizes that the corresponding carriage has reached its top position, marking it as the home position for that tower. The code lines mentioned above are: **#define USE_XMAX_PLUG**, **#define USE_YMAX_PLUG**, and **#define USE_ZMAX_PLUG**.

To ensure correct printer operation, it is important to introduce certain hardware parameters into the software. One key parameter is the number of steps per rotation of the stepper motor, which in this case is 200. This value is used to configure microstepping, which is essential for achieving high print quality through precise control of the extruder head's movement. For Delta printers, a common microstepping setting is 1/16 of a full step. The relevant lines of code implementing these settings are as follows:

#define XYZ_FULL_STEPS_PER_ROTATION 200;
#define XYZ_MICROSTEPS 16.

The next hardware parameters that should be introduced are those related to the pulley and belt system. The following lines of code define the belt pitch and the number of pulley teeth: **#define XYZ_BELT_PITCH 2**, and **#define XYZ_PULLEY_TEETH 16**.

Once all these parameters have been defined, it is necessary to calculate the number of impulses (steps) that must be sent to the stepper motors in order to move the corresponding carriage on each tower by exactly 1 mm. This is determined using the following formula:

#define DEFAULT_XYZ_STEPS_PER_UNIT ((XYZ_FULL_STEPS_PER_ROTATION) * (XYZ_MICROSTEPS) / double(XYZ_BELT_PITCH) / double(XYZ_PULLEY_TEETH)).

The next phase involves defining velocities and accelerations, such as the maximum homing speed and acceleration, as well as the speed and acceleration of the extruder head during rapid movement (G0 command). An example of such a directive is the following homing federate setting: **#define HOMING_FEEDRATE_MM_M { (2500), (2500), (2500) }**, where the speeds for each axis is represented in millimetres per minute (mm/min). The adjusted values for these parameters are presented in Table 2.

Table 2. Adjusted speed and acceleration values

***characteristic*:** **speed [mm/s] or acceleration [mm/s²]**	**value for stepper motor**			
	X	**Y**	**Z**	**E0**
DEFAULT_MAX_FEEDRATE *maximum speed for all three axes and filament feeding*	300	300	300	70
MAX_FEEDRATE_EDIT_VALUES *limit value of speed modifiable through the printer's display*	100	100	100	100
DEFAULT_MAX_ACCELERATION *maximum acceleration for all three axes and filament feeding*	3000	3000	3000	2000
MAX_ACCEL_EDIT_VALUES *limit value of acceleration modifiable through the printer's display*	1000	1000	1000	1000
DEFAULT_ACCELERATION *general axis and filament feeding acceleration during G1 commands*	2000	2000	2000	2000
DEFAULT_RETRACT_ACCELERATION *retraction acceleration during filament pullback*	/	/	/	1500
DEFAULT_TRAVEL_ACCELERATION *axis acceleration for non-printing (travel) moves*	2000	2000	2000	/

The default retract acceleration refers to the acceleration applied before or during travel moves, when the extruder head moves from one print section to another, helping to prevent stringing effects.

At this stage, the acceleration profile was set to S-curve acceleration, which provides a smoother transition between speed and acceleration shifts. Instead of sharp shifts, the motion follows a curved trajectory, resulting in more stable extruder head movement and reduced vibration during printing. This was done by implementing the function: **#define S_CURVE_ACCELERATION**. The differences between S-curve and trapezoidal acceleration profiles are illustrated in Figure 4.

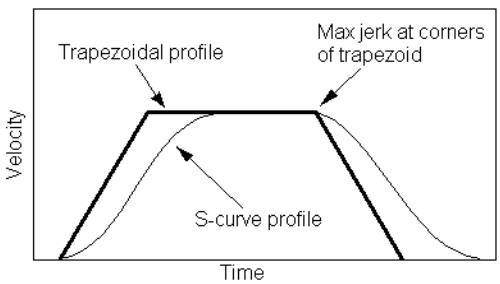

Figure 4. Difference between trapezoidal and S-curve acceleration profiles

The following directives are used to define the homing direction for each of the three towers – X, Y, and Z. The direction is defined with a value of 1 or -1, depending on whether the movement should be upward or downward. Since the home position in Delta printers is located at the top of the towers, and in accordance with previously mentioned directives **#define USE_XMAX_PLUG**, as well as Y and Z, a value of 1 is assigned to ensure that the extruder head moves upward toward the micro switches. These directives are: **#define X_HOME_DIR 1**, **#define Y_HOME_DIR 1**, and **#define Z_HOME_DIR 1**.

In the following step, it was necessary to adjust the reference voltages (**V_{ref}**) on the stepper motor drivers to ensure stable, quiet, and reliable motor operation, as well as to prolong the service life of stepper motors. Excessively high reference voltage values may result in motor overheating and potential driver damage. On the other hand, if the reference voltage values are too low, the motors may lose or skip steps, leading to printing errors and poor print quality.

One of the final steps involved defining the type of display used, which was specified using the directive **#define REPRAP_DISCOUNT_SMART_CONTROLLER**. It was also concluded that the automatic calibration process, based on the Allen key

probe, failed to achieve satisfactory results. Subsequently, this function was disabled, and it was decided that manual calibration would be a more suitable approach in this case. Up to this point, the printer's operation could only be controlled through a USB-B connection to a computer. To improve user experience, SD card support was added using the **#define SDSUPPORT** function.

Finally, the printer was personalized by assigning it a name that appears on the display when the device is turned on, using the following function: **#define CUSTOM_MACHINE_NAME "DELTA MAS PRO"**.

Following the software setup, the configuration was thoroughly tested and confirmed, resulting in successful printing of test parts.

3. AVAILABLE SLICER SOFTWARE EVALUATION

After successful testing of the Delta printer, several available slicing software options were analyzed. This included Orca, Cura, Slic3r, an older version of PrusaSlicer, and the latest PrusaSlicer version.

Figure 5 (top) shows the first printed layer using the Cura and Orca slicers, where trajectory errors of the extruder head during infill are clearly visible. In both cases, the areas surrounding the holes were not properly filled, resulting in gaps and incomplete coverage of certain printed zones. Similar issues were observed with Slic3r, where the first layer exhibited irregular extrusion paths around the holes (Figure 5, bottom left). Additionally, parts printed with Slic3r showed poor surface quality due to visible gaps between the infill lines (Figure 5, bottom right). While some issues can be addressed by tuning the print parameters, none of the slicers mentioned delivered satisfactory results using the default settings.

The older version of the PrusaSlicer also exhibited trajectory issues around openings in the initial layers (Figure 7, left), but achieved noticeably better surface quality compared to previously mentioned slicers (Figure 7, right).

Figure 5. Printing defects observed when using Cura, Orca, and Slic3r slicers

Figure 6. Surface finish obtained using PrusaSlicer

Given that slicer versions also have an impact on the overall print quality and performance, the latest version of PrusaSlicer (version 2.9.2) was installed and tested. This version produced optimal results: motion paths of the extruder head were accurate, all areas were consistently filled, and no defects were observed. Further improvements were achieved through parameter adjustments within the slicer, which offers extensive customization options for its users. A part printed using the updated PrusaSlicer is shown in Figure 8.

Figure 7. Part printed using the PrusaSlicer version 2.9.2

A dimensional analysis was conducted on the part sliced using PrusaSlicer v2.9.2. Table 3 presents a comparison between the nominal dimensions (from the CAD model) and the actual measurements of the printed part.

Table 3. CAD model and Printed Part Dimensions

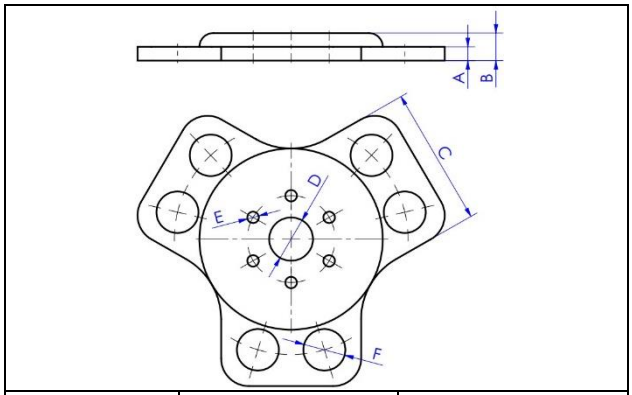

dimension label	nominal value [mm]	measured value [mm]
A	4	3.98 ÷ 4.03
B	8	8.05 ÷ 8.15
C	40	39.87 ÷ 40.10
D	Ø12.5	Ø12.45
E	Ø3.3	Ø3.28 ÷ 3.41
F	Ø12	Ø11.86 ÷ 12.10

4. CONCLUSION

The Cartesian configuration is the most widely used in the market, but introducing delta printers into educational settings represents a great advantage. It gives students the opportunity to compare different printer designs and understand both their strengths and limitations. Alongside practical experience in additive manufacturing, it also helps students grasp the basics of motion system mechanics.

The goal of the project was to restore the functionality of an outdated delta 3D printer, which was successfully achieved, as parts were printed reliably, with room left for further improvement. Of all the slicers tested, the latest version of PrusaSlicer (v2.9.2) delivered the best surface quality. Dimensional analysis showed that the deviations were within acceptable limits, confirming the device's precision. It was concluded that minor dimensional variations were caused by slight warping due to the absence of a heated bed. The next step in improving the system would be the integration of bed heating to further improve print quality and dimensional accuracy

ACKNOWLEDGEMENT

The research work is funded by the Ministry of Science, Technological Development and Innovation of Republic of Serbia. Project Contract 451-03-137/2025-03/ 200105 from 04.02.2025.

REFERENCES

[1] ASTM F2792-12a: *Standard Terminology for Additive Manufacturing Technologies*, ASTM International, DOI: 10.1520/F2792-12A

[2] J. Sun, W. Zhou, L. Yan, D. Huang, and L. Lin: Extrusion-based food printing for digitalized food design and nutrition control. Journal of Food Engineering, Vol. 220, pp. 1–11, doi: 10.1016/j.jfoodeng.2017.02.028, 2018

[3] X. Song, Y. Pan, Y. Chen: Development of a low-cost parallel kinematic machine for multidirectional additive technologies, *Journal of Manufacturing Science and Engineering*, Vol. 137, p. 021005, 2015.

[4] Y. Zhuk, T. Klotchko: Comparison of 3D-printed parts' quality using printers with "CoreXY" and "Delta" kinematics, *Visnyk KPI. Series: Instrumentation Engineering*, Vol. 68(2), 2024.

[5] B. M. Schmitt, C. F. Zirbes, C. Bonin, D. Lohmann, D. C. Lencina, A. C. S. Netto: A comparative study of Cartesian and Delta 3D printers on producing PLA parts, *Materials Research*, Vol. 19(8), 2016.

[6] O. V. Zakharov, K. G. Pugin, T. N.Ivanova: Modeling and analysis of Delta kinematics FDM printer, *Journal of Physics: Conference Series*, Vol. 2182, p. 01206, 2022.

Society of Production Engineering

ICPES 2025

40th INTERNATIONAL CONFERENCE ON PRODUCTION ENGINEERING - SERBIA 2025

DOI: 10.46793/ICPES25.372V

University of Nis Faculty of Mechanical Engineering

Nis, Serbia, 18 - 19th September 2025

THE INFLUENCE AND ADJUSTMENT OF 3D PRINTER TEMPERATURES DURING MODEL PRINTING WITH REFERENCE TO THE USED MATERIAL

Saša VASILJEVIĆ[1*], Milan ĐORĐEVIĆ[1], Marina KARIĆ[1], Milan RADENKOVIĆ[2], Marko MASLAĆ[3]

Orcid: 0000-0002-2235-1309; **Orcid:** 0000-0001-5941-3262; **Orcid:** 0009-0006-4180-1754;

[1] Academy of Professional Studies Šumadija, Kragujevac

[2] Faculty of Technical Sciences, University of Priština in Kosovska Mitrovica, Kosovska Mitrovica

[3] Academy of Professional Studies Šumadija, Kragujevac

*Corresponding author: svasiljevic@asss.edu.rs

Abstract: *The application of 3D printing is today one of the technologies that are applied due to its practical application and speed of production of parts. 3D printing is a representative of the concept of rapid prototyping, due to the ease of production of prototypes. In addition to the simplicity of production of parts, certain problems may arise related to the adjustment of the temperature of the extruder and the stand on which the model is printed. Temperatures and the adjustment of temperatures themselves may depend on the material or the part itself that is being produced. Thus, in this paper, an analysis of the temperatures that should be applied depending on the material used from which the part itself is made has been carried out. In addition to the fact that temperature can affect the success of model production or some incidental actions that would prevent printing, temperature can also affect the quality of model production. Thus, in this paper, the influence of temperature on models during printing has been carried out. On the other hand, a review of the temperature limit values that should be applied depending on the material used has been carried out.*

Keywords: *3D printer, extruder, material, platform, temperatures.*

1. INTRODUCTION

Printing a 3D model may seem like a simple process that depends on various factors that can affect the printing process itself and the printing success. The factors that are adjusted in the case of a 3D printer depend on the printer itself and its characteristics and capabilities [1]. At the same time, various factors that affect the printing process itself and the quality of the printed model. In this paper, the focus is on printers that use solid filaments as a working material [2].

Temperature is basically an important factor that can also affect the printing success of a model. If the temperatures are not set correctly, the model cannot be printed successfully [3]. There are basically two temperatures that need to be set, which are the extruder temperature and the temperature of the platform on which it is printed. Each of these temperatures is significant for the quality and printing capabilities, and the temperature setting directly depends primarily on the material used [4]. Incorrectly set temperature can lead to reduced print quality or even failure of the print.

The aim of this paper is to present the range of heated build plate (substrate, heating bad) and extruder temperatures for different materials and to analyze the impact of temperature on the printed model. In this case, the problems of both extruder and heated build plate temperatures in the case of Fused Deposition Modeling (FDM) i.e. Fused Filament Fabrication (FFF) 3D printers were analyzed.

2. FUSED DEPOSITION MODELING (FDM) OR FUSED FILAMENT FABRICATION (FFF)

When it comes to Fused Deposition Modeling (FDM) or Fused Filament Fabrication (FFF) 3D printers, it is important to note that these terms can be said to be the same technology, just two different terms [5]. Figure 1 shows the principle and basic elements of this type of printer. Generally, in this case, there is a filament, or plastic, that is drawn into the extruder, where the plastic is melted and then deposited in layers on the heated build plate.

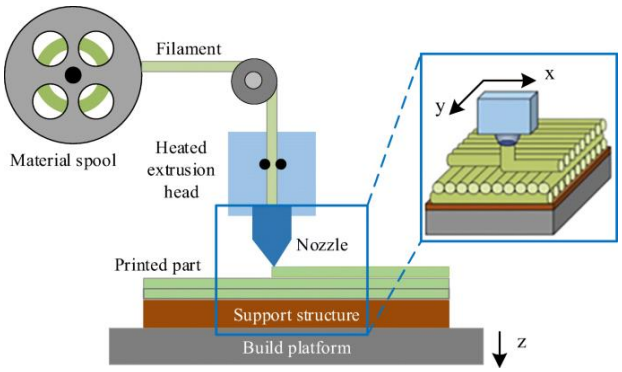

Figure 1. Simplified schematic of a 3D printer [6]

When it comes to heating plastic, which is the topic of this paper, and the elements that are heated, a representation of these elements is shown in Figure 2. In this case, heating is done specifically by two elements. The first element is the extruder, which is the element that has the task of heating and converting the plastic, or filament, from a solid to a semi-solid state. That is, the melted filament allows it to be applied to each layer and to be connected to it. Generally, the filament is initially applied to the heated build plate. The heated build plate is the second element that is heated. The model itself is formed on the heated build plate.

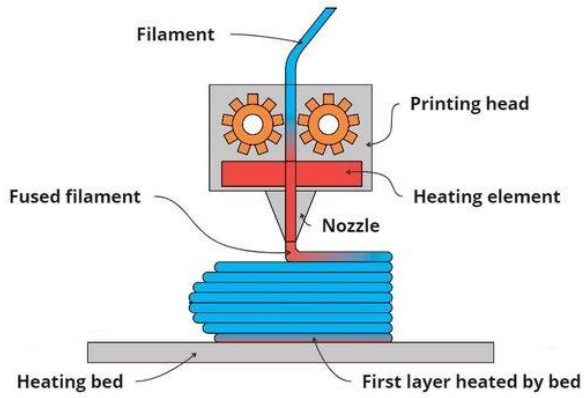

Figure 2. View of heated elements [7]

3. INFLUENCE OF TEMPERATURE ON THE PRINTED MODEL

The effect of temperature has a significant impact on the quality of the model's printing. Due to an increase or decrease in the extruder temperature, significant differences in the quality of the print itself can occur [8]. The simplest example of the difference in extruder temperature is shown in Figure 3. This example shows a model that is half printed with an extruder temperature of 230oC while the other half of the model is printed at a temperature of 220oC. In this case, it is noticeable how much the quality of the printing of the model's surface differs.

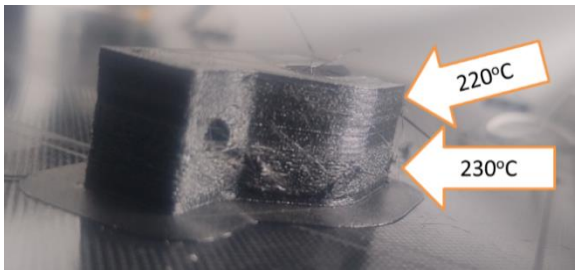

Figure 3. Difference in model print quality at two different extruder temperatures

If we look at a larger group of extruder temperature values, as shown in Figure 4, a clear difference in how much it means to optimize temperature values is noticeable. Sometimes, it is not only necessary to lower the temperature to obtain a quality printed model, but it is also not necessary to simply increase the temperature because it can also lead to a deterioration in print quality.

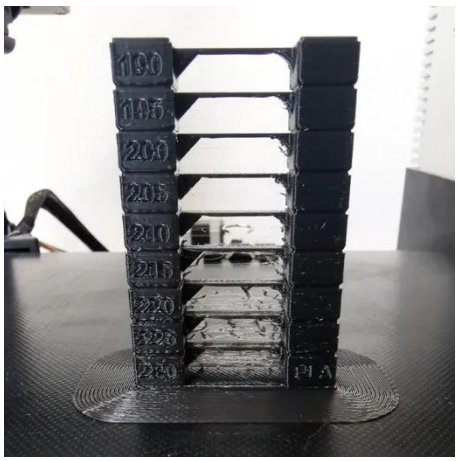

Figure 4. Difference in model print quality at two different extruder temperatures [9]

The temperature of the heated build plate on which the model is printed is also important for the printing process and the successful printing of the model. The heated build plate temperature in 3D printing is very important because it directly affects the adhesion of the first layer, the stability of the model during printing and the prevention of deformation (warping). Again, the heated build plate temperature depends on various factors that will be highlighted below. Figure 5 shows a model where models are printed on a stand with different temperatures. In general, the heated build plate and heated build plate temperature are very important for the correct printing of the model, but also in general for the model to be printed correctly in its entirety.

Figure 5. Printing at different build plate temperatures and the impact on the model [10]

Due to poor adhesion of the heated build plate on which the model is printed, it is possible that the model does not print as required or that the model prints incorrectly. Figure 6 shows an example where poor adhesion of the build plate caused the first layer to peel off, which pulled the entire model. In this case, the extruder still followed the print code, but only material was wasted.

Figure 6. Example of failed printing due to poor model adhesion [11, 12]

Moving the model does not necessarily result in a failed print in the sense that the model does not print, but it can result in incorrect printing due to the movement of a part of the model. Thus, Figure 7 shows a model that was not printed correctly, given that the model was moved.

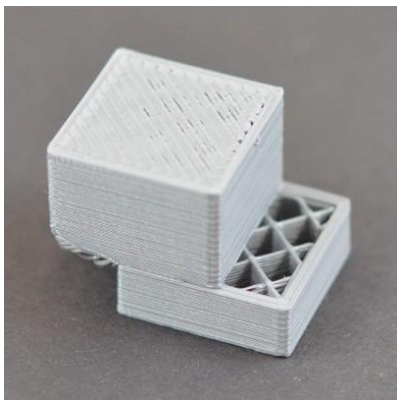

Figure 7. Example of poor printing and inaccurate printing when moving the model [13]

4. EXTRUDER TEMPERATURE AND MATERIAL

The extruder temperature is very important when it comes to the quality of a model. The extruder temperature certainly depends on the material used, each material has its own range in which the extruder temperature needs to be. The extruder temperature basically affects the melted material, if the temperature is set correctly, it ensures that it melts and flows evenly. The extruder temperature also has an impact on the cohesion and adhesion of the layers, so that the appropriate temperature allows the layers to stick well to each other. However, the choice of extruder temperature, in addition to the material itself, which has a

defined range in which the temperature needs to be, also depends on:

- The filament manufacturer, despite the fact that manufacturers of the same material define different temperature ranges;
- The nozzle diameter is also important, a wider nozzle (e.g. 0.6mm or 0.8mm) requires a higher temperature, because more material passes through it;
- The type or material from which the nozzle is made, e.g. metal nozzles require a higher temperature than brass nozzles;
- Printing speed, in the case of a higher printing speed, a higher extruder temperature is also required, while a lower extruder temperature can be used for slower printing;
- Cooling (fan cooling) so if more intensive cooling (fan) is used, the extruder temperature must be slightly higher to compensate for heat loss;
- If the filament is wet, then a higher temperature is often used, but care must be taken to avoid the opposite effect [14-16].

Thus, it is necessary to choose the optimal temperature to obtain the required model. However, depending on other parameters, some outcome may occur if the temperature is too low or too high [16-18]. If the extruder temperature is too low, it can lead to:

- Poor filament flow (under-extrusion),
- Poor layer adhesion (delamination),
- Rough or incomplete parts due to insufficiently melted layers and layers not forming well.

However, if the extruder temperature is too high, it can lead to:

- Filament leakage (stringing), i.e. the appearance of threads because excess material leaks from the nozzle,
- Damage or “burning” of the material or the appearance of bubbles,
- Distorted shape due to the material being too melted and spilling,
- Deformations due to the loss of precision in making the model because the layers are joining unevenly.

Considering all the above and based on this, Figure 8 shows an example of the importance of optimizing temperature in relation to other parameters. Each material has its own printing range, but it is also important to balance it with other parameters. Thus, Figure 7 illustrates the importance of temperature optimization to achieve maximum quality.

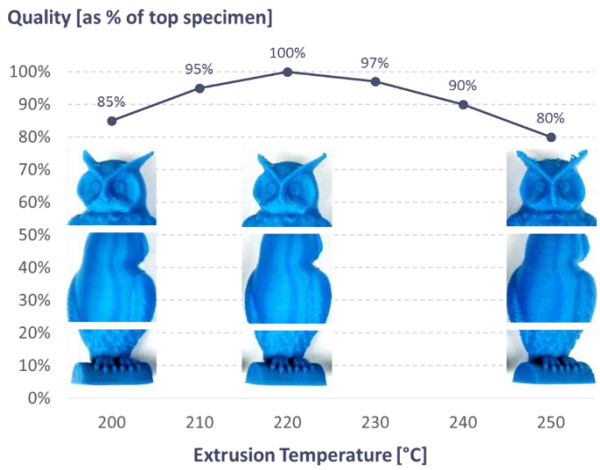

Figure 8. Effect of temperature on model build-up [19]

Since the topic itself is related to materials and temperatures that need to be used, and given the importance of extruder temperature, Table 1 shows extruder temperature values for different types of materials. It is important to note that the range of extruder temperature application is shown for each material, but it is certainly necessary to optimize the temperature according to other factors.

5. STAND TEMPERATURE AND MATERIAL

The heated build plate temperature is a key factor in 3D printing that directly affects the adhesion of the print, the quality of the surface and the success of a successful print. The build plate temperature in 3D printing is very important because it directly affects the adhesion of the first layer, the stability of the model during printing and the prevention of warping [25,26].

Table 1. Extruder temperature range depending on material [20 - 24]

Filament material	Extruder temperature range (°C)
ABS	220 - 250
ABS-GF	240 - 280
ABS-CF	240 - 270
Flexible	225 - 245
PLA	190 - 220
PLA-CF	210 - 240
PLA+ / PLA Pro	200 - 230
HIPS	230 - 245
PETG	220 - 250
PETG HF	230 - 260
PETG-CF	240 - 270
Nylon	220 - 270
Carbon Fiber Filled	200 - 230
Carbon Fiber Reinforced	240 - 280
ASA	235 - 255
ASA-CF	250 - 290
Polycarbonate	260 - 310
Polypropylene	220 - 250
Metal Filled	190 - 220
Wood Filled	190 - 220
PVA	185 - 200
PC	260 - 280
PC FR	260 - 280
TPU	210 - 230
TPU 95A HF	220 - 240
TPU for AMS	220 - 240
TPE	210 - 240
PET CF	260 - 300
PAHT CF	260 - 300
PA6 CF	260 - 300
PA6-GF	260 - 290
PPA-CF	280 - 310
PPS-CF	310 - 340

The heated build plate allows the first layer to adhere firmly to the heated build plate, if the temperature is not set correctly, the model may peel off during printing. This means that the build plate temperature allows for thermal stability at the bottom of the model, which prevents the model from peeling off, edge distortion and poor print accuracy [27].

As in the case of the extruder, there is again a range in which the build plate temperature needs to be adjusted[25-28]. However, which temperature should be chosen depends on several factors, including:

- Type of filament;
- Type of heated build plate where e.g. glass requires higher temperatures while PEI build plate have better adhesion, so lower temperatures can be used;
- Model size and design, where larger models require higher temperatures because they are more prone to peeling, while smaller models can use lower temperatures;
- Cooling speed, where in the case of using a fan, it is preferable to use a higher temperature,
- Printing speed, where a higher printing speed means that the material has less time to bond, so a higher temperature is required;
- Room conditions, where e.g. cold air can have a negative effect on the cooling of the material, so an additional heating temperature of the build plate is required;
- Software settings such as brim, raft or first layer temp can change the required heat at the beginning of the print.

As in the case of the extruder, a certain temperature range is recommended for each material. The problem of too low or too high temperatures can also occur with mixed materials. When the build plate temperature is too low:

- Poor adhesion of the first layer to the substrate;
- Lifting of the model edges (warping);
- Possibility of the model peeling off and shifting during printing;
- Unsuccessful or unstable printing;

- Need for additional adhesives (glue, tape, spray).

When the build plate temperature is too high:

- The lower layers of the model may become too soft and may deform;
- Loss of sharp edge details on the initial layers of the model;
- Slower cooling, which may affect the precision and quality of the upper layers;
- Problems with heat-sensitive materials;
- Possibility of the model sticking too tightly to the heated build plate, making it difficult to remove.

Thus, when setting up a printing model, it is necessary to take into account all the previously mentioned factors, since one of the most important factors of the heated build plate temperature source is the applied material, i.e. filament. Table 2 shows the heated build plate temperature values depending on the material.

Table 2. Heated build plate temperature range depending on material [20 - 24]

Filament material	Build plate temperature range (°C)
ABS	80 - 110
ABS-GF	100 - 110
ABS-CF	100 - 110
Flexible	45 - 60
PLA	45 - 60
PLA-CF	30 - 60
PLA+ / PLA Pro	50 - 60
HIPS	100 - 115
PETG	70 - 90
PETG HF	60 - 80
PETG-CF	60 - 100
Nylon	70 - 110
Carbon Fiber Filled	45 - 60
Carbon Fiber Reinforced	60 - 80
ASA	90 - 110
ASA-CF	90 - 100
Polycarbonate	80 - 120
Polypropylene	85 - 100
Metal Filled	45 - 60
Wood Filled	45 - 60
PVA	45 - 60
	0 – 60 [23]
PC	90 - 110
PC FR	90 - 110
TPU	30 - 60
TPU 95A HF	30 - 45
TPU for AMS	30 - 35
TPE	0 - 110
PET CF	60 - 100
PAHT CF	100 - 120
PA6 CF	100 - 120
PA6-GF	100 - 120
PPA-CF	100 - 120
PPS-CF	100 - 120

6. CONCLUSION

In addition to the fact that 3D printing is a seemingly simple process for creating physical models, it is still necessary to have certain knowledge and skills when setting up the printer in order to print the model correctly. Thus, this paper examines the influence of temperature on the model and the facts that need to be taken into account when determining the temperature setting. In the case of Fused Deposition Modeling (FDM) or Fused Filament Fabrication (FFF) printers, it is necessary to set the extruder temperature or heated build plate temperature. Setting the temperature can be a serious challenge where it is necessary to take into account all other factors that can affect the printing process itself, the quality of the print, as well as the success of printing the model.

Thus, it is necessary, first of all, to respect the temperature range prescribed by the manufacturer. The printing temperatures of the elements themselves when printing the model need to be determined based on experience and taking into account other factors during the printing process itself.

When choosing the printing temperature of the model, it is necessary to choose the optimal temperature in order to obtain the best print quality. If maximum model printing quality is not required, it is not necessary to choose the optimal temperature, but those that are approximate and allow successful printing with lower quality. However, choosing the wrong temperature, i.e. a lower or higher temperature, can lead not only to lower print quality or extremely poor quality, but also to failure in printing the model. Thus, choosing a lower or higher temperature can lead to various phenomena that prevent successful printing of the model, which can only lead to a waste of time, material wear, and damage to the elements on the printer.

The paper itself shows some of the materials and their temperature ranges. So it is necessary to use temperatures within the range that is provided, but with respect and taking into account other factors in order to determine the appropriate temperature for successful printing of the model. In future research, in addition to materials, other factors that can affect the quality and success in printing the model will be taken into account, with a review of this research and the parameters that are listed and analyzed in this paper.

REFERENCES

[1] K. Mencarelli, K. Sisella, L. Puggelli, B. Innocenti, Y. Volpe: Sensitivity Analysis of 3D Printing Parameters on Mechanical Properties of Fused Deposition Modeling-Printed Polylactic Acid Part, Applied Mechanics, Vol. 6, No. 1, pp. 17, 2025.

[2] L. Beníček, M. Vašina, P. Hrbáček: Influence of 3D Printing Conditions on Physical–Mechanical Properties of Polymer Materials. Polymers. Vol. 17, No. 1, pp. 43, 2025.

[3] D. Krapež, M. Jusufagić, M. Obućina, M. Kitek Kuzman, M. Kariž M.: Effect of Filament Material and Printing Temperature on 3D Printing Extrusion Force, Applied Sciences, Vol. 15, No. 4, pp. 2046, 2025.

[4] O. Ulkir, I. Ertugrul, S. Ersoy, B. Yağımlı: The Effects of Printing Temperature on the Mechanical Properties of 3D-Printed Acrylonitrile Butadiene Styrene, Applied Sciences, Vol. 14, No. 8, pp. 3376, 2025.

[5] K. Ruben Bayu, Imaduddin, F. Ariawan, Dody, Ubaidillah, A. Zainal: A review on the fused deposition modeling (FDM) 3D printing: Filament processing, materials, and printing parameters, Open Engineering, Vol. 11, No. 1, pp. 639-649, 2021.

[6] T. S. Tamir, G. Xiong, Q. Fang, X. Dong, Z. Shen, F. Y. Wang: A feedback-based print quality improving strategy for FDM 3D printing: an optimal design approach, The International Journal of Advanced Manufacturing Technology, Vol. 120, pp. 2777–2791, 2022.

[7] K. Erokhin, S. Naumov, V. Ananikov: Defects in 3D Printing and Strategies to Enhance Quality of FFF Additive Manufacturing A Review, Vol. 120, No 11, 2023.

[8] R. Pang, M. K. Lai, K. I. Ismail, T. C. Yap: The Effect of Printing Temperature on Bonding Quality and Tensile Properties of Fused Deposition Modelling 3d-Printed Parts, IOP Conference Series: Materials Science and Engineering, Vol. 1257, pp. 012031, 2022.

[9] Ender 3 PLA Temp Tower, available at: https://cults3d.com/en/3d-model/tool/ender-3-pla-temp-tower-bltouch-brim, accessed: 26.07.2025.

[10] Ender 3 PLA Temp Tower, available at: https://cults3d.com/en/3d-model/tool/ender-3-pla-temp-tower-bltouch-brim, accessed: 05.07.2025.

[11] How to fix 3D printer bed adhesion issues, available at: https://americanfilament.us/blogs/3d-printing-guide/how-to-fix-3d-printer-bed-adhesion-issues?srsltid=AfmBOorbfPSg3nAiGz2iXyuAH60cuBlYus9hubNDhbawXNqIpDp-NsA1, accessed: 07.07.2025.

[12] Bed adhesion problems, available at: https://www.reddit.com/r/BambuLab/comments/10vjbux/bed_adhesion_problems, accessed: 07.07.2025.

[13] How To Overcome The Most Common 3D Printing Failures, available at: https://additive-x.com/blog/how-to-overcome-the-most-common-3d-printing-failures?srsltid=AfmBOooZHzOQTsAYUXxMSBFbRbMjsavBQ4x4vpvvLath44zMl89_Fc8e, accessed: 08.07.2025.

[14] 10 Factors to Consider When Buying an FDM 3D Printer, available at: https://airwolf3d.com/3d-printer-buying-

guide/?srsltid=AfmBOopSZf64k2xt19UPiXMNCFE1r8ttibJzuzuhzzqiAxEqiaqxyfO9, accessed: 08.07.2025.

[15] Temperature Troubleshooting for 3D Printer Filament Extruders, available at: https://www.accextrusion.com/news/temperature-troubleshooting-for-3d-printer-filament-extruders, accessed: 08.07.2025.

[16] 3D Printing Temperature: Effects, Materials and Considerations, available at: https://www.raise3d.com/blog/3d-printing-temperature/#:~:text=If%20the%20temperature%20is%20too,to%20cracks%20or%20part%20failure., accessed: 08.07.2025.

[17] Thermal runaway (low temp extruder), available at: https://forum.prusa3d.com/forum/original-prusa-i3-mk3s-mk3-hardware-firmware-and-software-help/thermal-runaway-low-temp-extruder, accessed: 08.07.2025.

[18] Common print quality problems and solutions, available at: https://wiki.bambulab.com/en/knowledge-sharing/common-print-quality-problem, accessed: 08.07.2025.

[19] Color, Speed, Temperature, & Age: How Do These Factors Influence the 3D Printed Outcome, available at: https://3dprintingindustry.com/news/color-speed-temperature-and-age-how-do-these-factors-influence-the-outcome-57141, accessed: 08.07.2025.

[20] Filament Properties Table, available at: https://www.simplify3d.com/resources/materials-guide/properties-table, accessed: 11.07.2025.

[21] Bambu Filament Guide, available at: https://bambulab.com/en/filament-guide, accessed: 11.07.2025.

[22] Getting the Best Results: Optimal 3D Printing Temperatures for PLA, ABS, PETG, TPU, Nylon, available at: https://3d4create.com/3d-printing-temperatures-for-pla-abs-petg-tpu-nylon, accessed: 12.07.2025.

[23] Nozzle and Filament Temperature Guide, available at: https://www.3docity.com.au/pages/nozzle-and-filament-temperature-guide?srsltid=AfmBOooHT2XKqllnsicPpY5VaGFrhE8Ls9qJQSpmJ4eiWT8GdV1KAGcm, accessed: 12.07.2025.

[24] 3D Printing Temperature for Quality Outputs: Essential Guide, available at: https://www.eufymake.com/blogs/printing-guides/3d-printing-temperature?srsltid=AfmBOorYxBIkFp-ECZitnKZdXlX7RT_RwsLflqze-xWM4a4aV4ifV1cs, accessed: 12.07.2025.

[25] 3D print quality: Mastering 3D printing temperature settings, available at: https://azurefilm.com/2024/07/11/3d-printing-temperature-settings, accessed: 10.07.2025.

[26] How to Prevent Warping in Large 3D Prints, available at: https://kingroon.com/blogs/3d-print-101/how-to-prevent-warping-in-large-3d-prints, accessed: 10.07.2025.

[27] 3DLac - adhesive for 3D printing put to the test with PLA, available at: https://www.voxelfactory.com/blogs/news/3dlac-adhesive-for-3d-printing-put-to-the-test-with-pla, accessed: 10.07.2025.

[28] PLA Not Sticking to Print Bed: 9 Fixes and Causes, available at: https://www.wevolver.com/article/pla-not-sticking-to-bed, accessed: 11.07.2025.

Society of Production Engineering

ICPES 2025

40th INTERNATIONAL CONFERENCE ON PRODUCTION ENGINEERING - SERBIA 2025

DOI: 10.46793/ICPES25.380DJ

University of Nis Faculty of Mechanical Engineering

Nis, Serbia, 18 - 19th September 2025

INFLUENCE OF LAYER HEIGHT ON THE SURFACE ROUGHNESS OF FDM PRINTED PETG PARTS

Strahinja DJUROVIĆ[1]*, Nikolaj VELIKINAC[2], Milan IVKOVIĆ[3], Dragan LAZAREVIĆ[4], Milan MIŠIĆ[1], Bojan STOJČETOVIĆ[1], Martina Petkovic[1]

Orcid: 0000-0002-5629-6221; **Orcid:** 0009-0007-2115-5799; **Orcid:** 0000-0003-3971-7984; **Orcid:** 0000-0001-5106-554X; **Orcid:** 0000-0002-9695-7776; **Orcid:** 0000-0001-7418-6985; **Orcid:** 0000-0003-3210-3250

[1] Academy of applied studies Kosovo and Metohija, Republic of Serbia

[2]Faculty of Science & Engineering, Sorbonne University, French Republic

[3]Faculty of Engineering, University of Kragujevac, Republic of Serbia

[4]Faculty of Technical Sciences, University of Pristina, Republic of Serbia

*Corresponding author: strahinja.djurovic@akademijakm.edu.rs

Abstract: *This paper investigates the influence of layer height, one of the key parameters in Fused Deposition Modeling (FDM) 3D printing, on the surface roughness of parts manufactured using PETG (Polyethylene Terephthalate Glycol) material. Specimens were printed with different layer heights (0.1 mm, 0.2 mm, and 0.3 mm) under identical printing conditions to evaluate how this parameter affects surface quality. Surface roughness (Ra) was measured using a profilometer, and the results indicate that increased layer height leads to higher surface roughness values, resulting in a rougher surface finish. The findings highlight the importance of selecting an appropriate layer height to achieve the desired surface quality, particularly in applications where aesthetics or functional surface characteristics are critical. This study contributes to the optimization of PETG 3D printing processes in contexts where surface finish is of particular importance.*

Keywords: *3D printing, Fused Deposition Modeling, PETG, Surface Roughness.*

1. INTRODUCTION

Fused Deposition Modeling (FDM) is one of the most widely used additive manufacturing technologies due to its affordability, simplicity, and versatility in material selection [1]. Among the various thermoplastics used in FDM, Polyethylene Terephthalate Glycol (PETG) has gained significant attention for its excellent balance between mechanical properties and ease of printing. However, one of the main challenges in FDM is achieving a high-quality surface finish, which is critical for both functional and aesthetic applications.

Surface roughness is influenced by multiple process parameters, with layer height being one of the most critical. As the layer height determines the vertical resolution of a print, it directly affects the stair-stepping effect that contributes to surface irregularities. Lower layer heights typically result in smoother surfaces but also increase print time, while higher layer heights reduce production time at the cost of surface quality.

Many researchers have studied the effect of layer height on the surface roughness of PETG materials.

Taqdisillah et al. in their research examined the influence of layer height (0.1–0.3 mm), filling geometry and nozzle temperature on the surface roughness of PETG materials. Using the Taguchi method, it was determined that the height of the layer had a dominant effect on Ra, which ranged between 7.8 and 22.3 µm [2].

Christodoulou et al. studied the dimensional accuracy of parts printed with PETG as a function of layer height and print speed. It was found that layers with a thickness of 0.1 mm give the smallest deviations in dimensions and the least roughness, while 0.3 mm generates larger deviations and higher roughness [3].

Kadhum et al. investigated the effects of different printing parameters on the quality of PETG, PLA and PLA+ materials. PETG showed an average roughness of Ra = 6.4 µm, with the hexagon-shaped infill giving the best results [4].

Barrios and Romero specifically examined how printing parameters affect the surface quality of 3D-printed PETG. They investigated various parameters, including layer height, print temperature, print speed, print acceleration, and flow rate. Their results indicated that flow rate and print acceleration have the most significant impact on surface quality [5].

Akande et al. performed some experiments to optimize the parameters for two responses, dimensional accuracy and surface roughness. They assuemed layer height, fill density and speed of deposition as optimizing parameters. They observed that optimum factor level was different for dimensional accuracy and surface roughness. For good dimensional accuracy, layer height should be high but for low surface roughness, layer height should be low [6].

Anita et al. have analysed the effect of road width, layer height and printing speed on surface roughness of FDM build part using taguchi's technics. Objective of the experiment was to minimize the surface roughness (Ra value). They found out that the interaction between the layer height and speed of printing and, speed of deposition and road width have negligible contribution on surface roughness [7].

P. Vijay et al. conducted an investigation into the impact of orientation on surface roughness. Their findings revealed that as the orientation increases, there is an initial slight rise in surface roughness, followed by a gradual decrease. This nuanced relationship highlights the complexity of how orientation influences the texture of surfaces [8].

Che Mat et al. conducted a detailed study on the impact of layer height on surface roughness in additive manufacturing. Their findings revealed that the smoothest surface achieved a roughness measurement of Ra 4.2. This optimal surface quality was attained with a layer height of 0.1 mm and an infill density of 50%, highlighting the importance of these parameters in enhancing the finish of 3D-printed objects [9].

2. MATERIALS AND EQUIPMENTS

In this work, Solidworks 15x64 edition CAD software was used to model the test specimens. The 3D CAD model was saved as an STL file and imported into Ultimaker Cura 4.11.0 software (Figure 1), where layer heights were varied from 0.1 mm to 0.3 mm, while other parameters were standard.

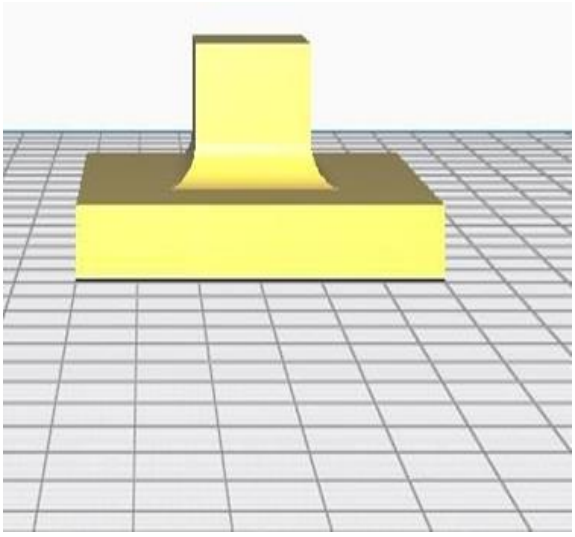

Figure 1. Model in UltimakerCura software

Specimens for surface roughness measurement were printed on low-cost Creality 10-s printer, which is located at Faculty

of Tehnical Science in Kosovska Mitrovica (Figure 2). Characteristics of printer are: Build area of 300x300x400mm, nozzle diameter 0.4, print speed normal60mm/s - max 100mm/s, and with wide range of materials like PLA, PETG, TPU, ABS, But ABS, PETG and PLA are definitely the most represented.

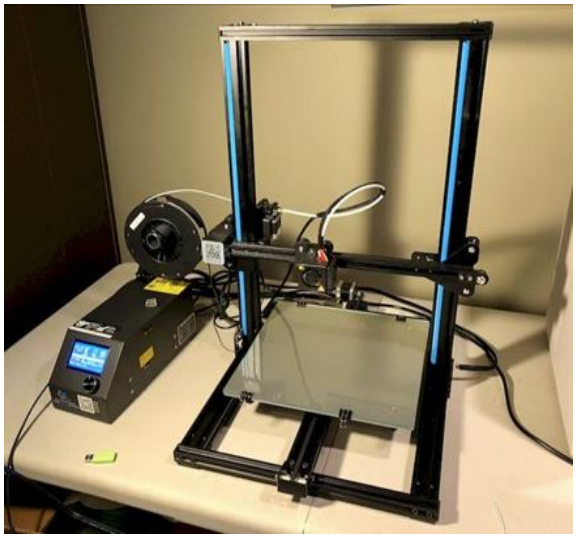

Figure 2. Creality CR 10-s 3D printer

Surface roughness was measured on a computerized measuring device Talysurf-6 (Figure 3) with an ISR-C002 INSIZE measuring device connected to a computer. Basic data about the device: device dimensions are 141x55x40 mm, measuring range 160 µm, measurement accuracy ±10 %, resolution 0.01 µm, movement speed 0.02 —/s, 0.04 —/s, measurement of 21 roughness parameters.

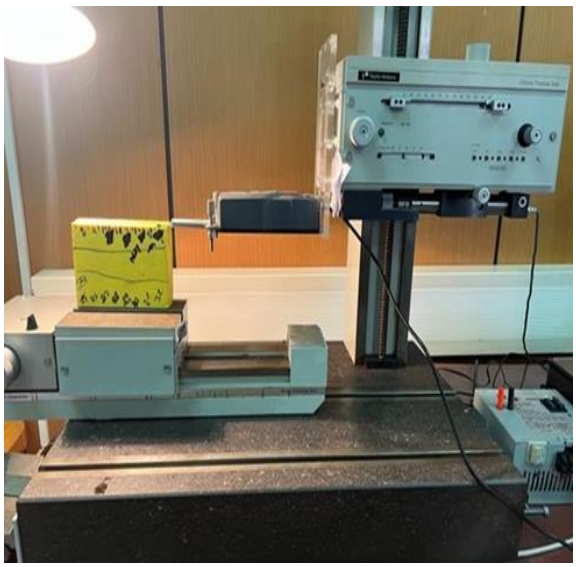

Figure 3. Talysurf-6 measuring system

3. EXPERIMENTAL RESULTS AND ANALYSIS

In Figure 4, we can see the effect of changing the layer height (from 0.1 mm to 0.3 mm), while the other parameters remained standard, on the surface roughness of the specimens made with PETG material.

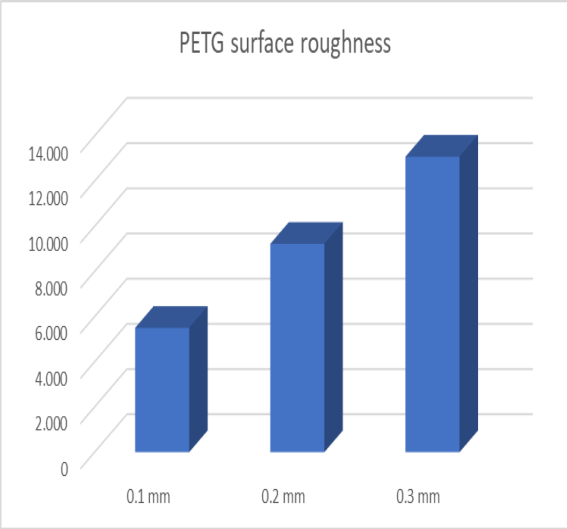

Figure 4. Surface roughness of PETG material

A layer height of 0.1 mm resulted in the lowest surface roughness (Ra=5,503 µm), which indicates a relatively good quality and smoother surface suitable for parts where aesthetic appearance is important.

A layer height of 0.2 mm resulted in a higher surface roughness (Ra=9.221 µm), which is in line with expectations, because higher layers create a step effect between the print layers.

The layer height of 0.3 mm resulted in the highest surface roughness (Ra=13,078 µm), which indicates an obvious decline in the quality of the final surface treatment. These values are characteristic for fast printing and printing with low resolution, where the aesthetic appearance and quality of the surface are sacrificed due to the manufacturing time of the parts.

The tendency for roughness to increase with increasing layer height is expected, and confirms previous research that dealt with these researches. In addition to layer height, surface quality can be affected by many other factors such as printing speed, extruder temperatures, filament quality, cooling conditions, print angle and orientation.

4. CONCLUSION

Based on the conducted analysis, it can be confirmed that the layer height has a significant influence on the surface roughness of the parts made with FDM technology and PETG material. With an increase in the of the layer height, there is a marked increase in the value of the surface roughness Ra, which is a consequence of the step effect that occurs when applying layers of a larger cross-section.

As expected, based on the insight into the literature, the lowest roughness was obtained at a layer height of 0.1 mm, while the highest roughness was obtained at a layer height of 0.3 mm.

In addition to layer height, additional factors such as printing speed, temperature, filament quality and others can have a great impact on the quality of the manufactured parts.

The obtained results can serve as a guideline for the selection of printing parameters, especially in cases where the aesthetic and functional requirements of the surface are critical.

REFERENCES

[1] S. Djurovic, D. Lazarević, Ž. Šarkoćević, M. Blagojević, B. Stojčetović: Fused Deposition Modeling in 3D Printing, in *Conference on advances in science and technology Coast*, 2022.

[2] D. Taqdissillah, A.Z. Muttaqin, M. Darsin, D. Dwilaksana, N. Ilminnafik: The effect of nozzle temperature, infill geometry, layer height and fan speed on roughness surface in PETG filament. *Journal of Mechanical Engineering Science and Technology*, 6(2), 74, (2022).

[3] I.T, Christodoulou, V.E. Alexopoulou, A.P. Markopoulos: Correlation of printing speed and layer height with the geometrical accuracy of FDM-fabricated PETG resolution ribs. *Acta Technica Napocensis – Applied Mathematics, Mechanics, and Engineering*, 65(4S), (2022).

[4] A.H. Kadhum, S. Al-Zubaidi, S. Abdulkareem: Effect of the Infill Patterns on the Mechanical and Surface Characteristics of 3D Printing of PLA, PLA+ and PETG Materials. *ChemEngineering*, *7*(3), 46, (2023).

[5] J.M. Barrios, P.E. Romero: Improvement of surface roughness and hydrophobicity in PETG parts manufactured via fused deposition modeling (FDM): An application in 3D printed self–cleaning parts. *Materials*, *12*(15), 2499, (2019)

[6] S.O. Akande: Dimensional accuracy and surface finish optimization of fused deposition modelling parts using desirability function analysis. *Int. J. Eng. Res. Technol*, *4*(4), 196-202, (2015).

[7] R. Anitha, S. Arunachalam, P. Radhakrishnan: Critical parameters influencing the quality of prototypes in fused deposition modelling. *Journal of materials processing technology*, *118*(1-3), 385-388, (2001).

[8] P. Vijay, P. Danaiah, K.V.D. Rajesh: Critical parameters effecting the rapid prototyping surface finish. *Journal of Mechanical Engineering and Automation*, *1*(1), 17-20, (2011).

[9] M.A. Che Mat, F. R. Ramli, M. R. Alkahari, M.N. Sudin, M.F. Abdollah, S. Mat: Influence of layer thickness and infill design on the surface roughness of PLA, PETG and metal copper materials, *Proceedings of Mechanical Engineering Research*, pp. 64-66, 2020.

Society of Production Engineering

ICPES 2025

40th INTERNATIONAL CONFERENCE ON PRODUCTION ENGINEERING - SERBIA 2025

DOI: 10.46793/ICPES25.384B

University of Nis Faculty of Mechanical Engineering

Nis, Serbia, 18 - 19th September 2025

ADVANCED DESIGN OF 3D-PRINTED COMPONENTS FOR ROBOTIC END-EFFECTORS: A TAGUCHI-BASED MASS AND VOLUME OPTIMIZATION

Dejan BOZIC[1], Mijodrag MILOSEVIC[1], Zeljko SANTOSI[1], Grigor STAMBOLOV[2], Dejan LUKIC[1]*

Orcid: 0009-0009-1095-8101; **Orcid:** 0000-0002-8950-4867; **Orcid:** 0000-0003-3975-0864; **Orcid:** 0000-0002-1566-282X

[1]University of Novi Sad, Faculty of Technical Sciences, Department of Production Engineering, Novi Sad, Serbia

[2]Technical University of Sofia, Faculty of Industrial Technology, Sofia, Bulgaria

*Corresponding author: lukicd@uns.ac.rs

Abstract: *This study investigates the optimization of mass and volume in 3D-printed components featuring internal lattice structures, using the Taguchi method and Fused Deposition Modeling (FDM) technology. A set of three design parameters-unit cell type, cell size, and shell thickness-was systematically varied across three levels using an L9 orthogonal array. The goal was to identify combinations that minimize material usage without compromising structural integrity. Lattice structures were designed and generated using nTop software, which enabled efficient modeling of complex geometries through implicit modeling and field-driven design techniques. Experimental results showed that cell size had the most significant effect on both mass and volume reduction, while the Diamond unit cell type and reduced shell thickness further contributed to performance improvement. Statistical analysis, including signal-to-noise (S/N) ratio evaluation and ANOVA, confirmed the robustness of the identified optimal configuration. The results underscore the potential of combining advanced design tools with structured experimental methods to accelerate material-efficient product development in additive manufacturing.*

Keywords: *robotic arm, 3D scan, Optimization, 3D Printing, Physical adaptation.*

1. INTRODUCTION

This paper presents a multidisciplinary approach to adapting an existing industrial robot for 3D scanning applications, involving the development of a custom-designed interface (gripper) to connect the robot with the scanner. The gripper was specifically engineered for this purpose and fabricated using additive manufacturing (3D printing). The primary aim of the project was to extend the functionality of existing industrial equipment through the integration of modern digital tools and advanced manufacturing technologies.

The second section provides a comprehensive literature review related to industrial robots, additive manufacturing technologies, and CAD model search engines. The third section, titled *Materials and Methods*, outlines the design workflow for the

gripper, introduces the selected robot and scanner, and describes the reverse engineering process. It also details the use of the 3DfindIT platform for identifying similar components, along with the final modified and adapted gripper design.

The fourth section presents the experimental setup and results, including a Taguchi design of experiments followed by ANOVA analysis for systematic parameter evaluation. Finally, the fifth section summarizes the key findings and implications of the study.

2. LITERATURE REVIEW

Industrial robots, defined by ISO 8373:2021 as reprogrammable, multipurpose manipulators controlled along three or more axes and capable of being either fixed or mobile [1], remain a key element in large-scale manufacturing processes [2]. They are widely categorized into six types: Polar, Cylindrical, Cartesian, SCARA, Vertically Articulated, and Parallel-Link robots [3,4]. Their economic efficiency has been demonstrated across various industrial fields, with validation from multiple studies and practical applications [2,5-7]. In the shift toward smart manufacturing, industrial robots are increasingly embedded within digital ecosystems such as Industry 4.0 [8], the Internet of Things (IoT), Cyber-Physical Systems, and Big Data frameworks [9,10]. This integration supports automation, predictive analytics, and real-time process control [11,12]. A critical part of this digital evolution involves 3D digital models, which are central to digital twins used for simulating real-world industrial scenarios [13,14,15]. The progression toward sustainability in robotics depends heavily on modernizing outdated robotic systems. One effective strategy involves replacing obsolete control units with newer ones that enhance motion planning and allow for complex operations [1]. Through IoT connectivity, robots can be monitored and even remotely operated via mobile applications [16]. Old robotic arms, which often remain unused, can be revitalized for simple industrial tasks such as sorting, welding, and assembly [17,18]. In educational settings, they also serve as practical tools for student training in programming, sensor systems, and automation logic [19]. Flexible deployment is becoming increasingly essential in manufacturing environments characterized by mass customization. Reconfigurable manufacturing systems (RMSs) promote adaptability, where robots and machines are repositioned as needed [20]. This evolution encourages the reuse of existing systems and contributes to circular technological practices. A major contributor to robotic adaptability is the design and functionality of end-effectors, particularly grippers. Traditional hard grippers are well suited to structured geometries but are limited when handling irregular shapes [21]. In contrast, soft robotic grippers, actuated by pneumatic systems, cable-driven mechanisms, or shape memory alloys, offer greater versatility and a gentler touch-ideal for fragile or non-uniform objects [9,22]. Robotic arms equipped with 3D scanning systems are instrumental in modern quality control processes, especially in metrology [23]. These systems help improve product accuracy, reduce manufacturing time, and lower operational costs [24-27]. A specialized method proposed by Ma et al. [28] combines a linear laser scanner and a laser cladding nozzle mounted on a robot to restore worn free-form surfaces. Another vision-based solution utilizes multiple cameras to reconstruct 3D point clouds and align them with CAD models, significantly increasing positioning accuracy in dynamic environments [29]. The versatility of industrial robots also enables their use in cutting-edge research. For instance, they have been used to study the effects of cutting parameters on fibber quality during ultrasonic cutting [30]. Additionally, the integration of robotic systems with additive manufacturing techniques like Fused Deposition Modelling (FDM) offers new opportunities for free-form fabrication [31]. This study addresses a unique and practical challenge-how to adapt older articulated

robotic arms to function with handheld 3D scanners. Unlike modern systems, these legacy robots lack direct compatibility with handheld devices, which are typically not intended for robotic integration. However, through a multidisciplinary approach that includes photogrammetry-based 3D digitization, reverse engineering (RE), CAD modelling using SolidWorks, the use of CAD component search engines (3Dfindit), and FDM 3D printing, aviable integration can be achieved.

3. MATERIALS AND METHODS

Figure 1. illustrates the workflow for designing a fully functional 3D-printed connector for robotic grippers. The process begins by querying online CAD platforms such as 3Dfindit (CADENAS GmbH, Augsburg, Germany) [32], which enables access to a wide range of verified 3D models from numerous manufacturer catalogues [33-35]. Searches can be refined using filters like file format, dimensions, category, or manufacturer, and can include inputs such as keywords, images, sketches, or existing CAD files [36].

If a suitable CAD model is located, it is downloaded and assessed for compatibility. In cases where adjustment is needed to suit 3D printing or ensure structural integrity, the model is modified-typically to improve strength-to-weight ratio or to match the unique geometry of a specific 3D scanner [37,38].

Once modified, a design verification stage checks if the gripper satisfies the requirements for integration with the robotic arm and the 3D scanner. If not, further refinements are made. Due to the variability in scanner shapes and materials (most commercial grippers are metal, unlike typical 3D-printed plastic ones), custom jaw modelling is often required. This step combines the scanner's CAD model with the verified gripper to design jaws that ensure a secure and ergonomic grip.

After successful validation, the finalized design is prepared for 3D printing and stored in a shared database for future use or distribution. If any issue is detected during verification, the design returns to the modelling phase for correction.

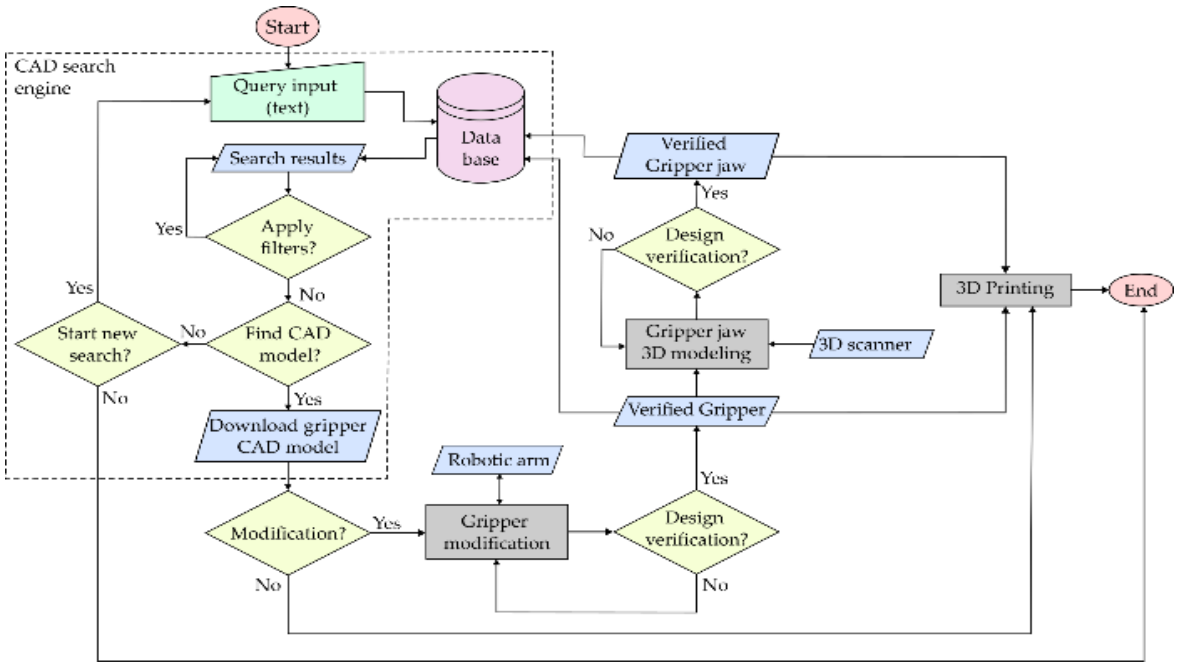

Figure 1. Workflow diagram illustrating the development process of a fully functional 3D-printed connection element [39]

To establish a precise mechanical connection between the Mitsubishi RV-3SDB-S15 robotic

arm (Figure 2a) and the EinScan Pro 2X handheld 3D scanner (Figure 2b), a photogrammetric 3D reconstruction methodology was employed. High-resolution images were captured using a Canon EOS 1200D camera, consistently mounted on a tripod to ensure stability and uniform image acquisition. The robotic arm was documented from five concentric levels to achieve full geometric coverage, while the scanner was photographed using a controlled rotary table setup. In total, 169 images were taken for the robot and 37 for the scanner. Coded markers with known, predefined distances were strategically positioned around both objects to provide spatial scale, enabling accurate 3D reconstruction. These markers were automatically detected by photogrammetry software. The resulting high-fidelity 3D models served as essential geometric references for designing a custom-fit connector, physically linking the robot and scanner. This approach enabled precise mechanical adaptation, overcoming the lack of standardized interface compatibility between the two components.

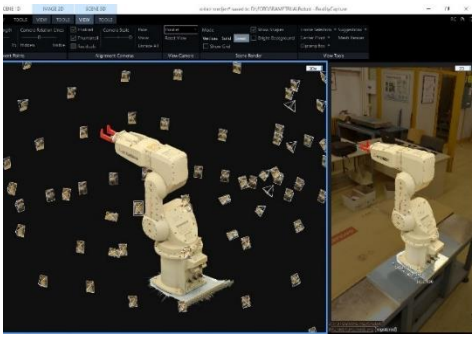

a) Mitsubishi RV-3SDB-S15

b) Shining 3D EinScan Pro 2X optical 3D scanner.

Figure 2. Physical components used for 3D digitization

Reverse engineering was performed utilizing a combination of CAD modeling techniques, based on 3D mesh references of both the robotic arm and the scanner. SolidWorks 2022 was employed to reconstruct geometric features by extracting precise distances and angles directly from the imported mesh data. Dimensionally accurate CAD models were subsequently generated, with particular attention given to the robotic arm's end-effector interface to ensure proper connector assembly and integration (Figure 3).

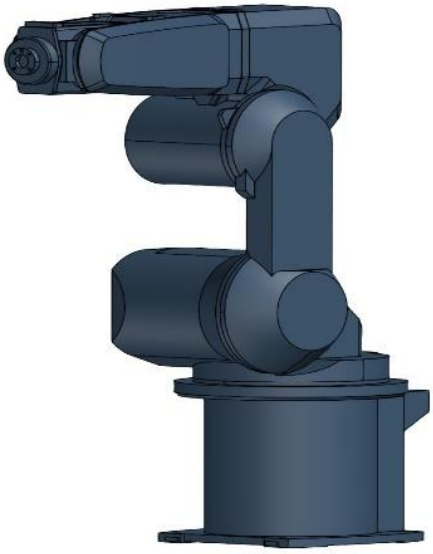

a) Robotic arm

b) Optical 3D scanner

Figure 3. Polygonal mesh models

To access the 3Dfindit platform, users are required to be registered and logged in. Figure 4 illustrates the interface showing the final search results. Initially, the term “gripper” was entered into the search bar (Frame 1), returning approximately 25,000 results. To narrow the selection, filters were applied using the keywords “flexible” and “robot” with the “AND” operator (Frame 2), which reduced the matches

to three. The first result was then selected for detailed review (Frame 3).

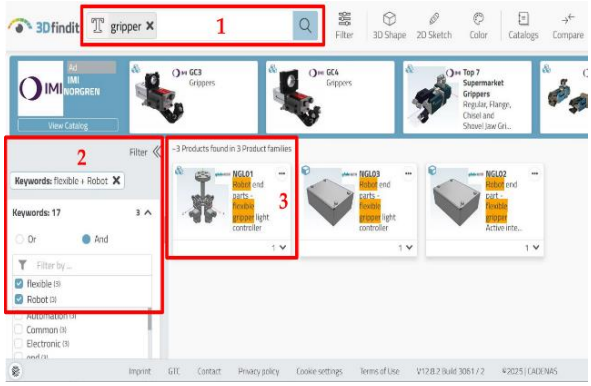

Figure 4. Gripper search results on 3Dfindit after applying filter criteria [39]

The selected gripper model was thoroughly examined; its dimensions and cross-sections were verified, and all available documentation was reviewed. After confirmation, the CAD file was downloaded for subsequent modification. Adjustments included resizing the gripper body to accommodate the fixing screws and removing the original flexible jaws. A new jaw block was then modeled to fit the 3D scanner handle with precision, followed by a Boolean intersection operation. The finalized jaw and complete gripper assembly (Figure 5) incorporated all essential geometric features.

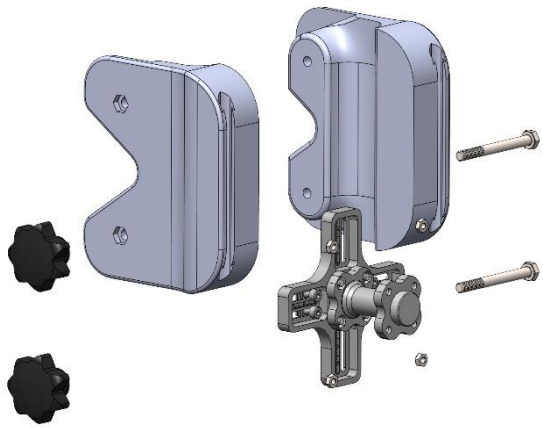

Figure 5. Gripper explode view

4. EXPERIMENTAL RESEARCH

In this study, three key design parameters were selected as control factors for the Taguchi experimental design: unit cell type, cell size, and shell thickness. Each factor was assigned three levels based on practical relevance and variation in structural behavior. The unit cell types (Octet, Diamond, and Hexagonal Honeycomb) represent distinct lattice geometries. Cell sizes of 2 mm, 4 mm, and 6 mm were chosen to evaluate the influence of scale, while shell thicknesses of 1 mm, 2 mm, and 3 mm reflect typical manufacturing boundaries in FDM printing. These combinations form the basis of the L9 orthogonal array used in the experiment (Table 1.).

Table 1. Factors and factor level

Factors	Level 1	Level 2	Level 3
Unit cell (mm)	Octet	Diamond	Hexagonal honeycomb
Cell size (mm)	2	4	6
Shell thickness (mm)	1	2	3

Software nTop was selected for this study due to its advanced capabilities in modeling complex geometries and supporting efficient design workflows, particularly in the context of additive manufacturing. In contrast to traditional CAD platforms, which are often limited when working with intricate lattice structures and organic forms, nTop employs an implicit modeling engine. This enables the generation and manipulation of highly complex structures with enhanced computational efficiency and robustness, regardless of geometry size or resolution. Its field-driven design methodology allows for the integration of performance data-such as stress, temperature, or displacement fields-directly into geometry creation, resulting in functionally optimized and adaptable parts. This is especially important for lattice structures, where performance is highly dependent on localized behavior. Furthermore, nTop supports parametric control and conditional logic, enabling users to build reusable, logic-based workflows that adapt to new design inputs. Additionally, its robust automation features facilitate rapid iteration and exploration of design variants, significantly reducing the time from concept to optimized part. This makes it particularly suitable for

research environments where multiple design configurations need to be evaluated quickly and systematically. The platform's scalability and stability also make it a valuable tool for developing lightweight, performance-driven components across industries such as aerospace, biomedical, and automotive (Figure 6).

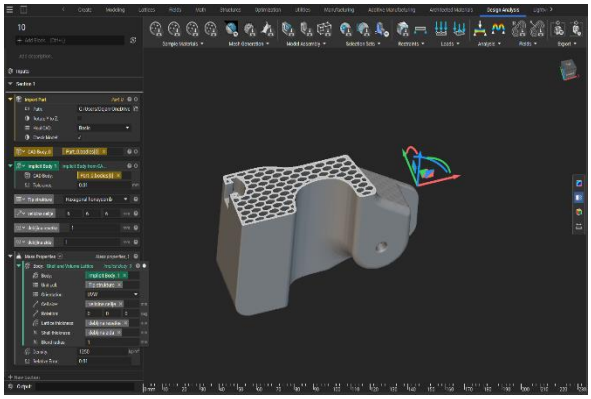

Figure 6. nTop interface

e

5. RESULTS AND DISCUSSION

Figure 7. shows the influence of each factor on the signal-to-noise (S/N) ratio for the response "mass". According to the “smaller is better” Taguchi criterion, higher S/N values indicate lower and more stable mass. The analysis reveals that cell size (CELL SIZE) has the most significant influence on the S/N ratio, followed by unit cell type, while shell thickness shows the least influence. The trend indicates that a larger cell size (6 mm) and a diamond-type unit cell contribute to a lower and more consistent mass. Shell thickness has a minor effect in this case.

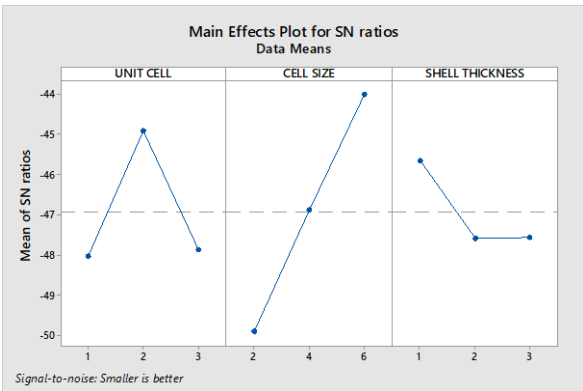

Figure 7. Main Effects Plot for SN ratios

Figure 8. presents the mean mass values for each level of the three input factors. It visually confirms the trends observed in the S/N ratio diagram. The lowest mean mass is achieved when the cell size is large (6 mm), the shell thickness is minimal (1 mm), and the unit cell type is Diamond (level 2). The cell size has the greatest effect on the reduction of part mass, with a clear decreasing trend from 2 mm to 6 mm.

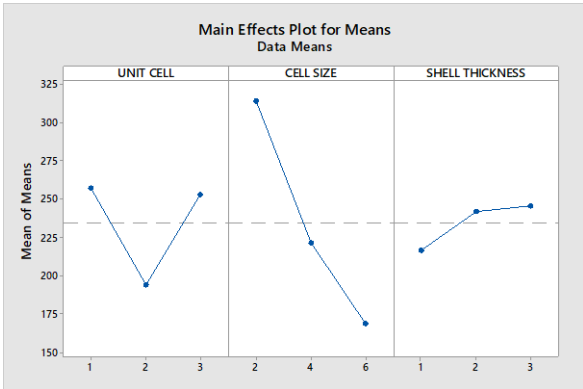

Figure 8. Main Effects Plot for Means

Although the same Taguchi analysis was performed for the response “volume”, the Main Effects Plots for S/N ratios and means for volume were found to be visually identical in shape to those for mass. This is expected, since mass and volume are directly proportional for a given material (PLA) with constant density. Therefore, only the plots for mass are shown, as they are fully representative of the trends in both responses.

Figure 9. assesses the normality of residuals in the regression model. The points approximately follow a straight line, indicating that the residuals are normally distributed. This validates the use of the general linear model and confirms the statistical adequacy of the Taguchi analysis for the response mass.

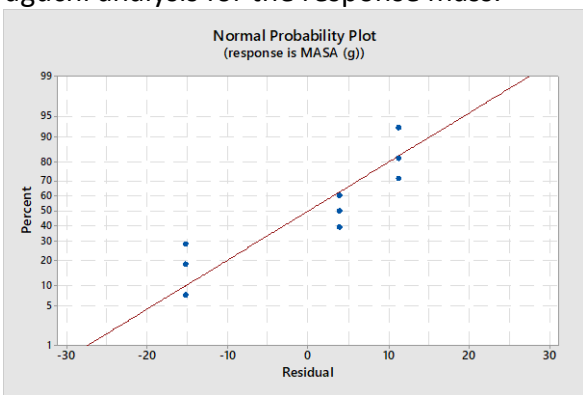

Figure 9. Normal Probability Plot

This diagram shows the residuals plotted against the fitted values from the model. The distribution of points is random, without any clear pattern, which indicates homoscedasticity (constant variance) and the absence of systematic error. This further confirms that the assumptions of the linear model are satisfied.

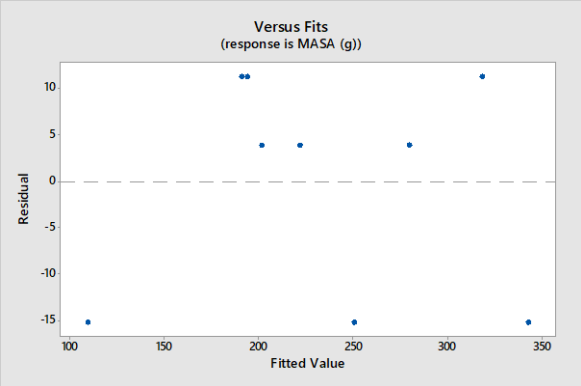

Figure 10. Versus Fits

Residual plots for the "volume" response are not shown because no general linear model was constructed for this response in Minitab. The ANOVA and regression analysis were only performed for the mass variable. As such, residual analysis is only valid and meaningful for mass.

Figure 11 provides a visual representation of the key stages in the additive manufacturing process, specifically utilizing Fused Deposition Modeling (FDM) technology. The image shows a 3D printer in operation, where thermoplastic filament is accurately extruded and deposited layer by layer following a digital model. This layer-by-layer approach enables the fabrication of geometrically complex parts, including intricate internal lattice structures that are often unachievable through traditional manufacturing techniques. The precise control of the extruder's movement ensures accurate material placement, which is essential for achieving the desired dimensional accuracy and mechanical performance of the printed component.

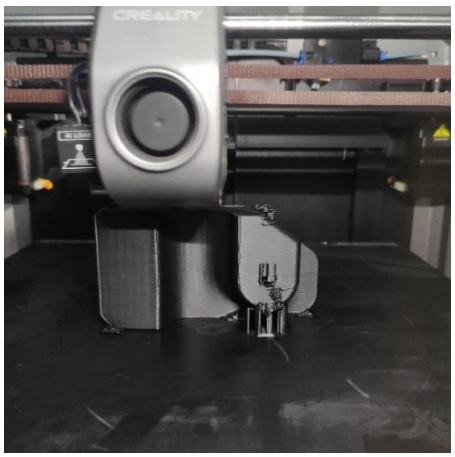

Figure 11. 3D printing process

Figure 12 displays the final output of the 3D printing process-prototype components incorporating optimized lattice structures. These parts reflect the effective application of the Taguchi method, specifically through an L9 orthogonal array, to minimize both mass and volume. The image distinctly illustrates different unit cell types (e.g., Diamond, Octet, and Hexagonal Honeycomb) and emphasizes variations in parameters such as cell size and shell thickness. This visual evidence highlights the capability of FDM technology to fabricate complex internal geometries that enhance material efficiency and contribute to improved overall part performance.

Figure 12. 3D Printing results

The final stage involved assembling the 3D scanner and the modified gripper onto the end-effector of the robotic arm. This integration ensured that all components were properly aligned and mechanically compatible. Figure 13a presents the fully assembled CAD model, serving as a digital twin for virtual validation

and simulation, while Figure 13b depicts the realized physical assembly, confirming the feasibility of the designed connection in real-world conditions.

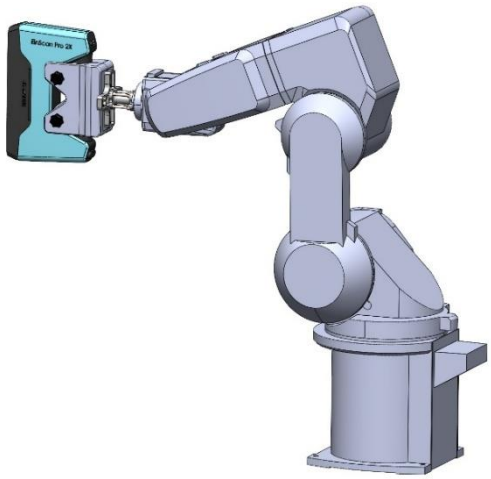

a) Digital Twin

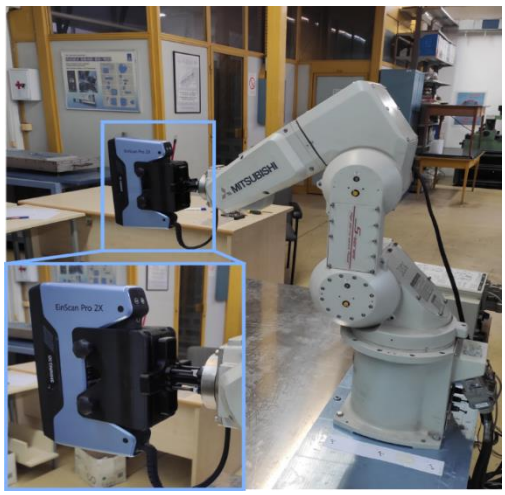

b) Real system

Figure 13. Adopted articulated robotic arm [39]

6. CONCLUSION

This study successfully demonstrated the application of the Taguchi method for optimizing the mass and volume of 3D-printed lattice structures using FDM technology. Among the evaluated parameters, cell size showed the most significant influence on performance. The use of advanced design tools such as nTop proved effective for generating complex, material-efficient geometries. Future research will focus on exploring additional unit cell configurations, incorporating mechanical testing, and integrating new software tools and simulation environments to further enhance optimization workflows and validate functional performance across a broader range of applications.

FUNDING

This research has been supported by the Ministry of Science, Technological Development and Innovation (Contract No. 451-03-137/2025-03/200156) and the Faculty of Technical Sciences, University of Novi Sad through project "Scientific and Artistic Research Work of Researchers in Teaching and Associate Positions at the Faculty of Technical Sciences, University of Novi Sad 2025" (No. 01-50/295. Also, this paper is part of a study in the project "Collaborative systems in the digital industrial environment" No. 142-451-3178/2022-01/01, supported by the Provincial Secretariat for Higher Education and Scientific Research of the Autonomous Province of Vojvodina.)

ACKNOWLEDGEMENT

This research has been supported by the Department of Production Engineering, Faculty of Technical Sciences, University of Novi Sad through project "The future of production engineering".

REFERENCES

[1] ISO 8373:2021; *Robotics—Vocabulary. International Organization for Standardization*: Geneva, Switzerland, 2021.

[2] Yin, X.; He, W.; Wang, J.; Peng, S.; Cao, Y.; Zhang, B. Health State Assessment Based on the Parallel–Serial Belief Rule Base for Industrial Robot Systems. Eng. Appl. Artif. Intell. 2025, 142, 109856. https://doi.org/10.1016/j.engappai.2024.109856.

[3] Singh, G.; Banga, V.K. Robots and Its Types for Industrial Applications. Mater. Today Proc. 2022, 60, 1779–1786. https://doi.org/10.1016/j.matpr.2021.12.426.

[4] The Basics of Industrial Robots|Industrial Robots by Kawasaki Robotics. Available online: https://kawasakirobotics.com/asia-oceania/industrial-robots/ (accessed on 4 January 2025).

[5] Onstein, I.F.; Bjerkeng, M.; Martinsen, K. Automated Tool Trajectory Generation for Robotized Deburring of Cast Parts Based on 3D Scans. Procedia CIRP 2023, 118, 507–512. https://doi.org/10.1016/j.procir.2023.06.087.

[6] Khoat, N.X.; Hoa, C.T.V.; Khoa, N.B.N.; Dung, N.M. Trajectory Planning and Tracking Control for 6-DOF Yaskawa Manipulator Based on Differential Inverse Kinematics. J. Robot. Control (JRC) 2024, 5, 2035–2047. https://doi.org/10.18196/jrc.v5i6.23109.

[7] Ulrich, M.; Steger, C.; Butsch, F.; Liebe, M. Vision-Guided Robot Calibration Using Photogrammetric Methods. ISPRS J. Photogramm. Remote Sens. 2024, 218, 645–662. https://doi.org/10.1016/j.isprsjprs.2024.09.037.

[8] Milošević, M.; Lukić, D.; Borojević, S.; Antić, A.; Đurđev, M. A Cloud-Based Process Planning System in Industry 4.0 Framework. In *Proceedings of the 4th International Conference on the Industry 4.0 Model for Advanced Manufacturing*; Lecture Notes in Mechanical Engineering; Springer: Cham, Switzerland, pp. 202–211, 2019. https://doi.org/10.1007/978-3-030-18180-2_16.

[9] Xu, Y.; Lv, M.; Xu, Q.; Xu, R. Design and Analysis of a Robotic Gripper Mechanism for Fruit Picking. Actuators 2024, 13, 338. https://doi.org/10.3390/act13090338.

[10] Oks, S.J.; Jalowski, M.; Lechner, M.; Mirschberger, S.; Merklein, M.; Vogel-Heuser, B.; Möslein, K.M. Cyber-Physical Systems in the Context of Industry 4.0: A Review, Categorization and Outlook. Inf. Syst. Front. 2024, 26, 1731–1772. https://doi.org/10.1007/s10796-022-10252-x.

[11] Stepanić, P.; Dučić, N.; Stanković, N. Development of Artificial Neural Network Models for Vibration Classification in Machining Process on Brownfield CNC Machining Center. J. Prod. Eng. 2024, 27, 16–20. https://doi.org/10.24867/JPE-2024-02-016.

[12] Hozdić, E.; Makovec, I. Evolution of the Human Role in Manufacturing Systems: On the Route from Digitalization and Cybernation to Cognitization. Appl. Syst. Innov. 2023, 6, 49. https://doi.org/10.3390/asi6020049.

[13] Kamali, M.; Atazadeh, B.; Rajabifard, A.; Chen, Y. Advancements in 3D Digital Model Generation for Digital Twins in Industrial Environments: Knowledge Gaps and Future Directions. Adv. Eng. Inform. 2024, 62, 102929. https://doi.org/10.1016/j.aei.2024.102929.

[14] Chen, K.; Zhao, B.; Zhang, Y.; Zhou, L.; Niu, K.; Jin, X.; Xu, B.; Yuan, Y.; Zheng, Y. Digital Twin-Based Vibration Monitoring of Plant Factory Transplanting Machine. Appl. Sci. 2023, 13, 12162. https://doi.org/10.3390/app132212162.

[15] Wang, Z.; Wang, L.; Martínez-Arellano, G.; Griffin, J.; Sanderson, D.; Ratchev, S. Digital Twin Based Photogrammetry Field-of-View Evaluation and 3D Layout Optimisation for Reconfigurable Manufacturing Systems. J. Manuf. Syst. 2024, 77, 1045–1061. https://doi.org/10.1016/j.jmsy.2024.11.001.

[16] Laman, E.; Maslan, M.N.; Ali, M.M.; Abdullah, L.; Zamri, R.; Syafiq, M.; Mohamed, S.; Zainon, M.; Noorazizi, M.S.; Sudianto, A. Design of an Internet of Things Based Electromagnetic Robotic Arm for Pick and Place Applications. Malays. J. Compos. Sci. Manuf. 2020, 2, 12–20.

[17] Fitria, S.; Nawawi, Z.; Kurnia, R.F.; Yuniarti, D.; Dewi, T. Simulation of Robot Arm System Control Using Fuzzy Logic. Sriwij. Electr. Comput. Eng. J. 2024, 1, 20–29. https://doi.org/10.62420/selco.v1i1.2.

[18] Elfasakhany, A.; Yanez, E.; Baylon, K.; Salgado, R. Design and Development of a Competitive Low-Cost Robot Arm with Four Degrees of Freedom. Mod. Mech. Eng. 2011, 01, 47–55. https://doi.org/10.4236/mme.2011.12007.

[19] Yusoff, Z.M.; Nordin, S.A.; Markom, A.M.; Mohammad, N.N. Wireless Hand Motion Controlled Robotic Arm Using Flex Sensors. Indones. J. Electr. Eng. Comput. Sci. 2023, 29, 133–140. https://doi.org/10.11591/ijeecs.v29.i1.

[20] Arnarson, H. *Intelligent Self- and Reconfigurable Manufacturing System*. Ph.D. Thesis, UiT The Arctic University of Norway, Tromsø, Norway, 2023.

[21] Diller, E.; Sitti, M. Three-Dimensional Programmable Assembly by Untethered Magnetic Robotic Micro-Grippers. Adv. Funct. Mater. 2014, 24, 4397–4404. https://doi.org/10.1002/adfm.201400275.

[22] Milojević, A.; Linß, S.; Ćojbašić, Ž.; Handroos, H. A Novel Simple, Adaptive, and Versatile Soft-Robotic Compliant Two-Finger Gripper With an Inherently Gentle Touch. J. Mech. Robot. 2021, 13, 011015. https://doi.org/10.1115/1.4048752.

[23] Dzedzickis, A.; Subačiūtė-Žemaitienė, J.; Šutinys, E.; Samukaitė-Bubnienė, U.; Bučinskas, V. Advanced Applications of Industrial Robotics: New Trends and Possibilities. Appl. Sci. 2021, 12, 135. https://doi.org/10.3390/app12010135.

[24] Vasiljević, S.; Rajković, D.; Đorđević, M.; Kostić, S.; Stanojević, M. Application of Innovative Mechatronic Systems in Product Design, Development and Production. J. Prod. Eng. 2024, 27, 13–21. https://doi.org/10.24867/jpe-2024-01-013.

[25] Zong, Y.; Liang, J.; Pai, W.; Ye, M.; Ren, M.; Zhao, J.; Tang, Z.; Zhang, J. A High-Efficiency and High-Precision Automatic 3D Scanning System for Industrial Parts Based on a Scanning Path Planning Algorithm. Opt. Lasers Eng. 2022, 158, 107176. https://doi.org/10.1016/j.optlaseng.2022.107176.

[26] Zheng, Y.; Liu, W.; Zhang, Y.; Ding, H.; Li, J.; Lu, Y. Laser In-Situ Measurement in Robotic Machining of Large-Area Complex Parts. Measurement 2025, 241, 115718. https://doi.org/10.1016/j.measurement.2024.115718.

[27] Itadera, S.; Domae, Y. Motion Priority Optimization Framework towards Automated and Teleoperated Robot Cooperation in Industrial Recovery Scenarios. Robot. Auton. Syst. 2025, 184, 104833. https://doi.org/10.1016/j.robot.2024.104833.

[28] Ma, W.; Hu, T.; Zhang, C.; Chen, Q. Adaptive Remanufacturing for Freeform Surface Parts Based on Linear Laser Scanner and Robotic Laser Cladding. Robot. Comput.-Integr. Manuf. 2025, 91, 102855. https://doi.org/10.1016/j.rcim.2024.102855.

[29] Wu, J.; Jiang, H.; Wang, H.; Wu, Q.; Qin, X.; Dong, K. Vision-Based Multi-View Reconstruction for High-Precision Part Positioning in Industrial Robot Machining. Measurement 2025, 242, 116042. https://doi.org/10.1016/j.measurement.2024.116042.

[30] Gu Kim, H.; Hwa Hong, T.; Kim, D.; Hyeon Kim, S. An Experimental Study of Ultrasonic-Knife Cutting for a Woven Carbon Fiber Preform by an Industrial Robot. Manuf. Lett. 2024, 41, 581–587. https://doi.org/10.1016/j.mfglet.2024.09.074.

[31] Toshev, R.; Bengs, D.; Helo, P.; Zamora, M. Advancing Free-Form Fabrication: Industrial Robots' Role in Additive Manufacturing of Thermoplastics. Procedia Comput. Sci. 2024, 232, 3131–3140. https://doi.org/10.1016/j.procs.2024.02.129.

[32] CAD Content Platform for Engineers, Architects, Purchasers. Available online: https://www.3dfindit.com/en/ (accessed on 15 December 2024).

[33] 3D Models and Modelling Software|MacOdrum Library. Available online: https://library.carleton.ca/services/3d-printing/3d-models-and-modelling-software (accessed on 10 January 2025).

[34] 3D Models Search Engines in 2024—Asseter. Available online: https://asseter.ai/3d-models-search-engines-in-2024/ (accessed on 10 January 2025).

[35] 7 Best Search Engines for 3d Printing Models. Available online: https://www.3ddrucklife.de/post/7-best-search-engines-for-3d-printing-models-stl-finder?srsltid=AfmBOoqasBLO9oMsiNokwx2T_uvyL1f2gU2rQsSOU6rttVIAZus7Z2hw (accessed on 10 January 2025).

[36] Get Started With 3Dfindit. Available online: https://www.3dfindit.com/en/engiclopedia/et-started-with-3-dfindit (accessed on 10 January 2025).

[37] Perak, V. Influence of infill density and number of layers on mechanical properties of 3D printed pla and abs sandwich. *Adv. Eng. Lett.* **2024**, *3*, 154–163.

[38] Hozdić, E. Characterization and Comparative Analysis of Mechanical Parameters of FDM- and SLA-Printed ABS Materials. *Appl. Sci.* **2024**, *14*, 649. https://doi.org/10.3390/app14020649.

Society of Production Engineering

ICPES 2025

40th INTERNATIONAL CONFERENCE ON PRODUCTION ENGINEERING - SERBIA 2025

DOI: 10.46793/ICPES25.397M

University of Nis Faculty of Mechanical Engineering

Nis, Serbia, 18 - 19th September 2025

EXPERIMENTAL EVALUATION OF TENSILE PROPERTIES OF 3D-PRINTED PLA THREADS

Miroslav MIJAJLOVIĆ[1*], Gordana JOVIĆ[2], Aleksandar TRAJKOVIĆ[1], Miloš MADIĆ[1], Jovan ARANĐELOVIĆ[1], Nikola KORUNOVIĆ[1]

Orcid: 0000-0001-9185-8296; **Orcid:** 0009-0006-1390-8167; **Orcid:** 0000-0002-2310-2590; **Orcid:** 0000-0001-9653-4119; **Orcid:** 0000-0002-9103-9300;

[1]University of Niš, Faculty of Mechanical Engineering in Niš, Niš, Serbia

[2]The Academy of Applied Technical and Preschool Studies, Niš, Serbia

*Corresponding author: miroslav.mijajlovic@masfak.ni.ac.rs

Abstract: *This study presents an experimental investigation into the tensile behavior of threads and specimens fabricated using polylactic acid (PLA) filament via fused deposition modeling (FDM). While tensile properties of bulk PLA samples and structural components have been widely explored, the mechanical performance of isolated, stand-alone printed threads remains underreported. Such analysis is vital given that the integrity of thin structural surfaces is heavily dependent on the strength and stability of their embedded threads. To investigate this topic, PLA threads were printed using controlled parameters and subjected to standardized tensile testing. Key mechanical properties, including ultimate tensile strength, elongation at break, number of threads and Young's modulus, were determined, compared and discussed. These results provide a foundation for optimizing printing procedures and techniques towards adaptive printing.*

Keywords: *Tensile Properties, PLA, Threads.*

1. INTRODUCTION

Tensile testing represents a fundamental and well-established technique for characterizing the mechanical properties of engineering materials and structural elements. The tensile-derived parameters, such as yield strength, ultimate tensile strength, elastic modulus, and strain, serve as a reliable foundation for extrapolating other material behaviors and for optimizing structural performance within specific geometrical and loading contexts. Tensile characterization of polylactic acid (PLA), a widely utilized biodegradable thermoplastic in additive manufacturing, is typically conducted in accordance with standardized protocols such as ASTM D638 [1] and ISO 527-1 [2]. Specimens are fabricated via fused deposition modeling (FDM) and subsequently subjected to uniaxial tensile loading until mechanical failure. This methodology enables the quantification of critical parameters, including ultimate tensile strength, elastic modulus, and elongation at break [3, 4]. The resulting mechanical behavior is highly dependent on process variables such as layer height, raster orientation, and infill density, which affect interlayer adhesion and internal microstructure. Tensile testing serves

as a foundational tool for optimizing printing conditions in structural/functional applications.

In recent studies, the tensile behavior of PLA has been extensively investigated under differing conditions. Poddar and Sarangi assessed how extrusion parameters influence the tensile strength of PLA filaments, applying Taguchi and ANOVA methodologies to quantify effects of temperature [5]. Complementarily, Domerg et al. examined the impact of ambient aging and specimen geometry on 3D-printed PLA, demonstrating notable variations in ductility and fracture response due to morphological and temporal factors [6]. Stojković and Turudija review how fiber type and thread overall, alignment, and printing conditions critically affect the tensile and structural performance of carbon fiber reinforced PLA composites fabricated via FFF [7]. Alparslan et al. demonstrated that PLA specimens printed via FDM with a 0.15 mm layer thickness and hexagonal infill showed optimal tensile strength, while increased layer height led to reduced strength and ductility [8].

2. SPECIMEN DESIGN, FABRICATION AND TESTING PROCEDURE

Tensile testing of PLA printed parts is performed according to standardized protocols to ensure accurate evaluation of mechanical properties. Specimens are designed and fabricated via FDM with controlled parameters, then conditioned under ambient conditions prior to mechanical testing. Using a universal testing machine, uniaxial load is applied on test specimens until fracture, while force and elongation data are captured to derive stress-strain behavior. Key metrics, such as tensile strength, modulus, and elongation, are determined, and post-fracture analysis reveal failure modes.

2.1 Determination of tensile properties

The general methodology for evaluating tensile properties is described in ISO 527-1. Specific testing conditions applicable to thin plastic films, defined as materials with a thickness $h \leqslant 1$ mm, are provided in ISO 527-3 [10]. Testing specimens should be strips (type 2), dimensioned as given in Figure 1.

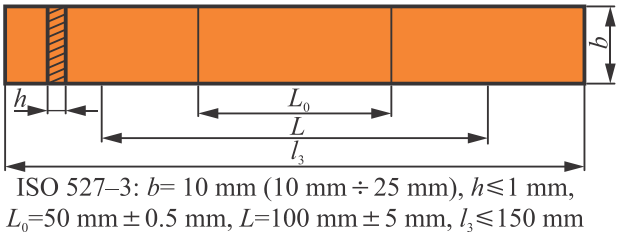

Figure 1. ISO 527-3: Test specimen, shape and dimensions

According to the ISO 527-3, test specimens shall be fabricated either through additive manufacturing or as cutouts, ensuring they remain unpolished, unbonded, and free from macroscopic defects. Each testing protocol shall be conducted on a minimum of five geometrically and materially identical specimens, conforming to the standards and specifications outlined in ISO 527-1.

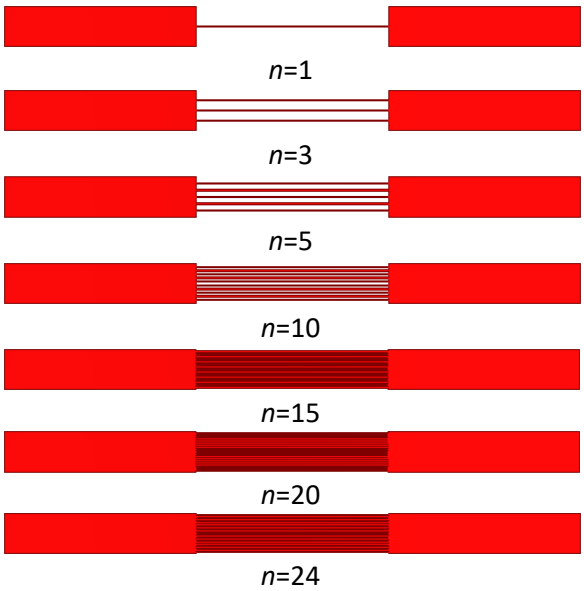

Figure 2. Virtual (CAD) specimens

2.1 CAD model of specimens

Virtual specimens (CAD models) were designed using Autodesk Inventor Academic, modeled as three-dimensional components with geometric parameters corresponding to those illustrated in Figure 1.

To investigate the load-bearing behavior of individual and grouped extruded threads (representing 3D printed lines), the central gauge section of each specimen (L_o) was systematically varied. This region was modeled to incorporate 1, 3, 5, 10, 15, 20, and 24 parallel threads, resulting in the generation of seven distinct specimen types (Figure 2).

2.2 3D printing

All 7 types of the testing specimens (35 specimens in total) are created/printed using the Creality Ender 3 V3 SE 3D printer (Figure 3).

Figure 3. Creality Ender 3 V3 SE 3D printer **Figure 4.** Filament type

The slicing of CAD models was performed using Ultimaker Cura 5.6.0. The printing process was conducted with the 0.4 mm diameter nozzle, at a nozzle temperature of 225 °C and a heated bed temperature of 70°C. The layer height was set to 0.2 mm, and the total height of each specimen corresponded to a single printed layer.

The printing speed was precisely defined for different parts of the model: outer wall, inner wall, and general wall speeds were all set to 90 mm/s, while the initial layer was printed at a reduced speed of 15 mm/s to improve adhesion to the build plate. The overall print speed was set to 180 mm/s. A 100% infill density with a lines infill pattern was used to ensure complete volumetric solidity of the specimens. No support structures were applied, nor were any build plate adhesion methods (skirt, brim, or raft) used. Prior to printing, automatic mesh bed levelling was enabled to ensure consistent layer height across the build surface.

Printing has been performed in two stages:

1. In the initial stage, the threads were printed in a single, uninterrupted pass to ensure continuity and structural integrity. Each thread measured l_3=150 mm in length, with a layer height of h=0.2 mm and a line width of b_1=0.4 mm.

2. During the second stage, the specimen's gripping regions were printed at full scale on both ends, each with a printed length of l=50 mm, a pass height of h=0.4 mm, and thread width b_1=0.4 mm. This additional layer thermally fused with the previously deposited filaments through material overlap, thereby securing their position within the sample geometry. Notably, the central threads, spanning the full length, remained virtually intact and unaffected by the secondary printing operation.

As a fillament material, HP Ultra – PLA is used (Figure 4). HP Ultra – PLA filament is degradable PLA (Polylactic Acid), material co-developed by Creality and BASF as a high-quality, reliable material known for its ease of printing, stable performance, giving high quality of the printed parts. The manufacturers report that HP Ultra PLA has Young's elasticity modulus of E=2970-3050 MPa (in plane), ultimate strength of maximal R_m=75 MPa and ultimate strain (strain at ultimate strength) ε_m=3 % [9].

2.3 Testing machine

The tensile testing procedure shall be conducted using a machine conforming to the requirements outlined in ISO 7500-1 [11] (verification of static uniaxial testing machines) and ISO 9513 [12]. Testing speeds shall be set at one of the following discrete values: v=5/50/100/200/300/500 mm/min, selected based on the material behavior and experimental protocol (in this case v=10 mm/min).

Quasi-static uniaxial tensile tests were carried out with a Shimadzu Table-top AGS-X 10 kN universal testing machine (UTM), which is shown in Figure 5. This UTM is comprised of a rigid frame (stroke distance 1200 mm), crosshead (speed range 0.001-1000 mm/min, with an accuracy of 0.1%), test grips (for holding the specimen), force sensors (load cell with a maximum of 10 kN), and a control unit (up to 1 kHz accuracy).

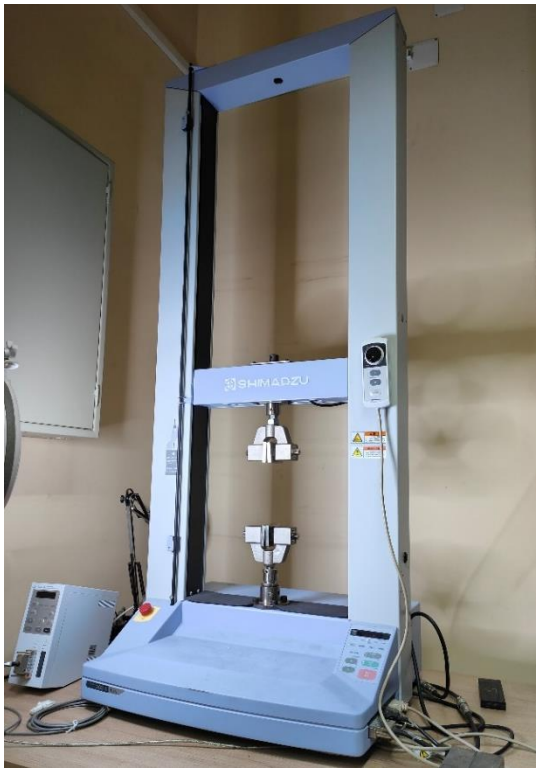

Figure 5. Shimadzu Table-top AGS-X UTM

With the mentioned characteristics this UTM ensures the uniform transfer of force to the test specimen which is fixed with the grips and subjected to pulling (tensile) forces in the axial direction until it breaks. During this process force-stroke points are recorded with the Shimadzu TrapeziumX software with a 100 Hz frequency, based on which the software can produce a force-stroke curve for each tested specimen.

2.4 Data acquisition

Dimensional accuracy at the initial gauge length (L_0=0 mm) is assumed to be within a tolerance of 1%. The data acquisition rate shall be maintained at f=100 Hz, ensuring adequate resolution for both force and strain measurements according to applicable metrological standards.

The use of dumb-bell shaped specimens that exhibit breakage or slippage within the gripping zones is strictly prohibited. A prestrain of $\varepsilon_0 \leq 0.05\%$ shall be applied to all test specimens prior to initiating the tensile test, in order to stabilize the material response and minimize initial slack.

The standardized report for each test shall be labeled in accordance with ISO nomenclature as ISO 527-3/2/50, reflecting the specimen type, test conditions, and measurement parameters.

2.5 Estimation of tension stress, strain and modulus

Since nominal cross section A_n of the fully printed test specimen shall be:

$$A_n = b \cdot h = 10 \cdot 0.2 = 20\,\text{mm}^2, \tag{1}$$

the maximal cross sections of the printed sample sets are 4%, 12%, 20%, 40%, 60%, 80% and 96% of A_n, for n=1, 3, 5, 10, 15, 20 and 24 threads. Since the number of unbroken threads $n(t)$ changes during testing ($n(t) \leqslant n$), the true cross section of the testing sample is:

$$A_{n(t)} = n(t) \cdot b_1 \cdot h. \tag{2}$$

Finally, the engineering stress σ_e [MPa] in the samples is estimated as:

$$\sigma_e = \sigma_{n(t)} = F / A_{n(t)}, \tag{3}$$

where F [N] is the measured tension force.

The engineering strain ε_e [-] is estimated as:

$$\varepsilon_e = \Delta L_0 / L_0, \quad (4)$$

where: L_0 [mm] is the gauge length of the test specimen, ΔL_0 [mm] is the increase of the specimen length between the gauge marks.

The tensile modulus E [MPa] is estimated using linear regression procedure applied on the stress/strain curve in the strain interval $0.0005 \leqslant \varepsilon \leqslant 0.0025$, using the expression:

$$E = \mathrm{d}\sigma_e / \mathrm{d}\varepsilon_e, \quad (5)$$

where $\mathrm{d}\sigma_e/\mathrm{d}\varepsilon_e$ is the slope of a least-squares regression line fit to the part of the stress/strain curve.

The true stress σ and true strain ε are estimated as:

$$\sigma = \sigma_e (1 + \varepsilon_e) \quad (6)$$

$$\varepsilon = \ln(1 + \varepsilon_e) \quad (7)$$

True stress/ strain are used for accurate definition of both elastic and plastic behaviour of materials by considering the actual cross section of the test specimens.

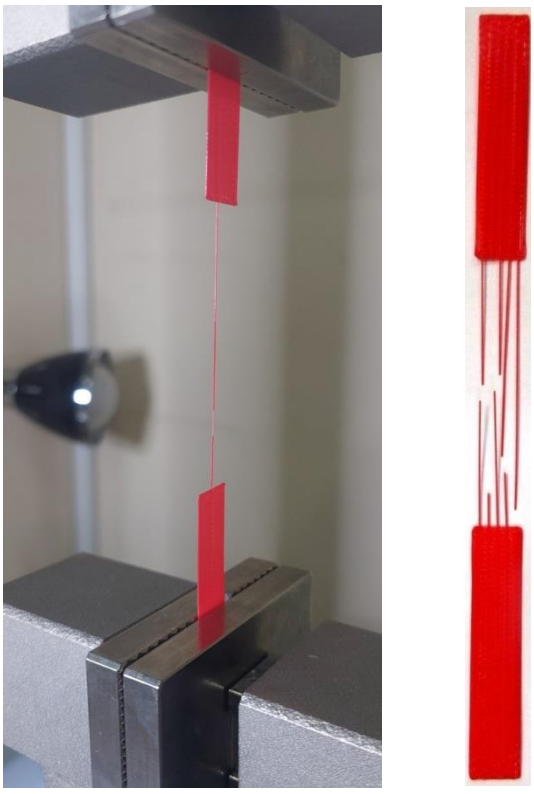

a) b)

Figure 6. Experimental testing: a) test specimen in testing machine, b) broken test specimen

3. RESULTS AND DISCUSSION

All specimens underwent experimental testing under standardized conditions. The same testing protocols, procedures, and measuring equipment were used throughout, ensuring consistency of the results (Figure 6).

All of the samples with n=1 threads exhibit typical stress-strain curve diagrams (Figure 7).

All specimens exhibited stress-strain behavior characteristic of tensile failure, wherein the applied stress reached the expected peak tensile strength prior to specimen fracture. This indicates that failure occurred post-maximum stress, confirming that the structural integrity of the samples was maintained up to the point of ultimate load-bearing capacity.

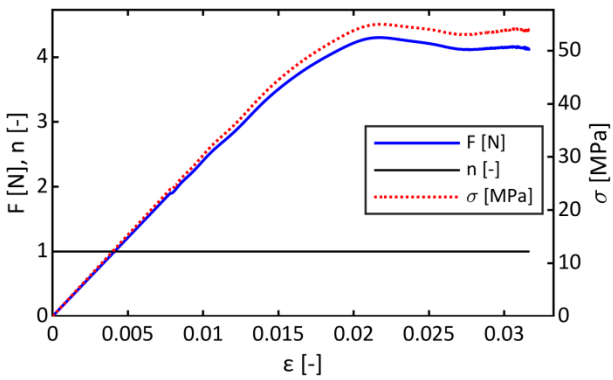

Figure 7. Tension force, number of unbroken treads, and true stress vs. true strain (n1/#1)

The specimen number (#), maximal tension force in the specimen (F_{max}), maximal tension force in the thread(s) ($F_{max'}$), stress at 0.2% strain (R_{p02}), strength (R_m), modulus (E), strain of 0.2% (ε_{p02}), strain at R_m (ε_m), median value (M), and standard deviation (SD) are shown in Table 1. The same nomenclature is used for all testing specimens.

Table 1. Test specimens #1-#5 with n=1 – results

#	F_{max}	$F_{max'}$	R_{p02}	R_m	E	ε_{p02}	ε_m
[-]	[N]	[N/thr]	[MPa]	[MPa]	[MPa]	[-]	[-]
1	4.355	4.355	53.250	55.660	2891	0.020	0.022
2	4.981	4.981	61.779	63.137	3063	0.022	0.024

3	4.970	4.970	58.708	62.994	3166	0.021	0.025
4	4.864	4.864	57.032	61.628	3267	0.019	0.023
5	4.355	4.355	53.045	54.962	3035	0.019	0.022
M:	4.705	4.705	56.763	59.676	3084	0.020	0.023
SD:	0.323	0.323	3.714	4.036	141.689	0.001	0.001

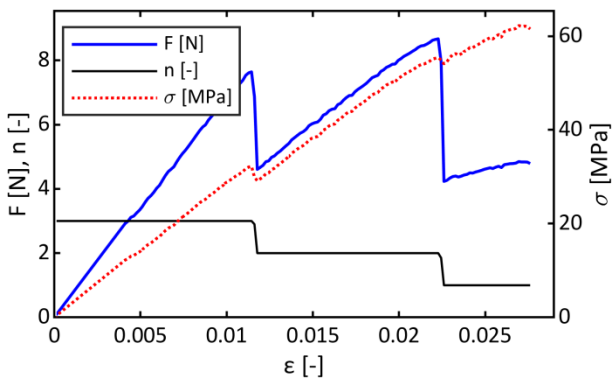

Figure 8. Tension force, number of unbroken treads, and true stress vs. true strain (n3/#3)

Test samples with *n*=3 threads exhibit typical stress-strain curve diagrams (Figures 8 and 9). Thread rupture occurred at random locations across specimens, indicating non-uniform failure initiation.

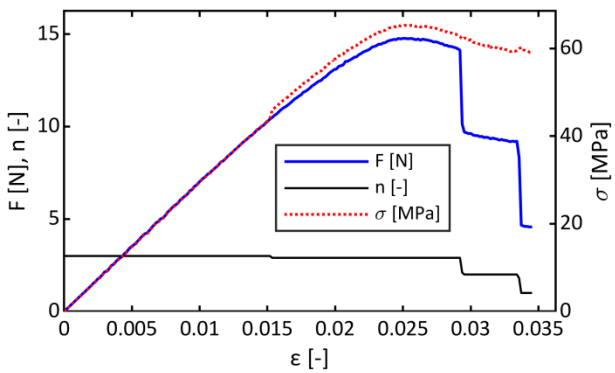

Figure 9. Tension force, number of unbroken treads, and true stress vs. true strain (n3/#4)

Test specimens n3/#1, n3/#2, n3/#3, and n3/#5 exhibit rupture and breakage of at least one thread before reaching the strength of the specimen. The specimen n3/#3 shows rupture of threads before reaching the maximal strength of the specimen; destruction of the treads appears afterwards, one thread after another. The summarized results are shown in the Table 2.

Table 2. Test specimens #1-#5 with *n*=3 – results

#	F_{max}	$F_{max'}$	R_{p02}	R_m	E	ε_{p02}	ε_m
[-]	[N]	[N/thr]	[MPa]	[MPa]	[MPa]	[-]	[-]
1	10.303	5.031	59.703	63.445	3005	0.022	0.026
2	10.516	4.963	63.295	63.375	2912	0.024	0.024
3	8.685	4.849	47.318	62.311	2968	0.018	0.027
4	14.774	5.093	64.075	65.289	2943	0.024	0.025
5	12.037	4.902	61.980	62.819	2982	0.023	0.025
M:	11.263	4.968	59.274	63.448	2962	0.022	0.026
SD:	2.294	0.098	6.886	1.127	35.868	0.002	0.001

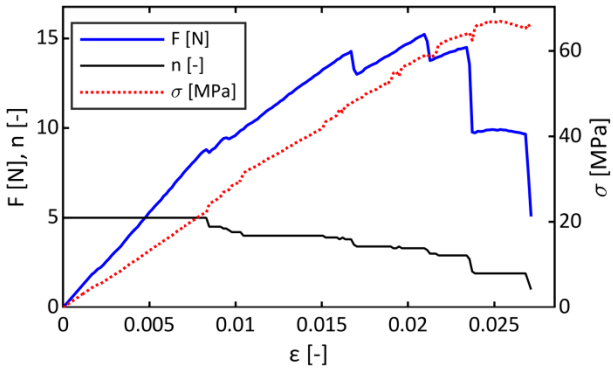

Figure 10. Tension force, number of unbroken treads, and true stress vs. true strain (n5/#4)

All test samples with *n*=5 threads exhibit rupture and breakage of the threads before reaching the strength of the specimen (Figure 10).

The strength of the specimens is comparable to the strength of the previously tested specimens. It is reached in all specimens (having $n(t) \geqslant 2$ treads unbroken at the moment of reaching strength). The summarized results are shown in the Table 3.

Table 3. Test specimens #1-#5 with *n*=5 – results

#	F_{max}	$F_{max'}$	R_{p02}	R_m	E	ε_{p02}	ε_m
[-]	[N]	[N/thr]	[MPa]	[MPa]	[MPa]	[-]	[-]
1	18.636	4.906	60.368	62.975	2712	0.024	0.026
2	23.648	4.951	56.474	63.452	2835	0.022	0.025
3	19.827	4.913	52.983	63.554	2501	0.023	0.034
4	15.246	5.222	66.184	66.948	2749	0.026	0.025
5	19.259	5.104	63.493	65.445	2810	0.025	0.025
M:	19.323	5.019	59.900	64.475	2721	0.024	0.027
SD:	3.002	0.139	5.296	1.673	132.459	0.002	0.004

All test samples with *n*=10 threads also exhibit rupture and breakage some of the threads before reaching the strength of the sample (Figure 11).

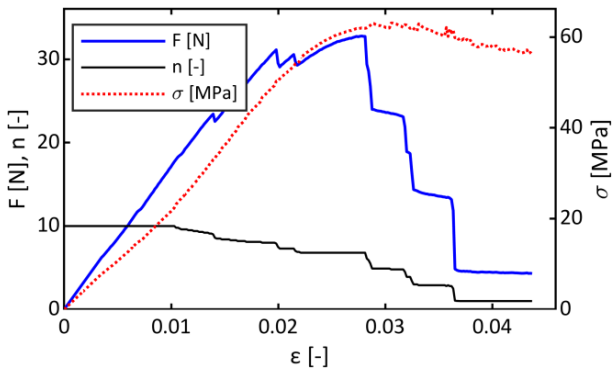

Figure 11. Tension force, number of unbroken treads, and true stress vs. true strain (n10/#2)

The strength of the specimens is comparable to the strength of the previously tested specimens. It is reached in all specimens (having $n(t) \geqslant 5$ unbroken treads at the moment of reaching strength). The summarized results are shown in the Table 4.

All test specimens with *n*=15 threads also exhibit rupture and breakage some of the threads before reaching the strength of the sample (Figures 12).

Table 4. Test specimens #1-#5 with *n*=10 – results

#	F_{max}	$F_{max'}$	R_{p02}	R_m	E	ε_{p02}	ε_m
[-]	[N]	[N/thr]	[MPa]	[MPa]	[MPa]	[-]	[-]
1	43.538	5.052	62.433	65.098	2548	0.027	0.030
2	32.808	4.896	62.229	63.092	2103	0.032	0.031
3	30.573	5.267	61.698	66.713	2042	0.032	0.028
4	34.626	5.124	65.127	65.929	2543	0.028	0.029
5	42.934	4.851	59.984	62.357	2531	0.026	0.028
M:	36.896	5.038	62.294	64.638	2353.4	0.029	0.029
SD:	5.967	0.169	1.853	1.856	257.405	0.003	0.001

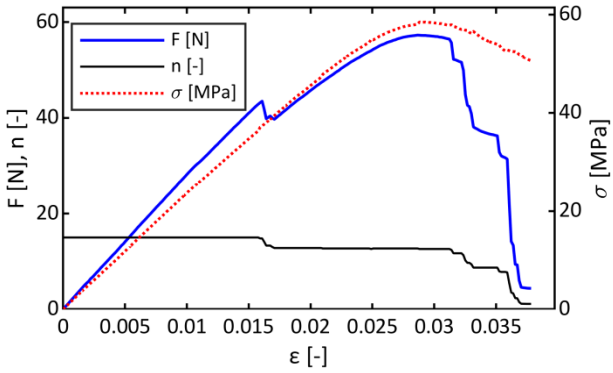

Figure 12. Tension force, number of unbroken treads, and true stress vs. true strain (n15/#1)

The strength of the specimens is comparable to the strength of the previously tested specimens. It is reached in all specimens (having $n(t) \geqslant 7$ unbroken threads at the moment of reaching strength). The summarized results are shown in the Table 5.

Table 5. Test specimens #1-#5 with *n*=15 – results

#	F_{max}	$F_{max'}$	R_{p02}	R_m	E	ε_{p02}	ε_m
[-]	[N]	[N/thr]	[MPa]	[MPa]	[MPa]	[-]	[-]
1	57.298	4.545	54.135	58.471	2372	0.025	0.029
2	54.433	5.092	64.456	65.481	2331	0.030	0.028
3	52.284	4.903	62.167	63.113	2421	0.028	0.029

4	49.046	4.706	57.070	60.501	2389	0.026	0.028
5	48.250	5.070	61.026	65.373	2381	0.028	0.032
M:	52.262	4.863	59.771	62.588	2378	0.027	0.029
SD:	3.759	0.236	4.133	3.070	32.484	0.002	0.002

All test samples containing n=20 threads showed signs of rupture, with several threads breaking prior to the sample reaching its full tensile strength (Figure 13).

The specimens demonstrated strength levels comparable to those observed in previously tested samples. In every case, the maximum strength was achieved with approximately $n(t) \geqslant 10$ threads remaining unbroken at the point of peak load. The summarized results are shown in the Table 6.

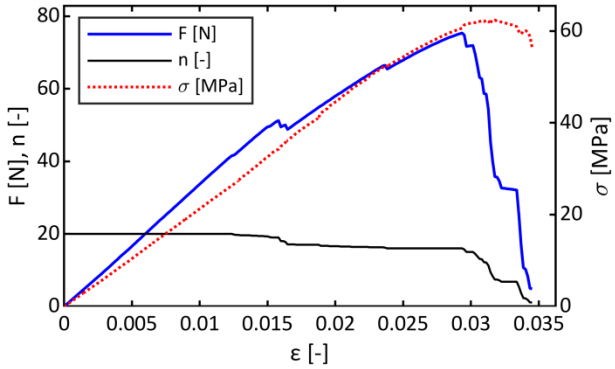

Figure 13. Tension force, number of unbroken treads, and true stress vs. true strain (n20/#5)

Table 6. Test specimens #1-#5 with n=20 – results

#	F_{max}	$F_{max'}$	R_{p02}	R_m	E	ε_{p02}	ε_m
[-]	[N]	[N/thr]	[MPa]	[MPa]	[MPa]	[-]	[-]
1	70.518	5.036	64.971	64.970	2217	0.031	0.032
2	84.162	4.771	56.191	61.475	2128	0.028	0.034
3	67.698	5.090	61.007	65.693	1947	0.033	0.032
4	59.579	4.866	60.320	62.620	2150	0.030	0.029
5	75.458	4.836	62.256	62.407	2156	0.031	0.032
M:	71.483	4.920	60.949	63.433	2119	0.031	0.032
SD:	9.131	0.136	3.199	1.804	101.977	0.002	0.002

All test samples with n=24 threads also exhibit rupture and breakage some of the threads before reaching the strength of the sample (Figures 14).

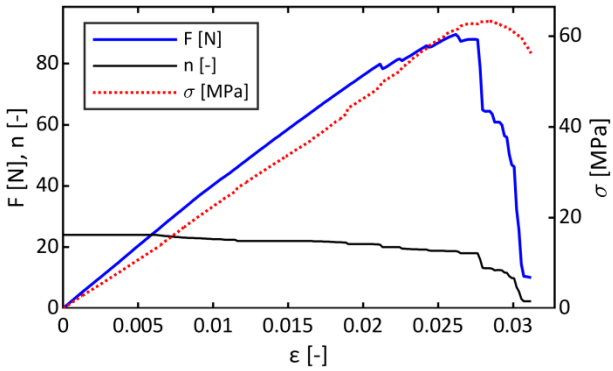

Figure 14. Tension force, number of unbroken treads, and true stress vs. true strain (n24/#2)

The tensile strength achieved in all specimens is consistent with that observed in previously tested samples. At the point of peak tensile load, each specimen retained at least $n(t) \geqslant 12$ unbroken threads, confirming uniform structural integrity across the test set. A summary of the results is presented in Table 7.

Table 7. Test specimens #1-#5 with n=24 – results

#	F_{max}	$F_{max'}$	R_{p02}	R_m	E	ε_{p02}	ε_m
[-]	[N]	[N/thr]	[MPa]	[MPa]	[MPa]	[-]	[-]
1	70.518	5.036	62.832	64.907	1985	0.032	0.031
2	89.695	4.919	60.444	63.257	2135	0.030	0.028
3	100.315	4.996	63.657	64.444	2144	0.032	0.031
4	94.387	4.941	63.129	63.869	2095	0.032	0.034
5	110.739	4.615	56.816	59.504	2128	0.029	0.031
M:	93.131	4.901	61.376	63.196	2097	0.031	0.031
SD:	14.886	0.166	2.831	2.155	65.500	0.001	0.002

The maximum force per thread ($F_{max'}$) is lowest for specimens with n=1 thread (4.705 N) and highest for those with n=10 threads (5.038 N). While the lower value at n=1 is expected, the elevated force observed at n=10 may be attributed to the greater number of unbroken threads present at the point of peak tensile strength.

The elastic modulus (E) exhibits a decreasing trend, with the highest value recorded in specimens containing a single thread (3084 MPa), and the lowest in specimens with 24 threads (2097 MPa). A slight deviation from this trend is observed at n=10 threads (2353 MPa), likely attributed to the increased number of unbroken threads.

The ultimate tensile strength (R_m) was lowest in single-threaded specimens (59.676 MPa) and highest in specimens with ten thread lines (64.638 MPa). Similarly, the 0.2% proof stress (R_{p02}) ranged from 56.763 MPa at n=1 to a maximum of 62.294 MPa at n=10. These increases are again attributable to the higher number of unbroken threads contributing to load-bearing during testing.

The 0.2% strain (ε_{p02}) was lowest in single-threaded specimens (0.020) and highest in specimens with 24 threads (0.031). A similar trend was observed for the strain at maximum tensile strength (ε_m), ranging from ε_m =0.020 at n=1 to a peak of ε_m =0.032 at n=20.

To define tensile properties of the samples, upon completing the full testing sequence for all 35 specimens, the data were aggregated, analyzed, normalized, and statistically refined (Table 8). Given the limited sample size, the Student's t-distribution was adopted as the appropriate statistical model.

Table 8. Estimated tension properties

Confidence: 99% T-Score: 2.728		M	SD	± Margin
$F_{max'}$	[N/thr]	4.916	0.205	0.095
R_{p02}	[MPa]	60.047	4.228	1.950
R_m	[MPa]	63.065	2.695	1.243
E	[MPa]	2531	390.505	180.094
ε_{p02}	[-]	0.026	0.004	0.002
ε_m	[-]	0.028	0.003	0.002

The experimental results indicate that a single PLA 3D-printed filament can sustain a maximum tensile force of 4.916±0.095 N with 99% statistical confidence. The stress-strain behavior does not exhibit a distinct yield point separating elastic and plastic deformation. However, the specimens demonstrate consistent values for 0.2% offset yield strength (R_{p02}), Young's modulus, and elongation at break, suggesting reproducible mechanical performance under tensile loading.

4. CONCLUSION

This research offers a focused tribute to the tensile characteristics of PLA filament, specifically in the form of isolated, printed threads, an aspect often overlooked in broader additive manufacturing research. By steering away from traditional bulk specimens and instead targeting individual thread lines, the study honors the material's micro-scale structural behavior and its contribution to the macro-scale integrity of printed components.

The testing approach was designed not only to evaluate mechanical parameters, such as ultimate tensile strength, elongation, and modulus, but also to highlight the crucial influence of thread survival throughout deformation. Observations reveal that the mechanical reliability of a PLA structure under tensile load is deeply tied to the ability of its embedded threads to remain unbroken up to the point of maximum strength. This insight emphasizes that preserving the continuity and cohesion of as many threads as possible during stress application is not just beneficial, it is essential for ensuring optimal performance in thin-walled or thread-reliant structures.

The experimental results revealed slightly lower overall tensile properties than anticipated for the specified filament manufacturer. While within acceptable variation ranges, this deviation suggests that material performance may be influenced by factors beyond standard specifications, such as batch consistency, thermal history during printing, or subtle variations in filament composition. Further work is should determine

whether these findings are systematic or anomalous, and to assess their impact on the mechanical properties.

Overall, the results lay the groundwork for refining FDM printing strategies aimed at thread-based optimization, offering meaningful implications for adaptive design and high-precision manufacturing where material efficiency and structural dependability converge.

ACKNOWLEDGEMENT

This research was financially supported by the Ministry of Science, Technological Development and Innovation of the Republic of Serbia (Contract No. 451-03-137/2025-03/200109).

REFERENCES

[1] ASTM D638-14 Standard Test Method for Tensile Properties of Plastics, 2022.

[2] ISO 527-1:2019 Plastics – Determination of tensile properties. Part 1: General principles, 2019.

[3] Yeole, Shivraj Narayan: Tensile Testing and Evaluation of 3D Printed PLA Specimens as per ASTM D638 Type-IV Standard, In book: Innovative Design, Analysis and Development Practices in Aerospace and Automotive Engineering (I-DAD 2018), pp.79-95, 2018.

[4] B. Salvatore, R. Torre. Tensile and Compressive Behavior in the Experimental Tests for PLA Specimens Produced via Fused Deposition Modelling Technique, Journal of Composites Science 4, no. 3: 140, 2020.

[5] Poddar, M. K., & Sarangi, S. K. An experimental analysis of poly-lactic acid (PLA) filament manufacturing for the 3D printer using Taguchi and analysis of variance (ANOVA). SSRG International Journal of Mechanical Engineering, 11(3), 1–10, 2024.

[6] Domerg, M., Ostre, B., Belec, L., Berlioz, S., Joliff, Y., & Grunevald, Y. H. Aging effects at room temperature and process parameters on 3D-printed PLA tensile properties. Progress in Additive Manufacturing, 9, 2427–2443, 2024.

[7] Stojković, J.R., Turudija, R. A Review of 3D Printed Carbon Fiber Reinforced PLA Composites in Fused Filament Fabrication. Innovative Mechanical Engineering, Vol. 1, No. 2, pp. 58–79, 2022.

[8] Alparslan, C., Bayraktar, Ş., & Gupta, K. A comparative study on mechanical performance of PLA, ABS, and CF materials fabricated by fused deposition modeling. Facta Universitatis, Series: Mechanical Engineering, 22(1), 1–12, 2024.

[9] https://www.crealitycloud.com, accessed: 07/22/2025.

[10] ISO 527-3:2018 Plastics – Determination of tensile properties – Part 3: Test conditions for films and sheets, 2018.

[11] ISO 7500-1:2018 Metallic materials – Calibration and verification of static uniaxial testing machines Part 1: Tension/compression testing machines – Calibration and verification of the force-measuring system, 2023.

[12] SRPS EN ISO 9513:2014 Metallic materials - Calibration of extensometer systems used in uniaxial testing (ISO 9513:2012, Corrected version 2015-06), 2014.

Society of Production Engineering

ICPES 2025

40th INTERNATIONAL CONFERENCE ON PRODUCTION ENGINEERING - SERBIA 2025

DOI: 10.46793/ICPES25.407V

University of Nis
Faculty of Mechanical Engineering

Nis, Serbia, 18 - 19th September 2025

PERSONALIZED CHRONIC WOUNDS TREATMENT BY APPLICATION OF ADDITIVE TECHNOLOGIES

Nikola VITKOVIĆ[1*], Sanja STOJANOVIĆ[2], Miloš MADIĆ[1], Zoran DAMNJANOVIĆ[2], Razvan PACURAR[3], Filip GORSKI[4], Joaquín Francisco ROCA GONZÁLEZ[5]

Orcid: 0000-0002-2310-2590;

[1]Faculty of Mechanical Engineering, University of Niš, Serbia
[2]Faculty of Medicine, University of Niš, Serbia
[3]Technical University of Cluj-Napoca, Romania
[4]Poznan University of Technology, Poland
[5]Technical University of Cartagena, Spain
*Corresponding author: nikola.vitkovic@masfak.ni.ac.rs

Abstract: *Chronic wounds are complex, non-healing conditions that require individualized therapeutic solutions. This paper presents a digital workflow that integrates advanced wound imaging, AI-based segmentation (DeepSkin), CAD modeling, and additive manufacturing (AM) to produce patient-specific wound care devices. High-precision wound boundary detection and peri-wound segmentation enable the generation of anatomically accurate 3D models, which are converted to STL and fabricated using FDM 3D printing. Personalized dressings and covers conform precisely to wound geometry, supporting moisture control, mechanical protection, and controlled drug release. In addition, porous scaffolds can be designed to mimic extracellular matrix structures and promote tissue regeneration. This personalized approach improves healing outcomes and enables rapid, point-of-care production, reducing treatment time and costs. The proposed workflow demonstrates the potential of combining AI-driven analysis and additive manufacturing for next-generation wound care solutions and lays the foundation for integrating smart sensors and automated clinical production systems.*

Keywords: *chronic wounds, personalized, CAD, image analysis, additive technologies, ROI, scaffolds*

1. INTRODUCTION

Chronic wounds, defined as wounds that do not progress through the standard stages of healing within a predictable time frame, are a significant and growing public health concern. These wounds often arise from underlying conditions such as diabetes mellitus, venous insufficiency, or prolonged pressure and are frequently complicated by infection, inflammation, and tissue necrosis. They affect millions of patients worldwide and place a substantial economic burden on healthcare systems due to their prolonged treatment periods, frequent hospital visits, and the need for specialized care. Despite advances in wound management, conventional treatment methods, such as debridement, topical antimicrobials, and pressure-relieving devices, often prove inadequate, particularly when dealing with extensive wounds, infections, or those located in anatomically complex areas.

These challenges necessitate the exploration of novel, patient-specific therapeutic solutions that can adapt to the unique characteristics of each wound. Recent developments in digital health technologies offer promising pathways toward personalized medicine in wound care. Among these, additive manufacturing (AM) commonly known as 3D printing, stands out as a particularly valuable innovation. AM enables the fabrication of customized medical devices and treatment tools by layering materials based on digital models derived from imaging data. In the context of chronic wound treatment, this capability can be utilized to design and produce wound-specific bandages, drug-eluting patches, and bioengineered scaffolds that facilitate tissue regeneration. This paper investigates the application of AM in chronic wound care, focusing on the integration of advanced imaging, computer-aided design (CAD), and biocompatible material printing to produce highly tailored therapeutic treatments.

2. LITERATURE REVIEW

Chronic wounds represent a failure in the normal healing cascade, often arrested in the inflammatory phase due to ischemia, infection, or immune dysregulation. As highlighted in [1], elevated protease levels and diminished growth factor expression sustain inflammation and obstruct tissue regeneration. Clinically, these wounds manifest as painful, slow-healing ulcerations with high recurrence risk. Conventional treatment methods are often inadequate, lacking the ability to adapt to the wound's unique morphology and environment. In [2], authors emphasized that standard dressings are often ineffective and advocated for personalized approaches that consider wound depth, geometry, and biochemical profile. Accurate wound assessment is critical for individualized care. Modalities such as digital photography, thermography, and 3D surface scanning are employed to capture wound features. More recently, machine learning techniques have improved wound characterization, including margin detection and tissue classification. For example, [3] showed that convolutional neural networks could delineate wound boundaries with over 90% accuracy, enabling the generation of high-fidelity digital wound models. These models form the basis for CAD processes, which drive the production of customized therapeutic devices through additive manufacturing (AM). AM technologies such as Fused Deposition Modelling (FDM), stereolithography (SLA), and inkjet bioprinting allow fabrication of wound dressings tailored to the patient's anatomy. In [4], researchers developed 3D-printed dressings equipped with sensors for monitoring pH, temperature, and moisture, combined with drug reservoirs for targeted release. Materials like polylactic acid (PLA) and polycaprolactone (PCL), blended with hydrogels or antimicrobial agents, enable biocompatible and functional designs. When tissue loss is significant, regenerative scaffolds fabricated via AM can support healing by mimicking the extracellular matrix (ECM). These porous structures are engineered for optimal cell adhesion, proliferation, and angiogenesis. As described in [5], stem cell–laden bioprinted scaffolds using ECM-mimicking hydrogels have shown promise in preclinical models of soft tissue regeneration. The true power of AM emerges when integrated into a digital workflow that includes wound imaging, CAD modeling, and 3D fabrication. This closed-loop process enables rapid prototyping, iterative improvements, and patient-specific interventions. Combined with telemedicine and cloud platforms, such workflows can enhance accessibility to advanced wound care technologies. Although still in early clinical adoption, the integration of imaging, CAD, and AM holds great promise for transforming chronic wound management with personalized, efficient, and biologically informed solutions.

3. METHODOLOGY

The methodology combines AI-driven wound segmentation with the DeepSkin framework and automated pixel-to-millimetre calibration for precise wound geometry extraction. Segmentation masks are converted into 3D point clouds and mesh models, which are then transformed into STL files for custom-fit dressing/cover design. These models are refined in Blender and prepared for FDM 3D printing using Cura [6], ensuring anatomically accurate, patient-specific wound dressings.

3.1 The DeepSkin Framework

Recent advances in artificial intelligence and computer vision have enabled powerful tools for medical image analysis, including wound care. A prominent example is the DeepSkin framework, a deep learning–based system designed for automatic recognition, segmentation, and classification of chronic wounds. By employing convolutional neural networks (CNNs), DeepSkin enhances wound assessment with greater consistency, speed, and objectivity compared to manual methods [6]. Architecturally, DeepSkin often uses encoder-decoder networks such as U-Net or DeepLabV3+, sometimes augmented with attention mechanisms or dense skip connections to preserve spatial detail. It is trained on annotated wound datasets collected under varying imaging conditions, promoting generalization across diverse clinical scenarios [3]. Although multi-class segmentation of tissue types, e.g., necrotic, sloughy, granulating, and epithelial, is still challenging, promising classification results have been achieved in controlled settings. To improve performance, pre-processing steps like color normalization and contrast adjustment are applied, along with data augmentation techniques such as flipping, rotation, and scaling. Post-processing methods, including morphological operations or conditional random fields (CRFs), further refine the wound masks to enhance boundary accuracy. These segmentation outputs can be converted into 3D models using techniques like photogrammetry or structured light, allowing integration with CAD tools. This enables the design of personalized interventions, such as custom-fit dressings or scaffolds fabricated through additive manufacturing (AM). Some experimental studies have combined these constructs with controlled drug-release profiles, pointing toward individualized wound therapies [7]. In addition, DeepSkin supports longitudinal monitoring by quantifying changes in wound area and tissue composition over time, making it a potentially valuable tool for evidence-based clinical decision-making and outcome prediction [8].

3.2 Applications of Additive Manufacturing in Chronic Wound Care

Additive manufacturing (AM) provides a transformative platform for producing highly customized therapeutic solutions for chronic wound management [9-11]. By leveraging patient-specific wound geometry obtained from imaging and segmentation (e.g., via DeepSkin), AM can be used to produce advanced wound care products that conform precisely to the affected area. One major application is the development of custom-fit wound dressings or anatomical sleeves that match the topography of irregular wound surfaces. These dressings can be designed with multilayered structures, integrating materials that regulate moisture, delivering antimicrobial agents, or promote cell proliferation through bioactive coatings. Additionally, AM enables the production of bioresorbable drug-delivery systems, such as patches and microneedle arrays, that can release therapeutic agents in a controlled manner tailored to the wound's healing stage. In more advanced applications, biocompatible scaffolds fabricated using polymers such as PCL, PLA, or gelatine-based hydrogels are used to support tissue regeneration. These scaffolds are engineered to mimic the extracellular matrix (ECM) by tuning porosity, surface texture, and mechanical strength, thus promoting angiogenesis, epithelialization, and collagen deposition in the wound bed.

Moreover, AM allows for the integration of sensor elements (e.g., pH, temperature, moisture) within smart wound dressings, enabling real-time monitoring of wound status and adaptive treatment strategies. These capabilities support the vision of personalized wound care, reducing healing times, minimizing infection risk, and improving patient comfort.

3.3 Custom-Fit Wound Dressings Created Through Additive Manufacturing

Additive manufacturing (AM) has revolutionized chronic wound care by enabling the production of custom-fit dressings tailored to a patient's wound shape. Unlike conventional products, AM uses 3D wound models from imaging tools like DeepSkin to guide the precise deposition of biocompatible materials [12]. This ensures a personalized fit that promotes healing by maintaining moisture, reducing dead space, and conforming to complex anatomical areas like joints [10]. AM also supports multi-material fabrication. Inner layers may incorporate hydrogels infused with antimicrobials or growth factors, while outer layers offer protection against external contaminants [11]. By adjusting parameters such as porosity, infill, and thickness, clinicians can fine-tune mechanical properties. Features like microchannels further support oxygen exchange and fluid drainage. This entire workflow, from imaging to fabrication, can be done on-site, reducing treatment delays and supply issues. AM extends to producing rigid and semi-rigid supports that redistribute pressure in conditions like diabetic foot ulcers (DFUs). Orthoses such as 3D-printed braces or wraps, based on detailed scans, are printed in biocompatible thermoplastics like TPU or PLA, enabling customization of elasticity and support [10]. These supports protect the wound by offloading pressure without creating new points of stress. CAD tools allow integration of complex geometries, such as honeycomb structures, to reduce weight and enhance breathability, with airflow channels aiding thermal and moisture control. Such supports can also include bioactive inner components, like hydrogel or medicated films, for simultaneous wound protection and treatment. This hybrid approach merges mechanical function with therapeutic delivery, enabling localized release of antimicrobial or regenerative agents. A major benefit of AM is its adaptability: as the wound heals, updated models can be reprinted with minimal waste and rapid turnaround. This decentralized, point-of-care production is feasible even in hospitals or clinics using desktop 3D printers, improving access in remote or underserved settings. Clinical evidence highlights improved healing outcomes, patient comfort, and adherence when using personalized AM solutions [10]. As adoption grows, AM holds strong promise for scalable, effective, and patient-specific wound care.

3.4 The workflow for the creation of custom fittings by using FDM printing

The workflow during the preprocessing phase automatically performs a pixel-to-millimetre calibration routine for wound-assessment images that include a plastic ruler (Figure 1). The images are captured with mobile phone cameras using a designated ruler to determine pixel spacing. The general procedure for processing images is described in detail in [12]. The initial images are pre-processed in GIMP, a free software, by rotating the ruler horizontally and cropping the image. The algorithm is:

1. Pre-processes the cropped ruler strip,
2. Extracts the tick marks by adaptive thresholding,
3. Projects the binary image onto the X-axis to obtain a 1-D signal,
4. Detects peaks in that signal to localize tick,
5. Computes the median inter-peak distance to yield pixels per millimetres, and
6. Optionally overlays the detected ticks for visual verification.

To create a custom fit for various ulcers, a workflow for designing the 3D model of the nylon dressing cover was developed. The workflow diagram is shown in the following Figure 2. This diagram presents a step-by-step

workflow for generating custom-fit wound covers. It integrates the DeepSkin deep learning framework and Fused Deposition Modeling (FDM)-based additive manufacturing. The process begins with an image database that serves as a source of chronic wounds images.

Figure 1. The definition of the millimeters lines

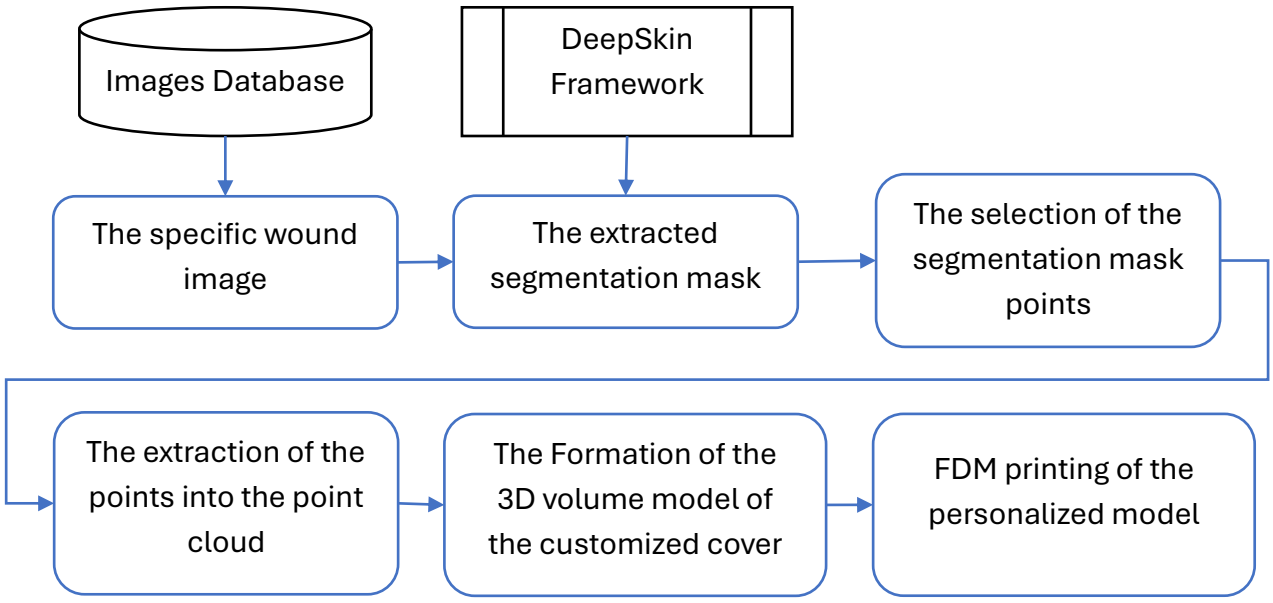

Figure 2. Workflow for Personalized Wound Dressing Cover Design Using DeepSkin and Additive Manufacturing

A specific wound image is selected and processed through the DeepSkin framework, which performs segmentation to isolate the wound region and generate a segmentation mask (Figure 3). The DeepSkin framework application is defined trough several steps:

A. Wound and Peri-Wound Surface Extraction Pipeline - We developed a Python-based pipeline using the DeepSkin framework for automated segmentation and 3D modeling of chronic wounds. The process consists of the following key stages:

B. Image Acquisition and Preprocessing - The input image of the wound is read using OpenCV and converted from BGR to RGB color space to maintain compatibility with visualization and analysis libraries.

C. Segmentation Using DeepSkin - DeepSkin's wound segmentation function is applied to the RGB image, generating a three-channel binary mask that identifies the wound, peri-wound area, and background.

D. Mask Extraction and Visualization - From the segmentation output, individual binary masks for the wound and body surface are extracted. The peri-wound region is then calculated using morphological expansion, and post-processed with an infill operation to ensure completeness. Visualization of each mask overlay on the original image is performed for verification.

E. Wound and Peri-Wound Area Estimation - Using cv2.findContours() and pixel spacing (set to 1/8 mm), the planar area of the wound and peri-wound masks is calculated and converted to real-world square millimetre units.

F. 3D Mesh Generation - The peri-wound mask is converted into a 3D model by turning it into a solid volume. We use the marching cubes method from skimage measure to generate a surface mesh from the volumetric representation of the binary mask. The mesh is scaled based on the real-world pixel spacing

and then exported to STL format using the trimesh lib.

G. Preservation of Real Dimensions - Unlike previous simplified methods, this pipeline ensures that the spatial dimensions of the extracted mesh are consistent with the real wound size by strictly applying calibrated pixel spacing and accounting for extrusion depth.

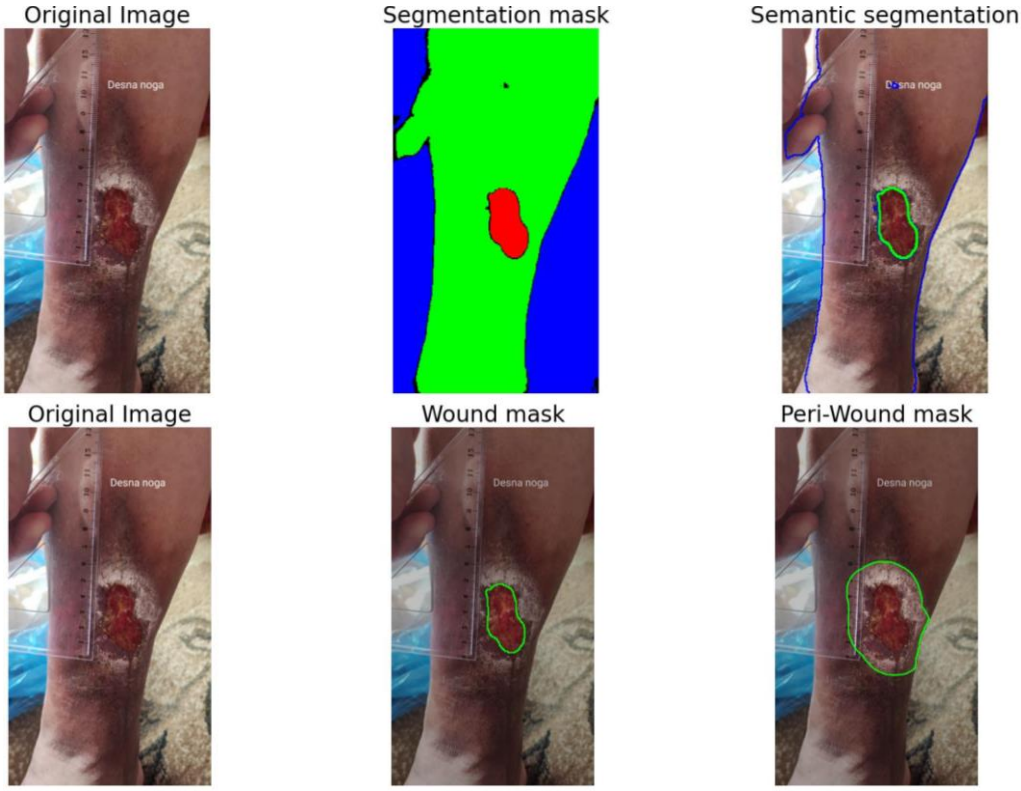

Figure 3. The process of segmentation masks and boundaries creation

In this case, we use a peripheral mask as a basis for the dressing development, to cover a wider wound area. After segmentation, the system allows for selecting relevant mask points that define the boundary, area, and shape of the wound. These points are then extracted and converted into a point cloud and respective mesh, which serves as the foundation for creating a 3D digital model. The point cloud provides an accurate spatial representation of the wound surface, used to generate a 3D volume model that matches the patient's wound and surrounding tissue. This 3D model is designed to conform to the anatomical contours, ensuring an optimal therapeutic fit. The final step in the process is FDM printing of the personalized model using elastomer material (nylon).

The calculated areas are: Wound boundary area: 36532.00 pixels (745.55 mm²); Peri Wound boundary area: 140643.50 pixels (2870.28 mm²). The 3D model designed for FDM was created by converting segmented peri-wound masks into printable geometries. Starting with clinical images, the wound and surrounding tissue were identified using a DeepSkin framework. The output mask was then processed to define both the wound boundaries and the extended peri-wound region. From this binary image, a contour-based approach was used to calculate the surface area and extract spatial information relevant for 3D modeling (Figure 4). The pixel-based area estimates were converted into real-world dimensions using calibrated pixel spacing. Based on the extracted wound geometry, a three-dimensional mesh was generated to represent the shape of the wound site (Figure 4). The mesh was formed by extruding the wound boundary to a set thickness, creating a volumetric shell that could serve as a custom-fit wound dressing. To better conform to

anatomical contours, an elevation profile was applied so that the central area of the wound cover gradually rose relative to the periphery. This design mimics the curvature of biological tissues, supporting therapeutic functions such as pressure distribution and fluid management. The digital mesh was exported in STL format and imported into a 3D modeling environment (Blender Software) for inspection and refinement [13]. In this environment, the model could be smoothed, adjusted, or structurally improved to ensure stability during printing and comfort during clinical use (Figure 4). Once finalized, the model was sliced using computer-aided manufacturing software (Cura, Figure 5), where printing parameters such as layer height, infill, and material type were configured. The resulting G-code was then used to produce the custom wound dressing cover using a medical-grade elastomeric material, Figure 6.

This workflow demonstrates a streamlined process for creating personalized, anatomically accurate wound care solutions, ready for production using low-cost and widely available FDM 3D printing technologies.

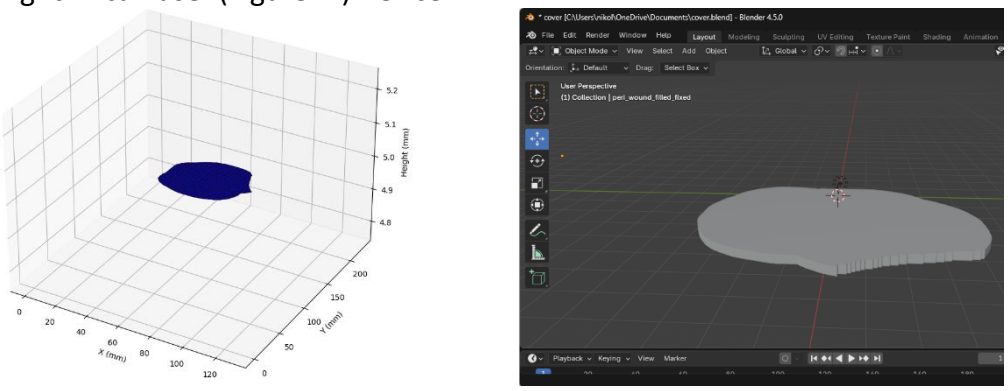

Figure 4. The mesh model of the per-wound segmentation mask (left) and The STL model processed in Blender Software (right)

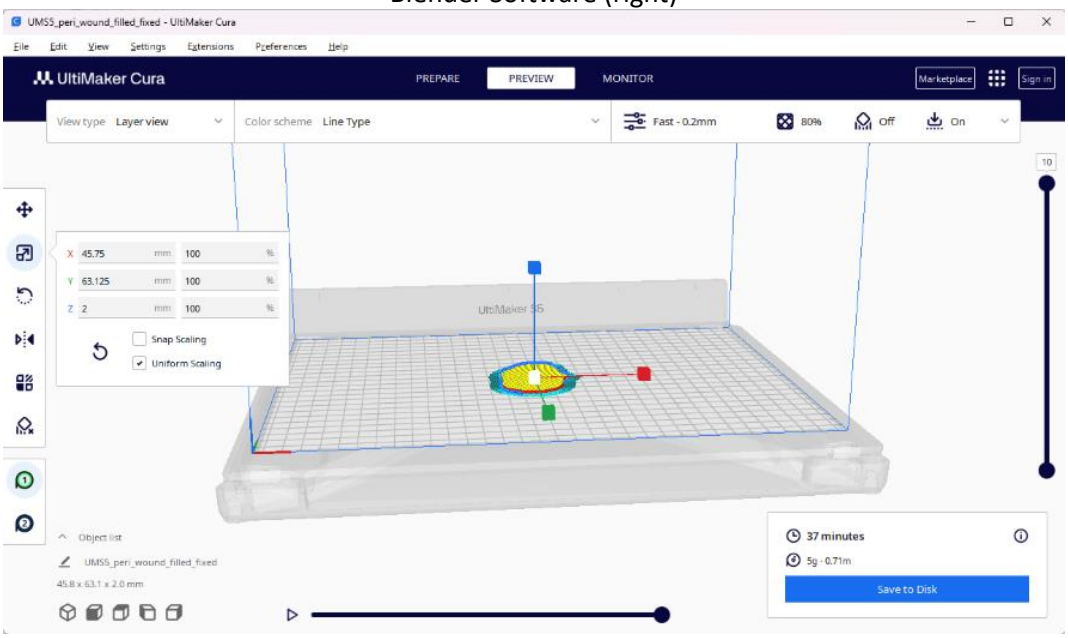

Figure 5. The model processed in Cura Software

Figure 6. The FDM printing process and Physical nylon model of personalized wound dressing cover

4. CONCLUSION

This study outlines a workflow for personalized treatment of chronic wounds using additive manufacturing technologies. By combining advanced imaging, AI-based segmentation (DeepSkin), CAD modeling, FDM 3D printing, and other additive technologies [14], it is possible to create custom-fit wound dressing and structural supports tailored to individual patient anatomy. The methodology ensures geometric accuracy, promotes healing through biomaterial design, and allows for real-time monitoring when paired with smart sensors. The approach shows potential to improve clinical outcomes, shorten healing times, and enhance patient comfort. Future work will focus on clinical validation and expanding capabilities toward automated, on-site wound care production systems.

ACKNOWLEDGMENT

This research was supported by the Science Fund of the Republic of Serbia, program PRISMA, #7617, “Multilevel approach to study chronic wounds based on clinical and biological assessment with development of novel personalized therapeutic approaches using in vitro and in vivo experimental models” – CHRONOWOUND and by the ERASMUS+ Partnerships for cooperation and exchanges of practices (KA220) - “Biomedical Innovations through Digital Transformation of Additive Technologies and Knowledge Exchange - BIOMEDIX” - Project No. 2024-1-LV01-KA220-HED-000255929.

REFERENCES

[1] S. Guo and L. A. DiPietro, “Factors affecting wound healing,” Journal of Dental Research, vol. 89, no. 3, pp. 219–229, 2010. DOI: 10.1177/0022034509359125

[2] R. G. Frykberg and J. Banks, “Challenges in the treatment of chronic wounds,” Advances in Wound Care, vol. 4, no. 9, pp. 560–582, 2015. DOI: 10.1089/wound.2015.0635

[3] N. Curti, C. Zengarini, Y. Merli, E. Marcelli, G. C. Castellani, T. Bianchi, and E. Giampieri, “Automated prediction of Photographic Wound Assessment Tool in chronic wound images,” Journal of Medical Systems, vol. 48, no. 2, pp. 1–10, 2024. DOI: 10.1007/s10916-024-02067-1

[4] P. Mostafalu, A. Tamayol, R. Rahimi et al., “Smart bandage for monitoring and treatment of chronic wounds,” Small, vol. 14, no. 33, art. 1703509, 2018. DOI: 10.1002/smll.201703509

[5] S. V. Murphy and A. Atala, “3D bioprinting of tissues and organs,” Nature Biotechnology, vol. 32, no. 8, pp. 773–785, 2014. DOI: 10.1038/nbt.2958

[6] M. H. Yap, B. Cassidy, N. D. Reeves, J. M. Pappachan, W. D. Gillespie, and R. Goyal, “Deep learning in diabetic foot ulcers detection: A comprehensive evaluation,” Computers in Biology and Medicine, vol. 135, art. 104596,

2021.
DOI: 10.1016/j.compbiomed.2021.104596

[7] P. Mostafalu, W. Lenk, M. R. Dokmeci, B. Ziaie, and A. Khademhosseini, "Wireless flexible smart bandage for continuous monitoring of wound oxygenation," IEEE Transactions on Biomedical Circuits and Systems, vol. 9, no. 5, pp. 670–677, 2015. DOI: 10.1109/TBCAS.2015.2488582

[8] R. S. Howell, H. H. Liu, A. A. Khan, J. S. Woods, L. J. Lin, M. Saxena, H. Saxena, M. Castellano, P. Petrone, E. Slone, E. S. Chiu, B. M. Gillette, and S. A. Gorenstein, "Development of a method for clinical evaluation of artificial intelligence–based digital wound assessment tools," JAMA Network Open, vol. 4, no. 5, art. e217234, 2021. DOI: 10.1001/jamanetworkopen.2021.7234

[9] R. Kumar and S. K. Sarangi, "3D-Printed Customized Diabetic Foot Insoles with Architecture-Designed Lattice Structures: A Case Study," Biomedical Physics & Engineering Express, vol. 10, no. 1, art. 015019, 2023. DOI: 10.1088/2057-1976/ad1732

[10] K.-W. Lin, L.-W. Chou, Y.-T. Su, S.-H. Wei, and C.-S. Chen, "Biomechanical Effect of 3D-Printed Foot Orthoses in Patients with Knee Osteoarthritis," Applied Sciences, vol. 11, no. 9, art. 4200, 2021. DOI: 10.3390/app11094200

[11] Alberts, D.-I. Tudorache, A.-G. Niculescu, and A. M. Grumezescu, "Advancements in wound dressing materials: Highlighting recent progress in hydrogels, foams, and antimicrobial dressings," Gels, vol. 11, no. 2, art. 123, 2025. DOI: 10.3390/gels11020123

[12] M. Tymrak, M. Krieger, and J. M. Pearce, "Mechanical properties of components fabricated with open-source 3-D printers under realistic environmental conditions," Materials & Design, vol. 58, pp. 242–246, 2014. DOI: 10.1016/j.matdes.2014.02.038

[13] Y. Wu, L. Wu, and M. Yu, "The clinical value of intelligent wound measurement devices in patients with chronic wounds: A scoping review," International Wound Journal, vol. 21, no. 3, art. e14843, 2024. DOI: 10.1111/iwj.14843

[14] J. Kühl, S. Gorb, M. Kern, T. Klüter, S. Kühl, A. Seekamp, and S. Fuchs, "Extrusion based 3D printing of osteoinductive scaffolds with a spongiosa inspired structure," Frontiers in Bioengineering and Biotechnology, vol. 11, art. 1268049, 2023. DOI: 10.3389/fbioe.2023.1268049

[15] N. Čatipović, J. Krolo, and N. Gjeldum, "An AI-driven approach for a comprehensive evaluation of 3D printed molds in aluminium casting, considering material, speed, precision, modeling time, and costs," Proceedings of the 13th International Conference Mechanical Technologies and Structural Materials, Split, Croatia, pp. 273–280, 2024.

Society of Production Engineering

ICPES 2025

40th INTERNATIONAL CONFERENCE ON PRODUCTION ENGINEERING - SERBIA 2025

DOI: 10.46793/ICPES25.416P

University of Nis Faculty of Mechanical Engineering

Nis, Serbia, 18 - 19th September 2025

INFLUENCE OF EXTRUSION TEMPERATURE ON THE INTERLAYER ADHESION OF PLA AND TPU IN FDM TECHNOLOGY

Milica PANIĆ[1], Dejan MOVRIN[1]*, Mladomir MILUTINOVIĆ[1], Sanja BOJIĆ[1]

Orcid: 0000-0001-7812-0713; **Orcid:** 0000-0002-2023-1215;

University of Novi Sad, Faculty of Technical Sciences, Novi Sad, Serbia

*Corresponding author: movrin@uns.ac.rs

Abstract: *This paper investigates the effect of extrusion temperature on the adhesion between polylactic acid (PLA) and thermoplastic polyurethane (TPU) in fused deposition modeling (FDM) technology. The study is motivated by the development of sensor-equipped insoles combining rigid and flexible materials to enable both structural support and sensor integration. The research aims to identify the optimal printing parameters, with particular attention to material compatibility and temperature settings, in order to ensure structural integrity and performance of multi-material printed components. Two TPU materials with Shore hardness ratings of 95A and 98A were tested at extrusion temperatures of 210 °C, 230 °C, and 250 °C. These results are intended to support the design and manufacturing of functional, wearable 3D printed products.*

Keywords: *FDM, 3D printing, PLA, TPU, adhesion, extrusion temperature.*

1. INTRODUCTION

Additive manufacturing, or 3D printing, is one of the leading technologies in modern industry, distinguished by its ability to produce parts with complex geometrical shapes, as well as by its cost-effectiveness and high level of precision [1].

Significant progress has been made in the field of 3D printing, particularly in combining multiple different polymeric materials to achieve desired properties such as strength, wear resistance, elasticity, and more. The wide range of available materials on the market allows for their effective combination.

Polylactic acid (PLA) is one of the most popular thermoplastic materials in 3D printing, known for its biodegradability and mechanical resistance [2]. In contrast, thermoplastic polyurethane (TPU) is used for fabricating parts that require properties such as elasticity and flexibility. By combining these materials, it becomes possible to produce functional parts with hybrid characteristics [3].

Obtaining such characteristics is most achieved using the Fused Deposition Modeling (FDM) method, the most widely used 3D printing technique. This technology enables the production of smaller and complex parts, which can be made from one or a combination of a couple of different materials. For this reason, special attention is given to adhesion, both between the printed materials themselves and between the first layer and the build surface [4].

When it comes to first-layer adhesion, the most influential parameters are:

- Bed temperature (heating the bed improves adhesion by preventing rapid cooling and shrinkage of the material);
- Bed leveling and first-layer settings (proper leveling ensures better contact between the filament and the build surface) [5].

The most important factors influencing inter-layer adhesion are:

- Extruder temperature (ensures proper melting of the filament and its bonding with the previous layer);
- Printing speed and cooling (slower printing allows for better layer bonding, while excessive cooling can solidify the layer too quickly and weaken the bond);
- Material type (different materials have different adhesion properties);
- Environmental factors (ambient temperature, drafts, and air humidity can affect adhesion, especially for materials that require high printing temperatures) [6].

Poor bed adhesion can lead to warping, shifting, and complete print failure, while poor inter-layer adhesion results in delamination, low mechanical strength, and structural defects [6].

In the research [7], methods for determining the best printing parameters for interlayer adhesion are presented in the case of PC/ABS polymers. Print speed and layer height are considered the most significant parameters, as bond strength shows an inversely proportional relationship with print speed. The negative influence of high print speed can be observed from several aspects. The most significant aspect is the reduction of print accuracy and the distortion of the printing pattern, which leads to poor quality of bonded layers and may also result from an uneven temperature gradient between successive layers. On the other hand, low print speed promotes layer fusion and allows for better bonding of the subsequent layer, thereby improving bond strength. The second printing parameter that individually affects bond strength is layer height, and its behavior shows similarities with print speed. As the layer height increases, bond strength gradually decreases, because increased layer height introduces gaps, meaning there is unwanted porosity within the specimen. These gaps are key factors that prevent rasters from properly adhering to each other. If lower layer height values are used, the gaps occur to a lesser extent, and there is a higher likelihood of strong interlayer adhesion. It has been proven that an infill density of around 85% and a low print speed of 20 mm/s are the most favorable printing conditions for achieving high bond strength. Conversely, maximum infill density combined with maximum print speed leads to the lowest bond strength values. This can be explained by the fact that at 100% infill density, there is a higher likelihood of stress accumulation due to restricted heat transfer, requiring the printed part more time to dissipate heat. If there is a minimal air gap in the print pattern, it can serve as a space for more efficient heat transfer [7].

This paper presents the effect of temperature on the adhesion between two materials, PLA and TPU, in FDM technology.

2. FUSED DEPOSITION MODELING (FDM)

FDM or Fused Deposition Modeling technology is one of the most widespread methods of 3D printing. This technology is based on the extrusion process of polymer materials. A thermoplastic material, in the form of a filament, is heated to its melting point and extruded through a nozzle with a diameter ranging from 0.1 to 2 mm, then deposited layer by layer onto the build surface, forming the final product in the shape of a three-dimensional object [8].

The advantage of this technology lies in the wide range of materials that can be used, such as PLA, ABS, TPU, and others, which enable product properties, ranging from rigidity and flexibility to resistance to chemical and mechanical influences. FDM is the leading 3D printing technology in experimental research due to its low cost, availability, and ease of use. Nozzle temperature, print speed, and layer thickness are the key parameters that must be adjusted appropriately in order for the final

product to achieve the desired quality and dimensional accuracy [9].

3. EXPERIMENTAL RESEARCH

The experimental research aimed to examine the adhesion between two different materials produced using FDM technology, through the creation of insoles with sensors designed to collect gait data. The insole consists of PLA material in which force-sensitive resistors (FSRs) are embedded, while TPU material is printed above the sensors to enhance comfort, as shown in Figure 1.

Figure 1. Sensoring insole fabricated from two materials: rigid PLA material (white part), and softer-elastic material TPU (black part)

The 3D printer used for sample fabrication was the Prusa Mk3 (Czech Republic), with one print head. Material changing was provided with a pause in the G-code, and the material was manually replaced. Adhesion testing was conducted on an Instron 34SC-2 universal testing machine (USA), with the data collection and processing supported by Bluehill Universal software. To ensure adequate precision and safety during the testing process, a custom fixture was designed. Its role was to hold the samples in the machine's standard flat grips. The fixture utilized metal pins for efficient force transfer from the machine to the samples, as shown in Figure 2.

Since standard adhesion tests are typically performed under shear stress—which is not present in the case of sensor-equipped insoles—a specially designed sample shape was used for testing. These samples were designed to evaluate material adhesion in 3D printing under conditions relevant to the actual use of the insoles. The sample dimensions are shown in Figure 3.

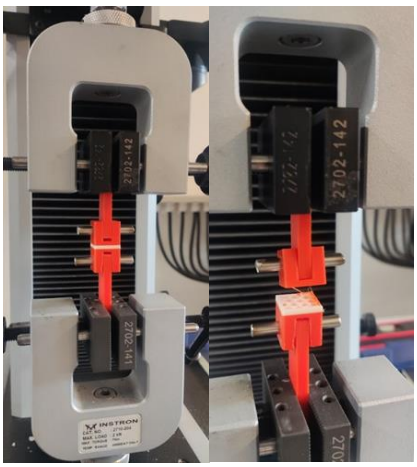

Figure 2. Specimen before and after testing on the Instron universal testing machine

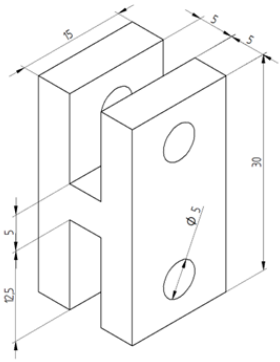

Figure 3. Dimensions of the specimens

3.1 Two different materials adhesion test

Two TPU materials from the manufacturer AzureFilm (Slovenia), with different hardness levels of 95A (softer) and 98A (harder) according to the Shore hardness scale, were used to fabricate 3D-printed insoles with sensors, and both were tested. The adhesion of TPU to PLA was tested for both hardness levels at varying temperature settings: 210°C, 230°C, and 250°C. In Figure 4, specimens for adhesion testing are presented, where white zones represent TPU material, and the orange zones are PLA.

For each temperature, three samples were produced and subsequently tested on a tensile testing machine. All specimens were printed with the same printing parameters (except nozzle temperatures): bed temperature 50 °C, printing speed 40mm/s, and layer thickness 0.2 mm.

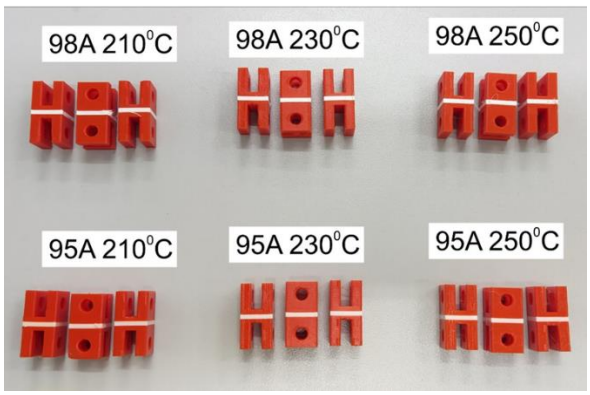

Figure 4. Testing specimens

The initial test results conducted at a temperature of 210 °C for the series of samples made from TPU materials with hardness levels of 98A and 95A are presented in Figure 5.

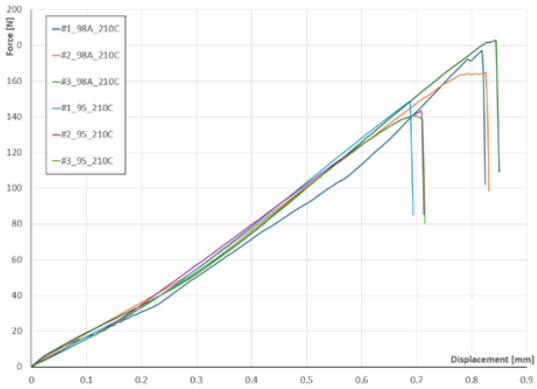

Figure 5. Diagram tensile test for determination of the maximal force for layer separation for temperature 210^{0}C

From the data shown, it can be concluded that the samples made from TPU with a hardness of 98A exhibit better adhesion properties, with an average layer separation force of 174 N, compared to 144 N for the 95A samples. The results indicate that the more rigid material demonstrates stronger interlayer bonding.

In Figure 6, the study was conducted at a temperature of 230 °C, where a decrease in the required force for layer separation was observed for the more rigid TPU material, with a value of approximately 74 N. Meanwhile, the softer TPU material maintained a similar value, with an average separation force of 148 N, compared to the previous test.

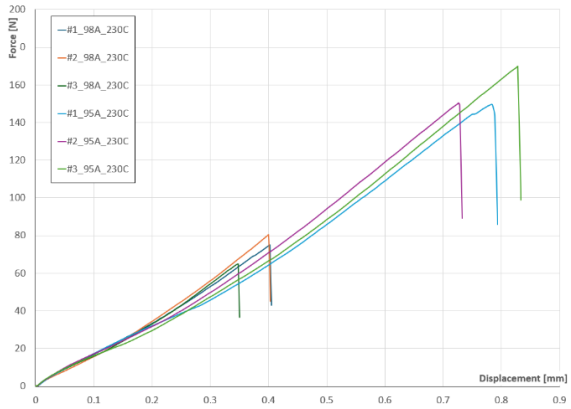

Figure 6. Diagram tensile test for determination of the maximal force for layer separation for temperature 230^{0}C

An increase in temperature to 250 °C for the softer TPU material indicates stability in the layer separation force, with a value of 151 N, while the TPU material with a hardness of 98A shows lower force values of around 84 N compared to the initial temperature of 210 °C (Figure 7).

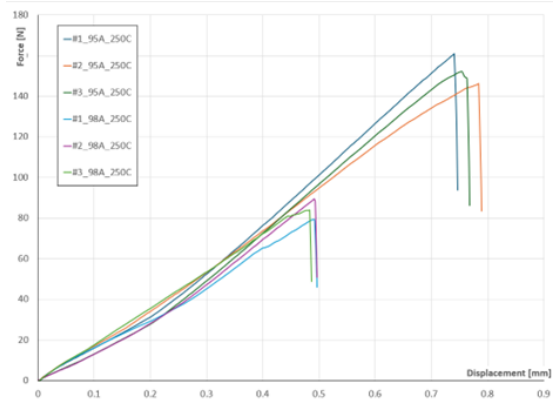

Figure 7. Diagram tensile test for determination of the maximal force for layer separation for temperature 250^{0}C

Figures 8 and 9 show the layer separation force diagrams as a function of temperature for each hardness level of the TPU material. In Figure 8, the results are combined, and an identical trend can be observed in the curves for all three temperature values.

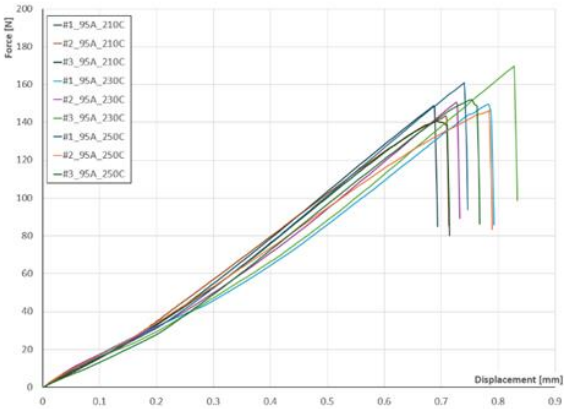

Figure 8. Layer separation force diagrams for TPU material, 95A hardness for temperatures 210^{0}C, 230^{0}C, and 250^{0}C

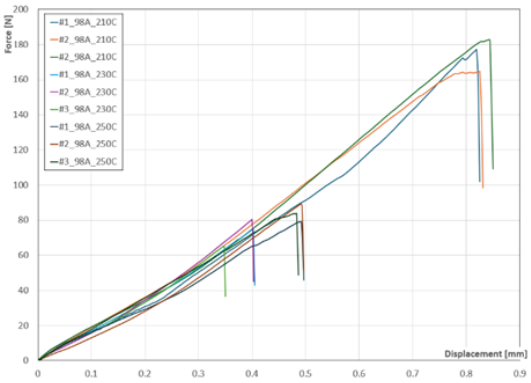

Figure 9. Layer separation force diagrams for TPU material, 98A hardness for temperatures 210^{0}C, 230^{0}C, and 250^{0}C

Figure 9 highlights the behavior of the TPU material with a hardness of 98A, showing a sharp drop in separation force with increasing temperature.

4. CONCLUSION

Adjusting the optimal temperature parameters is essential in the production of sensor-equipped insoles to.

ensure their protection from damage during use. The temperature setting is directly dependent on the desired hardness level of the thermoplastic polyurethane (TPU).

The TPU material with a hardness of 98A demonstrates sensitivity to temperature changes during the 3D printing process, with the best results observed at a temperature of 210 °C. Printing below this temperature is not acceptable due to the material's inability to melt and flow through the nozzle, which leads to extruder head clogging and potential damage. On the other hand, the TPU material with a hardness of 95A allows for a wider range of temperature processing, as it does not show significant variations in separation force at different temperatures.

ACKNOWLEDGEMENT

We would like to thank the European Union's Horizon programme for partly supporting the research project. This project has received funding from the European Union's Horizon Europe research and innovation program under grant agreement No.101086348.

REFERENCES

[1] Hopkinson, N.; Dickens, P.M. Analysis of rapid manufacturing—Using layer manufacturing processes for production. Proc. Inst. Mech. Eng. Part C J. Mech. Eng. Sci. 2003, 217, 31–39.

[2] Cicala, G. et al. Polylactide (PLA) filaments a biobased solution for additive manufacturing: correlating rheology and thermome-chanical properties with printing quality. Materials 11, 1191. https:// doi. org/ 10. 3390/ ma110 71191 (2018).

[3] Z.-W. Liu, H.-C. Chou, S.-H. Chen, C.-T. Tsao, C.-N. Chuang, L.-C. Cheng, C.-H. Yang, C.-K. Wang, K.-H. Hsieh, Mechanical and Thermal Properties of Thermoplastic Polyurethane-Toughened Polylactide-Based Nanocomposites, Polymer Composites 35/9 (2014) 1744-1757.

[4] Bergonzi L., Pirondi A., Moroni F., Frascio M., Avalle M., A study on additive manufacturing build parameters as bonded joint design factors, The Journal of Adhesion, 2021, pp. 1-30.

[5] Gonzalez-Gutierrez J (2017) Filler content & properties of highly flled flaments for fused flament fabrication of magents. Proc ANTEC 2017:1–4

[6] Genina N, Hollander J, Jukarainen H, Makila E, Salonen J, Sandler N (2016) Ethylene vinyl acetate (EVA) as a new drug carrier for 3D printed medical drug delivery devices. Eur J Pharm Sci 90:53–63

[7] Mohamed, O.A.; Masood, S.H.; Bhowmik, J.L.; Nikzad, M.; Azadmanjiri, J. Effect of Process Parameters on Dynamic Mechanical Performance of FDM PC/ABS Printed Parts

Through Design of Experiment. J. Mater. Eng. Perform. 2016, 25, 2922–2935.

[8] W.S.W. Harun, S. Safian, M.H. Idris WIT Trans. Eng. Sci., 64 (2009), pp. 319-328 Gibson, D.W. Rosen, and B. Stucker, Additive Manufacturing Technologies, DOI 10.1007/9784419-1120-9_5, Springer ScienceþBusiness Media, LLC 2010

Society of Production Engineering

ICPES 2025

40th INTERNATIONAL CONFERENCE ON PRODUCTION ENGINEERING - SERBIA 2025

DOI: 10.46793/ICPES25.422K

University of Nis Faculty of Mechanical Engineering

Nis, Serbia, 18 - 19th September 2025

EFFECT OF LAYER HEIGHT ON GEOMETRIC ACCURACY OF FDM 3D PRINTED POROUS STRUCTURES

Nikola KOTORČEVIĆ[1,*], Fatima ŽIVIĆ[1], Petar TODOROVIĆ[1], Nenad GRUJOVIC[1]

Orcid: 0000-0002-5664-9832; **Orcid:** 0000-0003-2509-187X; **Orcid:** 0000-0003-3260-1655; **Orcid:** 0000-0002-8765-2196

[1]Faculty of Engineering, University of Kragujevac

*Corresponding author: nikola.kotorcevic@uni.kg.ac.rs

Abstract: *This paper investigated the influence of FDM 3D printing input parameters and presented short analysis of various parameters on some specific properties of the printed parts. We examined the effect of layer height on dimensional precision of the printed parts made of polylactic acid (PLA). We experimentally tested three different layer heights (0.16 mm, 0.20 mm, 0.24 mm) and their influence on the geometric accuracy, using cross hatch infill pattern at 70% infill density. Simple 3D model of the printed structure was created to evaluate the porosity in printed part, depending on the layer height. Experimental study, as well as the computational model, both indicated that layer height showed significant influence on the dimensional precision of the printed parts. Layer height as input parameter in 3D printing also impact the accuracy of internal infill structures.*

Keywords: *additive manufacturing, FDM 3D printing, dimensional accuracy, layer height, Dragonfly software model*

1. INTRODUCTION

Additive manufacturing (AM) is a process that fabricates parts through the layer-by-layer deposition of material. It is widely used for prototyping and research applications [1], [2]. The advancement of AM has, to some extent, surpassed conventional manufacturing techniques. With further advancements in this technology, it is likely that this trend will continue, driven by AM cost-effectiveness and versatility, which provide a viable alternative to traditional processes such as injection molding and plastic forming [1]. Unlike subtractive methods, AM builds parts without removing material, reducing waste except for support structures [3]. Parts made by traditional methods often have better mechanical properties than 3D printed ones due to porosity and anisotropy in additive manufacturing [4]. However, with adequate optimisation and considering the influence of specific input parameters [5], [6], 3D printing has been used across various industries. Several additive manufacturing (AM) processes have been widely used, including: Selective Laser Melting (SLM), Laminated

Object Manufacturing (LOM), Selective Laser Sintering (SLS), Fused Deposition Modelling (FDM) etc. [6].

In Fused Deposition Modelling (FDM), a thermoplastic polymer filament is fed through an extruder nozzle onto a build platform under precisely controlled temperature conditions [7]. The filament is heated to a molten state within the nozzle, forming a viscous material that is precisely deposited onto the preceding layer. The interlayer bonding is achieved through heat transfer, which induces localized melting and fusion between adjacent layers [8]. The final object is constructed through the sequential deposition of material layers [7]. While elevated extrusion temperatures enhance material fluidity and improve interlayer adhesion, excessive temperatures can compromise mechanical properties. This occurs due to residual stress accumulation, irregular material deposition, surface imperfections, and reduced interlayer bonding strength [9].

FDM is widely used due to its simplicity, low cost and high speed [4]. This technology finds applications across diverse sectors, including medical, biomedical, electronics, automotive, and aerospace industries [10].

Most commonly used materials in FDM include: polylactic acid (PLA), poly carbonate (PC), acrylonitrile butadiene styrene (ABS), poly-ether-ether-ketone (PEEK) etc. [3].

PLA, a thermoplastic polymer derived from renewable resources (e.g., sugarcane, corn starch), is particularly notable for its eco-friendliness, biodegradability, and excellent melt flow properties [6]. While polymers dominate FDM material usage, advanced composites incorporating metals, ceramics, or hybrid materials can also be processed, expanding the technology’s functional scope [11].

2. INFLUENCE OF 3D PRINTING PARAMETERS ON THE PRINTED PART PROPERTIES

The process begins with the creation of a CAD (Computer-Aided Design) model [12]. This model is converted to a Standard Tessellation Language (STL) file [11] and then sliced in software, which provides the input data for the 3D printer. This means the model is divided into layers [1]. The G-code generated by the slicer software defines the movement of the printer head and nozzle [7]. FDM parts consist of multiple layers containing partially bonded rasters and voids [4]. The nozzle diameter in FDM usually ranges between 0,25 and 0,8 mm [12].

The characteristics of the output part - including dimensional accuracy, geometric precision, and mechanical properties - are influenced by process and machine parameters [13] [1]. Key input parameters such as layer resolution, build orientation, raster angle, temperature, and air gap significantly affect the part's mechanical properties [7].

Layer resolution refers to the thickness of a single layer deposited during one nozzle pass. It directly affects the staircasing effect. Higher layer resolution corresponds to smaller layer thickness values, which can improve surface finish but increase printing time. Studies show that increased layer thickness may reduce load-bearing capacity [7].

Build orientation defines the placement side of the part on the build platform, indicating the object's angular position relative to the platform's horizontal axis. This parameter affects layer arrangement and print quality, as the mechanical properties depend on interlayer fusion quality [7].

Raster angle determines filament alignment within a single layer and directly influences stress distribution under load [7].

Air gap refers to the distance between neighboring rasters [7].

Among the key slicing process parameters, the most significant are: infill density, number

of contours (walls), raster angle, raster pattern, and number of shells [1].

Infill density indicates the percentage of a layer's area that is filled with material relative to the total layer area [1]. Number of contours refers to the count of perimeter boundaries surrounding each layer [1].

Raster pattern determines the nozzle's specific deposition path during printing, which creates the part's internal structure [1].

Number of shells specifies the quantity of bottom and top surface layers covering the part [1].

Experimental studies and analytical models are typically used to predict the geometric quality of FDM-printed parts, though recent efforts have explored reverse CAD approaches [1], [14].

Numerous research studies have investigated the influence of printing parameters on the mechanical behavior of printed parts using various optimization techniques and design of experiment (DOE) methods [2], [3], [4], [5], [6], [11], [15], [16], [17].

The mechanical properties of printed parts are determined by void density, inter-fiber bond strength, and the material properties of the filament [4]. Consequently, printing and process parameters directly affect the quality of bonding between adjacent filaments [4]. Research indicates that parts printed with lower layer heights exhibit higher yield stress and increased elastic modulus [4], [5]. It was also observed that these parts had reduced void density [4].

Printing parameters such as infill percentage, geometric pattern, and layer height play an important role in 3D printing for producing defect-free parts with enhanced mechanical strength [9].

Table 2 presents the effects of key printing parameters on part behavior.

Research indicates that increasing infill percentage enhances tensile strength by reducing voids and improving stress distribution [9].

While higher infill density improves part strength, it also increases object weight. The infill pattern further influences FDM part performance [3]. However, we should keep in mind that higher infill density and lower layer height require longer printing time and higher material cost [3].

Other research shows that infill density and print speed have the greatest effect on flexural, compression, and tensile strength, followed by layer thickness [18].

Giri et al. indicate that increasing the number of contours improves tensile strength, while decreasing layer thickness and air gap enhances surface roughness [20].

Different infill patterns affect the mechanical properties of printed parts. For example, gyroid and honeycomb patterns show similar behavior under bending loads, while the grid pattern demonstrates a smaller increase in bending strength with increasing density [15]. Another study found that in grid and tri-hexagon infill patterns, volume inaccuracy increases with infill density [12].

Table 2. Influence of input parameters on final properties of the printed part

Printing parameter	Influenced parameter	Reference
Layer height	Dimensional accuracy, elastic modulus, surface roughness, mechanical strength (tensile, compression, flexural)	[1], [2], [7], [18]
Infill density	Mechanical strength, surface hardness	[18], [19]
Infill pattern	Mechanical strength	[9], [15]
Printing temperature	Mechanical strength (layer fusion)	[9]
Raster angle	Mechanical strength (load direction)	[7]

It was also proven that maximum hardness is achieved at maximum fill density levels. This occurs because fewer voids in subsurface layers reduce strength [19].

Although voids and spaces often decrease the mechanical strength of parts, FDM remains a valuable technology for creating porous structures. Proper input parameters can produce internal pores, which are required for applications like scaffolds, water filters [21], [22] and separators [23].

3. EXPERIMENTAL SETUP

Using Autodesk Inventor software, we created a 3D model of a syringe nozzle that serves for the positioning of the filter with dimensions of 10 mm diameter and 3.4 mm height, as shown in Figure.

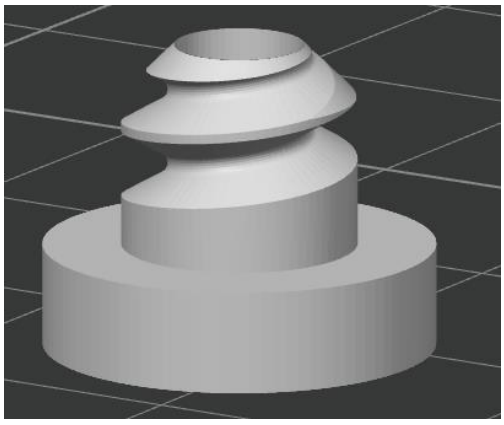

Figure 1. 3D model of syringe filter

In Bambu Studio slicing software, we created three different samples with Cross Hatch infill pattern at 70% infill density. The models contained no top/bottom shells or walls. Layer height was varied between 0.16 mm, 0.20 mm, 0.24 mm as specified in **Table** . Samples were manufactured using a Bambu Lab X1E 3D printer.

Table 2. Sample parameters

Sample	Pattern	Infill [%]	Layer height [mm]
1	Cross Hatch	70	0,16
2			0,20
3			0,24

Each sample was printed five times and measured with a vernier caliper to calculate average values of printed dimensional values. The material was PLA, with nozzle temperature ranging between 190°C and 240°C (automatically adjusted by the machine). All other parameters used default recommended values.

To better analyse subsurface processes, we created a model in Dragonfly software using optical images of each layer. For example: the first sample comprised 21 layers, the second had 17 layers and the third contained 14 layers. We used transparent PLA for the base (layer positioning reference) and red filament for the upper top layer, meaning that all layers were transparent except for the one at the top position (red colour PLA). Under light illumination, only the upper top layer is visible because light can pass through all other transparent layers (Figure 15 and Figure 3).

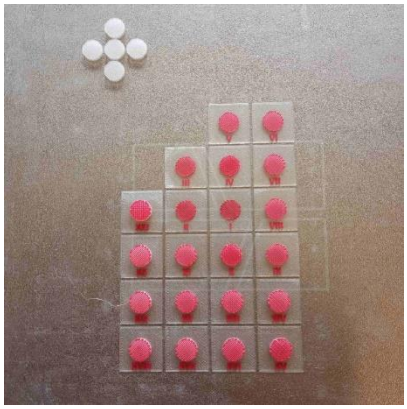

Figure 15. Printing plate; in the top left corner – 5 samples for measuring test with vernier caliper, on the right – layers for Dragonfly model

Figure 3. Layer for Dragonfly model under the light source

We photographed all layers, prepared the images in Photoshop software, and imported

them into Dragonfly software. For example, 21 layer images from Sample 1 were reconstructed into a single 3D model in Dragonfly. Each layer's height was set according to the input layer height parameters specified in Table for each sample.

To evaluate print accuracy, we calculated the percentage error using Formula (1) [24]:

$$\delta = \left|\frac{Dn-D}{Dn}\right| \times 100 \quad (1)$$

where: δ was error percent, Dn represents nominal value (target dimension from ideal model) and D was measured value. The sample with the lowest percent error was considered closest to the ideal model and therefore identified as the optimal result.

4. RESULTS
5.

The measurement results for all samples and their percentage errors (calculated using Formula 1) are presented in **Table** . Since a perfect circle cannot be achieved without wall contours, we considered the smallest measured diameter value. The ideal sample dimensions, as designed in Autodesk Inventor, were: 10 mm in diameter (d) and 3,4 mm in height (H). Any deviation from these values indicates inaccuracies in the printed model due to the selected parameters.

Table 3. Measuring results and percent of error δ

Sample	Average height [mm]	δ (H) [%]	Average diameter [mm]	δ (d) [%]
1	3,47	2,1	9,86	1,4
2	3,50	2,8	9,80	2
3	3,50	2,8	9,79	2,1

The results indicate that Sample 1, with the lowest layer height value, achieved the best dimensional accuracy. Samples 2 and 3 showed slightly lower accuracy with their chosen parameters.

In Dragonfly software, we created 3D models by importing optical images of the layers, as demonstrated in Figure .

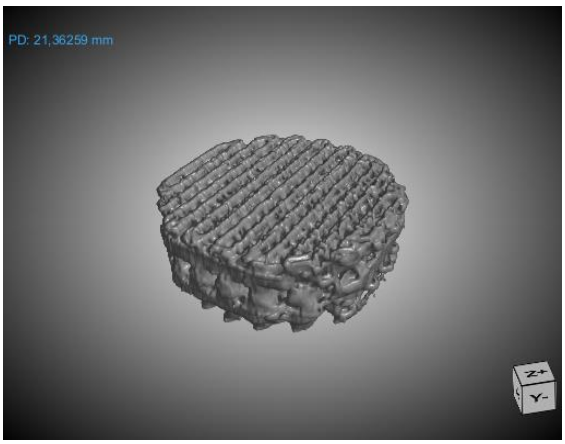

Figure 4. Dragonfly model of Sample 2

The model exhibited inaccuracies compared to the ideal reference sample as designed in CAD. The most significant deviation occurred in diameter dimensions. To determine infill percentage accuracy, we created an ideal reference model with a 10 mm diameter, as shown in **Figure** .

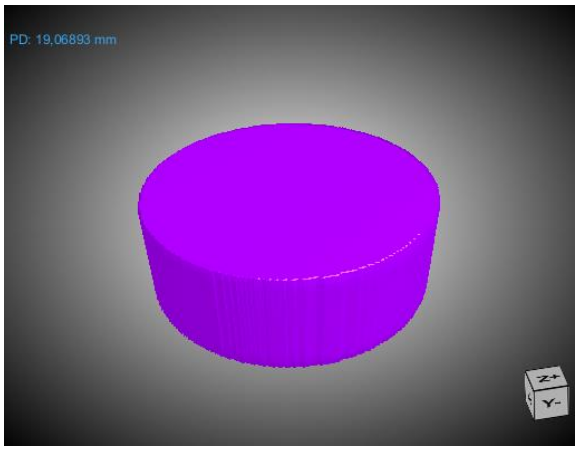

Figure 5. Ideal model

Then, the two regions of interest were considered: volume of pores (Figure) and volume of solid material (filament), as shown in Figure .

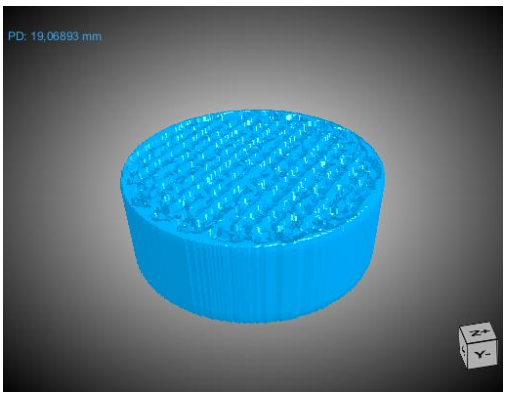

Figure 6. Volume of pores

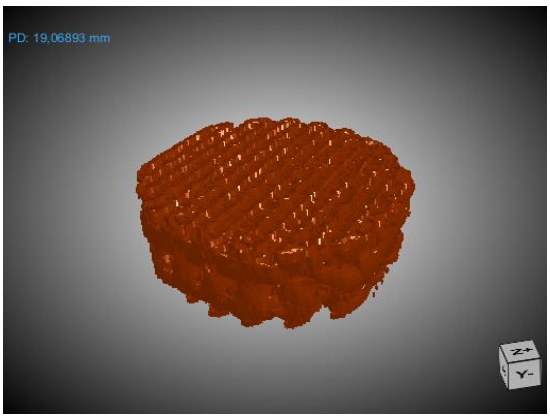

Figure 7. Volume of solid material

The infill percentage was determined by comparing the ideal model's volume with the solid material volume. The nominal value was set at 70% (**Table**). We calculated the error by subtracting the measured filament percentage from this ideal 70% value. The lowest error indicated the optimal print accuracy. All results are presented in

Table

Table 4. Volume percent as provided by the Dragonfly software and error

Sample	Volume of ideal model [mm^3]	Percent of pores [%]	Percent of filament [%]	Error [%]
1	263,8	56	44	26
2	266,7	62	38	32
3	263,8	69	31	39

Because the model does not account for internal material fusion processes or the geometric limitations of filament deposition, the ideal model's volume differed across samples. Sample 2 (17 layers × 0.2 mm) most closely matched the ideal model's volume, achieving the exact target height of 3.4 mm. Sample 1 (21 layers × 0.16 mm) and Sample 3 (14 layers × 0.24 mm) deviated from the target height, resulting in lower volumes. Consequently, we evaluated accuracy solely based on the filament percentage within each printed model, not the ideal dimensions.

The simplified Dragonfly model analysis indicates that Sample 1 achieved the best results, followed by Samples 2 and 3. This suggests that infill accuracy improves with reduced layer height.

In FDM 3D printing, infill percentage refers to how much of the internal volume of a printed part is filled with material, typically using a patterned structure. Porosity, on the other hand, measures the amount of void space (air) within the material or part. There is an inverse correlation between infill percentage and porosity. Higher infill percentage results in lower porosity and vice versa. However, this relationship is not strictly linear, and several factors affect the actual porosity of a part beyond just the infill percentage.

In ideal scenarios (perfect layer adhesion, no gaps, etc.), infill percentage of 70% infill should produce 30% porosity in the final printed part. However, in reality, porosity is usually higher than directly projected by the input infill percentage, due to inter-layer gaps or poor fusion, inconsistent extrusion, shell/wall settings and pattern inefficiencies (e.g., some infill types like "grid" vs "gyroid"). 100% infill does not guarantee 0% porosity, due to microscopic voids from imperfect bonding or filament gaps. In reality, a part with 70% infill might have actual porosity closer to 35–40%, especially if the print has only 1–2 perimeters or poorly tuned print parameters.

It can be seen from our experimental results and subsequent software model that porosity was higher than expected 30%, what is in accordance with work of other authors. Therefore, it is important to consider these deviations when designing porous structure for specific applications.

6. CONCLUSION

It can be concluded that higher layer resolution (i.e., lower layer height) improves the geometric precision of printed parts. Additionally, the simplified 3D model analysis of infill percentage showed that samples with

lower layer heights more closely matched the target infill values. This demonstrates that layer height affects not only surface geometry but also internal dimensional accuracy.

ACKNOWLEDGEMENT

This paper is supported through the EIT's Higher Education Initiative SMART-2M, DEEPTECH-2M and A-SIDE projects, coordinated by EIT RawMaterials, funded by the European Union and supported by the Ministry of Education and Ministry of Science, Technological Development and Innovation, Republic of Serbia, Grants: No. 451-03-137/2025-03/200107.

REFERENCES

[1] B. S. Rupal, K. G. Mostafa, Y. Wang, and A. J. Qureshi, "A Reverse CAD Approach for Estimating Geometric and Mechanical Behavior of FDM Printed Parts," Procedia Manuf., vol. 34, pp. 535–544, 2019, doi: 10.1016/j.promfg.2019.06.217.

[2] K. S. Patel, D. B. Shah, S. J. Joshi, F. K. Aldawood, and M. Kchaou, "Effect of process parameters on the mechanical performance of FDM printed carbon fiber reinforced PETG," J. Mater. Res. Technol., vol. 30, pp. 8006–8018, May 2024, doi: 10.1016/j.jmrt.2024.05.184.

[3] N. Lokesh, B. A. Praveena, J. Sudheer Reddy, V. K. Vasu, and S. Vijaykumar, "Evaluation on effect of printing process parameter through Taguchi approach on mechanical properties of 3D printed PLA specimens using FDM at constant printing temperature," Mater. Today Proc., vol. 52, pp. 1288–1293, 2022, doi: 10.1016/j.matpr.2021.11.054.

[4] S. Garzon-Hernandez, D. Garcia-Gonzalez, A. Jérusalem, and A. Arias, "Design of FDM 3D printed polymers: An experimental-modelling methodology for the prediction of mechanical properties," Mater. Des., vol. 188, p. 108414, Mar. 2020, doi: 10.1016/j.matdes.2019.108414.

[5] K. Almansoori and S. Pervaiz, "Effect of layer height, print speed and cell geometry on mechanical properties of marble PLA based 3D printed parts," Smart Mater. Manuf., vol. 1, p. 100023, 2023, doi: 10.1016/j.smmf.2023.100023.

[6] S. Sahoo, H. Sutar, P. Senapati, B. Shankar Mohanto, P. Ranjan Dhal, and S. Kumar Baral, "Experimental investigation and optimization of the FDM process using PLA," Mater. Today Proc., vol. 74, pp. 843–847, 2023, doi: 10.1016/j.matpr.2022.11.208.

[7] S. Khan, K. Joshi, and S. Deshmukh, "A comprehensive review on effect of printing parameters on mechanical properties of FDM printed parts," Mater. Today Proc., vol. 50, pp. 2119–2127, 2022, doi: 10.1016/j.matpr.2021.09.433.

[8] A. Equbal, A. K. Sood, Md. I. Equbal, I. A. Badruddin, and Z. A. Khan, "RSM based investigation of compressive properties of FDM fabricated part," CIRP J. Manuf. Sci. Technol., vol. 35, pp. 701–714, Nov. 2021, doi: 10.1016/j.cirpj.2021.08.004.

[9] K. Vijayananth, G. Pudhupalayam Muthukutti, A. Raju, and I. Barsoum, "Integrated optimization and prediction of mechanical properties in FDM printed polyamide/carbon fiber composites using PSI–VIKOR and ANN," Mater., vol. 8, p. 11, 2025, doi: 10.1016/j.nxmate.2025.100932.

[10] N. A. Fountas, I. Papantoniou, J. D. Kechagias, D. E. Manolakos, and N. M. Vaxevanidis, "Modeling and optimization of flexural properties of FDM-processed PET-G specimens using RSM and GWO algorithm," Eng. Fail. Anal., vol. 138, p. 106340, Aug. 2022, doi: 10.1016/j.engfailanal.2022.106340.

[11] M. R. Pratheesh Kumar, K. Saravanakumar, C. Arun Kumar, R. Saravanakumar, and B. Abimanyu, "Experimental investigation of the process parameters and print orientation on the dimensional accuracy of fused deposition modelling (FDM) processed carbon fiber reinforced ABS polymer parts," Mater. Today Proc., vol. 98, pp. 166–173, 2024, doi: 10.1016/j.matpr.2023.10.062.

[12] S. Maurya, B. Malik, P. Sharma, A. Singh, and R. Chalisgaonkar, "Investigation of different parameters of cube printed using PLA by FDM 3D printer," Mater. Today Proc., vol. 64, pp. 1217–1222, 2022, doi: 10.1016/j.matpr.2022.03.700.

[13] F. Zivic, S. Mitrovic, N. Grujovic, Z. Jovanovic, D. Dzunic, and S. Milenkovic, "The Influence of the 3D Printing Infill and Printing Direction on Friction and Wear of Polylactic Acid (PLA) under Rotational Sliding," J. Frict. Wear, vol. 42, no. 2, pp. 106–111, Mar. 2021, doi: 10.3103/S1068366621020124.

[14] S. M. Mora, J. C. Gil, and A. M. Camacho López, "Influence of manufacturing parameters in the dimensional characteristics of ABS parts obtained by FDM using reverse engineering techniques," Procedia Manuf., vol. 41, pp. 968–975, 2019, doi: 10.1016/j.promfg.2019.10.022.

[15] M. M. M. Haque et al., "Impact of process parameters and material selection on the mechanical performance of FDM 3D-Printed components," Hybrid Adv., vol. 10, p. 100502, Sep. 2025, doi: 10.1016/j.hybadv.2025.100502.

[16] B. Kartikeyan, A. Ponshanmugakumar, G. Saravanan, S. BharathGanesh, and V. Hemamalini, "Experimental and theoretical analysis of FDM AM PLA mechanical properties," Mater. Today Proc., May 2023, doi: 10.1016/j.matpr.2023.05.105.

[17] L. Kothandaraman and N. K. Balasubramanian, "Optimization of FDM printing parameters for square lattice structures: Improving mechanical characteristics," Mater. Today Proc., Apr. 2024, doi: 10.1016/j.matpr.2024.04.033.

[18] M. N. Bashir et al., "Investigation of process parameter influence on the mechanical properties of FDM-printed PEEK-carbon fiber composites using RSM and Taguchi methods," J. Mater. Res. Technol., vol. 36, pp. 10199–10209, May 2025, doi: 10.1016/j.jmrt.2025.05.217.

[19] M. Ramesh and K. Panneerselvam, "Mechanical investigation and optimization of parameter selection for Nylon material processed by FDM," Mater. Today Proc., vol. 46, pp. 9303–9307, 2021, doi: 10.1016/j.matpr.2020.02.697.

[20] J. Giri, P. Shahane, S. Jachak, R. Chadge, and P. Giri, "Optimization of FDM process parameters for dual extruder 3d printer using Artificial Neural network," Mater. Today Proc., vol. 43, pp. 3242–3249, 2021, doi: 10.1016/j.matpr.2021.01.899.

[21] N. Kotorčević et al., "Material Extrusion 3D Printing of Micro-Porous Copper-Based Structure for Water Filters," Machines, vol. 12, no. 7, p. 470, Jul. 2024, doi: 10.3390/machines12070470.

[22] N. Fijoł and A. P. Mathew, "Accelerated ageing of 3D printed water purification filters based on PLA reinforced with green nanofibers," Polym. Test., vol. 129, p. 108270, Dec. 2023, doi: 10.1016/j.polymertesting.2023.108270.

[23] N. Fijoł, A. Aguilar-Sánchez, M.-X. Ruiz-Caldas, J. Redlinger-Pohn, A. Mautner, and A. P. Mathew, "3D printed polylactic acid (PLA) filters reinforced with polysaccharide nanofibers for metal ions capture and microplastics separation from water," Chem. Eng. J., vol. 457, p. 141153, Feb. 2023, doi: 10.1016/j.cej.2022.141153.

[24] Y. F. Majd, M. S. G. Tsuzuki, and A. Barari, "A Machine Learning Approach to Find Density Percentage Error Resulting by Infill Patterns in Additive Manufacturing," IFAC-Pap., vol. 56, no. 2, pp. 4740–4745, 2023, doi: 10.1016/j.ifacol.2023.10.1236.

Society of Production Engineering

ICPES 2025

40th INTERNATIONAL CONFERENCE ON PRODUCTION ENGINEERING - SERBIA 2025

DOI: 10.46793/ICPES25.431V

University of Nis Faculty of Mechanical Engineering

Nis, Serbia, 18 - 19th September 2025

INFLUENCE OF STRUT CROSS-SECTION GEOMETRY ON THE MECHANICAL PROPERTIES OF MSLA-FABRICATED BONE SCAFFOLDS

Aleksandra VELIČKOVIĆ[1], Rajko TURUDIJA[2] *, Jovan ARANĐELOVIĆ[1], Jelena STOJKOVIĆ[1]*

Orcid: 0009-0006-8017-6787; **Orcid:** 0000-0002-6324-5967; **Orcid:** 0000-0001-9653-4119; **Orcid:** 0000-0002-8249-2816;

[1] Faculty of Mechanical Engineering, Niš, Serbia, andra0174@gmail.com

*Corresponding author: rajko.turudija@masfak.ni.ac.rs

Abstract: *Severe bone injuries often result in critical-sized defects that exceed the body's natural healing capacity, requiring engineered scaffolds to restore mechanical stability and promote bone regeneration. This study investigates how different strut cross-sectional geometries affect the mechanical properties of 3D-printed bone scaffolds. Six geometries (including square, rhomboid, circular, and three others) were designed and fabricated using Masked Stereolithography (MSLA) technology. Multiple samples of each geometry were produced and tested under uniaxial compression using a universal testing machine. Key parameters analyzed included engineering stress and elastic modulus. Results showed significant variation in mechanical properties depending on the cross-sectional shape. Scaffolds with rectangular strut cross-section exhibited the highest compressive strength of 33.39 MPa, while those with circular strut cross-section recorded the lowest value of 27.38 MPa. Additionally, scaffolds with a circular strut cross-section exhibited the highest elastic modulus of 1774.3 N/mm², while scaffolds with a cross-shaped strut cross-section exhibited the lowest elastic modulus of 1153.7 N/mm². These findings highlight the importance of geometric optimization in scaffold design for improved mechanical stability.*

Keywords: *lattice-like scaffolds, strut cross-section, mechanical properties, MSLA*

1. INTRODUCTION

At the global level, the incidence of bone fractures, defects, and tumors is steadily increasing [1]. Each year, approximately four million surgical procedures are performed to address bone loss using grafts and/or bone tissue replacements [2]. Although bone tissue has the capacity to regenerate, defects exceeding a critical size (approximately >2 cm) often exhibit significantly impaired healing and fail to repair spontaneously [3]. Tissue engineering employs integrated, multidisciplinary strategies to enhance or replace damaged biological tissues [4]. Within this field, scaffolds play a central role: they not only provide a temporary structure to support cell adhesion, proliferation, and differentiation, but also facilitate the formation of new tissue. Furthermore, scaffolds interact with cells and bioactive molecules that regulate tissue remodeling. As a result, scaffolds are commonly designed to mimic the structure and composition of the extracellular matrix (ECM), thereby reestablishing communication between cells and the ECM, and ultimately

promoting effective tissue regeneration [3]. The present study aims to evaluate the mechanical properties of such scaffolds.

The properties of bone scaffolds largely depend on their microstructure. Scaffold microstructures can be classified into three groups. First, scaffolds formed from periodic, regular lattice structures (Figure 1a), which are constructed from repeating units (cells) and are primarily used in the early stages of bone scaffold development. Second, scaffolds formed from irregular and non-periodic structures (Figure 1b), which closely resemble natural bone and may represent an ideal replacement for damaged bone tissue. Finally, scaffolds formed from bioinspired (bionic) microstructures (Figure 1c), such as Triply Periodic Minimal Surfaces (TPMS), which are widely employed in bone scaffold design [5].

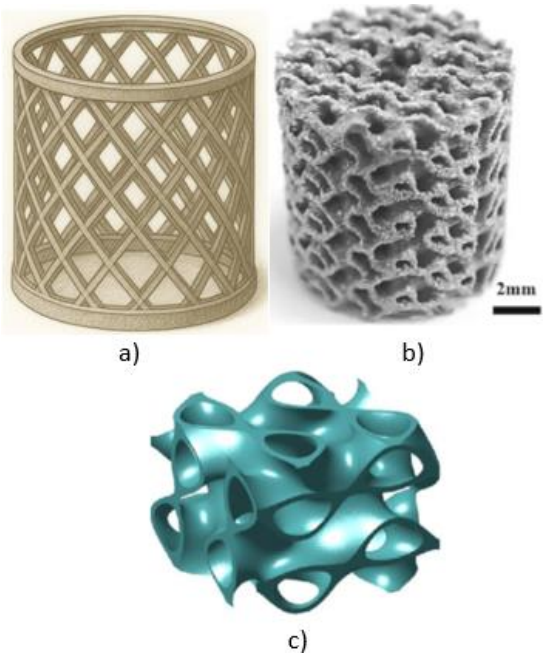

Figure 1. a) Lattice-like, b) Irregular and non-periodic, c) TPMS bone scaffold structures [5]

An ideal scaffold should be biodegradable, biocompatible, bioactive, osteoconductive, osteoinductive, and non-toxic, while also possessing optimal mechanical properties—such as stiffness, pore size, surface topology, and load-bearing capacity—to promote successful cell proliferation and osteogenic differentiation [1]. The main limitations in scaffold application include insufficient vascularization, inadequate mechanical strength, and difficulties in managing bone infections [6]. Biomaterials, which form the fundamental components of scaffolds, play a crucial role in bone tissue engineering. Materials such as metals, natural and synthetic polymers, ceramics, and their composites have been widely used for decades as scaffold materials in biomedical fields [4].

To be suitable for clinical use, scaffolds must comply with established mechanical performance standards. Numerous experimental studies have investigated the mechanical response of porous scaffolds through uniaxial compression testing [9], [10], [12] – [17], while other research has employed computational structural analyses to predict their behaviour under various loading conditions [7], [8], [10], [12] – [15], [17] – [19]. Taken together, these studies highlight consistent trends, showing that both scaffold geometry [10], [12], [15] – [17] and manufacturing parameters [8], [12] – [14] play a crucial role in determining overall mechanical behaviour.

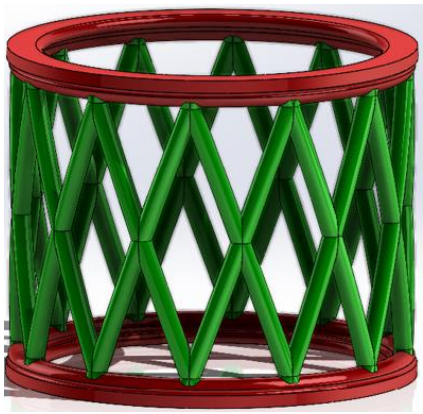

Figure 2. Lattice like scaffold

A review of the literature clearly highlights the need for further research into the structure and geometry of scaffolds, particularly lattice-like scaffolds composed of periodic, regular structures. One such scaffold design, developed and presented by the authors in a previous study [20], was specifically intended for the treatment of small segmental bone defects (Figure 2). The scaffold was fabricated using Masked Stereolithography (MSLA) 3D printing technology. This type of scaffold remains

insufficiently investigated in terms of its mechanical behavior, the optimization of various strut shapes, and the influence of strut cross-sectional geometry on its overall mechanical performance. The aim of this study is to advance knowledge regarding the mechanical characteristics of this type of scaffold by examining how strut cross-sectional geometry affects its mechanical behavior.

This paper includes an introduction and literature review, a description of the methodology, a presentation and discussion of the results, and a summary of the main conclusions.

2. METHODOLOGY

The aim of this research is to expand the understanding of the mechanical characteristics of lattice-structured scaffolds by analyzing the influence of strut cross-section on their mechanical performance.

The lattice scaffold models described in the previous section were designed for small bone defect segments and subjected to uniaxial compression testing to evaluate their mechanical performance. Twelve lattice scaffold models representing six different strut geometries (square, rhomboid, circular, two rectangular, and cross-shaped) were fabricated – two models for each geometry. These models were designed in SolidWorks CAD software (SolidWorks 2023) using fully parametric modeling. The scaffolds were constructed from beams at the top and bottom of the outer frame, connected by vertical struts. The outer frame beams have a diameter of 36 mm. The 12 vertical struts, evenly spaced around the frame, were cut at an angle of 35°. According to these dimensions, the scaffold is small, with a height of 30 mm and width of 40 mm. The scaffold models were made with six different cross-sectional shapes of the struts, oriented perpendicular to the strut direction (Figure 3). The cross-sectional areas were kept identical at 2.5 mm^2 to isolate the effect of shape on mechanical performance.

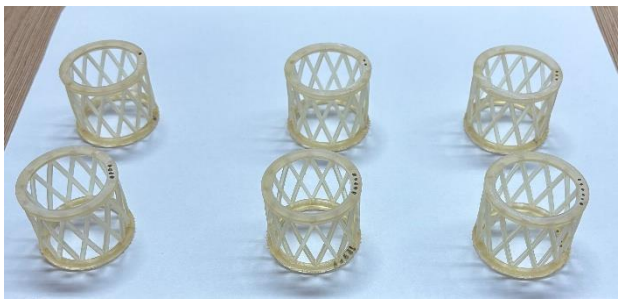

Figure 3. Lattice like scaffold used for the experiments

The previously mentioned scaffold models were fabricated using MSLA (Masked Stereolithography) 3D printing technology, which enables high precision and fine detail in complex microstructures. MSLA technology utilizes a UV LCD screen to mask individual layers of photopolymer resin, allowing selective curing of the material and achieving high printing resolution.

Figure 4. Anycubic Photom M3 Plus 3D printer

The scaffold models were prepared for printing using Anycubic Photon Workshop software (v.3.1.4), which facilitates optimization of printing parameters and precise control over the CAD model geometry. The scaffolds were printed on an Anycubic Photon M3 Plus 3D printer (Figure 4), which enables the production of scaffolds with high dimensional accuracy and microstructure control. This 3D printer features a build volume of 245 × 197 × 122 mm, an LCD screen resolution of 5760 × 3600 pixels, and a layer resolution of 34 microns. Additional technical specifications of the printer are provided in the Table 1. The material used for model fabrication is ECO UV RESIN Black — a

resin whose properties, detailed in the Table 2, contribute to the stability and mechanical resistance of the scaffold.

Table 1. Mechanical properties of Anycubic Photom M3 Plus 3D printer [21]

Mechanical Properties	Value
Exposure screen	9.25 inch monochrome screen
Printing volume	5.9 liters
Printing platform	Laser engraved aluminum alloy platform
Printing speed	≤100 mm/hour
Rated power	144W
Mechanical Properties	**Value**
Machine weight	~12kg
Machine dimensions	475 x 360 x 290 mm
Machine leveling	4-point manual leveling

Table 2. Material properties of ECO UV RESIN [22]

Property	Value
Material type	ECO UV RESIN
Manufacturing process	Masked Stereolithography (MSLA)
Color	Black
Tensile strength	59 – 70 Mpa
Elongation at break	11-20%
Density	1.05-1.25 g/cm3
Viscosity (25℃)	300 mPas
Print Layer Thickness	from 35 microns
Volume	1l
Recommended baking time for layers	6-10 seconds

Since the aim of this research is to analyze the influence of scaffold cross-section on their mechanical performance, quasi-static uniaxial compression tests were performed. These tests evaluate the behavior and mechanical properties of scaffold materials or structures under compressive force applied in a single direction. Additionally, the tests enable precise analysis of the scaffold's mechanical properties under compression, which is essential for optimizing its design and material selection. The quasi-static uniaxial compression tests were conducted on a Shimadzu Table-top AGS-X universal testing machine (Shimadzu, Kyoto, Japan) equipped with a 10 kN load cell. Testing was carried out at a crosshead speed of 0.5 mm/min with a speed accuracy of 0.1%. The universal testing machine and the test setup are shown in the Figure 5, while the technical specifications of the machine are presented in the Table 3. During the tests, data on force as a function of crosshead displacement (useful for generating force-displacement diagrams) were recorded at specific intervals and collected using Shimadzu TrapeziumX software at a sampling frequency of 100 Hz.

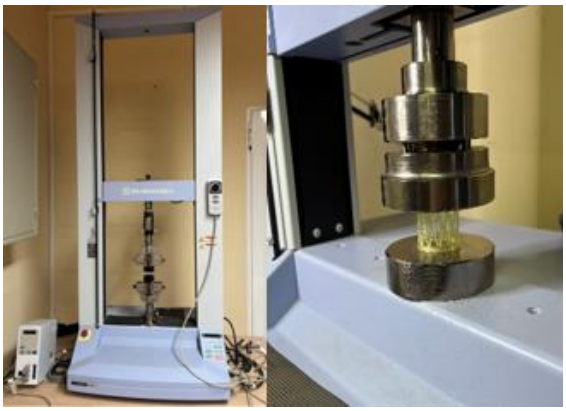

Figure 5. Shimadzu Table-top AGS-X 10 kN universal testing machine (left), experiment setup (right)

Table 3. Shimadzu Table-top AGS-X 10 kN universal testing machine characteristics [23]

Mechanical Properties	Value
Brand	Shimadzu
Model	Table-top AGS-X 10 kN
Weight	85 kg
Power	1.2 kW
Max load/capacity	10 kN
Dimensions	W653 × D520 × H1603 mm
Crosshead speed range	0.001 to 1000 mm/min
Crosshead speed accuracy	0.1%
Crosshead—table distance (tensile stroke)	1200 mm (760 mm, MWG)
Data capture rate	1000 Hz max

After the quasi-static uniaxial compression tests, experimental results consisting of stress-strain curves were obtained. Six scaffold models, differing in strut cross-section (square, rhomboid, circular, two rectangular, and cross-shaped), were subjected to these tests. Two independent tests were performed for each scaffold model to ensure the reliability and repeatability of the results. Based on this, the total number of quasi-static uniaxial compression tests conducted was 12.

3. RESULTS AND DISCUSSION

In the previous section, all six scaffold models, each characterized by a distinct strut cross-section, were described in detail. These models were subjected to quasi-static uniaxial compression tests (performed twice for each scaffold model) to evaluate the influence of strut cross-section on their mechanical properties. The tests yielded specific experimental results that served as the basis for generating the corresponding stress-strain curves. Figure 6 presents these curves (i.e., the relationship between stress and strain) obtained after performing all quasi-static uniaxial compression tests on the twelve tested scaffold specimens. Table 4 summarizes selected numerical data from the testing of all six scaffold models in two repeated trials. The table includes the maximum force recorded, the maximum stress, Young's modulus, and the coefficient of determination (R^2) for each scaffold model.

The stress–strain curves presented in Figure 6 clearly illustrate the differences in maximum stress values, the post-peak behavior (fracture of the scaffold models), and the variations in the deformation zone observed during the quasi-static uniaxial compression tests conducted on the twelve tested scaffold specimens. All these differences are directly related to the cross-sectional shape of the struts (circular, square, rhomboid, two rectangular, and cross-shaped). Scaffold models with rectangular strut cross-sections (4-1, 4-2, 5-1, and 5-2) reach the highest stress values and exhibit a steeper initial slope of the curve, which directly indicates greater stiffness of these models. Scaffolds with rhomboid and cross-shaped strut cross-sections (3-1, 3-2, 6-1, and 6-2) exhibit relatively high stress values and are characterized by an extended deformation zone prior to fracture, which makes them more resistant to sudden failure.

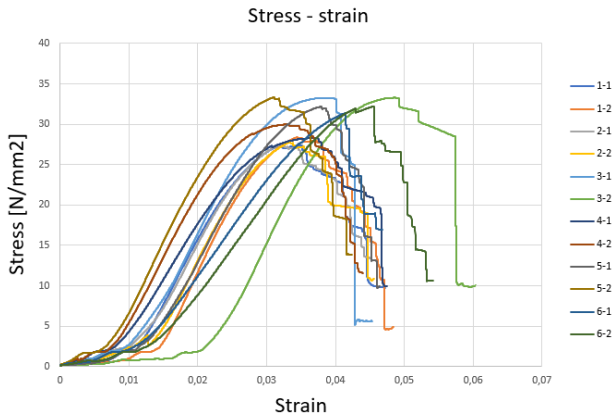

Figure 6. Stress–strain curves obtained after quasi-static uniaxial compression tests

Table 4. Numerical data obtained from testing all six scaffold models in two repeated trials

Scaffold models	F_{max} [N]	σ_{max} [N/mm^2]	E [N/mm^2]	R^2
1-1	821.54	27.38	1583.2	0.9993
1-2	852.26	28.41	1774.3	0.9992
2-1	830.38	27.68	1543.7	0.9984
2-2	834.84	27.83	1666.1	0.9993
3-1	997.82	33.26	1645.3	0.9993
3-2	998.72	33.29	1688.5	0.999
4-1	848.21	28.27	1368.6	0.9996
4-2	900.14	30.01	1638.1	0.9997
5-1	966.00	32.20	1523.8	0.9993
5-2	1001.6	33.39	1710.7	0.999
6-1	941.24	31.38	1180	0.9998
6-2	965.96	32.199	1153.7	0.9994

After reaching maximum stress, they gradually lose load-bearing capacity and are able to withstand loading for a longer period. In contrast, scaffolds with circular and square strut cross-sections (1-1, 1-2, 2-1, and 2-2) show the lowest stress values and have a more moderate initial slope on the curve, clearly indicating lower stiffness.

After reaching their peak stress, scaffolds with circular and square strut cross-sections (1-1, 1-2, 2-1, and 2-2) exhibit a sharp drop in stress, leading to a brittle fracture mode,

whereas scaffolds with rhomboid and cross-shaped strut cross-sections (3-1, 3-2, 6-1, and 6-2) retain a gradual decrease in stress and an extended deformation phase.

Table 4 presents the maximum force and stress values, elastic modulus, and coefficient of determination for all six scaffold models with different strut cross-sectional shapes (circular, square, rhomboid, two rectangular, and cross-shaped) in two repeated tests. The results indicate significant differences in mechanical performance depending on the cross-sectional geometry, despite all specimens being tested under identical conditions.

Scaffolds with rhomboid and rectangular strut geometries–model 3 (998.72 N) and model 5 (1001.6 N) – achieved the highest force values. Both scaffolds also exhibited the highest stress values, 33.29 N/mm² and 33.39 N/mm², indicating exceptional load-bearing capacity. In contrast, the lowest force values were recorded for scaffolds with circular and square strut cross-sections, model 1 (821.54 N) and model 2 (830.38 N), which also displayed the lowest stress values, 27.38 N/mm² and 27.68 N/mm², reflecting lower load capacity and reduced resistance to compression. Based on these results, a positive correlation between maximum force and maximum stress can be established. The elastic modulus values also vary depending on the strut geometry of the scaffolds. The highest elastic modulus values were observed for scaffolds with circular and rectangular strut cross-sections, model 1 (1774.2 N/mm²) and model 5 (1710.7 N/mm²), while the lowest elastic modulus was recorded for the scaffold with a cross-shaped strut cross-section, model 6 (1180 N/mm²). These findings demonstrate that certain strut geometries can simultaneously provide high strength and stiffness, whereas others offer greater elasticity at the expense of load-bearing capacity.

Based on all the presented results, it can be concluded that the geometry of the strut cross-section significantly impacts the mechanical performance of the scaffolds. Scaffolds with rhomboid and rectangular strut cross-sections (model 3 and 5) exhibited the best mechanical performance, showing an optimal balance of maximum force, stress, and elastic modulus, along with exceptional load-bearing capacity and good elasticity. In contrast, scaffolds with circular, square, and cross-shaped strut cross-sections (models 1, 2, and 6) showed the weakest mechanical performance — models 1 and 2 due to their lowest load-bearing capacity, and model 6 due to its lowest elastic modulus, indicating the greatest brittleness.

4. CONCLUSION

In this study, the influence of six different strut cross-sectional geometries (circular, square, rhomboid, two rectangular, and cross-shaped) on the mechanical performance of lattice scaffolds intended for small bone defect segments was thoroughly investigated. Twelve scaffold models (two for each geometry) were fabricated using an Anycubic Photon M3 Plus 3D printer with MSLA technology and tested on a Shimadzu Table-top AGS-X machine under quasi-static uniaxial compression.

The experimental results confirmed that strut cross-sectional geometry significantly affects scaffold performance in terms of load-bearing capacity, stiffness, strength, deformation behaviour, and fracture mode. Scaffolds with rhomboid and rectangular strut cross-sections exhibited the highest maximum force and stress values while simultaneously maintaining optimal elasticity. These scaffolds are characterized by exceptional load-bearing capability, making them particularly suitable for applications requiring high load capacity combined with a certain level of deformability. In contrast, scaffolds with circular and square strut cross-sections recorded the lowest force and stress values, and thus the lowest load-bearing capacity, along with a greater tendency toward brittle fracture. Scaffold models with cross-shaped strut cross-sections had the lowest elastic modulus, indicating increased flexibility but significantly lower resistance to load. Analysis of the stress–strain curves further revealed that the geometry of the strut cross-section influences not only the maximum values of stress, force, and elastic modulus but also the post-fracture behaviour of the

scaffolds. This influence is manifested as either a sudden loss of load-bearing capacity, as observed in scaffolds with circular and square strut cross-sections, or a gradual decrease in load, as in scaffolds with rhomboid and cross-shaped strut cross-sections.

The presented test results indicate that the choice of strut cross-sectional geometry can be a critical parameter in designing scaffolds for specific applications. This study forms part of a broader investigation aimed at identifying the mechanical property patterns of this particular lattice-structured scaffold. Future research will focus on incorporating numerical methods, such as finite element analysis (FEA), to more accurately assess stress distribution and optimize the structure for improved scaffold performance.

ACKNOWLEDGEMENT

The research activities are financed by the Ministry of Science, Technological Development and Innovation of the Republic of Serbia (Contract No. 451-03-47/2023-01/200109).

REFERENCES

[1] Seunghun S. Lee, Xiaoyu Du, Inseon Kim, Stephen J. Ferguson, "Scaffolds for bone-tussue engineering, Matter", Vol. 5, Issue 9, pp. 2722-2759, 2022.

[2] Tongyu Zhu, Hongbo Zhou, Xiaojing Chen, Yuanjing Zhu, "Rcent advances of responsive scaffolds in bone tissue engineering, Frontiers", Vol. 11, pp. 534–538, 2023.

[3] Chang Xu, Zhize Liu, Xi Chen, Yang Gao, Wenjun Wang, Xijing Zhuang, Hao Zhang, Xufeng Dong, "Bone tissue engineering scaffold materials: Fundamentals, advances, and challenges", ScienceDirect, Vol. 35, pp. 109-197, 2024.

[4] Huawei Qu, Hongya Fu, Zhenyu Hana, Yang Sun, "Biomaterials for bone tissue engineering scaffolds: a review", Publishing, Vol. 9, pp. 26252-26262, 2019.

[5] Yi Huo, Yongtao Lu, Lingfei Meng, Jiongyi Wu, Tingxiang Gong, Jia'ao Zou, Sergei Bosiakov, Liangliang Cheng, "A Critical Review on the Design, Manufacturing and Assessment of the Bone Scaffold for Large Bone Defects", PubMed Central, Vol. 9, pp. 404–411, 2021.

[6] Yuchun Liu, Jing Lim, Swee-Hin Teoh, "Review: development of clinically relevant scaffolds for vascularised bone tissue engineering", PubMed, Vol. 31, pp. 688-705, 2013.

[7] M. A. Wettergreen, B. S. Bucklen, B. Starly, E. Yuksel, W. Sun, and M. A. K. Liebschner, "Creation of a unit block library of architectures for use in assembled scaffold engineering," Comput. Des., vol. 37, no. 11, pp. 1141–1149, Sep. 2005.

[8] G. Ryan, P. McGarry, A. Pandit, and D. Apatsidis, "Analysis of the mechanical behavior of a titanium scaffold with a repeating unit-cell substructure," J. Biomed. Mater. Res. Part B Appl. Biomater., vol. 90B, no. 2, pp. 894–906, Aug. 2009.

[9] G. E. Ryan, A. S. Pandit, and D. P. Apatsidis, "Porous titanium scaffolds fabricated using a rapid prototyping and powder metallurgy technique," Biomaterials, vol. 29, no. 27, pp. 3625–3635, Sep. 2008

[10] M. Ramu, M. Ananthasubramanian, T. Kumaresan, R. Gandhinathan, and S. Jothi, "Optimization of the configuration of porous bone scaffolds made of Polyamide/Hydroxyapatite composites using Selective Laser Sintering for tissue engineering applications," Biomed. Mater. Eng., vol. 29, no. 6, pp. 739–755, Jan. 2018.

[11] C. Shi, N. Lu, Y. Qin, M. Liu, H. Li, and H. Li, "Study on mechanical properties and permeability of elliptical porous scaffold based on the SLM manufactured medical Ti6Al4V," PLoS One, vol. 16, no. 3, p. e0247764, Mar. 2021.

[12] M. Asadi-Eydivand, M. Solati-Hashjin, and N. A. Abu Osman, "Mechanical behavior of calcium sulfate scaffold prototypes built by solid free-form fabrication," Rapid Prototyp. J., vol. 24, no. 8, pp. 1392–1400, Nov. 2018.

[13] S. Eshraghi and S. Das, "Micromechanical finite-element modeling and experimental characterization of the compressive mechanical properties of polycaprolactone–hydroxyapatite composite scaffolds prepared by selective laser sintering for bone tissue engineering," Acta Biomater., vol. 8, no. 8, pp. 3138–3143, Aug. 2012.

[14] S. Cahill, S. Lohfeld, and P. E. McHugh, "Finite element predictions compared to experimental results for the effective modulus of bone tissue engineering scaffolds fabricated by selective laser sintering," J. Mater. Sci. Mater. Med. 2009 206, vol. 20, no. 6, pp. 1255–1262, Feb. 2009.

[15] J. Wieding, R. Souffrant, W. Mittelmeier, and R. Bader, "Finite element analysis on the biomechanical stability of open porous titanium scaffolds for large segmental bone defects under physiological load conditions," Med. Eng. Phys., vol. 35, no. 4, pp. 422–432, Apr. 2013.

[16] Z. Xu, A. M. Omar, and P. Bartolo, "Experimental and Numerical Simulations of 3D-Printed Polycaprolactone Scaffolds for Bone Tissue Engineering Applications," Mater. 2021, Vol. 14, Page 3546, vol. 14, no. 13, p. 3546, Jun. 2021.

[17] S. Naghieh, M. R. Karamooz Ravari, M. Badrossamay, E. Foroozmehr, and M. Kadkhodaei, "Numerical investigation of the mechanical properties of the additive manufactured bone scaffolds fabricated by FDM: The effect of layer penetration and post-heating," J. Mech. Behav. Biomed. Mater., vol. 59, pp. 241–250, Jun. 2016.

[18] C. Shi, N. Lu, Y. Qin, M. Liu, H. Li, and H. Li, "Study on mechanical properties and permeability of elliptical porous scaffold based on the SLM manufactured medical Ti6Al4V," PLoS One, vol. 16, no. 3, pp. 1–17, 2021.

[19] Z. Xu, A. M. Omar, and P. Bartolo, "Experimental and Numerical Simulations of 3D-Printed Polycaprolactone Scaffolds for Bone Tissue Engineering Applications," Materials (Basel)., vol. 14, no. 13, 2021.

[20] J. R. Milovanovic, M. S. Stojkovic, K. N. Husain, N. D. Korunovic, and J. Arandjelovic, "Holistic approach in designing the personalized bone scaffold: The case of reconstruction of large missing piece of mandible caused by congenital anatomic anomaly," J. Healthc. Eng., vol. 2020, 2020.

[21] Anycubic photon M3 Plus, available at: https://store.anycubic.com/products/photon-m3-plus, accessed: 10.08.2025.

[22] Anycubic-Grey/Gray Eco Plant-Based UV Resin 0.5kg, available at: https://anycubic.biz/grey-gray-eco-plant-based-uv-resin-anycubic-05kg, accessed: 10.08.2025.

[23] Rajko Turudija, Miloš Stojkovic, Jelena R. Stojkovic, Jovan Arandelovic and Dragan Marinkovic, "Stiffness of Anatomically Shaped Lattice Scaffolds Made by Direct Metal Laser Sintering of Ti-6Al-4V Powder: A Comparison of Two Different Design Variants", Metals. Eng., vol. 2024, 2024.

Society of Production Engineering

ICPES 2025

40th INTERNATIONAL CONFERENCE ON PRODUCTION ENGINEERING - SERBIA 2025

DOI: 10.46793/ICPES25.439T

University of Nis Faculty of Mechanical Engineering

Nis, Serbia, 18 - 19th September 2025

RELATIONSHIP BETWEEN POROSITY AND MECHANICAL PERFORMANCE OF CUSTOM LATTICE-LIKE BONE SCAFFOLDS

Rajko TURUDIJA[1*], Jovan ARANĐELOVIĆ[1], Miloš STOJKOVIĆ[1], Jelena STOJKOVIĆ[1], Nikola KORUNOVIĆ[1]

Orcid: 0000-0002-6324-5967; **Orcid:** 0000-0001-9653-4119; **Orcid:** 0000-0001-9020-125X; **Orcid:** 0000-0002-8249-2816; **Orcid:** 0000-0002-9103-9300;

[1]Faculty of Mechanical Engineering, Niš, Serbia

*Corresponding author: rajko.turudija@masfak.ni.ac.rs

Abstract: *Bone scaffolds for the treatment of large defects serve two primary functions: to replicate the mechanical properties of natural bone, particularly elasticity, thereby preventing complications such as stress shielding and implant failure, and to promote bone regeneration by incorporating bioactive agents that stimulate new tissue growth. To retain these substances in place and to prevent their diffusion or migration away from the targeted site, scaffolds must be sufficiently porous to allow substance delivery and vascularization but also mechanically stable enough to replicate the properties of the bone region they are intended for. This work presents an analysis of experimental results obtained by mechanical testing of custom-made lattice-like scaffolds, focusing on their porosity and mechanical performance. Porosity of scaffolds was varied by varying the design parameters of a custom CAD model of lattice-like scaffold (such as strut diameter, strut angle, etc.). These scaffolds were fabricated using SLS 3D printing technology and tested under uniaxial compression using a universal testing machine. The results reveal an almost linear negative correlation between scaffold porosity and compressive strength, which aligns with theoretical expectations. It was also observed that scaffolds with very similar porosity values (e.g., 76% vs. 77%) can exhibit significant differences in mechanical strength, with the difference sometimes exceeding 600 N, indicating that strut arrangement and geometry also play a crucial role beyond porosity alone.*

Keywords: *lattice-like scaffolds, bioengineering, mechanical properties, porosity*

1. INTRODUCTION

Bone scaffolds are widely used to provide mechanical support and structural integrity in cases of bone defects or large tissue loss. These scaffolds serve two primary functions: to mimic the mechanical properties of the surrounding bone in order to maintain the physiological load-bearing balance and prevent complications such as stress shielding or implant failure, and to promote bone regeneration by incorporating bioactive materials that stimulate new tissue growth. This study focuses exclusively on the mechanical behaviour of the scaffold.

Scaffold designs are typically categorized into two main groups [1]: porous scaffolds (Figure 1 - left), which emulate the morphology of cancellous bone, and lattice-like scaffolds (Figure 1 - right), which adopt more geometrically regular structures. In porous scaffolds, the design emphasis is placed on the

pore geometry—specifically the shape, size, and distribution of the voids. The connecting elements serve primarily to define and support these voids and are often formed as complex shell-like structures. In contrast, lattice-like scaffolds shift the design focus from the pores to the structural elements themselves—commonly referred to as struts. While lattice-like scaffolds also occupy a largely void-filled volume, their open and interconnected nature may in some cases allow for even greater permeability and airiness than porous scaffolds. However, due to the reduced surface area of the structural elements, the contact interface with the surrounding tissue may be significantly smaller compared to that of porous scaffolds.

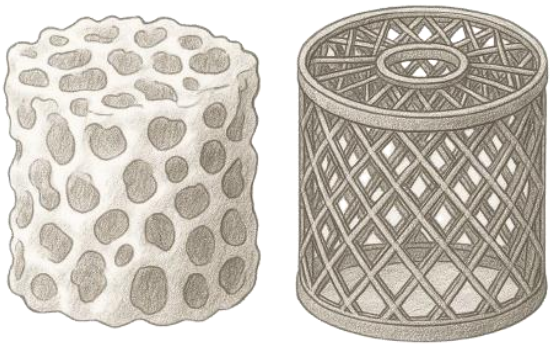

Figure 1. Porous (left) and lattice-like (right) bone scaffold structures

While porous scaffold designs dominate the literature, lattice-based concepts remain comparatively underexplored, primarily due to their more complex and time-consuming design procedures. Various computer-aided design (CAD) strategies have been employed in scaffold modelling. One common approach involves the use of unit cells micro-architectural elements that are replicated and assembled into a complete macrostructure [2, 3]. Alternatively, monolithic macro-scale designs can be created directly as a unified scaffold structure, [4, 5]. Both approaches can utilize different modelling techniques. For instance, scaffold geometry can be generated through Boolean operations, by subtracting predefined shapes from a base volume [2, 6], or by applying wireframe-based design principles, where struts define the structure's topology, [2, 4]. Furthermore, topology optimization techniques have been used to adapt scaffold geometry to specific loading and boundary conditions, enhancing structural performance.

Across multiple studies [4, 6, 7, 8], several recurring design parameters have been identified, regardless of the specific modelling approach. These include:

- Pore size or strut diameter,
- Pore density or number of struts,
- Strut orientation or angle, and
- Overall scaffold dimensions (e.g., height, width, diameter).

Although the choice of design methodology (whether the scaffolds are based on unit cells, macro-scale volumes, or patient-specific customization) introduces variability in scaffold geometry, these global design parameters consistently influence the scaffold's mechanical and biological performance.

To ensure clinical applicability, scaffolds must meet specific mechanical performance requirements. Numerous experimental studies have assessed the mechanical behaviour of porous scaffolds through uniaxial compression testing [7, 9] while others have employed computational structural analysis methods to simulate scaffold behaviour under loading conditions [2, 9, 10]. These investigations have revealed key trends regarding the influence of both geometrical parameters [6, 9] and manufacturing conditions [8, 10] on overall mechanical response.

As highlighted in the literature review, further investigation of lattice-like scaffolds is needed, and particularly of those featuring free-form and custom-made geometries. These complex designs, although promising, remain insufficiently explored in terms of their mechanical behaviour and practical application. One such scaffold design, developed and presented by the authors in a previous study [11], was specifically designed to address the challenges of large segmental defects in long bones (Figure 2). This structure features a tailored lattice configuration optimized for both anatomical compatibility and load-bearing capacity.

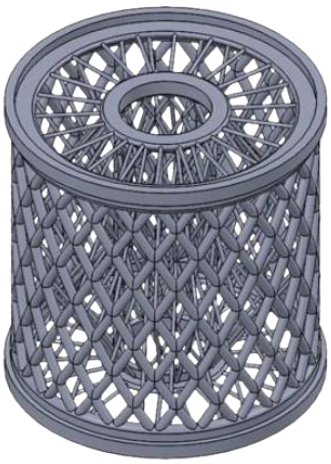

Figure 2. Custom lattice like scaffold

The present study builds upon earlier work of the authors as part of an ongoing research efforts focused on evaluating and optimizing the aforementioned scaffold design. The objective of this paper is to investigate the relationship between scaffold porosity and its mechanical performance, with the aim of establishing general design principles that can guide the development of structurally efficient and clinically viable lattice-like bone scaffolds.

2. METHODOLOGY

The custom lattice-like scaffold models described in the previous section were subjected to uniaxial compression testing to evaluate their mechanical performance. A total of 12 scaffold samples were fabricated, each featuring a distinct porosity level. The underlying CAD model was fully parametrized, enabling systematic variation of key geometrical features. By adjusting the following parameters:

- outer strut diameter,
- inner strut diameter,
- outer strut angle,
- inner strut angle, and
- number of outer struts,

twelve unique scaffold configurations were generated, each with a different porosity percentage. These configurations served as the basis for analysing the influence of scaffold porosity on its mechanical behaviour. An overview of the tested designs and their respective porosity values is provided in Table 1 and presented in Figure 3.

Table 1. Scaffold samples and their respective porosity values

#	Porosity	#	Porosity
1	76.01	7	74.18
2	82.68	8	79.78
3	78.47	9	83.83
4	80.32	10	77.41
5	86.33	11	83.28
6	79.68	12	76.85

Figure 3. Custom lattice like scaffold used for the experiments

Machine used for fabrication of the above-mentioned scaffolds was EOS Formiga P100 (Figure 4). It has the build volume of 200 x 250 x 330 mm and layer resolution from 100 micron to 60 micron. As scaffold material, PA2200 – polyamide 12 was used (PA12) (Table 2 provides some information about this material).

Figure 4. EOS Formiga P100 SLS 3D printer

Table 2. Material properties of PA12

Property	Value
Material type	Polyamide 12 (PA12)
Manufacturing process	Selective Laser Sintering (SLS)
Color	White
Tensile strength	~48 MPa
Elongation at break	~20%
Young's modulus	~1650 MPa
Density	~930 kg/m³ (solid)
Heat deflection temperature	~95 °C (at 1.8 MPa)

Quasi-static uniaxial compression tests were carried out on Shimadzu Table-top AGS-X universal testing machine with a 10 kN load cell (the load cell accuracy is within ±0.5% of the indicated test force, for forces between 20 N and 10 kN). During the tests, a crosshead speed of 1 mm/min was used (with a speed accuracy of 0.1%). The force-stroke points were collected with the Shimadzu TrapeziumX software with a 100 Hz frequency. The illustration of the machine and testing setup is presented in Figure 5. To ensure accurate and reliable measurements, custom-made compression plates were fabricated specifically for this study. The plates were manufactured from high-strength steel, significantly stronger than the PA12 material used for the scaffolds, in order to eliminate any deformation of the fixtures during testing and to preserve the integrity of the experimental data.

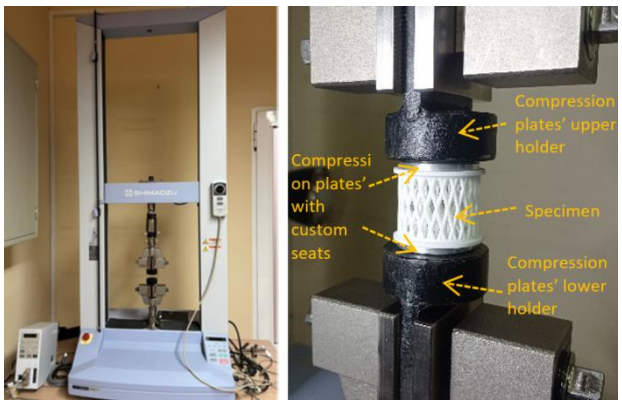

Figure 5. Shimadzu Table-top AGS-X 10 kN universal testing machine (left), experiment setup (right)

The experimental output obtained from the compression tests consisted of force–displacement curves. For each scaffold configuration, three independent tests were performed to ensure the reliability and repeatability of the results.

3. RESULTS AND DISCUSION

Figure 6 presents the force–displacement curves obtained during the second set of experimental trials for all tested specimens. The corresponding numerical results are summarized in Table 3, which lists the maximum force values recorded during testing for all twelve scaffold configurations, across all three repeated trials. Additionally, the table presents the average maximum force calculated from the three measurements for each individual scaffold design.

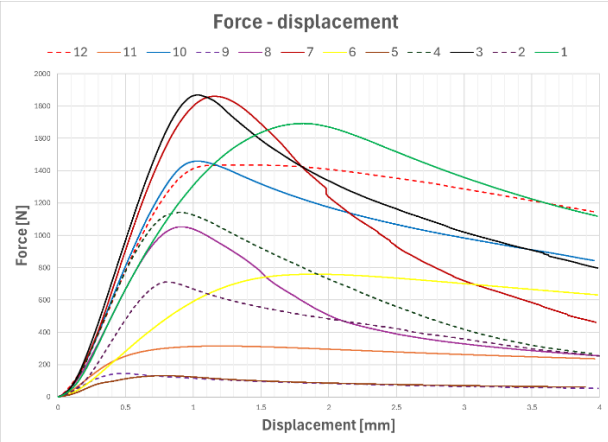

Figure 6. Force - displacement curves obtained during the second set of experimental trials

The curves (Figure 5) show noticeable differences in both maximum force and post-peak behaviour, which directly correlate with scaffold geometry and porosity. Scaffolds with lower porosity (e.g., samples 3 and 7) exhibit steeper initial slopes, indicating higher stiffness, and reach significantly higher peak forces before failure. In contrast, high-porosity scaffolds (e.g., samples 2, 5 and 11) display a more gradual force increase, lower peak forces, and an earlier onset of deformation, reflecting reduced load-bearing capacity. The shape of the curves after peak force also varies considerably. Some configurations (e.g., samples 12 and 6) maintain relatively high residual load capacity after peak force, suggesting a more gradual failure mode. Others

(e.g., samples 4 and 3) experience an abrupt load drop. These differences can be attributed not only to porosity but also to strut orientation, connection density, and load path continuity within the lattice structure.

Table 3. Maximum force values recorded during testing for all twelve scaffold configurations, across all three repeated trials

#	Porosity (%)	Fmax1 (N)	Fmax2 (N)	Fmax3 (N)	Average F (N)
1	76.01	1620.002	1691.573	1784.6	1698.725
2	82.68	539.1614	711.5094	743.38	664.6836
3	78.47	1879.869	1868.281	1563.94	1770.697
4	80.32	1335.344	1141.326	1653.7	1376.79
5	86.33	317.9026	131.6341	259.107	236.2146
6	79.68	968.0668	759.2185	859.218	862.1678
7	74.18	2813.004	1859.703	2590.22	2420.976
8	79.78	876.6985	1052.397	1433.87	1120.989
9	83.83	299.2614	145.9026	239.433	228.199
10	77.41	1674.898	1459.061	1468.97	1534.31
11	83.28	220.3528	315.0161	226.563	253.9773
12	76.85	975.0255	1434.867	1388.65	1266.181

The maximum force values obtained for all twelve scaffold configurations are summarized in Table 3. The results reveal a clear negative correlation between porosity and maximum compressive force (which can also be seen in Figure 7), where scaffolds with lower porosity generally exhibit higher load-bearing capacity. For example, the specimen with 74.18% porosity achieved the highest average maximum force (2420.976 N), while the most porous configuration (86.33% porosity) demonstrated the lowest mechanical strength (236.2146 N on average). However, the data also indicate that porosity alone does not fully determine mechanical performance. Certain scaffolds with very similar porosity values exhibited large differences in their maximum load capacity. For instance, the two samples with porosity levels of 76.01% and 76.85% showed average maximum forces of 1698.725 N and 1266.181 N, respectively, a difference of over 400 N. This suggests that other geometrical factors, such as strut arrangement, diameter, and orientation, play a significant role in defining the overall mechanical response. It is also notable that some mid-range porosity designs (e.g., 78.47%) outperformed certain lower-porosity scaffolds (e.g., 77.41% and 76.85%), again highlighting that structural topology and load distribution within the lattice network can offset the expected loss of strength due to increased void fraction.

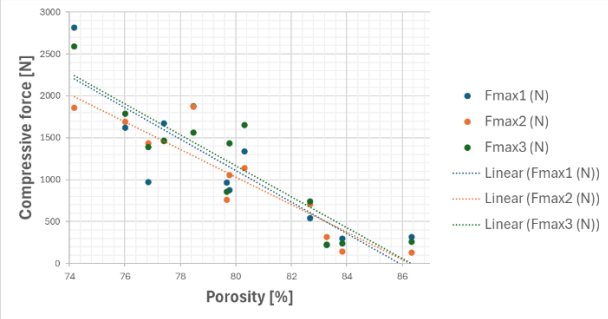

Figure 7. Correlation between porosity and maximum compressive force

4. CONCLUSION

This study investigated the relationship between porosity and mechanical performance of custom-designed lattice-like bone scaffolds, specifically tailored for large segmental defects in long bones. Twelve scaffold configurations with varying porosity levels were fabricated using SLS additive manufacturing and tested under uniaxial compression.

The results confirmed theoretical expectations of a general decrease in strength with increasing porosity. However, the findings also demonstrated that geometrical optimization at the strut and cell level can produce scaffolds with a large mechanical strength even at relatively high porosity levels. Furthermore, analysis of the force–deformation curves revealed that certain lattice designs are capable of retaining a portion of their load-bearing capacity even after the onset of structural failure. This characteristic may be advantageous in biomedical applications, where controlled failure and gradual load transfer to the surrounding bone tissue can facilitate the healing process and reduce the risk of catastrophic implant failure. However, there is a possibility that following unloading

and subsequent reloading, these scaffolds may also experience immediate failure. This aspect warrants further investigation and will be the subject of future research.

Future work will focus on more detailed stress–strain characterization, accounting for complex and variable cross-sections, and on exploring topological optimization methods to further refine scaffold performance for specific clinical requirements. Additionally, given the complexity of the stress distribution within lattice-like scaffolds, incorporating finite element analysis (FEA) will be essential for accurately assessing the internal stress state and identifying potential failure zones.

ACKNOWLEDGEMENT

The research activities are financed by the Ministry of Science, Technological Development and Innovation of the Republic of Serbia (Contract No. 451-03-47/2023-01/200109).

REFERENCES

[1] J. Milovanović, M. Stojković, M. Trifunović, and N. Vitković, “Review of Bone Scaffold Design Concepts and Design Methods,” Facta Univ. Ser. Mech. Eng., 2020.

[2] M. A. Wettergreen, B. S. Bucklen, B. Starly, E. Yuksel, W. Sun, and M. A. K. Liebschner, “Creation of a unit block library of architectures for use in assembled scaffold engineering,” Comput. Des., vol. 37, no. 11, pp. 1141–1149, Sep. 2005.

[3] R. M. Gorguluarslan, S. K. Choi, and C. J. Saldana, “Uncertainty quantification and validation of 3D lattice scaffolds for computer-aided biomedical applications,” J. Mech. Behav. Biomed. Mater., vol. 71, pp. 428–440, Jul. 2017.

[4] M. S. Stojkovic, N. D. Korunovic, M. D. Trajanovic, J. R. Milovanovic, M. B. Trifunovic, and N. M. Vitkovic, “Design study of anatomically shaped lattice scaffolds for the bone tissue recovery,” ECCOMAS Spec. Interes. Conf. - SEECCM 2013 3rd South-East Eur. Conf. Comput. Mech. Proc. - An IACM Spec. Interes. Conf., pp. 381–393, 2013.

[5] S. Eshraghi and S. Das, “Micromechanical finite-element modeling and experimental characterization of the compressive mechanical properties of polycaprolactone–hydroxyapatite composite scaffolds prepared by selective laser sintering for bone tissue engineering,” Acta Biomater., vol. 8, no. 8, pp. 3138–3143, Aug. 2012

[6] C. Shi, N. Lu, Y. Qin, M. Liu, H. Li, and H. Li, “Study on mechanical properties and permeability of elliptical porous scaffold based on the SLM manufactured medical Ti6Al4V,” PLoS One, vol. 16, no. 3, p. e0247764, Mar. 2021.

[7] G. E. Ryan, A. S. Pandit, and D. P. Apatsidis, “Porous titanium scaffolds fabricated using a rapid prototyping and powder metallurgy technique,” Biomaterials, vol. 29, no. 27, pp. 3625–3635, Sep. 2008.

[8] S. Cahill, S. Lohfeld, and P. E. McHugh, “Finite element predictions compared to experimental results for the effective modulus of bone tissue engineering scaffolds fabricated by selective laser sintering,” J. Mater. Sci. Mater. Med. 2009 206, vol. 20, no. 6, pp. 1255–1262, Feb. 2009.

[9] M. Ramu, M. Ananthasubramanian, T. Kumaresan, R. Gandhinathan, and S. Jothi, “Optimization of the configuration of porous bone scaffolds made of Polyamide/Hydroxyapatite composites using Selective Laser Sintering for tissue engineering applications,” Biomed. Mater. Eng., vol. 29, no. 6, pp. 739–755, Jan. 2018.

[10] G. Ryan, P. McGarry, A. Pandit, and D. Apatsidis, “Analysis of the mechanical behavior of a titanium scaffold with a repeating unit-cell substructure,” J. Biomed. Mater. Res. Part B Appl. Biomater., vol. 90B, no. 2, pp. 894–906, Aug. 2009.

[11] R. Turudija, J. Arandjelovic, M. Stojkovic, N. Korunovic, J. Milovanovic, “Novel approach to generic parametrized lattice scaffold model design”, Conference ICIST 2022, Kopaonik, Serbia.

Session 9:

Metrology and quality, cutting tools

Society of Production Engineering

ICPES 2025

40th INTERNATIONAL CONFERENCE ON PRODUCTION ENGINEERING - SERBIA 2025

DOI: 10.46793/ICPES25.446B

University of Nis Faculty of Mechanical Engineering

Nis, Serbia, 18 - 19th September 2025

COMPARISON OF LASER INTERFEROMETER SYSTEMS FOR MEASURING POSITIONAL ACCURACY OF MACHINE TOOLS

Alexander Buda BUDIMIR[1], Slobodan TABAKOVIĆ[1]*, Milan ZELJKOVIĆ[1], Saša ŽIVANOVIĆ[2], Zoran DIMIĆ[3]

Orcid: 0000-0001-6470-2376; **Orcid:** 0000-0002-8542-0535; **Orcid:** 0000-0003-4950-8203; **Orcid:** 0000-0002-1496-4981;

[1]University of Novi Sad, Faculty of Technical Sciences, Novi Sad, Serbia

[2] University of Belgrade, Faculty of Mechanical Engineering, Belgrade, Serbia

[3]LOLA Institute, Belgrade, Serbia

*Corresponding author: tabak@uns.ac.rs

Abstract: *Laser interferometers have become indispensable tools in the high-precision calibration of machine tools, offering sub-micron resolution and enhanced measurement reliability. Since the introduction of stabilized helium–neon (He–Ne) lasers in the 1960s, manufacturers like Hewlett-Packard (HP), Renishaw, and Lasertex have developed systems with increasingly advanced capabilities. This paper presents a technical and historical comparison of three key interferometric systems: HP's 5525A, Renishaw's XL-80, and Lasertex's HPI-3D. The analysis includes specifications such as laser stability, resolution, environmental compensation, and dynamic measurement capabilities. The HP 5525A, although historically significant, lacks modern portability and software integration. In contrast, Renishaw's XL-80 offers compactness, advanced environmental compensation, and compatibility with international metrology standards. Lasertex's HPI-3D introduces next-generation capabilities, such as real-time vibration analysis, nanometric resolution, and full 3D geometric evaluation. The comparative findings suggest a clear technological evolution toward higher precision, modularity, and software-driven diagnostics in laser interferometry.*

Keywords: *Laser interferometer, Machine tool accuracy, Displacement measurement, Positioning accuracy, Machine tool calibration*

1. INTRODUCTION

Laser interferometers have become essential tools for measuring the geometric accuracy of machine tools, offering significant advantages over traditional gauge meters. Laser interferometers for length measurement became prominent after the introduction of frequency-stabilized lasers, particularly the He-Ne laser, in the 1960s and 1970s. Early commercial systems used stabilized He-Ne lasers as primary wavelength references for high-accuracy measurements [1,2]. The earliest manufacturer identified in the literature of laser interferometric systems for measuring the geometric accuracy of the machine tools is Hewlett-Packard. They developed a helium–neon laser system featuring beam splitters and

benders, which achieved an accuracy of ±0,5 parts per million at velocities up to 18 meters per minute for position and contour measurements [3].

Laser interferometers are crucial because they provide high-precision, non-contact, and rapid measurements of geometric errors, which are vital for maintaining and improving the accuracy of modern CNC and high-precision machine tools [4-6]. According to [6-8] laser interferometers compared to gauge meters offer many advantages:

- Higher accuracy and resolution. They are capable of detecting nanometer-level deviations.
- Faster and more comprehensive measurements. Systems like the Renishaw XM-60 can measure all six degrees of freedom at once, significantly reducing setup and measurement time.
- Reduced human error. Automated and software-integrated systems minimize manual intervention and subjective interpretation.
- Ability to measure over long distances and large machines. Especially important as machine tools increase in size for industries like aerospace.

2. LASER INTERFEROMETER MANUFACTURERS

Today on the European market there are two main suppliers of laser interferometers for measuring the positional accuracy of the machine tools, Lasertex and Renishaw. In the possession of University of Novi Sad, Faculty of Technical Sciences (UNS, FTN) there is a laser interferometer from the manufacturer Hewlett-Packard, which was at the time of purchasing (in 1980's) the main supplier of the market.

2.1 Hewlett-Packard (HP)

HP introduced and developed laser interferometers from 1966 whit Zeeman two-frequency He-Ne laser, enabling heterodyne interferometry. Major models with upgrades were also many times introduced, like the 5525A (in 1970), 10565A (in 1972), 10690A (in 1973) and 5501A transducer (in 1975) [9].

In 1999, Hewlett-Packard underwent a major corporate restructuring. The computer and printer divisions remained under the HP brand, while the test and measurement, semiconductor, and life sciences businesses were spun off into a new company called Agilent Technologies. Agilent inherited HP's entire Electronic Measurement Group, including the legacy of precision metrology and laser interferometry systems, although by that time, many of these older interferometer models were aging or already phased out. By 2014, Agilent chose to sharpen its focus on life sciences and diagnostics, and decided to spin off its electronic measurement division into a new company. This resulted in the formation of Keysight Technologies in November 2014. In summary, HP was the originator of many foundational technologies in laser-based precision measurement. Through its corporate evolution—first into Agilent Technologies in 1999, and then into Keysight Technologies in 2014—its legacy in electronic measurement has continued, even though laser interferometers were phased out decades earlier [10].

Figure 1. shows the HP 5525A system mounted on a tripod during measurement sequence.

Figure 1. HP 5525A laserhead during measurements

It is based on a frequency-stabilized helium-neon (He–Ne) gas laser, which serves as a highly

stable optical source for interferometric measurement. The system provides a frequency stability of ±5 ppm, sufficient for sub-micron accuracy in typical industrial calibration environments at the time of its development.

The HP 5525A delivers a displacement resolution of 10 nm, which, although modest by today's standards, was a significant achievement during its operational peak. The system supports a maximum sampling rate of 40 Hz, and a maximum velocity measurement capability of 3 m/s. The interferometric range extends up to 60 meters, which makes it suitable for large-scale machine calibration and long-range displacement tracking applications.

Environmental compensation in the HP 5525A system is facilitated via the HP 5510A environmental compensator, which provides real-time correction based on temperature, pressure, and humidity readings. This allows the system to adjust the effective laser wavelength in accordance with the refractive index of air, thereby improving measurement accuracy under non-laboratory conditions.

The HP 5525A system is capable of multiple measurement types, including linear displacement, velocity, angular deviation, rotary axis positioning, straightness, and flatness.

Physically, the HP 5525A laser head is large and robust, with dimensions of 127 × 179 × 526 mm and a total mass of 8,94 kg, making it unsuitable for portable or in-situ applications without specialized mounting hardware. Its analog signal output and lack of digital interfaces further limit its direct integration into modern computer-based control and analysis environments [11].

2.2 Renishaw

Renishaw plc is a UK-based engineering and technology company founded in 1973 by Sir David McMurtry and John Deer. The company initially gained recognition for developing the touch-trigger probe, revolutionizing coordinate measuring machines (CMMs). One of Renishaw's flagship products in dimensional metrology is the XL-80 laser interferometer system, widely used for calibrating CNC machines and coordinate measuring machines.

One of Renishaw's most sophisticated products in the field of dimensional metrology is the XL-80 laser interferometer system. The XL-80 is designed for ultra-high-accuracy measurement and calibration of machine tools, CMMs, and motion systems. It employs a frequency-stabilized helium-neon (He–Ne) laser source, ensuring a wavelength stability of ±0,05 ppm over a three-year calibration interval, and ±0,02 ppm over 1 hour. This degree of stability is critical in maintaining nanometer-level resolution during high-speed linear displacement measurements, even under dynamic conditions. The system supports a measurement resolution of 1 nm and a maximum velocity measurement capability of 4 m/s, making it highly suitable for modern high-speed motion platforms. In Figure 2. the Renishaw XL-80 laserhead is presented.

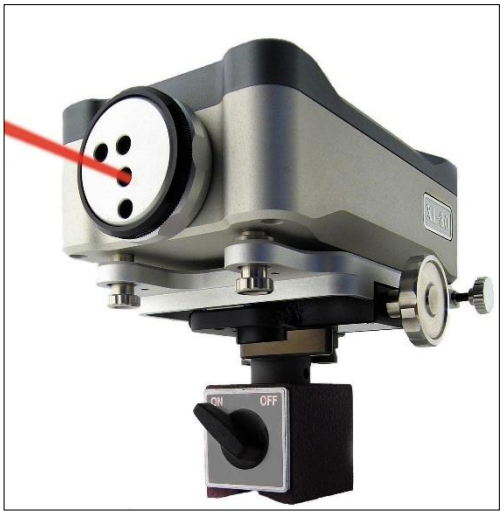

Figure 2. Renishaw XL-80 laserhead [12]

The XL-80 is modular and highly adaptable, supporting a wide range of optical accessories for linear, angular, straightness, rotary, flatness, and squareness measurement modes. Renishaw pairs this system with the XC-80 environmental compensator, which provides real-time correction for air temperature, pressure, humidity, and material temperature. This ensures that the refractive index of air and thermal expansion of components are appropriately accounted for, preserving measurement accuracy even in non-laboratory

conditions. The system's high sampling rate, up to 50 kHz, and real-time data processing capabilities enable accurate capture of dynamic behavior and vibration, which is essential in modern high-precision manufacturing environments.

Physically, the XL-80 is designed for portability and ease of integration, weighing only 1,85 kg for the laser unit and easily packaged in a transportable case with other components. The dimensions of the laser head are 127 x 179 x 526 mm. Connectivity via USB and compatibility with Renishaw's CARTO software suite streamline its deployment in both industrial and research settings. The system complies with international standards for laser safety and traceability, and its calibration procedures are ISO 17025-accredited, ensuring that measurement results meet rigorous traceability requirements [12,13].

2.3 Lasertex

Lasertex is a company originating from Poland and specializing in high-precision laser interferometry systems, primarily developed for the calibration and dynamic analysis of precision machinery, coordinate measuring machines (CMMs), CNC machines, and other motion platforms. The company has gained a reputation for innovation in the field of dimensional metrology by integrating compact form factors, advanced environmental sensing, and ultra-high-resolution measurement technologies. Among its most advanced offerings is the HPI-3D laser interferometer, a state-of-the-art system designed to meet the demands of next-generation manufacturing and scientific measurement environments.

The HPI-3D system employs a frequency-stabilized helium-neon (He–Ne) laser with an exceptional long- and short-term wavelength stability of ±0,001 ppm. This level of laser stability enables the HPI-3D to deliver measurement resolutions as fine as 0,1 nm in single-pass configurations and 0,05 nm in double-pass configurations, positioning it among the most precise commercially available systems. The system supports a maximum measurement range of up to 30 meters, with optional range extensions, and can measure velocities up to 7 m/s, or 20 m/s with an optional high-speed module. These specifications make the HPI-3D ideal for both laboratory-grade precision and high-speed industrial applications.

Figure 3. Lasertex HPI-3D laserhead [14]

A notable feature of the HPI-3D is its real-time environmental compensation system, which uses wireless sensors to monitor ambient air temperature, humidity, and pressure, along with material temperature. This ensures dynamic correction of the refractive index of air and thermal expansion effects, significantly enhancing measurement accuracy under varying environmental conditions. These corrections are processed in real-time, allowing the system to maintain its specified accuracy even outside controlled laboratory environments.

The system also supports high-frequency dynamic measurements, such as vibration and motion analysis, with sampling rates up to 100 kHz. This makes it suitable not only for static dimensional calibration but also for advanced dynamic diagnostics in high-speed motion systems. In addition to standard measurements such as linear displacement, angular deviation, straightness, flatness, squareness, and perpendicularity, the HPI-3D is capable of analysing geometric deviations in three dimensions, making it suitable for full 3D spatial metrology applications.

Physically, the HPI-3D is designed with compactness and portability in mind. The laser head measures approximately 76 × 70 × 310 mm and weighs only 2 kg, while the control and power unit is similarly compact. This modular architecture enables easy transport, field setup, and integration with various mechanical systems. The system includes a suite of high-precision optical components, including retroreflectors, beam splitters, and angular optics, all optimized for ultra-stable beam alignment and signal integrity.

Control and data acquisition are handled through a dedicated software suite developed by Lasertex, offering real-time visualization, statistical analysis, and exportable data formats for integration with CAD/CAM and CNC control platforms. The software supports user-defined measurement routines, automatic calibration sequences, and dynamic system modelling for complex geometric analysis. Calibration of the HPI-3D is traceable to international metrology standards, and the system adheres to ISO 17025 requirements for laboratory-grade calibration [14,15].

3. COMPARISON OF THE CHARACTERISTICS

In this chapter comparison of three laser interferometric systems is presented. It is made based on the key features of the measuring devices using the available data from their data sheets and based on user experience. In Table 1. the comparison of three systems is presented.

Table 1. Comparison data between three manufacturers

Parameter	HP 5525A	Renishaw XL-80	Lasertex HPI-3D
Laser type	He–Ne (frequency stabilized)		
Wavelenght stability	±5 ppm	±0,05 ppm	±0,001 ppm
Resolution	10 nm	1 nm	0,1 nm single pass, 0,05nm double pass
Max sampling rate	40 Hz	50 kHz	100 kHz
Max velocity	3 m/s	4 m/s	7 m/s standard; 20 m/s optional
Max measure-ment range	60 m	40m (80m)	30m (80m)
Env. com-pensation	Real time via 5510A compensat or	Real-time via XC-80 (Temp, Press., Humidity, Material)	Real-time via wireless sensors (Temp, Press., Humidity, Material)
Measure-ment types	Linear, velocity, angular, rotary, straightness , flatness	Linear, velocity, angular, rotary, straightness , flatness	Linear, velocity, angular, rotary, straightnes s, flatness, 3D
Vibration analysis	Not supported	Limited (via external software)	Yes
Software environ-ment	None -self made at UNS	CARTO suite	Lasertex software (CAD/CAM capable)
Dimension-laserhead	127 x 179 x 526 mm	214 x 120 x 70 mm	76 × 70 × 310 mm
Weight - laserhead	8,94 kg	1,85 kg	1,9 kg
Portability	Low - heavy and robust	High (portable case system)	Very high (modular, compact, wireless sensors)

Parameter	HP 5525A	Renishaw XL-80	Lasertex HPI-3D
Connec-tivity	Analog	USB-integrated	Modern digital with software and wireless interfaces

4. CONCLUSION

The comparative study of the HP 5525A, Renishaw XL-80, and Lasertex HPI-3D laser interferometers highlights the significant technological evolution in precision metrology systems over the past five decades. HP's early contributions, particularly with the 5525A, laid the groundwork for precision laser interferometry with features such as a stabilized He–Ne source, a 60-meter range, and analog displacement readout. However, this system's bulky form factor, limited sampling rate, and lack of digital interfaces restrict its relevance in contemporary measurement environments. Renishaw's XL-80 represents a major advancement, offering nanometric resolution, high sampling rates, and comprehensive environmental compensation within a portable and software-integrated architecture. The use of CARTO software and USB connectivity further enhances the system's usability for both research and industrial applications.

Lasertex's HPI-3D system demonstrates the forefront of modern interferometric technology, featuring an exceptional wavelength stability of ±0,001 ppm and sub-nanometric resolution capabilities. Its capacity for dynamic vibration analysis, real-time 3D spatial measurement, and wireless environmental sensing makes it highly adaptable for both laboratory and field environments. The HPI-3D also benefits from a modular and compact design, facilitating transport and integration across diverse measurement platforms. In terms of software environment, Lasertex offers a comprehensive suite supporting CAD/CAM systems, automated routines, and ISO-compliant calibration workflows.

Environmental compensation has become a critical aspect in maintaining measurement accuracy outside controlled conditions. Both Renishaw and Lasertex systems implement real-time, multi-parameter compensation strategies, whereas the HP 5525A relies on a separate analog compensator with limited responsiveness. Modern systems also offer superior velocity tracking and sampling rates, essential for applications involving high-speed axis motion and real-time diagnostics.

Overall, the analysis confirms that modern laser interferometers are not only more accurate but also more versatile, integrated, and user-friendly. As precision requirements in manufacturing and metrology continue to rise, systems like the XL-80 and HPI-3D exemplify the direction of future innovation. Nevertheless, the historical significance of the HP 5525A underscores the foundational role of early laser systems in shaping today's precision measurement landscape.

ACKNOWLEDGEMENT

This research has been supported by the Ministry of Science, Technological Development and Innovation (Contract No. 451-03-137/2025-03/200156) and the Faculty of Technical Sciences, University of Novi Sad through project "Scientific and Artistic Research Work of Researchers in Teaching and Associate Positions at the Faculty of Technical Sciences, University of Novi Sad 2025" (No. 01-50/295) and University of Belgrade Faculty of Mechanical Engineering by contract no. 451-03-137/2025-03/200105 for 2025, and LOLA Institute by contract no. 451-03-47/2025-01/200066 for 2025.

REFERENCES

[1] M. Frennberg, M. Johansson, S. Kaellberg, U. Karn, L. R. Pendrill: Long gauge block interferometer using two frequency-stabilized lasers, in: Recent Developments in Optical

Gauge Block Metrology, Vol. 3477, SPIE, pp. 35–44, 1998.

[2] J. Flügge, S. Kroker, H. Schnatz: Fundamental length metrology, in: Handbook of Laser Technology and Applications, CRC Press, pp. 3–22, 2021.

[3] W. E. Barkman: Use of the laser interferometer for position feedback, in: Interferometry, Vol. 192, SPIE, pp. 98–104, December 1979.

[4] X. Li, X. Liu: Efficient identification of geometric errors in CNC machine tools based on dual-frequency laser interferometry, Journal of Measurements in Engineering, Vol. 12, No. 4, pp. 622–637, 2024.

[5] A. Budimir, S. Tabakovic, M. Zeljković: The influence of the movement method on the results of machine tool positioning accuracy analysis, Measurement Science Review, Vol. 23, No. 3, pp. 136–145, 2023.

[6] N. Kuprin, J. Švéda, Š. Chládek, T. Havlan, L. Novotný, J. Koubek: New device for rapid measurement of machine tool geometric errors, MM Science Journal, 2022.

[7] F. Zheng, Q. Feng, B. Zhang, J. Li, Y. Zhao: A high-precision laser method for directly and quickly measuring 21 geometric motion errors of three linear axes of computer numerical control machine tools, The International Journal of Advanced Manufacturing Technology, Vol. 109, pp. 1285–1296, 2020.

[8] M. Holub, J. Rosenfeld: Geometric accuracy of large machine tools, Acta Mech. Slovaca, Vol. 24, No. 3, pp. 56–62, 2020.

[9] R. Kneppers, A. R. Amstelveen: HP laser interferometers, Vaisala News, No. 151, pp. 34–37, 1999.

[10] Keysight Technologies history, available at: https://www.keysight.com/nl/en/about/keysight-technologies-history.html/1000?utm_source=chatgpt.com, accessed: 10.07.2025.

[11] Hewlett-Packard: Laser measurement, Brochure (print), 1984.

[12] XL-80 laser system, available at: https://www.renishaw.com/en/xl-80-laser-system--8268?srsltid=AfmBOoqcVyaCHzDxYb7DqpP8Wy40PgSTA1JQFFTxXJp0XDB74ZX3rdqq, accessed: 10.07.2025.

[13] Renishaw: XL-80 laser system [Brochure]. Data sheet (online), 2004.

[14] HPI-3D laser system, available at: https://lasertex.eu/products/dmi-hpi-3d/, accessed: 10.07.2025.

[15] Lasertex: HPI-3D. Data sheet (print), 2025.

Society of Production Engineering

ICPES 2025

40th INTERNATIONAL CONFERENCE ON PRODUCTION ENGINEERING - SERBIA 2025

DOI: 10.46793/ICPES25.453K

University of Nis Faculty of Mechanical Engineering

Nis, Serbia, 18 - 19th September 2025

MULTISENSOR TECHNOLOGIES IN COORDINATE METROLOGY: MEASUREMENT DIMENSIONAL QUALITY CHARACTERISTICS

Vidoje KASALICA[1]*, Slavenko STOJADINOVIC[1], Radovan PUZOVIC[1]

Orcid: 0000-0002-4055-5874; **Orcid:** 0000-0003-0552-5247;

[1]University of Belgrade, Faculty of Mechanical Engineering, Belgrade, Serbia

*Corresponding author: vidoje.kasalica@gmail.com

Abstract: *The importance of multisensor coordinate metrology is becoming increasingly prominent, particularly with the advancement of smart manufacturing and digital quality control. It can be stated that multisensor coordinate metrology represents a modern extension of conventional coordinate metrology, whose foundation lies in the coordinate measuring machine (CMM). This approach integrates the measuring machine, optical sensors, and computed tomography, thereby enabling enhanced capabilities for performing a wide range of metrological tasks and operations. This paper presents the current state of research in multisensor measurement technologies, with the aim of fostering further advancements in the field. The justification for applying these technologies is well-established, however, several challenges remain regarding their practical implementation, especially in the integration and coordination of different measurement methods for specific tasks or groups of operations. Special attention is given to the characteristics of a measuring machine based on parallel kinematics, in order to assess its potential for upgrade with optical sensors and integration into a multisensor touch-optical system. The results of this study confirm the validity and benefits of such a system, particularly in terms of high measurement speed, excellent repeatability, resistance to temperature variations, flexibility, and reprogrammability. However, certain limitations have been identified, primarily related to lower absolute accuracy and reduced mechanical rigidity resulting from the use of a parallel mechanism.*

Keywords: *Coordinate metrology, Sensors, CMMs, Optical methods, Computer tomography.*

1. INTRODUCTION

Smart factories are defined by the use of advanced technologies such as the Internet of Things (IoT), artificial intelligence (AI), and big data analytics to enhance efficiency, effectiveness, flexibility, and product quality within the manufacturing process. From a metrological perspective, multisensor technologies play a crucial role in this process by providing real-time data on the geometric dimensions of machined components.

Multisensor technologies in coordinate measuring machines (CMMs) utilize a combination of contact and non-contact sensors. The characteristics of these sensors typically depend on their primary application area. The deployment of such systems is primarily determined by factors such as the size of the measured object, the required tolerance features (i.e., the measurement task), the type

and dimensions of the inspection features, and the need for rapid acquisition of a large number of measurement points (i.e., scanning).

To carry out complex measurement tasks, it is often necessary to use multiple sensor types within a single measurement cycle. Visual sensors that are mechanically compatible with the probe head can be easily integrated with contact sensors and exchanged or added using standard automatic changers. However, this concept limits overall system flexibility.

There are also specially designed multisensor systems for coordinate measuring machines that allow seamless integration of high-performance optical sensors with the required lighting systems, in combination with conventional tactile touch probes and other types of sensors. For example, such a system may integrate a tactile stylus, a laser sensor, and a so-called "fiber" probe within a unified measurement platform.

2. CLASIFICATION OF SENZORS FOR DIMENSIONAL QUALITY CHARACTERISTICS

2.1 Contact measurement sensors

Contact measurement sensors enable the acquisition of measurement points based on the probe's contact with the surface of the measured object. These sensors are classified into:

1) Discontinuous sensors,
2) Continuous sensors.

Discontinuous sensors, also referred to as "trigger" sensors, generate an electrical signal upon direct physical contact with the surface of the measured object. As previously mentioned, this signal is utilized within a feedback system to interrupt all machine axis movements and to record the coordinates of the probe tip's center by the control unit, based on the positional data acquired from the machine's axis measurement systems. Discontinuous contact sensors can be further categorized into the following groups:

1) Electro-contact sensors,
2) Inductive sensors,
3) Piezoelectric sensors,
4) Strain gauge-based sensors.

Continuous measurement sensors are classified into:

1) Active,
2) Passive.

In contrast to discontinuous measurement sensors, which acquire a measurement point only at the moment of contact between the probe and the surface of the measured object, continuous sensors remain in constant contact with the object's surface, following its profile and collecting measurement points according to predefined criteria (for instance, by maintaining a consistent contact force).

The primary function of an electro-contact sensor, Figure 1, is to establish or interrupt an electromotive force in the corresponding electrical circuit at the moment the probe contacts the measured object, even at contact forces lower than 0.01 N.

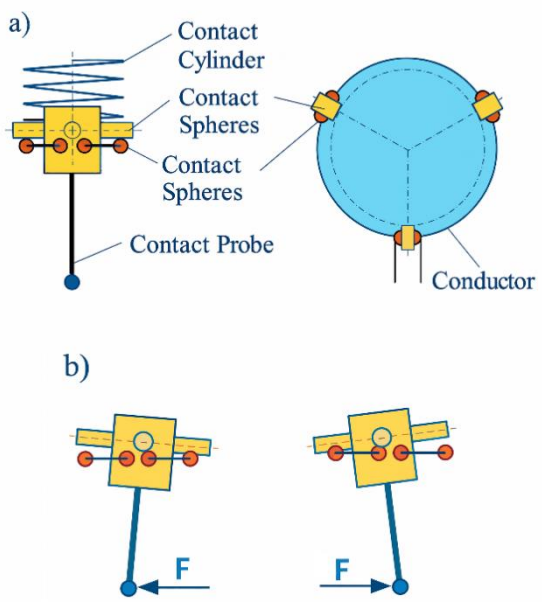

Figure 1. Electro-contact measurement sensor: a) basic components, b) principle of measurement signal generation.

These sensors operate based on a mechanism in which three pairs of contacts (Figure 1) are closed by the force of a spring. The contacts typically consist of three cylinders arranged in the same plane at angles of 120° to one another. In the resting state, the cylinders together with the contact spheres complete the electrical circuit.

Inductive measurement sensors operate based on the principle of electromagnetic induction and enable continuous tracking of the contour of the measured object (scanning). Continuous contour tracking is achieved by controlling the measuring force or contact force. When the measuring probe touches the surface of the measured object, the machine follows its contour, allowing motion in the required directions, with a constant contact force regulated by the value of the induced voltage U in the sensor.

2.2 Contact - optical sensors

A typical representative of this type of sensor is the fiber probe or stylus. The fiber probe consists of an optical fiber with a glass sphere at its tip. The position of the sphere is tracked by optical sensors independently of the deflection of the fiber. The diameter of the sphere can be as small as 10 µm. This type of sensor ranks among the most precise. It enables the measurement of small-diameter bores, gear tooth parameters of relatively small module, and similar features.

2.3 Visual sensors

The term visual sensor refers to all sensors that, similarly to the human eye, can "see" at least a two-dimensional image of the measured object by detecting and evaluating the distribution of color intensity in this optical image [1]. In other words, industrial visual sensors serve as an alternative to the human eye. According to Figure 2, visual sensors can be classified into the following categories:

1) Interferometers,
2) Image processing sensors,
3) Triangulation-based sensors, and
4) Contrast technique-based sensors.

A further subdivision within this classification is illustrated in Figure 2. It is also important to note an additional classification:

1) Axial,
2) Lateral.

A typical axial sensor is the interferometer, while image processing sensors are applicable for measuring lateral or profile surfaces of the measured object.

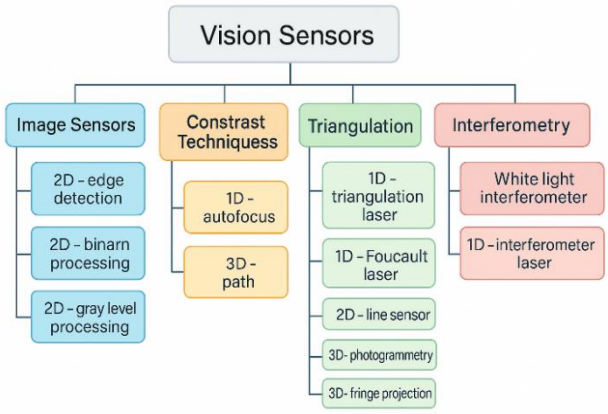

Figure 2. Visual sensors in coordinate measuring machines

However, visual sensors have limitations in their applicability when dealing with complex, three-dimensional measured objects, as for instance, a one-dimensional laser cannot measure the cylindrical geometry of a bore.

Image processing sensors operate based on the principles of light transmission and reflection. The measured object is captured by a CCD (charge-coupled device) camera, after which the matrix photosensitive diode converts the optical signal into an electrical signal, which is subsequently transformed into a digital image via an A/D converter. The resulting image is then processed and used to compute the measured points within a computer equipped with appropriate image processing software.

The measurement principle of a laser sensor is based on projecting a beam of light generated by a laser (light amplification by stimulated emission of radiation, typically a laser diode) onto the measured object (Figure 3). The point of the reflected beam is recorded by an optoelectronic sensor. The position of the measured point is then determined using an appropriate technique. The most commonly employed techniques generally fall into one of the following two categories:

1) Triangulation,
2) Interferometric techniques.

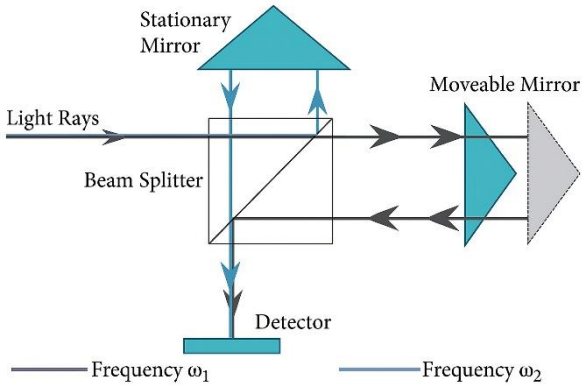

Figure 3. Michelson interferometer schematic [2]

Triangulation sensors, which are commonly used in metrology, operate on the following principle: the laser beam and the sensor's optical axis form an angle of several tens of degrees, thereby creating a triangle between the laser transmitter, the measuring point, and the sensor. This triangle can be used to determine distance using trigonometric formulas. The measurement result largely depends on the surface structure and inclination angle, leading to relatively high measurement uncertainties. Consequently, this technique is suitable primarily for less demanding measurement tasks. Improved results can be achieved with laser sensors operating on the Foucault's principle (Figure 4).

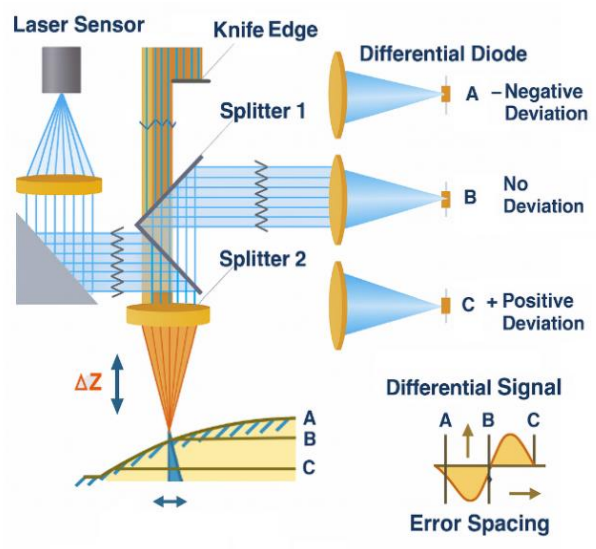

Figure 4. Laser sensor based on the Foucault's principle with an integrated image processing sensor [1].

This principle uses the aperture angle of the sensor's imaging optics as the triangulation angle. Instead of a laser spot, a Foucault's knife-edge is projected onto the object along the beam path. The signal is evaluated using a differential photodiode. The measured result is obtained by superimposing the values acquired by the laser sensor with those recorded by the CMM.

As with previous cases, the material and surface inclination significantly influence the measurement result for this type of sensor as well, thus requiring correction of these influencing factors. However, when appropriate software is used, the uncertainty can be reduced to a level that meets the requirements of high-precision coordinate measuring machines. In practical applications, the Foucault laser sensor can be integrated into image processing sensors. The greatest advantage of the laser spot sensor compared to focus-based techniques lies in its significantly higher measurement speed. This enables the acquisition of several hundred to a thousand points per second, making these sensors suitable for scanning profile surfaces.

2.4 Computer tomography

Computed tomography enables the measurement of both external and internal surfaces of the measured object. Initially, this technique was used in industry for coarse accuracy evaluation. Its combination with other sensors made it applicable to CMM.

X-ray tomography utilizes the property of X-rays to penetrate the material of the measured object. As the rays pass through the material, part of the radiation is absorbed [3]. The longer the radiographic path through the object, the less radiation emerges on the opposite side. Absorption also depends on the material itself. The X-ray detector (sensor) captures the exiting X-rays as a 2D radiographic image. To apply tomography, several hundred 2D radiographic images of the object must be acquired while the object is measured in various rotated positions (Figure 5).

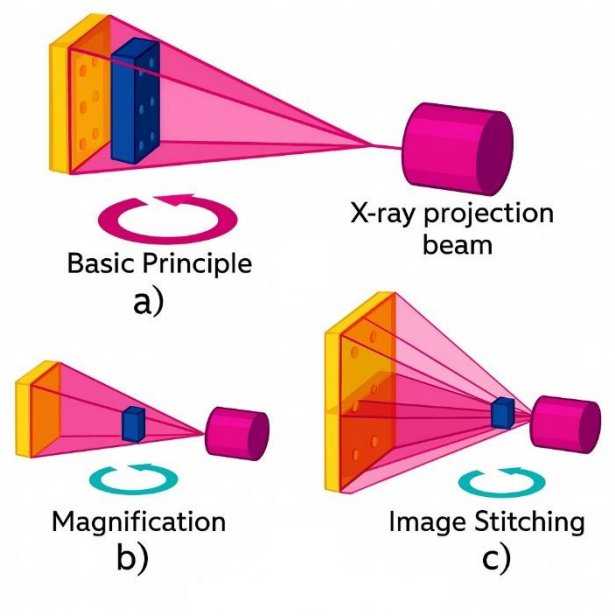

Figure 5. X-ray tomography [1]: (a) basic principle, (b) magnification adjustment, (c) image stitching.

3. MEASUREMENT USING CONTACT AND VISUAL SENSORS

In addition to the continuous and rapidly advancing development of modern technologies in the field of precision measurement and quality control, as discussed in the previous chapters, CMMs continue to hold a central position in industrial metrology. This subsection provides an overview of the operating principle of CMM systems and highlights the various effects and benefits of working with such equipment.

For inspection purposes, the machine employs contact sensors (based either on mechanical or piezoelectric principles for detecting contact), where measurements are performed by the tactile probe, i.e., the spherical tip of the stylus, coming into contact with a predefined surface of the measured geometric feature.

In addition to a technical description and illustration of the main components and functionalities of the system, this section also includes a simulation of the measurement inspection in a digital environment. Such a simulation enables interactive planning and optimization of the measurement process.

3.1 Measurement and simulation of measurements on CMM

For the purposes of this study, a dimensional inspection of the geometric features of the test part was carried out on a Mitutoyo CRYSTA Apex coordinate measuring machine. The configuration of the mentioned machine is based on a moving-bridge structure and operates within a Cartesian coordinate system, meaning it allows movement of the measuring system along three mutually orthogonal axes (X, Y, Z), thus enabling precise positioning and measurement in three-dimensional space.

For the proper operation of this type of coordinate measuring machine, three main components must work in synchronized coordination to enable the measurement process:

1) Machine base – Serves as the structural foundation of the system, ensuring mechanical stability and providing support for all other components of the CMM,
2) Measuring bridge – Enables controlled movement of the measuring probe along three orthogonal axes (X, Y, Z), allowing for precise positioning required during dimensional inspection processes.
3) Z-axis assembly – Houses the rotary head, the control unit (which functions as the central processing unit or "brain" of the CMM), and the measurement probe mounted at its uppermost point [4].

After completing the measurement inspection on the CMM under real-world conditions, the process continues with a simulation in a virtual environment, utilizing the PTC Creo Parametric software package. The simulation of dimensional inspection in a software environment such as PTC Creo represents a significant step toward enhancing the quality and efficiency of numerically controlled coordinate measurements in industrial production. This approach enables virtual planning, optimization, and validation of

measurement procedures, thereby eliminating potential errors prior to the actual execution of the inspection on the CMM.

For the purposes of this study, and with the aim of visualizing the specific existing configuration, a complete CAD model of the mentioned measuring machine was created, Figure 6. All kinematic links between key subsystems were established within this model, in order to enable a comprehensive simulation in a virtual environment.

The modelling and simulation procedure involve the following steps:

- Development of the 3D CAD model of the part (PW),
- Import of the modelled component into the CMM (Manufacturing) module,
- Configuration of the inspection setup, including:
  - Definition of the CMM workcell,
  - Selection of appropriate probes or measuring heads,
  - Specification of fixture elements,
- Initialization of the coordinate system used for the measurement process,
- Definition of individual measurement operations and inspection paths,
- Implementation of the measuring machine model within the environment and its positional definition relative to all inspection components,
- Generation of DMIS (.ncl) code followed by post-processing.

This structured approach enables accurate virtual simulation of CMM-based inspection processes and supports planning, verification, and optimization of measurement routines prior to physical implementation [5].

Verification of the accuracy of the simulated measurement inspection in the virtual environment is achieved through the analysis of the output code generated by the PTC Creo software. This code is produced following the successful execution of the simulation and validation of the planned measurement path. The generated DMIS (.dms) code, which represents the outcome of the simulation within the digital measurement system, is presented in Figure 6, alongside the complete simulation workflow in the software environment.

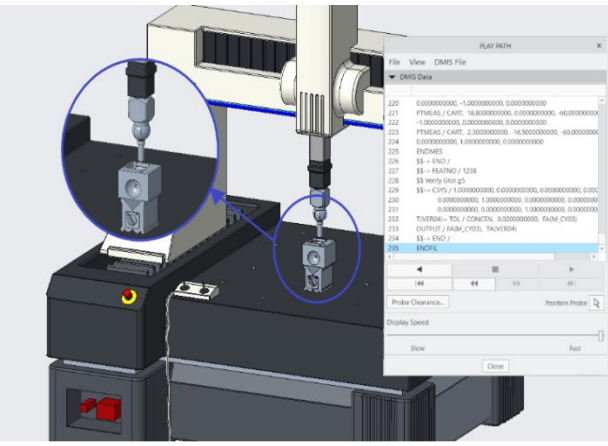

Figure 6. Measuring path simulation on virtual CMM [6].

The simulation in PTC Creo software is particularly beneficial when combined with advanced tactile and optical sensors, as it enables the determination of the optimal measurement strategy in accordance with the complexity of the geometry, tolerance requirements, and production time constraints.

3.2 Measurement on the 3D scanner

The paper [7] presents one example of a measurement on the GOM ATOS device and gives a complete data processing in the purpose to inspection the geometrical parameters of the sprocket tooth profile in the final (post-process machining) inspection. GOM ATOS it's an optical scanner allows you to perform inspection the geometrical parameters of the sprocket tooth profile.

As a workpiece's authors used real sprocket (Figure 7a) to inspection the geometrical parameters of the sprocket tooth profile (figure 6b). The measurement analysis is based on a comparison of the real and 3D CAD geometry (Figure 7b) of the sprocket, while data analysis was carried out in MATLAB software. The verification was done by comparing the nominal and measured (statistical) geometry [7]. The deviation results are shown in a spectrum of colors on the Figure 7c.

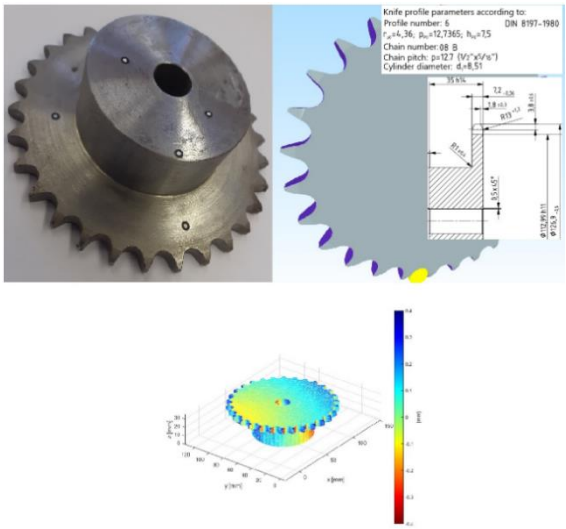

Figure 7. Measuring part: a) real sprocket; b) 3D CAD model of sprocket with parameters, c) result of deviation measurement [7]

3.3 Measurement on the CMM with parallel kinematics

This subsection provides a detailed description of a relatively novel approach to dimensional inspection, namely, the use of the Renishaw Equator 300, as shown in Figure 8. The Equator is a highly adaptable comparative measurement system used in industrial metrology for fast, repeatable, and reliable dimensional verification [8]. It is important to emphasize that the Equator is not intended to completely replace conventional CMM systems. Unlike traditional coordinate measuring machines that operate based on absolute coordinate reference points, the Equator performs relative (comparative) measurements, relying on a mastering process that compares a measured part to a previously calibrated reference (master) part.

The measurement principle is based on the comparative method, where the system measures the deviation between the measured part and the master part. The master part must first be accurately measured on a CMM, making these two types of systems complementary rather than interchangeable.

The Equator system operates using a mechanical contact-trigger probe, typically the Renishaw TP20 or TP200, and features a parallel kinematic structure that allows motion within a working volume of 300 mm in diameter and 150 mm in height (or up to 300 mm in Z-axis height in the Extended Height version). Measurement data is processed using the MODUS Equator software suite, which is fully compatible with DMIS code, enabling seamless integration into existing industrial inspection workflows.

Figure 8. Renishaw Equator 300 Extended Height

The advantages of the Equator system are primarily reflected in its high-speed inspection of defined tolerances, which is enabled by its parallel kinematic structure. The machine is resistant to temperature variations and is capable of automatic recalibration when ambient temperature exceeds the predefined range. Unlike traditional CMMs, the Equator can be installed directly on the production line without compromising measurement accuracy. In addition to thermal stability, the system also exhibits high resistance to vibrations, which is particularly important in demanding shop-floor environments. When its flexibility and reprogrammability are considered, it becomes evident that the Equator is an optimal solution for serial production and the inspection of large volumes of components.

Regarding the limitations, which have been partially mentioned already, the Equator system is not suitable for high-precision

measurements in the micron range as conventional CMM machines, particularly when dealing with complex geometries and tight tolerances. Its comparative method requires prior measurement of a reference (master) part on a CMM, which introduces an additional step in the inspection process. The workspace limitation can be mitigated by using the Equator 500 version, which offers expanded capabilities; however, the system remains confined to specific industrial sectors. The most significant drawback, from the user's perspective, lies in the reduced flexibility for those seeking deeper integration with their own systems or custom scripting. More specifically, while MODUS is a powerful and advanced software solution, it is not as open or customizable as some CMM platforms such as PC-DMIS or Zeiss Calypso.

6. CONCLUSION

Smart factories are defined by the use of advanced technologies such as the Internet of Things (IoT), artificial intelligence (AI), and big data analytics to improve efficiency, effectiveness, flexibility, and product quality in the manufacturing process. From a metrological perspective, multisensor technologies play a key role in this process, as they provide real-time data on the geometric dimensions of machine components. The data they generate can be used to enhance overall quality and accuracy in production, minimize disruptions in the supply chain, reduce delivery downtime, and increase productivity.

This paper offers a classification of sensors that can be integrated into multisensor systems, which are subsequently used in smart manufacturing for in-process and final inspection measurements. Depending on the measurement requirements, geometric variability, and planned measurement costs, the paper proposes several criteria for configuring multisensor systems.

Thus, the main result of the work is a classification of sensors used for measuring geometric dimensions, along with examples of multisensor system applications in smart manufacturing. Furthermore, the advantages and disadvantages of these systems are discussed to support their effective implementation in industrial metrology. Examples of measurements conducted on a CMM and with a 3D scanner illustrate the capabilities and characteristics of contact and optical measurement sensors.

ACKNOWLEDGEMENT

The presented research was supported by the Ministry of Science, Technological Development and Innovation of the Republic of Serbia under Grant No. 451-03-137/2025-03/ 200105.

REFERENCES

[1] Christoph, H. J. Neumann (2012), Multisensor Coordinate Metrology, in Coordinate Measuring Machines and Systems, Edited by Robert J. Hocken & Paulo H. Pereira, CRC Press, Taylor & Francis Group, ISBN 978-1-4200-1753-3.

[2] P. H. Pereira (2012), Cartesian Coordinate Measuring Machines, in Coordinate Measuring Machines and Systems, Edited by Robert J. Hocken & Paulo H. Pereira, CRC Press, Taylor & Francis Group, ISBN 978-1-4200-1753-3.

[3] Kak, A. Slaney (2001), Principles of Computerized Tomographic Imaging. Philadelphia, PA: Society for Industrial Mathematics, ISBN-10:089871494X.

[4] Kasalica, Vidoje, Stojadinović, Slavenko, "DATA INTEROPERABILITY IN COMMUNICATION BETWEEN REAL AND DIGITAL MEASURING TWIN." in Proceedings of the 39th International Conference on production Engineering of Serbia – ICPES 2023:48-54, 2023.

[5] Slavenko Stojadinović, Vidosav Majstorović, Srđan Živković, Vidoje Kasalica, Dušan Stanić, An Approach of Development Digital Twin Based on CMM as Support Industry 4.0, VII International Scientific Conference Industry 4.0 2022, SUMMER SESSION, vol 2, pp. 131-134, Varna, Bulgaria, Jun, 2022, ISSN: 2535-0161 (Online).

[6] Kasalica, V. , Zivanovic, S. , Stojadinovic, S. SIMULATION OF MEASUREMENT ON CMM BY

IMPLEMENTING A DIGITAL TWIN MODEL, XV INTERNATIONAL SCIENTIFIC CONFERENCE MMA 2024 – Flexible Technologies, Novi Sad, Serbia, September 24-26, 2024, 2024, 119-122

[7] S. Stojadinovic, M. Pjevic, N. Slavkovic, R. Puzovic (2024), 3D scaning and inspection geometrical parameters of sprocket tooth profile, Proceedings of the 7th International Scientific Conference ”Conference on Mechanical Engineering Technologies and Applications” COMETa2024, 14th – 16th November, B&H, East Sarajevo, ISBN 978-99976-085-2-9.

[8] Moschos Papananias, Simon Fletcher, Andrew Peter Longstaff, Alistair Barrie Forbes, Uncertainty evaluation associated with versatile automated gauging influenced by process variations through design of experiments approach, Precision Engineering, Volume 49, 2017, Pages 440-455, ISSN 0141-6359.

Society of Production Engineering

ICPES 2025

40th INTERNATIONAL CONFERENCE ON PRODUCTION ENGINEERING - SERBIA 2025

DOI: 10.46793/ICPES25.462P

University of Nis Faculty of Mechanical Engineering

Nis, Serbia, 18 - 19th September 2025

MEASUREMENT OF NOISE AND VIBRATION IN THE CUTTING ZONE DURING TURNING

Zvonko PETROVIĆ[1], Branko RADIČEVIĆ[2], Bogdan NEDIĆ[3], Radovan NIKOLIĆ[1]

Orcid: 0000-0002-4182-4095; **Orcid:** 0000-0002-4236-3833;

[1]Academy of Professional Studies Šumadija-Department in Trstenik, Kragujevac, Serbia

[2]Faculty of Engineering and Civil Engineering in Kraljevo, University of Kragujevac, Serbia

[3]Faculty of Engineering, University of Kragujevac, Serbia

*Corresponding author: zpetrovic@asss.edu.rs

Abstract: *Turning is a complex machining process due to the influence of numerous factors and is accompanied by the occurrence of noise as well as forced and self-excited vibrations. Measuring these quantities enables more accurate modeling of the cutting process and the determination of optimal machining conditions. In this study, sound energy and vibrations during the turning process were measured, and the measurement methodology was described. The selected input machining parameters were: cutting speed (v), depth of cut (a), and feed rate (s). Optimal machining conditions were then determined using the Particle Swarm Optimization (PSO) method.*

Keywords: *Noise, Vibrations, Particle Swarm Optimization (PSO)*

1. INTRODUCTION

The metal cutting process, particularly turning, represents one of the most widespread and significant technologies in modern mechanical engineering. Despite its long-standing application and continuous technological progress, the cutting process remains an extremely complex dynamic system, whose complete understanding presents a constant challenge for researchers and engineers. A particular problem in this context is the occurrence of noise and vibrations in the cutting zone, which directly affect product quality, process productivity, tool life, and also the health aspects of the working environment.

Noise and vibrations in the turning process arise as a consequence of complex physical phenomena involving elastic and plastic material deformations, friction on the contact surfaces of the tool and workpiece, and dynamic interactions in the tool-holder-workpiece system. These phenomena not only degrade the quality of the machined surface and reduce machining accuracy but can also lead to accelerated tool wear, machine tool damage, and long-term exposure to high noise levels can have serious consequences for the operator's health.

The relevance of this issue is particularly pronounced in the conditions of modern production, which strives for increased productivity, quality, and energy efficiency, while simultaneously ensuring ergonomically

acceptable working conditions. Growing demands for reducing production costs, increasing competitiveness, and implementing the principles of sustainable production necessitate a comprehensive study and optimization of the cutting process from the perspective of dynamics and acoustics.

2. PREVIOUS RESEARCH

A fundamental contribution to the study of the cutting process was made by A. D. Makarov in his work "Optimization of the Cutting Process" from 1976 [1]. Makarov thoroughly investigated the physical foundations of the cutting process, tool wear mechanisms, and the influence of temperature on the cutting process. His concept of a constant optimal cutting temperature represents a significant theoretical contribution that enabled the understanding of the basic principles of cutting process optimization. Although Makarov did not explicitly study noise and vibrations, his works on the mechanics of the cutting process and contact phenomena on tool surfaces provide valuable insights into the physical processes that are sources of noise and vibrations.

Vibrations in the cutting process can be classified as forced vibrations or self-excited vibrations (chatter).

Forced vibrations arise due to uneven movement of machine parts, imbalance, or periodic changes in the cutting force [2]. Self-excited vibrations arise due to the regenerative effect and nonlinearities in the cutting process [2].

Tobias [3] and Tlusty [4] developed models explaining the mechanism of self-excited vibration occurrence, emphasizing the role of the regenerative effect and system stiffness. Kudinov [5] highlighted the importance of chip thickness variation and the influence of friction. Modern approaches use statistical methods for vibration identification through analysis of the machined surface or direct measurement of machine structure oscillations.

Numerous studies have shown that modeling of the machining process can be successfully carried out using factorial design of experiments and artificial neural networks. Also, vibrations and noise during machining directly affect surface quality, accuracy, and tool wear. Papers emphasize the importance of acoustic emission and vibro-diagnostics in monitoring the cutting process.

Within the doctoral dissertation of Mirfad Tarić [6], significant contributions were made in the field of cutting process research, particularly in the context of machining parameter optimization. Tarić thoroughly analyzed the influence of various factors on the cutting process and developed a methodology for determining optimal machining regimes. His work is particularly important in the context of experimental determination of cutting process characteristics and understanding the interrelationships between machining parameters and process output characteristics. Tarić's contribution in applying modern methods of analysis and optimization of the cutting process represents a solid foundation for further research in this area.

Contemporary research in the field of cutting processes is directed towards the application of advanced measurement techniques, numerical modeling, and the application of artificial intelligence for process optimization. Numerous authors deal with the analysis of cutting process dynamics, identification of noise and vibration sources, and the development of methods for their suppression.

Particular attention is paid to the application of sensor technology, signal analysis in the time and frequency domain, and the development of adaptive control systems that adjust machining parameters in real time to minimize unwanted dynamic effects.

3. METHODOLOGY FOR MEASURING NOISE AND VIBRATIONS ON A CNC LATHEE

3.1. Eksperimental setup

For measuring vibrations on a CNC lathe, the following are used:

- Piezoelectric accelerometers (range: 0-10 kHz, sensitivity: 100 mV/g),
- Laser vibrometer for non-contact measurement of tool oscillations,
- Microphone for noise measurement (range: 20 Hz-20 kHz).

For measuring vibrations on a CNC lathe, the following are used:

- Piezoelectric accelerometers (range: 0-10 kHz, sensitivity: 100 mV/g),
- Laser vibrometer for non-contact measurement of tool oscillations,
- Microphone for noise measurement (range: 20 Hz-20 kHz).

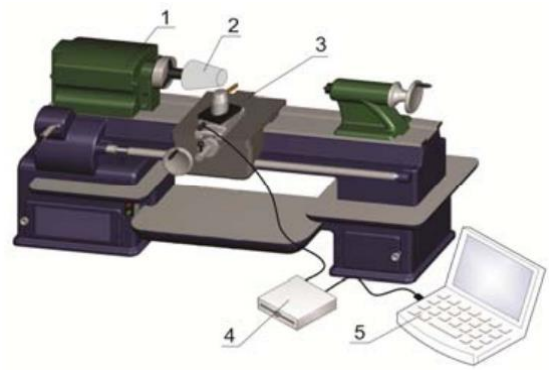

Figure 1. Vibration Measurement during Turning [7]

All sensors are connected to a data acquisition system (DAQ) and a computer with analysis software (e.g., LabVIEW or MATLAB). Measurements are conducted on the CNC lathe itself, equipped with a data acquisition system (DAQ) and sensors:

- Microphone for noise measurement (frequency range: 20 Hz – 20 kHz)
- Accelerometers for vibration measurement (mounted on the tool holder and spindle)
- Signal analysis system (e.g., LabVIEW or MATLAB with Signal Processing Toolbox).

3.2. Measurement procedure and locations

Before the actual measurement, sensor calibration must be performed according to standards (e.g., ISO 16063). Sensors are positioned such that the noise measurement microphone is at a distance of 1 m from the cutting zone, and accelerometers are at strategic points. Signal recording is performed during different cutting regimes (v, s, a). Signal analysis involves:

- FFT analysis for identifying dominant frequencies.
- RMS values for vibration and noise intensity.

Accelerometers are placed on:

- Tool holder
- Spindle
- Machine bed

During the experiment, turning parameters are varied:

- Cutting speed V [m/min]
- Depth of cut a [mm]
- Feed s [mm/rev]

3.3. Signal processing

Vibration and noise signals are analyzed in:

- Time domain (RMS, amplitude),
- Frequency domain (FFT, spectral analysis),
- Statistical domain (correlation function, power spectra).

4. RESULTS AND DISCUSSION

Using the PSO algorithm, optimal machining parameters that minimize noise and vibrations can be identified. Cutting speed has the greatest influence on process stability. Increasing the cutting speed above a critical value leads to the occurrence of self-excited vibrations, which is also confirmed by Tobias [3] and Tlusty [4].

Correlation analysis of the workpiece surface showed a good correlation between the presence of periodic components and the occurrence of self-excited vibrations [8].

Using a three-factor central composite design and neural networks, reliable models for predicting cutting forces, temperature, and roughness were obtained. The correlation between measured vibrations and tool wear parameters indicates the possibility of early detection of tool blunting.

4. CONCLUSION

The metal cutting process represents one of the most significant and prevalent operations in modern industry. Although tool materials and machining technologies are continuously improved, the existence of unwanted physical phenomena such as noise and vibrations remains a current and complex problem. These phenomena are inherently present in the cutting zone and have a direct impact on multiple aspects of the production process.

Noise and vibrations negatively affect: the quality of the machined surface, lead to accelerated tool wear and reduction of its durability, and can lead to damage to the machining systems themselves.

From the aspect of the working environment, operator exposure to excessive noise poses a serious health risk, requiring the application of additional protective measures. Therefore, the research, modeling, and control of noise and vibrations are not only a matter of technological efficiency but also of economic viability and workplace safety. Understanding their causes and mechanisms of occurrence is crucial for developing strategies to mitigate them and optimize the machining process.

REFERENCES

[1] D. Makarov: Optimization of the cutting process, Technologist's Library, Moscow, 1976.

[2] V.R. Milačić: *Forced and self-excited vibrations of machine tools, Proceedings of the Fifth Conference on Production Engineering*, *15-16. V 1969, Kragujevac, pp. AM1.1-AM1.14.*

[3] Tobias S.A.: *Machine Tool Vibration*, Blackie, (1965).

[4] Tlusty, J.: Selbsterregte Schwingungen an Werkzeugmaschinen, VEB Verlag Technik, (1962).

[5] Kudinov, V.A.:Dynamics of Machine Tools*. Mir Publishers, (1968).

[6] M. Zarić: *Modeling of the turning process of heat-treated steel*, PhD thesis, Faculty of Technical Sciences Novi Sad, Novi Sad, Srbija, 2018.

[7] Košarac A., Željković M., Mlađenović C., Živković A.: *Identification of self-excited vibrations during turning using modern diagnostic equipment*, IMK-14 – Research and Development in Heavy Machinery Engineering, pp.SR105-SR111 (2013).

[8] Peklenik, J., Gartner, J.: Workpiece Accuracy Criterion for the Dynamic Machine Tool Acceptance Test, MTDR, (1966) .

Society of Production Engineering

ICPES 2025

40th INTERNATIONAL CONFERENCE ON PRODUCTION ENGINEERING - SERBIA 2025

DOI: 10.46793/ICPES25.466S

University of Nis Faculty of Mechanical Engineering

Nis, Serbia, 18 - 19th September 2025

REVIEW OF METHODS AND APPROACHES FOR EVALUATING MEASUREMENT UNCERTAINTY OF CMM

Branko ŠTRBAC[1*], Miloš RANISAVLJEV[1], Biserka RUNJE[2], Goran JOTIĆ[3], Branislav DUDIĆ[4], Miodrag HADŽISTEVIĆ[1]

Orcid: 0000-0003-3892-2767; **Orcid:** 0000-0002-4159-8753; **Orcid:** 0000-0002-8882-982X; **Orcid:** 0000-0002-6753-3691;

[1]Faculty of Technical Sciences, University of Novi Sad, Serbia

[2]Faculty of Mechanical Engineering and Naval Architecture, University of Zagreb, Croatia

[3]Faculty of Mechanical Engineering, University of Banja Luka, BiH

[4]Comenius University Bratislava, Faculty of Management, Bratislava, Slovakia

*Corresponding author: strbacb@uns.ac.rs

Abstract: *For a long time, the evaluation of measurement uncertainty in coordinate measuring machines (CMMs) has been one of the most prominent research areas in the field of dimensional metrology. This is because coordinate measuring machines, whether equipped with contact or non-contact sensors, are dominant in assessing the conformity of workpieces with specifications. They are characterized primarily by a high degree of flexibility and accuracy, but they are also complex metrological systems with numerous sources contributing to measurement errors, i.e., measurement uncertainty. Numerous methods and approaches have been developed so far for the evaluation of CMM measurement uncertainty, and it is generally accepted that this is a highly challenging and complex task. Experimental methods, simulation-based methods, analytical approaches, as well as the ISO 15530 series of standards have proposed their own methodologies. The aim of this paper is to present the current state of research in this field. The authors of this paper have many years of experience in this area, and several case studies will be presented.*

Keywords: *dimensional metrology, CMM, quality control, accuracy, measurement uncertainty, accuracy.*

1. INTRODUCTION

Modern industrial demands increasingly call for the design of workpieces with extremely tight specifications in order to ensure the intended functionality of the final product. As a result and considering the inherent imperfections of manufacturing processes metrological systems used for quality control must operate as close to ideal conditions as possible. In other words, the quality of measurement results must be exceptionally high, allowing measurement imperfections to consume no more than 10 % of the given tolerance [1].

Due to their high flexibility and satisfactory accuracy, coordinate measuring machines (CMMs) have been the dominant measuring instruments for several decades when it comes to evaluating dimensional and geometrical characteristics of parts at the macroscopic level. The key performance parameter defined for

these instruments is the maximum permissible error (MPE) when measuring geometrical tolerances typically in the form of a hemisphere to assess sensor error. This includes MPE_P for contact sensors in "point-by-point" measurement mode and $MPE_{Tij/\tau}$ for contact sensors operating in scanning mode, as well as MPE_E for reference length measurements [2]. For industrial-grade CMMs, these maximum permissible errors typically range from 1 to 5 µm. However, due to the complexity of these measuring systems, such parameters alone are insufficient to fully define the quality of the measurement results. Therefore, it is highly desirable to evaluate the measurement uncertainty for each specific measuring task.

A measurement result is considered complete only when accompanied by a statement of the uncertainty—i.e., an interval within which the true value is reasonably expected to lie. Given the complexity of both the measuring system and the measurement process itself, numerous contributing factors and their interactions must be considered, all of which can affect measurement uncertainty. The main challenge lies in identifying and quantifying all sources of standard uncertainty and incorporating them into an uncertainty model—if such a model can even be reliably formulated. So far, research into CMM measurement uncertainty has applied various approaches, including the Guide to the Expression of Uncertainty in Measurement (GUM), experimental methods, computational simulations, and expert judgment. Some of these approaches have been standardized through the ISO 15530 series of standards. The most recent research in this area is discussed in the referenced publication [3]. The following section provides an overview of key studies and findings in this field.

2. EVALUATION OF CMM MEASUREMENT UNCERTAINTY USING THE GUM APPROACH

The consensus among researchers and experts is that the GUM approach has significant limitations when applied to CMM measurements, primarily due to the number of assumptions that must be introduced. Alternative methods for evaluating measurement uncertainty often require extensive experimental procedures, access to calibrated reference workpieces, or a detailed virtual model of the measurement process and the behaviour of the CMM. These approaches are frequently costly and complex, especially when applied to CMMs operating in a production environment.

As a result, the GUM method remains the most practical option provided that its use yields a reliable estimate of uncertainty. In some cases, the Maximum Permissible Error (MPE) can be accepted as a measure of uncertainty, particularly when evaluating simple dimensional characteristics such as the distance between two points. Even in such cases, however, the GUM framework is used to assess the uncertainty of that measurement.

The main drawbacks of applying the GUM methodology to CMM uncertainty evaluation can be summarized as follows:

- Assumption of independence – introduced to avoid complex covariance terms;
- Standard deviation distribution – the conventional GUM method uses standard deviation as a measure of uncertainty;
- First-order Taylor approximation – the GUM approach relies on the first-order Taylor series expansion of the measurement function;
- Analytical relationship – the method assumes that the measurement process can be expressed as an analytical function of a set of input quantities, each associated with its own uncertainty;
- Systematic errors – the GUM framework also assumes that all known systematic effects have been identified and appropriately compensated for.

The lack of an analytical relationship between input quantities and the measurement result is one of the main reasons why the conventional GUM method

is difficult to apply to CMM measurements. In the GUM-based approach, the starting point for determining measurement uncertainty in CMM applications involves formulating the equation of the substitute geometric primitive. However, commercial CMM software typically does not provide access to the equations of these reference (substitute) elements. To properly assess measurement uncertainty using GUM, it is necessary to develop independent software capable of generating both the reference equations and the extreme point coordinates. The application of GUM is most representative in the context of form error evaluation, since, as previously mentioned, the maximum permissible error can in some cases be considered as the measurement uncertainty—particularly when measuring lengths.

2.1 Evaluation of Measurement Uncertainty in Flatness Measurement on a CMM Using the GUM Method

The application of the GUM approach relies on principles of analytical geometry. The first step in evaluating the uncertainty of flatness measurement on a CMM is to define the reference plane from the sampled points. Since the relevant standard specifies that form error should be determined using the minimum zone method, the equation of the reference plane is obtained using a Bundle of Plains through One Point [4]. Flatness error is defined as the minimum distance between the points at the maximum (x_1, y_1, z_1) and minimum (x_2, y_2, z_2) deviation from the reference plane, as expressed in Equation (1):

$$\delta = \frac{(z_1 - z_2) - a(x_1 - x_2) - b(y_1 - y_2)}{\sqrt{1 + a^2 + b^2}}. \qquad (1)$$

To determine the uncertainty of the flatness error δ, it is necessary to evaluate the uncertainty and the propagation coefficient of each element in Equation (1). From this, it follows that the measurement uncertainty of the flatness error estimate is given by Equation (2):

$$u_\delta^2 = \left(\frac{\partial\delta}{\partial x_1}u_{x1}\right)^2 + \left(\frac{\partial\delta}{\partial x_2}u_{y1}\right) + \left(\frac{\partial\delta}{\partial y_1}u_{z1}\right) + \left(\frac{\partial\delta}{\partial y_1}u_{x2}\right) + \left(\frac{\partial\delta}{\partial z_1}u_{y1}\right) + \left(\frac{\partial\delta}{\partial z_2}u_{z2}\right) + \left(\frac{\partial\delta}{\partial a}u_a\right) + \left(\frac{\partial\delta}{\partial b}u_b\right) + 2\frac{\partial\delta}{\partial a}\frac{\partial\delta}{\partial b}\rho_{ab}u_{ab}. \qquad (2)$$

The uncertainty components denoted as u_{xi}, u_{yi} and u_{zi} represent the uncertainty of the sampled points, with the dominant influences arising primarily from the CMM's geometric errors and sampling system inaccuracies, as well as environmental conditions affecting both the CMM and the measurement process. The uncertainty components u_a, u_b, $u_a u_b$ and ρ_{ab} correspond to the uncertainty associated with the algorithm used to derive the substitute geometry. The coefficients defining the orientation of the reference plane, a and b, are correlated and represent the correlation coefficient. For a detailed case study on the evaluation of measurement uncertainty in flatness measurement on a CMM using the GUM method, refer to the study [5]. The same methodology can be applied to assess measurement uncertainty in other form errors on CMMs, such as roundness, straightness, and cylindricity.

3. EVALUATION OF CMM MEASUREMENT UNCERTAINTY USING ISO 15530-3:2011 STANDARD

The evaluation of CMM measurement uncertainty according to the guidelines of ISO 15530-3:2011 [6], is considered the most reliable method and is often used as the reference for validating simulation-based approaches [7]. This method involves repeated measurement—at least 20 times—of a calibrated workpiece that is geometrically identical to the part being inspected, positioned at different locations and orientations within the CMM's measurement volume. Furthermore, the conditions under which the calibrated part is measured must be identical to

those used for the actual workpiece, including the same probe configuration, measurement strategy, and environmental conditions. The differences between the measured results and the known calibrated values of the reference part are used to estimate the measurement uncertainty. The uncertainty components arise from the measurement procedure itself, the calibration of the reference part, and variations in the measured features such as deviations in form error, thermal expansion coefficients, and surface texture. The expanded measurement uncertainty is calculated according to Equation (3):

$$U = k\sqrt{u_{cal}^2+u_p^2+u_b^2+u_w^2} \quad (3)$$

where k is the coverage factor used to calculate the expanded uncertainty; u_{cal} represents the standard uncertainty associated with the calibration of the reference part, as stated in the calibration certificate, u_p is the standard uncertainty derived from the experimental measurements and includes uncertainty components related to the CMM hardware, u_b represents the standard uncertainty associated with systematic errors in the measurement process and u_w is the standard uncertainty linked to material and manufacturing variations. Since the systematic error b, defined as the difference between the mean value obtained from the CMM measurements and the calibrated value of the observed feature typically remains uncompensated, the total measurement result is expressed using Equation (4):

$$Y=y-b\pm U \quad (4)$$

where Y represents the total measurement result, y is the result obtained from the CMM, b is the systematic error and U is the expanded measurement uncertainty. An application of this approach to a specific case can be found in [8]. However, the standard in question has several limitations. First, the standard uncertainty u_w consists of two components, where u_{wp} accounts for uncertainty arising from the manufacturing process [9]. This component is particularly difficult to quantify, as it is inherent to the machining process of the workpiece and is therefore often neglected. Second, a point of ongoing discussion in the scientific community concerns the value of L which appears in the equations for the standard uncertainties u_w and u_b in the case of form error measurements [10]. Specifically, when measuring deviations from ideal form, the value of L is considered to be zero. As a result, both standard uncertainties are also evaluated as zero, which can misrepresent the true uncertainty. Third, the standard requires the application of the same measurement strategy across multiple orientations and positions of the workpiece within the CMM's working volume. This approach accounts only for uncertainties arising from the CMM hardware, such as geometric errors and sensor inaccuracies. To address these limitations, the International Organization for Standardization has worked on a draft of ISO 15530-2, which proposes multiple measurement strategies with variations in part orientation and position within the CMM's measurement space. Additionally, the draft standard suggested the use of uncalibrated parts, which may be one of the main reasons it was never formally published. Nevertheless, ISO 15530-3:2011 can be extended by incorporating various measurement strategies, using probing styli of different diameters, and varying scanning speeds when operating in scanning mode. In such cases, the application of design of experiments (DoE) techniques proves highly beneficial.

4. APPLICATION OF SIMULATION METHODS FOR EVALUATING CMM MEASUREMENT UNCERTAINTY

Numerous models have been developed for evaluating measurement uncertainty on CMMs, with most relying on simulation-based principles. The core idea behind these methods is to model both the machine and the measurement process in order to replicate the behaviour of a real coordinate measuring machine. Two main approaches can be distinguished: the first, more straightforward approach involves using simulation to

propagate the uncertainty of sampled points through a model that represents the equation of the substitute geometric primitive [11]. The second, more complex approach is based on constructing a virtual coordinate measuring machine (VCMM), which is a software-based solution designed to digitally replicate the operation of a specific CMM [12]. The use of simulation methods has been standardized under ISO 15530-4:2008, and several commercial software tools—known as Uncertainty Evaluating Software (UES)—are available for this purpose. These tools primarily use Monte Carlo simulation as the computational engine. Currently, there are only a few commercial and non-commercial software solutions available for uncertainty evaluation, most of which are developed and maintained by leading national metrology institutes and research centers. UES tools are capable of evaluating valid uncertainties for a wide range of measurement tasks, and as such, both the measurement procedures and the simulations can be considered as part of traceable calibration workflows [13]. Below are some representative examples of simulation-based methods for evaluating CMM measurement uncertainty:

- Virtual Coordinate Measuring Machine (VCMM) – The first software solution developed for evaluating the measurement uncertainty of coordinate measuring machines was named the Virtual Coordinate Measuring Machine [3]. This software tool was developed in the 1990s by PTB (Physikalisch-Technische Bundesanstalt, Germany)
- Virtual Coordinate Measuring Machine MCM PK – A virtual coordinate measuring machine named MCM PK was developed at the Cracow University of Technology (Poland) [12]. The operating principle of this software solution is similar to that of the classical VCMM, although different techniques were applied to model the real behaviour of the CMM;
- Virtual Coordinate Measuring Machine Extended with Form Error Uncertainty Source – At the Catholic University of Leuven (Belgium), a software solution was developed that, in addition to accounting for hardware-related CMM errors, also considered form error as one of the more significant sources of measurement uncertainty in CMM measurements [14]. It was also found that existing commercial software solutions at the time were not capable of incorporating this factor into uncertainty evaluation;
- Expert CMM (ECMM) – A group of authors [15] introduced a concept for evaluating CMM measurement uncertainty using Monte Carlo simulation, referred to as the Expert Coordinate Measuring Machine (ECMM). The operational principle of ECMM consists of two conceptual steps: first, the estimation of uncertainty for the individual point coordinates; and second, the propagation of this uncertainty through the part measurement program;
- Simulation by Constraints – PUNDIT/CMM – The National Institute of Standards and Technology (NIST) in the United States developed a simulation-based method for evaluating CMM measurement uncertainty, known as Simulation by Constraints (SBC) [16]. This approach allows both the CMM and its sensor to be modeled using results from tests prescribed by ISO 10360.

4.1 Application of Monte Carlo Simulation for Evaluating Measurement Uncertainty in Flatness Measurement on a CMM

This simulation approach is based on a simplified application of the Monte Carlo method, without the use of a virtual model of the coordinate measuring machine (CMM). In this model, the uncertainty of a sampled point is not described through calibration procedures, but rather through the corresponding repeatability of the sampled

point, determined experimentally. The model for evaluating measurement uncertainty in flatness measurements is illustrated in Figure 1. The inputs to the simulation model are probability distribution functions of the coordinates of the sampled points, obtained from ten repeated measurements on an actual, randomly selected workpiece. The repeatability of each sampled point (*x*, *y* and z coordinates) is described using a normal distribution, where the mean values $\overline{x_i}$, $\overline{y_i}$, $\overline{z_i}$ and standard deviations $\overline{\sigma x_i}$, $\overline{\sigma y_i}$, $\overline{\sigma z_i}$ are calculated from the experimental sampling data. Such input probability distributions of the point coordinates inherently include uncertainties arising from the interaction of the CMM hardware with the environment. All geometric and sensor-related errors, whether random or systematic, are embedded in the defined probability distribution function that describes the sampled point. Although defining the input based on the repeatability of the sampled point may pose challenges due to the need for repeated measurements, the time required for acquiring this repeatability is comparable to that needed for modeling geometric and sensor errors through measurements of specific calibration workpieces. The accuracy of such inputs to the simulation model is inherently higher, as they are based on real-world measurement conditions. Furthermore, the simulation model incorporates various sampling strategies, i.e., different numbers of sampling points distributed according to the Hammersley distribution on the measured surface. Specifically, this model for determining the flatness of a workpiece included sets of b=10, 20, 40, 75 and 140. It is assumed that flatness error increases with the number of sampling points in the measurement strategy, while the measurement uncertainty decreases. In order to investigate how flatness error and measurement uncertainty behave depending on the position of the workpiece within the CMM measuring volume, the *x*, *y*, and *z* coordinates were sampled according to a predefined sampling plan at five different positions within the measuring volume. Through these experiments, the CMM measuring space was calibrated for flatness measurements, providing the user with insights into specific regions of the machine where higher or lower flatness errors and, correspondingly, lower or higher measurement uncertainties may occur. Once the input parameters were defined, the Monte Carlo simulation was carried out. Due to its stochastic nature, the calculated uncertainty (expressed as a confidence interval) will vary between simulation runs. After generating M virtual samples from the defined input distribution functions, a criterion must be applied to determine the substitute geometry, i.e., to estimate the reference planes and flatness errors. For this purpose, a novel methodology based on the Minimum Zone (MZ) method—Bundle of Plains through One Point was employed. Specifically, the first sampled values (x_1, y_1, z_1)...(x_b, y_b, z_b) are taken to define coordinates for *b* points. Through these b points, using the MZ method with rotation through a single point, the equation of the plane and the flatness error are determined. Then, the second set of sampled values (x_1, y_1, z_1)...(x_b, y_b, z_b) is used to generate a new set of b points, which are input into the algorithm to estimate the reference plane and flatness error again. This procedure is repeated for all M equations of planes, resulting in M flatness error values. Additionally, the process is repeated for several positions within the available CMM measuring volume. Based on the M obtained flatness error values, a frequency distribution is constructed in the form of a histogram, from which the 95 % confidence interval is used to determine the expanded measurement uncertainty. After the simulation is completed, focus is placed on the influence of different numbers of sampling points and the position of the workpiece within the measuring volume on the values of expanded uncertainty and flatness error. Further results of this investigation are presented in [17]

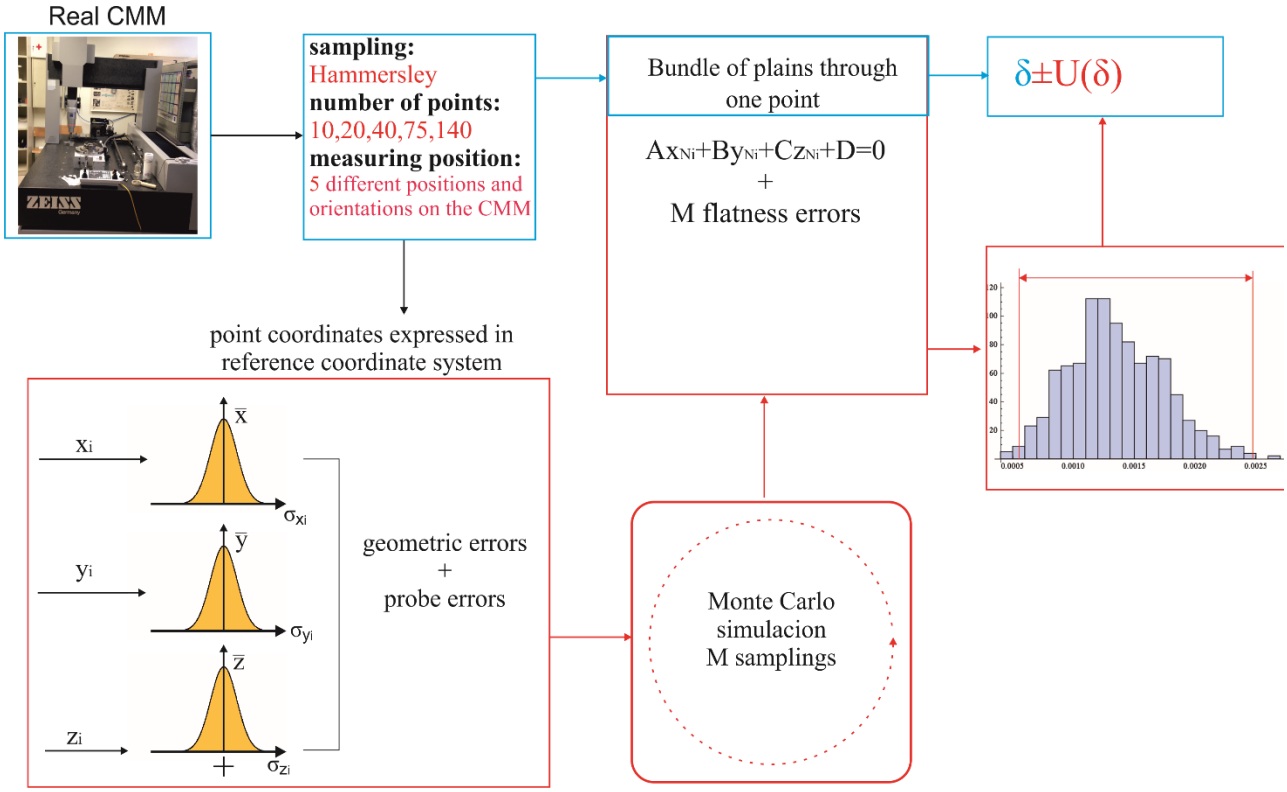

Figure 1. Model for estimating measurement uncertainty of CMM during flatness measurements based on Monte Carlo simulation

5. CONCLUSION

The accurate evaluation of measurement uncertainty in coordinate measuring machines (CMMs) is a critical factor in ensuring the reliability and traceability of dimensional measurements in modern manufacturing. This paper has presented a comprehensive review of existing methods and approaches used for uncertainty assessment, including ISO-based approaches, statistical methods, Monte Carlo simulations, and numerical modeling techniques.

Each method carries specific advantages and limitations depending on the measurement context, the complexity of the part, and the measurement environment. While ISO 15530 series offers a standardized framework—especially through substitution and simulation methods—alternative approaches such as Monte Carlo methods provide greater flexibility in complex and non-standard applications.

It is evident that the integration of multiple methods, combined with advanced software and sensor technologies, represents a promising direction for future development. Furthermore, the adoption of digital twins and machine learning techniques holds significant potential for real-time uncertainty estimation and process optimization.

ACKNOWLEDGEMENT

This research has been supported by the Ministry of Science, Technological Development and Innovation (Contract No. 451-03-137/2025-03/200156) and the Faculty of Technical Sciences, University of Novi Sad through project “Scientific and Artistic Research Work of Researchers in Teaching and Associate Positions at the Faculty of Technical Sciences, University of Novi Sad 2025” (No. 01-50/295).

REFERENCES

[1] Kunzmann, H., Pfeifer, T., Schmitt, R., Schwenke, H., & Weckenmann, A. Productive metrology-adding value to manufacture. CIRP annals, Vol. 54, No. 2, pp. 155-168. 2005.

[2] ISO 10360-1:2000 Geometrical Product Specifications (GPS) — Acceptance and

reverification tests for coordinate measuring machines (CMM)

[3] Wilhelm, R. G., Hocken, R., & Schwenke, H: Task specific uncertainty in coordinate measurement. CIRP annals, Vol. 50, No. 2, pp. 553-563. 2001.

[4] Radlovački, V., Hadžistević, M., Štrbac, B., Delić, M., & Kamberović, B. Evaluating minimum zone flatness error using new method—Bundle of plains through one point. Precision Engineering, Vol. 43, pp. 554-562. 2016.

[5] Štrbac, B., Radlovački, V., Spasić-Jokić, V., Delić, M., & Hadžistević, M. 2017. The difference between GUM and ISO/TC 15530-3 method to evaluate the measurement uncertainty of flatness by a CMM. Mapan, Vol. 32, No. 4, pp. 251-257. 2017.

[6] ISO/TS 15530-3:2011. Geometrical product specifications (GPS) – coordinate measuring machines (CMM): technique for determining the uncertainty of measurement – part 3: use of calibrated workpieces or standards.

[7] Gromczak, K., Gąska, A., Ostrowska, K., Sładek, J., Harmatys, W., Gąska, P.,& Kowalski, M. Validation model for coordinate measuring methods based on the concept of statistical consistency control. Precision Engineering, Vol. 45, pp. 414-422. 2016.

[8] Štrbac, B., Ačko, B., Havrlišan, S., Matin, I., Savković, B., & Hadžistević, M. Investigation of the effect of temperature and other significant factors on systematic error and measurement uncertainty in CMM measurements by applying design of experiments. Measurement, Vol. 158, pp. 107692. 2020.

[9] Štrbac, B., Ranisavljev, M., Zeljković, M., Knežev, M., & Hadžistević, M. Supplement to the Standard VDI/DGQ 3442 with Gage R&R Study. In International Conference “New Technologies, Development and Applications” (pp. 350-356). Springer, Cham.97. 2021

[10] Plowucha, W., & Jakubiec, W. Proposal for changes in the ISO 15530 series of standards. Calitatea, Vol. 13 No. 5, 2012.

[11] Wen, X. L., Zhu, X. C., Zhao, Y. B., Wang, D. X., & Wang, F. L. Flatness error evaluation and verification based on new generation geometrical product specification (GPS). Precision Engineering, Vol. 36, No. 1, pp. 70-76. 2012

[12] Sładek, J., & Gąska, A. Evaluation of coordinate measurementvuncertainty with use of virtual machine model based on Monte Carlo method. Measurement, Vol. 45, No. 6, 1564-157. 2012.

[13] Trenk, M., Franke, M., & Schwenke, H. The “Virtual CMM” a software tool for uncertainty evaluation–practical application in an accredited calibration lab. Proc. of ASPE: Uncertainty Analysis in Measurement and Design, 9, pp. 68-75. 2004.

[14] Kruth, J. P., Van Gestel, N., Bleys, P., & Welkenhuyzen, F. Uncertainty determination for CMMs by Monte Carlo simulation integrating feature form deviations. CIRP annals, Vol. 58, No. 1, pp. 463-466. 2009.

[15] Balsamo, A., Di Ciommo, M., Mugno, R., Rebaglia, B. I., Ricci, E., Grella, R. Evaluation of CMM uncertainty through Monte Carlo simulations. CIRP Annals, Vol. 48, No. 1, pp. 425-428. 1999.

[16] Baldwin, J. M., Summerhays, K. D., Campbell, D. A., & Henke, R. P. Application of simulation software to coordinate measurement uncertainty evaluations. NCSLI Measure, Vol. 2, No.4, pp. 40-52. 2007.

[17] Štrbac, B. (2017). Estimation of measurement uncertainty in flatness measurement on a coordinate measuring machine using Monte Carlo simulation. Doctoral thesis, University of Novi Sad. 2017.

Society of Production Engineering

ICPES 2025

40th INTERNATIONAL CONFERENCE ON PRODUCTION ENGINEERING - SERBIA 2025

DOI: 10.46793/ICPES25.475D

University of Nis
Faculty of Mechanical Engineering

Nis, Serbia, 18 - 19th September 2025

ACCURACY OF SOUND POWER DETERMINATION USING DIFFERENT SOUND INTENSITY METHODS: A CASE STUDY ON A VACUUM PUMP

Tanja DULOVIĆ[1*], Branko RADIČEVIĆ[1], Jovana PERIĆ[1], Mladen RASINAC[1], Vladan GRKOVIĆ[1]

Orcid: 0000-0003-3265-5661; **Orcid:** 0000-0002-4182-4095; **Orcid:** 0000-0003-4933-3756; **Orcid:** 0000-0003-1229-4678;

[1]University of Kragujevac, Faculty of Mechanical and Civil Engineering in Kraljevo, Serbia

*Corresponding author: dulovic.t@mfkv.kg.ac.rs

Abstract: *This study presents the measurement and analysis of the sound power emitted by a vacuum pump using two sound intensity-based methods in accordance with ISO 9614: the discrete point method and the scanning method. The sound intensity measurements were conducted under two airflow conditions (5 l/min, 15 l/min) in the frequency range from 200 to 6000 Hz range. The results indicate a high level of agreement between the two methods in terms of the frequency distribution of sound power, with the discrete point method yielding slightly higher values due to more detailed spatial sampling. The maximum observed difference between the methods was 2.4 dB, recorded at 250 Hz and 400 Hz. The highest sound power levels occurred between 1000 and 2000 Hz, which corresponds to the typical spectral range of mechanical noise. The result showed that noise emission's loudest source is the rear face of the pump, likely due to the position of the electric motor cooling fan. These findings validate both techniques for use in describing noise emissions from similar equipment.*

Keywords: *sound power, sound intensity, vacuum pump.*

1. INTRODUCTION

Effective noise control strategies are based on a clear understanding of the characteristics of the noise sources. Among these, sound power is considered a reliable parameter for evaluating and comparing different sources, as it is independent of the acoustic environment and allows for consistent definition of acceptable emission limits [1].

Traditional methods for determining sound power are most commonly based on sound pressure level measurements. However, these approaches often face significant limitations, particularly in terms of measurement accuracy and susceptibility to background noise [2]. In recent years, sound intensity measurement has gained increasing recognition as an alternative technique for estimating sound power, offering several advantages over conventional methods. Sound intensity is a vector quantity that include both the magnitude and direction of sound propagation, allowing for more accurate source localization and reduced influence of environmental conditions on the results [3,4]. This method allows the precise

identification of dominant noise sources and the visualization of spatial sound intensity distribution [5]. Overall, sound intensity measurement provides a practical and cost-effective alternative to traditional sound power determination techniques, eliminating the need for large investments in reverberation or anechoic chambers.

Diaphragm vacuum pumps are commonly used in various laboratory settings, industrial applications, and processes that require stable and controlled vacuum conditions. During operation, these pumps generate significant noise levels due to the characteristic vibrations of the diaphragm, further intensified by friction and interactions between moving components [6]. In addition, the pulsating nature creates pressure variation and turbulence, which directly affect noise emission [7,8]. Operating conditions, such as airflow rate and pump load, also affect significantly the noise dynamics. An increase in speed and load leads to higher noise levels, due to higher vibration effects and higher turbulence [9]. Due to these factors, the characterization and measurement of noise generated by vacuum pumps are of key importance for improving their performance, reliability, and environmental acceptability in the contexts in which they are used.

The research object in this study is the determination of the sound power level of the ZAMBELLI vacuum pump, model ZB1, using the sound intensity measurement method. Due to its compact design, precise flow control, and wide operating range (0.2–30 l/min), the ZAMBELLI ZB1 pump is a common choice for both laboratory and field measurements. In this research, two sound intensity measurement techniques were applied: the discrete point method [10], in accordance with ISO 9614-1, and the scanning method [11], in accordance with ISO 9614-2. The main objective of this work is to analyze and compare the applicability of these methods for accurate determination of the sound power level of the ZB1 pump and to discuss the results in terms of noise reduction and performance optimization.

2. INTENSITY MEASUREMENT METHODS

The most commonly used procedure in sound intensity measurement is based on the use of an intensity probe. This method involves two microphones placed at a small distance apart. Its main advantage involves the determination of sound intensity only in the direction given by the axis between the two microphones, allowing spatial selection of the analyzed sound sources and effectively minimizing the influence of background noise [12].

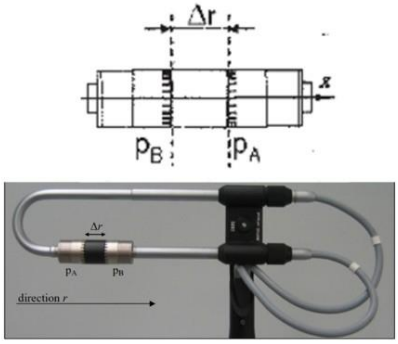

Figure 1. Face to face dual-microphone structure

Sound intensity can be estimated from the ratio of the pressures measured by microphones A and B, separated by a known distance, according to Equation (1):

$$I(t) = \frac{1}{2\rho_0 \Delta r}\left[p_A(t) + p_B(t)\right] \int \left[p_A(t) - p_B(t)\right] dt \quad (1)$$

where *I(t)* represents the sound intensity estimate in the direction (r) [W/m^2], $p_A(t)$ is the sound pressure in the time domain captured by microphone A [Pa]; $p_B(t)$ is the sound pressure in the time domain captured by microphone B [Pa]; Δ_r is the separation distance between microphones A and B [mm] and ρ is the volumetric density of the environment [kg/m^3].

The determination of sound power using sound intensity measurements is based on forming a measurement surface around the noise source, with the distance between the source and the probe being limited. Since sound power is proportional to the surface area of the measurement surface (equation (2)), it is used to calculate the power of the source. According to ISO 9614-1 and ISO 9614-2 standards, the minimum distance from the source to the measurement probe ranges from

200 to 500 mm, depending on the probe's orientation relative to the source [13].

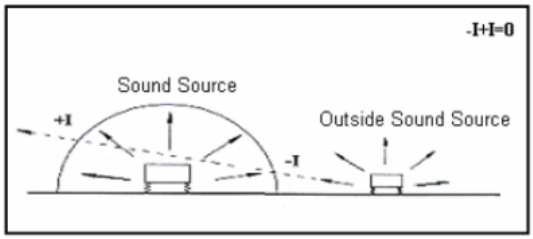

Figure 2. Illustration of the influence of external noise sources on sound power measurements

Figure 2 schematically illustrates how a source emits noise within the measurement surface, while background noise is also present. This represents a typical scenario when determining sound power using the sound intensity measurement technique [13].

The sound power generated by a noise source inside a surface is given by equation (2):

$$W_S = \int_S I_n dS. \quad (2)$$

where W_s represents the average sound power generated by the source inside of surface S, I_n is the sound intensity in the normal direction of the surface S.

Equation 2 allows the determination of the sound power of the source even in the presence of other sources or background noise, as the energy crossing the measurement surface is not taken into account [14].

In this study, two methods—discrete point measurement and scanning—were applied to ensure reliable determination of the sound power of a vacuum pump and to perform a comparison of the obtained results.

2.1 Discrete points method

The discrete point method involves measuring the normal component of the sound intensity at predefined positions on a measurement surface that fully encloses the noise source. The total sound power is then obtained by integrating the results over all surface segments. This method requires sampling of sound intensity at the central points of each segment over a sufficiently long time period to minimize statistical and sampling errors, in accordance with ISO 9614-1. The measurement time at each position is defined by the relation $B \cdot T \geq 400$, where B is the width of the lower band of interest and T is the sampling time in seconds. This method enables high measurement accuracy and detailed spatial analysis of sound intensity distribution, but it is time-consuming.

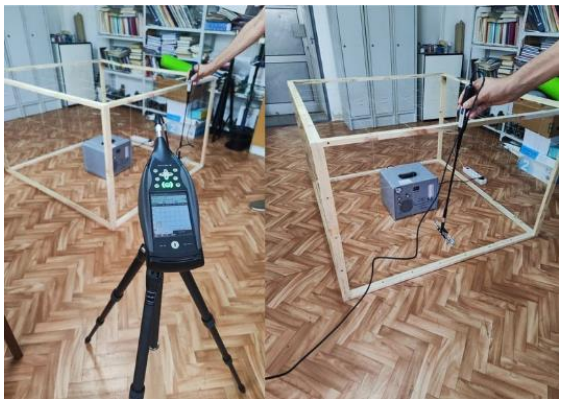

Figure 3. The measurement grid

In accordance with the standard [10] the measurement surface should enclose the noise source as completely as possible. Based on this requirement, measurement points were evenly distributed across all sides of the device, with a total of 161 points used. The measurement grid layout was defined to enable representative sampling of the sound field and is shown in Figure 3.

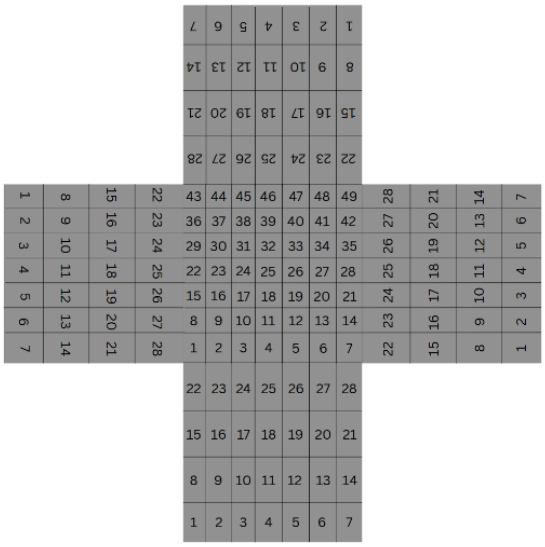

Figure 4. Orientation and sequence of the measurement points

During measurements, A-weighting was applied, as it best corresponds to the way the human ear perceives different frequencies. The sound intensity probe was positioned

perpendicularly to the surface at a distance of 0.5 m, and data were collected sequentially within the defined grid to capture the full sound radiation of the device.

2.2 Scanning method

The scanning method involves continuous movement of the probe along predefined paths on the measurement surface, resulting in a time–space averaged value of the sound intensity. This approach reduces the overall measurement time and enables faster estimation of total sound power, but it is more sensitive to irregularities in scanning speed and less suitable for sources with localized intensity maxima.

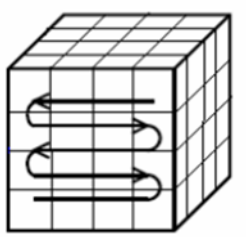

Figure 5. Measurement by scanning method [13]

In accordance with the standard [11], the device surfaces were scanned to capture the noise radiation as comprehensively as possible. A total of five surfaces were analyzed—front, rear, top, left, and right. On each surface, a measurement grid was defined, and the sound intensity was continuously recorded by moving the probe along predefined paths, as illustrated in Figure 6. This approach ensures efficient coverage of the entire sound field and reliable determination of the total sound power of the device [13].

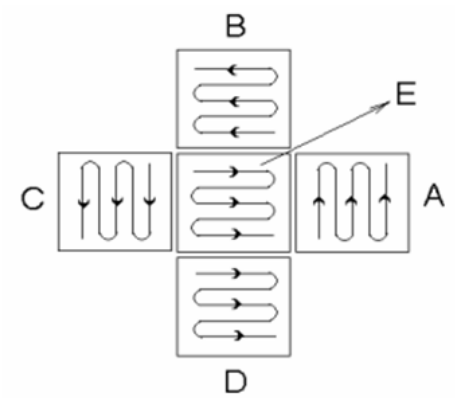

Figure 6. Orientation of sound intensity probe during measurement using the scanning method

The probe scanning speed is determined based on the total distance covered over each partial surface within the selected measurement time, as defined in ISO 9614-2.

3. RESULTS

Numerous studies have confirmed that the technique of determining sound power through sound intensity measurements represents a reliable and flexible alternative to classical methods in reverberant conditions. In the research [13] it was demonstrated that this technique yields results with deviations of less than ±2 dB compared to the reverberation method, with the additional advantage of identifying noise sources and the possibility of use in uncontrolled environments. Mohsen Aliabadi et al. [1] concluded that the sound intensity method is applicable even in high-background noise conditions, although accuracy may decrease when measuring non-uniformly radiating sources due to uneven sound fields and external noise interference. Similarly, Wittstock et al. [14] showed that despite the presence of background noise, it is possible to achieve high measurement accuracy using this method; however, sources that do not radiate uniformly present a challenge in terms of result reliability.

Based on the conclusions from these studies, this paper presents an analysis of the results obtained using both the discrete point method and the scanning method, with the available equipment at the Faculty of Mechanical and Civil Engineering in Kraljevo. The investigation included measurements of the overall sound power level as a function of frequency, as well as the spatial distribution of sound energy over the surfaces surrounding the noise source. The analysis was conducted under two airflow conditions (5 l/min and 15 l/min) to assess the influence of operating parameters on noise emission.

Measurement results at a frequency of 200 Hz (Figure 7) indicate that the rear surface generated the highest sound power level, with

values of 47.7 dB for an airflow rate of 15 l/min and 49.6 dB for 5 l/min. This indicates dominant noise radiation toward the rear side of the device, which is a direct consequence of the position of the cooling fan for the electric motor that draws in air during operation, thereby generating increased sound radiation in that direction. On the other hand, the lowest sound power levels were observed on the lateral surfaces, suggesting limited propagation of sound energy in those directions due to the pump housing geometry and reduced influence of vibrations.

Figure 7. Distribution of sound power over the measurement surfaces at a frequency of 200 Hz, for two different flow rates (left: 5 l/min, right: 15 l/min), obtained using the discrete points method

The contour maps of sound power on the rear surface of the device, shown in Figure 8, provide a visual representation of the spatial distribution of noise radiation. The most intense radiation zone is localized in the lower central part of the surface, which corresponds to the location of the pump's exhaust outlet.

At a flow rate of 15 l/min, a higher sound power level is observed in this zone—reaching 52 dB, compared to 31 dB at a flow rate of 5 l/min. This indicates an increase in noise emission due to higher dynamic pressure and air turbulence at increased flow, which is consistent with the expected behavior of the fan under such conditions.

The distribution of sound power extends concentrically from the center toward the edges, with a gradual decrease in noise levels, which is characteristic of localized and directional sources such as fans or compressor components. These results further support the findings obtained from the surface-based sound power analysis, emphasizing the significance of the rear surface as the primary noise-radiating segment of the device.

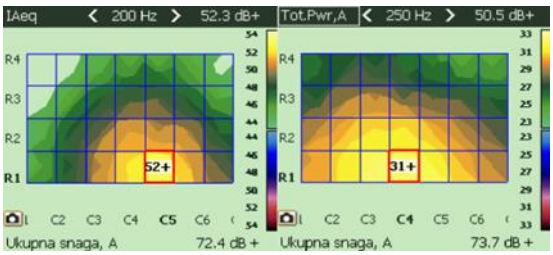

Figure 8. Contour map of sound power on the rear surface of the device – comparison for flow rates of 5 l/min and 15 l/min

A similar trend is observed for both methods – sound power increases with frequency in the low-frequency range, reaches a maximum between 1000 and 2000 Hz, and then gradually decreases toward higher frequencies (Figure 9). This spectrum indicates dominant noise radiation in the mid-frequency range, which is typical for mechanical noise sources such as vacuum pump.

When comparing the results for the two flow rates, it can be noted that, in most frequency bands, the total sound power at the lower flow rate (5 l/min) is slightly higher than at the higher flow rate (15 l/min), especially in the high-frequency range (≥ 4000 Hz). This can be explained by the higher local air velocity at lower flow, due to the narrowed cross-section inside the rotameter, which leads to intensified turbulence and more pronounced noise emission. Similar effects have been reported in previous studies [9], which showed that flow dynamics and diaphragm mechanism stability significantly affect the level of emitted noise.

The discrete point method shows a slightly higher sound power level compared to the scanning method across most frequency bands, which is expected given the more detailed sampling this method involves. On the other hand, both methods display a similar frequency distribution and strong agreement in overall trends, indicating the reliability of the measured values.

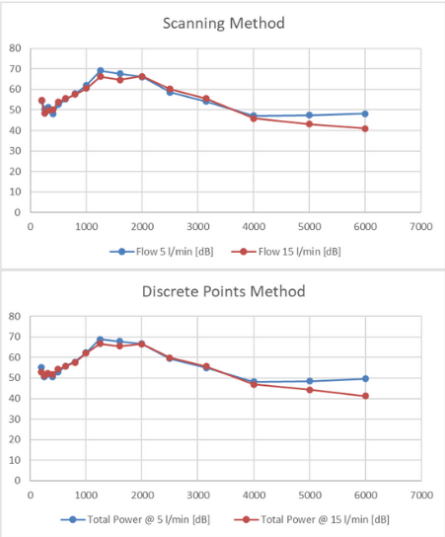

Figure 9. Total sound power measurement results for two flow regimes (5 l/min and 15 l/min), obtained using the scanning method and the discrete point method

4. CONCLUSION

This study analyzed the sound power of a vacuum pump using two sound intensity-based measurement methods – the discrete-point method (ISO 9614-1) and the scanning method (ISO 9614-2). Both methods produced results consistent with the expected frequency spectrum of mechanical noise sources, with a maximum occurring in the 1000 to 2000 Hz range. A comparison of results at different flow rates (5 and 15 l/min) indicated the influence of operating conditions on the intensity of emitted noise, with sound power generally being higher at the lower flow rate.

The discrete point method enabled high measurement precision and a detailed analysis of the spatial distribution of noise, which proved particularly useful in identifying zones of highest emission, such as the rear surface of the pump in this case. However, this method is more time-consuming due to the requirement to position the probe at a large number of individual points.

The scanning method proved more efficient in terms of measurement duration and ease of use. When properly executed and field-controlled, the results were comparable to those of the discrete-point method, as confirmed by the good agreement in overall sound power across frequencies. Still, the method shows increased sensitivity to background noise and requires skilled equipment handling.

Taking all aspects into account – accuracy, applicability, measurement duration, and processing complexity – it can be concluded that the choice of method depends on the specific measurement requirements. When detailed emission analysis and source localization are needed, the discrete-point method is preferable. Conversely, in situations where efficiency and simplicity are priorities, the scanning method offers a more practical solution. Both approaches, when properly implemented, provide results that comply with ISO 9614 and are sufficiently reliable for practical application.

ACKNOWLEDGEMENT

The authors acknowledge the support of Ministry of Science, Technological Development and Innovation of Republic of Serbia (contract no. 451-03-136/2025-03/200108) . This research contributes to the United Nations 2030 Agenda for Sustainable Development, specifically to Sustainable Development Goal 9: Buid resilient infrastructure, promote inclusive and sustainable industrialization and foster innovation.

REFERENCES

[1] M. Aliabadi, R. Golmohammadi, A. Ohad: Empirical Comparison of the In Situ Methods for Determining Sound Power of Typical Embroidery Machine Located in Industrial Workroom, International Journal of Occupational Hygiene, Vol. 5, No. 3, pp. 89-95, 2013.

[2] W. Mickiewicz, M. Raczyński, A. Parus: Performance Analysis of Cost-Effective Miniature Microphone Sound Intensity 2D Probe, Physical Sensors , Vol. 20, No. 1, p. 271, 2020.

[3] N. Knežević, M. Bjelić, K. Jovanović: Performance Analysis of Cost-Effective Miniature Microphone Sound Intensity 2D Probe, International Journal of Electrical Engineering and Computing, Vol. 2, No. 1, pp. 20-28, 2019.

[4] R. Girgis, K. Garner, M. Bernesjö, J. Anger, D. Chu: Measuring no - load and load noise of power transformers using the Sound Pressure and Sound Intensity methods — Part - I: Outdoors measurements, in: *2008 IEEE Power and Energy Society General Meeting - Conversion and Delivery of Electrical Energy in the 21st Century*, 2008, Pittsburgh, PA, USA, pp. 1-8.

[5] S. Nagata, F. Kenji, T. Wada, D. Asano, T. Yanagisawa: A three-dimensional sound intensity measurement system for sound source identification and sound power determination by ln models, The Journal of the Acoustical Society of America, Vol. 118, No. 6, pp. 3691-3705, 2005.

[6] K. Zhao, Y. Lou, G. Peng, C. Liu, H. Chang: A Review of the Development and Research Status of Symmetrical Diaphragm Pumps, Symmetry in Micro/Nanofluid and Fluid Flow, Vol. 15, No. 1, p. 2091, 2023.

[7] Y. Liang, Z. Chen, J. Liao: Numerical simulation and experimental evaluation of flow ripple characteristics of Truninger pump, Scientific Reports, Vol. 12, No. 1, 2022.

[8] Q. Si, C. Shen, X. He, H. Li, K. Huang, J. Yuan, Numerical and experimental study on the flow-induced noise characteristics of high-speed centrifugal pumps, Applied Sciences, Vol. 10, No. 9, p.3105, 2020.

[9] M. Ibrahim, M. Mahat, CFD Analysis of Electromagnetic Based Valveless Pump, Procedia Engineering, Vol. 41, pp. 1524-1532, 2012.

[10] ISO 9614-1, Acoustics — Determination of sound power levels of noise sources using sound intensity — Part 1: Measurement at discrete points, 1993

[11] ISO 9614-2, Acoustics — Determination of sound power levels of noise sources using sound intensity, Part 2: Measurement by scanning, 1996

[12] M. Bjelić, N. Knezević, K. Jovanović: Automatizovano merenje intenziteta zvuka pomoću robota i intenzitetske sonde, in: *Proceedings of the 17th International Symposium INFOTEH*, 21-23 March 2018, Jahorina, BiH, pp. 17-22.

[13] C. M. de Souza, L. C. S. Góes: SOUND POWER DETERMINATION USING ACOUSTIC INTENSIMETRY,APPLYING DISCRETE POINTS AND SCANNING METHODS, in: *Proceedings o*f *COBEM 2007*, 5-9 November 2007, Brasília, DF

[14] V. Wittstock, S. Brezas, F. Heisterkamp: Sound power determination by intensity—are field indicators and criteria in iso 9614 meaningful?, The Journal of the Acoustical Society of America, Vol. 155, No. 1, pp. 588-599, 2024.

Society of Production Engineering

ICPES 2025

40th INTERNATIONAL CONFERENCE ON PRODUCTION ENGINEERING - SERBIA 2025

DOI: 10.46793/ICPES25.482S

University of Nis
Faculty of Mechanical Engineering

Niš, Serbia, 18-19th September 2025

IMPLEMENTATION OF INDUSTRY 4.0 IN THE AUTOMOTIVE INDUSTRY ACCORDING TO ISO 16949

Natalija STANKOVIĆ[1], Saša S. RANĐELOVIĆ[1], Goran STANKOVIĆ[2], Branislav MARKOVIĆ[2], Radoslav VUČUREVIĆ[3]

Orcid: 0000-0002-2334-8929; **Orcid:** 0000-0002-2334-8929; **Orcid:** 0000-0002-5979-674X;

[1]Faculty of Mechanical Engineering, University of Niš, Serbia

[2]LEONI, Niš, Serbia

[3]Faculty of Production and Management Trebinje, University of East Sarajevo, Bosnia and Herzegovina

*Corresponding author: stankovicnatalija023@gmail.com

Abstract: *This paper examines the implementation of Industry 4.0 elements in enhancing the quality of cables and connectors in the automotive industry, with a focus on meeting ISO 16949 requirements. Modern quality control solutions are presented, including smart sensors, digital twins, and predictive analytics. Special emphasis is placed on multi-stage testing methods and process digitalization for quality monitoring. Through a case study from the company Leoni, the impact of QRQC, Q4.0, and Q-Loop systems on defect reduction in the production of BMW components is analyzed. The paper demonstrates how the integration of Industry 4.0 technologies enhances reliability, efficiency, and compliance with automotive industry standards.*

Keywords: *automotive industry, Industry 4.0, quality control, predictive analytics, SPC, ISO 16949, connectors, cables.*

1. INTRODUCTION

Electrical and electronic systems are increasingly attracting the attention of customers in the highly demanding automotive market. A modern car represents a complex technological system, where the transfer of energy and information is considered one of the most reliable subsystems and assemblies. Essential electrical cables and connectors form the foundation of such advanced electronic systems in next-generation vehicles, industrial machines, and devices, ensuring stable transmission of energy and data between various components. Their technical design and reliability directly affect the safety and functionality of the entire system, making quality control in this segment crucial.

With the growing implementation of electric drive systems and the development of autonomous technologies, wiring systems are becoming increasingly complex, which further complicates fault detection and raises the risk of serious consequences, from reduced

performance to complete system failure. Traditional approaches, which primarily rely on technical trials, electrical and electronic tests, manual inspections, and statistical process control, are no longer sufficient to detect all deviations in the finished product that occur during production. In this context, Industry 4.0 elements bring new possibilities through automated inspection, digitalized control, artificial intelligence, and predictive analytics, enabling timely error detection and a more stable production process.

This paper analyzes the application of Industry 4.0 technologies in the company Leoni and the ways in which they contribute to improving the quality of cables and connectors for the automotive industry.

2. SHORT ANALYSIS OF THE CABLE INDUSTRY

Recent research and industrial practice indicate the increasing application of multi-stage testing methods for wiring harnesses to ensure their reliability under real operating conditions. These methods include visual inspection, continuity testing, insulation resistance measurement, dielectric strength testing, and mechanical testing under simulated extreme conditions such as high temperatures, vibrations, and humidity. Critical tests such as the High Voltage Test, Insulation Resistance Test, and Functional Testing [1] enable the detection of hidden defects that manual inspections often cannot identify.

Figure 1. Multifunctional wiring harness with circular and rectangular connectors

Although traditional testing methods are still present, they rely heavily on human involvement and are therefore prone to errors. On the other hand, modern automated systems increase the accuracy and repeatability of measurements, contributing to a higher level of quality and reduced production losses.

Parallel to the development of testing methods, modern industry is increasingly integrating the principles of Industry 4.0 into its quality control processes. By using technologies such as the Internet of Things (IoT), Artificial Intelligence (AI), Big Data, and Digital Twins, it becomes possible to monitor and analyze key production parameters in real time [2]. Smart sensors record data and automatically send alerts in case of deviations, while predictive analytics enables error prevention before they even occur.

This approach is based on the concept of Cyber-Physical Systems (CPS), which represents the foundation of smart manufacturing within Industry 4.0. According to Lee, Bagheri, and Kao (2015), CPS enables the integration of the physical and digital worlds through continuous data collection, processing, and real-time analysis, ensuring full process control and improved product quality [7].

Modern testing systems also employ specialized software tools, such as LabVIEW for managing testing stations, Q-DAS for statistical process control, and ANSYS for simulating cable and connector load conditions. These tools allow for integrated data analysis and efficient process optimization.

Among the most commonly used tools in practice are:

- **SPC (Statistical Process Control)** – for real-time variation monitoring,
- **6S methodology** – for workplace organization and waste elimination,
- **7-Point Measurement Method** – ensuring quality control across all critical stages of production [1][5],
- Additionally, systems such as **ASP (Automated Smart Processing)** enable early detection of irregularities and significantly improve quality in cable and connector production [2].

- For example, the company **Leoni**, a supplier for **BMW**, uses automated testing stations for wiring harnesses that transmit real-time data to a central system. These data are analyzed using AI algorithms to predict potential issues and optimize the process, ensuring high precision and reduced waste.

2.1 Types of Connectors in the Automotive Industry

Connectors in the automotive industry are classified according to various criteria, one of the most common being the housing shape – circular and rectangular – depending on technical requirements and specific areas of application.

Figure 2. Circular Connectors

Circular Connectors

Circular connectors, such as M12, M23, and D38999 (MIL-standard), are used for power and signal transmission in demanding conditions due to their resistance to moisture, vibrations, and mechanical stress. For example, the M12 connector with a metal housing and rubber seal is commonly used in industrial machinery and vehicles where high reliability and resistance to external factors are required.

Rectangular connectors, such as D-sub, Fakra, and Amphenol AT06, are widely used in electronics and the automotive industry. Due to easier integration, modularity, and reliability, they are often employed for communication modules, infotainment systems, power connections, and safety components.

Besides the basic classification by shape, connectors also differ by function and performance:

- **High-speed connectors** – designed for fast data transmission,
- **High-voltage connectors** – used in high-voltage systems,
- **Waterproof connectors** – for components exposed to external influences (moisture, dust).

Modern trends include miniaturization, modular design, and the use of environmentally friendly materials, in compliance with REACH and RoHS directives.

Figure 3. Rectangular Connector

Figure 4. Rectangular Automotive Fakra Connector

The selection of connectors directly affects product design, connection reliability, assembly quality, and the applied control methods. Connectors must comply with the requirements of vehicle manufacturers (OEMs) and international standards, particularly ISO 16949 [3], which defines the quality management system requirements in the automotive industry.

3. BRIEF PROBLEM DESCRIPTION

One of the key challenges in modern cable and connector manufacturing is the timely detection of defects before the product reaches the final assembly stage. In high-volume production environments, such as in the case of the company Leoni, traditional control methods, which rely on manual inspection, are often insufficient to detect deviations such as incorrect lengths, weak connections, or improperly formed contacts. The lack of real-time automated monitoring further complicates the maintenance of stable quality and increases the risk of customer complaints and additional costs [4].

The development of electric and smart vehicles adds further complexity, as the increased intricacy of electrical circuits demands greater precision and reliability of cable systems. In this context, the traditional

"wire-to-wire" connection system is being replaced by the concept of "one wire – multiple functions" [5], which saves space, reduces the number of components, and increases the overall efficiency of the system.

Figure 5 Example of a Standard Wire Harness with Multiple Connectors (RCCN)

Figure 5 shows a wire harness with multiple types of connectors, commonly used in automotive and industrial production. These harnesses enable the connection of various functional systems, including power supply, signaling, and communication. Their reliability largely depends on the quality of the connections as well as adequate protection from external influences such as moisture, dust, and mechanical wear.

Modern technological advancements in the automotive industry are placing increasing demands on the manufacturing process of wire harnesses and connectors. To ensure system reliability, it is essential to carefully select input materials by strict internal and international standards, such as ISO 16949, as well as specific performance requirements for automotive applications. Special attention is given to the properties of the materials used – their resistance to heat, moisture, chemicals, and mechanical stress – both in standard and extreme operating conditions.

In addition to proper material selection, every stage of the production process must be subjected to strict and multilayered control, both process-based and physical, in compliance with ISO 16949 requirements. Without a systematic and digitalized approach to quality management, it is difficult to meet the challenges posed by intelligent vehicle systems and the high expectations of end users.

4. PROPOSED SOLUTIONS

In response to the challenges of modern manufacturing, companies are implementing integrated quality control strategies that combine multi-level testing, digitalization, and automation. The process begins with CAD simulation, the selection of high-quality materials, and precise production by the ISO 16949 standard. Quality is ensured through multiple stages of electrical, mechanical, and environmental testing, as well as final visual inspection. Software tools for automatic data collection enable real-time process monitoring, deviation detection, and fast decision-making. Systems such as digital twins and SPC (Statistical Process Control) tools allow for the simulation of production conditions and defect prevention.

In the production of connectors for BMW, Statistical Process Control (SPC) plays a key role, enabling continuous monitoring of the stability of dimensional and functional characteristics of the product. By using control charts and Cp/Cpk analysis, processes can be timely adjusted to ensure compliance with ISO 16949 requirements.

Table 1. Key Parameters of SPC Quality Control for Connectors

Parameter	Measuring Device	Control Chart	Response to Deviations
Housing dimension	Modern optical CMM	X̄-R chart	Tool calibration, line stoppage
Insertion force	Force tester	X̄-R chart	Die replacement, press inspection
Electrical resistance	4-point ohmmeter	P chart	Contact cleaning, batch recall
Cp/Cpk process value	SPC software	Cp/Cpk monitoring	Process analysis, corrective actions

In addition to SPC, the 7 Point Method also plays an important role, covering all key stages – from incoming material inspection to final process analysis. This combination of methods

provides a comprehensive approach to quality and reduces the risk of defective products.

Qin, Liu, and Grosvenor (2016) emphasize that such an approach enables more flexible and intelligent production flows that can quickly adapt to changes in market demands and quality standards [8].

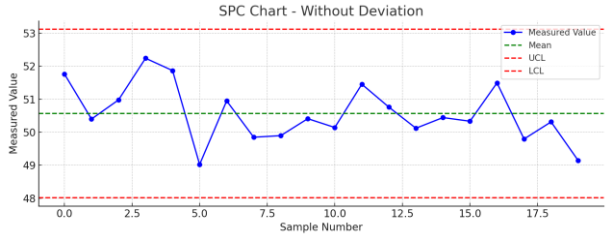

Figure 6. Change in Force Outside Control Limits

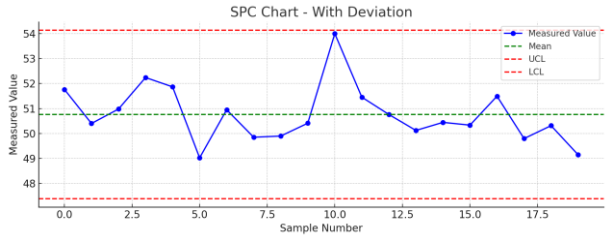

Figure 7. Force Within Control Limits

In the presented SPC charts (Figures 6 and 7), the monitored parameter is the connector insertion force, which is one of the most critical indicators of connection reliability. The insertion force is measured using specialized force testers under real production conditions, and the results are displayed on X̄-R control charts. When values remain within the control limits (LCL and UCL), the process is considered stable, whereas any deviation—as shown in Figure 6—requires immediate analysis and corrective action.

Additional methods for improving quality control include:

- Automatic scanning and digitalization of components using systems such as InspecVision Planar 2D and RPS Measuring Arms.
- Software support through High QA Inspection Manager for complete traceability and rapid response.
- Surface and contour analysis using Waveline and Formline systems.
- Intelligent crimping systems with real-time automatic correction.
- Use of digital twins and predictive analytics for process optimization and defect prevention.

This approach ensures a high level of quality and reliability, meeting the strict requirements of the automotive industry and ensuring compliance with international standards, including ISO 16949.

Table 2. Seven Critical Quality Control Points

Control Point	What Is Checked	Response to Deviations
1. Incoming material inspection	Quality of plastic and metal	Supplier replacement, material rejection
2. Dimensional control	Length, width, tolerances	Tool correction, process stoppage
3. Insertion force control	Minimum and maximum insertion force	Connector rejection
4. Electrical testing	Continuity, resistance	Batch blocking, additional analysis
5. Visual and surface inspection	Damage, roughness, contamination	Cleaning, tool replacement
6. Functional fit test	Connection with matching components	Batch recall, corrective actions
7. Final SPC analysis	Cp, Cpk, process stability	Parameter adjustment, process optimization

4.1. Case study: LEONI – implementation of industry 4.0 in quality control

Leoni Wiring Systems represents a successful example of Industry 4.0 implementation in the field of quality control for cables and connectors used in BMW vehicles. Through its *Zero Defect Mindset* strategy, the company has introduced automated and digitalized systems that enable early defect detection and rapid response, thereby increasing production stability and reliability.

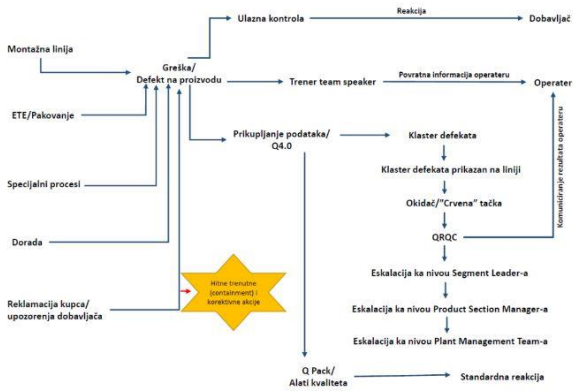

Figure 8. Flow of quality issue escalation and corrective actions in Leoni – Industry 4.0 application

Figure 8 illustrates the escalation flow of quality issues within Leoni's Industry 4.0 framework, starting from incoming inspection and supplier reaction, continuing through defect detection on the line and data collection via Q4.0, all the way to QRQC activation and corrective actions. Reischauer (2018) further points out that the concept of Industry 4.0 is increasingly used not only as a technological framework but also as a strategic tool for institutionalizing innovation systems within manufacturing organizations [9]. This role of Industry 4.0 as a strategic factor is reflected in how companies like Leoni manage quality by modern requirements.

Leoni employs three key methods for quality management:

- **QRQC (Quick Response Quality Control)** – enables rapid defect resolution directly on the production line, including root cause analysis (5Why), implementation of corrective actions, and full traceability;
- **Q-Loop** – a seven-phase cycle covering the entire process from planning to continuous improvement, incorporating SPC software, CMM measurements, and digital twins;
- **5Why & 2How analysis** – used to identify the root cause of problems and define preventive and verification measures.

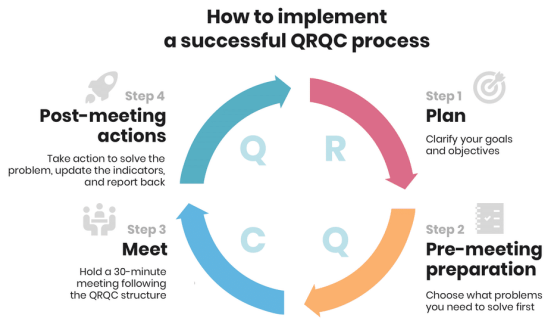

Figure 9. Four-step method for rapid quality problem resolution

As shown in Figure 9, the company applies a four-step method for rapid quality problem resolution, beginning with defect identification and escalating toward management-level intervention.

The quality system at Leoni includes central databases (QDE and SE Masterdata) that enable full traceability of connectors. The assembly process is digitally controlled, and each component undergoes electrical, mechanical, environmental, and visual testing. Regular QRQC meetings ensure continuous improvement, while deeper analyses utilize tools such as PDCA, FTA, 8D, and A3.

The implementation of Industry 4.0 has brought:

-a reduction in defect rates and increased product reliability,

-faster decision-making and automated quality analysis,

-Improved collaboration with BMW and a stronger market position.

To OEM specifications and offer nearly identical dimensions and functionality as original products from well-known brands (Molex, TE Connectivity, Delphi, Deutsch), but at lower cost and with significantly shorter lead times.

Alternative connectors provide greater flexibility in the supply chain and cost reduction without compromising quality, provided that they meet all technical and certification requirements (e.g., ISO 16949). Although there may be technical limitations in certain specialized cases, their use is increasingly common in the industry, especially when a

rapid response is needed in case of original component shortages. [3]

5. CONCLUSION

The implementation of Industry 4.0 in the automotive industry, specifically in the production of electrical cables and connectors for BMW, represents a significant advancement toward improving the quality, reliability, and efficiency of manufacturing processes. Through the integration of advanced technologies such as smart sensors, digital twins, predictive analytics, and Statistical Process Control (SPC), the company Leoni successfully applies digitalization principles to achieve a high level of automation and precision.

The QRQC and Q-Loop methodologies enable rapid response to defects and thorough analysis, minimizing the likelihood of recurring issues and reducing the number of defective products. By establishing the digitalized Q4.0 system, Leoni ensures complete traceability and control over every segment of production, contributing to compliance with the stringent requirements of ISO 16949 standards and the expectations of prestigious customers like BMW.

The results confirm that Industry 4.0 is not only a technological but also a strategic key to achieving zero defect tolerance and long-term competitiveness in the automotive industry. This work can serve as a foundation for applying similar approaches in other sectors with complex manufacturing processes.

REFERENCES

[1] https://konnra.com/wire-harness-quality-testing-methods-ensuring-product-safety-and-reliability/

[2] AUTOMOTIVE SMART PRODUCTION: MEASUREMENT SYSTEMS IN THE INDUSTRY 4.0 ERA

[3] https://www.ql-custom.com/what-is-equal-substitute-connector.html

[4] PRIRUČNIK ZA PROIZVODNJU, LEONI NIŠ, 2023.

[5] HOW TO CONTROL THE QUALITY OF AUTOMOTIVE WIRING HARNESSES IN THE MANUFACTURING PROCESS – INDUSTRIA INFORMAZIONI – NEWS – WIRING DUCT, CABLE GLAND, CABLE TIE, TERMINALS, RCCN

[6] http://tqmkonsalting.com/usluge/standardi/sistemi-menadzmenta/isots-16949-sistem-menadzmenta-kvalitetom/

[7] LEE, J., BAGHERI, B., & KAO, H. A. (2015). A CYBER-PHYSICAL SYSTEMS ARCHITECTURE FOR INDUSTRY 4.0-BASED MANUFACTURING SYSTEMS. *MANUFACTURING LETTERS*, 3, 18–23. https://doi.org/10.1016/j.mfglet.2014.12.001

[8] Qin, J., Liu, Y., & Grosvenor, R. (2016). A Categorical Framework of Manufacturing for Industry 4.0 and Beyond. *Procedia CIRP*, 52, 173–178. https://doi.org/10.1016/j.procir.2016.08.005

[9] Reischauer, G. (2018). Industry 4.0 is a policy-driven discourse to institutionalize innovation systems in manufacturing. *Technological Forecasting and Social Change*, 132, 26–33. https://doi.org/10.1016/j.techfore.2018.02.012

Society of Production Engineering

ICPES 2025

40th INTERNATIONAL CONFERENCE ON PRODUCTION ENGINEERING - SERBIA 2025

DOI: 10.46793/ICPES25.489J

University of Nis Faculty of Mechanical Engineering

Nis, Serbia, 18 - 19th September 2025

ANALYSIS OF MEASUREMENT SYSTEM CAPABILITY WITH NEGLIGIBLE OPERATOR INFLUENCE: A CASE STUDY USING A COORDINATE MEASURING MACHINE

Predrag JANKOVIĆ[1]*, Miloš MADIĆ[1]
Orcid: 0000-0001-9951-4500; **Orcid:** 0000-0002-2310-2590
[1] University of Niš, Faculty of Mechanical Engineering, Niš, Serbia
*Corresponding author: predrag.jankovic@masfak.ni.ac.rs

Abstract: *In modern industrial metrology, the ability to assess the reliability and precision of measurement systems is of critical importance. This study presents a measurement system analysis (MSA) focused on scenarios where operator influence is negligible, particularly applicable when using coordinate measuring machines (CMMs) operating in automated or highly standardized conditions. Unlike classical GRR (Gage Repeatability and Reproducibility) studies that assess both repeatability and reproducibility — often require multiple operators — this approach isolates repeatability as the dominant component of measurement variation.The experimental part of the research was conducted using a CNC-controlled CMM to measure key dimensional characteristics on a series of precision-machined cylindrical parts. A fixed measurement program was used to eliminate variability due to operator actions. Statistical analysis included repeatability studies, calculation of %GRR, and evaluation of measurement system capability indexes (such as P/T ratio).*

Keywords: *Product quality, Measurement system analysis, GR&R, CMM*

1. INTRODUCTION

Coordinate Measuring Machines (CMMs) represent a cornerstone of modern dimensional metrology, primarily due to their ability to minimize the influence of human operators on measurement outcomes. Traditional manual measurement techniques, such as calipers, micrometers, or gauges, are highly dependent on operator skill, consistency, and subjective judgment, which introduces variability into the measurement system. By contrast, CMMs automate the measurement process through programmable probing strategies, controlled motion systems, and integrated software environments. This automation reduces operator-dependent sources of error, ensuring that measurements are executed in a repeatable and standardized manner. From a theoretical perspective, CMMs can be considered as instruments that effectively decouple the measurement process from human factors, allowing researchers to focus on machine-related uncertainty components such as repeatability, probe performance, fixturing, and environmental

stability. In industrial practice, this translates into improved measurement reliability, higher productivity, and a stronger foundation for objective decision-making in quality assurance.

In past years, CMMs have evolved from high-precision laboratory measuring devices into shop floor systems. This trend is observed in high-tech processes, a typical example being the automotive industry. Standardized procedures for quality assurance in the automotive industry require proof of the quality of the control processes and of the measuring devices, for which the MSA methodology is applied.

Measurement System Analysis has been extensively standardized and documented, most notably in the AIAG MSA manual and in ISO 22514-7 [1], which provide guidelines for evaluating the capability of measurement systems across different industrial applications. According to international standards, m*easurement system analysis* is defined as "a series of studies that explains how a measurement system performs" (ISO 13053-2 2011 [2]) and consists of "a set of methods used to evaluate the uncertainty of a measurement process under the range of conditions in which the process operates" (ISO 22514-1 2014) [3]. The core idea is to decompose total observed variation into repeatability, reproducibility, and part-to-part components, using either range-based methods or variance analysis (ANOVA). Within academic literature, several studies have emphasized the importance of adapting MSA methodologies to advanced metrology systems, including CMMs, where the traditional assumption of significant operator influence no longer applies. Instead, the focus shifts toward quantifying machine-related uncertainty sources such as probe calibration, thermal effects, and the stability of fixturing and alignment strategies. Research contributions in this field highlight that, while CMMs inherently reduce human variability, they still require rigorous system capability studies to ensure measurement validity, particularly when measurements are employed for process control or capability analysis. This dual perspective, rooted in both industrial standards and academic investigation, establishes a sound methodological foundation for applying MSA in the CMM environment.

A measurement system analysis initially aims to verify if the right measurement is being applied to the system. It evaluates if the chosen method is appropriate considering all potential variables. Next, it assesses the measuring instruments. Often, tools like gages and fixtures deteriorate or malfunction, compromising their efficiency. The MSA checks whether these tools require calibration, replacement, or an upgrade.

Furthermore, the MSA evaluates the staff's proficiency in implementing the measurement system's guidelines and any environmental elements that could impact the procedure. Inconsistencies in the process can lead to inaccurate outcomes and potentially defective products. The primary objective of the MSA is to pinpoint and reduce these inconsistencies [4].

A comprehensive review of different methods and techniques used for measuring system analysis is given as an in-depth analysis in many scientific articles. In [5] the authors discuss the sources of measurement variation, such as bias, linearity, and stability, and provide insights into how to assess and improve measurement systems.

There are also studies in which it is examined, and the impact of various factors on the quality of measurement results from a coordinate measuring machine (CMM) being explored, with a particular focus on the role of temperature [6].

Measurement system analysis methods are used to analyze measurement systems for continuous and attribute data. It is important to mention that all elements of a measurement system (gages, standards, operators, software, measurement equipment, procedures, environmental components, as well as others) can affect the variation of results and contribute to the measurement system capability. Capability of the measurement system can be characterized by quantifying its accuracy and precision [7].

Measurement System Analysis (MSA) is critical in ensuring the reliability of data used in manufacturing and quality assurance. Traditional systems often suffer from operator-induced variability. CMMs, especially in automated configurations, offer a solution by reducing human influence. This paper aims to evaluate the capability of such systems through a structured case study.

2. MEASUREMENT SYSTEM ANALYSIS

Quality control is an essential component of modern manufacturing, ensuring that products consistently meet design specifications and customer expectations. At the heart of every quality control process lies the measurement system, which provides the quantitative basis for evaluating conformity and process stability. A reliable measurement system not only enables the detection of nonconformities but also supports continuous improvement initiatives, process optimization, and cost reduction. Conversely, if the measurement system itself introduces significant variation or uncertainty, the validity of quality decisions is compromised, leading to incorrect acceptance or rejection of parts, inefficiencies, and potential customer dissatisfaction. For this reason, the evaluation and validation of measurement systems represent a critical step in establishing an effective quality management framework, particularly in industries where high precision and tight tolerances are required.

Measurement Systems Analysis (MSA) is a tool for analyzing the variation present in each type of inspection, measurement, and test equipment. It is the system used to assess the quality of the measurement system. In other words, it allows us to ensure that the variation in our measurement is minimal compared to the variation in our process.

Every day our lives are being impacted by more and more data. We have become a data driven society. In business and industry, we are using data in more ways than ever before. Today manufacturing companies gather massive amounts of information through measurement and inspection. When this measurement data is being used to make decisions regarding the process and the business in general it is vital that the data is accurate. If there are errors in our measurement system, we will be making decisions based on incorrect data. We could be making incorrect decisions or producing non-conforming parts. A properly planned and executed measurement system analysis can help build a strong foundation for any data-based decision-making process [8].

3. COORDINATE MEASURING MACHINES

A Coordinate Measuring Machine (CMM) is a device designed to measure the geometry of physical objects by detecting discrete points on their surfaces using a probing system (Figure 12). CMMs are most commonly applied in the inspection of parts or assemblies to verify whether they conform to the original design intent. They are integrated into quality assurance and quality control processes to check the dimensions of manufactured components and to prevent or resolve quality-related issues. In addition, CMMs are widely used in production and assembly operations to verify parts and assemblies against design specifications. The measured points can be utilized to validate distances between characteristic features, as well as to construct geometric elements such as cylinders or planes, enabling the evaluation of aspects like roundness, flatness, and perpendicularity. Compared to manual inspections or conventional measuring tools such as micrometers and height gauges, CMMs offer significant advantages, including higher accuracy, faster measurement cycles, and a considerable reduction of human error [9].

Although CMMs significantly reduce operator-induced variability, the application of Measurement System Analysis (MSA) remains essential to ensure the overall reliability of the measurement process. The reason lies in the fact that measurement variation is never completely eliminated; instead, its sources shift from human factors to machine- and process-

related components. In the case of CMMs, repeatability is primarily influenced by probe performance, machine kinematics, fixturing conditions, and environmental stability, while part-to-part variation reflects the actual dimensional differences of the workpieces under study. By applying MSA, it becomes possible to quantitatively separate these components of variation, evaluate the proportion of measurement error relative to the studied tolerance, and determine whether the CMM system is capable of supporting process control decisions. From both academic and industrial perspectives, conducting an MSA study in the CMM environment provides a systematic framework for validating the measurement system, identifying dominant error sources, and establishing confidence in the data used for product and process quality assurance.

MSA is a process used to evaluate the suitability of a measuring system for use. A measuring system can be any combination of a transducer, signal conditioner, display, recorder, or data acquisition system used to obtain a measurement. A measuring system is capable if it meets the required technical performance specifications.

With increasing demands for accuracy and precision in industries such as aerospace, automotive, medical, tooling, semiconductor, electronics, shipbuilding, and other manufacturing sectors, it has become essential to develop new procedures and machines capable of performing complex measurements. In this context, the Coordinate Measuring Machine (CMM), due to its high accuracy and repeatability of measurement results, represents a logical choice for enhancing the quality of the production process. However, the CMM must efficiently and effectively provide the necessary information regarding part dimensions and tolerances. Furthermore, it is crucial that CMM users understand and apply proper procedures and techniques to improve the reliability of measurement results. Evaluating the performance of the CMM and determining the uncertainties associated with measurement outcomes are of fundamental importance for maintaining repeatability and reliability in measurement processes.

4. STUDIES FOR ASSESSING THE ABILITY OF THE MEASURING SYSTEM

Measurement System Analysis (MSA) is a standardized methodology used to statistically evaluate the capability of a measurement system to deliver accurate, repeatable, and stable measurement results. This analysis is essential for ensuring product and process quality, as it enables the identification of sources of variability in measurement—whether they originate from the device itself, the operator, the measurement method, or environmental conditions. In modern industrial systems, particularly in the automotive and precision manufacturing sectors, MSA is regarded as an indispensable tool for qualifying control processes [10].

MSA studies are conducted as a form of “mini experiment” aimed at assessing the overall variability within the measurement system. When a variable (quantitative) characteristic is being measured—such as length, angle, temperature, pressure, or resistance—specific MSA methods are applied depending on the study’s objective and the presence of operator influence. The fundamental types of MSA studies for quantitative data include [11]:

- Evaluation of instrument bias, linearity, and stability over an extended period of time.
- **Type I Study** – assessment of the measuring device alone (excluding the operator), where Cg and Cgk indices are calculated, analogous to process capability indices (Cp, Cpk).
- **Type II Study** – classical GR&R analysis (Repeatability and Reproducibility), in which variability is assessed by involving multiple operators.
- **Type III Study** – GR&R study without operator influence, suitable when the same operator measures multiple samples and differences between operators are considered negligible.

Type II and Type III studies utilize two primary calculation methods: the Average and

Range Method (ARM) and Analysis of Variance (ANOVA). Although the ARM method is simpler and widely used, the ANOVA method is increasingly required in practice due to its higher precision and ability to clearly isolate sources of variation [12]. The MSA methodology received its standardized form in the early 1990s, when the Automotive Industry Action Group (AIAG), in collaboration with leading American automotive manufacturers such as Chrysler Motors, General Motors, and Ford Motor Company, developed the MSA manual as the official guide for conducting these analyses. Within this manual, specific rules for evaluating GR&R (Gage Repeatability and Reproducibility) studies are defined, along with threshold values that enable straightforward interpretation of results.

Based on the percentage contribution of GR&R variation to the total tolerance, it is possible to determine whether a measurement system is acceptable, marginally acceptable, or unacceptable for a given application. This allows engineers to quickly decide whether a particular measuring device (gage) can be used in serial production, or whether replacement or further process optimization is required [13]. The most used criterion is the so-called %GRR, which represents the percentage of total tolerance "consumed" by measurement uncertainty. According to AIAG guidelines, the system is considered [13]:

According to AIAG guidelines, the system is considered:

- **Acceptable** if %GRR is less than 10% – the measurement system is suitable for use in production without further modification.
- **Marginally acceptable** if %GRR is between 10% and 30% – the system may be used, but improvement is recommended.
- **Unacceptable** if %GRR exceeds 30% – the measurement system is not suitable for the intended application and requires corrective action, such as equipment replacement or process optimization.

Total Variation (TV) of a measurement system represents the sum of several components that collectively describe the quality and reliability of the measurement process. These components include repeatability (EV), reproducibility (AV), stability, and linearity. Repeatability refers to the ability of a measuring device to consistently produce similar results under the same conditions and with the same operator, and it is quantified by the standard deviation of a set of measurements. In contrast, reproducibility reflects the variation caused by different operators, time intervals, or other external factors, thereby measuring the influence of human factors on the measurement results.

5. EXAMPLE OF A STUDY FOR ASSESSING THE ABILITY OF A MEASURING SYSTEM WHERE THE IMPACT OF THE MEASURE IS NEGLIGIBLE

Stability refers to the ability of the measurement system to maintain its accuracy over time, while linearity indicates how the instrument's deviation changes across the entire measurement range [10]. In cases where reproducibility, i.e., AV = 0, the operator's influence is considered negligible. This is a specific scenario that typically occurs with automated measuring equipment. In such cases, the adequacy of the measurement system is determined by evaluating the precision of the measuring device (EV) [14].

To successfully conduct a case study for assessing the capability of a measurement system where operator influence is negligible, the following conditions must be met [14]:

The following conditions must be met in order to successfully conduct a case study for evaluating the capability of a measurement system where operator influence is negligible:

- The measurement process must be fully automated or consistently performed by a single operator whose influence is statistically insignificant.
- The measured characteristic must be quantitative and stable over time, without significant fluctuations due to environmental or process-related factors.

- The measurement equipment must be properly calibrated and maintained, ensuring consistent performance throughout the study.
- A sufficient number of repeated measurements must be taken to allow for reliable statistical evaluation of repeatability.
- The measurement results must be analyzed using appropriate statistical methods, such as standard deviation or control charts, to assess the precision of the device.

These conditions ensure that the study focuses solely on the intrinsic performance of the measuring instrument, allowing engineers to determine whether the system meets the required standards for precision and reliability in production environments.

- Repeated measurements must be performed (r ≥ 2).

- A sufficient number of measurement items must be included (n = 5–25), and the condition n·r > 20 must be satisfied.

- All measurements must be conducted using the same measuring device under consistent measurement conditions.

Using a coordinate measuring machine (SPECIFICATION and image provided), repeated measurements (r = 3) of the relay housing depth were performed on a sample of 10 measurement items. The specified nominal value for the relay housing depth is 175.58 mm with a tolerance of ±0.7 mm. Based on the measurement results presented in Table 1, it is necessary to evaluate the capability of the measurement process for the intended application using the Average and Range Method.

The measurement results for the relay housing depth, obtained using a 3D coordinate measuring machine, are presented in Table 1. The numerical calculation of the study for evaluating the capability of the measurement system, where operator influence is considered negligible, using the Average and Range Method, is presented in Report (Table 2).

Table 1. Results of measuring the depth of the relay housing [14]

	Measurement results of the depth of the relay housing (mm)									
Rep	1	2	3	4	5	6	7	8	9	10
1	175.7657	175.7163	175.8471	175.8074	175.7991	175.7414	175.7898	175.8534	175.7827	175.7790
2	175.7738	175.7222	175.8507	175.8120	175.8028	175.7436	175.7928	175.8538	175.7868	175.7815
3	175.7762	175.7252	175.8515	175.8155	175.7343	175.7844	175.8489	175.8036	175.7872	175.7750

Table 2. Report on the ability of the measuring system where the influence of the measure is negligible

Statistics obtained based on measurement results: $\overline{R}$ = 0.02637 R_p = 0.12853	
Analysis of the measuring system where the influence of the measure is negligible	**% Total variation (TV)**
Repeatability - precision of the measuring device (EV) - σ_E $EV = \overline{R} * K_1$ =0.02637 * 0.5908 = 0.01558 mm	$\% EV = 100\ [EV/TV]$ = 100 * [0.01558/0.2333] = 6.68%
Reproductiveness - precision of martyrs (AV) - σ_A	

AV = 0	$\% AV = 100\ [AV/TV]$ = 0%
Repeatability and reproductive (GRR) - σ_M $GRR = \sqrt{EV^2 + AV^2} = \sqrt{0.01558^2 + 0^2} =$ = 0.01558 mm	$\% GRR = 100\ [GRR/TV] =$ 100 * [0.01558/0.2333] = 6.68%
Process variation (PV) - σ_P $PV = R_p * K_3 =$ 0.12853 * 0.3146 = = 0.04044 mm	$\% PV = 100\ [PV/TV] =$ 100* [0.04044/0.2333] = = 17.33%
Total variation (TV) - σ_T $TV = \frac{GGT-DGT}{6} = \frac{176.28-174.88}{6} = 0.23333\ mm$	$ndc = 1.41\ \frac{PV}{GRR} =$ = 1.41* (0.04044/0.01558) = 4

In the report (Table 2), deviations were included in the calculation. Although the measurement system is considered unreliable (since ndc < 5), the %GRR value is now within acceptable limits, i.e., %GRR < 10%. This indicates that the system, while not ideal, is sufficiently adequate for the specific application, particularly in cases where wide tolerances are defined, as in this example.

6. CONCLUSION

In modern manufacturing environments, the demand for precision and reliability in measurement processes has become increasingly critical, especially in industries such as aerospace, automotive, medical devices, and electronics. Coordinate Measuring Machines (CMMs) have emerged as a key solution for performing complex dimensional inspections due to their high accuracy and repeatability. However, the effectiveness of a CMM is not solely determined by its technical specifications—it also depends on the robustness of the measurement system as a whole.

The application of MSA methodology to a CMM-based measurement process has demonstrated the importance of evaluating system capability beyond mere equipment specifications. Through a structured study using the Average and Range Method, it was shown that even when operator influence is statistically insignificant, key metrics such as %GRR and ndc must be carefully interpreted to determine system adequacy.

Although the number of distinct categories (ndc) was below the recommended threshold, indicating limited resolution, the %GRR value remained below 10%, suggesting that the measurement system is sufficiently capable for the specific application—particularly when wide tolerances are defined. This highlights a practical insight: a system that may not meet ideal statistical criteria can still be acceptable for certain industrial contexts, provided its

limitations are understood and aligned with process requirements.

The results confirm that automated CMMs can deliver highly repeatable and reproducible measurements with negligible operator influence. This enhances confidence in quality control decisions and reduces risks of Type I and Type II errors.

Automated CMMs represent a robust solution for high-precision measurement tasks. Their ability to minimize operator-induced variability makes them ideal for modern manufacturing environments. Future work should explore integration with AI-driven inspection systems and real-time process feedback.

ACKNOWLEDGEMENT

This research was financially supported by the Ministry of Science, Technological Development and Innovation of the Republic of Serbia (Contract No. 451-03-136/2025-03/ 200109)

REFERENCES

[1] H. Czichos, D. Klaffke, E. Santner, M. Woydt: Advances in tribology: the materials point of view, Wear, Vol. 190, No. 2, pp. 155-161, 1995.

[2] A.W. Gross: *Gas Film Lubrication*, John Wiley and Sons, New York, 1992.

[3] G.W. Stachowiak: Numerical characterization of wear particle morphology, in: I.M. Hutchings (Ed.): *New Directions in Tribology*, Mechanical Engineering Publications Ltd., Bury St Edmunds, pp. 371-389, 1997.

[4] J. Stokes: *Production of Coated and Free-Standing Engineering Components using the HVOF (High Velocity Oxy-Fuel) Process*, PhD thesis, School of Mechanical and Manufacturing Engineering, Dublin City University, Dublin, 2003.

[5] J.K. Lancaster: Severe metallic wear, in: *Proceedings of the Conference on Lubrication and Wear*, 01-03.10.1957, London, UK, pp. 1-7 or Paper 7

[6] ASTM G77-98 *Standard Test Method for Ranking Resistance of Materials to Sliding Wear Using Block-on-Ring Wear Test*, 1998.

[7] ISO 14577-1, *Metallic Materials – Instrumented Indentation Test for Hardness and Materials Parameters – Part 1: Test Method*, 2002.

[8] Fluid bearing, available at: http://en.wikipedia.org/wiki/Fluid_bearing, accessed: 29.06.2005.

Session 10:

Management for sustainable manufacturing

Society of Production Engineering

ICPES 2025

40th INTERNATIONAL CONFERENCE ON PRODUCTION ENGINEERING - SERBIA 2025

DOI: 10.46793/ICPES25.498T

University of Nis Faculty of Mechanical Engineering

Nis, Serbia, 18 - 19th September 2025

SMART ENERGY PRODUCTION AND INDUSTRY 5.0: XAI AND IRREGULAR TIME SERIES FORECASTING

Milica TASIC[1], Ivan CIRIC[1], Predrag RAJKOVIC[1], Vladan JOVANOVIC[1], Milos SIMONOVIC[1], Marko IGNJATOVIC[1]

Orcid: 0000-0002-5399-2870; **Orcid:** 0000-0002-2914-0985; **Orcid:** 0000-0003-1364-7764, **Orcid:** 0000-0001-7205-7987

[1]Faculty of Mechanical Engineering, University of Nis, Serbia

*Corresponding author: milica.tasic@masfak.ni.ac.rs

Abstract: *Modern energy production systems, particularly in the district heating sector, face challenges caused by irregularly sampled time series resulting from asynchronous measurements, missing values, and variable operating conditions. These issues complicate the application of traditional forecasting methods. In this context, interpolation procedures play an important role, where the error depends on the curvature of the function and indicates the extent to which a polynomial of a given degree can approximate the observed signal, which is particularly important in irregular time series. In this way, a theoretical foundation is provided for understanding the limitations of data regularization and the irregularity of time series. The proposed work combines the theoretical analysis of interpolation with advanced time series processing and machine learning methods in order to support reliable forecasting, process optimization, and decision-making. The results highlight how theoretical insights into interpolation errors can guide the design of explainable and transparent forecasting models, thereby advancing smart energy production strategies aligned with Industry 5.0.*

Keywords: *irregular time series, polynomial interpolation error, artificial intelligence, explainable artificial intelligence, energy consumption forecasting, industry 5.0, smart energy production*

1. INTRODUCTION

Energy systems in transition, particularly district heating systems, rely on heterogeneous SCADA data streams that are often irregularly sampled due to asynchronous measurements, missing readings, and variable operating conditions. Although modern machine learning and deep learning models achieve high predictive accuracy, their lack of transparency hinders trust and limits their practical application in critical infrastructure. These challenges further emphasize the need for transparent and explainable models, in line with the principles of Industry 5.0, which are based on human-centricity, resilience, and sustainability[1,2]. Recent reviews of XAI approaches in the energy sector highlight issues of traceability, accountability, and certifiability, offering guidelines and principles for the implementation of explainable solutions in areas such as demand and production forecasting, as well as grid

management [3-5]. In the context of irregular time series, interpolation plays a crucial role in filling gaps and regularizing data. However, the accuracy of such procedures depends on the local curvature of the function, which directly affects the interpolation error and the limits of polynomial approximation of a given order [6]. At the same time, the application of XAI techniques, particularly SHAP and LIME, has been gaining increasing attention, as they enable deeper insights into the functioning of predictive models and the importance of individual features. At the household level, research confirms that XAI contributes to the reliable identification of consumption patterns (both current and historical) and the validation of model architectures using standard performance metrics (R^2, RMSE, MAE) [7]. Nevertheless, model explainability has no real value unless it is grounded in high-quality data and methodologically consistent approaches. Inadequate regularization or excessive interpolation may generate convincing but misleading model interpretations. For this reason, modern XAI frameworks emphasize the necessity of aligning technical solutions with organizational and societal requirements, including transparency, accountability, and security—the core principles of Industry 5.0.

Building on these challenges, this paper makes threefold contributions: (I) it links the theoretical framework of interpolation errors, derived from function curvature, with preprocessing procedures for irregular time series, (II) it integrates these insights into a modeling pipeline that seeks to preserve the authenticity of real system dynamics, and (III) it extends this pipeline with XAI analyses (SHAP/LIME) that enable the interpretation of predictions in the context of energy variables and operational decisions. In this way, the study contributes to the development of transparent and explainable predictive models that enhance trust, usability, and sustainability in line with the Industry 5.0 paradigm.

2. THEORETICAL FOUNDATIONS OF INTERPOLATION

The theoretical analysis of interpolation errors provides not only a mathematical framework but also a practical tool for processing consumption data and forecasting load demand in district heating systems. The curvature of a function, expressed through higher-order derivatives, together with the distribution of interpolation nodes and multidimensional data processing, directly determines the limits of prediction accuracy. In the context of energy systems, and particularly district heating networks, interpolation techniques are applied during the processing of SCADA data, where missing or irregularly sampled values frequently occur.

A classical result states that if

$$f \in C^{n+1}[a,b] \tag{1}$$

the interpolation polynomial $p_n\,(x)$ satisfies the relation:

$$f(x) - p_n(x) = \frac{f^{(n+1)}(\xi_x)}{(n+1)!} \prod_{i=1}^{n}(x - x_i) \tag{2}$$

which indicates that the error magnitude depends both on the higher-order derivative of the function and on the choice of interpolation nodes [8,9]. This formula is analogous to the Taylor expansion, but differs in that the polynomial is constructed from function values at several distinct points, making it particularly suitable for time series characterized by discreteness and irregular sampling. The error f interpolation is often smaller if we increase the number of nodes. But, there are some counterexamples.

2.1 Example 1. Consider the Runge function:

$$f(x) = \frac{1}{1+x^2}\ , \quad x \in [-5,5]. \tag{3}$$

In contrast to our expectations, increasing the number of nodes especially in the segments [-5,-3] and [3,5], has the consequence that the interpolation (blue curve) gives significant error. Even more,

$$\max_{-5\le x\le 5} \|f(x) - Q_n(x)\| \to \infty, \quad n \to \infty \qquad (4)$$

On the Figure 1, the divergence is obvious for n=10. This example illustrates that interpolation error may increase despite using more nodes. This naturally raises the question of how the choice of interpolation nodes affects the error. Until now, the discussion has been based on the assumption that the interpolation nodes are fixed.

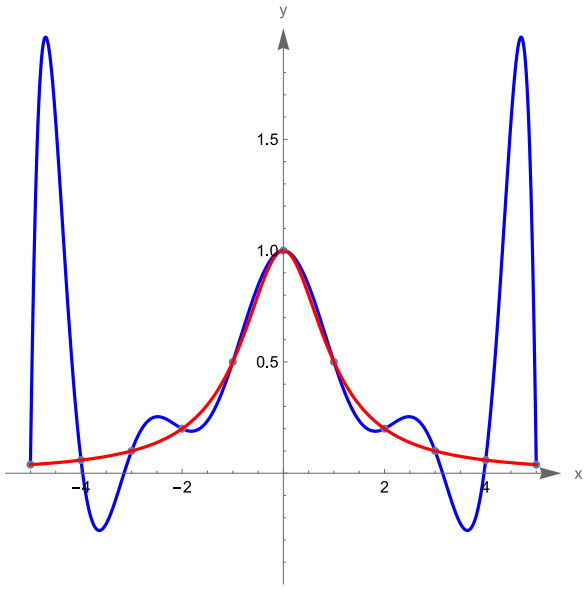

Figure 1. Illustration of Runge's phenomenon

In the entire discussion up to now, it is assumed that the interpolation nodes are given.

If this is the case, it would be reasonable to use this degree of freedom to minimize the interpolation error.

The distribution of error strongly depends on the selection of interpolation nodes. For uniformly distributed nodes, oscillations and significant growth of error occur near the interval boundaries, a phenomenon known as Runge's phenomenon. In energy applications, particularly in heat demand analysis, such an effect may lead to inaccurate forecasts during periods of sudden outdoor temperature changes. Therefore, special node distributions, such as Chebyshev nodes, are employed to provide a more balanced error distribution and to minimize the maximum deviation of the interpolation polynomial from the actual data [10-12].

Apart from node selection, the nature of the underlying function also plays an important role. Rapid growth of higher-order derivatives (e.g., sudden changes in heat load) can significantly increase the interpolation error, demonstrating that increasing the number of interpolation points does not necessarily improve the approximation. This demonstrates that increasing the number of interpolation points does not necessarily improve the approximation and that, in real district heating operations, a compromise must be made between complexity and stability [12].

In such circumstances, the use of spline functions becomes particularly relevant, as they enable stable interpolation through local low-degree polynomials. Unlike global polynomials, splines ensure smoothness of the function and continuity of derivatives, which is especially important in energy systems where changes in load and temperature must remain physically consistent. In this way, the risk of oscillations and error accumulation is reduced, and the reconstructed data provide a more reliable basis for modeling heat substations [13,14].

On some real interval $[a, b]$ notice its partition $\mathbb{P}$ with nodes

$\mathbb{P}: a = x_0 < x_1 < \cdots < x_{n-1} < x_n = b, \ (n \in N)$

Suppose that for a function $f(x)$ are known values $f_k = f(x_k) \ (k = 0,1, \dots, n)$

The function $S_m(x) = S_{m,k}(x; f; \mathbb{P})$ is polynomial spline with degree m and defect k $(1 \le k \le m)$ for $f(x)$ if

1) For every $i \in \{1,2, \dots, n\}$, and for every $x \in (x_{i-1}, x_i)$, $S_m(x)$ is a polynomial with degree at most m;

2) $S_m(x)$ is a part-by-part interpolating polynomial, i.e. $S_m(x_i) = f_i \ (i = 0,1, \dots, n)$;

3) $S_m(x)$ is a continuously differentiable function with its derivatives until order $m - k$ on $[a, b]$, i.e.

$$S_m^{(k)}(x_i^-) = S_m^{(k)}(x_i^+)$$
$$(k = 1, \dots, m - k; \ i = 1, \dots, n - 1).$$

Figure 2 illustrates the concept of a spline as a piecewise polynomial that maintains smoothness across interval boundaries.

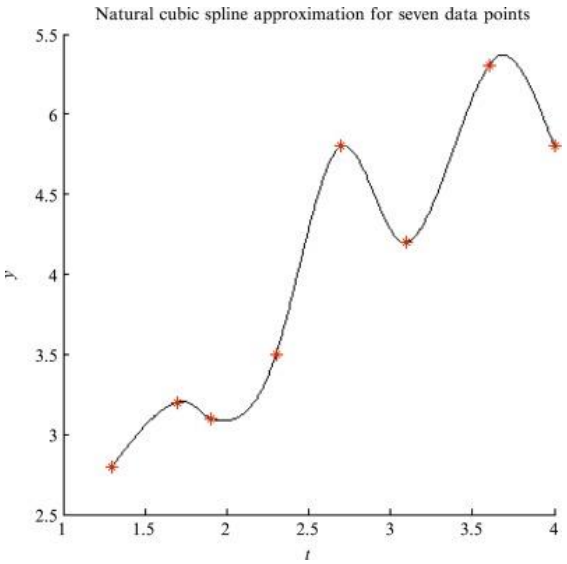

Figure 2. Natural cubic spline interpolation

These insights form the foundation for subsequent methods in this work that combine interpolation with machine learning and explainable artificial intelligence (XAI) to enhance transparency and reliability in district heating operations.

3. RELATED WORK

3.1 Data characteristics and preprocessing of irregular time series

Research focusing on data processing in district heating systems highlights that SCADA and smart meters typically provide key variables such as supply and return water temperatures, thermal energy, flow, and outdoor temperature. For example, Cvetković et al. document a publicly available SCADA dataset in which measurements were collected at the substation level and standardized to hourly time steps after cleaning, resulting in time series without errors or missing values [15]. Similarly, Schaffer et al. present a three-year dataset from 3,021 smart meters, where raw readings deviated by up to ±30 minutes from the full hour and were therefore subjected to initial screening, linear interpolation, and imputation to obtain a fully equidistant hourly series [16].

Typical challenges include irregularity and missing values. In practice, timestamps are not always aligned due to communication delays or technical faults, which leads to gaps in the series. Chatterjee et al. emphasize that raw smart meter data are often irregularly spaced and therefore require interpolation and resampling before being used in predictive models [17]. In addition, Steindl et al. point out that the transition from daylight saving time (DST) to standard time can produce incorrect measurement order, so it is recommended to explicitly remove readings recorded between 02:00–02:59 during this transition [18].

The proposed preprocessing procedures form a clear pipeline. In the first stage, data are checked for inconsistencies, especially cumulative variables such as energy or flow, where monotonicity is required (each new value must be greater than or equal to the previous one). A similar approach was applied in studies on fault detection based on smart meter data [19]. Interpolation and resampling are then performed—most often linear—in order to form an equidistant time grid (hourly or 15-minute). Short gaps up to one hour are typically filled by linear interpolation, while longer gaps are usually excluded from analysis [18]. Afterward, the remaining small fraction of missing values is imputed using moving-window methods. Schaffer et al. conducted a systematic comparison of different techniques and demonstrated that a weighted moving average with a 48-hour symmetric window, combined with scaling that respects the cumulative trend, yields the best results for smart meters [16]. Finally, when measurements are quantized or truncated at the hourly level (e.g., due to utility data storage practices), aggregation to daily values is recommended to reduce rounding errors and provide a more stable series for anomaly detection [20].

Beyond classical procedures, the importance of documenting the entire process through formal data-curation

guidelines is emphasized. Stecher et al. recommend an approach inspired by the CRISP-DM methodology, adapted to the DHS domain: defining objectives, understanding the data, integrating multiple sources (SCADA and meteorology), and performing systematic cleaning and annotation.

3.2 Forecasting heat demand in district heating systems

Conventional approaches to heat demand forecasting in district heating systems (DHS) are primarily rule-based, relying heavily on weather forecasts and, in particular, ambient temperature. This control strategy, known as weather compensation, can provide acceptable decisions in certain circumstances but rarely achieves optimality. In practice, this often results in overheating, observable through elevated supply line water temperatures and decreased heat load. While end-user comfort is usually unaffected, such inefficiencies lead to increased fuel consumption and negative environmental impacts.

Several empirical studies highlight the progress from conventional to advanced data-driven models.

Potočnik et al. [21] pioneered the use of Gaussian Process Regression (GPR) in Slovenia's largest DHS, demonstrating that nonlinear models substantially improve short-term forecasting accuracy. Building on this, Zdravković et al. [22] proposed a proactive control strategy based on deep learning, where different LSTM architectures enabled more adaptive and responsive system operation. In a complementary study, Kurek et al. [23] combined traditional approaches with fuzzy logic models, adapted to seasonal variations, to manage Warsaw's large district heating network, underlining the potential of ANNs in complex urban environments.

The scope of AI applications has been further expanded in comparative studies. Runge and Saloux [24] investigated predictive versus forecasting paradigms, showing that advanced machine learning methods, particularly LSTM and XGBoost, yield significant accuracy improvements in Canadian DHS. Along similar lines, Shakeel et al. [25] introduced a hybrid LightGBM–FB Prophet model, demonstrating the ability to overcome sparse-data challenges and providing superior accuracy in operational heat demand forecasting. In China, Liu et al. [26] implemented a dynamic integrated control strategy, which incorporated multiple correction factors to better align supply with demand, achieving notable improvements in energy efficiency and emission reduction. Finally, Morteza et al. [27] explored Deep Recurrent Neural Networks (DRNNs) for medium- to long-term forecasting, emphasizing the importance of hyperparameter optimization. Their work confirmed that tailored deep learning architectures significantly outperform conventional models in energy demand prediction.

3.3 Explainable AI in district heating

Explainable AI in district heating has been advancing along two complementary tracks: data-centric XAI readiness—i.e., curated SCADA datasets and platforms that ensure reliable, interpretable inputs—and model-centric explainability—i.e., forecasting models whose inner workings (features, lags, temporal focus) can be understood and trusted by operators.

Recent work formalizes the data backbone needed for explainable control in DHS. An integrated data-acquisition platform aggregates SCADA, IoT, and weather streams into a unified time-series repository, enabling real-time monitoring and predictive control; the platform is positioned as the core of an explainable control approach (XAI4HEAT) that combines XAI algorithms with model-based predictive control for dynamic heat-supply adjustment. This line of work explicitly motivates explainability for operator trust, situational awareness, and decision support [28]. Building on the same program, the platform's conclusions emphasize that

curated, multi-source data ingestion is prerequisite to intelligent, explainable DHS operation [28].

Complementing the platform perspective, a curated SCADA dataset for enhanced explainability documents five years of substation-level measurements (supply/return temperatures on both primary and secondary circuits, energy transmission, local meteorology) and, crucially, standardizes the data to uniform hourly resolution without errors or missing values—a property that directly supports reliable model interpretation and feature attribution [29]. The dataset is explicitly positioned to facilitate explainable analyses in smart-energy research and DHS practice [29].

On the modeling side, Neubauer et al. develop a multi-step heating-load forecaster that marries an Encoder–Decoder architecture with SHAP feature attributions and temporal attention. They show that attention weights and SHAP values increase interpretability; feature selection guided by Deep SHAP reduces training time and error; and future weather features materially improve accuracy—findings that connect XAI directly to both performance and operator insight [30].

Going beyond post-hoc explanations, Souza et al. (HELIOS) embed explainability into the model structure by combining physics and expert knowledge. The approach decomposes heat load into space heating, domestic hot water, and transmission losses, links them through a causal graph, and leverages contextual mixture-of-experts to encode domain priors—yielding transparent predictions and superior accountability relative to black-box baselines [30]. The authors further argue that such inherent interpretability fosters stakeholder trust and supports operational decision-making [30].

Together, these strands outline a practical XAI framework for DHS: curate XAI-ready data (platform + dataset) to ensure valid, aligned inputs; adopt interpretable forecasting (SHAP + attention) to expose feature and temporal contributions; and, where possible, encode physics/expert knowledge to make explanations intrinsic rather than purely post-hoc. This triangulation supports transparent forecasting, operator trust, and integration with predictive control in real networks [30].

4. METHODOLOGY

The data used in this study were obtained from the SCADA system of the Faculty of Mechanical Engineering in Nis, specifically from the heat substation in Lamela L8. For the purpose of this analysis, two input variables were selected: outdoor air temperature (t_amb) and supply water temperature in the primary circuit (t_sup_prim). These variables were chosen due to their direct physical influence on heat consumption and district heating system operation.

A specific characteristic of the dataset is that it is irregularly sampled, meaning that measurements were not always recorded at equal time intervals. The causes of such irregularities may be of a technical nature (interruptions in data acquisition, communication issues) but can also result from the dynamic operation of the system. In addition to irregular sampling, the dataset also contains missing values, which further complicates the analysis process. These challenges require the application of special preprocessing procedures to ensure a uniform time grid and consistent inputs for the prediction model. The focus of this study is precisely on addressing these issues, as the quality of preprocessing directly determines the reliability and accuracy of the subsequent forecasting model. By carefully regularizing the time series and handling missing values, the study emphasizes the importance of preparing real-world SCADA data for robust and interpretable predictive modeling.

4.1 Data Preprocessing

The dataset contains time-stamped measurements with irregular sampling intervals and occasional missing values. To enable numerical processing:

1. Time conversion: Original timestamps were transformed into numerical values expressed as the elapsed hours from the initial timestamp. This was calculated as the difference between serial date numbers, which allows the time variable to be treated as a continuous numerical input in the model.
2. Regularization of the time grid: The entire dataset was resampled to a 15-minute resolution to ensure comparability of observations.
3. Handling missing values: A local Lagrange interpolation method with barycentric weights was applied. The interpolation order was limited to a maximum of **n = 2**, with a fallback to lower orders if the data density was insufficient. Additionally, a guardrail mechanism was used to prevent interpolation across gaps longer than 90 minutes, where missing values were preserved as NaN.
4. Value clipping: Interpolated results were restricted within physically meaningful ranges (e.g., outdoor temperature between −40 °C and 80 °C) to prevent unrealistic estimates.

In this context, preprocessing is the central contribution of the research. The methodology demonstrates how irregular and incomplete SCADA data can be systematically transformed into a structured form suitable for machine learning, thereby ensuring both model accuracy and interpretability.

5. RESULTS AND DISCUSSION

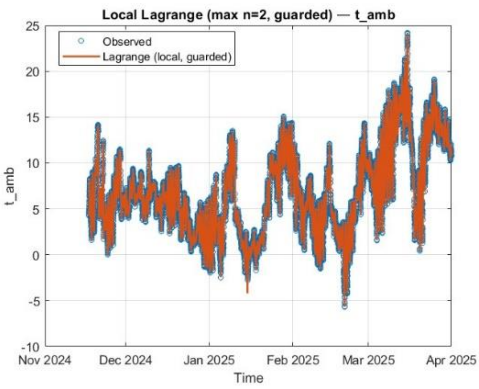

Figure 3. Observed and interpolated outdoor air temperature

The interpolation results reveal substantial differences in accuracy between the outdoor air temperature (t_amb) and the supply water temperature in the primary circuit (t_sup_prim).

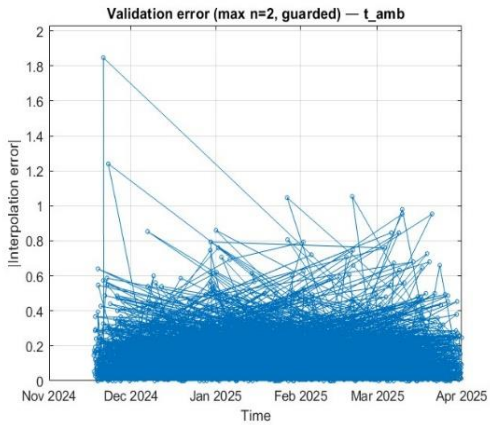

Figure 4. Validation error of local Lagrange interpolation for outdoor air temperature

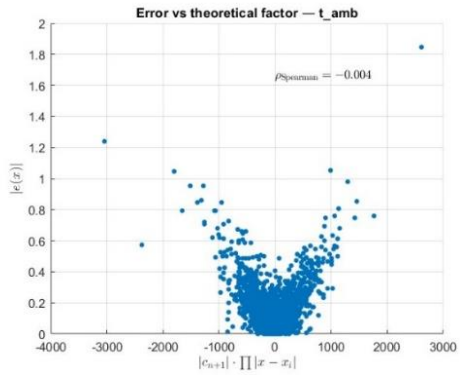

Figure 5. Interpolation error versus theoretical factor for outdoor air temperature

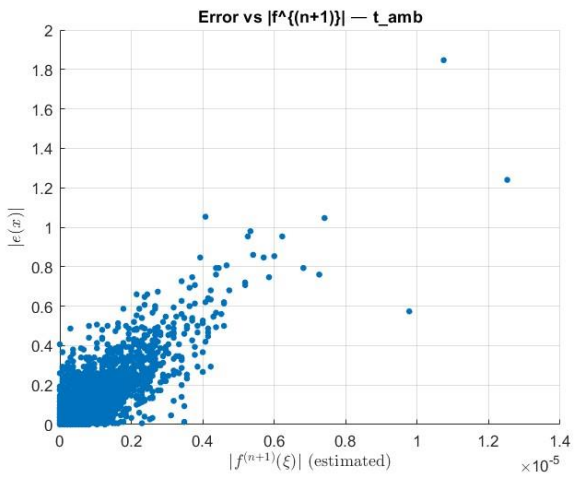

Figure 6. Interpolation error versus estimated higher-order derivative term for outdoor air temperature

For outdoor temperature, the local Lagrange interpolation (n=2) demonstrated very good agreement with the observed data. The interpolated curve (Fig.1) smoothly follows seasonal variations, while deviations remain minor. In most cases, the interpolation error remained below 0.5, with occasional peaks up to 1.8. The analysis with respect to the estimated curvature of the function $f^{(n+1)}$confirms the expected positive correlation – errors increase as curvature grows, consistent with interpolation theory. This indicates that the method is sufficiently robust for processing meteorological data.

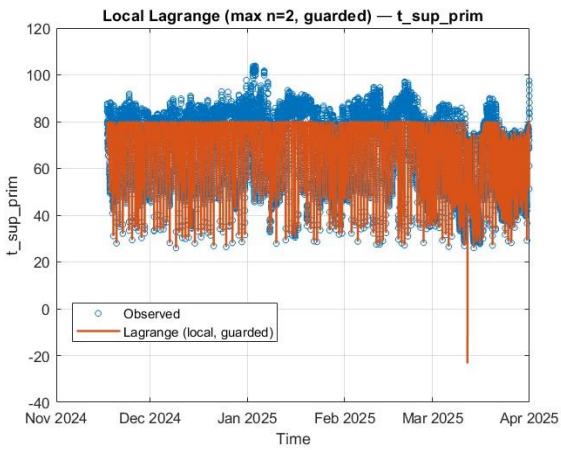

Figure 7. Observed and interpolated primary supply water temperature using local Lagrange method

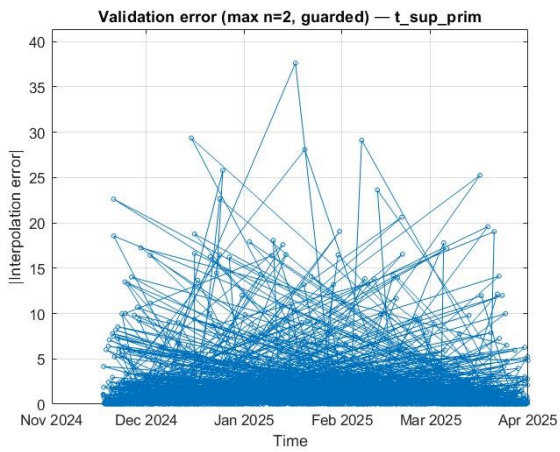

Figure 8. Validation error of local Lagrange interpolation for primary supply water temperature

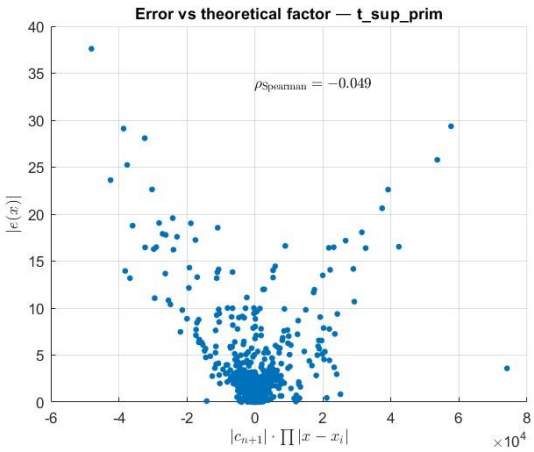

Figure 9. Interpolation error versus theoretical factor for primary supply water temperature

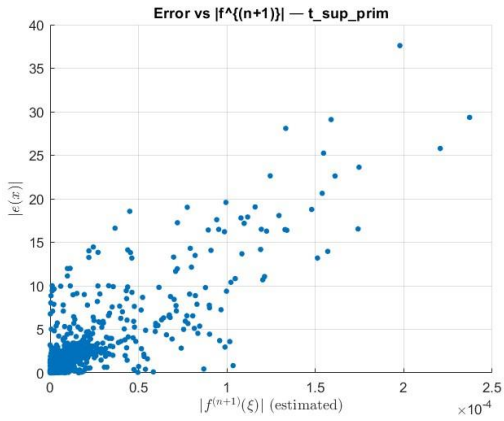

Figure 10. Interpolation error versus estimated higher-order derivative term for primary supply water temperature

In contrast, for supply water temperature in the primary circuit, interpolation accuracy is significantly lower. The results exhibit larger deviations between observed and interpolated values, as well as anomalies, including sudden drops that the method failed to capture. The interpolation error ranged widely, with values reaching up to 35–37, which is several times higher than for the outdoor temperature. The correlation with the theoretical factor proved negligible, while the dependency on the estimated curvature of the function was present but with considerable scattering.

Based on these findings, it can be concluded that the local Lagrange interpolation method is suitable and sufficiently accurate for outdoor temperature, while for the supply water temperature in the

primary circuit it requires refinement or replacement with more advanced approaches (e.g., spline interpolation, data filtering, or machine learning–based reconstruction). These results emphasize the importance of carefully selecting and combining preprocessing methods depending on the physical nature of the variables and the dynamics of the system.

6. CONCLUSION

This study demonstrated how the challenges of irregularly sampled SCADA data in district heating systems can be addressed through advanced preprocessing techniques and the application of explainable machine learning models. By focusing on outdoor air temperature and primary supply water temperature, the analysis highlighted substantial differences in interpolation accuracy, showing that some variables can be reliably reconstructed while others require more sophisticated approaches.

Beyond the specific case of district heating, the presented methodology illustrates a general framework applicable to production engineering systems, where data irregularities, missing values, and operational variability are common. The integration of mathematical interpolation theory with explainable AI provides not only accurate forecasts but also transparent insights into system behavior, which is essential for decision-making, process optimization, and sustainable operation. Future research will focus on the careful selection of prediction models and the systematic application of XAI methods fully aligned with Industry 5.0 principles, further enhancing predictive accuracy, interpretability, and operator trust in complex production systems.

REFERENCES

[1] C. Trivedi, P. Bhattacharya, V. K. Prasad, *et al.*, "Explainable AI for Industry 5.0: Vision, Architecture, and Potential Directions," *IEEE Open Journal of Industry Applications*, vol. PP, no. 99, pp. 1–12, Sep. 2023, doi: 10.1109/OJIA.2024.3399057.

[2] J.-L. Hu, Y. Li, and J.-C. Chew, "Industry 5.0 and Human-Centered Energy System: A Comprehensive Review with Socio-Economic Viewpoints," *Energies*, vol. 18, no. 9, p. 2345, 2025. doi: 10.3390/en18092345.

[3] R. Alsaigh, R. Mehmood, and I. Katib, "AI Explainability and Governance in Smart Energy Systems: A Review," *arXiv preprint*, arXiv:2211.00069, Nov. 2022.

[4] R. Machlev, L. Heistrene, M. Perl, *et al.*, "Explainable Artificial Intelligence (XAI) techniques for energy and power systems: Review, challenges and opportunities," *Energy and AI*, vol. 9, p. 100169, May 2022, doi: 10.1016/j.egyai.2022.100169

[5] T. Rojat, R. Puget, D. Filliat, J. Del Ser, R. Gelin, and N. Díaz-Rodríguez, "Explainable AI on Time Series Data: A Survey," *arXiv preprint*, arXiv:2104.00950, 2021.

[6] J. Chen, J. Yuan, W. Chen, A. Zeb, M. Suzauddola, and Y. A. Nanehkaran, "Research on Interpolation Method for Missing Electricity Consumption Data," *Computers, Materials & Continua*, vol. 78, no. 2, pp. 2576–2591, Feb. 2024, doi:10.32604/cmc.2024.050414.

[7] Bhandary, V. Dobariya, G. Yenduri, S. K. Pasupuleti, S. K. Maddikunta, and F. Benedetto, "Enhancing Household Energy Consumption Predictions Through Explainable AI Frameworks," *IEEE Access*, vol. 12, pp. 1–1, Jan.2024, doi: 10.1109/ACCESS.2024.3373552.

[8] Lecture Notes, *Errors in Polynomial Interpolation*, Lecture 15–16, 2010.

[9] D. Levy, *Numerical Analysis – Interpolation*, University of Maryland, 2010.

[10] Kværnø, *Polynomial Interpolation: Error Theory*, NTNU, 2021.

[11] Ron, Y. Li, M. Cowlishaw, and N. Fillmore, "Polynomial Interpolation: Error Analysis and Introduction to Splines," *Lecture Notes in Numerical Analysis*, Univ. of Wisconsin, 2010.

[12] Runge, "Über empirische Funktionen und die Interpolation zwischen äquidistanten Ordinaten," *Zeitschrift für Mathematik und Physik*, vol. 46, pp. 224–243, 1901.

[13] Y. Mehari, "Easy Way to Find Multivariate Interpolation," *Int. J. Emerging Trends in Science and Technology*, vol. 4, no. 5, pp. 5189–5193, 2017.

[14] M. Aldroubi and A. Papoulis, "Two-dimensional polynomial interpolation from nonuniform samples," *IEEE Trans. Signal Processing*, vol. 40, no. 2, pp. 333–339, 1992.

[15] S. Cvetković, M. Zdravković, and M. Ignjatović, "Exploring district heating systems: A SCADA dataset for enhanced explainability," *Data in Brief*, vol. 59, p. 111320, 2025, doi: 10.1016/j.dib.2025.111320.

[16] M. Schaffer, T. Tvedebrink, and A. Marszal-Pomianowska, "Three years of hourly data from 3021 smart heat meters installed in Danish residential buildings," *Scientific Data*, vol. 9, p. 420, 2022, doi: 10.1038/s41597-022-01502-3.

[17] S. Chatterjee, P. K. Jana, and A. Bandyopadhyay, "Prediction of household-level heat consumption using PSO-kSVR with accumulated smart meter data," *arXiv preprint*, arXiv:2112.01908, Dec. 2021.

[18] G. Steindl, M. Kathan, and G. N. Almbauer, "Comparison of black box models for load profile generation of district heating substations," *Proceedings of the 11th International Modelica Conference*, 2015, pp. 711–719, doi: 10.3384/ecp15118711.

[19] F. Theusch, P. Diaconescu, J. Tuschy, and R. T. Stankovic, "Fault detection and condition monitoring in district heating using smart meter data," *Proceedings of the European Conference of the PHM Society*, vol. 6, no. 1, pp. 1–11, 2021, doi: 10.36001/phme.2021.v6i1.2786.

[20] Stecher, A. A. Nielsen, M. K. Andersen, and H. Madsen, "Creating a labeled district heating data set: From anomaly detection towards fault detection," *Energy*, vol. 313, p. 134016, 2024, doi: 10.1016/j.energy.2024.134016.

[21] Potočnik, P., Škerl, P., and E. Govekar. 2021. Machine-learning-based multi-step heademand forecasting in a district heating system. Energy & Buildings 233:110673

[22] Zdravković, M., Ćirić, I., and M. Ignjatović. 2022. Explainable heat demand forecasting for the novel control strategies of district heating systems. Annual Reviews in Control 53:405–413.

[23] Kurek, T., Bielecki, A., Świrski, K., Wojdan, K., Guzek, M., Białek, J., Brzozowski, R., and R. Serafin. 2021. Heat demand forecasting algorithm for a Warsaw district heating network. Energy 217:119347.

[24] Runge, J., and E. Saloux. 2023. A comparison of prediction and forecasting artificial intelligence models to estimate the future energy demand in a district heating system. Energy 269:126661.

[25] Shakeel, A., Chong, D., and J. Wang. 2023. District heating load forecasting with a hybrid model based on LightGBM and FB-prophet. Journal of Cleaner Production 409:137130.

[26] Liu, G., Zhou, X., Yan, J., and G. Yan. 2023. Dynamic integrated control for Chinese district heating system to balance the heat supply and heat demand. Sustainable Cities and Society 88:104286.

[27] Morteza, A., Yahyaeian, A.A., Mirzaeibonehkhater, M., Sadeghi, S., Mohaimeni, A., and S. Taheri. 2023. Deep learning hyperparameter optimization: Application to electricity and heat demand prediction for buildings. Energy and Buildings 289:113036.

[28] S. Cvetković, D. Stojiljković, I. Ćirić, R. Turudija, and M. Špeletić, "Integrated data acquisition platform for explainable control in district heating systems," *Facta Universitatis, Series: Automatic Control and Robotics*, vol. 23, no. 2, pp. 133–143, 2024.

[29] S. Cvetković, M. Zdravković, and M. Ignjatović, "Exploring district heating systems: A SCADA dataset for enhanced explainability," *Data in Brief*, vol. 59, p. 111320, Jan. 2025.

[30] Neubauer, S. Brandt, and M. Kriegel, "Explainable multi-step heating load forecasting: Using SHAP values and temporal attention mechanisms for enhanced interpretability," *Energy and AI*, vol. 20, p. 100480, Feb. 2025.

Society of Production Engineering

ICPES 2025

40th INTERNATIONAL CONFERENCE ON PRODUCTION ENGINEERING - SERBIA 2025

DOI: 10.46793/ICPES25.510B

University of Nis Faculty of Mechanical Engineering

Nis, Serbia, 18 - 19th September 2025

PACKAGING OPTIMIZATION AS A TOOL FOR SUSTAINABLE PRODUCTION ON A GLOBAL SCALE

Maja BRANKOVIĆ[1], Miloš PAUNOVIĆ[1], Saša S. RANĐELOVIĆ[2]

Orcid: 0000-0002-2334-8929

[1]Robert Bosch d.o.o, Republic of Serbia

[2]Faculty of Mechanical Engineering, University of Nis, Republic of Serbia

*Corresponding author: maja.brankovic@bosch.com

Abstract: *Packaging optimization is a key strategy for achieving sustainability, especially as global consumption and packaging use continue to rise. In the automotive industry, packaging ensures safe storage and transport of components but traditionally relies on resource-intensive materials that generate significant waste. Sustainable solutions include reducing material use, adopting recyclable and biodegradable inputs, and introducing modular, reusable, and collapsible systems to improve logistics and efficiency. These practices lower CO_2 emissions, energy use, and costs while supporting circular economy principles. Successful examples, such as Bosch's carbon-neutral operations, show that optimized packaging can cut waste and emissions by up to 30%. Overall, packaging optimization is both a technical and strategic tool for sustainable development in the automotive sector.*

Keywords: *Packaging, Automotive Industry, Optimization, Sustainability, Lean, Logistics*

1. INTRODUCTION

Packaging is the science, art and technology of preparing a product for appropriate transportation, storage, sale and use. [1]

Packaging is an important component of many facets of modern consumption in that it has become part of the delivery system for products and it is generally seen to fulfil four key functions, namely to 'preserve and protect the product', 'to communicate brand image', to 'convey information', and 'offer convenience' (PricewaterhouseCoopers 2010, p.4). Packaging plays a vital role in the protection, storage and hygienic handling of products. At the same time packaging materials require the use of a wide range of natural resources whose disposal has a direct impact on the environment and widespread concerns have been expressed about the negative environmental impact of packaging systems. [2]

Packaging also plays a vital role in conveying a wide range of product information to customers, including information on use by dates, ingredients and health and safety. Packaging is also seen to be vitally important marketing tool in that it is seen to enhance product appeal, to create and enhance brand awareness and to influence consumer buying behaviour. [2]

Due to the currently widespread transformation in the methods of energy production, distribution, and consumption—specifically, the shift from traditional fossil energy sources (such as coal, oil, and gas) to renewable and sustainable energy sources (such as solar, geothermal energy, hydropower, biomass.etc.)—the global supply of materials in various industries is also changing and adapting to new conditions. [3]

Changes in technologies, infrastructure, policies, and social norms, with a focus on reducing negative environmental impact, have posed challenges for the materials industry over the past two to three years. [3]. These changes in material supply and production methods, the transition to digital business practices, and the emphasis on sustainability and environmental protection have directly impacted the packaging industry, which is the topic of this paper and will be discussed further below.

2. CORPORATE SUSTAINABILITY

As investors, consumers, governments, interests groups and the media have become more acutely aware about the environmental, social and economic impacts of business activities so corporate sustainability initiatives have assumed ever increasing importance. KPMG (2012, webpage), for example, suggested that 'the evidence that sustainability is becoming a core consideration for successful businesses around the world grows stronger every day. [2]

More generally corporate sustainability is also increasingly seen to incorporate the more recently developed concept of the creation of shared value. This concept has been 'defined as policies and practices that enhance the competitiveness of a company while simultaneously addressing the economic and social conditions in the communities in which it operates' [4]

This paper will examine the case of the company Bosch, which is focused on packaging optimization for the purpose of sustainable development. Based on the company's 2024 annual report Bosch aims to minimize the environmental impact of its operations through the implementation of a comprehensive, Group-wide environmental management system, supported by clearly defined targets. The company prioritizes climate protection, water conservation—particularly in regions where water is scarce—and the promotion of a circular economy through targeted initiatives. [8]

To achieve these goals, Bosch seeks to ensure that all relevant facilities operate under certified environmental management systems. As of the latest reporting period, 97% of the company's relevant manufacturing and development sites have implemented such systems, with 98% of them certified in accordance with the ISO 14001 standard. Additionally, 90% of the energy management systems in use across the company are aligned with these environmental objectives. [5]

Bosch has clearly defined environmental criteria for the design, planning, and acquisition or construction of facilities, machinery, and manufacturing equipment, for example with regard to energy efficiency and the use of renewable energy sources. These criteria also play a role in the decision-making process when choosing new company locations.[5]

Bosch's sustainability efforts encompass the entire value chain — from the procurement of materials and goods, through production processes at its own facilities, to the use phase of its products and their end-of-life management. This holistic approach ensures that environmental and social considerations are integrated at every stage of the product lifecycle.

The following section presents an overview of all key aspects addressed by Bosch in its pursuit of sustainable development, along with the corresponding activities implemented within each area.

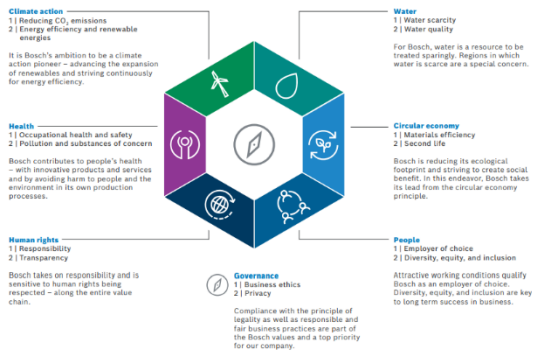

Figure 1. Sustainability strategy

This paper presents a case study of Bosch's successful product *packaging optimization* as part of its sustainable development strategy. The analysis includes an overview of achieved results, relevant key performance indicators (KPIs), and other related metrics.

Explained case study includes segments from both stated Bosch's activities – *climate action* and *circular economy*.

With its more than 450 locations worldwide, the Bosch Group has been carbon-neutral overall since 2020. Four levers were used to achieve carbon neutrality: increasing energy efficiency, generating our own energy from renewable sources (new clean power), purchasing electricity from renewable sources (green electricity), and – as the last resort – offsetting residual CO_2 emissions with carbon credits. In 2024, residual emissions of roughly 531,300 metric tons of CO_2 were offset by carbon credits. This represents a decrease of 8.5 percent on the prior year's level.

Since 2018, Bosch has cut scope 3 emissions by around 27 percent, down to 335 million metric tons of CO_2 in 2023. In this process, company is focusing on the categories that make up around 98 percent of their scope 3 emissions: upstream emissions in the Bosch value chain primarily concern purchased goods and services as well as logistics. Downstream emissions are mainly caused by the use of their products. [7]

For years, materials efficiency has been a fixed criterion in the Bosch product development process, where it is anchored in their Design for Environment (DfE) principle. Company's activities range from reusing products and their components to repairs and right through to remanufacturing – in each case with the objective of extending product and component life cycles. The individual divisions of Bosch each have their own objectives in this regard, depending on market and product-specific framework conditions

Important aspects of sustainable packaging operations involve finding the right balance between cost-efficiency, practical functionality, and environmental responsibility. As more companies aim to adopt greener packaging practices, it becomes crucial to manage these factors thoughtfully to ensure effective results. The main challenge is to choose materials and methods that reduce environmental harm without compromising the performance or affordability needed for regular business activities. [6].

3. CASE STUDY: OPTIMIZATION OF WINDSHIELD WIPER PACKAGING AT BOSCH AS A CONTRIBUTION TO SUSTAINABLE DEVELOPMENT

In line with its commitment to sustainable development and environmental protection, Bosch has implemented a range of initiatives focused on reducing resource consumption and minimizing waste across its value chain. A notable example is the optimization of packaging for windshield wipers—an initiative that significantly contributed to material savings, reduced environmental impact, and increased operational efficiency.

3.1. Initial Packaging Challenges

Prior to the optimization project, Bosch's windshield wipers were packaged in rectangular cardboard boxes that included an internal insert designed to hold the wiper in place. Each package also contained a smaller box with four plastic adapters, even though only one adapter was necessary for the specific vehicle model owned by the customer. This led to the disposal of excess components—three plastic adapters, the insert, and the outer cardboard packaging—

immediately after installation, contributing to unnecessary material waste.

Figure 2. Initial Packaging **3.2. Optimized Packaging Solution**

Through a targeted redesign, Bosch introduced a more compact and aerodynamically shaped packaging solution. The new packaging is tailored to fit the wiper blade securely without the need for additional inserts. Moreover, the adapter is now sold separately, enabling customers to purchase only the specific adapter required for their vehicle model. These adapters are distributed in bulk packaging units of 30, 50, or 70 pieces and are available for individual sale.

Figure 3. Optimized Packaging Solution

3.2. Measurable Results and Key Performance Indicators (KPIs)

This packaging optimization yielded measurable environmental and operational benefits. Key performance indicators used to assess the success of the initiative include:

- Material savings: Reduction of plastic usage by up to 35 metric tons per year and cardboard usage by approximately 50 metric tons per year.
- Packaging weight reduction: A single package's weight decreased from 69 grams to 34 grams, representing a 50.7% reduction in material per unit.
- Waste reduction: Fewer surplus components (adapters) are discarded post-purchase.
- Resource efficiency: Improved ratio of packaging weight to product weight and reduction in packaging volume per unit transported.

These KPIs are aligned with Bosch's internal environmental management goals and are regularly monitored as part of the company's ISO 14001-certified environmental management system. The majority of Bosch's manufacturing and development locations operate under this standard, which provides a structured framework for managing environmental responsibilities in a systematic and transparent manner.

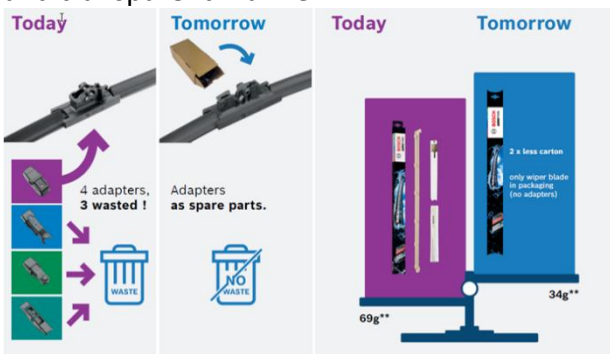

Figure 4. Waste reduction and results

3.3. Alignment with Sustainability Goals and Standards

Bosch is committed to implementing good practices and meeting the requirements of international standards that support the SDGs, and additional procedures have been developed, i.e. calculations in accordance with ISO 14067, and the process of critical review and issuing CO2 reduction signs is ongoing. Independent third party critical review according to ISO 14067 will enable Bosch to communicate results or reduction achievements internally and externally.

The packaging optimization project directly contributes to the United Nations Sustainable Development Goals (SDGs), particularly:

- SDG 12: Responsible Consumption and Production – by reducing material inputs and minimizing waste generation.
- SDG 13: Climate Action – by lowering the environmental footprint associated with packaging materials and logistics.
- SDG 9: Industry, Innovation and Infrastructure – through the application of innovative design for sustainability.

Additionally, the initiative supports Bosch's broader corporate sustainability strategy, which includes objectives related to climate action, circular economy enhancement, and resource efficiency across the product lifecycle.

4. CONCLUSION

The case of Bosch's windshield wiper packaging optimization illustrates how targeted, well-executed design changes can significantly contribute to environmental sustainability while maintaining functionality and economic efficiency. By reducing the use of plastic and cardboard, minimizing surplus components, and improving the weight-to-product ratio, Bosch has demonstrated a strong commitment to sustainable development. The company's alignment with ISO 14001 standards and the broader United Nations Sustainable Development Goals underscores the strategic integration of sustainability into its operations.

Looking to the future, companies like Bosch are expected to further embed sustainability across all levels of their value chains, driven by tightening environmental regulations, evolving consumer expectations, and increasing investor scrutiny. In this context, packaging will remain a key area for innovation and improvement. To sustain momentum, companies should invest in life-cycle thinking, adopt advanced digital tools to monitor and analyze environmental impacts, and foster cross-sector collaboration for circular packaging solutions. Continued focus on eco-design principles, reusable and biodegradable materials, and supply chain optimization will be crucial.

Furthermore, transparency and accountability—achieved through standardized reporting and third-party verification—will play an essential role in validating sustainability claims and building stakeholder trust. As global supply chains become more interconnected and resource constraints more pressing, packaging optimization will no longer be an isolated activity but a central pillar of responsible corporate strategy. By continuously innovating and expanding its sustainability framework, Bosch sets a compelling example for how industrial leaders can balance operational efficiency with environmental responsibility.

REFERENCES

[1] A. Cordeiro, M. Hussain, T Ramacha-ndran, N. Beemkumar· R. Kumar, · A. Karthikeyan, V. K. Bupesh Raja, D. N. Thatoi, A. Mahapatro, J. Nanda, · C. Prakash, A. Y. Patil, Advancements in Packaging Materials: Trends, Sustainability, and Future Prospects, May 2025, Circular Economy and Sustanibility, 5(4) pp. 2959-2990

[2] Hillier, David, Comfort, Daphne and Jones, Peter (2017) - The Packaging Industry and Sustainability. Athens Journal of Business and Economics

[3] C.W. Chen, F.X. Yang, J. Xie, D.D. YangPackaging Solution Optimization of Automotive Parts and Its Ocean Shipping Test, January 2015, DOI:10.2991/aiie-15.2015.149, Conference: 2015 International Conference on Artificial Intelligence and Industrial Engineering

[4] Megan Kelly, How smarter packaging design is becoming a competitive advantage in autonomous automotive logistics, 20 February, 2025, AUTOMOTIVE Logistics

[5] Bosch sustainability report 2024. https://assets.bosch.com/media/global/sustainability/reporting_and_data/2024/bosch-sustainability-report-2024.pdf

[6] Addy, et al., 2024, Nwatu, Folorunso & Babalola, 2024, Olutimehin, et al., 2024, Paul & Iyelolu, 2024

[7] Invented for life | Bosch Global

[8] Augustus Jones, Yingdan Catherine Cai, Rifat Kamasak, Examining Sustainable Packaging

Designs in the Automotive Industry: A Case Study of a Luxury Car Manufacturer Examining Sustainable Packaging Designs in the Automotive Industry, March 2024, DOI:10.4018/979-8-3693-0669-7.ch010, In book: Strategies for Environmentally Responsible Supply Chain and Production Management (pp.206-227) , IGI Global

Society of Production Engineering

ICPES 2025

40th INTERNATIONAL CONFERENCE ON PRODUCTION ENGINEERING - SERBIA 2025

DOI: 10.46793/ICPES25.516A

University of Nis Faculty of Mechanical Engineering

Nis, Serbia, 18 - 19th September 2025

ANALYSIS OF TECHNICAL RISKS IN SMALL HYDROPOWER PLANTS IN THE CONTEXT OF SUSTAINABLE DEVELOPMENT

Natalija ANĐELKOVIĆ[1]*, Saša S. RANĐELOVIĆ[1], Radica STOJANOVIĆ[2]

Orcid: 0000-0002-2334-8929

[1] University of Nis Faculty of Mechanical Engineering, Serbia

[2]Hydropower plants "Đerdap", Surdulica, Serbia

*Corresponding author: natalija.andjelkovicc@gmail.com

Abstract: *Small hydropower plants in areas with suitable hydroenergetic conditions have become important resources for producing increasingly demanded electricity. These small systems are susceptible to both external and internal disruptions, which significantly increase their level of technical risk. Managing such systems in real-time is the subject of many studies that take all influencing factors into account to ensure the optimal exploitation of natural resources. These energy systems represent fully integrated technical units that demonstrate strong robustness under various operating and exploitation conditions.*

Keywords: *small hydropower plants, technical risks, sustainable development, SCADA system, FMEA analysis.*

1. INTRODUCTION

The issue of small hydropower plants (SHPs) is becoming increasingly relevant both globally and locally as the energy crisis deepens. In regions with high energy consumption, every new energy source helps alleviate peak demands and sudden changes in energy markets. In this sense, analyzing technical risks of such facilities becomes essential to ensure that these hydroenergy systems are ready and responsive to market disruptions in energy supply.

SHPs play a key role in the renewable energy system by contributing to the reduction of harmful gas emissions and the diversification of energy sources. Additionally, such facilities allow for localized energy production that is both economical and environmentally friendly. However, despite these advantages, SHPs face a number of technical challenges and risks that can threaten their reliability, operational safety, and efficienciy.

Managing technical risks in SHPs includes various methods and approaches used to identify, analyze, assess, and control risks. The primary purpose of these methods is to minimize operational errors, increase system safety, and reduce unplanned downtime. Modern technologies such as SCADA (Supervisory Control and Data Acquisition) systems play a significant role in this process by

enabling real-time monitoring and timely detection of malfunction.

This paper focuses on a specific technical problem at the Vrla 3 hydropower plant, which is part of the Vlasina hydropower system—namely, the inadequate monitoring of the generator cooling system. This problem presents a significant risk because it leads to generator overheating and potential damage. Using the Failure Mode and Effects Analysis (FMEA) method, the study demonstrates how the implementation of a SCADA system can significantly reduce the risk of failure and improve system efficiency.

2. REVIEW OF EXISTING SOLUTIONS

Risk management in SHPs requires a comprehensive approach that includes technical, organizational, and environmental aspects. ISO 31000 (2018) defines risk management as coordinated activities to direct and control an organization regarding risks, covering identification, analysis, evaluation, and treatment, with ongoing communication and monitoring systematic approach that reduces uncertainty and increases operational safety in infrastructure systems, including SHPs [1].

For large infrastructure facilities like hydropower plants, risk management must be applied throughout the entire lifecycle—from planning and construction to operation and maintenance. Mikić (2015) emphasizes the importance of the timely identification of vulnerabilities as a key element in preventing accidents and ensuring sustainability. He highlights that integrating risk in the planning phase is crucial for reducing operational issues and improving facility safety [1].

Safety risk assessment in automated systems, especially in industrial facilities using remote control, is extremely important. Marković-Petrović (2018) warns that inadequate assessment can lead to serious incidents and operational interruptions with major economic and safety consequences. Her analysis shows that implementing comprehensive safety protocols and real-time performance monitoring using automated tools is key to reducing risks [2].

Although SHPs in Serbia have great potential in producing renewable and clean energy, their reliability can be compromised due to technical problems and a lack of modern monitoring systems. Jovanović et al. (2019) emphasize the need for advanced control and monitoring technologies to enhance SHP efficiency and safety [3].

They stress the importance of integrated management systems for better equipment condition monitoring and accident prevention. Stojković and Petrović (2020) describe in detail the application of FMEA in power systems, including SHPs. This method identifies possible failure modes and their consequences, which is essential for improving safety and reliability. The authors note that combining FMEA with SCADA systems significantly reduces operational errors and improves maintenance planning, as SCADA collects real-time data for identifying risk situations [4].

Petrović and Nikolić (2021) highlight the advantages of SCADA systems as modern control solutions in hydropower plants. They state that SCADA enables timely detection of technical issues, automatic responses to critical situations, and fast decision-making, thus reducing accident risks and extending equipment lifespan. Moreover, SCADA enhances operational efficiency by optimizing work parameters and reducing human errors [5].

Grigoraș et al. (2024) present an innovative approach integrating SCADA systems with data-mining technologies for predictive maintenance in SHPs. This combination enables early detection of potential failures before major issues arise, significantly reducing risks and unplanned downtime costs. Their work shows how smart SCADA systems can be at the core of modern SHP risk management solutions [6].

Kaur et al. (2015) analyze SHP automation through SCADA systems, focusing on real-time monitoring and remote control. They stress that such systems not only increase safety and efficiency but also allow further integration

with other IT systems, enhancing coordination and control of electricity production [7].

Radojević and Petrović (2020) describe the application of SCADA systems in Serbian hydropower facilities, emphasizing that these systems are essential for efficient monitoring and control. They particularly note the adaptation of SCADA systems to local conditions, enabling better management of specific risks in Serbian SHPs, along with lower operational costs and improved work safety [8].

3. CASE STUDY: VRLA 3 HPP

One of the key technical problems at Vrla 3 Hydropower Plant during operation is the high temperature of the inlet water from Lake Vlasina, especially during the summer months.

Table 1. FMEA analysis before introduction of the SCADA system

ID	Function	Failure mode	Consequence	Cause	S	O	D	RPN
1	Generator Cooling	No alarm when pump stops working	Overheating, downtime	Mechanical pump failure	7	9	6	378
2	Monitoring	Lack of temperature sensors	Late fault detection	Incomplete equipment	6	8	5	240

This water is used to cool the generator, but elevated temperatures lead to increased bearing temperatures. If this process is not detected and addressed in time, it can result in bearing overheating, reduced cooling efficiency, and potential mechanical damage to the generator. Previously, without the SCADA system, such situations often went unnoticed due to manual inspections and analog instruments. The absence of an alarm system further increased the risk of a malfunction escalating into a serious technical issue. This problem represents a real and measurable technical risk and can be identified as a critical point for SCADA-based risk management. An FMEA analysis revealed a high risk of serious consequences resulting from the improper functioning of the cooling system. The FMEA analysis SCADA system implementation is presented in the following table:

With the implementation of the SCADA system in Vrla 3 in 2022, significant progress was made in managing technical risks. The SCADA system enabled continuous monitoring of key parameters, automatic alarm generation upon fault detection, and rapid response in case of failure.

The SCADA system enables:

- Real-time monitoring of generator and cooling system temperatures
- Automatic alarm activation and system shutdown in case of a fault
- Remote control of cooling pumps
- Data archiving and report generation

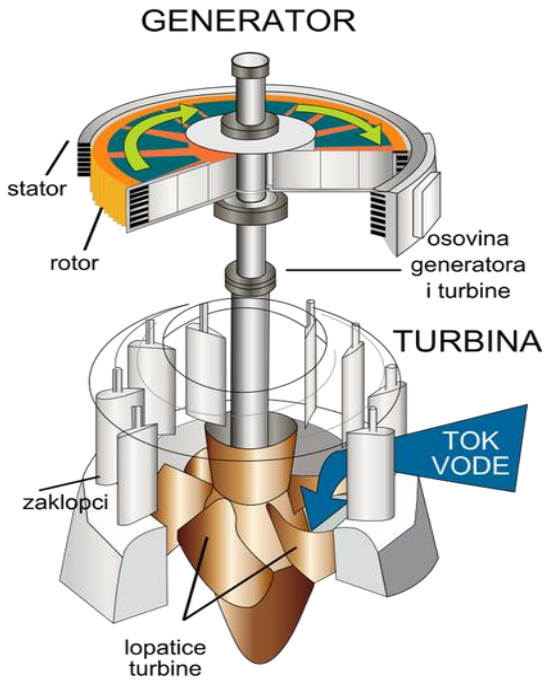

Figure 1. View of the generator and turbines

Table 2. FMEA analysis after SCADA system implementation

ID	Function	Failure mode	Consequence	Cause	S	O	D	RPN
1	Generator Cooling	The pump stops working	Alarm, no downtime	Pump failure	4	5	3	60
2	Monitoring	Sensor fails	Backup channel takes over	Sensor failure	3	4	2	24

An analysis of the FMEA tables before and after the implementation of the SCADA system in HE Vrla 3 clearly shows a significant reduction in risk. Prior to the implementation of the SCADA system, the RPN (Risk Priority Number) values for key functions were extremely high – 378 for the generator cooling system and 240 for the monitoring system. These high values were the result of a combination of high occurrence probability (O), severe consequences (S), and limited detectability (D), indicating a high level of technical vulnerability and the need for enhanced supervision.

After the implementation of the SCADA system, the RPN values significantly decreased – to 60 for cooling and only 24 for monitoring. This drastic reduction is the result of the following improvements:

- Reduction in Occurrence (O): The SCADA system enables earlier fault detection, thereby reducing the frequency of critical failures.
- Reduction in Severity (S): Automatic alarm generation and rapid response help mitigate the potential consequences, such as overheating and system shutdowns.
- Improved Detectability (D): With the integration of sensors and an alarm system, faults are detected in real-time, allowing timely interventions.

To gain a more detailed understanding of the benefits of using the SCADA system in reducing technical risks at HE Vrla 3, a time series analysis was conducted using data collected over 12 months following the system's implementation. A clear decrease was observed in the frequency of emergency shutdowns of the generator units due to overheating, from an average of 7 incidents per year before 2022 to only 1 incident in 2023. The analysis of SCADA system log files revealed that in as many as 80% of cases, the alarm was triggered before the temperature reached a critical point, which enabled preventive shutdown of the cooling system and timely technician intervention.

In addition to the technical improvements, the introduction of the SCADA system also significantly contributed to the organizational aspects of HE operations, especially in enhancing the procedures for planned and preventive maintenance. Based on data from the SCADA archive, the maintenance team now plans the replacement of critical components (pumps, sensors, valves) by the actual condition of the equipment, rather than using fixed time intervals. This increases equipment utilization and reduces costs.

One of the key factors in the successful implementation was the training of operators, who, through working with the system's interfaces, developed skills in quickly identifying and solving problems. A dedicated SCADA software module was used to simulate crisis scenarios, which further improved staff readiness.

A comparative analysis was also conducted with HE Vrla 2, which had not implemented a SCADA monitoring system for the cooling system by 2024. During the summer of the same year, Vrla 2 recorded three overheating incidents and two generator shutdowns, while Vrla 3 had none. This difference further confirms the practical benefits of real-time digital monitoring.

Based on the results mentioned, a standardized procedure for SCADA system implementation in other plants within the Vlasinske HE system was developed, with the following clear steps:

1. Analysis of critical points and definition of the sensor system,

2. Installation of equipment and alarm testing,
3. Database setup and definition of reporting parameters,
4. Staff training and operational deployment of the SCADA system,
5. Continuous performance monitoring and system optimization.

Based on these findings, it can be concluded that SCADA not only contributes to technical safety but is becoming a key tool for comprehensive risk management, operational efficiency, and sustainable plant operation.

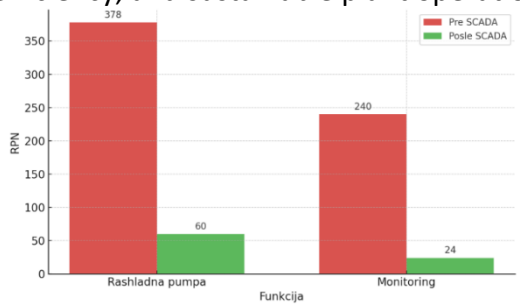

Figure 2. Change in RPN values before and after SCADA system implementation

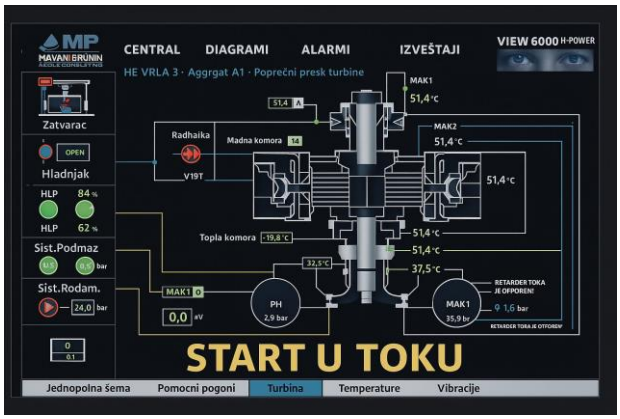

Figure 3. SCADA Interface Display for Unit A1 at HE Vrla 3

Key displayed parameters and elements:

- START IN PROGRESS — Indicates that the unit is in the startup phase and that the turbine and associated systems are operating.
- Turbine — A visual representation of the turbine with indicators for maximum (MAX) and minimum (MIN) allowable values for various parameters.
- Temperature — Display of temperature readings in different parts of the plant, e.g., in the cold chamber (14.8 °C), hot chamber (17.5 °C), and cooling water (1.1 °C). These values are important for controlling thermal loads and ensuring safe operation.
- Vibrations — Measurement of unit vibrations, shown on screen (e.g., values in green boxes), enabling early detection of mechanical issues and preventive maintenance.
- Water pressure and flow — Parameters such as flow and pressure in the pipelines, important for efficient turbine power control and equipment protection.
- Component status — Status display of gates, pumps, regulators, and other auxiliary systems, with indicators for activity and functionality (green symbols indicate the system is operational).
- Alarms and reports — Option to view active alarms and generate reports for system operation analysis and documentation.

Additional menus:

- CENTRAL, DIAGRAMS, ALARMS, H.R.D., REPORTS — Main menu for navigating through the system's functionalities.
- Single-line diagram, Auxiliary drives, Turbine, Temperatures, Vibrations — Detailed views and settings for specific parts of the plant.

The implementation of SCADA reduced the RPN from 378 to 60, indicating a significant risk reduction. Real-time parameter monitoring allows for faster responses and mitigated consequences. Future development may include:

- Implementation of predictive analytics for anomaly detection and failure prediction
- Multiple sensor redundancies to reduce the risk of sensor failure

4. CONCLUSION

The technical risk analysis at Vrla 3 HPP, part of the Vlasina hydropower system, identified a critical issue in the generator cooling system—speci cally, the absence of alarms and monitoring sensors—posing a real threat to the plant's safe and continuous operation. The FMEA analysis before SCADA implementation indicated a high RPN, confirming the need for technical supervision improvements.

SCADA system implementation at Vrla 3, as part of a broader modernization of the Vlasina HPPs, provided precise and automated monitoring of all key parameters—temperature, pressure, and cooling water flow. It enabled timely responses to pump failures, real-time alarm generation, and remote control from the central control room. After SCADA installation, the RPN values significantly decreased (from 378 to 60), substantially improving plant technical safety.

What makes this case particularly significant is the fact that the SCADA system was not part of a new investment, but rather a revitalization of an existing plant operating for over 60 years. This demonstrates that even older hydropower plants, such as Vrla 3, have realistic modernization potential that delivers measurable results in terms of safety and efficiency.

REFERENCES

[1] Miljan S. Mikić, "Risk Management in the Construction of Major Infrastructure Projects to improve Their Sustainability", Belgrade (2015), Doctoral Dissertation, Faculty of Civil Engineering, University of Belgrade.

[2] Jasna D. Marković-Petrović, "Safety Risk Assessment in Industrial Remote Control Systems", Belgrade (2018), Doctoral Dissertation, Faculty of Transport and Traffic Engineering – University of Belgrade.

[3] Milan Jovanović et al., "Energy Potential of Small Hydropower Plants in Serbia" (2019), Internal document of EPS or professional-analytical report.

[4] Dragan Stojković and Bojan Petrović, "Application of the FMEA Method in the Power Sector" (2020), Internal technical material of the "Đerdap" Hydropower Plant, Vlasina HPP Branch. (internal document)

[5] Ivana Petrović and Aleksandar Nikolić, "Modernization of Control Systems in Hydropower Plants" (2021), Internal report of the Đerdap / Vlasina HPPs. (practical source document)

[6] Grigoraș, G. et al. (2024). "Toward Smart SCADA Systems in Hydropower Plants: Integration of SCADA and Data-Mining for Predictive Maintenance in Small Hydropower Plants." Applied Sciences, 14(18), 8228. MDPI.

[7] Kaur, S. et al. (2015). "Role of SCADA in Hydro Power Plant Automation." ResearchGate, International Journal of Advanced Research in Electrical, Electronics and Instrumentation Engineering, Vol. 4, Issue 10, October 2015.

[8] Radojević, B. & Petrović, D. (2020). "SCADA Systems for Supervision and Control of Hydropower Facilities in Serbia." Internal document / presentation from professional practice within EPS HE Vlasina.

Society of Production Engineering

ICPES 2025

40th INTERNATIONAL CONFERENCE ON PRODUCTION ENGINEERING - SERBIA 2025

DOI: 10.46793/ICPES25.522G

University of Nis
Faculty of Mechanical Engineering

Nis, Serbia, 18 - 19th September 2025

INTEGRATING RENEWABLE ENERGY SOURCES INTO INDUSTRIAL MANUFACTURING: TECHNOLOGIES, CHALLENGES, AND BEST PRACTICES

Milan GROZDANOVIĆ[1,*], Dejan TANIKIĆ[1], Ana KITIĆ[2]

Orcid: 0000-0002-5618-9274; **Orcid:** 0000-0003-0702-5721; **Orcid:** 0000-0001-6465-3471;

[1] University of Belgrade – Technical Faculty in Bor, Bor, Serbia

[2] University of Niš, Faculty of Mechanical Engineering, Niš, Serbia

*Corresponding author: mgrozdanovic@tfbor.bg.ac.rs

Abstract: *The industrial sector is one of the largest consumers of energy and contributors to global greenhouse gas emissions. As pressure mounts to reduce environmental impact and comply with increasingly strict regulations, the integration of renewable energy sources (RES) into manufacturing systems is gaining momentum as a pathway toward sustainable production. This paper presents a concise review of available RES technologies applicable to industrial environments, with a particular focus on photovoltaic systems, heat pumps, waste heat recovery, and bioenergy. The technical feasibility, integration strategies, and primary challenges associated with each solution are discussed, along with relevant economic and regulatory considerations. Additionally, examples of successful implementation in manufacturing are highlighted to illustrate current trends and practical benefits. The review reveals that successful RES deployment requires a holistic approach that combines technological adaptation, financial planning, and supportive policy frameworks. The findings emphasize that while technical and financial barriers remain, RES integration represents a key opportunity for decarbonizing the industrial sector and advancing toward the objectives of circular economy and net-zero emissions.*

Keywords: *Industrial decarbonization, Waste heat recovery, Solar PV systems, Industrial heat pumps, Renewable energy sources*

1. INTRODUCTION

The manufacturing industry plays a central role in global economic development but also represents a significant source of energy consumption and greenhouse gas (GHG) emissions. According to the International Energy Agency, the industrial sector accounts for approximately 38% of final energy use worldwide, with fossil fuels still dominating the energy mix in many regions. The urgent need to reduce carbon emissions, coupled with increasing energy costs and regulatory pressures, is compelling manufacturers to explore cleaner and more sustainable energy solutions.

In this context, the integration of renewable energy sources (RES) into industrial production systems has emerged as a viable strategy to support the transition toward low-carbon manufacturing [1]. Renewable technologies such as solar photovoltaic (PV) systems, industrial heat pumps, waste heat recovery units, and biomass-based cogeneration offer

opportunities not only for reducing emissions but also for enhancing energy security and operational resilience.

Beyond the environmental imperative, the alignment with international policy frameworks, such as the European Union's *Fit for 55* package and the introduction of mechanisms like the Carbon Border Adjustment Mechanism (CBAM), is further accelerating the decarbonization of industrial sectors. These policies emphasize the need for systemic energy transitions, especially within energy-intensive industries such as metal processing, cement, and chemicals. For example, CBAM specifically targets imports from sectors like cement, aluminium, iron and steel, fertilisers, and hydrogen while reducing free allowances through the EU Emissions Trading System as part of a broader strategy to cut greenhouse gas emissions by at least 55% by 2030 and reach climate neutrality by 2050.

However, while the potential of RES integration in industry is widely acknowledged, its practical implementation is constrained by a range of technical, financial, and infrastructural barriers [2]. Intermittency of energy supply, limited space for on-site installations, high upfront investment costs, and the complexity of retrofitting legacy systems are among the key challenges facing manufacturers.

The purpose of this paper is to give a succinct summary of renewable energy technologies that can be incorporated into manufacturing systems. It examines implementation's technical and financial facets, pinpoints typical roadblocks, and offers a few chosen instances of industry best practices. The study adds to the larger conversation on sustainable production and industrial decarbonization by charting the present state of RES applications in manufacturing.

2. TYPES OF RENEWABLE ENERGY SOURCES FOR INDUSTRIAL APPLICATIONS

The transition toward sustainable manufacturing involves the strategic integration of RES that are technically feasible, economically viable, and environmentally beneficial. The choice of technology depends on multiple factors, including energy demand patterns, site-specific conditions, available infrastructure, and regulatory incentives. This section provides an overview of the key RES technologies applicable to industrial environments [3].

Solar PV systems are among the most accessible renewable technologies for manufacturing facilities, particularly due to the availability of large roof areas on industrial buildings. These systems convert sunlight directly into electricity and can be used either to supplement grid power or to operate in partially off-grid configurations. Industrial users benefit from predictable daytime energy loads, which align well with solar generation patterns, making self-consumption strategies highly effective. Additionally, falling PV module prices and favorable policies, such as net metering and tax incentives, have improved the return on investment for solar integration in industry [4].

Despite these advantages, challenges include intermittency of solar radiation, space limitations in high-density industrial zones, and the need for inverters and storage systems to manage peak loads and variability.

Heat pumps have gained traction as a low-carbon solution for providing thermal energy in the form of hot water, process heat, or space heating. Unlike conventional boilers, heat pumps operate on the principle of transferring heat from a low-temperature source (e.g., air, water, or waste heat) to a higher-temperature sink, typically using electricity. Their coefficient of performance (COP) often exceeds 3.0, meaning that for every unit of electricity consumed, they can deliver three or more units of heat energy. Industrial heat pumps are particularly useful in processes with moderate temperature requirements (<150°C), such as washing, drying, or pre-heating [5].

The main limitation lies in their inability to provide very high process temperatures, as required in metallurgical or chemical applications. Nevertheless, ongoing technological developments are extending their application range.

While not a renewable source per se, waste heat recovery is a critical component of industrial energy efficiency and can complement RES strategies [6]. Many manufacturing processes emit substantial quantities of low- to medium-grade waste heat, which often goes unused. Technologies such as recuperators, economizers, and heat exchangers can be employed to capture this heat and redirect it into useful applications, such as space heating, water pre-heating, or even electricity generation via Organic Rankine Cycles (ORC). This improves overall system efficiency and reduces fuel consumption.

Implementation requires careful process integration and feasibility analysis, especially when retrofitting existing plants. However, waste heat recovery can often achieve short payback periods due to direct energy savings.

Industries that generate organic waste—such as food, wood processing, and agricultural sectors—can harness biomass and biogas as internal energy resources. Biomass can be combusted directly or converted into syngas and bio-oil, while biogas is typically produced via anaerobic digestion and used in combined heat and power (CHP) systems.

These technologies support circular economy principles by converting waste streams into usable energy, thereby reducing both environmental impact and energy costs [7].

Barriers include high capital costs, logistical complexities of biomass supply, and emissions control. Nonetheless, in sectors where biomass is abundant and regulations favor bioenergy, these systems can offer competitive advantages.

3. TECHNICAL INTEGRATION OF RENEWABLE ENERGY SOURCES IN INDUSTRIAL SYSTEMS

The integration of RES into industrial systems requires more than the mere installation of green technologies—it involves the adaptation of existing infrastructure, operational strategies, and energy management practices. This section outlines key technical considerations and integration strategies for deploying RES within manufacturing environments.

Table 1. Overview of RES Technologies for Industrial Applications

Technology	Primary Use in Industry	Main Advantages	Key Challenges
Solar PV	Electricity generation for machinery, lighting	- Reduces electricity bills - Low maintenance - Scalable	- Intermittent production - Roof space limitations - Need for storage/inverters
Heat Pumps	Process heat, space heating, hot water	- High efficiency (COP > 3) - Electrification of heat - Reduced emissions	- Limited to moderate temperatures - High initial cost
Waste Heat Recovery	Reuse of thermal energy from processes	- Improves energy efficiency - Quick payback in many cases	- Requires careful integration - Often process-specific
Biomass/Biogas	Heat and electricity (via CHP), waste valorization	- Utilizes internal waste - Supports circular economy - On-site generation	- Logistics and fuel preparation - Emission control - High CAPEX

Most industrial facilities adopt grid-connected RES systems, where renewable energy complements the grid supply. This approach allows flexibility: excess energy can be exported to the grid under net metering or feed-in tariff schemes, while deficits can be covered from the grid. Grid-connected systems are especially common in solar PV applications, as they reduce the need for costly storage systems. Standalone systems, on the other

hand, are relevant in remote industrial operations or in facilities aiming for energy independence. These often require a combination of RES (e.g., PV + biomass) and battery storage or backup generators to ensure reliability.

The fluctuating nature of RES, particularly solar and wind, necessitates real-time Energy Management Systems (EMS) that can balance generation, storage, and demand. EMS can dynamically adjust load profiles, prioritize self-consumption, and reduce peak demand charges. Smart EMS platforms are typically integrated with Industrial Internet of Things (IIoT) technologies, enabling remote monitoring and predictive maintenance [8]. This not only improves system performance but also extends equipment lifespan and helps with demand-side management.

In many cases, RES must be integrated into existing production processes without disrupting productivity. This can be particularly challenging when retrofitting older facilities. For example, heat pumps may require modifications in process temperature levels and distribution systems, waste heat recovery systems demand a thorough thermal audit to identify viable heat sources and match them to nearby sinks, and biomass boilers require dedicated fuel handling and emissions control infrastructurs. Process integration also involves matching energy supply profiles with demand, e.g., aligning solar PV output with peak machine operation hours.

Because RES such as solar and wind are intermittent, energy storage systems are often required to ensure continuity and reliability in industrial settings. Options include electrical storage (e.g., lithium-ion batteries) for PV integration, thermal storage (e.g., hot water tanks, phase-change materials) for processes with heating demands, hydrogen production via electrolysis is emerging as a long-term storage solution and can be used in high-temperature industrial applications.

In addition to physical storage, flexibility measures such as load shifting, demand response, or hybrid RES systems contribute to more efficient integration [9].

Continuous monitoring is critical for maximizing the benefits of RES. The use of digital twins, virtual models of energy systems, allows for real-time simulation, performance prediction, and optimization under variable operating conditions.

Digitalization thus plays a key enabling role, especially in complex manufacturing environments where interactions between energy and production processes are dynamic and multidimensional.

4. ECONOMIC AND REGULATORY ASPECTS OF RES INTEGRATION IN MANUFACTURING

While the technical feasibility of renewable energy integration in manufacturing continues to improve, the decision to invest in such systems is often governed by economic considerations and regulatory frameworks. This chapter outlines key financial drivers, cost-related barriers, and policy instruments that shape industrial adoption of RES technologies [1, 3, 4].

The initial capital expenditure (CAPEX) for renewable energy installations, especially for solar PV systems, industrial heat pumps, and biomass boilers, can be substantial. However, decreasing equipment costs and improved efficiency have made many technologies economically attractive over time. For example, the global average cost of installed utility-scale solar PV dropped by over 80% between 2010 and 2020.

The return on investment (ROI) varies depending on energy prices, self-consumption rates, system sizing, and available incentives. In some regions, ROI for industrial PV systems can be achieved within 5–7 years, particularly when electricity tariffs are high and peak shaving is enabled. However, uncertainty about long-term policy stability, fluctuating energy markets, and lack of awareness about lifecycle savings still act as deterrents for some manufacturers.

Compared to conventional systems, RES technologies typically offer lower operating costs (OPEX) due to reduced fuel dependency and fewer moving parts (e.g., in PV systems). Maintenance requirements are also lower,

though periodic cleaning, performance monitoring, and inverter replacement are necessary [3, 4].

In contrast, biomass systems may have higher OPEX, driven by fuel logistics, combustion system upkeep, and emission control requirements.

Many governments and international institutions offer financial incentives to support RES deployment in industry. These include investment subsidies and grants, feed-in tariffs or premium tariffs, accelerated depreciation schemes, carbon credits and tax breaksm, and net metering and virtual net metering for grid-connected PV. These mechanisms significantly improve the financial viability of RES projects and encourage early adoption. For example, the European Union's Recovery and Resilience Facility (RRF) earmarks billions of euros for green industrial upgrades, including RES integration.

However, access to funding may be limited for small and medium-sized enterprises (SMEs) due to administrative complexity, lack of technical capacity, or insufficient upfront capital.

RES deployment in manufacturing must comply with a variety of local, national, and supranational regulations. These include grid connection standards, environmental permits (especially for bioenergy systems, energy performance reporting, building codes for rooftop PV, and emissions monitoring and reporting.

In the European Union, the *Fit for 55* legislative package mandates stricter emissions reductions across industrial sectors, alongside the introduction of the Carbon Border Adjustment Mechanism (CBAM). This mechanism imposes a carbon cost on imported goods from countries with less stringent climate policies, thereby incentivizing domestic industries to decarbonize.

Beyond regulatory compliance, manufacturers are increasingly subject to market-driven decarbonization pressures. Many large buyers, investors, and financial institutions now require Environmental, Social, and Governance (ESG) disclosures. A company's energy mix and emissions profile are key ESG metrics that influence supply chain decisions and investment attractiveness. As a result, integrating RES can enhance not only environmental performance but also brand value, access to green financing, and competitive positioning in global markets [10].

5. CASE STUDIES AND BEST PRACTICES

To illustrate the practical implementation of renewable energy technologies in manufacturing, this chapter presents selected case studies and examples from leading industrial companies. These cases highlight both the potential benefits and real-world challenges associated with the integration of RES into production systems.

Siemens has implemented solar photovoltaic (PV) systems in several of its manufacturing plants worldwide. In its Kalwa plant in India, Siemens installed a 1 MW rooftop solar system that supplies up to 25% of the facility's daytime electricity demand, reducing annual CO_2 emissions by approximately 1,200 tons. The company reports a payback period of fewer than six years, supported by national feed-in tariffs and tax incentives. This case demonstrates the compatibility of PV with facilities that have large roof surfaces and stable energy loads during daylight hours [10].

Bosch has implemented a comprehensive energy efficiency strategy that includes waste heat recovery systems across its European plants. In its Homburg factory (Germany), Bosch uses heat exchangers and thermal storage to capture and reuse process heat for space heating and hot water, reducing fossil fuel use by over 20% [6]. The success of this approach relies on thorough thermal audits and integration planning. Bosch's experience illustrates that even legacy facilities can achieve significant improvements through targeted retrofitting.

A major pharmaceutical manufacturer in France implemented a waste-heat recovery heat pump in one of its production facilities. This industrial heat pump captures low-grade waste heat and upgrades it to useful process

heat, reducing reliance on fossil fuels and improving the site's carbon footprint. This case demonstrates that industrial heat pumps can be effectively deployed even in energy-intensive manufacturing settings, provided that temperature requirements are suitable and the process integration is carefully engineered.

Interface Inc., a global flooring manufacturer, integrates biogas-fueled CHP systems at its manufacturing facilities in Europe. By using directed biogas for thermal energy and combined heat & power, the company captures renewable thermal energy and implements circular economy practices—recycling production waste—and aligns its operations with ambitious carbon neutrality goals [7].

Despite differences in technology and scale, several common factors emerge across these best practices: top management commitment and alignment with long-term sustainability goals, thorough energy audits and feasibility studiesm, use of public incentives and regulatory frameworks to reduce investment risk, digital monitoring systems for performance tracking and optimization, and integration with broader decarbonization strategies (e.g., circular economy, waste valorization).

These cases underscore that RES integration is not limited to specific sectors or company sizes; rather, it is a viable strategy for any manufacturer with the vision and capacity to invest in long-term energy and environmental performance.

6. CONCLUSION

The integration of RES into manufacturing systems represents a critical step toward achieving industrial decarbonization, improving energy security, and aligning with broader sustainability goals. As the industrial sector faces increasing pressure from regulatory frameworks, market expectations, and environmental imperatives, renewable energy technologies offer a viable path forward.

This paper has presented an overview of key RES technologies applicable to industrial environments, including solar PV, heat pumps, waste heat recovery, and biomass-based systems. Technical integration requires careful planning, process compatibility assessments, and energy management strategies—particularly when retrofitting existing facilities. While economic challenges persist—such as high upfront costs and administrative complexity—available financial incentives and policy support can significantly improve project viability.

Real-world case studies demonstrate that manufacturers across various sectors and geographies have successfully adopted RES technologies, resulting in reduced emissions, operational savings, and enhanced ESG performance. These examples highlight the importance of strategic planning, strong leadership commitment, and the use of digital tools for performance monitoring and optimization.

Looking ahead, further progress will depend on the continued evolution of enabling technologies (e.g., energy storage, smart grids), regulatory clarity, and increased awareness within the industrial community. Integrating RES is not merely an environmental measure—it is an opportunity to future-proof industrial operations and create resilient, sustainable production systems.

ACKNOWLEDGEMENT

This research was financially supported by the Ministry of Science, Technological Development and Innovation of the Republic of Serbia (Contract No. 451-03-137/2025-03/ 200131 and 451-03-137/2025-03/ 200109).

REFERENCES

[1] F. O. Usman, E. l. Chigozie Ani, W. Ebirim, D. J. P. Montero, K. A. Olu-lawal, N. Ninduwezuor-Ehiobu, Integrating Renewable Energy Solutions in the Manufacturing Industry: Chalenges and Opportunities: A Review, Engineering Science & Technology Journal, Volume 5, Issue 3, pp. 674-703, 2024

[2] E. Obuseh, J. Eyenubo, J. Alele, A. Okpare, I. Oghogo, *A Systematic Review of Barriers to*

Renewable Energy Integration and Adoption, Journal of Asian Energy Studies, 9, pp. 26–45, 2025

[3] IRENA, *Renewable Power Generation Costs in 2020*, International Renewable Energy Agency, Abu Dhabi, 2021

[4] N. García-Morales, López-González, E. Fernández, *Economic Evaluation of PV Installations for Self-Consumption in Industrial Park*s, Energies, 14(3), 728, 2021

[5] R. de Boer, A. Marina, B. Zühlsdorf, C. Arpagaus, M. Bantle, V. Wilk, B. Elmegaard, J. Corberán, J. Benson, *Strengthening Industrial Heat Pump Innovation: Decarbonizing Industrial Heat*, 2020

[6] S. O. Oyedepo, B. A. Fakeye, Waste heat recovery technologies: a pathway to sustainable energy development, Journal of Thermal Engineering, 7(1), pp. 324–348, 2021

[7] S. Rezania, B. Oryani, V. R. Nasrollahi, N. Darajeh, M. Lotfi Ghahroud, K. Mehranzamir, *Review on Waste-to-Energy Approaches toward a Circular Economy in Developed and Developing Countries*, Processes, 11(9), 2566, 2023

[8] S. Lee, J. Seon, B. Hwang, S. Kim, Y. Sun, J. Kim, *Recent Trends and Issues of Energy Management Systems Using Machine Learning*, Energies, 17, 624, 2024

[9] P. D. Lund, J. Lindgren, J. Mikkola, J. Salpakari, *Review of energy system flexibility measures to enable high levels of variable renewable electricity*, Renewable and Sustainable Energy Reviews, Volume 45, pp. 785-807, 2015

[10] https://www.siemens.com/global/en/company/about/businesses/real-estate/info-center/green-greener-kalwa.html?utm_source=chatgpt.com accessed: 08.07.2025

Society of Production Engineering

ICPES 2025

40. INTERNATIONAL CONFERENCE ON PRODUCTION ENGINEERING - SERBIA 2025

DOI: 10.46793/ICPES25.529K

University of Nis Faculty of Mechanical Engineering

Nis, Serbia, 18 - 19. September 2025

ROADMAP FOR SUSTAINABLE MANUFACTURING IN THE INDUSTRY 4.0 AND 5.0 ERA: CONCEPTS, METRICS, AND OPPORTUNITIES FOR SMES

Ana KITIĆ[1]*, Mladen RADIŠIĆ[2], Milan GROZDANOVIĆ[3], Ivana JANKOVIĆ[4]

Orcid: 0000-0001-6465-3471; **Orcid:** 0000-0002-6689-7717; **Orcid:** 0000-0002-5618-9274

[1]University of Niš, Faculty of Mechanical Engineering, Niš, Serbia

[2]University of Novi Sad, Faculty of Technical Science, Novi Sad, Serbia

[3] University of Belgrade, Technical Faculty in Bor, Bor, Serbia

[4]University of Niš, Faculty of Mechanical Engineering, Niš, Serbia

*Corresponding author: ana.kitic@masfak.ni.ac.rs

Abstract: *This paper discusses about how Industry 4.0 and the new Industry 5.0 paradigm make it possible for small and medium-sized businesses (SMEs) to make things in a way that is good for the environment. We put together a taxonomy of technology, sustainability lever, KPI by combining the economic, environmental, and social streams of the literature (PLM/LCA, lean–green practices, sustainable supply chains, RMS/modularity, and digitalization/AI/IoT) into a structured narrative review. Based on this synthesis, we suggest a SME-friendly metric set and a useful roadmap that puts human-machine collaboration, green and circular technologies, data-driven operations, flexible and resilient production, smart workplaces, ethical governance, and ecosystem support in the right order. The roadmap makes it clear how digital skills can lead to triple-bottom-line results and where policy and funding can speed up adoption. The paper gives SME managers and policymakers a clear framework and useful metrics to help them plan and assess digitally enabled sustainability transitions.*

Keywords: *sustainable manufacturing, Industry 4.0, Industry 5.0, SMEs, digital twin/IoT/AI, circular economy, KPIs, roadmap*

1. INTRODUCTION

The need for a new model of production and consumption that considers its effects on society and the environment is becoming more widely recognised. Stakeholders are putting more pressure on the industry to report openly about these effects. In this sense, sustainable manufacturing means reducing damage to the environment and energy and natural resource consumption while being both socially and financially responsible. As a result, organisations and the research community, especially in the industrial sector, are paying more attention to the idea of sustainable manufacturing.[1]

Social sustainability and ecosystem degradation have emerged as major concerns in the business world in recent decades. However, most corporate social responsibility research focusses on large corporations, frequently ignoring the unique characteristics of small and medium-sized businesses (SMEs). [2]

When the effects of SMEs are considered collectively, it becomes easier to understand the crucial role that they play in global sustainability. [3]

Although small and medium-sized enterprises are widespread, it is not easy for them to adapt to the requirements of Industry 5.0 while also adhering to sustainability principles. In this paper, we present a clear framework and a metric that can help SMEs more easily align with the requirements of Industry 5.0.

2. INDUSTRY 4.0 AND SUSTAINABILITY

Authors argue that the surge of expectations surrounding Industry 4.0's contribution to sustainable development is accompanied by a lack of clear understanding of how digital technologies actually deliver economic, environmental, and social benefits in manufacturing. Drawing on a systematic literature review, the authors distill 15 "sustainability functions" (e.g., energy-consumption optimization via IoT sensors, digital twins for waste reduction, predictive maintenance for higher reliability) and use Interpretive Structural Modeling (ISM) to map their interdependencies and implementation sequence. The outcome is a visual roadmap that shows the steps companies can follow to leverage Industry 4.0 technologies for strengthening all three pillars of sustainability, economic, environmental, and social thus providing managers and scholars with a practical guide for planning digitally driven, triple-bottom-line transformations.[4]

Digital transformation of Industry 4.0 technologies helps small and medium-sized businesses (SMEs) make their manufacturing more sustainable by making it more efficient, optimising resources, doing business in an ethical way, and being more competitive. Using sensor-based IoT devices to keep an eye on how machines are being used, how much energy they use, and the skills of the workers makes it possible to make decisions based on real-time data that cut down on waste and make the best use of resources.

By combining cyber-physical systems, AI, big data analytics, and automated quality control tools that cut down on defects, energy use, and operational costs, you can make production more efficient and sustainable.

Allow for flexibility and quick response to changing market needs and the need for customisation, which is very important for small and medium-sized businesses that have to deal with complicated customer needs.

Help small and medium-sized businesses move from linear to sustainable manufacturing models by using fewer resources and making less waste.

Even though there are problems with cost, skills, and adoption, better communication, information flow, and collaboration across supply chains can help businesses become more ethical and sustainable.[5–7]

2.1 Industry 5.0, sustainability and SMEs

Industry 5.0 is an improvement on Industry 4.0 that focusses more on people, the environment, and resilience. This makes it very useful for small and medium-sized businesses in sustainable manufacturing. Industry 4.0 was all about automation and efficiency. In contrast, Industry 5.0 uses collaborative robotics (cobots), renewable energy, circular economy principles, and digital technologies to support production models that are sustainable, customised, and adaptable.[8]

3. INDUSTRY 5.0 ENHANCE SUSTAINABILITY IN SME MANUFACTURING PRACTICES

Industry 5.0 utilises the small and medium-sized enterprises (SMEs) more sustainable by combining human-centered design, advanced technology, and circular economy ideas to make a production system that is more durable, eco-friendly, and socially responsible. Industry 5.0 prioritizes eco-friendly manufacturing by incorporating green technologies, renewable energy sources (like bioenergy), and energy-efficient production systems. It promotes material reuse, waste minimization, and closed-loop production models that reduce

environmental impact and resource consumption. IoT and big data analytics allow real-time monitoring for better resource efficiency and waste reduction. AI and machine learning optimize production quality and energy use. These technologies support predictive maintenance and flexible manufacturing, increasing adaptability and reducing downtime. Industry 5.0 uses AI, IoT, and blockchain to enhance supply chain transparency and responsiveness, helping SMEs quickly adjust to disruptions such as supply delays or market changes without compromising operational efficiency. By combining human creativity with machine precision, SMEs can offer personalized products at scale, which aligns with customer demand and enhances competitiveness while maintaining sustainability [8].

4. METRICS OF SUSTAINABLE MANUFACTURING

The most effective KPIs (Key Performance Indicators) for measuring SME sustainability in manufacturing focus on economic, environmental, and social dimensions, enabling SMEs to track and improve their sustainability performance comprehensively.

The Triple Bottom Line (TBL) is a fundamental metric framework utilized to assess sustainable manufacturing by analyzing performance across three equally significant dimensions: economic, environmental, and social. For SMEs in manufacturing, TBL facilitates the equilibrium of profitability (economic), environmental stewardship (planet), and social responsibility (people) to attain comprehensive sustainability.[9, 10]

4.1 Economic sustainability

The literature shows that manufacturing companies can improve economic sustainability through life-cycle thinking (PLM/LCA) to spread costs and value across product-process-system levels; logistics and supply-chain optimisation; and digitalization / global integration (e-products, mass customisation, digital manufacturing, integration of design management with ERP, STEP-NC) that boost productivity and decision-making. A lot of work has been done on reconfigurable manufacturing systems (RMS), which include modular, scalable machines, feasibility models, reconfiguration policies, and indices for measuring reconfigurability. These systems are more flexible, can respond to changes in the market or product faster, have better CAPEX/OPEX profiles, and are more competitive. The corpus also emphasises the need for disciplined energy cost management, the flexibility to adapt to crises, and choosing suppliers who are aware of sustainability (for example, AHP+QFD) to lower the total cost of ownership and risk. When you put them all together, principles like eco-design, reuse/repair/recycling, lean operations, and sustainable supply chains help businesses become more efficient, keep their margins steady, and stay in business for a long time.

4.2 Environmental sustainability

In manufacturing shows that recycling, waste reduction, pollution prevention, and ISO 14000 certification boost plant efficiency. Supply chains adopt “green” techniques and performance metrics due to regulatory, market, and reputational constraints. Environmental cost accounting (e.g., extended activity-based costing) promotes waste reduction for productivity and sustainability. Lean techniques and environmental management increase business outcomes, while reduced raw-material consumption, redesign products for environmental performance, and solid-waste recycling lower production costs and improve product quality [11].

4.3 Social sustainability

An analysis of **social sustainability** in manufacturing focusses on the larger value generation for society, transparency and

disclosure, and the conditions and well-being of workers. It appears at the social effects of designing a logistics network and uses criteria that cover internal human resources, external populations, macro-level social performance, and stakeholder participation. Impact assessments often look at things from a life-cycle point of view, separating effects on workers, local communities, and society.

7. INDUSTRY 5.0 OPPORTUNITIES FOR SUSTAINABLE MANUFACTURING IN SMES

Industry 5.0 differs from Industry 4.0 in several key respects. Industry 5.0 is a human-centered, sustainable, and resilient approach to business. Implementing 5.0 reduces operating costs, makes operations "greener," and improves product quality. Small and medium enterprises need to adopt advanced technologies like AI, IoT and robots to improve productivity and stay ahead of the competition [12].

In Industry 5.0, people and machines work together (for example, with cobots and AR interfaces) to make things more accurate, efficient, and safe while still allowing people to do meaningful work.

SMEs can make sustainability a key competitive advantage by using green and circular technologies like renewables, zero-waste processes, and digital material passports.

AI/ML and IoT analytics make it possible to optimise resources in real time, predict when maintenance will be needed, forecast demand, and reduce scrap, which lowers both costs and carbon.

Flexible, reconfigurable production and blockchain-enabled supply-chain visibility make it easy to adapt quickly to changes in the market, disruptions, and mass customisation.

Smart building and EHS technologies (BMS, sensors, wearables) make workplaces safer, more comfortable, and more energy-efficient. They also help social sustainability.

Combining human creativity with digital twins and additive manufacturing lets small and medium-sized businesses make products that are unique to each customer and help speed up the process of coming up with new ideas.

Digital operations and supplier relationships that are ethical and responsible include social responsibility, human-centered design, and open governance.

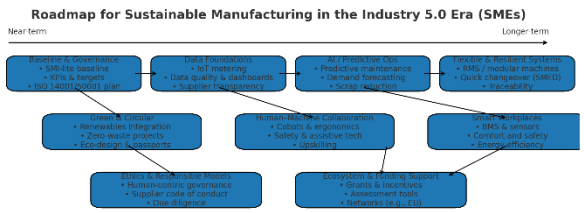

Figure 1. Roadmap for Sustainable Manufacturing in the Industry 5.0 Era (SMEs). Sequence is indicative; tracks may run in parallel. Progress should be monitored with SMI-lite KPIs.

Ecosystem programs and funding, like EU SURE5.0, give small and medium-sized businesses (SMEs) the money, tools for evaluation, and networks they need to make the switch to sustainable Industry 5.0 faster and with less risk [13].

Figure 2 shows a way to put the literature synthesis into action by linking industry 4.0/5.0 technologies to sustainability levers and example kpis that are important for small and medium-sized businesses. The taxonomy puts seven technology groups (iot/sensors, ai/ml, digital twins, rms/modular automation, additive manufacturing, blockchain traceability, and smart building/ehs) against five levers: energy and resource efficiency, circularity and waste, safety and well-being, transparency and compliance, and resilience and flexibility. It also links each lever to practical kpis, such as energy intensity and renewables share, waste-to-landfill and recycled content, trir and training coverage, suppli the figure doesn't tell smes what to do; it helps them choose a set of kpis that works for their industry and level of maturity.

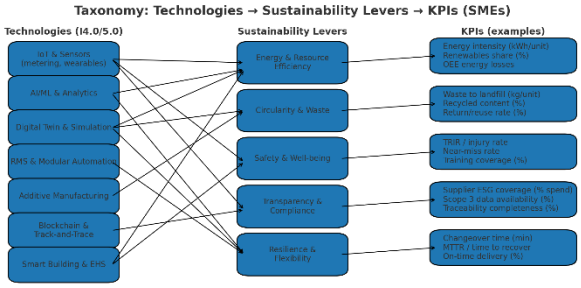

Figure 2. Taxonomy linking Industry 4.0/5.0 technologies to sustainability levers and example KPIs for SMEs. Links are indicative; KPIs should be adapted to sector context.

8. CONLCULISON

The review shows that Industry 4.0 capabilities, which are made even better in Industry 5.0 by principles that focus on people and resilience, can help businesses do well on all three bottom lines when they are put in the right order and measured with the right KPIs. For small and medium-sized businesses (SMEs), short-term wins come from being more efficient with energy and materials, being able to predict when maintenance will be needed, and having a clear view of the supply chain. Medium-term gains come from using circular design, reconfigurable systems, and training the workforce. The suggested roadmap and taxonomy make measurement and governance work, which helps companies connect projects to results and lets policymakers focus their support. Because this is a desk review, future work should test the roadmap in the real world (through case studies and surveys in different sectors) and measure the effect sizes of the most important interventions.

REFERENCES

[11] Sartal, A., Bellas, R., Mejías, A.M., García-Collado, A.: The Sustainable Manufacturing Concept, Evolution And Opportunities Within Industry 4.0: A Literature Review. Advances In Mechanical Engineering. 12, (2020).

[12] Jansson, J., Nilsson, J., Modig, F., Hed Vall, G.: Commitment To Sustainability In Small And Medium-Sized Enterprises: The Influence Of Strategic Orientations And Management Values. Bus Strategy Environ. 26, 69–83 (2017).

[13] Ayyagari Asli Demirguc-Kunt Vojislav Maksimovic The World Bank, M.: Small Vs. Young Firms Across The World Contribution To Employment, Job Creation, And Growth. (2011)

[14] Ching, N.T., Ghobakhloo, M., Iranmanesh, M., Maroufkhani, P., Asadi, S.: Industry 4.0 Applications For Sustainable Manufacturing: A Systematic Literature Review And A Roadmap To Sustainable Development. J Clean Prod. 334, 130133 (2022).

[15] Jamwal, A., Palit, N., Kumari, S., Agrawal, R., Sharma, M.: A Decision Framework For Smes To Address Sustainability Issues With Industry 4.0 Technologies. Ann Oper Res. (2025).

[16] Santos, A. De M., Sant'anna, Â.M.O.: Industry 4.0 Technologies For Sustainability Within Small And Medium Enterprises: A Systematic Literature Review And Future Directions. J Clean Prod. 467, 143023 (2024).

[17] Kumar, R., Singh, R.Kr., Dwivedi, Y.Kr.: Application Of Industry 4.0 Technologies In Smes For Ethical And Sustainable Operations: Analysis Of Challenges. J Clean Prod. 275, 124063 (2020).

[18] Shabur, M.A., Shahriar, A., Ara, M.A.: From Automation To Collaboration: Exploring The Impact Of Industry 5.0 On Sustainable Manufacturing, (2025)

[19] Vasconcelos, A.F., González, I.A.R., Fernández, M.A., Santiago, A.Z., Romage, G.R.: Applying A Delphi Method To Assess The Sustainability In Smes: An Approach Of Triple Bottom Line. Revista De Gestão Social E Ambiental. 18, E09690 (2024).

[20] Sethi, R., Rajesh, M.: 444-464; 2022 For The Manufacturing Industries. (2022)

[21] Garbie, I.H.: An Analytical Technique To Model And Assess Sustainable Development Index In Manufacturing Enterprises. Int J Prod Res. 52, 4876–4915 (2014).

[22] Takawira, B., Pooe, D.: Sme Readiness For Industry 5.0: A Systematic Literature Review. Southern African Journal Of Entrepreneurship And Small Business Management. 17, 1–14 (2025).

[23] Aviable at: https://www.eitmanufacturing.eu/news-events/activities/sure5-0/ 20.05.2025

Society of Production Engineering

ICPES 2025

40th INTERNATIONAL CONFERENCE ON PRODUCTION ENGINEERING - SERBIA 2025

DOI: 10.46793/ICPES25.535N

University of Nis Faculty of Mechanical Engineering

Nis, Serbia, 18 - 19th September 2025

SUSTAINABLE WATER MANAGEMENT IN THE COSMETIC INDUSTRY

Jelena NEDELJKOVIĆ[1], Neda DESIĆ[1], Iva JEVTIĆ[1], Jelena NIKOLIĆ[1], Saša S. RANĐELOVIĆ[1]

Orcid: 0000-0002-2334-8929

[1] Faculty of Mechanical Engineering, University of Niš, Serbia

*Corresponding author: jelenanedeljkovic527@gmail.com

Abstract: *One of the key issues of the 21st century is sustainable water management, as we are witnessing an increasing water shortage caused by uncontrolled consumption. This is a global problem that poses a major challenge of the modern era, affecting individuals, the general population, and large corporations alike. The aim of this paper is to present how companies are responding to this growing problem by implementing sustainable practices and innovative systems that enable water consumption reduction in industrial settings. Through a case study, an environmentally friendly shower system is presented, which applies water fragmentation technology to ensure reduced water usage while maintaining rinsing efficiency. It is concluded that the application of technological solutions and sustainable practices in business processes has the potential to become a standard within environmentally responsible industrial operations.*

Keywords*: sustainability, water, industrial consumption, eco-friendly shower system, fragmentation*

1. INTRODUCTION TO SUSTAINABLE WATER MANAGEMENT

Sustainable water management entails the balanced use, protection, and preservation of water resources to meet the needs of current generations without compromising the ability of future generations to meet their own needs. This approach integrates ecological, economic, and social aspects into water resource planning and management.

According to the United Nations, “sustainable water management means using water in a way that meets the needs of people and ecosystems today without compromising the ability of future generations to use the same resources” (UN-Water, 2021). [1]

Water scarcity is one of the most serious global challenges today. According to the World Health Organization (WHO, 2023), more than two billion people worldwide still lack access to safe drinking water, and projections suggest that by 2025, as much as half of the world's population could be living in areas experiencing severe water shortages.

Industry consumes about one-fifth of the world’s available freshwater, and in developed countries, that share can reach up to 50% (OECD, 2020), further worsening the situation by degrading ecosystems and reducing resources available to local communities.

In addition, according to the World Resources Institute (WRI), a significant number of aquifers are being depleted faster than they can naturally recharge, threatening the sustainability of water supplies (WRI, 2019).

Water pollution further complicates the situation, as agricultural chemicals enter rivers and lakes, causing eutrophication—a process that diminishes water quality and destroys

aquatic ecosystems (UNEP, 2022). Industrial and municipal waste exacerbates this problem, altering the chemical composition of surface and groundwater.

Unequal distribution of water resources also contributes to the problem. While some regions enjoy abundance—often used inefficiently—others, such as Africa and the Middle East, face severe shortages that threaten basic human needs (FAO, 2020). This imbalance clearly indicates the urgent need for coordinated global action focused on conservation and equitable water distribution.

Despite the growing number of declarations, policies, and corporate sustainability reports, the question remains whether sustainable water management has truly become practice—or if it remains merely an image.

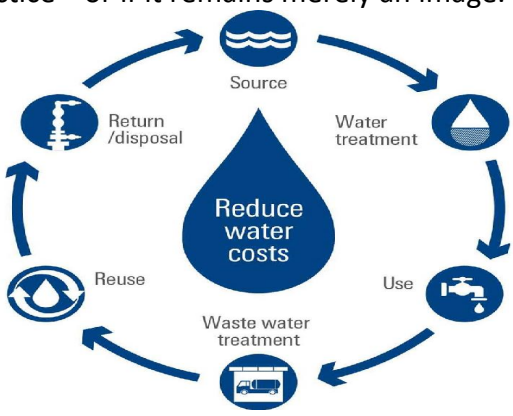

Figure 1. *Reduce water costs*

Many companies and governments promote "sustainability" in their strategies, but concrete measures are often lacking or limited to symbolic actions with little real effect. As McKinsey & Company (2021) noted, "many companies invest more in sustainability marketing than in actual changes to their water supply chains." [2]

Although there are success stories of local initiatives, smart technologies, and participatory planning, on a global scale, sustainable water use is still the exception rather than the rule.

2. INDUSTRIAL WATER CONSUMPTION

Water is a key raw material in the cosmetics industry, not only as a base ingredient in many products (e.g., lotions, shampoos, creams) but also in the manufacturing process, equipment cleaning, and plant hygiene. On average, water makes up 70–80% of the formulation of products like lotions and toners. It is also used in cooling systems, raw material rinsing, and as a solvent in various production stages. Without it, mass production of cosmetic products is virtually impossible.

This intensive water use becomes particularly problematic in regions where water resources are limited or already under stress. Industries that heavily rely on water, such as cosmetics, must reassess their practices to preserve local resources and meet ecological standards. According to research by the Water Footprint Network, the industrial sector consumes over 20% of the world's available freshwater, with the cosmetics sector having a high "hidden water footprint" through raw materials and production processes. Moreover, wastewater from production often contains chemicals, preservatives, and microplastics that degrade the quality of surface and groundwater. [3]

As awareness of climate change and sustainability grows, so does social pressure on cosmetics companies to reduce their water impact. Stakeholders—including investors, NGOs, and regulatory bodies—are demanding that companies adopt strategies for efficient water management, measure their water footprint, and publicly disclose their environmental impact. Meanwhile, consumers increasingly choose brands that operate sustainably and communicate their environmental initiatives transparently.

Irresponsible water use can damage brand reputation, lead to product boycotts, and result in market losses. Society now expects not only quality products from cosmetics companies but also responsible behavior toward shared resources, with water being one of the most vital. Sustainability is no longer a bonus—it is becoming the standard.

The environmental consequences of unsustainable water use are serious. The most direct effect is water scarcity—depleting local water sources reduces availability for

households, agriculture, and ecosystems. This is especially harmful in arid and vulnerable areas, where every liter plays a key role in sustaining life and food production.

However, there are solutions. One of the most significant is the development of waterless formulations—products that contain little to no water. These include solid shampoos, stick balms, facial powders, and oil-based serums. Such products not only save water in production but also reduce the need for preservatives. Another key solution is recycling and reusing process water within facilities using closed-loop systems and advanced purification technologies. These systems enable multiple uses of the same water, thereby reducing total consumption.

Figure 2. *Sustainable water management*

By implementing these solutions, the industry not only minimizes its environmental footprint but also achieves long-term resource savings and meets market demands that increasingly value sustainability. Another major issue is water pollution. In addition to local impacts, unsustainable water use contributes to global environmental challenges, as water treatment and transportation systems consume significant energy, increasing greenhouse gas emissions. Therefore, rational water use is essential not only for resource conservation but also for protecting the entire environment.

3. WATER TREATMENT (RECYCLING) AND REUSE

In today's industrial environment, where resources are increasingly limited and environmental standards more stringent, sustainable water management is essential. Industries around the world are increasingly implementing systems for water recycling and reuse to reduce their environmental footprint, save resources, and meet international standards and regulations. Of particular importance are so-called waterloop factories—production facilities where water is continuously treated and reused in the process, without being discharged into the external environment.

Almost 20% of the world's water is used by industries, and that percentage continues to rise. Typical factories use far more water than they actually need, after which the water is discharged into sewage systems. In waterloop factories, the same water is treated and reused. Water drawn from the environment is reserved for drinking and as a product ingredient.

There are many benefits to this system, including significant water savings; at L'Oréal's factory in Jichang, water consumption has been reduced by 85% compared to 2005. The factory saves approximately 16,758 tons of water annually. There is also a notable reduction in wastewater released into the environment, directly contributing to ecosystem protection and reducing environmental footprints. [4]

Companies that invest in responsible water management send a clear message of concern for social and environmental issues, thereby strengthening their brand image and customer trust. Although initial investments may be high, long-term savings on water, energy, and wastewater treatment positively affect overall business efficiency.

However, implementing waterloop factories comes with challenges such as high upfront costs and technical system complexities. Integration into existing facilities often requires infrastructure adjustments and process modifications, which may cause disruptions and additional expenses. Also, system maintenance and water quality control require ongoing attention and expertise to ensure safety and effectiveness.

Beyond technical aspects, employee education and a shift in organizational culture

are necessary to adopt new water conservation practices. Furthermore, regulatory requirements and local laws may pose additional obstacles.

Waterloop factories adhere to international standards such as ISO 14001 for environmental management and ISO 22716 for good manufacturing practices in the cosmetics industry, reducing environmental impact and complying with strict regulations for production processes.

The Water Framework Directive (WFD) focuses on maintaining good water quality and quantity, reducing and eliminating pollution, and ensuring sufficient water for both nature and human needs. [5]

4. GJOSA & L'ORÉAL WATER SAVER

L'Oréal Water Saver is the first handheld showerhead to use patented water fragmentation technology, designed for hair salons. This shower system was developed in response to the need for efficient and sustainable rinsing systems in professional cosmetic treatments. Traditional rinsing systems use large amounts of water, leading to resource waste and higher energy costs. This showerhead offers a solution that not only reduces environmental impact but also provides high service quality and adaptability for professional use.

The technology is based on colliding water streams that produce droplets 10 times smaller than standard ones. This results in greater coverage, lower overall consumption, and maintained rinsing efficiency. In addition to fragmentation, the system also uses aeration—injection of air into the water stream—to increase the sense of water pressure and coverage without raising actual flow. This creates a "water curtain" that evenly covers the hair, enabling quick and effective rinsing.

The image is a contour map showing how fluid velocity changes across a surface or space. This is actually the average velocity as a parameter being monitored, denoted as Umean. The X and Y axes represent position in millimeters, showing a cross-section of the water jet.

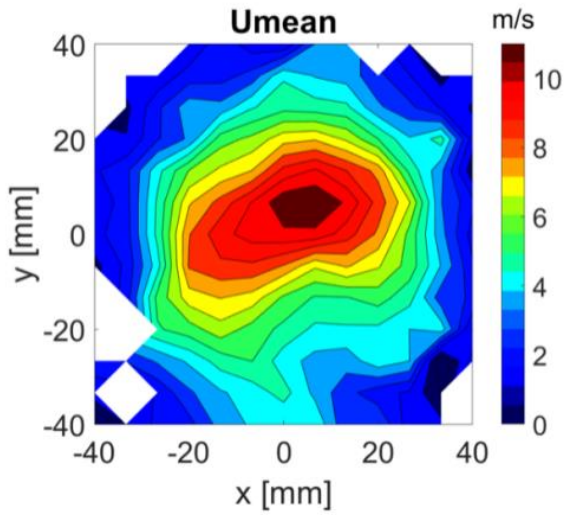

Figure 3. *Contour map of fluid velocity*

The red and dark red areas in the center show the highest speeds—over 10 m/s—while blue and dark blue areas show lower speeds, from 0 to 2 m/s. The gradient from blue to red represents the change in speed from the edges to the center. Based on this image, it can be determined whether jet design should be changed—either if speed is too low in the center or if flow needs optimization.

According to fluid mechanics principles, an optimal velocity distribution across the jet cross-section enables controlled direction of energy to where it is most needed-in the central part of the jet. The goal is to maintain a high velocity at the center to maximize the transferable impulse, while velocities at the edges are reduced to prevent uncontrolled splashing and water loss. Such velocity profile controle ensures that the fragmented droplets have enough energy to remove impurities, while remaining gentle enough to provide a comfortable rinsing experience.

Gjosa designs shower to concentrate water energy in the center while reducing it where it1`s not needed. This leads to efficient hair rinsing with less water and energy without compromising wash quality.

The system includes:

- precisely directed water jet collisions,

- controlled and uniform flow ensuring consistent rinsing performance,
- a wide, curtain-like spray for optimal hair coverage, and
- an ergonomic rotating nozzle for easy scalp access.

L'Oréal Water Saver was first implemented in hair salons worldwide as part of a pilot project for sustainable operations in the cosmetics industry. By the end of 2023, more than 10,000 salons globally had adopted this system. It has also been integrated into L'Oréal's manufacturing plants, particularly waterloop factories, where water is recycled and reused.

The image shows, on the left, a compact hemisphere of water—i.e., a part of the stream exiting the showerhead.

Figure 4. *Contour map of fluid velocity*

On the right are finely dispersed droplets moving slower and more evenly spread. While conventional showers emit a continuous strong stream, Gjosa uses a mist of small droplets that move slowly, better cover the scalp, and use less water.

The application of this technology has led to numerous positive environmental effects, including:

- up to 69% water savings per user,
- reduced CO_2 emissions from lower energy use to heat water,
- faster and better-quality treatments, and
- improved working experience for salon professionals.

5. CONCLUSION

Are technical solutions, innovations, new technologies, and artificial intelligence the right path to resource preservation in the near and distant future?

In a world facing increasing water scarcity, growing industrial consumption, and stronger societal pressure, sustainable business practices and water management are becoming essential. As shown in this paper, high water consumption in the cosmetics industry and irresponsible use of water resources lead to long-term environmental and social consequences. Therefore, many companies, such as L'Oréal, are implementing technological solutions and innovations to enable more rational consumption and reduce environmental impact. This also includes the use of artificial intelligence, which is becoming increasingly important for data analysis, identifying bottlenecks, and optimizing business processes. Together, these measures enable a proactive approach to environmental protection, which is becoming almost inevitable today.

L'Oréal Water Saver is an ideal example of innovation responding to the need to reduce ecological footprints and preserve local resources. It allows the company to balance economic goals with ecological responsibility. This raises the question: do companies truly apply sustainable practices out of environmental concern, or to preserve their image and respond to public pressure?

Although it is difficult for consumers to determine companies' true intentions, it can be said that, for most, sustainable business represents a combination of strategic, ecological, and regulatory goals. While some companies merely market environmental messages, others take sustainability seriously, publishing strategic plans, transparent reports, and measurable goals.

Regardless, one cannot ignore the fact that in today's world, sustainability has become an essential tool for industry survival on the market.

REFERENCES

[1] UN-Water (2021). *Sustainable Water Management*. Retrieved from

[2] Klemes, J. J. (2012). Industrial water recycle/reuse. *Procedia CIRP*, 1, 3–10.

[3] Gupta, R. (2020). Water and Sustainability in Cosmetics Manufacturing

[4] Anderson, J. (2003). The environmental benefits of water recycling and reuse. *Water Science & Technology Water Supply*, 3(4), 1–10.

[5] Aguilar, J. B. 2022. "Water Sustainability: A Waterless Life Cycle for Cosmetic Products." *Cleaner* .

SPONSORS:

The publication of this Conference program was financially supported by:

The Ministry of Education, Science and Technological Development of the Republic of Serbia

and :

MING Industry of hot forging

LOLA Institute d.o.o. Belgrade, Serbia

Philip Morris Operations a.d., Niš

Zijin Mining Group, Bor, Srbija

vossloh
enabling green mobility **Vossloh MIN Skretnice**

ZUMTOBEL

ZG Ligting Srb d.o.o.

EXIT ltd Prokuplje

JOHNSON ELECTRIC Niš

TEHNICOM INFORMATIKA

TEHNIKM INFORMATIKA DOO Niš

9 788660 551971